

MACHINE DESIGN

An Integrated Approach

Fourth Edition



Robert L. Norton

MACHINE DESIGN

An Integrated Approach

Fourth Edition

Robert L. Norton

Worcester Polytechnic Institute

Worcester, Massachusetts

Prentice Hall

Boston Columbus Indianapolis New York San Francisco Upper Saddle River
Amsterdam Cape Town Dubai London Madrid Milan Munich Paris Montreal Toronto
Delhi Mexico City Sao Paulo Sydney Hong Kong Seoul Singapore Taipei Tokyo

VP/Editorial Director, Engineering/Computer Science: *Marcia J. Horton*
Senior Editor: *Tacy Quinn*
Director of Marketing: *Margaret Waples*
Senior Marketing Manager: *Tim Galligan*
Marketing Assistant: *Mack Patterson*
Senior Managing Editor: *Scott Disanno*
Senior Operations Supervisor *Alan Fischer*
Manufacturing Buyer: *Lisa McDowell*
Creative Director: *Jayne Conte*
Cover Designer: *Margaret Kenselaar*
Media Editor: *Daniel Sandin*

Copyright © 2011, 2006, 2000, 1998 Pearson Education, Inc., publishing as Prentice Hall, One Lake Street, Upper Saddle River, New Jersey 07458. All rights reserved. Manufactured in the United States of America. This publication is protected by Copyright, and permission should be obtained from the publisher prior to any prohibited reproduction, storage in a retrieval system, or transmission in any form or by any means, electronic, mechanical, photocopying, recording, or likewise. To obtain permission(s) to use material from this work, please submit a written request to Pearson Education, Inc., Permissions Department, One Lake Street, Upper Saddle River, New Jersey 07458.

The author and publisher of the book have used their best efforts in preparing this book and the accompanying computer programs. These efforts include the development, research, and testing of the theories and programs to determine their effectiveness. The author and publisher make no warranty of any kind, expressed or implied, with regard to these programs or the documentation contained in this book. The author and publisher shall not be liable in any event for incidental or consequential damages in connection with, or arising out of, the furnishing, performance, or use of these programs.

Mathcad is a registered trademark of Mathsoft, Cambridge, MA. MATLAB® is a registered trademark of The MathWorks, Inc. Microsoft is a registered trademark or trademark of Microsoft Corporation in the United States and/or other countries. TK Solver is a trademark of UTS Corporation in the U.S. and/or other countries.

The cover photograph by the author is of Tom Norton, seven-time New England Trail Riders Association (NETRA) Hare Scrambles Champion (and the author's son).

Library of Congress Cataloging-in-Publication Data
Norton, Robert L.

Machine Design An Integrated Approach 4ed /
Robert L. Norton
p. cm.
Includes bibliographical references and index.
ISBN: 0-13-612370-8 (hard cover)
1. Machine design. I. Title
TJ230.N64 2010
621.8'15--dc22 97-19522 CIP 2005045847

10 9 8 7 6 5 4 3 2 1

Prentice Hall
is an imprint of



www.pearsonhighered.com

**ISBN 0-13-612370-8
ISBN 978-0-13-612370-5**

ABOUT THE AUTHOR

Robert L. Norton earned undergraduate degrees in both mechanical engineering and industrial technology at Northeastern University and an MS in engineering design at Tufts University. He is a registered professional engineer in Massachusetts. He has extensive industrial experience in engineering design and manufacturing and many years' experience teaching mechanical engineering, engineering design, computer science, and related subjects at Northeastern University, Tufts University, and Worcester Polytechnic Institute.

At Polaroid Corporation for 10 years, he designed cameras, related mechanisms, and high-speed automated machinery. He spent three years at Jet Spray Cooler Inc., designing food-handling machinery and products. For five years he helped develop artificial-heart and noninvasive assisted-circulation (counterpulsation) devices at the Tufts New England Medical Center and Boston City Hospital. Since leaving industry to join academia, he has continued as an independent consultant on engineering projects ranging from disposable medical products to high-speed production machinery. He holds 13 U.S. patents.

Norton has been on the faculty of Worcester Polytechnic Institute since 1981 and is currently the Milton P. Higgins II Distinguished Professor of Mechanical Engineering, Russell P. Searle Distinguished Instructor, Head of the Design Group in that department, and the Director of the Gillette Project Center at WPI. He teaches undergraduate and graduate courses in mechanical engineering with emphasis on design, kinematics, vibrations, and dynamics of machinery.

He is the author of numerous technical papers and journal articles covering kinematics, dynamics of machinery, cam design and manufacturing, computers in education, and engineering education and of the texts *Design of Machinery*, *Machine Design: An Integrated Approach* and the *Cam Design and Manufacturing Handbook*. He is a Fellow of the American Society of Mechanical Engineers and a member of the Society of Automotive Engineers. But, since his main interest is in teaching, he is most proud of the fact that, in 2007, he was chosen as *U. S. Professor of the Year* for the State of Massachusetts by the *Council for the Advancement and Support of Education (CASE)* and the *Carnegie Foundation for the Advancement of Teaching*, who jointly present the only national awards for teaching excellence given in the United States of America.

This book is dedicated to:

Donald N. Zwiep

Provost, Department Head, and Professor Emeritus
Worcester Polytechnic Institute

A gentleman and a leader,
without whose faith and foresight,
this book would never have been written.

Contents

PART I FUNDAMENTALS 1

CHAPTER 1 INTRODUCTION TO DESIGN

1.1	Design	3
	Machine Design	3
	Machine	4
	Iteration	5
1.2	A Design Process	5
1.3	Problem Formulation and Calculation	8
	Definition Stage	8
	Preliminary Design Stage	8
	Detailed Design Stage	9
	Documentation Stage	9
1.4	The Engineering Model	9
	Estimation and First-Order Analysis	10
	The Engineering Sketch	10
1.5	Computer-Aided Design and Engineering	11
	Computer-Aided Design (CAD)	11
	Computer-Aided Engineering (CAE)	14
	Computational Accuracy	16
1.6	The Engineering Report	16
1.7	Factors of Safety and Design Codes	16
	Factor of Safety	17
	Choosing a Safety Factor	18
	Design and Safety Codes	19
1.8	Statistical Considerations	20
1.9	Units	21
1.10	Summary	25
1.11	References	26
1.12	Web References	27
1.13	Bibliography	27
1.14	Problems	28

CHAPTER 2 MATERIALS AND PROCESSES	29
2.0 Introduction	29
2.1 Material-Property Definitions	29
The Tensile Test	31
Ductility and Brittleness	33
The Compression Test	35
The Bending Test	35
The Torsion Test	35
Fatigue Strength and Endurance Limit	37
Impact Resistance	38
Fracture Toughness	40
Creep and Temperature Effects	40
2.2 The Statistical Nature of Material Properties	41
2.3 Homogeneity and Isotropy	42
2.4 Hardness	42
Heat Treatment	44
Surface (Case) Hardening	45
Heat Treating Nonferrous Materials	46
Mechanical Forming and Hardening	46
2.5 Coatings and Surface Treatments	48
Galvanic Action	49
Electroplating	50
Electroless Plating	50
Anodizing	51
Plasma-Sprayed Coatings	51
Chemical Coatings	51
2.6 General Properties of Metals	52
Cast Iron	52
Cast Steels	53
Wrought Steels	53
Steel Numbering Systems	54
Aluminum	56
Titanium	58
Magnesium	59
Copper Alloys	59
2.7 General Properties of Nonmetals	60
Polymers	60
Ceramics	62
Composites	62
2.8 Selecting Materials	63
2.9 Summary	64
2.10 References	68
2.11 Web References	68
2.12 Bibliography	68
2.13 Problems	69

CHAPTER 3 LOAD DETERMINATION	73
3.0 Introduction	73
3.1 Loading Classes	73
3.2 Free-Body Diagrams	75
3.3 Load Analysis	76
Three-Dimensional Analysis	76
Two-Dimensional Analysis	77
Static Load Analysis	78
3.4 Two-Dimensional, Static Loading Case Studies	78
Case Study 1A: Bicycle Brake Lever Loading Analysis	79
Case Study 2A: Hand-Operated Crimping-Tool Loading Analysis	84
Case Study 3A: Automobile Scissors-Jack Loading Analysis	88
3.5 Three-Dimensional, Static Loading Case Study	93
Case Study 4A: Bicycle Brake Arm Loading Analysis	94
3.6 Dynamic Loading Case Study	98
Case Study 5A: Fourbar Linkage Loading Analysis	98
3.7 Vibration Loading	101
Natural Frequency	102
Dynamic Forces	104
Case Study 5B: Fourbar Linkage Dynamic Loading Measurement	105
3.8 Impact Loading	106
Energy Method	107
3.9 Beam Loading	111
Shear and Moment	111
Singularity Functions	112
Superposition	122
3.10 Summary	123
3.11 References	125
3.12 Web References	126
3.13 Bibliography	126
3.14 Problems	126
CHAPTER 4 STRESS, STRAIN, AND DEFLECTION	139
4.0 Introduction	139
4.1 Stress	139
4.2 Strain	143
4.3 Principal Stresses	143
4.4 Plane Stress and Plane Strain	146
Plane Stress	146
Plane Strain	146
4.5 Mohr's Circles	146
4.6 Applied Versus Principal Stresses	151
4.7 Axial Tension	152

4.8	Direct Shear Stress, Bearing Stress, and Tearout	153
	Direct Shear	153
	Direct Bearing	154
	Tearout Failure	154
4.9	Beams and Bending Stresses	154
	Beams in Pure Bending	155
	Shear Due to Transverse Loading	158
4.10	Deflection in Beams	162
	Deflection by Singularity Functions	164
	Statically Indeterminate Beams	171
4.11	Castigliano's Method	173
	Deflection by Castigliano's Method	175
	Finding Redundant Reactions with Castigliano's Method	175
4.12	Torsion	177
4.13	Combined Stresses	183
4.14	Spring Rates	185
4.15	Stress Concentration	186
	Stress Concentration Under Static Loading	187
	Stress Concentration Under Dynamic Loading	188
	Determining Geometric Stress-Concentration Factors	188
	Designing to Avoid Stress Concentrations	191
4.16	Axial Compression - Columns	193
	Slenderness Ratio	193
	Short Columns	193
	Long Columns	193
	End Conditions	195
	Intermediate Columns	197
	Eccentric Columns	200
4.17	Stresses in Cylinders	203
	Thick-Walled Cylinders	204
	Thin-Walled Cylinders	205
4.18	Case Studies in Static Stress and Deflection Analysis	205
	Case Study 1B: Bicycle Brake Lever Stress and Deflection Analysis	206
	Case Study 2B: Crimping-Tool Stress and Deflection Analysis	209
	Case Study 3B: Automobile Scissors-Jack Stress and Deflection Analysis	214
	Case Study 4B: Bicycle Brake Arm Stress Analysis	217
4.19	Summary	221
4.20	References	227
4.21	Bibliography	228
4.22	Problems	228
CHAPTER 5 STATIC FAILURE THEORIES		243
5.0	Introduction	243
5.1	Failure of Ductile Materials Under Static Loading	245
	The von Mises-Hencky or Distortion-Energy Theory	246
	The Maximum Shear-Stress Theory	252
	The Maximum Normal-Stress Theory	254
	Comparison of Experimental Data with Failure Theories	254

5.2	Failure of Brittle Materials Under Static Loading	258
	Even and Uneven Materials	258
	The Coulomb-Mohr Theory	259
	The Modified-Mohr Theory	260
5.3	Fracture Mechanics	265
	Fracture-Mechanics Theory	266
	Fracture Toughness K_c	269
5.4	Using The Static Loading Failure Theories	273
5.5	Case Studies in Static Failure Analysis	274
	Case Study 1C: Bicycle Brake Lever Failure Analysis	274
	Case Study 2C: Crimping Tool Failure Analysis	277
	Case Study 3C: Automobile Scissors-Jack Failure Analysis	280
	Case Study 4C: Bicycle Brake Arm Factors of Safety	282
5.6	Summary	285
5.7	References	288
5.8	Bibliography	289
5.9	Problems	290
CHAPTER 6 FATIGUE FAILURE THEORIES		303
6.0	Introduction	303
	History of Fatigue Failure	303
6.1	Mechanism of Fatigue Failure	306
	Crack Initiation Stage	307
	Crack Propagation Stage	307
	Fracture	308
6.2	Fatigue-Failure Models	309
	Fatigue Regimes	309
	The Stress-Life Approach	311
	The Strain-Life Approach	311
	The LEFM Approach	311
6.3	Machine-Design Considerations	312
6.4	Fatigue Loads	313
	Rotating Machinery Loading	313
	Service Equipment Loading	314
6.5	Measuring Fatigue Failure Criteria	315
	Fully Reversed Stresses	316
	Combined Mean and Alternating Stress	322
	Fracture-Mechanics Criteria	323
	Testing Actual Assemblies	326
6.6	Estimating Fatigue Failure Criteria	327
	Estimating the Theoretical Fatigue Strength S_f' or Endurance Limit S_e'	328
	Correction Factors to the Theoretical Fatigue Strength	330
	Calculating the Corrected Fatigue Strength S_f	337
	Creating Estimated S-N Diagrams	337
6.7	Notches and Stress Concentrations	342
	Notch Sensitivity	343
6.8	Residual Stresses	347

6.9	Designing for High-Cycle Fatigue	352
6.10	Designing for Fully Reversed Uniaxial Stresses	352
	Design Steps for Fully Reversed Stresses with Uniaxial Loading:	353
6.11	Designing for Fluctuating Uniaxial Stresses	360
	Creating the Modified-Goodman Diagram	361
	Applying Stress-Concentration Effects with Fluctuating Stresses	364
	Determining the Safety Factor with Fluctuating Stresses	366
	Design Steps for Fluctuating Stresses	369
6.12	Designing for Multiaxial Stresses in Fatigue	376
	Frequency and Phase Relationships	377
	Fully Reversed Simple Multiaxial Stresses	377
	Fluctuating Simple Multiaxial Stresses	378
	Complex Multiaxial Stresses	379
6.13	A General Approach to High-Cycle Fatigue Design.....	381
6.14	A Case Study in Fatigue Design	386
	Case Study 6: Redesign of a Failed Laybar for a Water-Jet Power Loom	387
6.15	Summary	399
6.16	References	403
6.17	Bibliography	406
6.18	Problems	407
CHAPTER 7 SURFACE FAILURE		419
7.0	Introduction	419
7.1	Surface Geometry	421
7.2	Mating Surfaces	423
7.3	Friction	424
	Effect of Roughness on Friction	425
	Effect of Velocity on Friction	425
	Rolling Friction	425
	Effect of Lubricant on Friction	426
7.4	Adhesive Wear	426
	The Adhesive-Wear Coefficient	429
7.5	Abrasive Wear	430
	Abrasive Materials	433
	Abrasion-Resistant Materials	433
7.6	Corrosion Wear	434
	Corrosion Fatigue	435
	Fretting Corrosion	435
7.7	Surface Fatigue	436
7.8	Spherical Contact	438
	Contact Pressure and Contact Patch in Spherical Contact	438
	Static Stress Distributions in Spherical Contact	440

7.9	Cylindrical Contact	444
	Contact Pressure and Contact Patch in Parallel Cylindrical Contact	444
	Static Stress Distributions in Parallel Cylindrical Contact	445
7.10	General Contact	448
	Contact Pressure and Contact Patch in General Contact	448
	Stress Distributions in General Contact	450
7.11	Dynamic Contact Stresses	453
	Effect of a Sliding Component on Contact Stresses	453
7.12	Surface Fatigue Failure Models—Dynamic Contact.....	461
7.13	Surface Fatigue Strength	464
7.14	Summary	470
	Designing to Avoid Surface Failure	471
7.15	References	474
7.16	Problems	476
CHAPTER 8 FINITE ELEMENT ANALYSIS		481
8.0	Introduction	481
	Stress and Strain Computation	482
8.1	Finite Element Method.....	483
8.2	Element Types	485
	Element Dimension and Degree of Freedom (DOF)	485
	Element Order	486
	H-Elements Versus P-Elements	487
	Element Aspect Ratio	487
8.3	Meshing	487
	Mesh Density	488
	Mesh Refinement	488
	Convergence	488
8.4	Boundary Conditions	492
8.5	Applying Loads	502
8.6	Testing the Model	503
8.7	Modal Analysis	506
8.8	Case Studies	508
	Case Study 1D: FEA Analysis of a Bicycle Brake Lever	509
	Case Study 2D: FEA Analysis of a Crimping Tool	511
	Case Study 4D: FEA Analysis of a Bicycle Brake Arm	513
	Case Study 7: FEA Analysis of a Trailer Hitch	516
8.9	Summary	518
8.10	References	519
8.11	Bibliography	519
8.12	Web Resources	519
8.13	Problems	520

PART II MACHINE DESIGN 521**CHAPTER 9 DESIGN CASE STUDIES 523**

9.0	Introduction	523
9.1	Case Study 8A: Preliminary Design of a Compressor Drive Train	526
9.2	Case Study 9A: Preliminary Design of a Winch Lift.....	528
9.3	Case Study 10A: Preliminary Design of a Cam Dynamic Test Fixture ...	532
9.4	Summary	537
9.5	References	537
9.6	Design Projects	538

CHAPTER 10 SHAFTS, KEYS, AND COUPLINGS 549

10.0	Introduction	549
10.1	Shaft Loads	549
10.2	Attachments and Stress Concentrations	551
10.3	Shaft Materials	553
10.4	Shaft Power	553
10.5	Shaft Loads	554
10.6	Shaft Stresses	554
10.7	Shaft Failure in Combined Loading.....	555
10.8	Shaft Design	556
	General Considerations	556
	Design for Fully Reversed Bending and Steady Torsion	557
	Design for Fluctuating Bending and Fluctuating Torsion	559
10.9	Shaft Deflection	566
	Shafts as Beams	567
	Shafts as Torsion Bars	567
10.10	Keys and Keyways	570
	Parallel Keys	570
	Tapered Keys	571
	Woodruff Keys	572
	Stresses in Keys	572
	Key Materials	573
	Key Design	573
	Stress Concentrations in Keyways	574
10.11	Splines.....	578
10.12	Interference Fits	580
	Stresses in Interference Fits	580
	Stress Concentration in Interference Fits	581
	Fretting Corrosion	582
10.13	Flywheel Design.....	585
	Energy Variation in a Rotating System	586
	Determining the Flywheel Inertia	588
	Stresses in Flywheels	590
	Failure Criteria	591

10.14 Critical Speeds of Shafts	593
Lateral Vibration of Shafts and Beams—Rayleigh's Method	596
Shaft Whirl	597
Torsional Vibration	599
Two Disks on a Common Shaft	600
Multiple Disks on a Common Shaft	601
Controlling Torsional Vibrations	602
10.15 Couplings	604
Rigid Couplings	605
Compliant Couplings	606
10.16 Case Study	608
Case Study 8B: Preliminary Design of Shafts for a Compressor Drive Train	608
10.17 Summary	612
10.18 References	614
10.19 Problems	615
CHAPTER 11 BEARINGS AND LUBRICATION	623
11.0 Introduction	623
11.1 Lubricants	625
11.2 Viscosity	627
11.3 Types of Lubrication	628
Full-Film Lubrication	629
Boundary Lubrication	631
11.4 Material Combinations in Sliding Bearings	631
11.5 Hydrodynamic Lubrication Theory	632
Petroff's Equation for No-Load Torque	633
Reynolds' Equation for Eccentric Journal Bearings	634
Torque and Power Losses in Journal Bearings	639
11.6 Design of Hydrodynamic Bearings	640
Design Load Factor—The Ocvirk Number	640
Design Procedures	642
11.7 Nonconforming Contacts	646
11.8 Rolling-element bearings	653
Comparison of Rolling and Sliding Bearings	654
Types of Rolling-Element Bearings	654
11.9 Failure of Rolling-Element bearings	658
11.10 Selection of Rolling-Element bearings	659
Basic Dynamic Load Rating C	659
Modified Bearing Life Rating	660
Basic Static Load Rating C_0	661
Combined Radial and Thrust Loads	662
Calculation Procedures	663
11.11 Bearing Mounting Details	665
11.12 Special Bearings	666
11.13 Case Study	668
Case Study 10B: Design of Hydrodynamic Bearings for a Cam Test Fixture	668

11.14 Summary	670
11.15 References	673
11.16 Problems	675
CHAPTER 12 SPUR GEARS	681
12.0 Introduction	681
12.1 Gear Tooth Theory	683
The Fundamental Law of Gearing	683
The Involute Tooth Form	684
Pressure Angle	685
Gear Mesh Geometry	686
Rack and Pinion	687
Changing Center Distance	687
Backlash	689
Relative Tooth Motion	689
12.2 Gear Tooth Nomenclature	689
12.3 Interference and Undercutting	692
Unequal-Addendum Tooth Forms	693
12.4 Contact Ratio	694
12.5 Gear Trains	696
Simple Gear Trains	696
Compound Gear Trains	697
Reverted Compound Trains	698
Epicyclic or Planetary Gear Trains	699
12.6 Gear Manufacturing	702
Forming Gear Teeth	702
Machining	703
Roughing Processes	703
Finishing Processes	705
Gear Quality	705
12.7 Loading on Spur Gears	706
12.8 Stresses in Spur Gears	708
Bending Stresses	709
Surface Stresses	718
12.9 Gear Materials	722
Material Strengths	723
AGMA Bending-Fatigue Strengths for Gear Materials	724
AGMA Surface-Fatigue Strengths for Gear Materials	725
12.10 Lubrication of Gearing	732
12.11 Design of Spur Gears	732
12.12 Case Study	734
Case Study 8C: Design of Spur Gears for a Compressor Drive Train	734
12.13 Summary	738
12.14 References	741
12.15 Problems	742

CHAPTER 13 HELICAL, BEVEL, AND WORM GEARS	747
13.0 Introduction	747
13.1 Helical Gears	747
Helical Gear Geometry	749
Helical-Gear Forces	750
Virtual Number of Teeth	751
Contact Ratios	752
Stresses in Helical Gears	752
13.2 Bevel Gears	760
Bevel-Gear Geometry and Nomenclature	761
Bevel-Gear Mounting	762
Forces on Bevel Gears	762
Stresses in Bevel Gears	763
13.3 Wormsets	768
Materials for Wormsets	770
Lubrication in Wormsets	770
Forces in Wormsets	770
Wormset Geometry	770
Rating Methods	771
A Design Procedure for Wormsets	773
13.4 Case Study	774
Case Study 9B: Design of a Wormset Speed Reducer for a Winch Lift	774
13.5 Summary	777
13.6 References	781
13.7 Problems	782
CHAPTER 14 SPRING DESIGN	785
14.0 Introduction	785
14.1 Spring Rate	785
14.2 Spring Configurations	788
14.3 Spring Materials	790
Spring Wire	790
Flat Spring Stock	793
14.4 Helical Compression Springs	795
Spring Lengths	796
End Details	796
Active Coils	797
Spring Index	797
Spring Deflection	797
Spring Rate	797
Stresses in Helical Compression Spring Coils	798
Helical Coil Springs of Nonround Wire	799
Residual Stresses	800
Buckling of Compression Springs	802
Compression-Spring Surge	802
Allowable Strengths for Compression Springs	803
The Torsional-Shear S-N Diagram for Spring Wire	804
The Modified-Goodman Diagram for Spring Wire	806

14.5 Designing Helical Compression Springs for Static Loading	808
14.6 Designing Helical Compression Springs for Fatigue Loading	812
14.7 Helical Extension Springs	820
Active Coils in Extension Springs	821
Spring Rate of Extension Springs	821
Spring Index of Extension Springs	821
Coil Preload in Extension Springs	821
Deflection of Extension Springs	822
Coil Stresses in Extension Springs	822
End Stresses in Extension Springs	822
Surging in Extension Springs	823
Material Strengths for Extension Springs	823
Design of Helical Extension Springs	824
14.8 Helical Torsion Springs	831
Terminology for Torsion Springs	832
Number of Coils in Torsion Springs	832
Deflection of Torsion Springs	832
Spring Rate of Torsion Springs	833
Coil Closure	833
Coil Stresses in Torsion Springs	833
Material Parameters for Torsion Springs	834
Safety Factors for Torsion Springs	835
Designing Helical Torsion Springs	836
14.9 Belleville Spring Washers	838
Load-Deflection Function for Belleville Washers	840
Stresses in Belleville Washers	841
Static Loading of Belleville Washers	842
Dynamic Loading	842
Stacking Springs	842
Designing Belleville Springs	843
14.10 Case Studies	845
Case Study 10C: Design of a Return Spring for a Cam-Follower Arm	846
14.11 Summary	850
14.12 References	853
14.13 Problems	854
CHAPTER 15 SCREWS AND FASTENERS	859
15.0 Introduction	859
15.1 Standard Thread Forms	862
Tensile Stress Area	863
Standard Thread Dimensions	864
15.2 Power Screws	865
Square, Acme, and Buttress Threads	865
Power Screw Application	866
Power Screw Force and Torque Analysis	868
Friction Coefficients	869
Self-Locking and Back-Driving of Power Screws	870
Screw Efficiency	871
Ball Screws	872

15.3	Stresses in Threads	874
	Axial Stress	875
	Shear Stress	875
	Torsional Stress	876
15.4	Types of Screw Fasteners	876
	Classification by Intended Use	877
	Classification by Thread Type	877
	Classification by Head Style	877
	Nuts and Washers	879
15.5	Manufacturing Fasteners	880
15.6	Strengths of Standard Bolts and Machine Screws	881
15.7	Preloaded Fasteners in Tension	882
	Preloaded Bolts Under Static Loading	885
	Preloaded Bolts Under Dynamic Loading	890
15.8	Determining the Joint Stiffness Factor	895
	Joints With Two Plates of the Same Material	897
	Joints With Two Plates of Different Materials	898
	Gasketed Joints	899
15.9	Controlling Preload	904
	The Turn-of-the-Nut Method	905
	Torque-Limited Fasteners	905
	Load-Indicating Washers	905
	Torsional Stress Due to Torquing of Bolts	906
15.10	Fasteners in Shear	907
	Dowel Pins	908
	Centroids of Fastener Groups	909
	Determining Shear Loads on Fasteners	910
15.11	Case Study	912
	Designing Headbolts for an Air Compressor	912
	Case Study 8D: Design of the Headbolts for an Air Compressor	912
15.12	Summary	917
15.13	References	920
15.14	Bibliography	921
15.15	Problems	921
CHAPTER 16	WELDMENTS	927
16.0	Introduction	927
16.1	Welding Processes	929
	Types of Welding in Common Use	930
	Why Should a Designer Be Concerned with the Welding Process?	931
16.2	Weld Joints and Weld Types	931
	Joint Preparation	933
	Weld Specification	933
16.3	Principles of Weldment Design	934
16.4	Static Loading of Welds	936

16.5 Static Strength of Welds	936
Residual Stresses in Welds	937
Direction of Loading	937
Allowable Shear Stress for Statically Loaded Fillet and PJP Welds	937
16.6 Dynamic Loading of Welds	940
Effect of Mean Stress on Weldment Fatigue Strength	940
Are Correction Factors Needed For Weldment Fatigue Strength?	940
Effect of Weldment Configuration on Fatigue Strength	941
Is There an Endurance Limit for Weldments?	945
Fatigue Failure in Compression Loading?	945
16.7 Treating a Weld as a Line	947
16.8 Eccentrically Loaded Weld Patterns	952
16.9 Design Considerations for Weldments in Machines	954
16.10 Summary	955
16.11 References	956
16.12 Problems	956
CHAPTER 17 CLUTCHES AND BRAKES	959
17.0 Introduction	959
17.1 Types of Brakes and Clutches	961
17.2 Clutch/Brake Selection and Specification	966
17.3 Clutch and Brake Materials	968
17.4 Disk Clutches	968
Uniform Pressure	969
Uniform Wear	969
17.5 Disk Brakes	971
17.6 Drum Brakes	972
Short-Shoe External Drum Brakes	973
Long-Shoe External Drum Brakes	975
Long-Shoe Internal Drum Brakes	979
17.7 Summary	979
17.8 References	982
17.9 Bibliography	982
17.10 Problems	983
APPENDIX A MATERIAL PROPERTIES	987
APPENDIX B BEAM TABLES	995
APPENDIX C STRESS-CONCENTRATION FACTORS	999
APPENDIX D ANSWERS TO SELECTED PROBLEMS	1007
INDEX	1017

Preface

Introduction

This text is intended for the *Design of Machine Elements* courses typically given in the junior year of most mechanical engineering curricula. The usual prerequisites are a first course in *Statics and Dynamics*, and one in *Strength of Materials*. The purpose of this book is to present the subject matter in an up-to-date manner with a strong design emphasis. The level is aimed at junior-senior mechanical engineering students. A primary goal was to write a text that is very easy to read and that students will enjoy reading despite the inherent dryness of the subject matter.

This textbook is designed to be an improvement over others currently available and to provide methods and techniques that take full advantage of computer-aided analysis. It emphasizes design and synthesis as well as analysis. Example problems, case studies, and solution techniques are spelled out in detail and are self-contained. All the illustrations are done in two colors. Short problems are provided in each chapter and, where appropriate, longer unstructured design-project assignments are given.

The book is independent of any particular computer program. Computer files for the solution of all the examples and case studies written in several different languages (Mathcad, MATLAB, Excel, and TK Solver) are provided on the CD-ROM. Several other programs written by the author are also provided as executable files. These include a Mohr's circle generator (MOHR.exe), dynamic surface stress calculator (CONTACT.exe), matrix solver (MATRIX.exe) and several linkage and cam design programs. An index of the CD-ROM's content is on the CD.

While this book attempts to be thorough and complete on the engineering-mechanics topics of failure theory and analysis, it also emphasizes the synthesis and design aspects of the subject to a greater degree than most other texts in print on this subject. It points out the commonality of the analytical approaches needed to design a wide variety of elements and emphasizes the use of computer-aided engineering as an approach to the design and analysis of these classes of problems. The author's approach to this course is based on 50 years of practical experience in mechanical engineering design, both in industry and as a consultant. He has taught mechanical engineering design at the university level for 30 of those years as well.

What's New in the Fourth Edition?

- A new chapter on the design of weldments presents the latest data and methods on this topic.
- The chapter on finite element analysis (FEA) has been moved from Chapter 16 to Chapter 8 and augmented with additional FEA solutions for case studies that are developed in earlier chapters.
- Solidworks models with FEA solutions to several of the case studies are provided on the CD-ROM.
- Solidworks models of many assigned problems' geometry are provided on the CD-ROM to expedite FEA solutions of those problems at the instructor's option.
- A new technique for the computation of bolted-joint stiffness is presented in Chapter 15 on Fasteners.
- Over 150 problems are added or revised with an emphasis on SI units.

Philosophy

This is often the first course that mechanical engineering students see that presents them with design challenges rather than set-piece problems. Nevertheless, the type of design addressed in this course is that of *detailed design*, which is only one part of the entire design-process spectrum. In detailed design, the general concept, application, and even general shape of the required device are typically known at the outset. We are not trying to invent a new device so much as define the shape, size, and material of a particular machine element such that it will not fail under the loading and environmental conditions expected in service.

The traditional approach to the teaching of the *Elements* course has been to emphasize the design of individual machine parts, or elements, such as gears, springs, shafts, etc. One criticism that is sometimes directed at the *Elements* course (or textbook) is that it can easily become a “cookbook” collection of disparate topics that does not prepare the student to solve other types of problems not found in the recipes presented. There is a risk of this happening. It is relatively easy for the instructor (or author) to allow the course (or text) to degenerate into the mode “Well it’s Tuesday, let’s design springs—on Friday, we’ll do gears.” If this happens, it may do the student a disservice because it doesn’t necessarily develop a fundamental understanding of the practical application of the underlying theories to design problems.

However, many of the machine elements typically addressed in this course provide superb examples of the underlying theory. If viewed in that light, and if presented in a general context, they can be an excellent vehicle for the development of student understanding of complex and important engineering theories. For example, the topic of preloaded bolts is a perfect vehicle to introduce the concept of prestressing used as a foil against fatigue loading. The student may never be called upon in practice to design a preloaded bolt, but he or she may well utilize the understanding of prestressing gained from the experience. The design of helical gears to withstand time-varying loads provides an excellent vehicle to develop the student’s understanding of combined stresses, Hertzian stresses, and fatigue failure. Thus the *elements* approach is a valid and defensible one as long as the approach taken in the text is sufficiently global. That is, it should not be allowed to degenerate into a collection of apparently unrelated exercises, but rather provide an integrated approach.

Another area in which the author has found existing texts (and *Machine Elements* courses) to be deficient is the lack of connection made between the dynamics of a system and the stress analysis of that system. Typically, these texts present their machine elements with (magically) predefined forces on them. The student is then shown how to determine the stresses and deflections caused by those forces. In real machine design, the forces are not always predefined and can, in large part, be due to the accelerations of the masses of the moving parts. However, the masses cannot be accurately determined until the geometry is defined and a stress analysis done to determine the strength of the assumed part. Thus an impasse exists that is broken only by iteration, i.e., assume a part geometry and define its geometric and mass properties, calculate the dynamic loads due in part to the material and geometry of the part. Then calculate the stresses and deflections resulting from those forces, find out it fails, redesign, and repeat.

An Integrated Approach

The text is divided into two parts. The first part presents the fundamentals of stress, strain, deflection, materials properties, failure theories, fatigue phenomena, fracture mechanics, FEA, etc. These theoretical aspects are presented in similar fashion to other texts. The second part presents treatments of specific, common design elements used as examples of applications of the theory but also attempts to avoid presenting a string of disparate topics in favor of an integrated approach that ties the various topics together via *case studies*.

Most *Elements* texts contain many more topics and more content than can possibly be covered in a one-semester course. Before writing the first edition of this book, a questionnaire was sent to 200 U.S. university instructors of the *Elements* course to solicit their opinions on the relative importance and desirability of the typical set of topics in an *Elements* text. With each revision to second, third, and fourth editions, users were again surveyed to determine what should be changed or added. The responses were analyzed and used to influence the structure and content of this book in all editions. One of the strongest desires originally expressed by the respondents was for *case studies* that present realistic design problems.

We have attempted to accomplish this goal by structuring the text around a series of ten case studies. These case studies present different aspects of the same design problem in successive chapters, for example, defining the static or dynamic loads on the device in Chapter 3, calculating the stresses due to the static loads in Chapter 4, and applying the appropriate failure theory to determine its safety factor in Chapter 5. Later chapters present more complex case studies, with more design content. The case study in Chapter 6 on fatigue design is one such example a real problem taken from the author's consulting practice. Chapter 8 presents FEA analyses of several of these case studies and compares those results to the classical solutions done in prior chapters.

The case studies provide a series of machine design projects throughout the book that contain various combinations of the elements normally dealt with in this type of text. The assemblies contain some collection of elements such as links subjected to combined axial and bending loads, column members, shafts in combined bending and torsion, gearsets under alternating loads, return springs, fasteners under fatigue loading, rolling element bearings, etc. This integrated approach has several advantages. It presents the student with a generic design problem in context rather than as a set of disparate, unrelated entities. The student can then see the interrelationships and the rationales for the design decisions that affect the individual elements. These more comprehensive case studies are in Part II of the text. The case studies in Part I are more limited in scope and directed to the engineering mechanics topics of the chapter. In addition to the case studies, each chapter has a selection of worked-out examples to reinforce particular topics.

Chapter 9, Design Case Studies, is devoted to the setup of three design case studies that are used in the following chapters to reinforce the concepts behind the design and analysis of shafts, springs, gears, fasteners, etc. Not all aspects of these design case studies are addressed as worked-out examples since another purpose is to provide material for student-project assignments. The author has used these case study topics as multi-week or term-long project assignments for groups or individual students with good success. Assigning open-ended project assignments serves to reinforce the design and analysis aspects of the course much better than set-piece homework assignments.

Problem Sets

Most of the 790 problem sets (590, or 75%) are independent within a chapter, responding to requests by users of the first edition to decouple them. The other 25% of the problem sets are still built upon in succeeding chapters. These linked problems have the same dash number in each chapter and their problem number is **boldface** to indicate their commonality among chapters. For example, Problem 3-4 asks for a static force analysis of a trailer hitch; Problem 4-4 requests a stress analysis of the same hitch based on the forces calculated in Problem 3-4; Problem 5-4 asks for the static safety factor for the hitch using the stresses calculated in Problem 4-4; Problem 6-4 requests a fatigue-failure analysis of the same hitch, and Problem 7-4 requires a surface stress analysis. The same trailer hitch is used as an FEA case study in Chapter 8. Thus, the complexity of the underlying design problem is unfolded as new topics are introduced. An

instructor who wishes to use this approach can assign problems with the same dash number in succeeding chapters. If one does not want to assign an earlier problem on which a later one is based, the solution manual data from the earlier problem can be provided to the students. Instructors who do not like interlinked problems can avoid them entirely and select from the 590 problems with nonbold problem numbers that are independent within their chapters.

Text Arrangement

Chapter 1 provides an introduction to the design process, problem formulation, safety factors, and units. Material properties are reviewed in Chapter 2 since even the student who has had a first course in material science or metallurgy typically has but a superficial understanding of the wide spectrum of engineering material properties needed for machine design. Chapter 3 presents a review of static and dynamic loading analysis, including beam, vibration, and impact loading, and sets up a series of case studies that are used in later chapters to illustrate the stress and deflection analysis topics with some continuity.

The *Design of Machine Elements* course, at its core, is really an intermediate-level, applied stress-analysis course. Accordingly, a review of the fundamentals of stress and deflection analysis is presented in Chapter 4. Static failure theories are presented in detail in Chapter 5 since the students have typically not yet fully digested these concepts from their first stress-analysis course. Fracture-mechanics analysis for static loads is also introduced.

The *Elements* course is typically the student's first exposure to fatigue analysis since most introductory stress-analysis courses deal only with statically loaded problems. Accordingly, fatigue-failure theory is presented at length in Chapter 6 with the emphasis on stress-life approaches to high-cycle fatigue design, which is commonly used in the design of rotating machinery. Fracture-mechanics theory is further discussed with regard to crack propagation under cyclic loading. Strain-based methods for low-cycle fatigue analysis are not presented but their application and purpose are introduced to the reader and bibliographic references are provided for further study. Residual stresses are also addressed. Chapter 7 presents a thorough discussion of the phenomena of wear mechanisms, surface contact stresses, and surface fatigue.

Chapter 8 provides an introduction to Finite Element Analysis (FEA). Many instructors are using the machine elements course to introduce students to FEA as well as to instruct them in the techniques of machine design. The material presented in Chapter 8 is not intended as a substitute for education in FEA theory. That material is available in many other textbooks devoted to that subject and the student is urged to become familiar with FEA theory through coursework or self-study. Instead Chapter 8 presents proper techniques for the application of FEA to practical machine design problems. Issues of element selection, mesh refinement, and the definition of proper boundary conditions are developed in some detail. These issues are not usually addressed in books on FEA theory. Many engineers in training today will, in their professional practice, use CAD solid modeling software and commercial finite element analysis code. It is important that they have some knowledge of the limitations and proper application of those tools. This chapter can be taken up earlier in the course if desired, especially if the students are expected to use FEA to solve assigned tasks. It is relatively independent of the other chapters. Many of various chapters' problem assignments have Solidworks models of their geometry provided on the CD-ROM.

These eight chapters comprise Part I of the text and lay the analytical foundation needed for design of machine elements. They are arranged to be taken up in the order presented and build upon each other with the exception of Chapter 8 on FEA.

Part II of the text presents the design of machine elements in context as parts of a whole machine. The chapters in Part II are essentially independent of one another and can be taken (or skipped) in any order that the instructor desires (except that Chapter 12 on spur gears should be studied before Chapter 13 on helical, bevel, and worm gears). It is unlikely that all topics in the book can be covered in a one-term or one semester course. Uncovered chapters will still serve as a reference for engineers in their professional practice.

Chapter 9 presents a set of design case studies to be used as assignments and as example case studies in the following chapters and also provides a set of suggested design project assignments in addition to the detailed case studies as described above. Chapter 10 investigates shaft design using the fatigue-analysis techniques developed in Chapter 6. Chapter 11 discusses fluid-film and rolling-element bearing theory and application using the theory developed in Chapter 7. Chapter 12 gives a thorough introduction to the kinematics, design and stress analysis of spur gears using the latest AGMA recommended procedures. Chapter 13 extends gear design to helical, bevel, and worm gearing. Chapter 14 covers spring design including helical compression, extension and torsion springs, as well as a thorough treatment of Belleville springs. Chapter 15 deals with screws and fasteners including power screws and preloaded fasteners. Chapter 16 presents an up-to-date treatment of the design of weldments for both static and dynamic loading. Chapter 17 presents an introduction to the design and specification of disk and drum clutches and brakes. The appendices contain material-strength data, beam tables, and stress-concentration factors, as well as answers to selected problems.

Supplements

A **Solutions Manual** is available to instructors from the publisher and **PowerPoint slides** of all figures and tables in the text are available on the publisher's website (password protected) at:

<http://www.pearsonhighered.com/>

To download these resources, choose the **Instructor Support** tab to register as an instructor and follow instructions on the site to obtain the resources provided. Mathcad files for all the problem solutions are available with the solutions manual. This computerized approach to problem solutions has significant advantages to the instructor who can easily change any assigned problem's data and instantly solve it. Thus an essentially infinite supply of problem sets is available, going far beyond those defined in the text. The instructor also can easily prepare and solve exam problems by changing data in the supplied files.

Anyone may download supplemental information about the author's course organization and operation (syllabi, project assignments, etc.) from the author's university web site at:

<http://www.me.wpi.edu/People/Norton/design.html>

As errata are discovered they will be posted on the author's personal website at:

<http://www.designofmachinery.com/MD/errata.html>

Professors who adopt the book may register at the author's personal website to obtain additional information relevant to the subject and the text and to download updated software (password protected). Go to:

<http://www.designofmachinery.com/registered/professor.html>

Anyone who purchases the book may register at the author's personal website to request updated software for the current edition (password protected). Go to:

<http://www.designofmachinery.com/registered/student.html>

Acknowledgments

The author expresses his sincere appreciation to all those who reviewed the first edition of the text in various stages of development including Professors J. E. Beard, Michigan Tech; J. M. Henderson, U. California, Davis; L. R. Koval, U. Missouri, Rolla; S. N. Kramer, U. Toledo; L. D. Mitchell, Virginia Polytechnic; G. R. Pennock, Purdue; D. A. Wilson, Tennessee Tech; Mr. John Lothrop; and Professor J. Ari-Gur, Western Michigan University, who also taught from a class-test version of the book. Robert Herrmann (WPI-ME '94) provided some problems and Charles Gillis (WPI-ME '96) solved most of the problem sets for the first edition.

Professors John R. Steffen of Valparaiso University, R. Jay Conant of Montana State, Norman E. Dowling of Virginia Polytechnic, and Francis E. Kennedy of Dartmouth made many useful suggestions for improvement and caught many errors. Special thanks go to Professor Hartley T. Grandin of WPI, who provided much encouragement and many good suggestions and ideas throughout the book's gestation, and also taught from various class-test versions.

Three former and the current Prentice Hall editors deserve special mention for their efforts in developing this book: Doug Humphrey, who wouldn't take no for an answer in persuading me to write it, Bill Stenquist, who usually said yes to my requests and expertly shepherded the book through to completion in its first edition, and Eric Svendsen who helped get the third edition into print and added value to the book. Tacy Quinn's support has helped marshall the fourth edition into print.

Since the book's first printing in 1995, several users have kindly pointed out errors and suggested improvements. My thanks go to Professors R. Boudreau of U. Moncton, Canada, V. Glozman of Cal Poly Pomona, John Steele of Colorado School of Mines, Burford J. Furman of San Jose State University, and Michael Ward of California State University, Chico.

Several other faculty have been kind enough to point out errors and offer constructive criticisms and suggestions for improvement in the later editions. Notable among these are: Professors Cosme Furlong of Worcester Polytechnic Institute, Joseph Rencis of University of Arkansas, Annie Ross of Universite de Moncton, Andrew Ruina of Cornell University, Douglas Walcerz of York College, and Thomas Dresner of Mountain City, CA.

Dr. Duane Miller of Lincoln Electric Company provided invaluable help with Chapter 16 on weldments and reviewed several drafts. Professor Stephen Covey of St. Cloud State University, and engineers Gregory Aviza and Charles Gillis of P&G Gillette also provided valuable feedback on the weldment chapter. Professor Robert Cornwell of Seattle University reviewed the discussion in Chapter 15 of his new method for the calculation of bolted joint stiffness and his method for computing stress concentration in rectangular wire springs discussed in Chapter 14.

Professors Fabio Marcelo Peña Bustos of Universidad Autónoma de Manizales, Caldas, Colombia, and Juan L. Balsevich-Prieto of Universidad Católica Nuestra Señora de la Asunción, Asunción, Paraguay, were kind enough to point out errata in the Spanish translation.

Special thanks are due to William Jolley of The Gillette Company who created the FEA models for the examples and reviewed Chapter 8, and to Edwin Ryan, retired Vice President of Engineering at Gillette, who provided invaluable support. Donald A. Jacques of the UTC Fuel Cells division of the United Technologies Company also reviewed Chapter 8 on Finite Element Analysis and made many useful suggestions. Professor Eben C. Cobb of Worcester Polytechnic Institute and his student Thomas Watson created the Solidworks models of many problem assignments and case studies and solved the FEA for the case studies that are on the CD-ROM.

Thanks are due several people who responded to surveys for the fourth edition and made many good suggestions: Kenneth R. Halliday of Ohio State University, Mohamed B. Trabia of University of Nevada Las Vegas, H. J. Summer III of Penn State University, Rajeev Madhavan Nair of Iowa State University, Ali P. Gordon of University of Central Florida, Robert Jackson of Auburn University, Cara Coad of Colorado School of Mines, Burford J. Furman of San Jose State University, Steven J. Covey of St. Cloud State University, Nathan Crane of University of Central Florida, César Augusto Álvarez Vargas of Universidad Autónoma de Manizales, Caldas, Colombia, Naser Nawayseh of Dhofar University, Oman, Hodge E. Jenkins of Mercer University, John Lee of San Jose State University, Mahmoud Kadkhodaei of Isfahan University of Technology, Steve Searcy of Texas A&M University, Yesh P. Singh of University of Texas at San Antonio, and Osornio C. Cuitláhuac of Universidad Iberoamericana Santa Fe, Mexico.

The author is greatly indebted to Thomas A. Cook, Professor Emeritus, Mercer University, who did the Solutions Manual for this book, updated the Mathcad examples, and contributed most of the new problem sets for this edition. Thanks also to Dr. Adriana Hera of Worcester Polytechnic Institute who updated the MATLAB and Excel models of all the examples and case studies and thoroughly vetted their correctness.

Finally, Nancy Norton, my infinitely patient wife for the past fifty years, deserves renewed kudos for her unfailing support and encouragement during many summers of “book widowhood.” I could not have done it without her.

Every effort has been made to eliminate errors from this text. Any that remain are the author’s responsibility. He will greatly appreciate being informed of any errors that still remain so they can be corrected in future printings. An e-mail to norton@wpi.edu will be sufficient.

*Robert L. Norton
Mattapoisett, Mass.
August 1, 2009*

Part

I

FUNDAMENTALS

1



INTRODUCTION TO DESIGN

*Learning without thought is labor lost;
thought without learning is perilous.*

CONFUCIUS, 6TH CENTURY B.C.

1.1 DESIGN

What is design? Wallpaper is designed. You may be wearing “designer” clothes. Automobiles are “designed” in terms of their external appearance. The term *design* clearly encompasses a wide range of meaning. In the above examples, design refers primarily to the object’s aesthetic appearance. In the case of the automobile, all of its other aspects also involve design. Its mechanical internals (engine, brakes, suspension, etc.) must be designed, more likely by engineers than by artists, though even the engineer gets to exhibit some artistry when designing machinery.

The word *design* is from the Latin word *designare* meaning “*to designate, or mark out.*” Webster’s dictionary gives several definitions of the word **design**, the most applicable of which is “*to outline, plot, or plan as action or work . . . to conceive, invent, contrive.*” We are more concerned here with engineering design than with artistic design. **Engineering design** can be defined as “*The process of applying the various techniques and scientific principles for the purpose of defining a device, a process, or a system in sufficient detail to permit its realization.*”

Machine Design

This text is concerned with one aspect of engineering design—**machine design**. Machine design deals with the creation of machinery that works safely, reliably, and well. A **machine** can be defined in many ways. The Random House dictionary^[1] lists twelve definitions, among which are these two:

Machine

1. An apparatus consisting of interrelated units, or
2. A device that modifies force or motion.

The **interrelated parts** referred to in the definition are also sometimes called **machine elements** in this context. The notion of **useful work** is basic to a machine's function, as there is almost always some energy transfer involved. The mention of **forces** and **motion** is also critical to our concerns, as, in converting energy from one form to another, machines **create motion** and **develop forces**. It is the engineer's task to define and calculate those motions, forces, and changes in energy in order to determine the sizes, shapes, and materials needed for each of the interrelated parts in the machine. This is the essence of **machine design**.

While one must, of necessity, design a machine one part at a time, it is crucial to recognize that each part's function and performance (and thus its design) are dependent on many other interrelated parts within the same machine. Thus, we are going to attempt to "design the whole machine" here, rather than simply designing individual elements in isolation from one another. To do this we must draw upon a common body of engineering knowledge encountered in previous courses, e.g., statics, dynamics, mechanics of materials (stress analysis), and material properties. Brief reviews and examples of these topics are included in the early chapters of this book.

The ultimate goal in machine design is to size and shape the parts (machine elements) and choose appropriate materials and manufacturing processes so that the resulting machine can be expected to perform its intended function without failure. This requires that the engineer be able to calculate and predict the mode and conditions of failure for each element and then design it to prevent that failure. This in turn requires that a **stress and deflection analysis** be done for each part. Since stresses are a function of the applied and inertial loads, and of the part's geometry, an analysis of the forces, moments, torques, and the dynamics of the system must be done before the stresses and deflections can be completely calculated.

If the "machine" in question has no moving parts, then the design task becomes much simpler, because only a static force analysis is required. But if the machine has no moving parts, it is not much of a machine (and doesn't meet the definition above); it is then a **structure**. Structures also need to be designed against failure, and, in fact, large external structures (bridges, buildings, etc.) are also subjected to dynamic loads from wind, earthquakes, traffic, etc., and thus must also be designed for these conditions. Structural dynamics is an interesting subject but one which we will not address in this text. We will concern ourselves with the problems associated with machines that move. If the machine's motions are very slow and the accelerations negligible, then a static force analysis will suffice. But if the machine has significant accelerations within it, then a dynamic force analysis is needed and the accelerating parts become "victims of their own mass."

In a static structure, such as a building's floor, designed to support a particular weight, the safety factor of the structure can be increased by adding appropriately distributed material to its structural parts. Though it will be heavier (more "dead" weight), if properly designed it may nevertheless carry more "live" weight (payload) than it did before, still without failure. In a dynamic machine, adding weight (mass) to moving parts may have the opposite effect, reducing the machine's safety factor, its allowable

speed, or its payload capacity. This is because some of the loading that creates stresses in the moving parts is due to the inertial forces predicted by **Newton's second law**, $F = ma$. Since the accelerations of the moving parts in the machine are dictated by its kinematic design and by its running speed, adding mass to moving parts will increase the inertial loads on those same parts unless their kinematic accelerations are reduced by slowing its operation. Even though the added mass may increase the strength of the part, that benefit may be reduced or cancelled by the resultant increases in inertial forces.

Iteration

Thus, we face a dilemma at the initial stages of machine design. Generally, before reaching the stage of sizing the parts, the kinematic motions of the machine will have already been defined. External forces provided by the “outside world” on the machine are also often known. Note that in some cases, the external loads on the machine will be very difficult to predict—for example, the loads on a moving automobile. The designer cannot predict with accuracy what environmental loads the user will subject the machine to (potholes, hard cornering, etc.) In such cases, statistical analysis of empirical data gathered from actual testing can provide some information for design purposes.

What remain to be defined are the inertial forces that will be generated by the known kinematic accelerations acting on the as yet undefined masses of the moving parts. The dilemma can be resolved only by **iteration**, which means *to repeat, or to return to a previous state*. We must assume some trial configuration for each part, use the mass properties (mass, CG location, and mass moment of inertia) of that trial configuration in a dynamic force analysis to determine the forces, moments, and torques acting on the part, and then use the cross-sectional geometry of the trial design to calculate the resulting stresses. In general, accurately determining all the loads on a machine is the most difficult task in the design process. If the loads are known, the stresses can be calculated.

Most likely, on the first trial, we will find that our design fails because the materials cannot stand the levels of stress presented. We must then redesign the parts (iterate) by changing shapes, sizes, materials, manufacturing processes, or other factors in order to reach an acceptable design. It is generally not possible to achieve a successful result without making several iterations through this design process. Note also that a change to the mass of one part will also affect the forces applied to parts connected to it and thus require their redesign also. It is truly the design of **interrelated parts**.

1.2 A DESIGN PROCESS*

The process of design is essentially an exercise in applied creativity. Various “design processes” have been defined to help organize the attack upon the “unstructured problem,” i.e., one for which the problem definition is vague and for which many possible solutions exist. Some of these design process definitions contain only a few steps and others a detailed list of 25 steps. One version of a design process is shown in Table 1-1, which lists ten steps. The initial step, **Identification of Need**, usually consists of an ill-defined and vague problem statement. The development of **Background Research** information (step 2) is necessary to fully define and understand the problem, after which it is possible to restate the **Goal** (step 3) in a more reasonable and realistic way than in the original problem statement.

* Adapted from Norton, *Design of Machinery*, 3ed. McGraw-Hill, New York, 2004, with the publisher's permission.

Table 1-1 A Design Process

1	Identification of need
2	Background research
3	Goal statement
4	Task specifications
5	Synthesis
6	Analysis
7	Selection
8	Detailed design
9	Prototyping and testing
10	Production

Step 4 calls for the creation of a detailed set of **Task Specifications** which bound the problem and limit its scope. The **Synthesis** step (5) is one in which as many alternative design approaches as possible are sought, usually without regard (at this stage) for their value or quality. This is also sometimes called the **Ideation and Invention** step in which the largest possible number of creative solutions are generated.

In step 6, the possible solutions from the previous step are **Analyzed** and either accepted, rejected, or modified. The most promising solution is **Selected** at step 7. Once an acceptable design is selected, the **Detailed Design** (step 8) can be done, in which all the loose ends are tied up, complete engineering drawings made, vendors identified, manufacturing specifications defined, etc. The actual construction of the working design is first done as a **Prototype** in step 9 and finally in quantity in **Production** at step 10. A more complete discussion of this design process can be found in reference 2, and a number of references on the topics of creativity and design are provided in the bibliography at the end of this chapter.

The above description may give an erroneous impression that this process can be accomplished in a linear fashion as listed. On the contrary, **iteration is required within the entire process**, moving from any step back to any previous step, in all possible combinations, and doing this repeatedly. The best ideas generated at step 5 will invariably be discovered to be flawed when later analyzed. Thus a return to at least the Ideation step will be necessary in order to generate more solutions. Perhaps a return to the Background Research phase may be necessary to gather more information. The Task Specifications may need to be revised if it turns out that they were unrealistic. In other words, anything is “fair game” in the design process, including a redefinition of the problem, if necessary. One cannot design in a linear fashion. It’s three steps forward and two (or more) back, until you finally emerge with a working solution.

Theoretically, we could continue this iteration on a given design problem forever, continually creating small improvements. Inevitably, the incremental gains in function or reductions in cost will tend toward zero with time. At some point, we must declare the design “good enough” and ship it. Often someone else (most likely, the boss) will snatch it from our grasp and ship it over our protests that it isn’t yet “perfect.” Machines that have been around a long time and that have been improved by many designers reach a level of “perfection” that makes them difficult to improve upon. One

example is the ordinary bicycle. Though inventors continue to attempt to improve this machine, the basic design has become fairly static after more than a century of development.

In machine design, the early design-process steps usually involve the **Type Synthesis** of suitable kinematic configurations which can provide the necessary motions. Type synthesis involves the choice of the *type of mechanism best suited to the problem*. This is a difficult task for the student, as it requires some experience and knowledge of the various types of mechanisms that exist and that might be feasible from a performance and manufacturing standpoint. As an example, assume that the task is to design a device to track the constant-speed, straight-line motion of a part on a conveyor belt and attach a second part to it as it passes by. This has to be done with good accuracy and repeatability and must be reliable and inexpensive. You might not be aware that this task could be accomplished by any of the following devices:

- a straight-line linkage
- a cam and follower
- an air cylinder
- a hydraulic cylinder
- a robot
- a solenoid

Each of these solutions, while possible, may not be optimal or even practical. Each has good and bad points. The straight-line linkage is large and may have undesirable accelerations, the cam and follower is expensive but is accurate and repeatable. The air cylinder is inexpensive but noisy and unreliable. The hydraulic cylinder and the robot are more expensive. The inexpensive solenoid has high impact loads and velocities. So, the choice of device type can have a big effect on design quality. A bad choice at the type-synthesis stage can create major problems later on. The design might have to be changed after completion, at great expense. Design is essentially an exercise in trade-offs. There is usually no clear-cut solution to a real engineering design problem.

Once the type of required mechanism is defined, its detailed kinematics must be synthesized and analyzed. The motions of all moving parts and their time derivatives through acceleration must be calculated in order to be able to determine the dynamic forces on the system. (See reference 2 for more information on this aspect of machine design.)

In the context of machine design addressed in this text, we will not exercise the entire design process as described in Table 1-1. Rather, we will propose examples, problems, and case studies that already have had steps 1–4 defined. The type synthesis and kinematic analysis will already be done, or at least set up, and the problems will be structured to that degree. The tasks remaining will largely involve steps 5 through 8, with a concentration on **synthesis** (step 5) and **analysis** (step 6).

Synthesis and analysis are the “two faces” of machine design, like two sides of the same coin. **Synthesis** means *to put together* and **analysis** means *to decompose, to take apart, to resolve into its constituent parts*. Thus they are opposites, but they are symbiotic. We cannot take apart “nothing,” thus we must first synthesize something in order to analyze it. When we analyze it, we will probably find it lacking, requiring further

synthesis, and then further analysis *ad nauseam*, finally iterating to a better solution. You will need to draw heavily upon your understanding of statics, dynamics, and mechanics of materials to accomplish this.

1.3 PROBLEM FORMULATION AND CALCULATION

It is extremely important for every engineer to develop good and careful computational habits. Solving complicated problems requires an organized approach. Design problems also require good record-keeping and documentation habits in order to record the many assumptions and design decisions made along the way so that the designer's thought process can be later reconstructed if redesign is necessary.

A suggested procedure for the designer is shown in Table 1-2, which lists a set of subtasks appropriate to most machine-design problems of this type. These steps should be documented for each problem in a neat fashion, preferably in a bound notebook in order to maintain their chronological order.*

Definition Stage

In your design notebook, first **Define the Problem** clearly in a concise statement. The “**givens**” for the particular task should be clearly listed, followed by a record of the **assumptions** made by the designer about the problem. Assumptions expand upon the given (known) information to further constrain the problem. For example, one might assume the effects of friction to be negligible in a particular case, or assume that the weight of the part can be ignored because it will be small compared to the applied or dynamic loads expected.

Preliminary Design Stage

Once the general constraints are defined, some **Preliminary Design Decisions** must be made in order to proceed. The reasons and justifications for these decisions should be documented. For example, we might decide to try a solid, rectangular cross section for a connecting link and choose aluminum as a trial material. On the other hand, if we recognized from our understanding of the problem that this link would be subjected to significant accelerations of a time-varying nature that would repeat for millions of cycles, a better design decision might be to use a hollow or I-beam section in order to reduce its mass and also to choose steel for its infinite fatigue life. Thus, these design decisions can have significant effect on the results and will often have to be changed or abandoned as we iterate through the design process. It has often been noted that 90% of a design’s characteristics may be determined in the first 10% of the total project time, during which these preliminary design decisions are made. If they are bad decisions, it may not be possible to save the bad design through later modifications without essentially starting over. The preliminary design concept should be documented at this stage with clearly drawn and labeled **Design Sketches** that will be understandable to another engineer or even to oneself after some time has passed.

* If there is a possibility of a patentable invention resulting from the design, then the notebook should be permanently bound (not loose-leaf), and its pages should be consecutively numbered, dated, and witnessed by someone who understands the technical content.

Table 1-2 Problem Formulation and Calculation

1	Define the problem	
2	State the givens	
3	Make appropriate assumptions	
4	Preliminary design decisions	
5	Design sketches	
6	Mathematical models	
7	Analysis of the design	
8	Evaluation	
9	Document results	

Detailed Design Stage

With a tentative design direction established we can create one or more **engineering** (mathematical) **models** of the element or system in order to analyze it. These models will usually include a loading model consisting of free-body diagrams which show all forces, moments, and torques on the element or system and the appropriate equations for their calculation. Models of the stress and deflection states expected at locations of anticipated failure are then defined with appropriate stress and deflection equations.

Analysis of the design is then done using these models and the safety or failure of the design determined. The results are **evaluated** in conjunction with the properties of the chosen **engineering materials** and a decision made whether to proceed with this design or iterate to a better solution by returning to an earlier step of the process.

Documentation Stage

Once sufficient iteration through this process provides satisfactory results, the **documentation** of the element's or system's design should be completed in the form of detailed engineering drawings, material and manufacturing specifications, etc. If properly approached, a great deal of the documentation task can be accomplished concurrent with the earlier stages simply by keeping accurate and neat records of all assumptions, computations, and design decisions made throughout the process.

1.4 THE ENGINEERING MODEL

The success of any design is highly dependent on the validity and appropriateness of the engineering models used to predict and analyze its behavior in advance of building any hardware. Creating a useful engineering model of a design is probably the most difficult and challenging part of the whole process. Its success depends a great deal on experience as well as skill. Most important is a thorough understanding of the first principles and fundamentals of engineering. The engineering model that we are describing here is an amorphous thing which may consist of some sketches of the geometric configuration and some equations that describe its behavior. It is a mathematical model

that describes the physical behavior of the system. This engineering model invariably requires the use of computers to exercise it. Using computer tools for analyzing engineering models is discussed in the next section. A physical model or prototype usually comes later in the process and is necessary to prove the validity of the engineering model through experiments.

Estimation and First-Order Analysis

The value of making even very simplistic engineering models of your preliminary designs cannot be overemphasized. Often, at the outset of a design, the problem is so loosely and poorly defined that it is difficult to develop a comprehensive and thorough model in the form of equations that fully describe the system. The engineering student is used to problems that are fully structured, of a form such as “*Given A, B, and C, find D.*” If one can identify the appropriate equations (model) to apply to such a problem, it is relatively easy to determine an answer (which might even match the one in the back of the book).

Real-life engineering design problems are not of this type. They are very **unstructured** and must be structured by you before they can be solved. Also, there is no “*back of the book*” to refer to for the answer.* This situation makes most students and beginning engineers very nervous. They face the “blank paper syndrome,” not knowing where to begin. A useful strategy is to recognize that

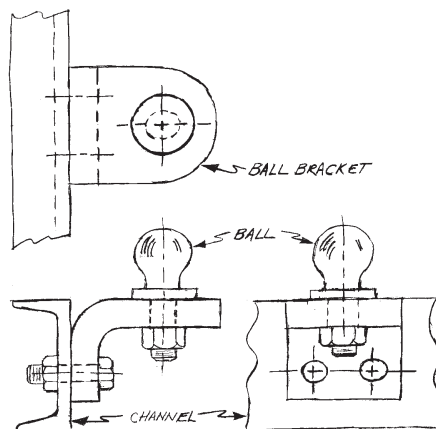
- 1 You must begin somewhere.
- 2 Wherever you begin, it will probably not be the “best” place to do so.
- 3 The magic of iteration will allow you to back up, improve your design, and eventually succeed.

With this strategy in mind, you can feel free to make some estimation of a design configuration at the outset, assume whatever limiting conditions you think appropriate, and do a “first-order analysis,” one that will be only an estimate of the system’s behavior. These results will allow you to identify ways to improve the design. Remember that it is preferable to get a reasonably approximate but quick answer that tells you whether the design does or doesn’t work rather than to spend more time getting the same result to more decimal places. With each succeeding iteration, you will improve your understanding of the problem, the accuracy of your assumptions, the complexity of your model, and the quality of your design decisions. Eventually, you will be able to refine your model to include all relevant factors (or identify them as irrelevant) and obtain a higher-order, final analysis in which you have more confidence.

The Engineering Sketch

A sketch of the concept is often the starting point for a design. This may be a freehand sketch, but it should always be made reasonably to scale in order to show realistic geometric proportions. This sketch often serves the primary purpose of communicating the concept to other engineers and even to yourself. It is one thing to have a vague concept in mind and quite another to define it in a sketch. This sketch should, at a minimum, contain three or more orthographic views, aligned according to proper drafting convention, and may also include an isometric or trimetric view. Figure 1-1 shows a freehand sketch of a simple design for one subassembly of a trailer hitch for a tractor.

* A student once commented that “*Life is an odd-numbered problem.*” This (slow) author had to ask for an explanation, which was: “*The answer is not in the back of the book.*”

**FIGURE 1-1**

A Freehand Sketch of a Trailer Hitch Assembly for a Tractor

While often incomplete in terms of detail needed for manufacture, the engineering sketch should contain enough information to allow the development of an engineering model for design and analysis. This may include critical, if approximate, dimensional information, some material assumptions, and any other data germane to its function that is needed for further analysis. The engineering sketch captures some of the givens and assumptions made, even implicitly, at the outset of the design process.

1.5 COMPUTER-AIDED DESIGN AND ENGINEERING

The computer has created a true revolution in engineering design and analysis. Problems whose solution methods have literally been known for centuries but that only a generation ago were practically unsolvable due to their high computational demands can now be solved in minutes on inexpensive microcomputers. Tedious graphical solution methods were developed in the past to circumvent the lack of computational power available from slide rules. Some of these graphical solution methods still have value in that they can show the results in an understandable form. But one can no longer “do engineering” without using its latest and most powerful tool, the computer.

Computer-Aided Design (CAD)

As the design progresses, the crude freehand sketches made at the earliest stages will be supplanted by formal drawings made either with conventional drafting equipment or, as is increasingly common, with computer-aided design or computer-aided drafting software. If the distinction between these two terms (both of which share the acronym CAD) was ever clear (a subject for debate which will be avoided here), then that distinction is fading as more sophisticated CAD software becomes available. The original CAD systems of a generation ago were essentially drafting tools that allowed the creation of computer-generated multiview drawings similar to those done for centuries before by hand on a drafting board. The data stored in these early CAD systems were

strictly two-dimensional representations of the orthographic projections of the part's true 3-D geometry. Only the edges of the part were defined in the database. This is called a **wireframe model**. Some 3-D CAD packages use wireframe representation as well.

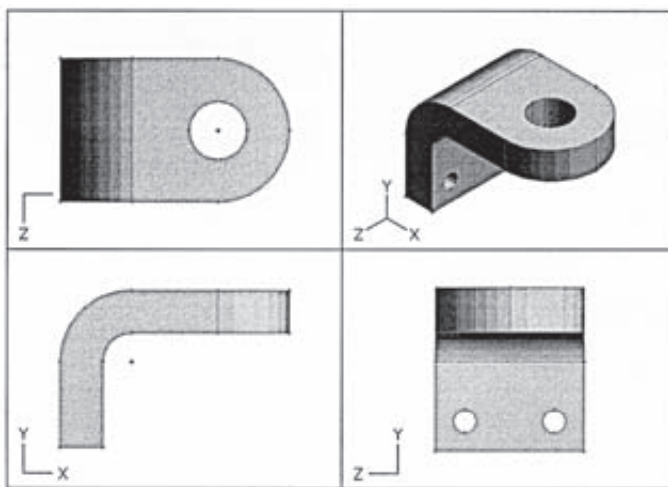
Present versions of most CAD software packages allow (and sometimes require) that the geometry of the parts be encoded in a 3-D data base as **solid models**. In a solid model the edges and the faces of the part are defined. From this 3-D information, the conventional 2-D orthographic views can be automatically generated if desired. The major advantage of creating a 3-D solid-model geometric data base for any design is that its mass-property information can be rapidly calculated. (This is not possible in a 2-D or 3-D wireframe model.) For example, in designing a machine part, we need to determine the location of its center of gravity (CG), its mass, its mass moment of inertia, and its cross-sectional geometries at various locations. Determining this information from a 2-D model must be done outside the CAD package. That is tedious to do and can only be approximate when the geometry is complex. But, if the part is designed in a solid modeling CAD system such as *ProEngineer*,^[7] *Unigraphics*,^[4] or one of many others, the mass properties can be calculated for the most complicated part geometries.

Solid modeling systems usually provide an interface to one or more Finite Element Analysis (FEA) programs and allow direct transfer of the model's geometry to the FEA package for stress, vibration, and heat transfer analysis. Some CAD systems include a mesh-generation feature which creates the FEA mesh automatically before sending the data to the FEA software. This combination of tools provides an extremely powerful means to obtain superior designs whose stresses are more accurately known than would be possible by conventional analysis techniques when the geometry is complex.

While it is highly likely that the students reading this textbook will be using CAD tools including finite element or boundary element analysis (BEA) methods in their professional practice, it is still necessary that the fundamentals of applied stress analysis be thoroughly understood. That is the purpose of this text. FEA techniques will be discussed in Chapters 4 and 8 but will not be emphasized in this text. Rather we will concentrate on the classical stress-analysis techniques in order to lay the foundation for a thorough understanding of the fundamentals and their application to machine design.

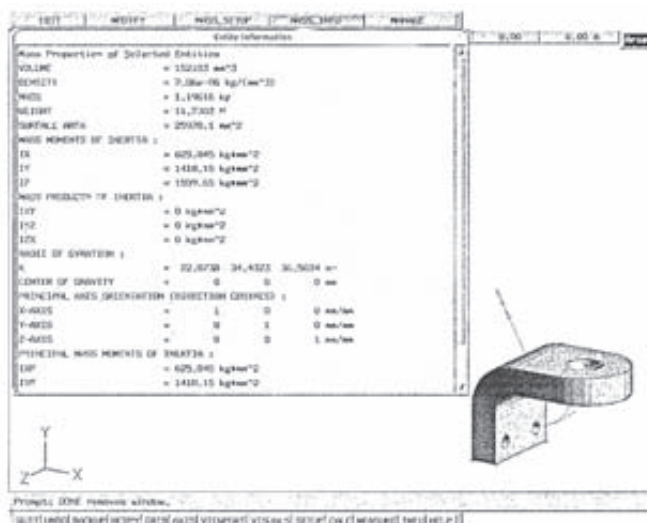
FEA and BEA methods are rapidly becoming the methods of choice for the solution of complicated stress-analysis problems. However, there is danger in using those techniques without a solid understanding of the theory behind them. These methods will always give *some* results. Unfortunately, those results can be incorrect if the problem was not well formulated and well meshed with proper boundary conditions applied. Being able to recognize incorrect results from a computer-aided solution is extremely important to the success of any design. Chapter 8 provides a brief introduction to FEA. The student should take courses in FEA and BEA to become familiar with these tools.

Figure 1-2 shows a solid model of the ball bracket from Figure 1-1 that was created in a CAD software package. The shaded, isometric view in the upper right corner shows that the solid volume of the part is defined. The other three views show orthographic projections of the part. Figure 1-3 shows the mass-properties data which are calculated by the software. Figure 1-4 shows a wireframe rendering of the same part generated from the solid geometry data base. A wireframe version is used principally to speed up the screen-drawing time when working on the model. There is much less wireframe display information to calculate than for the solid rendering of Figure 1-2.

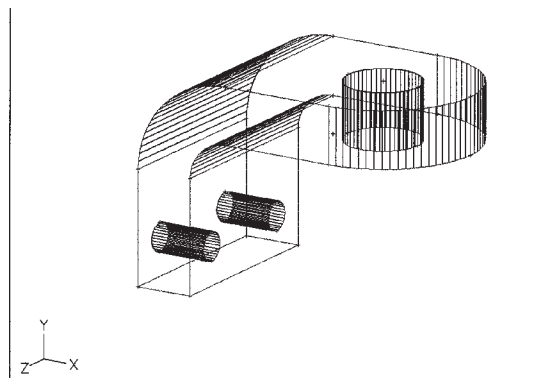
**FIGURE 1-2**

A CAD Solid Model of the Ball Bracket from the Trailer Hitch Assembly of Figure 1-1

Figure 1-5 shows a fully dimensioned, orthographic, multiview drawing of the ball bracket that was generated in the CAD software package. Another major advantage of creating a solid model of a part is that the dimensional and tool-path information needed for its manufacture can be generated in the CAD system and sent over a network to a computer-controlled machine on the manufacturing floor. This feature allows the production of parts without the need for paper drawings such as Figure 1-5. Figure 1-6 shows the same part after a finite element mesh was applied to it by the CAD software before sending it to the FEA software for stress analysis.

**FIGURE 1-3**

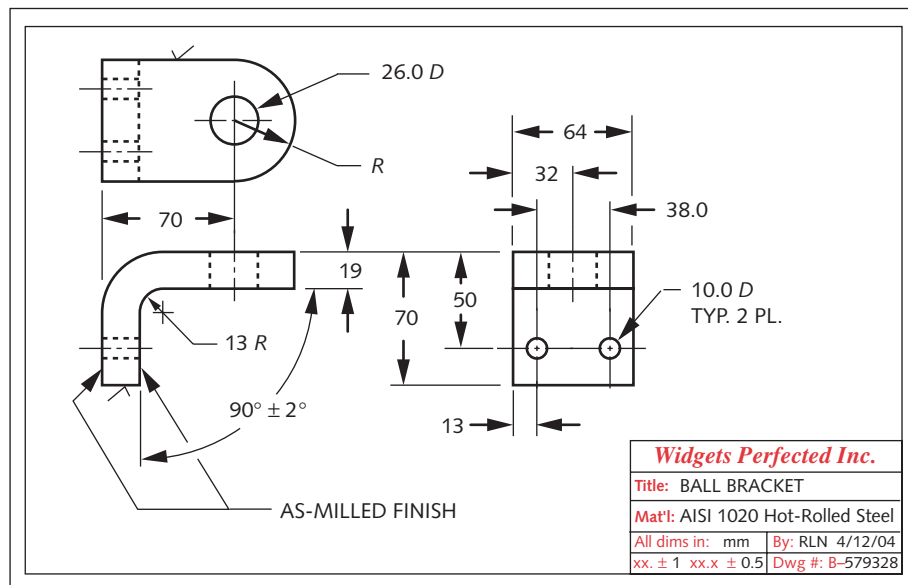
Mass Properties of the Ball Bracket Calculated Within the CAD System from Its Solid Model

**FIGURE 1-4**

A Wireframe Representation of the Ball Bracket Generated from Its Solid Model in a CAD System

Computer-Aided Engineering (CAE)

The techniques generally referred to above as CAD are a subset of the more general topic of computer-aided engineering (CAE), which term implies that more than just the geometry of the parts is being dealt with. However, the distinctions between CAD and CAE continue to blur as more sophisticated software packages become available. In fact, the description of the use of a solid modeling CAD system and an FEA package together as described in the previous section is an example of CAE. When some analysis of forces, stresses, deflections, or other aspects of the physical behavior of the design

**FIGURE 1-5**

A Dimensioned, 3-View Orthographic Drawing Done in a 2-D CAD Drawing Package

**FIGURE 1-6**

An FEA Mesh Applied to the Solid Model of the Ball Bracket in the CAD System

is included, with or without the solid geometry aspects, the process is called CAE. Many commercial software packages do one or more aspects of CAE. The FEA and BEA software packages mentioned above are in this category. See Chapter 8 for more information on FEA. Dynamic force simulations of mechanisms can be done with such packages as *ADAMS*^[5] and *Working Model*.^[6] Some software packages such as *ProEngineer*,^[7] *Solidworks*,^[12] *Unigraphics*,^[4] and others combine aspects of a CAD system with general analysis capabilities. These constraint-based programs allow constraints to be applied to the design which can control the part geometry as the design parameters are varied.

Other classes of tools for CAE are equation solvers such as *MATLAB*^[11], *Mathcad*,^[9] *TK Solver*,^[8] and spreadsheets such as *Excel*.^[10] These are general-purpose tools that will allow any combination of equations to be encoded in a convenient form and then will manipulate the equation set (i.e., the engineering model) for different trial data and conveniently display tabular and graphic output. Equation solvers are invaluable for the solution of force, stress, and deflection equations in machine-design problems because they allow rapid “what-if” calculations to be done. The effects of dimensional or material changes on the stresses and deflections in the part can be seen instantly. In the absence of a true solid modeling system, an equation solver also can be used to approximate the part’s mass properties while iterating the geometry and material properties of trial part designs. Rapid iteration to an acceptable solution is thus enhanced.

The CD-ROM included with the text contains a large number of models for various equation solvers that support the examples and case studies presented in the text. Introductions to the use of *TK Solver* and *Mathcad* along with examples of their use are provided as PDF files on the CD-ROM. In addition, some custom-written computer programs, MOHR, CONTACT, ASDEQ, FOURBAR, FIVEBAR, SIXBAR, SLIDER, DYNACAM, and MATRIX are provided on the CD-ROM to aid in the calculation of dynamic loads and stresses when solving the open-ended design problems assigned.

However, one must be aware that these computer tools are just tools and are not a substitute for the human brain. Without a thorough understanding of the engineering fundamentals on the part of the user, the computer will not give good results. Garbage in, garbage out. *Caveat Lector.*

Computational Accuracy

Computers and calculators make it very easy to obtain numerical answers having many significant figures. Before writing down all those digits, you are advised to recall the accuracy of your initial assumptions and given data. If, for example, your applied loads were known to only two significant figures, it is incorrect and misleading to express the calculated stresses to more significant figures than your input data possessed. However, it is valid and appropriate to make all intermediate calculations to the greatest accuracy available in your computational tools. This will minimize computational round-off errors. But, when done, round off the results to a level consistent with your known or assumed data.

1.6 THE ENGINEERING REPORT*

Communication of your ideas and results is a very important aspect of engineering. Many engineering students picture themselves in professional practice spending most of their time doing calculations of a nature similar to those they have done as students. Fortunately, this is seldom the case, as it would be very boring. Actually, engineers spend a large percentage of their time communicating with others, either orally or in writing. Engineers write proposals and technical reports, give presentations, and interact with support personnel. When your design is done, it is usually necessary to present the results to your client, peers, or employer. The usual form of presentation is a formal engineering report. In addition to a written description of the design, these reports will usually contain engineering drawings or sketches as described earlier, as well as tables and graphs of data calculated from the engineering model.

It is very important for engineering students to develop their communication skills. *You may be the cleverest person in the world, but no one will know that if you cannot communicate your ideas clearly and concisely.* In fact, if you cannot explain what you have done, you probably don't understand it yourself. The design-project assignments in Chapter 9 are intended to be written up in formal engineering reports to give you some experience in this important skill of technical communication. Information on writing engineering reports can be found in the suggested readings listed in the bibliography.

1.7 FACTORS OF SAFETY AND DESIGN CODES

* Excerpted from Norton,
Design of Machinery, 3ed
McGraw-Hill, New York, 2004,
with the publisher's permission.

The quality of a design can be measured by many criteria. It is always necessary to calculate one or more factors of safety to estimate the likelihood of failure. There may be legislated, or generally accepted, design codes that must be adhered to as well.

Factor of Safety*

A factor of safety or safety factor can be expressed in many ways. It is typically a ratio of two quantities that have the same units, such as strength/stress, critical load/applied load, load to fail part/expected service overload, maximum cycles/applied cycles, or maximum safe speed/operating speed. A safety factor is always unitless.

The form of expression for a safety factor can usually be chosen based on the character of loading on the part. For example, consider the loading on the side wall of a cylindrical water tower that can never be “more than full” of a liquid of known density within a known temperature range. Since this loading is highly predictable over time, a comparison of the strength of the material to the stress in the wall of a full tank might be appropriate as a safety factor. Note in this example that the possibility of rust reducing the thickness of the wall over time must be considered. (See Section 4.17 for a discussion of stresses in cylinder walls and Section 7.6 for a discussion of corrosion.)

If this cylindrical water tower is standing on legs loaded as columns, then a safety factor for the legs based on a ratio of the column’s critical buckling load over the applied load from a full water tower would be appropriate. (See Section 4.16 for a discussion of column buckling.)

If a part is subjected to loading that varies cyclically with time, it may experience fatigue failure. The resistance of a material to some types of fatigue loading can be expressed as a maximum number of cycles of stress reversal at a given stress level. In such cases, it may be appropriate to express the safety factor as a ratio of the maximum number of cycles to expected material failure over the number of cycles applied to the part in service for its desired life. (See Chapter 6 for a discussion of fatigue-failure phenomena and several approaches to the calculation of safety factors in such situations.)

The safety factor of a part such as a rotating sheave (pulley) or flywheel is often expressed as a ratio of its maximum safe speed over the highest expected speed in service. In general, if the stresses in the parts are a linear function of the applied service loads and those loads are predictable, then a safety factor expressed as strength/stress or failure load/applied load will give the same result. Not all situations fit these criteria. Some require a nonlinear ratio. A column is one example, because its stresses are a nonlinear function of the loading (see Section 4.16). Thus a critical (failure) load for the particular column must be calculated for comparison to the applied load.

Another complicating factor is introduced when the magnitudes of the expected applied loads are not accurately predictable. This can be true in virtually any application in which the use (and thus the loading) of the part or device is controlled by humans. For example, there is really no way to prevent someone from attempting to lift a 10-ton truck with a jack designed to lift a 2-ton automobile. When the jack fails, the manufacturer (and designer) may be blamed even though the failure was probably due more to the “nut behind the jack handle.” In situations where the user may subject the device to overloading conditions, an assumed overload may have to be used to calculate a safety factor based on a ratio of the load that causes failure over the assumed service overload. Labels warning against inappropriate use may be needed in these situations as well.

Since there may be more than one potential mode of failure for any machine element, it can have more than one value of safety factor N . The smallest value of N for

* Also called safety factor. We will use both terms interchangeably in this text.

any part is of greatest concern, since it predicts the most likely mode of failure. When N becomes reduced to 1, the stress in the part is equal to the strength of the material (or the applied load is equal to the load that fails it, etc.) and failure occurs. Therefore, we desire N to be always greater than 1.

Choosing a Safety Factor

Choosing a safety factor is often a confusing proposition for the beginning designer. The safety factor can be thought of as a measure of the designer's uncertainty in the analytical models, failure theories, and material-property data used, and should be chosen accordingly. How much greater than one N must be depends on many factors, including our level of confidence in the model on which the calculations are based, our knowledge of the range of possible in-service loading conditions, and our confidence in the available material-strength information. If we have done extensive testing on physical prototypes of our design to prove the validity of our engineering model and of the design, and have generated test data on the particular material's strengths, then we can afford to use a smaller safety factor. If our model is less well proven or the material-property information is less reliable, a larger N is in order. In the absence of any design codes that may specify N for particular cases, the choice of factor of safety involves engineering judgment. A reasonable approach is to determine the largest loads expected in service (including possible overloads) and the minimum expected material strengths and base the safety factors on these data. The safety factor then becomes a reasonable measure of uncertainty.

If you fly, it may not give you great comfort to know that safety factors for commercial aircraft are in the range of 1.2 to 1.5. Military aircraft can have $N < 1.1$, but their crews wear parachutes. (Test pilots deserve their high salaries.) Missiles have $N = 1$ but have no crew and aren't expected to return anyway. These small factors of safety in aircraft are necessary to keep weight low and are justified by sophisticated analytical modeling (usually involving FEA), testing of the actual materials used, extensive testing of prototype designs, and rigorous in-service inspections for incipient failures of the equipment. The opening photograph of this chapter shows an elaborate test rig used by the Boeing Aircraft Co. to mechanically test the airframe of full-scale prototype or production aircraft by applying dynamic forces and measuring their effects.

It can be difficult to predict the kinds of loads that an assembly will experience in service, especially if those loads are under the control of the end-user, or Mother Nature. For example, what loads will the wheel and frame of a bicycle experience? It depends greatly on the age, weight, and recklessness of the rider, whether used on- or off-road, etc. The same problem of load uncertainty exists with all transportation equipment, ships, aircraft, automobiles, etc. Manufacturers of these devices engage in extensive test programs to measure typical service loads. See Figures 3-16 (p. 106) and 6-7 (p. 315) for examples of such service-load data.

Some guidelines for the choice of a safety factor in machine design can be defined based on the quality and appropriateness of the material-property data available, the expected environmental conditions compared to those under which the material test data were obtained, and the accuracy of the loading- and stress-analysis models developed for the analyses. Table 1-3 shows a set of factors for ductile materials which can be chosen in each of the three categories listed based on the designer's knowledge or judg-

Table 1-3 Factors Used to Determine a Safety Factor for Ductile Materials

Information	Quality of Information	Factor
Material-property data available from tests	The actual material used was tested	<i>F1</i> 1.3
	Representative material test data are available	2
	Fairly representative material test data are available	3
	Poorly representative material test data are available	5+
Environmental conditions in which it will be used	Are identical to material test conditions	<i>F2</i> 1.3
	Essentially room-ambient environment	2
	Moderately challenging environment	3
Analytical models for loading and stress	Extremely challenging environment	5+
	Models have been tested against experiments	<i>F3</i> 1.3
	Models accurately represent system	2
	Models approximately represent system	3
	Models are crude approximations	5+

ment of the quality of information used. The overall safety factor is then taken as the largest of the three factors chosen. Given the uncertainties involved, a safety factor typically should not be taken to more than 1 decimal place accuracy.

$$N_{ductile} \cong \text{MAX}(F1, F2, F3) \quad (1.1a)$$

The ductility or brittleness of the material is also a concern. Brittle materials are designed against the ultimate strength, so failure means fracture. Ductile materials under static loads are designed against the yield strength and are expected to give some visible warning of failure before fracture, unless cracks indicate the possibility of a fracture-mechanics failure (see Sections 5-3 and 6-5). For these reasons, the safety factor for brittle materials is often made twice that which would be used for a ductile material in the same situation:

$$N_{brittle} \cong 2 * \text{MAX}(F1, F2, F3) \quad (1.1b)$$

This method of determining a safety factor is only a guideline to obtain a starting point and is obviously subject to the judgment of the designer in selecting factors in each category. The designer has the ultimate responsibility to ensure that the design is safe. A larger safety factor than any shown in Table 1-3 may be appropriate in some circumstances.

Design and Safety Codes

Many engineering societies and government agencies have developed codes for specific areas of engineering design. Most are only recommendations, but some have the force of law. The ASME provides recommended guidelines for safety factors to be used in particular applications such as steam boilers and pressure vessels. Building codes are

legislated in most U.S.A. states and cities and usually deal with publicly accessible structures or their components, such as elevators and escalators. Safety factors are sometimes specified in these codes and may be quite high. (The code for escalators in one state called for a factor of safety of 14.) Clearly, where human safety is involved, high values of N are justified. However, they come with a weight and cost penalty, as parts must often be made heavier to achieve large values of N . The design engineer must always be aware of these codes and standards and adhere to them where applicable.

The following is a partial list of engineering societies and governmental, industrial, and international organizations that publish standards and codes of potential interest to the mechanical engineer. Addresses and data on their publications can be obtained in any technical library or from the internet.

- American Gear Manufacturers Association (AGMA) <http://www.agma.org/>
- American Institute of Steel Construction (AISC) <http://www.aisc.org/>
- American Iron and Steel Institute (AISI) <http://www.steel.org/>
- American National Standards Institute (ANSI) <http://www.ansi.org/>
- American Society for Metals (ASM International) <http://www.asm-intl.org/>
- American Society of Mechanical Engineers (ASME) <http://www.asme.org/>
- American Society of Testing and Materials (ASTM) <http://www.astm.org/>
- American Welding Society (AWS) <http://www.aws.org/>
- Anti-Friction Bearing Manufacturers Association (AFBMA)
- International Standards Organization (ISO) <http://www.iso.ch/iso/en>
- National Institute for Standards and Technology (NIST)* <http://www.nist.gov/>
- Society of Automotive Engineers (SAE) <http://www.sae.org/>
- Society of Plastics Engineers (SPE) <http://www.4spe.org/>
- Underwriters Laboratories (UL) <http://www.ul.com/>

1.8 STATISTICAL CONSIDERATIONS

Nothing is absolute in engineering any more than in any other endeavor. The strengths of materials will vary from sample to sample. The actual size of different examples of the “same” part made in quantity will vary due to manufacturing tolerances. As a result, we should take the statistical distributions of these properties into account in our calculations. The published data on the strengths of materials may be stated either as minimum values or as average values of tests made on many specimens. If it is an average value, there is a 50% chance that a randomly chosen sample of that material will be weaker or stronger than the published average value. To guard against failure, we can reduce the material-strength value that we will use in our calculations to a level that will include a larger percentage of the population. To do this requires some understanding of statistical phenomena and their calculation. All engineers should have this understanding and should include a statistics course in their curriculum. We briefly discuss some of the fundamental aspects of statistics in Chapter 2.

* Formerly the National Bureau of Standards (NBS).

1.9 UNITS*

Several different systems of units are used in engineering. The most common in the United States are the U.S. *foot-pound-second system (fps)*, the U.S. *inch-pound-second system (ips)*, and the *Système Internationale (SI)*. The metric *centimeter, gram, second (cgs)* system is being used more frequently in the U.S., particularly in international companies, e.g., the automotive industry. All systems are created from the choice of three of the quantities in the general expression of Newton's second law

$$F = \frac{mL}{t^2} \quad (1.2a)$$

where F is force, m is mass, L is length, and t is time. The units for any three of these variables can be chosen and the other is then derived in terms of the chosen units. The three chosen units are called *base units*, and the remaining one is a *derived unit*.

Most of the confusion that surrounds the conversion of computations between either one of the U.S. systems and the *SI* system is due to the fact that the *SI* system uses a different set of base units than the U.S. systems. Both U.S. systems choose *force*, *length*, and *time* as the base units. Mass is then a derived unit in the U.S. systems, which are referred to as *gravitational systems* because the value of mass is dependent on the local gravitational constant. The *SI* system chooses *mass*, *length*, and *time* as the base units, and force is the derived unit. *SI* is then referred to as an *absolute system*, since the mass is a base unit whose value is not dependent on local gravity.

The U.S. *foot-pound-second (fps)* system requires that all lengths be measured in feet (ft), forces in pounds (lb), and time in seconds (sec). Mass is then derived from Newton's law as

$$m = \frac{Ft^2}{L} \quad (1.2b)$$

and its units are pounds seconds squared per **foot** (lb sec²/ft) = **slugs**.

The U.S. *inch-pound-second (ips)* system requires that all lengths be measured in inches (in), forces in pounds (lb), and time in seconds (sec). Mass is still derived from Newton's law, equation 1.2b, but the units are now

$$\text{pounds seconds squared per } \text{inch} \text{ (lb sec}^2/\text{in}) = \text{blobs}^\dagger$$

This mass unit is not slugs! It is worth twelve slugs or one "blob"!

Weight is defined as the force exerted on an object by gravity. Probably the most common units error that students make is to mix up these two unit systems (*fps* and *ips*) when converting weight units (which are pounds force) to mass units. Note that the gravitational acceleration constant (g or g_c) on earth at sea level is approximately 32.17 **feet** per second squared, which is equivalent to 386 **inches** per second squared. The relationship between mass and weight is

$$\text{mass} = \text{weight} / \text{gravitational acceleration}$$

$$m = \frac{W}{g_c} \quad (1.3)$$

* Excerpted from Norton, *Design of Machinery*, 3ed, 2004, McGraw-Hill, New York, with the publisher's permission.

† It is unfortunate that the mass unit in the *ips* system has never officially been given a name such as the term *slug* used for mass in the *fps* system. The author boldly suggests (with tongue only slightly in cheek) that this unit of mass in the *ips* system be called a *blob* (bl) to distinguish it more clearly from the *slug* (sl), and to help the student avoid some of the common errors listed below. Twelve *slugs* = one *blob*. *Blob* does not sound any sillier than *slug*, is easy to remember, implies mass, and has a convenient abbreviation (bl) which is an anagram for the abbreviation for pound (lb). Besides, if you have ever seen a garden *slug*, you know it looks just like a "little *blob*."

It should be obvious that if you measure all your lengths in **inches** and then use $g = g_c = 32.17 \text{ feet/sec}^2$ to compute mass, you will have an error of *a factor of 12* in your results. This is a serious error, large enough to crash the airplane you designed. Even worse off is the student who neglects to convert weight to mass *at all*. The results of this calculation will have an error of either 32 or 386, which is enough to sink the ship!*

The value of mass is needed in Newton's second-law equation to determine forces due to accelerations:

$$F = ma \quad (1.4a)$$

The units of mass in this equation are either g , kg , **slugs**, or **blobs** depending on the units system used. Thus, in either English system, the weight W (lbf) must be divided by the acceleration due to gravity g_c as indicated in equation 1.3 to get the proper mass quantity for equation 1.4a.

Adding further to the confusion is the common use of the unit of **pounds mass** (lb_m). This unit, often used in fluid dynamics and thermodynamics, comes about through the use of a slightly different form of Newton's equation:

$$F = \frac{ma}{g_c} \quad (1.4b)$$

where m = mass in lb_m , a = acceleration, and g_c = the gravitational constant. On earth, the value of the **mass** of an object measured in **pounds mass** (lb_m) is *numerically equal* to its **weight** in **pounds force** (lbf). However, the student *must remember to divide* the value of m in lb_m by g_c when using this form of Newton's equation. Thus the lb_m will be divided either by 32.17 or by 386 when calculating the dynamic force. The result will be the same as when the mass is expressed in either slugs or blobs in the $F = ma$ form of the equation. Remember that in round numbers at sea level on earth

* A 125-million-dollar space probe was lost because NASA failed to convert data that had been supplied in *ips* units by its contractor, Lockheed Aerospace, into the metric units used in the NASA computer programs that controlled the spacecraft. It was supposed to orbit the planet Mars, but instead either burned up in the Martian atmosphere or crashed into the planet because of this units error. Source: *The Boston Globe*, October 1, 1999, p. 1.

† A valuable resource for information on the proper use of SI units can be found at the U. S. Government NIST site at <http://physics.nist.gov/cuu/Units/units.html>

Another excellent resource on the proper use of metric units in machine design can be found in a pamphlet "Metric Is Simple," published and distributed by the fastener company Bossard International Inc., 235 Heritage Avenue, Portsmouth, NH 03801 <http://www.bossard.com/>

$$1 \text{ lb}_m = 1 \text{ lbf} \qquad 1 \text{ slug} = 32.17 \text{ lbf} \qquad 1 \text{ blob} = 386 \text{ lbf}$$

The **SI system** requires that lengths be measured in meters (m), mass in kilograms (kg), and time in seconds (sec). This is sometimes also referred to as the **mks** system. Force is derived from Newton's law and the units are:

$$\text{kg m/sec}^2 = \text{newtons}$$

In the **SI** system there are distinct names for mass and force, which helps alleviate confusion.[†] When converting between **SI** and U.S. systems, be alert to the fact that mass converts from kilograms (kg) to either slugs (sl) or blobs (bl), and force converts from newtons (N) to pounds (lb). The gravitational constant (g_c) in the **SI** system is approximately 9.81 m/sec^2 .

The **cgs** system requires that lengths be measured in centimeters (cm), mass in grams (g), and time in seconds (sec). Force is measured in dynes. The **SI** system is generally preferred over the **cgs** system.

The systems of units used in this textbook are the U.S. *ips* system and the **SI** system. Much of machine design in the United States is still done in the *ips* system, though the **SI** system is becoming more common.[†] Table 1-4 shows some of the variables used in this text and their units. Table 1-5 shows a number of conversion factors between commonly used units. The student is cautioned always to check the units in any equa-

Table 1-4 Variables and Units

Base Units in Boldface - Abbreviations in ()

Variable	Symbol	ips unit	fps unit	SI unit
Force	<i>F</i>	pounds (lb)	pounds (lb)	newtons (N)
Length	<i>l</i>	inches (in)	feet (ft)	meters (m)
Time	<i>t</i>	seconds (sec)	seconds (sec)	seconds (sec)
Mass	<i>m</i>	lb-sec ² /in (bl)	lb-sec ² /ft (sl)	kilograms (kg)
Weight	<i>W</i>	pounds (lb)	pounds (lb)	newtons (N)
Pressure	<i>p</i>	psi	psf	N/m ² = Pa
Velocity	<i>v</i>	in/sec	ft/sec	m/sec
Acceleration	<i>a</i>	in/sec ²	ft/sec ²	m/sec ²
Stress	σ , τ	psi	psf	N/m ² = Pa
Angle	θ	degrees (deg)	degrees (deg)	degrees (deg)
Angular velocity	ω	radians/sec	radians/sec	radians/sec
Angular acceleration	α	radians/sec ²	radians/sec ²	radians/sec ²
Torque	<i>T</i>	lb-in	lb-ft	N-m
Mass moment of inertia	<i>I</i>	lb-in-sec ²	lb-ft-sec ²	kg-m ²
Area moment of inertia	<i>I</i>	in ⁴	ft ⁴	m ⁴
Energy	<i>E</i>	in-lb	ft-lb	joules = N-m
Power	<i>P</i>	in-lb/sec	ft-lb/sec	N-m/sec = watt
Volume	<i>V</i>	in ³	ft ³	m ³
Specific weight	<i>v</i>	lb/in ³	lb/ft ³	N/m ³
Mass density	ρ	bl/in ³	sl/ft ³	kg/m ³

tion written for a problem solution, whether in school or in professional practice. If properly written, an equation should cancel all units across the equal sign. If it does not, then you can be *absolutely sure it is incorrect*. Unfortunately, a unit balance in an equation does not guarantee that it is correct, as many other errors are possible. Always double-check your results. You might save a life.

EXAMPLE 1-1

Units Conversion

Problem The weight of an automobile is known in lb_f . Convert it to mass units in the *SI*, *cgs*, *fps*, and *ips* systems. Also convert it to lb_m .

Given The weight = 4 500 lb_f .

Assumptions The automobile is on earth at sea level.

Table 1-5 Selected Units Conversion Factors

These conversion factors (and others) are built into the files UNITMAST and STUDENT

Multiply this	by	this	to get	this	Multiply this	by	this	to get	this
acceleration									
in/sec ²	x	0.0254	=	m/sec ²	lb-in.sec ²	x	0.1138	=	N-m.sec ²
ft/sec ²	x	12	=	in/sec ²	in-lb	x	0.1138	=	N-m
angles									
radian	x	57.2958	=	deg	ft-lb	x	12	=	in-lb
area									
in ²	x	645.16	=	mm ²	N-m	x	8.7873	=	in-lb
ft ²	x	144	=	in ²	N-m	x	0.7323	=	ft-lb
area moment of inertia									
in ⁴	x	416 231	=	mm ⁴	power	x	550	=	ft-lb/sec
in ⁴	x	4.162E-07	=	m ⁴	hp	x	33 000	=	ft-lb/min
m ⁴	x	1.0E+12	=	mm ⁴	hp	x	6 600	=	in-lb/sec
m ⁴	x	1.0E+08	=	cm ⁴	hp	x	745.7	=	watts
ft ⁴	x	20 736	=	in ⁴	N-m/sec	x	8.7873	=	in-lb/sec
density									
lb/in ³	x	27.6805	=	g/cc	pressure and stress				Pa
lb/in ³	x	1 728	=	lb/ft ³	psi	x	6 894.8	=	Pa
g/cc	x	0.001	=	g/mm ³	psi	x	6.895E-3	=	MPa
kg/m ³	x	1.0E-06	=	g/mm ³	psi	x	144	=	psf
force									
lb	x	4.448	=	N	kpsi	x	1 000	=	psi
N	x	1.0E+05	=	dyne	N/m ²	x	1	=	Pa
ton (short)	x	2 000	=	lb	N/mm ²	x	1	=	MPa
length									
in	x	25.4	=	mm	spring rate				N/m
ft	x	12	=	in	lb/in	x	175.126	=	N/m
mass									
blob	x	386	=	lb	lb/ft	x	0.08333	=	lb/in
slug	x	32.17	=	lb	stress intensity				Pa
blob	x	12	=	slug	MPa-m ^{0.5}	x	0.909	=	kpsi-in ^{0.5}
kg	x	2.205	=	lb	velocity				m/sec
kg	x	9.8083	=	N	in/sec	x	0.0254	=	in/sec
kg	x	1 000	=	g	ft/sec	x	12	=	in/sec
volume									
in ³	x	16 387.2	=	mm ³	rad/sec	x	9.5493	=	rpm
ft ³	x	1 728	=	in ³	in ³	x	16 387.2	=	mm ³
cm ³	x	0.061023	=	in ³	ft ³	x	1 728	=	in ³
m ³	x	1.0E+09	=	mm ³	cm ³	x	0.061023	=	in ³
Solution									

Solution

- 1 Equation 1.4a (p. 22) is valid for the first four systems listed.

For the *fps* system:

$$m = \frac{W}{g} = \frac{4500 \text{ lb}_f}{32.17 \text{ ft/sec}^2} = 139.9 \frac{\text{lb}_f - \text{sec}^2}{\text{ft}} = 139.9 \text{ slugs} \quad (a)$$

For the *ips* system:

$$m = \frac{W}{g} = \frac{4500 \text{ lb}_f}{386 \text{ in/sec}^2} = 11.66 \frac{\text{lb}_f - \text{sec}^2}{\text{in}} = 11.66 \text{ blobs} \quad (b)$$

For the *SI* system:

$$\begin{aligned} W &= 4500 \text{ lb} \frac{4.448 \text{ N}}{\text{lb}} = 20016 \text{ N} \\ m &= \frac{W}{g} = \frac{20016 \text{ N}}{9.81 \text{ m/sec}^2} = 2040 \frac{\text{N} - \text{sec}^2}{\text{m}} = 2040 \text{ kg} \end{aligned} \quad (c)$$

For the *cgs* system:

$$\begin{aligned} W &= 4500 \text{ lb} \frac{4.448E5 \text{ dynes}}{\text{lb}} = 2.002E9 \text{ dynes} \\ m &= \frac{W}{g} = \frac{2.002E9 \text{ dynes}}{981 \text{ cm/sec}^2} = 2.04E6 \frac{\text{dynes} - \text{sec}^2}{\text{cm}} = 2.04E6 \text{ g} \end{aligned} \quad (d)$$

- 2 For mass expressed in lb_m , equation 1.4b (p. 22) must be used.

$$m = W \frac{g_c}{g} = 4500 \text{ lb}_f \frac{386 \text{ in/sec}^2}{386 \text{ in/sec}^2} = 4500 \text{ lb}_m \quad (e)$$

Note that lb_m is numerically equal to lb_f and so must not be used as a mass unit unless you are using the form of Newton's law expressed as equation 1.4b.

1.10 SUMMARY

Design can be fun and frustrating at the same time. Because design problems are very unstructured, a large part of the task is creating sufficient structure to make it solvable. This naturally leads to multiple solutions. To students used to seeking an answer that matches the one in the “back of the book” this exercise can be frustrating. There is no “one right answer” to a design problem, only answers that are arguably better or worse than others. The marketplace has many examples of this phenomenon. How many different makes and models of new automobiles are available? Don’t they all do more or less the same task? But you probably have your own opinion about which ones do the task better than others. Moreover, the task definition is not exactly the same for all examples. A four-wheel-drive automobile is designed for a slightly different problem definition than is a two-seat sports car (though some examples incorporate both those features).

The message to the beginning designer then is to be open-minded about the design problems posed. Don’t approach design problems with the attitude of trying to find “the right answer,” as there is none. Rather, be daring! Try something radical. Then test it

with analysis. When you find it doesn't work, don't be disappointed; instead realize that you have learned something about the problem you didn't know before. Negative results are still results! We learn from our mistakes and can then design a better solution the next time. This is why *iteration* is so crucial to successful design.

The computer is a necessary tool to the solution of contemporary engineering problems. Problems can be solved more quickly and more accurately with proper use of computer-aided engineering (CAE) software. However, the results are only as good as the quality of the engineering models and data used. The engineer should not rely on computer-generated solutions without also developing and applying a thorough understanding of the fundamentals on which the model and the CAE tools are based.

Important Equations Used in This Chapter

See the referenced sections for information on the proper use of these equations.

Mass (see Section 1.9):

$$m = \frac{W}{g_c} \quad (1.3)$$

Dynamic Force—for use with standard mass units (kg, slugs, blobs) (see Section 1.9):

$$F = ma \quad (1.4a)$$

Dynamic Force—for use with mass in lb_m = lb_f (see Section 1.9):

$$F = \frac{ma}{g_c} \quad (1.4b)$$

1.11 REFERENCES

- 1 *Random House Dictionary of the English Language*. 2nd ed. unabridged, S.B. Flexner, ed., Random House: New York, 1987, pp. 1151.
- 2 **R. L. Norton**, *Design of Machinery: An Introduction to the Synthesis and Analysis of Mechanisms and Machines*, 3ed. McGraw-Hill: New York, 2004, pp. 7-14.
- 3 **Autocad**, Autodesk Inc., <http://usa.autodesk.com>
- 4 **Unigraphics**, EDS, Cypress, CA, <http://www.eds.com>
- 5 **ADAMS**, Mechanical Dynamics, MSC Software, <http://www.krev.com>
- 6 **Working Model**, MSC Software, <http://www.krev.com>.
- 7 **Pro/Engineer**, Parametric Technology Corp., Waltham, MA, <http://www.ptc.com>
- 8 **TK Solver**, Universal Technical Systems, Rockford, IL, <http://www.uts.com>
- 9 **Mathcad**, Mathsoft Inc., Cambridge, MA, <http://www.mathsoft.com>
- 10 **Excel**, Microsoft Corp., Redmond, WA, <http://www.microsoft.com>
- 11 **MATLAB**, Mathworks Inc., Natick, MA, <http://www.mathworks.com>
- 12 **Solidworks**, Solidworks Corp., Concord, MA, <http://www.solidworks.com>

1.12 WEB REFERENCES

<http://www.onlineconversion.com>

Convert just about anything to anything else. Over 5,000 units, and 50,000 conversions.

<http://www.katmarsoftware.com/uconeer.htm>

Download a free units converter program for engineers.

<http://global.ihs.com>

Search a collection of technical standards with over 500,000 documents available for electronic download.

<http://www.thomasnet.com>

An online resource for finding companies and products manufactured in North America.

1.13 BIBLIOGRAPHY

For information on creativity and the design process, the following are recommended:

J. L. Adams, *The Care and Feeding of Ideas*. 3rd ed. Addison Wesley: Reading, Mass., 1986.

J. L. Adams, *Conceptual Blockbusting*. 3rd ed. Addison Wesley: Reading, Mass., 1986.

J. R. M. Alger and C. V. Hays, *Creative Synthesis in Design*. Prentice-Hall: Englewood Cliffs, N.J., 1964.

M. S. Allen, *Morphological Creativity*. Prentice-Hall: Englewood Cliffs, N.J., 1962.

H. R. Buhl, *Creative Engineering Design*. Iowa State University Press: Ames, Iowa, 1960.

W. J. J. Gordon, *Synectics*. Harper and Row: New York, 1962.

J. W. Haefele, *Creativity and Innovation*. Reinhold: New York, 1962.

L. Harrisberger, *Engineersmanship*. 2nd ed. Brooks/Cole: Monterey, Calif., 1982.

D. A. Norman, *The Psychology of Everyday Things*. Basic Books: New York, 1986.

A. F. Osborne, *Applied Imagination*. Scribners: New York, 1963.

C. W. Taylor, *Widening Horizons in Creativity*. John Wiley: New York, 1964.

E. K. Von Fange, *Professional Creativity*. Prentice-Hall: Englewood Cliffs, N.J., 1959.

For information on writing engineering reports, the following are recommended:

R. Barrass, *Scientists Must Write*. Chapman and Hall: New York, 1978.

W. G. Crouch and R. L. Zetler, *A Guide to Technical Writing*. 3rd ed. The Ronald Press Co.: New York, 1964.

D. S. Davis, *Elements of Engineering Reports*. Chemical Publishing Co.: New York, 1963.

D. E. Gray, *So You Have to Write a Technical Report*. Information Resources Press: Washington, D.C., 1970.

H. B. Michaelson, *How to Write and Publish Engineering Papers and Reports*. ISI: Philadelphia, Pa., 1982.

J. R. Nelson, *Writing the Technical Report*. 3rd ed. McGraw-Hill: New York, 1952.

Table P1-0

Topic/Problem Matrix

1.4 Engineering Model

1-1, 1-2, 1-3

1.9 Units

1-4, 1-5, 1-6, 1-7, 1-8

1.14 PROBLEMS

- 1-1 It is often said, “*Build a better mousetrap and the world will beat a path to your door.*” Consider this problem and write a goal statement and a set of at least 12 task specifications that you would apply to its solution. Then suggest 3 possible concepts to achieve the goal. Make annotated, freehand sketches of the concepts.

- 1-2 A bowling machine is desired to allow quadriplegic youths, who can only move a joystick, to engage in the sport of bowling at a conventional bowling alley. Consider the factors involved, write a goal statement, and develop a set of at least 12 task specifications that constrain this problem. Then suggest 3 possible concepts to achieve the goal. Make annotated, freehand sketches of the concepts.

- 1-3 A quadriplegic needs an automated page-turner to allow her to read books without assistance. Consider the factors involved, write a goal statement, and develop a set of at least 12 task specifications that constrain this problem. Then suggest 3 possible concepts to achieve the goal. Make annotated, freehand sketches of the concepts.

*1-4 Convert a mass of 1000 lb_m to (a) lb_f, (b) slugs, (c) blobs, (d) kg.

*1-5 A 250-lb_m mass is accelerated at 40 in/sec². Find the force in lb needed for this acceleration.

*1-6 Express a 100 kg mass in units of slugs, blobs, and lb_m. How much does this mass weigh in lb_f and in N?

- 1-7 Prepare an interactive computer program (using, for example, *Excel, Mathcad, MATLAB*, or *TK Solver*) from which the cross-sectional properties for the shapes shown on the inside front cover can be calculated. Arrange the program to deal with both *ips* and *SI* units systems and convert the results between those systems.

- 1-8 Prepare an interactive computer program (using, for example, *Excel, Mathcad, MATLAB*, or *TK Solver*) from which the mass properties for the solids shown on the page opposite the inside front cover can be calculated. Arrange the program to deal with both *ips* and *SI* units systems and convert the results between those systems.

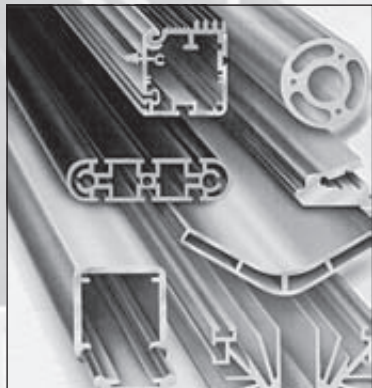
- 1-9 Convert the program written for Problem 1-7 to have and use a set of functions or subroutines that can be called from within any program in that language to solve for the cross-sectional properties of the shapes shown on the inside front cover.

- 1-10 Convert the program written for Problem 1-8 to have and use a set of functions or subroutines that can be called from within any program in that language to solve for the mass properties for the solids shown on the page opposite the inside front cover.

* Answers to these problems are provided in Appendix D.

2

MATERIALS AND PROCESSES



There is no subject so old that something new cannot be said about it.

Dostoevsky

2.0 INTRODUCTION

Whatever you design, you must make it out of some material and be able to manufacture it. A thorough understanding of material properties, treatments, and manufacturing processes is essential to good machine design. It is assumed that the reader has had a first course in material science. This chapter presents a brief review of some basic metallurgical concepts and a short summary of engineering material properties to serve as background for what follows. This is not intended as a substitute for a text on material science, and the reader is encouraged to review references such as those listed in the bibliography of this chapter for more detailed information. Later chapters of this text will explore some of the common material-failure modes in more detail.

Table 2-0 shows the variables used in this chapter and references the equations, figures, or sections in which they are used. At the end of the chapter, a summary section is provided which groups the significant equations from this chapter for easy reference and identifies the chapter section in which they are discussed.

2.1 MATERIAL-PROPERTY DEFINITIONS

Mechanical properties of a material are generally determined through destructive testing of samples under controlled loading conditions. The test loadings do not accurately duplicate actual service loadings experienced by machine parts except in certain special cases. Also, there is no guarantee that the particular piece of material you purchase for your part will exhibit the same strength properties as the samples of similar materials tested previously. There will be some statistical variation in the strength of any par-

Table 2-0 Variables Used in This Chapter

Symbol	Variable	ips units	SI units	See
A	area	in ²	m ²	Sect. 2.1
A_0	original area, test specimen	in ²	m ²	Eq. 2.1a
E	Young's modulus	psi	Pa	Eq. 2.2
el	elastic limit	psi	Pa	Figure 2-2
f	fracture point	none	none	Figure 2-2
G	shear modulus, modulus of rigidity	psi	Pa	Eq. 2.4
HB	Brinell hardness	none	none	Eq. 2.10
HRB	Rockwell B hardness	none	none	Sect. 2.4
HRC	Rockwell C hardness	none	none	Sect. 2.4
HV	Vickers hardness	none	none	Sect. 2.4
J	polar second moment of area	in ⁴	m ⁴	Eq. 2.5
K	stress intensity	kpsi-in ^{0.5}	MPa-m ^{0.5}	Sect. 2.1
K_c	fracture toughness	kpsi-in ^{0.5}	MPa-m ^{0.5}	Sect. 2.1
l_0	gage length, test specimen	in	m	Eq. 2.3
N	number of cycles	none	none	Figure 2-10
P	force or load	lb	N	Sect. 2.1
pl	proportional limit	psi	Pa	Figure 2-2
r	radius	in	m	Eq. 2.5a
S_d	standard deviation	any	any	Eq. 2.9
S_e	endurance limit	psi	Pa	Figure 2-10
S_{el}	strength at elastic limit	psi	Pa	Eq. 2.7
S_f	fatigue strength	psi	Pa	Figure 2-10
S_{us}	ultimate shear strength	psi	Pa	Eq. 2.5
S_{ut}	ultimate tensile strength	psi	Pa	Figure 2-2
S_y	tensile yield strength	psi	Pa	Figure 2-2
S_{ys}	shear yield strength	psi	Pa	Eq. 2.5c
T	torque	lb-in	N-m	Sect. 2.1
U_R	modulus of resilience	psi	Pa	Eq. 2.7
U_T	modulus of toughness	psi	Pa	Eq. 2.8
y	yield point	none	none	Figure 2-2
ϵ	strain	none	none	Eq. 2.1b
σ	tensile stress	psi	Pa	Sect. 2.1
τ	shear stress	psi	Pa	Eq. 2.3
θ	angular deflection	rad	rad	Eq. 2.3
μ	arithmetic mean value	any	any	Eq. 2.9b
ν	Poisson's ratio	none	none	Eq. 2.4

ticular sample compared to the average tested properties for that material. For this reason, many of the published strength data are given as minimum values. It is with these caveats that we must view all published material-property data, as it is the engineer's responsibility to ensure the safety of his or her design.

The best material-property data will be obtained from destructive or nondestructive testing under actual service loadings of prototypes of your actual design, made from the actual materials by the actual manufacturing process. This is typically done only when the economic and safety risks are high. Manufacturers of aircraft, automobiles, motorcycles, snowmobiles, farm equipment, and other products regularly instrument and test finished assemblies under real or simulated service conditions.

In the absence of such specific test data, the engineer must adapt and apply published material-property data from standard tests to the particular situation. The *American Society for Testing and Materials* (ASTM) defines standards for test specimens and test procedures for a variety of material-property measurements.* The most common material test used is the tensile test.

The Tensile Test

A typical tensile test specimen is shown in Figure 2-1. This tensile bar is machined from the material to be tested in one of several standard diameters d_o and gage lengths l_o . The gage length is an arbitrary length defined along the small-diameter portion of the specimen by two indentations so that its increase can be measured during the test. The larger-diameter ends of the bar are threaded for insertion into a tensile test machine which is capable of applying either controlled loads or controlled deflections to the ends of the bar, and the gage-length portion is mirror polished to eliminate stress concentrations from surface defects. The bar is stretched slowly in tension until it breaks, while the load and the distance across the gage length (or alternatively the strain) are continuously monitored. The result is a stress-strain plot of the material's behavior under load as shown in Figure 2-2a, which depicts a curve for a low-carbon or "mild" steel.

STRESS AND STRAIN Note that the parameters measured are load and deflection, but those plotted are stress and strain. **Stress** (σ) is defined as *load per unit area* (or *unit load*) and for the tensile specimen is calculated from

$$\sigma = \frac{P}{A_o} \quad (2.1a)$$

where P is the applied load at any instant and A_o is the original cross-sectional area of the specimen. The stress is assumed to be uniformly distributed across the cross section. The stress units are psi or Pa.

Strain is the *change in length per unit length* and is calculated from

$$\epsilon = \frac{l - l_o}{l_o} \quad (2.1b)$$

where l_o is the original gage length and l is the gage length at any load P . The strain is unitless, being length divided by length.

MODULUS OF ELASTICITY This tensile stress-strain curve provides us with a number of useful material parameters. Point pl in Figure 2-2a is the **proportional limit** below which the stress is proportional to the strain, as expressed by the one-dimensional form of **Hooke's law**:

$$E = \frac{\sigma}{\epsilon} \quad (2.2)$$

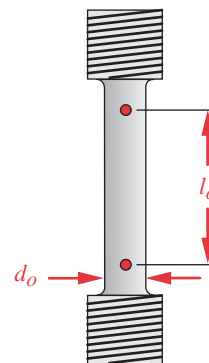
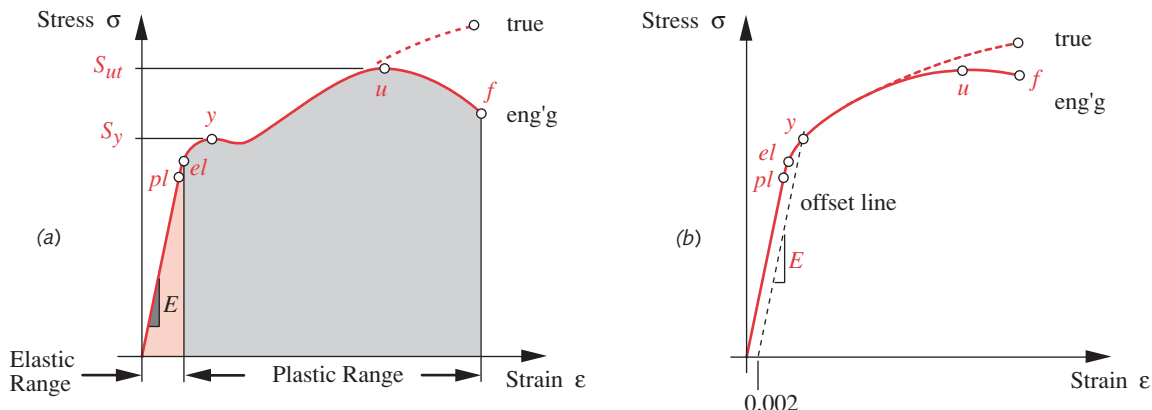


FIGURE 2-1

A Tensile Test Specimen

* ASTM, 1994 Annual Book of ASTM Standards, Vol. 03.01, Am. Soc. for Testing and Materials, Philadelphia, PA.

**FIGURE 2-2**

Engineering and True Stress-Strain Curves for Ductile Materials: (a) Low-Carbon Steel (b) Annealed High-Carbon Steel

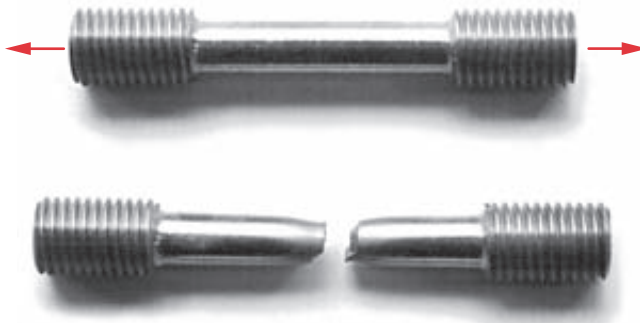
where E defines the slope of the stress-strain curve up to the proportional limit and is called **Young's modulus** or the **modulus of elasticity** of the material. E is a measure of the stiffness of the material in its elastic range and has the units of stress. Most metals exhibit this linear stiffness behavior and also have elastic moduli that vary very little with heat treatment or with the addition of alloying elements. For example, the highest-strength steel has the same E as the lowest-strength steel at about 30 Mpsi (207 GPa). For most ductile materials (defined below), the modulus of elasticity in compression is the same as in tension. This is not true for cast irons and other brittle materials (defined below) or for magnesium.

ELASTIC LIMIT The point labeled el in Figure 2-2a is the **elastic limit**, or the point beyond which the material will take a permanent set, or plastic deformation. The elastic limit marks the boundary between the **elastic-behavior** and **plastic-behavior** regions of the material. Points el and pl are typically so close together that they are often considered to be the same.

YIELD STRENGTH At a point y slightly above the elastic limit, the material begins to yield more readily to the applied stress, and its rate of deformation increases (note the lower slope). This is called the **yield point**, and the value of stress at that point defines the **yield strength** S_y of the material.

Materials that are very ductile, such as low-carbon steels, will sometimes show an apparent drop in stress just beyond the yield point, as shown in Figure 2-2a. Many less ductile materials, such as aluminum and medium- to high-carbon steels, will not exhibit this apparent drop in stress and will look more like Figure 2-2b. The yield strength of a material that does not exhibit a clear yield point has to be defined with an offset line, drawn parallel to the elastic curve and offset some small percentage along the strain axis. An offset of 0.2% strain is most often used. The yield strength is then taken at the intersection of the stress-strain curve and the offset line as shown in Figure 2-2b.

ULTIMATE TENSILE STRENGTH The stress in the specimen continues to increase non-linearly to a peak or **ultimate tensile strength** value S_{ut} at point u . This is considered to be the largest tensile stress the material can sustain before breaking. However, for

**FIGURE 2-3**

A Tensile Test Specimen of Mild, Ductile Steel Before and After Fracture

the ductile steel curve shown, the stress appears to fall off to a smaller value at the fracture point f . The drop in apparent stress before the fracture point (from u to f in Figure 2-2a) is an artifact caused by the “necking-down” or reduction in area of the ductile specimen. The reduction of cross-sectional area is nonuniform along the length of the specimen as can be seen in Figure 2-3.

Because the stress is calculated using the original area A_o in equation 2.1a, it understates the true value of stress after point u . It is difficult to accurately monitor the dynamic change in cross-sectional area during the test, so these errors are accepted. The strengths of different materials can still be compared on this basis. When based on the uncorrected area A_o this is called the **engineering stress-strain curve**, as shown in Figure 2-2.

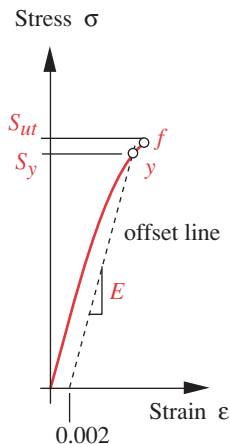
The stress at fracture is actually larger than shown. Figure 2-2 also shows the **true stress-strain curve** that would result if the change in area were accounted for. The **engineering stress-strain** data from Figure 2-2 are typically used in practice. The most commonly used strength values for **static loading** are the yield strength S_y and the ultimate tensile strength S_{ut} . The material stiffness is defined by Young’s modulus, E .

In comparing the properties of different materials, it is quite useful to express those properties normalized to the material’s density. Since light weight is nearly always a goal in design, we seek the lightest material that has sufficient strength and stiffness to withstand the applied loads. The **specific strength** of a material is defined as *the strength divided by the density*. Unless otherwise specified, strength in this case is assumed to mean ultimate tensile strength, though any strength criterion can be so normalized. The **strength-to-weight ratio** (SWR) is another way to express the specific strength. **Specific stiffness** is the *Young’s modulus divided by material density*.

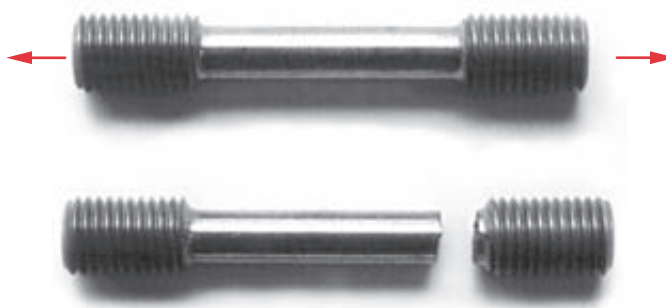
Ductility and Brittleness

The tendency for a material to deform significantly before fracturing is a measure of its ductility. The absence of significant deformation before fracture is called brittleness.

DUCTILITY The stress-strain curve in Figure 2-2a is of a ductile material, mild steel. Take a common paper clip made of mild-steel wire. Straighten it out with your fingers.

**FIGURE 2-4**

Stress-Strain Curve of a Brittle Material

**FIGURE 2-5**

A Tensile Test Specimen of Brittle Cast Iron Before and After Fracture

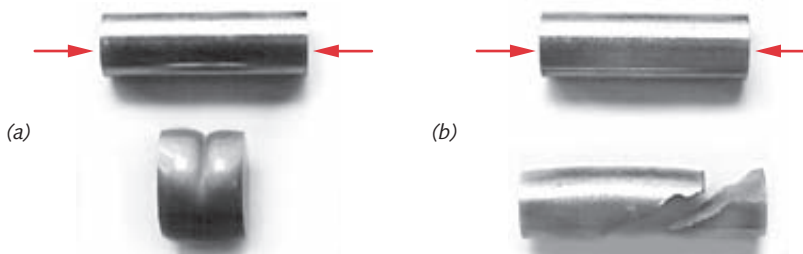
Bend it into some new shape. You are yielding this ductile steel wire but not fracturing it. You are operating between point y and point f on the stress-strain curve of Figure 2-2a. The presence of a significant plastic region on the stress-strain curve is evidence of ductility.

Figure 2-3 shows a test specimen of ductile steel after fracture. The distortion called *necking-down* can clearly be seen at the break. The fracture surface appears torn and is laced with hills and valleys, also indicating a ductile failure. The **ductility** of a material is measured by its percent elongation to fracture, or percent reduction in area at fracture. Materials with more than 5% elongation at fracture are considered ductile.

BRITTLENESS Figure 2-4 shows a stress-strain curve for a brittle material. Note the lack of a clearly defined yield point and the absence of any plastic range before fracture. Repeat your paper-clip experiment, this time using a wooden toothpick or matchstick. Any attempt to bend it results in fracture. Wood is a brittle material.

Brittle materials do not exhibit a clear yield point, so the yield strength has to be defined at the intersection of the stress-strain curve and an offset line, drawn parallel to the elastic curve and offset some small percentage such as 0.2% along the strain axis. Some brittle materials like cast iron do not have a linear elastic region, and the offset line is taken at the average slope of the region. Figure 2-5 shows a cast iron test specimen after fracture. The break shows no evidence of necking and has the finer surface contours typical of a brittle fracture.

The same metals can be either ductile or brittle depending on the way they are manufactured, worked, and heat treated. Metals that are **wrought** (meaning drawn or pressed into shape in a solid form while either hot or cold) can be more ductile than metals that are cast by pouring molten metal into a mold or form. There are many exceptions to this broad statement, however. The cold working of metal (discussed below) tends to reduce its ductility and increase its brittleness. Heat treatment (discussed below) also has a marked effect on the ductility of steels. Thus it is difficult to generalize about the relative ductility or brittleness of various materials. A careful look at all the mechanical properties of a given material will tell the story.

**FIGURE 2-6**

Compression Test Specimens Before and After Failure (a) Ductile Steel (b) Brittle Cast Iron

The Compression Test

The tensile test machine can be run in reverse to apply a compressive load to a specimen that is a constant-diameter cylinder as shown in Figure 2-6. It is difficult to obtain a useful stress-strain curve from this test because a ductile material will yield and increase its cross-sectional area, as shown in Figure 2-6a, eventually stalling the test machine. The ductile sample will not fracture in compression. If enough force were available from the machine, it could be crushed into a pancake shape. Most ductile materials have compressive strengths similar to their tensile strengths, and the tensile stress-strain curve is used to represent their compressive behavior as well. A material that has essentially equal tensile and compressive strengths is called an **even material**.

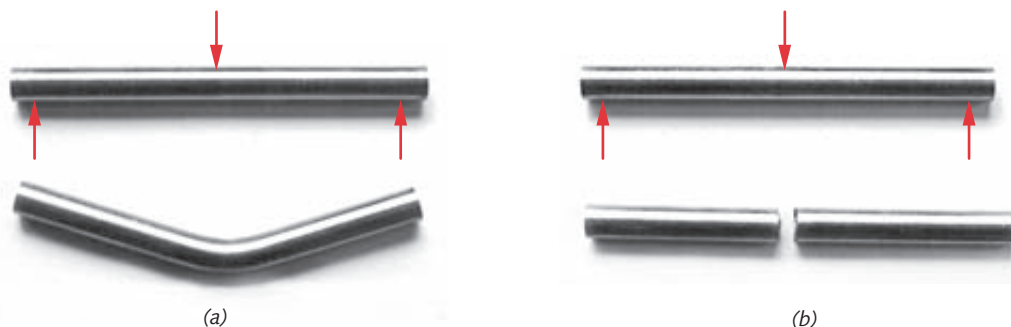
Brittle materials will fracture when compressed. A failed specimen of brittle cast iron is shown in Figure 2-6b. Note the rough, angled fracture surface. The reason for the failure on an angled plane is discussed in Chapter 4. Brittle materials generally have much greater strength in compression than in tension. Compressive stress-strain curves can be generated, since the material fractures rather than crushes and the cross-sectional area doesn't change appreciably. A material that has different tensile and compressive strengths is called an **uneven material**.

The Bending Test

A thin rod, as shown in Figure 2-7, is simply supported at each end as a beam and loaded transversely in the center of its length until it fails. If the material is ductile, failure is by yielding, as shown in Figure 2-7a. If the material is brittle, the beam fractures as shown in Figure 2-7b. Stress-strain curves are not generated from this test because the stress distribution across the cross section is not uniform. The tensile test's σ - ϵ curve is used to predict failure in bending, since the bending stresses are tensile on the convex side and compressive on the concave side of the beam.

The Torsion Test

The shear properties of a material are more difficult to determine than its tensile properties. A specimen similar to the tensile test specimen is made with noncircular details on its ends so that it can be twisted axially to failure. Figure 2-8 shows two such samples, one of ductile steel and one of brittle cast iron. Note the painted lines along

**FIGURE 2-7**

Bending Test Specimens Before and After Failure (a) Ductile Steel (b) Brittle Cast Iron

their lengths. The lines were originally straight in both cases. The helical twist in the ductile specimen's line after failure shows that it wound up for several revolutions before breaking. The brittle, torsion-test specimen's line is still straight after failure as there was no significant plastic distortion before fracture.

Table 2-1

Poisson's Ratio v

Material	v
Aluminum	0.34
Copper	0.35
Iron	0.28
Steel	0.28
Magnesium	0.33
Titanium	0.34

MODULUS OF RIGIDITY The stress-strain relation for pure torsion is defined by

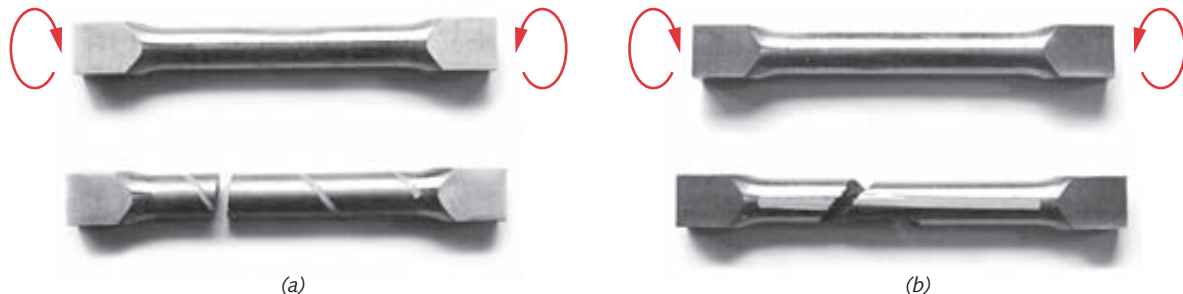
$$\tau = \frac{Gr\theta}{l_o} \quad (2.3)$$

where τ is the shear stress, r is the radius of the specimen, l_o is the gage length, θ is the angular twist in radians, and G is the shear modulus or **modulus of rigidity**. G can be defined in terms of Young's modulus E and Poisson's ratio v :

$$G = \frac{E}{2(1+v)} \quad (2.4)$$

Poisson's ratio (v) is the ratio between lateral and longitudinal strain and for most metals is around 0.3 as shown in Table 2-1.

ULTIMATE SHEAR STRENGTH The breaking strength in torsion is called the ultimate shear strength or modulus of rupture S_{us} and is calculated from

**FIGURE 2-8**

Torsion Test Specimens Before and After Failure (a) Ductile Steel (b) Brittle Cast Iron

$$S_{us} = \frac{Tr}{J} \quad (2.5a)$$

where T is the applied torque necessary to break the specimen, r is the radius of the specimen, and J is the polar second moment of area of the cross section. The distribution of stress across the section loaded in torsion is not uniform. It is zero at the center and maximum at the outer radius. Thus the outer portions have already plastically yielded while the inner portions are still below the yield point. This nonuniform stress distribution in the torsion test (unlike the uniform distribution in the tension test) is the reason for calling the measured value at failure of a solid bar in torsion a *modulus of rupture*. A thin-walled tube is a better torsion-test specimen than a solid bar for this reason and can give a better measure of the ultimate shear strength.

In the absence of available data for the ultimate shear strength of a material, a reasonable approximation can be obtained from tension test data:^{*}

steels :	$S_{us} \cong 0.80S_{ut}$	(2.5b)
other ductile metals :	$S_{us} \cong 0.75S_{ut}$	

Note that the shear yield strength has a different relationship to the tensile yield strength:

$$S_{ys} \cong 0.577S_y \quad (2.5c)$$

This relationship is derived in Chapter 5, where failure of materials under static loading is discussed in more detail.

Fatigue Strength and Endurance Limit

The tensile test and the torsion test both apply loads slowly and only once to the specimen. These are static tests and measure static strengths. While some machine parts may see only static loads in their lifetime, most will see loads and stresses that vary with time. Materials behave very differently in response to loads that come and go (called **fatigue loads**) than they do to loads that remain static. Most of machine design deals with the design of parts for time-varying loads, so we need to know the **fatigue strength** of materials under these loading conditions.

One test for fatigue strength is the R. R. Moore rotating-beam test in which a similar, but slightly smaller, test specimen than that shown in Figure 2-1 is loaded as a beam in bending while being rotated by a motor. Recall from your first course in strength of materials that a bending load causes tension on one side of a beam and compression on the other. (See Sections 4-9 and 4-10 for a review of beams in bending.) The rotation of the beam causes any one point on the surface to go from compression to tension to compression each cycle. This creates a load-time curve as shown in Figure 2-9.

The test is continued at a particular stress level until the part fractures, and the number of cycles N is then noted. Many samples of the same material are tested at various stress levels S until a curve similar to Figure 2-10 is generated. This is called a Wohler strength-life diagram or an $S-N$ diagram. It depicts the breaking strength of a particular material at various numbers of repeated cycles of fully reversed stress.

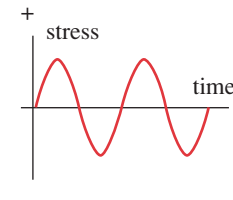
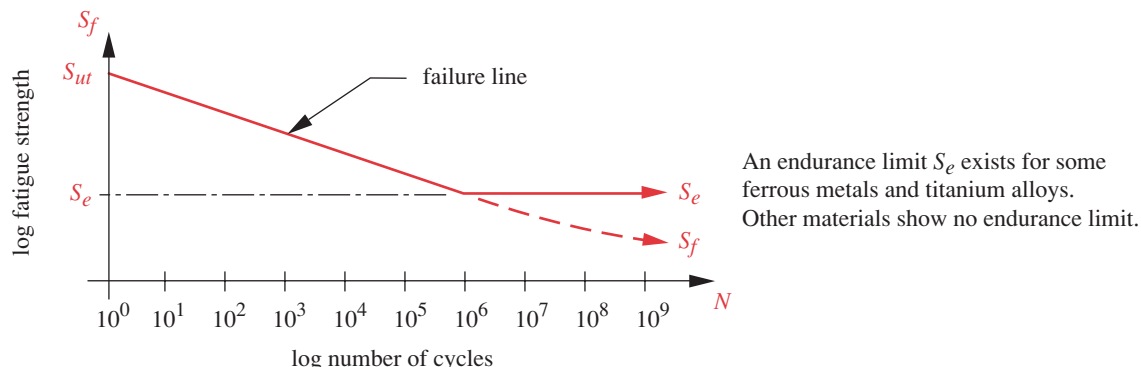


FIGURE 2-9

Time-Varying Loading

* In Chapter 14 on helical spring design, an empirical relationship for the ultimate shear strength of small diameter steel wire, based on extensive testing of wire in torsion, is presented in equation 14.4 (p. 793) and is $S_{us} = 0.67 S_{ut}$. This is obviously different than the general approximation for steel in equation 2.5b. The best data for material properties will always be obtained from tests of the same material, geometry, and loading as the part will be subjected to in service. In the absence of direct test data we must rely on approximations of the sort in equation 2.5b and apply suitable safety factors based on the uncertainty of these approximations.

**FIGURE 2-10**

Wohler Strength-Life or S-N Diagram Plots Fatigue Strength Against Number of Fully Reversed Stress Cycles

Note in Figure 2-10 that the **fatigue strength** S_f at one cycle is the same as the static strength S_{ut} , and it decreases steadily with increasing numbers of cycles N (on a log-log plot) until reaching a plateau at about 10^6 cycles. This plateau in fatigue strength exists only for certain metals (notably steels and some titanium alloys) and is called the endurance limit S_e . Fatigue strengths of other materials keep falling beyond that point. While there is considerable variation among materials, their raw (or uncorrected) fatigue strengths at about $N = 10^6$ cycles tend to be no more than about 40–50% of their static tensile strength S_{ut} . This is a significant reduction and, as we will learn in Chapter 6, further reductions in the fatigue strengths of materials will be necessary due to other factors such as surface finish and type of loading.

It is important at this stage to remember that the tensile stress-strain test does not tell the whole story and that a material's static strength properties are seldom adequate by themselves to predict failure in a machine-design application. This topic of fatigue strength and endurance limit is so important and fundamental to machine design that we devote Chapter 6 exclusively to a study of fatigue failure.

The rotating-beam test is now being supplanted by axial-tension tests performed on modern test machines which can apply time-varying loads of any desired character to the axial-test specimen. This approach provides more testing flexibility and more accurate data because of the uniform stress distribution in the tensile specimen. The results are consistent with (but slightly lower-valued than) the historical rotating-beam test data for the same materials.

Impact Resistance

The stress-strain test is done at very low, controlled strain rates, allowing the material to accommodate itself to the changing load. If the load is suddenly applied, the energy absorption capacity of the material becomes important. The energy in the differential element is its **strain energy density** (strain energy per unit volume U_0), or the area under the stress-strain curve at any particular strain.

$$U_0 = \int_0^{\epsilon} \sigma d\epsilon \quad (2.6a)$$

The strain energy U is equal to the strain energy density integrated over the volume v .

$$U = \int_v U_0 dv \quad (2.6b)$$

The **resilience** and **toughness** of the material are measures, respectively, of the strain energy present in the material at the elastic limit or at the fracture point.

RESILIENCE The ability of a material to absorb energy per unit volume without permanent deformation is called its **resilience** U_R (also called **modulus of resilience**) and is equal to the area under the stress-strain curve up to the elastic limit, shown as the color-shaded area in Figure 2-2a. Resilience is defined as:

$$\begin{aligned} U_R &= \int_0^{\varepsilon_{el}} \sigma d\varepsilon = \frac{1}{2} S_{el} \varepsilon_{el} \\ &= \frac{1}{2} S_{el} \frac{S_{el}}{E} = \frac{1}{2} \frac{S_{el}^2}{E} \\ U_R &\approx \frac{1}{2} \frac{S_y^2}{E} \end{aligned} \quad (2.7)$$

where S_{el} and ε_{el} represent, respectively, the strength and strain at the elastic limit. Substitution of Hooke's law from equation 2.2 expresses the relationship in terms of strength and Young's modulus. Since the S_{el} value is seldom available, a reasonable approximation of resilience can be obtained by using the yield strength S_y instead.

This relationship shows that a stiffer material of the same elastic strength is less resilient than a more compliant one. A rubber ball can absorb more energy without permanent deformation than one made of glass.

TOUGHNESS The ability of a material to absorb energy per unit volume without fracture is called its **toughness** U_T (also called **modulus of toughness**) and is equal to the area under the stress-strain curve up to the fracture point, shown as the entire shaded area in Figure 2-2a. Toughness is defined as:

$$\begin{aligned} U_T &= \int_0^{\varepsilon_f} \sigma d\varepsilon \\ &\approx \left(\frac{S_y + S_{ut}}{2} \right) \varepsilon_f \end{aligned} \quad (2.8)$$

where S_{ut} and ε_f represent, respectively, the ultimate tensile strength and the strain at fracture. Since an analytical expression for the stress-strain curve is seldom available for actual integration, an approximation of toughness can be obtained by using the average of the yield and ultimate strengths and the strain at fracture to calculate an area. The units of toughness and resilience are energy per unit volume (in-lb/in³ or joules/m³). Note that these units are numerically equivalent to psi or Pa.

A ductile material of similar ultimate strength to a brittle one will be much more tough. A sheet-metal automobile body will absorb more energy from a collision through plastic deformation than will a brittle, fiberglass body.*

* It is interesting to note that one of the toughest and strongest materials known is that of *spider webs*! These tiny arachnids spin a monofilament that has an ultimate tensile strength of 200 to 300 kpsi (1380 to 2070 MPa) and 35% elongation to fracture! It also can absorb more energy without rupture than any fiber known, absorbing 3 times as much energy as Kevlar, the man-made fiber used for bullet-proof vests. According to the *Boston Globe*, January 18, 2002, researchers in Canada and the U.S. have synthesized a material with similar properties to spider silk in strands up to 10-ft long with strengths of 1/4 to 1/3 that of natural silk fiber, "stronger than a steel wire of similar weight," and one that has greater elasticity than organic silk fiber.

IMPACT TESTING Various tests have been devised to measure the ability of materials to withstand impact loading. The **Izod** and the **Charpy** tests are two such procedures which involve striking a notched specimen with a pendulum and recording the kinetic energy needed to break the specimen at a particular temperature. While these data do not directly correlate with the area under the stress-strain curve, they nevertheless provide a means to compare the energy absorption capacity of various materials under controlled conditions. Materials handbooks such as those listed in this chapter's bibliography give data on the impact resistance of various materials.

Fracture Toughness

Fracture toughness K_c (not to be confused with the modulus of toughness defined above) is a *material property that defines its ability to resist stress at the tip of a crack*. The fracture toughness of a material is measured by subjecting a standardized, pre-cracked test specimen to cyclical tensile loads until it breaks. Cracks create very high local stress concentrations which cause local yielding (see Section 4.15). The effect of the crack on the local stress is measured by a **stress intensity factor** K which is defined in Section 5.3. When the stress intensity K reaches the fracture toughness K_c , a sudden fracture occurs with no warning. The study of this failure phenomenon is called **fracture mechanics** and it is discussed in more detail in Chapters 5 and 6.

Creep and Temperature Effects

The tensile test, while slow, does not last long compared to the length of time an actual machine part may be subjected to constant loading. All materials will, under the right environmental conditions (particularly elevated temperatures), slowly creep (deform) under stress loadings well below the level (yield point) deemed safe in the tensile test. Ferrous metals tend to have negligible creep at room temperature or below. Their creep rates increase with increasing ambient temperature, usually becoming significant around 30–60% of the material's absolute melting temperature.

Low-melt-temperature metals such as lead, and many polymers, can exhibit significant creep at room temperature as well as increasing creep rates at higher temperatures. Creep data for engineering materials are quite sparse due to the expense and time required to develop the experimental data. The machine designer needs to be aware of the creep phenomenon and obtain the latest manufacturer's data on the selected materials if high ambient temperatures are anticipated or if polymers are specified. The creep phenomenon is more complex than this simple description implies. See the bibliography to this chapter for more complete and detailed information on creep in materials.

It is also important to understand that all material properties are a function of temperature, and published test data are usually generated at room temperature. Increased temperature usually reduces strength. Many materials that are ductile at room temperature can behave as brittle materials at low temperatures. Thus, if your application involves either elevated or low temperatures, you need to seek out relevant material-property data for your operating environment. Material manufacturers are the best source of up-to-date information. Most manufacturers of polymers publish creep data for their materials at various temperatures.

2.2 THE STATISTICAL NATURE OF MATERIAL PROPERTIES

Some published data for material properties represent average values of many samples tested. (Other data are stated as minimum values.) The range of variation of the published test data is sometimes stated, sometimes not. Most material properties will vary about the average or mean value according to some statistical distribution such as the *Gaussian* or *normal distribution* shown in Figure 2-11. This curve is defined in terms of two parameters, the *arithmetic mean* μ and the *standard deviation* S_d . The equation of the Gaussian distribution curve is

$$f(x) = \frac{1}{\sqrt{2\pi}S_d} \exp\left[-\frac{(x-\mu)^2}{2S_d^2}\right], \quad -\infty \leq x \leq \infty \quad (2.9a)$$

where x represents some material parameter, $f(x)$ is the frequency with which that value of x occurs in the population, and μ and S_d are defined as

$$\mu = \frac{1}{n} \sum_{i=1}^n x_i \quad (2.9b)$$

$$S_d = \sqrt{\frac{1}{n-1} \sum_{i=1}^n (x_i - \mu)^2} \quad (2.9c)$$

The *mean* μ defines the most frequently occurring value of x at the peak of the curve, and the *standard deviation* S_d is a measure of the “spread” of the curve about the *mean*. A small value of S_d relative to μ means that the entire population is clustered closely about the mean. A large S_d indicates that the population is widely dispersed about the mean. We can expect to find 68% of the population within $\mu \pm 1S_d$, 95% within $\mu \pm 2S_d$, and 99% within $\mu \pm 3S_d$.

There is considerable scatter in multiple tests of the same material under the same test conditions. Note that there is a 50% chance that the samples of any material that you buy will have a strength less than that material’s published mean value. Thus, you may not want to use the mean value alone as a predictor of the strength of a randomly chosen sample of that material. If the standard deviation of the test data is published along with the mean, we can “factor it down” to a lower value that is predictive of some larger percentage of the population based on the ratios listed above. For example, if you want to have a 99% probability that all possible samples of material are stronger than your assumed material strength, you will subtract $3S_d$ from μ to get an allowable value for your design. This assumes that the material property’s distribution is Gaussian and not skewed toward one end or the other of the spectrum. If a minimum value of the material property is given (and used), then its statistical distribution is not of concern.

Usually, no data are available on the standard deviation of the material samples tested. But you can still choose to reduce the published mean strength by a reliability factor based on an assumed S_d . One such approach assumes S_d to be some percentage of μ based on experience. Haugen and Wirsching^[1] report that the standard deviations of strengths of steels seldom exceed 8% of their mean values. Table 2-2 shows reliability reduction factors based on an assumption of $S_d = 0.08 \mu$ for various reliabilities. Note that a 50% reliability has a factor of 1 and the factor reduces as you choose higher reli-

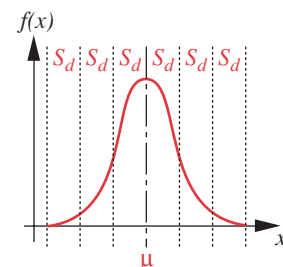


FIGURE 2-11

The Gaussian (Normal) Distribution

Table 2-2

Reliability Factors
for $S_d = 0.08 \mu$

Reliability %	Factor
50	1.000
90	0.897
95	0.868
99	0.814
99.9	0.753
99.99	0.702
99.999	0.659
99.9999	0.620

ability. The reduction factor is multiplied by the mean value of the relevant material property. For example, if you wish 99.99% of your samples to meet or exceed the assumed strength, multiply the mean strength value by 0.702.

In summary, the safest approach is to develop your own material-property data for the particular materials and loading conditions relevant to your design. Since this approach is usually prohibitively expensive in both time and money, the engineer often must rely on published material-property data. Some published strength data are expressed as the minimum strength to be expected in a statistical sample, but other data may be given as the average value for the samples tested. In that case, some of the tested material samples failed at stresses lower than the average value, and your design strength may need to be reduced accordingly.

2.3 HOMOGENEITY AND ISOTROPY

All discussion of material properties so far has assumed that the material is homogeneous and isotropic. **Homogeneous** means that the *material properties are uniform throughout its continuum*, e.g., they are not a function of position. This ideal state is seldom attained in real materials, many of which are subject to the inclusion of discontinuities, precipitates, voids, or bits of foreign matter from their manufacturing process. However, most metals and some nonmetals can be considered, for engineering purposes, to be macroscopically homogeneous despite their microscopic deviations from this ideal.

An **isotropic** material is one whose *mechanical properties are independent of orientation or direction*. That is, the strengths across the width and thickness are the same as along the length of the part, for example. Most metals and some nonmetals can be considered to be macroscopically isotropic. Other materials are **anisotropic**, meaning that *there is no plane of material-property symmetry*. **Orthotropic** materials have three mutually perpendicular planes of property symmetry and can have different material properties along each axis. Wood, plywood, fiberglass, and some cold-rolled sheet metals are orthotropic.

One large class of materials that is distinctly nonhomogeneous (i.e., heterogeneous) and nonisotropic is that of **composites** (also see below). Most composites are man-made, but some, such as wood, occur naturally. Wood is a composite of long fibers held together in a resinous matrix of lignin. You know from experience that it is easy to split wood along the grain (fiber) lines and nearly impossible to do so across the grain. Its strength is a function of both orientation and position. The matrix is weaker than the fibers, and it always splits between fibers.

2.4 HARDNESS

The hardness of a material can be an indicator of its resistance to wear (but is not a guarantee of wear resistance). The strengths of some materials such as steels are also closely correlated to their hardness. Various treatments are applied to steels and other metals to increase hardness and strength. These are discussed below.

Hardness is most often measured on one of three scales: *Brinell*, *Rockwell*, or *Vickers*. These hardness tests all involve the forced impression of a small probe into the surface of the material being tested. The **Brinell test** uses a 10-mm hardened steel or tungsten-carbide* ball impressed with either a 500- or 3000-kg load depending on the range of hardness of the material. The diameter of the resulting indent is measured under a microscope and used to calculate the Brinell hardness number, which has the units of kgf/mm². The **Vickers test** uses a diamond-pyramid indenter and measures the width of the indent under the microscope. The **Rockwell test** uses a 1/16-in ball or a 120° cone-shaped diamond indenter and measures the depth of penetration.

Hardness is indicated by a number followed by the letter H, followed by letter(s) to identify the method used, e.g., 375 HB or 396 HV. Several lettered scales (A, B, C, D, F, G, N, T) are used for materials in different Rockwell hardness ranges and it is necessary to specify both the letter and number of a Rockwell reading, such as 60 HRC. In the case of the Rockwell N scale, a narrow-cone-angle diamond indenter is used with loads of 15, 30, or 40 kg and the specification must include the load used as well as the letter specification, e.g., 84.6 HR15N. This Rockwell N scale is typically used to measure the “superficial” hardness of thin or case-hardened materials. The smaller load and narrow-angle N-tip give a shallow penetration that measures the hardness of the case without including effects of the soft core.

All these tests are nondestructive in the sense that the sample remains intact. However, the indentation can present a problem if the surface finish is critical or if the section is thin, so they are actually considered destructive tests. The Vickers test has the advantage of having only one test setup for all materials. Both the Brinell and Rockwell tests require selection of the tip size or indentation load, or both, to match the material tested. The Rockwell test is favored for its lack of operator error, since no microscope reading is required and the indentation tends to be smaller, particularly if the N-tip is used. But, the Brinell hardness number provides a very convenient way to quickly estimate the ultimate tensile strength (S_{ut}) of the material from the relationship

$$\begin{aligned} S_{ut} &\approx 500 \text{ HB} \pm 30 \text{ HB } \text{psi} \\ S_{ut} &\approx 3.45 \text{ HB} \pm 0.2 \text{ HB } \text{MPa} \end{aligned} \tag{2.10}$$

where HB is the Brinell hardness number. This gives a convenient way to obtain a rough experimental measure of the strength of any low- or medium-strength carbon or alloy steel sample, even one that has already been placed in service and cannot be truly destructively tested.

Microhardness tests use a low force on a small diamond indenter and can provide a profile of microhardness as a function of depth across a sectioned sample. The hardness is computed on an absolute scale by dividing the applied force by the area of the indent. The units of **absolute hardness** are kgf/mm². Brinell and Vickers hardness numbers also have these hardness units, though the values measured on the same sample can differ with each method. For example, a Brinell hardness of 500 HB is about the same as a Rockwell C hardness of 52 HRC and an absolute hardness of 600 kgf/mm². Note that these scales are not linearly related, so conversion is difficult. Table 2-3 shows approximate conversions between the Brinell, Vickers, and Rockwell B and C hardness scales for steels and their approximate equivalent ultimate tensile strengths.

* Tungsten carbide is one of the hardest substances known.

Table 2-3 Approximate Equivalent Hardness Numbers and Ultimate Tensile Strengths for Steels

Brinell <i>HB</i>	Vickers <i>HV</i>	Rockwell		Ultimate, σ_u	
		<i>HRB</i>	<i>HRC</i>	MPa	ksi
627	667	—	58.7	2393	347
578	615	—	56.0	2158	313
534	569	—	53.5	1986	288
495	528	—	51.0	1813	263
461	491	—	48.5	1669	242
429	455	—	45.7	1517	220
401	425	—	43.1	1393	202
375	396	—	40.4	1267	184
341	360	—	36.6	1131	164
311	328	—	33.1	1027	149
277	292	—	28.8	924	134
241	253	100	22.8	800	116
217	228	96.4	—	724	105
197	207	92.8	—	655	95
179	188	89.0	—	600	87
159	167	83.9	—	538	78
143	150	78.6	—	490	71
131	137	74.2	—	448	65
116	122	67.6	—	400	58

Note: Load 3000 kg for HB.

Source: Table 5-10, p.185, in N. E. Dowling, *Mechanical Behavior of Materials*, Prentice Hall, Englewood Cliffs, N.J., 1993, with permission.

Heat Treatment

The steel heat-treatment process is quite complicated and is dealt with in detail in materials texts such as those listed in the bibliography at the end of this chapter. The reader is referred to such references for a more complete discussion. Only a brief review of some of the salient points is provided here.

The hardness and other characteristics of many steels and some nonferrous metals can be changed by heat treatment. Steel is an alloy of iron and carbon. The weight percent of carbon present affects the alloy's ability to be heat-treated. A low-carbon steel will have about 0.03 to 0.30% of carbon, a medium-carbon steel about 0.35 to 0.55%, and a high-carbon steel about 0.60 to 1.50%. (Cast irons will have greater than 2% carbon.) Hardenability of steel increases with carbon content. Low-carbon steel has too little carbon for effective through-hardening so other surface-hardening methods must be used (see below). Medium- and high-carbon steels can be through-hardened by appropriate heat treatment. The depth of hardening will vary with alloy content.

QUENCHING To harden a medium- or high-carbon steel, the part is heated above a critical temperature (about 1 400°F {760°C}), allowed to equilibrate for some time, and then suddenly cooled to room temperature by immersion in a water or oil bath. The rapid cooling creates a supersaturated solution of iron and carbon called martensite,

which is extremely hard and much stronger than the original soft material. Unfortunately it is also very brittle. In effect, we have traded off the steel's ductility for its increased strength. The rapid cooling also introduces strains to the part. The change in the shape of the stress-strain curve as a result of quenching a ductile, medium-carbon steel is shown in Figure 2-12 (not to scale). While the increased strength is desirable, the severe brittleness of a fully quenched steel usually makes it unusable without tempering.

TEMPERING Subsequent to quenching, the same part can be reheated to a lower temperature (400–1300°F {200–700°C}), heat-soaked, and then allowed to cool slowly. This will cause some of the martensite to convert to ferrite and cementite, which reduces the strength somewhat but restores some ductility. A great deal of flexibility is possible in terms of tailoring the resulting combination of properties by varying time and temperature during the tempering process. The knowledgeable materials engineer or metallurgist can achieve a wide variety of properties to suit any application. Figure 2-12 also shows a stress-strain curve for the same steel after tempering.

ANNEALING The quenching and tempering process is reversible by annealing. The part is heated above the critical temperature (as for quenching) but now allowed to cool slowly to room temperature. This restores the solution conditions and mechanical properties of the unhardened alloy. Annealing is often used even if no hardening has been previously done in order to eliminate any residual stresses and strains introduced by the forces applied in forming the part. It effectively puts the part back into a “relaxed” and soft state, restoring its original stress-strain curve as shown in Figure 2-12.

NORMALIZING Many tables of commercial steel data indicate that the steel has been normalized after rolling or forming into its stock shape. Normalizing is similar to annealing but involves a shorter soak time at elevated temperature and a more rapid cooling rate. The result is a somewhat stronger and harder steel than a fully annealed one but one that is closer to the annealed condition than to any tempered condition.

Surface (Case) Hardening

When a part is large or thick, it is difficult to obtain uniform hardness within its interior by through hardening. An alternative is to harden only the surface, leaving the core soft. This also avoids the distortion associated with quenching a large, through-heated part. If the steel has sufficient carbon content, its surface can be heated, quenched, and tempered as would be done for through hardening. For low-carbon (mild) steels other techniques are needed to obtain a hardened condition. These involve heating the part in a special atmosphere rich in either carbon, nitrogen or both and then quenching it, a process called *carburizing*, *nitriding*, or *cyaniding*. In all situations, the result is a hard surface (i.e., *case*) on a soft core, referred to as being **case-hardened**.

Carburizing heats low-carbon steel in a carbon monoxide gas atmosphere, causing the surface to take up carbon in solution. **Nitriding** heats low-carbon steel in a nitrogen-gas atmosphere and forms hard iron nitrides in the surface layers. **Cyaniding** heats the part in a cyanide salt bath at about 1 500°F (800°C), and the low-carbon steel takes up both carbides and nitrides from the salt.

For medium- and high-carbon steels no artificial atmosphere is needed, as the steel has sufficient carbon for hardening. Two methods are in common use. **Flame hard-**

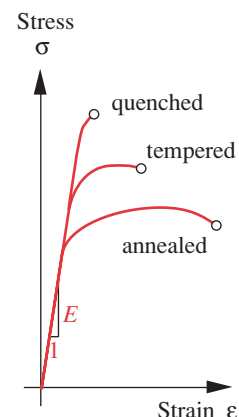


FIGURE 2-12

Stress-Strain Curves for Annealed, Quenched, and Tempered Steel

Flame hardening passes an oxyacetylene flame over the surface to be hardened and follows it with a water jet for quenching. This results in a somewhat deeper hardened case than obtainable from the artificial-atmosphere methods. **Induction hardening** uses electric coils to rapidly heat the part surface, which is then quenched before the core can get hot.

Case hardening by any appropriate method is a very desirable hardening treatment for many applications. It is often advantageous to retain the full ductility (and thus the toughness) of the core material for better energy absorption capacity while also obtaining high hardness on the surface in order to reduce wear and increase surface strength. Large machine parts such as cams and gears are examples of elements that can benefit more from case hardening than from through hardening, as heat distortion is minimized and the tough, ductile core can better absorb impact energy.

Heat Treating Nonferrous Materials

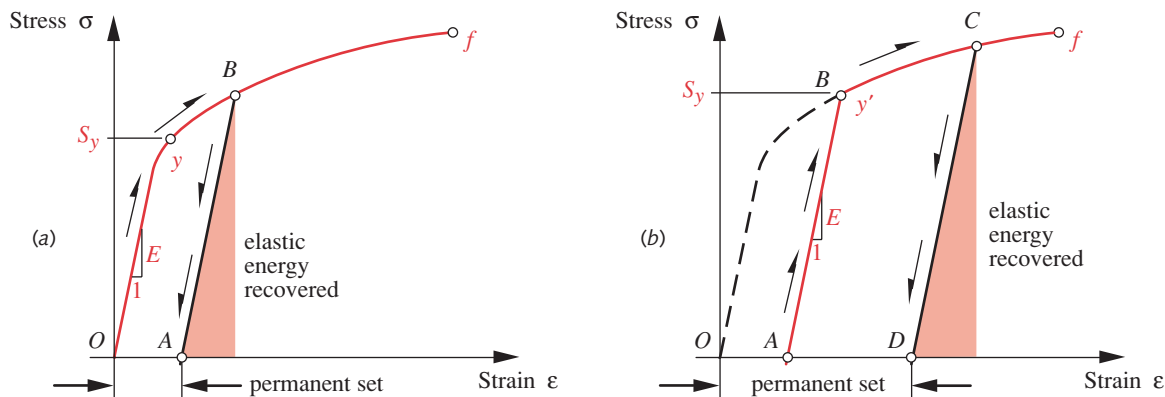
Some nonferrous alloys are hardenable and others are not. Some of the aluminum alloys can be **precipitation hardened**, also called **age hardening**. An example is aluminum alloyed with up to about 4.5% copper. This material can be hot-worked (rolled, forged, etc.) at a particular temperature and then heated and held at a higher temperature to force a random dispersion of the copper in the solid solution. It is then quenched to capture the supersaturated solution at normal temperature. The part is subsequently reheated to a temperature below the quenching temperature and held for an extended period of time while some of the supersaturated solution precipitates out and increases the material's hardness.

Other aluminum alloys, magnesium, titanium, and a few copper alloys are amenable to similar heat treatment. The strengths of the hardened aluminum alloys approach those of medium-carbon steels. Since all aluminum is about 1/3 the density of steel, the stronger aluminum alloys can offer better strength-to-weight ratios than low-carbon (mild) steels.

Mechanical Forming and Hardening

COLD WORKING The mechanical working of metals at room temperature to change their shape or size will also work-harden them and increase their strength at the expense of ductility. Cold working can result from the rolling process in which metal bars are progressively reduced in thickness by being squeezed between rollers, or from any operation that takes the ductile metal beyond the yield point and permanently deforms it. Figure 2-13 shows the process as it affects the material's stress-strain curve. As the load is increased from the origin at *O* beyond the yield point *y* to point *B*, a permanent set *OA* is introduced.

If the load is removed at that point, the stored elastic energy is recovered and the material returns to zero stress at point *A* along a new elastic line *BA* parallel to the original elastic slope *E*. If the load is now reapplied and brought to point *C*, again yielding the material, the new stress-strain curve is *ABCf*. Note that there is now a new yield point *y'* which is at a higher stress than before. The material has **strain-hardened**, increasing its yield strength and reducing its ductility. This process can be repeated until the material becomes brittle and fractures.

**FIGURE 2-13**

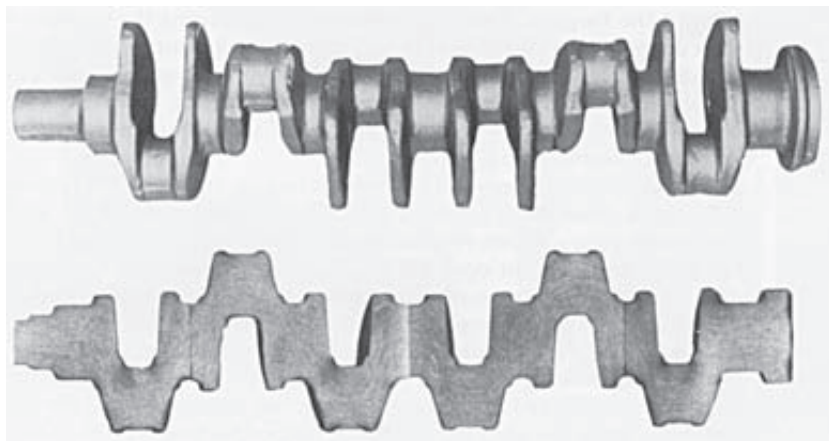
Strain Hardening a Ductile Material by Cold Working (a) First Working (b) Second Working

If significant plastic deformation is required for manufacture, such as in making deep-drawn metal pots or cylinders, it is necessary to cold form the material in stages and anneal the part between successive stages to avoid fracture. The annealing resets the material to more nearly the original ductile stress-strain curve, allowing further yielding without fracture.

HOT WORKING All metals have a recrystallization temperature below which the effects of mechanical working will be as described above, e.g., cold worked. If the material is mechanically worked above its recrystallization temperature (hot working), it will tend to at least partially anneal itself as it cools. Thus hot working reduces the strain-hardening problem but introduces its own problems of rapid oxidation of the surface due to the high temperatures. Hot-rolled metals tend to have higher ductility, lower strength and poorer surface finish than cold-worked metals of the same alloy. Hot working does not increase the hardness of the material appreciably, though it can increase the strength by improving grain structure and aligning the “grain” of the metal with the final contours of the part. This is particularly true of forged parts.

FORGING is an automation of the ancient art of blacksmithing. The blacksmith heats the part red-hot in the forge, then beats it into shape with a hammer. When it cools too much for forming, it is reheated and the process is repeated. Forging uses a series of hammer dies shaped to gradually form the hot metal into the final shape. Each stage’s die shape represents an achievable change in shape from the original ingot form to the final desired part shape. The part is reheated between blows from the hammer dies which are mounted in a forging press. The large forces required to plastically deform the hot metal require massive presses for parts of medium to large size. Machining operations are required to remove the large “flash” belt at the die parting line and to machine holes, mounting surfaces, etc. The surface finish of a forging is as rough as any hot-rolled part due to oxidation and decarburization of the heated metal.

Virtually any wrought, ductile metal can be forged. Steel, aluminum, and titanium are commonly used. Forging has the advantage of creating stronger parts than casting or machining can. Casting alloys are inherently weaker in tension than wrought alloys. The hot forming of a wrought material into the final forged shape causes the material’s

**FIGURE 2-14**

Forged Steel Crankshaft for a Diesel-Truck Engine - Courtesy of Wyman-Gordon Corp., Grafton, MA

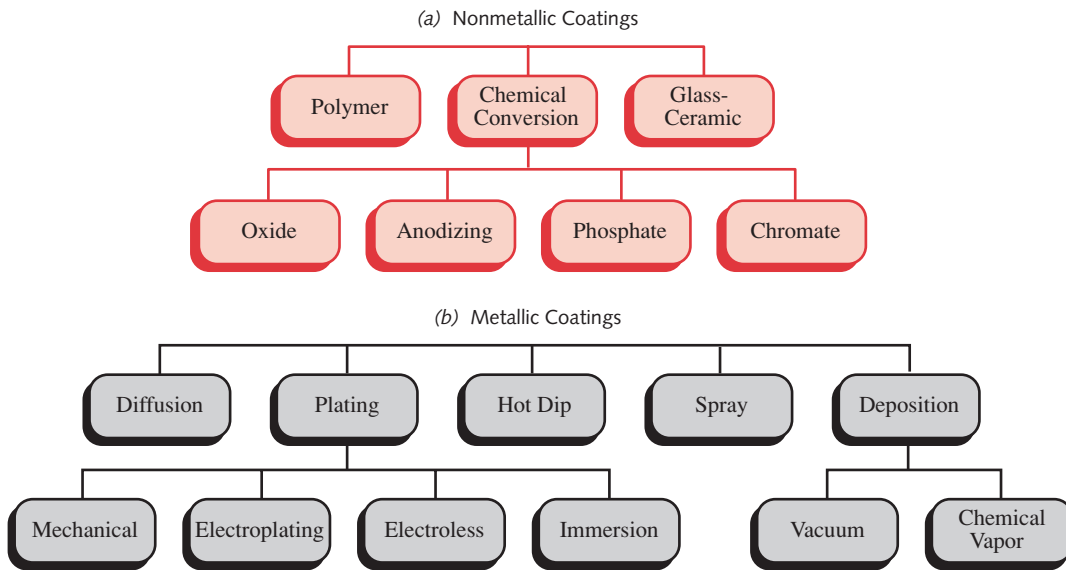
internal “flow lines” or “grain” to approximate the contours of the part, which can result in greater strength than if a stock shape’s flow lines were severed by machining to the final contour. forgings are used in highly stressed parts, such as aircraft wing and fuselage structures, engine crankshafts and connecting rods, and vehicle suspension links. Figure 2-14 shows a forged truck crankshaft. In the cross section, the grain lines can be seen to follow the crankshaft’s contours. The high cost of the multiple dies needed for forged shapes makes it an impractical choice unless production quantities are large enough to amortize the tooling cost.

EXTRUSION is used principally for nonferrous metals (especially aluminum) as it typically uses steel dies. The usual die is a thick, hardened-tool-steel disk with a tapered “hole” or orifice ending in the cross-sectional shape of the finished part. A billet of the extrudate is heated to a soft state and then rammed at fairly high speed through the die, which is clamped in the machine. The billet flows, or extrudes, into the die’s shape. The process is similar to the making of macaroni. A long strand of the material in the desired cross section is extruded from the billet. The extrusion then passes through a water-spray cooling station. Extrusion is an economical way to obtain custom shapes of constant cross section since the dies are not very expensive to make. Dimensional control and surface finish are good. Extrusion is used to make aluminum mill shapes such as angles, channels, I-beams, and custom shapes for storm-door and -window frames, sliding-door frames, etc. The extrusions are cut and machined as necessary to assemble them into the finished product. Some extruded shapes are shown in Figure 2-15.

**FIGURE 2-15**Extrusions - Courtesy of
The Aluminum Extruders
Council

2.5 COATINGS AND SURFACE TREATMENTS

Many coatings and surface treatments are available for metals. Some have the prime purpose of inhibiting corrosion while others are intended to improve surface hardness and wear resistance. Coatings are also used to change dimensions (slightly) and to alter physical properties such as reflectance, color, and resistivity. For example, piston

**FIGURE 2-16**

Coating Methods Available for Metals

rings are chrome-plated to improve wear resistance, fasteners are plated to reduce corrosion, and automobile trim is chrome-plated for appearance and corrosion resistance. Figure 2-16 shows a chart of various types of coatings for machine applications. These divide into two major classes, metallic and nonmetallic, based on the type of coating, not substrate. Some of the classes divide into many subclasses. We will discuss only a few of these here. The reader is encouraged to seek more information from the references in the bibliography.

Galvanic Action

When a coating of one metal is applied to another dissimilar metal, a galvanic cell may be created. All metals are electrolytically active to a greater or lesser degree and if sufficiently different in their electrolytic potential will create a battery in the presence of a conductive electrolyte such as seawater or even tap water. Table 2-4 lists some common metals ordered in terms of their galvanic action potential from the least noble (most electrolytically active) to the most noble (least active). Combinations of metals that are close to each other in the galvanic series, such as cast iron and steel, are relatively safe from galvanic corrosion. Combinations of metals far apart on this scale, such as aluminum and copper, will experience severe corrosion in an electrolyte or even in a moist environment.

In a conductive medium, the two metals become anode and cathode, with the less-noble metal acting as the anode. The self-generated electrical current flow causes a loss of material from the anode and a deposition of material on the cathode. The less-noble metal gradually disappears. This problem occurs whenever two metals sufficiently far apart in the galvanic series are present in an electrically conductive medium. Thus, not only coatings but fasteners and mating parts must be made of metal combinations that will not create this problem.

Table 2-4

Galvanic Series
of Metals in Seawater

Least noble

Magnesium
Zinc
Aluminum
Cadmium
Steel
Cast iron
Stainless steel
Lead
Tin
Nickel
Brass
Copper
Bronze
Monel
Silver
Titanium
Graphite
Gold
Platinum

Most noble

Electroplating

Electroplating involves the deliberate creation of a galvanic cell in which the part to be plated is the cathode and the plating material is the anode. The two metals are placed in an electrolyte bath and a direct current applied from anode to cathode. Ions of the plating material are driven to the plating substrate through the electrolyte and cover the part with a thin coating of the plating material. Allowance must be made for the plating thickness, which is controllable. Plating thickness is uniform except at sharp corners or in holes and crevices. The plating builds up on the outside corners and will not go into holes or narrow crevices. Thus, grinding may be necessary after plating to restore dimensions. Worn parts (or mistakes) can sometimes be repaired by plating on a coating of suitable material, then regrinding to dimension.

Steels, nickel- and copper-based alloys, as well as other metals are readily electroplatable. Two approaches are possible. If a more noble (less active) metal is plated onto the substrate, it can reduce the tendency to oxidize as long as the plating remains intact to protect the substrate from the environment. Tin, nickel, and chromium are often used to electroplate steel for corrosion resistance. Chrome plating also offers an increase in surface hardness to HRC 70, which is above that obtainable from many hardened alloy steels.* Unfortunately, any disruptions or pits in the plating can provide nodes for galvanic action if conductive media (such as rainwater) are present. Because the substrate is less noble than the plating, it becomes the sacrificial anode and rapidly corrodes. Electroplating with metals more noble than the substrate is seldom used for parts that will be immersed in water or other electrolytes.

Alternatively, a less-noble metal can be plated onto the substrate to serve as a sacrificial anode which will corrode instead of the substrate. The most common example of this is zinc coating of steel, also called galvanizing. (Cadmium can be used instead of zinc and will last longer in saltwater or salt-air environments.) The zinc or cadmium coating will gradually corrode and protect the more noble steel substrate until the coating is used up, after which the steel will oxidize. Zinc coating can be applied by a process called “hot dipping” rather than by electroplating, which will result in a thicker and more protective coating recognizable by its “mother-of-pearl” appearance. Galvanizing is often applied by manufacturers to automobile body panels to inhibit corrosion. Sacrificial zinc anodes are also attached to aluminum outboard motors and aluminum boat hulls to short-circuit corrosion of the aluminum in seawater.

A caution about electroplated coatings is that hydrogen embrittlement of the substrate can occur, causing significant loss of strength. Electroplated finishes should not be used on parts that are fatigue loaded. Experience has shown that electroplating severely reduces the fatigue strength of metals and can cause early failure.

Electroless Plating

Electroless plating puts a coating of nickel on the substrate without any electric current needed. The substrate “cathode” in this case (there is no anode) acts as a catalyst to start a chemical reaction that causes nickel ions in the electrolyte solution to be reduced and deposited on the substrate. The nickel coating also acts as a catalyst and keeps the reaction going until the part is removed from the bath. Thus, relatively thick coatings can be developed. Coatings are typically between 0.001 in and 0.002 in thick. Unlike elec-

* It is interesting to note that chromium in the pure form is softer than hardened steel but when electroplated onto steel, it becomes harder than the steel substrate. Nickel and iron also increase their hardness when electroplated on metal substrates. The mechanism is not well understood, but it is believed that internal microstrains are developed in the plating process that harden the coating. The hardness of the plating can be controlled by changes in process conditions.

troplating, the electroless nickel plate is completely uniform and will enter holes and crevices. The plate is dense and fairly hard at around 43 HRC. Other metals can also be electroless plated but nickel is most commonly used.

Anodizing

While aluminum can be electroplated (with difficulty), it is more common to treat it by anodizing. This process creates a very thin layer of aluminum oxide on the surface. The aluminum oxide coating is self-limiting in that it prevents atmospheric oxygen from further attacking the aluminum substrate in service. The anodized oxide coating is naturally colorless but dyes can be added to color the surface and provide a pleasing appearance in a variety of hues. This is a relatively inexpensive surface treatment with good corrosion resistance and negligible distortion. Titanium, magnesium, and zinc can also be anodized.

A variation on conventional anodizing of aluminum is so-called “hard anodizing.” Since aluminum oxide is a ceramic material, it is naturally very hard and abrasion resistant. **Hard anodizing** provides a thicker (but not actually harder) coating than conventional anodizing and is often used to protect the relatively soft aluminum parts from wear in abrasive contact situations. The hardness of this surface treatment exceeds that of the hardest steel, and hard-anodized aluminum parts can be run against hardened steel though the somewhat abrasive aluminum oxide surface is not kind to the steel.

Plasma-Sprayed Coatings

A variety of very hard ceramic coatings can be applied to steel and other metal parts by a plasma-spray technique. The application temperatures are high, which limits the choice of substrate. The coatings as sprayed have a rough “orange-peel” surface finish which requires grinding or polishing to obtain a fine finish. The main advantage is a surface with extremely high hardness and chemical resistance. However, the ceramic coatings are brittle and subject to chipping under mechanical or thermal shock.

Chemical Coatings

The most common chemical treatments for metals range from a phosphoric acid wash on steel (or chromatic acid on aluminum) that provides limited and short-term oxidation resistance, to paints of various types designed to give more lasting corrosion protection. Paints are available in a large variety of formulations for different environments and substrates. One-part paints give somewhat less protection than two-part epoxy formulations, but all chemical coatings should be viewed as only temporary protection against corrosion, especially when used on corrosion-prone materials such as steel. Baked enamel and porcelain finishes on steel have longer lives in terms of corrosion resistance, though they suffer from brittleness. New formulations of paints and protective coatings are continually being developed. The latest and best information will be obtained from vendors of these products.

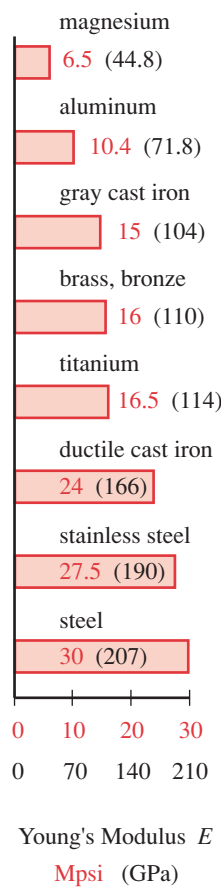


FIGURE 2-17

Young's Moduli for Various Metals

2.6 GENERAL PROPERTIES OF METALS

The large variety of useful engineering materials can be confusing to the beginning engineer. There is not space enough in this book to deal with the topic of material selection in complete detail. Several references are provided in this chapter's bibliography which the reader is encouraged to use. Tables of mechanical property data are also provided for a limited set of materials in Appendix A of this book. Figure 2-17 shows the Young's moduli for several engineering metals.

The following sections attempt to provide some general information and guidelines for the engineer to help identify what types of materials might be suitable in a given design situation. It is expected that the practicing engineer will rely heavily on the expertise and help available from materials manufacturers in selecting the optimum material for each design. Many references are also published which list detailed property data for most engineering materials. Some of these references are listed in the bibliography to this chapter.

Cast Iron

Cast irons constitute a whole family of materials. Their main advantages are relatively low cost and ease of fabrication. Some are weak in tension compared to steels but, like most cast materials, have high compressive strengths. Their densities are slightly lower than steel at about 0.25 lb/in^3 ($6\,920 \text{ kg/m}^3$). Most cast irons do not exhibit a linear stress-strain relationship below the elastic limit; they do not obey Hooke's law. Their modulus of elasticity E is estimated by drawing a line from the origin through a point on the curve at $1/4$ the ultimate tensile strength and is in the range of $14\text{--}25 \text{ Mpsi}$ ($97\text{--}172 \text{ MPa}$). Cast iron's chemical composition differs from steel principally in its higher carbon content, being between 2 and 4.5% . The large amount of carbon, present in some cast irons as graphite, makes some of these alloys easy to pour as a casting liquid and also easy to machine as a solid. The most common means of fabrication is sand casting with subsequent machining operations. Cast irons are not easily welded, however.

WHITE CAST IRON is a very hard and brittle material. It is difficult to machine and has limited uses, such as in linings for cement mixers where its hardness is needed.

GRAY CAST IRON is the most commonly used form of cast iron. Its graphite flakes give it its gray appearance and name. The ASTM grades gray cast iron into seven classes based on the minimum tensile strength in kpsi. Class 20 has a minimum tensile strength of 20 kpsi (138 MPa). The class numbers of $20, 25, 30, 35, 40, 50$, and 60 then represent the tensile strength in kpsi. Cost increases with increasing tensile strength. This alloy is easy to pour, easy to machine, and offers good acoustical damping. This makes it the popular choice for machine frames, engine blocks, brake rotors and drums, etc. The graphite flakes also give it good lubricity and wear resistance. Its relatively low tensile strength recommends against its use in situations where large bending or fatigue loads are present, though it is sometimes used in low-cost engine crankshafts. It runs reasonably well against steel if lubricated.

MALLEABLE CAST IRON has superior tensile strength to gray cast iron but does not wear as well. The tensile strength can range from 50 to 120 kpsi (345 to 827 MPa) depending on formulation. It is often used in parts where bending stresses are present.

NODULAR (DUCTILE) CAST IRON has the highest tensile strength of the cast irons, ranging from about 70 to 135 kpsi (480 to 930 MPa). The name *nodular* comes from the fact that its graphite particles are spheroidal in shape. Ductile cast iron has a higher modulus of elasticity (about 25 Mpsi {172 GPa}) than gray cast iron and exhibits a linear stress-strain curve. It is tougher, stronger, more ductile, and less porous than gray cast iron. It is the cast iron of choice for fatigue-loaded parts such as crankshafts, pistons, and cams.

Cast Steels

Cast steel is similar to wrought steel in terms of its chemical content, i.e., it has much less carbon than cast iron. The mechanical properties of cast steel are superior to cast iron but inferior to wrought steel. Its principal advantage is ease of fabrication by sand or investment (lost wax) casting. Cast steel is classed according to its carbon content into low carbon (< 0.2%), medium carbon (0.2–0.5%) and high carbon (> 0.5%). Alloy cast steels are also made containing other elements for high strength and heat resistance. The tensile strengths of cast steel alloys range from about 65 to 200 kpsi (450 to 1380 MPa).

Wrought Steels

The term “wrought” refers to all processes that manipulate the shape of the material without melting it. Hot rolling and cold rolling are the two most common methods used though many variants exist, such as wire drawing, deep drawing, extrusion, and cold-heading. The common denominator is a deliberate yielding of the material to change its shape either at room or at elevated temperatures.

HOT-ROLLED STEEL is produced by forcing hot billets of steel through sets of rollers or dies which progressively change their shape into I-beams, channel sections, angle irons, flats, squares, rounds, tubes, sheets, plates, etc. The surface finish of hot-rolled shapes is rough due to oxidation at the elevated temperatures. The mechanical properties are also relatively low because the material ends up in an annealed or normalized state unless deliberately heat-treated later. This is the typical choice for low-carbon structural steel members used for building- and machine-frame construction. Hot-rolled material is also used for machine parts that will be subjected to extensive machining (gears, cams, etc.) where the initial finish of the stock is irrelevant and uniform, non-cold-worked material properties are desired in advance of a planned heat treatment. A wide variety of alloys and carbon contents are available in hot-rolled form.

COLD-ROLLED STEEL is produced from billets or hot-rolled shapes. The shape is brought to final form and size by rolling between hardened steel rollers or drawing through dies at room temperature. The rolls or dies burnish the surface and cold work the material, increasing its strength and reducing its ductility as was described in the section on mechanical forming and hardening above. The result is a material with good surface finish and accurate dimensions compared to hot-rolled material. Its strength and hardness are increased at the expense of significant built-in strains, which can later be released during machining, welding, or heat treating, then causing distortion. Cold-rolled shapes commonly available are sheets, strips, plates, round and rectangular bars, tubes, etc. Structural shapes such as I-beams are typically available only as hot rolled.

Steel Numbering Systems

Several steel numbering systems are in general use. The ASTM, AISI, and SAE* have devised codes to define the alloying elements and carbon content of steels. Table 2-5 lists some of the AISI/SAE designations for commonly used steel alloys. The first two digits indicate the principal alloying elements. The last two digits indicate the amount of carbon present, expressed in hundredths of a percent. ASTM and the SAE have developed a new Unified Numbering System for all metal alloys, which uses the prefix UNS followed by a letter and a 5-digit number. The letter defines the alloy category, *F* for cast iron, *G* for carbon and low-alloy steels, *K* for special-purpose steels, *S* for stainless steels, and *T* for tool steels. For the *G* series, the numbers are the same as the AISI/SAE designations in Table 2-5 with a trailing zero added. For example, SAE 4340 becomes UNS G43400. See reference 2 for more information on metal numbering systems. We will use the AISI/SAE designations for steels.

* ASTM is the American Society for Testing and Materials, AISI is the American Iron and Steel Institute, and SAE is the Society of Automotive Engineers. AISI and SAE both use the same designations for steels.

PLAIN CARBON STEEL is designated by a first digit of 1 and a second digit of 0, since no alloys other than carbon are present. The low-carbon steels are those numbered AISI 1005 to 1030, medium-carbon from 1035 to 1055, and high-carbon from 1060 to 1095. The AISI 11xx series adds sulphur, principally to improve machinability. These are called free-machining steels and are not considered alloy steels as the sulphur does

Table 2-5 AISI/SAE Designations of Steel Alloys

A partial list - other alloys are available - consult the manufacturers

Type	AISI/SAE Series	Principal Alloying Elements
Carbon Steels		
Plain	10xx	Carbon
Free-cutting	11xx	Carbon plus Sulphur (resulphurized)
Alloy Steels		
Manganese	13xx	1.75% Manganese
	15xx	1.00 to 1.65% Manganese
Nickel	23xx	3.50% Nickel
	25xx	5.00% Nickel
Nickel-Chrome	31xx	1.25% Nickel and 0.65 or 0.80% Chromium
	33xx	3.50% Nickel and 1.55% Chromium
Molybdenum	40xx	0.25% Molybdenum
	44xx	0.40 or 0.52% Molybdenum
Chrome-Moly	41xx	0.95% Chromium and 0.20% Molybdenum
Nickel-Chrome-Moly	43xx	1.82% Nickel, 0.50 or 0.80% Chromium, and 0.25% Molybdenum
	47xx	1.45% Nickel, 0.45% Chromium, and 0.20 or 0.35% Molybdenum
Nickel-Moly	46xx	0.82 or 1.82% Nickel and 0.25% Molybdenum
	48xx	3.50% Nickel and 0.25% Molybdenum
Chrome	50xx	0.27 to 0.65% Chromium
	51xx	0.80 to 1.05% Chromium
	52xx	1.45% Chromium
Chrome-Vanadium	61xx	0.60 to 0.95% Chromium and 0.10 to 0.15% Vanadium minimum

not improve the mechanical properties and also makes it brittle. The ultimate tensile strength of plain carbon steel can vary from about 60 to 150 kpsi (414 to 1 034 MPa) depending on heat treatment.

ALLOY STEELS have various elements added in small quantities to improve the material's strength, hardenability, temperature resistance, corrosion resistance, and other properties. Any level of carbon can be combined with these alloying elements. Chromium is added to improve strength, ductility, toughness, wear resistance, and hardenability. Nickel is added to improve strength without loss of ductility, and it also enhances case hardenability. Molybdenum, used in combination with nickel and/or chromium, adds hardness, reduces brittleness, and increases toughness. Many other alloys in various combinations, as shown in Table 2-5, are used to achieve specific properties. Specialty steel manufacturers are the best source of information and assistance for the engineer trying to find the best material for any application. The ultimate tensile strength of alloy steels can vary from about 80 to 300 kpsi (550 to 2 070 MPa), depending on its alloying elements and heat treatment. Appendix A contains tables of mechanical property data for a selection of carbon and alloy steels. Figure 2-18 shows approximate ultimate tensile strengths of some normalized carbon and alloy steels and Figure 2-19 shows engineering stress-strain curves from tensile tests of three steels.

TOOL STEELS are medium- to high-carbon alloy steels especially formulated to give very high hardness in combination with wear resistance and sufficient toughness to resist the shock loads experienced in service as cutting tools, dies and molds. There is a very large variety of tool steels available. Refer to the bibliography and to manufacturers' literature for more information.

STAINLESS STEELS are alloy steels containing at least 10% chromium and offer much improved corrosion resistance over plain or alloy steels, though their name should not be taken too literally. Stainless steels will stain and corrode (slowly) in severe environments such as seawater. Some stainless-steel alloys have improved resistance to high

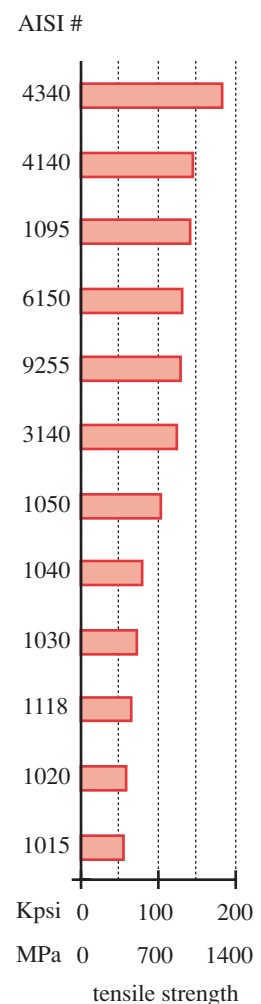


FIGURE 2-18

Approximate Ultimate Tensile Strengths of Some Normalized Steels

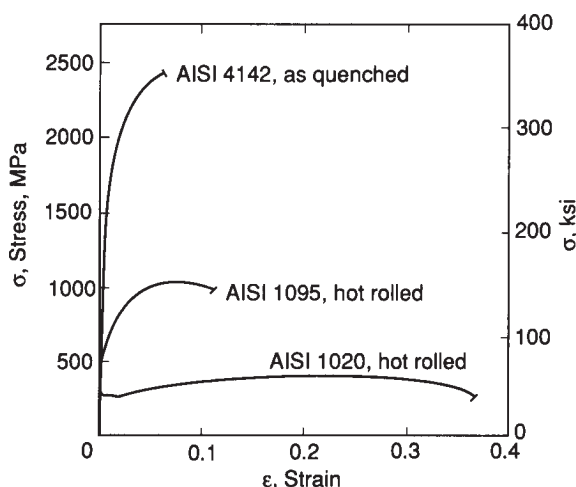


FIGURE 2-19

Tensile Test Stress-Strain Curves of Three Steel Alloys (From Fig. 5.16, p. 160, in N. E. Dowling, *Mechanical Behavior of Materials*, Prentice-Hall, Englewood Cliffs, N.J., 1993, with permission)

temperature. There are four types of stainless steel, called **martensitic**, **ferritic**, **austenitic**, and **precipitation hardening**.

Martensitic stainless steel contains 11.5 to 15% Cr and 0.15 to 1.2% C, is magnetic, can be hardened by heat treatment, and is commonly used for cutlery. **Ferritic** stainless steel has over 16% Cr and a low carbon content, is magnetic, soft, and ductile, but is not heat treatable though its strength can be increased modestly by cold working. It is used for deep-drawn parts such as cookware and has better corrosion resistance than the martensitic SS. The ferritic and martensitic stainless steels are both called **400 series** stainless steel.

Austenitic stainless steel is alloyed with 17 to 25% chromium and 10 to 20% nickel. It has better corrosion resistance due to the nickel, is nonmagnetic, and has excellent ductility and toughness. It cannot be hardened except by cold working. It is classed as **300 series** stainless steel.

Precipitation-hardening stainless steels are designated by their alloy percentages followed by the letters PH, as in 17-4 PH which contains 17% chromium and 4% nickel. These alloys offer high strength and high temperature and corrosion resistance.

The **300 series** stainless steels are very weldable but the 400 series are less so. All grades of stainless steel have poorer heat conductivity than regular steel and many of the stainless alloys are difficult to machine. All stainless steels are significantly more expensive than regular steel. See Appendix A for mechanical property data.

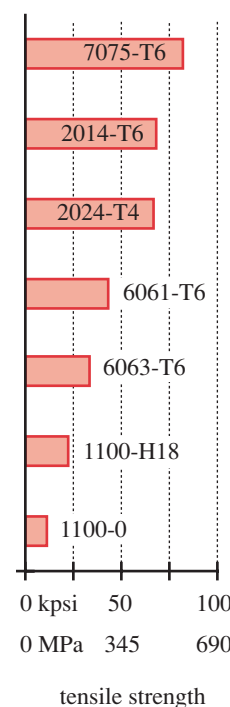


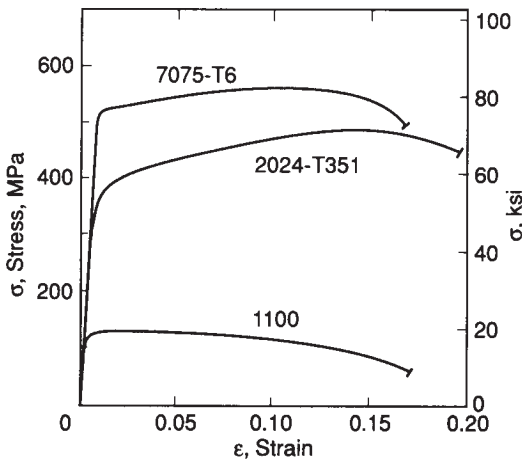
FIGURE 2-20

Ultimate Tensile Strengths of Some Aluminum Alloys

Aluminum

Aluminum is the most widely used nonferrous metal, being second only to steel in world consumption. Aluminum is produced in both “pure” and alloyed forms. Aluminum is commercially available up to 99.8% pure. The most common alloying elements are copper, silicon, magnesium, manganese, and zinc, in varying amounts up to about 5%. The principal advantages of aluminum are its low density, good strength-to-weight ratio (SWR), ductility, excellent workability, castability, and weldability, corrosion resistance, high conductivity, and reasonable cost. Compared to steel it is 1/3 as dense (0.10 lb/in³ versus 0.28 lb/in³), about 1/3 as stiff ($E = 10.3 \text{ Mpsi}$ {71 GPa} versus 30 Mpsi {207 GPa}), and generally less strong. If you compare the strengths of low-carbon steel and pure aluminum, the steel is about three times as strong. Thus the specific strength is approximately the same in that comparison. However, pure aluminum is seldom used in engineering applications. It is too soft and weak. Pure aluminum’s principal advantages are its bright finish and good corrosion resistance. It is used mainly in decorative applications.

The aluminum alloys have significantly greater strengths than pure aluminum and are used extensively in engineering, with the aircraft and automotive industries among the largest users. The higher-strength aluminum alloys have tensile strengths in the 70 to 90 kpsi (480 to 620 MPa) range, and yield strengths about twice that of mild steel. They compare favorably to medium-carbon steels in specific strength. Aluminum competes successfully with steel in some applications, though few materials can beat steel if very high strength is needed. See Figure 2-20 for tensile strengths of some aluminum alloys. Figure 2-21 shows tensile-test engineering stress-strain curves for three aluminum alloys. Aluminum’s strength is reduced at low temperatures as well as at elevated temperatures.

**FIGURE 2-21**

Tensile Test Stress-Strain Curves of Three Aluminum Alloys (From Fig. 5.17, p. 160, in N. E. Dowling, *Mechanical Behavior of Materials*, Prentice-Hall, Englewood Cliffs, N.J., 1993, with permission)

Some aluminum alloys are hardenable by heat treatment and others by strain hardening or precipitation and aging. High-strength aluminum alloys are about 1.5 times harder than soft steel, and surface treatments such as *hard anodizing* can bring the surface to a condition harder than the hardest steel.

Aluminum is among the most easily worked of the engineering materials, though it tends to work harden. It casts, machines, welds,* and hot and cold forms† easily. It can also be extruded. Alloys are specially formulated for both sand and die casting as well as for wrought and extruded shapes and for forged parts.

WROUGHT-ALUMINUM ALLOYS are available in a wide variety of stock shapes such as I-beams, angles, channels, bars, strip, sheet, rounds, and tubes. Extrusion allows relatively inexpensive custom shapes as well. The Aluminum Association numbering system for alloys is shown in Table 2-6. The first digit indicates the principal alloying element and defines the series. Hardness is indicated by a suffix containing a letter and up to 3 numbers as defined in the table. The most commonly available and most-used aluminum alloys in machine-design applications are the 2000 and 6000 series.

The oldest aluminum alloy is 2024, which contains 4.5% copper, 1.5% magnesium, and 0.8% manganese. It is among the most machinable of the aluminum alloys and is heat treatable. In the higher tempers, such as -T3 and -T4, it has a tensile strength approaching 70 ksi (483 MPa), which also makes it one of the strongest of the aluminum alloys. It also has high fatigue strength. However, it has poor weldability and formability compared to the other aluminum alloys.

The 6061 alloy contains 0.6% silicon, 0.27% copper, 1.0% manganese, and 0.2% chromium. It is widely used in structural applications because of its excellent weldability. Its strength is about 40 to 45 ksi (276 to 310 MPa) in the higher tempers. It has lower fatigue strength than 2024 aluminum. It is easily machined and is a popular alloy for extrusion, which is a hot-forming process.

The 7000 series is called aircraft aluminum and is used mostly in airframes. These are the strongest alloys of aluminum with tensile strengths up to 98 ksi (676 MPa) and

* The heat of welding causes localized annealing, which can remove the desirable strengthening effects of cold work or heat treatment in any metal.

† Some aluminum alloys will cold-work when formed to the degree that trying to bend them again (without first annealing) will cause fractures. Some bicycle racers prefer steel frames over aluminum despite their added weight because, once an aluminum frame is bent in a fall, it cannot be straightened without cracking. Damaged steel tube frames can be straightened and reused.

Table 2-6 Aluminum Association Designations of Aluminum Alloys

A partial list - other alloys are available - consult the manufacturers

Series	Major Alloying Elements	Secondary Alloys
1xxx	Commercially pure (99%)	None
2xxx	Copper (Cu)	Mg, Mn, Si
3xxx	Manganese (Mn)	Mg, Cu
4xxx	Silicon (Si)	None
5xxx	Magnesium (Mg)	Mn, Cr
6xxx	Magnesium and Silicon	Cu, Mn
7xxx	Zinc (Zn)	Mg, Cu, Cr
Hardness Designations		
xxxx-F	As fabricated	
xxxx-O	Annealed	
xxxx-Hyyy	Work hardened	
xxxx-Tyyy	Thermal/age hardened	

the highest fatigue strength of about 22 kpsi (152 MPa) @ 10^8 cycles. Some alloys are also available in an *alclad* form which bonds a thin layer of pure aluminum to one or both sides to improve corrosion resistance.

CAST-ALUMINUM ALLOYS are differently formulated than the wrought alloys. Some of these are hardenable but their strength and ductility are less than those of the wrought alloys. Alloys are available for sand casting, die casting, or investment casting. See Appendix A for mechanical properties of wrought- and cast-aluminum alloys.

Titanium

Though discovered as an element in 1791, commercially produced titanium has been available only since the 1940s, so it is among the newest of engineering metals. Titanium can be the answer to an engineer's prayer in some cases. It has an upper service-temperature limit of 1 200 to 1 400°F (650 to 750°C), weighs half as much as steel (0.16 lb/in³ {4 429 kg/m³}), and is as strong as a medium-strength steel (135 kpsi {930 MPa} typical). Its Young's modulus is 16 to 18 Mpsi (110 to 124 GPa), or about 60% that of steel. Its specific strength approaches that of the strongest alloy steels and exceeds that of medium-strength steels by a factor of 2. Its specific stiffness is greater than that of steel, making it as good or better in limiting deflections. It is also nonmagnetic.

Titanium is very corrosion resistant and is nontoxic, allowing its use in contact with acidic or alkaline foodstuffs and chemicals, and in the human body as replacement heart valves and hip joints, for example. Unfortunately, it is expensive compared to aluminum and steel. It finds much use in the aerospace industry, especially in military aircraft structures and in jet engines, where strength, light weight, and high temperature and corrosion resistance are all required.

Titanium is available both pure and alloyed with combinations of aluminum, vanadium, silicon, iron, chromium, and manganese. Its alloys can be hardened and anodized. Limited stock shapes are available commercially. It can be forged and wrought, though it is quite difficult to cast, machine, and cold form. Like steel and unlike most other metals, some titanium alloys exhibit a true endurance limit, or leveling off of the fatigue strength, beyond about 10^6 cycles of repeated loading, as shown in Figure 2-10. See Appendix A for mechanical property data.

Magnesium

Magnesium is the lightest of commercial metals but is relatively weak. The tensile strengths of its alloys are between 10 and 50 kpsi (69 and 345 MPa). The most common alloying elements are aluminum, manganese, and zinc. Because of its low density (0.065 lb/in^3 { $1\ 800 \text{ kg/m}^3$ }), its specific strength approaches that of aluminum. Its Young's modulus is 6.5 Mpsi (45 GPa) and its specific stiffness exceeds those of aluminum and steel. It is very easy to cast and machine but is more brittle than aluminum and thus is difficult to cold form.

It is nonmagnetic and has fair corrosion resistance, better than steel, but not as good as aluminum. Some magnesium alloys are hardenable, and all can be anodized. It is the most active metal on the galvanic scale and cannot be combined with most other metals in a wet environment. It is also extremely flammable, especially in powder or chip form, and its flame cannot be doused with water. Machining requires flooding with oil coolant to prevent fire. It is roughly twice as costly per pound as aluminum. Magnesium is used where light weight is of paramount importance such as in castings for chain-saw housings and other hand-held items. See Appendix A for mechanical property data.

Copper Alloys

Pure copper is soft, weak, and malleable and is used primarily for piping, flashing, electrical conductors (wire) and motors. It cold works readily and can become brittle after forming, requiring annealing between successive draws.

Many alloys are possible with copper. The most common are brasses and bronzes which themselves are families of alloys. **Brasses**, in general, are alloys of copper and zinc in varying proportions and are used in many applications, from artillery shells and bullet shells to lamps and jewelry.

Bronzes were originally defined as alloys of copper and tin, but now also include alloys containing no tin, such as silicon bronze and aluminum bronze, so the terminology is somewhat confusing. **Silicon bronze** is used in marine applications such as ship propellers.

Beryllium copper is neither brass nor bronze and is the strongest of the alloys, with strengths approaching those of alloy steels (200 kpsi { $1\ 380 \text{ MPa}$ }). It is often used in springs that must be nonmagnetic, carry electricity, or exist in corrosive environments. **Phosphor bronze** is also used for springs but unlike beryllium copper, it cannot be bent along the grain or heat treated.

Copper and its alloys have excellent corrosion resistance and are nonmagnetic. All copper alloys can be cast, hot or cold formed, and machined, but pure copper is difficult to machine. Some alloys are heat treatable and all will work harden. The Young's modulus of most copper alloys is about 17 Mpsi (117 GPa) and their weight density is slightly higher than that of steel at 0.31 lb/in³ (8 580 kg/m³). Copper alloys are expensive compared to other structural metals. See Appendix A for mechanical property data.

2.7 GENERAL PROPERTIES OF NONMETALS

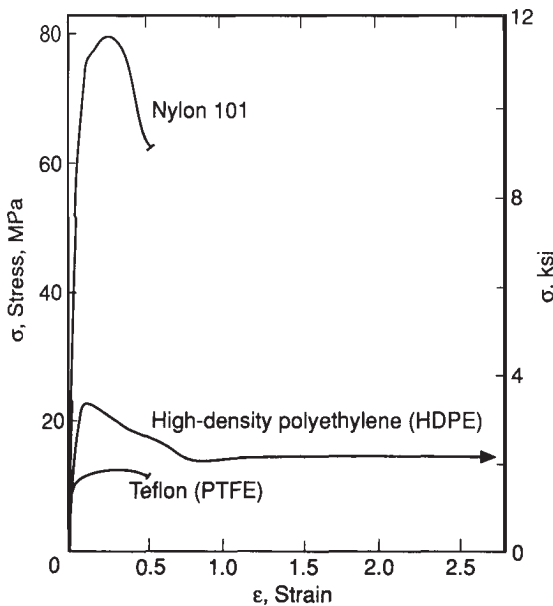
The use of nonmetallic materials has increased greatly in the last 50 years. The usual advantages sought are light weight, corrosion resistance, temperature resistance, dielectric strength, and ease of manufacture. Cost can range from low to high compared to metals depending on the particular nonmetallic material. There are three general categories of nonmetals of general engineering interest: **polymers** (plastics), **ceramics**, and **composites**.

Polymers have a wide variety of properties, principally low weight, relatively low strength and stiffness, good corrosion and electrical resistance, and relatively low cost per unit volume. **Ceramics** can have extremely high compressive (but not tensile) strengths, high stiffness, high temperature resistance, high dielectric strength (resistance to electrical current), high hardness, and relatively low cost per unit volume. **Composites** can have almost any combination of properties you want to build into them, including the highest specific strengths obtainable from any materials. Composites can be low or very high in cost. We briefly discuss nonmetals and some of their applications. Space does not permit a complete treatment of these important classes of materials. The reader is directed to the bibliography for further information. Appendix A also provides some mechanical property data for polymers.

Polymers

The word polymers comes from **poly** = *many* and **mers** = *molecules*. Polymers are long-chain molecules of organic materials or carbon-based compounds. (There is also a family of silicon-based polymeric compounds.) The source of most polymers is oil or coal, which contains the carbon or hydrocarbons necessary to create the polymers. While there are many natural polymer compounds (wax, rubber, proteins, ...), most polymers used in engineering applications are man-made. Their properties can be tailored over a wide range by copolymerization with other compounds or by alloying two or more polymers together. Mixtures of polymers and inorganic materials such as talc or glass fiber are also common.

Because of their variety, it is difficult to generalize about the mechanical properties of polymers, but compared to metals they have low density, low strength, low stiffness, nonlinear elastic stress-strain curves as shown in Figure 2-22 (with a few exceptions), low hardness, excellent electrical and corrosion resistance, and ease of fabrication. Their apparent moduli of elasticity vary widely from about 10 kpsi (69 MPa) to about 400 kpsi (2.8 GPa), all much less stiff than any metals. Their ultimate tensile strengths range from about 4 kpsi (28 MPa) for the weakest unfilled polymer to about 22 kpsi (152 MPa) for the strongest glass-filled polymers. The specific gravities of most polymers range from about 0.95 to 1.8 compared to about 2 for magnesium, 3 for alu-

**FIGURE 2-22**

Tensile Test Stress-Strain Curves of Three Thermoplastic Polymers (From Fig. 5.18, p. 161 in N. E. Dowling, *Mechanical Behavior of Materials*, Prentice-Hall, 1993, with permission)

minimum, 8 for steel, and 13 for lead. So, even though the absolute strengths of polymers are low, their specific strengths are respectable due to their low densities.

Polymers are divided into two classes, **thermoplastic** and **thermosets**. **Thermoplastic polymers** can be repeatedly melted and solidified, though their properties can degrade due to the high melt temperatures. Thermoplastics are easy to mold and their rejects or leftovers can be reground and remolded. **Thermosetting polymers** become cross-linked when first heated and will burn, not melt, on reheating. Cross-linking creates connections (like the rungs of a ladder) between the long-chain molecules which wind and twist through a polymer. These cross-connections add strength and stiffness.

Another division among polymers can be made between filled and unfilled compounds. The fillers are usually inorganic materials, such as carbon black, graphite, talc, chopped glass fibers, and metal powders. Fillers are added to both thermoplastic and thermosetting resins, though they are more frequently used in the latter. These filled compounds have superior strength, stiffness, and temperature resistance over that of the raw polymers but are more difficult to mold and to fabricate.

A confusing array of polymers is available commercially. The confusion is increased by a proliferation of brand names for similar compounds made by different manufacturers. The generic chemical names of polymers tend to be long, complex, and hard to remember. In some cases a particular polymer brand name has been so widely used that it has become generic. Nylon, plexiglass, and fiberglass are examples. Learning the generic chemical names and associated brand names of the main families of engineering polymers will eliminate some of the confusion. Table 2-7 shows a number of important polymer families. The mechanical properties of a few of these that have significant engineering applications are included in Appendix A.

Table 2-7
Families of Polymers

Thermoplastics

- Cellulosics
- Ethylenics
- Polyamides
- Polyacetals
- Polycarbonates
- Polyphenylene oxides
- Polysulfones

Thermosets

- Aminos
- Elastomers
- Epoxies
- Phenolics
- Polyesters
- Silicones
- Urethanes

Ceramics

Ceramic materials are finding increasing application in engineering, and a great deal of effort is being devoted to the development of new ceramic compounds. Ceramics are among the oldest known engineering materials; clay bricks are ceramic materials. Though still widely used in building, clay is not now considered an engineering ceramic. Engineering ceramics are typically compounds of metallic and nonmetallic elements. They may be single oxides of a metal, mixtures of metallic oxides, carbides, borides, nitrides, or other compounds such as Al_2O_3 , MgO , SiC , and Si_3N_4 , for example. The principal properties of ceramic materials are high hardness and brittleness, high temperature and chemical resistance, high compressive strength, high dielectric strength, and potentially low cost and weight. Ceramic materials are too hard to be machined by conventional techniques and are usually formed by compaction of powder, then fired or sintered to form bonds between particles and increase their strength. The powder compaction can be done in dies or by hydrostatic pressure. Sometimes, glass powder is mixed with the ceramic and the result is fired to melt the glass and fuse the two together. Attempts are being made to replace traditional metals with ceramics in such applications as cast engine blocks, pistons, and other engine parts. The low tensile strength, porosity, and low fracture toughness of most ceramics can be problems in these applications. Plasma-sprayed ceramic compounds are often used as hard coatings on metal substrates to provide wear- and corrosion-resistant surfaces.

Composites

Most composites are man-made, but some, such as wood, occur naturally. Wood is a composite of long cellulose fibers held together in a resinous matrix of lignin. Man-made composites are typically a combination of some strong, fibrous material such as glass, carbon, or boron fibers glued together in a matrix of resin such as epoxy or polyester. The fiberglass material used in boats and other vehicles is a common example of a glass-fiber reinforced polyester (GFRP) composite. The directional material properties of a composite can be tailored to the application by arranging the fibers in different juxtapositions such as parallel, interwoven at random or particular angles, or wound around a mandrel. Custom composites are finding increased use in highly stressed applications such as airframes due to their superior strength-to-weight ratios compared to the common structural metals. Temperature and corrosion resistance can also be designed into some composite materials. These composites are typically neither homogeneous nor isotropic as was discussed in Section 2.3.

Table 2-8

Iron and Steel Strengths

Form	S_{ut} kpsi (MPa)
Theoretical	2 900 ($20E3$)
Whisker	1 800 ($12E3$)
Fine wire	1 400 ($10E3$)
Mild steel	60 (414)
Cast iron	40 (276)

It is interesting to note that if one calculates the theoretical strength of any “pure” elemental crystalline material based on the interatomic bonds of the element, the predicted strengths are orders of magnitude larger than those seen in any test of a “real” material, as seen in Table 2-8. The huge differences in actual versus theoretical strengths are attributed to disruptions of the atomic bonds due to crystal defects in the real material. That is, it is considered impossible to manufacture “pure anything” on any realistic superatomic scale. It is presumed that if we could make a “wire” of pure iron only one atom in diameter, it would exhibit its theoretical “super strength.” Crystal “whiskers” have been successfully made of some elemental materials and exhibit very high tensile strengths which approach their theoretical values (Table 2-8).

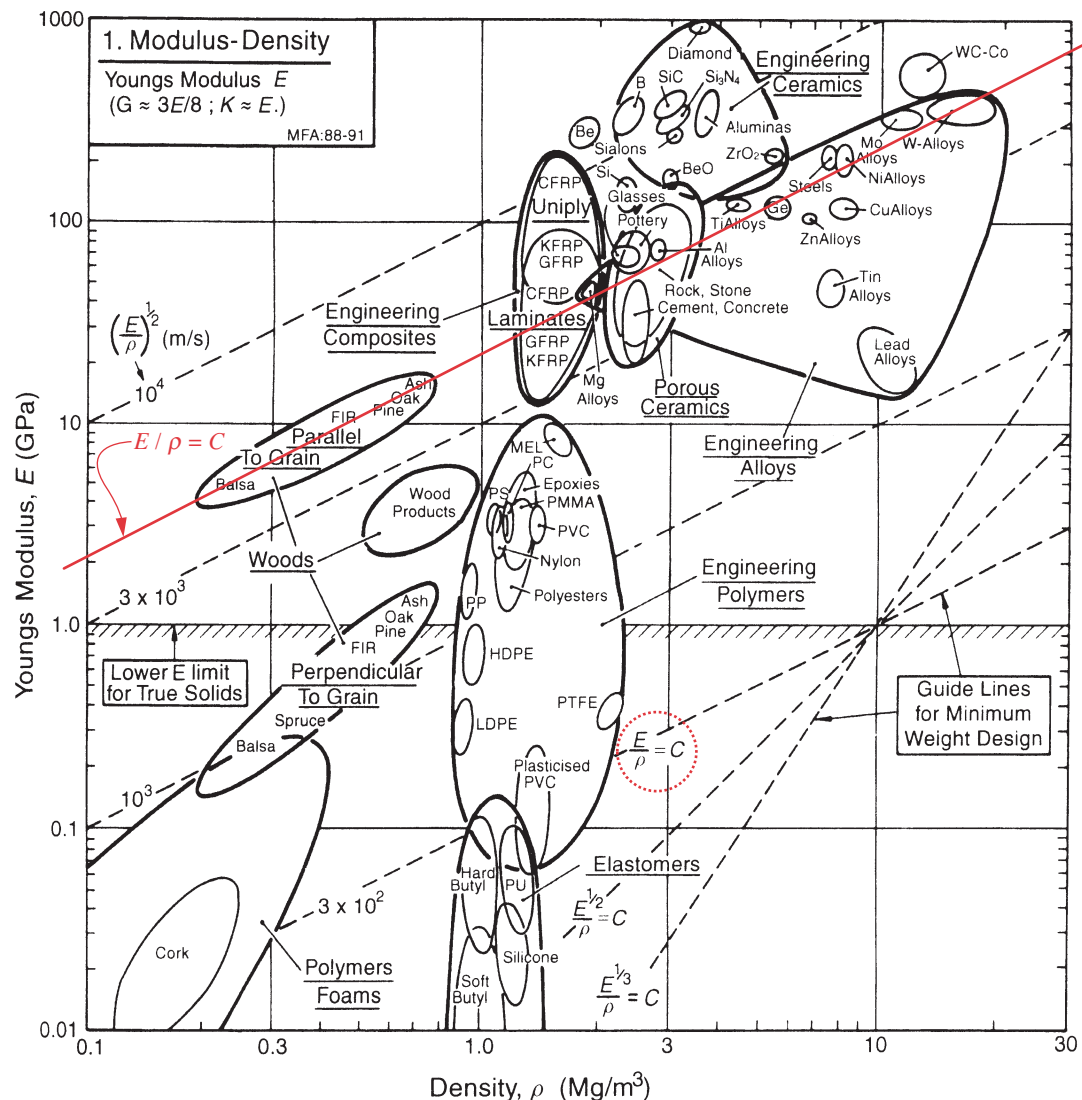
Other empirical evidence for this theory comes from the fact that fibers of any material made in very small diameters exhibit much higher tensile strengths than would be expected from stress-strain tests of larger samples of the same material. Presumably, the very small cross sections are approaching a “purer” material state. For example, it is well known that glass has poor tensile strength. However, small-diameter glass fibers show much larger tensile strength than sheet glass, making them a practical (and inexpensive) fiber for use in boat hulls, which are subjected to large tensile stresses in use. Small-diameter fibers of carbon and boron exhibit even higher tensile strengths than glass fiber, which explains their use in composites for spacecraft and military aircraft applications, where their relatively high cost is not a barrier.

2.8 SELECTING MATERIALS

One of the most important design decisions is the proper choice of material. Materials limit design and new materials are still being invented that open new design possibilities. It would help if there were a systematic way to select a material for an application. M. F. Ashby has proposed such an approach that plots various material properties against one another to form “materials selection charts.”^[3] Materials can be roughly divided into six classes, metals, ceramics, polymers (solid or foam), elastomers, glasses, and composites (which include wood). Members of these classes and sub-classes tend to cluster together on a plot of this type.

Figure 2-23 shows such a chart that plots Young’s modulus against density, which is called *specific stiffness*. By drawing lines of constant slope on such a chart, one can see which materials possess similar properties. A line of specific stiffness $E / \rho = C$ has been drawn in color on Figure 2-23 and shows that some woods have equivalent specific stiffness to steel and some other metals. The line also passes through the lower range of the engineering composites’ “bubble” indicating that fiberglass (GFRP) has about the same specific stiffness as wood and steel, while the nonreinforced thermoplastics such as nylon and polyester have lower specific stiffness. So if you seek the stiffest/lightest material, you want to move up and to the left on the chart. Other lines are shown that have slopes equal to $E^n / \rho = C$ where n is a fraction such as 1/2 or 1/3. These represent loading situations, such as beams in bending, for which the parameter of interest is a nonlinear function of specific stiffness. Since the chart is a log-log plot, exponential functions also plot as straight lines allowing simple comparisons to be made.

Figure 2-24 shows a chart of strength versus density (called *specific strength*) for a number of materials. In this chart, the particular material strength used varies with the material depending on its character. For example, ductile metals and polymers show their yield strength, brittle ceramics their crushing compressive strength, and elastomers their tear strength. The vertical elongation of a material’s “bubble” indicates the range of strength values that can obtain due to thermal or work hardening, alloying elements, etc. The colored line drawn on the chart represents a particular value of specific strength or $\sigma / \rho = C$ and shows that the strength-to-weight ratio of some woods are as good as high-strength steel and better than most other metals. It should be no surprise that wood is a popular material in building construction. Note also the high specific strength of engineering ceramics. Unfortunately, their tensile strengths are at best only about 10% of these compressive strengths, which is why you seldom see them used in structures where tensile stresses are commonly encountered.

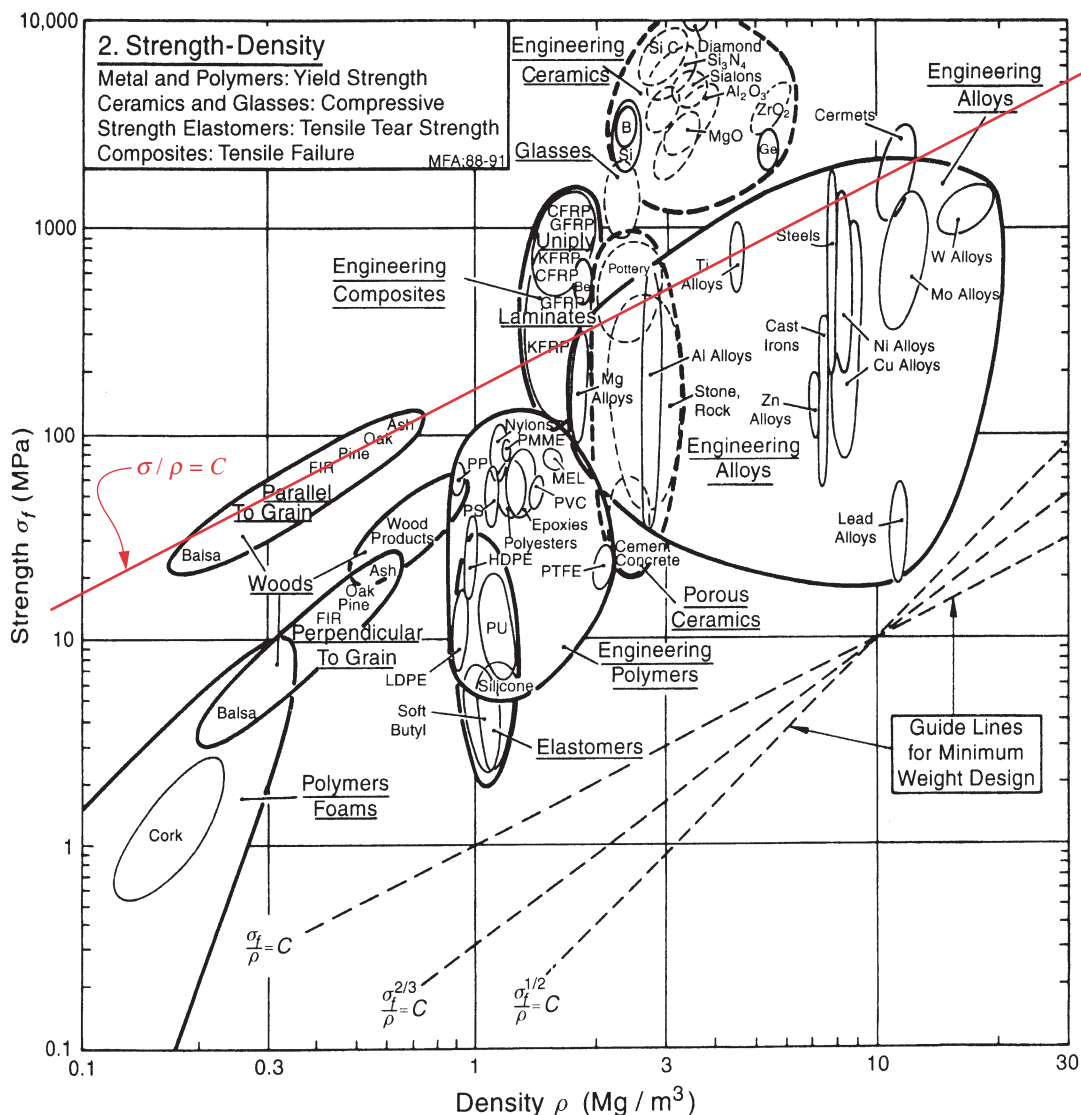
**FIGURE 2-23**

Young's Modulus Plotted Against Density for Engineering Materials (From Fig. 4-3, p. 37 in M. F. Ashby, *Materials Selection in Mechanical Design*, 2ed, Butterworth-Heinemann 1999, with permission)

Ashby's book^[3] is a very useful reference for the practicing engineer. It has dozens of charts of the type shown here that plot various properties against one another in a manner that enhances their comparison and develops good understanding.

2.9 SUMMARY

There are many different kinds of material strengths. It is important to understand which ones are important in particular loading situations. The most commonly measured and

**FIGURE 2-24**

Strength Plotted Against Density for Engineering Materials (From Fig. 4-4, p. 39 in M. F. Ashby, *Materials Selection in Mechanical Design*, 2ed, Butterworth-Heinemann 1999, with permission)

reported strengths are the **ultimate tensile strength** S_{ut} and the **tensile yield strength** S_y . The S_{ut} indicates the largest stress that the material will accept before fracture, and S_y indicates the stress beyond which the material will take a permanent set. Many materials have **compressive strengths** about equal to their tensile strengths and are called **even materials**. Most wrought metals are in the *even* category. Some materials have significantly different compressive and tensile strengths and these are called **uneven materials**. Cast metals are usually in the *uneven* category, with compressive strengths much greater than their tensile strengths. The **shear strengths** of even materials tend

to be about half their tensile strengths, while shear strengths of uneven materials tend to be between their tensile and compressive strengths.

One or more of these strengths may be of interest when the loading is static. If the material is ductile, then S_y is the usual criterion of failure, as a ductile material is capable of significant distortion before fracture. If the material is brittle, as are most cast materials, then the S_{ut} is a more interesting parameter, because the material will fracture before any significant yielding distortion takes place. Yield strength values are nevertheless reported for brittle materials, but are usually calculated based on an arbitrary, small value of strain rather than on any measured yielding of the specimen. Chapter 5 deals with the mechanisms of material failure for both ductile and brittle materials in more detail than does this chapter.

The **tensile test** is the most common measure of these static strength parameters. The **stress-strain curve** (σ - ϵ) generated in this test is shown in Figure 2-2. The so-called **engineering σ - ϵ curve** differs from the **true σ - ϵ curve** due to the reduction in area of a ductile test specimen during the failure process. Nevertheless, the **engineering σ - ϵ curve** is the standard used to compare materials, since the true σ - ϵ curve is more difficult to generate.

The slope of the σ - ϵ curve in the elastic range, called **Young's modulus** or the **modulus of elasticity** E , is a very important parameter as it defines the material's stiffness or resistance to elastic deflection under load. If you are designing to control deflections as well as stresses, the value of E may be of more interest than the material's strength. While various alloys of a given base material may vary markedly in terms of their strengths, they will have essentially the same E . If deflection is the prime concern, a low-strength alloy is as good as a high-strength one of the same base material.

When the loading on the part varies with time it is called **dynamic** or **fatigue loading**. Then the static strengths do not give a good indication of failure. Instead, the **fatigue strength** is of more interest. This strength parameter is measured by subjecting a specimen to dynamic loading until it fails. Both the magnitude of the stress and the number of cycles of stress at failure are reported as the strength criterion. The fatigue strength of a given material will always be lower than its static strength, and often is less than half its S_{ut} . Chapter 6 deals with the phenomenon of fatigue failure of materials in more detail than does this chapter.

Other material parameters of interest to the machine designer are **resilience**, which is the ability to absorb energy without permanent deformation, and **toughness** or the ability to absorb energy without fracturing (but *with* permanent deformation). **Homogeneity** is the uniformity of a material throughout its volume. Many engineering materials, especially metals, can be assumed to be macroscopically homogeneous even though at a microscopic level they are often heterogeneous. **Isotropism** means having properties that are the same regardless of direction within the material. Many engineering materials are reasonably isotropic in the macro and are assumed so for engineering purposes. However, other useful engineering materials such as wood and composites are neither homogeneous nor isotropic and their strengths must be measured separately in different directions. **Hardness** is important in wear resistance and is also related to strength. **Heat treatment**, both through and surface, as well as **cold working** can increase the hardness and strength of some materials.

Important Equations Used in This Chapter

See the referenced sections for information on the proper use of these equations.

Axial tensile stress (Section 2.1):

$$\sigma = \frac{P}{A_o} \quad (2.1a)$$

Axial tensile strain (Section 2.1):

$$\epsilon = \frac{l - l_o}{l_o} \quad (2.1b)$$

Modulus of elasticity (Young's modulus) (Section 2.1):

$$E = \frac{\sigma}{\epsilon} \quad (2.2)$$

Modulus of rigidity (Section 2.1):

$$G = \frac{E}{2(1+\nu)} \quad (2.4)$$

Ultimate shear strength (Section 2.1):

steels :	$S_{us} \cong 0.80 S_{ut}$	(2.5b)
other ductile metals :	$S_{us} \cong 0.75 S_{ut}$	

Shear yield strength (Section 2.1):

$$U = \int_0^{\epsilon} \sigma d\epsilon \quad (2.6)$$

Modulus of resilience (Section 2.1):

$$U_R \cong \frac{1}{2} \frac{S_y^2}{E} \quad (2.7)$$

Modulus of toughness (Section 2.1):

$$U_T \cong \left(\frac{S_y + S_{ut}}{2} \right) \epsilon_f \quad (2.8)$$

Arithmetic mean (Section 2.2):

$$\mu = \frac{1}{n} \sum_{i=1}^n x_i \quad (2.9b)$$

Standard deviation (Section 2.2):

$$S_d = \sqrt{\frac{1}{n-1} \sum_{i=1}^n (x_i - \mu)^2} \quad (2.9c)$$

Ultimate tensile strength as a function of Brinell hardness (Section 2.4):

$$\begin{aligned} S_{ut} &\geq 500 \text{ HB} \pm 30 \text{ HB} \text{ psi} \\ S_{ut} &\geq 3.45 \text{ HB} \pm 0.2 \text{ HB MPa} \end{aligned} \quad (2.10)$$

2.10 REFERENCES

- 1 **E. B. Haugen and P. H. Wirsching**, "Probabilistic Design." *Machine Design*, v. 47, nos. 10-14, Penton Publishing, Cleveland, Ohio, 1975.
- 2 **H. E. Boyer and T. L. Gall**, eds. *Metals Handbook*. Vol. 1. American Society for Metals: Metals Park, Ohio, 1985.
- 3 **M. F. Ashby**, *Materials Selection in Mechanical Design*, 2ed., Butterworth and Heinemann, 1999.

2.11 WEB REFERENCES

The web is a useful resource for up-to-date material property information at these and other sites that can be found with a search engine.

<http://www.matweb.com>

Properties data sheets for over 41,000 metals, plastics, ceramics, and composites.

<http://metals.about.com>

Material properties and data.

2.12 BIBLIOGRAPHY

For general information on materials, consult the following:

Metals & Alloys in the Unified Numbering System. 6th ed. ASTM/SAE: Philadelphia, Pa., 1994.

Brady, ed. *Materials Handbook*. 13th ed. McGraw-Hill: New York. 1992.

H. E. Boyer, ed. *Atlas of Stress-Strain Curves*. Amer. Soc. for Metals: Metals Park, Ohio, 1987.

K. Budinski, *Engineering Materials: Properties and Selection*. 4th ed. Reston-Prentice-Hall: Reston, Va., 1992.

M. M. Farag, *Selection of Materials and Manufacturing Processes for Engineering Design*. Prentice-Hall International: Hertfordshire, U.K., 1989.

I. Granet, *Modern Materials Science*. Reston-Prentice-Hall: Reston, Va., 1980.

H. W. Pollack, *Materials Science and Metallurgy*. 2nd ed. Reston-Prentice-Hall: Reston, Va., 1977.

S. P. Timoshenko, *History of Strength of Materials*. McGraw-Hill: New York, 1983.

L. H. V. Vlack, *Elements of Material Science and Engineering*. 6th ed. Addison-Wesley: Reading, Mass., 1989.

M. M. Schwartz, ed. *Handbook of Structural Ceramics*. McGraw-Hill: New York. 1984.

For specific information on material properties, consult the following:

H. E. Boyer and T. L. Gall, ed. *Metals Handbook*. Vol. 1. American Society for Metals: Metals Park, Ohio, 1985.

U. S. Department of Defense. *Metallic Materials and Elements for Aerospace Vehicles and Structures* MIL-HDBK-5H, 1998.

R. Juran, ed. *Modern Plastics Encyclopedia*. McGraw-Hill: New York, 1988.

J. D. Lubahn and R. P. Felgar, *Plasticity and Creep of Metals*. Wiley: New York, 1961.

For information on failure of materials, consult the following:

J. A. Collins, *Failure of Materials in Mechanical Design*. Wiley: New York, 1981.

N. E. Dowling, *Mechanical Behavior of Materials*. Prentice-Hall: Englewood Cliffs, N.J., 1992.

R. C. Juvinall, *Stress, Strain and Strength*. McGraw-Hill: New York, 1967.

For information on plastics and composites, consult the following:

ASM, *Engineered Materials Handbook: Composites*. Vol. 1. American Society for Metals: Metals Park, Ohio, 1987.

ASM, *Engineered Materials Handbook: Engineering Plastics*. Vol. 2. American Society for Metals: Metals Park, Ohio, 1988.

Harper, ed. *Handbook of Plastics, Elastomers and Composites*. 2nd ed. McGraw-Hill: New York, 1990.

J. E. Hauck, "Long-Term Performance of Plastics." *Materials in Design Engineering*, pp. 113-128, November, 1965.

M. M. Schwartz, *Composite Materials Handbook*. McGraw-Hill: New York, 1984.

For information on manufacturing processes, see:

R. W. Bolz, *Production Processes: The Productivity Handbook*. Industrial Press: New York, 1974.

J. A. Schey, *Introduction to Manufacturing Processes*. McGraw-Hill: New York, 1977.

2.13 PROBLEMS

- 2-1 Figure P2-1 shows stress-strain curves for three failed tensile-test specimens. All are plotted on the same scale.
 - (a) Characterize each material as brittle or ductile.
 - (b) Which is the stiffest?
 - (c) Which has the highest ultimate strength?
 - (d) Which has the largest modulus of resilience?
 - (e) Which has the largest modulus of toughness?
- 2-2 Determine an approximate ratio between the yield strength and ultimate strength for each material shown in Figure P2-1.
- 2-3 Which of the steel alloys shown in Figure 2-19 would you choose to obtain
 - (a) Maximum strength
 - (b) Maximum modulus of resilience
 - (c) Maximum modulus of toughness
 - (d) Maximum stiffness

Table P2-0

Topic/Problem Matrix

2.1 Material Properties

2-1, 2-2, 2-3, 2-4, 2-5, 2-6, 2-7,
2-8, 2-9, 2-10, 2-11, 2-12, 2-18,
2-19, 2-20, 2-21, 2-22, 2-23

2.4 Hardness

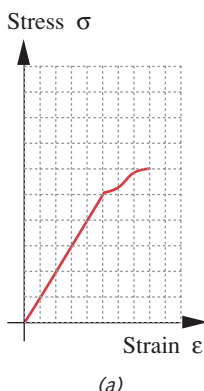
2-13, 2-14

2.6 General Properties

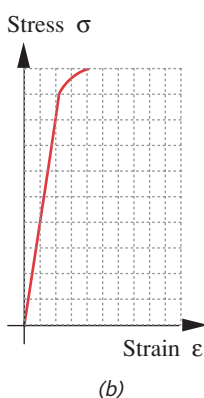
2-15, 2-16, 2-17, 2-24, 2-25,
2-26

2.8 Selecting Materials

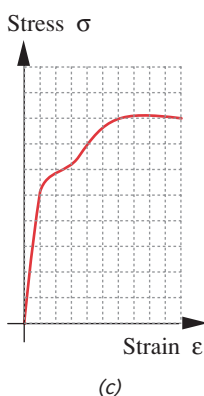
2-37, 2-38, 2-39, 2-40



(a)



(b)



(c)

FIGURE P2-1

Stress-Strain Curves

- 2-4 Which of the aluminum alloys shown in Figure 2-21 would you choose to obtain
- Maximum strength
 - Maximum modulus of resilience
 - Maximum modulus of toughness
 - Maximum stiffness
- 2-5 Which of the thermoplastic polymers shown in Figure 2-22 would you choose in order to obtain
- Maximum strength
 - Maximum modulus of resilience
 - Maximum modulus of toughness
 - Maximum stiffness
- *2-6 A metal has a strength of 414 MPa at its elastic limit and the strain at that point is 0.002. Assume the test specimen is 12.8-mm dia and has a 50-mm gage length. What is its modulus of elasticity? What is the strain energy at the elastic limit? Can you define the type of metal based on the given data?
- 2-7 A metal has a strength of 41.2 kpsi (284 MPa) at its elastic limit and the strain at that point is 0.004. Assume the test specimen is 0.505-in dia and has a 2-in gage length. What is the strain energy at the elastic limit? Can you define the type of metal based on the given data?
- *2-8 A metal has a strength of 134 MPa at its elastic limit and the strain at that point is 0.003. What is its modulus of elasticity? Assume the test specimen is 12.8-mm dia and has a 50-mm gage length. What is its modulus of elasticity? What is the strain energy at the elastic limit? Can you define the type of metal based on the given data?
- *2-9 A metal has a strength of 100 kpsi (689 MPa) at its elastic limit and the strain at that point is 0.006. What is its modulus of elasticity? What is the strain energy at the elastic limit? Assume the test specimen is 0.505-in dia and has a 2-in gage length. Can you define the type of metal based on the given data?
- 2-10 A material has a yield strength of 689 MPa at an offset of 0.6% strain. What is its modulus of resilience?
- 2-11 A material has a yield strength of 60 kpsi (414 MPa) at an offset of 0.2% strain. What is its modulus of resilience?
- *2-12 A steel has a yield strength of 414 MPa, an ultimate tensile strength of 689 MPa, and an elongation at fracture of 15%. What is its approximate modulus of toughness? What is its approximate modulus of resilience?
- 2-13 The Brinell hardness of a steel specimen was measured to be 250 HB. What is the material's approximate tensile strength? What is its hardness on the Vickers scale? The Rockwell scale?
- *2-14 The Brinell hardness of a steel specimen was measured to be 340 HB. What is the material's approximate tensile strength? What is its hardness on the Vickers scale? The Rockwell scale?
- 2-15 What are the principal alloy elements of an AISI 4340 steel? How much carbon does it have? Is it hardenable? By what techniques?
- *2-16 What are the principal alloy elements of an AISI 1095 steel? How much carbon does it have? Is it hardenable? By what techniques?
- 2-17 What are the principal alloy elements of an AISI 6180 steel? How much carbon does it have? Is it hardenable? By what techniques?
- 2-18 Which of the steels in Problems 2-15, 2-16, and 2-17 is the stiffest?

* Answers to these problems are provided in Appendix D.

- 2-19 Calculate the *specific strength* and *specific stiffness* of the following materials and pick one for use in an aircraft wing spar.
- (a) Steel $S_{ut} = 80 \text{ kpsi (552 MPa)}$
(b) Aluminum $S_{ut} = 60 \text{ kpsi (414 MPa)}$
(c) Titanium $S_{ut} = 90 \text{ kpsi (621 MPa)}$
- 2-20 If maximum *impact resistance* were desired in a part, which material properties would you look for?
- 2-21 Refer to the tables of material data in Appendix A and determine the strength-to-weight ratios of the following material alloys based on their tensile yield strengths: heat-treated 2024 aluminum, SAE 1040 cold-rolled steel, Ti-75A titanium, type 302 cold-rolled stainless steel.
- 2-22 Refer to the tables of material data in Appendix A and determine the strength-to-weight ratios of the following material alloys based on their ultimate tensile strengths: heat-treated 2024 aluminum, SAE 1040 cold-rolled steel, unfilled acetal plastic, Ti-75A titanium, type 302 cold-rolled stainless steel.
- 2-23 Refer to the tables of material data in Appendix A and calculate the specific stiffnesses of aluminum, titanium, gray cast iron, ductile iron, bronze, carbon steel, and stainless steel. Rank them in increasing order of this property and discuss the engineering significance of these data.
- 2-24 Call your local steel and aluminum distributors (consult the Yellow Pages) and obtain current costs per pound for round stock of consistent size in low-carbon (SAE 1020) steel, SAE 4340 steel, 2024-T4 aluminum, and 6061-T6 aluminum. Calculate a strength/dollar ratio and a stiffness/dollar ratio for each alloy. Which would be your first choice on a cost-efficiency basis for an axial-tension-loaded round rod
- (a) If maximum strength were needed?
(b) If maximum stiffness were needed?
- 2-25 Call your local plastic stock-shapes distributors (consult the Yellow Pages) and obtain current costs per pound for round rod or tubing of consistent size in plexiglass, acetal, nylon 6/6, and PVC. Calculate a strength/dollar ratio and a stiffness/dollar ratio for each alloy. Which would be your first choice on a cost-efficiency basis for an axial-tension-loaded round rod or tube of particular diameters. (Note: material parameters can be found in Appendix A.)
- (a) If maximum strength were needed?
(b) If maximum stiffness were needed?
- 2-26 A part has been designed and its dimensions cannot be changed. To minimize its deflections under the same loading in all directions irrespective of stress levels, which of these materials would you choose: aluminum, titanium, steel, or stainless steel? Why?
- *2-27 Assuming that the mechanical properties data given in Appendix Table A-9 for some carbon steels represents mean values, what is the value of the tensile yield strength for 1050 steel quenched and tempered at 400F if a reliability of 99.9% is required?
- 2-28 Assuming that the mechanical properties data given in Appendix Table A-9 for some carbon steels represents mean values, what is the value of the ultimate tensile strength for 4340 steel quenched and tempered at 800F if a reliability of 99.99% is required?
- 2-29 Assuming that the mechanical properties data given in Appendix Table A-9 for some carbon steels represents mean values, what is the value of the ultimate tensile strength for 4130 steel quenched and tempered at 400F if a reliability of 90% is required?
- 2-30 Assuming that the mechanical properties data given in Appendix Table A-9 for some carbon steels represents mean values, what is the value of the tensile yield strength for 4140 steel quenched and tempered at 800F if a reliability of 99.999% is required?

* Answers to these problems are provided in Appendix D.

- 2-31 A steel part is to be plated to give it better corrosion resistance. Two materials are being considered: cadmium and nickel. Considering only the problem of galvanic action, which would you choose? Why?
- 2-32 A steel part with many holes and sharp corners is to be plated with nickel. Two processes are being considered: electroplating and electroless plating. Which process would you choose? Why?
- 2-33 What is the common treatment used on aluminum to prevent oxidation? What other metals can also be treated with this method? What options are available with this method?
- *2-34 Steel is often plated with a less noble metal that acts as a sacrificial anode that will corrode instead of the steel. What metal is commonly used for this purpose (when the finished product will not be exposed to saltwater), what is the coating process called, and what are the common processes used to obtain the finished product?
- 2-35 A low-carbon steel part is to be heat-treated to increase its strength. If an ultimate tensile strength of approximately 550 MPa is required, what mean Brinell hardness should the part have after treatment? What is the equivalent hardness on the Rockwell scale?
- 2-36 A low-carbon steel part has been tested for hardness using the Brinell method and is found to have a hardness of 220 HB. What are the approximate lower and upper limits of the ultimate tensile strength of this part in MPa?
- 2-37 Figure 2-24 shows “guide lines” for minimum weight design when failure is the criterion. The guide line, or index, for minimizing the weight of a beam in bending is $\sigma_f^{2/3} / \rho$, where σ_f is the yield strength of a material and ρ is its mass density. For a given cross-section shape the weight of a beam with given loading will be minimized when this index is maximized. The following materials are being considered for a beam application: 5052 aluminum, cold rolled; CA-170 beryllium copper, hard plus aged; and 4130 steel, Q&T @ 1200F. The use of which of these three materials will result in the least-weight beam?
- 2-38 Figure 2-24 shows “guide lines” for minimum weight design when failure is the criterion. The guide line, or index, for minimizing the weight of a member in tension is σ_f / ρ , where σ_f is the yield strength of a material and ρ is its mass density. The weight of a member with given loading will be minimized when this index is maximized. For the three materials given in Problem 2-37, which will result in the lowest weight tension member?
- 2-39 Figure 2-23 shows “guide lines” for minimum weight design when stiffness is the criterion. The guide line, or index, for minimizing the weight of a beam in bending is $E^{1/2} / \rho$, where E is the modulus of elasticity of a material and ρ is its mass density. For a given cross-section shape the weight of a beam with given stiffness will be minimized when this index is maximized. The following materials are being considered for a beam application: 5052 aluminum, cold rolled; CA-170 beryllium copper, hard plus aged; and 4130 steel, Q&T @ 1200F. The use of which of these three materials will result in the lowest-weight beam?
- 2-40 Figure 2-24 shows “guide lines” for minimum weight design when stiffness is the criterion. The guide line, or index, for minimizing the weight of a member in tension is E / ρ , where E is the modulus of elasticity of a material and ρ is its mass density. The weight of a member with given stiffness will be minimized when this index is maximized. For the three materials given in Problem 2-39, which will result in the lowest-weight tension member?

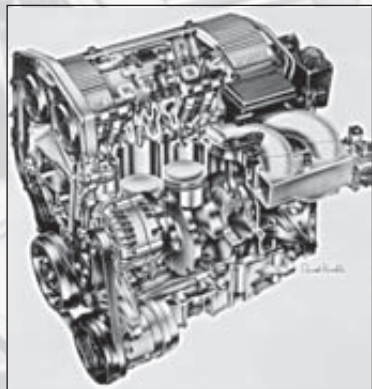
* Answers to these problems are provided in Appendix D.

3

LOAD DETERMINATION

If a builder has built a house for a man and his work is not strong and the house falls in and kills the householder, that builder shall be slain.

FROM THE CODE OF HAMMURABI, 2150 BC



3.0 INTRODUCTION

This chapter provides a review of the fundamentals of static and dynamic force analysis, impact forces, and beam loading. The reader is assumed to have had first courses in statics and dynamics. Thus, this chapter presents only a brief, general overview of those topics but also provides more powerful solution techniques, such as the use of singularity functions for beam calculations. The Newtonian solution method of force analysis is reviewed and a number of case-study examples are presented to reinforce understanding of this subject. The case studies also set the stage for analysis of these same systems for stress, deflection, and failure modes in later chapters.

Table 3-0 shows the variables used in this chapter and references the equations, sections, or case studies in which they are used. At the end of the chapter, a summary section is provided which groups all the significant equations from this chapter for easy reference and identifies the chapter section in which their discussion can be found.

3.1 LOADING CLASSES

The type of loading on a system can be divided into several classes based on the character of the applied loads and the presence or absence of system motion. Once the general configuration of a mechanical system is defined and its kinematic motions calculated, the next task is to determine the magnitudes and directions of all the forces and couples present on the various elements. These loads may be constant or may be varying over time. The elements in the system may be stationary or moving. The most general class is that of a moving system with time-varying loads. The other combinations are subsets of the general class.

Table 3-0 Variables Used in This Chapter

Symbol	Variable	ips units	SI units	See
<i>a</i>	distance to load	in	m	Sect. 3.9
<i>b</i>	distance to load	in	m	Sect. 3.9
<i>d</i>	damping	lb-sec/in	N-sec/m	Eq. 3.6
<i>E</i>	energy	in-lb	joules	Eq. 3.9, 3.10
<i>F</i>	force or load	lb	N	Sect. 3.3
<i>f_d</i>	damped natural frequency	Hz	Hz	Eq. 3.7
<i>f_n</i>	natural frequency	Hz	Hz	Eq. 3.4
<i>g</i>	gravitational acceleration	in/sec ²	m/sec ²	Eq. 3.12
<i>I_x</i>	mass moment of inertia about x axis	lb-in-sec ²	kg-m ²	Sect. 3.3
<i>I_y</i>	mass moment of inertia about y axis	lb-in-sec ²	kg-m ²	Sect. 3.3
<i>I_z</i>	mass moment of inertia about z axis	lb-in-sec ²	kg-m ²	Sect. 3.3
<i>k</i>	spring rate or spring constant	lb/in	N/m	Eq. 3.5
<i>l</i>	length	in	m	Sect. 3.9
<i>m</i>	mass	lb-sec ² /in	kg	Sect. 3.3
<i>N</i>	normal force	in	m	Case 4A
<i>M</i>	moment, moment function	lb-in	N-m	Sect. 3.3, 3.9
<i>q</i>	beam loading function	lb	N	Sect. 3.9
R	position vector	in	m	Sect. 3.4
<i>R</i>	reaction force	lb	N	Sect. 3.9
<i>v</i>	linear velocity	in/sec	m/sec	Eq. 3.10
<i>V</i>	beam shear function	lb	N	Sect. 3.9
<i>W</i>	weight	lb	N	Eq. 3.14
<i>x</i>	generalized length variable	in	m	Sect. 3.9
<i>y</i>	displacement	in	m	Eq. 3.5, 3.8
δ	deflection	in	m	Eq. 3.5
η	correction factor	none	none	Eq. 3.10
μ	coefficient of friction	none	none	Case 4A
ω	rotational or angular velocity	rad/sec	rad/sec	Case 5A
ω_d	damped natural frequency	rad/sec	rad/sec	Eq. 3.7
ω_n	natural frequency	rad/sec	rad/sec	Eq. 3.4

Table 3-1 shows the four possible classes. Class 1 is a stationary system with constant loads. One example of a Class 1 system is the base frame for an arbor press used in a machine shop. The base is required to support the dead weight of the arbor press which is essentially constant over time, and the base frame does not move. The parts brought to the arbor press (to have something pressed into them) temporarily add their weight to the load on the base, but this is usually a small percentage of the dead weight. A static load analysis is all that is necessary for a Class 1 system.

Table 3-1 Load Classes

	Constant Loads	Time-Varying Loads
Stationary Elements	Class 1	Class 2
Moving Elements	Class 3	Class 4

3

Class 2 describes a stationary system with time-varying loads. An example is a bridge which, though essentially stationary, is subjected to changing loads as vehicles drive over it and wind impinges on its structure. Class 3 defines a moving system with constant loads. Even though the applied external loads may be constant, any significant accelerations of the moving members can create time-varying reaction forces. An example might be a powered rotary lawn mower. Except for the case of mowing the occasional rock, the blades experience a nearly constant external load from mowing the grass. However, the accelerations of the spinning blades can create high loads at their fastenings. A dynamic load analysis is necessary for Classes 2 and 3.

Note however that, if the motions of a Class 3 system are so slow as to generate negligible accelerations on its members, it could qualify as a Class 1 system and then would be called *quasi-static*. An automobile scissors jack (see Figure 3-5, p. 88) can be considered to be a Class 1 system since the external load (when used) is essentially constant, and the motions of the links are slow with negligible accelerations. The only complexity introduced by the motions of the elements in this example is that of determining in which position the internal loads on the jack's elements will be maximal, since they vary as the jack is raised, despite the essentially constant external load.

Class 4 describes the general case of a rapidly moving system subjected to time-varying loads. Note that even if the applied external loads are essentially constant in a given case, the dynamic loads developed on the elements from their accelerations will still vary with time. Most machinery, especially if powered by a motor or engine, will be in Class 4. An example of such a system is the engine in your car. The internal parts (crankshaft, connecting rods, pistons, etc.) are subjected to time-varying loads from the gasoline explosions, and also experience time-varying inertial loads from their own accelerations. A dynamic load analysis is necessary for Class 4.

3.2 FREE-BODY DIAGRAMS

In order to correctly identify all potential forces and moments on a system, it is necessary to draw accurate free-body diagrams (FBDs) of each member of the system. These FBDs should show a general shape of the part and display all the forces and moments that are acting on it. There may be external forces and moments applied to the part from outside the system, and there will be interconnection forces and/or moments where each part joins or contacts adjacent parts in the assembly or system.

In addition to the known and unknown forces and couples shown on the FBD, the dimensions and angles of the elements in the system are defined with respect to local coordinate systems located at the **centers of gravity** (CG) of each element.* For a dynamic load analysis, the kinematic accelerations, both angular and linear (at the CG), need to be known or calculated for each element prior to doing the load analysis.

* While it is not a requirement that the local coordinate system for each element be located at its CG, this approach provides consistency and simplifies the dynamic calculations. Further, most solid modeling CAD/CAE systems will automatically calculate the mass properties of parts with respect to their CGs. The approach taken here is to apply a consistent method that works for both static and dynamic problems and that is also amenable to computer solution.

3.3 LOAD ANALYSIS

This section presents a brief review of Newton's laws and Euler's equations as applied to dynamically loaded and statically loaded systems in both 3-D and 2-D. The method of solution presented here may be somewhat different than that used in your previous statics and dynamics courses. The approach taken here in setting up the equations for force and moment analysis is designed to facilitate computer programming of the solution.

This approach assumes all *unknown* forces and moments on the system to be positive in sign, regardless of what one's intuition or an inspection of the free-body diagram might indicate as to their probable directions. However, all *known* force components are given their proper signs to define their directions. The simultaneous solution of the set of equations that results will cause all the unknown components to have the proper signs when the solution is complete. This is ultimately a simpler approach than the one often taught in statics and dynamics courses which requires that the student assume directions for all unknown forces and moments (a practice that does help the student develop some intuition, however). Even with that traditional approach, an incorrect assumption of direction results in a sign reversal on that component in the solution. Assuming all unknown forces and moments to be positive allows the resulting computer program to be simpler than would otherwise be the case. The simultaneous equation solution method used is extremely simple in concept, though it requires the aid of a computer to solve. Software is provided with the text to solve the simultaneous equations. See program MATRIX on the CD-ROM.

Real dynamic systems are three dimensional and thus must be analyzed as such. However, many 3-D systems can be analyzed by simpler 2-D methods. Accordingly, we will investigate both approaches.

Three-Dimensional Analysis

Since three of the four cases potentially require dynamic load analysis, and because a static force analysis is really just a variation on the dynamic analysis, it makes sense to start with the dynamic case. Dynamic load analysis can be done by any of several methods, but the one that gives the most information about internal forces is the Newtonian approach based on Newton's laws.

NEWTON'S FIRST LAW *A body at rest tends to remain at rest and a body in motion at constant velocity will tend to maintain that velocity unless acted upon by an external force.*

NEWTON'S SECOND LAW *The time rate of change of momentum of a body is equal to the magnitude of the applied force and acts in the direction of the force.*

Newton's second law can be written for a rigid body in two forms, one for linear forces and one for moments or torques:

$$\sum \mathbf{F} = m\mathbf{a} \quad \sum \mathbf{M}_G = \dot{\mathbf{H}}_G \quad (3.1a)$$

where \mathbf{F} = force, m = mass, \mathbf{a} = acceleration, \mathbf{M}_G = moment about the center of gravity, and $\dot{\mathbf{H}}_G$ = the time rate of change of the moment of momentum, or the angular mo-

mentum about the CG. The left sides of these equations respectively sum all the forces and moments that act on the body, whether from known applied forces or from interconnections with adjacent bodies in the system.

For a three-dimensional system of connected rigid bodies, this vector equation for the linear forces can be written as three scalar equations involving orthogonal components taken along a local x, y, z axis system with its origin at the CG of the body:

$$\sum F_x = ma_x \quad \sum F_y = ma_y \quad \sum F_z = ma_z \quad (3.1b)$$

If the x, y, z axes are chosen coincident with the principal axes of inertia of the body,* the angular momentum of the body is defined as

$$\mathbf{H}_G = I_x \omega_x \hat{\mathbf{i}} + I_y \omega_y \hat{\mathbf{j}} + I_z \omega_z \hat{\mathbf{k}} \quad (3.1c)$$

where I_x, I_y , and I_z are the principal centroidal mass moments of inertia (second moments of mass) about the principal axes. This vector equation can be substituted into equation 3.1a to yield the three scalar equations known as **Euler's equations**:

$$\begin{aligned} \sum M_x &= I_x \alpha_x - (I_y - I_z) \omega_y \omega_z \\ \sum M_y &= I_y \alpha_y - (I_z - I_x) \omega_z \omega_x \\ \sum M_z &= I_z \alpha_z - (I_x - I_y) \omega_x \omega_y \end{aligned} \quad (3.1d)$$

where M_x, M_y, M_z are moments about those axes and $\alpha_x, \alpha_y, \alpha_z$ are the angular accelerations about the axes. This assumes that the inertia terms remain constant with time, i.e., the mass distribution about the axes is constant.

NEWTON'S THIRD LAW states that *when two particles interact, a pair of equal and opposite reaction forces will exist at their contact point. This force pair will have the same magnitude and act along the same direction line, but have opposite sense.*

We will need to apply this relationship as well as applying the second law in order to solve for the forces on assemblies of elements that act upon one another. The six equations in equations 3.1b and 3.1d can be written for each rigid body in a 3-D system. In addition, as many (third-law) reaction force equations as are necessary will be written and the resulting set of equations solved simultaneously for the forces and moments. The number of second-law equations will be up to six times the number of individual parts in a three-dimensional system (plus the reaction equations), meaning that even simple systems result in large sets of simultaneous equations. A computer is needed to solve these equations, though high-end pocket calculators will solve large sets of simultaneous equations also. The reaction (third-law) equations are often substituted into the second-law equations to reduce the total number of equations to be solved simultaneously.

Two-Dimensional Analysis

All real machines exist in three dimensions but many three-dimensional systems can be analyzed two dimensionally if their motions exist only in one plane or in parallel planes.

* This is a convenient choice for symmetric bodies but may be less convenient for other shapes. See F. P. Beer and E. R. Johnson, *Vector Mechanics for Engineers*, 3rd ed., 1977, McGraw-Hill, New York, Chap. 18, "Kinetics of Rigid Bodies in Three Dimensions."

Euler's equations 3.1d show that if the rotational motions (ω, α) and applied moments or couples exist about only one axis (say the z axis), then that set of three equations reduces to one equation,

$$\sum M_z = I_z \alpha_z \quad (3.2a)$$

because the ω and α terms about the x and y axes are now zero. Equation 3.1b is reduced to

$$\sum F_x = ma_x \quad \sum F_y = ma_y \quad (3.2b)$$

Equations 3.2 can be written for all the connected bodies in a two-dimensional system and the entire set solved simultaneously for forces and moments. The number of second-law equations will now be up to three times the number of elements in the system plus the necessary reaction equations at connecting points, again resulting in large systems of equations for even simple systems. Note that even though all motion is about one (z) axis in a 2-D system, there may still be loading components in the z direction due to external forces or couples.

Static Load Analysis

The difference between a dynamic loading situation and a static one is the presence or absence of accelerations. If the accelerations in equations 3.1 and 3.2 are all zero, then for the three-dimensional case these equations reduce to

$$\begin{array}{lll} \sum F_x = 0 & \sum F_y = 0 & \sum F_z = 0 \\ \sum M_x = 0 & \sum M_y = 0 & \sum M_z = 0 \end{array} \quad (3.3a)$$

and for the two-dimensional case,

$$\sum F_x = 0 \quad \sum F_y = 0 \quad \sum M_z = 0 \quad (3.3b)$$

Thus, we can see that the static loading situation is just a special case of the dynamic loading one, in which the accelerations happen to be zero. A solution approach based on the dynamic case will then also satisfy the static one with appropriate substitutions of zero values for the absent accelerations.

3.4 TWO-DIMENSIONAL, STATIC LOADING CASE STUDIES

This section presents a series of three case studies of increasing complexity, all limited to two-dimensional static loading situations. A bicycle handbrake lever, a crimping tool, and a scissors jack are the systems analyzed. These case studies provide examples of the simplest form of force analysis, having no significant accelerations and having forces acting in only two dimensions.

CASE STUDY 1A**Bicycle Brake Lever Loading Analysis**

Problem: Determine the forces on the elements of the bicycle brake lever assembly shown in Figure 3-1 during braking.

3

Given: The geometry of each element is known. The average human's hand can develop a grip force of about 267 N (60 lb) in the lever position shown.

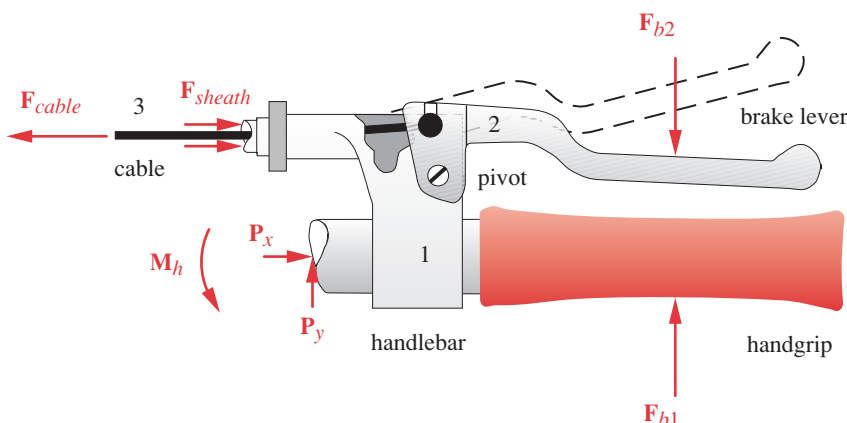
Assumptions: The accelerations are negligible. All forces are coplanar and two dimensional. A Class 1 load model is appropriate and a static analysis is acceptable.

Solution: See Figures 3-1, 3-2, and Table 3-2, parts 1 and 2.

- Figure 3-1 shows the handbrake lever assembly, which consists of three subassemblies: the handlebar (1), the lever (2), and the cable (3). The lever is pivoted to the handlebar and the cable is connected to the lever. The cable runs within a plastic-lined sheath (for low friction) down to the brake caliper assembly at the bicycle's wheel rim. The sheath provides a compressive force to balance the tension in the cable ($F_{sheath} = -F_{cable}$). The user's hand applies equal and opposite forces at some points on the lever and handgrip. These forces are transformed to a larger force in the cable by the lever ratio of part 2.

Figure 3-1 is a free-body diagram of the entire assembly since it shows all the forces and moments potentially acting on it except for its weight, which is small compared to the applied forces and is thus neglected for this analysis. The "broken away" portion of the handlebar can provide x and y force components and a moment if required for equilibrium. These reaction forces and moments are arbitrarily shown as positive in sign. Their actual signs will "come out in the wash" in the calculations. The known applied forces are shown acting in their actual directions and senses.

- Figure 3-2 shows the three subassembly elements separated and drawn as free-body diagrams with all relevant forces and moments applied to each element, again neglect-

**FIGURE 3-1**

Bicycle Brake Lever Assembly

Table 3-2 - part 1

Case Study 1A
Given Data

Variable	Value	Unit
F_{13x}	0.0	N
F_{b2x}	0.0	N
F_{b2y}	-267.0	N
θ	184.0	deg
ϕ	180.0	deg
R_{b2x}	39.39	mm
R_{b2y}	2.07	mm
R_{32x}	-50.91	mm
R_{32y}	4.66	mm
R_{12x}	-47.91	mm
R_{12y}	-7.34	mm
R_{21x}	7.0	mm
R_{21y}	19.0	mm
R_{b1x}	47.5	mm
R_{b1y}	-14.0	mm
R_{31x}	-27.0	mm
R_{31y}	30.0	mm
R_{px}	-27.0	mm
R_{py}	0.0	mm
R_{dx}	-41.0	mm
R_{dy}	27.0	mm

* Actually, for a simple static analysis such as the one in this example, any point (on or off the element) can be taken as the origin of the local coordinate system. However, in a dynamic force analysis it simplifies the analysis if the coordinate system is placed at the CG. So, for the sake of consistency, and to prepare for the more complicated dynamic analysis problems ahead, we will use the CG as the origin even in the static cases here.

† You may not have done this in your statics class but this approach makes the problem more amenable to a computer solution. Note that regardless of the direction shown for any unknown force on the FBD, we will assume its components to be positive in the equations. The angles of the known (given) forces (or the signs of their components) do have to be correctly input to the equations, however.

ing the weights of the parts. The lever (part 2) has three forces on it, \mathbf{F}_{b2} , \mathbf{F}_{32} , and \mathbf{F}_{12} . The two-character subscript notation used here should be read as, force of element 1 on 2 (\mathbf{F}_{12}) or force at B on 2 (\mathbf{F}_{b2}), etc. This defines the source of the force (first subscript) and the element on which it acts (second subscript).

This notation will be used consistently throughout this text for both forces and position vectors such as \mathbf{R}_{b2} , \mathbf{R}_{32} , and \mathbf{R}_{12} in Figure 3-2 which serve to locate the above three forces in a local, nonrotating coordinate system whose origin is at the center of gravity (CG) of the element or subassembly being analyzed.*

On this brake lever, \mathbf{F}_{b2} is an applied force whose magnitude and direction are known. \mathbf{F}_{32} is the force in the cable. Its direction is known but not its magnitude. Force \mathbf{F}_{12} is provided by part 1 on part 2 at the pivot pin. Its magnitude and direction are both unknown. We can write equations 3.3b for this element to sum forces in the x and y directions and sum moments about the CG. Note that all unknown forces and moments are initially assumed positive in the equations. Their true signs will come out in the calculation.† However, all known or given forces must carry their proper signs.

$$\begin{aligned}\sum F_x &= F_{12x} + F_{b2x} + F_{32x} = 0 \\ \sum F_y &= F_{12y} + F_{b2y} + F_{32y} = 0 \\ \sum M_z &= (\mathbf{R}_{12} \times \mathbf{F}_{12}) + (\mathbf{R}_{b2} \times \mathbf{F}_{b2}) + (\mathbf{R}_{32} \times \mathbf{F}_{32}) = 0\end{aligned}\quad (a)$$

The cross products in the moment equation represent the “turning forces” or moments created by the application of these forces at points remote from the CG of the element. Recall that these cross products can be expanded to

$$\begin{aligned}\sum M_z &= (R_{12x}F_{12y} - R_{12y}F_{12x}) + (R_{b2x}F_{b2y} - R_{b2y}F_{b2x}) \\ &\quad + (R_{32x}F_{32y} - R_{32y}F_{32x}) = 0\end{aligned}\quad (b)$$

We have three equations and four unknowns (F_{12x} , F_{12y} , F_{32x} , F_{32y}) at this point, so we need another equation. It is available from the fact that the direction of \mathbf{F}_{32} is known. (The cable can pull only along its axis.) We can express one component of the cable force \mathbf{F}_{32} in terms of its other component and the known angle, θ of the cable.

$$F_{32y} = F_{32x} \tan \theta \quad (c)$$

We could now solve the four unknowns for this element, but will wait to do so until the equations for the other two links are defined.

- 3 Part 3 in Figure 3-2 is the cable which passes through a hole in part 1. This hole is lined with a low-friction material which allows us to assume no friction at the joint between parts 1 and 3. We will further assume that the three forces \mathbf{F}_{13} , \mathbf{F}_{23} , and \mathbf{F}_{cable} form a concurrent system of forces acting through the CG and thus create no moment. With this assumption only a summation of forces is necessary for this element.

$$\begin{aligned}\sum F_x &= F_{cable_x} + F_{13x} + F_{23x} = 0 \\ \sum F_y &= F_{cable_y} + F_{13y} + F_{23y} = 0\end{aligned}\quad (d)$$

- 4 The assembly of elements labeled part 1 in Figure 3-2 can have both forces and moments on it (i.e., it is not a concurrent system), so the three equations 3.3b are needed.

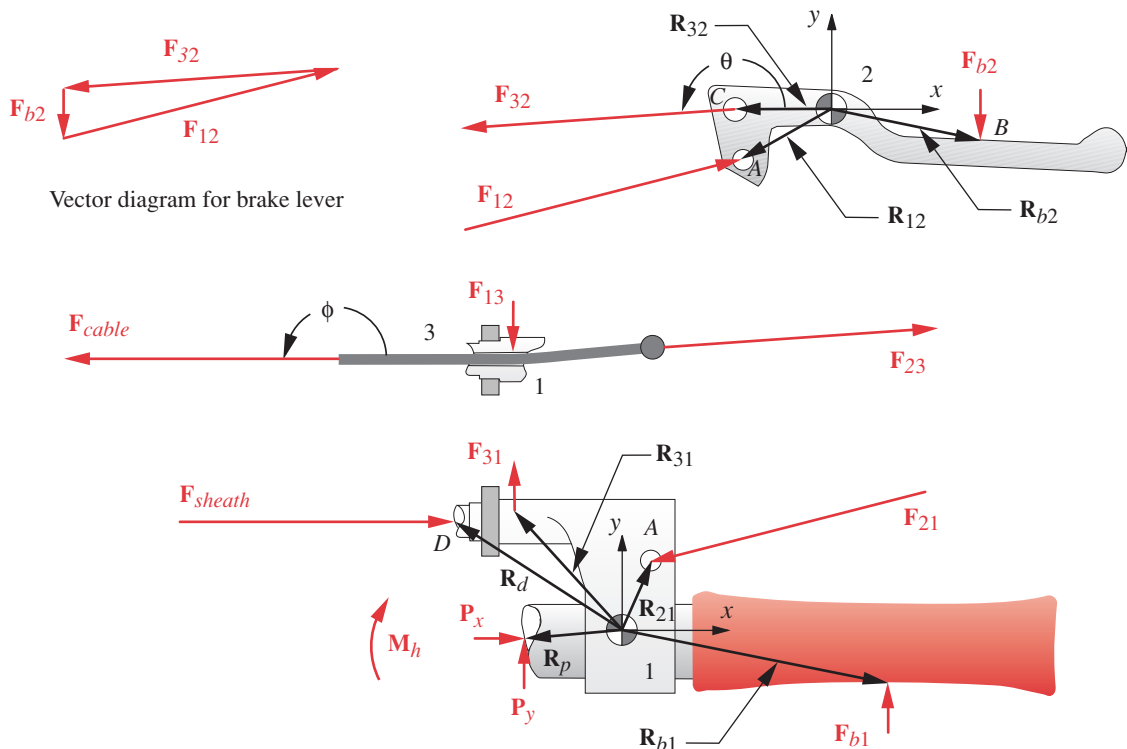


FIGURE 3-2

Bicycle Brake Lever Free-Body Diagrams

$$\sum F_x = F_{21x} + F_{b1x} + F_{31x} + P_x + F_{sheath_x} = 0$$

$$\sum F_y = F_{21y} + F_{b1y} + F_{31y} + P_y = 0 \quad (e)$$

$$\sum \mathbf{M}_z = M_h + (\mathbf{R}_{21} \times \mathbf{F}_{21}) + (\mathbf{R}_{b1} \times \mathbf{F}_{b1}) + (\mathbf{R}_{31} \times \mathbf{F}_{31}) + (\mathbf{R}_p \times \mathbf{P}) + (\mathbf{R}_d \times \mathbf{F}_{sheath}) = 0$$

Expanding cross products in the moment equation gives the moment magnitude as

$$\begin{aligned} \sum M_z = M_h + & (R_{21x}F_{21y} - R_{21y}F_{21x}) + (R_{b1x}F_{b1y} - R_{b1y}F_{b1x}) + (R_{31x}F_{31y} - R_{31y}F_{31x}) \\ & + (R_{Px}P_y - R_{Py}P_x) + (R_{dx}F_{sheath_y} - R_{dy}F_{sheath_x}) = 0 \end{aligned} \quad (f)$$

- 5 The total of unknowns at this point (including those listed in step 2 above) is 21: F_{b1x} , F_{b1y} , F_{12x} , F_{12y} , F_{21x} , F_{21y} , F_{23x} , F_{23y} , F_{13x} , F_{13y} , F_{31x} , F_{31y} , F_{cable_x} , F_{cable_y} , F_{sheath_x} , F_{sheath_y} , P_x , P_y , and M_h . We have only nine equations so far, three in equation set (a), one in set (c), two in set (d) and three in set (e). We need twelve more equations to solve this system. We can get seven of them from the Newton's third-law relationships between contacting elements:

$$\begin{aligned} F_{23x} &= -F_{32x} & F_{23y} &= -F_{32y} \\ F_{21x} &= -F_{12x} & F_{21y} &= -F_{12y} & (g) \\ F_{31x} &= -F_{13x} & F_{31y} &= -F_{13y} \\ F_{sheath_x} &= -F_{cable_x} \end{aligned}$$

Table 3-2 - part 1 repeated

Case Study 1A
Given Data

Variable	Value	Unit
F_{13x}	0.0	N
F_{b2x}	0.0	N
F_{b2y}	-267.0	N
θ	184.0	deg
ϕ	180.0	deg
R_{b2x}	39.39	mm
R_{b2y}	2.07	mm
R_{32x}	-50.91	mm
R_{32y}	4.66	mm
R_{12x}	-47.91	mm
R_{12y}	-7.34	mm
R_{21x}	7.0	mm
R_{21y}	19.0	mm
R_{b1x}	47.5	mm
R_{b1y}	-14.0	mm
R_{31x}	-27.0	mm
R_{31y}	30.0	mm
R_{px}	-27.0	mm
R_{py}	0.0	mm
R_{dx}	-41.0	mm
R_{dy}	27.0	mm

Two more equations come from the assumption (shown in Figure 3-1) that the two forces provided by the hand on the brake lever and handgrip are equal and opposite.*

$$\begin{aligned} F_{b1x} &= -F_{b2x} \\ F_{b1y} &= -F_{b2y} \end{aligned} \quad (h)$$

The remaining three equations come from the given geometry and the assumptions made about the system. The direction of the forces F_{cable} and F_{sheath} are known to be in the same direction as that end of the cable. In the figure it is seen to be horizontal, so we can set

$$F_{cable_y} = 0; \quad F_{sheath_y} = 0 \quad (i)$$

Because of our no-friction assumption, the force F_{31} can be assumed to be normal to the surface of contact between the cable and the hole in part 1. This surface is horizontal in this example, so F_{31} is vertical and

$$F_{31x} = 0 \quad (j)$$

- 6 This completes the set of 21 equations (equation sets *a*, *c*, *d*, *e*, *g*, *h*, *i*, and *j*), and they can be solved for the 21 unknowns simultaneously “as is,” that is, all 21 equations could be put into matrix form and solved with a matrix-reduction computer program. However, the problem can be simplified by manually substituting equations *c*, *g*, *h*, *i*, and *j* into the others to reduce them to a set of eight equations in eight unknowns. The known or given data are as shown in Table 3-2, part 1.
- 7 As a first step, for link 2, substitute equations *b* and *c* in equation *a* to get:

$$\begin{aligned} F_{12x} + F_{b2x} + F_{32x} &= 0 \\ F_{12y} + F_{b2y} + F_{32x} \tan \theta &= 0 \end{aligned} \quad (k)$$

- $$(R_{12x}F_{12y} - R_{12y}F_{12x}) + (R_{b2x}F_{b2y} - R_{b2y}F_{b2x}) + (R_{32x}F_{32x} \tan \theta - R_{32y}F_{32x}) = 0$$
- 8 Next, take equations *d* for link 3 and substitute equation *c* and also $-F_{32x}$ for F_{23x} , and $-F_{32y}$ for F_{23y} from equation *g* to eliminate those variables.

$$\begin{aligned} F_{cable_x} + F_{13x} - F_{32x} &= 0 \\ F_{cable_y} + F_{13y} - F_{32x} \tan \theta &= 0 \end{aligned} \quad (l)$$

- 9 For link 1, substitute equation *f* in *e* and replace F_{21x} with $-F_{12x}$, F_{21y} with $-F_{12y}$, F_{31x} with $-F_{13x}$, F_{31y} with $-F_{13y}$, and F_{sheath_x} with $-F_{cable_x}$ from equation *g*,

$$\begin{aligned} -F_{12x} + F_{b1x} - F_{13x} + P_x - F_{cable_x} &= 0 \\ -F_{12y} + F_{b1y} - F_{32x} \tan \theta + P_y &= 0 \end{aligned} \quad (m)$$

$$\begin{aligned} M_h + (-R_{21x}F_{12y} + R_{21y}F_{12x}) + (R_{b1x}F_{b1y} - R_{b1y}F_{b1x}) \\ + (-R_{31x}F_{13y} + R_{31y}F_{13x}) + (R_{px}P_y - R_{py}P_x) + R_{dy}F_{cable_x} &= 0 \end{aligned}$$

- 10 Finally, substitute equations *h*, *i*, and *j* into equations *k*, *l*, and *m* to yield the following set of eight simultaneous equations in the eight remaining unknowns: F_{12x} , F_{12y} , F_{32x} , F_{32y} , F_{cable_x} , P_x , P_y , and M_h . Put them in the standard form which has all unknown terms on the left and all known terms to the right of the equal signs.

* But not necessarily colinear.

$$\begin{aligned}
 F_{12x} + F_{32x} &= -F_{b2x} \\
 F_{12y} + F_{32x} \tan\theta &= -F_{b2y} \\
 F_{cable_x} - F_{32x} &= 0 \\
 F_{13y} - F_{32x} \tan\theta &= 0 \quad (n) \\
 -F_{12x} + P_x - F_{cable_x} &= F_{b2x} \\
 -F_{12y} - F_{13y} + P_y &= F_{b2y}
 \end{aligned}$$

3

$$R_{12x}F_{12y} - R_{12y}F_{12x} + (R_{32x} \tan\theta - R_{32y})F_{32x} = -R_{b2x}F_{b2y} + R_{b2y}F_{b2x}$$

$$M_h - R_{21x}F_{12y} + R_{21y}F_{12x} - R_{31x}F_{13y} + R_{Px}P_y - R_{Py}P_x + R_{dy}F_{cable_x} = R_{b1x}F_{b2y} - R_{b1y}F_{b2x}$$

11 Form the matrices from equation *n*.

$$\left[\begin{array}{ccccccc|c}
 1 & 0 & 1 & 0 & 0 & 0 & 0 & 0 \\
 0 & 1 & \tan\theta & 0 & 0 & 0 & 0 & 0 \\
 0 & 0 & -1 & 0 & 1 & 0 & 0 & 0 \\
 0 & 0 & -\tan\theta & 1 & 0 & 0 & 0 & 0 \\
 -1 & 0 & 0 & 0 & -1 & 1 & 0 & 0 \\
 0 & -1 & 0 & -1 & 0 & 0 & 1 & 0 \\
 -R_{12y} & R_{12x} & R_{32x} \tan\theta - R_{32y} & 0 & 0 & 0 & 0 & 0 \\
 R_{21y} & -R_{21x} & 0 & -R_{31x} & R_{dy} & -R_{Py} & R_{Px} & 1
 \end{array} \right] \times \begin{bmatrix} F_{12x} \\ F_{12y} \\ F_{32x} \\ F_{13y} \\ F_{cable_x} \\ P_x \\ P_y \\ M_h \end{bmatrix} = \quad (o)$$

$$\begin{bmatrix} -F_{b2x} \\ -F_{b2y} \\ 0 \\ 0 \\ F_{b2x} \\ F_{b2y} \\ -R_{b2x}F_{b2y} + R_{b2y}F_{b2x} \\ R_{b1x}F_{b2y} - R_{b1y}F_{b2x} \end{bmatrix}$$

Table 3-2 - part 2

Case Study 1A
Calculated Data

Variable	Value	Unit
F_{32x}	-1 909	N
F_{32y}	-133	N
F_{12x}	1 909	N
F_{12y}	400	N
F_{23x}	1 909	N
F_{23y}	133	N
F_{13y}	-133	N
F_{cable_x}	-1 909	N
F_{cable_y}	0	N
F_{b1x}	0	N
F_{b1y}	267	N
F_{31x}	0	N
F_{31y}	133	N
F_{21x}	-1 909	N
F_{21y}	-400	N
P_x	0	N
P_y	0	N
M_h	9	N-m
F_{sheath_x}	1 909	N

12 Substitute the known data as shown in Table 3-2 part 1 (repeated opposite).

$$\left[\begin{array}{ccccccc|c}
 1 & 0 & 1 & 0 & 0 & 0 & 0 & 0 \\
 0 & 1 & 0.070 & 0 & 0 & 0 & 0 & 0 \\
 0 & 0 & -1 & 0 & 1 & 0 & 0 & 0 \\
 0 & 0 & -0.070 & 1 & 0 & 0 & 0 & 0 \\
 -1 & 0 & 0 & 0 & -1 & 1 & 0 & 0 \\
 0 & -1 & 0 & -1 & 0 & 0 & 1 & 0 \\
 7.34 & -47.91 & -0.324 & 0 & 0 & 0 & 0 & 0 \\
 19 & -7 & 0 & 27 & 27 & 0 & -27 & 1
 \end{array} \right] \times \begin{bmatrix} F_{12x} \\ F_{12y} \\ F_{32x} \\ F_{13y} \\ F_{cable_x} \\ P_x \\ P_y \\ M_h \end{bmatrix} = \begin{bmatrix} 0 \\ 267 \\ 0 \\ 0 \\ 0 \\ -267 \\ 93.08 \\ -112.25 \end{bmatrix} \quad (p)$$

13 The solution is shown in Table 3-2 part 2. This matrix equation can be solved with any one of a number of commercially available matrix solvers such as *Mathcad*, *MATLAB*, *Maple*, or *Mathematica*, as well as with many engineering pocket calculators. A custom-written program called MATRIX is provided on the CD-ROM in this

Table 3-2 - part 2 repeatedCase Study 1A
Calculated Data

Variable	Value	Unit
F_{32x}	-1 909	N
F_{32y}	-133	N
F_{12x}	1 909	N
F_{12y}	400	N
F_{23x}	1 909	N
F_{23y}	133	N
F_{13y}	-133	N
F_{cable_x}	-1 909	N
F_{cable_y}	0	N
F_{b1x}	0	N
F_{b1y}	267	N
F_{31x}	0	N
F_{31y}	133	N
F_{21x}	-1 909	N
F_{21y}	-400	N
P_x	0	N
P_y	0	N
M_h	9	N-m
F_{sheath_x}	1 909	N

book that can be used to solve a linear system of up to 16 equations. Equation p was solved with program MATRIX to find the 8 unknowns listed in step 10. Those results were then substituted into the other equations to solve for the previously eliminated variables.

- 3 14 Table 3-2 part 2 shows the solution data for the data given in Figure 3-2 and Table 3-2 part 1. This assumes a 267-N (60-lb) force is applied by the person's hand normal to the brake lever. The force generated in the cable (F_{cable}) is then 1 909 N (429 lb) and the reaction force against the handlebar (F_{21}) is 1 951 N (439 lb) at -168° .

CASE STUDY 2 A

Hand-Operated Crimping-Tool Loading Analysis

Problem: Determine the forces on the elements of the crimping tool shown in Figure 3-3 during a crimp operation.

Given: The geometry is known and the tool develops a crimp force of 2 000 lb (8 896 N) at closure in the position shown.

Assumptions: The accelerations are negligible. All forces are coplanar and two dimensional. A Class 1 load model is appropriate and a static analysis acceptable.

Solution: See Figures 3-3 and 3-4, and Table 3-3, parts 1 and 2.

- 1 Figure 3-3 shows the tool in the closed position in the process of crimping a metal connector onto a wire. The user's hand provides the input forces between links 1 and 2, shown as the reaction pair F_h . The user can grip the handle anywhere along its length, but we are assuming a nominal moment arm of R_h for the application of the resultant of the user's grip force (see Figure 3-4). The high mechanical advantage of the tool transforms the grip force to a large force at the crimp.

Figure 3-3 is a free-body diagram of the entire assembly, neglecting the weight of the tool which is small compared to the crimp force. There are four elements, or links, in the assembly, all pinned together. Link 1 can be considered to be the "ground" link, with the other links moving with respect to it as the jaw is closed. The desired magnitude of the crimp force F_c is defined and its direction will be normal to the surfaces at the crimp. The third law relates the action-reaction pair acting on links 1 and 4:

$$\begin{aligned} F_{c1x} &= -F_{c4x} \\ F_{c1y} &= -F_{c4y} \end{aligned} \quad (a)$$

- 2 Figure 3-4 shows the elements of the crimping-tool assembly separated and drawn as free-body diagrams with all forces applied to each element, again neglecting their weights as being insignificant compared to the applied forces. The centers of gravity of the respective elements are used as the origins of the local, nonrotating coordinate systems in which the points of application of all forces on the elements are located.*
- 3 We will consider link 1 to be the ground plane and analyze the remaining moving links. Note that all unknown forces and moments are initially assumed positive. Link 2 has three forces acting on it: F_h is the unknown force from the hand, and F_{12} and F_{32} are

* Again, in a static analysis it is not necessary to take the CG as the coordinate system origin (any point can be used), but we do so to be consistent with the dynamic analysis approach in which it is quite useful to do so.

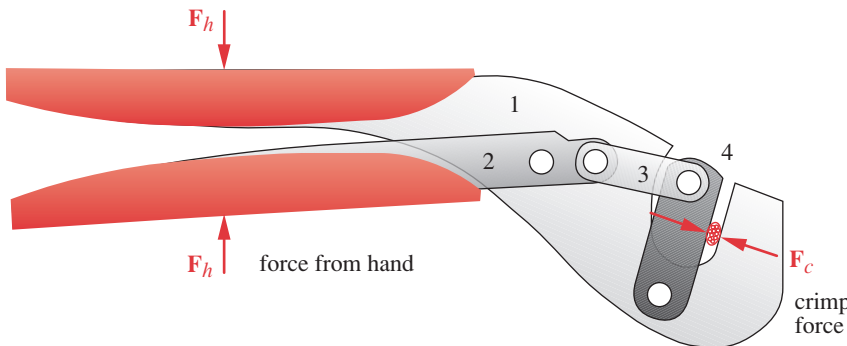


FIGURE 3-3

Wire Connector Crimping Tool

the reaction forces from links 1 and 3, respectively. Force \mathbf{F}_{12} is provided by part 1 on part 2 at the pivot pin and force \mathbf{F}_{32} is provided by part 3 acting on part 2 at their pivot pin. The magnitudes and directions of both these pin forces are unknown. We can write equations 3.3b for this element to sum forces in the x and y directions and sum moments about the CG (with cross products expanded).

$$\begin{aligned}\sum F_x &= F_{12x} + F_{32x} = 0 \\ \sum F_y &= F_{12y} + F_{32y} + F_h = 0 \\ \sum M_z &= F_h R_h + (R_{12x} F_{12y} - R_{12y} F_{12x}) + (R_{32x} F_{32y} - R_{32y} F_{32x}) = 0\end{aligned}\quad (b)$$

- 4 Link 3 has two forces on it, \mathbf{F}_{23} and \mathbf{F}_{43} . Write equations 3.3b for this element:

$$\begin{aligned}\sum F_x &= F_{23x} + F_{43x} = 0 \\ \sum F_y &= F_{23y} + F_{43y} = 0 \\ \sum M_z &= (R_{23x} F_{23y} - R_{23y} F_{23x}) + (R_{43x} F_{43y} - R_{43y} F_{43x}) = 0\end{aligned}\quad (c)$$

- 5 Link 4 has three forces acting on it: \mathbf{F}_{c4} is the known (desired) force at the crimp, and \mathbf{F}_{14} and \mathbf{F}_{34} are the reaction forces from links 1 and 3, respectively. The magnitudes and directions of both these pin forces are unknown. Write equations 3.3b for this element:

$$\begin{aligned}\sum F_x &= F_{14x} + F_{34x} + F_{c4x} = 0 \\ \sum F_y &= F_{14y} + F_{34y} + F_{c4y} = 0 \\ \sum M_z &= (R_{14x} F_{14y} - R_{14y} F_{14x}) + (R_{34x} F_{34y} - R_{34y} F_{34x}) \\ &\quad + (R_{c4x} F_{c4y} - R_{c4y} F_{c4x}) = 0\end{aligned}\quad (d)$$

- 6 The 9 equations in sets b through d have 13 unknowns: F_{12x} , F_{12y} , F_{32x} , F_{32y} , F_{23x} , F_{23y} , F_{43x} , F_{43y} , F_{14x} , F_{14y} , F_{34x} , F_{34y} , and F_h . We can write the third-law relationships between action-reaction pairs at each of the joints to obtain the four additional equations needed:

$$F_{32x} = -F_{23x}; \quad F_{34x} = -F_{43x}; \quad F_{32y} = -F_{23y}; \quad F_{34y} = -F_{43y} \quad (e)$$

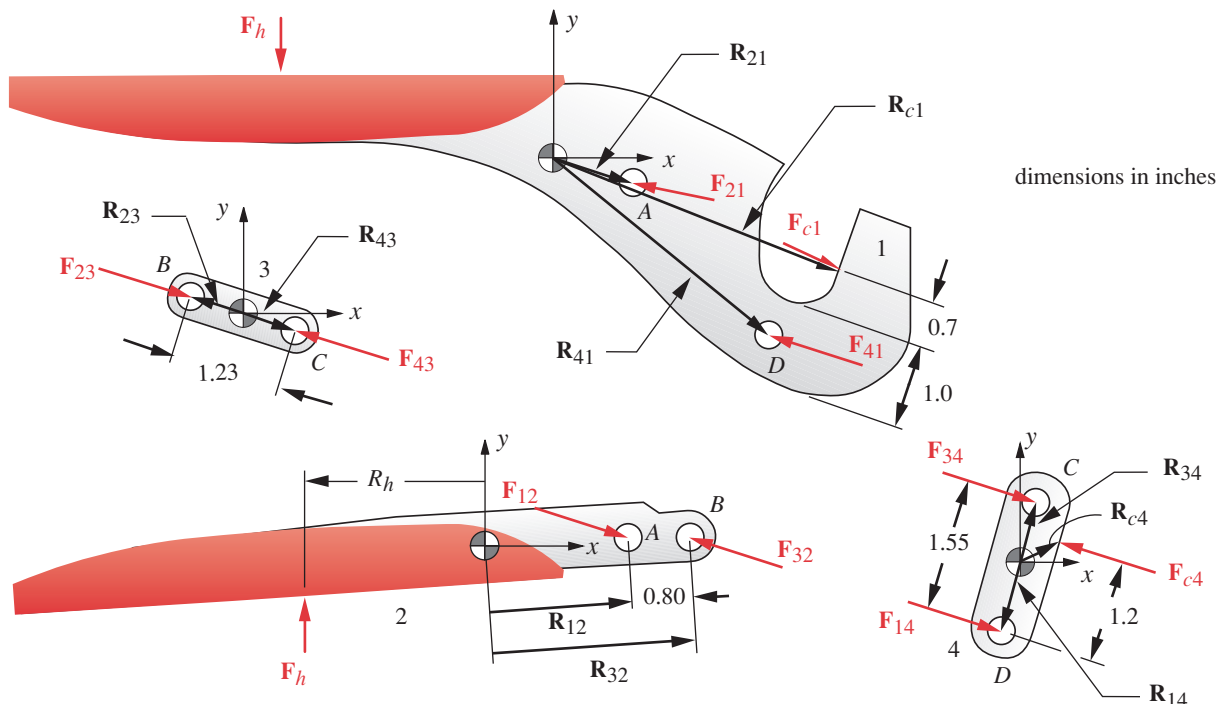
Table 3-3 - part 1

Case Study 2A
Given Data

Variable	Value	Unit
F_{c4x}	-1 956.30	lb
F_{c4y}	415.82	lb
R_{c4x}	0.45	in
R_{c4y}	0.34	in
R_{12x}	1.40	in
R_{12y}	0.05	in
R_{32x}	2.20	in
R_{32y}	0.08	in
R_h	-4.40	in
R_{23x}	-0.60	in
R_{23y}	0.13	in
R_{43x}	0.60	in
R_{43y}	-0.13	in
R_{14x}	-0.16	in
R_{14y}	-0.76	in
R_{34x}	0.16	in
R_{34y}	0.76	in

3

3

**FIGURE 3-4**

Free-Body Diagrams of a Wire Connector Crimping Tool

Table 3-3 - part 2Case Study 2A
Calculated Data

Variable	Value	Unit
F_h	53.1	lb
F_{12x}	1 513.6	lb
F_{12y}	-381.0	lb
F_{32x}	-1 513.6	lb
F_{32y}	327.9	lb
F_{43x}	-1 513.6	lb
F_{43y}	327.9	lb
F_{23x}	1 513.6	lb
F_{23y}	-327.9	lb
F_{34x}	1 513.6	lb
F_{34y}	-327.9	lb
F_{14x}	442.7	lb
F_{14y}	-87.9	lb
F_{21x}	-1 513.6	lb
F_{21y}	381.0	lb
F_{41x}	-442.7	lb
F_{41y}	87.9	lb

- 7 The 13 equations *b–e* can be solved simultaneously by matrix reduction or by iteration with a root-finding algorithm. For a matrix solution, the unknown terms are placed on the left and known terms on the right of the equal signs.

$$\begin{aligned}
 F_{12x} + F_{32x} &= 0 \\
 F_{12y} + F_{32y} + F_h &= 0 \\
 R_h F_h + R_{12x} F_{12y} - R_{12y} F_{12x} + R_{32x} F_{32y} - R_{32y} F_{32x} &= 0 \\
 F_{23x} + F_{43x} &= 0 \\
 F_{23y} + F_{43y} &= 0 \\
 R_{23x} F_{23y} - R_{23y} F_{23x} + R_{43x} F_{43y} - R_{43y} F_{43x} &= 0 \\
 F_{14x} + F_{34x} &= -F_{c4x} \\
 F_{14y} + F_{34y} &= -F_{c4y} \\
 R_{14x} F_{14y} - R_{14y} F_{14x} + R_{34x} F_{34y} - R_{34y} F_{34x} &= -R_{c4x} F_{c4y} + R_{c4y} F_{c4x} \\
 F_{32x} + F_{23x} &= 0 \\
 F_{34x} + F_{43x} &= 0 \\
 F_{32y} + F_{23y} &= 0 \\
 F_{34y} + F_{43y} &= 0
 \end{aligned} \tag{f}$$

- 8 Substitute the given data from Table 3-3 part 1.

$$\begin{aligned}
 F_{12x} + F_{32x} &= 0 \\
 F_{12y} + F_{32y} + F_h &= 0 \\
 -4.4F_h + 1.4F_{12y} - 0.05F_{12x} + 2.2F_{32y} - 0.08F_{32x} &= 0 \\
 F_{23x} + F_{43x} &= 0 \\
 F_{23y} + F_{43y} &= 0 \\
 -0.6F_{23y} - 0.13F_{23x} + 0.6F_{43y} + 0.13F_{43x} &= 0 \\
 F_{14x} + F_{34x} &= 1956.3 \quad (g) \\
 F_{14y} + F_{34y} &= -415.82 \\
 -0.16F_{14y} + 0.76F_{14x} + 0.16F_{34y} - 0.76F_{34x} &= -0.45(415.82) - 0.34(1956.3) \\
 &= -852.26 \\
 F_{32x} + F_{23x} &= 0 \\
 F_{34x} + F_{43x} &= 0 \\
 F_{32y} + F_{23y} &= 0 \\
 F_{34y} + F_{43y} &= 0
 \end{aligned}$$

9 Form the matrices for solution.

$$\left[\begin{array}{cccccccccccccc|c|c}
 1 & 0 & 1 & 0 & 0 & 0 & 0 & 0 & 0 & 0 & 0 & 0 & 0 & 0 & F_{12x} & 0 \\
 0 & 1 & 0 & 1 & 1 & 0 & 0 & 0 & 0 & 0 & 0 & 0 & 0 & 0 & F_{12y} & 0 \\
 -0.05 & 1.4 & -0.08 & 2.2 & -4.4 & 0 & 0 & 0 & 0 & 0 & 0 & 0 & 0 & 0 & F_{32x} & 0 \\
 0 & 0 & 0 & 0 & 0 & 1 & 0 & 1 & 0 & 0 & 0 & 0 & 0 & 0 & F_{32y} & 0 \\
 0 & 0 & 0 & 0 & 0 & 0 & 1 & 0 & 1 & 0 & 0 & 0 & 0 & 0 & F_h & 0 \\
 0 & 0 & 0 & 0 & 0 & -0.13 & -0.6 & 0.13 & 0.6 & 0 & 0 & 0 & 0 & 0 & F_{23x} & 0 \\
 0 & 0 & 0 & 0 & 0 & 0 & 0 & 0 & 0 & 1 & 0 & 1 & 0 & 0 & F_{23y} & 1956.30 \\
 0 & 0 & 0 & 0 & 0 & 0 & 0 & 0 & 0 & 0 & 1 & 0 & 1 & 1 & F_{43x} & -415.82 \\
 0 & 0 & 0 & 0 & 0 & 0 & 0 & 0 & 0 & 0.76 & -0.16 & -0.76 & 0.16 & 0 & F_{43y} & -852.26 \\
 0 & 0 & 1 & 0 & 0 & 1 & 0 & 0 & 0 & 0 & 0 & 0 & 0 & 0 & F_{14x} & 0 \\
 0 & 0 & 0 & 0 & 0 & 0 & 0 & 1 & 0 & 0 & 0 & 1 & 0 & 0 & F_{14y} & 0 \\
 0 & 0 & 0 & 1 & 0 & 0 & 1 & 0 & 0 & 0 & 0 & 0 & 0 & 0 & F_{34x} & 0 \\
 0 & 0 & 0 & 0 & 0 & 0 & 0 & 0 & 1 & 0 & 0 & 0 & 1 & 0 & F_{34y} & 0
 \end{array} \right] = \left[\begin{array}{c} 0 \\ 0 \\ 0 \\ 0 \\ 0 \\ 0 \\ 0 \\ 1956.30 \\ -415.82 \\ -852.26 \\ 0 \\ 0 \\ 0 \\ 0 \\ 0 \\ 0 \end{array} \right] \quad (h)$$

- 10 Table 3-3 part 2 shows the solution to this problem for the data given in Table 3-3 part 1, assuming a 2000-lb (8 896-N) force applied at the crimp, normal to the crimp surface. Program MATRIX (on the CD-ROM) was used. The force generated in link 3 is 1 547 lb (6 888 N), the reaction force against link 1 by link 2 (F_{21}) is 1 561 lb (6 943 N) at 166° , the reaction force against link 1 by link 4 (F_{41}) is 451 lb (2 008 N) at 169° , and a -233.5 lb-in (-26.6 -N-m) moment must be applied to the handles to generate the specified crimp force. This moment can be obtained with a 53.1-lb (236-N) force applied at mid-handle. This force is within the physiological grip-force capacity of the average human.

CASE STUDY 3A

Automobile Scissors-Jack Loading Analysis

3

Problem: Determine the forces on the elements of the scissors jack in the position shown in Figure 3-5.

Given: The geometry is known and the jack supports a force of $P = 1\,000 \text{ lb}$ ($4\,448 \text{ N}$) in the position shown.

Assumptions: The accelerations are negligible. The jack is on level ground. The angle of the elevated car chassis does not impart an overturning moment to the jack. All forces are coplanar and two dimensional. A Class 1 load model is appropriate and a static analysis is acceptable.

Solution: See Figures 3-5 through 3-8 and Table 3-4, parts 1 and 2.

- Figure 3-5 shows a schematic of a simple scissors jack used to raise a car. It consists of six links which are pivoted and/or geared together and a seventh link in the form of a lead screw which is turned to raise the jack. While this is clearly a three-dimensional device, it can be analyzed as a two-dimensional one if we assume that the applied load (from the car) and the jack are exactly vertical (in the z direction). If so, all forces will be in the xy plane. This assumption is valid if the car is jacked from a level surface. If not, then there will be some forces in the yz and xz planes as well. The jack designer needs to consider the more general case, but for our simple example we will initially assume two-dimensional loading. For the overall assembly as shown in Figure 3-5, we can solve for the reaction force F_g , given force P , by summing forces: $F_g = -P$.
- Figure 3-6 shows a set of free-body diagrams for the entire jack. Each element or subassembly of interest has been separated from the others and the forces and moments shown acting on it (except for its weight, which is small compared to the applied forces and is thus neglected for this analysis). The forces and moments can be either internal reactions at interconnections with other elements or external loads from the “out-

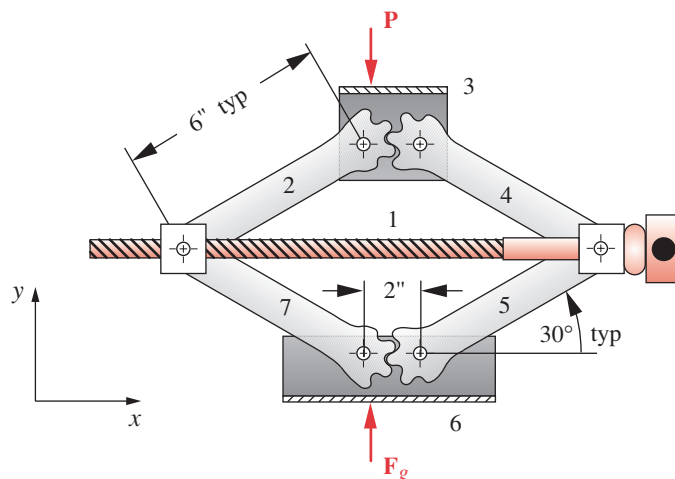
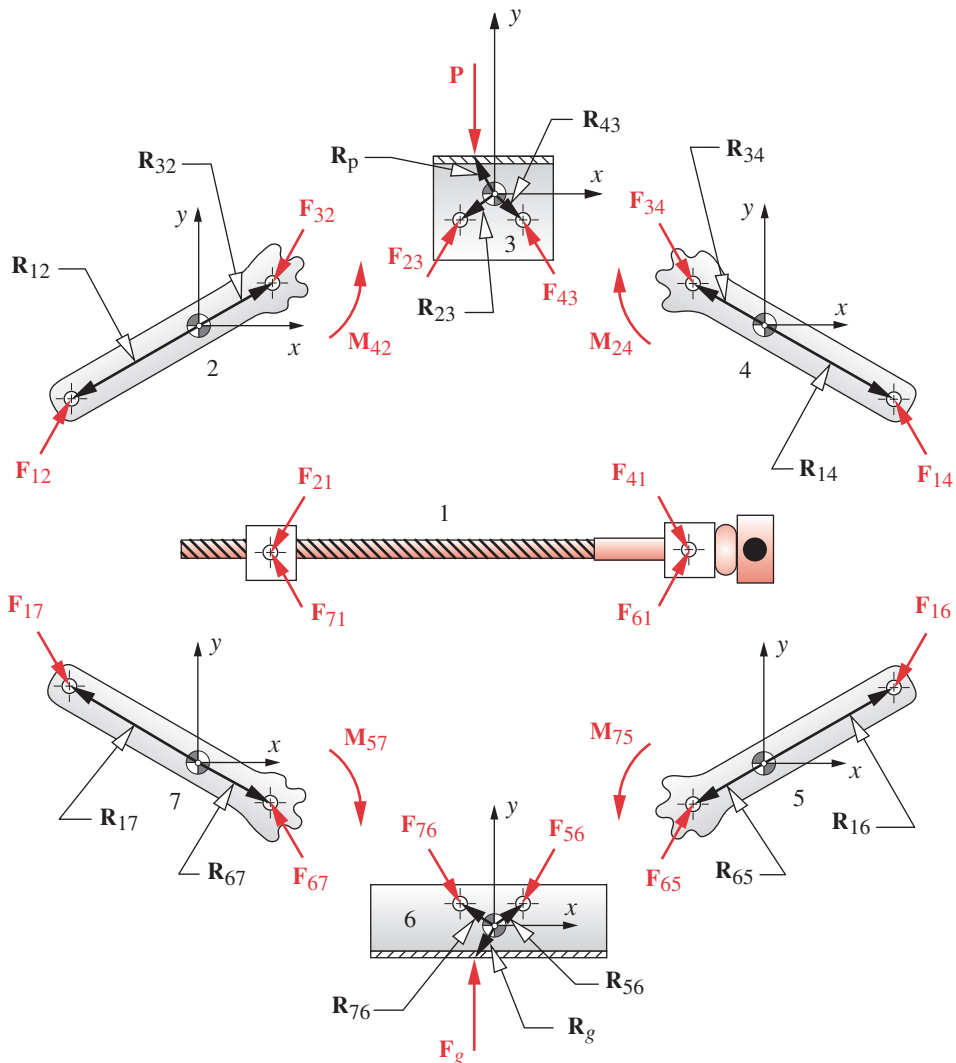


FIGURE 3-5

An Automobile Scissors Jack

**FIGURE 3-6**

Free-Body Diagrams of the Complete Scissors Jack

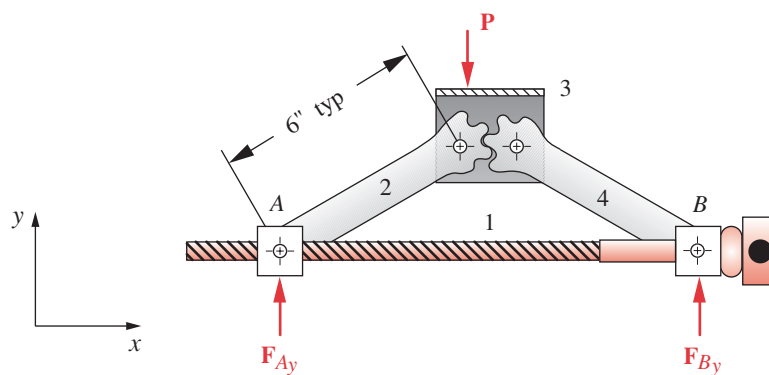
side world.” The centers of gravity of the respective elements are used as the origins of the local, nonrotating coordinate systems in which the points of application of all forces on the elements are located. In this design, stability is achieved by the mating of two pairs of crude (noninvolute) gear segments acting between links 2 and 4 and between links 5 and 7. These interactions are modeled as forces acting along a *common normal* shared by the two teeth. This common normal is perpendicular to the common tangent at the contact point.

There are 3 second-law equations available for each of the seven elements, allowing 21 unknowns. An additional 10 third-law equations will be needed for a total of 31. This is a cumbersome system to solve for such a simple device, but we can use its symmetry to advantage in order to simplify the problem.

Table 3-4 - part 1

Case Study 3A
Given Data

Variable	Value	Unit
P_x	0.00	lb
P_y	-1 000.00	lb
R_{px}	-0.50	in
R_{py}	0.87	in
θ	-45.00	deg
R_{12x}	-3.12	in
R_{12y}	-1.80	in
R_{32x}	2.08	in
R_{32y}	1.20	in
R_{42x}	2.71	in
R_{42y}	1.00	in
R_{23x}	-0.78	in
R_{23y}	-0.78	in
R_{43x}	0.78	in
R_{43y}	-0.78	in
R_{14x}	3.12	in
R_{14y}	-1.80	in
R_{24x}	-2.58	in
R_{24y}	1.04	in
R_{34x}	-2.08	in
R_{34y}	1.20	in

**FIGURE 3-7**

Free-Body Diagram of the Symmetrical Upper Half of an Automobile Scissors Jack

- 3 Figure 3-7 shows the upper half of the jack assembly. Because of the mirror symmetry between the upper and lower portions, the lower half can be removed to simplify the analysis. The forces calculated for this half will be duplicated in the other. If we wished, we could solve for the reaction forces at A and B using equations 3.3b from this free-body diagram of the half-jack assembly.
- 4 Figure 3-8a shows the free-body diagrams for the upper half of the jack assembly which are essentially the same as those of Figure 3-6. We now have four elements but can consider the subassembly labeled 1 to be the “ground,” leaving three elements on which to apply equations 3.3. Note that all unknown forces and moments are initially assumed positive in the equations.
- 5 Link 2 has three forces acting on it: F_{42} is the unknown force at the gear tooth contact with link 4; F_{12} and F_{32} are the unknown reaction forces from links 1 and 3 respectively. Force F_{12} is provided by part 1 on part 2 at the pivot pin, and force F_{32} is provided by part 3 acting on part 2 at their pivot pin. The magnitudes and directions of these pin forces and the magnitude of F_{42} are unknown. The direction of F_{42} is along the common normal shown in Figure 3-8b. Write equations 3.3b for this element to sum forces in the x and y directions and sum moments about the CG (with the cross products expanded):*

$$\begin{aligned}\sum F_x &= F_{12x} + F_{32x} + F_{42x} = 0 \\ \sum F_y &= F_{12y} + F_{32y} + F_{42y} = 0 \\ \sum M_z &= R_{12x}F_{12y} - R_{12y}F_{12x} + R_{32x}F_{32y} - R_{32y}F_{32x} + R_{42x}F_{42y} - R_{42y}F_{42x} = 0\end{aligned}\quad (a)$$

- 6 Link 3 has three forces acting on it: the applied load P , F_{23} , and F_{43} . Only P is known. Writing equations 3.3b for this element gives

$$\begin{aligned}\sum F_x &= F_{23x} + F_{43x} + P_x = 0 \\ \sum F_y &= F_{23y} + F_{43y} + P_y = 0 \\ \sum M_z &= R_{23x}F_{23y} - R_{23y}F_{23x} + R_{43x}F_{43y} - R_{43y}F_{43x} + R_{Px}P_y - R_{Py}P_x = 0\end{aligned}\quad (b)$$

* Note the similarity to equations (b) in Case Study 2A. Only the subscript for the reaction moment is different because a different link is providing it. The consistent notation of this force analysis method makes it easy to write the equations for any system.

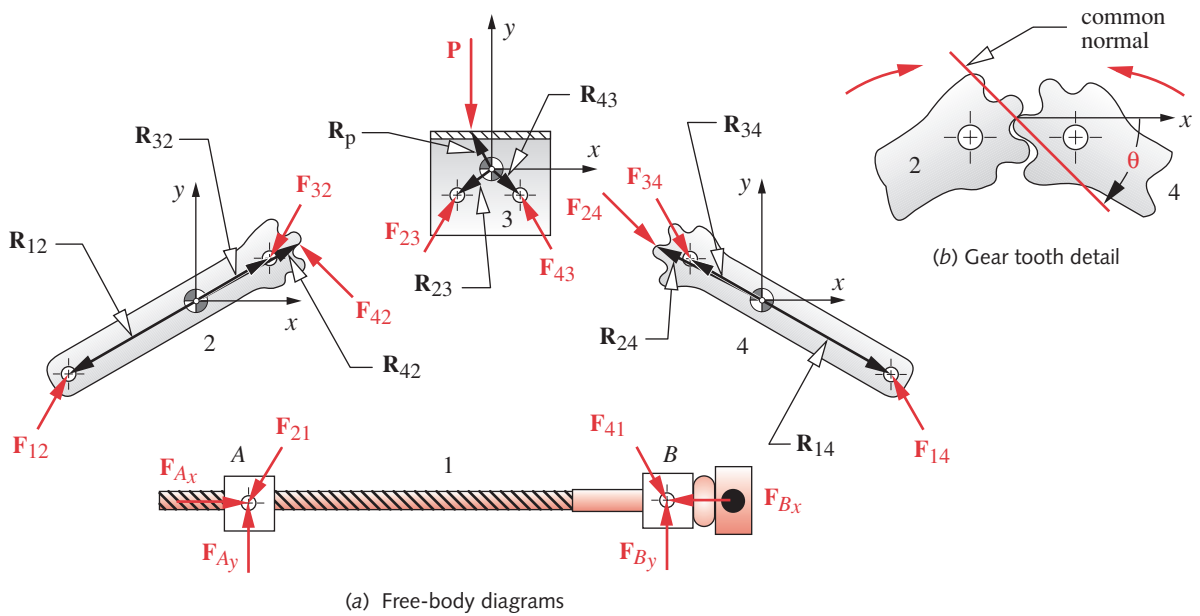


FIGURE 3-8

Free-Body Diagrams of Elements of the Half Scissors Jack

- 7 Link 4 has three forces acting on it: \mathbf{F}_{24} is the unknown force from link 2; \mathbf{F}_{14} and \mathbf{F}_{34} are the unknown reaction forces from links 1 and 3 respectively.

$$\sum F_x = F_{14x} + F_{24x} + F_{34x} = 0$$

$$\sum F_y = F_{14y} + F_{24y} + F_{34y} = 0 \quad (c)$$

$$\sum M_z = R_{14x}F_{14y} - R_{14y}F_{14x} + R_{24x}F_{24y} - R_{24y}F_{24x} + R_{34x}F_{34y} - R_{34y}F_{34x} = 0$$

- 8 The nine equations in sets *a* through *c* have 16 unknowns in them, F_{12x} , F_{12y} , F_{32x} , F_{32y} , F_{23x} , F_{23y} , F_{43x} , F_{43y} , F_{14x} , F_{14y} , F_{34x} , F_{34y} , F_{24x} , F_{24y} , F_{42x} , and F_{42y} . We can write the third-law relationships between action-reaction pairs at each of the joints to obtain six of the seven additional equations needed:

$$\begin{array}{ll} F_{32x} = -F_{23x} & F_{32y} = -F_{23y} \\ F_{34x} = -F_{43x} & F_{34y} = -F_{43y} \\ F_{42x} = -F_{24x} & F_{42y} = -F_{24y} \end{array} \quad (d)$$

- 9 The last equation needed comes from the relationship between the *x* and *y* components of the force \mathbf{F}_{24} (or \mathbf{F}_{42}) at the tooth/tooth contact point. Such a contact (or half) joint can transmit force (excepting friction force) only along the **common normal**^[4] which is perpendicular to the joint's common tangent as shown in Figure 3-8b. The common normal is also called the **axis of transmission**. The tangent of the angle of this common normal relates the two components of the force at the joint:

$$F_{24y} = F_{24x} \tan \theta \quad (e)$$

Table 3-4 - part 2

Case Study 3A
Calculated Data

Variable	Value	Unit
F_{12x}	877.8	lb
F_{12y}	530.4	lb
F_{32x}	-587.7	lb
F_{32y}	-820.5	lb
F_{42x}	-290.1	lb
F_{42y}	290.1	lb
F_{23x}	587.7	lb
F_{23y}	820.5	lb
F_{43x}	-587.7	lb
F_{43y}	179.5	lb
F_{14x}	-877.8	lb
F_{14y}	469.6	lb
F_{24x}	290.1	lb
F_{24y}	-290.1	lb
F_{34x}	587.7	lb
F_{34y}	-179.5	lb

- 10 Equations (a) through (e) comprise a set of 16 simultaneous equations that can be solved either by matrix reduction or by iterative root-finding methods. Putting them in standard form for a matrix solution gives:

$$\begin{aligned}
 F_{12x} + F_{32x} + F_{42x} &= 0 \\
 F_{12y} + F_{32y} + F_{42y} &= 0 \\
 R_{12x}F_{12y} - R_{12y}F_{12x} + R_{32x}F_{32y} - R_{32y}F_{32x} + R_{42x}F_{42y} - R_{42y}F_{42x} &= 0 \\
 F_{23x} + F_{43x} &= -P_x \\
 F_{23y} + F_{43y} &= -P_y \\
 R_{23x}F_{23y} - R_{23y}F_{23x} + R_{43x}F_{43y} - R_{43y}F_{43x} &= -R_{Px}P_y + R_{Py}P_x \\
 F_{14x} + F_{24x} + F_{34x} &= 0 \\
 F_{14y} + F_{24y} + F_{34y} &= 0 \\
 R_{14x}F_{14y} - R_{14y}F_{14x} + R_{24x}F_{24y} - R_{24y}F_{24x} + R_{34x}F_{34y} - R_{34y}F_{34x} &= 0 \quad (f) \\
 F_{32x} + F_{23x} &= 0 \\
 F_{32y} + F_{23y} &= 0 \\
 F_{34x} + F_{43x} &= 0 \\
 F_{34y} + F_{43y} &= 0 \\
 F_{42x} + F_{24x} &= 0 \\
 F_{42y} + F_{24y} &= 0 \\
 F_{24y} - F_{24x} \tan\theta &= 0
 \end{aligned}$$

- 11 Substituting the given data from Table 3-4 part 1 gives:

$$\begin{aligned}
 F_{12x} + F_{32x} + F_{42x} &= 0 \\
 F_{12y} + F_{32y} + F_{42y} &= 0 \\
 -3.12F_{12y} + 1.80F_{12x} + 2.08F_{32y} - 1.20F_{32x} + 2.71F_{42y} - 0.99F_{42x} &= 0 \\
 F_{23x} + F_{43x} &= 0.0 \\
 F_{23y} + F_{43y} &= 1.000 \\
 -0.78F_{23y} + 0.78F_{23x} + 0.78F_{43y} + 0.78F_{43x} &= -500 \\
 F_{14x} + F_{24x} + F_{34x} &= 0 \\
 F_{14y} + F_{24y} + F_{34y} &= 0 \\
 3.12F_{14y} + 1.80F_{14x} - 2.58F_{24y} - 1.04F_{24x} - 2.08F_{34y} - 1.20F_{34x} &= 0 \quad (g) \\
 F_{32x} + F_{23x} &= 0 \\
 F_{32y} + F_{23y} &= 0 \\
 F_{34x} + F_{43x} &= 0 \\
 F_{34y} + F_{43y} &= 0 \\
 F_{42x} + F_{24x} &= 0 \\
 F_{42y} + F_{24y} &= 0 \\
 F_{24y} + 1.0F_{24x} &= 0
 \end{aligned}$$

- 12 Put these equations into matrix form.

$$\begin{bmatrix}
 1 & 0 & 1 & 0 & 1 & 0 & 0 & 0 & 0 & 0 & 0 & 0 & 0 & 0 & 0 & 0 \\
 0 & 1 & 0 & 1 & 0 & 1 & 0 & 0 & 0 & 0 & 0 & 0 & 0 & 0 & 0 & 0 \\
 1.80 & -3.12 & -1.20 & 2.08 & -1.00 & 2.71 & 0 & 0 & 0 & 0 & 0 & 0 & 0 & 0 & 0 & 0 \\
 0 & 0 & 0 & 0 & 0 & 0 & 1 & 0 & 1 & 0 & 0 & 0 & 0 & 0 & 0 & 0 \\
 0 & 0 & 0 & 0 & 0 & 0 & 0 & 1 & 0 & 1 & 0 & 0 & 0 & 0 & 0 & 0 \\
 0 & 0 & 0 & 0 & 0 & 0 & 0.78 & -0.78 & 0.78 & 0.78 & 0 & 0 & 0 & 0 & 0 \\
 0 & 0 & 0 & 0 & 0 & 0 & 0 & 0 & 0 & 0 & 1 & 0 & 1 & 0 & 1 & 0 \\
 0 & 0 & 0 & 0 & 0 & 0 & 0 & 0 & 0 & 0 & 1 & 0 & 1 & 0 & 1 & 0 \\
 0 & 0 & 0 & 0 & 0 & 0 & 0 & 0 & 0 & 0 & 1.80 & 3.12 & -1.04 & -2.58 & -1.20 & -2.08 \\
 0 & 0 & 1 & 0 & 0 & 0 & 1 & 0 & 0 & 0 & 0 & 0 & 0 & 0 & 0 & 0 \\
 0 & 0 & 0 & 1 & 0 & 0 & 0 & 1 & 0 & 0 & 0 & 0 & 0 & 0 & 0 & 0 \\
 0 & 0 & 0 & 0 & 0 & 0 & 0 & 0 & 1 & 0 & 0 & 0 & 0 & 1 & 0 & 0 \\
 0 & 0 & 0 & 0 & 0 & 0 & 0 & 0 & 0 & 1 & 0 & 0 & 0 & 0 & 1 & 0 \\
 0 & 0 & 0 & 0 & 1 & 0 & 0 & 0 & 0 & 0 & 0 & 1 & 0 & 0 & 0 & 0 \\
 0 & 0 & 0 & 0 & 0 & 1 & 0 & 0 & 0 & 0 & 0 & 0 & 1 & 0 & 0 & 0 \\
 0 & 0 & 0 & 0 & 0 & 0 & 0 & 0 & 0 & 0 & 0 & 1 & 1 & 0 & 0 & 0 \\
 0 & 0 & 0 & 0 & 0 & 0 & 0 & 0 & 0 & 0 & 0 & 1 & 1 & 0 & 0 & 0 \\
 0 & 0 & 0 & 0 & 0 & 0 & 0 & 0 & 0 & 0 & 0 & 0 & 0 & 0 & 0 & 0
 \end{bmatrix} \times \begin{bmatrix}
 F_{12x} \\
 F_{12y} \\
 F_{32x} \\
 F_{32y} \\
 F_{42x} \\
 F_{42y} \\
 F_{23x} \\
 F_{23y} \\
 F_{43x} \\
 F_{43y} \\
 F_{14x} \\
 F_{14y} \\
 F_{24x} \\
 F_{24y} \\
 F_{34x} \\
 F_{34y}
 \end{bmatrix} = \begin{bmatrix}
 0 \\
 0 \\
 0 \\
 0 \\
 1000 \\
 -500 \\
 0 \\
 0 \\
 0 \\
 0 \\
 0 \\
 0 \\
 0 \\
 0 \\
 0 \\
 0
 \end{bmatrix} \quad (h)$$

3

- 13 Table 3-4 part 2 shows the solution to this problem from program MATRIX for the given data in Table 3-4 part 1, which assumes a vertical 1 000-lb (4 448-N) applied force \mathbf{P} .

- 14 The forces on link 1 can also be found from Newton's third law.

$$\begin{aligned}
 F_{Ax} &= -F_{21x} = F_{12x} \\
 F_{Ay} &= -F_{21y} = F_{12y} \\
 F_{Bx} &= -F_{41x} = F_{14x} \\
 F_{By} &= -F_{41y} = F_{14y}
 \end{aligned} \quad (i)$$

3.5 THREE-DIMENSIONAL, STATIC LOADING CASE STUDY

This section presents a case study involving three-dimensional static loading on a bicycle brake caliper assembly. The same techniques used for two-dimensional load analysis also work for the three-dimensional case. The third dimension requires more equations, which are available from the summation of forces in the z direction and the summation of moments about the x and y axes as defined in equations 3.1 and 3.3 for the dynamic and static cases, respectively. As an example, we will now analyze the bicycle brake arm that is actuated by the handbrake lever that was analyzed in Case Study 1A.

CASE STUDY 4 A

Bicycle Brake Arm Loading Analysis

3

Problem: Determine the forces acting in three dimensions on the bicycle brake arm in its actuated position as shown in Figure 3-9. This brake arm has been failing in service and may need to be redesigned.

Given: The existing brake arm geometry is known and the arm is acted on by a cable force of 1 046 N in the position shown. (See also Case Study 1A.)

Assumptions: The accelerations are negligible. A Class 1 load model is appropriate and a static analysis is acceptable. The coefficient of friction between the brake pad and wheel rim has been measured and is 0.45 at room temperature and 0.40 at 150°F.

Solution: See Figures 3-9 and 3-10, and Table 3-5.

- Figure 3-9 shows a center-pull brake arm assembly commonly used on bicycles. It consists of six elements or subassemblies, the frame and its pivot pins (1), the two brake arms (2 and 4), the cable spreader assembly (3), the brake pads (5), and the wheel rim (6). This is clearly a three-dimensional device and must be analyzed as such.
- The cable is the same one that is attached to the brake lever in Figure 3-1. The 267-N (60-lb) hand force is multiplied by the mechanical advantage of the hand lever and transmitted via this cable to the pair of brake arms as was calculated in Case Study

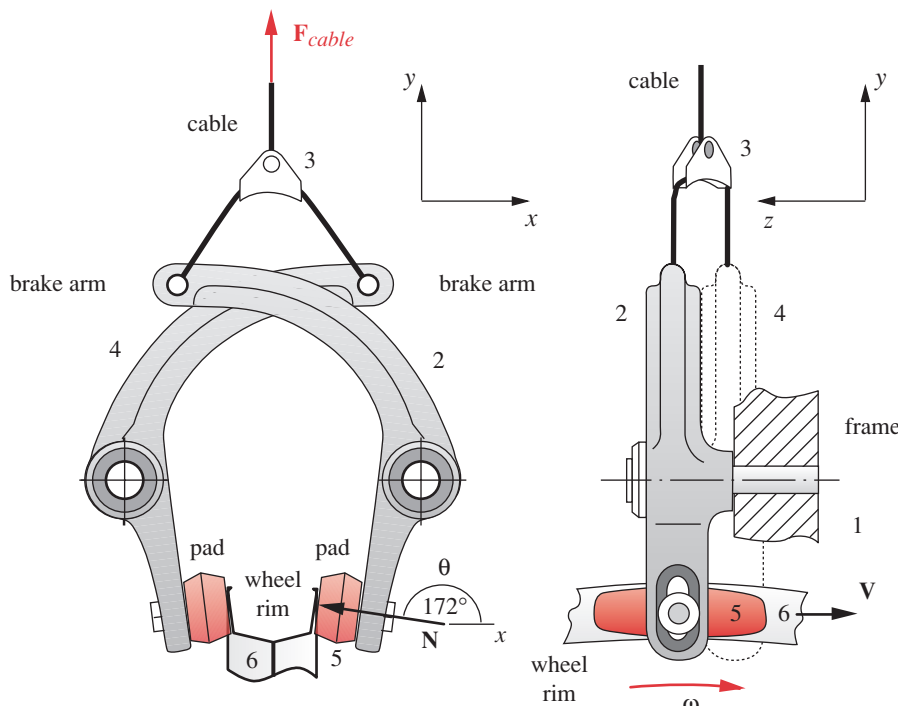


FIGURE 3-9

Center-Pull Bicycle Brake Arm Assembly

- 1A. We will assume no loss of force in the cable guides, thus the full 1 046-N (235-lb) cable force is available at this end.
- 3 The direction of the normal force between the brake pad and the wheel rim is shown in Figure 3-9 to be at $\theta = 172^\circ$ with respect to the positive x axis, and the friction force is directed along the z axis. (See Figures 3-9 and 3-10 for the xyz axis orientations.)
- 4 Figure 3-10 shows free-body diagrams of the arm, frame, and cable spreader assembly. We are principally interested in the forces acting on the brake arm. However, we first need to analyze the effect of the cable spreader geometry on the force applied to the arm at A. This analysis can be two dimensional if we ignore the small z -offset between the two arms for simplicity. A more accurate analysis would require that the z -directed components of the cable-spreader forces acting on the arms be included. Note that the cable subassembly (3) is a concurrent force system. Writing equations 3.3b in two dimensions for this subassembly, and noting the symmetry about point A, we can write from inspection of the FBD:

$$\begin{aligned}\sum F_x &= F_{23x} + F_{43x} = 0 \\ \sum F_y &= F_{23y} + F_{43y} + F_{cable} = 0\end{aligned}\quad (a)$$

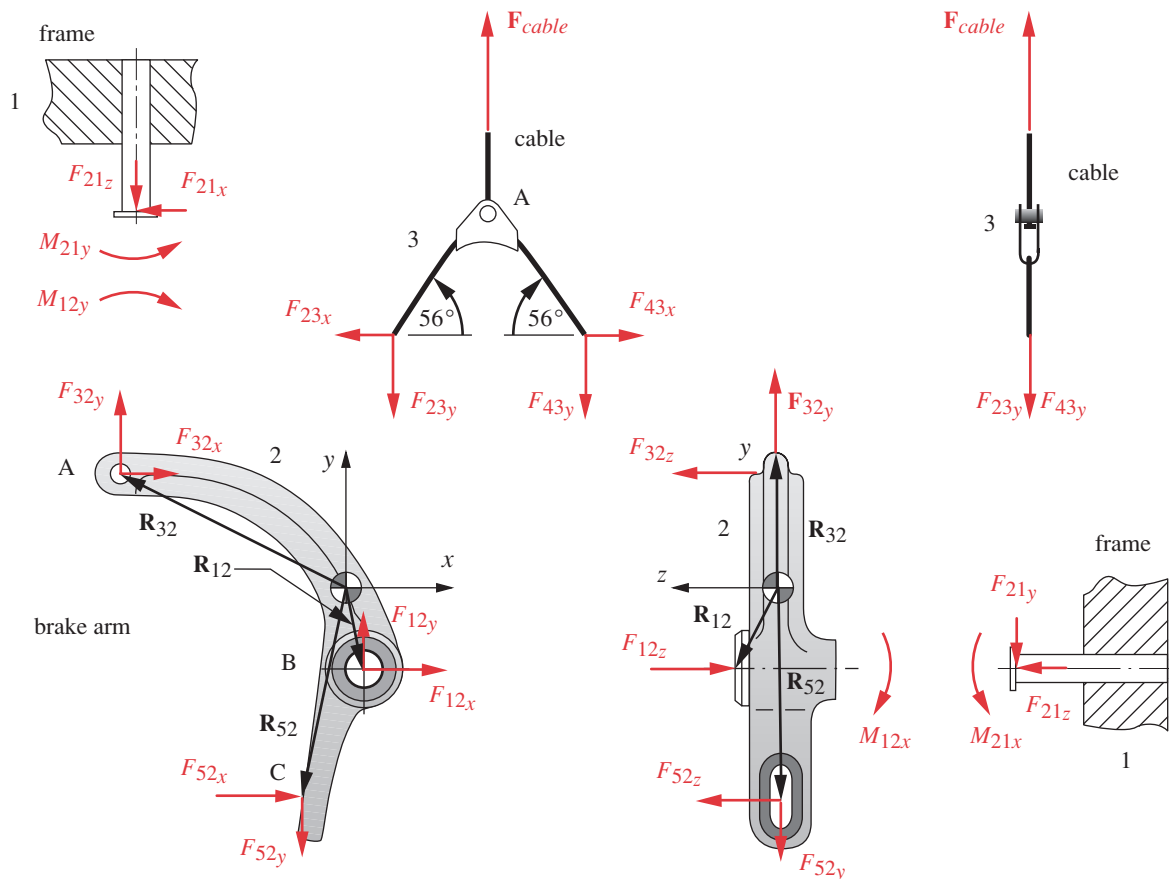


FIGURE 3-10

Brake Arm Free-Body Diagrams

This equation set can be easily solved to yield

$$\begin{aligned} F_{23y} &= F_{43y} = -\frac{F_{cable}}{2} = -\frac{1046}{2} = -523 \text{ N} \\ F_{23x} &= \frac{F_{23y}}{\tan(56^\circ)} = \frac{-523}{1.483} = -353 \text{ N} \\ F_{43x} &= -F_{23x} = 353 \text{ N} \end{aligned} \quad (b)$$

Newton's third law relates these forces to their reactions on the brake arm at point A:

$$\begin{aligned} F_{32x} &= -F_{23x} = 353 \text{ N} \\ F_{32y} &= -F_{23y} = 523 \text{ N} \\ F_{32z} &= 0 \end{aligned} \quad (c)$$

5 We can now write equations 3.3a for the arm (link 2).

For the forces:

$$\begin{aligned} \sum F_x &= F_{12x} + F_{32x} + F_{52x} = 0; & F_{12x} + F_{52x} &= -353 \\ \sum F_y &= F_{12y} + F_{32y} + F_{52y} = 0; & F_{12y} + F_{52y} &= -523 \\ \sum F_z &= F_{12z} + F_{32z} + F_{52z} = 0; & F_{12z} + F_{52z} &= 0 \end{aligned} \quad (d)$$

For the moments:

$$\begin{aligned} \sum M_x &= M_{12x} + (R_{12y}F_{12z} - R_{12z}F_{12y}) + (R_{32y}F_{32z} - R_{32z}F_{32y}) \\ &\quad + (R_{52y}F_{52z} - R_{52z}F_{52y}) = 0 \\ \sum M_y &= M_{12y} + (R_{12z}F_{12x} - R_{12x}F_{12z}) + (R_{32z}F_{32x} - R_{32x}F_{32z}) \\ &\quad + (R_{52z}F_{52x} - R_{52x}F_{52z}) = 0 \\ \sum M_z &= (R_{12x}F_{12y} - R_{12y}F_{12x}) + (R_{32x}F_{32y} - R_{32y}F_{32x}) \\ &\quad + (R_{52x}F_{52y} - R_{52y}F_{52x}) = 0 \end{aligned} \quad (e)$$

Note that all unknown forces and moments are initially assumed positive in the equations, regardless of their apparent directions on the FBDs. The moments M_{12x} and M_{12y} are due to the fact that there is a moment joint between the arm (2) and the pivot pin (1) about the x and y axes. We assume negligible friction about the z axis, thus allowing M_{12z} to be zero.

6 The joint between the brake pad (5) and the wheel rim (6) transmits a force normal to the plane of contact. The friction force magnitude, F_f , in the contact plane is related to the normal force by the Coulomb friction equation,

$$F_f = \mu N \quad (f)$$

where μ is the coefficient of friction and N is the normal force. The velocity of the point on the rim below the center of the brake pad is in the z direction. The force components F_{52x} and F_{52y} are due entirely to the normal force being transmitted through the pad to the arm and are therefore related by Newton's third law.

$$\begin{aligned} F_{52x} &= -N_x = -N \cos \theta = -N \cos 172^\circ = 0.990N \\ F_{52y} &= -N_y = -N \sin \theta = -N \sin 172^\circ = -0.139N \end{aligned} \quad (g)$$

The direction of the friction force F_f must always oppose motion and thus it acts in the negative z direction on the wheel rim. Its reaction force on the arm has the opposite sense.

$$F_{52z} = -F_f \quad (h)$$

- 7 We now have 10 equations (in the sets labeled d, e, f, g , and h) containing 10 unknowns: $F_{12x}, F_{12y}, F_{12z}, F_{52x}, F_{52y}, F_{52z}, M_{12x}, M_{12y}, N$, and F_f . Forces F_{32x}, F_{32y} , and F_{32z} are known from equations c . These 10 equations can be solved simultaneously either by matrix reduction or by iterative root-finding methods. First arrange the equations with all unknowns on the left and all known or assumed values on the right.

$$\begin{aligned} F_{12x} + F_{52x} &= -353 \\ F_{12y} + F_{52y} &= -523 \\ F_{12z} + F_{52z} &= 0 \\ M_{12x} + R_{12y}F_{12z} - R_{12z}F_{12y} + R_{52y}F_{52z} - R_{52z}F_{52y} &= R_{32z}F_{32y} - R_{32y}F_{32z} \\ M_{12y} + R_{12z}F_{12x} - R_{12x}F_{12z} + R_{52z}F_{52x} - R_{52x}F_{52z} &= R_{32x}F_{32z} - R_{32z}F_{32x} \quad (i) \\ R_{12x}F_{12y} - R_{12y}F_{12x} + R_{52x}F_{52y} - R_{52y}F_{52x} &= R_{32y}F_{32x} - R_{32x}F_{32y} \\ F_f - \mu N &= 0 \\ F_{52x} + N \cos \theta &= 0 \\ F_{52y} + N \sin \theta &= 0 \\ F_{52z} + F_f &= 0 \end{aligned}$$

- 8 Substitute the known and assumed values from Table 3-5 part 1:

$$\begin{aligned} F_{12x} + F_{52x} &= -353 \\ F_{12y} + F_{52y} &= -523 \\ F_{12z} + F_{52z} &= 0 \\ M_{12x} - 27.2F_{12z} - 23.1F_{12y} - 69.7F_{52z} - 0F_{52y} &= 0(523) - 38.7(0) = 0 \\ M_{12y} + 23.1F_{12x} - 5.2F_{12z} + 0F_{52x} + 13F_{52z} &= -75.4(0) - 0(353) = 0 \quad (j) \\ 5.2F_{12y} + 27.2F_{12x} - 13F_{52y} + 69.7F_{52x} &= 38.7(353) + 75.4(523) = 53\,095 \\ F_f - 0.4N &= 0 \\ F_{52x} - 0.990N &= 0 \\ F_{52y} + 0.139N &= 0 \\ F_{52z} + F_f &= 0 \end{aligned}$$

- 9 Form the matrices for solution.

Table 3-5 - part 1

Case Study 4A
Given and Assumed Data

Variable	Value	Unit
μ	0.4	none
θ	172.0	deg
R_{12x}	5.2	mm
R_{12y}	-27.2	mm
R_{12z}	23.1	mm
R_{32x}	-75.4	mm
R_{32y}	38.7	mm
R_{32z}	0.0	mm
R_{52x}	-13.0	mm
R_{52y}	-69.7	mm
R_{52z}	0.0	mm
F_{32x}	353.0	N
F_{32y}	523.0	N
F_{32z}	0.0	N
M_{12z}	0.0	N-m

Table 3-5 - part 2Case Study 4A
Calculated Data

Variable	Value	Unit
F_{12x}	-1 805	N
F_{12y}	-319	N
F_{12z}	587	N
F_{52x}	1 452	N
F_{52y}	-204	N
F_{52z}	-587	N
M_{12x}	32 304	N-mm
M_{12y}	52 370	N-mm
N	1 467	N
F_f	587	N

$$\begin{bmatrix} 1 & 0 & 0 & 1 & 0 & 0 & 0 & 0 & 0 \\ 0 & 1 & 0 & 0 & 1 & 0 & 0 & 0 & 0 \\ 0 & 0 & 1 & 0 & 0 & 1 & 0 & 0 & 0 \\ 0 & -23.1 & -27.2 & 0 & 0 & -69.7 & 1 & 0 & 0 \\ 23.1 & 0 & -5.2 & 0 & 0 & 13 & 0 & 1 & 0 \\ 27.2 & 5.2 & 0 & 69.7 & -13 & 0 & 0 & 0 & 0 \\ 0 & 0 & 0 & 0 & 0 & 0 & 0 & 0 & 1 \\ 0 & 0 & 0 & 1 & 0 & 0 & 0 & 0 & -0.4 \\ 0 & 0 & 0 & 0 & 1 & 0 & 0 & 0 & 0.139 \\ 0 & 0 & 0 & 0 & 0 & 1 & 0 & 0 & 1 \end{bmatrix} \times \begin{bmatrix} F_{12x} \\ F_{12y} \\ F_{12z} \\ F_{52x} \\ F_{52y} \\ F_{52z} \\ M_{12x} \\ M_{12y} \\ F_f \\ N \end{bmatrix} = \begin{bmatrix} -353 \\ -523 \\ 0 \\ 0 \\ 0 \\ 53 095 \\ 0 \\ 0 \\ 0 \\ 0 \end{bmatrix} \quad (k)$$

- 10 Table 3-5 part 2 shows the solution to this problem from program MATRIX for the given data in Table 3-5 part 1. This problem can be solved using any one of several commercial equation-solver programs such as *Mathcad*, *MATLAB*, *Maple*, *Mathematica* or with the program **MATRIX** provided with the text.

3.6 DYNAMIC LOADING CASE STUDY

This section presents a case study involving two-dimensional dynamic loading on a four-bar linkage designed as a dynamic-load demonstration device. A photograph of this machine is shown in Figure 3-11. This machine can be analyzed in two dimensions since all elements move in parallel planes. The presence of significant accelerations on the moving elements in a system requires that a dynamic analysis be done with equations 3.1. The approach is identical to that used in the preceding static load analyses except for the need to include the mA and $I\alpha$ terms in the equations.

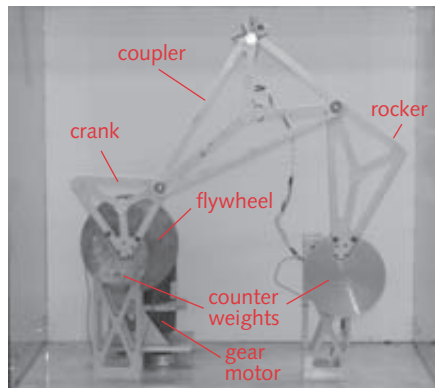
CASE STUDY 5A

Fourbar Linkage Loading Analysis

Problem: Determine the theoretical rigid-body forces acting in two dimensions on the fourbar linkage shown in Figure 3-11.

Given: The linkage geometry, masses, and mass moments of inertia are known and the linkage is driven at up to 120 rpm by a speed-controlled electric motor.

Assumptions: The accelerations are significant. A Class 4 load model is appropriate and a dynamic analysis is required. There are no external loads on the system; all loads are due to the accelerations of the links. The weight forces are insignificant compared to the inertial forces and will be neglected. The links are assumed to be ideal rigid bodies. Friction and the effects of clearances in the pin joints also will be ignored.

**FIGURE 3-11**

Fourbar Linkage Dynamic Model

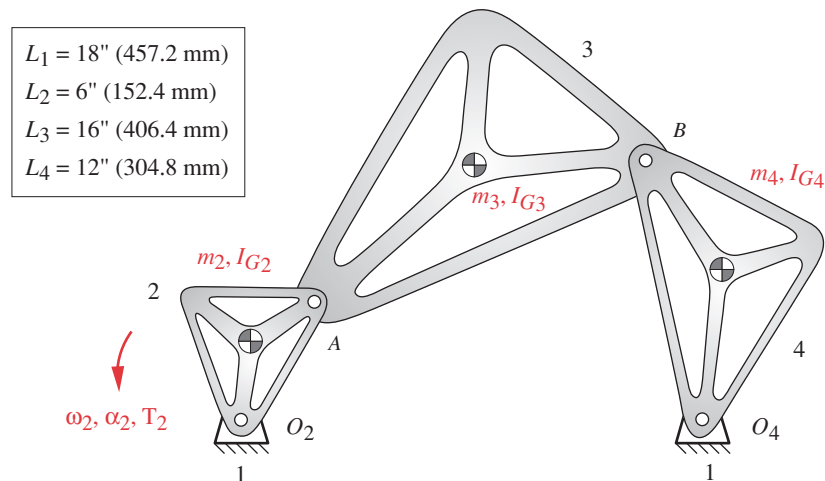
Solution: See Figures 3-11 through 3-13 and Table 3-6.

- Figures 3-11 and 3-12 show the fourbar linkage demonstrator model. It consists of three moving elements (links 2, 3, and 4) plus the frame or ground link (1). The motor drives link 2 through a gearbox. The two fixed pivots are instrumented with piezoelectric force transducers to measure the dynamic forces acting in x and y directions on the ground plane. A pair of accelerometers is mounted to a point on the floating coupler (link 3) to measure its accelerations.
- Figure 3-12 shows a schematic of the linkage. The links are designed with lightening holes to reduce their masses and mass moments of inertia. The input to link 2 can be an angular acceleration, a constant angular velocity, or an applied torque. Link 2 rotates fully about its fixed pivot at O_2 . Even though link 2 may have a zero angular acceleration α_2 , if run at constant angular velocity ω_2 , there will still be time-varying angular accelerations on links 3 and 4 since they oscillate back and forth. In any case, the CGs of the links will experience time-varying linear accelerations as the linkage moves. These angular and linear accelerations will generate inertia forces and torques

Table 3-6 - part 1Case Study 5A
Given and Assumed Data

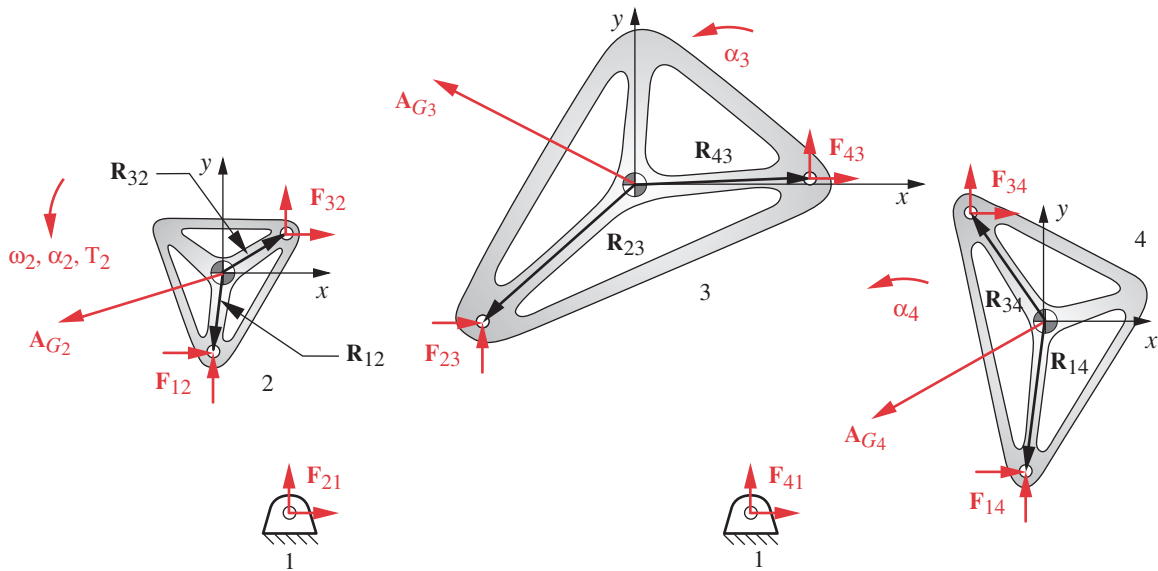
Variable	Value	Unit
θ_2	30.00	deg
ω_2	120.00	rpm
$mass_2$	0.525	kg
$mass_3$	1.050	kg
$mass_4$	1.050	kg
I_{cg2}	0.057	$kg \cdot m^2$
I_{cg3}	0.011	$kg \cdot m^2$
I_{cg4}	0.455	$kg \cdot m^2$
R_{12x}	-46.9	mm
R_{12y}	-71.3	mm
R_{32x}	85.1	mm
R_{32y}	4.9	mm
R_{23x}	-150.7	mm
R_{23y}	-177.6	mm
R_{43x}	185.5	mm
R_{43y}	50.8	mm
R_{14x}	-21.5	mm
R_{14y}	-100.6	mm
R_{34x}	-10.6	mm
R_{34y}	204.0	mm

3

**FIGURE 3-12**

Fourbar Linkage Schematic and Basic Dimensions (See Table 3-6 for more information)

3

**FIGURE 3-13**

Free-Body Diagrams of Elements in a Fourbar Linkage

as defined by Newton's second law. Thus, even with no external forces or torques applied to the links, the inertial forces will create reaction forces at the pins. It is these forces that we wish to calculate.

- 3 Figure 3-13 shows the free-body diagrams of the individual links. The local, nonrotating, coordinate system for each link is set up at its CG. The kinematic equations of motion must be solved to determine the linear accelerations of the CG of each link and the link's angular acceleration for every position of interest during the cycle. (See reference 1 for an explanation of this procedure.) These accelerations, A_{Gn} and α_n , are shown acting on each of the n links. The forces at each pin connection are shown as xy pairs, numbered as before, and are initially assumed to be positive.
- 4 Equations 3.1 can be written for each moving link in the system. The masses and the mass moments of inertia of each link about its CG must be calculated for use in these equations. In this case study, a solid modeling CAD system was used to design the links' geometries and to calculate their mass properties.

- 5 For link 2:

$$\begin{aligned}\sum F_x &= F_{12x} + F_{32x} = m_2 A_{G2_x} \\ \sum F_y &= F_{12y} + F_{32y} = m_2 A_{G2_y} \\ \sum M_z &= T_2 + (R_{12x}F_{12y} - R_{12y}F_{12x}) + (R_{32x}F_{32y} - R_{32y}F_{32x}) = I_{G2}\alpha_2\end{aligned}\quad (a)$$

- 6 For link 3:

$$\begin{aligned}\sum F_x &= F_{12x} + F_{32x} = m_2 A_{G3_x} \\ \sum F_y &= F_{12y} + F_{32y} = m_2 A_{G3_y} \\ \sum M_z &= T_3 + (R_{12x}F_{12y} - R_{12y}F_{12x}) + (R_{32x}F_{32y} - R_{32y}F_{32x}) = I_{G3}\alpha_3\end{aligned}\quad (a)$$

7 For link 4:

$$\begin{aligned}\sum F_x &= F_{14x} + F_{34x} = m_4 A_{G4_x} \\ \sum F_y &= F_{14y} + F_{34y} = m_4 A_{G4_y} \\ \sum M_z &= (R_{14x}F_{14y} - R_{14y}F_{14x}) + (R_{34x}F_{34y} - R_{34y}F_{34x}) = I_{G4}\alpha_4\end{aligned}\quad (c)$$

8 There are 13 unknowns in these nine equations: F_{12x} , F_{12y} , F_{32x} , F_{32y} , F_{23x} , F_{23y} , F_{43x} , F_{43y} , F_{14x} , F_{14y} , F_{34x} , F_{34y} , and T_2 . Four third-law equations can be written to equate the action-reaction pairs at the joints.

$$\begin{aligned}F_{32x} &= -F_{23x} \\ F_{32y} &= -F_{23y} \\ F_{34x} &= -F_{43x} \\ F_{34y} &= -F_{43y}\end{aligned}\quad (d)$$

9 The set of thirteen equations in *a* through *d* can be solved simultaneously to determine the forces and driving torque either by matrix reduction or by iterative root-finding methods. This case study was solved by both techniques and files for both are on the CD. Note that the masses and mass moments of inertia of the links are constant with time and position, but the accelerations are time-varying. Thus, a complete analysis requires that equations *a-d* be solved for all positions or time steps of interest. The models use *lists* or *arrays* to store the calculated values from equations *a-d* for 13 values of the input angle θ_2 of the driving link (0 to 360° by 30° increments). The model also calculates the kinematic accelerations of the links and their CGs which are needed for the force calculations. The largest and smallest forces present on each link during the cycle can then be determined for use in later stress and deflection analyses. The given data and results of this force analysis for one crank position ($\theta_2 = 30^\circ$) are shown in Table 3-6, parts 1 and 2. Plots of the forces at the fixed pivots for one complete revolution of the crank are shown in Figure 3-14.

Table 3-6 - part 2

Case Study 5A
Calculated Data

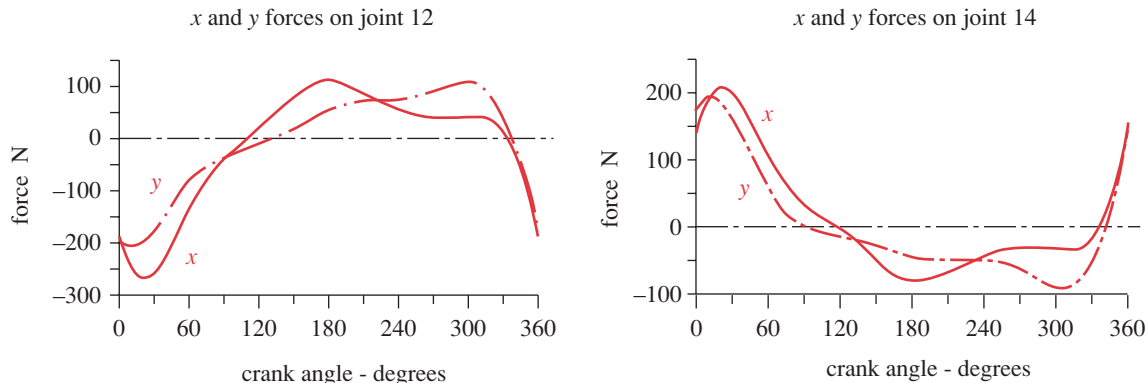
Variable	Value	Unit
F_{12x}	-255.8	N
F_{12y}	-178.1	N
F_{32x}	252.0	N
F_{32y}	172.2	N
F_{34x}	-215.6	N
F_{34y}	-163.9	N
F_{14x}	201.0	N
F_{14y}	167.0	N
F_{43x}	215.6	N
F_{43y}	163.9	N
F_{23x}	-252.0	N
F_{23y}	-172.2	N
T_{12}	-3.55	N-m
α_3	56.7	rad/sec ²
α_4	138.0	rad/sec ²
A_{cg2x}	-7.4	rad/sec ²
A_{cg2y}	-11.3	rad/sec ²
A_{cg3x}	-34.6	rad/sec ²
A_{cg3y}	-7.9	rad/sec ²
A_{cg4x}	-13.9	rad/sec ²
A_{cg4y}	2.9	rad/sec ²

3

3.7 VIBRATION LOADING

In systems that are dynamically loaded, there will usually be vibration loads superimposed on the theoretical loads predicted by the dynamic equations. These vibration loads can be due to a variety of causes. If the elements in the system were infinitely stiff, then vibrations would be eliminated. But all real elements, of any material, have elasticity and thus act as springs when subjected to forces. The resulting deflections can cause additional forces to be generated from the inertial forces associated with the vibratory movements of elements or, if clearances allow contact of mating parts, to generate impact (shock) loads (see below) during their vibrations.

A complete discussion of vibration phenomena is beyond the scope of this text and will not be attempted here. References are provided in the bibliography at the end of this chapter for further study. The topic is introduced here mainly to alert the machine designer to the need to consider vibration as a source of loading. Often the only way to get an accurate measure of the effects of vibration on a system is to do testing of prototypes or production systems under service conditions. The discussion of safety fac-

**FIGURE 3-14**

Calculated Rigid-Body Dynamic Forces in the Fourbar Linkage of Case Study 5A

tors in Section 1.7 mentioned that many industries (automotive, aircraft, etc.) engage in extensive test programs to develop realistic loading models of their equipment. This topic will be discussed further in Section 6.4 when fatigue loading is introduced. Modern finite element (FEA) and boundary element (BEA) analysis techniques also allow vibration effects on a system or structure to be modeled and calculated. It is still difficult to obtain a computer model of a complex system that is as accurate as a real, instrumented prototype. This is especially true when clearances (gaps) between moving parts allow impacts to occur in the joints when loads reverse. Impacts create nonlinearities which are very difficult to model mathematically.

Natural Frequency

When designing machinery, it is desirable to determine the natural frequencies of the assembly or subassemblies in order to predict and avoid resonance problems in operation. Any real system can have an infinite number of natural frequencies at which it will readily vibrate. The number of natural frequencies that are necessary or desirable to calculate will vary with the situation. The most complete approach to the task is to use Finite Element Analysis (FEA) to break the assembly into a large number of discrete elements. See Chapter 8 for more information on FEA. The stresses, deflections, and number of natural frequencies that can be calculated by this technique are mainly limited by time and the computer resources available.

If not using FEA, we would like to determine, at a minimum, the system's lowest, or fundamental, natural frequency, since this frequency will usually create the largest magnitude of vibrations. The undamped fundamental natural frequency ω_n , with units of rad/sec, or f_n , with units of Hz, can be computed from the expressions

$$\omega_n = \sqrt{\frac{k}{m}} \quad (3.4)$$

$$f_n = \frac{1}{2\pi} \omega_n$$

where ω_n is the fundamental natural frequency, m is the moving mass of the system in true mass units (e.g., kg, g, blob, or slug, not lb_m), and k is the effective spring constant of the system. (The period of the natural frequency is its reciprocal in seconds, $T_n = 1/f_n$.)

Equation 3.4 is based on a single-degree-of-freedom, lumped model of the system. Figure 3-15 shows such a model of a simple cam-follower system consisting of a cam, a sliding follower, and a return spring. The simplest lumped model consists of a mass connected to ground through a single spring and a single damper. All the moving mass in the system (follower, spring) is contained in m and all the “spring” including the physical spring and the springiness of all other parts is lumped in the effective spring constant k .

SPRING CONSTANT A spring constant k is an assumed linear relationship between the force, F , applied to an element and its resulting deflection δ (see Figure 3-17):

$$k = \frac{F}{\delta} \quad (3.5a)$$

If an expression for the deflection of an element can be found or derived, it will provide this spring-constant relationship. This topic is revisited in the next chapter. In the example of Figure 3-15, the spring deflection δ is equal to the displacement y of the mass.

$$k = \frac{F}{y} \quad (3.5b)$$

DAMPING All the damping, or frictional, losses are lumped in the damping coefficient d . For this simple model, damping is assumed to be inversely proportional to the velocity y_{dot} of the mass.

$$d = \frac{F}{\dot{y}} \quad (3.6)$$

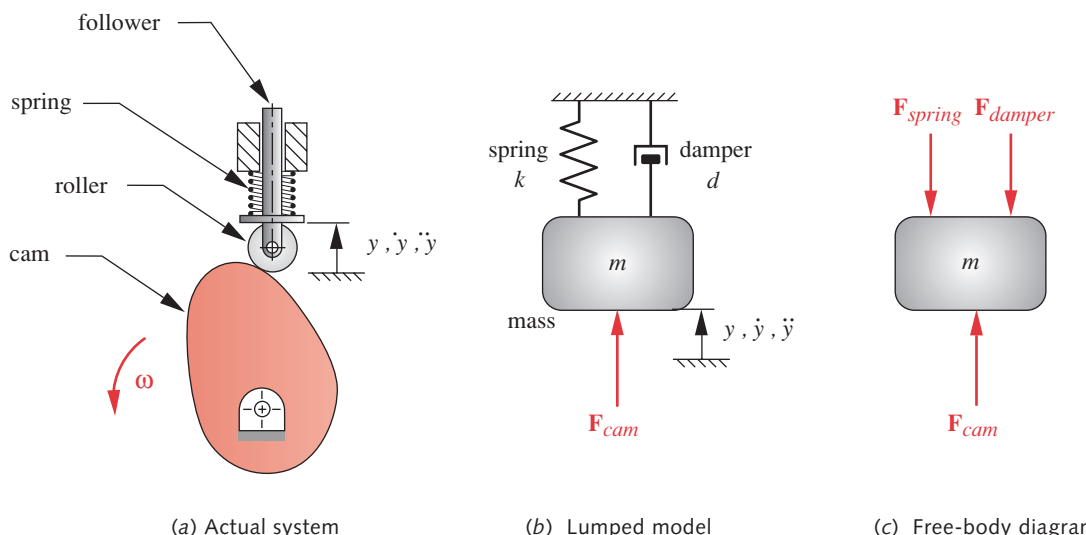


FIGURE 3-15

Lumped Model of a Cam-Follower Dynamic System

Equation 3.4 simplifies this model even further by assuming the damping d to be zero. If damping is included, the expressions for the fundamental, damped natural frequency ω_d with units of radians/sec, or f_d , with units of Hz, become

$$\begin{aligned}\omega_d &= \sqrt{\frac{k}{m} - \left(\frac{d}{2m}\right)^2} \\ f_d &= \frac{1}{2\pi} \omega_d\end{aligned}\quad (3.7)$$

This damped frequency ω_d will be slightly lower than the undamped frequency ω_n .

EFFECTIVE VALUES Determining the effective mass for a lumped model is straightforward and requires only summing all the values of the connected, moving masses in appropriate mass units. Determining the values of the effective spring constant and the effective damping coefficient is more complicated and will not be addressed here. See reference 2 for an explanation.

RESONANCE A condition called resonance can be experienced if the operating or forcing frequency applied to the system is the same as any one of its natural frequencies. That is, if the input angular velocity applied to a rotating system is the same as, or close to, ω_n , the vibratory response will be very large. This can create large forces and cause failure. Thus it is necessary to avoid operation at or near the natural frequencies if possible.

Dynamic Forces

If we write equation 3.1 for the simple, one-DOF model of the dynamic system in Figure 3-15 and substitute equations 3.5 and 3.6, we get

$$\begin{aligned}\sum F_y &= ma = m\ddot{y} \\ F_{cam} - F_{spring} - F_{damper} &= m\ddot{y} \\ F_{cam} &= m\ddot{y} + d\dot{y} + ky\end{aligned}\quad (3.8)$$

If the kinematic parameters of displacement, velocity, and acceleration are known for the system, this equation can be solved directly for the force on the cam as a function of time. If the cam force is known and the kinematic parameters are desired, then the well-known solution to this linear, constant-coefficient differential equation can be applied. See reference 3 for a detailed derivation of that solution. Though the coordinate system used for a dynamic analysis can be arbitrarily chosen, it is important to note that both the kinematic parameters (displacement, velocity, and acceleration) and the forces in equation 3.8 must be defined in the **same** coordinate system.

As an example of the effect of vibration on the dynamic forces of a system, we now revisit the fourbar linkage of Case Study 5A and see the results of actual measurements of dynamic forces under operating conditions.

C A S E S T U D Y 5 B**Fourbar Linkage Dynamic Loading Measurement**

Problem: Determine the actual forces acting on the fixed pivots of the fourbar linkage in Figure 3-11 (p. 99) during one revolution of the input crank.

3

Given: The linkage is driven at 60 rpm by a speed-controlled electric motor, and force transducers are placed between the fixed pivot bearings and the ground plane.

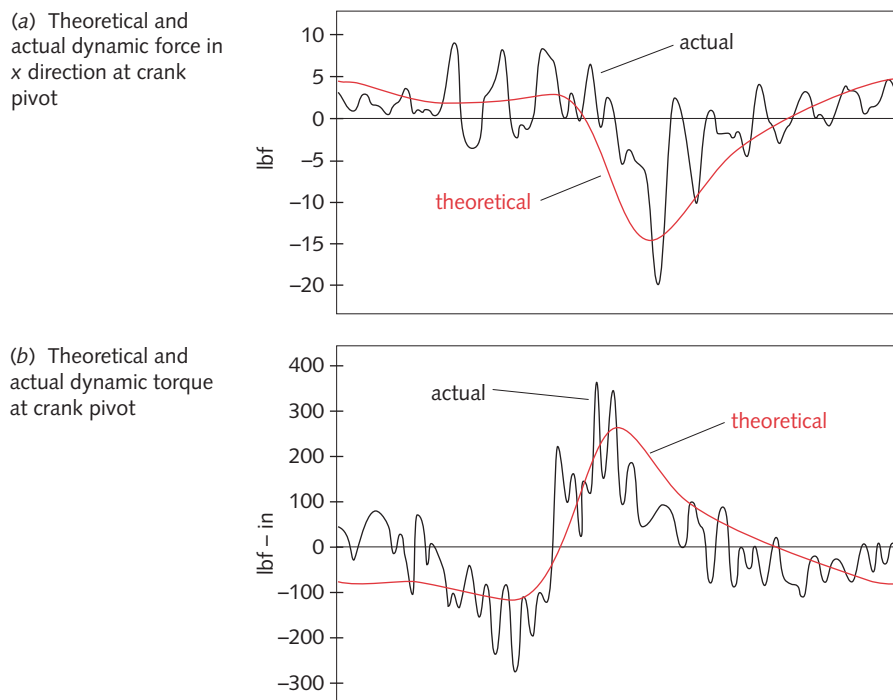
Assumptions: There are no applied external loads on the system; all loads are due to the accelerations of the links. The weight forces are insignificant compared to the inertial forces and will be neglected. The force transducers measure only dynamic forces.

Solution: See Figures 3-12 (p. 99) and 3-16 (p. 106).

- 1 Figure 3-11 shows the fourbar linkage. It consists of three moving elements (links 2, 3, and 4) plus the frame or ground link (1). The shock-mounted motor drives link 2 through a gearbox and shaft coupling. The two fixed pivots are instrumented with piezoelectric force transducers to measure the dynamic forces acting in x and y directions on the ground plane.
- 2 Figure 3-16 shows an actual force and torque measured while the linkage was running at 60 rpm and compares them to the theoretical force and torque predicted by equations *a-d* in Case Study 5A.^[5] Only the x component of force at the pivot between link 2 and the ground and the torque on link 2 are shown as examples. The other pin forces and components show similar deviations from their predicted theoretical values. Some of these deviations are due to variations in instantaneous angular velocity of the drive motor. The theoretical analysis assumes constant input shaft velocity. Vibrations and impacts account for other deviations.

This example of deviations from theoretical forces in a very simple dynamic system is presented to point out that our best calculations of forces (and thus the resulting stresses) on a system may be in error due to factors not included in a simplified force analysis. It is common for the theoretical predictions of forces in a dynamic system to underestimate reality, which is, of course, a nonconservative result. Wherever feasible, the testing of physical prototypes will give the most accurate and realistic results.

The effects of vibration on a system can cause significant loadings and are difficult to predict without test data of the sort shown in Figure 3-16, where the actual loads are seen to be double their predicted values; this will obviously double the stresses. A traditional, and somewhat crude, approach used in machine design has been to apply overload factors to the theoretical calculated loads based on experience with the same or similar equipment. As an example, see Table 12-17 (p. 715) in the chapter on spur-gear design. This table lists industry-recommended overload factors for gears subjected to various types of shock loading. These sorts of factors should be used only if one cannot develop more accurate test data of the type shown in Figure 3-16 (p. 106).

**FIGURE 3-16**

Theoretical and Measured Dynamic Forces and Torques in a Fourbar Linkage

3.8 IMPACT LOADING

The loading considered so far has either been static or, if time-varying, has been assumed to be gradually and smoothly applied, with all mating parts continually in contact. Many machines have elements that are subjected to sudden loads or impacts. One example is the crank-slider mechanism which forms the heart of an automobile engine. The piston head is subjected to an explosive rise in pressure every two crank revolutions when the cylinder fires, and the clearance between the circumference of the piston and the cylinder wall can allow an impact of these surfaces as the load is reversed each cycle. A more extreme example is a jackhammer, whose purpose is to impact pavement and break it up. The loads that result from impact can be much greater than those that would result from the same elements contacting gradually. Imagine trying to drive a nail by gently placing the hammer head on the nail rather than by striking it.

What distinguishes impact loading from static loading is the time duration of the application of the load. If the load is applied slowly, it is considered static; if applied rapidly, then it is impact. One criterion used to distinguish the two is to compare the time of load application t_l (defined as the time it takes the load to rise from zero to its peak value) to the period of the natural frequency T_n of the system. If t_l is less than half T_n , it is considered to be impact. If t_l is greater than three times T_n , it is considered static. Between those limits is a gray area in which either condition can exist.

Two general cases of impact loading are considered to exist, though we will see that one is just a limiting case of the other. Burr^[6] calls these two cases *striking impact* and

force impact. **Striking impact** refers to an actual collision of two bodies, such as in hammering or the taking up of clearance between mating parts. **Force impact** refers to a suddenly applied load with no velocity of collision, as in a weight suddenly being taken up by a support. This condition is common in friction clutches and brakes (see Chapter 17). These cases can occur independently or in combination.

Severe collisions between moving objects can result in permanent deformation of the colliding bodies as in an automobile accident. In such cases the permanent deformation is desirable in order to absorb the large amount of energy of the collision and protect the occupants from more severe harm. We are concerned here only with impacts that do not cause permanent deformation; that is, the stresses will remain in the elastic region. This is necessary to allow continued use of the component after impact.

If the mass of the striking object m is large compared to that of the struck object m_b and if the striking object can be considered rigid, then the kinetic energy possessed by the striking object can be equated to the energy stored elastically in the struck object at its maximum deflection. This energy approach gives an **approximate value** for the impact loading. It is not exact because it assumes that the stresses throughout the impacted member reach peak values at the same time. However, waves of stress are set up in the struck body, travel through it at the speed of sound, and reflect from the boundaries. Calculating the effects of these longitudinal waves on the stresses in elastic media gives exact results and is necessary when the ratio of mass of the striking object to that of the struck object is small. The wave method will not be discussed here. The reader is directed to reference 6 for further information.

Energy Method

The kinetic energy of the striking body will be converted to stored potential energy in the struck body, assuming that no energy is lost to heat. If we assume that all particles of the combined bodies come to rest at the same instant, then just before rebound, the force, stress, and deflection in the struck body will be maximal. The elastic energy stored in the struck body will be equal to the area under the force-deflection curve defined by its particular spring constant. A generalized force-deflection curve for a linear spring element is shown in Figure 3-17. The elastic energy stored is the area under the curve between zero and any combination of force and deflection. Because of the linear relationship, this is the area of a triangle, $A = 1/2bh$. Thus, the energy stored at the point of peak impact deflection, δ_i , is

$$E = \frac{1}{2} F_i \delta_i \quad (3.9a)$$

Substituting equation 3.5 gives

$$E = \frac{F_i^2}{2k} \quad (3.9b)$$

HORIZONTAL IMPACT Figure 3-18a shows a mass about to impact the end of a horizontal rod. This device is sometimes called a *slide hammer* and is used to remove dents from automobile sheet metal among other uses. At the point of impact, the portion of the kinetic energy of the moving mass that is imparted to the struck mass is

$$E = \eta \left(\frac{1}{2} m v_i^2 \right) \quad (3.10)$$

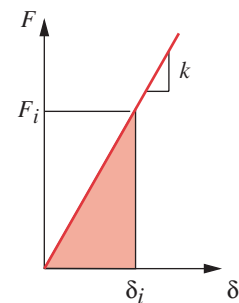


FIGURE 3-17

Energy Stored in a Spring

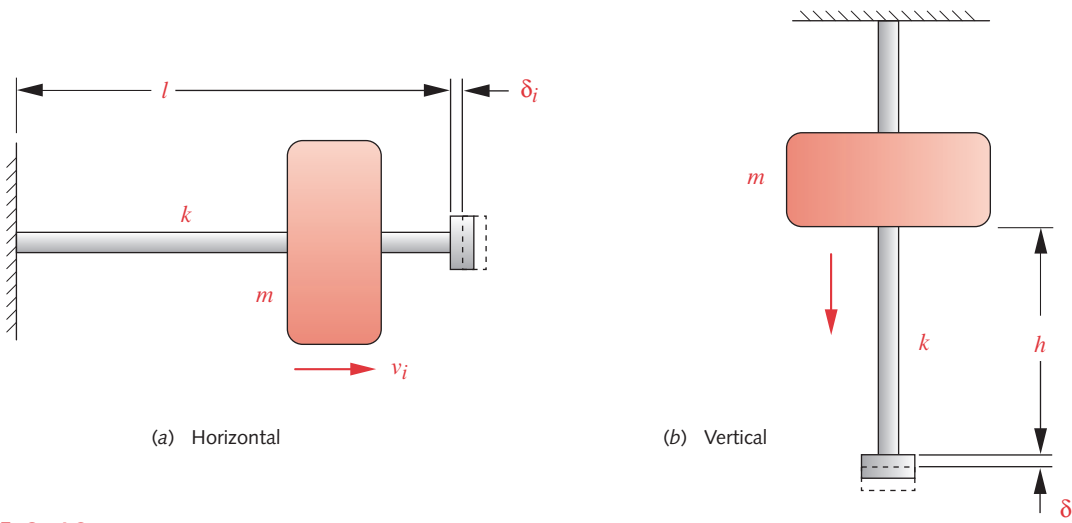


FIGURE 3-18

Axial Impact on a Slender Rod

where m is its mass and v_i its velocity at impact. We need to modify the kinetic energy term by a correction factor η to account for the energy dissipation associated with the particular type of elastic member being struck. If the dissipation is negligible, η will be 1.

Assuming that all the kinetic energy transferred from the moving mass is converted to elastic energy stored in the struck member allows us to equate equations 3.9 and 3.10:

$$\frac{F_i^2}{2k} = \eta \frac{mv_i^2}{2}$$

$$F_i = v_i \sqrt{\eta mk} \quad (3.11)$$

If the mass were allowed to statically load the struck member, the resulting static deflection would be $\delta_{st} = W/k$ where $W = mg$. Substituting these into equation 3.11 gives a ratio of dynamic force to static force or dynamic deflection to static deflection:

$$\frac{F_i}{W} = \frac{\delta_i}{\delta_{st}} = v_i \sqrt{\frac{\eta}{g\delta_{st}}} \quad (3.12)$$

The term on the right side of this equation is called the impact factor which provides a ratio of impact to static force or deflection. Thus if the static deflection can be calculated for the application of a force equal to the weight of the mass, an estimate of the dynamic force and dynamic deflection can be obtained. Note that equations 3.11 and 3.12 are valid for any case of horizontal impact, whether the object is loaded axially as shown here, in bending, or in torsion. Methods for calculating the deflections of various cases are addressed in the next chapter. The spring rate k for any object can be found by rearranging its deflection equation according to equation 3.5.

VERTICAL IMPACT For the case of a mass falling through a distance h onto a rod as shown in Figure 3-18b, equation 3.11 also applies with the impact velocity $v_i^2 = 2gh$. The potential energy for a drop through distance h is:

$$E = \eta \frac{mv_i^2}{2} = \eta mgh = W\eta h \quad (3.13a)$$

If the deflection at impact is small compared to the drop distance h , this equation is sufficient. But, if the deflection is significant compared to h , the energy of impact needs to include an amount due to the deflection through which the weight falls beyond h . The total potential energy given up by the mass on impact is then

$$E = W\eta h + W\delta_i = W(\eta h + \delta_i) \quad (3.13b)$$

Equate this potential energy to the elastic energy stored in the struck member and substitute equation 3-9b and the expression $W = k\delta_{st}$

$$\begin{aligned} \frac{F_i^2}{2k} &= W(\eta h + \delta_i) \\ F_i^2 &= 2kW(\eta h + \delta_i) = 2\frac{W}{\delta_{st}}W(\eta h + \delta_i) \\ \left(\frac{F_i}{W}\right)^2 &= \frac{2\eta h}{\delta_{st}} + \frac{\delta_i}{\delta_{st}} = \frac{2\eta h}{\delta_{st}} + 2\left(\frac{F_i}{W}\right) \\ \left(\frac{F_i}{W}\right)^2 - 2\left(\frac{F_i}{W}\right) &- \frac{2\eta h}{\delta_{st}} = 0 \end{aligned} \quad (3.14a)$$

giving a quadratic equation in F_i/W whose solution is:

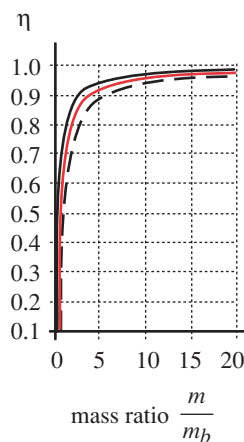
$$\frac{F_i}{W} = \frac{\delta_i}{\delta_{st}} = 1 + \sqrt{1 + \frac{2\eta h}{\delta_{st}}} \quad (3.14b)$$

The right side expression is the impact ratio for the falling weight case. Equation 3-14b can be used for any impact case involving a falling weight. For example, if the weight is dropped on a beam, the static deflection of the beam at the point of impact is used.

If the distance h to which the mass is raised is set to zero, equation 3.14b becomes equal to 2. This says that if the mass is held **in contact** with the “struck” member (with the weight of the mass separately supported) and then allowed to suddenly impart its weight to that member, the dynamic force will be twice the weight. This is the case of “force impact” described earlier, in which there is no actual collision between the objects. A more accurate analysis, using wave methods, predicts that the dynamic force will be more than doubled even in this noncollision case of sudden application of load.^[6] Many designers use 3 or 4 as a more conservative estimate of this dynamic factor for the case of sudden load application. This is only a crude estimate, however, and, if possible, experimental measurements or a wave-method analysis should be made to determine more suitable dynamic factors for any particular design.

Burr derives the correction factors η for several impact cases in reference 6. Roark and Young provide factors for additional cases in reference 7. For the case of a mass axially impacting a rod as shown in Figure 3-18, the correction factor is^[6]

$$\eta = \frac{1}{1 + \frac{m_b}{3m}} \quad (3.15)$$

**FIGURE 3-19**

Correction Factor η as a Function of Mass Ratio

EXAMPLE 3-1

Impact Loading on an Axial Rod

Problem: The axial rod shown in Figure 3-18a is hit by a mass moving at 1 m/sec.

- Determine the sensitivity of the impact force to the length/diameter ratio of the rod for a constant 1-kg moving mass.
- Determine the sensitivity of the impact force to the ratio of moving mass to rod mass for a constant length/diameter ratio of 10.

Given: The round rod is 100 mm long. The rod and moving mass are steel with $E = 207 \text{ Gpa}$ and a mass density of 7.86 g/cm^3 .

Assumptions: An approximate energy method will be acceptable. The correction factor for energy dissipation will be applied.

Solution: See Figures 3-18a, 3-20, and 3-21.

- Figure 3-18a shows the system. The moving mass strikes the flange on the end of the rod with the stated velocity of 1 m/sec.
- For part (a), we will keep the moving mass constant at 1 kg, and the rod length constant at 100 mm and vary the rod diameter to obtain l/d ratios in the range of 1 to 20. In the equations that follow we will show only one calculation made for the l/d ratio of 10. We can also compute all the values for a list of l/d ratios. The static deflection that would result from application of the weight force of the mass is calculated from the expression for the deflection of a bar in tension. (See equation 4.8 in the next chapter for the derivation.)

$$\delta_{st} = \frac{Wl}{AE} = \frac{9.81 \text{ N}(100 \text{ mm})}{78.54 \text{ mm}^2(2.07E5 \text{ N/mm}^2)} = 0.06 \mu\text{m} \quad (a)$$

The correction factor η is calculated here for an assumed mass ratio of 16.2,

$$\eta = \frac{1}{1 + \frac{m_b}{3m}} = \frac{1}{1 + \frac{0.0617}{3(1)}} = 0.98 \quad (b)$$

These values (calculated for each different rod diameter d) are then substituted into equation 3.12 to find the force ratio F_i/W and the dynamic force F_i . For $d = 10 \text{ mm}$

$$\frac{F_i}{W} = v_i \sqrt{\frac{\eta}{g\delta_{st}}} = 1 \frac{\text{m}}{\text{s}} \sqrt{\frac{0.98}{9.81 \frac{\text{m}}{\text{s}^2} (0.00006 \text{m})}} = 1285.9$$

$$F_i = 1285.9(9.81 \text{N}) = 12612 \text{ N} \quad (c)$$

The variation in force ratio with changes in l/d ratio for a constant amount of moving mass and a constant impact velocity (i.e., constant input energy) is shown in Figure 3-20. As the l/d ratio is reduced, the rod becomes much stiffer and generates much larger dynamic forces from the same impact energy. This clearly shows that impact forces can be reduced by increasing the compliance of the impacted system.

- 3 For part (b), we will keep the l/d ratio constant at 10 and vary the ratio between the moving mass and the rod mass over the range of 1 to 20. The files EX03-01B on the CD-ROM calculate all values for a range of mass ratios. The results for a mass ratio of 16.2 are the same as in part (a) above. Figure 3-21a shows that the dynamic force ratio F_i/W varies inversely with the mass ratio. However, the value of the dynamic force is increasing with mass ratio as shown in Figure 3-21b, because the static force W is also increasing with mass ratio.

3.9 BEAM LOADING

A beam is any element that carries loads transverse to its long axis and may carry loads in the axial direction as well. A beam supported on pins or narrow supports at each end is said to be **simply supported**, as shown in Figure 3-22a. A beam fixed at one end and unsupported at the other is a **cantilever beam** (Figure 3-22b). A simply supported beam that overhangs its supports at either end is an **overhung beam** (Figure 3-22c). If a beam has more supports than are necessary to provide kinematic stability (i.e., make the kinematic degree of freedom zero), then the beam is said to be overconstrained or indeterminate, as shown in Figure 3-22d. An **indeterminate beam** problem cannot be solved for its loads using only equations 3.3 (p. 78). Other techniques are necessary. This problem is addressed in the next chapter.

Beams are typically analyzed as static devices, though vibrations and accelerations can cause dynamic loading. A beam may carry loads in three dimensions, in which case equations 3.3a apply. For the two-dimensional case, equations 3.3b suffice. The review examples used here are limited to 2-D cases for brevity.

Shear and Moment

A beam may be loaded with some combination of distributed and/or concentrated forces or moments as in Figure 3-22. The applied forces will create both shearing forces and bending moments in the beam. A load analysis must find the magnitudes and spatial distributions of these shear forces and bending moments on the beam. The shear forces V and the moment M in a beam are related to the loading function $q(x)$ by

$$q(x) = \frac{dV}{dx} = \frac{d^2M}{dx^2} \quad (3.16a)$$

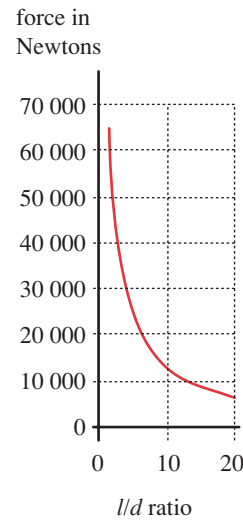
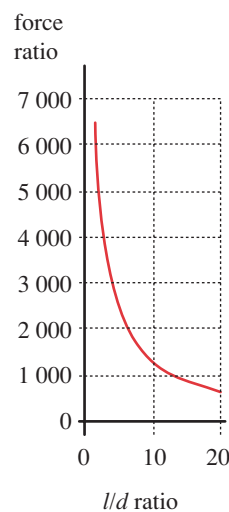
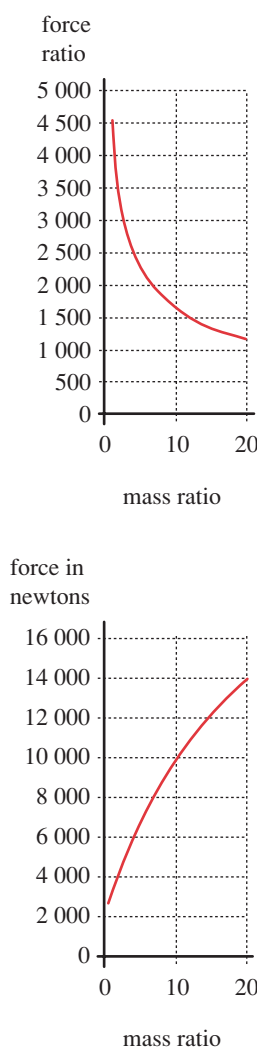


FIGURE 3-20

Dynamic Force and Force Ratio as a Function of l/d Ratio for the System in Example 3-1

**FIGURE 3-21**

Dynamic Force and Force Ratio as a Function of Mass Ratio for the System in Example 3-1

The loading function $q(x)$ is typically known and the shear V and moment M distributions can be found by integrating equation 3.16a:

$$\int_{V_A}^{V_B} dV = \int_{x_A}^{x_B} qdx = V_B - V_A \quad (3.16b)$$

Equation 3.16b shows that the difference in the shear forces between any two points, A and B , is equal to the area under the graph of the loading function, equation 3.16a.

Integrating the relationship between shear and moment gives

$$\int_{M_A}^{M_B} dM = \int_{x_A}^{x_B} Vdx = M_B - M_A \quad (3.16c)$$

showing that the difference in the moment between any two points, A and B , is equal to the area under the graph of the shear function, equation 3.16b.

SIGN CONVENTION The usual (and arbitrary) sign convention used for beams is to consider a moment positive if it causes the beam to deflect concave downward (as if to collect water). This puts the top surface in compression and the bottom surface in tension. The shear force is considered positive if it causes a clockwise rotation of the section on which it acts. These conventions are shown in Figure 3-23 and result in positive moments being created by negative applied loads. All the applied loads shown in Figure 3-22 are negative. For example, in Figure 3-22a, the distributed load magnitude from a to l is $q = -w$.

EQUATION SOLUTION The solution of equations 3.3 (p. 78) and 3.16 for any beam problem may be carried out by one of several approaches. Sequential and graphical solutions are described in many textbooks on statics and mechanics of materials. One classical approach to these problems is to find the reactions on the beam using equations 3.3 and then draw the shear and moment diagrams using a graphical integration approach combined with calculations for the significant values of the functions. This approach has value from a pedagogical standpoint as it is easily followed, but it is cumbersome to implement. The approach most amenable to computer solution uses a class of mathematical functions called **singularity functions** to represent the loads on the beam. We present the classical approach as a pedagogical reference and also introduce the use of singularity functions which offer some computational advantages. While this approach may be new to some students, when compared to the methods usually learned in other courses, it has significant advantages in computerizing the solution.

Singularity Functions

Because the loads on beams typically consist of collections of discrete entities, such as point loads or segments of distributed loads that can be discontinuous over the beam length, it is difficult to represent these discrete functions with equations that are valid over the entire continuum of beam length. A special class of functions called **singularity functions** was invented to deal with these mathematical situations. Singularity functions are often denoted by a binomial in angled brackets as shown in equations 3.17. The first quantity in the brackets is the variable of interest, in our case x , the distance along the beam length. The second quantity a is a user-defined parameter that denotes where in x the singularity function either acts or begins to act. For example, for a point

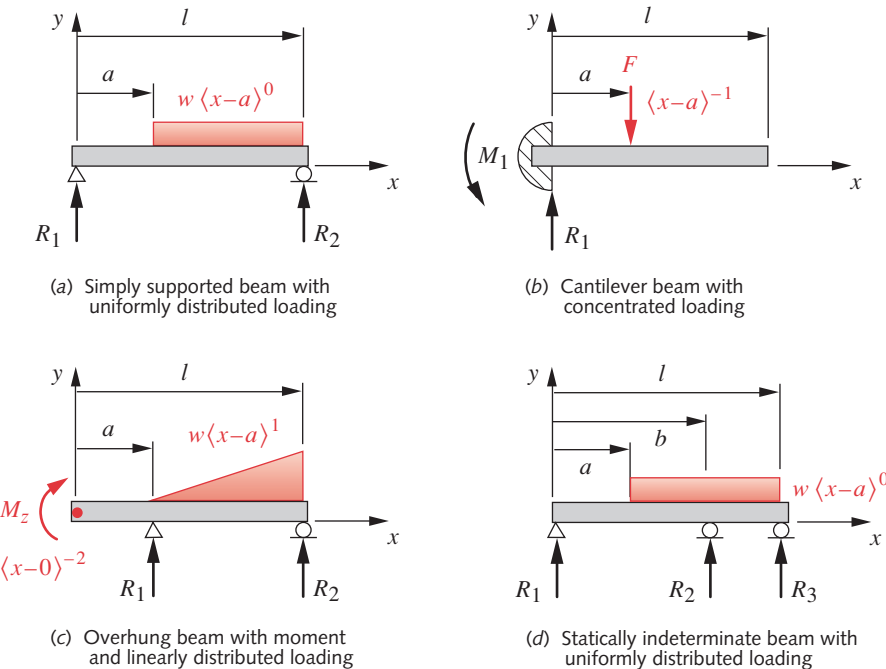


FIGURE 3-22

Types of Beams and Beam Loadings

load, the quantity a represents the particular value of x at which the load acts (see Figure 3-22b). The definition of this singularity function, called the **unit impulse** or **Dirac delta function**, is given in equation 3.17d. Note that all singularity functions involve a conditional constraint. The unit impulse evaluates to ∞ if $x = a$ and is 0 at any other value of x . The **unit step** function or **Heaviside step function** (Eq. 3.17c) evaluates to 0 for all values of x less than a and to 1 for all other x .

Since these functions are defined to evaluate to unity, multiplying them by a coefficient creates any magnitude desired. Their application is shown in the following three examples and is explained in the most detail in Example 3-2B. If a loading function both starts and stops within the range of x desired, it needs two singularity functions to describe it. The first defines the value of a_1 at which the function begins to act and has a positive or negative coefficient as appropriate to its direction. The second defines the value a_2 at which the function ceases to act and has a coefficient of the same magnitude but opposite sign as the first. These two functions will cancel beyond a_2 , making the load zero. Such a case is shown in Example 4-6 in the next chapter.

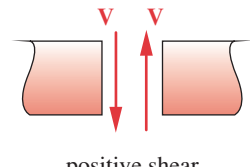
Quadratically distributed loads can be represented by a **unit parabolic function**,

$$\langle x - a \rangle^2 \quad (3.17a)$$

which is defined as 0 when $x \leq a$, and equal to $(x - a)^2$ when $x > a$.

Linearly distributed loads can be represented by a **unit ramp function**,

$$\langle x - a \rangle^1 \quad (3.17b)$$



3

FIGURE 3-23
Beam Sign Convention

which is defined as 0 when $x \leq a$, and equal to $(x - a)$ when $x > a$.

A uniformly distributed load over a portion of a beam can be represented mathematically by a **unit step** function,

$$\langle x - a \rangle^0 \quad (3.17c)$$

which is defined as 0 when $x < a$, unity when $x > a$, and is undefined at $x = a$.

A concentrated force can be represented by the **unit impulse** function,

$$\langle x - a \rangle^{-1} \quad (3.17d)$$

which is defined as 0 when $x < a$, ∞ when $x = a$, and 0 when $x > a$. Its integral evaluates to unity at a .

A concentrated moment can be represented by the **unit doublet** function,

$$\langle x - a \rangle^{-2} \quad (3.17e)$$

which is defined as 0 when $x < a$, indeterminate when $x = a$, and 0 when $x > a$. It generates a unit couple moment at a .

This process can be extended to obtain polynomial singularity functions of any order $\langle x - a \rangle^n$ to fit distributed loads of any shape. Four of the five singularity functions described here are shown in Figure 3-22, as applied to various beam types. A computer program is needed to evaluate these functions. Table 3-7 shows five of the singularity functions implemented in a “BASIC-like” pseudocode. The *For* loops run the variable x from zero to the beam length l . The *If* test determines whether x has reached the value of a which is the location of the start of the singularity function. Depending on this test, the value of $y(x)$ is set either to zero or to the specified magnitude of the singularity function. This type of code can easily be implemented in any computer language (e.g., C+, Fortran, BASIC) or in an equation solver (e.g., Mathcad, MATLAB, TK Solver, EES).

The integrals of these singularity functions have special definitions that, in some cases, defy common sense but nevertheless provide the desired mathematical results. For example, the unit impulse function (Eq. 3.17d) is defined in the limit as having zero width and infinite magnitude, yet its area (integral) is defined as equal to one (Eq. 3.18d). (See reference 8 for a more complete discussion of singularity functions.) The integrals of the singularity functions in equations 3.17 are defined as

$$\int_{-\infty}^x \langle \lambda - a \rangle^2 d\lambda = \frac{\langle x - a \rangle^3}{3} \quad (3.18a)$$

$$\int_{-\infty}^x \langle \lambda - a \rangle^1 d\lambda = \frac{\langle x - a \rangle^2}{2} \quad (3.18b)$$

$$\int_{-\infty}^x \langle \lambda - a \rangle^0 d\lambda = \langle x - a \rangle^1 \quad (3.18c)$$

$$\int_{-\infty}^x \langle \lambda - a \rangle^{-1} d\lambda = \langle x - a \rangle^0 \quad (3.18d)$$

Table 3-7 Pseudocode to Evaluate Singularity Functions

' Pulse Singularity Function

For $x = 0$ to l If ABS $(x - a) < 0.0001$ Then $y(x) = magnitude$, Else $y(x) = 0^*$ Next x

' Step Singularity Function

For $x = 0$ to l If $x < a$ Then $y(x) = 0$, Else $y(x) = magnitude$ Next x

' Ramp Singularity Function

For $x = 0$ to l If $x \leq a$ Then $y(x) = 0$, Else $y(x) = magnitude * (x - a)$ Next x

' Parabolic Singularity Function

For $x = 0$ to l If $x \leq a$ Then $y(x) = 0$, Else $y(x) = magnitude * (x - a)^2$ Next x

' Cubic Singularity Function

For $x = 0$ to l If $x \leq a$ Then $y(x) = 0$, Else $y(x) = magnitude * (x - a)^3$ Next x

* Note: This routine does not generate the infinite value of the Dirac delta function. Rather, it generates the magnitude of a point load applied at location a for use in plotting a beam's loading function.

$$\int_{-\infty}^x \langle \lambda - a \rangle^{-2} d\lambda = \langle x - a \rangle^{-1} \quad (3.18e)$$

where λ is just an integration variable running from $-\infty$ to x . These expressions can be used to evaluate the shear and moment functions that result from any loading function that is expressed as a combination of singularity functions.

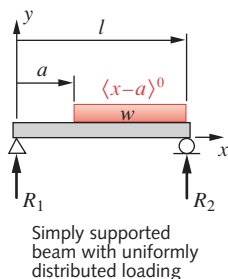
EXAMPLE 3-2A**Shear and Moment Diagrams of a Simply Supported Beam Using a Graphical Method**

Problem: Determine and plot the shear and moment functions for the simply supported beam with uniformly distributed load shown in Figure 3-22a.

Given: Beam length $l = 10$ in, and load location $a = 4$ in. The magnitude of the uniform force distribution is $w = 10$ lb/in.

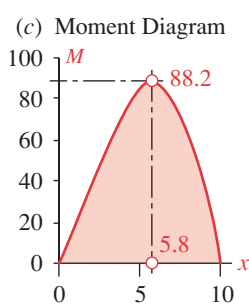
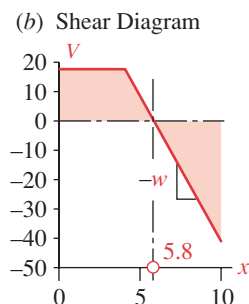
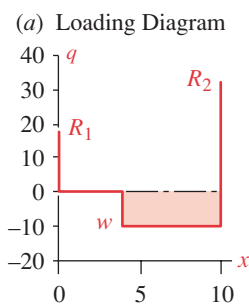
Assumptions: The weight of the beam is negligible compared to the applied load and so can be ignored.

Solution: See Figures 3-22a and 3-24.

**FIGURE 3-22a**

Repeated

3

**FIGURE 3-24**

Example 3-2 Plots

- 1 Solve for the reaction forces using equations 3.3 (p. 78). Summing moments about the right end and summing forces in the y direction gives

$$\sum M_z = 0 = R_1 l - \frac{w(l-a)^2}{2} \quad (a)$$

$$R_1 = \frac{w(l-a)^2}{2l} = \frac{10(10-4)^2}{2(10)} = 18$$

$$\sum F_y = 0 = R_1 - w(l-a) + R_2 \quad (b)$$

$$R_2 = w(l-a) - R_1 = 10(10-4) - 18 = 42$$

- 2 The shape of the shear diagram can be sketched by graphically integrating the loading diagram shown in Figure 3-24a. As a “device” to visualize this graphical integration process, imagine that you walk backward across the loading diagram of the beam, starting from the left end and taking small steps of length dx . You will record on the shear diagram (Figure 3-24b) the area ($\text{force} \cdot dx$) of the loading diagram that you can see as you take each step. As you take the first step backward from $x = 0$, the shear diagram rises immediately to the value of R_1 . As you walk from $x = 0$ to $x = a$, no change occurs, since you see no additional forces. As you step beyond $x = a$, you begin to see strips of area equal to $-w \cdot dx$, which subtract from the value of R_1 on the shear diagram. When you reach $x = l$, the total area $w \cdot (l-a)$ will have taken the value of the shear diagram to $-R_2$. As you step backward off the beam’s loading diagram (Figure 3-24a) and plummet downward, you can now see the reaction force R_2 which closes the shear diagram to zero. The largest value of the shear force in this case is then R_2 at $x = l$.
- 3 If your reflexes are quick enough, you should try to catch the shear diagram (Figure 3-24b) as you fall, climb onto it, and repeat this backward-walking trick across it to create the moment diagram which is the integral of the shear diagram. Note in Figure 3-24c that from $x = 0$ to $x = a$ this moment function is a straight line with slope $= R_1$. Beyond point a , the shear diagram is triangular, and so integrates to a parabola. The peak moment will occur where the shear diagram crosses zero (i.e., zero slope on the moment diagram). The value of x at $V = 0$ can be found with a little trigonometry, noting that the slope of the triangle is $-w$:

$$x_{@V=0} = a + \frac{R_1}{w} = 4 + \frac{18}{10} = 5.8 \quad (c)$$

Positive shear area adds to the moment value and negative area subtracts. So the value of the peak moment can be found by adding the areas of the rectangular and triangular portions of the shear diagram from $x = 0$ to the point of zero shear at $x = 5.8$:

$$M_{@x=5.8} = R_1(a) + R_1 \frac{1.8}{2} = 18(4) + 18 \frac{1.8}{2} = 88.2 \quad (d)$$

The above method gives the magnitudes and locations of the maximum shear and moment on the beam and is useful for a quick determination of those values. However, all that walking and falling can become tiresome, and it would be useful to have a method that can be conveniently computerized to give accurate and complete information on the shear and moment diagrams of any beam-loading case. Such a method will

also allow us to obtain the beam's deflection curve with little additional work. The simple method shown above is not as useful for determining deflection curves, as will be seen in the next chapter. We will now repeat this example using singularity functions to determine the loading, shear, and moment diagrams.

EXAMPLE 3-2B

Shear and Moment Diagrams of a Simply Supported Beam Using Singularity Functions

Problem: Determine and plot the shear and moment functions for the simply supported beam with uniformly distributed load shown in Figure 3-22a.

Given: Beam length $l = 10$ in, and load location $a = 4$ in. The magnitude of the uniform force distribution is $w = 10$ lb/in.

Assumptions: The weight of the beam is negligible compared to the applied load and so can be ignored.

Solution: See Figures 3-22a and 3-24.

- 1 Write equations for the load function in terms of equations 3.17 (pp. 113–114) and integrate the resulting function twice using equations 3.18 (pp. 114–115) to obtain the shear and moment functions. For the beam in Figure 3-22a,

$$q = R_1 \langle x - 0 \rangle^{-1} - w \langle x - a \rangle^0 + R_2 \langle x - l \rangle^{-1} \quad (a)$$

$$V = \int q dx = R_1 \langle x - 0 \rangle^0 - w \langle x - a \rangle^1 + R_2 \langle x - l \rangle^0 + C_1 \quad (b)$$

$$M = \int V dx = R_1 \langle x - 0 \rangle^1 - \frac{w}{2} \langle x - a \rangle^2 + R_2 \langle x - l \rangle^1 + C_1 x + C_2 \quad (c)$$

There are two reaction forces and two constants of integration to be found. We are integrating along a hypothetical infinite beam from $-\infty$ to x . The variable x can take on values both before and beyond the end of the beam. If we consider the conditions at a point infinitesimally to the left of $x = 0$ (denoted as $x = 0^-$), the shear and moment will both be zero there. The same conditions apply at a point infinitesimally to the right of $x = l$ (denoted as $x = l^+$). These observations provide the four boundary conditions needed to evaluate the four constants C_1 , C_2 , R_1 , R_2 : when $x = 0^-$, $V = 0$, $M = 0$; when $x = l^+$, $V = 0$, $M = 0$.

- 2 The constants C_1 and C_2 are found by substituting the boundary conditions $x = 0^-$, $V = 0$, and $x = l^+$, $M = 0$ in equations (b) and (c), respectively:

$$\begin{aligned} V(0^-) &= 0 = R_1 \langle 0^- - 0 \rangle^0 - w \langle 0^- - a \rangle^1 + R_2 \langle 0^- - l \rangle^0 + C_1 \\ C_1 &= 0 \end{aligned} \quad (d)$$

$$\begin{aligned} M(0^-) &= 0 = R_1 \langle 0^- - 0 \rangle^1 - \frac{w}{2} \langle 0^- - a \rangle^2 + R_2 \langle 0^- - l \rangle^1 + C_1 \langle 0^- \rangle + C_2 \\ C_2 &= 0 \end{aligned}$$

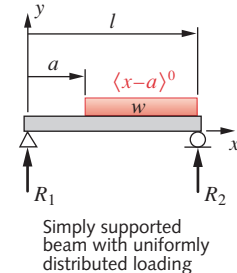


FIGURE 3-22a

Repeated

Note that in general, the constants C_1 and C_2 will always be zero if the reaction forces and moments acting on the beam are included in the loading function, because the shear and moment diagrams must close to zero at each end of the beam.

- 3 The reaction forces R_1 and R_2 can be calculated from equations (c) and (b) respectively by substituting the boundary conditions $x = l^+$, $V = 0$, $M = 0$. Note that we can substitute l for l^+ to evaluate it since their difference is vanishingly small.

$$\begin{aligned} M(l^+) &= R_1(l^+ - 0)^1 - w \frac{(l^+ - a)^2}{2} + R_2(l^+ - l)^1 = 0 \\ 0 &= R_1 l^+ - \frac{w(l^+ - a)^2}{2} \\ R_1 &= \frac{w(l^+ - a)^2}{2l^+} = \frac{w(l - a)^2}{2l} = \frac{10(10 - 4)^2}{2(10)} = 18 \end{aligned} \quad (e)$$

$$\begin{aligned} V(l^+) &= R_1(l^+ - 0)^0 - w(l^+ - a)^1 + R_2(l^+ - l)^0 = 0 \\ 0 &= R_1 - w(l - a) + R_2 \\ R_2 &= w(l - a) - R_1 = 10(10 - 4) - 18 = 42 \end{aligned} \quad (f)$$

Since w , l , and a are known from the given data, equation (e) can be solved for R_1 , and this result substituted in equation (f) to find R_2 . Note that equation (f) is just $\Sigma F = 0$, and equation (e) is the sum of moments taken about point l and set to 0.

- 4 To generate the shear and moment functions over the length of the beam, equations (b) and (c) must be evaluated for a range of values of x from 0 to l , after substituting the above values of C_1 , C_2 , R_1 , and R_2 in them. The independent variable x was run from 0 to $l = 10$ at 0.1 increments. The reactions, loading function, shear-force function, and moment function were calculated from equations (a) through (f) above and are plotted in Figure 3-24. The files EX03-02 that generate these plots are on the CD-ROM.
- 5 The largest absolute values of the shear and moment functions are of interest for the calculation of stresses in the beam. The plots show that the shear force is largest at $x = l$ and the moment has a maximum M_{max} near the center. The value of x at M_{max} can be found by setting V to 0 in equation (b) and solving for x . (The shear function is the derivative of the moment function and so must be zero at each of its minima and maxima.) This gives $x = 5.8$ at M_{max} . The function values at these points of maxima or minima can then be calculated from equations b and c respectively by substituting the appropriate values of x and evaluating the singularity functions. For the maximum absolute value of shear force at $x = l$,

$$\begin{aligned} V_{max} &= V_{@x=l^-} = R_1(l^- - 0)^0 - w(l^- - a)^1 + R_2(l^- - l)^0 \\ &= R_1 - w(l^- - a) + 0 \\ &= 18 - 10(10 - 4) + 0 = -42 \end{aligned} \quad (g)$$

Note that the first singularity term evaluates to 1 since $l^- > 0$ (see Eq. 3.17c, p. 114), the second singularity term evaluates to $(l - a)$ because $l^- > a$ in this problem (see Eq. 3.17b), and the third singularity term evaluates to 0 as defined in equation 3.17c. The maximum moment is found in similar fashion:

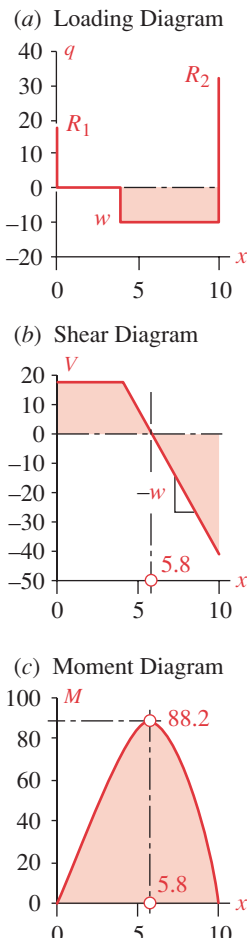


FIGURE 3-24 Repeated

Example 3-2 Plots

$$\begin{aligned}
 M_{max} = M_{@x=5.8} &= R_1(5.8 - 0)^1 - w \frac{(5.8 - a)^2}{2} + R_2(5.8 - l)^1 \\
 &= R_1(5.8)^1 - w \frac{(5.8 - 4)^2}{2} + R_2(5.8 - 10)^1 \\
 &= 18(5.8) - 10 \frac{(5.8 - 4)^2}{2} + 0 = 88.2
 \end{aligned} \tag{h}$$

The third singularity term evaluates to 0 because $5.8 < l$ (see Eq. 3.17b).

6 The results are

$$R_1 = 18 \quad R_2 = 42 \quad V_{max} = -42 \quad M_{max} = 88.2 \tag{i}$$

EXAMPLE 3-3A

Shear and Moment Diagrams of a Cantilever Beam Using a Graphical Method

Problem: Determine and plot the shear and moment functions for the cantilever beam with a concentrated load as shown in Figure 3-22b.

Given: Beam length $l = 10$ in, and load location $a = 4$ in. The magnitude of the applied force is $F = 40$ lb.

Assumptions: The weight of the beam is negligible compared to the applied load and so can be ignored.

Solution: See Figures 3-22b and 3-25.

- 1 Solve for the reaction forces using equations 3.3 (p. 78). Summing moments about the left end and summing forces in the y direction gives

$$\sum M_z = 0 = Fa - M_1 \tag{a}$$

$$M_1 = Fa = 40(4) = 160$$

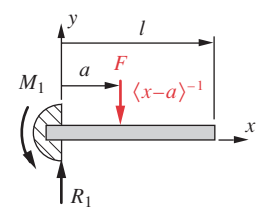
$$\sum F_y = 0 = R_1 - F \tag{b}$$

$$R_1 = F = 40$$

- 2 By the sign convention, the shear is positive and the moment is negative in this example. To graphically construct the shear and moment diagrams for a cantilever beam take an imaginary “backward walk” starting at the fixed end of the beam and moving toward the free end (from left to right in Figure 3-24).

In this example, that results in the first observed force being the reaction force R_1 acting upward. This shear force remains constant until the downward force F at $x = a$ is reached, which closes the shear diagram to zero.

- 3 The moment diagram is the integral of the shear diagram, which in this case is a straight line of slope = 40.



Cantilever beam with concentrated loading

FIGURE 3-22b

Repeated

- 4 Both the shear and moment are maximum at the wall in a cantilever beam. Their maximum magnitudes are as shown in equations (a) and (b) above.

This example will now be repeated using singularity functions.

3

EXAMPLE 3-3B

Shear and Moment Diagrams of a Cantilever Beam Using Singularity Functions

Problem: Determine and plot the shear and moment functions for the cantilever beam with a concentrated load as shown in Figure 3-22b.

Given: Beam length $l = 10$ in, and load location $a = 4$ in. The magnitude of the applied force is $F = 40$ lb.

Assumptions: The weight of the beam is negligible compared to the applied load and so can be ignored.

Solution: See Figures 3-22b and 3-25.

- 1 Write equations for the load function in terms of equations 3.17 (pp. 113–114) and integrate the resulting function twice using equations 3.18 (pp. 114–115) to obtain the shear and moment functions. Note the use of the unit doublet function to represent the moment at the wall. For the beam in Figure 3-22b,

$$q = -M_1(x-0)^{-2} + R_1(x-0)^{-1} - F(x-a)^{-1} \quad (a)$$

$$V = \int q dx = -M_1(x-0)^{-1} + R_1(x-0)^0 - F(x-a)^0 + C_1 \quad (b)$$

$$M = \int V dx = -M_1(x-0)^0 + R_1(x-0)^1 - F(x-a)^1 + C_1x + C_2 \quad (c)$$

The reaction moment M_1 at the wall is in the z direction and the forces R_1 and F are in the y direction in equation (b). All moments in equation (c) are in the z direction.

- 2 Because the reactions have been included in the loading function, the shear and moment diagrams both close to zero at each end of the beam, making $C_1 = C_2 = 0$.
- 3 The reaction force R_1 and reaction moment M_1 are calculated from equations (b) and (c) respectively by substituting the boundary conditions $x = l^+$, $V = 0$, $M = 0$. Note that we can substitute l for l^+ since their difference is vanishingly small. M_1 does not appear in equation (d) because its singularity function is not defined at $l = l^+$.

$$V = M(l)^{-1} + R_1(l-0)^0 - F(l-a)^0 = 0 \quad (d)$$

$$0 = M(0) + R_1 - F \quad (d)$$

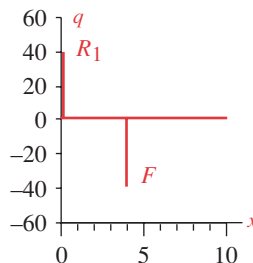
$$R_1 = F = 40 \text{ lb}$$

$$M = -M_1(l-0)^0 + R_1(l-0)^1 - F(l-a)^1 = 0 \quad (e)$$

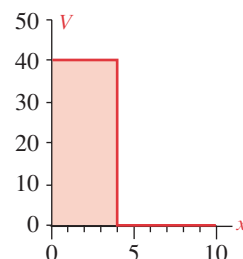
$$0 = -M_1 + R_1(l) - F(l-a) \quad (e)$$

$$M_1 = R_1(l) - F(l-a) = 40(10) - 40(10-4) = 160 \text{ lb-in cw}$$

(a) Loading Diagram



(b) Shear Diagram



(c) Moment Diagram

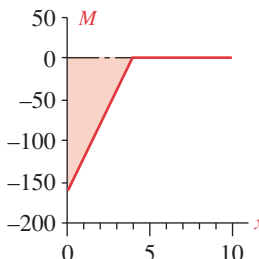


FIGURE 3-25

Example 3-3 Plots

Since F , l , and a are known from the given data, equation (d) can be solved for R_1 , and this result substituted in equation (e) to find M_1 . Note that equation (d) is just $\Sigma F_y = 0$, and equation (e) is $\Sigma M_z = 0$.

- 4 To generate the shear and moment functions over the length of the beam, equations (b) and (c) must be evaluated for a range of values of x from 0 to l , after substituting the above values of C_1 , C_2 , R_1 , and M_1 in them. The independent variable x was varied from 0 to $l = 10$ at 0.1 increments. The reactions, loading function, shear-force function and moment function were calculated from equations (a) through (e) above and are plotted in Figure 3-25. The files EX03-03 that generate these plots are on the CD-ROM.
- 5 The largest absolute values of the shear and moment functions are of interest for the calculation of stresses in the beam. The plots show that the shear force and the moment are both largest at $x = 0$. The function values at these points can be calculated from equations (b) and (c) respectively by substituting $x = 0$ and evaluating the singularity functions:

$$R_1 = 40 \quad V_{max} = 40 \quad |M_{max}| = 160 \quad (f)$$

EXAMPLE 3-4

Shear and Moment Diagrams of an Overhung Beam Using Singularity Functions

Problem: Determine and plot the shear and moment functions for the overhung beam with an applied moment and ramp load as shown in Figure 3-22c.

Given: Beam length $l = 10$ in, and load location $a = 4$ in. The magnitude of the applied moment $M = 20$ lb-in, and the slope of the force distribution is $w = 10$ lb/in/in.

Assumptions: The weight of the beam is negligible compared to the applied load and so can be ignored.

Solution: See Figures 3-22c and 3-26.

- 1 Write equations for the load function in terms of equations 3.17 (pp. 113–114) and integrate the resulting function twice using equations 3.18 (pp. 114–115) to obtain the shear and moment functions. For the beam in Figure 3-22c,

$$q = M\langle x - 0 \rangle^{-2} + R_1\langle x - a \rangle^{-1} - w\langle x - a \rangle^1 + R_2\langle x - l \rangle^{-1} \quad (a)$$

$$V = \int q dx = M\langle x - 0 \rangle^{-1} + R_1\langle x - a \rangle^0 - \frac{w}{2}\langle x - a \rangle^2 + R_2\langle x - l \rangle^0 + C_1 \quad (b)$$

$$M = \int V dx = M\langle x - 0 \rangle^0 + R_1\langle x - a \rangle^1 - \frac{w}{6}\langle x - a \rangle^3 + R_2\langle x - l \rangle^1 + C_1x + C_2 \quad (c)$$

- 2 As demonstrated in the previous two examples, the constants of integration C_1 and C_2 will always be zero if the reaction forces are included in the equations for shear and moment. So we will set them to zero.

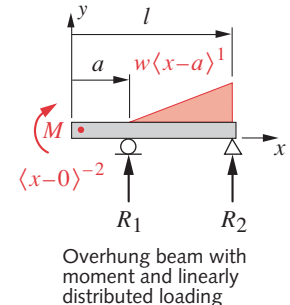
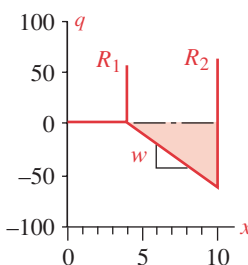


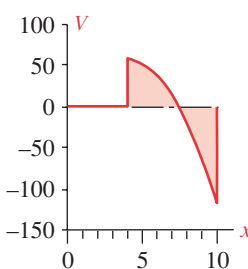
FIGURE 3-22c

Repeated

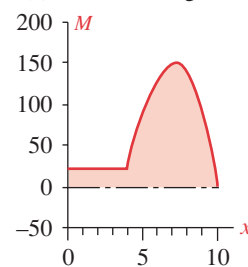
(a) Loading Diagram



(b) Shear Diagram



(c) Moment Diagram

**FIGURE 3-26**

Example 3-4 Plots

3

- 3 The reaction forces R_1 and R_2 can be calculated from equations (c) and (b) respectively by substituting the boundary conditions $x = l^+$, $V = 0$, $M = 0$. Note that we can substitute l for l^+ since their difference is vanishingly small.

$$M = M_1 \langle l \rangle^0 + R_1 \langle l - a \rangle^1 - \frac{w}{6} \langle l - a \rangle^3 + R_2 \langle l - l \rangle^1 = 0$$

$$0 = M_1 + R_1(l - a) - \frac{w}{6}(l - a)^3$$

$$R_1 = \frac{w}{6}(l - a)^2 - \frac{M_1}{(l - a)} \quad (d)$$

$$= \frac{10}{6}(10 - 4)^2 - \frac{20}{(10 - 4)} = 56.67 \text{ lb}$$

$$V = M \langle l \rangle^{-1} + R_1 \langle l - a \rangle^0 - \frac{w}{2} \langle l - a \rangle^2 + R_2 \langle l - l \rangle^0 = 0$$

$$0 = M(0) + R_1 - \frac{w}{2}(l - a)^2 + R_2 \quad (e)$$

$$R_2 = \frac{w}{2}(l - a)^2 - R_1 = \frac{10}{2}(10 - 4)^2 - 56.67 = 123.33 \text{ lb}$$

Note that equation (d) is just $\sum M_z = 0$, and equation (e) is $\sum F_y = 0$.

- 4 To generate the shear and moment functions over the length of the beam, equations (b) and (c) must be evaluated for a range of values of x from 0 to l , after substituting the values of $C_1 = 0$, $C_2 = 0$, R_1 , and R_2 in them. The independent variable x was varied from 0 to $l = 10$ at 0.1 increments. The reactions, loading function, shear-force function, and moment function were calculated from equations (a) through (f) above and are plotted in Figure 3-26.*
- 5 The largest absolute values of the shear and moment functions are of interest for the calculation of stresses in the beam. The plots show that the shear force is largest at $x = l$ and the moment has a maximum to the right of the beam center. The value of x at M_{max} can be found by setting V to 0 in equation (b) and solving for x . The shear function is the derivative of the moment function and so must be zero at each of its minima and maxima. This gives $x = 7.4$ at M_{max} . The function values at these points of maxima or minima can be calculated from equations (b) and (c) respectively by substituting the appropriate values of x and evaluating the singularity function:

$$R_1 = 56.7 \quad R_2 = 123.3 \quad V_{max} = -120 \quad M_{max} = 147.2 \quad (f)$$

Superposition

These examples of beam systems represent only a small fraction of all the possible combinations of beam loadings and constraints that one will encounter in practice. Rather than having to write and integrate the loading functions for every new beam situation from scratch, the particular problem can often be solved by using superposition, which simply means adding the individual results together. For small deflections, it is safe to assume linearity in these problems, and linearity is a requirement for superposition to be valid. For example, the load due to the weight of a beam (ignored in the above examples) can be accounted for by superposing a uniform load over the beam's entire length on whatever other applied loads may be present.

* The files EX03-04 that generate these plots are on the CD-ROM.

The effects on the shear and moment diagrams of multiple loads on a beam can also be determined by superposition of the individual loadings. If, for example, the beam of Example 3-3 had two point loads applied to it, each at a different distance a , their combined effect could be found by applying the equations of that example twice, once for each load and position, and then adding (superposing) the two results. Appendix B contains a collection of common beam-loading situations solved for shear and moment functions giving their equations and plots. These solutions can be combined by superposition to accommodate more complicated situations. They can be superposed within your model to obtain and plot the total shear and moment diagrams, their maxima and minima.

3.10 SUMMARY

Though the student learning about stress analysis for the first time may not think so, the subject of load analysis can often be more difficult and complicated than that of stress analysis. Ultimately, the accuracy of any stress analysis is limited by the quality of our knowledge about the loads on the system, since the stresses are generally proportional to the loads as will be discussed in Chapter 4. This chapter has presented a review of Newtonian methods of force and moment analysis for both dynamically and statically loaded systems of a few types. It is by no means a complete treatment of the complex subject of load analysis, and the references in the bibliography of this chapter should be consulted for more detail and for cases not covered here.

The following factors should be kept in mind when attempting to determine loads on a system:

- 1 Determine the character of the loading in terms of its load class as defined in Section 3.1 in order to decide on whether a static or dynamic load analysis is in order.
- 2 Draw complete free-body diagrams (FBD) of the system and of as many subsystems within it as are necessary to define the loads acting on its elements. Include all applied moments and torques as well as forces. The importance of a carefully drawn FBD cannot be overemphasized. Most errors in force analysis occur at this step because the FBD is often incorrectly drawn.
- 3 Write the relevant equations using Newton's laws to define the unknown forces and moments acting on the system. The solution of these equations for most real problems requires some sort of computer tool such as an equation solver or spreadsheet to get satisfactory results in a reasonable time. This is especially true for dynamic systems, which must be solved for a multiplicity of positions in order to determine the maximum loads.
- 4 The presence of impact forces can significantly increase the loads on any system. The accurate calculation of forces due to impact is quite difficult. The energy method for impact-force estimation presented in this chapter is crude and should be considered an approximation. Detailed information about the deformations of the bodies at impact is needed for a more accurate result, and this may not be available without testing of the actual system under impact. More sophisticated analysis techniques exist for impact-force analysis but are beyond the scope of this introductory design text. The reader is referred to the bibliography for more information.

5 Vibration loading can also severely increase the actual loading above the theoretically calculated levels as shown in Case Study 5B and Figure 3-16 (p. 106). Experimental measurements made under real loading conditions are the best way to develop information in these cases.

The case studies in this chapter are designed to set up realistic problems for stress and failure analysis in the following chapters. Though their complexity may be a bit daunting to the student at first encounter, much benefit can be gained from time spent studying them. This effort will be rewarded with a better understanding of the stress-analysis and failure-theory topics in succeeding chapters.

Important Equations Used in This Chapter

See the referenced sections for information on the proper use of these equations.

Newton's Second Law (Section 3.3):

$$\sum F_x = ma_x \quad \sum F_y = ma_y \quad \sum F_z = ma_z \quad (3.1b)$$

Euler's Equations (Section 3.3):

$$\begin{aligned} \sum M_x &= I_x \alpha_x - (I_y - I_z) \omega_y \omega_z \\ \sum M_y &= I_y \alpha_y - (I_z - I_x) \omega_z \omega_x \\ \sum M_z &= I_z \alpha_z - (I_x - I_y) \omega_x \omega_y \end{aligned} \quad (3.1d)$$

Static Loading (Section 3.3):

$$\begin{aligned} \sum F_x &= 0 & \sum F_y &= 0 & \sum F_z &= 0 \\ \sum M_x &= 0 & \sum M_y &= 0 & \sum M_z &= 0 \end{aligned} \quad (3.3a)$$

Undamped Natural Frequency (Section 3.7):

$$\begin{aligned} \omega_n &= \sqrt{\frac{k}{m}} \\ f_n &= \frac{1}{2\pi} \omega_n \end{aligned} \quad (3.4)$$

Damped Natural Frequency (Section 3.7):

$$\begin{aligned} \omega_d &= \sqrt{\frac{k}{m} - \left(\frac{d}{2m}\right)^2} \\ f_d &= \frac{1}{2\pi} \omega_d \end{aligned} \quad (3.7)$$

Spring Constant (Section 3.7):

$$k = \frac{F}{\delta} \quad (3.5a)$$

Viscous Damping (Section 3.7):

$$d = \frac{F}{\dot{y}} \quad (3.6)$$

Dynamic Force Ratio (Section 3.8):

$$\frac{F_i}{W} = \frac{\delta_i}{\delta_{st}} = 1 + \sqrt{1 + \frac{2\eta h}{\delta_{st}}} \quad (3.14b)$$

3

Beam-Loading, Shear, and Moment Functions (Section 3.9):

$$q(x) = \frac{dV}{dx} = \frac{d^2M}{dx^2} \quad (3.16a)$$

Integrals of Singularity Functions (Section 3.9):

$$\int_{-\infty}^x \langle \lambda - a \rangle^2 d\lambda = \frac{\langle x - a \rangle^3}{3} \quad (3.18a)$$

$$\int_{-\infty}^x \langle \lambda - a \rangle^1 d\lambda = \frac{\langle x - a \rangle^2}{2} \quad (3.18b)$$

$$\int_{-\infty}^x \langle \lambda - a \rangle^0 d\lambda = \langle x - a \rangle^1 \quad (3.18c)$$

$$\int_{-\infty}^x \langle \lambda - a \rangle^{-1} d\lambda = \langle x - a \rangle^0 \quad (3.18d)$$

$$\int_{-\infty}^x \langle \lambda - a \rangle^{-2} d\lambda = \langle x - a \rangle^{-1} \quad (3.18e)$$

3.11 REFERENCES

- 1 **R. L. Norton**, *Design of Machinery: An Introduction to the Synthesis and Analysis of Mechanisms and Machines*, 3ed. McGraw-Hill: New York, pp. 162–196, 265–355, 2004.
- 2 *Ibid.*, pp. 537-549.
- 3 *Ibid.*, pp. 730-753.
- 4 *Ibid.*, p. 279.
- 5 **R. L. Norton, et al.**, “Bearing Forces as a Function of Mechanical Stiffness and Vibration in a Fourbar Linkage,” in *Effects of Mechanical Stiffness and Vibration on Wear*, R. G. Bayer, ed. American Society for Testing and Materials: Philadelphia, Pa., 1995.
- 6 **A. H. Burr and J. B. Cheatham**, *Mechanical Analysis and Design*. 2nd ed. Prentice-Hall: Englewood Cliffs, N.J., pp. 835–863, 1995.
- 7 **R. J. Roark and W. C. Young**, *Formulas for Stress and Strain*. 6th ed. McGraw-Hill: New York, 1989.
- 8 **C. R. Wylie and L. C. Barrett**, *Advanced Engineering Mathematics*. 5th ed. McGraw-Hill: New York, 1982.

3.12 WEB REFERENCES

Free-body diagrams

<http://laser.phys.ualberta.ca/~freeman/enph131/fbdex1.html>

<http://eta.physics.uoguelph.ca/tutorials/fbd/Q.fbd.html>

<http://www.ac.wwu.edu/~vawter/PhysicsNet/Topics/Dynamics/Forces/FreeBodyDiagram.html>

Singularity functions

<http://www.ce.berkeley.edu/Courses/CE130/Sing.pdf>

3.13 BIBLIOGRAPHY

Table P3-0[†]

Topic/Problem Matrix

3.1 Loading Classes

3-1

3.2 Free-Body Diagrams

3-2, 3-43, 3-45, 3-50, 3-52

3.3 Load Analysis

3-3, 3-4, 3-5, 3-7, 3-9, 3-15,
3-16, 3-17, 3-18, 3-19, 3-21,
3-29, 3-30, 3-31, 3-44, 3-46,
3-51, 3-53

3.7 Vibration Loading

3-8, 3-47, 3-48, 3-49

3.8 Impact Loading

3-6, 3-14, 3-20, 3-22, 3-42

3.9 Beams—Static

3-10, 3-12, 3-23, 3-24, 3-26,
3-27, 3-28, 3-32, 3-33, 3-34, 3-
35, 3-36, 3-37, 3-38, 3-39, 3-40,
3-41

3.9 Beams—Dynamic

3-11, 3-13

* Answers to these problems are provided in Appendix D.

[†] Problem numbers in **boldface** are extended with similar problems in later chapters having the same dash number, e.g., Problem 4-4 is based on Problem 3-4, etc.

For further review of static and dynamic force analysis see:

R. C. Hibbeler, *Engineering Mechanics: Statics*. 7th ed. Prentice-Hall: Englewood Cliffs, N.J., 1995.

R. C. Hibbeler, *Engineering Mechanics: Dynamics*. 7th ed. Prentice-Hall: Englewood Cliffs, N.J., 1995.

I. H. Shames, *Engineering Mechanics: Statics and Dynamics*. 3rd ed. Prentice-Hall: Englewood Cliffs, N.J., 1980.

For further information on impact see:

A. H. Burr and J. B. Cheatham, *Mechanical Analysis and Design*. 2nd ed., Prentice-Hall, Englewood Cliffs, N.J., Chapter 14, 1995.

W. Goldsmith, *Impact*. Edward Arnold Ltd.: London, 1960.

H. Kolsky, *Stress Waves in Solids*. Dover Publications: New York, 1963.

For further information on vibrations see:

L. Meirovitch, *Elements of Vibration Analysis*. McGraw-Hill: New York, 1975.

For beam loading formulas and tables see:

R. J. Roark and W. C. Young, *Formulas for Stress and Strain*. 6th ed. McGraw-Hill: New York, 1989.

3.14 PROBLEMS

3-1 Which load class from Table 3-1 best suits these systems?

- | | | |
|-------------------|-----------------|---------------|
| (a) Bicycle frame | (b) Flagpole | (c) Boat oar |
| (d) Diving board | (e) Pipe wrench | (f) Golf club |

3-2 Draw free-body diagrams for the systems of Problem 3-1.

***3-3** Draw a free-body diagram of the pedal-arm assembly from a bicycle with the pedal arms in the horizontal position and dimensions as shown in Figure P3-1. (Consider the two arms, pedals, and pivot as one piece.) Assuming a rider-applied force of 1500 N at the pedal, determine the torque applied to the chain sprocket and the maximum bending moment and torque in the pedal arm.

- 3-4** The trailer hitch from Figure 1-1 (p. 11) has loads applied as shown in Figure P3-2. The tongue weight of 100 kg acts downward and the pull force of 4 905 N acts horizontally. Using the dimensions of the ball bracket in Figure 1-5 (p. 14), draw a free-body diagram of the ball bracket and find the tensile and shear loads applied to the two bolts that attach the bracket to the channel in Figure 1-1.

- 3-5** For the trailer hitch of Problem 3-4, determine the horizontal force that will result on the ball from accelerating a 2000-kg trailer to 60 m/sec in 20 sec. Assume a constant acceleration.

- *3-6** For the trailer hitch of Problem 3-4, determine the horizontal force that will result on the ball from an impact between the ball and the tongue of the 2000-kg trailer if the hitch deflects 2.8 mm dynamically on impact. The tractor weighs 1 000 kg. The velocity at impact is 0.3 m/sec.

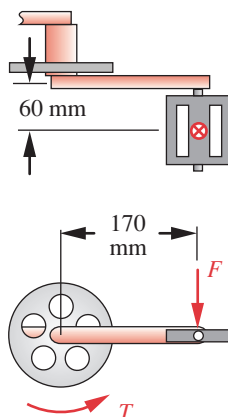
- *3-7** The piston of an internal-combustion engine is connected to its connecting rod with a “wrist pin.” Find the force on the wrist pin if the 0.5-kg piston has an acceleration of 2 500 g.

- *3-8** A cam-follower system similar to that shown in Figure 3-15 (p. 103) has a mass $m = 1$ kg, a spring constant $k = 1\,000$ N/m, and a damping coefficient $d = 19.4$ N-s/m. Find the undamped and damped natural frequencies of this system.

- 3-9** A ViseGrip® plier-wrench is drawn to scale in Figure P3-3. Scale the drawing for dimensions. Find the forces acting on each pin and member of the assembly for an assumed clamping force of $P = 4\,000$ N in the position shown. What force F is required to keep it in the clamped position shown? *Note: A similar tool is probably available for inspection in your school's machine shop.*

- *3-10** An overhung diving board is shown in Figure P3-4a. Find the reaction forces and construct the shear and moment diagrams for this board with a 100-kg person standing at the free end. Determine the maximum shear force, maximum moment, and their locations.

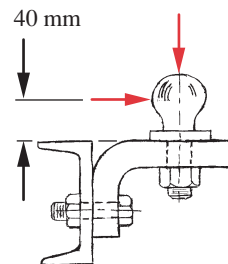
- *3-11** Determine the impact force and dynamic deflection that will result when the 100-kg person in Problem 3-10 jumps up 25 cm and lands back on the board. Assume that the board weighs 29 kg and deflects 13.1 cm statically when the person stands on it. Find the reaction forces and construct the shear and moment diagrams for this dynamic



3

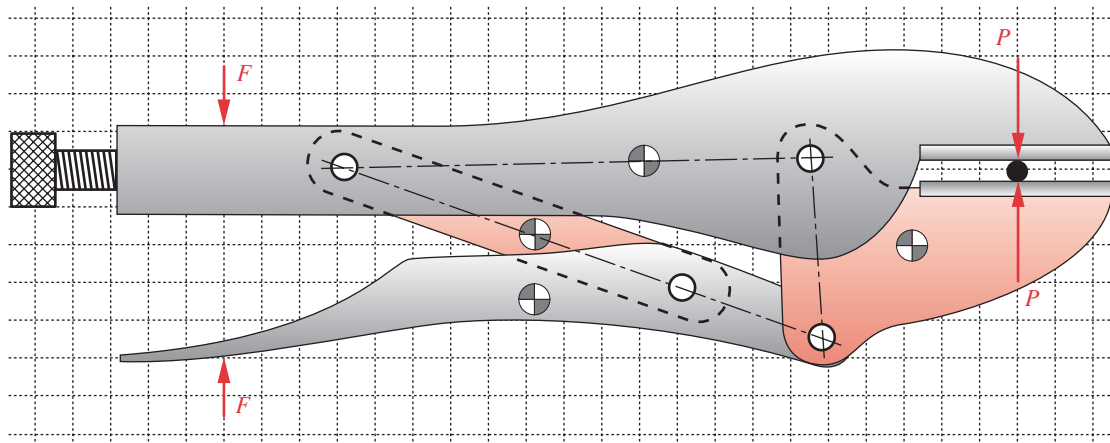
FIGURE P3-1

Problem 3-3 (A Solidworks model of this is on the CD)

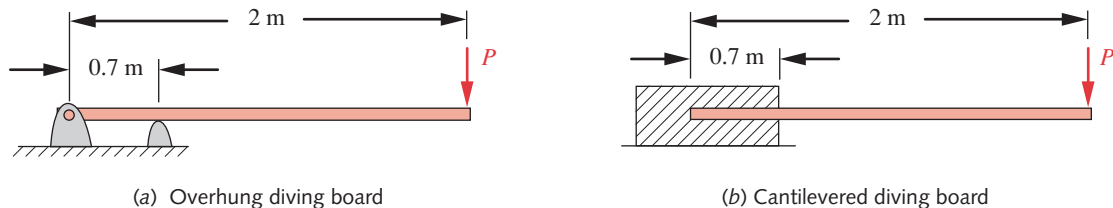
**FIGURE P3-2**

Problems 3-4, 3-5, 3-6
(A Solidworks model of this is on the CD)

* Answers to these problems are provided in Appendix D.

**FIGURE P3-3**

Problem 3-9 (A Solidworks model of this is on the CD)

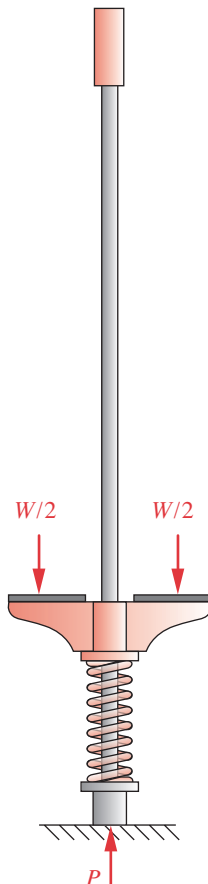
**FIGURE P3-4**

Problems 3-10 through 3-13

loading. Determine the maximum shear force, maximum moment, and their locations along the length of the board.

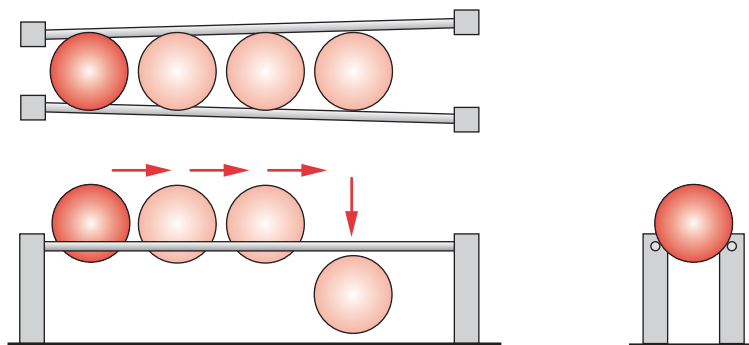
- 3-12** Repeat Problem 3-10 using the cantilevered diving board design in Figure P3-4b.
- 3-13** Repeat Problem 3-11 using the diving board design shown in Figure P3-3b. Assume that the board weighs 19 kg and deflects 8.5 cm when the person stands on it.
- 3-14** Figure P3-5 shows a child's toy called a *pogo stick*. The child stands on the pads, applying half her weight on each side. She jumps up off the ground, holding the pads up against her feet, and bounces along with the spring cushioning the impact and storing energy to help each rebound. Assume a 60-lb child and a spring constant of 100 lb/in. The pogo stick weighs 5 lb. Find the natural frequency of the system, the static deflection of the spring with the child standing still, and the dynamic force and deflection when the child lands after jumping 2 in off the ground.
- *3-15** A pen plotter imparts a constant acceleration of 2.5 m/sec^2 to the pen assembly, which travels in a straight line across the paper. The moving pen assembly weighs 0.5 kg. The plotter weighs 5 kg. What coefficient of friction is needed between the plotter feet and the table top on which it sits to prevent the plotter from moving when the pen accelerates?
- 3-16** A track to guide bowling balls is designed with two round rods as shown in Figure P3-6. The rods are not parallel to one another but have a small angle between them. The balls roll on the rods until they fall between them and drop onto another track. The angle between the rods is varied to cause the ball to drop at different locations. Each rod's unsupported length is 30 in and the angle between them is 3.2° . The balls are 4.5 in dia and weigh 2.5 lb. The center distance between the 1-in-dia rods is 4.2 in at the narrow end. Find the distance from the narrow end at which the ball drops through and determine the worst-case shear and moment maxima for the rods as the ball rolls a distance from the narrow end that is 98% of the distance to drop. Assume the rods are simply supported at each end and have zero deflection under the applied loading. (Note that assuming zero deflection is unrealistic. This assumption will be relaxed in the next chapter after deflection has been discussed.)
- 3-17** A pair of ice tongs is shown in Figure P3-7. The ice weighs 50 lb and is 10 in wide across the tongs. The distance between the handles is 4 in, and the mean radius r of a tong is 6 in. Draw free-body diagrams of the two tongs and find all forces acting on them. Determine the bending moment at point A.

- *3-18** A tractor-trailer tipped over while negotiating an on-ramp to the New York Thruway. The road has a 50-ft radius at that point and tilts 3° toward the outside of the curve. The 45-ft-long by 8-ft-wide by 8.5-ft-high trailer box (13 ft from ground to top) was loaded with 44 415 lb of paper rolls in two rows by two high as shown in Figure P3-8. The rolls are 40 in dia by 38 in long and weigh about 900 lb each. They are wedged against backward rolling but not against sideways sliding. The empty trailer weighed 14 000 lb. The driver claims that he was traveling at less than 15 mph and that the load of paper

**FIGURE P3-5**

Problem 3-14

* Answers to these problems are provided in Appendix D. Problem numbers in **boldface** are extended with similar problems in later chapters having the same dash number, e.g., Problem 4-4 is based on Problem 3-4, etc.



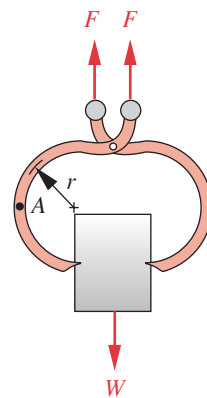
3

FIGURE P3-6

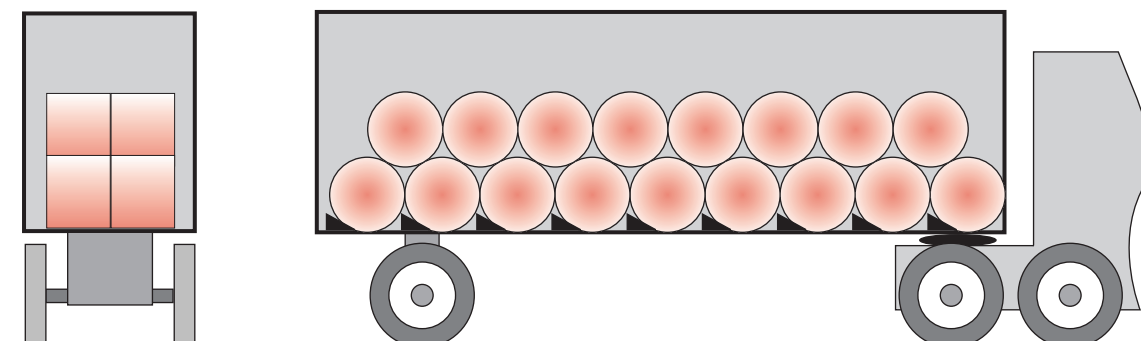
Problem 3-16

shifted inside the trailer, struck the trailer sidewall, and tipped the truck. The paper company that loaded the truck claims the load was properly stowed and would not shift at that speed. Independent tests of the coefficient of friction between similar paper rolls and a similar trailer floor give a value of 0.43 ± 0.08 . The composite center of gravity of the loaded trailer is estimated to be 7.5 ft above the road. Determine the truck speed that would cause the truck to just begin to tip and the speed at which the rolls will just begin to slide sideways. What do you think caused the accident?

- 3-19 Assume that the CG of the paper rolls in the truck of Problem 3-18 is 2.5 ft above the floor of the trailer. At what speed on the same curve will the pile of rolls tip over (not slide) with respect to the trailer?
- 3-20 Assume that the load of paper rolls in Problem 3-18 will slide sideways at a truck speed of 20 mph on the curve in question. Estimate the impact force of the cargo against the trailer wall. The force-deflection characteristic of the trailer wall has been measured as approximately 400 lb/in.
- 3-21 Figure P3-9 shows an automobile wheel with two common styles of lug wrench being used to tighten the wheel nuts, a single-ended wrench in (a), and a double-ended wrench in (b). In each case two hands are required to provide forces respectively at A and B as shown. The distance between points A and B is 1 ft in both cases. The wheel nuts

**FIGURE P3-7**

Problem 3-17

**FIGURE P3-8**

Problem 3-18

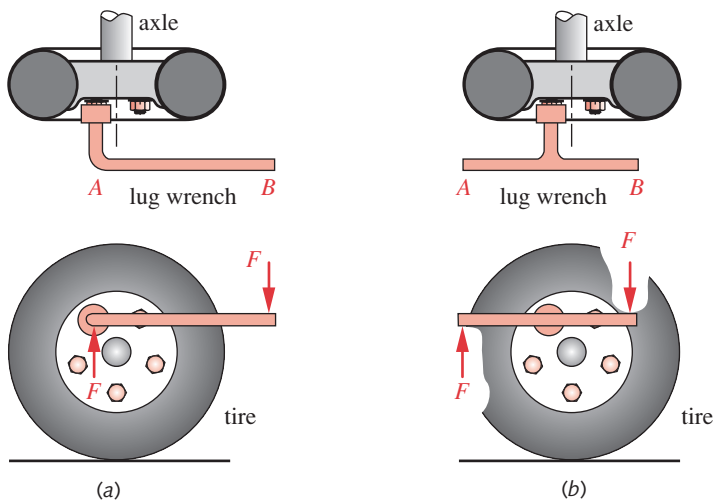


FIGURE P3-9

Problem 3-21

require a torque of 70 ft-lb. Draw free-body diagrams for both wrenches and determine the magnitudes of all forces and moments on each wrench. Is there any difference between the way these two wrenches perform their assigned task? Is one design better than the other? If so, why? Explain.



FIGURE P3-10

Problem 3-22

- *3-22** A roller-blade skate is shown in Figure P3-10. The polyurethane wheels are 72 mm dia. The skate-boot-foot combination weighs 2 kg. The effective “spring rate” of the person-skate system is 6 000 N/m. Find the forces on the wheels’ axles for a 100-kg person landing a 0.5-m jump on one foot. (a) Assume that all 4 wheels land simultaneously. (b) Assume that one wheel absorbs all the landing force.

- *3-23** A beam is supported and loaded as shown in Figure P3-11a. Find the reactions, maximum shear, and maximum moment for the data given in the row(s) assigned from Table P3-1.

- *3-24** A beam is supported and loaded as shown in Figure P3-11b. Find the reactions, maximum shear, and maximum moment for the data given in the row(s) assigned from Table P3-1.

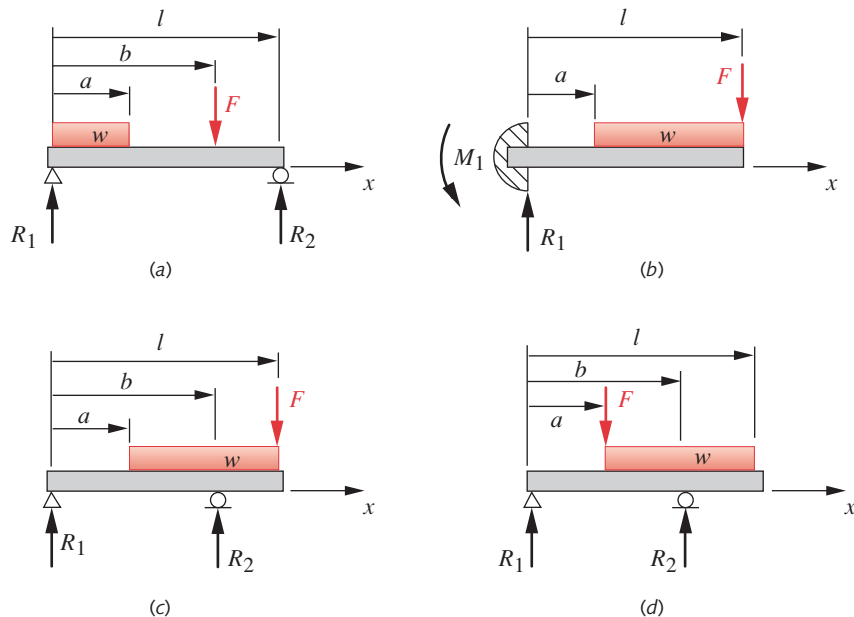
- *3-25** A beam is supported and loaded as shown in Figure P3-11c. Find the reactions, maximum shear, and maximum moment for the data given in the row(s) assigned from Table P3-1.

- 3-26** A beam is supported and loaded as shown in Figure P3-11d. Find the reactions, maximum shear, and maximum moment for the data given in the row(s) assigned from Table P3-1.

- *3-27** A storage rack to hold the paper roll of Problem 3-18 is shown in Figure P3-12. Determine the reactions and draw the shear and moment diagrams for the mandrel that extends 50% into the roll.

- 3-28** Figure P3-13 shows a forklift truck negotiating a 15° ramp to drive onto a 4-ft-high loading platform. The truck weighs 5 000 lb and has a 42-in wheelbase. Determine the reactions and draw the shear and moment diagrams for the worst case of loading as the truck travels up the ramp.

* Answers to these problems are provided in Appendix D. Problem numbers in **boldface** are extended with similar problems in later chapters having the same dash number, e.g., Problem 4-4 is based on Problem 3-4, etc.

**FIGURE P3-11**

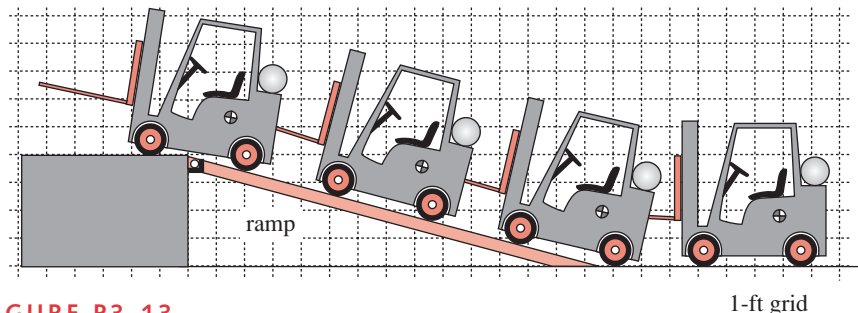
Beams and Beam Loadings for Problems 3-23 to 3-26 - see Table P3-1 for Data

- 3-29 Run the computer model CASE1A for Case Study 1A (on the CD-ROM in several languages) and move the point of application of the hand force along the lever by changing the values of R_{b2} , recalculate, and observe the changes to the forces and moments.

Table P3-1 Data for Problems 3-23 through 3-26Use only data relevant to the particular problem. Lengths in m, forces in N, I in m^4 .

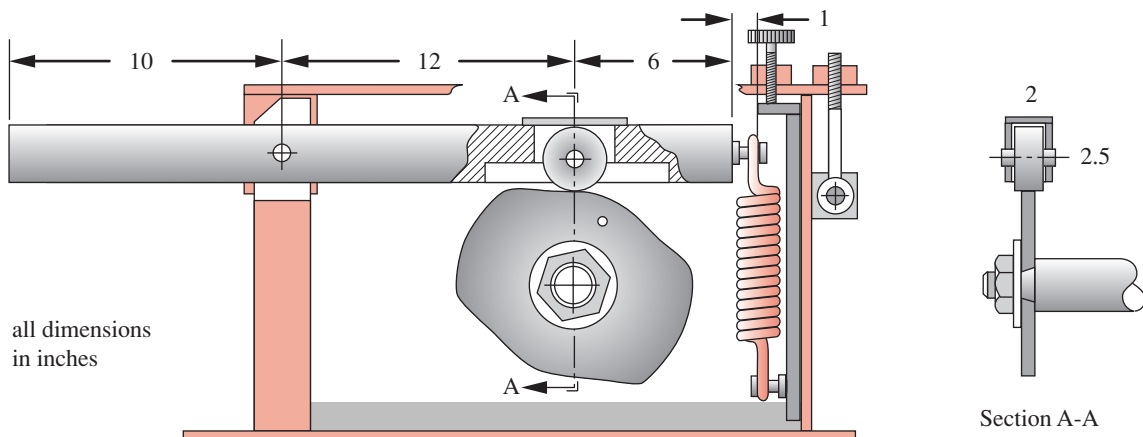
Row	<i>l</i>	<i>a</i>	<i>b</i>	<i>w</i> *	<i>F</i>	<i>I</i>	<i>c</i>	<i>E</i>
<i>a</i>	1.00	0.40	0.60	200	500	$2.85E-08$	$2.00E-02$	steel
<i>b</i>	0.70	0.20	0.40	80	850	$1.70E-08$	$1.00E-02$	steel
<i>c</i>	0.30	0.10	0.20	500	450	$4.70E-09$	$1.25E-02$	steel
<i>d</i>	0.80	0.50	0.60	65	250	$4.90E-09$	$1.10E-02$	steel
<i>e</i>	0.85	0.35	0.50	96	750	$1.80E-08$	$9.00E-03$	steel
<i>f</i>	0.50	0.18	0.40	450	950	$1.17E-08$	$1.00E-02$	steel
<i>g</i>	0.60	0.28	0.50	250	250	$3.20E-09$	$7.50E-03$	steel
<i>h</i>	0.20	0.10	0.13	400	500	$4.00E-09$	$5.00E-03$	alum
<i>i</i>	0.40	0.15	0.30	50	200	$2.75E-09$	$5.00E-03$	alum
<i>j</i>	0.20	0.10	0.15	150	80	$6.50E-10$	$5.50E-03$	alum
<i>k</i>	0.40	0.16	0.30	70	880	$4.30E-08$	$1.45E-02$	alum
<i>l</i>	0.90	0.25	0.80	90	600	$4.20E-08$	$7.50E-03$	alum
<i>m</i>	0.70	0.10	0.60	80	500	$2.10E-08$	$6.50E-03$	alum
<i>n</i>	0.85	0.15	0.70	60	120	$7.90E-09$	$1.00E-02$	alum

3

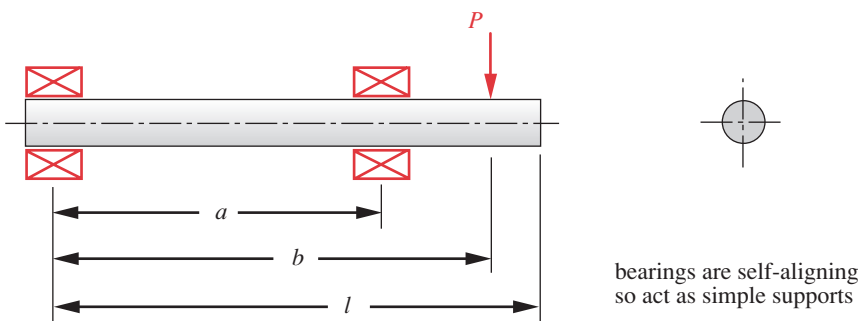
**FIGURE P3-13**

Problem 3-28

- 3-30 Run the computer model CASE2A for Case Study 2A (on the CD-ROM in several languages) and move the point of application of the crimp force along the jaw, recalculate, and observe the changes to the forces and moments.
- 3-31 Run the computer model CASE3A for Case Study 3A (on the CD-ROM in several languages) and move the point of application of \mathbf{P} along the x direction, recalculate, and observe the changes to the forces and moments on the links. What happens when the vertical force \mathbf{P} is centered on link 3? Also, change the angle of the applied force \mathbf{P} to create an x component and observe the effects on the forces and moments on the elements.
- 3-32 Figure P3-14 shows a cam and cam-follower arm. If the load $P = 200$ lb, what spring force is needed at the right end to maintain a minimum load between cam and follower of 25 lb? Find the maximum shear force and bending moment in the follower arm. Plot the shear and moment diagrams.
- 3-33 Write a computer program or equation-solver model to calculate all the singularity functions listed in equations 3.17. Set them up as functions that can be called from within any other program or model.
- 3-34 A beam is supported and loaded as shown in Figure P3-15. Find the reactions, maximum shear, and maximum moment for the data given in the row(s) assigned from Table P3-2.

**FIGURE P3-14**

Problem 3-32

**FIGURE P3-15**

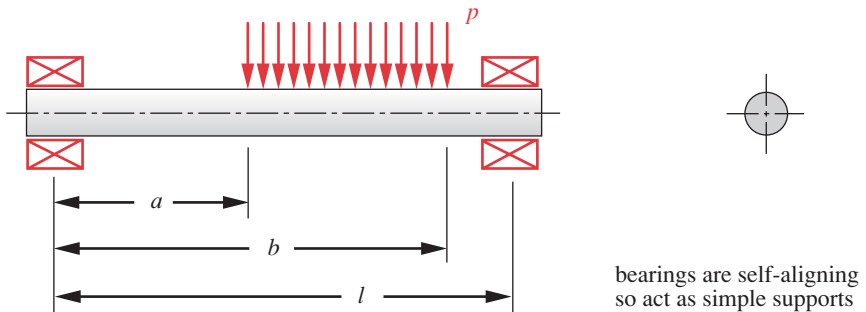
Problems 3-34 and 3-35

- *3-35 A beam is supported and loaded as shown in Figure P3-15. Write a computer program or equation-solver model to find the reactions and calculate and plot the loading, shear, and moment functions. Test the program with the data given in the row(s) assigned from Table P3-2.
- 3-36 A beam is supported and loaded as shown in Figure P3-16. Find the reactions, maximum shear, and maximum moment for the data given in the row(s) assigned from Table P3-2.
- 3-37 A beam is supported and loaded as shown in Figure P3-16. Write a computer program or equation-solver model to find the reactions and calculate and plot the loading, shear, and moment functions. Test the program with the data given in the row(s) assigned from Table P3-2.
- 3-38 A beam is supported and loaded as shown in Figure P3-17. Find the reactions, maximum shear, and maximum moment for the data given in the row(s) assigned from Table P3-2.
- 3-39 A beam is supported and loaded as shown in Figure P3-17. Write a computer program or equation-solver model to find the reactions and calculate and plot the loading, shear, and moment functions. Test the program with the data given in the row(s) assigned from Table P3-2.
- 3-40 A beam is supported and loaded as shown in Figure P3-18. Find the reactions, maximum shear, and maximum moment for the data given in the row(s) assigned from Table P3-2.
- 3-41 A beam is supported and loaded as shown in Figure P3-18. Write a computer program or equation-solver model to find the reactions and calculate and plot the loading, shear, and moment functions. Test the program with the data given in the row(s) assigned from Table P3-2.

Table P3-2 Data for Problems 3-34 Through 3-41

Row	<i>l</i> (in)	<i>a</i> (in)	<i>b</i> (in)	<i>P</i> (lb) or <i>p</i> (lb/in)
<i>a</i>	20	16	18	1 000
<i>b</i>	12	2	7	500
<i>c</i>	14	4	12	750
<i>d</i>	8	4	8	1 000
<i>e</i>	17	6	12	1 500
<i>f</i>	24	16	22	750

* Answers to these problems are provided in Appendix D.

**FIGURE P3-16**

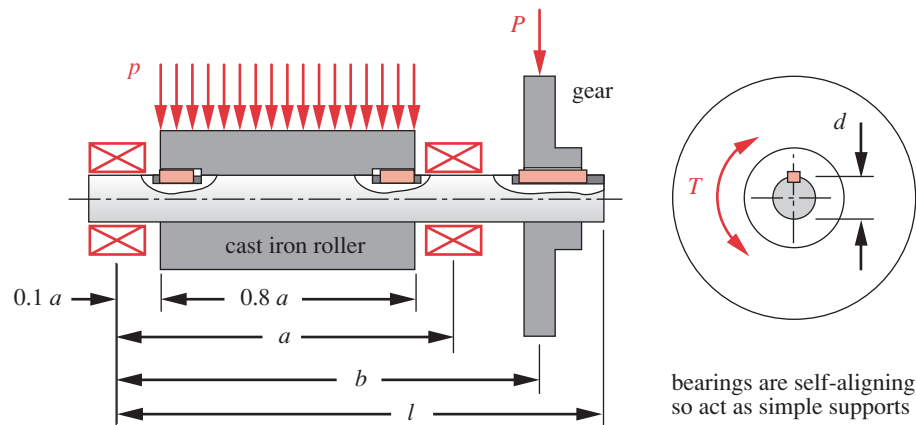
Problems 3-36 and 3-37

Table P3-3

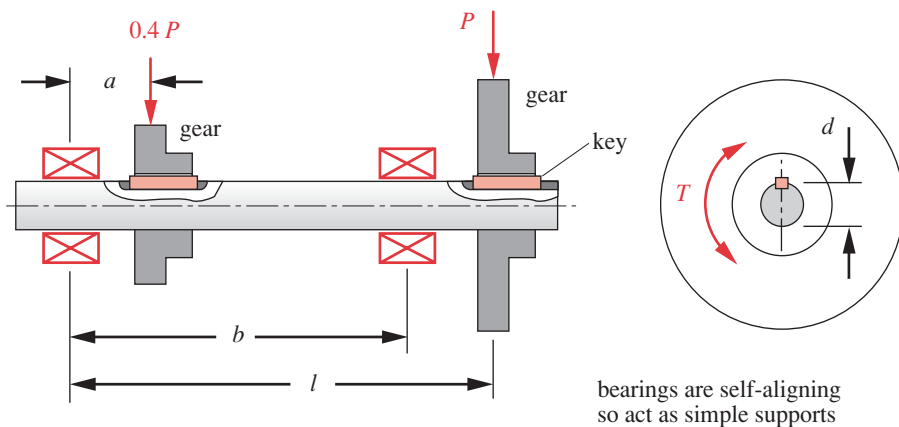
Problem 3-44

R_{12}	13.20 in @ 135°
R_{14}	79.22 in @ 196°
R_{32}	0.80 in @ 45°
R_{34}	32.00 in @ 169°
R_P	124.44 in @ 185°
F_{cable}	2970 lb
W_2	598 lb
W_4	2706 lb
θ_3	98.5°

- 3-42 A 1000-kg speedboat reaches a speed of 16 kph at the instant it takes up the slack in a 100-m-long tow rope attached to a surfboard carrying a 100-kg passenger. If the rope has $k = 5 \text{ N/m}$, what is the dynamic force exerted on the surfboard?
- 3-43 Figure P3-19 shows an oil-field pump jack. For the position shown, draw free-body diagrams of the crank (2), connecting rod (3) and walking beam (4) using variable names similar to those used in Case Studies 1A and 2A. Assume that the crank turns slowly enough that accelerations can be ignored. Include the weight acting at the CG of the walking beam and the crank but not the connecting rod.
- 3-44 For the pump jack of Problem 3-43 and the data of Table P3-3, determine the pin forces on the walking beam, connecting rod, and crank and the reaction torque on the crank.
- 3-45 Figure P3-20 shows an aircraft overhead bin mechanism in end view. For the position shown, draw free-body diagrams of links 2 and 4 and the door (3) using variable names similar to those used in Case Studies 1A and 2A. There are stops that prevent further clockwise motion of link 2 (and the identical link behind it at the other end of the door) resulting in horizontal forces being applied to the door at points A. Assume that the mechanism is symmetrical so that each set of links 2 and 4 carry one half of the door weight. Ignore the weight of links 2 and 4 as they are negligible.

**FIGURE P3-17**

Problems 3-38 and 3-39

**FIGURE P3-18**

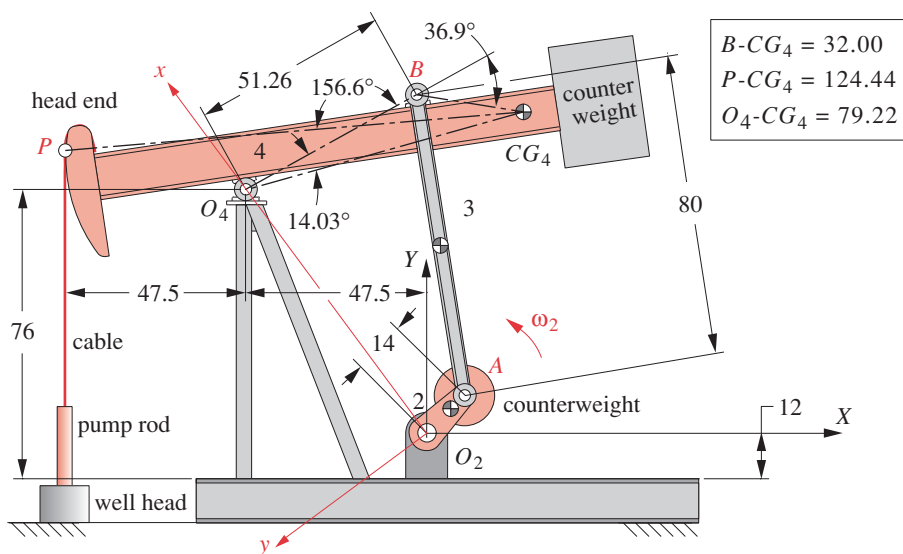
Problems 3-40 and 3-41

- 3-46 For the overhead bin mechanism of Problem 3-45 and the data of Table P3-4, determine the pin forces on the door (3), and links 2 & 4 and the reaction force on each of the two stops.
- 3-47 A particular automobile wheel suspension consists of two A-arms, the wheel (with tire), a coil spring, and a shock absorber (damper). The effective stiffness of the suspension (called the "ride rate") is a function of the coil spring stiffness and the tire stiffness. The A-arms are designed to give the wheel a nearly vertical displacement as the tire rides over bumps in the road. The entire assembly can be modeled as a spring-mass-damper system as shown in Figure 3-15(b). If the sprung mass (mass of the portion of the vehicle supported by the suspension system) weighs 675 lb, determine the ride rate that

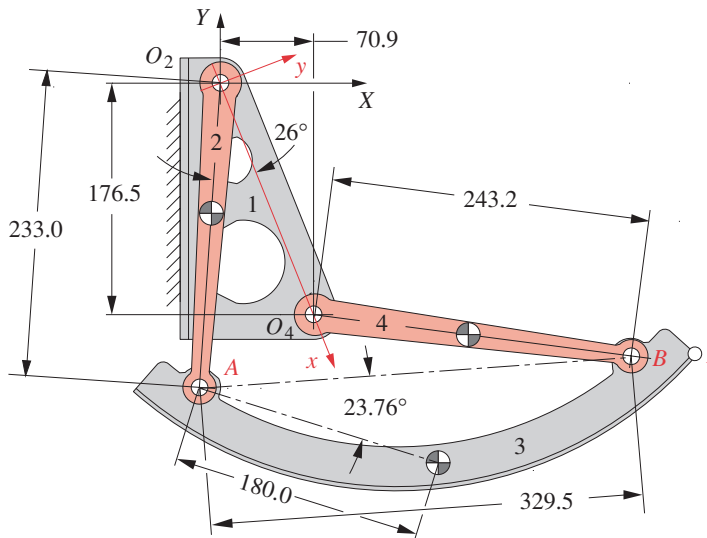
Table P3-4

Problem 3-46

R_{23}	180 mm @ 160.345°
R_{43}	180 mm @ 27.862°
W_3	45 N
θ_2	85.879°
θ_4	172.352°

**FIGURE P3-19**

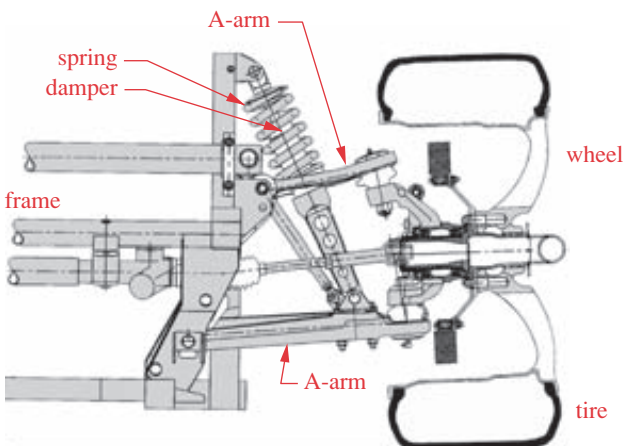
Problems 3-43 and 44

**FIGURE P3-20**

Problems 3-45 and 46

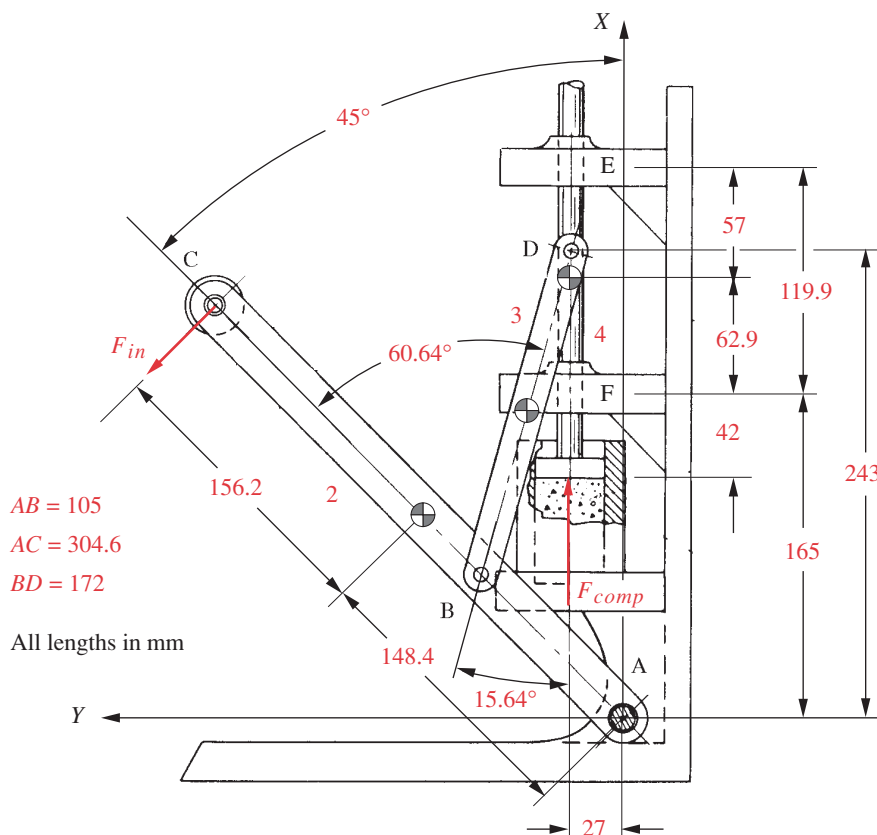
is required to achieve an undamped natural frequency of 1.4 Hz. What is the static deflection of the suspension for the calculated ride rate?

- *3-48 The independent suspension system of Problem 3-47 has an unsprung weight (the weight of the axle, wheel, A-arms, etc.) of 106 lb. Calculate the natural frequency (hop resonance) of the unsprung mass if the combined tire and coil spring stiffness (ride rate) is 1100 lb/in.
- 3-49 The independent suspension system of Problem 3-47 has a sprung weight of 675 lb and a ride rate of 135 lb/in. Calculate the damped natural frequency of the sprung mass if the damping coefficient of the shock absorber is a constant 12 lb-sec/in.

**FIGURE P3-21**

* Answers to these problems are provided in Appendix D.

Problems 3-47 through 49 Viper suspension - Courtesy of DaimlerChrysler Corporation

**FIGURE P3-22**

Problems 3-50 and 3-51

- 3-50 Figure P3-22 shows a powder compaction mechanism. For the position shown, draw free-body diagrams of the input arm (2), connecting rod (3) and compacting ram (4) using variable names similar to those used in Case Studies 1A and 2A. Assume that the input arm turns slowly enough that accelerations can be ignored. Ignore the weights of the arm, connecting rod, and compacting ram. Neglect friction. All links are symmetrical with CG in the center.
- 3-51 For the compaction mechanism of Problem 3-50 and the data of Table P3-5, determine the pin forces on the compacting ram, connecting rod, and input arm. The position vectors (R_{xx}) in the table locate points of force application on a link versus the CG of the link on which the force acts. All links are symmetrical with CG in the center.
- 3-52 Figure P3-23 shows a drag link slider crank mechanism. For the position shown, draw free-body diagrams of links 2 through 6 using variable names similar to those used in Case Studies 1A and 2A. Assume that the crank turns slowly enough that accelerations can be ignored. Ignore the weights of the links and any friction forces or torques. All links are symmetrical with CG in the center.
- 3-53 For the drag link slider crank mechanism of Problem 3-52 and the data of Table P3-6, determine the pin forces on the slider, connecting rods, and crank and the reaction torque on the crank. The position vectors (R_{xx}) in the table locate points of force application on a link versus the CG of the link on which the force acts. All links are symmetrical with CG in the center.

Table P3-5

Problem 3-51

R_{12}	148.4 mm @ 315°
R_{14E}	57.0 mm @ 90°
R_{14F}	62.9 mm @ 270°
R_{32}	42.9 mm @ 74.36°
R_{23}	87.6 mm @ 254.36°
R_{34}	15.0 mm @ 90°
R_{43}	87.6 mm @ 74.36°
R_{in}	152.6 mm @ 225°
R_P	105.0 mm @ 270°
F_{comp}	100 N
θ_3	254.36°

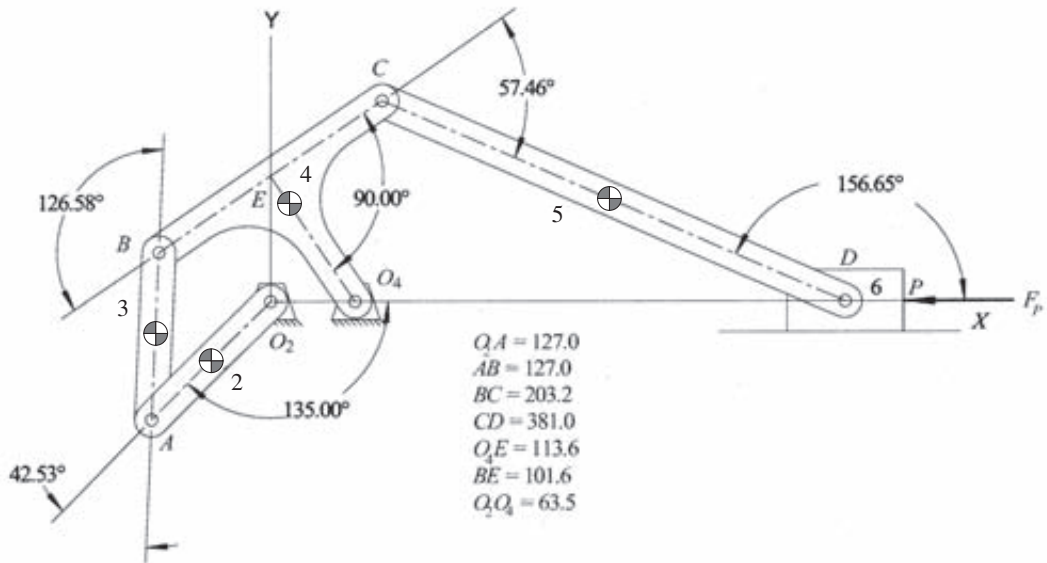
3

Table P3-6

Problem 3-53

R_{12}	63.5 mm @ 45.38°
R_{14}	93.6 mm @ -55.89°
R_{23}	63.5 mm @ 267.80°
R_{32}	63.5 mm @ 225.38°
R_{34}	103.5 mm @ 202.68°
R_{43}	63.5 mm @ 87.80°
R_{45}	190.5 mm @ 156.65°
R_{54}	103.5 mm @ 45.34°
R_{65}	190.5 mm @ -23.35°
F_P	85 N
θ_3	87.80°
θ_5	156.65°

3

**FIGURE P3-23**

Problems 3-52 and 3-53

4

STRESS, STRAIN, AND DEFLECTION

*'Tis not knowing much, but what is useful
that makes a wise man.*

THOMAS FULLER, M.D.



4.0 INTRODUCTION

You have probably had a first course in stress analysis (perhaps called *Strength of Materials* or *Mechanics of Materials*) and thus should understand the fundamentals of that subject. Nevertheless, this chapter will present a review of the basics in order to set the stage for the topic of fatigue analysis in later chapters. Stress and strain were discussed in Chapter 2 on materials properties but were incompletely defined at that juncture. In this chapter we will present a more complete definition of what is meant by the terms stress, strain, and deflection.

Table 4-0 shows the variables used in this chapter and references the equations, tables, or sections in which they are used. At the end of the chapter a summary section is provided that also groups all the significant equations from this chapter for easy reference and identifies the chapter section in which their discussion can be found.

4.1 STRESS

Stress was defined in Chapter 2 as force per unit area with units of psi or MPa. In a part subjected to some forces, stress is generally distributed as a continuously varying function within the continuum of material. Every infinitesimal element of the material can conceivably experience different stresses at the same time. Thus, we must look at stresses as acting on vanishingly small elements within the part. These infinitesimal elements are typically modeled as cubes, shown in Figure 4-1 (p. 142). The stress components are considered to be acting on the faces of these cubes in two different manners. **Normal stresses** act perpendicular (i.e., normal) to the face of the cube and tend

Table 4-0 Variables Used in This Chapter

Part 1 of 2

Symbol	Variable	ips units	SI units	See
<i>A</i>	area	in ²	m ²	Sect. 4.7 - 4.9, 4.11
<i>b</i>	width of beam cross section	in	m	Sect. 4.9
<i>c</i>	distance to outer fiber - straight beam	in	m	Eq. 4.11b
<i>c_i</i>	distance to inner fiber - curved beam	in	m	Eq. 4.12
<i>c_o</i>	distance to outer fiber - curved beam	in	m	Eq. 4.12
<i>d</i>	diameter of cross section	in	m	Sect. 4.10, 4.11
<i>E</i>	Young's modulus	psi	Pa	Sect. 4.7 - 4.12
<i>e</i>	eccentricity of a column	in	m	Sect. 4.14
<i>e</i>	shift of neutral axis - curved beam	in	m	Sect. 4.9, Eq. 4.12a
<i>F</i>	force or load	lb	N	Sect. 4.11
<i>G</i>	shear modulus, modulus of rigidity	psi	Pa	Sect. 4.11
<i>h</i>	depth of beam cross section	in	m	Sect. 4.9
<i>I</i>	second moment of area	in ⁴	m ⁴	Eq. 4.11a
<i>K</i>	geometry parameter - torsion	in ⁴	m ⁴	Eq. 4.26b, Table 4-7
<i>k</i>	radius of gyration	in	m	Sect. 4.16
<i>K_t</i>	geometric stress conc. factor - normal stress	none	none	Sect. 4.15
<i>K_{ts}</i>	geometric stress conc. factor - shear stress	none	none	Sect. 4.15
<i>l</i>	length	in	m	Sect. 4.7 - 4.12
<i>M</i>	moment, moment function	lb-in	N-m	Sect. 4.9
<i>P</i>	force or load	lb	N	Sect. 4.7
<i>P_{cr}</i>	critical column load	lb	N	Sect. 4.16
<i>q</i>	beam loading function	lb	N	Sect. 4.10
<i>Q</i>	integral of first moment of area - beam	in ³	m ³	Eq. 4.13
<i>Q</i>	geometry parameter - torsion	in ³	m ³	Eq. 4.26a, Table 4-3
<i>r</i>	radius - general	in	m	Sect. 4.9, Eq. 4.12
<i>r_i</i>	inside radius of curved beam	in	m	Eq. 4.12
<i>r_o</i>	outside radius of curved beam	in	m	Eq. 4.12
<i>S_r</i>	slenderness ratio - column	none	none	Sect. 4.16
<i>S_y</i>	yield strength	psi	Pa	Sect. 4.16
<i>T</i>	torque	lb-in	N-m	Sect. 4.12
<i>V</i>	beam shear function	lb	N	Sect. 4.9, 4.10
<i>x</i>	generalized length variable	in	m	Sect. 4.10
<i>y</i>	distance from neutral axis - beam	in	m	Eq. 4.11a
<i>y</i>	deflection - general	in	m	Sect. 4.10, 4.14
<i>Z</i>	section modulus	in ³	m ³	Eq. 4.11d
<i>x, y, z</i>	generalized coordinates	any	any	Sect. 4.1, 4.2
ϵ	strain	none	none	Sect. 4.2
θ	beam slope	rad	rad	Sect. 4.10
θ	angular deflection - torsion	rad	rad	Sect. 4.12

Table 4-0 Variables Used in This Chapter

Part 2 of 2

Symbol	Variable	ips units	SI units	See
σ	normal stress	psi	Pa	Sect. 4.1
σ_1	principal stress	psi	Pa	Sect. 4.3
σ_2	principal stress	psi	Pa	Sect. 4.3
σ_3	principal stress	psi	Pa	Sect. 4.3
τ	shear stress	psi	Pa	Sect. 4.1
τ_{13}	maximum shear stress	psi	Pa	Sect. 4.3
τ_{21}	principal shear stress	psi	Pa	Sect. 4.3
τ_{32}	principal shear stress	psi	Pa	Sect. 4.3

to either pull it out (tensile normal stress) or push it in (compressive normal stress). **Shear stresses** act parallel to the faces of the cubes, in pairs (couples) on opposite faces, which tends to distort the cube into a rhomboidal shape. This is analogous to grabbing both pieces of bread of a peanut-butter sandwich and sliding them in opposite directions. The peanut butter will be sheared as a result. These normal and shear components of stress acting on an infinitesimal element make up the terms of a **tensor**.*

Stress is a tensor of order two[†] and thus requires nine values or components to describe it in three dimensions. The 3-D stress tensor can be expressed as the matrix:

$$\begin{bmatrix} \sigma_{xx} & \tau_{xy} & \tau_{xz} \\ \tau_{yx} & \sigma_{yy} & \tau_{yz} \\ \tau_{zx} & \tau_{zy} & \sigma_{zz} \end{bmatrix} \quad (4.1a)$$

where the notation for each stress component contains three elements, a magnitude (either σ or τ), the direction of a normal to the reference surface (first subscript), and a direction of action (second subscript). We will use σ to refer to normal stresses and τ for shear stresses.

Many elements in machinery are subjected to three-dimensional stress states and thus require the stress tensor of equation 4.1a. There are some special cases, however, which can be treated as two-dimensional stress states.

The stress tensor for 2-D is

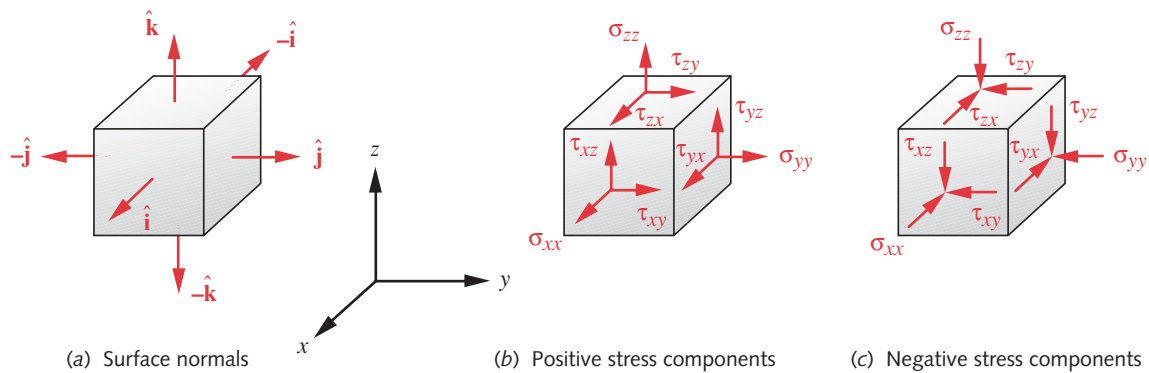
$$\begin{bmatrix} \sigma_{xx} & \tau_{xy} \\ \tau_{yx} & \sigma_{yy} \end{bmatrix} \quad (4.1b)$$

Figure 4-1 shows an infinitesimal cube of material taken from within the material continuum of a part that is subjected to some 3-D stresses. The faces of this infinitesimal cube are made parallel to a set of xyz axes taken in some convenient orientation. The orientation of each face is defined by its surface normal vector[‡] as shown in Figure 4-1a. The x face has its surface normal parallel to the x axis, etc. Note that there are thus two x faces, two y faces, and two z faces, one of each being positive and one negative as defined by the sense of its surface normal vector.

* For a discussion of tensor notation, see C. R. Wylie and L. C. Barrett, *Advanced Engineering Mathematics*, 5th ed., McGraw-Hill, New York, 1982.

† Equation 4.1a more correctly shows a tensor for rectilinear Cartesian coordinates. The more general tensor notation for curvilinear coordinate systems will not be used here.

‡ A surface normal vector is defined as "growing out of the surface of the solid in a direction normal to that surface." Its sign is defined as the sense of this surface normal vector in the local coordinate system.

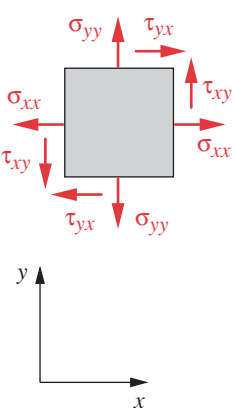
**FIGURE 4-1**

The Stress Cube, Its Surface Normals, and Its Stress Components

The nine stress components are shown acting on the surfaces of this infinitesimal element in Figure 4-1b and c. The components σ_{xx} , σ_{yy} , and σ_{zz} are the normal stresses, so called because they act, respectively, in directions normal to the x , y , and z surfaces of the cube. The components τ_{xy} and τ_{xz} , for example, are shear stresses that act on the x face and whose directions of action are parallel to the y and z axes, respectively. The sign of any one of these components is defined as positive if the signs of its surface normal and its stress direction are the same, and as negative if they are different. Thus the components shown in Figure 4-1b are all positive because they are acting on the positive faces of the cube and their directions are also positive. The components shown in Figure 4-1c are all negative because they are acting on the positive faces of the cube and their directions are negative. This sign convention makes tensile normal stresses positive and compressive normal stresses negative.

For the 2-D case, only one face of the stress cube may be drawn. If the x and y directions are retained and z eliminated, we look normal to the xy plane of the cube of Figure 4-1 and see the stresses shown in Figure 4-2, acting on the unseen faces of the cube. The reader should confirm that the stress components shown in Figure 4-2 are all positive by the sign convention stated above.

Note that the definition of the dual subscript notation given above is consistent when applied to the normal stresses. For example, the normal stress σ_{xx} acts on the x face and is also in the x direction. Since the subscripts are simply repeated for normal stresses, it is common to eliminate one of them and refer to the normal components simply as σ_x , σ_y , and σ_z . Both subscripts are needed to define the shear-stress components and they will be retained. It can also be shown^[1] that the stress tensor is symmetric, which means that

**FIGURE 4-2**

Two-Dimensional Stress Element

$$\begin{aligned}\tau_{xy} &= \tau_{yx} \\ \tau_{yz} &= \tau_{zy} \\ \tau_{zx} &= \tau_{xz}\end{aligned}\tag{4.2}$$

This reduces the number of stress components to be calculated.

4.2 STRAIN

Stress and strain are linearly related by Hooke's law in the elastic region of most engineering materials as discussed in Chapter 2. Strain is also a second-order tensor and can be expressed for the 3-D case as

$$\begin{bmatrix} \epsilon_{xx} & \epsilon_{xy} & \epsilon_{xz} \\ \epsilon_{yx} & \epsilon_{yy} & \epsilon_{yz} \\ \epsilon_{zx} & \epsilon_{zy} & \epsilon_{zz} \end{bmatrix} \quad (4.3a)$$

and for the 2-D case as

$$\begin{bmatrix} \epsilon_{xx} & \epsilon_{xy} \\ \epsilon_{yx} & \epsilon_{yy} \end{bmatrix} \quad (4.3b)$$

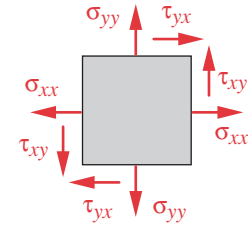
where ϵ represents either a normal or a shear strain, the two being differentiated by their subscripts. We will also simplify the repeated subscripts for normal strains to ϵ_x , ϵ_y , and ϵ_z for convenience while retaining the dual subscripts to identify shear strains. The same symmetric relationships shown for shear stress components in equation 4.2 also apply to the strain components.

4.3 PRINCIPAL STRESSES

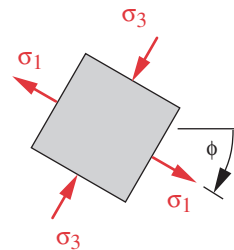
The axis systems taken in Figures 4-1 and 4-2 are arbitrary and are usually chosen for convenience in computing the applied stresses. For any particular combination of applied stresses, there will be a continuous distribution of the stress field around any point analyzed. The normal and shear stresses at the point will vary with direction in any coordinate system chosen. There will always be planes on which the shear-stress components are zero. The normal stresses acting on these planes are called the principal stresses. The planes on which these principal stresses act are called the **principal planes**. The directions of the surface normals to the principal planes are called the **principal axes**, and the normal stresses acting in those directions are the **principal normal stresses**. There will also be another set of mutually perpendicular axes along which the shear stresses will be maximal. The **principal shear stresses** act on a set of planes that are at 45° angles to the planes of the principal normal stresses. The principal planes and principal stresses for the 2-D case of Figure 4-2 are shown in Figure 4-3.

Since, from an engineering standpoint, we are most concerned with designing our machine parts so that they will not fail, and since failure will occur if the stress at any point exceeds some safe value, we need to find the largest stresses (both normal and shear) that occur anywhere in the continuum of material that makes up our machine part. We may be less concerned with the directions of those stresses than with their magnitudes as long as the material can be considered to be at least macroscopically isotropic, thus having strength properties that are uniform in all directions. Most metals and many other engineering materials meet these criteria, although wood and composite materials are notable exceptions.

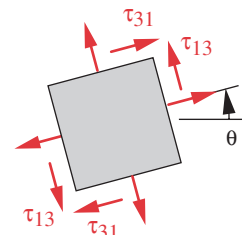
The expression relating the applied stresses to the principal stresses is



(a) Applied stresses



(b) Principal normal stresses



(c) Principal shear stresses



FIGURE 4-3

Principal Stresses on a Two-Dimensional Stress Element

$$\begin{bmatrix} \sigma_x - \sigma & \tau_{xy} & \tau_{xz} \\ \tau_{yx} & \sigma_y - \sigma & \tau_{yz} \\ \tau_{zx} & \tau_{zy} & \sigma_z - \sigma \end{bmatrix} \begin{bmatrix} n_x \\ n_y \\ n_z \end{bmatrix} = \begin{bmatrix} 0 \\ 0 \\ 0 \end{bmatrix} \quad (4.4a)$$

where σ is the principal stress magnitude and n_x , n_y , and n_z are the direction cosines of the unit vector \mathbf{n} , which is normal to the principal plane:

$$\begin{aligned} \hat{\mathbf{n}} \cdot \hat{\mathbf{n}} &= 1 \\ \hat{\mathbf{n}} &= n_x \hat{\mathbf{i}} + n_y \hat{\mathbf{j}} + n_z \hat{\mathbf{k}} \end{aligned} \quad (4.4b)$$

For the solution of equation 4.4a to exist, the determinant of the coefficient matrix must be zero. Expanding this determinant and setting it to zero, we obtain

$$\sigma^3 - C_2\sigma^2 - C_1\sigma - C_0 = 0 \quad (4.4c)$$

where

$$\begin{aligned} C_2 &= \sigma_x + \sigma_y + \sigma_z \\ C_1 &= \tau_{xy}^2 + \tau_{yz}^2 + \tau_{zx}^2 - \sigma_x\sigma_y - \sigma_y\sigma_z - \sigma_z\sigma_x \\ C_0 &= \sigma_x\sigma_y\sigma_z + 2\tau_{xy}\tau_{yz}\tau_{zx} - \sigma_x\tau_{yz}^2 - \sigma_y\tau_{zx}^2 - \sigma_z\tau_{xy}^2 \end{aligned}$$

Equation 4.4c is a cubic polynomial in σ . The coefficients C_0 , C_1 , and C_2 are called the tensor invariants, because they have the same values regardless of the initial choice of xyz axes in which the applied stresses were measured or calculated. The units of C_2 are psi (MPa), of C_1 psi² (MPa²), and of C_0 psi³ (MPa³). The three principal (normal) stresses σ_1 , σ_2 , σ_3 are the three roots of this cubic polynomial. The roots of this polynomial are always real^[2] and are usually ordered such that $\sigma_1 > \sigma_2 > \sigma_3$. If needed, the directions of the principal stress vectors can be found by substituting each root of equation 4.4c into 4.4a and solving for n_x , n_y , and n_z for each of the three principal stresses. The directions of the three principal stresses are mutually orthogonal.

The principal shear stresses can be found from the values of the principal normal stresses using

$$\begin{aligned} \tau_{13} &= \frac{|\sigma_1 - \sigma_3|}{2} \\ \tau_{21} &= \frac{|\sigma_2 - \sigma_1|}{2} \\ \tau_{32} &= \frac{|\sigma_3 - \sigma_2|}{2} \end{aligned} \quad (4.5)$$

If the principal normal stresses have been ordered as shown above, then $\tau_{max} = \tau_{13}$. The directions of the planes of the principal shear stresses are 45° from those of the principal normal stresses and are also mutually orthogonal.

The solution of equation 4.4c for its three roots can be done trigonometrically by Viète's method* or using an iterative root-finding algorithm. The file STRESS3D provided solves equation 4.4c and finds the three principal stress roots by Viète's

* See *Numerical Recipes* by W. H. Press et al., Cambridge Univ. Press, 1986, p. 146, or *Standard Mathematical Tables*, CRC Press, 22d ed., 1974, p. 104, or any collection of standard mathematical formulas.

method and orders them by the above convention. STRESS3D also computes the stress function (Eq. 4.4c) for a list of user-defined values of σ and then plots that function. The root crossings can be seen on the plot. Figure 4-4 shows the stress function for an arbitrary set of applied stresses plotted over a range of values of σ that includes all three roots. Table 4-1 shows the results of the computation.

For the special case of a two-dimensional stress state, the equations 4.4c for principal stress reduce to*

$$\sigma_a, \sigma_b = \frac{\sigma_x + \sigma_y}{2} \pm \sqrt{\left(\frac{\sigma_x - \sigma_y}{2}\right)^2 + \tau_{xy}^2}$$

$$\sigma_c = 0 \quad (4.6a)$$

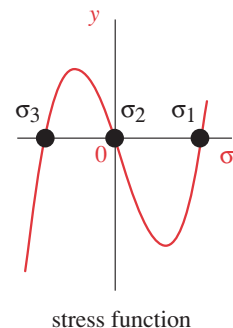
The two nonzero roots calculated from equation 4.6a are temporarily labeled σ_a and σ_b , and the third root σ_c is always zero in the 2-D case. Depending on their resulting values, the three roots are then labeled according to the convention: *algebraically largest* = σ_1 , *algebraically smallest* = σ_3 , and *other* = σ_2 . Using equation 4.6a to solve the example shown in Figure 4-4 would yield values of $\sigma_1 = \sigma_a$, $\sigma_3 = \sigma_b$, and $\sigma_2 = \sigma_c = 0$ as labeled in the figure.[†] Of course, equation 4.4c for the 3-D case can still be used to solve any two-dimensional case. One of the three principal stresses found will then be zero. The example in Figure 4-4 is of a two-dimensional case solved with equation 4.4c. Note the root at $\sigma = 0$.

Once the three principal stresses are found and ordered as described above, the maximum shear stress is found from equation 4.5:

$$\tau_{max} = \tau_{13} = \frac{|\sigma_1 - \sigma_3|}{2} \quad (4.6b)$$

Table 4-1 Solution to the Cubic Stress Function for a Plane Stress Case
From File STRESS3D

Input	Variable	Output	Unit	Comments
1 000	σ_{xx}		psi	applied normal stress in x direction
-750	σ_{yy}		psi	applied normal stress in y direction
0	σ_{zz}		psi	applied normal stress in z direction
500	τ_{xy}		psi	applied shear stress in xy direction
0	τ_{yz}		psi	applied shear stress in yz direction
0	τ_{zx}		psi	applied shear stress in zx direction
C ₂	250		psi	coefficient of σ^2 term
C ₁	1.0E6		psi ²	coefficient of σ^1 term
C ₀	0		psi ³	coefficient of σ^0 term
σ_1	1 133	psi		principal stress root #1
σ_2	0	psi		principal stress root #2
σ_3	-883	psi		principal stress root #3

**FIGURE 4-4**

The Three Roots of the Stress Function for a Plane Stress Case

* Equations 4.6 can also be used when one principal stress is nonzero but is directed along one of the axes of the xyz coordinate system chosen for calculation. The stress cube of Figure 4-1 is then rotated about one principal axis to determine the angles of the other two principal planes.

[†] If the 3-D numbering convention is strictly observed in the 2-D case, then sometimes the two nonzero principal stresses will turn out to be σ_1 and σ_3 if they are opposite in sign (as in Example 4-1). Other times they will be σ_1 and σ_2 when they are both positive and the smallest (σ_3) is zero (as in Example 4-2). A third possibility is that both nonzero principal stresses are negative (compressive) and the algebraically largest of the set (σ_1) is then zero. Equation 4.6a arbitrarily calls the two nonzero 2-D principal stresses σ_a and σ_b with the remaining one (σ_c) reserved for the zero member of the trio. Application of the standard convention can result in σ_a and σ_b being called any of the possible combinations σ_1 and σ_2 , σ_1 and σ_3 , or σ_2 and σ_3 depending on their relative values. See Examples 4-1 and 4-2.

4.4 PLANE STRESS AND PLANE STRAIN

The general state of stress and strain is three-dimensional but there exist particular geometric configurations that can be treated differently.

Plane Stress

The two-dimensional, or biaxial, stress state is also called plane stress. **Plane stress** requires that one principal stress be zero. This condition is common in some applications. For example, a thin plate or shell may also have a state of plane stress away from its boundaries or points of attachment. These cases can be treated with the simpler approach of equations 4.6.

Plane Strain

There are principal strains associated with the principal stresses. If one of the principal strains (say ϵ_3) is zero, and if the remaining strains are independent of the dimension along its principal axis, n_3 , it is called **plane strain**. This condition occurs in particular geometries. For example, if a long, solid, prismatic bar is loaded only in the transverse direction, regions within the bar that are distant from any end constraints will see essentially zero strain in the direction along the axis of the bar and be in plane strain. (However, the stress is not zero in the zero-strain direction.) A long, hydraulic dam can be considered to have a plane strain condition in regions well removed from its ends or base at which it is attached to surrounding structures.

4.5 MOHR'S CIRCLES

Mohr's circles* have long provided a means to do a graphical solution of equation 4.6 and find the principal stresses for the plane stress case. Many textbooks on machine design present the Mohr's circle method as a primary solution technique for determining principal stresses. Before the advent of programmable calculators and computers, Mohr's graphical method was a reasonable and practical way to solve equation 4.6. Now, however, it is more practical to find the principal stresses numerically. Nevertheless, we present the graphical method for several reasons. It can serve as a quick check on a numerical solution, and it may be the only viable method if the power to your computer fails or your calculator's batteries go dead. It also serves the useful purpose of providing a visual presentation of the stress state at a point.

Mohr's circles exist for the three-dimensional stress case as well, but a graphical construction method is not available to create them directly from the applied-stress data except for the special case where one of the principal stresses is coincident with an axis of the xyz coordinate system chosen, i.e., where one plane is a plane of principal stress. However, once the principal stresses are calculated from equation 4.4c (p. 144) by a suitable root-finding technique, the 3-D Mohr's circles can be drawn by using the calculated principal stresses. A computer program called MOHR is provided on disk for that purpose. In the special 3-D stress case where one principal stress lies along a coordinate axis, the three Mohr's circles can be graphically constructed.

* Devised by the German engineer, Otto Mohr (1835–1918). His circles are also used for the coordinate transformation of strains, and area moments and products of inertia.

The Mohr plane, on which Mohr's circles are drawn, is arranged with its axes drawn mutually perpendicular, but the angle between them represents 180° in real space. All angles drawn on the Mohr plane are double their value in real space. The abscissa is the axis of all normal stresses. The applied normal stresses σ_x , σ_y , and σ_z are plotted along this axis and the principal stresses σ_1 , σ_2 , and σ_3 are also found on this axis. The ordinate is the axis of all shear stresses. It is used to plot the applied shear stresses τ_{xy} , τ_{yx} , and τ_{xz} and to find the maximum shear stress.* Mohr used a sign convention for shear stresses that makes *cw* shear couples positive, *which is not consistent with the now-standard right-hand rule*. Nevertheless, this left-handed convention is still used for his circles. The best way to demonstrate the use of Mohr's circle is with examples.

EXAMPLE 4-1

Determining Principal Stresses Using Mohr's Circles

Problem: A biaxial stress element as shown in Figure 4-2 has $\sigma_x = 40\,000$ psi, $\sigma_y = -20\,000$ psi, and $\tau_{xy} = 30\,000$ psi *ccw*. Use Mohr's circles to determine the principal stresses. Check the result with a numerical method.

Solution: See Figures 4-2 (p. 142) and 4-5.

- 1 Construct the Mohr-plane axes as shown in Figure 4-5b and label them σ and τ .
- 2 Lay off the given applied stress σ_x (as line *OA*) to any convenient scale along the normal-stress (horizontal) axis. Note that σ_x is a tensile (positive) stress in this example.
- 3 Lay off the given applied stress σ_y (as line *OB*) to scale along the normal-stress axis. Note that σ_y is a compressive (negative) stress in this example.
- 4 Figure 4-2 shows that the pair of shear stresses τ_{xy} create a *ccw* couple on the element. This couple is balanced for equilibrium by the *cw* couple provided by the shear stresses τ_{yx} . Recall that both of these shear stresses, τ_{xy} and τ_{yx} , are equal in magnitude according to equation 4.2 (p. 142) and are positive according to the stress sign convention. But, instead of using the stress sign convention, they are plotted on the Mohr circle according to the rotation that they imply to the element, using Mohr's left-handed sign convention of *cw+* and *ccw-*.
- 5 Draw a vertical line downward (*ccw-*) from the tip of σ_x (as line *AC*) to represent the scaled magnitude of τ_{xy} . Draw a vertical line upward (*cw+*) from the tip of σ_y (as line *BD*) to represent the scaled magnitude of τ_{yx} .
- 6 The diameter of one Mohr's circle is the distance from point *C* to point *D*. Line *AB* bisects *CD*. Draw the circle using this intersection as a center.
- 7 Two of the three principal normal stresses are then found at the two intersections that this Mohr's circle makes with the normal stress axis at points *P*₁ and *P*₃: $\sigma_1 = 52\,426$ psi at *P*₁ and $\sigma_3 = -32\,426$ psi at *P*₃.
- 8 Since there were no applied stresses in the *z* direction in this example, it is a 2-D stress state, and the third principal stress, σ_2 , is zero, located at point *O*, which is also labeled *P*₂.

* The fact that Mohr used the same axes to plot more than one variable is one of the sources of confusion to students when they first encounter this method. Just remember that all σ 's are plotted on the horizontal axis whether they are applied normal stresses (σ_x , σ_y , σ_z) or principal stresses (σ_1 , σ_2 , σ_3), and all τ 's are plotted on the vertical axis whether they are applied shear stresses (τ_{xy} , etc.) or maximum shear stresses (τ_{12} , etc.). The Mohr axes are **not** conventional Cartesian axes.

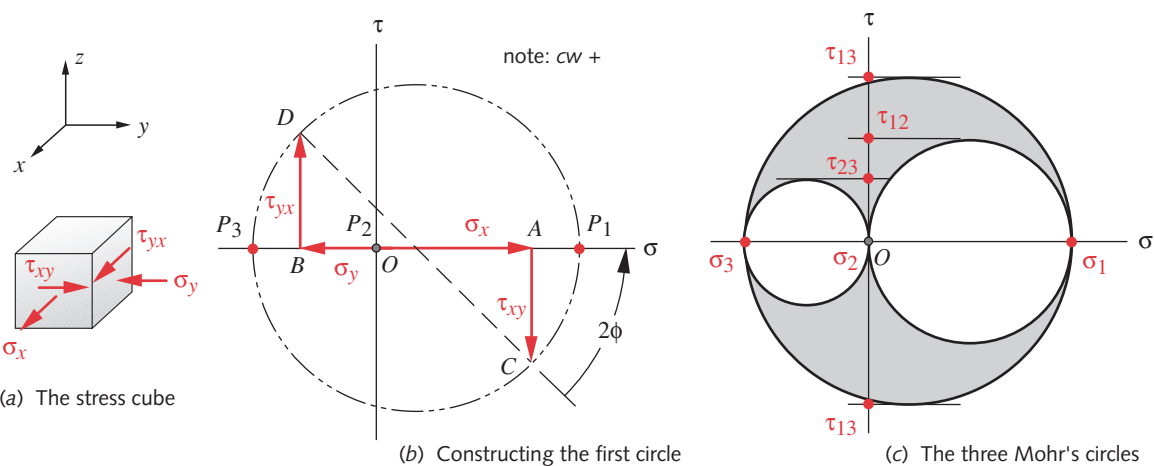


FIGURE 4-5

The Stress Cube and Mohr's Circles for Example 4-1

- 9 There are still two other Mohr's circles to be drawn. The three Mohr's circles are defined by the diameters $(\sigma_1 - \sigma_3)$, $(\sigma_1 - \sigma_2)$, and $(\sigma_2 - \sigma_3)$, which are the lines P_1P_3 , P_2P_1 , and P_2P_3 . The three circles are shown in Figure 4-5c.
- 10 Extend horizontal tangent lines from the top and bottom extremes of each Mohr's circle to intersect the shear (vertical) axis. This determines the values of the principal shear stresses associated with each pair of principal normal stresses: $\tau_{13} = 42.426$, $\tau_{12} = 26.213$, and $\tau_{23} = 16.213$ psi. Note that despite having only two nonzero principal normal stresses, there are three nonzero principal shear stresses. However, only the largest of these, $\tau_{max} = \tau_{13} = 42.426$ psi, is of interest for design purposes.
- 11 We can also determine the angles (with respect to our original xyz axes) of the principal normal and principal shear stresses from the Mohr's circle. These angles are only of academic interest if the material is homogeneous and isotropic. If it is not isotropic, its material properties are direction dependent and the directions of the principal stresses are then important. The angle $2\phi = -45^\circ$ in Figure 4-5a represents the orientation of the principal normal stress with respect to the x axis of our original system. Note that the line DC on the Mohr plane is the x axis in real space and the angles are measured according to Mohr's left-handed convention (*cw+*). Since angles on the Mohr plane are double those in real space, the angle of the principal stress σ_1 with respect to the real-space x axis, is $\phi = -22.5^\circ$. The stress σ_3 will be 90° from σ_1 and the maximum shear stress τ_{13} will be 45° from the σ_1 axis in real space.

A computer program called MOHR has been written and is included with this text. Program MOHR allows the input of any set of applied stresses and computes the principal normal and shear stresses using equations 4.4 and 4.5 (p. 144). The program then plots the Mohr's circles and will also display the stress function in the vicinity of the three principal stress roots. Data files that can be read into this program are also supplied. Open the file EX04-01.moh in MOHR to see the analytical solution to that example. Additional files with the name EX04-01 can be input to various commercial programs (identified by suffix) and will also calculate the principal stresses and plot the cubic stress function for Example 4-1. See the book's CD-ROM.

We will now change the previous example only slightly to show the need for drawing all three Mohr's circles, even in the plane stress case. The change of significance makes the applied stresses σ_x and σ_y both positive, instead of opposite in sign.

EXAMPLE 4-2

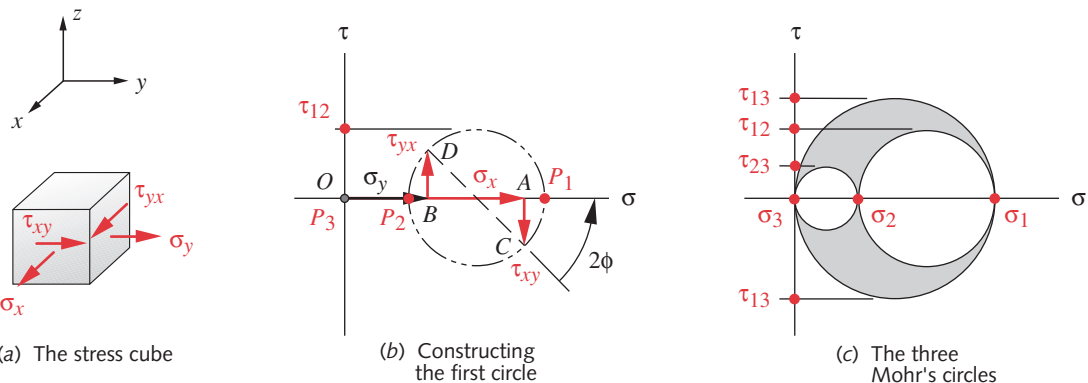
Determining Plane Stresses Using Mohr's Circles

4

Problem: A biaxial stress element as shown in Figure 4-2 has $\sigma_x = 40\,000$ psi, $\sigma_y = 20\,000$ psi, and $\tau_{xy} = 10\,000$ psi ccw. Use Mohr's circles to determine the principal stresses. Check the result with a numerical method.

Solution: See Figures 4-2 (p. 142) and 4-6.

- 1 Construct the Mohr-plane axes as shown in Figure 4-6 and label them σ and τ .
- 2 Lay off the given applied stress σ_x (as line OA) to scale along the normal-stress (horizontal) axis. Note that σ_x is a tensile (positive) stress in this example.
- 3 Lay off the given applied stress σ_y (as line OB) to scale along the normal-stress axis. Note that σ_y is also a tensile (positive) stress in this example and so lies in the same direction as σ_x along the σ axis.
- 4 Figure 4-2 shows that the shear stresses τ_{xy} create a ccw couple on the element. This couple is balanced for equilibrium by the cw couple provided by the shear stresses τ_{yx} . Recall that both of these shear stresses, τ_{xy} and τ_{yx} , are equal according to equation 4.2 (p. 142) and are positive according to the stress sign convention. But, instead of using the stress sign convention, they are plotted on the Mohr circle according to the rotation that they imply to the element, using Mohr's left-handed sign convention of cw+ and ccw-.
- 5 Draw a vertical line downward (ccw-) from the tip of σ_x (as line AC) to represent the scaled magnitude of τ_{xy} . Draw a vertical line upward (cw+) from the tip of σ_y (as line BD) to represent the scaled magnitude of τ_{yx} .
- 6 The diameter of one Mohr's circle is the distance from point C to point D . Line AB bisects CD . Draw the circle using this intersection as a center.
- 7 Two of the three principal normal stresses are then found at the two intersections that this Mohr's circle makes with the normal-stress axis at points P_1 and P_2 : $\sigma_1 = 44\,142$ and $\sigma_2 = 15\,858$ psi. Note that if we stop at this point, the maximum shear stress appears to be $\tau_{12} = 14\,142$ psi as defined by the projection of a horizontal tangent from the top of the one circle to the τ axis, as shown in Figure 4-6b.
- 8 Since there were no applied stresses in the z direction in this example, it is a 2-D stress state, and the third principal stress, σ_3 , is known to be zero, thus is located at point O , also labeled P_3 .
- 9 There are still two other Mohr's circles to be drawn. The three Mohr's circles are defined by the diameters $(\sigma_1 - \sigma_3)$, $(\sigma_1 - \sigma_2)$, and $(\sigma_2 - \sigma_3)$, which in this case are the lines P_1P_3 , P_1P_2 , and P_2P_3 as shown in Figure 4-6.

**FIGURE 4-6**

The Stress Cube and Mohr's Circles for Example 4-2

- 10 Extend horizontal tangent lines from the top and bottom extremes of each Mohr's circle to intersect the shear (vertical) axis. This determines the value of the principal shear stress associated with each pair of principal normal stresses: i.e., $\tau_{13} = 22\ 071$, $\tau_{12} = 14\ 142$, and $\tau_{23} = 7\ 929$ psi. The largest of these is $\tau_{max} = 22\ 071$, not the value 14 142 found in step 7.
- 11 Note that it is always the circle lying between the largest and smallest principal stresses that determines the maximum shear stress. In the previous example the zero principal stress was not the smallest of the three, because one principal stress was negative. In the present example the zero principal stress is the smallest. Thus, failing to draw all three circles would have led to a serious error in the value of τ_{max} .
- 12 The files EX04-02 can be opened in program MOHR and others. See the CD-ROM.

The previous two examples point out some uses and limitations of the Mohr's circle approach to plane stress calculations. From a practical standpoint, as long as computational resources (at least in the form of a programmable pocket calculator) are available to the modern engineer, the analytical solution (Eq. 4.4c, p. 144) is the preferred method of solution for determining principal stresses. It is universal (serving for plane stress, plane strain or any general stress case) and it yields all three principal stresses.

EXAMPLE 4-3

Determining 3-D Stresses Using Analytical Methods

Problem: A triaxial stress element as shown in Figure 4-1 (p. 142) has $\sigma_x = 40\ 000$, $\sigma_y = -20\ 000$, $\sigma_z = -10\ 000$, $\tau_{xy} = 5\ 000$, $\tau_{yz} = -1\ 500$, $\tau_{zx} = 2\ 500$ psi. Find the principal stresses using a numerical method and draw the resulting Mohr's circles.

Solution: See Figures 4-2 (p. 142) and 4-7.

- 1 Calculate the tensor invariants C_0 , C_1 , and C_2 from equation 4.4c.

$$C_2 = \sigma_x + \sigma_y + \sigma_z = 40\ 000 - 20\ 000 - 10\ 000 = 10\ 000 \quad (a)$$

$$\begin{aligned} C_1 &= \tau_{xy}^2 + \tau_{yz}^2 + \tau_{zx}^2 - \sigma_x \sigma_y - \sigma_y \sigma_z - \sigma_z \sigma_x \\ &= (5\ 000)^2 + (-1\ 500)^2 + (2\ 500)^2 - (40\ 000)(-20\ 000) \\ &\quad - (-20\ 000)(-10\ 000) - (-10\ 000)(40\ 000) = 10.335E8 \end{aligned} \quad (b)$$

$$\begin{aligned} C_0 &= \sigma_x \sigma_y \sigma_z + 2\tau_{xy}\tau_{yz}\tau_{zx} - \sigma_x \tau_{yz}^2 - \sigma_y \tau_{zx}^2 - \sigma_z \tau_{xy}^2 \\ &= 40\ 000(-20\ 000)(-10\ 000) + 2(5\ 000)(-1\ 500)(2\ 500) \\ &\quad - 40\ 000(-1\ 500)^2 - (-20\ 000)(2\ 500)^2 \\ &\quad - (-10\ 000)(5\ 000)^2 = 8.248E12 \end{aligned} \quad (c)$$

- 2 Substitute the invariants into equation 4.4c (p. 144) and solve for its three roots using Viete's or a numerical method.

$$\sigma^3 - C_2\sigma^2 - C_1\sigma - C_0 = 0$$

$$\sigma^3 - 10\ 000\ \sigma^2 - 10.335E8\ \sigma - 8.248E12 = 0 \quad (d)$$

$$\sigma_1 = 40\ 525; \quad \sigma_2 = -9\ 838; \quad \sigma_3 = -20\ 687$$

- 3 The principal shear stresses can now be found from equation 4.5 (p. 144).

$$\begin{aligned} \tau_{13} &= \frac{|\sigma_1 - \sigma_3|}{2} = \frac{|40\ 525 - (-20\ 687)|}{2} = 30\ 606 \\ \tau_{21} &= \frac{|\sigma_2 - \sigma_1|}{2} = \frac{|-9\ 838 - 40\ 525|}{2} = 25\ 182 \quad (e) \\ \tau_{32} &= \frac{|\sigma_3 - \sigma_2|}{2} = \frac{|-20\ 687 - (-9\ 838)|}{2} = 5\ 425 \end{aligned}$$

- 4 The files EX04-03 can be opened in program MOHR and others. See the CD-ROM.

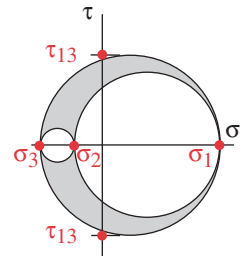
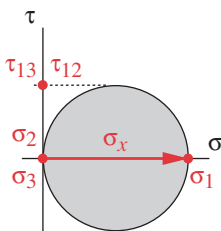


FIGURE 4-7

Mohr's Circles for Example 4-3

4.6 APPLIED VERSUS PRINCIPAL STRESSES

We now want to summarize the differences between the stresses **applied to an element** and the principal stresses that may occur on other planes as a result of the applied stresses. The **applied stresses** are the nine *components of the stress tensor* (Eq. 4.4a, p. 144) that result from whatever loads are applied to the particular geometry of the object as defined in a coordinate system chosen for convenience. The **principal stresses** are the three *principal normal stresses* and the three *principal shear stresses* defined in Section 4.3. Of course, many of the applied-stress terms may be zero in a given case. For example, in the tensile-test specimen discussed in Chapter 2, the only nonzero applied stress is the σ_x term in equation 4.4a (p. 144), which is unidirectional and normal. There are no applied shear stresses on the surfaces normal to the force axis in pure tensile loading. However, the principal stresses are **both normal and shear**.



4

FIGURE 4-8

Mohr's Circles for Unidirectional Tensile Stress (Two Circles are Coincident and the Third is a Point, Since $\sigma_2 = \sigma_3 = 0$)

Figure 4-8 shows the Mohr's circle for a tensile-test specimen. In this case, the applied stress is pure tensile and the maximum principal normal stress is equal to it in magnitude and direction. But a principal shear stress of half the magnitude of the applied tensile stress acts on a plane 45° from the plane of the principal normal stress. Thus, the principal shear stresses will typically be nonzero even in the absence of any applied shear stress. This fact is important to an understanding of why parts fail, and it will be discussed in more detail in Chapter 5. The examples in the previous section also reinforce this point. The most difficult task for the machine designer in this context is to correctly determine the locations, types, and magnitudes of all the applied stresses acting on the part. The calculation of the principal stresses is then *pro forma* using equations 4.4 to 4.6 (pp. 144–145).

**FIGURE 4-9**

A Bar in Axial Tension

4.7 AXIAL TENSION

Axial loading in tension (Figure 4-9) is one of the simplest types of loading that can be applied to an element. It is assumed that the load is applied through the area centroid of the element and that the two opposing forces are colinear along the x axis. At some distance away from the ends where the forces are applied, the stress distribution across the cross section of the element is essentially uniform, as shown in Figure 4-10. This is one reason that this loading method is used to test material properties, as was described in Chapter 2. The applied normal stress for pure axial tension can be calculated from

$$\sigma_x = \frac{P}{A} \quad (4.7)$$

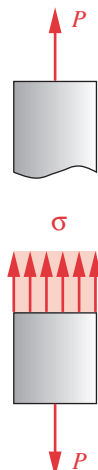
where P is the applied force and A is the cross-sectional area at the point of interest. This is an applied normal stress. The principal normal stresses and the maximum shear stress can be found from equations 4-6 (p. 145). The Mohr's circle for this case was shown in Figure 4-8. The allowable load for any particular tension member can be determined by a comparison of the principal stresses with the appropriate strength of the material. For example, if the material is ductile, then the tensile yield strength, S_y , could be compared to the principal normal stress and the safety factor calculated as $N = S_y / \sigma_1$. Failure criteria will be dealt with in detail in Chapter 5.

The change in length Δs of a member of uniform cross section loaded in pure axial tension is given by

$$\Delta s = \frac{Pl}{AE} \quad (4.8)$$

where P is the applied force, A is the cross-sectional area, l is the loaded length, and E is Young's modulus for the material.

Tension loading is very common, occurring in cables, struts, bolts, and many other axially loaded elements. The designer needs to check carefully for the presence of other loads on the member that, if present in combination with the tensile load, will create a different stress state than the pure axial tension described here.

**FIGURE 4-10**

Stress Distribution Across a Bar in Axial Tension

4.8 DIRECT SHEAR STRESS, BEARING STRESS, AND TEAROUT

These types of loading occur mainly in pin-jointed, bolted, or riveted connections. Possible modes of failure are direct shear of the connector (pin, rivet, or bolt), bearing failure of connector or surrounding material, or a tearing out of the material surrounding the connector. See the Case Studies later in this chapter for examples of the calculation of these types of stresses.

Direct Shear

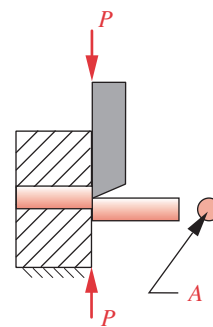
Direct shear occurs in situations where there is no bending present. A pair of scissors (also called a *pair of shears*) is designed to produce direct shear on the material being cut. A poor-quality or worn-out pair of scissors will not cut well (even if sharp) if it allows a gap to exist between the two blades in a direction perpendicular to the blades' motion. Figure 4-11 shows a condition of direct shear and also one in which bending occurs instead. If the gap between the two shearing "blades" or surfaces can be kept close to zero, then a state of direct shear can be assumed and the resulting average stress on the shear face can be estimated from

$$\tau_{xy} = \frac{P}{A_{shear}} \quad (4.9)$$

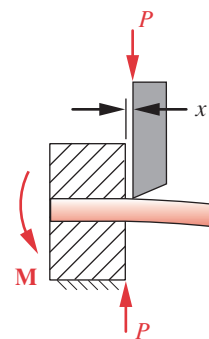
where P is the applied load and A_{shear} is the shear-area being cut, i.e., the cross-sectional area being sheared. The assumption here is that the shear stress is uniformly distributed over the cross section. This is not accurate, since higher local stresses occur at the blade.

In Figure 4-11a the shear blade is tight against the jaws that hold the workpiece. Thus, the two forces P are in the same plane and do not create a couple. This provides a condition of direct shear with no bending. Figure 4-11b shows the same workpiece with a small gap (x) between the shear blade and the jaws. This creates a moment arm, turning the pair of forces P into a couple and thus bending, rather than directly shearing the part. Of course, there will still be significant shearing stresses developed in addition to the bending stresses in this case. Note that it is difficult to create situations in which pure direct shear is the only loading. Even the slight clearances necessary for function can superimpose bending stresses on the applied shear stresses. We will discuss stresses due to bending in the next section.

The situation depicted in Figures 4-11a and 4-12a is also called *single shear*, because only one cross-sectional area of the part needs to be severed to break it. Figure 4-12b shows a pivot pin in *double shear*. Two areas must fail before it separates. This is called a *clevis-pin joint*, where the yoke-shaped link is the *clevis*. The area to be used in equation 4-9 is now $2A$. Double shear is preferred over single shear for pivot-pin designs. Single-shear pivots should only be used where it is impossible to support both ends of the pin as in some linkage cranks, which must pass over adjacent links on one side. Bolted and riveted joints are in single shear when only two flat pieces are fastened together.



(a) Direct shear



(b) Shear with bending

FIGURE 4-11

Shear Loading

Direct Bearing

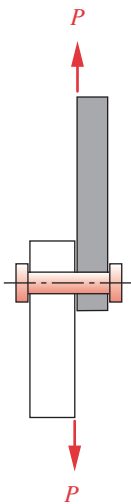
A pivot pin in a hole such as is depicted in Figure 4-12 may fail in other ways than in direct shear. The surfaces of the pin and hole are subjected to a direct *bearing stress*, which is compressive in nature. Bearing stress occurs whenever two surfaces are pressed together. This stress tends to crush the hole or pin rather than to shear it. The bearing stress is normal, compressive, and can be calculated from equation 4.7 (p. 152). If the pin is a close fit in the hole with essentially no clearance, the area used for this calculation is typically taken as the **projected area of contact** of pin and hole, **not the circumferential area**. That is,

$$A_{bearing} = l d \quad (4.10a)$$

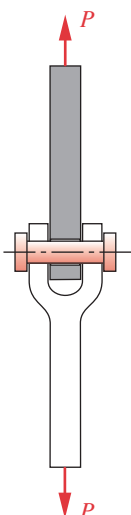
where l is the length of the bearing contact and d is the diameter of the hole or pin. If there is clearance between the pin and hole then the area of contact is reduced. Grandin^[7] has shown that for this case the bearing area can be approximated by

$$A_{bearing} = \frac{\pi}{4} l d \quad (4.10b)$$

Figure 4-13a shows the bearing areas for the clevis-pin joint of Figure 4-12. Each of the two links joined must be checked separately for bearing failure, as either can fail independent of the other. The length l (i.e., link thickness) as well as the pin diameter can be adjusted to create sufficient bearing area and avoid failure.



(a) Pivot in single shear
(less than ideal)



(b) Pivot in double shear
(preferred)

FIGURE 4-12

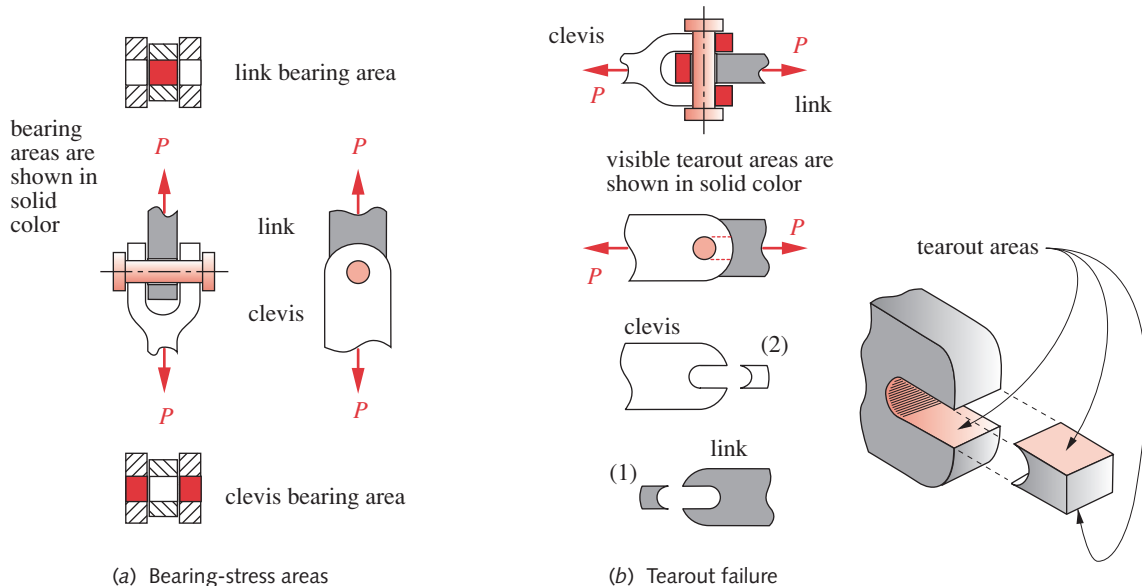
Single and Double Shear

Tearout Failure

Another possible mode of failure for pinned joints is tearout of the material surrounding the hole. This will occur if the hole is placed too close to the edge. This is a double-shear failure, as it requires both sides of the hole to separate from the parent material. Equation 4.9 is applicable to this case, provided that the correct shear area is used. Figure 4-13b shows the tearout areas for the clevis-pin joint from Figure 4-12. It appears that the area could be calculated as the product of the link thickness and the distance from the center of the hole to the outer edge of the part, doubled to account for both sides of the hole. However, this assumption implies that the very thin wedge of material within the hole diameter adds significant shear strength. A more common and conservative assumption is to use twice the product of the total link thickness and the dimension from the **edge of the hole to the outside of the part** for the tearout area. It is a simple matter to provide sufficient material around holes to prevent tearout failure. A minimum of one pin-diameter of material between edge of hole and the part outer edge is a reasonable starting point for your design calculations.

4.9 BEAMS AND BENDING STRESSES

Beams are very common elements in structures and machines of all kinds. Any intermittently supported member subjected to loads transverse to its length will act as a beam. Structural floor joists, roof rafters, machinery shafts, springs, and frames are a few examples of elements that are often loaded as beams. Beams will usually have some combination of normal and shear stresses distributed over their cross sections. It is important

**FIGURE 4-13**

Bearing and Tearout Failures

for the designer to understand how stresses are distributed within beams in order to choose the correct locations for the calculation of maximum stresses. Memorization of the beam stress formulas, while useful, is not sufficient without also gaining an understanding of how and where to properly apply them.

Beams in Pure Bending

While it is rare in practice to encounter a beam that is loaded strictly in “pure” bending, it is nevertheless useful to explore this simplest loading case as a means of developing the theory of stresses due to bending loads. Most real beams will also be subjected to shear loading in combination with the bending moment. That case will be addressed in the next section.

STRAIGHT BEAMS As an example of a pure bending case, consider the simply supported, straight beam shown in Figure 4-14. Two identical, concentrated loads P are applied at points A and B , which are each the same distance from either end of the beam. The shear and bending moment diagrams for this loading show that the center section of the beam, between points A and B , has zero shear force and a constant bending moment of magnitude M . The absence of a shear force makes it pure bending.

Figure 4-15 shows a removed and enlarged segment of the beam taken between points A and B . The assumptions for the analysis are as follows:

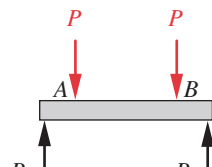
- 1 The segment analyzed is distant from applied loads or external constraints on the beam.
- 2 The beam is loaded in a plane of symmetry.

- 3 Cross sections of the beam remain plane and perpendicular to the neutral axis during bending.
- 4 The material of the beam is homogeneous and obeys Hooke's law.
- 5 Stresses remain below the elastic limit and deflections are small.
- 6 The segment is subjected to pure bending with no axial or shear loads.
- 7 The beam is initially straight.

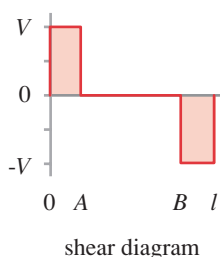
4

The unloaded segment in Figure 4-15a is straight but, as the bending moment is applied in Figure 4-15b, the segment becomes curved (shown exaggerated). The line from N to N along the neutral axis does not change length, but all other lines along the x direction must either shorten or lengthen in order to keep all cross sections perpendicular to the neutral axis. The outer fibers of the beam at $A-A$ are shortened, which puts them in compression, and the outer fibers at $B-B$ are lengthened and put in tension. This causes the bending stress distribution shown in Figure 4-15b. The bending stress magnitude is zero at the neutral axis and is linearly proportional to the distance y from the neutral axis. This relationship is expressed by the familiar bending stress equation:

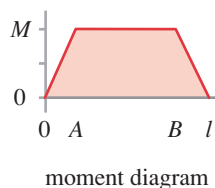
$$\sigma_x = -\frac{My}{I} \quad (4.11a)$$



loading diagram



shear diagram



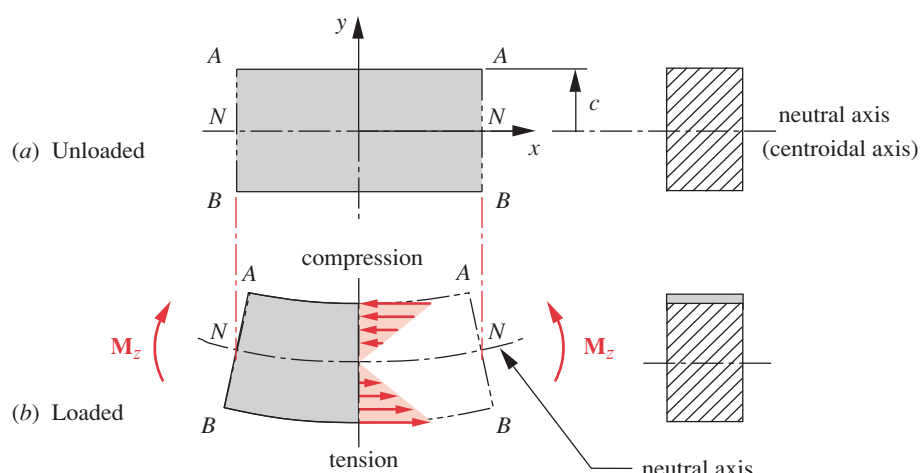
moment diagram

FIGURE 4-14

Pure Bending in a Beam

FIGURE 4-15

Segment of a Straight Beam in Pure Bending



symmetrical about the neutral plane. The value of c is usually taken as positive for both top and bottom surfaces, and the proper sign is then applied to the stress based on inspection of the beam loading to determine which surface is in compression (−) and which is in tension (+).

An alternate form of equation 4.11b is often used:

$$\sigma_{max} = \frac{M}{Z} \quad (4.11c)$$

where Z is the beam's *section modulus*:

$$Z = \frac{I}{c} \quad (4.11d)$$

These equations, though developed for the case of pure bending, are nevertheless applicable to cases, where shear strain is negligible, in which other loads in addition to the moment are applied to the beam. In such situations the effects of the combined loadings must be properly accounted for. This will be discussed in later sections. Formulas for the geometric properties (A , I , Z) of typical beam cross sections can be found in Appendix A and are also provided as computer files on disk.

CURVED BEAMS Many machine parts such as crane hooks, C-clamps, punch-press frames, etc., are loaded as beams, but are not straight. They have a radius of curvature. The first six assumptions listed above for straight beams still apply. If a beam has significant curvature, then the neutral axis will no longer be coincident with the centroidal axis and equations 4.11 do not directly apply. The neutral axis shifts toward the center of curvature by a distance e as shown in Figure 4-16.

$$e = r_c - \int \frac{dA}{r} \quad (4.12a)$$

where r_c is the radius of curvature of the centroidal axis of the curved beam, A is the cross-sectional area, and r is the radius from the beam's center of curvature to the differential area dA . Numerical evaluation of the integral can be done for complex shapes.*

* Expressions for this integral for many common cross-sectional shapes can be found in reference [4]. For example, for a rectangular cross section, $e = r_c - (r_o - r_i) / \ln(r_o / r_i)$

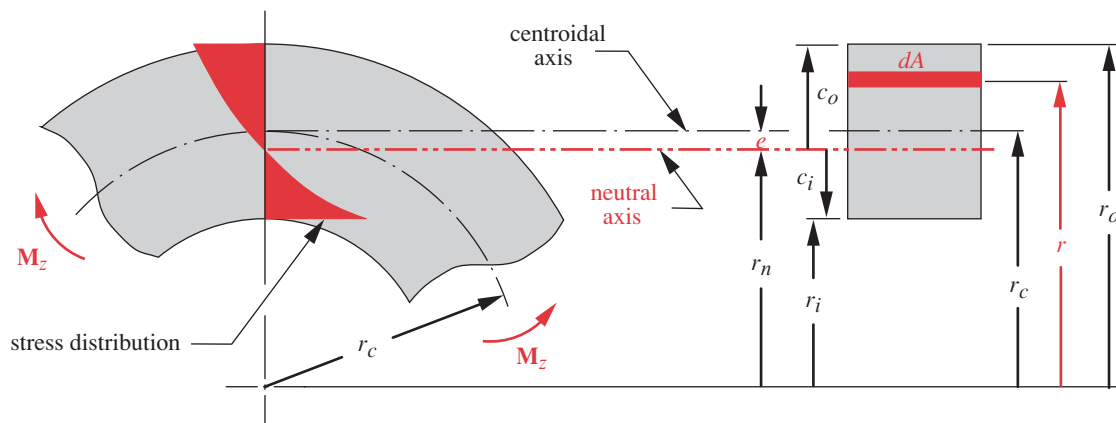
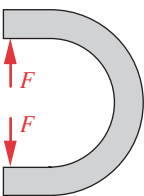


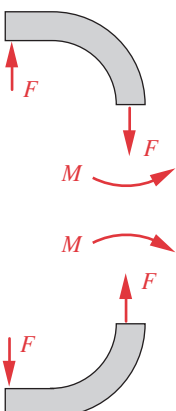
FIGURE 4-16

Segment of a Curved Beam in Pure Bending



4

(a) Force-loaded curved beam



(b) Free-body diagrams

FIGURE 4-17

A Curved Beam with Force Loading

The stress distribution across the section is no longer linear but is now hyperbolic, and it is greatest on the inner surface of a rectangular cross section as shown in Figure 4-16. The convention is to define a positive moment as one that tends to straighten the beam. This creates tension on the inside and compression on the outside surface from a positive applied moment and vice versa. For pure bending loads, the expressions for the maximum stresses at inner and outer surfaces of a curved beam now become:

$$\sigma_i = +\frac{M}{eA} \left(\frac{c_i}{r_i} \right) \quad (4.12b)$$

$$\sigma_o = -\frac{M}{eA} \left(\frac{c_o}{r_o} \right) \quad (4.12c)$$

where the subscript *i* denotes the inside surface and *o* the outside, *M* is the applied moment at the section in question, *A* is the cross-sectional area, and *r_i* and *r_o* are the radii of curvature of the inner and outer surfaces. These expressions contain the ratio *c/r*. If the radius of curvature *r* is large compared to *c*, then the beam looks more “straight” than “curved.” When *c/r* becomes less than about 1:10, the stresses will be only about 10% greater than those of a straight beam of the same dimensions and loading. (Note that this is not a linear relationship, as *e* is also a function of *c* and *r*.)

It is more common to have applied forces loading a curved beam, as shown in Figure 4-17a. An example is a clamp or a hook. The free-body diagrams in Figure 4-17b show that there is now an axial force as well as a moment on the cut section. The equations for stress at the inside and outside of the beam become

$$\sigma_i = +\frac{M}{eA} \left(\frac{c_i}{r_i} \right) + \frac{F}{A} \quad (4.12d)$$

$$\sigma_o = -\frac{M}{eA} \left(\frac{c_o}{r_o} \right) + \frac{F}{A} \quad (4.12e)$$

The second terms in equations 4.12d and 4.12e represent the direct axial tensile stress on the midsection of the beam. The file CURVBEAM provided computes equations 4.12 for five common shapes of curved beam cross sections: round, elliptical, trapezoidal, rectangular, and tee. This program uses numerical integration to evaluate equation 4.12a and to find the area and centroid of the cross section.

Shear Due to Transverse Loading

The more common condition in beam loading is a combination of both shear force and bending moment applied to a particular section. Figure 4-18 shows a point-loaded, simply supported beam and its shear and moment diagrams. We need to now consider how the shear loading affects the stress state within the beam’s cross sections.

Figure 4-19a shows a segment taken from the beam around point *A* in Figure 4-18. An element labeled *P* is shown cut out of the beam at point *A*. This element is *dx* wide and is cut in from the outer fiber at *c* to a depth *y₁* from the neutral axis. Note that the magnitude of the moment *M(x₁)* on the left-hand side of *P* (face *b₁-c₁*) is less than the moment *M(x₂)* on the right-hand side (face *b₂-c₂*), and their difference is the differen-

tial moment dM . Figure 4-18 shows that at point A, the moment $M(x)$ is increasing as a function of beam length x , due to the presence of the nonzero shear force V at that point. The normal stresses on the vertical faces of P are found from equation 4.11a. Since the normal stress due to bending is proportional to $M(x)$, the stress σ on the left-hand face of P is less than on its right-hand face, as shown in Figure 4-19b. For equilibrium, this stress imbalance must be counteracted by some other stress component, which is shown as the **shear stress** τ in Figure 4-19b.

The force acting on the left-hand face of P at any distance y from the neutral axis can be found by multiplying the stress by the differential area dA at that point.

$$\sigma dA = \frac{My}{I} dA \quad (4.13a)$$

The total force acting on the left-hand face is found by integrating

$$F_{1x} = \int_{y_1}^c \frac{My}{I} dA \quad (4.13b)$$

and similarly for the right-hand face:

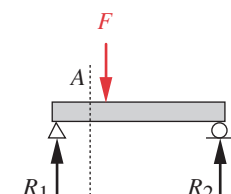
$$F_{2x} = \int_{y_1}^c \frac{(M + dM)y}{I} dA \quad (4.13c)$$

The shear force on the top face at distance y_1 from the neutral axis is found from

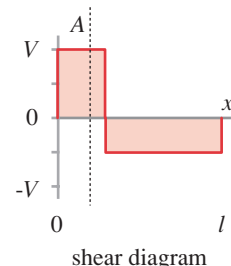
$$F_{xy} = \tau b dx \quad (4.13d)$$

where the product $b dx$ is the area of the top face of element P .

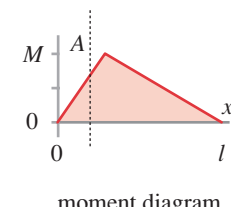
For equilibrium, the forces acting on P must sum to zero,



loading diagram



shear diagram



moment diagram

FIGURE 4-18

Shear Force and Bending Moment in a Beam

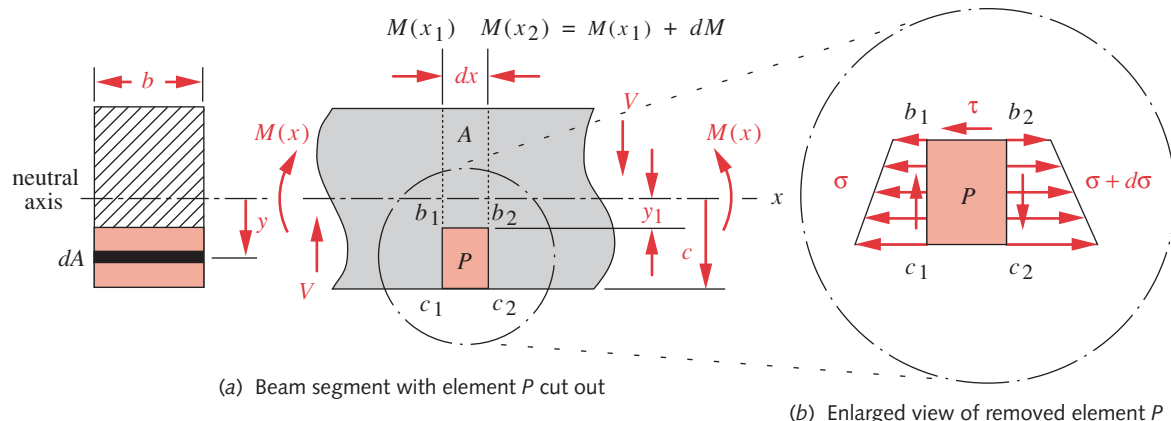


FIGURE 4-19

Segment of a Beam in Bending and Transverse Shear - Shown Removed at Point A in Figure 4-18

$$F_{xy} = F_{2x} - F_{1x}$$

$$\tau b dx = \int_{y_1}^c \frac{(M + dM)y}{I} dA - \int_{y_1}^c \frac{My}{I} dA \quad (4.13e)$$

$$\tau = \frac{dM}{dx} \frac{1}{Ib} \int_{y_1}^c y dA$$

which gives an expression for the shear stress τ as a function of the change in moment with respect to x , the distance y from the neutral axis, the second moment of area I of the cross section, and the width b of the cross section at y . Equation 3.16a (p. 111) shows that the slope of the moment function dM/dx is equal to the magnitude of the shear function V at any point, so:

$$\tau_{xy} = \frac{V}{Ib} \int_{y_1}^c y dA \quad (4.13f)$$

The integral in equation 4.13f represents the first moment about the neutral axis of that portion of the cross-sectional area that exists outside of the value of y_1 for which the shear stress is being calculated. It is conventional to assign the variable Q to the value of this integral.

$$Q = \int_{y_1}^c y dA \quad (4.13g)$$

and then

$$\tau_{xy} = \frac{VQ}{Ib}$$

The integral Q will obviously vary with the shape of the beam's cross section and also with the distance y_1 from the neutral axis. Thus, for any particular cross section, we should expect the shear stress to vary across the beam. It will always be zero at the outer fibers because Q vanishes when y_1 becomes equal to c . This makes sense, as there is no material to shear against at the outer fiber. The shear stress due to transverse loading will be a maximum at the neutral axis. These results are very fortuitous, since the normal stress due to bending is maximum at the outer fiber and zero at the neutral axis. Thus their combination on any particular element within the cross section seldom creates a worse stress state than exists at the outer fibers.

The shear stress due to transverse loading will be small compared to the bending stress Mc / I if the beam is long compared to its depth. The reason for this can be seen in equation 3.16 and in the shear and moment diagrams, one example of which is shown in Figure 4-18. Since the magnitude of the moment function is equal to the area under the shear function, for any given value of V in Figure 4-18, the area under the shear function and thus the maximum moment will increase with beam length. So, while the maximum shear-stress magnitude remains constant, the bending stress increases with beam length, eventually dwarfing the shear stress. A commonly used rule of thumb says that the shear stress due to transverse loading in a beam will be small enough to ignore if the length-to-depth ratio of the beam is 10 or more. Short beams below that ratio should be investigated for transverse shear stress as well as for bending stress.

RECTANGULAR BEAMS The calculation of shear stress due to transverse loading typically becomes an exercise in evaluating the integral Q for the particular beam cross section. Once that is done, the maximum value of τ is easily found. For a beam with a rectangular cross section of width b and depth h , $dA = b dy$, and $c = h / 2$.

$$Q = \int_{y_1}^c y dA = b \int_{y_1}^c y dy = \frac{b}{2} \left(\frac{h^2}{4} - y_1^2 \right) \quad (4.14a)$$

and

$$\tau = \frac{V}{2I} \left(\frac{h^2}{4} - y_1^2 \right)$$

The shear stress varies parabolically across a rectangular beam as shown in Figure 4-20a. When $y_1 = h / 2$, $\tau = 0$ as expected. When $y_1 = 0$, $\tau_{max} = Vh^2 / 8I$. For a rectangle, $I = bh^3 / 12$, which gives

$$\tau_{max} = \frac{3V}{2A} \quad (4.14b)$$

This is valid **only for rectangular cross-sectional beams** and is shown in Figure 4-20a.

ROUND BEAMS Equations 4.13g apply to any cross section. The integral Q for a circular cross section is

$$Q = \int_{y_1}^c y dA = 2 \int_{y_1}^c y \sqrt{r^2 - y^2} dy = \frac{2}{3} (r^2 - y_1^2)^{\frac{3}{2}} \quad (4.15a)$$

and the shear-stress distribution is

$$\tau = \frac{VQ}{bI} = \frac{V \left[\frac{2}{3} (r^2 - y_1^2)^{\frac{3}{2}} \right]}{2\sqrt{r^2 - y^2} \left(\frac{\pi r^4}{4} \right)} = \frac{4}{3} \frac{V}{\pi r^2} \left(1 - \frac{y_1^2}{r^2} \right) \quad (4.15b)$$

This is also a parabolic distribution but has a smaller peak value than the rectangular section, as shown in Figure 4-20b. The maximum shear stress in a **solid, circular cross-sectional beam** is, at the neutral axis:

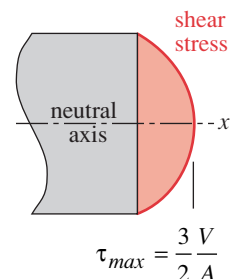
$$\tau_{max} = \frac{4V}{3A} \quad (4.15c)$$

If the **round beam is hollow and thin walled** (wall thickness $<$ about 1/10 the outside radius), the maximum shear stress at the neutral axis will be approximately

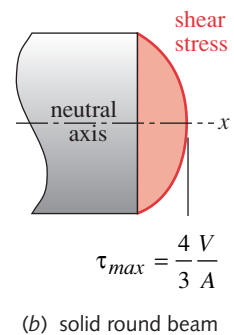
$$\tau_{max} \approx \frac{2V}{A} \quad (4.15d)$$

as shown in Figure 4-20c.

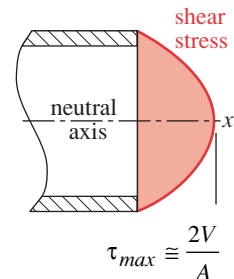
I-BEAMS It can be shown mathematically that the I-beam configuration in Figure 4-21a is the optimal cross-sectional shape for a beam in terms of strength-to-weight



(a) rectangular beam



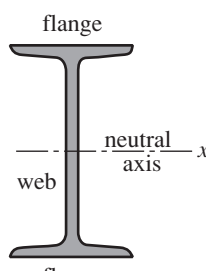
(b) solid round beam



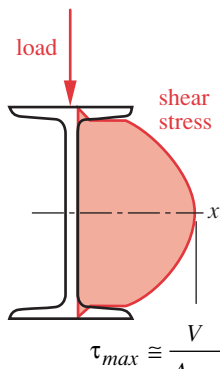
(c) hollow round beam

FIGURE 4-20

Shear-Stress Distribution and Maxima in Round, Round-Hollow, and Rectangular Beams



(a) I-beam shape



(b) Stress distribution

FIGURE 4-21

Shear-Stress Distribution and Maximum in an I-Beam

ratio. This explains why I-beams are commonly used as floor and roof beams in large structures. Their shape puts most of the material at the outer fibers where the bending stress is maximum. This gives a large area moment of inertia to resist the bending moment. As the shear stress is maximum at the neutral axis, the narrow web connecting the flanges (called the shear web) serves to resist the shear forces in the beam. In a long beam, the shear stresses due to bending are small compared to the bending stresses, which allows the web to be thin, reducing weight. An approximate expression for the maximum shear stress in an I-beam uses only the area of the web and ignores the flanges:

$$\tau_{max} \approx \frac{V}{A_{web}} \quad (4.16)$$

Figure 4-21b shows the shear-stress distribution across the I-beam section depth. Note the discontinuities at the flange-web interfaces. The shear stress in the flange is small due to its large area. The shear stress jumps to a larger value on entering the web, then rises parabolically to a maximum at the neutral axis.

4.10 DEFLECTION IN BEAMS

In addition to the stresses in a beam, a designer also needs to be concerned with its deflections. Any applied bending load will cause a beam to deflect, since it is made of an elastic material. If the deflection does not create strains in excess of the material's strain at its yield point, the beam will return to its undeflected state when the load is removed. If the strain exceeds that of the material's yield point, the beam will yield and "take a set" if ductile, or possibly fracture if brittle. If the beam is sized to prevent stresses that exceed the material's yield point (or other appropriate strength criterion), then no permanent set or fracture should occur. However, elastic deflections at stresses well below the material's failure levels may still cause serious problems in a machine.

Deflections can cause interferences between moving parts or misalignments that destroy the required accuracy of the device. In general, designing to minimize deflections will lead to larger beam cross sections than will designing only against stress failure. Even in static structures such as buildings, deflection can be the limiting criterion in sizing floor or roof beams. You have probably walked across a residential floor that bounced noticeably with each step. The floor was undoubtedly safe against collapse due to excessive stresses, but had not been designed stiff enough to prevent undesirable deflections under normal working loads.

The bending deflection of a beam is calculated by double integration of the beam equation,

$$\frac{M}{EI} = \frac{d^2y}{dx^2} \quad (4.17)$$

which relates the applied moment M , the material's modulus of elasticity E , and the cross section's area moment of inertia I to the second derivative of the beam deflection y . The independent variable x is the position along the beam length. Equation 4.17 is only valid for small deflections, which is not a limitation in most cases of beam design for machine or structural applications. Sometimes beams are used as springs, and their deflections may then exceed the limitations of this equation. Spring design will be covered in a later

chapter. Equation 4.17 also does not include the effects of deflection due to transverse shear loads. The transverse-shear component of deflection in long beams is small compared to that due to bending and is typically ignored unless the beam's length/depth ratio is < about 10.

Equation 4.17 can be differentiated twice and integrated twice to create the set of five equations 4.18 (including Eq. 4.17 repeated as Eq. 4.18c), which define beam behavior. Section 3.9 showed the relationship between the loading function $q(x)$, the shear function $V(x)$, and the moment function $M(x)$. V is the first derivative and q the second derivative of equation 4.17 with respect to x . Integrating equation 4.17 once gives the beam slope θ and integrating a second time gives the beam deflection y . These relationships form the following set of beam equations:

$$\frac{q}{EI} = \frac{d^4 y}{dx^4} \quad (4.18a)$$

$$\frac{V}{EI} = \frac{d^3 y}{dx^3} \quad (4.18b)$$

$$\frac{M}{EI} = \frac{d^2 y}{dx^2} \quad (4.18c)$$

$$\theta = \frac{dy}{dx} \quad (4.18d)$$

$$y = f(x) \quad (4.18e)$$

The only material parameter in these equations is Young's modulus E , which defines its stiffness. Since most alloys of a given base metal have essentially the same modulus of elasticity, equations 4.18 show why there is no advantage in using a stronger and more expensive alloy when designing to minimize deflection. Higher-strength alloys typically only provide higher yield or break strengths, and designing against a deflection criterion will usually result in relatively low stresses. This is the reason that I-beams and other structural-steel shapes are made primarily in low-strength, low-carbon steels.

Determining the deflection function of a beam is an exercise in integration. The loading function q is typically known and can be integrated by any one of several methods, analytical, graphical, or numerical. The constants of integration are evaluated from the boundary conditions of the particular beam configuration. Changes in section modulus across the beam require creating the M/EI function from the moment diagram before integrating for the beam slope. If the beam's area moment of inertia I and material E is uniform across its length, the moment function can just be divided by the constant EI . If the beam's cross section changes over its length, then the integration must be done piecewise to accommodate the changes in I . The integral forms of the beam equations are

$$V = \int q \, dx + C_1 \quad 0 < x < l \quad (4.19a)$$

$$M = \int V \, dx + C_1 x + C_2 \quad 0 < x < l \quad (4.19b)$$

$$\theta = \int \frac{M}{EI} \, dx + C_1 x^2 + C_2 x + C_3 \quad 0 < x < l \quad (4.19c)$$

$$y = \int \theta \, dx + C_1 x^3 + C_2 x^2 + C_3 x + C_4 \quad 0 < x < l \quad (4.19d)$$

The constants C_1 and C_2 can be found from boundary conditions on the shear and moment functions. For example, the moment will be zero at a simply supported beam end and either zero (or known if applied) at an unsupported free end of a beam. The shear force will be zero at an unloaded free end. Note that if the reaction forces are included in the loading function $q(x)$, then $C_1 = C_2 = 0$.

4

The constants C_3 and C_4 can be found from boundary conditions on the slope and deflection functions. For example, the deflection will be zero at any rigid support, and the beam slope will be zero at a moment joint. Substitute two known combinations of values of x and y or x and θ along with C_1 and C_2 in equations 4.19c and 4.19d and solve for C_3 and C_4 . Many techniques for solution of these equations have been developed such as graphical integration, the area-moment method, energy methods, and singularity functions. We will explore the last two of these.

Deflection by Singularity Functions

Section 3.9 presented the use of singularity functions to represent loads on the beam. These functions make it relatively simple to perform the integration analytically and can easily be programmed for computer solution. Section 3.9 also applied this approach to obtain the shear and moment functions from the loading function. We will now extend that technique to develop the beam's slope and deflection functions. The best way to explore this method is by way of examples. Accordingly, we will calculate the beam shear, moment, slope, and deflection functions for the beams shown in Figure 4-22.

EXAMPLE 4-4

Finding Beam Slope and Deflection of a Simply Supported Beam Using Singularity Functions

Problem: Determine and plot the slope and deflection functions for the simply supported beam shown in Figure 4-22a.

Given: The load is uniform over part of the beam length. Let beam length $l = 10$ in, and load location $a = 4$ in. The beam's $I = 0.163$ in 4 and $E = 30$ Mpsi. The distributed force is $w = 100$ lb/in.

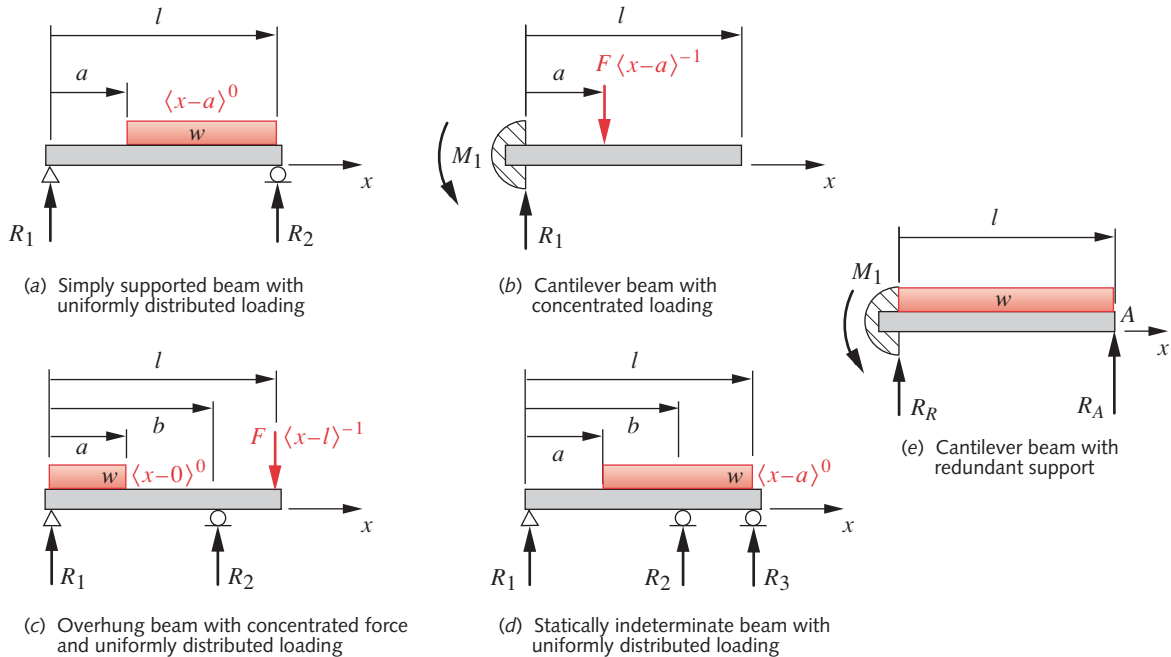
Assumptions: The weight of the beam is negligible compared to the applied load and so can be ignored.

Solution: See Figures 4-22a and 4-23.

- 1 Solve for the reaction forces using equations 3.3 (p. 78). Summing moments about the right-hand end and summing forces in the y direction:

$$\sum M_z = 0 = R_l l - \frac{w(l-a)^2}{2} \quad (a)$$

$$R_l = \frac{w(l-a)^2}{2l} = \frac{100(10-4)^2}{2(10)} = 180$$

**FIGURE 4-22**

Various Beams and Beam Loadings

$$\sum F_y = 0 = R_1 - w(l-a) + R_2 \quad (b)$$

$$R_2 = w(l-a) - R_1 = 100(10-4) - 180 = 420$$

- 2 Write equations for the load function in terms of equations 3.17 (pp. 113–114) and integrate the resulting function four times using equations 3.18 (pp. 114–115) to obtain the shear, moment, slope, and deflection functions. For the simply supported beam with a distributed load over part of its length:

$$q = R_1 \langle x-0 \rangle^{-1} - w \langle x-a \rangle^0 + R_2 \langle x-l \rangle^{-1} \quad (c)$$

$$V = \int q dx = R_1 \langle x-0 \rangle^0 - w \langle x-a \rangle^1 + R_2 \langle x-l \rangle^0 + C_1 \quad (d)$$

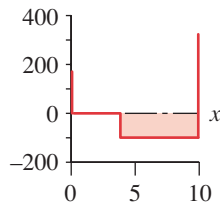
$$M = \int V dx = R_1 \langle x-0 \rangle^1 - \frac{w}{2} \langle x-a \rangle^2 + R_2 \langle x-l \rangle^1 + C_1 x + C_2 \quad (e)$$

$$\theta = \int \frac{M}{EI} dx = \frac{1}{EI} \left(\begin{array}{l} \frac{R_1}{2} \langle x-0 \rangle^2 - \frac{w}{6} \langle x-a \rangle^3 + \frac{R_2}{2} \langle x-l \rangle^2 \\ + \frac{C_1 x^2}{2} + C_2 x + C_3 \end{array} \right) \quad (f)$$

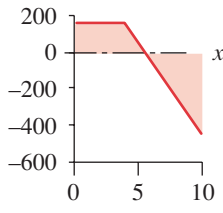
$$y = \int \theta dx = \frac{1}{EI} \left(\begin{array}{l} \frac{R_1}{6} \langle x-0 \rangle^3 - \frac{w}{24} \langle x-a \rangle^4 + \frac{R_2}{6} \langle x-l \rangle^3 \\ + \frac{C_1 x^3}{6} + \frac{C_2 x^2}{2} + C_3 x + C_4 \end{array} \right) \quad (g)$$

4

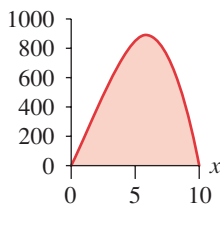
Loading Diagram (lb)



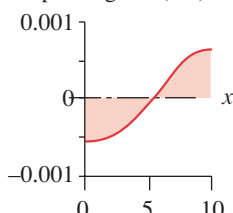
Shear Diagram (lb)



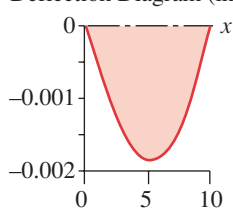
Moment Diagram (lb-in)



Slope Diagram (rad)



Deflection Diagram (in)

**FIGURE 4-23**

Example 4-4 Plots

* Because the value of x at the maximum deflection of a simply supported beam must be less than the length between supports, l , the third term in equation (f) is zero.

- 3 There are four constants of integration to be found. The constants C_1 and C_2 are zero because the reaction forces and moments acting on the beam are included in the loading function. The deflection y is zero at the supports. The constants C_3 and C_4 are found by substituting the boundary conditions $x = 0, y = 0$ and $x = l, y = 0$ into equation (g).

$$\begin{aligned}y(0) = 0 &= \frac{1}{EI} \left(\frac{R_1}{6} (0-0)^3 - \frac{w}{24} (0-a)^4 + \frac{R_2}{6} (0-l)^3 + C_3(0) + C_4 \right) \\C_4 &= -\frac{R_1}{6} (0-0)^3 + \frac{w}{24} (0-4)^4 - \frac{R_2}{6} (0-10)^3 - C_3(0) \\C_4 &= -\frac{R_1}{6} (0) + \frac{w}{24} (0) - \frac{R_2}{6} (0) - C_3(0) = 0\end{aligned}\quad (h)$$

$$\begin{aligned}y(l) = 0 &= \frac{1}{EI} \left(\frac{R_1}{6} (l-0)^3 - \frac{w}{24} (l-a)^4 + \frac{R_2}{6} (l-l)^3 + C_3 l + C_4 \right) \\C_3 &= \frac{w}{24l} [(l-a)^4 - 2l^2(l-a)^2] \\C_3 &= \frac{100}{24(10)} [(10-4)^4 - 2(10)^2(10-4)^2] = -2460\end{aligned}\quad (i)$$

- 4 Substitution of the values or expressions for C_3 , C_4 , R_1 , and R_2 from equations (a), (b), (h), and (i) into equation (g) gives the resulting deflection equation for the beam in part (a) of Figure 4-22 (p. 165):

$$y = \frac{w}{24EI} \left\{ [2(l-a)^2]x^3 + [(l-a)^4 - 2l^2(l-a)^2]x - l(x-a)^4 \right\} \quad (j)$$

- 5 The maximum deflection will occur at the point in x where the slope of the deflection curve is zero. Set the beam-slope equation (f) to zero and solve for x :

$$\begin{aligned}\theta &= \frac{1}{EI} \left(\frac{R_1}{2} x^2 - \frac{w}{6} (x-a)^3 + C_3 \right) = 0 \\0 &= \frac{1}{3E7(0.163)} (90x^2 - 16.67(x-4)^3 - 2460)\end{aligned}$$

$$x = 5.264 \quad (k)$$

Note that either Viete's method or a numerical root-finding algorithm is needed to find the roots of this cubic equation.

- 6 Use this value of x in equation (g) to find the largest deflection magnitude, either positive or negative.

$$y_{max} = \frac{100}{24(10)(4.883E6)} \left\{ \begin{aligned} &[2(10-4)^2](5.264)^3 + [(10-4)^4 - 2(10)^2(10-4)^2](5.264) \\ &- 10(5.264-4)^4 \end{aligned} \right\}$$

$$y_{max} = -0.00176 \text{ in} \quad (l)$$

- 7 Plots of the loading, shear, moment, slope, and deflection functions for part (a) are shown in Figure 4-23. The files EX04-04 can be opened in the program of your choice to examine the model and see larger-scale plots of the functions in Figure 4-23.

EXAMPLE 4-5**Finding Beam Slope and Deflection of a Cantilever Beam Using Singularity Functions**

Problem: Determine and plot the slope and deflection functions for the beam shown in Figure 4-22b (repeated here).

Given: The load is the concentrated force shown. Let beam length $l = 10$ in, and load location $a = 4$ in. The beam's $I = 0.5 \text{ in}^4$ and $E = 30 \text{ Mpsi}$. The magnitude of the applied force is $F = 400 \text{ lb}$.

Assumptions: Ignore the beam weight as negligible compared to the applied load.

Solution: See Figures 4-22b and 4-24.

- 1 Write equations for the load function in terms of equations 3.17 (pp. 113–114) and integrate the resulting function twice using equations 3.18 (pp. 114–115) to obtain the shear and moment functions. Note the use of the unit doublet function to represent the moment at the wall. For the beam in Figure 4-22b,

$$q = -M_1(x-0)^{-2} + R_1(x-0)^{-1} - F(x-a)^{-1} \quad (a)$$

$$V = \int q dx = -M_1(x-0)^{-1} + R_1(x-0)^0 - F(x-a)^0 + C_1 \quad (b)$$

$$M = \int V dx = -M_1(x-0)^0 + R_1(x-0)^1 - F(x-a)^1 + C_1x + C_2 \quad (c)$$

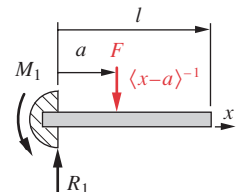
$$\theta = \int \frac{M}{EI} dx = \frac{1}{EI} \left(\begin{array}{l} -M_1(x-0)^1 + \frac{R_1}{2}(x-0)^2 - \frac{F}{2}(x-a)^2 \\ \quad + \frac{C_1x^2}{2} + C_2x + C_3 \end{array} \right) \quad (d)$$

$$y = \int \theta dx = \frac{1}{EI} \left(\begin{array}{l} -\frac{M_1}{2}(x-0)^2 + \frac{R_1}{6}(x-0)^3 - \frac{F}{6}(x-a)^3 \\ \quad + \frac{C_1x^3}{6} + \frac{C_2x^2}{2} + C_3x + C_4 \end{array} \right) \quad (e)$$

The reaction moment M_1 at the wall is in the z direction and the forces R_1 and F are in the y direction in equation (b). All moments in equation (c) are in the z direction.

- 2 Because the reactions have been included in the loading function, the shear and moment diagrams both close to zero at each end of the beam, making $C_1 = C_2 = 0$.
- 3 The reaction force R_1 and reaction moment M_1 are calculated from equations (b) and (c), respectively, by substituting the boundary conditions $x = l+$, $V = 0$, $M = 0$. Note that we can substitute l for $l+$ since their difference is vanishingly small.

$$\begin{aligned} V(l^+) &= 0 = R_1(l-0)^0 - F(l-a)^0 \\ 0 &= R_1 - F \\ R_1 &= F = 400 \text{ lb} \end{aligned} \quad (f)$$

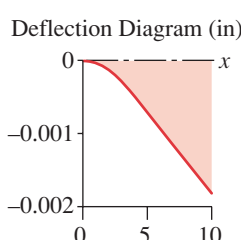
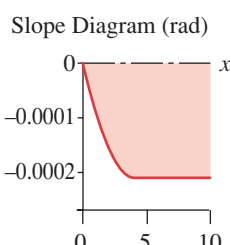
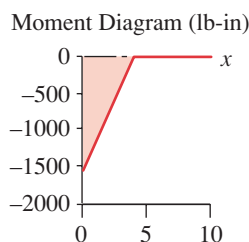
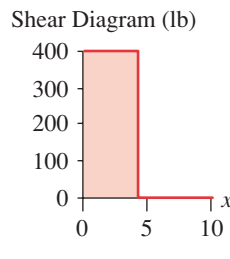
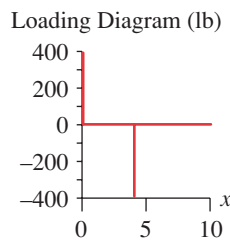


Cantilever beam with concentrated loading

FIGURE 4-22b

Repeated

4



$$\begin{aligned} M(l^+) &= 0 = -M_1(l-0)^0 + R_1(l-0)^1 - F(l-a)^1 \\ 0 &= -M_1 + lR_1(l) - F(l-a) \\ M_1 &= R_1(l) - F(l-a) = 400(10) - 400(10-4) = 1600 \text{ lb-in cw} \end{aligned} \quad (g)$$

Since w , l , and a are known from the given data, equation (f) can be solved for R_1 , and this result substituted in equation (g) to find M_1 . Note that equation (f) is just $\sum F_y = 0$, and equation (g) is $\sum M_z = 0$. M_1 does not appear in equation (f) because it is in a different vector direction than the y forces.

- 4 Substitute $x = 0$, $\theta = 0$ and $x = 0$, $y = 0$ in (d) and (e) and solve for C_3 and C_4 :

$$\begin{aligned} \theta(0) = 0 &= \frac{1}{EI} \left(-M_1(0-0)^1 + \frac{R_1}{2}(0-0)^2 - \frac{F}{2}(0-a)^2 + C_3 \right) \\ C_3 &= M_1(0-0)^1 - \frac{R_1}{2}(0-0)^2 + \frac{F}{2}(0-4)^2 = 0 \\ y(0) = 0 &= \frac{1}{EI} \left(-\frac{M_1}{2}(0-0)^2 + \frac{R_1}{6}(0-0)^3 - \frac{F}{6}(0-a)^3 + C_3(0) + C_4 \right) \\ C_4 &= \frac{M_1}{2}(0-0)^2 - \frac{R_1}{6}(0-0)^3 + \frac{F}{6}(0-4)^3 = 0 \end{aligned} \quad (h)$$

- 5 Substitution of the expressions for C_3 , C_4 , R_1 , and M_1 from (f), (g), (h), and (i) into equation (e) gives the deflection equation for the cantilever beam in Figure 4-22b (p. 165):

$$y = \frac{F}{6EI} [x^3 - 3ax^2 - (x-a)^3] \quad (j)$$

- 6 The maximum deflection of a cantilever beam is at its free end. Substitute $x = l$ in equation (j) to find y_{max} .

$$\begin{aligned} y_{max} &= \frac{F}{6EI} [l^3 - 3al^2 - (l-a)^3] = \frac{Fa^2}{6EI} (a-3l) \\ y_{max} &= \frac{400(4)^2}{6(3E7)(0.5)} [4 - 3(10)] = -0.00185 \text{ in} \end{aligned} \quad (k)$$

- 7 Plots of the loading, shear, moment, slope, and deflection functions are shown in Figure 4-24. Note that the beam slope becomes increasingly negative for the portion of beam between the support and the load and then becomes constant to the right of the load. While not very apparent at the small scale of the figure, the beam deflection becomes a straight line to the right of the point of application of the load.

The files EX04-05 can be opened in the program of your choice to examine the model and see larger-scale plots of the functions in Figure 4-24.

FIGURE 4-24

Example 4-5 Plots

EXAMPLE 4-6**Finding Beam Slope and Deflection of an Overhung Beam Using Singularity Functions****Problem:**

Determine and plot the slope and deflection functions for an overhung beam with a uniformly distributed load over part of its length and a concentrated force at its end as shown in Figure 4-22c (p. 165).

Given:

Beam length $l = 10$ in, and load locations $a = 4$ in and $b = 7$ in. The beam's $I = 0.2 \text{ in}^4$ and $E = 30 \text{ Mpsi}$. The magnitude of the concentrated force is $F = 200 \text{ lb}$ and the distributed force is $w = 100 \text{ lb/in}$.

Assumptions:

The weight of the beam is negligible compared to the applied loads and so can be ignored.

Solution:

See Figures 4-22c (repeated here), 4-25, 4-26.

- 1 The distributed load does not extend over the entire length of this beam. All singularity functions extend from their initial point to the end of the beam. So, to terminate the uniform load's step function at some point short of the end of the beam it is necessary to apply another step function of equal amplitude and opposite sign in order to cancel it for all points beyond length a as shown in Figure 4-25. The sum of the two step functions of opposite sign is then zero to the right of distance a .

$$q = R_1 \langle x - 0 \rangle^{-1} - w \langle x - 0 \rangle^0 + w \langle x - a \rangle^0 + R_2 \langle x - b \rangle^{-1} - F \langle x - l \rangle^{-1} \quad (a)$$

$$V = \int q dx = R_1 \langle x - 0 \rangle^0 - w \langle x - 0 \rangle^1 + w \langle x - a \rangle^1 + R_2 \langle x - b \rangle^0 - F \langle x - l \rangle^0 + C_1 \quad (b)$$

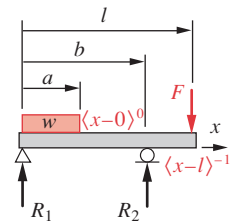
$$M = \int V dx = \left(R_1 \langle x - 0 \rangle^1 - \frac{w}{2} \langle x - 0 \rangle^2 + \frac{w}{2} \langle x - a \rangle^2 + R_2 \langle x - b \rangle^1 - F \langle x - l \rangle^1 + C_1 x + C_2 \right) \quad (c)$$

$$\theta = \int \frac{M}{EI} dx = \frac{1}{EI} \left(\frac{R_1}{2} \langle x - 0 \rangle^2 - \frac{w}{6} \langle x - 0 \rangle^3 + \frac{w}{6} \langle x - a \rangle^3 + \frac{R_2}{2} \langle x - b \rangle^2 - \frac{F}{2} \langle x - l \rangle^2 + \frac{C_1}{2} x^2 + C_2 x + C_3 \right) \quad (d)$$

$$y = \int \theta dx = \frac{1}{EI} \left(\frac{R_1}{6} \langle x - 0 \rangle^3 - \frac{w}{24} \langle x - 0 \rangle^4 + \frac{w}{24} \langle x - a \rangle^4 + \frac{R_2}{6} \langle x - b \rangle^3 - \frac{F}{6} \langle x - l \rangle^3 + \frac{C_1}{6} x^3 + \frac{C_2}{2} x^2 + C_3 x + C_4 \right) \quad (e)$$

- 2 Because the reactions have been included in the loading function, the shear and moment diagrams both close to zero at each end of the beam, making $C_1 = C_2 = 0$.
- 3 Since both the shear and moment are zero at $x = l^+$, the reactions R_1 and R_2 can be calculated simultaneously from (b) and (c) with $x = l^+ = l$:

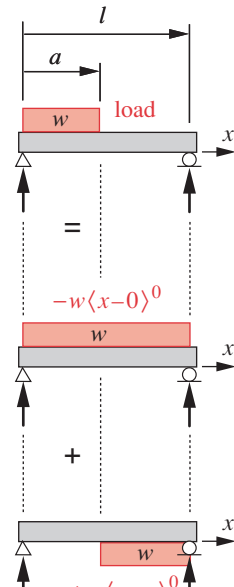
$$\begin{aligned} V(l) &= 0 = R_1 \langle l - 0 \rangle^0 - w \langle l - 0 \rangle^1 + w \langle l - a \rangle^1 + R_2 \langle l - b \rangle^0 - F \langle l - l \rangle^0 \\ 0 &= R_1 - wl + w(l - a) + R_2 - F \\ R_2 &= -R_1 + wl - w(l - a) + F = 400 \text{ lb} \end{aligned} \quad (f)$$



Overhung beam with concentrated force and uniformly distributed loading

FIGURE 4-22c

Repeated



$$\text{load} = -w \langle x - 0 \rangle^0 + w \langle x - a \rangle^0$$

FIGURE 4-25

Interrupted Singularity Functions Are Formed by Combining Functions of Opposite Sign That Start at Different Points Along the Beam

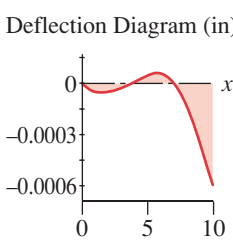
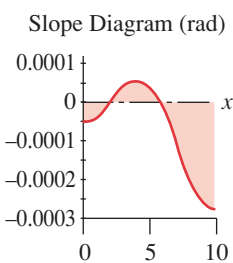
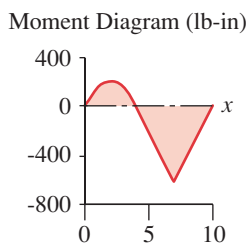
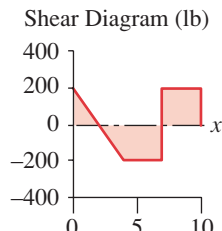
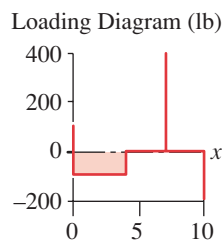


FIGURE 4-26

Example 4-6 Plots

$$\begin{aligned}
 M(l) = 0 &= \left(R_1 l^1 - \frac{w}{2} l^2 + \frac{w}{2} (l-a)^2 + R_2 (l-b)^1 - F (l-l)^1 \right) \\
 0 &= R_1 l - \frac{wl^2}{2} + \frac{w(l-a)^2}{2} + R_2 (l-b) \\
 R_1 &= \frac{1}{l} \left[\frac{wl^2}{2} - \frac{w(l-a)^2}{2} - R_2 (l-b) \right] = 200 \text{ lb}
 \end{aligned} \tag{g}$$

Note that the equations (f) are just the sum of forces = 0, and the sum of moments taken about point l and set to 0.

- 4 Substitute $x = 0, y = 0$, and $x = b, y = 0$ in equation (e) and solve for C_3 and C_4 :

$$\begin{aligned}
 y(0) = 0 &= \frac{1}{EI} \left(\frac{R_1}{6} (0-0)^3 - \frac{w}{24} (0-0)^4 + \frac{w}{24} (0-a)^4 + \frac{R_2}{6} (0-b)^3 \right. \\
 &\quad \left. - \frac{F}{6} (0-l)^3 + \frac{C_1}{6} (0)^3 + \frac{C_2}{2} (0)^2 + C_3(0) + C_4 \right) \\
 C_4 &= 0
 \end{aligned} \tag{h}$$

$$\begin{aligned}
 y(b) = 0 &= \frac{1}{EI} \left(\frac{R_1}{6} (b-0)^3 - \frac{w}{24} (b-0)^4 + \frac{w}{24} (b-a)^4 + \frac{R_2}{6} (b-b)^3 \right. \\
 &\quad \left. - \frac{F}{6} (b-l)^3 + \frac{C_1}{6} (b)^3 + \frac{C_2}{2} (b)^2 + C_3(b) + C_4 \right) \\
 C_3 &= \frac{1}{b} \left[-\frac{R_1}{6} b^3 + \frac{w}{24} b^4 - \frac{w}{24} (b-a)^4 \right] \\
 &= \frac{1}{7} \left[-\frac{200}{6} (7)^3 + \frac{100}{24} (7)^4 - \frac{100}{24} (7-4)^4 \right] = -252.4
 \end{aligned} \tag{i}$$

- 5 Substitution of the expressions for C_1, C_2, C_3, C_4, R_1 , and R_2 from equations (f), (g), (h), and (i) into equation (e) gives the resulting deflection equation

$$y = \frac{1}{EI} \left(\frac{R_1}{6} x^3 - \frac{w}{24} x^4 + \frac{w}{24} (x-a)^4 + \frac{R_2}{6} (x-b)^3 - \frac{F}{6} (x-l)^3 \right. \\
 \left. + \frac{1}{b} \left[-\frac{R_1}{6} (b)^3 + \frac{w}{24} (b)^4 - \frac{w}{24} (b-a)^4 \right] x \right) \tag{j}$$

- 6 Since an overhung beam is a form of cantilever beam, the maximum deflection is most likely at the free end. Substitute $x = l$ in equation (f) to find y_{max} .

$$\begin{aligned}
 y_{max} &= \frac{1}{EI} \left(\frac{R_1}{6} l^3 - \frac{w}{24} l^4 + \frac{w}{24} (l-a)^4 + \frac{R_2}{6} (l-b)^3 - \frac{F}{6} (l-l)^3 \right. \\
 &\quad \left. + \frac{1}{b} \left[-\frac{R_1}{6} (b)^3 + \frac{w}{24} (b)^4 - \frac{w}{24} (b-a)^4 \right] l \right) \\
 &= \frac{1}{3E7(0.2)} \left(\frac{200}{6} 10^3 - \frac{100}{24} 10^4 + \frac{100}{24} (10-4)^4 + \frac{400}{6} (10-7)^3 \right. \\
 &\quad \left. - \frac{200}{6} 0^3 + \frac{1}{7} \left[-\frac{200}{6} (7)^3 + \frac{100}{24} (7)^4 - \frac{100}{24} (7-4)^4 \right] 10 \right) \\
 y_{max} &= -0.0006 \text{ in}
 \end{aligned} \tag{k}$$

- 7 Plots of the loading, shear, moment, slope, and deflection functions for part (c) are shown in Figure 4-26. The files EX04-06 can be opened in the program of your choice to examine the model and see larger-scale plots of the functions in Figure 4-26.

Statically Indeterminate Beams

When a beam has redundant supports as shown in Figure 4-22d (repeated below) it is said to be statically indeterminate. This example is also called a continuous beam and is quite common. Supporting beams for buildings often have multiple columns distributed under a long beam span. The magnitudes of more than two reaction forces or moments cannot be found using only the two equations of static equilibrium, $\Sigma F = 0$ and $\Sigma M = 0$. To find more than two reactions requires additional equations, and the deflection function can be used for this purpose. The deflection can be assumed to be zero at each simple support (as a first approximation), and the beam slope is known or can be closely estimated at a moment support.* These provide an additional boundary condition for each added reaction, allowing the solution to be calculated.

SOLVING INDETERMINATE BEAMS WITH SINGULARITY FUNCTIONS The singularity functions provide a convenient way to set up and evaluate the equations for the loading, shear, moment, slope, and deflection functions as was demonstrated in the previous example. This approach can also be used to solve the indeterminate beam problem and is best demonstrated by another example.

EXAMPLE 4-7

Finding Reactions and Deflection of Statically Indeterminate Beams Using Singularity Functions

Problem: Determine and plot the loading, shear, moment, slope, and deflection functions for the beam in Figure 4-22d. Find maximum deflection.

Given: The load is uniformly distributed over part of the beam as shown. Length $l = 10$ in, $a = 4$ in, and $b = 7$ in. The beam's $I = 0.08 \text{ in}^4$ and $E = 30 \text{ Mpsi}$. The magnitude of the distributed force is $w = 500 \text{ in/lb}$.

Assumptions: Ignore the beam weight as negligible compared to the applied load.

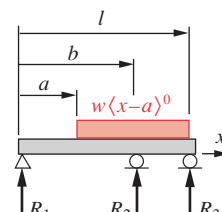
Solution: See Figures 4-22d (repeated here) and 4-27 (p. 173).

- 1 Write an equation for the load function in terms of equations 3.17 (pp. 113–114) and integrate the resulting function four times using equations 3.18 (pp. 114–115) to obtain the shear, moment, slope, and deflection functions.

$$q = R_1(x-0)^{-1} - w(x-a)^0 + R_2(x-b)^{-1} + R_3(x-l)^{-1} \quad (a)$$

$$V = \int q dx = R_1(x-0)^0 - w(x-a)^1 + R_2(x-b)^0 + R_3(x-l)^0 + C_1 \quad (b)$$

$$M = \int V dx = R_1(x-0)^1 - \frac{w}{2}(x-a)^2 + R_2(x-b)^1 + R_3(x-l)^1 + C_1x + C_2 \quad (c)$$



Indeterminate beam with uniformly distributed loading

FIGURE 4-22d

Repeated

* Since nothing is truly rigid, the beam's supports may deflect (compress) under the applied loads. However, if the supports are suitably stiff, this support movement will usually be small compared to the beam deflection and can be assumed to be zero for beam analysis.

$$\theta = \int \frac{M}{EI} dx = \frac{1}{EI} \left(\frac{R_1}{2} \langle x - 0 \rangle^2 - \frac{w}{6} \langle x - a \rangle^3 + \frac{R_2}{2} \langle x - b \rangle^2 + \frac{R_3}{2} \langle x - l \rangle^2 + \frac{C_1 x^2}{2} + C_2 x + C_3 \right) \quad (d)$$

$$y = \int \theta dx = \frac{1}{EI} \left(\frac{R_1}{6} \langle x - 0 \rangle^3 - \frac{w}{24} \langle x - a \rangle^4 + \frac{R_2}{6} \langle x - b \rangle^3 + \frac{R_3}{6} \langle x - l \rangle^3 + \frac{C_1 x^3}{6} + \frac{C_2 x^2}{2} + C_3 x + C_4 \right) \quad (e)$$

- 4
- 2 There are 3 reaction forces and 4 constants of integration to be found. The constants C_1 and C_2 are zero because the reaction forces and moments acting on the beam are included in the loading function. This leaves 5 unknowns to be found.
 - 3 If we consider the conditions at a point infinitesimally to the left of $x = 0$ (denoted as $x = 0^-$), the shear and moment will both be zero. The same conditions obtain at a point infinitesimally to the right of $x = l$ (denoted as $x = l^+$). Also, the deflection y must be zero at all three supports. These observations provide the 5 boundary conditions needed to evaluate the 3 reaction forces and 2 remaining integration constants: i.e., when $x = 0^-$, $V = 0$, $M = 0$; when $x = 0$, $y = 0$; when $x = b$, $y = 0$; when $x = l$, $y = 0$; when $x = l^+$, $V = 0$, $M = 0$.
 - 4 Substitute the boundary conditions $x = 0$, $y = 0$, $x = b$, $y = 0$, and $x = l$, $y = 0$ into (e).

Table 4-2Example 4-7
Calculated Data

Variable	Value	Unit
R_1	158.4	lb
R_2	2471.9	lb
R_3	369.6	lb
C_1	0.0	lb
C_2	0.0	lb-in
C_3	-1052.7	rad
C_4	0.0	in
V_{\min}	-1291.6	lb
V_{\max}	1130.4	lb
M_{\min}	-1141.1	lb-in
M_{\max}	658.7	lb-in
θ_{\min}	-0.025	deg
θ_{\max}	0.027	deg
y_{\min}	-0.0011	in
y_{\max}	0.0001	in

for $x = 0$:

$$y(0) = 0 = \frac{1}{EI} \left(\frac{R_1}{6} \langle 0 - 0 \rangle^3 - \frac{w}{24} \langle 0 - a \rangle^4 + \frac{R_2}{6} \langle 0 - b \rangle^3 + \frac{R_3}{6} \langle 0 - l \rangle^3 + C_3(0) + C_4 \right) \\ C_4 = 0 \quad (f)$$

for $x = b$:

$$y(b) = 0 = \frac{1}{EI} \left(\frac{R_1}{6} \langle b - 0 \rangle^3 - \frac{w}{24} \langle b - a \rangle^4 + \frac{R_2}{6} \langle b - b \rangle^3 + \frac{R_3}{6} \langle b - l \rangle^3 + C_3 b + C_4 \right) \\ C_3 = \frac{1}{b} \left(-\frac{R_1}{6} b^3 + \frac{w}{24} \langle b - a \rangle^4 \right) = \frac{1}{7} \left(-\frac{R_1}{6} 7^3 + 100(7 - 4)^4 \right) = 385.7 - 8.17R_1 \quad (g)$$

for $x = l$:

$$y(l) = 0 = \frac{1}{EI} \left(\frac{R_1}{6} \langle l - 0 \rangle^3 - \frac{w}{24} \langle l - a \rangle^4 + \frac{R_2}{6} \langle l - b \rangle^3 + \frac{R_3}{6} \langle l - l \rangle^3 + C_3 l + C_4 \right) \\ C_3 = \frac{1}{l} \left(-\frac{R_1}{6} l^3 + \frac{w}{24} \langle l - a \rangle^4 - \frac{R_2}{6} \langle l - b \rangle^3 \right) \\ C_3 = \frac{1}{10} \left(-\frac{R_1}{6} 10^3 + \frac{100}{24} \langle 10 - 4 \rangle^4 - \frac{R_2}{6} \langle 10 - 7 \rangle^3 \right) = 540 - 16.67R_1 - 4.5R_2 \quad (h)$$

- 5 Two more equations can be written using equations (c) and (b) and noting that at a point l^+ , infinitesimally beyond the right end of the beam, both V and M are zero. We can substitute l for l^+ since their difference is vanishingly small.

$$\begin{aligned}
 M(l) = 0 &= R_1(l-0)^1 - \frac{w}{2}(l-a)^2 + R_2(l-b)^1 + R_3(l-l)^1 \\
 0 &= R_1 l - \frac{w}{2}(l-a)^2 + R_2(l-b) \\
 R_1 &= \frac{1}{l} \left[\frac{w}{2}(l-a)^2 - R_2(l-b) \right] \\
 R_1 &= \frac{1}{10} \left[\frac{100}{2}(10-4)^2 - R_2(10-7) \right] = 180 - 0.3R_2 \quad (i)
 \end{aligned}$$

$$\begin{aligned}
 V(l) = 0 &= R_1(l)^0 - w(l-a)^1 + R_2(l-b)^0 + R_3(l-l)^0 = 0 \\
 0 &= R_1 - w(l-a) + R_2 + R_3 \\
 R_2 &= w(l-a) - R_1 - R_3 = 600 - R_1 - R_3 \quad (j)
 \end{aligned}$$

- 6 Equations (f) through (j) provide 5 equations in the 5 unknowns, R_1, R_2, R_3, C_3, C_4 and can be solved simultaneously. The deflection function can be expressed in terms of the geometry plus the loading and reaction forces, but, in this case, a simultaneous solution is necessary.

$$y = \frac{1}{EI} \left(\begin{array}{l} \left(\frac{R_1}{6}x^3 + \frac{1}{b} \left(\frac{w}{24}(b-a)^4 - \frac{R_1}{6}b^3 \right)x - \frac{w}{24}(x-a)^4 \right) \\ + \frac{R_2}{6}(x-b)^3 + \frac{R_3}{6}(x-l)^3 \end{array} \right) \quad (k)$$

- 7 Plots of the loading, shear, moment, slope, and deflection functions are shown in Figure 4-27 and their extreme values in Table 4-2. The files EX04-07 can be opened in the program of your choice to examine the model and see larger-scale plots of the functions shown in Figure 4-27.

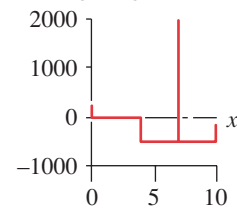
This example shows that singularity functions provide a good way to solve beam problems for reactions and deflections simultaneously when there are redundant reactions present. The singularity functions allow the writing of a single expression for each function that applies across the entire beam. They also are inherently computerizable in conjunction with an equation solver that will solve simultaneous equations. The singularity function method presented here is universal and will solve any problems of the types presented.

There are other techniques for the solution of deflection and redundant reaction problems. **Finite element analysis** (FEA) will solve these problems (see Chapter 8). The **area-moment method** treats the moment function as if it were a “loading” function and integrates twice to obtain the deflection function. The reader is referred to this chapter’s bibliography for additional information on these topics. **Castigliano’s method** uses strain energy equations to determine the deflection at any point.

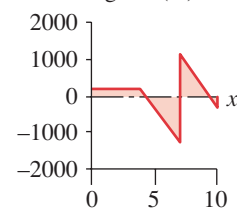
4.11 CASTIGLIANO’S METHOD

Energy methods often provide simple and rapid solutions to problems. One such method useful for the solution of beam deflections is that of Castigliano. It can also provide a

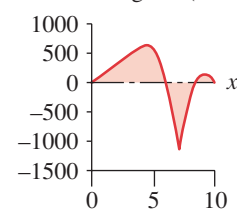
Loading Diagram (lb)



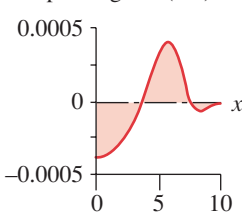
Shear Diagram (lb)



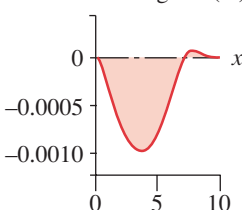
Moment Diagram (lb-in)



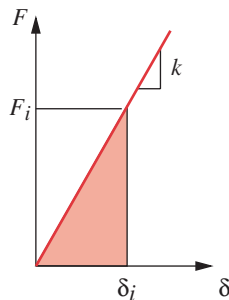
Slope Diagram (rad)



Deflection Diagram (in)

**FIGURE 4-27**

Example 4-7 Plots



4

FIGURE 3-17 Repeated
Energy Stored in a Spring

solution to indeterminate beam problems. When an elastic member is deflected by the application of a force, torque, or moment, strain energy is stored in the member. For small deflections of most geometries, the relationship between the applied force, moment, or torque and the resulting deflection can be assumed to be linear as shown in Figure 3-17, repeated here. This relationship is often called the spring rate k of the system. The area under the load deflection curve is the strain energy U stored in the part. For a linear relationship, this is the area of a triangle.

$$U = \frac{F\delta}{2} \quad (4.20)$$

where F is the applied load and δ is the deflection.

Castigliano observed that when a body is elastically deflected by any load, the deflection in the direction of that load is equal to the partial derivative of the strain energy with respect to that load. Letting Q represent a generalized load and Δ a generalized deflection,

$$\Delta = \frac{\partial U}{\partial Q} \quad (4.21)$$

This relationship can be applied to any loading case, whether axial, bending, shear, or torsion. If more than one such loading case exists on the same part, their effects can be superposed using equation 4.21 for each case.

STRAIN ENERGY IN AXIAL LOADING For axial loading, the strain energy is found by substituting the expression for axial deflection (Eq. 4.8, p. 152) into equation 4.20:

$$U = \frac{1}{2} \frac{F^2 l}{EA} \quad (4.22a)$$

which is valid only if neither E nor A varies over the length l . If they do vary with the distance x along the member, then an integration is necessary:

$$U = \frac{1}{2} \int_0^l \frac{F^2}{EA} dx \quad (4.22b)$$

STRAIN ENERGY IN TORSIONAL LOADING For torsional loading (see next section) the strain energy is

$$U = \frac{1}{2} \int_0^l \frac{T^2}{GK} dx \quad (4.22c)$$

where T is the applied torque, G is the modulus of rigidity, and K is a geometric property of the cross section as defined in Table 4-2 (p. 172).

STRAIN ENERGY IN BENDING LOADING For bending, the strain energy is

$$U = \frac{1}{2} \int_0^l \frac{M^2}{EI} dx \quad (4.22d)$$

where M is the bending moment, which may be a function of x .

STRAIN ENERGY IN TRANSVERSE SHEAR LOADING For transverse shear loading in a beam, the strain energy will be a function of the cross-sectional shape as well as the load and length. For a rectangular cross-sectional beam the strain energy is

$$U = \frac{3}{5} \int_0^L \frac{V^2}{GA} dx \quad (4.22e)$$

where V is the shear loading, which may be a function of x . For cross sections other than rectangular, the fraction 3/5 will be different.

The effects of transverse shear loads on deflections in beams typically will be less than 6% of the effects due to bending moments when the beam's length-to-depth ratio is >10 . Thus, only short beams will have significant transverse shear effects. For non-rectangular beam cross sections, 1/2 is often used in equation 4.22e rather than 3/5 to get a quick approximation of the strain energy due to transverse shear loads. Such a rough calculation will give an indication as to whether the order of magnitude of the deflection due to transverse shear is sufficient to justify a more accurate calculation.

Deflection by Castigliano's Method

This method is useful for calculating deflections at particular points on a system. Equation 4.21 relates force and deflection through strain energy. For a system deflected by more than one type of load, the individual effects can be superposed using a combination of equations 4.21 and 4.22. When bending and torsional loads are present, their deflection components will often be significantly larger than those due to any axial loading present. For this reason the axial effects are sometimes ignored.

The deflection at points where no actual load is applied can be found by applying a "dummy load" at that point and solving equation 4.21 with the dummy load set to zero. The computation is made easier if the partial differentiation of equation 4.21 is done before performing the integration defined in equations 4.22.

To find the maximum deflection, some knowledge of its location along the beam is needed. The singularity function method, on the other hand, provides the deflection function over the entire beam, from which the maxima and minima are easily found.

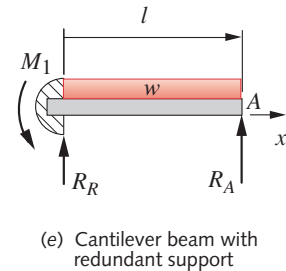
Finding Redundant Reactions with Castigliano's Method

Castigliano's method provides a convenient way to solve statically indeterminate problems. Reaction forces at redundant supports on a beam can be found from equation 4.22d by setting the deflection at the redundant support to zero and solving for the force.

EXAMPLE 4-8

Finding Reactions of a Statically Indeterminate Beam Using Castigliano's Method

Problem: Find the reaction forces for the indeterminate beam in Figure 4-22e.



4

FIGURE 4-22e

Indeterminate Beam

Given: The load is uniformly distributed over the beam as shown. Length is l . The magnitude of the distributed force is w .

Assumptions: Ignore the beam weight as negligible compared to the applied load.

Solution: See Figure 4-22e.

- 1 Consider the reaction force at A to be redundant and remove it temporarily. The beam will then be statically determinate and will deflect at A . Now consider the reaction force R_A to be an unknown applied load that will force the deflection to be zero (as it must be if point A is supported). If we write an equation for the deflection at A in terms of the force R_A and then solve it for R_A with the deflection set to zero, we will determine the necessary reaction force R_A .
- 2 Write equation 4.21 for the deflection y_A at the unknown applied load R_A in terms of the strain energy in the beam at that point.

$$y_A = \frac{\partial U}{\partial R_A} \quad (a)$$

- 3 Substitute equation 4.22d and differentiate:

$$y_A = \frac{\partial \left(\frac{1}{2} \int_0^l \frac{M^2}{EI} dx \right)}{\partial R_A} = \int_0^l \frac{M}{EI} \frac{\partial M}{\partial R_A} dx \quad (b)$$

- 4 Write an expression for the bending moment at a distance x from A :

$$M = R_A x - \frac{1}{2} w x^2 \quad (c)$$

- 5 Its derivative with respect to R_A is:

$$\frac{\partial M}{\partial R_A} = x \quad (d)$$

- 6 Substitute (c) and (d) in (b) to get:

$$y_A = \frac{1}{EI} \int_0^l \left(R_A x^2 - \frac{1}{2} w x^3 \right) dx = \frac{1}{EI} \left(\frac{R_A l^3}{3} - \frac{w l^4}{8} \right) \quad (e)$$

- 7 Set $y_A = 0$ and solve for R_A to get:

$$R_A = \frac{3}{8} w l \quad (f)$$

- 8 From sum of forces and sum of moments we get:

$$R_R = \frac{5}{8} w l \quad M_1 = \frac{1}{8} w l^2 \quad (g)$$

4.12 TORSION

When members are loaded with a moment about a longitudinal axis, they are said to be in **torsion**, and the applied moment is then called a **torque**. This situation is common in shafts that transmit power, in screw fasteners, and in any situation where the applied moment vector is parallel to the long axis of a part rather than transverse to it as in the case of bending. Many machine parts are loaded with combinations of torques and bending moments, and these situations will be dealt with in later chapters. Here we wish to consider only the simple case of **pure torsional loading**.

Figure 4-28a shows a straight bar having uniform circular cross section with a pure torque applied in such manner that no bending moment or other forces are present. This can be accomplished with a two-handled wrench such as a tap-handle, which allows a pure couple to be applied with no net transverse force. The fixed end of the bar is embedded in a rigid wall. The bar twists about its long axis, and its free end deflects through an angle θ . The assumptions for this analysis are as follows:

- 1 The element analyzed is distant from applied loads or external constraints on the bar.
- 2 The bar is subjected to pure torsion in a plane normal to its axis, and no axial, bending, or direct shear loads are present.
- 3 Cross sections of the bar remain plane and perpendicular to the axis.
- 4 The material of the bar is homogeneous, isotropic, and obeys Hooke's law.
- 5 Stresses remain below the elastic limit.
- 6 The bar is initially straight.

CIRCULAR SECTIONS A differential element taken anywhere on the outer surface will be sheared as a result of the torque loading. The stress τ is pure shear and varies from zero at the center to a maximum at the outer radius, as shown in Figure 4-28b,

$$\tau = \frac{T\rho}{J} \quad (4.23a)$$

where T = applied torque, ρ = radius to any point, and J = the polar area moment of inertia of the cross section. The stress is maximum at the outer surface, at radius r ,

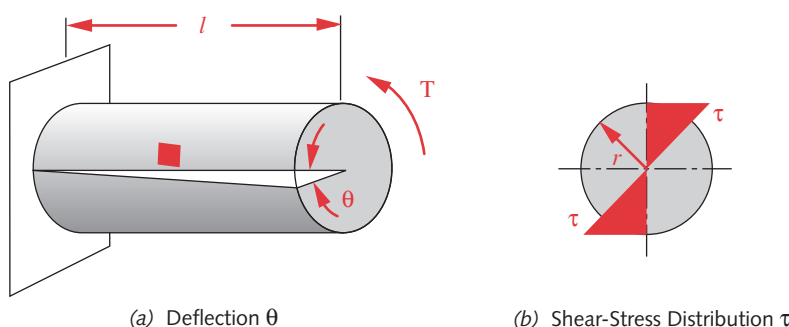


FIGURE 4-28

A Round Bar in Pure Torsion

$$\tau_{max} = \frac{Tr}{J} \quad (4.23b)$$

The angular deflection due to the applied torque is

$$\theta = \frac{Tl}{JG} \quad (4.24)$$

where l is length of the bar and G is the shear modulus (modulus of rigidity) of the material as defined in equation 2.5.

4

Note that **equations 4.24 apply only to circular cross sections**. Any other cross-sectional shape will behave quite differently. The polar area moment of inertia of a solid circular cross section of diameter d is

$$J = \frac{\pi d^4}{32} \quad (4.25a)$$

and for a hollow circular cross section of outside dia d_o and inside dia d_i is

$$J = \frac{\pi(d_o^4 - d_i^4)}{32} \quad (4.25b)$$

The circular cross section is the optimum shape for any bar subjected to torsional loading and should be used in all torsion situations if possible.

NONCIRCULAR SECTIONS In some cases, other shapes may be necessary for design reasons. Noncircular cross sections subjected to torsion exhibit behavior that violates some of the assumptions listed above. Sections do not remain plane, and will warp. Radial lines do not remain straight, and the shear-stress distribution is not necessarily linear across the section. A general expression for the **maximum shear stress due to torsion in noncircular sections** is

$$\tau_{max} = \frac{T}{Q} \quad (4.26a)$$

where Q is a function of cross-section geometry. The angular deflection is

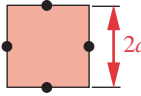
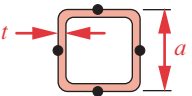
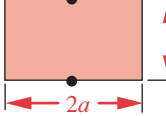
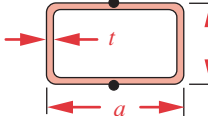
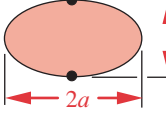
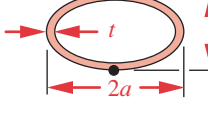
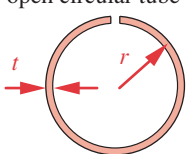
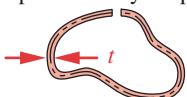
$$\theta = \frac{Tl}{KG} \quad (4.26b)$$

where K is a function of cross-sectional geometry. Note the similarity between this equation and equation 4.24. For a closed-circular section (only), the geometry factor K is the polar moment of inertia, J . For any closed cross-sectional shape other than circular, the factor K will be less than J for the same section dimensions, which is an indication of the value of using a closed-circular section for torsional loading. This fact will be demonstrated in the next example.

Expressions for Q and K for various cross sections can be found in reference 3 as well as in other sources. Table 4-3 shows expressions for Q and K for a few common cross sections and also shows the locations of the maximum shear stress.

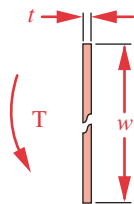
Table 4-3 Expressions for K and Q for Some Cross-Section Shapes in Torsion

The Black Dots Indicate Points of Maximum Shear Stress (Source: Ref. 4 with Permission)

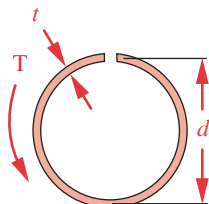
Shape	K	Q
solid square 	$K = 2.25a^4$	$Q = \frac{a^3}{0.6}$
hollow square 	$K = \frac{2t^2(a-t)^4}{2at-2t^2}$	$Q = 2t(a-t)^2$
solid rectangle 	$K = ab^3 \left[\frac{16}{3} - 3.36 \frac{b}{a} \left(1 - \frac{b^4}{12a^4} \right) \right]$	$Q = \frac{8a^2b^2}{3a+1.8b}$
hollow rectangle 	$K = \frac{2t^2(a-t)^2(b-t)^2}{at+bt-2t^2}$	$Q = 2t(a-t)(b-t)$
solid ellipse 	$K = \frac{\pi a^3 b^3}{a^2 + b^2}$	$Q = \frac{\pi a b^2}{2}$
hollow ellipse 	$K = \frac{\pi a^3 b^3}{a^2 + b^2} \left[1 - \left(1 - \frac{t}{a} \right)^4 \right]$	$Q = \frac{\pi a b^2}{2} \left[1 - \left(1 - \frac{t}{a} \right)^4 \right]$
open circular tube 	$K = \frac{2}{3}\pi r t^3; \quad t \ll r$	$Q = \frac{4\pi^2 r^2 t^2}{6\pi r + 1.8t}; \quad t \ll r$
open arbitrary shape 	$K = \frac{1}{3}U t^3; \quad t \ll U$	$Q = \frac{U^2 t^2}{3U + 1.8t}; \quad t \ll U$
U = length of median line		t must be much smaller than minimum radius of curvature

EXAMPLE 4-9**Design of a Torsion Bar**

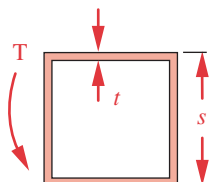
4



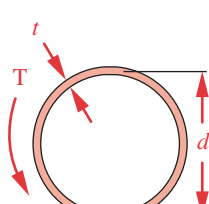
(a) Flat plate



(b) Open-circular



(c) Closed-square



(d) Closed-circular

Problem:

Determine the best cross-sectional shape for a hollow torsion bar to be made from a sheet of steel of known dimensions in order to withstand a pure torsional load with minimum angular deflection. Also find the maximum shear stress.

Given:

The applied torque is 10 N-m. The sheet of steel has length $l = 1$ m, width $w = 100$ mm, and thickness $t = 1$ mm. $G = 80.8$ GPa.

Assumptions:

Try four different cross-sectional shapes: unformed flat plate, open-circular section, closed-circular section, and closed-square section. The open-circular shape is rolled but is not welded at the seam. The closed shapes' seams are welded to create a continuous cross section. Assume a mean diameter or mean perimeter consistent with the sheet width.

Solution:

See Figure 4-29 and Table 4-3.

- 1 Equations 4.26 will apply for all sections, provided that we substitute J for K and J/r for Q in the case of the closed-circular section.
- 2 The unformed flat plate behaves as a solid rectangular section as shown in Figure 4-29a and Table 4-3. It has dimensions $a = w / 2 = 0.05$ m and $b = t / 2 = 0.0005$ m:

$$\begin{aligned} K &= ab^3 \left[\frac{16}{3} - 3.36 \frac{b}{a} \left(1 - \frac{b^4}{12a^4} \right) \right] \\ &= (0.05)(0.0005)^3 \left[5.333 - 3.36 \frac{0.0005}{0.05} \left(1 - \frac{(0.0005)^4}{12(0.05)^4} \right) \right] \quad (a) \\ K &= 3.312E-11 \text{ m}^4 = 33.123 \text{ mm}^4 \\ \theta &= \frac{Tl}{GK} = \frac{(10)(1)}{(8.08E10)(3.312E-11)} = 3.736 \text{ rad} = 214.1^\circ \end{aligned}$$

This is obviously a rather large angular deflection, indicating that the flat plate has been wound into a corkscrew by this torsional load.

$$\begin{aligned} Q &= \frac{8a^2b^2}{3a+1.8b} \\ &= \frac{8(0.05)^2(0.0005)^3}{3(0.05)+1.8(0.0005)} \quad (b) \\ Q &= 3.313E-8 \text{ m}^3 = 33.13 \text{ mm}^3 \\ \tau &= \frac{T}{Q} = \frac{10}{3.313E-8} = 301.8 \text{ MPa} = 43772 \text{ psi} \end{aligned}$$

The maximum shear stress is 300 MPa, which would require a material with a tensile yield strength of over 520 MPa (75 000 psi) in order not to yield and take a set. This

FIGURE 4-29

Cross-sections for Example 4-9

requires a high-strength steel. (See Section 5.1 for discussion of this relationship between tensile and shear strength as defined in equation 5.9b. on p. 251.)

- 3 The open-circular shape is now formed into a 3.18-cm diameter tube, but its longitudinal seam is left unwelded and open as shown in Figure 4-29b. The expressions for K and Q from Table 4-3 are

$$\begin{aligned} K &= \frac{2}{3}\pi r t^3 \\ &= \frac{2}{3}\pi \left(\frac{\frac{w}{\pi} - t}{2}\right) t^3 = \frac{1}{3}(w - \pi t)t^3 = \frac{1}{3}(0.1 - 0.001\pi)0.001^3 \quad (c) \\ K &= 3.2286E - 11 \text{ m}^4 = 32.286 \text{ mm}^4 \\ \theta &= \frac{Tl}{GK} = \frac{(10)(1)}{(8.08E10)(3.2286E - 11)} = 3.833 \text{ rad} = 219.6^\circ \end{aligned}$$

This is as large an angular deflection as that of the flat plate.

$$\begin{aligned} Q &= \frac{4\pi^2 r^2 t^2}{6\pi r + 1.8t} \\ &= \frac{4\pi^2 (0.01542)^2 (0.001)^3}{6\pi(0.01542) + 1.8(0.001)} \quad (d) \\ Q &= 3.209E - 8 \text{ m}^3 = 32.09 \text{ mm}^3 \\ \tau &= \frac{T}{Q} = \frac{10}{3.209E - 8} = 311.6 \text{ MPa} = 45,201 \text{ psi} \end{aligned}$$

The stress and deflection are unacceptable. It is just as bad a design as the flat plate.

- 4 The closed-square tube is formed by folding the sheet into a square section with side dimension $s = a = w / 4$. The seam is welded as shown in Figure 4-29c. From Table 4-3, K and Q , and the stress and deflection are now

$$\begin{aligned} K &= \frac{2t^2(a-t)^4}{2at-2t^2} = \frac{2t^2\left(\frac{w}{4}-t\right)^4}{2\frac{w}{4}t-2t^2} = \frac{2(0.001)^2\left(\frac{0.1}{4}-0.001\right)^4}{2\left(\frac{0.1}{4}\right)(0.001)-2(0.001)^2} \\ K &= 1.382E - 8 \text{ m}^4 = 13,824 \text{ mm}^4 \quad (e) \end{aligned}$$

$$\begin{aligned} \theta &= \frac{Tl}{GK} = \frac{(10)(1)}{(8.08E10)(1.382E - 8)} = 0.00895 \text{ rad} = 0.51^\circ \\ Q &= 2t(a-t)^2 = 2t\left(\frac{w}{4}-t\right)^2 = 2(0.001)\left(\frac{0.1}{4}-0.001\right)^2 \\ Q &= 1.152E - 6 \text{ m}^3 \quad (f) \end{aligned}$$

$$\tau = \frac{T}{Q} = \frac{10}{1.152E - 6} = 8.7 \text{ MPa} = 1,259 \text{ psi}$$

This angular deflection of the square tube is much less than that of either open section, and the maximum shear stress is now much more reasonable.

- 5 The closed-circular shape is formed into a 3.18-cm outside diameter tube and its longitudinal seam is welded shut as shown in Figure 4-29d. We can either use equations 4.24 and 4.25 (p. 178) or use the general equations 4.26 (p. 178) involving K and Q , which are now a function of J for this circular shape. For the deflection,

$$K = J = \frac{\pi(d_o^4 - d_i^4)}{32}; \quad d_o = \frac{w}{\pi}, \quad d_i = d_o - 2t \\ = \frac{\pi\left[\left(\frac{w}{\pi}\right)^4 - \left(\frac{w}{\pi} - 2t\right)^4\right]}{32} = \frac{\pi\left[\left(\frac{0.1}{\pi}\right)^4 - \left(\frac{0.1}{\pi} - 2\{0.001\}\right)^4\right]}{32} \quad (g)$$

$$K = J = 2.304E - 8 \text{ m}^4 = 23,041 \text{ mm}^4$$

$$\theta = \frac{Tl}{GK} = \frac{(10)(1)}{(8.08E10)(2.304E - 8)} = 0.0054 \text{ rad} = 0.31^\circ$$

and for the maximum shear stress at the outer surface,

$$Q = \frac{J}{r} = \frac{\pi(d_o^4 - d_i^4)}{32r_o} = \frac{\pi\left[\left(\frac{w}{\pi}\right)^4 - \left(\frac{w}{\pi} - 2t\right)^4\right]}{32\left(\frac{w}{2\pi}\right)} = \frac{\pi\left[\left(\frac{0.1}{\pi}\right)^4 - \left(\frac{0.1}{\pi} - 2\{0.001\}\right)^4\right]}{32\left(\frac{0.1}{2\pi}\right)} \\ Q = 1.448E - 6 \text{ m}^3 \quad (h) \\ \tau = \frac{T}{Q} = \frac{10}{1.448E - 6} = 6.91 \text{ MPa} = 1,002 \text{ psi}$$

- 6 This closed circular design has the smallest stress and deflection and is clearly the best choice of the four designs presented. The wall thickness could be increased to further reduce stress and deflection if desired. The design needs to be checked for possible torsional buckling as well. The files EX04-09 can be opened in the program of your choice if desired.

The previous example points out the advantage of using circular sections whenever torsional loads are present. Remember that the amount of material and thus the weight is identical in all four designs in this example. The closed-square section has 1.6 times the angular deflection of the closed-circular section (tube). The flat plate has 691 times the deflection of the closed-circular tube. Note that the open-circular section is no better in torsion than the flat plate; it has 708 times the angular deflection of the closed tube. This kind of result is true of any open section in torsion, whether I-beam, channel, angle, square, circle, or arbitrary shape. **Any open section is generally no better in torsion than a flat plate of the same cross-sectional dimensions.** Obviously, **open sections should be avoided for all torsionally loaded applications.** Even noncircular-closed sections should be avoided, as they are less efficient in torsion than closed-circular sections. **Only closed-circular sections, either hollow or solid, are recommended for torsional loading applications.**

4.13 COMBINED STRESSES

It is very common in machine parts to have combinations of loadings that create both normal and shear stresses on the same part. There may be locations within the part where these applied stresses must be combined to find the principal stresses and maximum shear stress. The best way to demonstrate this is with an example.

EXAMPLE 4-10

Combined Bending and Torsional Stresses

Problem Find the most highly stressed locations on the bracket shown in Figure 4-30 and determine the applied and principal stresses at those locations.

Given The rod length $l = 6$ in and arm $a = 8$ in. The rod outside diameter $d = 1.5$ in. Load $F = 1\,000$ lb.

Assumptions The load is static and the assembly is at room temperature. Consider shear due to transverse loading as well as other stresses.

Solution See Figures 4-30 to 4-33.

- We will limit our investigation to the rod which is loaded both in bending (as a cantilever beam) and in torsion. (The arm would also need to be analyzed for a complete design.) First, the load distributions over the rod's length need to be determined by drawing shear, moment, and torque diagrams for the rod.
- The shear and moment diagrams will look similar to those for the cantilever beam in Example 4-5, the difference being that this force is at the end of the beam rather than at some intermediate point. Figure 4-31 shows that the shear force is uniform across the beam length and its magnitude is equal to the applied load $V_{max} = F = 1\,000$ lb. The maximum moment occurs at the wall and its magnitude is $M_{max} = Fl = (1\,000)(6) = 6\,000$ lb-in. (See Example 4-5 for derivations.)

The torque applied to the rod is due to the force F acting at the end of the 8-in arm and is $T_{max} = Fa = (1\,000)(8) = 8\,000$ lb-in. Note that this torque is uniform over the length of the rod as it can only be reacted against by the wall. Figure 4-31 shows all three of these loading functions. It is clear from these plots that the most heavily loaded cross section is at the wall, where all three loads are maximum.

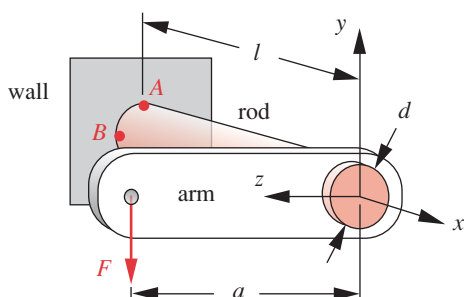


FIGURE 4-30

Bracket for Example 4-9

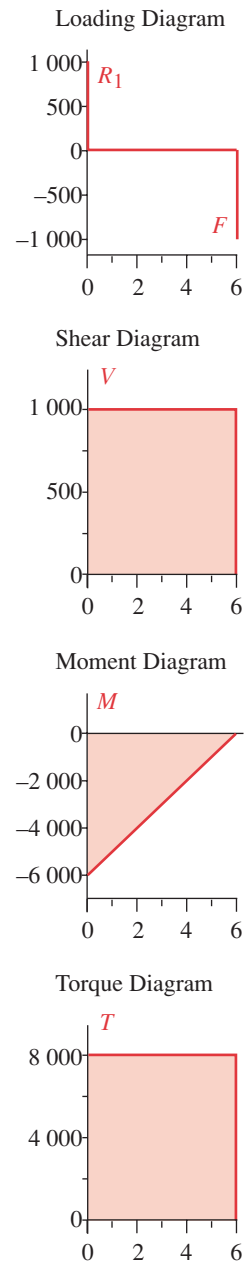
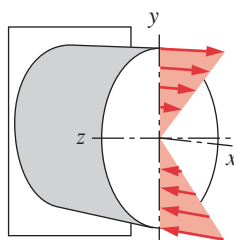


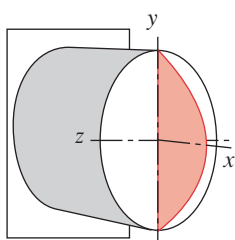
FIGURE 4-31

Loading Diagrams for Bending Shear, Moment, and Torque in Example 4-10

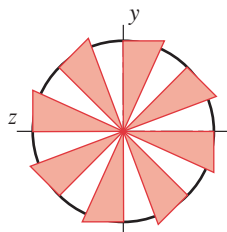
4



(a) Bending normal-stress distribution across section



(b) Transverse shear-stress distribution across section



(c) Torsional shear-stress distribution across section

FIGURE 4-32

Cross Sections of Rod for Example 4-10

- 3 We will now take a section through the rod at the wall and examine the stress distributions within it due to these external loads. Figure 4-32a shows the distribution across the section of the normal bending stresses, which are a maximum (+/-) at the outer fibers and zero at the neutral axis. The shear stress due to transverse loading is a maximum at all points in the neutral (xz) plane and zero at the outer fibers (Figure 4-32b).

The shear stress due to torsion is proportional to the radius so is zero at the center and a maximum at all points on the outer surface as shown in Figure 4-32c. Note the differences between the distributions of the normal bending stress and the torsional shear stress. The bending stress magnitude is proportional to the distance y from the neutral plane and so is maximum at only the top and bottom of the section, whereas the torsional shear stress is maximal all around the perimeter.

- 4 We choose two points, A and B of Figure 4-30, to analyze (also shown in Figure 4-33a) because they have the worst combinations of stresses. The largest tensile bending stress will be in the top outer fiber at point A, and it combines with the largest torsional shear stress that is all around the outer circumference of the rod. A differential element taken at point A is shown in Figure 4-33b. Note that the normal stress (σ_x) acts on the x face in the x direction and the torsional shear stress (τ_{xz}) acts on the x face in the $+z$ direction.

At point B the torsional shear stress has the same magnitude as at point A, but the direction of the torsional shear stress (τ_{xy}) at point B is 90° different than at point A. The shear stress due to transverse loading (τ_{xy}) is a maximum at point B. Note that these shear stresses both act in the $-y$ direction on the x face at point B as shown in Figure 4-33c. The transverse and torsional shear stresses then add at point B.

- 5 Find the normal bending stress and torsional shear stress on point A using equations 4.11b (p. 156) and 4.19b (p. 163), respectively.

$$\sigma_x = \frac{Mc}{I} = \frac{(Fl)c}{I} = \frac{1\ 000(6)(0.75)}{0.249} = 18\ 108 \text{ psi} \quad (a)$$

$$\tau_{xz} = \frac{Tr}{J} = \frac{(Fa)r}{J} = \frac{1\ 000(8)(0.75)}{0.497} = 12\ 072 \text{ psi} \quad (b)$$

- 6 Find the maximum shear stress and principal stresses that result from this combination of applied stresses using equations 4.6 (p. 145).

$$\begin{aligned} \tau_{max} &= \sqrt{\left(\frac{\sigma_x - \sigma_z}{2}\right)^2 + \tau_{xz}^2} = \sqrt{\left(\frac{18\ 108 - 0}{2}\right)^2 + 12\ 072^2} = 15\ 090 \text{ psi} \\ \sigma_1 &= \frac{\sigma_x + \sigma_z}{2} + \tau_{max} = \frac{18\ 108}{2} + 15\ 090 = 24\ 144 \text{ psi} \\ \sigma_2 &= 0 \\ \sigma_3 &= \frac{\sigma_x + \sigma_z}{2} - \tau_{max} = \frac{18\ 108}{2} - 15\ 090 = -6\ 036 \text{ psi} \end{aligned} \quad (c)$$

- 7 Find the shear due to transverse loading at point B on the neutral axis. The maximum transverse shear stress at the neutral axis of a round rod was given as equation 4.15c (p. 161).

$$\tau_{transverse} = \frac{4V}{3A} = \frac{4(1\ 000)}{3(1.767)} = 755 \text{ psi} \quad (d)$$

Point *B* is in pure shear. The total shear stress at point *B* is the algebraic sum of the transverse shear stress and the torsional shear stress, which both act on the same planes of the differential element.

$$\tau_{max} = \tau_{torsion} + \tau_{transverse} = 12\,072 + 755 = 12\,827 \text{ psi} \quad (e)$$

which from equation 4.6 or the Mohr's circle can be shown to be equal to the largest principal stress for this point.

- 8 Point *A* has the larger principal stress in this case, but note that the relative values of the applied torque and moment determine which of these two points will have the higher principal stress. Both points must then be checked. See files EX04-10 on CD.

4.14 SPRING RATES

Every part made of material having an elastic range can behave as a spring. Some parts are designed to function as springs, giving a controlled and predictable deflection in response to an applied load or vice versa. The "springiness" of a part is defined by its spring rate *k*, which is the load per unit deflection. For rectilinear motion springs,

$$k = \frac{F}{y} \quad (4.27a)$$

where *F* is the applied load and *y* is the resulting deflection. Typical units are lb/in or N/m. For angular motion springs the general expression is

$$k = \frac{T}{\theta} \quad (4.27b)$$

where *T* is the applied torque and *θ* is the resulting angular deflection. Typical units are in-lb/rad or N-m/rad, or sometimes expressed as in-lb/rev or N-m/rev.

The spring rate equation for any part is easily obtained from the relevant deflection equation, which provides a relationship between force (or torque) and deflection. For example, for a uniform bar in axial tension, the deflection is given by equation 4.8 (p. 152), rearranged to define its axial spring rate.

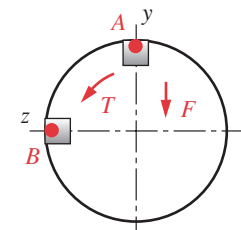
$$k = \frac{F}{y} : \quad \text{but } y = \frac{Fl}{AE}, \quad \text{so } k = \frac{AE}{l} \quad (4.28)$$

This is a constant spring rate, dependent only on the bar's geometry and its material properties.

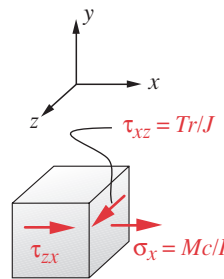
For a uniform-section round bar in pure torsion, the deflection is given by equation 4.24 (p. 178), rearranged to define its torsional spring rate:

$$k = \frac{T}{\theta} : \quad \text{but } \theta = \frac{Tr}{GJ}, \quad \text{so } k = \frac{GJ}{l} \quad (4.29)$$

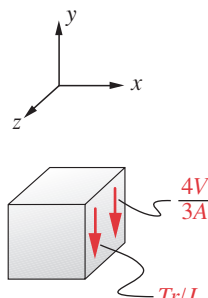
This is also a constant spring rate, dependent only on the bar's geometry and material properties.



(a) Two points of interest for stress calculations



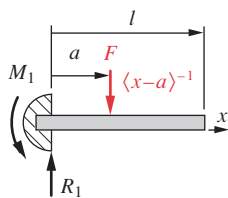
(b) Stress element at point *A*



(c) Stress element at point *B*

FIGURE 4-33

Stress Elements at Points *A* and *B* within Cross Section of Rod for Example 4-10



Cantilever beam with concentrated loading

4

FIGURE 4-22b

Repeated

For a cantilever beam with a concentrated point load as shown in Figure 4-22b (repeated here), the deflection is given by equation (j) in Example 4-5, rearranged here to define the beam's spring rate with the force applied at the end of the beam ($a = l$):

$$\begin{aligned} y &= \frac{F}{6EI} [x^3 - 3ax^2 - (x-a)^3] \\ \text{but, when } a=l, \quad y &= \frac{F}{6EI} (x^3 - 3lx^2 - 0) = \frac{Fx^2}{6EI} (x-3l) \\ \text{for } F \text{ at } x=l: \quad y &= \frac{Fl^2}{6EI} (l-3l) = -\frac{Fl^3}{3EI} \\ \text{then} \quad k &= \frac{F}{y} = \frac{3EI}{l^3} \end{aligned} \quad (4.30)$$

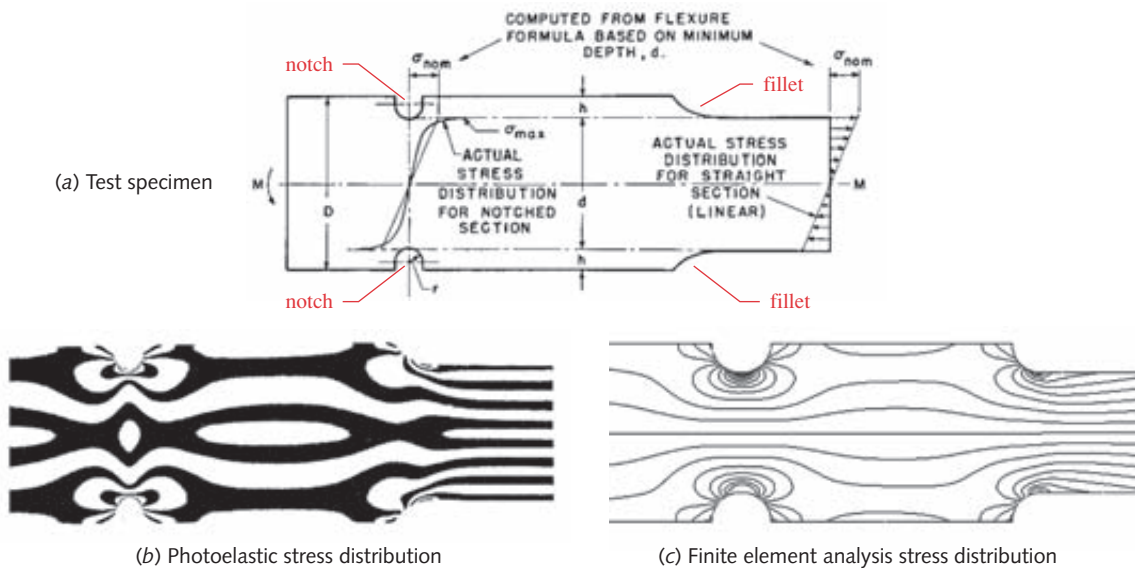
Note that the spring rate k of a beam is unique to its manner of support and its loading distribution, since k depends on the particular beam's deflection equation and point of load application. We will investigate spring design in more detail in a later chapter.

4.15 STRESS CONCENTRATION

All the discussion of stress distributions within loaded members has, up to now, assumed that the members' cross sections were uniform throughout. However, most real machine parts will have varying cross sections. For example, shafts often are stepped to different diameters to accommodate bearings, gears, pulleys, etc. A shaft may have grooves for snap-rings or O-rings, or have keyways and holes for the attachment of other parts. Bolts are threaded and have heads bigger than their shank. Any one of these changes in cross-sectional geometry will cause localized stress concentrations.

Figure 4-34 shows the stress concentration introduced by notches and fillets in a flat bar subjected to a bending moment. Figure 4-34b shows the stress effects as measured using photoelastic techniques. Photoelastic stress analysis involves making a physical model of the part in a particular type of transparent plastic, loading it in a fixture and photographing it under polarized light, which causes the stresses to show up as "fringes" that depict the stress distribution in the part. Figure 4-34c shows a finite-element model (FEM) of a part with the same geometry that is constrained and loaded the same way as the photoelastic specimen. Its lines denote isobars of stress levels. Note that, at the right end of the part where the cross section is uniform, the fringe lines of Figure 4-34b are straight, of uniform width, and equispaced. The FEM isobars in Figure 4-24c show a similar pattern.* This indicates a linear stress distribution across this portion of the bar well away from the notches, but at the changes in geometry the stress distribution is very nonlinear and is larger in magnitude. At the fillets where the width of the part is reduced from D to d , the fringe lines and the FEM isobars indicate a disruption and concentration of stresses at this sudden change in geometry. The same effect is seen near the left-hand end around the two notches. Figure 4-34b provides experimental evidence, and Figure 4-34c computational evidence, of the existence of stress concentration at any change in geometry. Such geometric changes are often called "stress-raiser" and should be avoided or at least minimized as much as possible in design. Unfortunately, it is not practical to eliminate all such stress-raiser, since such geometric details are needed to connect mating parts and provide functional part shapes.

* The finite element model was actually longer than shown and had the loads applied at the ends, well away from the section shown. This was done so as not to show the local stress concentrations at the points of load application and to match the stress fields of the photoelastic example, which probably also was longer than shown for the same reason.

**FIGURE 4-34**

Photoelastic and Finite Element Analysis Measurement of Stress Concentration in a Flat, Stepped, Notched Bar in Bending
Parts (a) and (b) reproduced from reference 5, Fig. 2, p. 3, reprinted by permission of John Wiley & Sons, Inc.

The amount of stress concentration in any particular geometry is denoted by a geometric stress-concentration factor K_t for normal stresses, or by K_{ts} for shear stresses. The maximum stress at a local stress-raiser is then defined as

$$\begin{aligned}\sigma_{max} &= K_t \sigma_{nom} \\ \tau_{max} &= K_{ts} \tau_{nom}\end{aligned}\quad (4.31)$$

where σ_{nom} and τ_{nom} are the nominal stresses calculated for the particular applied loading and net cross section, assuming a stress distribution across the section that would obtain for a uniform geometry. For example, in the beam of Figure 4-34, the nominal stress distribution is linear and at the outer fiber, $\sigma_{nom} = Mc / I$. The stress at the notches would then be $\sigma_{max} = K_t Mc / I$. In an axial-tension case, the nominal stress distribution would be as defined in Figure 4-10 (p. 152) and for torsion as defined in Figure 4-28 (p. 177). Note that the nominal stresses are calculated using the **net cross section**, which is *reduced by the notch geometry*, i.e., using d instead of D as the width at the notches in Figure 4-34.

The factors K_t and K_{ts} only take the effects of part geometry into account and do not consider how the material behaves in the face of stress concentrations. The ductility or brittleness of the material and the type of loading, whether static or dynamic, also affects how it responds to stress concentrations.

Stress Concentration Under Static Loading

The ductility or brittleness of the material has a pronounced effect on its response to stress concentrations under static loads. We will discuss each of these cases in turn.

DUCTILE MATERIALS will yield locally at the stress-raiser while the lower-stressed material further from the geometric discontinuity remains below the yield point. When the material yields locally, its stress-strain curve becomes nonlinear and of low slope (see Figure 2-2, p. 32), which prevents further significant increase in stress at that point. As the load is increased, more material is yielded, bringing more of the cross section to that stress. Only when the entire cross section has been brought to the yield point will the part continue up the σ - ϵ curve to fracture. Thus, it is common to ignore the effects of geometric stress concentration in *ductile materials under static loading*. The stress for the net cross section is calculated as if the stress concentration were not there. However, the reduction in net cross-sectional area or in area moment of inertia due to the removed material is accounted for, thus producing higher stresses than for an unnotched part of the same overall dimensions.

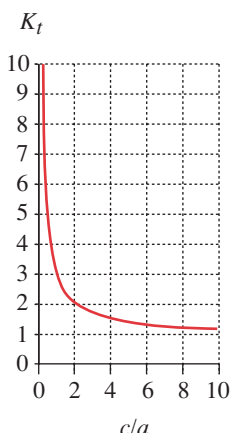
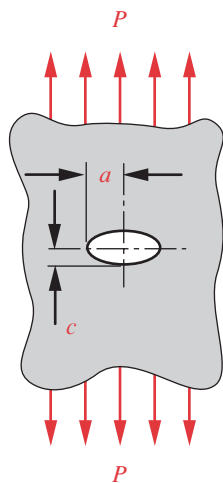


FIGURE 4-35

Stress Concentration at the Edge of an Elliptical Hole in a Plate

BRITTLE MATERIALS will not yield locally, since they do not have a plastic range. Thus, stress concentrations do have an effect on their behavior even under static loads. Once the stress at the stress-raiser exceeds the fracture strength, a crack begins to form. This reduces the material available to resist the load and also increases the stress concentration in the narrow crack. The part then goes quickly to failure. So, for brittle materials under static loads, the stress-concentration factor should be applied to increase the apparent maximum stress according to equation 4.31.

The one exception to this is for brittle, cast materials that tend to contain many disruptions and discontinuities within their structure due to graphite flakes in the alloy, or air bubbles, foreign matter, sand particles, etc., which found their way into the molten material in the mold. These discontinuities within the material create many stress-raisers, which are also present in the test specimens used to establish the material's basic strengths. Thus the published strength data include the effects of stress concentration. Adding geometric stress-raisers to the part design, it is argued, adds little to the overall statistical effect of those already in the material. Thus, the geometric stress-concentration factor is often ignored for cast-brittle materials or any material with known defects distributed throughout its interior. But, it should be applied to stresses in other brittle materials.

Stress Concentration Under Dynamic Loading

Ductile materials under dynamic loading behave and fail as if they were brittle. So, regardless of the ductility or brittleness of the material, the stress-concentration factor should be applied when dynamic loads (fatigue or impact) are present. However, there are still material-related parameters to account for. While all materials are affected by stress concentrations under dynamic loads, some materials are more sensitive than others. A parameter called notch sensitivity q is defined for various materials and used to modify the geometric factors K_t and K_{ts} for a given material under dynamic loading. These procedures will be discussed in detail in Chapter 6.

Determining Geometric Stress-Concentration Factors

The theory of elasticity can be used to derive stress-concentration functions for some simple geometries. Figure 4-35 shows an elliptical hole in a **semi-infinite plate** subjected to axial tension. The hole is assumed to be small compared to the plate and far

removed from the plate boundaries. The nominal stress is calculated based on the applied force and the total area, $\sigma_{nom} = P / A$. The theoretical stress-concentration factor at the edge of the hole was developed by Inglis in 1913* and is

$$K_t = 1 + 2\left(\frac{a}{c}\right) \quad (4.32a)$$

where a is the half-width of the ellipse and c is the half-height. Clearly, as the height of the elliptical hole approaches zero, creating a sharp-edged crack, the stress concentration goes to infinity. When the hole is a circle, $a = c$ and $K_t = 3$. Figure 4-35 also shows a plot of K_t as a function of c/a , the reciprocal of the ratio in equation 4.32a. The function is asymptotic to $K_t = 1$ at large values of c/a .

STRESS CONCENTRATION MEASUREMENT The theory of elasticity can provide stress-concentration values for some cases as above. Other stress-concentration factors have come from experimental investigations of parts under controlled loading. Experimental measurements can be made with strain gages, photoelastic techniques, laser holography, or other means. Finite element analysis (FEA) and boundary element analysis (BEA) techniques are increasingly being used to develop stress-concentration factors. When a stress analysis is done with these numerical techniques, the stress concentrations “come out in the wash” as long as the mesh is made sufficiently fine around areas of geometric stress raisers. (See Figure 4-51, p. 214.)

EFFECT OF LENGTH-WIDTH RATIO Note that Inglis’ classic 1913 analysis of this stress concentration case described above assumed a “semi-infinite plate,” meaning that the loads are applied far from the hole. Recently, FEA analysis of the circular-hole-in-plate case has shown that the stress concentration factor is larger for very short plates, as defined by the ratio of the plate length in the direction of loading to its width, L/W . Troyani et al.^[8] show that for L/W ratios less than about 2, and for a uniform tensile load applied over width W , the K_t values vary from around Inglis’ value of 3 up to as high as 11 depending on the ratio of hole radius to plate width r/W in combination with the L/W ratio. If your design uses a very short plate with hole(s), and is loaded in tension, this reference should probably be consulted to obtain a better value of K_t . This study also showed that if the tensile loading applied to the plate is the result of a uniform displacement across width W rather than a uniform force, then the value of K_t is reduced. This is because the stiffer webs around the hole are forced to carry the load when the cross section at the displaced end is kept undeformed by the uniform displacement. This points out the effect of boundary conditions on stresses in a part. Other studies by the same authors show similar sensitivity of K_t to the L/W ratio of the part. Reference [9] analyzes flat stepped bars in tension and [10] covers round stepped bars in tension. In this last case they show that uniformly loading the large diameter end and fixing the small end of a stepped rod gives *increasing* K_t with reduced L/W ratio, while applying a uniform load to the small diameter end of the rod and fixing the large end gives *decreasing* K_t with reduced L/W . While these results are quite interesting, the changes in K_t do not occur until the L/W ratio has become quite small (< 2) in which case the stepped bar or rod begins to take on the appearance of a stack of pancakes (hotcakes). This geometric configuration may seldom be encountered in practical machine design.

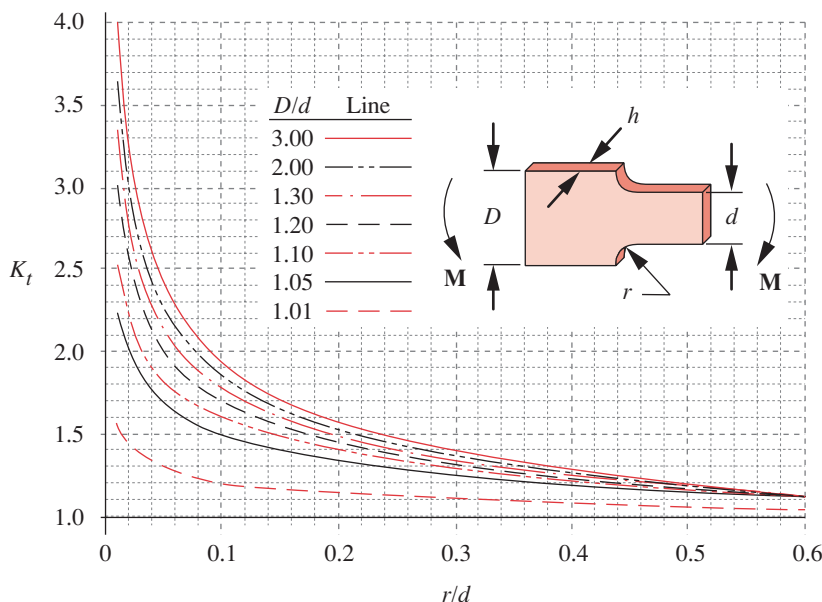
STRESS CONCENTRATION DATA The best-known and most-referenced set of stress-concentration factor data is in Peterson^[3, 5]. This book compiles the theoretical and experimental results of many researchers into useful design charts from which the values

* C. E. Inglis, 1913, “Stresses in a Plate Due to the Presence of Cracks and Sharp Corners,” *Engineering* (London), v. 95, p. 415.

of K_t and K_{ts} for various geometric parameters and types of loading can be read. Roark and Young^[4] also provide tables of stress-concentration factors for a number of cases.

Figure 4-36 and Appendix C contain stress-concentration functions and their plots based on data from the technical literature for a set of cases representing commonly encountered situations in machine design. In some cases, mathematical functions have been derived to fit the various empirical curves as closely as possible. In other cases list functions (table lookups) have been created that allow interpolation and automatic retrieval of the value of K_t in the process of a stress calculation. While these stress-concentration functions (SCF) are approximations of the data in the literature, they go beyond the originals in terms of usefulness, since they can be incorporated into a mathematical model of a machine-design problem. These SCF are supplied with this text as *TK Solver* files, which can be merged with other models or used as stand-alone tools to calculate K_t and K_{ts} for any supplied geometry. This is preferable to looking up data from charts for each calculation.

As an example, Figure 4-36 shows the stress-concentration function for the case of a stepped, flat bar in bending. (It and other cases are also shown in Appendix C.) The reduction in width from D to d at the step creates a stress-raiser, and the size of the fillet radius r is also a factor. These two geometric parameters are expressed as the dimensionless ratios r/d and D/d . The first of these is used as the independent variable in the equation and the second determines the member of the family of curves that result. This stress-concentration function is really a three-dimensional surface with the axes, r/d , D/d , and K_t . In Figure 4-36, we are looking at lines on that 3-D surface computed at different values of D/d and projected forward to the $r/d-K_t$ plane. The geometry of the part and its stress equation are defined in the figure, as is the function that defines each stress-concentration curve. In Figure 4-36 it is an exponential function of the form



$$\sigma_{nom} = \frac{Mc}{I} = 6 \frac{M}{hd^2}$$

$$\sigma_{max} = K_t \sigma_{nom}$$

and :

$$K_t = A \left(\frac{r}{d} \right)^b$$

where :

D/d	A	b
3.00	0.907 20	-0.333 33
2.00	0.932 32	-0.303 04
1.30	0.958 80	-0.272 69
1.20	0.995 90	-0.238 29
1.10	1.016 50	-0.215 48
1.05	1.022 60	-0.191 56
1.01	0.966 89	-0.154 17

FIGURE 4-36

Geometric Stress-Concentration Factors and Functions for a Stepped Flat Bar in Bending - Also see the File APP_C-10

Source: Fig. 73, p. 98, R. E. Peterson, Stress Concentration Factors, John Wiley & Sons, 1975, with the publisher's permission

$$K_t = Ax^b \quad (4.32b)$$

where x represents the independent variable or r/d in this case. The values of the coefficient A and exponent b for any one value of D/d are determined by nonlinear regression on several data points taken from the experimental data. The resulting values of A and b for various magnitudes of the second independent variable D/d are given in the table within the figure. A and b for other values of D/d can be interpolated. The file name that evaluates these functions and interpolates between them is also noted in this figure and in Appendix C for each of the 14 cases shown there.

The stress-concentration plots and functions provided in Appendix C along with their corresponding files will prove useful in the design of machine parts throughout this text and in your practice of engineering. For loading and geometry cases not covered in Appendix C of this text, see references 3 and 4.

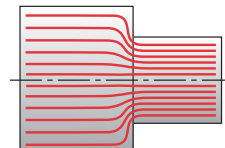
Designing to Avoid Stress Concentrations

Complicated geometry is often necessary for the proper function of machine parts. For example, a crankshaft must have particular contours for its purpose. The designer is always faced with the problem of stress concentrations at sections having abrupt changes of shape. The best that can be done is to minimize their effects. A study of the stress-concentration curves for various geometries in Appendix C will show that, in general, the sharper the corner and the larger in magnitude the change in contour, the worse will be the stress concentration. For the stepped bar in Figure 4-36, larger D/d ratios and smaller r/d ratios give worse stress concentration. From these observations, we can state some general guidelines for designing to minimize stress concentrations.

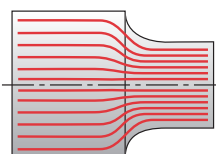
- 1 Avoid abrupt and/or large-magnitude changes in cross section if possible.
- 2 Avoid sharp corners completely and provide the largest possible transition radii between surfaces of different contours.

These guidelines are fine to state and better to observe, but practical design constraints often intervene to preclude strict adherence to them. Some examples of good and bad designs for stress concentration are shown in Figures 4-37 through 4-39 along with some common tricks used by experienced designers to improve the situation.

FORCE-FLOW ANALOGY Figure 4-37a shows a shaft with an abrupt step and a sharp corner, while Figure 4-37b shows the same step in a shaft with a large transition radius. A useful way to visualize the difference in the stress states in contoured parts such as these is to use a “force-flow” analogy, which considers the forces (and thus the stresses) to flow around contours in a way similar to the flow of an ideal incompressible fluid inside a pipe or duct of changing contour. (See also Figure 4-34.) A sudden narrowing of the pipe or duct causes an increase in fluid velocity at the neckdown to maintain constant flow. The velocity profile is then “concentrated” into a smaller region. Streamlined shapes are used in pipes and ducts (and on objects that are pushed through a fluid medium, such as aircraft and boats) to reduce turbulence and resistance to flow. “Streamlining” our part contours (at least internally) can have similar beneficial effects in reducing stress concentrations. The force-flow contours at the abrupt step transition in Figure 4-37a are more concentrated than in the design of Figure 4-37b.



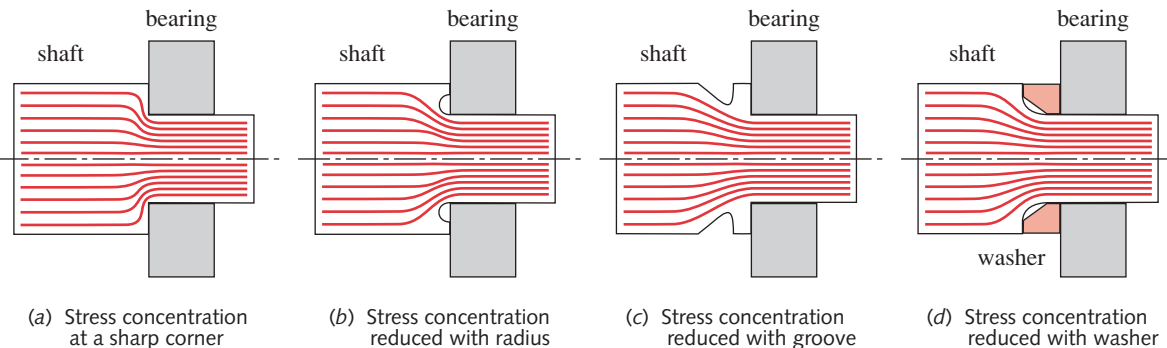
(a) Force flow around a sharp corner



(b) Force flow around a radiused corner

FIGURE 4-37

The Force-Flow Analogy for Contoured Parts

**FIGURE 4-38**

Design Modifications to Reduce Stress Concentrations at a Sharp Corner

The example in Figure 4-38 is a stepped shaft to which a ball bearing is to be fitted. A step is needed to locate the bearing axially as well as radially on the shaft diameter. Commercial ball- and roller bearings have quite small radii on their corners, which forces the designer to create a fairly sharp corner at the shaft step. To reduce the stress concentration at the step (a), a larger radius is needed than the bearing will allow. Three possible design modifications to create a better force flow around the step are shown in the figure. The first design (b) removes additional material at the corner in order to increase the radius and then “returns” the contour to provide the needed axial locating surface for the bearing. The second approach (c) removes material behind the step to improve the force streamlines. The third approach (d) provides a suitably large corner radius and adds a special washer that bridges the radius to provide the bearing seat. The stress concentration is reduced in each case versus the original sharp-cornered design.

A similar approach of removing material to improve the force flow is seen in Figure 4-39a, which shows a snap-ring groove in a shaft with additional relief grooves provided on each side to smooth the effective transition of the cross-sectional dimension. The effect on the force flow lines is similar to that shown in Figure 4-38c. Another common source of stress concentration is a key needed to torque-couple gears, pulleys, fly-wheels, etc., to a shaft. The keyway groove creates sharp corners at locations of maximum bending and torsional stresses. Different key styles are available, the most common being the square key and the circular-segment Woodruff key as shown in Figures 4-38b and 4-38c. See Section 10.10 for more information on keys and keyways.

Another example of removing material to reduce stress concentration (not shown) is the reduction of the unthreaded portion of a bolt shank’s diameter to a dimension less than that of the root diameter of the thread. Since the thread contours create large stress concentrations, the strategy is to keep the force-flow lines within the solid (unthreaded) portion of the bolt.

These examples show the usefulness of the *force-flow analogy* in providing a means to qualitatively improve the design of machine parts for reduced stress concentration. The designer should attempt to minimize sharp changes in the contours of internal force-flow lines by suitable choice of part shape.

4.16 AXIAL COMPRESSION - COLUMNS

Section 4.7 discussed stress and deflection due to axial tension and developed equations for their calculation, which are repeated here for convenience.

$$\sigma_x = \frac{P}{A} \quad (4.7)$$

$$\Delta s = \frac{Pl}{AE} \quad (4.8)$$

When the axial load direction is reversed so as to put the member in compression, equation 4.7 alone may not be sufficient to determine the safe load for the member. It is now a **column** and may fail by buckling rather than by compression. **Buckling** occurs suddenly and without warning, even in ductile materials, and as such is one of the more dangerous modes of failure. You can demonstrate buckling for yourself by taking a common rubber eraser between the palms of your two hands and gradually loading it in axial compression. It will resist the load until at some point it suddenly buckles into a bowed shape and collapses. (If you are feeling stronger, you can do the same with an aluminum beverage can.)

Slenderness Ratio

A **short column** will fail in compression as shown in Figure 2-6 (p. 35), and its compressive stress can be calculated from equation 4.7. An **intermediate** or a **long column** will fail by buckling when the applied axial load exceeds some critical value. The compressive stress can be **well below** the material's yield strength at the time of buckling. The factor that determines if a column is short or long is its **slenderness ratio** S_r ,

$$S_r = \frac{l}{k} \quad (4.33)$$

where l is the length of the column and k is its *radius of gyration*. **Radius of gyration** is defined as

$$k = \sqrt{\frac{I}{A}} \quad (4.34)$$

where I is the smallest *area moment of inertia* (*second moment of area*) of the column's cross section (about any neutral axis), and A is its *area at the same cross section*.

Short Columns

A short column is usually defined as one whose slenderness ratio is less than about 10. The material's yield strength in compression is then used as the limiting factor to compare to the stress calculated in equation 4.7.

Long Columns

A long column requires the calculation of its **critical load**. Figure 4-40 shows a slender column with rounded ends acted upon by compressive forces at either end, which

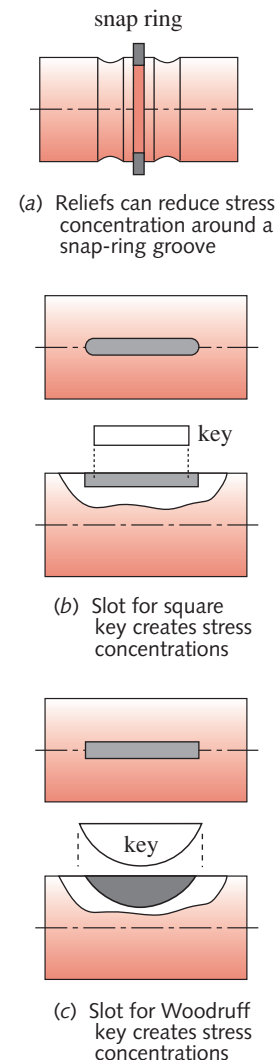


FIGURE 4-39

Stress Concentrations in Shafts

are coaxial and initially act through the area centroid of the column. (A section has been removed to show a reaction force and moment within the column.) The column is shown slightly deflected in the negative y direction, which shifts its area centroid out of collinearity with the applied forces at its ends. This shift of the area centroid creates a moment arm for the force to act about and puts the member in bending as well as in compression. The bending moment tends to increase the lateral deflection, which then also increases the moment arm! Once a critical value of load P_{cr} is exceeded, the positive feedback of this mechanism causes a sudden, catastrophic buckling. There is no visible warning.

The bending moment is given by

$$M = Py \quad (4.35)$$

For small deflections of a beam (using equation 4.17 repeated from p. 162),

$$\frac{M}{EI} = \frac{d^2y}{dx^2} \quad (4.17)$$

Combining 4.35 and 4.17 yields a familiar differential equation:

$$\frac{d^2y}{dx^2} + \frac{P}{EI}y = 0 \quad (4.36)$$

which has the well-known solution:

$$y = C_1 \sin \sqrt{\frac{P}{EI}}x + C_2 \cos \sqrt{\frac{P}{EI}}x \quad (4.37a)$$

where C_1 and C_2 are constants of integration that depend on the boundary conditions defined for the column of Figure 4-40 as $y = 0$ at $x = 0$; $y = 0$ at $x = l$. Substitution of these conditions shows that $C_2 = 0$ and

$$C_1 \sin \sqrt{\frac{P}{EI}}l = 0 \quad (4.37b)$$

This equation will hold if $C_1 = 0$, but that is a null solution. So C_1 must be nonzero and

$$\sin \sqrt{\frac{P}{EI}}l = 0 \quad (4.37c)$$

which will be true for

$$\sqrt{\frac{P}{EI}}l = n\pi; \quad n = 1, 2, 3, \dots \quad (4.37d)$$

The first critical load will occur for $n = 1$, which gives

$$P_{cr} = \frac{\pi^2 EI}{l^2} \quad (4.38a)$$

This is known as the **Euler-column formula** for rounded-end or pinned-end columns. Note that the critical load is a function only of the column's cross-sectional geometry I , its length l , and the material's modulus of elasticity E . **The strength of the**

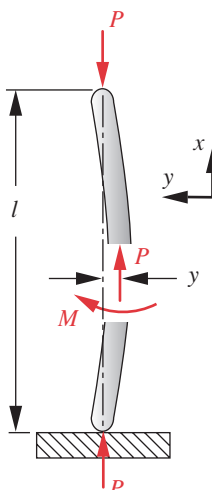


FIGURE 4-40

Buckling of an Euler Column

material is not a factor. Using a stronger (higher yield strength) steel, for example, will not help matters, because all steel alloys have essentially the same modulus of elasticity and will thus fail at the same critical load regardless of yield strength.

Substitute equation 4.33 and the expression $I = Ak^2$ from equation 4.34 into 4.38a:

$$P_{cr} = \frac{\pi^2 EAk^2}{l^2} = \frac{\pi^2 EA}{\left(\frac{l}{k}\right)^2} = \frac{\pi^2 EA}{S_r^2} \quad (4.38b)$$

Normalizing equation 4.38b by the cross-sectional area of the column, we get an expression for the **critical unit load**,

$$\frac{P_{cr}}{A} = \frac{\pi^2 E}{S_r^2} \quad (4.38c)$$

which has the same units as stress, or strength. It is the **load per unit area** of a rounded-(or pinned-) end column that will cause buckling to occur. Thus, it represents the strength of the particular column rather than the strength of the material from which it is made.

Substituting 4.38a in 4.37a gives the deflection curve for this column as

$$y = C_1 \sin \frac{\pi x}{l} \quad (4.39)$$

which is a half-period sine wave. Note that applying different boundary or **end conditions** will yield a different deflection curve and a different critical load.

End Conditions

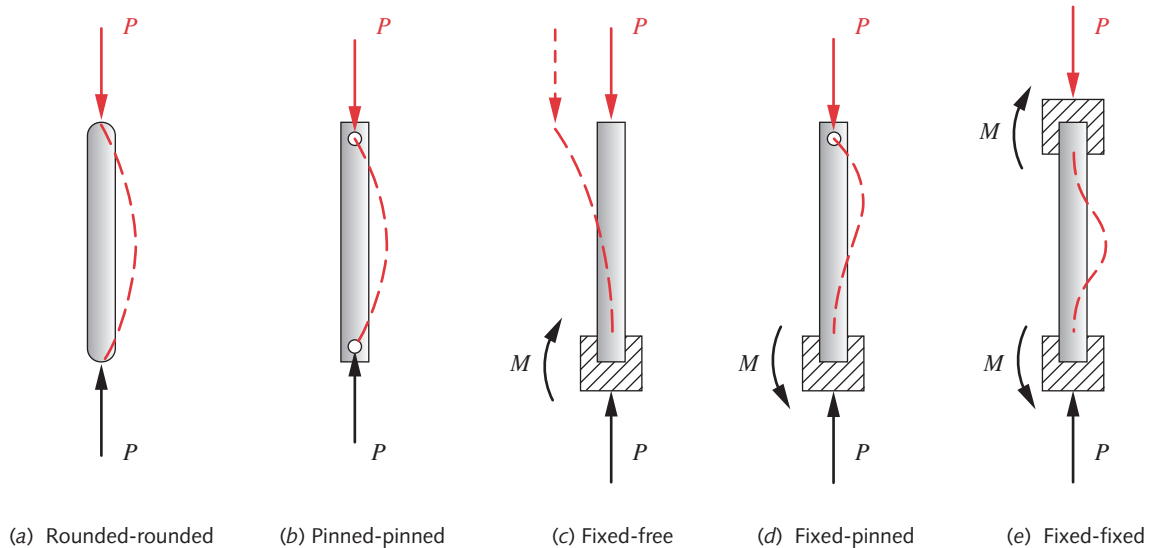
Several possible end conditions for columns are shown in Figure 4-41. The *rounded-rounded* and *pinned-pinned* conditions of Figures 4-41a and 4-41b are essentially the same. They each allow forces but not moments to be supported at their ends. Their boundary conditions are identical, as described above. Their critical unit load is defined in equation 4.38c and their deflection in equation 4.39.

The *fixed-free* column of Figure 4-41c supports a moment and a force at its base and thus controls both the deflection, y , and the slope, y' , at that end, but it controls neither x nor y movement at its tip. Its boundary conditions are $y = 0$ and $y' = 0$ at $x = 0$. Substitution of these conditions in equation 4.37a gives

$$\frac{P_{cr}}{A} = \frac{\pi^2 E}{4S_r^2} \quad (4.40a)$$

$$y = C_1 \sin \frac{\pi x}{2l} \quad (4.40b)$$

The deflection curve of a fixed-free Euler column is a quarter sine wave, making it effectively twice as long as a pinned-pinned column having the same cross section. This column can only support 1/4 the critical load of a pinned-pinned column. This reduction can be accounted for by using an effective length l_{eff} for a column with end conditions other than the pinned-pinned conditions used to derive the critical-load equations.

**FIGURE 4-41**

Various End Conditions for Columns and Their Resultant Deflection Curves (Applied Loads Shown in Color - Reactions in Black)

The *fixed-pinned* column (Figure 4-41d) has an $l_{eff} = 0.707l$ and the *fixed-fixed* column (Figure 4-41e) has an $l_{eff} = 0.5l$. The more rigid end constraints make these columns behave as if they were shorter (i.e., stiffer) than a pinned-pinned version and they will thus support more load. Substitute the appropriate effective length in equation 4.33 (p. 193) to obtain the proper slenderness ratio to use in any of the critical-load formulas:

$$S_r = \frac{l_{eff}}{k} \quad (4.41)$$

where l_{eff} takes the values shown in Table 4-4 for various end conditions. Note that the *fixed-pinned* and *fixed-fixed* conditions have theoretical l_{eff} values of $0.5l$ and $0.707l$, respectively, but these values are seldom used because it is very difficult to obtain a joint fixation that does not allow **any** change in slope at the column end. Welded joints will usually allow some angular deflection, which is dependent on the stiffness of the structure to which the column is welded.

Table 4-4 Column End-Condition Effective Length Factors

End Conditions	Theoretical Value	AISC* Recommends	Conservative Value
Rounded-Rounded	$l_{eff} = l$	$l_{eff} = l$	$l_{eff} = l$
Pinned-Pinned	$l_{eff} = l$	$l_{eff} = l$	$l_{eff} = l$
Fixed-Free	$l_{eff} = 2l$	$l_{eff} = 2.1l$	$l_{eff} = 2.4l$
Fixed-Pinned	$l_{eff} = 0.707l$	$l_{eff} = 0.80l$	$l_{eff} = l$
Fixed-Fixed	$l_{eff} = 0.5l$	$l_{eff} = 0.65l$	$l_{eff} = l$

Also, the theoretical analysis assumes that the loading is perfectly centered on the column axis. This condition is seldom realized in practice. Any loading eccentricity will cause a moment and create larger deflections than this model predicts. For these reasons, the AISC* suggests higher values for l_{eff} than the theoretical ones, and some designers use even more conservative values as shown in the third column of Table 4-4. The problem of eccentrically loaded columns is discussed in a later section.

Intermediate Columns

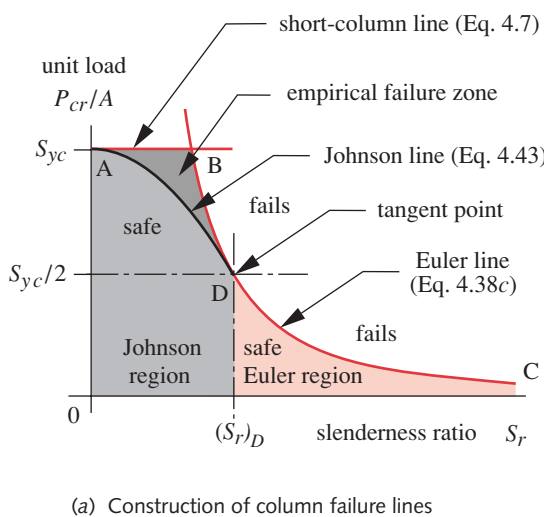
4

Equations 4.7 (p. 152) and 4.38c (p. 195) are plotted in Figure 4-42 as a function of slenderness ratio. The material's compressive yield strength, S_{yc} , is used as the value of σ_x in equations 4.7 and the critical unit load from equation 4.38c is plotted on the same axis as the material strength. The envelope $OABC$ defined by these two lines and the axes would seem to describe a safe region for column unit loads. However, experiments have demonstrated that columns loaded within this apparently safe envelope will sometimes fail. The problem occurs when the unit loads are in the region $ABDA$ near the intersection of the two curves at point B . J. B. Johnson suggested fitting a parabolic curve between point A and a tangent point D on the Euler curve (Eq. 4.38c, p. 195), which excluded the empirical failure zone. Point D is usually taken at the intersection of the Euler curve and a horizontal line at $S_{yc}/2$. The value of $(S_r)_D$ corresponding to this point can be found from equation 4.38c.

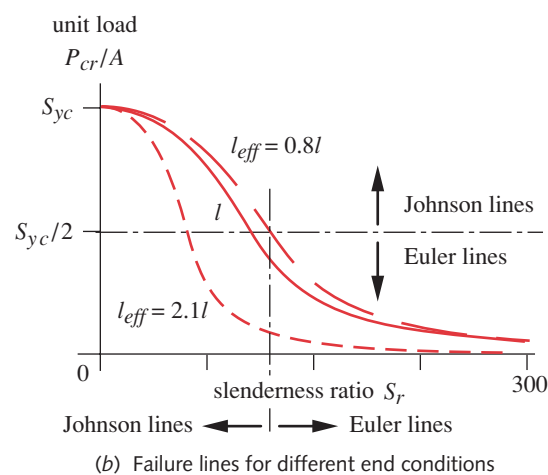
$$\frac{S_{yc}}{2} = \frac{\pi^2 E}{S_r^2}$$

$$(S_r)_D = \pi \sqrt{\frac{2E}{S_{yc}}} \quad (4.42)$$

* The American Institute of Steel Construction, in their *Manual of Steel Construction*.



(a) Construction of column failure lines



(b) Failure lines for different end conditions

FIGURE 4-42

Euler-, Johnson-, and Short-Column Failure Lines

The equation of the parabola fitted between points *A* and *D* is

$$\frac{P_{cr}}{A} = S_{yc} - \frac{1}{E} \left(\frac{S_{yc} S_r}{2\pi} \right)^2 \quad (4.43)$$

Equations 4.38c and 4.43 taken together over their appropriate regions then provide a reasonable failure model for all concentrically loaded columns. If the slenderness ratio is $\leq (S_r)_D$, use equation 4.43, else use equation 4.38c. Note that equation 4.43 is both valid and conservative for short columns as well. Equations 4.38c and 4.43 predict failure at the calculated critical unit loads, so an appropriate safety factor must be applied to the result to reduce the allowable load accordingly.

The file COLMPLOT will compute the critical load and plot the column failure curves of Figure 4-42 for any choices of S_{yc} , S_r , E , and end-condition factor. It can be used to check the design of any concentrically loaded column or to investigate trial designs. The reader may experiment with this program file by changing the values of the above factors and observing the effects on the plotted curves.

EXAMPLE 4-11

Column Design for Concentric Loading

Problem: A beachfront house is to be jacked up 10 ft above grade and placed on a set of steel columns. The weight to be supported by each column is estimated to be 200 000 lb. Two designs are to be considered, one using square steel tubes and the other using round steel tubes.

Given: Design the columns using a safety factor of 4. Determine the columns' outer dimensions for each shape, assuming a 0.5-in-thick tube wall in each case. The steel alloy has a compressive yield stress $S_{yc} = 60$ ksi.

Assumptions: The loading is concentric and the columns are vertical. Their bases are set in concrete and their tops are free, creating a *fixed-free* end-constraint condition. Use AISC recommended end-condition factors.

Solution: See Table 4-5, parts 1 and 2.

- 1 This problem, as stated, requires an iterative solution because the allowable load is specified and the column cross-sectional dimensions are requested. If the reverse were desired, equations 4.38c (p. 195), 4.42 (p. 197), and 4.43 (p. 198) could be solved directly to determine the allowable load for any chosen geometry.
- 2 To solve this problem using only a calculator requires choosing a trial cross-section dimension, such as the outside diameter, calculating its cross-sectional properties of area A , second moment of area I , radius of gyration k , and the slenderness ratio l_{eff}/k , then using these values in equations 4.38c, 4.42, and 4.43 to determine the allowable load after applying a safety factor. It is not known at the outset whether the column will turn out to be a Johnson or Euler one, so the slenderness ratio $(S_r)_D$ at the tangent point should be found from Eq 4.42 and compared to the column's actual S_r to decide whether Euler's or Johnson's equation is required.

- 3 Assume an 8-in outside diameter for a first-trial, round column. The area A , second moment of area I , and radius of gyration k for a 0.5-in wall-thickness round tube of that outside diameter are then

$$A = \frac{\pi(d_o^2 - d_i^2)}{4} = \frac{\pi(64 - 49)}{4} = 11.781 \text{ in}^2$$

$$I = \frac{\pi(d_o^4 - d_i^4)}{64} = \frac{\pi(4096 - 2401)}{64} = 83.203 \text{ in}^4 \quad (a)$$

$$k = \sqrt{\frac{I}{A}} = \sqrt{\frac{83.203}{11.781}} = 2.658 \text{ in}$$

- 4 Calculate the slenderness ratio S_r for this column and compare it to the value of $(S_r)_D$ corresponding to the tangent point between the Euler and Johnson curves (Eq. 4.42). Use the AISC recommended value (Table 4-4, p. 196) for a *fixed-free* column of $l_{eff} = 2.1 l$.

$$S_r = \frac{l_{eff}}{k} = \frac{120(2.1)}{2.658} = 94.825 \quad (b)$$

$$(S_r)_D = \pi \sqrt{\frac{2E}{S_y}} = \pi \sqrt{\frac{2(30E6)}{60000}} = 99.346$$

- 5 This column's slenderness ratio is to the left of the tangent point and thus is in the Johnson region of Figure 4-42 (p. 197), so use equation 4.43 (p. 198) to find the critical load P_{cr} and apply the safety factor to determine the allowable load P_{allow} .

$$P_{cr} = A \left[S_y - \frac{1}{E} \left(\frac{S_y S_r}{2\pi} \right)^2 \right] = 11.8 \left\{ 6E4 - \frac{1}{3E7} \left[\frac{6E4(94.825)}{2\pi} \right]^2 \right\} = 384\,866 \text{ lb} \quad (c)$$

$$P_{allow} = \frac{P_{cr}}{SF} = \frac{384\,866}{4} = 96\,217 \text{ lb}$$

- 6 This load is substantially below the required 200 000 lb, so we must repeat the calculations in steps 3–5 using larger outside diameters (or wall thicknesses) until we obtain a suitable allowable load. The problem also requests the design of a square-section column, which will only change the equations (a) in step 3 above.
- 7 This is clearly a tedious solution process when using only a calculator, and it cries out for a better approach. An equation solver or spreadsheet package can provide such a tool. An iterative-solver is needed for this problem that lets us specify the desired allowable load and have the program iterate until it converges to a value for the outside diameter (D_{out}) that will support the desired load, given an assumed wall thickness. Guess values for one or more of the unknown parameters are needed to start the iteration. The files EX04-10 are on the CD-ROM.
- 8 These programs allow for the solution of either a square or round cross section design and choose whether to use the Euler or Johnson equations based on the relative values of the slenderness ratios calculated in step 4 above. The complete solution takes only a few seconds. Table 4-5 part 1 shows the solution for the circular column and Table 4-5 part 2 shows the solution for the square column.

Table 4-5 Example 4-11 – Column Design

Part 1 of 2

Round Column Design

Input	Variable	Output	Unit	Comment
Input Data				
'circle	<i>Shape</i>			column shape 'square or 'circle
120	<i>L</i>		in	length of column
0.5	<i>Wall</i>		in	column wall thickness
2.1	<i>end</i>			AISC end condition factor
$30E6$	<i>E</i>		psi	Young's modulus
60 000	<i>Sy</i>		psi	compressive yield stress
4	<i>FS</i>			safety factor
200 000	<i>Allow</i>		lb	allowable load desired
Output Data				
<i>G</i> *	<i>Dout</i>	11.35	in	outside dia of column
	<i>Leff</i>	252	in	effective length of column
	<i>Sr</i>	65.60		slenderness ratio
	<i>Srd</i>	99.35		tangency point in <i>Sr</i>
	<i>Load</i>	46 921	lb	critical unit load
	<i>Johnson</i>	46 921	lb	Johnson unit load
	<i>Euler</i>	68 811	lb	Euler unit load
	<i>Din</i>	10.35	in	inside dia of column
	<i>k</i>	3.84	in	radius of gyration
	<i>I</i>	251.63	in ⁴	second moment of area
	<i>A</i>	17.05	in ²	area of cross section

* Indicates that a guess value is required to start the iteration.

- 9 A round column of 11.3-in diameter and 0.5-in wall is adequate to carry the specified load. This is a Johnson column with an effective slenderness ratio of 65.6 and a weight of 579 lb. The Euler formula predicts a critical load nearly 1.5 times that of the Johnson formula, so this column would be in the “danger region” labeled *ABDA* in Figure 4-42 (p. 197) if the Euler formula were used. If a 0.5-in wall, square column cross section is chosen, its outside dimension will be 9.3 in for the same slenderness ratio and allowable load, but the column will weigh more at 600 lb. A square column will always be stronger than a round one of the same outside dimension and wall thickness because its area, second moment of area, and radius of gyration are larger due to the material in the corners being at a larger radius. The additional weight of material also makes it more expensive than a round column of the same strength.

Eccentric Columns

The above discussion of column failure assumed that the applied load was concentric with the column and passed exactly through its centroid. Even though this condition

Table 4-5 Example 4-11 – Column Design

Part 2 of 2 Square Column Design

Input	Variable	Output	Unit	Comment
Input Data				
'square	<i>Shape</i>			column shape 'square or 'circle
120	<i>L</i>		in	length of column
0.5	<i>Wall</i>		in	column wall thickness
2.1	<i>end</i>			AISC end condition factor
30E6	<i>E</i>		psi	Young's modulus
60 000	<i>Sy</i>		psi	compressive yield stress
4	<i>FS</i>			safety factor
200 000	<i>Allow</i>		lb	allowable load desired
Output Data				
G*	<i>Dout</i>	9.34	in	outside dim of column
	<i>Leff</i>	252	in	effective length of column
	<i>Sr</i>	69.69		slenderness ratio
	<i>Srd</i>	99.35		tangency point in <i>Sr</i>
	<i>Load</i>	45 235	lb	critical unit load
	<i>Johnson</i>	45 235	lb	Johnson unit load
	<i>Euler</i>	60 956	lb	Euler unit load
	<i>Din</i>	8.34	in	inside dim of column
	<i>k</i>	3.62	in	radius of gyration
	<i>I</i>	231.21	in ⁴	second moment of area
	<i>A</i>	17.69	in ²	area of cross section

* Indicates that a guess value is required to start the iteration.

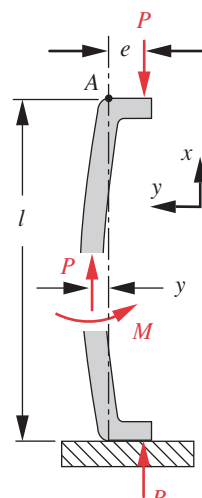
is desirable, it is seldom achieved in practice, as manufacturing tolerances will usually cause the load to be somewhat eccentric to the centroidal axis of the column. In other cases, the design may deliberately introduce an eccentricity *e* as shown in Figure 4-43. Whatever the cause, the eccentricity changes the loading situation significantly by superposing a bending moment *Pe* on the axial load *P*. The bending moment causes a lateral deflection *y*, which in turn increases the moment arm to *e* + *y*. Summing moments about point A gives

$$\sum M_A = -M + Pe + Py = -M + P(e + y) = 0 \quad (4.44a)$$

Substituting equation 4.17 (p. 162) yields the differential equation:

$$\frac{d^2y}{dx^2} + \frac{P}{EI}y = -\frac{Pe}{EI} \quad (4.44b)$$

The boundary conditions are *x* = 0, *y* = 0, and *x* = *l* / 2, *dy/dx* = 0, which give the solution for the deflection at midspan as

**FIGURE 4-43**

An Eccentrically Loaded Column

$$y = e \left[\sec \left(\frac{l}{2} \sqrt{\frac{P}{EI}} \right) - 1 \right] \quad (4.45a)$$

and for the maximum bending moment as

$$M_{max} = -P(e + y) = -Pe \sec \left(\frac{l}{2} \sqrt{\frac{P}{EI}} \right) \quad (4.45b)$$

The compressive stress is

$$\sigma_c = \frac{P}{A} - \frac{Mc}{I} = \frac{P}{A} - \frac{Mc}{Ak^2} \quad (4.46a)$$

Substituting the expression for maximum moment from equation 4.45b:

$$\sigma_c = \frac{P}{A} \left[1 + \left(\frac{ec}{k^2} \right) \sec \left(\frac{l}{k} \sqrt{\frac{P}{4EA}} \right) \right] \quad (4.46b)$$

Failure will occur at midspan when the maximum compressive stress exceeds the yield strength of the material if ductile, or its fracture strength if brittle. Setting σ_c equal to the compressive yield strength for a ductile material gives an expression for the critical unit load of an eccentric column:

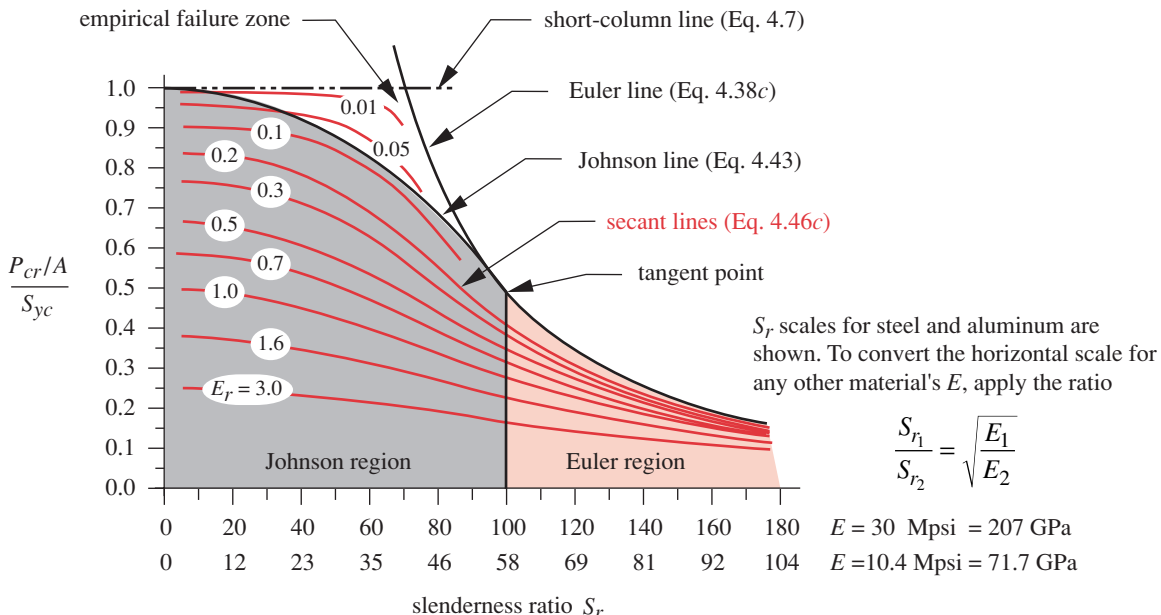
$$\frac{P}{A} = \frac{S_{yc}}{1 + \left(\frac{ec}{k^2} \right) \sec \left(\frac{l_{eff}}{k} \sqrt{\frac{P}{4EA}} \right)} \quad (4.46c)$$

This is called the **secant column formula**. The appropriate end-condition factor from Table 4-4 (p. 196) is used to obtain an effective length l_{eff} , which accounts for the column's boundary conditions. The radius of gyration k for equation 4.46c is taken with respect to the axis about which the applied bending moment acts. If the column cross section is asymmetrical and the bending moment does not act about the weakest axis, it must be checked for concentric-column failure about the axis having the smallest k as well as for failure due to eccentric loading in the bending plane.

The fraction ec / k^2 in equation 4.46c is called the **eccentricity ratio** E_r of the column. A 1933 study* concluded that assuming a value of 0.025 for the eccentricity ratio would account for typical variations in loading eccentricity of concentrically loaded Euler columns. However, if the column is in the Johnson range, Johnson's formula will apply for E_r 's of less than about 0.1. (See Figure 4-44 and its discussion below.)

Equation 4.46c is a difficult function to evaluate. Not only does it require an iterative solution, but the secant function goes to $\pm\infty$, causing computation problems. It also yields incorrect results when the secant function goes negative. The file SECANT computes and plots equation 4.46c (as well as the Euler and Johnson formulas) over a range of slenderness ratios for any choice of eccentricity ratio and round column cross-sectional parameters. Nonround columns can also be calculated in this program by declaring the area A and moment of inertia I to be input values instead of using the column's linear dimensions. When using this program, take care to plot the resulting function and note the regions, if any, in which the results are incorrect due to the secant's behavior. It will be obvious from the plots.

* Report of a Special Committee on Steel Column Research, *Trans. Amer. Soc. Civil Engrs.*, 98 (1933).

**FIGURE 4-44**

Secant Lines (in color) Superimposed on Euler-, Johnson-, and Short-Column Failure Lines

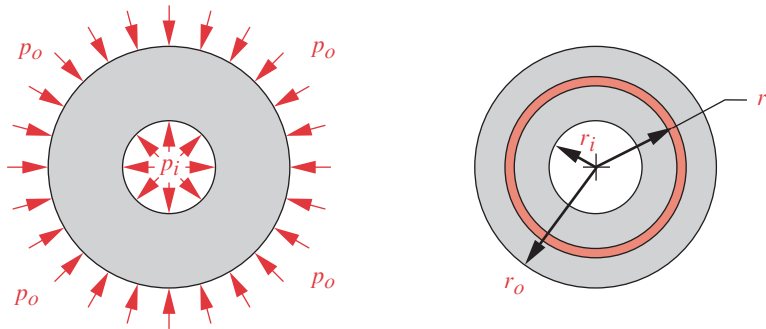
Figure 4-44 shows plots of equation 4.46c from SECANT (over valid ranges[†]) superimposed on the Euler-, Johnson-, and short-column plots from Figure 4-42. These curves are normalized to the compressive yield strength of the material. The curve shapes are the same for any material modulus of elasticity E ; only the horizontal scale changes. The ratio of the S_r scales to the ratio of E values of different materials is given in the figure.

The secant curves are all asymptotic to the Euler curve at large S_r 's. At an eccentricity ratio of zero, the secant curve becomes coincident with the Euler curve up to nearly the level of the short-column line. When the eccentricity ratio becomes smaller than about 0.1, the secant functions protrude into the concentric-column empirical failure region labeled ABDA in Figure 4-42 (p. 197), i.e., they move above the Johnson line. This indicates that **for eccentric intermediate columns with small eccentricity ratios, the Johnson concentric-column formula (rather than the secant formula) may be the failure criterion and should also be computed.**

4.17 STRESSES IN CYLINDERS

Cylinders are often used as pressure vessels or pipelines and can be subjected to internal and/or external pressure as shown in Figure 4-45. Some common applications are air or hydraulic cylinders, fluid storage tanks and pipes, and gun barrels. Some of these devices are open-ended and some are closed-ended. If open-ended, a two-dimensional stress state will exist in the cylinder walls, with radial and tangential (hoop) stress components. If close-ended, a third-dimensional stress called longitudinal or axial will also be present. These three applied stresses are mutually orthogonal and are principal, since there is no applied shear from the uniformly distributed pressure.

[†] Note in Figure 4-44 that the secant curves for eccentricity ratios of 0.01, 0.05, and 0.1 abruptly end short of the Euler line. This is where the first discontinuity in the secant function occurs, and the data beyond those points is invalid until the secant again goes positive. See the plots in file SECANT for further edification.

**FIGURE 4-45**

A Cylinder Subjected to Internal and External Pressure

Thick-Walled Cylinders

In Figure 4-45, an annular differential element is shown at radius r . The radial and tangential stresses on that element for an open-ended cylinder are given by Lame's equation:

$$\sigma_t = \frac{p_i r_i^2 - p_o r_o^2}{r_o^2 - r_i^2} + \frac{r_i^2 r_o^2 (p_i - p_o)}{r^2 (r_o^2 - r_i^2)} \quad (4.47a)$$

$$\sigma_r = \frac{p_i r_i^2 - p_o r_o^2}{r_o^2 - r_i^2} - \frac{r_i^2 r_o^2 (p_i - p_o)}{r^2 (r_o^2 - r_i^2)} \quad (4.47b)$$

where r_i and r_o are the inside and outside radii, p_i and p_o are the internal and external pressures, respectively, and r is the radius to the point of interest. Note that these stresses vary nonlinearly throughout the wall thickness.

If the ends of the cylinder are closed, the axial stress in the walls is:

$$\sigma_a = \frac{p_i r_i^2 - p_o r_o^2}{r_o^2 - r_i^2} \quad (4.47c)$$

Note the absence of r in this equation as the axial stress is uniform throughout the wall thickness.

If the external pressure $p_o = 0$, then the equations reduce to

$$\sigma_t = \frac{r_i^2 p_i}{r_o^2 - r_i^2} \left(1 + \frac{r_o^2}{r^2} \right) \quad (4.48a)$$

$$\sigma_r = \frac{r_i^2 p_i}{r_o^2 - r_i^2} \left(1 - \frac{r_o^2}{r^2} \right) \quad (4.48b)$$

and if closed-ended:

$$\sigma_a = \frac{p_i r_i^2}{r_o^2 - r_i^2} \quad (4.48c)$$

The distributions of these stresses across the wall thickness for $p_o = 0$ are shown in Figure 4-46. Under internal pressure, both are maximum at the inside surface. The tangential (hoop) stress is tensile and the radial stress is compressive. When two parts are press- or shrink-fitted together with an interference, the stresses developed in the two parts are defined by equations 4.47. Their mutual elastic deflections create internal pressure on the outer part and external pressure on the inner part. Interference fits are discussed further in Section 10.12.

Thin-Walled Cylinders

When the wall thickness is less than about 1/10 of the radius, the cylinder can be considered thin-walled. The stress distribution across the thin wall can be approximated as uniform, and the expressions for stress simplify to

$$\sigma_t = \frac{pr}{t} \quad (4.49a)$$

$$\sigma_r = 0 \quad (4.49b)$$

and if closed-ended:

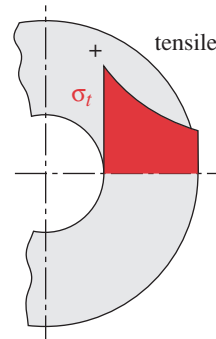
$$\sigma_a = \frac{pr}{2t} \quad (4.49c)$$

All of these equations are valid only at locations removed from any local stress concentrations or changes in section. For true pressure-vessel design, consult the ASME Boiler Code for more complete information and guidelines to safe design. Pressure vessels can be extremely dangerous even at relatively low pressures if the stored volume is large and the pressurized medium is compressible. Large amounts of energy can be released suddenly at failure, possibly causing serious injury.

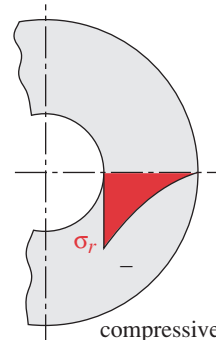
4.18 CASE STUDIES IN STATIC STRESS AND DEFLECTION ANALYSIS

We will now present some case studies that continue the design of devices whose forces were analyzed in the case studies of Chapter 3. The same case-study number will be retained for a given design throughout the text, and successive installments will be designated by a series of letter suffixes. For example, Chapter 3 presented six case studies labeled 1A, 2A, 3A, 4A, 5A, and 5B. This chapter will continue case studies 1 through 4 as 1B, 2B, 3B, and 4B. Some of these will be continued in later chapters and given successive letter designators. Thus, the reader can review the earlier installments of any case study by referring to its common case number. See the list of case studies in the table of contents to locate each part.

Since stresses vary continuously over a part, we must make some engineering judgment as to where they will be the largest and calculate for those locations. We do not



(a) Tangential stress



(b) Radial stress

FIGURE 4-46

Tangential and Radial Stress Distributions in Wall of Internally Pressurized Cylinder

have time to calculate the stresses at an infinity of locations. Since the geometries of these parts are fairly complicated, short of doing a complete finite element stress analysis, we must make some reasonable simplifications in order to model them. The aim is to quickly generate some information about the stress state of the design in order to determine its viability before investing more time in a complete analysis.

CASE STUDY 1B

Bicycle Brake Lever Stress and Deflection Analysis

Problem Determine the stresses and deflections at critical points in the brake lever shown in Figures 3-1 (repeated here) and 4-47.

Given The geometry and loading are known from Case Study 1A (p. 79). The pivot pin is 8-mm dia. The average human's hand can develop a grip force of about 267 N (60 lb) in the lever position shown.

Assumptions The most likely failure points are the two holes where the pins insert and at the root of the cantilever-beam lever handle. The cross section of the lever handle is essentially circular.

Solution See Figures 4-47 to 4-48.

- 1 The 14.3-mm-diameter portion of the handle can be modeled as a cantilever beam with an intermediate concentrated load as shown in Figure 4-48 if we assume that the more massive block at its left end serves as a "ground plane." The location of likely failure is the root of the round-handle portion where the shear and moment are both maximum, as shown in Figure 4-24 (p. 168) for this model that was analyzed for reactions, moments, and deflections in Examples 3-3 and 4-5. From $\Sigma F = 0$ and $\Sigma M = 0$, we find that $R_1 = 267$ N and $M_1 = 20.34$ N-m. The tensile bending stress at the root of the cantilever is maximum at the outer fiber (at point P as shown in Figure 4-47) and is found from equation 4.11b:

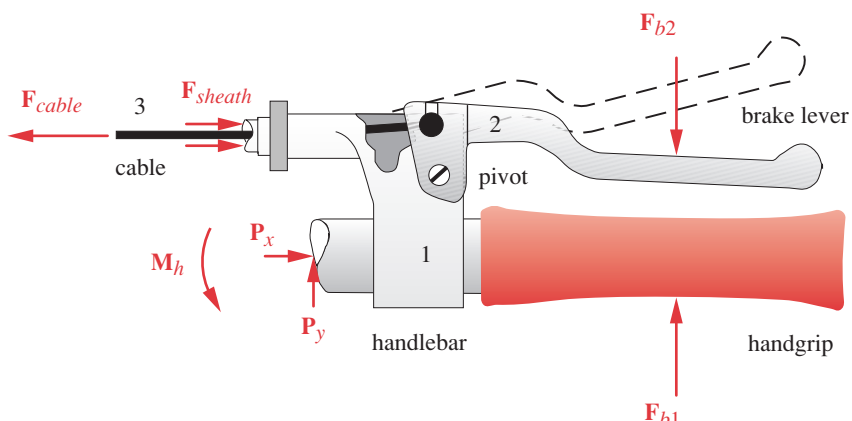


FIGURE 3-1 Repeated

Bicycle Brake Lever Assembly

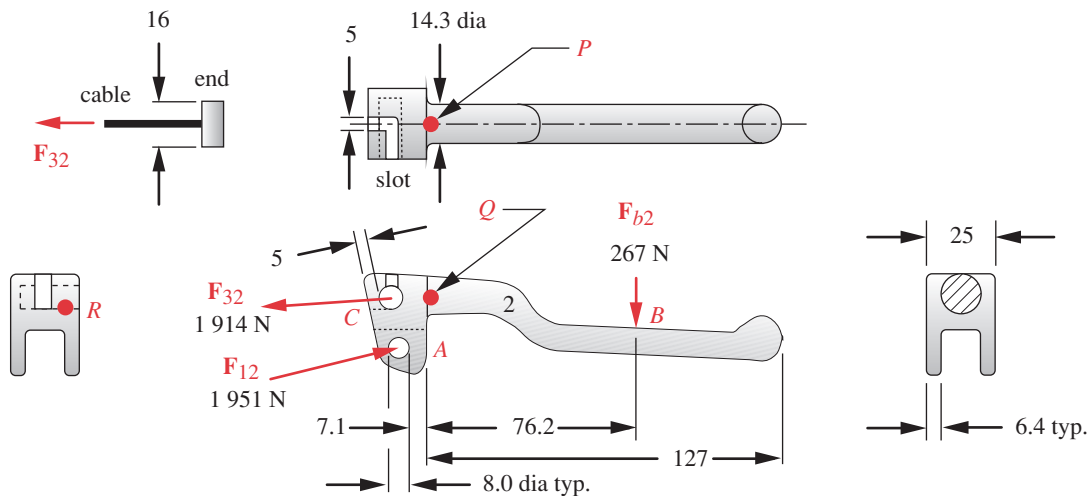


FIGURE 4-47

Bicycle Brake Lever Free-Body Diagram with Forces in N and Dimensions in mm

$$\sigma_x = \frac{Mc}{I} = \frac{(F \cdot a)c}{I} = \frac{(267 \text{ N} \cdot 0.0762 \text{ m})\left(\frac{0.0143}{2}\right) \text{ m}}{\frac{\pi(0.0143)^4}{64} \text{ m}^4} = 70.9 \text{ MPa} \quad (a)$$

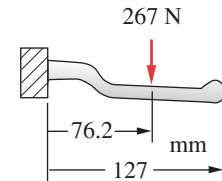
This is a relatively low stress for this material. There is some stress concentration due to the small radius at the root of the beam but since this is made of a marginally ductile cast material (5% elongation to fracture) we can ignore the stress concentrations on the basis that local yielding will relieve them.

- 2 The effective length-to-depth ratio of this beam is small at $76.2 / 14.3 = 5.3$. Since this ratio is less than 10, the shear stress due to transverse loading will be calculated. For this solid-circular section, it is found from equation 4.15c (p. 161) to be:

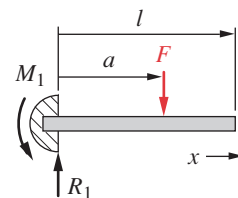
$$\tau_{xy} = \frac{4V}{3A} = \frac{4(267) \text{ N}}{\frac{3\pi(14.3)^2}{4} \text{ mm}^2} = 2.22 \text{ MPa} \quad (b)$$

The shear stress is maximum at the neutral axis (point Q) and the normal bending stress is maximum at the outer fiber (point P). The largest principal stress (equation 4.6, p. 145) at the top outer fiber is then $\sigma_1 = \sigma_x = 70.9 \text{ MPa}$, $\sigma_2 = \sigma_3 = 0$, and $\tau_{max} = 35.45 \text{ MPa}$. The Mohr circle for this stress element looks like the one in Figure 4-8 (repeated overleaf for convenience).

- 3 The deflection calculation for the handle is complicated by its curved geometry and its slight taper from root to end. A first approximation of the deflection can be obtained by simplifying the model to a straight beam of constant cross section as shown in Figure 4-48b. The deflection due to transverse shear will also be neglected. This will be in slight error in a nonconservative direction but will nevertheless give an order-of-magnitude indication of the deflection. If this result shows a problem with excessive deflection, it will be necessary to improve the model. Equation (i) from Example 4-5 provides the deflection equation for our simple model. In this case, $l = 127 \text{ mm}$, $a = 76.2 \text{ mm}$, and $x = l$ for the maximum deflection at the end of the beam.



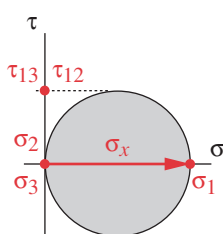
(a) The handle as a cantilever beam



(b) The cantilever-beam model

FIGURE 4-48

Cantilever-Beam Model of Handle



4

FIGURE 4-8 Repeated

Mohr's Circles for Unidirectional Tensile Stress
(Two Circles are Coincident and the Third is a Point, Since $\sigma_2 = \sigma_3 = 0$)

$$\begin{aligned} y &= \frac{F}{6EI} [x^3 - 3ax^2 - (x-a)^3] \\ &= \frac{267}{6(71.7E3)(2.04E3)} [127^3 - 3(76.2)127^2 - (127-76.2)^3] \\ &= -0.54 \text{ mm} \end{aligned} \quad (c)$$

This is about a 0.02-in deflection at the handle-end, which is not considered excessive in this application. See Figure 4-24 (p. 168) for a plot of the general shape of this beam's deflection curve, though the values are different in that example.

- 4 Other locations of likely failure must also be checked. The material around the two holes may experience any of several modes of failure due to bearing stress, direct shear stress, or tearout. The hole at point A in Figure 4-47 contains a pivot pin which bears against the handle with the 1951-N force shown. We will check this for the three modes listed above.
- 5 Bearing stress is compressive and is considered to act upon the projected area of the hole, which, in this case, is the 8-mm hole diameter times the total length of the bearing (two 6.4-mm-thick flanges).

$$\begin{aligned} A_{bearing} &= \text{dia} \cdot \text{thickness} = 8(2)(6.4) = 102.4 \text{ mm}^2 \\ \sigma_{bearing} &= \frac{F_{12}}{A_{bearing}} = \frac{1951 \text{ N}}{102.4 \text{ mm}^2} = 19.1 \text{ MPa} \end{aligned} \quad (d)$$

- 6 Tearout in this case requires that (4) 6.4-mm-thick sections fail in shear through the 5-mm length of material between hole and edge. (See also Figure 4-13, p. 155, for a definition of tearout area.)

$$\begin{aligned} A_{tearout} &= \text{length} \cdot \text{thickness} = 7.1(4)(6.4) = 181.8 \text{ mm}^2 \\ \tau_{tearout} &= \frac{F_{12}}{A_{tearout}} = \frac{1951 \text{ N}}{181.8 \text{ mm}^2} = 10.7 \text{ MPa} \end{aligned} \quad (e)$$

- 7 These are very low stresses for the specified material but remember that the applied force used is based on typical human-hand force capability and does not anticipate abuse due to impact or other means.
- 8 The cable-end inserts in a blind hole, which is half-slotted to allow the cable to pass through at assembly as shown in Figure 4-47. This slot weakens the part and makes the section at C the most likely failure location at this joint. We will assume that failure of the open (slotted) half of the material around the hole is sufficient to disable the part, since the cable-end could then slip out. The small section that retains the cable pin can be modeled to a first approximation as a cantilever beam with a cross-sectional width of $(25 - 5) / 2 = 10$ mm and a depth of 5 mm. This is a conservative assumption, as it ignores the increase in depth due to the radius of the hole. The moment arm of the force will be assumed to be equal to the radius of the pin or 4 mm. The force on the slotted half of the width is taken as half of the total force of 1914 N on the cable. The bending stress at the outer fiber at point C is then

$$\sigma_x = \frac{Mc}{I} = \frac{\frac{1914}{2} \left(\frac{5}{2}\right)(4)}{\frac{10(5)^3}{12}} = 91.9 \text{ MPa} \quad (f)$$

and the shear due to transverse loading at the neutral axis is (Eq. 4.14b, p. 161)

$$\tau_{xy} = \frac{3V}{2A} = \frac{3(957)}{2(10)(5)} = 28.7 \text{ MPa} \quad (g)$$

- 9 The normal stress is principal here, as shown in Figure 4-8 (p. 152), and the maximum shear stress is then half of the principal normal stress. These are the highest stresses found for the three sections checked. A failure analysis of this part will be done in the continuation of this case study in the next chapter.
- 10 This preliminary analysis shows some of the areas that might benefit from further investigation. A more complete stress analysis of this case study is done in Chapter 8 using Finite Element Analysis (FEA). You may examine the model for this case study by opening the file CASE1B in the program of your choice.

CASE STUDY 2B

Crimping-Tool Stress and Deflection Analysis

Problem	Determine the stresses and deflections at critical points in the crimping tool shown in Figures 3-3 (repeated here) and 4-49.
Given	The geometry and loading are known from Case Study 2A on p. 84. The thickness of link 1 is 0.313 in, of links 2 and 3 is 0.125 in and of link 4, 0.187 in. All material is 1095 steel with $E = 30 \text{ Mpsi}$.
Assumptions	The most likely failure points are link 3 as a column, the holes where the pins insert, the connecting pins in shear, and link 4 in bending. The number of cycles expected over the life of the tool is low, so a static analysis is acceptable. Stress concentration can be ignored due to the material's ductility and the static loading assumption.
Solution	See Figures 3-3, and 4-49 to 4-51.

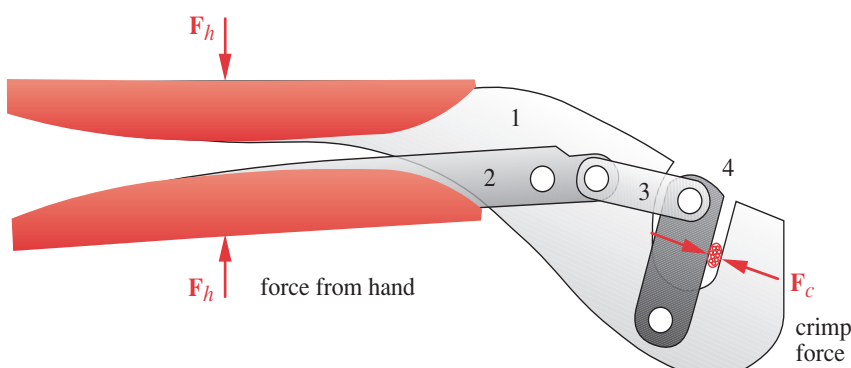
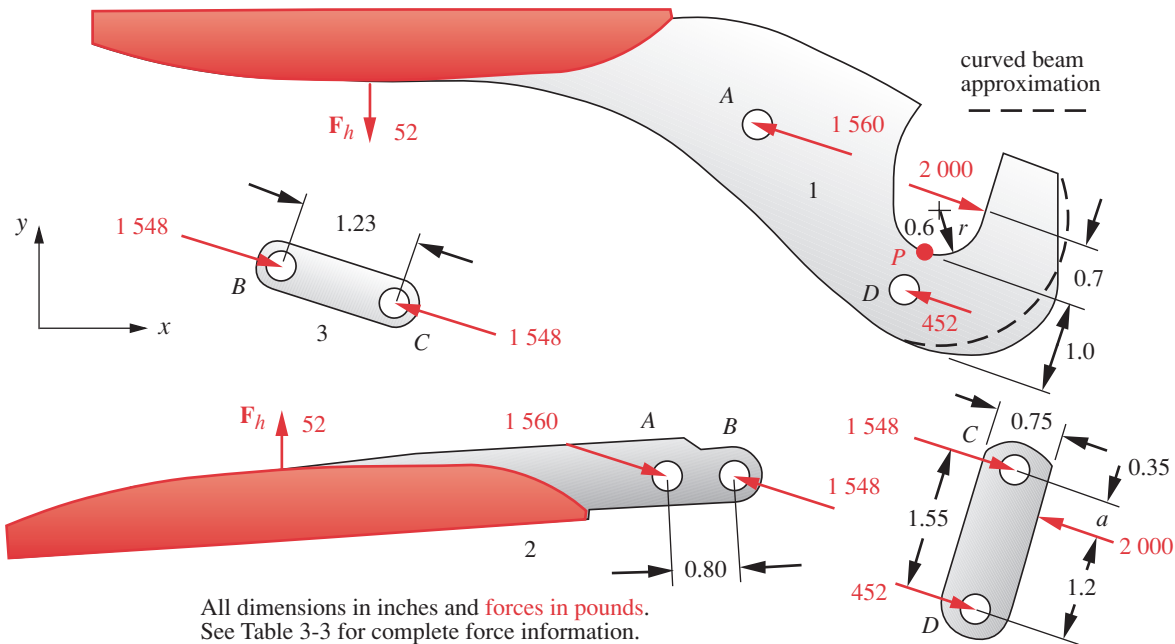


FIGURE 3-3 Repeated

Wire Connector Crimping Tool

**FIGURE 4-49**

Free-Body Diagrams, Dimensions, and Force Magnitudes for a Wire Connector Crimping Tool

- 1 Link 3 is a pinned-pinned column loaded with $F_{43} = 1\ 548$ lb as calculated in Case Study 2A (p. 84) and shown in Figure 4-49. Note that $l_{eff} = l$ from Table 4-4. We need to first check its slenderness ratio (Eq. 4.41). This requires the radius of gyration (Eq. 4.34, p. 193) for the weakest buckling direction (the z direction in this case).*

$$k = \sqrt{\frac{I}{A}} = \sqrt{\frac{bh^3/12}{bh}} = \sqrt{\frac{h^2}{12}} = \sqrt{\frac{0.125^2}{12}} = 0.036 \text{ in} \quad (a)$$

The slenderness ratio for z -direction buckling is then

$$S_r = \frac{l_{eff}}{k} = \frac{1.228}{0.036} = 34 \quad (b)$$

which is >10 , making it other than a short column. Calculate the slenderness ratio of the tangent point between the Johnson and Euler lines of Figure 4-42 (p. 197).

$$(S_r)_D = \pi \sqrt{\frac{2E}{S_y}} = \pi \sqrt{\frac{2(30E6)}{83E3}} = 84.5 \quad (c)$$

The slenderness ratio of this column is less than that of the tangent point between the Johnson and Euler lines shown in Figure 4-42. It is thus an intermediate-column and the Johnson-column formula (Eq. 4.43, p. 198) should be used to find the critical load.

* Even a small amount of clearance in the holes will prevent the pins from acting as a moment joint along their axes, thus creating an effective pinned-pinned connection in two dimensions.

$$\begin{aligned}
 P_{cr} &= A \left[S_y - \frac{1}{E} \left(\frac{S_y S_r}{2\pi} \right)^2 \right] \\
 &= 0.125(.5) \left[83\,000 - \frac{1}{30E6} \left(\frac{83\,000(34)}{2\pi} \right)^2 \right] = 4\,765 \text{ lb}
 \end{aligned} \tag{d}$$

The critical load is 3.1 times larger than the applied load. It is safe against buckling. Link 2 is a shorter, wider column than link 3 and has lower axial forces so can be assumed to be safe against buckling based on the link 3 calculations.

- 2 Since it does not buckle, the deflection of link 3 in axial compression is (Eq. 4.7, p. 152):

$$x = \frac{Pl}{AE} = \frac{1\,548(1.23)}{0.0625(30E6)} = 0.001 \text{ in} \tag{e}$$

- 3 Any of the links could also fail in bearing in the 0.25-in-dia holes. The largest force on any pin is 1 560 lb. This worst-case bearing stress (Eqs. 4.7 and 4.10, p. 154) is then

$$\sigma_b = \frac{P}{A_{bearing}} = \frac{P}{length(dia)} = \frac{1\,560}{0.125(0.25)} = 49\,920 \text{ psi} \tag{f}$$

There is no danger of tearout failure in links 2 or 3, since the loading is toward the center of the part. Link 1 has ample material around the holes to prevent tearout.

- 4 The 0.25-in-dia pins are in single shear. The worst-case direct shear stress from equation 4.9 (p. 153) is:

$$\tau = \frac{P}{A_{shear}} = \frac{1\,560}{\frac{\pi(0.25)^2}{4}} = 31\,780 \text{ psi} \tag{g}$$

- 5 Link 4 is a 1.55-in-long beam, simply supported at the pins and loaded with the 2 000-lb crimp force at 0.35 in from point C. Write the equations for the load, shear, moment, slope, and deflection using singularity functions, noting that the integration constants C_1 and C_2 will be zero:

$$\begin{aligned}
 q &= R_1 \langle x - 0 \rangle^{-1} - F \langle x - a \rangle^{-1} + R_2 \langle x - l \rangle^{-1} \\
 V &= R_1 \langle x - 0 \rangle^0 - F \langle x - a \rangle^0 + R_2 \langle x - l \rangle^0 \\
 M &= R_1 \langle x - 0 \rangle^1 - F \langle x - a \rangle^1 + R_2 \langle x - l \rangle^1
 \end{aligned} \tag{h}$$

$$\begin{aligned}
 \theta &= \frac{1}{EI} \left(\frac{R_1}{2} \langle x - 0 \rangle^2 - \frac{F}{2} \langle x - a \rangle^2 + \frac{R_2}{2} \langle x - l \rangle^2 + C_3 \right) \\
 y &= \frac{1}{EI} \left(\frac{R_1}{6} \langle x - 0 \rangle^3 - \frac{F}{6} \langle x - a \rangle^3 + \frac{R_2}{6} \langle x - l \rangle^3 + C_3x + C_4 \right)
 \end{aligned} \tag{i}$$

- 6 The reaction forces can be found from $\Sigma M = 0$ and $\Sigma F = 0$. (See Appendix B.)

$$R_1 = \frac{F(l-a)}{l} = \frac{2\,000(1.55-0.35)}{1.55} = 1\,548 \text{ lb} \tag{j}$$

$$R_2 = \frac{Fa}{l} = \frac{2\,000(0.35)}{1.55} = 452 \text{ lb} \tag{k}$$

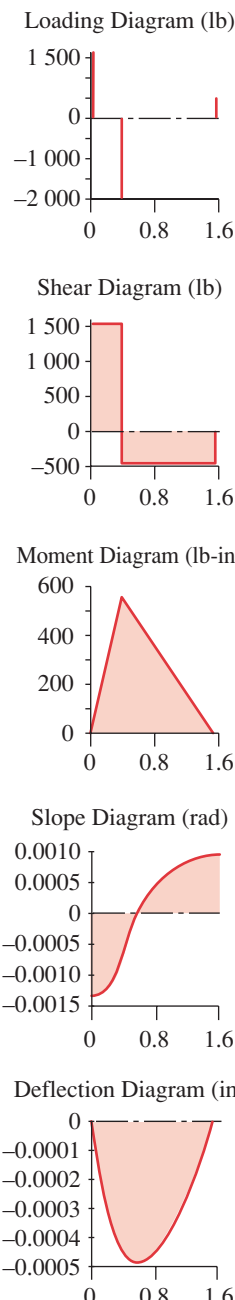


FIGURE 4-50

Link 4 Plots - Case 2B

The maximum moment is $1548(0.35) = 541.8$ lb-in at the applied load. The shear and moment diagrams for link 4 are shown in Figure 4-50.

- 7 The beam depth at the point of maximum moment is 0.75 in and the thickness is 0.187. The bending stress is then

$$\sigma = \frac{Mc}{I} = \frac{\frac{541.8}{12} \left(\frac{0.75}{2}\right)}{0.187(0.75)^3} = 30905 \text{ psi} \quad (l)$$

- 8 The beam slope and deflection functions require calculation of the integration constants C_3 and C_4 , which are found by substituting the boundary conditions $x = 0, y = 0$ and $x = l, y = 0$ in the deflection equation.

$$0 = \frac{1}{EI} \left(\frac{R_1}{6} (0-0)^3 - \frac{F}{6} (0-a)^3 + \frac{R_2}{6} (0-l)^3 + C_3(0) + C_4 \right) \quad (m)$$

$$0 = \frac{1}{EI} \left(\frac{R_1}{6} (l-0)^3 - \frac{F}{6} (l-a)^3 + \frac{R_2}{6} (l-l)^3 + C_3(l) \right) \quad (n)$$

$$C_3 = \frac{1}{6l} [F(l-a)^3 - R_1 l^3] = \frac{1}{6(1.55)} [2000(1.55-0.35)^3 - 1548(1.55)^3] = -248.4$$

- 9 The deflection equation is found by combining equations *i*, *j*, *k*, *m*, and *n*:

$$y = \frac{F}{6lEI} \left\{ (l-a) \left[x^3 + [(l-a)^2 - l^2]x \right] - l(x-a)^3 + a(x-l)^3 \right\} \quad (o)$$

and the maximum deflection at $x = 0.68$ in is

$$y_{max} = \frac{Fa(l-a)}{6lEI} (a^2 + (l-a)^2 - l^2) \\ = \frac{2000(0.35)(1.55-0.35)}{6(1.55)(30E6)(0.0066)} [0.35^2 + (1.55-0.35)^2 - 1.55^2] = 0.0005 \text{ in}$$

Only a very small deflection is allowed here to guarantee the proper crimp stroke, and this amount is acceptable. The slope and deflection diagrams are shown in Figure 4-50. Also see the file CASE2B-1.

- 10 Link 1 is relatively massive compared to the others and the only area of concern is the jaw, which is loaded by the 2000-lb crimp force and has a hole in the cross section at its root. While the shape of this element is not exactly that of a curved beam with concentric inside and outside radii, this assumption will be acceptably conservative if we use an outer radius equal to the smallest section dimension as shown in Figure 4-49 (p. 210). This makes its inside radius 0.6 in and its approximate outside radius 1.6 in. The eccentricity e of the curved beam's neutral axis versus the beam's centroidal axis r_c is found from equation 4.12a (p. 157), while accounting for the section's hole in the integration.

$$e = r_c - \frac{A}{\int_0^{r_o} \frac{dA}{r}} = 1.1 - \frac{0.313(1-0.25)}{0.313 \left(\int_{0.600}^{0.975} \frac{dr}{r} + \int_{1.225}^{1.600} \frac{dr}{r} \right)} = 0.103 \quad (q)$$

The radius to the neutral axis (r_n) and the distances (c_i and c_o) from the inner and outer fiber radii (r_i and r_o) to the neutral axis are then (see Figure 4-16, p. 157)

$$\begin{aligned} r_n &= r_c - e = 1.10 - 0.103 = 0.997 \\ c_i &= r_n - r_i = 0.997 - 0.600 = 0.397 \\ c_o &= r_o - r_n = 1.600 - 0.997 = 0.603 \end{aligned} \quad (r)$$

- 11 The applied bending moment on the curved beam section is taken as the applied load times its distance to the beam's centroidal axis.

$$M = Fl = 2\,000(0.7 - 0.6 + 1.1) = 2\,400 \text{ lb-in} \quad (s)$$

- 12 Find stresses at the inner and outer fibers from equations 4.12b and 4.12c (p. 158). Reduce the beam cross sectional area by the hole area.

$$\begin{aligned} \sigma_i &= +\frac{M}{eA} \left(\frac{c_i}{r_i} \right) = \frac{2\,400}{0.103[(1.0 - 0.25)(0.313)]} \left(\frac{0.397}{0.60} \right) = 65 \text{ kpsi} \\ \sigma_o &= -\frac{M}{eA} \left(\frac{c_o}{r_o} \right) = -\frac{2\,400}{0.103[(1.0 - 0.25)(0.313)]} \left(\frac{0.603}{1.60} \right) = -37 \text{ kpsi} \end{aligned} \quad (t)$$

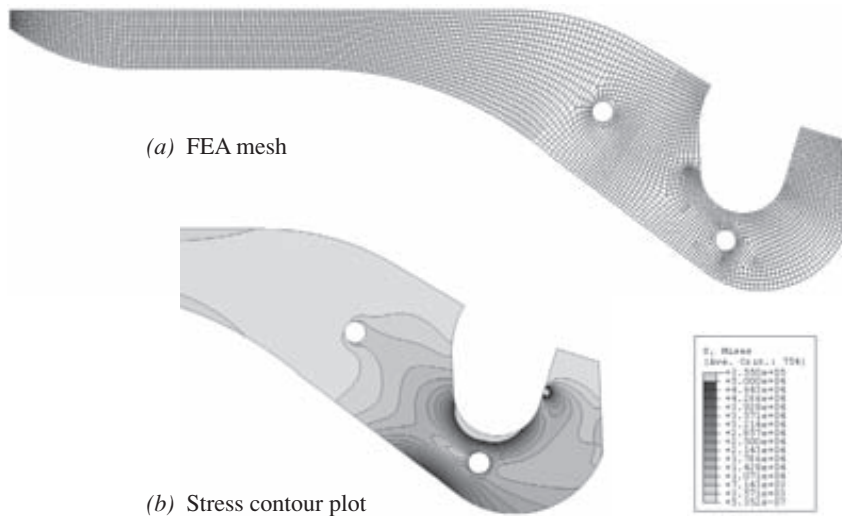
- 13 There is also a direct axial tensile stress, which adds to the bending stress in the inner fiber at point P :

$$\begin{aligned} \sigma_a &= \frac{F}{A} = \frac{2\,000}{(1.0 - 0.25)(0.313)} = 8.5 \text{ kpsi} \\ \sigma_{max} &= \sigma_a + \sigma_i = 65 + 8.5 = 74 \text{ kpsi} \end{aligned} \quad (u)$$

This is the principal stress for point P , since there is no applied shear or other normal stress at this edge point. The maximum shear stress at point P is half this principal stress or 37 kpsi. The bending stress at the outer fiber is compressive and thus subtracts from the axial tensile stress for a net of $-37 + 8.5 = -28.5$ kpsi.

- 14 There is significant stress concentration at the hole. The theoretical stress-concentration factor for the case of a circular hole in an infinite plate is $K_t = 3$ as defined in equation 4.32a (p. 189) and Figure 4-35 (p. 188). For a circular hole in a finite plate, K_t is a function of the ratio of the hole diameter to the plate width. Peterson gives a chart of stress-concentration factors for a round hole in a flat plate under tension^[5] from which we find that $K_t = 2.42$ for a dia / width ratio = 1/4. The local axial tensile stress at the hole is then $2.42(8.5) = 20.5$ kpsi, which is less than the tensile stress at the inner fiber.
- 15 While this is far from a complete stress and deflection analysis of these parts, the calculations done address the areas judged to be most likely to fail or to have problem deflections. The stresses and deflections in link 1 were also computed using the ABAQUS finite element analysis program, which gave an estimated maximum principal stress at point P of 81 kpsi compared to our estimate of 74 kpsi. The FEA mesh and stress distribution calculated by the FEA model is shown in Figure 4-51. Case Study 2D in Chapter 8 (p. 511) presents the complete FEA analysis of this assembly.

Our analysis simplified the part geometry in order to allow the use of a known closed-form model (the curved beam) whereas the FEA model included all the material in the actual part but discretized its geometry. Both analyses should be recognized as only estimates of the stress states in the parts, not exact solutions.

**FIGURE 4-51**

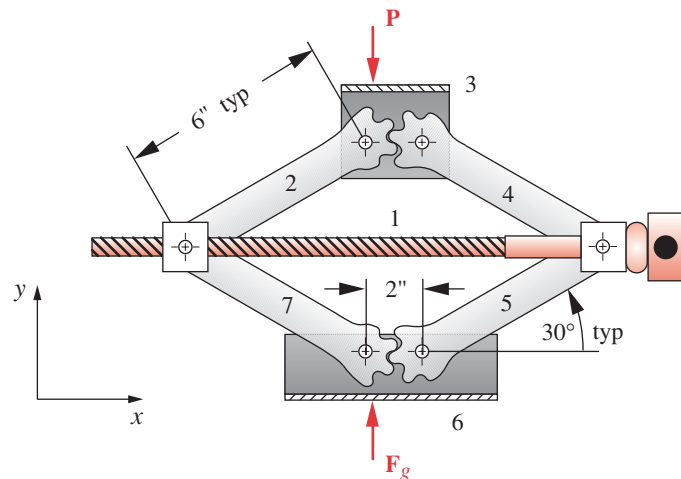
Finite Element Analysis of the Stresses in the Crimping Tool of Case Study 2B

- 16 Redesign may be needed to reduce these stresses and deflections, based on a failure analysis. This case study will be revisited in the next chapter after various failure theories are presented. You may examine the models for this case study by opening the files CASE2B-1, CASE2B-2, and CASE2B-3 in the program of your choice. A stress analysis of this case study is done in Chapter 8 using Finite Element Analysis (FEA).

CASE STUDY 3B

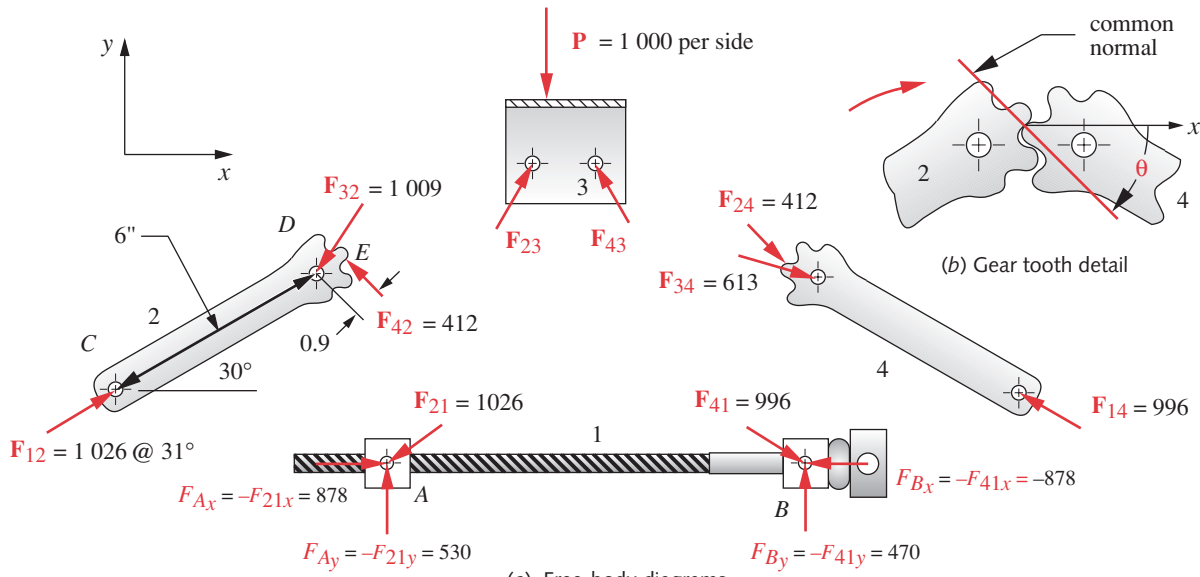
Automobile Scissors-Jack Stress and Deflection Analysis

Problem	Determine the stresses and deflections at critical points in the scissors-jack assembly shown in Figures 3-5 (repeated here) and 4-52.
Given	The geometry and loading are known from Case Study 3A (p. 88). The design load is 2 000 lb total or 1 000 lb per side. The width of the links is 1.032 in and their thickness is 0.15 in. The screw is a 1/2-13 UNC thread with root dia = 0.406 in. The material of all parts is ductile steel with $E = 30E6$ psi and $S_y = 60\ 000$ psi.
Assumptions	The most likely failure points are the links as columns, the holes in bearing where the pins insert, the connecting pins in shear, the gear teeth in bending, and the screw in tension. There are two sets of links, one set on each side. Assume the two sides share the load equally. The jack is typically used for very few cycles over its lifetime, so a static analysis is appropriate.
Solution	See Figures 4-52 to 4-53 and the files CASE3B-1 and CASE3B-2.

**FIGURE 3-5** Repeated

An Automobile Scissors Jack

- 1 The forces on this jack assembly for the position shown were calculated in the previous installment of this case study (3A) in Chapter 3 (p. 88). Please see that section and Table 3-4 (pp. 90–92) for additional force data.
- 2 The force in the jack screw is four times the 878-lb component F_{21x} at point A because that force is from the upper half of the jack in one plane only. The lower half exerts an equal force on the screw, and the back side doubles their sum. These forces put the screw in axial tension. The tensile stress is found from equation 4.7 (p. 152) using the 0.406-in root diameter of the thread to calculate the cross-sectional area. This is a conservative assumption, as we shall see when analyzing threaded fasteners in Chapter 15.

**FIGURE 4-52**

Free-Body Diagrams, Dimensions, and Forces for Elements of the Scissors Jack

$$\sigma_x = \frac{P}{A} = \frac{\frac{4(878)}{\pi(0.406)^2}}{4} = \frac{3512}{0.129} = 27128 \text{ psi} \quad (a)$$

The axial deflection of the screw is found from equation 4.8 (p. 152).

$$x = \frac{Pl}{AE} = \frac{4(878)(12.55)}{0.129(30E6)} = 0.011 \text{ in} \quad (b)$$

4

- 3 Link 2 is the most heavily loaded of the links due to the applied load P being slightly offset to the left of center, so we will calculate its stresses and deflections. This link is loaded as a beam-column with both an axial compressive force P between points C and D and a bending couple applied between D and E . Note that the force F_{12} is virtually colinear with the link axis. The axial load is equal to $F_{12} \cos(1^\circ) = 1026 \text{ lb}$ and the bending couple created by F_{42} acting about point D is $M = 412(0.9) = 371 \text{ in-lb}$. This couple is equivalent to the axial load being eccentric at point D by distance $e = M/P = 371 / 1026 = 0.36 \text{ in}$.

The secant-column formula (Eq. 4.46c, p. 202) can be used with this effective eccentricity e accounting for the applied couple in the plane of bending; c is 1/2 of the 1.032-in width of the link. Since it is a pinned-pinned column, $l_{eff} = l$ from Table 4-4. The radius of gyration k is taken in the xy plane of bending for this calculation (Eq. 4.34, p. 193):

$$k = \sqrt{\frac{I}{A}} = \sqrt{\frac{bh^3}{12bh}} = \sqrt{\frac{0.15(1.032)^3}{12(0.15)(1.032)}} = 0.298 \quad (c)$$

The slenderness ratio is $l_{eff}/k = 20.13$. The secant formula can now be applied and iterated for the value of P . (See Figure 4-53.)

$$\frac{P}{A} = \frac{S_{yc}}{1 + \left(\frac{ec}{k^2}\right) \sec\left(\frac{l_{eff}}{k} \sqrt{\frac{P}{4EA}}\right)} = 18975 \text{ psi} \quad (d)$$

$$P_{crit} = 0.155(18975) = 2937 \text{ lb}$$

The column also has to be checked for concentric-column buckling in the weaker (z) direction with $c = 0.15 / 2$. The radius of gyration in the z direction is found from

$$k = \sqrt{\frac{I}{A}} = \sqrt{\frac{bh^3}{12bh}} = \sqrt{\frac{1.032(0.15)^3}{12(1.032)(0.15)}} = 0.043 \quad (e)$$

The slenderness ratio in the z direction is

$$S_r = \frac{l_{eff}}{k} = \frac{6}{0.043} = 138.6 \quad (f)$$

This needs to be compared to the slenderness ratio (S_r)_D at the tangency between the Euler and Johnson lines to determine which buckling equation to use for this column:

$$(S_r)_D = \pi \sqrt{\frac{2E}{S_y}} = \pi \sqrt{\frac{2(30E6)}{60000}} = 99.3 \quad (g)$$

The S_r for this column is greater than $(S_r)_D$, making it an Euler column (see Figure 4-53). The critical Euler load is then found from equation 4.38a (p. 194).

$$P_{cr} = \frac{\pi^2 EI}{l^2} = \frac{\pi^2 (30E6)(1.032)(0.15)^3}{12(6)^2} = 2387 \text{ lb} \quad (h)$$

Thus it is more likely to buckle in the weaker z direction than in the plane of the applied moment. Its safety factor against buckling is 2.3.

- 4 The pins are all 0.437-in dia. The bearing stress in the most heavily loaded hole at C is

$$\sigma_{bearing} = \frac{P}{A_{bearing}} = \frac{1026}{0.15(0.437)} = 15652 \text{ psi} \quad (i)$$

The pins are in single shear and their worst shear stress is

$$\tau = \frac{P}{A_{shear}} = \frac{1026}{\frac{\pi(0.437)^2}{4}} = 6841 \text{ psi} \quad (j)$$

- 5 The gear tooth on link 2 is subjected to a force of 412 lb applied at a point 0.22 in from the root of the cantilevered tooth. The tooth is 0.44 in deep at the root and 0.15 in thick. The bending moment is $412(0.22) = 91$ in-lb and the bending stress at the root is

$$\sigma = \frac{Mc}{I} = \frac{91(0.22)}{\frac{0.15(0.44)^3}{12}} = 18727 \text{ psi} \quad (k)$$

- 6 This analysis could be continued, looking at other points in the assembly and, more importantly, at stresses when the jack is in different positions. We have used an arbitrary position for this case study but, as the jack moves to the lowered position, the link and pin forces will increase due to poorer transmission angles. A complete stress analysis should be done for multiple positions.

This case study will be revisited in the next chapter for the purpose of failure analysis. You may examine the models for this case study by opening the files CASE3B-1 and CASE3B-2 in the program of your choice.

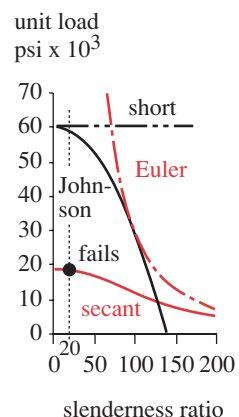


FIGURE 4-53

Solution to Eccentric Column in Case Study 3B

CASE STUDY 4B

Bicycle Brake Arm Stress Analysis

Problem Determine the stresses at critical points in the bicycle brake arm shown in Figures 3-9 (repeated here) and 4-54.

Given The geometry and loading are known from Case Study 4A (p. 94) and are shown in Table 3-5 (p. 97). The cast-aluminum arm is a tee-section curved beam whose dimensions are shown in Figure 4-54. The pivot pin is ductile steel. The loading is three-dimensional.

Assumptions The most likely failure points are the arm as a double-cantilever beam (one end of which is curved), the hole in bearing, and the connect-

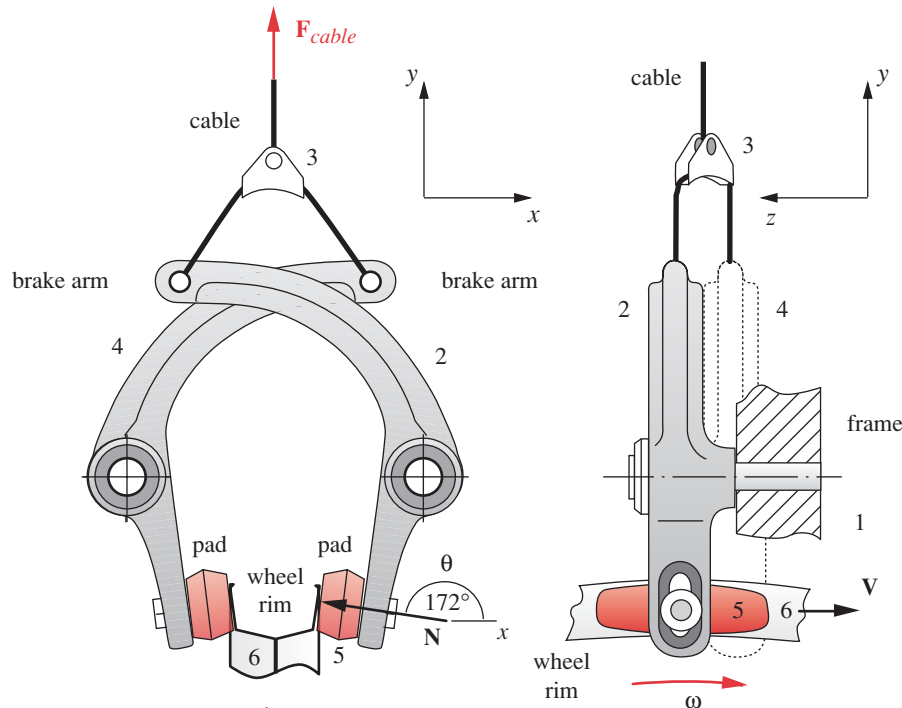


FIGURE 3-9 Repeated

Center-Pull Bicycle Brake Arm Assembly

ing pin in bending as a cantilever beam. Since this is a marginally ductile cast material (5% elongation to fracture), we can ignore the stress concentration on the basis that local yielding will relieve it.

Solution

See Figures 4-54 to 4-56.

- 1 The brake arm is a double-cantilever beam. Each end can be treated separately. The curved-beam portion has a tee-shaped cross section as shown in Section X-X of Figure 4-54. The neutral axis of a curved beam shifts from the centroidal axis toward the center of curvature a distance e as described in Section 4-9 and in equation 4.12a (p. 157). To find e requires an integration of the beam cross section and knowledge of its centroidal radius. Figure 4-55 shows the tee-section broken into two rectangular segments, flange and web. The radius of the centroid of the tee is found by summing moments of area for each segment about the center of curvature:

$$\sum M = A_1 r_{c_1} + A_2 r_{c_2} = A_t r_{c_t}$$

$$r_{c_t} = \frac{A_1 r_{c_1} + A_2 r_{c_2}}{A_t} = \frac{A_1(r_i + y_1) + A_2(r_i + y_2)}{A_1 + A_2} \quad (a)$$

$$r_{c_t} = \frac{(20)(7.5)(58 + 3.75) + (10)(7.5)(58 + 11.25)}{(20)(7.5) + (10)(7.5)} = 64.25 \text{ mm}$$

See Figures 4-53 and 4-54 for dimensions and variable names. The integral dA/r for equation 4.12a can be found in this case by adding the integrals for web and flange.

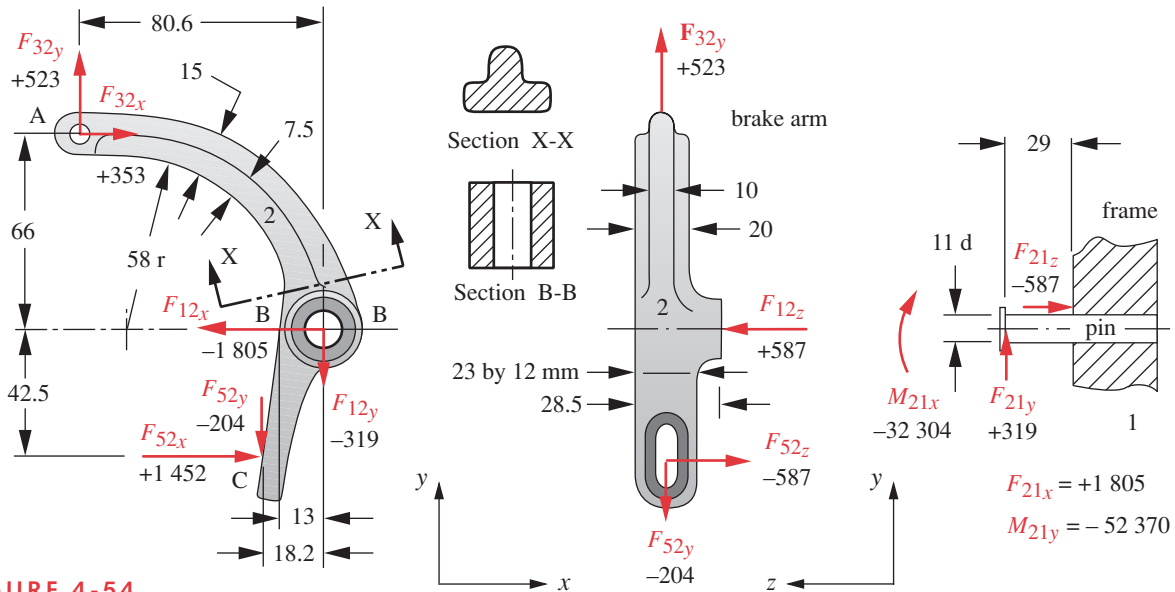


FIGURE 4-54

Brake-Arm Free-Body Diagrams, Forces in N, Moments in N-mm, and Dimensions in mm

$$\int_0^{r_o} \frac{dA}{r} = \frac{A_1}{r_{c_1}} + \frac{A_2}{r_{c_2}} = \frac{(20)(7.5)}{58 + 3.75} + \frac{(10)(7.5)}{58 + 11.25} = 3.51 \text{ mm} \quad (b)$$

The radius of the neutral axis and the distance e are then

$$r_n = \frac{A_t}{\int_0^{r_o} \frac{dA}{r}} = \frac{225}{3.51} = 64.06 \text{ mm} \quad (c)$$

$$e = r_c - r_n = 64.25 - 64.06 = 0.187 \text{ mm}$$

The magnitude of the bending moment acting on the curved section of the beam at Section X-X can be approximated by taking the cross product of the force F_{32} and its position vector R_{AB} referenced to the pivot at B in Figure 4-54.

$$|M_{AB}| = \left| R_{AB_x} F_{32_y} - R_{AB_y} F_{32_x} \right| = \left| -80.6(523) - 66(353) \right| = 65\,452 \text{ N-mm} \quad (d)$$

The stresses at the inner and outer fibers can now be found using equations 4.12b and 4.12c (p. 158) (with lengths in mm and moments in N-mm for proper unit balance):

$$\sigma_i = +\frac{M}{eA} \left(\frac{c_i}{r_i} \right) = \frac{65\,452(6.063)}{(0.1873)(225)(58)} = 162 \text{ MPa} \quad (e)$$

$$\sigma_o = -\frac{M}{eA} \left(\frac{c_o}{r_o} \right) = \frac{65\,452(8.937)}{(0.1873)(225)(73)} = -190 \text{ MPa}$$

- 2 The hub cross section, shown as Section B-B in Figure 4-54, is a possible location of failure, since there is a combination of bending and axial tension stresses here and the pin hole removes substantial material. The bending stress is due to the maximum moment acting on the curved beam at its root and the tensile stress is due to the y com-

ponent of the force at A. There is also a shear stress due to transverse loading, but this will be zero at the outer fiber where the sum of the bending and axial stresses is maximum. The area and area moment of inertia of the hub cross section are needed:

$$A_{hub} = \text{length}(d_{out} - d_{in}) = 28.5(25 - 11) = 399 \text{ mm}^2 \quad (f)$$

$$I_{hub} = \frac{\text{length}(d_{out}^3 - d_{in}^3)}{12} = \frac{28.5(25^3 - 11^3)}{12} = 33\,948 \text{ mm}^4$$

The stress on the left half of Section B-B is the sum of the bending and axial stresses:

$$\sigma_{hub} = \frac{Mc}{I_{hub}} + \frac{F_{32y}}{A_{hub}} = \frac{65\,452(12.5)}{33\,948} + \frac{523}{399} = 25.4 \text{ MPa} \quad (g)$$

The stress on the right half of Section B-B is lower, because the compression due to bending is reduced by the axial tension.

- 3 The straight portion of the brake arm is a cantilever beam loaded in two directions, in the xy plane and in the yz plane. The section moduli and moments are different in these bending directions. The z moment in the xy plane is equal and opposite to the moment on the curved section. The cross section at the root of the cantilever is a rectangle of 23 by 12 mm as shown in Figure 4-54. The bending stress at the outer fiber of the 23-mm side due to this moment is

$$\sigma_{y_1} = \frac{Mc}{I} = \frac{65\,452\left(\frac{12}{2}\right)}{\underline{23(12)^3}} = 118.6 \text{ MPa} \quad (h)$$

The x moment is due to force F_{52z} acting at the 42.5 radius, bending the link in the z direction. The bending stress at the surface of the 12-mm side is

$$\sigma_{y_2} = \frac{Mc}{I} = \frac{589 \cdot 42.5\left(\frac{23}{2}\right)}{\underline{12(23)^3}} = 23.7 \text{ MPa} \quad (i)$$

These two y -direction normal stresses add at the corners of the two faces to give

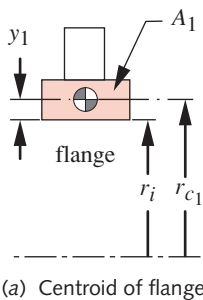
$$\sigma_y = \sigma_{y_1} + \sigma_{y_2} = 118.6 + 23.7 = 142.2 \text{ MPa} \quad (j)$$

- 4 Another possible failure point is the slot in the cantilever arm. Though the moment is zero there, the shear force is present and can cause tearout in the z direction. The tearout area is the shear area between the slot and edge.

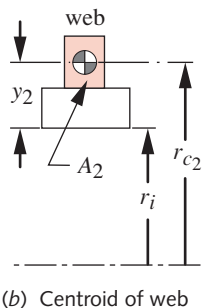
$$A_{tearout} = \text{thickness}(\text{width}) = 8(4) = 32 \text{ mm}^2 \quad (k)$$

$$\tau = \frac{F_{52z}}{A_{tearout}} = \frac{589}{32} = 18.4 \text{ MPa}$$

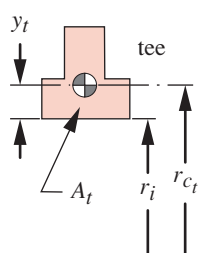
- 5 The pivot pin is subjected to force F_{21} , which has both x and y components and to a couple M_{21} due to the forces F_{12z} and F_{52z} . The force F_{21} creates a bending moment having components $F_{21x}l$ and $F_{21y}l$ in the yz and xz planes, respectively, where $l = 29$ mm is the length of the pin.



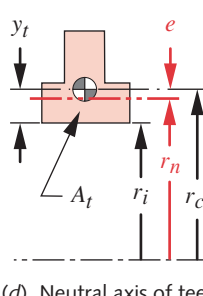
(a) Centroid of flange



(b) Centroid of web



(c) Centroid of tee



(d) Neutral axis of tee

FIGURE 4-55

Finding Neutral Axis of a Tee-Section Curved Beam - Case Study 4B

$$\begin{aligned}
 M_{pin} &= \sqrt{(M_{21_x} - F_{12_y} \cdot l)^2 + (-M_{21_y} + F_{12_x} \cdot l)^2} \\
 &= \sqrt{(-32\ 304 + 319 \cdot 29)^2 + (52\ 370 - 1805 \cdot 29)^2} \\
 &= \sqrt{(-32\ 304 + 9\ 251)^2 + (52\ 370 - 52\ 345)^2} \\
 &= \sqrt{(-23\ 053)^2 + (25)^2} = 23\ 053 \text{ N-mm} \quad (l) \\
 \theta_{M_{pin}} &= \tan^{-1}\left(\frac{25}{-23\ 053}\right) \approx 0^\circ \quad (m)
 \end{aligned}$$

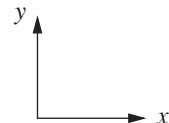


Figure 4-56a shows the moment of the couple M_{21} and Figure 4-56b shows the moment of the force F_{21} . Their combination is shown in Figure 4-56c.

It is this combined moment that creates the largest bending stresses in the pin at 0° and 180° around its circumference. The maximum bending stress in the pin (with lengths in mm and moments in N-mm for unit balance) is

$$\sigma_{pin} = \frac{M_{pin} c_{pin}}{I_{pin}} = \frac{23\ 053 \left(\frac{11}{2}\right)}{\frac{\pi(11)^4}{64}} = \frac{23\ 053(5.5)}{718.7} = 176 \text{ MPa} \quad (n)$$

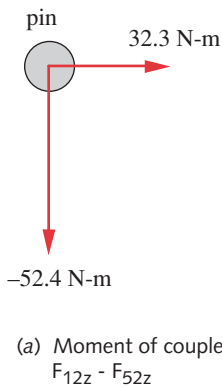
- 6 A more complete analysis could be done using finite element methods to determine the stresses and deformations at many other locations on the part. You may examine the model for this case study by opening the file CASE4B in the program of your choice. A stress analysis of this case study is also done in Chapter 8 using Finite Element Analysis (FEA).

4.19 SUMMARY

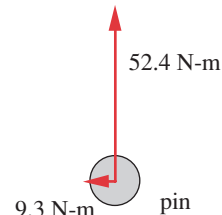
The equations used for stress analysis are relatively few and are fairly easy to remember. (See the equation summary later in this section.) The major source of confusion among students seems to be in understanding when to use which stress equation and how to determine where in the part's continuum to calculate the stresses, since they vary over the part's internal geometry.

There are two types of applied stresses of interest, **normal stress** σ and **shear stress** τ . Each may be present on the same stress element and they will combine to create a set of principal normal stresses and maximum shear stress, as evidenced on the Mohr's circle plane. It is ultimately these principal stresses that we need to find in order to determine the safety of the design. So, regardless of the source of loading or type of stress that may be applied to the part, you should always determine the principal stresses and maximum shear stress that result from their combination. (See Sections 4.3 and 4.5.)

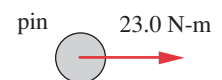
There are only a few types of loading that commonly occur on machine parts, but they may occur in combination on the same part. Loading types that create **applied normal stresses** are **bending loads**, **axial loads**, and **bearing loads**. Bending loads will



(a) Moment of couple $F_{12z} - F_{52z}$



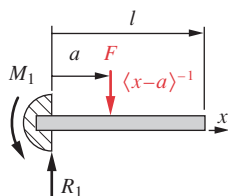
(b) Moment of force F_{21}



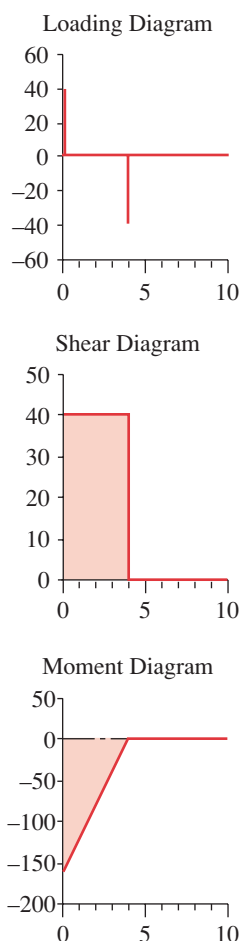
(c) Combined moments

FIGURE 4-56

Bending Moments on Pivot Pin - Case Study 4B

**FIGURE 4-57**

Cantilever Beam with Concentrated Load

**FIGURE 4-58**

Load Distributions

always create both tensile and compressive normal stresses at different locations within the part. Beams provide the most common example of bending loads. (See Section 4.9.) Axial loads create normal stresses that can be either tensile or compressive (but not both at once), depending on whether the axial load is in a tensile or compressive direction. (See Section 4.7.) Fasteners such as bolts often have significant axial-tension loads. If the axial load is compressive, then there may be a danger of **column buckling**, and the equations of Section 4.16 must also be applied. Bearing loads create compressive normal stresses in the shaft and bushing (bearing).

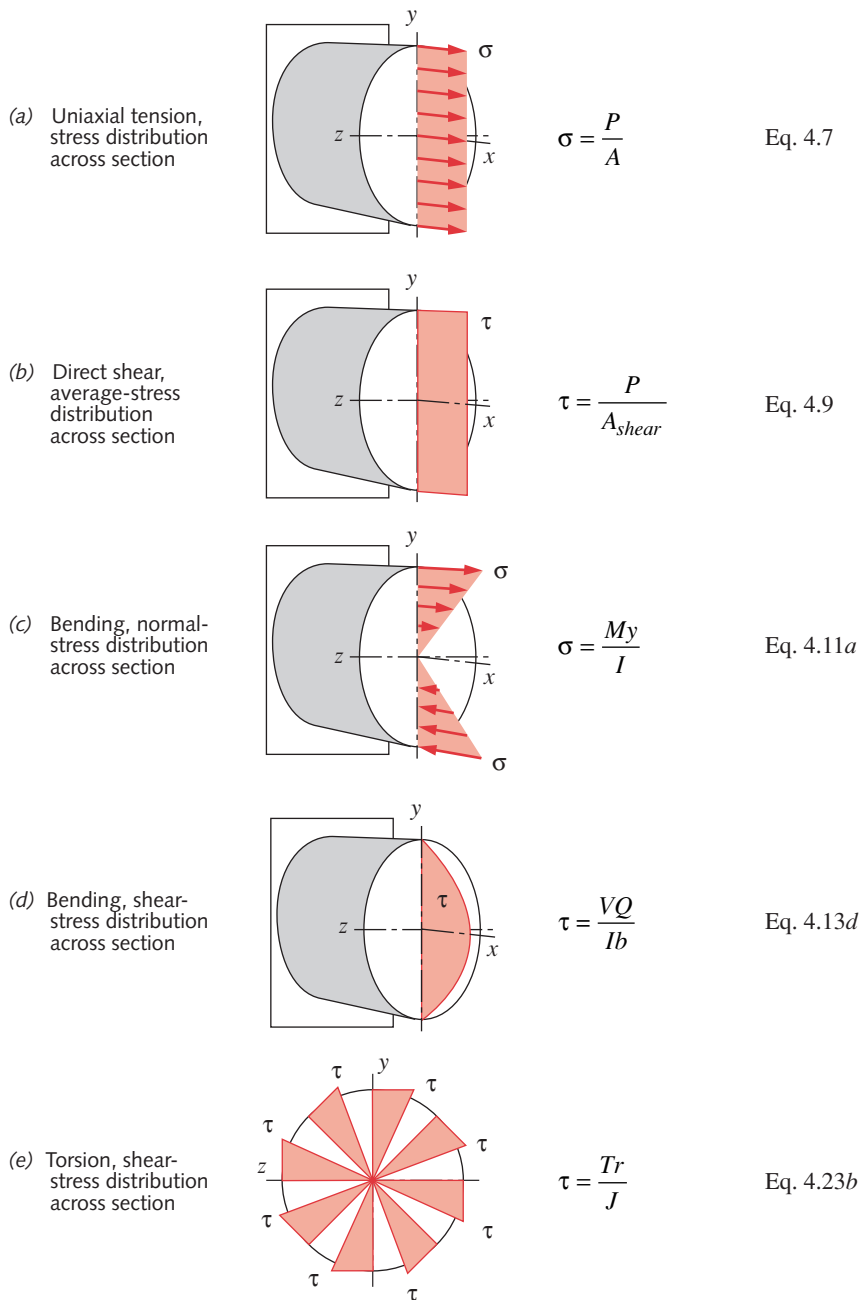
Loading types that create **applied shear stresses** are **torsional loads**, **direct shear loads**, and **bending loads**. Torsional loads involve the twisting of a part around its long axis by application of a torque. A transmission shaft is a typical example of a torsionally loaded part. (Chapter 10 deals with the design of transmission shafts.)

Direct shear can be caused by loads that tend to slice the part transversely. Fasteners such as rivets or pins sometimes experience direct shear loads. A pin trying to tear its way out of its hole also causes direct shear on the tearout area. (See Section 4.8.) Bending loads also cause transverse shear stresses on the cross section of the beam. (See Section 4.9.)

Stresses can vary continuously over the internal continuum of a part's geometry and are calculated as acting at an infinitesimally small point within that continuum. To do a complete analysis of the stresses at all the infinite number of potential sites within the part would require infinite time, which we obviously do not have. So, we must intelligently select a few sites for our calculations such that they represent the worst-case situations.

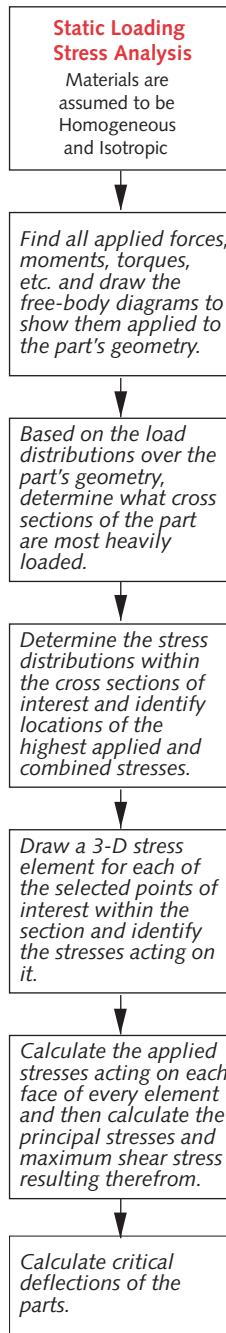
The student needs to understand how the various stresses are distributed within the continuum of a loaded part. There are two aspects to determining appropriate locations on a given part at which to make the stress calculations. The first aspect concerns the load distribution over the part's geometry and the second concerns the stress distribution within the part's cross section. For example, consider a straight cantilever beam loaded with a single force at some point along its length as shown in Figure 4-57. The first aspect requires some knowledge of the way the loads on the beam are distributed in response to the applied force. This comes from an analysis of the beam's shear and moment diagrams as shown in Figure 4-58, which indicate that in this case, the section with greatest load is at the wall. We would then concentrate our attention on a vanishingly thin "bologna slice" taken from this beam at the wall. Note that the presence of stress concentrations at other locations having lower nominal stresses would require their investigation too.

The second aspect is then to determine where in this cross-sectional "bologna slice" the stresses will be greatest. Figures in the relevant sections of this chapter show the stress distributions across sections for various types of loadings. These stress-distribution diagrams are collected in Figure 4-59, which also shows the relevant stress equations for each case. Since the loading in this beam example creates bending stresses, we must understand that there will be a normal stress that is maximally compressive at one extreme fiber and maximally tensile at the other extreme fiber as shown in Figures 4-15 (p. 156) and 4-59c. Thus we would take a stress element at the outer fiber of this slice of the beam to calculate the worst-case bending normal stress from equation 4.11b (p. 156).

**FIGURE 4-59**

Distribution of Stresses Across a Cross Section Under Various Types of Loading

Bending loads also cause shear stress, but its distribution is maximum at the neutral plane and zero at the outer fiber as shown in Figures 4-19 (p. 159) and 4-59d. So, a different stress element is taken at the neutral plane of the cross-sectional slice for calculation of the shear stress due to transverse loading, using the appropriate equation such as equation 4.14b (p. 161) for a rectangular cross section. Each of these two stress el-



ements will have its own set of principal stresses and maximum shear stress, which can be calculated from equation 4.6a (p. 145) for this 2-D case.

More complicated loadings on more complicated geometries may have multiple stresses applied to the same infinitesimal stress element. It is very common in machine parts to have loadings that create both bending and torsion on the same part. Example 4-9 deals with such a case and should be studied carefully.

Stress is only one consideration in design. The deflections of parts must also be controlled for proper function. Often, a requirement for small deflections will dominate the design and require thicker sections than would be necessary to guard against excessive stress. The deflections of a designed part, as well as its stresses, should always be checked. Equations for deflection under various loadings are given in the relevant sections and are also collected in Appendix B for beams of various types and loadings.

Figure 4-60 shows a flow chart depicting a set of steps that can be followed to analyze stresses and deflections under static loading.

Important Equations Used in This Chapter

See the referenced sections for information on the proper use of these equations.

The Stress Cubic - its roots are the 3-D principal stresses (Section 4.3):

$$\sigma^3 - C_2\sigma^2 - C_1\sigma - C_0 = 0 \quad (4.4c)$$

where

$$C_2 = \sigma_x + \sigma_y + \sigma_z$$

$$C_1 = \tau_{xy}^2 + \tau_{yz}^2 + \tau_{zx}^2 - \sigma_x\sigma_y - \sigma_y\sigma_z - \sigma_z\sigma_x$$

$$C_0 = \sigma_x\sigma_y\sigma_z + 2\tau_{xy}\tau_{yz}\tau_{zx} - \sigma_x\tau_{yz}^2 - \sigma_y\tau_{zx}^2 - \sigma_z\tau_{xy}^2$$

Maximum Shear Stresses (Section 4.3):

$$\begin{aligned} \tau_{13} &= \frac{|\sigma_1 - \sigma_3|}{2} \\ \tau_{21} &= \frac{|\sigma_2 - \sigma_1|}{2} \\ \tau_{32} &= \frac{|\sigma_3 - \sigma_2|}{2} \end{aligned} \quad (4.5)$$

Two-Dimensional Principal Stresses (Section 4.3):

$$\begin{aligned} \sigma_a, \sigma_b &= \frac{\sigma_x + \sigma_y}{2} \pm \sqrt{\left(\frac{\sigma_x - \sigma_y}{2}\right)^2 + \tau_{xy}^2} \\ \sigma_c &= 0 \end{aligned} \quad (4.6a)$$

$$\tau_{max} = \tau_{13} = \frac{|\sigma_1 - \sigma_3|}{2} \quad (4.6b)$$

FIGURE 4-60

Flow Chart for Static Stress Analysis

Axial Tension Stress (Section 4.7):

$$\sigma_x = \frac{P}{A} \quad (4.7)$$

Axial Deflection (Section 4.7):

$$\Delta s = \frac{Pl}{AE} \quad (4.8)$$

Direct Shear Stress (Section 4.8):

$$\tau_{xy} = \frac{P}{A_{shear}} \quad (4.9)$$

Direct Bearing Area (Section 4.8):

$$A_{bearing} = \frac{\pi}{4} l d \quad (4.10b)$$

Maximum Bending Stress - Straight Beams (Section 4.9):

$$\sigma_{max} = \frac{Mc}{I} \quad (4.11b)$$

Maximum Bending Stress - Curved Beams (Section 4.9):

$$\sigma_i = + \frac{M}{eA} \left(\frac{c_i}{r_i} \right) \quad (4.12b)$$

Transverse Shear Stress in Beams - General Formula (Section 4.9):

$$\tau_{xy} = \frac{V}{Ib} \int_{y_1}^c y dA \quad (4.13f)$$

Maximum Transverse Shear Stress - Rectangular Beam (Section 4.9):

$$\tau_{max} = \frac{3}{2} \frac{V}{A} \quad (4.14b)$$

Maximum Transverse Shear Stress - Round Beam (Section 4.9):

$$\tau_{max} = \frac{4}{3} \frac{V}{A} \quad (4.15c)$$

Maximum Transverse Shear Stress - I-Beam (Section 4.9):

$$\tau_{max} \cong \frac{V}{A_{web}} \quad (4.16)$$

The General Beam Equations (Section 4.9):

$$\frac{q}{EI} = \frac{d^4 y}{dx^4} \quad (4.18a)$$

$$\frac{V}{EI} = \frac{d^3 y}{dx^3} \quad (4.18b)$$

$$\frac{M}{EI} = \frac{d^2y}{dx^2} \quad (4.18c)$$

$$\theta = \frac{dy}{dx} \quad (4.18d)$$

$$y = f(x) \quad (4.18e)$$

4

Maximum Torsional Shear Stress - Round Section (Section 4.12):

$$\tau_{max} = \frac{Tr}{J} \quad (4.23b)$$

Maximum Torsional Deflection - Round Section (Section 4.12):

$$\theta = \frac{Tl}{JG} \quad (4.24)$$

Maximum Torsional Shear Stress - Nonround Section (Section 4.12):

$$\tau_{max} = \frac{T}{Q} \quad (4.26a)$$

Maximum Torsional Deflection - Nonround Section (Section 4.12):

$$\theta = \frac{Tl}{KG} \quad (4.26b)$$

Spring Rate or Spring Constant - linear (a), angular (b) (Section 4.14):

$$k = \frac{F}{y} \quad (4.27a)$$

$$k = \frac{T}{\theta} \quad (4.27b)$$

Stress with Stress Concentration (Section 4.15):

$$\begin{aligned} \sigma_{max} &= K_t \sigma_{nom} \\ \tau_{max} &= K_{ts} \tau_{nom} \end{aligned} \quad (4.31)$$

Column Radius of Gyration (Section 4.16):

$$k = \sqrt{\frac{I}{A}} \quad (4.34)$$

Column Slenderness Ratio (Section 4.16):

$$S_r = \frac{l}{k} \quad (4.33)$$

Column Critical Unit Load - Euler Formula (Section 4.16):

$$\frac{P_{cr}}{A} = \frac{\pi^2 E}{S_r^2} \quad (4.38c)$$

Column Critical Unit Load - Johnson Formula (Section 4.16):

$$\frac{P_{cr}}{A} = S_{yc} - \frac{1}{E} \left(\frac{S_{yc} S_r}{2\pi} \right)^2 \quad (4.43)$$

Column Critical Unit Load - Secant Formula (Section 4.16):

$$\frac{P}{A} = \frac{S_{yc}}{1 + \left(\frac{ec}{k^2} \right) \sec \left(\frac{l_{eff}}{k} \sqrt{\frac{P}{4EA}} \right)} \quad (4.46c)$$

Pressurized Cylinder (Section 4.17)

$$\sigma_t = \frac{p_i r_i^2 - p_o r_o^2}{r_o^2 - r_i^2} + \frac{r_i^2 r_o^2 (p_i - p_o)}{r^2 (r_o^2 - r_i^2)} \quad (4.47a)$$

$$\sigma_r = \frac{p_i r_i^2 - p_o r_o^2}{r_o^2 - r_i^2} - \frac{r_i^2 r_o^2 (p_i - p_o)}{r^2 (r_o^2 - r_i^2)} \quad (4.47b)$$

$$\sigma_a = \frac{p_i r_i^2 - p_o r_o^2}{r_o^2 - r_i^2} \quad (4.47c)$$

4.20 REFERENCES

- 1 **I. H. Shames and C. L. Dym**, *Energy and Finite Element Methods in Structural Mechanics*. Hemisphere Publishing: New York, Sect. 1.6, 1985.
- 2 **I. H. Shames and F. A. Cossarelli**, *Elastic and Inelastic Stress Analysis*. Prentice-Hall: Englewood Cliffs, N.J., pp. 46-50, 1991.
- 3 **R. E. Peterson**, *Stress Concentration Factors*. John Wiley & Sons: New York, 1974.
- 4 **R. J. Roark and W. C. Young**, *Formulas for Stress and Strain*. 6th ed. McGraw-Hill: New York, 1989.
- 5 **R. E. Peterson**, *Stress Concentration Factors*. John Wiley & Sons: New York, p. 150, 1974.
- 6 **W. D. Pilkey**, *Peterson's Stress Concentration Factors*, John Wiley & Sons: New York, 1997.
- 7 **H. T. Grandin and J. J. Rencis**, *Mechanics of Materials*, John Wiley & Sons: New York, pp. 144-147, 2006.
- 8 **N. Troyani, C. Gomes, and G. Sterlacci**, "Theoretical Stress Concentration Factors for Short Rectangular Plates With Centered Circular Holes." *ASME J. Mech. Design*, V. 124, pp. 126-128, 2002.
- 9 **N. Troyani, et al.**, "Theoretical Stress Concentration Factors for Short Shouldered Plates Subjected to Uniform Tensions." *IMechE J. Strain Analysis*, V. 38, pp. 103-113, 2003.
- 10 **N. Troyani, G. Sterlacci, and C. Gomes**, "Simultaneous Considerations of Length and Boundary Conditions on Theoretical Stress Concentration Factors." *Int. J. Fatigue*, V. 25, pp. 353-355, 2003.

Table P4-0[†]

Topic/Problem Matrix

Sect. 4.1, 4.2 Stress, Strain

4-55, 4-56, 4-57, 4-58

Sect. 4.5 Mohr's Circles

4-1, 4-79

Sect. 4.7 Axial Tension

4-2, 4-18, 4-61, 4-74a

Sect. 4.8 Direct Shear, Bearing, and Tearout4-4, 4-5, 4-6, 4-7, 4-9, 4-15, 4-19, 4-20, **4-22**, 4-47, 4-59, 4-60, 4-74f**Sect. 4.9 Straight Beams**

4-10, 4-11, 4-12, 4-13, 4-14, 4-27, 4-40, 4-43a, 4-64, 4-65, 4-66, 4-67, 4-68, 4-74b, 4-74 c, 4-74g

Sect. 4.9 Curved Beams4-17, 4-37, 4-62, 4-63, **4-69 to 4-72**, 4-73, 4-74e**Sect. 4.10 Deflection**4-8, 4-16, 4-23, 4-24, 4-25, **4-26**, 4-28, 4-43b, **4-44**, 4-48**Sect. 4.11 Castigliano's Method**

4-84, 4-85, 4-86

Sect. 4.12 Torsion

4-21, 4-34, 4-46, 4-74d, 4-74h, 4-81, 4-82

Sect. 4.13 Combined Stresses

4-3, 4-34, 4-46

Sect. 4.14 Spring Rates

4-29, 4-30, 4-31, 4-32, 4-35, 4-38, 4-39

Sect. 4.15 Stress Conc.

4-36, 4-75 to 4-78

Sect. 4.16 Columns

4-45, 4-49, 4-50, 4-51, 4-52, 4-53, 4-54

Sect. 4.17 Cylinders

4-41, 4-42, 4-80, 4-83

4.21 BIBLIOGRAPHY

For general information on stress and deflection analysis see:

F. P. Beer and E. R. Johnston, *Mechanics of Materials*. 2nd ed. McGraw-Hill: New York, 1992.**J. P. D. Hartog**, *Strength of Materials*. Dover: New York, 1961.**R. J. Roark and W. C. Young**, *Formulas for Stress and Strain*. 6th ed. McGraw-Hill: New York, 1989.**I. H. Shames**, *Introduction to Solid Mechanics*. Prentice-Hall: Englewood Cliffs, N.J., 1989.**I. H. Shames and F. A. Cossarelli**, *Elastic and Inelastic Stress Analysis*. Prentice-Hall: Englewood Cliffs, N.J., 1991.**S. Timoshenko and D. H. Young**, *Elements of Strength of Materials*. 5th ed. Van Nostrand: New York, 1968.**4.22 PROBLEMS**

***4-1** A differential stress element has a set of applied stresses on it as indicated in each row of Table P4-1. For the row(s) assigned, draw the stress element showing the applied stresses, find the principal stresses and maximum shear stress analytically, and check the results by drawing Mohr's circles for that stress state.

4-2 A 400-lb chandelier is to be hung from two 10-ft-long solid steel cables in tension. Choose a suitable diameter of cable which will not exceed an allowable stress of 5 000 psi. What will be the deflection of the cables? State all assumptions.

†4-3 For the bicycle pedal arm assembly in Figure P4-1 with a rider-applied force of 1500 N at the pedal, determine the maximum principal stress in the pedal arm if its cross section is 15 mm in dia. The pedal attaches to the pedal arm with a 12-mm screw thread. What is the stress in the pedal screw?

†*4-4 The trailer hitch shown in Figure P4-2 and Figure 1-1 (p. 11) has loads applied as defined in Problem 3-4. The 100-kg tongue weight acts downward and the pull force of 4 905 N acts horizontally. Using the dimensions of the ball bracket shown in Figure 1-5 (p. 14), determine:

- (a) The principal stresses in the shank of the ball where it joins the ball bracket.
- (b) The bearing stress in the ball bracket hole.
- (c) The tearout stress in the ball bracket.
- (d) The normal and shear stresses in the attachment bolts if they are 19-mm dia.
- (e) The principal stresses in the ball bracket as a cantilever.

†4-5 Repeat Problem 4-4 for the loading conditions of Problem 3-5.

†*4-6 Repeat Problem 4-4 for the loading conditions of Problem 3-6.

†*4-7 Design the wrist pin of Problem 3-7 for a maximum allowable principal stress of 20 kpsi if the pin is hollow and loaded in double shear.

†*4-8 A paper mill processes rolls of paper having a density of 984 kg/m^3 . The paper roll is 1.50 m outside dia (OD) \times 22 cm inside dia (ID) \times 3.23-m long and is on a simply supported, hollow, steel shaft. Find the shaft ID needed to obtain a maximum deflection at the center of 3 mm if the shaft OD is 22 cm. Assume the shaft to be the same length between supports as the length of the paper roll.

* Answers to these problems are provided in Appendix D.

[†] Numbers in **boldface** are extended from problems in earlier chapters with the same dash number. Problem numbers in *italics* are design problems.

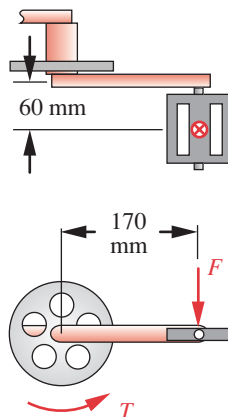
Table P4-1 Data for Problem 4-1 (in psi)

Rows a–g and k–m are two-dimensional, others are 3-D problems

Row	σ_x	σ_y	σ_z	τ_{xy}	τ_{yz}	τ_{zx}
a	1 000	0	0	500	0	0
b	-1 000	0	0	750	0	0
c	500	-500	0	1 000	0	0
d	0	-1 500	0	750	0	0
e	750	250	0	500	0	0
f	-500	1 000	0	750	0	0
g	1 000	0	-750	0	0	250
h	750	500	250	500	0	0
i	1 000	-250	-750	250	500	750
j	-500	750	250	100	250	1 000
k	1 000	0	0	0	0	0
l	1 000	0	0	0	500	0
m	1 000	0	0	0	0	500
n	1 000	1 000	1 000	500	0	0
o	1 000	1 000	1 000	500	500	0
p	1 000	1 000	1 000	500	500	500

- 4-9** For the ViseGrip® plier-wrench drawn to scale in Figure P4-3 (on previous page), and for which the forces were analyzed in Problem 3-9, find the stresses in each pin for an assumed clamping force of $P = 4\,000\text{ N}$ in the position shown. The pins are 8-mm dia and are all in double shear.

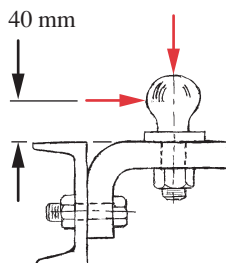
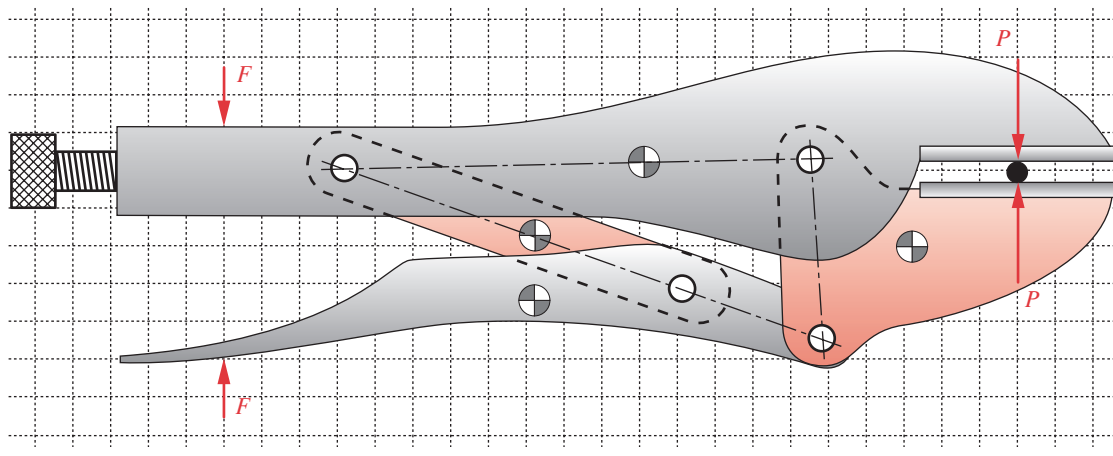
- *4-10** The overhung diving board of Problem 3-10 is shown in Figure P4-4a. Assume cross-section dimensions of 305 mm \times 32 mm. The material has $E = 10.3\text{ GPa}$. Find the largest principal stress at any location in the board when a 100-kg person is standing in the center of the width of the board at the free end. What is the maximum deflection?



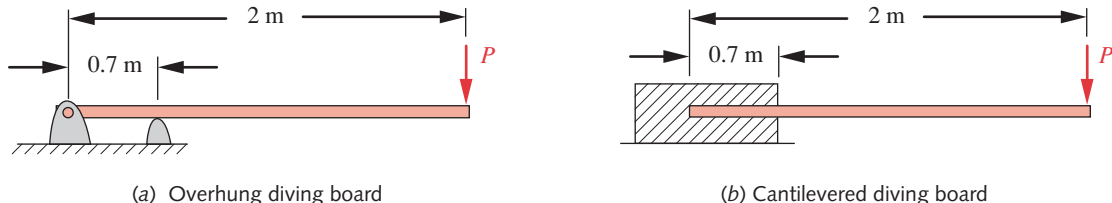
4

FIGURE P4-1

Problem 4-3 (A Solidworks model of this is on the CD)

**FIGURE P4-2**Problems 4-4, 4-5, 4-6
(A Solidworks model of this is on the CD)**FIGURE P4-3**

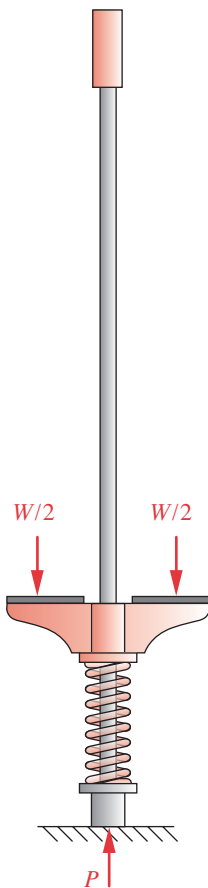
Problem 4-9 (A Solidworks model of this is on the CD)

**FIGURE P4-4**

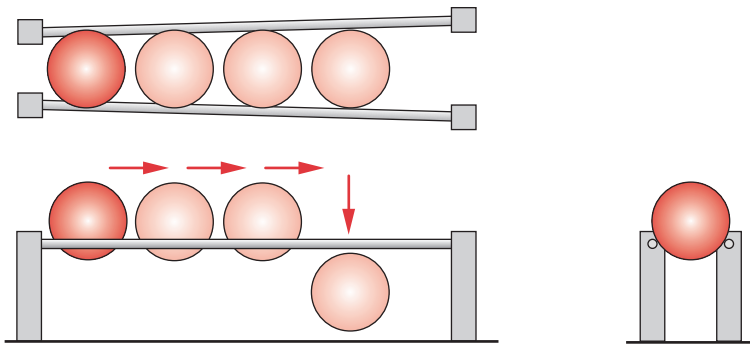
4

Problems 4-10 through 4-13

- *4-11** Repeat Problem 4-10 using the loading conditions of Problem 3-11. Assume the board weighs 29 kg and deflects 13.1 cm statically when the person stands on it. Find the largest principal stress at any location in the board when the 100-kg person in Problem 4-10 jumps up 25 cm and lands back on the board. Find the maximum deflection.
- 4-12** Repeat Problem 4-10 using the cantilevered diving board design in Figure P4-4b.
- 4-13** Repeat Problem 4-11 using the diving board design shown in Figure P4-4b. Assume the board weighs 19 kg and deflects 8.5 cm statically when the person stands on it.
- 4-14** Figure P4-5 shows a child's toy called a *pogo stick*. The child stands on the pads, applying half her weight on each side. She jumps up off the ground, holding the pads up against her feet, and bounces along with the spring cushioning the impact and storing energy to help each rebound. Assume a 60-lb child and a spring constant of 100 lb/in. The pogo stick weighs 5 lb. Design the aluminum cantilever beam sections on which she stands to survive jumping 2 in off the ground. Assume an allowable stress of 20 kpsi. Define the beam shape and size it appropriately.
- *4-15** Design a shear pin for the propeller shaft of an outboard motor if the shaft through which the pin is placed is 25-mm diameter, the propeller is 200-mm diameter, and the pin must fail when a force > 400 N is applied to the propeller tip. Assume an ultimate shear strength for the pin material of 100 MPa.
- 4-16** A track to guide bowling balls is designed with two round rods as shown in Figure P4-6. The rods are not parallel to one another but have a small angle between them. The balls roll on the rods until they fall between them and drop onto another track. The angle between the rods is varied to cause the ball to drop at different locations. Each rod's unsupported length is 30 in and the angle between them is 3.2° . The balls are 4.5-in dia and weigh 2.5 lb. The center distance between the 1-in-dia rods is 4.2 in at the narrow end. Find the maximum stress and deflection in the rods.
- Assume the rods are simply supported at each end.
 - Assume the rods are fixed at each end.
- 4-17** A pair of ice tongs is shown in Figure P4-7. The ice weighs 50 lb and is 10 in wide across the tongs. The distance between the handles is 4 in, and the mean radius r of a tong is 6 in. The rectangular cross-sectional dimensions are 0.75 in deep \times 0.312 in wide. Find the stress in the tongs.
- *4-18** A set of steel reinforcing rods is to be stretched axially in tension to create a tensile stress of 30 kpsi prior to being cast in concrete to form a beam. Determine how much force will be required to stretch them the required amount and how much deflection is required. There are 10 rods; each is 0.75-in dia and 30 ft long.
- *4-19** The clamping fixture used to pull the rods in Problem 4-18 is connected to the hydraulic ram by a clevis like that shown in Figure P4-8. Determine the size of the clevis pin needed to withstand the applied force. Assume an allowable shear stress of 20 000 psi

**FIGURE P4-5**

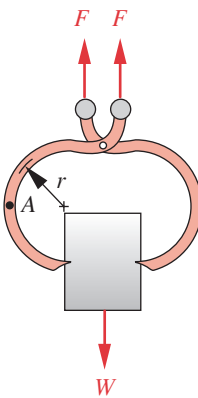
Problem 4-14

**FIGURE P4-6**

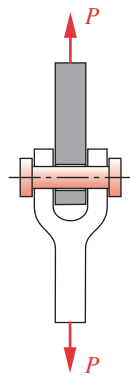
Problem 4-16

and an allowable normal stress of 40 000 psi. Determine the required outside radius of the clevis end to not exceed the above allowable stresses in either tearout or bearing if the clevis flanges are each 0.8 in thick.

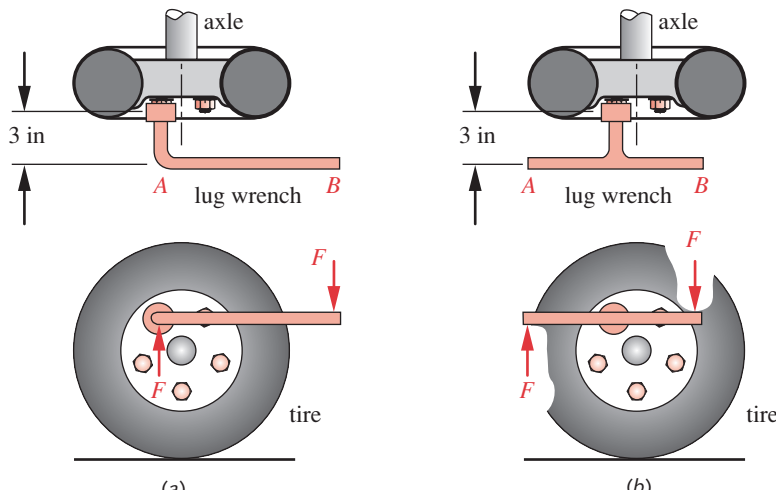
- 4-20** Repeat Problem 4-19 for 12 rods each 1-cm dia and 10 m long. The desired rod stress is 200 MPa. The allowable normal stress in the clevis and pin is 280 MPa and their allowable shear stress is 140 MPa. Each clevis flange is 2 cm wide.
- 4-21** Figure P4-9 shows an automobile wheel with two common styles of lug wrench being used to tighten the wheel nuts, a single-ended wrench in (a), and a double-ended wrench in (b). In each case two hands are required to provide forces, respectively, at A and B as shown. The distance between points A and B is 1 ft in both cases and the handle diameter is 0.625 in. The wheel nuts require a torque of 70 ft-lb. Find the maximum principal stress and maximum deflection in each wrench design.
- *4-22** An in-line “roller-blade” skate is shown in Figure P4-10. The polyurethane wheels are 72-mm dia and spaced on 104-mm centers. The skate-boot-foot combination weighs 2 kg. The effective “spring rate” of the person-skate system is 6 000 N/m. The axles are

**FIGURE P4-7**

Problem 4-17

**FIGURE P4-8**

Problems 4-19 and 4-20

**FIGURE P4-9**

Problem 4-21

* Answers to these problems are provided in Appendix D. Problem numbers in *italics* are design problems. Problem numbers in **boldface** are extended from similar problems in earlier chapters with the same dash number. Problems in succeeding chapters may also continue and extend these problems.

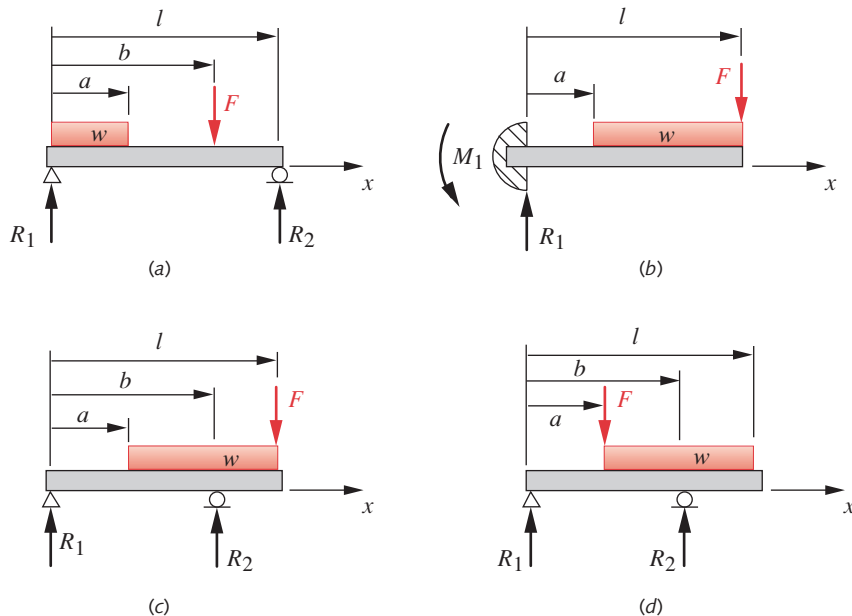
**FIGURE P4-10**

Problem 4-22

4

10-mm-dia steel pins in double shear. Find the stress in the pins for a 100-kg person landing a 0.5-m jump on one foot. (a) Assume that all four wheels land simultaneously. (b) Assume that one wheel absorbs all the landing force.

- ***4-23** A beam is supported and loaded as shown in Figure P4-11a. Find the reactions, maximum shear, maximum moment, maximum slope, maximum bending stress, and maximum deflection for the data given in the assigned row(s) in Table P4-2.
- ***4-24** A beam is supported and loaded as shown in Figure P4-11b. Find the reactions, the maximum shear, maximum moment, maximum slope, maximum bending stress, and maximum deflection for the data given in the assigned row(s) in Table P4-2.
- ***4-25** A beam is supported and loaded as shown in Figure P4-11c. Find the reactions, the maximum shear, maximum moment, maximum slope, maximum bending stress, and maximum deflection for the data given in the assigned row(s) in Table P4-2.
- ***4-26** A beam is supported and loaded as shown in Figure P4-11d. Find the reactions, maximum shear, maximum moment, maximum slope, maximum bending stress, and maximum deflection for the data given in the assigned row(s) in Table P4-2.
- 4-27** A storage rack is to be designed to hold the paper roll of Problem 4-8 as shown in Figure P4-12. Determine suitable values for dimensions a and b in the figure. Consider bending, shear, and bearing stresses. Assume an allowable tensile/compressive stress of 100 MPa and an allowable shear stress of 50 MPa for both stanchion and mandrel, which are steel. The mandrel is solid and inserts halfway into the paper roll. Balance the design to use all of the material strength. Calculate the deflection at the end of the roll.
- †**4-28** Figure P4-13 shows a forklift truck negotiating a 15° ramp to drive onto a 4-ft-high loading platform. The truck weighs 5 000 lb and has a 42-in wheelbase. Design two (one for each side) 1-ft-wide ramps of steel to have no more than 1-in deflection in the worst case of loading as the truck travels up them. Minimize the weight of the ramps by using a sensible cross-sectional geometry.

**FIGURE P4-11**

Beams and Beam Loadings for Problems 4-23 to 4-26 and 4-29 to 4-32 - See Table P4-2 for Data

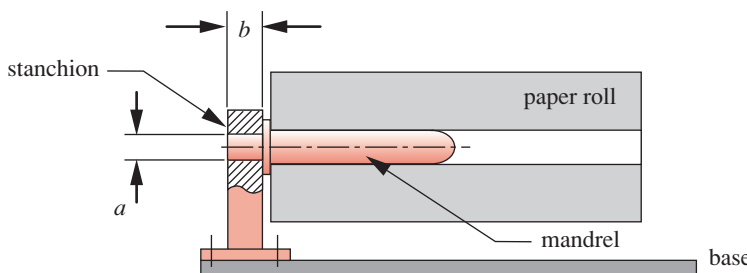
* Answers to these problems are provided in Appendix D. Problem numbers in *italics* are design problems. Problem numbers in **boldface** are extended from similar problems in earlier chapters with the same dash number. Problems in succeeding chapters may also continue and extend these problems.

Table P4-2 Data for Problems 4-23 through 4-26 and 4-29 through 4-32Use only data relevant to the particular problem. Lengths in m, forces in N, I in m^4 .

Row	l	a	b	w^*	F	I	c	E
<i>a</i>	1.00	0.40	0.60	200	500	$2.85E-08$	$2.00E-02$	steel
<i>b</i>	0.70	0.20	0.40	80	850	$1.70E-08$	$1.00E-02$	steel
<i>c</i>	0.30	0.10	0.20	500	450	$4.70E-09$	$1.25E-02$	steel
<i>d</i>	0.80	0.50	0.60	65	250	$4.90E-09$	$1.10E-02$	steel
<i>e</i>	0.85	0.35	0.50	96	750	$1.80E-08$	$9.00E-03$	steel
<i>f</i>	0.50	0.18	0.40	450	950	$1.17E-08$	$1.00E-02$	steel
<i>g</i>	0.60	0.28	0.50	250	250	$3.20E-09$	$7.50E-03$	steel
<i>h</i>	0.20	0.10	0.13	400	500	$4.00E-09$	$5.00E-03$	alum
<i>i</i>	0.40	0.15	0.30	50	200	$2.75E-09$	$5.00E-03$	alum
<i>j</i>	0.20	0.10	0.15	150	80	$6.50E-10$	$5.50E-03$	alum
<i>k</i>	0.40	0.16	0.30	70	880	$4.30E-08$	$1.45E-02$	alum
<i>l</i>	0.90	0.25	0.80	90	600	$4.20E-08$	$7.50E-03$	alum
<i>m</i>	0.70	0.10	0.60	80	500	$2.10E-08$	$6.50E-03$	alum
<i>n</i>	0.85	0.15	0.70	60	120	$7.90E-09$	$1.00E-02$	alum

* Note that w is a unit force of N/m

- *4-29 Find the spring rate of the beam in Problem 4-23 at the applied concentrated load for the row(s) assigned in Table P4-2.
- *4-30 Find the spring rate of the beam in Problem 4-24 at the applied concentrated load for the row(s) assigned in Table P4-2.
- *4-31 Find the spring rate of the beam in Problem 4-25 at the applied concentrated load for the row(s) assigned in Table P4-2.
- *4-32 Find the spring rate of the beam in Problem 4-26 at the applied concentrated load for the row(s) assigned in Table P4-2.
- *4-33 For the bracket shown in Figure P4-14 and the data in the row(s) assigned from Table P4-3, determine the bending stress at point A and the shear stress due to transverse loading at point B. Also find the torsional shear stress at both points. Then determine the principal stresses at points A and B.
- *4-34 For the bracket shown in Figure P4-14 and the data in the row(s) assigned from Table P4-3, determine the deflection at load F .

**FIGURE P4-12**

Problem 4-27

* Answers to these problems are provided in Appendix D. Problem numbers in *italics* are design problems. Problem numbers in **boldface** are extended from similar problems in earlier chapters with the same dash number. Problems in succeeding chapters may also continue and extend these problems.

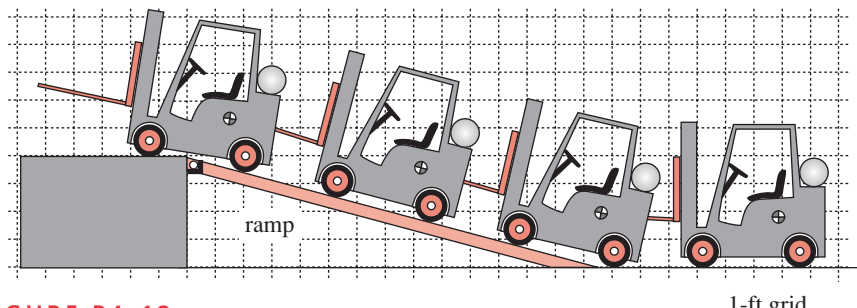


FIGURE P4-13

Problem 4-28

- *4-35 For the bracket shown in Figure P4-14 and the data in the row(s) assigned from Table P4-3, determine the spring rate of the tube in bending, the spring rate of the arm in bending, and the spring rate of the tube in torsion. Combine these into an overall spring rate in terms of the force F and the linear deflection at force F .
- 4-36 For the bracket shown in Figure P4-14 and the data in the row(s) assigned from Table P4-3, redo Problem 4-33 considering the stress concentration at points A and B. Assume a stress-concentration factor of 2.5 in both bending and torsion.
- *4-37 A semicircular curved beam as shown in Figure P4-15 has OD = 150 mm, ID = 100 mm, and $t = 25$ mm. For a load pair $F = 14$ kN applied along the diameter, find the eccentricity of the neutral axis and the stress at the inner and outer fibers.
- 4-38 Design a solid, straight, steel torsion bar to have a spring rate of 10 000 in-lb per radian per foot of length. Compare designs of solid round and solid square cross sections. Which is more efficient in terms of material use?
- 4-39 Design a 1-ft-long steel, end-loaded cantilever spring for a spring rate of 10 000 lb/in at the load. Compare designs of solid round and solid square cross sections. Which is more efficient in terms of material use?
- 4-40 Redesign the roll support of Problem 4-8 to be like that shown in Figure P4-16. The stub mandrels insert to 10% of the roll length at each end. Choose appropriate dimensions a and b to fully utilize the material's strength, which is the same as in Problem 4-27. See Problem 4-8 for additional data.
- *4-41 A 10-mm ID steel tube carries liquid at 7 MPa. Determine the principal stresses in the wall if its thickness is: (a) 1 mm, (b) 5 mm.

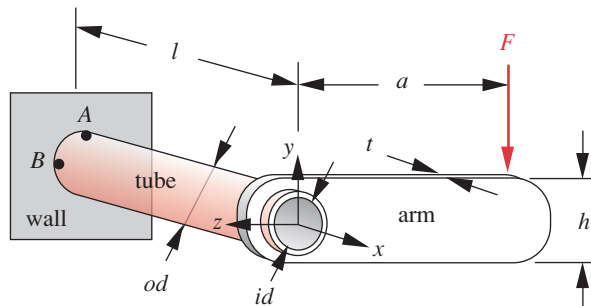


FIGURE P4-14

Problems 4-33 to 4-36 (A Solidworks model of this is on the CD)

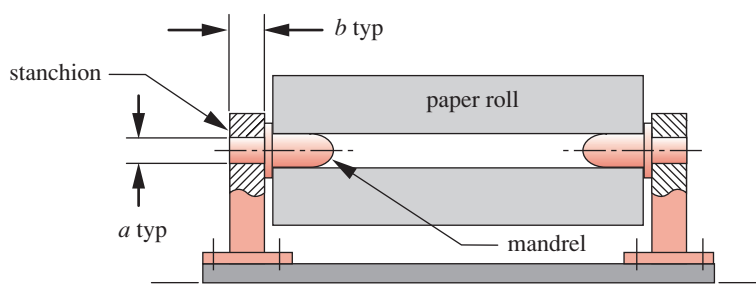
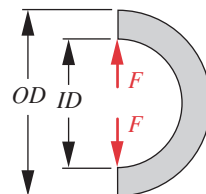
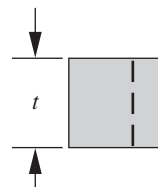
* Answers to these problems are provided in Appendix D.

Table P4-3 Data for Problems 4-33 through 4-36 and 4-49 through 4-52

Use only data that are relevant to the particular problem. Lengths in mm, forces in N.

Row	<i>l</i>	<i>a</i>	<i>t</i>	<i>h</i>	<i>F</i>	<i>OD</i>	<i>ID</i>	<i>E</i>
<i>a</i>	100	400	10	20	50	20	14	steel
<i>b</i>	70	200	6	80	85	20	6	steel
<i>c</i>	300	100	4	50	95	25	17	steel
<i>d</i>	800	500	6	65	160	46	22	alum
<i>e</i>	85	350	5	96	900	55	24	alum
<i>f</i>	50	180	4	45	950	50	30	alum
<i>g</i>	160	280	5	25	850	45	19	steel
<i>h</i>	200	100	2	10	800	40	24	steel
<i>i</i>	400	150	3	50	950	65	37	steel
<i>j</i>	200	100	3	10	600	45	32	alum
<i>k</i>	120	180	3	70	880	60	47	alum
<i>l</i>	150	250	8	90	750	52	28	alum
<i>m</i>	70	100	6	80	500	36	30	steel
<i>n</i>	85	150	7	60	820	40	15	steel

- 4-42 A cylindrical tank with hemispherical ends is required to hold 150 psi of pressurized air at room temperature. Find the principal stresses in the 1-mm-thick wall if the tank diameter is 0.5 m and its length is 1 m.
- 4-43 Figure P4-17 shows an off-loading station at the end of a paper rolling machine. The finished paper rolls are 0.9-m OD by 0.22-m ID by 3.23-m long and have a density of 984 kg/m³. The rolls are transferred from the machine conveyor (not shown) to the forklift truck by the V-linkage of the off-load station which is rotated through 90° by an air cylinder. The paper then rolls onto the waiting forks of the truck. The forks are 38-mm thick by 100-mm wide by 1.2-m long and are tipped at a 3° angle from the horizontal. Find the stresses in the two forks on the truck when the paper rolls onto it under two different conditions (state all assumptions):
- The two forks are unsupported at their free end.
 - The two forks are contacting the table at point A.
- 4-44 Determine a suitable thickness for the V-links of the off-loading station of Figure P4-17 to limit their deflections at the tips to 10 mm in any position during their rotation. Assume that there are two V-links supporting the roll, arranged at the 1/4 and 3/4 points along the roll's length, and that each of the V arms is 10 cm wide by 1 m long. The V

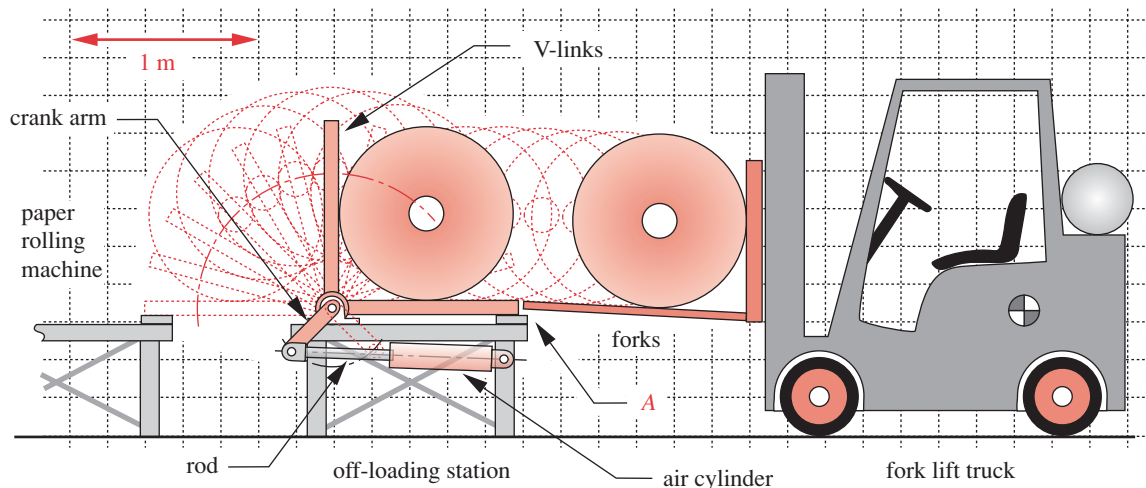
**FIGURE P4-16**

Problem 4-40 (A Solidworks model of this is on the CD)

FIGURE P4-15

Problem 4-37 (A Solidworks model of this is on the CD)

* Answers to these problems are provided in Appendix D.

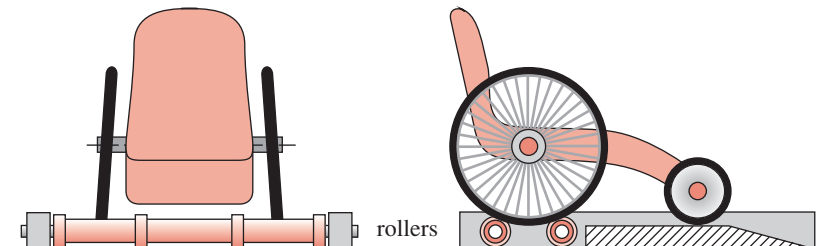
**FIGURE P4-17**

Problems 4-43 to 4-47

arms are welded to a steel tube that is rotated by the air cylinder. See Problem 4-43 for more information.

- 4-45 Determine the critical load on the air-cylinder rod in Figure P4-17 if the crank arm that rotates is 0.3 m long and the rod has a maximum extension of 0.5 m. The 25-mm-dia rod is solid steel with a yield strength of 400 MPa. State all assumptions.
- 4-46 The V-links of Figure P4-17 are rotated by the crank arm through a shaft that is 60-mm dia by 3.23 m long. Determine the maximum torque applied to this shaft during the motion of the V-linkage and find the maximum stress and deflection for the shaft. See Problem 4-43 for more information.
- 4-47 Determine the maximum forces on the pins at each end of the air cylinder of Figure P4-17. Determine the stress in these pins if they are 30-mm dia and in single shear.
- 4-48 A 100-kg wheelchair marathon racer wants an exerciser that will allow indoor practicing in any weather. The design shown in Figure P4-18 is proposed. Two free-turning rollers on bearings support the rear wheels. A platform supports the front wheels. Design the 1-m-long rollers as hollow tubes of aluminum to minimize the height of the platform and also limit the roller deflections to 1 mm in the worst case. The wheelchair has 65-cm-dia drive wheels separated by a 70-cm track width. The flanges shown on the rollers limit the lateral movement of the chair while exercising and thus the wheels can be anywhere between those flanges. Specify suitably sized steel axles to support the tubes on bearings. Calculate all significant stresses.
- *4-49 A hollow, square column has a length l and material E , as shown in the row(s) assigned in Table P4-3. Its cross-sectional dimensions are 4 mm outside and 3 mm inside. Use $S_y = 150$ MPa for aluminum and 300 MPa for steel. Determine if it is a Johnson or an Euler column and find the critical load:
- If its boundary conditions are pinned-pinned.
 - If its boundary conditions are fixed-pinned.
 - If its boundary conditions are fixed-fixed.
 - If its boundary conditions are fixed-free.
- *4-50 A hollow, round column has a length of 1.5 m, material E , and cross-sectional dimensions OD and ID as shown in the row(s) assigned in Table P4-3. Use $S_y = 150$ MPa for

* Answers to these problems are provided in Appendix D. Problem numbers in *italics* are design problems.

**FIGURE P4-18**

Problem 4-48

aluminum and 300 MPa for steel. Determine if it is a Johnson or an Euler column and find the critical load:

- (a) If its boundary conditions are pinned-pinned.
- (b) If its boundary conditions are fixed-pinned.
- (c) If its boundary conditions are fixed-fixed.
- (d) If its boundary conditions are fixed-free.

*4-51 A solid, rectangular column has a length l , material E , and cross-sectional dimensions h and t as shown in the row(s) assigned in Table P4-3. Use $S_y = 150$ MPa for aluminum and 300 MPa for steel. Determine if it is a Johnson or an Euler column and find the critical load:

- (a) If its boundary conditions are pinned-pinned.
- (b) If its boundary conditions are fixed-pinned.
- (c) If its boundary conditions are fixed-fixed.
- (d) If its boundary conditions are fixed-free.

*4-52 A solid, circular column has a length l , material E , diameter OD, and an eccentricity t as shown in the row(s) assigned in Table P4-3. Use $S_y = 150$ MPa for aluminum and 300 MPa for steel. Determine if it is a Johnson or an Euler column and find the critical load:

- (a) If its boundary conditions are pinned-pinned.
- (b) If its boundary conditions are fixed-pinned.
- (c) If its boundary conditions are fixed-fixed.
- (d) If its boundary conditions are fixed-free.

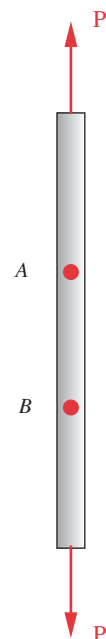
4-53 Design an aluminum, hollow, circular column for the following data: 3 m long, 5 mm wall thickness, 900 N concentric load, material yield strength of 150 MPa, and safety factor of 3.

- (a) If its boundary conditions are pinned-pinned.
- (b) If its boundary conditions are fixed-free.

4-54 Three round, 1.25-in-dia bars are made of SAE 1030 hot-rolled steel but are of different lengths, 5 in, 30 in, and 60 in, respectively. They are loaded axially in compression. Compare the load-supporting capability of the three bars if the ends are assumed to be:

- (a) Pinned-pinned.
- (b) Fixed-pinned.
- (c) Fixed-fixed.
- (d) Fixed-free.

4-55 Figure P4-19 shows a 1.5-in-dia, 30-in-long steel rod subjected to tensile loads $P = 10\,000$ lb applied at each end of the rod, acting along its longitudinal Y axis and through the centroid of its circular cross section. Point A is 12 in below the upper end and point B is 8 in below A. For this bar with this loading find:

**FIGURE P4-19**

Problems 4-55 and 4-56

* Answers to these problems are provided in Appendix D. Problem numbers in *italics* are design problems.

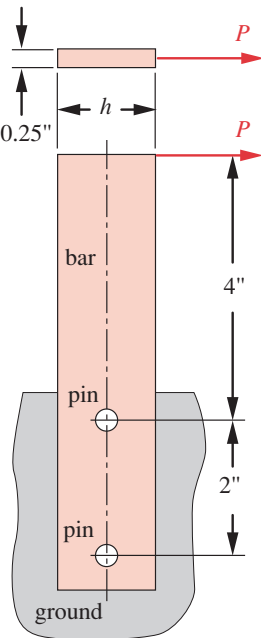
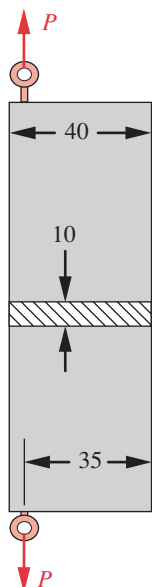


FIGURE P4-20

Problems 4-57 and 4-58
(A Solidworks model of this is on the CD)



dimensions in mm

FIGURE P4-21

Problem 4-59 (A Solidworks model of this is on the CD)

- (a) All components of the stress tensor matrix (equation 4.1a) for a point midway between A and B.

- (b) The displacement of point B relative to point A.
- (c) The elastic strain in the section between A and B.
- (d) The total strain in the section between A and B.

- 4-56 The rod in Figure P4-19, with the loading of Problem 4-55, is subjected to a reduction in temperature from 80°F to 20°F after the load is applied. The coefficient of thermal expansion for steel is approximately $6 \mu\text{in/in}/^\circ\text{F}$. Find:

- (a) All components of the stress tensor matrix (equation 4.1a) for a point midway between A and B.

- (b) The displacement of point B relative to point A.
- (c) The elastic strain in the section between A and B.
- (d) The total strain in the section between A and B.

- 4-57 Figure P4-20 shows a steel bar fastened to a rigid ground plane with two 0.25-in-dia hardened steel dowel pins. For $P = 1500$ lb, find:

- (a) The shear stress in each pin.
- (b) The direct bearing stress in each pin and hole.
- (c) The minimum value of dimension h to prevent tearout failure if the steel bar has a shear strength of 32.5 kpsi.

- 4-58 Repeat Problem 4-57 for $P = 2200$ lb.

- 4-59 Figure P4-21 shows a rectangular section aluminum bar subjected to off-center forces $P = 4000$ N applied as shown.

- (a) Solve for the maximum normal stress in the mid-region of the bar well away from the eyes where the loads are applied.
- (b) Plot the normal stress distribution across the cross section at this mid-region of the bar.
- (c) Sketch a "reasonable" plot of the normal stress distribution across the cross section at the ends, close to the applied loads.

- 4-60 Figure P4-22 shows a bracket machined from 0.5-in-thick steel flat stock. It is rigidly attached to a support and loaded with $P = 5000$ lb at point D. Find:

- (a) The magnitude, location, and the plane orientation of the maximum normal stress at section A-A.
- (b) The magnitude, location, and the plane orientation of the maximum shear stress at section A-A.
- (c) The magnitude, location, and the plane orientation of the maximum normal stress at section B-B.
- (d) The magnitude, location, and the plane orientation of the maximum shear stress at section B-B.

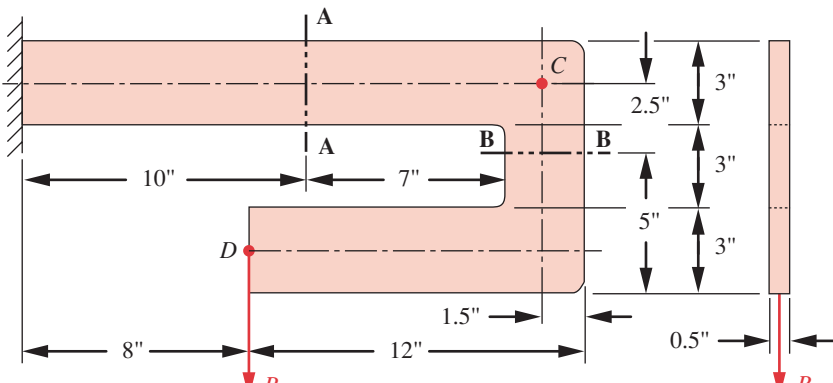
- 4-61 For the bracket of Problem 4-60, solve for the deflection and slope of point C.

- 4-62 Figure P4-23 shows a 1-in-dia steel bar supported and subjected to the applied load $P = 500$ lb. Solve for the deflection at the load and the slope at the roller support.

- 4-63 Figure P4-24 shows a 1.25-in-dia solid steel shaft with several twisting couples applied in the directions shown. For $T_A = 10000$ lb-in, $T_B = 20000$ lb-in, $T_C = 30000$ lb-in, find:

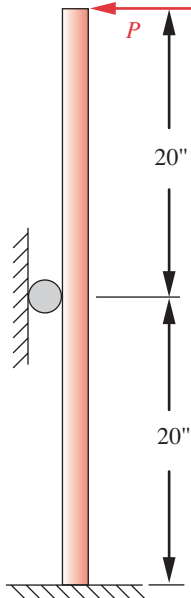
- (a) The magnitude and location of the maximum torsional shear stress in the shaft.
- (b) The corresponding principal stresses for the location determined in part (a).
- (c) The magnitude and location of the maximum shear strain in the shaft.

- 4-64 If the shaft of Problem 4-63 were rigidly attached to fixed supports at each end (A and D) and loaded only by the applied couples T_B , and T_C , then find:

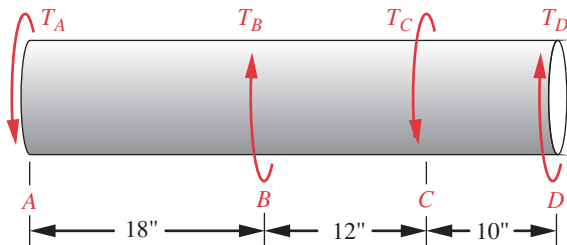
**FIGURE P4-22**

Problems 4-60 and 4-61 (A Solidworks model of this is on the CD)

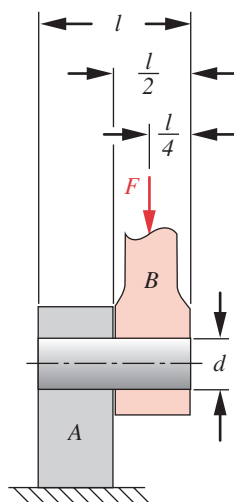
- (a) The reactions T_A and T_D at each end of the shaft.
 (b) The rotation of section B with respect to section C.
 (c) The magnitude and location of the maximum shear strain.
- [†]4-65 Figure P4-25 shows a pivot pin that is a press fit in part A and a slip fit in part B. If $F = 100$ lb and $l = 1.5$ in, what pin diameter is needed to limit the maximum stress in the pin to 50 ksi?
- 4-66 Figure P4-25 shows a pivot pin that is a press fit in part A and a slip fit in part B. If $F = 100$ N and $l = 64$ mm, what pin diameter is needed to limit the maximum stress in the pin to 250 MPa?
- [†]4-67 Figure P4-25 shows a pivot pin that is a press fit in part A and a slip fit in part B. Determine the l/d ratio that will make the pin equally strong in shear and bending if the shear strength is equal to one-half the bending strength.
- 4-68 Write a computer program in any language, or use an equation-solver program or spreadsheet to calculate and plot the variation in cross-sectional area, area moment of inertia, radius of gyration, slenderness ratio, and critical load with respect to the inside diameter of both a Euler and a Johnson column having round-hollow cross sections. Assume that the outside diameter of each column is 1 in. The effective length of the Euler column is 50 in. The effective length of the Johnson column is 10 in. Both are made of steel with $S_y = 36\,000$ psi. Let the inside diameter vary from 10% to 90% of the

**FIGURE P4-23**

Problem 4-62

**FIGURE P4-24**

Problems 4-63 and 4-64

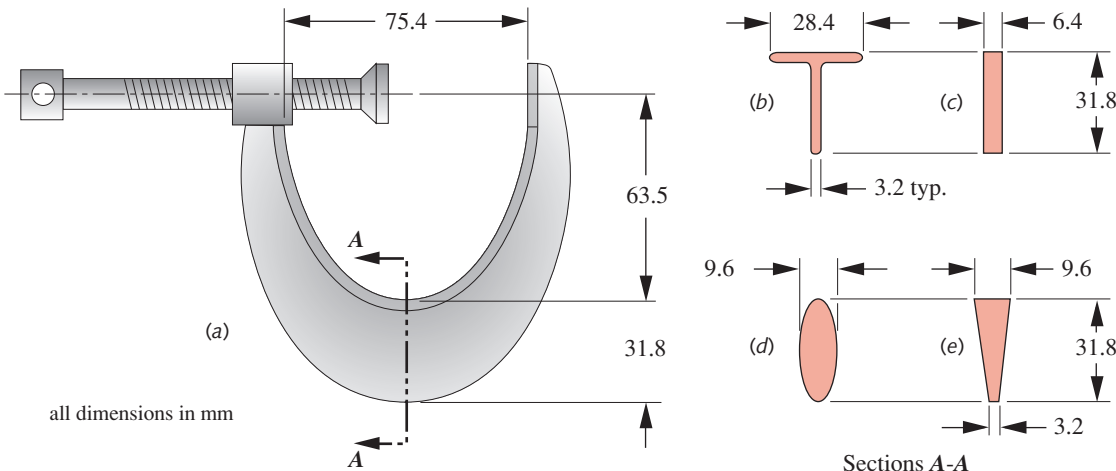
**FIGURE P4-25**

Problems 4-65 to 4-67

[†] Problem numbers in *italics* are design problems.

outside diameter for this parametric study. Comment on the advantages of hollow-round columns over solid-round columns of each type (Euler and Johnson) that have the same outer diameters, respective lengths, and materials.

- *4-69 Figure P4-26a shows a C-clamp with an elliptical body dimensioned as shown. The clamp has a T-section with a uniform thickness of 3.2 mm at the throat as shown in Figure P4-26b. Find the bending stress at the inner and outer fibers of the throat if the clamp force is 2.7 kN.
- 4-70 A C-clamp as in Figure P4-26a has a rectangular cross section as in Figure P4-26c. Find the bending stress at the inner and outer fibers of the throat if the clamp force is 1.6 kN.
- 4-71 A C-clamp as in Figure P4-26a has an elliptical cross section as in Figure P4-26d. Dimensions of the major and minor axes of the ellipse are given. Determine the bending stress at the inner and outer fibers of the throat if the clamping force is 1.6 kN.
- 4-72 A C-clamp as in Figure P4-26a has a trapezoidal cross section as in Figure P4-26e. Determine the bending stress at the inner and outer fibers of the throat if the clamping force is 1.6 kN.
- 4-73 We want to design a C-clamp with a T-section similar to the one shown in Figures P4-26a and b. The depth of the section will be 31.8 mm as shown but the width of the flange (shown as 28.4 mm) is to be determined. Assuming a uniform thickness of 3.2 mm and a factor of safety against static yielding of 2, determine a suitable value for the width of the flange if the C-clamp is to be made from 60-40-18 ductile iron and the maximum design load is 1.6 kN.
- 4-74 A round steel bar is 10 in long and has a diameter of 1 in.
- Calculate the stress in the bar when it is subjected to a 1000-lb force in tension.
 - Calculate the bending stress in the bar if it is fixed at one end (as a cantilever beam) and has a 1000-lb transverse load at the other end.
 - Calculate the transverse shear stress in the bar of part (b).
 - Determine how short the bar must be when loaded as a cantilever beam for its maximum flexural bending stress and its maximum transverse shear stress to provide equal tendency to failure. Find the length as a fraction of the diameter if the failure stress in shear is half the failure stress in bending.

**FIGURE P4-26**

Problems 4-69 to 4-73 (A Solidworks model of this is on the CD)

- (e) Calculate the torsional shear stress when a 10 000 in-lb couple is applied about the centerline (axis) of the cantilever beam at its free end.
- (f) If the force on the cantilever beam in (b) is eccentric, inducing torsional as well as bending stress, what fraction of the diameter would the eccentricity need to be in order to give a torsional stress equal to the transverse shear stress?
- (g) Calculate the direct shear stress that would result in the bar of (a) if it were the pin in a pin-and-clevis connection as in Figure P4-8 that is subjected to a 1000-lb pull.
- (h) Calculate the direct bearing stress that would result on the bar of (a) if it were the pin in a pin-and-clevis connection as in Figure P4-8 that is subjected to a 1000-lb pull if the center part (the eye or tongue) is 1-in wide.
- (i) Calculate the maximum bending stress in the bar if it is formed into a semicircle with a centroidal radius of $10/\pi$ in and 1000-lb opposing forces are applied at the ends and in the plane of the ends similar to Figure P4-15. Assume that there is no distortion of the cross section during bending.
- *4-75 For a filleted flat bar loaded in tension similar to that shown in Figure C-9 (Appendix C) and the data from the row(s) assigned from Table P4-4, determine the nominal and maximum axial stress in the bar.
- 4-76 For a filleted flat bar loaded in bending similar to that shown in Figure C-10 (Appendix C) and the data from the row(s) assigned from Table P4-4, determine the nominal and maximum bending stress in the bar.
- 4-77 For a shaft, with a shoulder fillet, loaded in tension similar to that shown in Figure C-1 (Appendix C) and the data from the row(s) assigned from Table P4-4, determine the nominal and maximum axial stress in the shaft.
- 4-78 For a shaft, with a shoulder fillet, loaded in bending similar to that shown in Figure C-2 (Appendix C) and the data from the row(s) assigned from Table P4-4, determine the nominal and maximum bending stress in the shaft.
- 4-79 A differential stress element has a set of applied stresses on it as shown in Figure 4-1 (p. 142). For $\sigma_x = 850$, $\sigma_y = -200$, $\sigma_z = 300$, $\tau_{xy} = 450$, $\tau_{yz} = -300$, and $\tau_{zx} = 0$; find the principal stresses and maximum shear stress and draw the Mohr's circle diagram for this three-dimensional stress state.
- 4-80 Write expressions for the normalized (stress/pressure) tangential stress as a function of the normalized wall thickness (wall thickness/outside radius) at the inside wall of a thick-wall cylinder and for a thin-wall cylinder, both with internal pressure only. Plot the percent difference between these two expressions and determine the range of the wall

Table P4-4 Data for Problems 4-75 through 4-78

Use only data that are relevant to the particular problem
Lengths are in mm, forces in N, and moments in N-m

Row	D	d	r	h	M	P
a	40	20	4	10	80	8000
b	26	20	1	12	100	9500
c	36	30	1.5	8	60	6500
d	33	30	1	8	75	7200
e	21	20	1	10	50	5500
f	51	50	1.5	7	80	8000
g	101	100	5	8	400	15000

* Answers to these problems are provided in Appendix D. Problem numbers in *italics* are design problems.

† Problem numbers in *italics* are design problems.

thickness to outside radius-ratio for which the stress predicted by the thin-wall expression is at least 5% greater than that predicted by the thick-wall expression.

- 4-81 A hollow square torsion bar such as that shown in Table 4-3 (p. 179) has dimensions $a = 25$ mm, $t = 3$ mm, and $l = 300$ mm. If it is made of steel with a modulus of rigidity of $G = 80.8$ GPa, determine the maximum shear stress in the bar and the angular deflection under a torsional load of 500 N-m.
- 4-82 Design a hollow rectangular torsion bar such as that shown in Table 4-3 (p. 179) that has dimensions $a = 45$ mm, $b = 20$ mm, and $l = 500$ mm. It is made of steel with a shear yield strength of 90 MPa and has an applied torsional load of 135 N-m. Use a factor of safety against yielding of 2.
- 4-83 A pressure vessel with closed ends has the following dimensions: outside diameter, $OD = 450$ mm, and wall thickness, $t = 6$ mm. If the internal pressure is 690 kPa, find the principal stresses on the inside surface away from the ends. What is the maximum shear stress at the point analyzed?
- 4-84 A simply supported steel beam of length l with a concentrated load, F , acting at midspan has a rectangular cross-section of width, b , and depth, h . If the strain energy due to transverse shear loading is U_s and that due to bending loading is U_b , derive an expression for the ratio U_s / U_b and plot it as a function of h / l over the range 0.0 to 0.10.
- 4-85 A beam is supported and loaded as shown in Figure P4-27a. Find the reactions for the data given in row a from Table P4-2.
- 4-86 A beam is supported and loaded as shown in Figure P4-27b. Find the reactions for the data given in row a from Table P4-2.

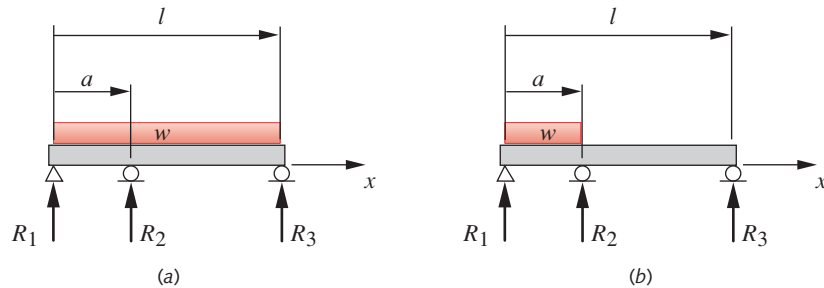


FIGURE P4-27

Beams and Beam Loadings for Problem 4-85 to 4-86 - see Table P4-2 for Data

5



STATIC FAILURE THEORIES

The whole of science is nothing more than a refinement of everyday thinking.

Albert Einstein

5.0 INTRODUCTION

Why do parts fail? This is a question that has occupied scientists and engineers for centuries. Much more is understood about various failure mechanisms today than was known even a few decades ago, largely due to improved testing and measuring techniques. If you were asked to respond to the above question based on what you have learned so far, you would probably say something like “Parts fail because their stresses exceed their strength,” and you would be right up to a point. The follow-up question is the critical one; what kind of stresses cause the failure: Tensile? Compressive? Shear? The answer to this one is the classic, “It depends.” It depends on the material in question and its relative strengths in compression, tension, and shear. It also depends on the character of the loading (whether static or dynamic) and on the presence or absence of cracks in the material.

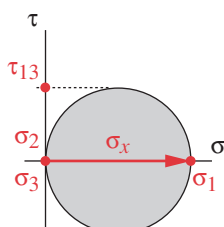
Table 5-0 shows the variables used in this chapter and references the equations or sections in which they are used. At the end of the chapter, a summary section is provided that also groups all the significant equations from this chapter for easy reference and identifies the chapter section in which their discussion can be found.

Figure 5-1a shows the Mohr’s circle for the stress state in a tensile test specimen. The tensile test (see Section 2-1) slowly applies a pure tensile loading to the part and causes a tensile, normal stress. However, the Mohr’s circle shows that a shear stress is also present, which happens to be exactly half as large as the normal stress. Which stress failed the part, the normal stress or the shear stress?

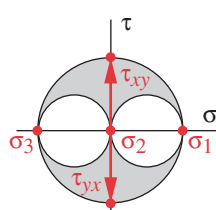
Figure 5-1b shows the Mohr’s circle for the stress state in a torsion test specimen. The torsion test (see Section 2-1) slowly applies a pure torsion loading to the part and

Table 5-0 Variables Used in This Chapter

Symbol	Variable	ips units	SI units	See
a	half-width of crack	in	m	Sect. 5.3
b	half-width of cracked plate	in	m	Sect. 5.3
E	Young's modulus	psi	Pa	Sect. 5.1
K	stress intensity	kpsi-in ^{0.5}	MPa-m ^{0.5}	Sect. 5.3
K_c	fracture toughness	kpsi-in ^{0.5}	MPa-m ^{0.5}	Sect. 5.3
N	safety factor	none	none	Sect. 5.1
N_{FM}	safety factor for fracture-mechanics failure	none	none	Sect. 5.3
S_{uc}	ultimate compressive strength	psi	Pa	Sect. 5.2
S_{ut}	ultimate tensile strength	psi	Pa	Sect. 5.2
S_y	tensile yield strength	psi	Pa	Eq. 5.8a, 5.9b
S_{ys}	shear yield strength	psi	Pa	Eq. 5.9b, 5.10
U	total strain energy	in-lb	Joules	Eq. 5.1
U_d	distortion strain energy	in-lb	Joules	Eq. 5.2
U_h	hydrostatic strain energy	in-lb	Joules	Eq. 5.2
β	stress-intensity geometry factor	none	none	Eq. 5.14c
ϵ	strain	none	none	Sect. 5.1
ν	Poisson's ratio	none	none	Sect. 5.1
σ_1	principal stress	psi	Pa	Sect. 5.1
σ_2	principal stress	psi	Pa	Sect. 5.1
σ_3	principal stress	psi	Pa	Sect. 5.1
$\tilde{\sigma}$	Modified-Mohr effective stress	psi	Pa	Eq. 5.12
σ'	von Mises effective stress	psi	Pa	Eq. 5.7



(a)



(b)

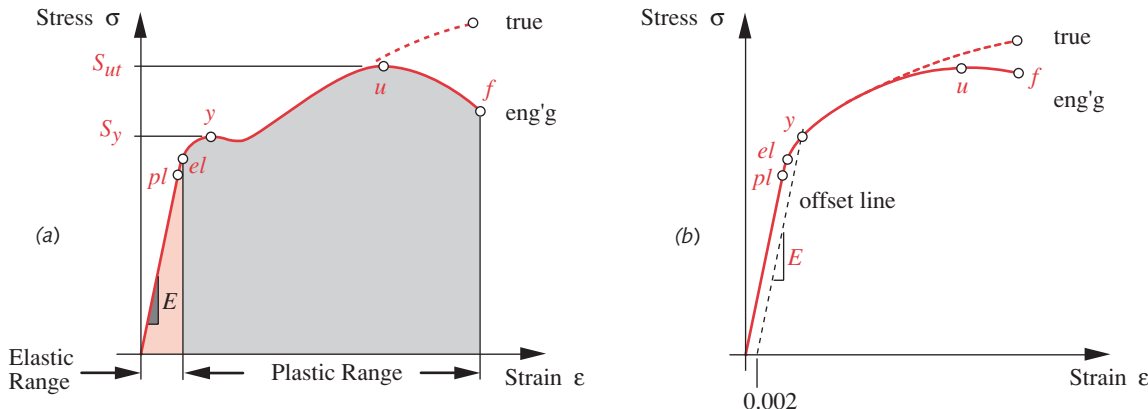
FIGURE 5-1

Mohr's Circles for Unidirectional Tensile Stress (a) and Pure Torsion (b)

causes a shear stress. However, the Mohr's circle shows that a normal stress is also present, which happens to be exactly equal to the shear stress. Which stress failed the part, the normal stress or the shear stress?

In general, ductile, isotropic materials in static tensile loading are limited by their shear strengths while brittle materials are limited by their tensile strengths (though there are exceptions to this rule when ductile materials can behave as if brittle). This situation requires that we have different failure theories for the two classes of materials, ductile and brittle. Recall from Chapter 2 that ductility can be defined in several ways, the most common being a material's percent elongation to fracture, which, if >5%, is considered ductile. Most ductile metals have elongations to fracture >10%.

Most importantly, we must carefully define what we mean by failure. A part may fail if it yields and distorts sufficiently to not function properly. Also, a part may fail by fracturing and separating. Either of these conditions is a failure, but the mechanisms causing them can be very different. Only ductile materials may yield significantly before fracturing. Brittle materials proceed to fracture without significant shape change. The stress-strain curves of each type of material reflect this difference, as shown in Figures 2-2 and 2-4, which are reproduced here for your convenience. Note that if cracks

**FIGURE 2-2** Repeated

Engineering and True Stress-Strain Curves for Ductile Materials: (a) Low-Carbon Steel (b) Annealed High-Carbon Steel

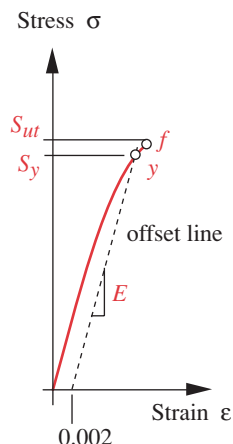
are present in a ductile material, it can suddenly fracture at nominal stress levels well below the yield strength, even under static loads.

Another significant factor in failure is the character of the loading, whether it is static or dynamic. Static loads are slowly applied and remain essentially constant with time. Dynamic loads are either suddenly applied (impact loads) or repeatedly varied with time (fatigue loads), or both. The failure mechanisms are quite different in either case. Table 3-1 (p. 75) defined four classes of loading based on the motion of the loaded parts and the time dependence of the loading. By that definition, only Class 1 loading is static. The other three classes are dynamic to a greater or lesser degree. When the loading is dynamic, the distinction between ductile and brittle materials' failure behavior blurs, and ductile materials fail in a "brittle" manner. Because of the significant differences in failure mechanisms under static and dynamic loading, we will consider them each separately, discussing failures due to static loading in this chapter and failures due to dynamic loading in the next chapter. For the static loading case (Class 1), we will consider the theories of failure separately for each type of material, ductile and brittle.

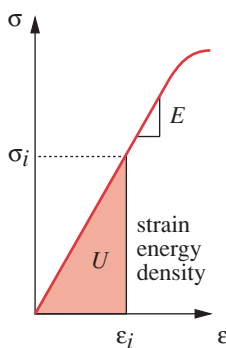
5.1 FAILURE OF DUCTILE MATERIALS UNDER STATIC LOADING

While ductile materials will fracture if statically stressed beyond their ultimate tensile strength, their failure in machine parts is generally considered to occur when they yield under static loading. The yield strength of a ductile material is appreciably less than its ultimate strength.

Historically, several theories have been formulated to explain this failure: *the maximum normal-stress theory, the maximum normal-strain theory, the total strain-energy theory, the distortion-energy (von Mises-Hencky) theory, and the maximum shear-stress theory*. Of these only the last two agree closely with experimental data for this case, and of those, the von Mises-Hencky theory is the most accurate. We will discuss only the last two in detail, starting with the most accurate (and preferred) approach.

**FIGURE 2-4** Repeated

Stress-Strain Curve of a Brittle Material



5

FIGURE 5-2

Internal Strain Energy Density in a Deflected Part

The von Mises-Hencky or Distortion-Energy Theory

The microscopic yielding mechanism is now understood to be due to relative sliding of the material's atoms within their lattice structure. This sliding is caused by shear stress and is accompanied by distortion of the shape of the part. The energy stored in the part from this distortion is an indicator of the magnitude of the shear stress present.

TOTAL STRAIN ENERGY It was once thought that the total strain energy stored in the material was the cause of yield failure, but experimental evidence did not bear this out. The strain energy U in a unit volume (strain energy density) associated with any stress is the area under the stress-strain curve up to the point of the applied stress, as shown in Figure 5-2 for a unidirectional stress state. Assuming that the stress-strain curve is essentially linear up to the yield point, then we can express the total strain energy in a unit volume at any point in that range as

$$U = \frac{1}{2} \sigma \epsilon \quad (5.1a)$$

Extending this to a three-dimensional stress state gives

$$U = \frac{1}{2} (\sigma_1 \epsilon_1 + \sigma_2 \epsilon_2 + \sigma_3 \epsilon_3) \quad (5.1b)$$

using the principal stresses and principal strains that act on planes of zero shear stress.

This expression can be put in terms of principal stresses alone by substituting the relationships

$$\begin{aligned} \epsilon_1 &= \frac{1}{E} (\sigma_1 - v\sigma_2 - v\sigma_3) \\ \epsilon_2 &= \frac{1}{E} (\sigma_2 - v\sigma_1 - v\sigma_3) \\ \epsilon_3 &= \frac{1}{E} (\sigma_3 - v\sigma_1 - v\sigma_2) \end{aligned} \quad (5.1c)$$

where v is Poisson's ratio, giving

$$U = \frac{1}{2E} [\sigma_1^2 + \sigma_2^2 + \sigma_3^2 - 2v(\sigma_1\sigma_2 + \sigma_2\sigma_3 + \sigma_1\sigma_3)] \quad (5.1d)$$

HYDROSTATIC LOADING Very large amounts of strain energy can be stored in materials without failure if they are hydrostatically loaded to create stresses that are uniform in all directions. This can be done in compression very easily by placing the specimen in a pressure chamber. Many experiments have shown that materials can be hydrostatically stressed to levels well beyond their ultimate strengths in compression without failure, as this just reduces the volume of the specimen without changing its shape. P. W. Bridgman subjected water ice to 1 Mpsi hydrostatic compression with no failure. The explanation is that uniform stresses in all directions, while creating volume change and potentially large strain energies, cause no distortion of the part and thus no shear stress. Consider the Mohr's circle for a specimen subjected to $\sigma_x = \sigma_y = \sigma_z = 1$ Mpsi compressive stress. The Mohr's "circle" is a point on the σ axis at -1 Mpsi and $\sigma_1 = \sigma_2 = \sigma_3$. The shear stress is zero, so there is no distortion and no failure. This is true for ductile or brittle materials when the principal stresses are identical in magnitude and sign.

Den Hartog^[1] describes the condition of rocks at great depth in the earth's crust where they withstand uniform, hydrostatic compressive stresses of 5 500 psi/mile of depth due to the weight of the rock above. This is in excess of their typical 3 000 psi ultimate compressive strength as measured in a compression test. While it is much more difficult to create hydrostatic tension, Den Hartog^[1] also describes such an experiment done by the Russian scientist Joffe in which he slowly cooled a glass marble in liquid air, allowed it to equilibrate to a stress-free state at the low temperature, then removed it to a warm room. As the marble warmed from the outside in, the temperature differential versus its cold core created uniform tensile stresses calculated to be well in excess of the material's tensile strength, but it did not crack. Thus, it appears that distortion is the culprit in tensile failure as well.

COMPONENTS OF STRAIN ENERGY The total strain energy in a loaded part (Eq. 5.1d) can be considered to consist of two components—one due to hydrostatic loading which changes its volume, and one due to distortion, which changes its shape. If we separate the two components, the **distortion-energy** portion will give a measure of the shear stress present. Let U_h represent the hydrostatic or volumetric component and U_d the **distortion-energy component**, then

$$U = U_h + U_d \quad (5.2)$$

We can also express each of the principal stresses in terms of a hydrostatic (or volumetric) component σ_h that is common to each face and a distortion component σ_{id} that is unique to each face, where the subscript i represents the principal stress direction, 1, 2, or 3:

$$\begin{aligned} \sigma_1 &= \sigma_h + \sigma_{1_d} \\ \sigma_2 &= \sigma_h + \sigma_{2_d} \\ \sigma_3 &= \sigma_h + \sigma_{3_d} \end{aligned} \quad (5.3a)$$

Adding the three principal stresses in equation 5.3a gives:

$$\begin{aligned} \sigma_1 + \sigma_2 + \sigma_3 &= \sigma_h + \sigma_{1_d} + \sigma_h + \sigma_{2_d} + \sigma_h + \sigma_{3_d} \\ \sigma_1 + \sigma_2 + \sigma_3 &= 3\sigma_h + (\sigma_{1_d} + \sigma_{2_d} + \sigma_{3_d}) \\ 3\sigma_h &= \sigma_1 + \sigma_2 + \sigma_3 - (\sigma_{1_d} + \sigma_{2_d} + \sigma_{3_d}) \end{aligned} \quad (5.3b)$$

For a volumetric change with no distortion, the term in parentheses in equation 5.3b must be zero, giving an expression for the volumetric or hydrostatic component of stress σ_h :

$$\sigma_h = \frac{\sigma_1 + \sigma_2 + \sigma_3}{3} \quad (5.3c)$$

which you will note is merely the average of the three principal stresses.

Now, the strain energy U_h associated with the hydrostatic volume change can be found by replacing each principal stress in equation 5.1d with σ_h :

$$\begin{aligned} U_h &= \frac{1}{2E} [\sigma_h^2 + \sigma_h^2 + \sigma_h^2 - 2v(\sigma_h \sigma_h + \sigma_h \sigma_h + \sigma_h \sigma_h)] \\ &= \frac{1}{2E} [3\sigma_h^2 - 2v(3\sigma_h^2)] \\ U_h &= \frac{3}{2} \frac{(1-2v)}{E} \sigma_h^2 \end{aligned} \quad (5.4a)$$

and substituting equation 5.3c:

$$\begin{aligned} U_h &= \frac{3}{2} \frac{(1-2v)}{E} \left(\frac{\sigma_1 + \sigma_2 + \sigma_3}{3} \right)^2 \\ &= \frac{1-2v}{6E} [\sigma_1^2 + \sigma_2^2 + \sigma_3^2 + 2(\sigma_1\sigma_2 + \sigma_2\sigma_3 + \sigma_1\sigma_3)] \end{aligned} \quad (5.4b)$$

DISTORTION ENERGY The distortion energy U_d is now found by subtracting equation 5.4b from 5.1d in accordance with equation 5.2:

$$\begin{aligned} U_d &= U - U_h \\ &= \left\{ \frac{1}{2E} [\sigma_1^2 + \sigma_2^2 + \sigma_3^2 - 2v(\sigma_1\sigma_2 + \sigma_2\sigma_3 + \sigma_1\sigma_3)] \right\} \\ &\quad - \left\{ \frac{1-2v}{6E} [\sigma_1^2 + \sigma_2^2 + \sigma_3^2 + 2(\sigma_1\sigma_2 + \sigma_2\sigma_3 + \sigma_1\sigma_3)] \right\} \\ U_d &= \frac{1+v}{3E} [\sigma_1^2 + \sigma_2^2 + \sigma_3^2 - \sigma_1\sigma_2 - \sigma_2\sigma_3 - \sigma_1\sigma_3] \end{aligned} \quad (5.5)$$

To obtain a failure criterion, we will compare the distortion energy per unit volume given by equation 5.5 to the distortion energy per unit volume present in a tensile test specimen at failure, because the tensile test is our principal source of material-strength data. The failure stress of interest here is the yield strength S_y . The tensile test is a **uniaxial stress state** where, at yield, $\sigma_1 = S_y$ and $\sigma_2 = \sigma_3 = 0$. The distortion energy associated with yielding in the tensile test is found by substituting these values in equation 5.5:

$$U_d = \frac{1+v}{3E} S_y^2 \quad (5.6a)$$

and the failure criterion is obtained by equating the general expression 5.5 with the specific failure expression 5.6a to get

$$\begin{aligned} \frac{1+v}{3E} S_y^2 &= U_d = \frac{1+v}{3E} [\sigma_1^2 + \sigma_2^2 + \sigma_3^2 - \sigma_1\sigma_2 - \sigma_2\sigma_3 - \sigma_1\sigma_3] \\ S_y^2 &= \sigma_1^2 + \sigma_2^2 + \sigma_3^2 - \sigma_1\sigma_2 - \sigma_2\sigma_3 - \sigma_1\sigma_3 \\ S_y &= \sqrt{\sigma_1^2 + \sigma_2^2 + \sigma_3^2 - \sigma_1\sigma_2 - \sigma_2\sigma_3 - \sigma_1\sigma_3} \end{aligned} \quad (5.6b)$$

which applies to the three-dimensional stress state.

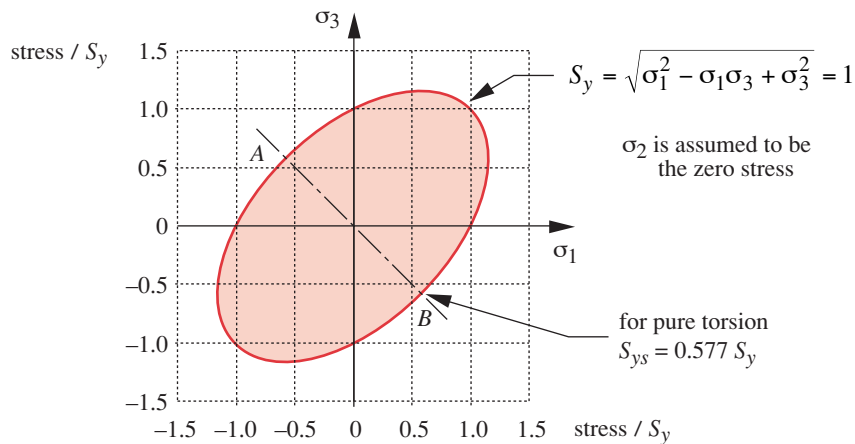
For a two-dimensional stress state, $\sigma_2 = 0^*$ and equation 5.6b reduces to:

$$S_y = \sqrt{\sigma_1^2 - \sigma_1\sigma_3 + \sigma_3^2} \quad (5.6c)$$

The two-dimensional distortion-energy equation 5.6c describes an ellipse, which when plotted on the σ_1 , σ_3 axes is as shown in Figure 5-3. The interior of this ellipse defines the region of combined biaxial stresses safe against yielding under static loading.

The three-dimensional distortion-energy equation 5.6b describes a circular cylinder, inclined to the σ_1 , σ_2 , σ_3 axes with each of its three Euler angles 45° as shown in Figure 5-4. The interior of this cylinder defines the region safe against yielding for combined stresses σ_1 , σ_2 , σ_3 . The axis of the cylinder is the locus of all hydrostatic stress

* Note that this assumption will be consistent with the conventional ordering of principal stresses in the 3-D case ($\sigma_1 > \sigma_2 > \sigma_3$) only if $\sigma_3 < 0$. If both nonzero principal stresses are positive, then the assumption that $\sigma_2 = 0$ violates the ordering convention. Nevertheless we will use σ_1 and σ_3 to represent the two nonzero principal stresses in the 2-D case regardless of their signs in order to simplify their representation in figures and equations.

**FIGURE 5-3**

The 2-D Distortion-Energy Ellipse Normalized to the Yield Strength of the Material

and extends to $\pm\infty$, further indication that hydrostatic stress alone will not fail a ductile material. The intersections of this cylinder with each of the three principal planes are ellipses as shown in Figures 5-3 and 5-4b.

VON MISES EFFECTIVE STRESS It is often convenient in situations involving combined tensile and shear stresses acting on the same point to define an effective stress that can be used to represent the stress combination. The distortion-energy approach provides a good means to do this for ductile materials. The **von Mises effective stress** σ' is defined as *the uniaxial tensile stress that would create the same distortion energy as is created by the actual combination of applied stresses*. This approach allows us to treat cases of combined, multiaxial tension and shear stresses as if they were due to pure tensile loading.

The von Mises effective stress σ' for the three-dimensional case is, from equation 5.6b:

$$\sigma' = \sqrt{\sigma_1^2 + \sigma_2^2 + \sigma_3^2 - \sigma_1\sigma_2 - \sigma_2\sigma_3 - \sigma_1\sigma_3} \quad (5.7a)$$

This can also be expressed in terms of the applied stresses:

$$\sigma' = \sqrt{\frac{(\sigma_x - \sigma_y)^2 + (\sigma_y - \sigma_z)^2 + (\sigma_z - \sigma_x)^2 + 6(\tau_{xy}^2 + \tau_{yz}^2 + \tau_{zx}^2)}{2}} \quad (5.7b)$$

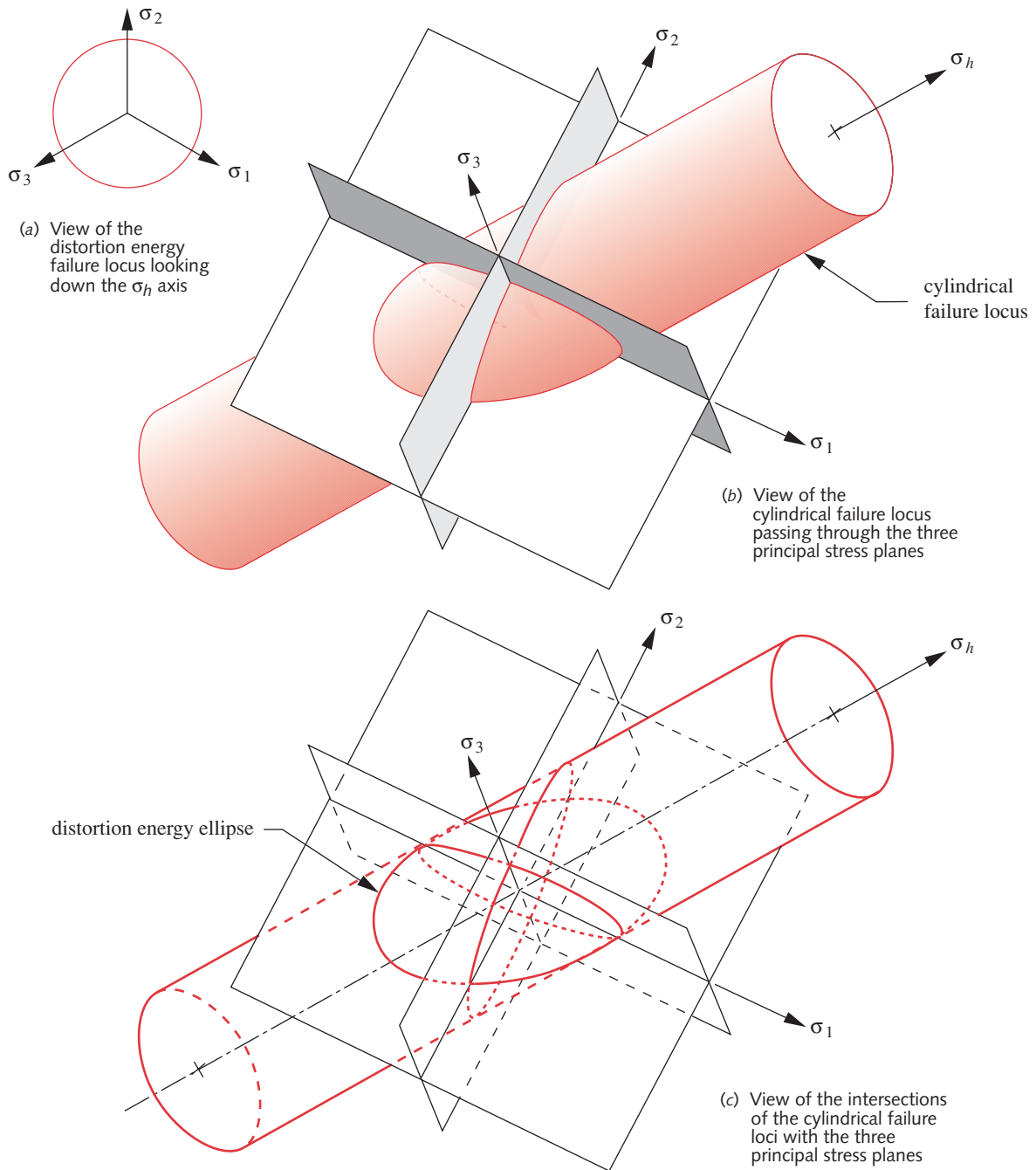
and for the two-dimensional case from equation 5.6c (with $\sigma_2 = 0$):

$$\sigma' = \sqrt{\sigma_1^2 - \sigma_1\sigma_3 + \sigma_3^2} \quad (5.7c)$$

and if expressed in terms of the applied stresses:

$$\sigma' = \sqrt{\sigma_x^2 + \sigma_y^2 - \sigma_x\sigma_y + 3\tau_{xy}^2} \quad (5.7d)$$

Use these effective stresses for any combined stress situation. (See Example 5-1 on p. 256.) This von Mises effective stress will be revisited later when examples of combined stresses are encountered.

**FIGURE 5-4**

Three-Dimensional Failure Locus for the Distortion Energy Theory

SAFETY FACTOR Equations 5.6b and 5.6c define the conditions at failure. For design purposes it is convenient to include a chosen safety factor N in the calculation so that the stress state will be safely inside the failure-stress ellipse of Figure 5-3.

$$N = \frac{S_y}{\sigma'} \quad (5.8a)$$

For the three-dimensional stress case this becomes

$$\frac{S_y}{N} = \sqrt{\sigma_1^2 + \sigma_2^2 + \sigma_3^2 - \sigma_1\sigma_2 - \sigma_2\sigma_3 - \sigma_1\sigma_3} \quad (5.8b)$$

and for the two-dimensional stress case:

$$\frac{S_y}{N} = \sqrt{\sigma_1^2 - \sigma_1\sigma_3 + \sigma_3^2} \quad (5.8c)$$

PURE SHEAR For the case of pure shear as encountered in pure torsional loading the principal stresses become $\sigma_1 = \tau = -\sigma_3$ and $\sigma_2 = 0$ as shown in Figure 5-1b (p. 244). Figure 5-3 also shows the pure torsional stress state plotted on the σ_1, σ_3 axes. The locus of pure torsional shear stress is a straight line through the origin at -45° . This line intersects the failure ellipse at two points, A and B. The absolute values of σ_1 and σ_3 at these points are found from equation 5.6c (p. 248) for the two-dimensional case.

$$\begin{aligned} S_y^2 &= \sigma_1^2 + \sigma_1\sigma_3 + \sigma_3^2 = 3\sigma_1^2 = 3\tau_{max}^2 \\ \sigma_1 &= \frac{S_y}{\sqrt{3}} = 0.577 S_y = \tau_{max} \end{aligned} \quad (5.9a)$$

This relationship defines the **shear yield strength** S_{ys} of any ductile material as a fraction of its yield strength in tension S_y determined from the tensile test.

$$S_{ys} = 0.577 S_y \quad (5.9b)$$

DUCTILE FAILURE THEORY We can now answer the question posed in the first paragraph of this chapter as to whether the shear stress or the tensile stress was responsible for the failure of a ductile specimen in the tensile test. Based on experiments and the distortion energy theory, *failure in the case of ductile materials in static tensile loading is considered to be due to shear stress*.

A HISTORICAL NOTE The distortion-energy approach to failure analysis has many fathers. In fact, equations 5.7 can be derived by five different approaches^[2]. The distortion-energy method presented here was originally proposed by James Clerk Maxwell^[3] in 1856 but not further developed until additional contributions were made in 1904 by Hueber, in 1913 by von Mises, and in 1925 by Hencky. Today it is most often credited to von Mises and Hencky, and sometimes only to von Mises. The effective stress defined in equations 5.7 is usually referred to as the von Mises or just the Mises (pronounced mees) stress. Eichinger (in 1926) and Nadai (in 1937) independently developed equations 5.7 by a different method involving **octahedral stresses**, and others have arrived at the same result by still different routes. The number of independent developments of this theory using different approaches, in combination with the very close correlation of experimental data to its predictions, make it the *best choice for predicting failure in the case of static loading of ductile materials in which the tensile and compressive strengths are equal*.

The Maximum Shear-Stress Theory

The role of shear stress in static failure was recognized prior to the development of the von Mises approach to the failure analysis of ductile materials under static loading. The maximum shear-stress theory was first proposed by Coulomb (1736–1806) and later described by Tresca in an 1864 publication. Around the turn of the twentieth century, J. Guest performed experiments in England that confirmed the theory. It is sometimes called the Tresca-Guest theory.

5

The **maximum shear-stress theory** (or just **maximum shear theory**) states that *failure occurs when the maximum shear stress in a part exceeds the shear stress in a tensile specimen at yield (one-half of the tensile yield strength)*. This predicts that the shear yield strength of a ductile material is

$$S_{ys} = 0.50 S_y \quad (5.10)$$

Note that this is a more conservative limit than that of the distortion-energy theory given in equation 5.9b.

Figure 5-5 shows the hexagonal failure envelope for the two-dimensional maximum shear theory superposed on the distortion-energy ellipse. It is inscribed within the ellipse and contacts it at six points. Combinations of principal stresses σ_1 and σ_3 that lie within this hexagon are considered safe, and failure is considered to occur when the combined stress state reaches the hexagonal boundary. This is obviously a more conservative failure theory than distortion energy, as it is contained within the latter. The conditions for torsional (pure) shear are shown at points C and D.

For the three-dimensional stress state, Figures 5-6a and 5-6b show the hexagonal prism of the maximum shear-stress theory fitted into the distortion-energy cylinder. The intersections of the shear-stress hexagon with the three planes of principal stress are shown in Figure 5-6c, inscribed within the distortion-energy ellipses.

To use this theory for either two- or three-dimensional static stress in homogeneous, isotropic, ductile materials, first compute the three principal normal stresses σ_1 , σ_2 , σ_3

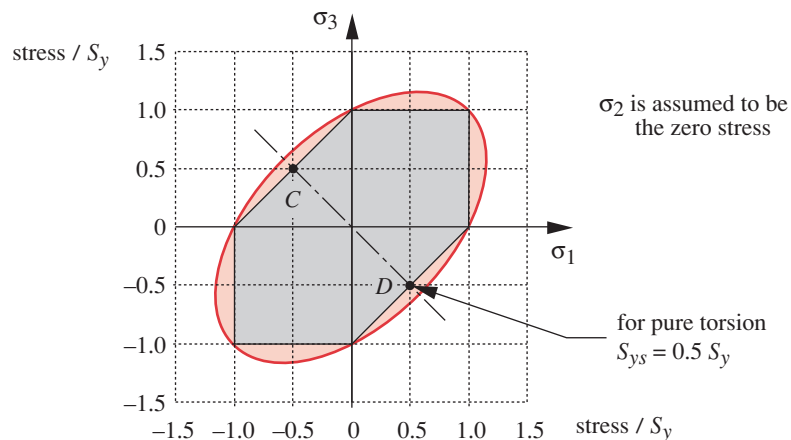
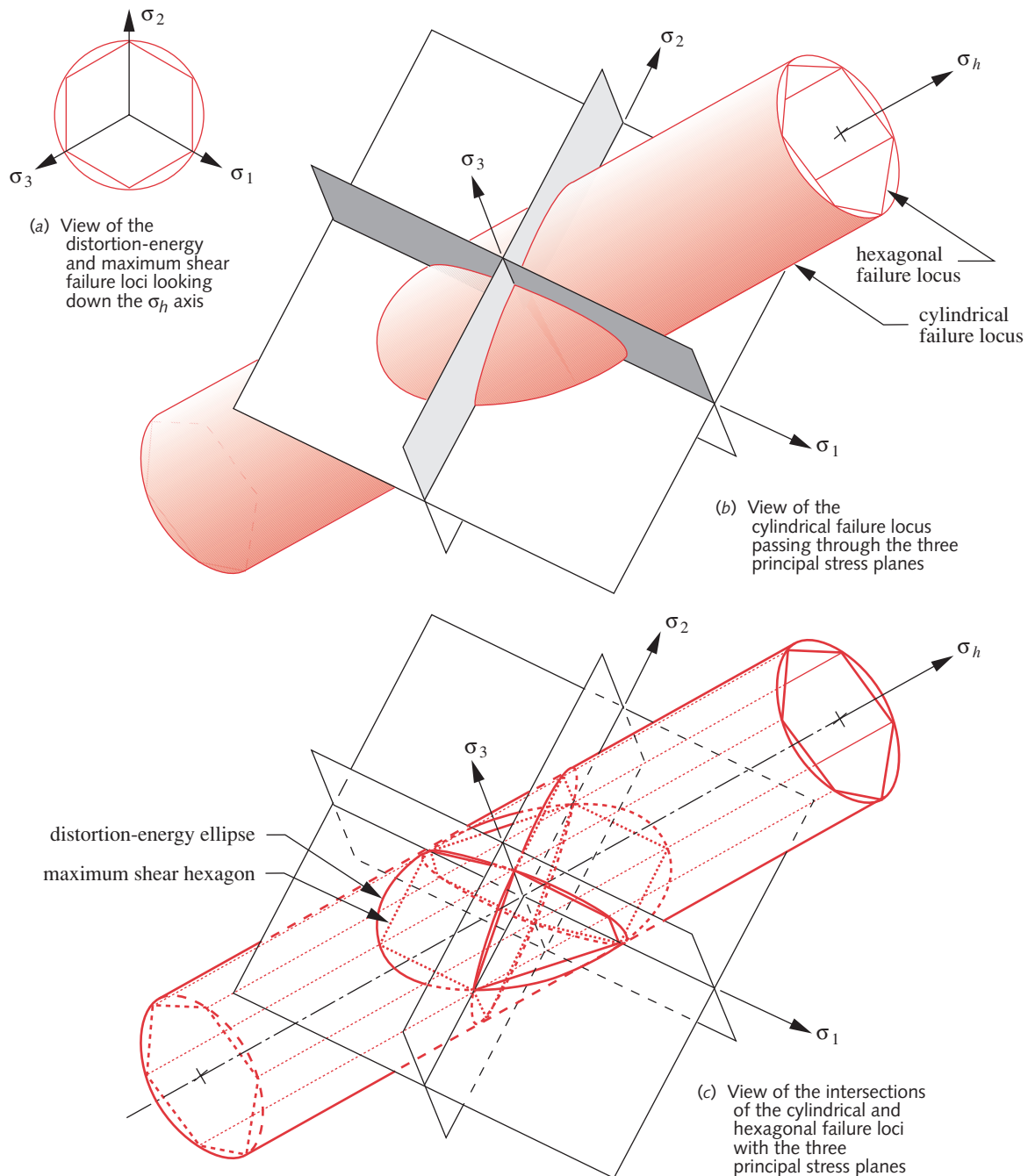


FIGURE 5-5

The 2-D Shear-Stress Theory Hexagon Inscribed Within the Distortion-Energy Ellipse

**FIGURE 5-6**

Three-Dimensional Failure Loci for the Distortion-Energy and Maximum Shear-Stress Theories

(one of which will be zero for a 2-D case) and the **maximum shear stress**, τ_{13} , as defined in equation 4.5 (p. 144). Then compare the maximum shear stress to the failure criterion in equation 5.10. The **safety factor** for the **maximum shear-stress theory** is found from

$$N = \frac{S_{ys}}{\tau_{max}} = \frac{0.50 S_y}{\tau_{max}} = \frac{S_y/2}{(\sigma_1 - \sigma_3)/2} = \frac{S_y}{(\sigma_1 - \sigma_3)} \quad (5.11)$$

where τ_{max} is the largest result from equations 4.5. Remember that in a two-dimensional applied-stress case, there can be three principal shear stresses, the largest of which is τ_{max} .

The Maximum Normal-Stress Theory

This theory is presented for historical interest and completeness **but it must be noted that it is not a safe theory to use for ductile materials.** Modifications of this theory will shortly be discussed that are valid and useful for brittle materials whose ultimate tensile strengths are lower than their shear and compressive strengths. The **maximum normal-stress theory** states that *failure will occur when the normal stress in the specimen reaches some limit on normal strength such as tensile yield strength or ultimate tensile strength.* For ductile materials, yield strength is the desired criterion.

Figure 5-7 shows the two-dimensional failure envelope for the maximum normal-stress theory. It is a square. Compare this square envelope to those shown in Figure 5-5 (p. 252). In the first and third quadrants, the maximum normal-stress theory envelope is coincident with that of the maximum shear theory. But, in the second and fourth quadrants, the normal-stress theory envelope is well outside of both the distortion-energy ellipse and its inscribed maximum-shear-theory hexagon. Since experiments show that ductile materials fail in static loading when their stress states are outside of the ellipse, the normal-stress theory is an unsafe failure criterion in the second and fourth quadrants. **The wise designer will avoid using the normal-stress theory with ductile materials.**

Comparison of Experimental Data with Failure Theories

Many tensile tests have been done on various materials. The data show statistical scatter but in the aggregate tend to fit the distortion-energy ellipse fairly well. Figure 5-8 shows experimental data for two ductile steels, two ductile aluminum alloys, and a brittle cast iron superposed on the failure envelopes for the three failure theories discussed above.

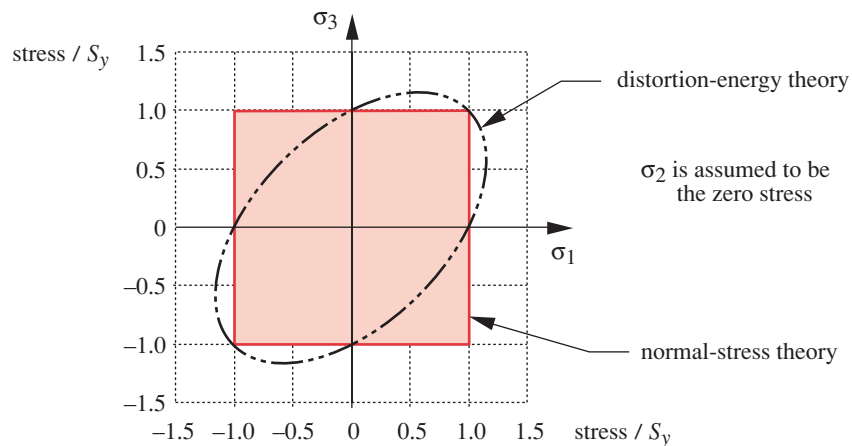


FIGURE 5-7

The Maximum Normal-Stress Theory - Incorrect for Ductile Materials in 2nd and 4th Quadrants

Note how the ductile-yield data cluster on or near the distortion-energy ellipse (labeled *oct shear*) with a few data points falling between the maximum-shear-theory hexagon and the ellipse, both of which are normalized to the yield strength of the material. The brittle cast-iron fracture (not yield) data are seen to cluster more closely about the (square) maximum normal-stress envelope, which in this figure is normalized to the ultimate tensile strength, not the yield strength.

These data are typical. From them we can see that the distortion-energy theory most closely approximates the ductile yield data and the maximum shear theory provides a more conservative criterion that is safely inside virtually all of the data points for yielding of the ductile materials. Since a safety factor will always be applied, the actual stress state can be expected to fall inside of these failure lines by some margin.

It was common in the past to recommend that the maximum shear theory be used in design rather than the more accurate distortion-energy theory because it was considered easier to calculate results using the former. This argument may (or may not) have been justified in the days of slide rules but is not defensible in an age of programmable calculators and computers. The distortion-energy method is very easy to use, even with only a pocket calculator, and provides a theoretically more accurate result. Nevertheless, since some experimental data fall inside the ellipse but outside the shear hexagon, some designers prefer the more conservative approach of the maximum shear theory. As the engineer in charge, the choice is ultimately your decision.

Both the distortion-energy theory and the maximum shear theory are acceptable as failure criteria in the case of static loading of ductile, homogeneous, isotropic materials whose compressive and tensile strengths are of the same magnitude. Most wrought engineering metals and some polymers are in this category of so-called **even materials**. **Uneven materials** such as cast-brittle metals and composites that do not exhibit these uniform properties require more complex failure theories, some of which are described in a later section and some in reference 4. See the next section for a discussion of even and uneven materials.

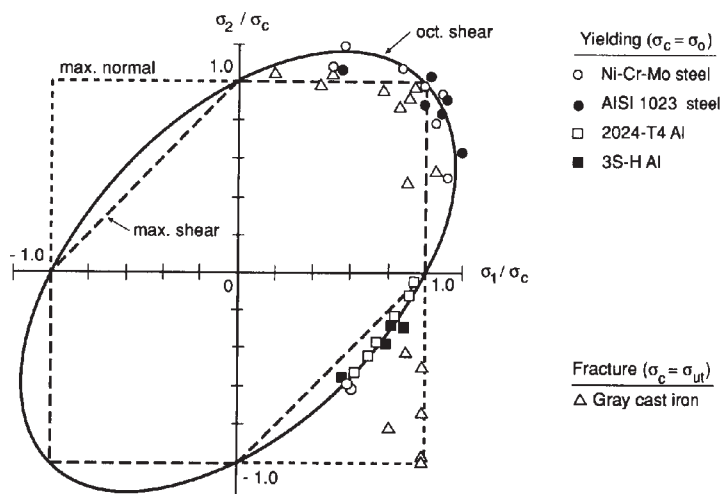
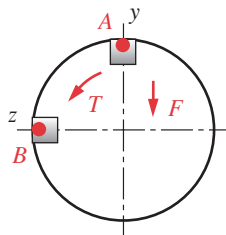
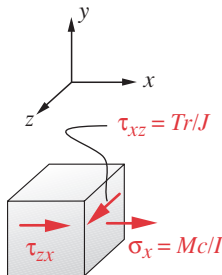


FIGURE 5-8

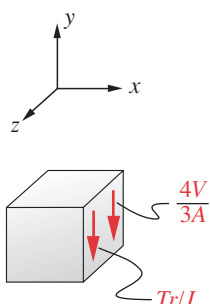
Experimental Data from Tensile Tests Superposed on Three Failure Theories (Reproduced from Fig. 7.11, p. 252, in *Mechanical Behavior of Materials* by N. E. Dowling, Prentice-Hall, Englewood Cliffs, NJ, 1993)

EXAMPLE 5-1**Failure of Ductile Materials Under Static Loading**

(a) Two points of interest for stress calculations



(b) Stress element at point A



(c) Stress element at point B

Problem

Determine the safety factors for the bracket rod shown in Figure 5-9 based on both the distortion-energy theory and the maximum shear theory and compare them.

Given

The material is 2024-T4 aluminum with a yield strength of 47 000 psi. The rod length $l = 6$ in and arm $a = 8$ in. The rod outside diameter $d = 1.5$ in. Load $F = 1\,000$ lb.

Assumptions

The load is static and the assembly is at room temperature. Consider shear due to transverse loading as well as other stresses.

Solution

See Figures 5-9 and 4-33 (repeated here). Also see Example 4-9 (p. 180) for a more complete explanation of the stress analysis for this problem.

- 1 The rod is loaded in both bending (as a cantilever beam) and in torsion. The largest tensile bending stress will be in the top outer fiber at point A. The largest torsional shear stress will be all around the outer circumference of the rod. (See Example 4-9 for more detail.) First take a differential element at point A where both of these stresses combine as shown in Figure 4-33b. Find the normal bending stress and torsional shear stress on point A using equations 4.11b (p. 156) and 4.23b (p. 178) respectively.

$$\sigma_x = \frac{Mc}{I} = \frac{(Fl)c}{I} = \frac{1\,000(6)(0.75)}{0.249} = 18\,108 \text{ psi} \quad (a)$$

$$\tau_{xz} = \frac{Tr}{J} = \frac{(Fa)r}{J} = \frac{1\,000(8)(0.75)}{0.497} = 12\,072 \text{ psi} \quad (b)$$

- 2 Find the maximum shear stress and principal stresses that result from this combination of applied stresses using equations 4.6 (p. 145).

$$\begin{aligned} \tau_{max} &= \sqrt{\left(\frac{\sigma_x - \sigma_z}{2}\right)^2 + \tau_{xz}^2} = \sqrt{\left(\frac{18\,108 - 0}{2}\right)^2 + 12\,072^2} = 15\,090 \text{ psi} \\ \sigma_1 &= \frac{\sigma_x + \sigma_z + \tau_{max}}{2} = \frac{18\,108}{2} + 15\,090 = 24\,144 \text{ psi} \\ \sigma_2 &= 0 \\ \sigma_3 &= \frac{\sigma_x + \sigma_z - \tau_{max}}{2} = \frac{18\,108}{2} - 15\,090 = -6\,036 \text{ psi} \end{aligned} \quad (c)$$

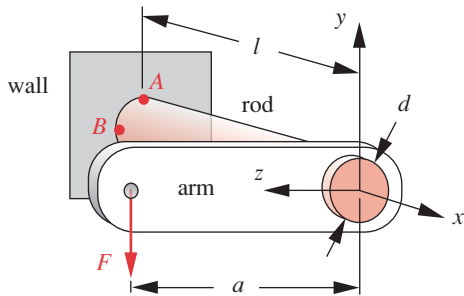
- 3 Find the von Mises effective stress from the principal stresses using equation 5.7a (p. 249) with $\sigma_2 = 0$, which is also shown as equation 5.7c (p. 249) for the 2-D case.

$$\begin{aligned} \sigma' &= \sqrt{\sigma_1^2 - \sigma_1\sigma_3 + \sigma_3^2} \\ \sigma' &= \sqrt{24\,144^2 - 24\,144(-6\,036) + (-6\,036)^2} = 27\,661 \text{ psi} \end{aligned} \quad (d)$$

- 4 The safety factor using the distortion-energy theory can now be found using equation 5.8a (p. 251).

FIGURE 4-33 Repeated

Stress Elements at Points A and B within Cross Section of Rod for Example 4-10

**FIGURE 5-9**

Bracket for Examples 5-1 and 5-2

$$N = \frac{S_y}{\sigma'} = \frac{47\,000}{27\,661} = 1.7 \quad (e)$$

- 5 The safety factor using the maximum shear-stress theory can be found from equation 5.10 (p. 252).

$$N = \frac{0.50 S_y}{\tau_{max}} = \frac{0.50(47\,000)}{15\,090} = 1.6 \quad (f)$$

- 6 Comparing these two results shows the more conservative nature of the maximum shear-stress theory, which gives a slightly lower safety factor.
- 7 Since the rod is a short beam, we need to check the shear due to transverse loading at point *B* on the neutral axis. The maximum transverse shear stress at the neutral axis of a round rod was given as equation 4.15c (p. 161).

$$\tau_{bending} = \frac{4V}{3A} = \frac{4(1\,000)}{3(1.767)} = 755 \text{ psi} \quad (g)$$

Point *B* is in pure shear. The total shear stress at point *B* is the algebraic sum of the transverse shear stress and the torsional shear stress, which both act on the same planes of the differential element in this case, in the same direction as shown in Figure 4-33c.

$$\tau_{max} = \tau_{torsion} + \tau_{bending} = 12\,072 + 755 = 12\,827 \text{ psi} \quad (h)$$

- 8 The safety factor for point *B* using the distortion energy theory for pure shear (Eq. 5.9b, p. 251) is

$$N = \frac{S_{ys}}{\tau_{max}} = \frac{0.577 S_y}{\tau_{max}} = \frac{0.577(47\,000)}{12\,827} = 2.1 \quad (i)$$

and for the maximum shear theory using equation 5.10 (p. 252) is

$$N = \frac{S_{ys}}{\tau_{max}} = \frac{0.50 S_y}{\tau_{max}} = \frac{0.50(47\,000)}{12\,827} = 1.8 \quad (j)$$

Again, the latter is more conservative.

- 9 The files EX05-01 are on the CD-ROM.

5.2 FAILURE OF BRITTLE MATERIALS UNDER STATIC LOADING

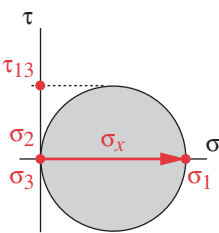
Brittle materials fracture rather than yield. **Brittle fracture in tension** is considered to be due to the normal tensile stress alone and thus the maximum normal-stress theory is applicable in this case. **Brittle fracture in compression** is due to some combination of normal compressive stress and shear stress and requires a different theory of failure. To account for all loading conditions a combination of theories is used.

Even and Uneven Materials

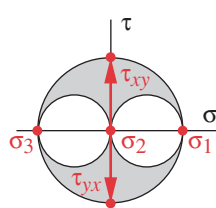
5

Some wrought materials, such as fully hardened tool steel, can be brittle. These materials tend to have compressive strengths equal to their tensile strengths and so are called *even materials*. Many cast materials, such as gray cast iron, are brittle but have compressive strengths much greater than their tensile strengths. These are called *uneven materials*. Their low tensile strength is due to the presence of microscopic flaws in the casting, which, when subjected to tensile loading, serve as nuclei for crack formation. But when subjected to compressive stress, these flaws are pressed together, increasing the resistance to slippage from the shear stress. Gray cast irons typically have compressive strengths 3 to 4 times their tensile strengths, and ceramics have even larger ratios.

Another characteristic of **some cast, brittle materials** is that their *shear strength can be greater than their tensile strength*, falling between their compressive and tensile values. This is quite different than ductile materials, in which the shear strength is about one-half the tensile strength. The effects of the stronger shear strength in cast materials can be seen in their failure characteristics in the tension and torsion tests. Figure 2-3 (p. 33) shows a ductile-steel tensile specimen whose failure plane is at 45° to the applied tensile stress, indicating a shear failure occurred, which we also know to be true from the distortion-energy theory. Figure 2-5 (p. 34) shows a brittle cast-iron tensile specimen whose failure plane is normal to the applied tensile stress, indicating that a tensile failure occurred. The Mohr's circle for this stress state is shown in Figure 5-1a, repeated here, **and is the same for both specimens**. The different failure mode is due to the difference in relative shear and tensile strengths between the two materials.



(a)



(b)

FIGURE 5-1 Repeated

Mohr's Circles for Unidirectional Tensile Stress (a) and Pure Torsion (b)

Figure 2-8 (p. 36) shows two torsion-test specimens. The Mohr's circle for the stress state in both specimens is shown in Figure 5-1b, repeated here. The ductile-steel specimen fails on a plane normal to the axis of the applied torque. The applied stress here is pure shear acting in a plane normal to the axis. The applied shear stress is also the maximum shear stress, and the failure is along the maximum shear plane because the ductile material is weakest in shear. The brittle, cast-iron specimen fails in a spiral fashion along planes inclined 45° to the specimen axis. The failure is on the planes of maximum (principal) normal stress because this material is weakest in tension.

Figure 5-10 shows Mohr's circles for both compression and tensile tests of an *even material* and an *uneven material*. The lines tangent to these circles constitute failure lines for all combinations of applied stresses between the two circles. The area enclosed by the circles and the failure lines represents a safe zone. In the case of the even material, the failure lines are independent of the normal stress and are defined by the maximum shear strength of the material. This is consistent with the maximum shear-stress theory for ductile materials (which tend also to be even materials). For the uneven material, the failure lines are a function of both the normal stress σ and the shear stress τ .

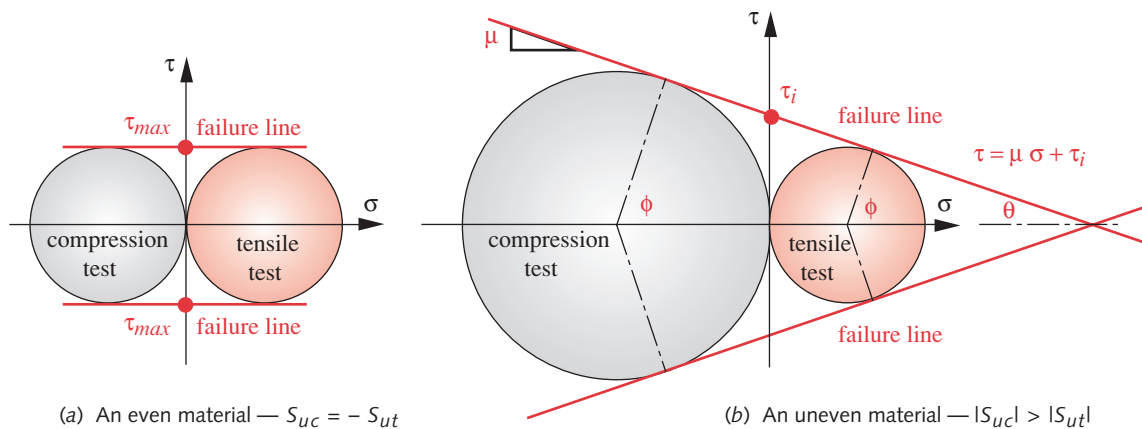


FIGURE 5-10

Mohr's Circles for Both Compression and Tensile Tests Showing the Failure Envelopes for (a) Even and (b) Uneven Materials

For the compressive regime, as the normal compressive stress component becomes increasingly negative (i.e., more compression), the material's resistance to shear stress increases. This is consistent with the idea expressed above that compression makes it more difficult for shear slippage to occur along fault lines within the material's internal flaws. The equation of the failure line can be found for any material from the test data shown in Figure 5-10. The slope μ and the intercept τ_i can be found from geometry using only the radii of the Mohr's circles from the tensile and compressive tests.

The interdependence between shear and normal stress shown in Figure 5-10b is confirmed by experiment for cases where the compressive stress is dominant, specifically where the principal stress having the largest absolute value is compressive. However, experiments also show that, in tensile-stress-dominated situations with uneven, brittle materials, failure is due to tensile stress alone. The shear stress appears not to be a factor in uneven materials if the principal stress with the largest absolute value is tensile.

The Coulomb-Mohr Theory

These observations lead to the Coulomb-Mohr theory of brittle failure, which is an adaptation of the maximum normal-stress theory. Figure 5-11 shows the two-dimensional case plotted on the σ_1 , σ_3 axes and normalized to the ultimate tensile strength, S_{ut} . The maximum normal-stress theory is shown for an *even material* as the dotted square of half-dimensions $\pm S_{ut}$. This could be used as the failure criterion for a brittle material in static loading if its compressive and tensile strengths were equal (an even material).

The maximum normal-stress theory envelope is also shown (gray-shaded) for an *uneven material* as the asymmetric square of half-dimensions S_{ut} , $-S_{uc}$. This failure envelope is only valid in the first and third quadrants as it does not account for the interdependence of the normal and shear stresses shown in Figure 5-10, which affects the second and fourth quadrants. The Coulomb-Mohr envelope (light-color shaded area) attempts to account for the interdependence by connecting opposite corners of these two quadrants with diagonals. Note the similarity of the shape of the Coulomb-Mohr hexagon to the maximum-shear-theory hexagon for ductile materials in Figure 5-5 (p. 252).

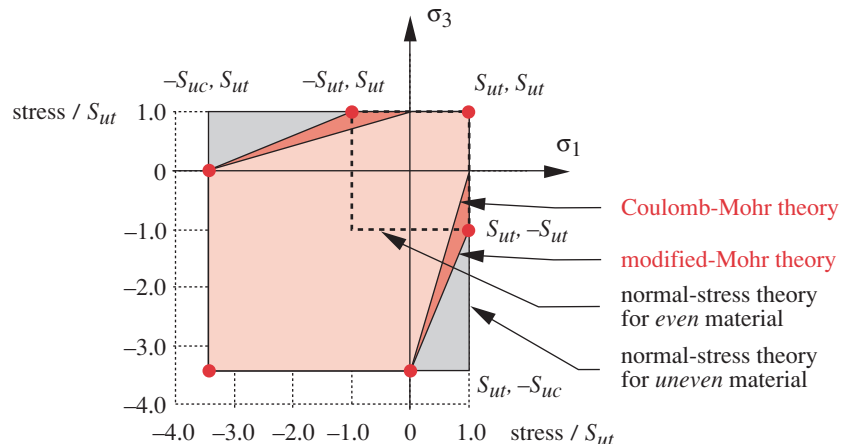


FIGURE 5-11

Coulomb-Mohr, Modified-Mohr, and Maximum Normal-Stress Theories for Uneven Brittle Materials

The only differences are the Coulomb Mohr's asymmetry due to the uneven material properties and its use of ultimate (fracture) strengths instead of yield strengths.

Figure 5-12 shows some gray cast-iron experimental test data superposed on the theoretical failure envelopes. Note that the failures in the first quadrant fit the maximum normal-stress theory line (which is coincident with the other theories). The failures in the fourth quadrant fall **inside** the maximum normal-stress line (indicating its unsuitability) and also fall well outside the Coulomb-Mohr line (indicating its conservative nature). This observation leads to a modification of the Coulomb-Mohr theory to make it better fit the observed data.

The Modified-Mohr Theory

The actual failure data in Figure 5-12 follow the even materials' maximum normal-stress theory envelope down to a point $S_{ut}, -S_{ut}$ below the σ_1 axis and then follow a straight line to $0, -S_{uc}$. This set of lines, shown as the combined light- and dark-color shaded portions of Figure 5-11 (also marked by colored dots), is the **modified-Mohr failure-theory envelope**. *It is the preferred failure theory for uneven, brittle materials in static loading.*

If the 2-D principal stresses are ordered $\sigma_1 > \sigma_3, \sigma_2 = 0$, then only the first and fourth quadrants of Figure 5-12 need to be drawn, as shown in Figure 5-13, which plots the stresses normalized by N/S_{ut} where N is the safety factor. Figure 5-13 also depicts three plane-stress conditions labeled *A*, *B*, and *C*. Point *A* represents any stress state in which the two nonzero principal stresses, σ_1, σ_3 are positive. Failure will occur when the load line *OA* crosses the failure envelope at *A'*. The safety factor for this situation can be expressed as

$$N = \frac{S_{ut}}{\sigma_1} \quad (5.12a)$$

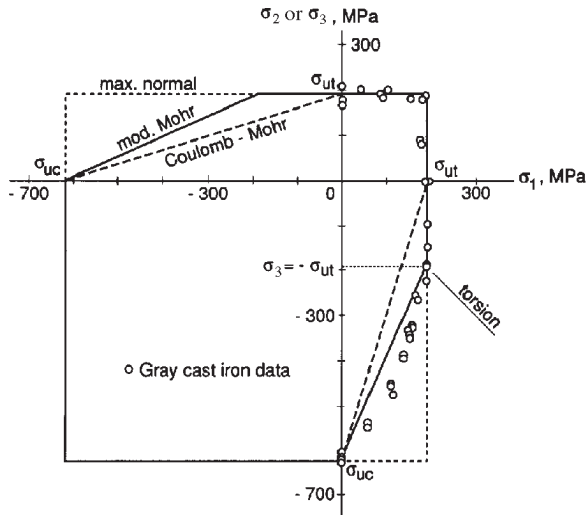


FIGURE 5-12

Biaxial Fracture Data of Gray Cast Iron Compared to Various Failure Criteria. (From Fig 7.13, p. 255, in *Mechanical Behavior of Materials* by N. E. Dowling, Prentice-Hall, Englewood Cliffs, NJ, 1993. Data from R. C. Grassi and I. Cornet, "Fracture of Gray Cast Iron Tubes under Biaxial Stresses," *J. App. Mech.*, v. 16, p.178, 1949)

If the two nonzero principal stresses have opposite sign, then two possibilities exist for failure, as depicted by points *B* and *C* in Figure 5-13. The only difference between these two points is the relative values of their two stress components σ_1, σ_3 . The load line *OB* exits the failure envelope at *B'* above the point $S_{ut}, -S_{ut}$, and the safety factor for this case is given by equation 5.12a above.

If the stress state is as depicted by point *C*, then the intersection of the load line *OC* and the failure envelope occurs at *C'* below point $S_{ut}, -S_{ut}$. The safety factor can be found by solving for the intersection between the load line *OC* and the failure line. Write the equations for these lines and solve simultaneously to get the **modified Mohr equation**.

$$N = \frac{S_{ut}|S_{uc}|}{|S_{uc}|\sigma_1 - S_{ut}(\sigma_1 + \sigma_3)} \quad (5.12b)$$

If the stress state is in the fourth quadrant, both equations 5.12a and 5.12b should be checked and the smaller resulting safety factor used.

Compare equation 5.12b to the less-accurate equation for the unmodified **Coulomb-Mohr theory** (which is not recommended for use).

$$N = \frac{S_{ut}|S_{uc}|}{|S_{uc}|\sigma_1 - S_{ut}\sigma_3}$$

To use the preferred modified Mohr theory of equation 5.12b, it would be convenient to have expressions for an **effective stress** that would account for all the applied stresses and allow direct comparison to a material-strength property, as was done for ductile materials with the von Mises stress. Dowling^[5] develops a set of expressions for this effective stress involving the three principal stresses:^{*}

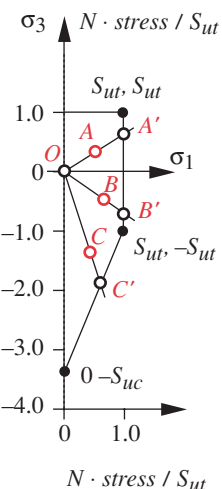


FIGURE 5-13

Modified-Mohr Failure Theory for Brittle Material

* See reference 5 for a complete derivation for both two- and three-dimensional Coulomb-Mohr and modified-Mohr theories and the effective stress.

$$\begin{aligned} C_1 &= \frac{1}{2} \left[|\sigma_1 - \sigma_2| + \frac{2S_{ut} - |S_{uc}|}{-|S_{uc}|} (\sigma_1 + \sigma_2) \right] \\ C_2 &= \frac{1}{2} \left[|\sigma_2 - \sigma_3| + \frac{2S_{ut} - |S_{uc}|}{-|S_{uc}|} (\sigma_2 + \sigma_3) \right] \\ C_3 &= \frac{1}{2} \left[|\sigma_3 - \sigma_1| + \frac{2S_{ut} - |S_{uc}|}{-|S_{uc}|} (\sigma_3 + \sigma_1) \right] \end{aligned} \quad (5.12c)$$

The largest of the set of six values (C_1, C_2, C_3 , plus the three principal stresses) is the desired effective stress as suggested by Dowling.

5

$$\begin{aligned} \tilde{\sigma} &= \text{MAX}(C_1, C_2, C_3, \sigma_1, \sigma_2, \sigma_3) \\ \tilde{\sigma} &= 0 \quad \text{if } \text{MAX} < 0 \end{aligned} \quad (5.12d)$$

where the signed function MAX denotes the algebraically largest of the six supplied arguments. If all of the arguments are negative, then the effective stress is zero.

This *modified-Mohr effective stress* can now be compared to the ultimate tensile strength of the material to determine a safety factor.

$$N = \frac{S_{ut}}{\tilde{\sigma}} \quad (5.12e)$$

This approach allows easy computerization of the process.

EXAMPLE 5-2

Failure of Brittle Materials Under Static Loading

Problem Determine the safety factors for the bracket rod shown in Figure 5-9 (repeated on next page) based on the modified-Mohr theory.

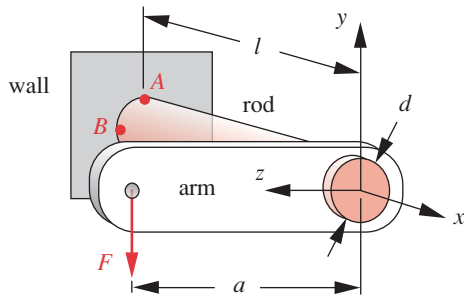
Given The material is class 50 gray cast iron with $S_{ut} = 52\ 500$ psi and $S_{uc} = -164\ 000$ psi. The rod length $l = 6$ in and arm $a = 8$ in. The rod outside diameter $d = 1.5$ in. Load $F = 1\ 000$ lb.

Assumptions The load is static and the assembly is at room temperature. Consider shear due to transverse loading as well as other stresses.

Solution See Figures 5-9 and 4-33 (opp. page) and Examples 4-9 (p. 180) and 5-1.

- 1 The rod of Figure 5-9 is loaded both in bending (as a cantilever beam) and in torsion. The largest tensile bending stress will be in the top outer fiber at point A. The largest torsional shear stress will be all around the outer circumference of the rod. First take a differential element at point A where both of these stresses combine. Find the normal bending stress and torsional shear stress on point A using equations 4.11b (p. 156) and 4.23b (p. 178), respectively.

$$\sigma_x = \frac{Mc}{I} = \frac{(Fl)c}{I} = \frac{1\ 000(6)(0.75)}{0.249} = 18\ 108 \text{ psi} \quad (a)$$

**FIGURE 5-9** Repeated

Bracket for Examples 5-1 and 5-2

$$\tau_{xz} = \frac{Tr}{J} = \frac{(Fa)r}{J} = \frac{1\ 000(8)(0.75)}{0.497} = 12\ 072 \text{ psi} \quad (b)$$

- 2 Find the maximum shear stress and principal stresses that result from this combination of applied stresses using equations 4.6.

$$\tau_{\max} = \sqrt{\left(\frac{\sigma_x - \sigma_z}{2}\right)^2 + \tau_{xz}^2} = \sqrt{\left(\frac{18\ 108 - 0}{2}\right)^2 + 12\ 072^2} = 15\ 090 \text{ psi}$$

$$\sigma_1 = \frac{\sigma_x + \sigma_z}{2} + \tau_{\max} = \frac{18\ 108}{2} + 15\ 090 = 24\ 144 \text{ psi}$$

$$\sigma_2 = 0$$

$$\sigma_3 = \frac{\sigma_x + \sigma_z}{2} - \tau_{\max} = \frac{18\ 108}{2} - 15\ 090 = -6\ 036 \text{ psi}$$

Note that these stresses are identical to those of Example 5-1.

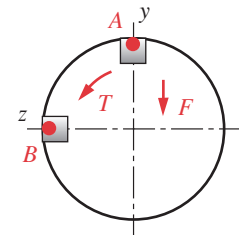
- 3 The principal stresses for point A can now be plotted on a modified-Mohr diagram as shown in Figure 5-14a (p. 264). This shows that the load line crosses the failure envelope above the $S_{ut}, -S_{ut}$ point, making equation 5.12a (p. 260) appropriate for the safety-factor calculation.

$$N = \frac{S_{ut}}{\sigma_1} = \frac{52\ 400}{24\ 144} = 2.2 \quad (d)$$

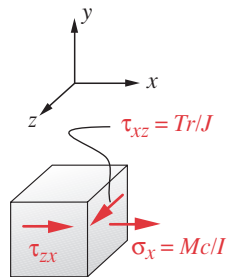
- 4 An alternative approach that does not require drawing the modified-Mohr diagram is to find the Dowling factors C_1, C_2, C_3 using equation 5.12c (p. 262).

$$C_1 = \frac{1}{2} \left[|\sigma_1 - \sigma_2| + \frac{2S_{ut} - |S_{uc}|}{-|S_{uc}|} (\sigma_1 + \sigma_2) \right] \\ = \frac{1}{2} \left[|24\ 144 - 0| + \frac{2(52\ 500) - 164\ 000}{-164\ 000} (24\ 144 + 0) \right] = 16\ 415 \text{ psi} \quad (e)$$

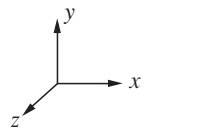
$$C_2 = \frac{1}{2} \left[|\sigma_2 - \sigma_3| + \frac{2S_{ut} - |S_{uc}|}{-|S_{uc}|} (\sigma_2 + \sigma_3) \right] \\ = \frac{1}{2} \left[|0 - (-6\ 036)| + \frac{2(52\ 500) - 164\ 000}{-164\ 000} (0 - 6\ 036) \right] = 1\ 932 \text{ psi} \quad (f)$$



(a) Two points of interest for stress calculations



(b) Stress element at point A



(c) Stress element at point B

FIGURE 4-33 Repeated

Stress Elements at Points A and B within Cross Section of Rod for Example 4-10

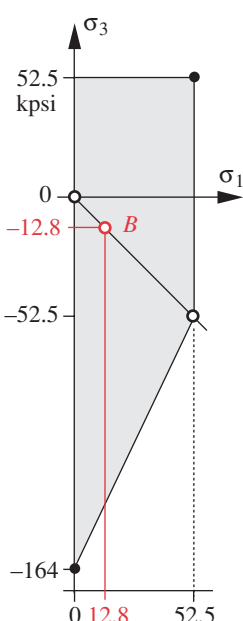
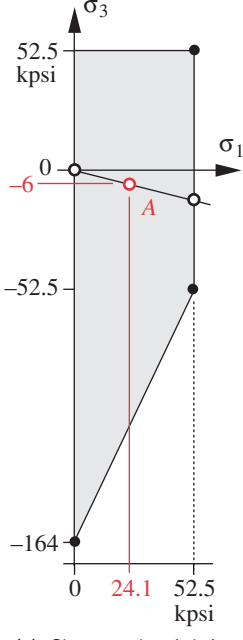


FIGURE 5-14

Example 5-2

$$\begin{aligned} C_3 &= \frac{1}{2} \left[|\sigma_3 - \sigma_1| + \frac{2S_{ut} - |S_{uc}|}{-|S_{uc}|} (\sigma_3 + \sigma_1) \right] \\ &= \frac{1}{2} \left[|24\ 144 - (-6\ 036)| + \frac{2(52\ 500) - 164\ 000}{-164\ 000} (24\ 144 - 6\ 036) \right] = 18\ 348 \quad (g) \end{aligned}$$

- 5 Then find the largest of the six stresses $C_1, C_2, C_3, \sigma_1, \sigma_2, \sigma_3$:

$$\begin{aligned} \tilde{\sigma} &= \text{MAX}(C_1, C_2, C_3, \sigma_1, \sigma_2, \sigma_3) \quad (h) \\ \tilde{\sigma} &= \text{MAX}(16\ 415, 1\ 932, 18\ 348, 24\ 144, 0, -6\ 036) = 24\ 144 \end{aligned}$$

which is the modified-Mohr effective stress.

- 6 The safety factor for point A can now be found using equation 5.12e (p. 262):

$$N = \frac{S_{ut}}{\tilde{\sigma}} = \frac{52\ 500}{24\ 144} = 2.2 \quad (i)$$

which is the same as was found in step 3.

- 7 Since the rod is a short beam, we need to check the shear stress due to transverse loading at point B on the neutral axis. The maximum transverse shear stress at the neutral axis of a solid round rod was given as equation 4.15c (p. 161).

$$\tau_{bending} = \frac{4V}{3A} = \frac{4(1\ 000)}{1.767} = 755 \text{ psi} \quad (j)$$

Point B is in pure shear. The total shear stress at point B is the algebraic sum of the transverse shear stress and the torsional shear stress, which both act on the same planes of the differential element and, in this case, act in the same direction as shown in Figure 4-33b (p. 185).

$$\tau_{max} = \tau_{torsion} + \tau_{bending} = 12\ 072 + 755 = 12\ 827 \text{ psi} \quad (k)$$

- 8 Find the principal stresses for this pure shear loading:

$$\begin{aligned} \sigma_1 &= \tau_{max} = 12\ 827 \text{ psi} \\ \sigma_2 &= 0 \\ \sigma_3 &= -\tau_{max} = -12\ 827 \text{ psi} \end{aligned} \quad (l)$$

- 9 These principal stresses for point B can now be plotted on a modified-Mohr diagram as shown in Figure 5-14b. Because this is a pure shear loading, the load line crosses the failure envelope at the $S_{ut}' - S_{ut}$ point, making equation 5.12a (p. 260) appropriate for the safety-factor calculation.

$$N = \frac{S_{ut}}{\sigma_1} = \frac{52\ 400}{12\ 827} = 4.1 \quad (m)$$

- 10 To avoid drawing the modified-Mohr diagram, find the Dowling factors C_1, C_2, C_3 using equations 5.12c:

$$\begin{aligned} C_1 &= 8\ 721 \text{ psi} \\ C_2 &= 4106 \text{ psi} \\ C_3 &= 12\ 827 \text{ psi} \end{aligned} \quad (n)$$

- 11 And find the largest of the six stresses $C_1, C_2, C_3, \sigma_1, \sigma_2, \sigma_3$:

$$\tilde{\sigma} = 12\,827 \text{ psi} \quad (o)$$

which is the modified-Mohr effective stress.

- 12 The safety factor for point B can now be found using equation 5.12e (p. 262):

$$N = \frac{S_{ut}}{\tilde{\sigma}} = \frac{52\,500}{12\,827} = 4.1 \quad (p)$$

and it is the same as was found in step 9.

- 13 The files EX05-02 are on the CD-ROM.
-

5.3 FRACTURE MECHANICS

The static failure theories discussed so far have all assumed that the material is perfectly homogeneous and isotropic, and thus free of any defects such as cracks, voids, or inclusions, which could serve as stress-raisers. This is seldom true for real materials. Actually, all materials are considered to contain microcracks too small to be seen with the naked eye. Dolan^[6] says that "... every structure contains small flaws whose size and distribution are dependent upon the material and its processing. These may vary from nonmetallic inclusions and microvoids to weld defects, grinding cracks, quench cracks, surface laps, etc." Scratches or gouges in the surface due to mishandling can also serve as incipient cracks. Functional geometric contours that are designed into the part may raise local stresses in predictable ways and can be taken into account in the stress calculations as was discussed in Chapter 4 (and will be further discussed in the next chapter). Cracks that occur spontaneously in service, due to damage or material flaws, are more difficult to predict and account for.

The presence of a sharp crack in a stress field creates stress concentrations that theoretically approach infinity. See Figure 4-35 and equation 4.32a, which are repeated here for your convenience.

$$K_t = 1 + 2\left(\frac{a}{c}\right) \quad (4.32a)$$

Note that when the value of c approaches zero, the stress concentration, and thus the stress, approaches infinity. Since no material can sustain such high stresses, local yielding (for ductile materials), local microfracture (for brittle materials), or local crazing (for polymers) will occur at the crack tip^[7]. If stresses are high enough at the tip of a crack of sufficient size, a sudden, "brittle-like" failure can result, even in ductile materials under static loads. The science of **fracture mechanics** has been developed to explain and predict this sudden-failure phenomenon.

Cracks commonly occur in welded structures, bridges, ships, aircraft, land vehicles, pressure vessels, etc. Many catastrophic failures of tankers and Liberty Ships built during World War II occurred.* [8], [9] Twelve of these failures occurred shortly after the ships were launched and before they had sailed anywhere. They simply split in half

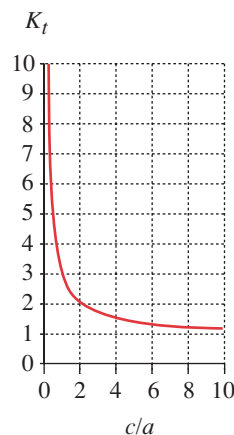
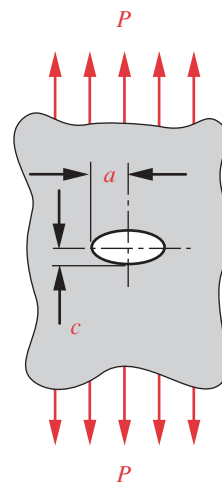


FIGURE 4-35 Repeated

Stress Concentration at the Edge of an Elliptical Hole in a Plate

* "Nearly 80 ships broke in two, and almost 1000 were found to have deck plates with long brittle fractures." D. A. Canonic, "Adjusting the Boiler Code," *Mechanical Engineering*, Feb. 2000, p.56.

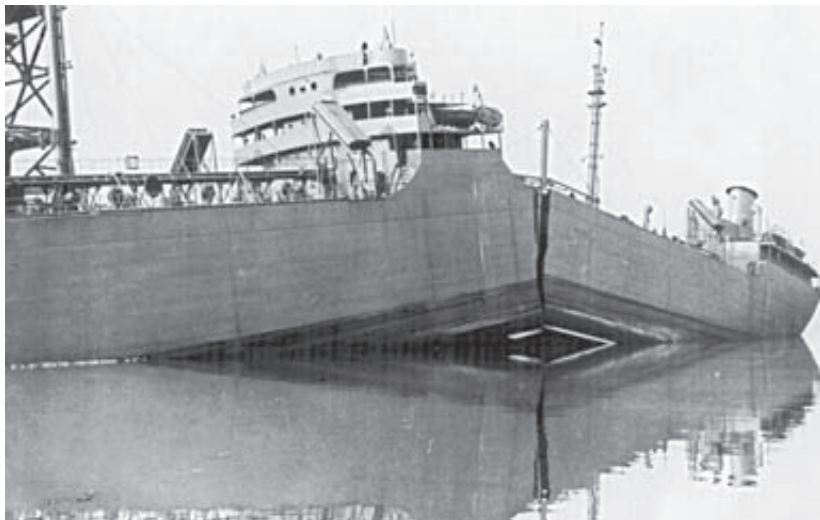


FIGURE 5-15

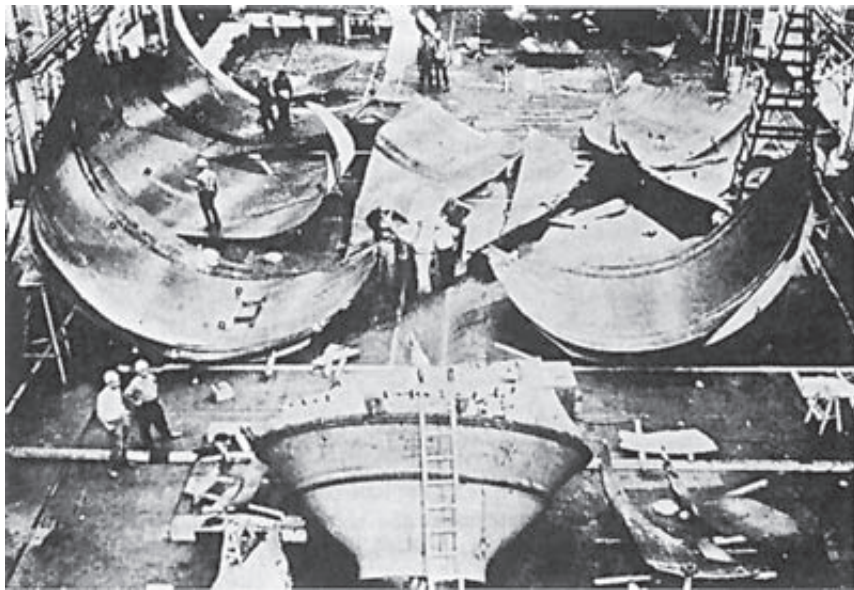
WW II Tanker Cracked in Two While Berthed Prior to Being Placed in Service, Portland, Oregon, January 16, 1943 (Courtesy of the Ship Structures Committee, U. S. Government)

while tied to the pier. One such ship is shown in Figure 5-15. The hull material was welded, ductile steel and the ship had not yet been dynamically loaded to any significant degree. The nominal stresses were well below the material's yield strength. Other examples of sudden failure at stresses below yield strength have occurred in this century, such as the Boston molasses-tank rupture in January 1919, which drowned 21 people and many horses under 2.3 million gallons of the sticky liquid.^[10] A more recent example is the failure of a 22-ft-dia rocket-motor case while being pressure tested by the manufacturer. Figure 5-16 shows the pieces of the rocket case after failure. It "... was designed to stand proof pressures of 960 psi (but) failed ... at 542 psi."^[11] These and other sudden "brittle-like" failures of ductile materials under static loading led researchers to seek better failure theories, since the ones then available could not adequately explain the observed phenomena.

Where human life is at risk, as in bridges, aircraft, etc., periodic structural-safety inspections for cracks are required by law or government regulation. These inspections can be by X-ray, ultrasonic energy, or just be visual. When cracks are discovered, an engineering judgment must be made whether to repair or replace the flawed part, retire the assembly, or to continue it in service for a further time subject to more frequent inspection. (Many commercial aircraft currently flying contain structural cracks.) These decisions can now be made sensibly through the use of fracture-mechanics theory.

Fracture-Mechanics Theory

Fracture mechanics presumes the presence of a crack. The stress state in the region of the crack may be one of plane strain or plane stress (see Section 4.4, p. 146). If the zone of yielding around the crack is small compared to the dimensions of the part, then **linear-elastic fracture-mechanics** (LEFM) theory is applicable. LEFM assumes that the

**FIGURE 5-16**

Failed Rocket-Motor Case (Courtesy of NASA-Lewis Research Center)

bulk of the material is behaving according to Hooke's law. However, if a significant portion of the bulk material is in the plastic region of its stress-strain behavior, then a more complicated approach is required than that described here. For the following discussion, we will assume that LEFM applies.

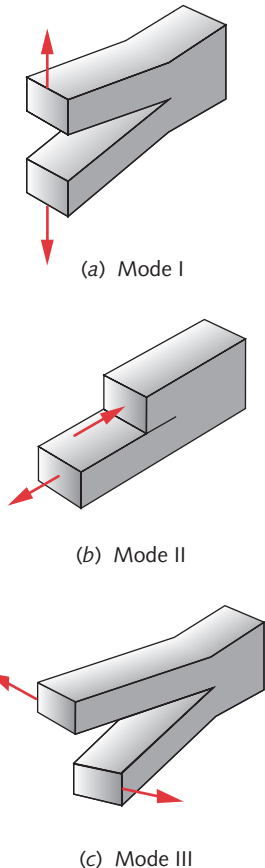
MODES OF CRACK DISPLACEMENT Depending on the orientation of the loading versus the crack, the applied loads may tend to pull the crack open in tension (Mode I), shear the crack in-plane (Mode II), or shear (tear) it out-of-plane (Mode III) as shown in Figure 5-17. Most of the fracture-mechanics research and testing has been devoted to the tensile loading case (Mode I), and we will limit our discussion to it.

STRESS INTENSITY FACTOR K Figure 5-18a shows a plate (not to scale) of width $2b$ under tension with a through crack of width $2a$ in the center. The crack is assumed to be sharp at its ends, and b is much larger than a . The crack's cross section is in the xy plane. An $r-\theta$ polar coordinate system is also set up in the xy plane with its origin at the crack tip as shown in Figure 5-18b. From the *theory of linear elasticity*, for $b \gg a$ the stresses around the crack tip, expressed as a function of the polar coordinates, are

$$\sigma_x = \frac{K}{\sqrt{2\pi r}} \cos \frac{\theta}{2} \left[1 - \sin \frac{\theta}{2} \sin \frac{3\theta}{2} \right] + \dots \quad (5.13a)$$

$$\sigma_y = \frac{K}{\sqrt{2\pi r}} \cos \frac{\theta}{2} \left[1 + \sin \frac{\theta}{2} \sin \frac{3\theta}{2} \right] + \dots \quad (5.13b)$$

$$\tau_{xy} = \frac{K}{\sqrt{2\pi r}} \sin \frac{\theta}{2} \cos \frac{\theta}{2} \cos \frac{3\theta}{2} + \dots \quad (5.13c)$$

**FIGURE 5-17**

Three Modes of Crack Displacement

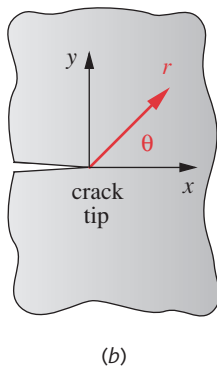
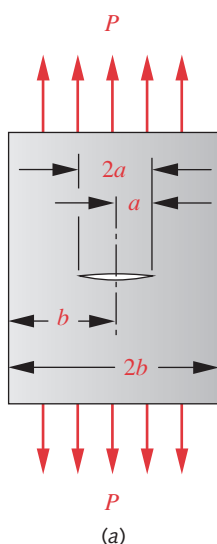


FIGURE 5-18

A Through-Crack in a Plate in Tension

$$\begin{aligned} \sigma_z &= 0 && \text{for plane stress} \\ \text{or} \\ \sigma_z &= v(\sigma_x + \sigma_y) && \text{for plane strain} \\ \tau_{yz} = \tau_{zx} &= 0 && (5.13e) \end{aligned}$$

with higher-order terms of small value omitted. Note that, when the radius r is zero, the xy stresses are infinite, which is consistent with equation 4.32b and Figure 4-36 (p. 190). The stresses diminish rapidly as r increases. The angle θ defines the geometric distribution of the stresses around the crack tip at any radius. **The quantity K is called the stress intensity factor.** (A subscript can be added to designate the mode I, II, III of loading as in K_I , K_{II} , K_{III} . Since we are dealing only with mode I loading, we will eliminate the subscript and let $K = K_I$.)

If we take the plane-stress case and compute the von Mises stress σ' from the x , y , and shear components (Eqs. 5.13a, -b, -c), we can plot the distribution of σ' versus θ for any chosen r as shown in Figure 5-19a for $r = 1E-5$ in and $K = 1$. The maximum occurs at 71° . If we set θ to that angle and compute the distribution of σ' as a function of r , it looks like Figure 5-19b, which plots r from $1E-5$ to 1 in on a log scale.

The high stresses near the crack tip cause local yielding and create a plastic zone of radius r_y as shown (not to scale) in Figure 5-19c. For any radius r and angle θ , the stress state in this plastic zone at the crack tip is directly proportional to the **stress intensity factor K** . If $b \gg a$, then K can be defined for the center-cracked plate as

$$K = \sigma_{nom} \sqrt{\pi a} \quad a \ll b \quad (5.14a)$$

where σ_{nom} is the nominal stress* in the absence of the crack, a is the crack half-width, and b is the plate half-width (see Figure 5-18, p. 268). This equation will be accurate within 10% if $a/b \leq 0.4$. Note that the stress intensity factor K is directly proportional to the applied nominal stress and proportional to the square root of the crack width. The units of K are either MPa-m^{0.5} or kpsi-in^{0.5}.

If the crack width a is not small compared to the plate width b , and/or if the geometry of the part is more complicated than the simple cracked plate shown in Figure 5-18, then an additional factor β is needed to calculate K .

$$K = \beta \sigma_{nom} \sqrt{\pi a} \quad (5.14b)$$

where β is a dimensionless quantity that depends on the part's geometry, the type of loading and the ratio a/b . Its value is also affected by the manner in which σ_{nom} is calculated. It is customary to use the gross stress for σ_{nom} calculated from the original section dimensions unreduced by the crack dimensions. Using the net stress would be more accurate but is less convenient to calculate, and the difference can be accounted for when determining the geometry factor β . Values of β for various geometries and loadings can be found in handbooks, some of which are noted in the bibliography at the end of this chapter. For example, the value of β for the center-cracked plate of Figure 5-18a is

$$\beta = \sqrt{\sec\left(\frac{\pi a}{2b}\right)} \quad (5.14c)$$

This asymptotically approaches 1 for small values of a/b and is ∞ for $a/b = 1$.

* The nominal stress for a fracture-mechanics analysis is calculated based on the gross cross-sectional area, without any reduction for the crack area. Note that this is different from the procedure used for calculation of nominal stress when using stress-concentration factors in a regular stress analysis. Then, the net cross section is used to find the nominal stress.

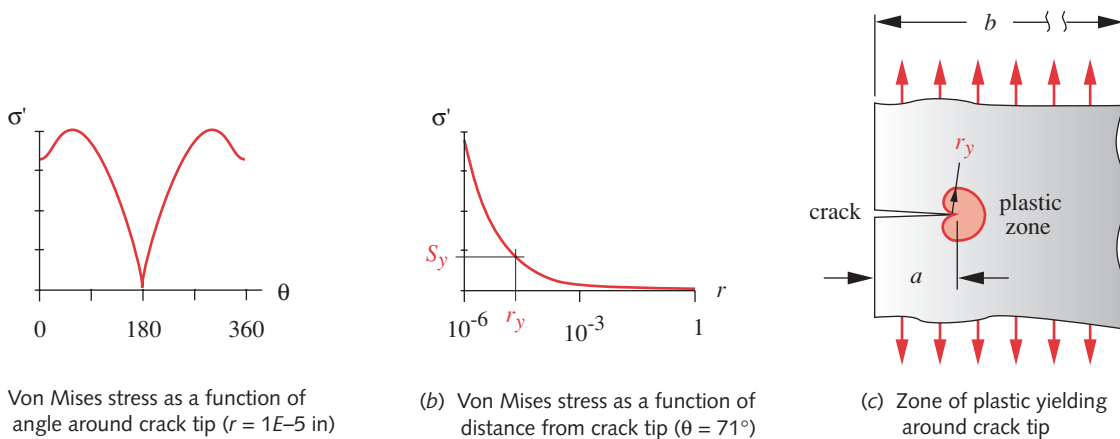


FIGURE 5-19

Von Mises Plane Stress Field Around an Edge Crack in a Plate Subject to Axial Tension for Stress Intensity Factor $K = 1$

For example, if the crack is at the edge rather than in the center of the plate, as shown in Figure 5-19c, the factor $\beta = 1.12$:

$$K = 1.12\sigma_{nom}\sqrt{\pi a} \quad a \ll b \quad (5.14d)$$

This equation will be accurate within 10% if $a/b \leq 0.13$. This equation is also accurate within 10% for a plate cracked on both edges if $a/b \leq 0.6$, and for an edge-cracked plate in bending if $a/b \leq 0.4$.

Fracture Toughness K_c

As long as the stress intensity factor K is below a critical value called the **fracture toughness** K_c * (which is a property of the material) the crack can be considered to be in a *stable mode* (if the load is static *and* the environment is noncorrosive), in a *slow-growth mode* (if the load is time-varying *and* the environment is noncorrosive), or in a *fast-growth mode* (if the environment is corrosive).^[13] When K reaches K_c , by reason of an increase in the nominal stress or by growth of the crack width, ***the crack will propagate suddenly to failure***. The rate of this unstable crack propagation can be spectacular, reaching velocities as high as 1 mile/sec!^[14] The structure effectively “unzips.”[†] The factor of safety for fracture-mechanics failure is defined as

$$N_{FM} = \frac{K_c}{K} \quad (5.15)$$

Note that this can be a moving target if cracks are in a growth mode because K is a function of crack width. If the current, or typical, crack width is known for the part and the fracture toughness K_c is known for the material, then the maximum allowable nominal stress can be determined for any chosen safety factor or vice versa. The allowable stress for any chosen safety factor calculated from the appropriate version of equation 5.14c will typically be lower than that calculated based on yield strength using equations 5.8 (p. 251) or 5.11 (p. 254). The effect of time-varying (dynamic) stresses on the stress intensity factor K and on failure will be addressed in the next chapter.

* More correctly called K_{Ic} where the I refers to mode I loading. Fracture toughness values for the other modes of loading are designated K_{IIc} and K_{IIIc} . Since we are discussing only mode I loading here, it is shortened to K_c .

† On the occasion of the 75th anniversary of the Boston molasses tank rupture described earlier, a 91-year-old Boston resident was interviewed and described what he saw and heard as a 16-year-old boy in January 1919 when he witnessed the tank failure from atop Cobb's Hill in Boston's North End. He recalled a sudden popping sound, like machine-gun fire, followed quickly by a loud explosion. The “machine-gun sound” was quite likely the sound of the crack propagating across the tank wall at up to 1 mile/second and the loud explosion was probably that of the molasses pressure bursting and disintegrating the tank, large pieces of which landed on and destroyed houses hundreds of yards away.

To determine the fracture toughness, K_c , ASTM-standardized specimens,* containing a crack of defined dimensions, are tested to failure. For axial tests, the specimen is gripped in a servo-hydraulic testing machine such that it can be tensioned across the crack. (Bending tests place the crack on the tension side of the beam.) The specimen is loaded dynamically with increasing displacements and its load-displacement characteristic (effective spring rate) is monitored. The load-displacement function becomes nonlinear at the start of rapid crack growth. The fracture toughness K_c is measured at this point.

Fracture toughness K_c for engineering metals ranges from 20 to 200 MPa-m^{0.5}; engineering polymers' and ceramics' K_c ranges from 1 to 5 MPa-m^{0.5}.^[15] Fracture toughness generally parallels ductility and increases substantially at high temperatures. Higher-strength steels tend to be less ductile and have lower K_c than lower-strength steels. Substitution of a high-strength steel for a low-strength steel has led to failures in some applications due to the reduction in fracture toughness that accompanied the material change.

Fracture toughness of a material typically varies with grain direction. Figure 5-20 shows the specimen and crack orientations and their symbols per the ASTM E-399 standard. The first character specifies the grain direction normal to the crack plane and the second character the grain direction parallel to the fracture plane. Test data for fracture toughness will usually define the specimen orientation by this method as shown in Table 5-1, which shows fracture toughness values for some steel and aluminum alloys used in aircraft structures.

Another example of a fracture-mechanics failure is shown in Figure 5-21a, which is a photograph of the low-carbon-steel trailer hitch ball bracket of Figures 1-2 through 1-6 (pp. 13-15). This part failed suddenly while being bent to shape at a red heat. The fracture surface can be seen to be relatively smooth, and the edges of the crack are extremely sharp. Since elevated temperature increases both ductility and fracture toughness, a sudden brittle failure is unusual under these circumstances. A closer inspection

* See ASTM E-399-83 "Standard Test Method for Plane Strain Fracture Toughness of Metallic Materials."

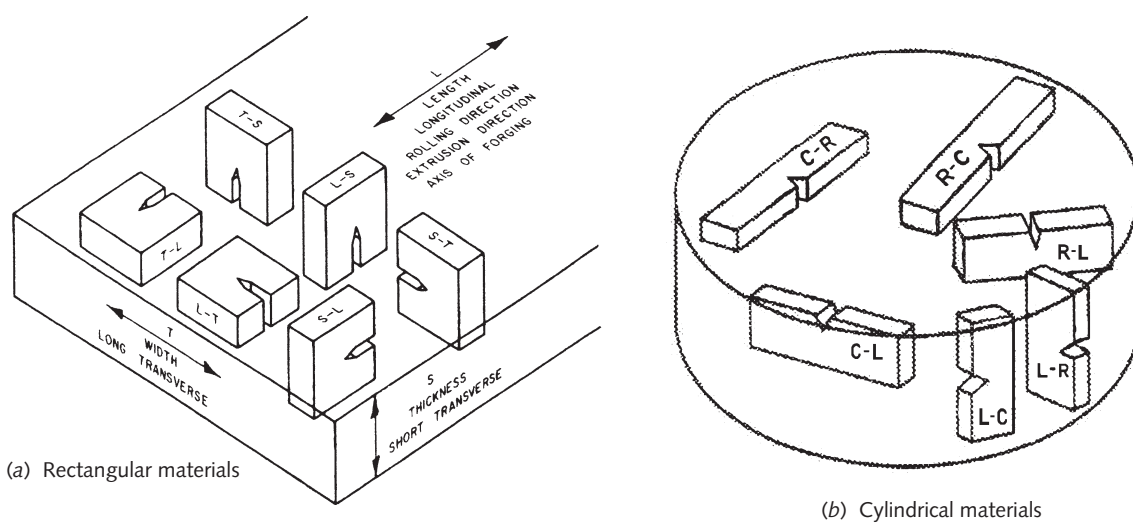


FIGURE 5-20

Typical Principal Fracture Path Directions - Source: MIL-HDBK-5J, p. 1-21, January 31, 2003

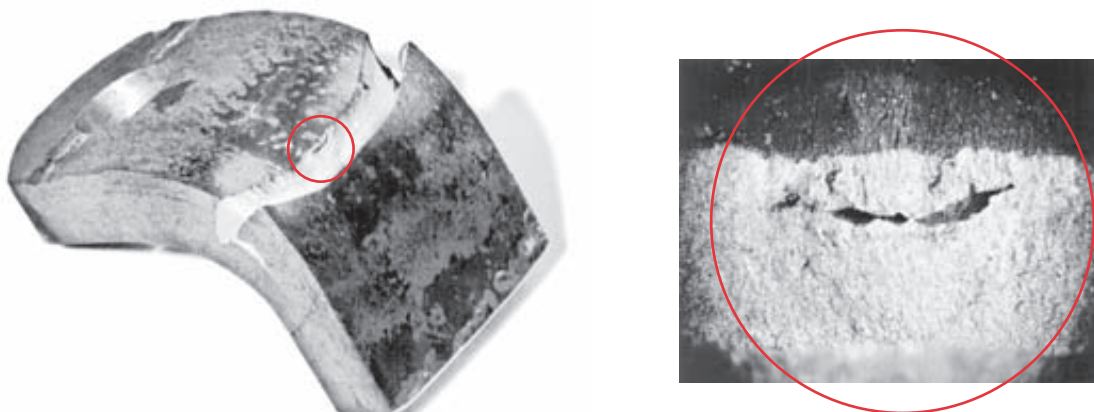
Table 5-1 Fracture Toughness Values for Selected Materials [16]

Material	Alloy	Heat Treatment	Form	Orientation	Yield Strength kpsi	K_{IC} , kpsi-in ^{0.5}		
						Max	Avg	Min
Steel	AerMet 100	Anneal, HT to 280 kpsi	Bar	L-R	236-281	146	121	100
Steel	AerMet 100	Anneal, HT to 280 kpsi	Bar	C-R	223-273	137	112	90
Steel	AerMet 100	Anneal, HT to 290 kpsi	Bar	L-R	251-265	110	99	88
Steel	AerMet 100	Anneal, HT to 290 kpsi	Bar	C-R	250-268	101	88	73
Steel	Custom 465	H1000	Bar	L-R	212-227	131	120	108
Steel	Custom 465	H1000	Bar	R-L	212-225	118	109	100
Steel	9Ni-4Co-0.20C	Quench & Temper (Q&T)	Forging	L-T	185-192	147	129	107
Steel	D6AC	Q&T [see ref. 16]	Plate	L-T	217	88	62	40
Aluminum	2024-T351		Plate	L-T		43	31	27
Aluminum	2024-T852		Forging	T-L		25	19	15
Aluminum	7075-T651		Plate	T-L		27	22	18
Aluminum	7075-T6510		Extrusion	L-T		32	27	23
Aluminum	7075-T6510		Forged Bar	L-T		35	29	24
Aluminum	7475-T651		Plate	T-L		60	47	34

of the failure surface (shown at 12.5X magnification in Figure 5-21b) shows a small crack that was apparently a flaw in the hot-rolled bar of steel. The stress intensity at this crack tip exceeded the fracture toughness of the material at its elevated temperature and a sudden brittle failure resulted.*

This brief discussion of fracture mechanics has barely *scratched the surface* of this complex topic. The reader is encouraged to read further on this subject. Sources for general information on fracture mechanics, stress intensity factors, and fracture-toughness properties of materials are noted in the bibliography of this chapter.

* Note that LEFM cannot be used to analyze this failure because it was not in the linear elastic range. The entire cross section was being plastically deformed at the time of failure. A nonlinear fracture-mechanics analysis would be needed here.



(a) Ball bracket failed suddenly while bending at red heat (b) 12.5x magnification of preexisting crack within material

FIGURE 5-21

Ductile Steel Trailer Hitch Fractured While Being Bent at Red Heat. Note Preexisting Crack and Sharpness of the Failure Edges.
(Courtesy of Steven Taylor, Mobile Logic Inc., Port Townsend, Wash.)

EXAMPLE 5-3**Failure of Cracked Materials Under Static Loading**

5

Problem

A steel support strap designed to hold a 60 000-N static load in axial tension was accidentally sawcut during production and now has an edge crack in it. Determine the safety factor of the original, uncracked strap based on yielding and its new “cracked” safety factor based on fracture mechanics. How large could the crack get before it fails? Would heat-treating the part compensate for the loss of strength due to the crack?

Given

The material is steel with $S_y = 540 \text{ MPa}$ and $K_c = 66 \text{ MPa}\cdot\text{m}^{0.5}$. The length $l = 6 \text{ m}$, width $b = 80 \text{ mm}$, and thickness $t = 3 \text{ mm}$. The crack width $a = 10 \text{ mm}$. The crack is completely through the thickness at one edge of the 80-mm width, similar to Figure 5-19c (p. 269).

Assumptions

The load is static and the assembly is at room temperature. The ratio $a / b < 0.13$, which allows use of equation 5.14d (p. 269).

Solution

- First calculate the nominal stress in the uncracked part based on total cross section.

$$\sigma_{nom} = \frac{P}{A} = \frac{60\,000}{3(80)} = 250 \text{ MPa} \quad (a)$$

- This is a uniaxial stress so is both the principal and the von Mises stress as well. The safety factor against yielding using the distortion-energy theory is (Eq 5.8a, p. 251):

$$N_{vm} = \frac{S_y}{\sigma'} = \frac{540}{250} = 2.16 \quad (b)$$

- The stress intensity K at the crack tip can be found for this case from equation 5.14d (p. 269) if the ratio $a / b < 0.13$:

$$\frac{a}{b} = \frac{10}{80} = 0.125$$

and

$$K = 1.12\sigma_{nom}\sqrt{\pi a} = 1.12(250)\sqrt{10\pi} = 49.63 \text{ MPa}\sqrt{\text{m}}$$

- The safety factor against sudden crack propagation is found from equation 5.15 (p. 269).

$$N_{FM} = \frac{K_c}{K} = \frac{66}{49.63} = 1.33 \quad (d)$$

Note that failure is now predicted to be sudden at a 33% overload, at which point the nominal stress in the part is still below the yield strength. This is too small a safety factor to allow the part to be used in the face of possible sudden fracture.

- The crack size necessary for failure can be found approximately by substituting K_c for K in equation 5.14b (p. 268) and solving for a . The result is a crack of about 18-mm width. Note, however, that the a / b ratio would now exceed that recommended for 10% accuracy with this equation. A more accurate equation for this case could be obtained from one of the references if desired.

- 6 Assuming the steel has enough carbon to allow heat treatment, through hardening will increase the yield strength but the **ductility and the fracture toughness K_c will decrease**, making the part **less safe** against a fracture-mechanics failure.
 - 7 The files EX05-03 are on the CD-ROM.
-

5.4 USING THE STATIC LOADING FAILURE THEORIES

It is neither practical nor possible to test all engineering materials under all combinations of applied stresses. The failure theories for static loading presented here provide a means to relate the stress states present in parts subjected to combined stresses to the stress state of the simple, uniaxial tensile test. The concept of an effective stress that “converts” the combination of applied stresses to an equivalent value that can be compared to a tensile-test result is extremely useful. However, the designer must be aware of its limitations in order to properly apply the effective-stress concept.

5

A fundamental assumption in this chapter is that the materials in question are macroscopically homogeneous and isotropic. Most engineering metals and many engineering polymers are in this category. The assumed presence of microscopic cracks does not preclude the use of conventional failure theories as long as detectable, macroscopic cracks are not in evidence. If so, fracture-mechanics theory should be used.

Composite materials are finding increased use in applications requiring high strength-to-weight ratios. These materials are typically nonhomogeneous and anisotropic (or orthotropic) and thus require different and more complicated failure theories than those presented here. For more information, the reader is directed to the literature on composite materials, some of which is noted in this chapter’s bibliography.

Another fundamental assumption of these static failure theories is that the loads are slowly applied and remain essentially constant with time. That is, they are static loads. **When the loads (and thus the stresses) vary with time or are suddenly applied, the failure theories of this chapter may not be the limiting factor.** The next chapter will discuss other failure theories suited to the dynamic loading case and extend the consideration of fracture mechanics to dynamic loading. When fracture mechanics is used in dynamic loading situations, a dynamic fracture toughness value K_d (K_{IId} , K_{IId} , or K_{IIId}) is used instead of the static fracture toughness K_c discussed above.

STRESS CONCENTRATION due to geometric discontinuities or sharp contours needs to be taken into account in some cases of static loading before applying the appropriate failure theory. The concept of stress concentration was explained and discussed in Section 4.15 (p. 186). It was pointed out that, **under static loading**, stress concentration can be ignored if the material is ductile, because the high stress at the discontinuity will cause local yielding that reduces its effect. However, it is worth repeating that for brittle materials under static loading, the effects of stress concentration should be applied to the calculated stresses before converting them to effective stresses for comparison to the failure theories described here. The one exception to this is with some cast materials (such as gray cast iron) in which the number of inherent stress-raisers within the cast material is so large that the addition of a few more geometric stress-raisers is considered to have little additional effect.

TEMPERATURE AND MOISTURE are also factors in failure. Most of the available test data for materials are generated at room temperature and low humidity. Virtually all material properties are a function of temperature. Metals typically become less strong and more ductile at elevated temperatures. A ductile material can become brittle at low temperatures. Polymers exhibit similar trends over much smaller ranges of temperature than metals. Boiling water is hot enough to soften some polymers, and a cold winter day can make them extremely brittle. If your application involves either high or low temperatures or aqueous/corrosive environments, you need to obtain strength data for these conditions from the material manufacturer before applying any failure theories.

CRACKS If macroscopic cracks are present, or are anticipated in service, then the fracture-mechanics (FM) theory should be applied. Once actual cracks are discovered in the field, FM should be used to predict failure and determine the safety of the particular part. If previous experience with similar equipment indicates that service cracking is a problem, then FM should be used in the design of future assemblies, and regular field inspections should be done to detect cracks as they occur.

5.5 CASE STUDIES IN STATIC FAILURE ANALYSIS

We will now continue some case studies whose forces were analyzed in Chapter 3 and whose stresses were analyzed in Chapter 4. The same case-study number is retained for a given design throughout the text, and successive installments are designated by a letter suffix. For example, Chapter 4 presented four case studies labeled 1B, 2B, 3B, and 4B. This chapter will continue these case studies as 1C, 2C, 3C, and 4C. The reader can review the earlier installments of any case study by referring to its common case number. See the list of case studies in the table of contents to locate each part. Since stresses vary continuously over a part, we made an engineering judgment in Chapter 4 as to where the stresses would be the largest and calculated them for those locations. We wish now to determine their safety factors using the appropriate failure theories.

CASE STUDY 1C

Bicycle Brake Lever Failure Analysis

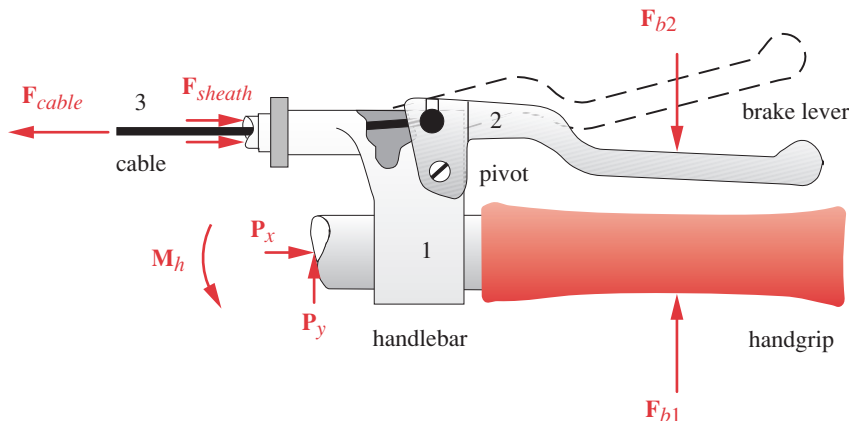
Problem Determine the factors of safety at critical points in the brake lever shown in Figures 3-1 (repeated here) and 5-22.

Given The stresses are known from Case Study 1B (p. 206). The material of the brake lever is die-cast aluminum alloy ASTM G8A with $S_{ut} = 310 \text{ MPa}$ (45 ksi) and $S_y = 186 \text{ MPa}$ (27 ksi). The elongation to fracture is 8%, making it a marginally ductile material.

Assumptions The most likely failure points are the two holes where the pins insert and at the root of the cantilever-beam lever handle.

Solution See Figures 3-1 and 5-22, and file CASE1C.

- 1 The bending stress at point P in Figure 5-22 at the root of the cantilever was found from equation 4.11b in Case Study 1B and is

**FIGURE 3-1** Repeated

Bicycle Brake Lever Assembly

5

$$\sigma_x = \frac{Mc}{I} = \frac{(267 \text{ N} \cdot 0.0762 \text{ m}) \left(\frac{0.0143}{2} \right) \text{ m}}{\frac{\pi(0.0143)^4}{64} \text{ m}^4} = 70.9 \text{ MPa} \quad (a)$$

- 2 This is the only applied stress at this point, so it is also the principal stress. The von Mises effective stress $\sigma' = \sigma_1$ in this case (see equation 5.7c, p. 249). The safety factor against yielding at point P is then (from equation 5.8a, p. 249),

$$N_{yield} = \frac{S_y}{\sigma'} = \frac{186}{70.9} = 2.6 \quad (b)$$

This design is safe at the average load but there is not a large margin to protect from overloads. Note that in this simple stress situation, the distortion-energy theory gives identical results to the maximum shear theory because the ellipse and hexagon are coincident at the point $x = \sigma_1, y = 0$ in Figure 5-5 (p. 252).

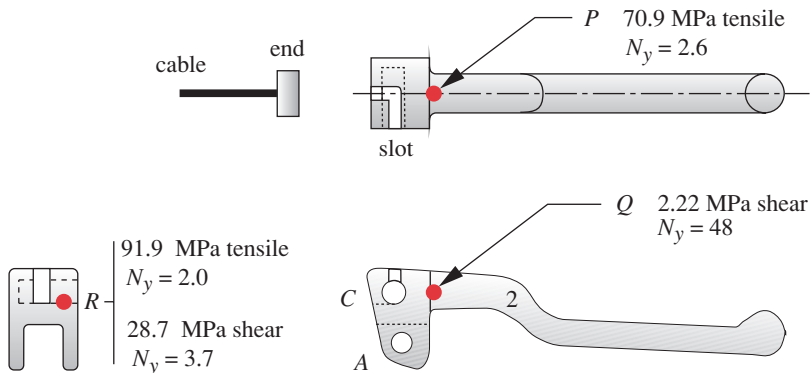
- 3 Since this is a cast material with limited ductility, it would be interesting to also compute the modified-Mohr safety factor against brittle fracture from equation 5.12a (p. 260). It could be argued that the brake handle might still be usable despite slight yielding having occurred:

$$N_{fracture} = \frac{S_{ut}}{\sigma_1} = \frac{310}{70.9} = 4.4 \quad (c)$$

Note that we have not accounted for stress concentrations at the root of the cantilever, which could reduce this fracture safety factor. Case Study 1D in Chapter 8 determines the stress concentration factor at point P by using Finite Element Analysis.

- 4 The transverse shear stress at point Q in Figure 5-22 was calculated from equation 4.15c (p. 161) as

$$\tau_{xy} = \frac{4V}{3A} = \frac{4(267) \text{ N}}{\frac{3\pi(14.3)^2}{4} \text{ mm}^2} = 2.22 \text{ MPa} \quad (d)$$

**FIGURE 5-22**

Stresses and Factors of Safety at Selected Points on the Bicycle Brake Lever

This shear stress is also the maximum, since no other stresses act at that point. The safety factor using the distortion-energy theory for pure shear at point *Q* is

$$N_{transverse} = \frac{S_{ys}}{\tau_{max}} = \frac{0.577S_y}{\tau_{max}} = \frac{0.577(186)}{2.22} = 48 \quad (e)$$

Clearly, there is no danger of transverse-shear failure at point *Q*.

- 5 The compressive bearing stress in the hole at point *A* in Figure 5-22 is

$$A_{bearing} = \text{dia} \cdot \text{thickness} = 8(2)(6.4) = 102 \text{ mm}^2$$

$$\sigma_{bearing} = \frac{F_{12}}{A_{bearing}} = \frac{1951}{102} = 19.2 \text{ MPa} \quad (f)$$

and this stress, acting alone, is also the principal and the von Mises stress. Assuming that the compressive strength of this material is equal to its tensile strength (an even material), the safety factor against bearing failure in the hole is

$$N_{bearing} = \frac{S_{yc}}{\sigma'} = \frac{186}{19.2} = 9.7 \quad (g)$$

- 6 Tearout in this case requires that (4) 6.4-mm-thick sections fail in shear through the material between hole *A* and the edge. (See also Figure 4-13 on p. 155.)

$$A_{tearout} = \text{length} \cdot \text{thickness} = 7.1(4)(6.4) = 181.8 \text{ mm}^2$$

$$\tau_{tearout} = \frac{F_{12}}{A_{tearout}} = \frac{1951}{181.8} = 10.7 \text{ MPa} \quad (h)$$

This is a pure shear case and the safety factor is found from

$$N_{tearout} = \frac{S_{ys}}{\tau_{max}} = \frac{0.577S_y}{\tau_{max}} = \frac{0.577(186)}{10.7} = 10.0 \quad (i)$$

- 7 The cable-end inserts in a blind hole which is half-slotted to allow the cable to pass through at assembly as shown in Figure 5-22. This slot weakens the part and makes the section at *R* the most likely failure location at this joint. The bending stress at the outer fiber is

$$\sigma_x = \frac{Mc}{I} = \frac{\frac{1914}{2} \left(\frac{5}{2}\right)(4)}{\frac{10(5)^3}{12}} = 91.9 \text{ MPa} \quad (j)$$

As the only applied stress at the outer fiber of this section, this is also the principal stress and the von Mises stress. The bending safety factor at point *R* is

$$N = \frac{S_{yc}}{\sigma'} = \frac{186}{91.9} = 2.0 \quad (k)$$

- 8 The shear due to transverse loading at the neutral axis in the section at *R* is (Eq. 4.14b, p. 161):

$$\tau_{xy} = \frac{3V}{2A} = \frac{3(957)}{2(10)(5)} = 28.7 \text{ MPa} \quad (l)$$

This is the maximum shear stress at the neutral axis, and the transverse-shear safety factor at point *R* is

$$N = \frac{S_{ys}}{\tau_{max}} = \frac{0.577S_y}{\tau_{max}} = \frac{0.577(186)}{28.7} = 3.7 \quad (m)$$

It is interesting to note that the transverse-shear safety factor is only about twice the bending safety factor at point *R* because the beam is so short. Compare this result with that at point *P* in equations (b) and (e), where the bending and transverse shear safety factors differ by about a factor of 18 in the longer beam. See Figure 5-22.

- 9 The die-cast aluminum alloy chosen is one of the strongest aluminum casting alloys available. If additional protection against overloads (as from the bicycle falling) is desired, either a change of geometry to increase the section size and/or reduce stress concentrations or a change in material or manufacturing method could be made. A forged-aluminum part would be stronger but would increase the cost. Thicker sections would increase the weight slightly, but probably not prohibitively. Increasing the diameter of the handle around point *P* by 26% to 18 mm (with perhaps a more generous transition radius also) would double the safety factor there, since the section modulus is a function of d^3 .

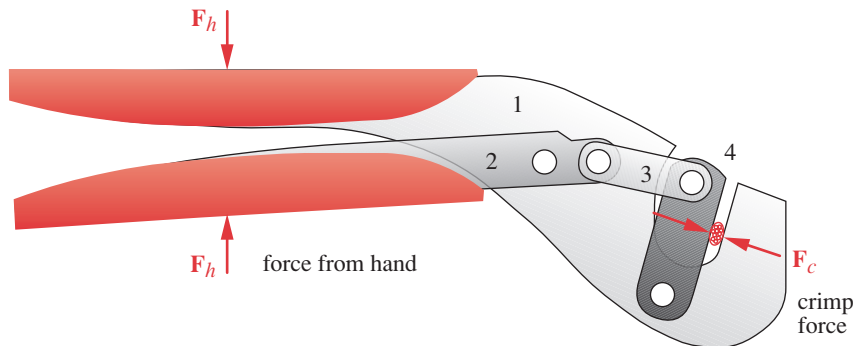
Even though some of the other safety factors may seem excessive, it may be impractical to reduce those sections due to difficulties in casting thin sections. Other considerations may take into account the appearance of a part intended for a consumer application such as a bicycle. If the dimensions do not look "right" to the customer, it may give an undesired impression of cheapness. Sometimes it is better economics to provide more thickness than is necessary for a suitable safety factor in order to provide a quality appearance.

CASE STUDY 2 C

Crimping Tool Failure Analysis

Problem

Determine the factors of safety at critical points in the crimping tool shown in Figures 3-3 (repeated on next page) and 5-23.



5

FIGURE 3-3 Repeated

Wire Connector Crimping Tool

Given

The stresses are known from Case Study 2B on p. 209. All material is AISI 1095 steel Q & T @ 800 °F with $S_y = 112$ kpsi (see Table A-9 in Appendix A). It is an even material.

Assumptions

The most likely failure points are link 3 as a column, the holes where the pins insert, the connecting pins in shear, and link 4 in bending.

Solution

See Figures 3-3 and 5-23, and files CASE2C-1 and CASE2C-2.

- 1 The previous case study found the critical column load in link 3 to be 3.1 times larger than the applied load. This is the safety factor against buckling, which is expressed in terms of load rather than stress.
- 2 Any link can fail in bearing in the 0.25-dia holes. The bearing stress (Eqs. 4.7, p. 152, and 4.10, p. 154) is:

$$\sigma_b = \frac{P}{A_{bearing}} = \frac{1560}{0.125(0.25)} = 50 \text{ kpsi} \quad (a)$$

- 3 As the only applied stress at this element, this is the principal stress and also the von Mises stress. The safety factor for bearing stress on either hole or pin is then

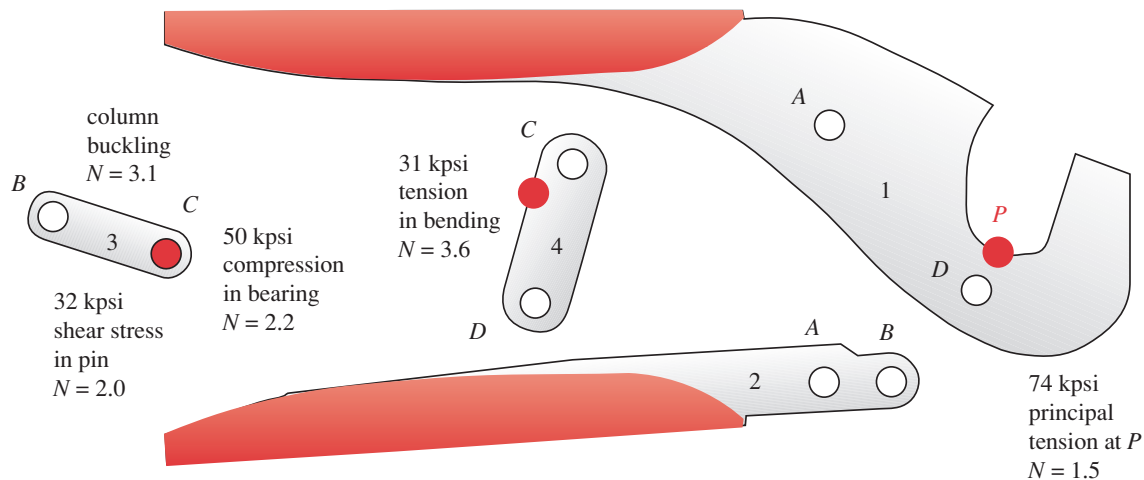
$$N = \frac{S_y}{\sigma'} = \frac{112}{50} = 2.2 \quad (b)$$

- 4 The 0.25-in-dia pins are in single shear. The worst-case direct-shear stress from equation 4.9 (p. 153) is

$$\tau = \frac{P}{A_{shear}} = \frac{1560}{\frac{\pi(0.25)^2}{4}} = 32 \text{ kpsi} \quad (c)$$

As the only stress on this section, this is also the maximum shear stress. The safety factor for the pins in single shear from equation 5.9a (p. 251) is

$$N = \frac{0.577S_y}{\tau_{max}} = \frac{(0.577)112}{32} = 2.0 \quad (d)$$

**FIGURE 5-23**Significant Stresses and Safety Factors (N) at Critical Points in a Crimping Tool

- 5 Link 4 is a 1.55-in-long beam, simply supported at the pins and loaded with the 2 000-lb crimp force at 0.35 in from point C. The beam depth at the point of maximum moment is 0.75 in and the thickness is 0.187. The bending stress is then

$$\sigma = \frac{Mc}{I} = \frac{541.8 \left(\frac{0.75}{2} \right)}{\underline{0.187(0.75)^3}} = 31 \text{ kpsi} \quad (e)$$

As the only applied stress on this element at the outer fiber of the beam, this is the principal stress and also the von Mises stress. The safety factor for link 4 in bending is then

$$N = \frac{S_y}{\sigma'} = \frac{112}{31} = 3.6 \quad (f)$$

- 6 Link 1 has a tensile stress due to bending in the inner fiber at point P on the curved beam superposed on an axial tensile stress at the same point. Their sum is the maximum principal stress:

$$\begin{aligned} \sigma_i &= +\frac{M}{eA} \left(\frac{c_i}{r_i} \right) = \frac{2400}{0.103[(1.0 - 0.25)(0.313)]} \left(\frac{0.397}{0.600} \right) = 65 \text{ kpsi} \\ \sigma_a &= \frac{F}{A} = \frac{2000}{(1.0 - 0.25)(0.313)} = 8.5 \text{ kpsi} \\ \sigma_1 &= \sigma_a + \sigma_i = 65 + 8.5 = 74 \text{ kpsi} \end{aligned} \quad (g)$$

There is no applied shear stress at point P, so this is the principal stress and also the von Mises stress. The safety factor for bending at the inner fiber of the curved beam at point P from equation 5.8a (p. 251) is

$$N = \frac{S_y}{\sigma'} = \frac{112}{74} = 1.5 \quad (h)$$

- 7 At the hole in link 1, there is an axial tensile stress σ_a from equation (g) increased by the stress-concentration factor (see Case Study 2B, step 14, p. 213). The safety factor is found from equation 5.8a:

$$N = \frac{S_y}{\sigma} = \frac{112}{2.42(8.5)} = 5.4 \quad (i)$$

Note that there is also a transverse shear stress at the hole which, when combined with the axial tension, reduces the safety factor at the hole to about 3.7.

- 8 Some of these safety factors, such as the $N = 1.5$ for bending in link 1 at point P , are somewhat low to guard against user-induced overloads. The safety factors for the pins in shear could also be increased. Either a stronger steel such as SAE 4140 could be selected or the section sizes of the parts could be increased slightly. A small change in link thickness would achieve acceptable safety factors in the existing material. Note that the geometry of this tool has been simplified for this example from that of the actual device. The stresses and safety factors calculated here are not necessarily the same as those in the actual tool, which is a well-tested and safe design.

CASE STUDY 3C

Automobile Scissors-Jack Failure Analysis

Problem Determine safety factors at critical points in a scissors jack.

Given The stresses are known from Case Study 3B on p. 214. The design load is 2 000 lb total or 1 000 lb per side. The width of the links is 1.032 in and their thickness is 0.15 in. The screw is a 1/2-13 UNC thread with root dia = 0.406 in. The material of all parts is ductile steel with $E = 30$ Mpsi and $S_y = 60$ kpsi.

Assumptions The most likely failure points are the links as columns, the holes in bearing where the pins insert, the connecting pins in shear, the gear teeth in bending, and the screw in tension. There are two sets of links, one set on each side. Assume the two sides share the load equally. The jack is typically used for very few cycles over its lifetime so a static analysis is appropriate.

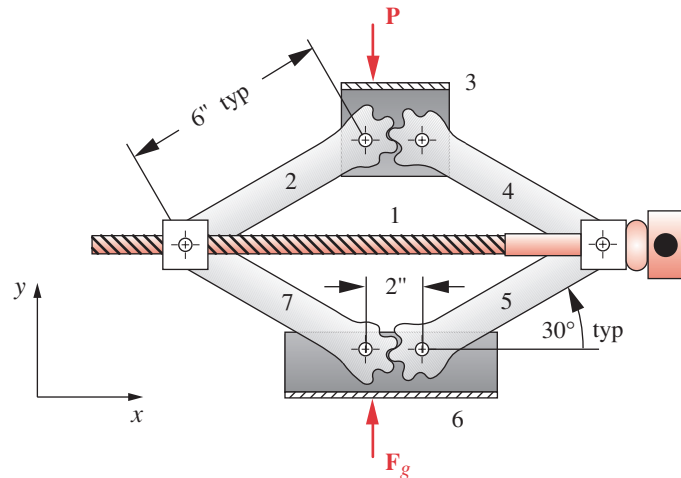
Solution See Figures 3-5 (opp. page) and 5-24, and the file CASE3C.

- The stresses on this jack assembly for the position shown were calculated in the previous installment of this case study in Chapter 4 (p. 214). Please see that case also.
- The jack screw is in axial tension. The tensile stress was found from equation 4.7 (p. 152).

$$\sigma_x = \frac{P}{A} = \frac{4(878)}{0.129} = 27\,128 \text{ psi} \quad (a)$$

This is a uniaxial tension stress, so is also the principal and the von Mises stress. The safety factor is

$$N = \frac{S_y}{\sigma} = \frac{60\,000}{27\,128} = 2.2 \quad (b)$$

**FIGURE 3-5** Repeated

An Automobile Scissors Jack

5

- 3 Link 2 is loaded as a beam-column. Its safety factor against buckling was calculated in the last installment of this case study and is $N = 2.3$.
- 4 The bearing stress in the most heavily loaded hole at C is

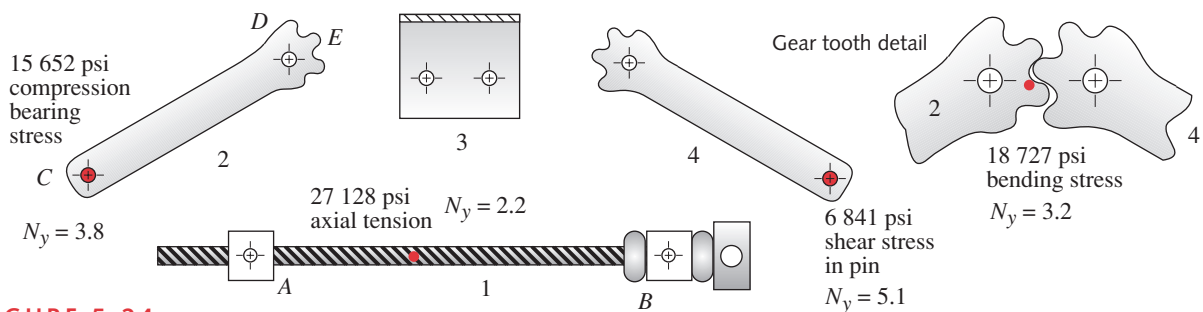
$$\sigma_{bearing} = \frac{P}{A_{bearing}} = \frac{1026}{0.15(0.437)} = 15652 \text{ psi} \quad (c)$$

This is a uniaxial compression stress, so is also the principal and the von Mises stress. The safety factor is

$$N_{bearing} = \frac{S_y}{\sigma'} = \frac{60000}{15652} = 3.8 \quad (d)$$

The pins' shear stress is

$$\tau = \frac{P}{A_{shear}} = \frac{1026}{\frac{\pi(0.437)^2}{4}} = 6841 \text{ psi} \quad (e)$$

**FIGURE 5-24**

Selected Stresses and Factors of Safety in the Scissors-Jack Assembly

This is a pure shear stress, so is also the maximum shear stress. The safety factor is

$$N = \frac{0.577S_y}{\tau_{max}} = \frac{0.577(60\ 000)}{6\ 841} = 5.1 \quad (f)$$

- 5 The bending stress at the root of the gear tooth on link 2 is

$$\sigma = \frac{Mc}{I} = \frac{91(0.22)}{\frac{0.15(0.44)^3}{12}} = 18\ 727 \text{ psi} \quad (g)$$

This is a uniaxial bending stress, so is also the principal and the von Mises stress. The safety factor is

$$N = \frac{S_y}{\sigma'} = \frac{60\ 000}{18\ 727} = 3.2 \quad (h)$$

- 6 This analysis should be continued, looking at other points in the assembly and, more importantly, at stresses and safety factors when the jack is in different positions. We have used an arbitrary position for this case study, but, as the jack moves to the lowered position, the link and pin forces will increase due to poorer transmission angles. A complete stress and safety-factor analysis should be done for multiple positions. You may examine the models for this case study by opening the files CASE3C-1 and CASE3C-2 in the program of your choice.

5

CASE STUDY 4 C

Bicycle Brake Arm Factors of Safety

Problem Choose appropriate material alloys to obtain a safety factor against fracture of at least 2 at critical points in the bicycle brake arm in Figures 3-9 (repeated here) and 5-25.

Given The stresses are known from Case Study 4B (p. 217). The arm is cast aluminum and the pivot pin is steel.

Assumptions Since the arm is a cast (uneven) material, the modified-Mohr theory will be used to find a safety factor against fracture. The pin is ductile, so the maximum distortion-energy theory will be used for it.

Solution See Figures 3-9 and 5-25, and the file CASE4C.

- 1 The bending stresses of the arm, σ_i at the inner fibers (point A in Figure 5-25) and σ_o at the outer fibers (point B in Figure 5-25), were found to be

$$\sigma_i = +\frac{M}{eA} \left(\frac{c_i}{r_i} \right) = \frac{65\ 452(6.063)}{(0.1873)(225)(58)} = 162 \text{ MPa} \quad (a)$$

$$\sigma_o = -\frac{M}{eA} \left(\frac{c_o}{r_o} \right) = \frac{65\ 452(8.937)}{(0.1873)(225)(73)} = -190 \text{ MPa}$$

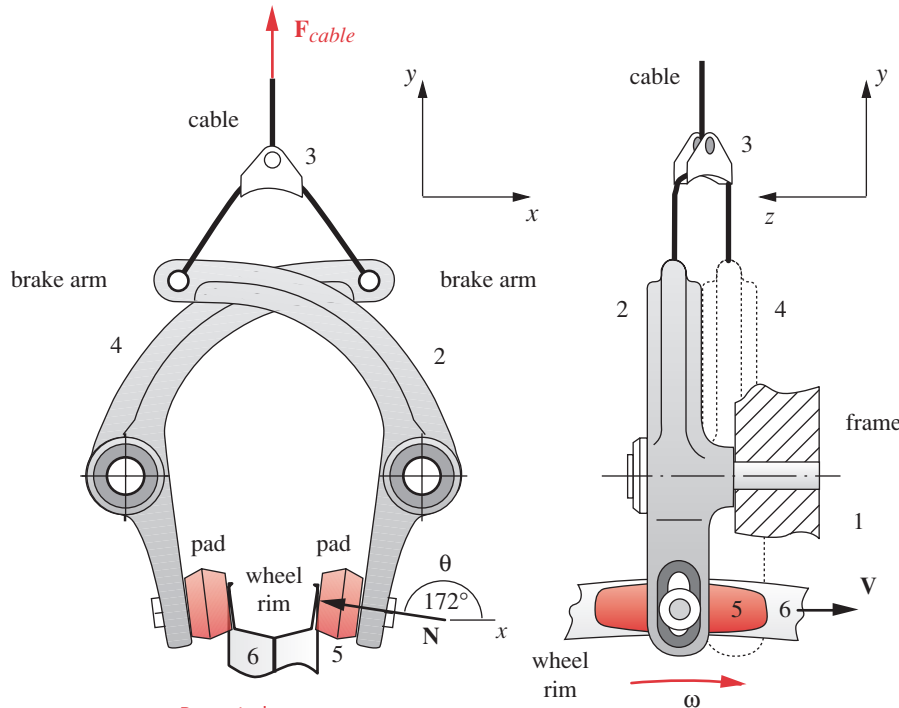


FIGURE 3-9 Repeated

Center-Pull Bicycle Brake Arm Assembly

5

For a safety factor of 2 at this point we need a material with an ultimate tensile strength of at least 325 MPa and a compressive strength of at least 380 MPa.

- 2 The stress on the left half of Section B-B at point C in Figure 5-25 is the sum of the bending stress and the axial-tension stress:

$$\sigma_{hub} = \frac{Mc}{I_{hub}} + \frac{F_{32_y}}{A_{hub}} = \frac{65\,452(12.5)}{33\,948} + \frac{523}{399} = 25.4 \text{ MPa} \quad (b)$$

This needs a material tensile strength of about 52 MPa to have a safety factor of 2.

- 3 The bending stress at the outer fiber of the 23-mm side of the straight portion of the brake arm (point D in Figure 5-25) is

$$\sigma_y = \sigma_{y_1} + \sigma_{y_2} = 118.6 + 23.7 = 142 \text{ MPa} \quad (c)$$

For a safety factor of 2 at this point we need a material with an S_{ut} of at least 284 MPa.

- 4 Another possible failure point is the slot in the arm (point E in Figure 5-25). The tearout shear stress is

$$\tau = \frac{F_{52_z}}{A_{tearout}} = \frac{589}{32} = 18.4 \text{ MPa} \quad (d)$$

For a uniaxial applied shear stress, the stresses are all in the first quadrant of Figure 5-11 (p. 260) and the modified-Mohr theory is identical to the maximum normal-stress theory. The equivalent tensile stress is then twice the maximum shear stress, which requires an ultimate tensile strength greater than 75 MPa for a safety factor of 2 in this case.

- 5 The worst-stress case among the points calculated on the arm is point A with $\sigma_y = 162$ MPa. This is a uniaxial stress, so is principal. Table A-3 in Appendix A shows an A132 permanent-mold-casting aluminum alloy, heat treated at 340°F, with an S_{ut} of 324 MPa. This material satisfies the requirement for a fracture safety factor ≥ 2 in this case.

$$N_f = \frac{S_{ut}}{\sigma_{b_A}} = \frac{324 \text{ MPa}}{162 \text{ MPa}} = 2.0 \quad (e)$$

- 6 The 0.2% offset tensile yield strength of this cast material is given as 296 MPa. Since point A has a uniaxial stress, the von Mises effective stress $\sigma' = \sigma_y$. The safety factor against tensile yielding at point A is

$$N_y = \frac{S_y}{\sigma'_A} = \frac{296 \text{ MPa}}{162 \text{ MPa}} = 1.8 \quad (f)$$

5

- 7 The 11-mm-dia steel pivot pin has a maximum bending stress at point F of

$$\sigma_{pin} = \frac{M_{pin}c_{pin}}{I_{pin}} = \frac{23\,053 \left(\frac{11}{2}\right)}{\frac{\pi(11)^4}{64}} = 176 \text{ MPa} \quad (g)$$

For a ductile yielding safety factor of 2, this requires a steel with a yield strength of at least 352 MPa. An AISI 1040 steel has $S_y = 372$ MPa in the normalized condition. This gives the desired safety factor of just over 2.

- 8 Figure 5-25 shows a summary of the stresses at various critical points in the part. You may examine the model for this case study by opening the file CASE4C in the program of your choice.

Note that in most of these case studies, some redesign was necessary after (and only after) getting to the “bottom line” of determining safety factors for the geometry and loading assumed at the outset. Some of the safety factors were found to be low. This

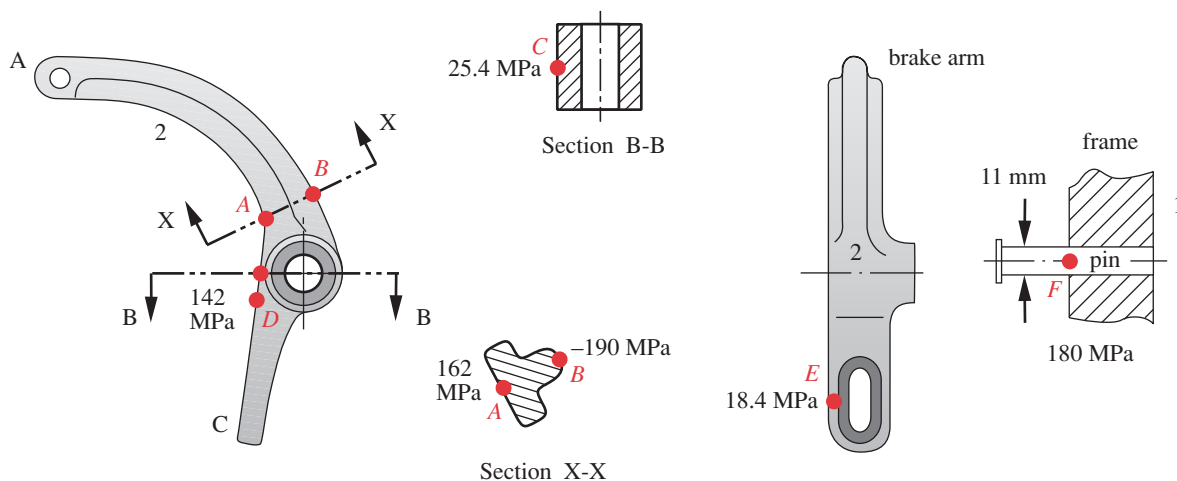


FIGURE 5-25

Brake Arm Stresses at Selected Points

is typical of design problems and demonstrates their iterative nature. We cannot know whether our assumptions are valid until we spend the considerable time and energy required to thoroughly analyze the proposed design. We should not be too disappointed when we find that our first design doesn't work. That is not necessarily a reflection on the designer's abilities. It is rather just the "nature of the beast." The value of setting up the analytical model in a computer tool such as a spreadsheet or equation solver should by now be obvious. The analysis of redesigned geometry as proposed in these latest case studies above can literally be accomplished in minutes if the time was taken initially to computerize the model. If not, we are faced with a much larger amount of work to reanalyze the modified design.

5.6 SUMMARY

This chapter has presented several theories of failure for materials under static loading. Two of these theories seem to fit the experimental data best. Both assume that the material is reasonably homogeneous and isotropic in the macro. In addition, the mechanism of crack propagation based on fracture-mechanics theory is presented.

The **distortion-energy theory**, also called the **von Mises theory**, is best for ductile, even materials whose compressive and tensile strengths are approximately the same and whose shear strengths are smaller than their tensile strengths. These materials are considered to fail from shear stress, and the distortion-energy theory best predicts their failure.

Uneven, brittle materials such as cast iron typically have tensile strengths that are much lower than their compressive strengths, and their shear strengths are between those two values. They are weakest in tension, and the **modified-Mohr theory** best describes their failure.

Note that when the loading is not static, but varies with time, *then neither of these theories is appropriate to describe failure*. A different set of criteria for time-varying loading is discussed in the next chapter. If known cracks are present, then the possibility of sudden failure due to crack propagation must be investigated using fracture-mechanics theory. The crack can suddenly open at stress levels much lower than the yield strength of the material under certain circumstances.

EFFECTIVE STRESS For loading situations with combined stresses (such as tensile and shear stresses applied at the same point), which stress should be used to compare to what material strength to obtain a safety factor? Should the applied shear stress be compared to a shear strength or the applied normal stress to a tensile strength? The answer is neither. An **effective stress**, which combines the effects of all the applied stresses combined at the point, must be calculated that can be compared to the "pure" normal-stress state of the tensile-test specimen. These effective stresses are a useful means to create a stress-loading criterion for comparison with published material-strength data on an "apples for apples" basis, even when the applied-stress situation is quite different from the test specimen's loading. The effective-stress approach is also valid when only one stress is applied at the point and so can be universally used. The calculation for the effective stress differs with the type of material, either ductile or brittle, however.

For ductile, even materials, the **von Mises effective stress** is calculated either directly from the applied stresses (Eq. 5.7b, 5.7d, p. 249) or from the principal stresses

that result from those applied stresses (Eq. 5.7a, 5.7c, p. 249). Note that this effective-stress calculation converts **any combination** of 2-D or 3-D applied stresses at a point into a **single stress value** σ' that can be compared with a suitable strength criterion in order to obtain a safety factor. For ductile materials under static loads, the desired strength criterion is the **tensile yield strength**. (See Section 5.1, p. 245.)

For brittle, uneven materials, a **modified-Mohr effective stress** can be calculated using the principal stresses that result from the particular combination of applied stresses at the point in question (Eq. 5.12a-d, pp. 260–262). The resulting effective stress is compared to the ultimate tensile strength of the material (not the yield strength) to obtain a safety factor. (See Section 5.2, p. 258.)

5

FRACTURE MECHANICS In addition to possible failure by yielding or breaking, a part can fail at much lower stresses by crack propagation if a crack of sufficient size is present. The theory of fracture mechanics provides a means to predict such sudden failure based on a calculated **stress intensity factor** compared to a tested **fracture toughness** criterion for the material. (See Section 5.3, p. 265.)

The failure-analysis process for static loading can be summarized in a series of steps as shown in the flow chart of Figure 5-26. Note that the first five steps are the same as those in the chart of Figure 4-60 (p. 224).

Important Equations Used in This Chapter

See the referenced sections for information on the proper use of these equations.

Von Mises Effective Stress for 3 Dimensions (Section 5.1):

$$\sigma' = \sqrt{\sigma_1^2 + \sigma_2^2 + \sigma_3^2 - \sigma_1\sigma_2 - \sigma_2\sigma_3 - \sigma_1\sigma_3} \quad (5.7a)$$

$$\sigma' = \sqrt{\frac{(\sigma_x - \sigma_y)^2 + (\sigma_y - \sigma_z)^2 + (\sigma_z - \sigma_x)^2 + 6(\tau_{xy}^2 + \tau_{yz}^2 + \tau_{zx}^2)}{2}} \quad (5.7b)$$

Von Mises Effective Stress for 2 Dimensions (Section 5.1):

$$\sigma' = \sqrt{\sigma_1^2 - \sigma_1\sigma_3 + \sigma_3^2} \quad (5.7c)$$

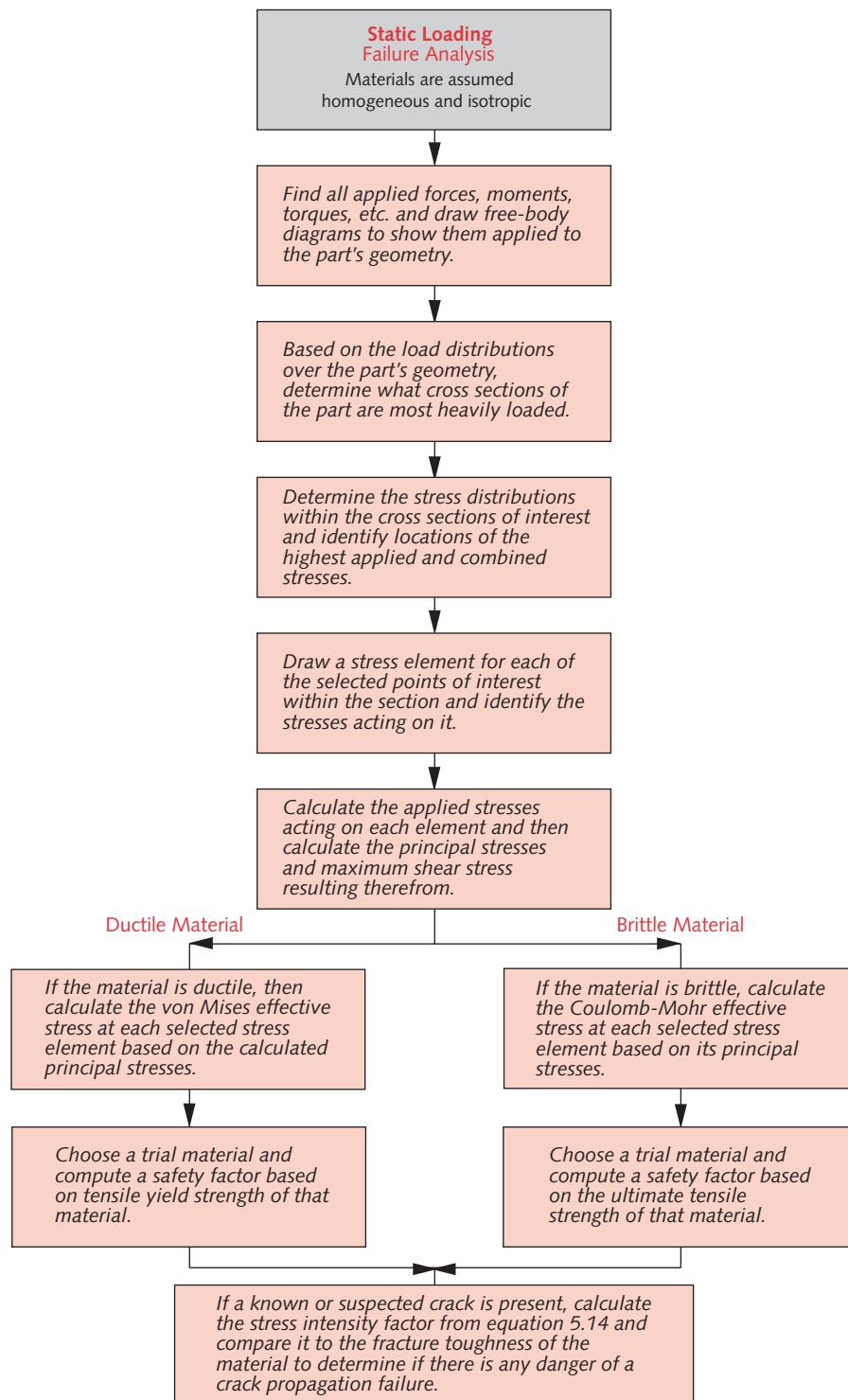
$$\sigma' = \sqrt{\sigma_x^2 + \sigma_y^2 - \sigma_x\sigma_y + 3\tau_{xy}^2} \quad (5.7d)$$

Safety Factor for Ductile Materials Under Static Loading (Section 5.1):

$$N = \frac{S_y}{\sigma'} \quad (5.8a)$$

Shear Yield Strength as a Function of Tensile Yield Strength (Section 5.1):

$$S_{ys} = 0.577 S_y \quad (5.9b)$$

**FIGURE 5-26**

Flow Chart for Static Failure Analysis

Modified-Mohr Effective Stress for 3 Dimensions (Section 5.2):

$$\begin{aligned} C_1 &= \frac{1}{2} \left[|\sigma_1 - \sigma_2| + \frac{2S_{ut} - |S_{uc}|}{-|S_{uc}|} (\sigma_1 + \sigma_2) \right] \\ C_2 &= \frac{1}{2} \left[|\sigma_2 - \sigma_3| + \frac{2S_{ut} - |S_{uc}|}{-|S_{uc}|} (\sigma_2 + \sigma_3) \right] \\ C_3 &= \frac{1}{2} \left[|\sigma_3 - \sigma_1| + \frac{2S_{ut} - |S_{uc}|}{-|S_{uc}|} (\sigma_3 + \sigma_1) \right] \end{aligned} \quad (5.12c)$$

$$\begin{aligned} \tilde{\sigma} &= \text{MAX}(C_1, C_2, C_3, \sigma_1, \sigma_2, \sigma_3) \\ \tilde{\sigma} &= 0 \quad \text{if } \text{MAX} < 0 \end{aligned} \quad (5.12d)$$

5

Safety Factor for Brittle Materials Under Static Loading (Section 5.2):

$$N = \frac{S_{ut}}{\tilde{\sigma}} \quad (5.12e)$$

Stress Intensity Factor (Section 5.3):

$$K = \beta \sigma_{nom} \sqrt{\pi a} \quad (5.14b)$$

Safety Factor for Crack Propagation (Section 5.3):

$$N_{FM} = \frac{K_c}{K} \quad (5.15)$$

5.7 REFERENCES

- 1 **J. P. D. Hartog**, *Strength of Materials*. Dover Press: New York, p. 222, 1961.
- 2 **J. Marin**, *Mechanical Behavior of Engineering Materials*. Prentice-Hall: Englewood Cliffs, N.J., pp. 117-122, 1962.
- 3 **S. P. Timoshenko**, *History of Strength of Materials*. McGraw-Hill: New York, 1953.
- 4 **N. E. Dowling**, *Mechanical Behavior of Materials*. Prentice-Hall: Englewood Cliffs, N.J., p. 252, 1993.
- 5 **Ibid.**, pp. 262-264.
- 6 **T. J. Dolan**, *Preclude Failure: A Philosophy for Material Selection and Simulated Service Testing*. SESA J. Exp. Mech., Jan. 1970.
- 7 **N. E. Dowling**, *Mechanical Behavior of Materials*. Prentice-Hall: Englewood Cliffs N.J., p. 280, 1993.
- 8 *Interim Report of a Board of Investigation to Inquire into the Design and Methods of Construction of Welded Steel Merchant Vessels*, USCG Ship Structures Committee, Wash., D.C. 20593-0001, June 3, 1944.
- 9 **C. F. Tipper**, *The Brittle Fracture Story*. Cambridge University Press: New York, 1962.
- 10 **R. C. Juvinall**, *Engineering Considerations of Stress, Strain, and Strength*. McGraw-Hill: New York, p. 71, 1967.
- 11 **J. M. Barsom and S. T. Rolfe**, *Fracture and Fatigue Control in Structures*. 2nd ed. Prentice-Hall: Englewood Cliffs, N.J., p. 203, 1987.

- 12 **J. A. Bannantine, J. J. Comer, and J. L. Handrock**, *Fundamentals of Metal Fatigue Analysis*. Prentice-Hall: Englewood Cliffs, N.J., p. 94, 1990.
- 13 **D. Broek**, *The Practical Use of Fracture Mechanics*. Kluwer Academic Publishers: Dordrecht, The Netherlands, pp. 8-10, 1988.
- 14 **Ibid**, p. 11.
- 15 **N. E. Dowling**, *Mechanical Behavior of Materials*. Prentice-Hall: Englewood Cliffs, N.J., pp. 306-307, 1993.
- 16 *Metallic Materials and Elements for Aerospace Vehicle Structures*, Department of Defense Handbook MIL-HDBK-5J, January 31, 2003.

5.8 BIBLIOGRAPHY

For further information on fracture mechanics see:

J. M. Barsom and S. T. Rolfe, *Fracture and Fatigue Control in Structures*. 2nd ed. Prentice-Hall: Englewood Cliffs, N.J., 1987.

D. Broek, *The Practical Use of Fracture Mechanics*. Kluwer: Dordrecht, The Netherlands, 1988.

R. C. Rice, ed. *Fatigue Design Handbook*. 2nd ed. SAE: Warrendale, PA. 1988.

For information on stress intensity factors see:

Y. Murakami, ed. *Stress Intensity Factors Handbook*. Pergamon Press: Oxford, U.K. 1987.

D. P. Rooke and D. J. Cartwright, *Compendium of Stress Intensity Factors*. Her Majesty's Stationery Office: London, 1976.

H. Tada, P. C. Paris, and G. R. Irwin, *The Stress Analysis of Cracks Handbook*. 2nd ed. Paris Productions Inc.: 226 Woodbourne Dr., St. Louis, Mo., 1985.

For information on fracture toughness of materials see:

Battelle, *Aerospace Structural Metals Handbook*. Metals and Ceramics Information Center, Battelle Columbus Labs: Columbus Ohio, 1991.

J. P. Gallagher, ed. *Damage Tolerant Design Handbook*. Metals and Ceramics Information Center, Battelle Columbus Labs: Columbus, Ohio, 1983.

C. M. Hudson and S. K. Seward, *A Compendium of Sources of Fracture Toughness and Fatigue Crack Growth Data for Metallic Alloys*. Int. J. of Fracture, **14**(4): R151-R184, 1978.

B. Marandet and G. Sanz, *Evaluation of the Toughness of Thick Medium Strength Steels, in Flaw Growth and Fracture*. Am. Soc. for Testing and Materials: Philadelphia, Pa. pp. 72-95, 1977.

For information on failure of composite materials see:

R. Juran, ed., *Modern Plastics Encyclopedia*. McGraw-Hill: New York. 1992.

A. Kelly, ed., *Concise Encyclopedia of Composite Materials*. Pergamon Press: Oxford, U.K. 1989.

M. M. Schwartz, *Composite Materials Handbook*. McGraw-Hill: New York, 1984.

Table P5-0[†]

Topic/Problem Matrix

5.1 Ductile Materials

**5-1, 5-2, 5-3, 5-4, 5-6, 5-7, 5-8,
5-9, 5-14, 5-15, 5-16, 5-17,
5-19, 5-20, 5-21, 5-22, 5-27a,
5-28, 5-29, 5-31, 5-33, 5-34,
5-36, 5-41, 5-42, 5-43, 5-44,
5-45, 5-46, 5-47, 5-48, 5-49,
5-56, 5-57, 5-58, 5-60, 5-67,
5-68, 5-73, 5-74, 5-78, 5-79,
5-80, 5-81**

5.2 Brittle Materials

**5-10, 5-11, 5-12, 5-13, 5-18,
5-23, 5-24, 5-25, 5-26, 5-27b,
5-30, 5-32, 5-35, 5-37, 5-59,
5-40, 5-61, 5-62, 5-63, 5-64,
5-65, 5-66, 5-69, 5-70, 5-71,
5-72, 5-75, 5-82, 5-83, 5-84,
5-85**

5.3 Fracture Mechanics

**5-38, 5-39, 5-50, 5-51, 5-52,
5-53, 5-54, 5-55, 5-76, 5-77**

5.9 PROBLEMS

- *[†]**5-1** A differential stress element has a set of applied stresses on it as indicated in each row of Table P5-1. For the row(s) assigned, draw the stress element showing the applied stresses. Find the principal stresses and von Mises stresses.
- 5-2** A 400-lb chandelier is to be hung from two 10-ft-long solid, low-carbon steel cables in tension. Size the cables for a safety factor of 4. State all assumptions.
- 5-3** For the bicycle pedal arm assembly in Figure P5-1 with a rider-applied force of 1 500 N at the pedal, determine the von Mises stress in the 15-mm-dia pedal arm. The pedal attaches to the arm with a 12-mm thread. Find the von Mises stress in the screw. Find the safety factor against static failure if the material has $S_y = 350$ MPa.
- ***5-4** The trailer hitch shown in Figure P5-2 and Figure 1-1 (p. 11) has loads applied as shown. The tongue weight of 100 kg acts downward and the pull force of 4 905 N acts horizontally. Using the dimensions of the ball bracket shown in Figure 1-5 (p. 14) and $S_y = 300$ MPa ductile steel, determine static safety factors for
 (a) The shank of the ball where it joins the ball bracket.
 (b) Bearing failure in the ball bracket hole.
 (c) Tearout failure in the ball bracket.
 (d) Tensile failure in the attachment bolts if they are 19-mm dia.
 (e) Bending failure in the ball bracket as a cantilever.
- 5-5** Repeat Problem 5-4 for the loading conditions of Problem 3-5 on p. 127.
- ***5-6** Repeat Problem 5-4 for the loading conditions of Problem 3-6 on p. 127.
- ***5-7** Design the wrist pin of Problem 3-7 (p. 127) for safety factor = 3.0 if $S_y = 100$ kpsi.
- ***5-8** A paper mill processes rolls of paper having a density of 984 kg/m³. The paper roll is 1.50-m outside dia. (*OD*) × 0.22-m inside diameter (*ID*) × 3.23-m long and is on a simply supported, hollow, steel shaft with $S_y = 300$ MPa. Find the shaft *ID* needed to obtain a static safety factor of 5 if the shaft *OD* is 22 cm.
- 5-9** For the ViseGrip® plier-wrench drawn to scale in Figure P5-3, and for which the forces were analyzed in Problem 3-9 and the stresses in Problem 4-9, find the safety factors for each pin for an assumed clamping force of $P = 4\ 000$ N in the position shown. The pins are 8-mm dia, $S_y = 400$ MPa, and are all in double shear.

Table P5-1 Data for Problem 5-1

Rows a-g are two-dimensional, others are 3-D problems

Row	σ_x	σ_y	σ_z	τ_{xy}	τ_{yz}	τ_{zx}
a	1 000	0	0	500	0	0
b	-1 000	0	0	750	0	0
c	500	-500	0	1 000	0	0
d	0	-1 500	0	750	0	0
e	750	250	0	500	0	0
f	-500	1 000	0	750	0	0
g	1 000	0	-750	0	0	250
h	750	500	250	500	0	0
i	1 000	-250	-750	250	500	750
j	-500	750	250	100	250	1 000

* Answers to these problems are provided in Appendix D.

† Problem numbers in *italics* are design problems. Problem numbers in **boldface** are extended from similar problems in earlier chapters with the same dash number. Problems in succeeding chapters may also continue and extend these problems.

- *5-10** An overhung diving board is shown in Figure P5-4a. Assume cross-sectional dimensions of 305 mm \times 32 mm. Find the largest principal stress in the board when a 100-kg person is standing at the free end. What is the static safety factor if the material is brittle fiberglass with $S_{ut} = 130$ MPa in the longitudinal direction?

- *5-11** Repeat Problem 5-10 assuming the 100-kg person in Problem 5-10 jumps up 25 cm and lands back on the board. Assume the board weighs 29 kg and deflects 13.1 cm statically when the person stands on it. What is the static safety factor if the material is brittle fiberglass with $S_{ut} = 130$ MPa in the longitudinal direction?

- 5-12** Repeat Problem 5-10 using the cantilevered diving-board design in Figure P5-4b.

- 5-13** Repeat Problem 5-11 using the diving-board design shown in Figure P5-4b. Assume the board weighs 19 kg and deflects 8.5 cm statically when the person stands on it.

- 5-14** Figure P5-5 shows a child's toy called a *pogo stick*. The child stands on the pads, applying half her weight on each side. She jumps up off the ground, holding the pads up against her feet, and bounces along with the spring cushioning the impact and storing energy to help each rebound. Assume a 60-lb child and a spring constant of 100 lb/in. The pogo stick weighs 5 lb. Design the aluminum cantilever beam sections on which she stands to survive jumping 2 in off the ground with a safety factor of 2. Use 1100 series aluminum. Define the beam shape and size.

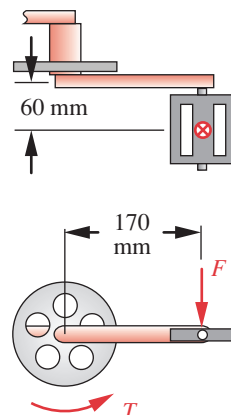
- *5-15** What is the safety factor for the shear pin as defined in Problem 4-15?

- 5-16** A track to guide bowling balls is designed with two round rods as shown in Figure P5-6. The rods have a small angle between them. The balls roll on the rods until they fall between them and drop onto another track. Each rod's unsupported length is 30 in and the angle between them is 3.2°. The balls are 4.5-in dia and weigh 2.5 lb. The center distance between the rods is 4.2 in at the narrow end. Find the static safety factor for the 1-in-dia SAE 1045 normalized steel rods.

- (a) Assume the rods are simply supported at each end.
(b) Assume the rods are fixed at each end.

- *5-17** A pair of ice tongs is shown in Figure P5-7. The ice weighs 50 lb and is 10 in wide across the tongs. The distance between the handles is 4 in, and the mean radius r of a tong is 6 in. The rectangular cross-sectional dimensions are 0.750 in deep \times 0.312 in wide. Find the safety factor for the tongs if their $S_y = 30$ kpsi.

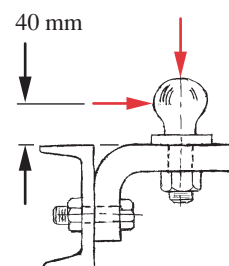
- 5-18 Repeat Problem 5-17 with the tongs made of Class 20 gray cast iron.



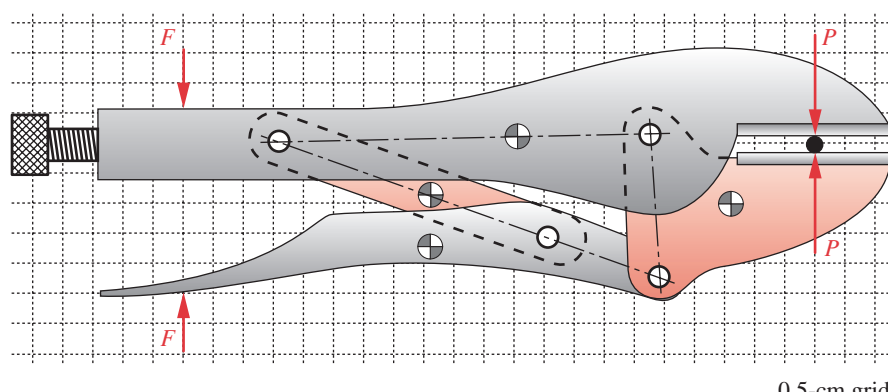
5

FIGURE P5-1

Problem 5-3 (A Solidworks model of this is on the CD)

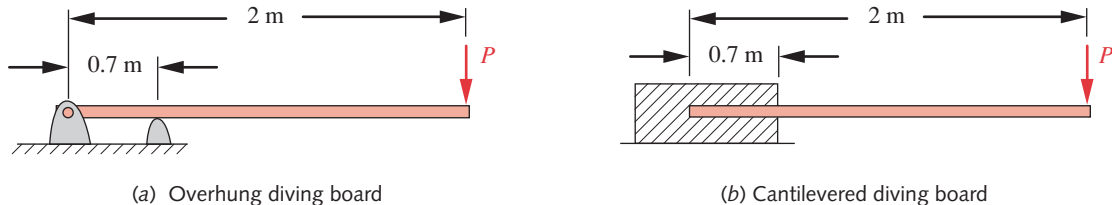
**FIGURE P5-2**

Problems 5-4, 5-5, 5-6
(A Solidworks model of this is on the CD)

**FIGURE P5-3**

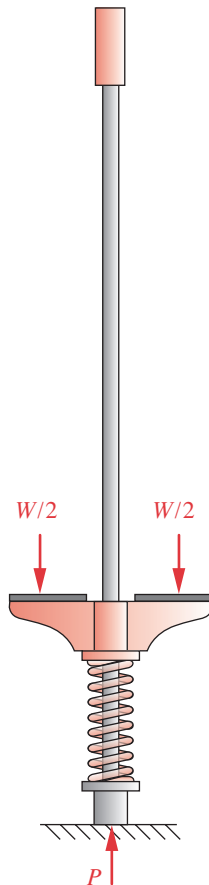
Problem 5-9 (A Solidworks model of this is on the CD)

* Answers to these problems are provided in Appendix D. Problem numbers in *italics* are design problems. Problem numbers in **boldface** are extended from similar problems in earlier chapters with the same dash number. Problems in succeeding chapters may also continue and extend these problems.

**FIGURE P5-4**

Problems 5-10 through 5-13

5

**FIGURE P5-5**

Problem 5-14

* Answers to these problems are provided in Appendix D. Problem numbers in *italics* are design problems. Problem numbers in **boldface** are extended from similar problems in earlier chapters with the same dash number. Problems in succeeding chapters may also continue and extend these problems.

- *5-19** Determine the size of the clevis pin shown in Figure P5-8 needed to withstand an applied force of 130 000 lb. Also determine the required outside radius of the clevis end to not fail in either tearout or bearing if the clevis flanges are each 2.5 in thick. Use a safety factor of 3 for all modes of failure. Assume $S_y = 89.3$ ksi for the pin and $S_y = 35.5$ ksi for the clevis.

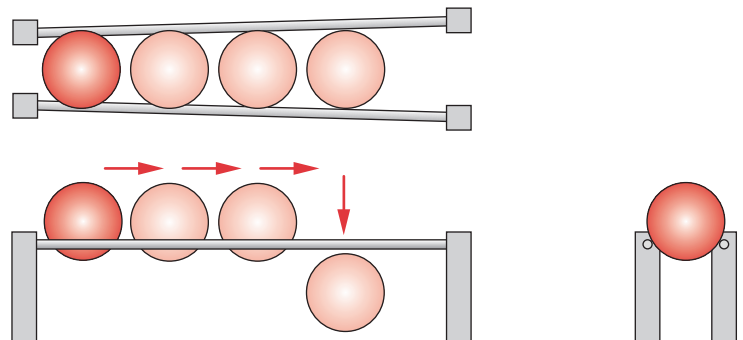
- 5-20** A 100 N-m torque is applied to a 1-m-long, solid, round shaft. Design it to limit its angular deflection to 2° and select a steel alloy to have a yielding safety factor of 2.

- 5-21** Figure P5-9 shows an automobile wheel with two styles of lug wrench, a single-ended wrench in (a) and a double-ended wrench in (b). The distance between points A and B is 1 ft in both cases and the handle diameter is 0.625 in. What is the maximum force possible before yielding the handle if the material $S_y = 45$ ksi?

- *5-22** An in-line “roller-blade” skate is shown in Figure P5-10. The polyurethane wheels are 72-mm dia and spaced on 104-mm centers. The skate-boot-foot combination weighs 2 kg. The effective “spring rate” of the person-skate system is 6 000 N/m. The axles are 10-mm-dia steel pins in double shear with $S_y = 400$ MPa. Find the safety factor for the pins when a 100-kg person lands a 0.5-m jump on one foot.

- (a) Assume that all four wheels land simultaneously.
 (b) Assume that one wheel absorbs all the landing force.

- *5-23** A beam is supported and loaded as shown in Figure P5-11a. For the data given in the assigned row(s) in Table P5-2, find the static safety factor:
- (a) If the beam is a ductile material with $S_y = 300$ MPa,
 (b) If the beam is a cast-brittle material with $S_{ut} = 150$ MPa, $S_{uc} = 570$ MPa.

**FIGURE P5-6**

Problem 5-16

***5-24** A beam is supported and loaded as shown in Figure P5-11b. For the data given in the assigned row(s) in Table P5-2, find the static safety factor:

- If the beam is a ductile material with $S_y = 300 \text{ MPa}$,
- If the beam is a cast-brittle material with $S_{ut} = 150 \text{ MPa}$, $S_{uc} = 570 \text{ MPa}$.

***5-25** A beam is supported and loaded as shown in Figure P5-11c. For the data given in the assigned row(s) in Table P5-2, find the static safety factor:

- If the beam is a ductile material with $S_y = 300 \text{ MPa}$,
- If the beam is a cast-brittle material with $S_{ut} = 150 \text{ MPa}$, $S_{uc} = 570 \text{ MPa}$.

***5-26** A beam is supported and loaded as shown in Figure P5-11d. For the data given in the assigned row(s) in Table P5-2, find the static safety factor:

- If the beam is a ductile material with $S_y = 300 \text{ MPa}$,
- If the beam is a cast-brittle material with $S_{ut} = 150 \text{ MPa}$, $S_{uc} = 570 \text{ MPa}$.

***5-27** A storage rack is to be designed to hold the paper roll of Problem 5-8 as shown in Figure P5-12. Determine suitable values for dimensions a and b in the figure. Make the static safety factor at least 1.5. The mandrel is solid and inserts halfway into the paper roll.

- The beam is a ductile material with $S_y = 300 \text{ MPa}$,
- The beam is a cast-brittle material with $S_{ut} = 150 \text{ MPa}$, $S_{uc} = 570 \text{ MPa}$.

5-28 Figure P5-13 shows a forklift truck negotiating a 15° ramp to drive onto a 4-ft-high loading platform. The truck weighs 5 000 lb and has a 42-in wheelbase. Design two (one for each side) 1-ft-wide ramps of steel to have a safety factor of 3 in the worst case of loading as the truck travels up them. Minimize the weight of the ramps by using a sensible cross-section geometry. Choose an appropriate steel or aluminum alloy.

5-29 A differential element is subjected to the stresses (in kpsi): $\sigma_1 = 10$, $\sigma_2 = 0$, $\sigma_3 = -20$. A ductile material has the strengths (in kpsi) $S_{ut} = 50$, $S_y = 40$, $S_{uc} = 50$. Calculate the safety factor and draw $\sigma_1 - \sigma_3$ diagrams of each theory showing the stress state using:

- Maximum shear-stress theory
- Distortion-energy theory

5-30 A differential element is subjected to the stresses (in kpsi): $\sigma_1 = 10$, $\sigma_2 = 0$, $\sigma_3 = -20$. A brittle material has the strengths (in kpsi) $S_{ut} = 50$, $S_{uc} = 90$. Calculate the safety factor and draw $\sigma_1 - \sigma_3$ diagrams of each theory showing the stress state using:

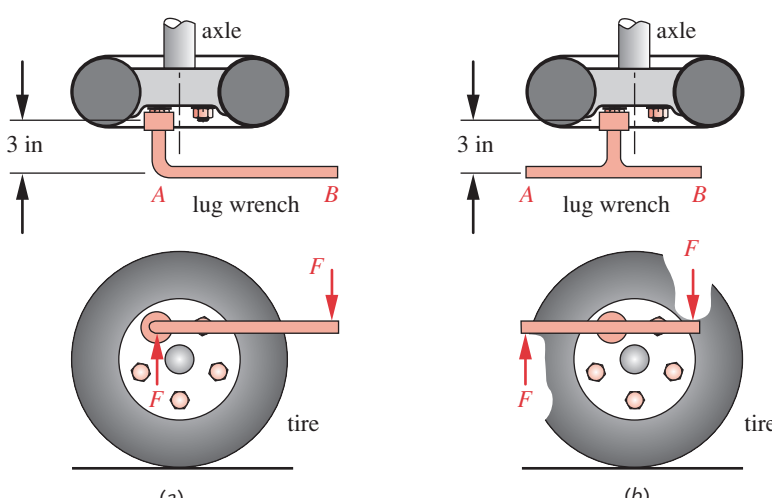
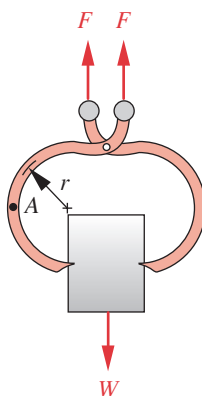


FIGURE P5-9

Problem 5-21



5

FIGURE P5-7

Problem 5-17

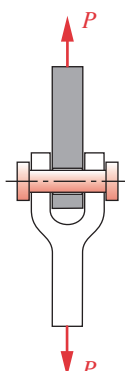


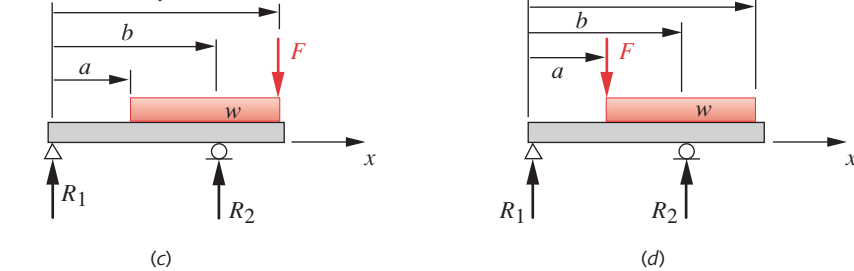
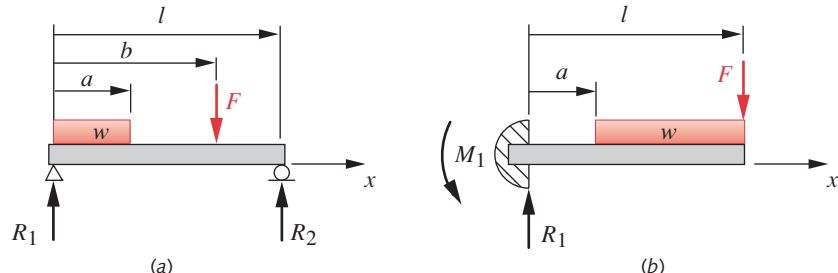
FIGURE P5-8

Problem 5-19

* Answers to these problems are provided in Appendix D. Problem numbers in *italics* are design problems. Problem numbers in **boldface** are extended from similar problems in earlier chapters with the same dash number. Problems in succeeding chapters may also continue and extend these problems.

**FIGURE P5-10**

Problem 5-22

**FIGURE P5-11**

Beams and Beam Loadings for Problems 5-23 to 5-26 — see Table P5-2 for Data

- (a) Coulomb-Mohr theory
 (b) Modified-Mohr theory

- 5-31** Design a jack-stand in a tripod configuration that will support 2 tons of load with a safety factor of 3. Use SAE 1020 steel and minimize its weight.

Table P5-2 Data for Problems 5-23 through 5-26Use only data relevant to the particular problem. Lengths in m, forces in N, I in m^4 .

Row	<i>l</i>	<i>a</i>	<i>b</i>	<i>w</i> [*]	<i>F</i>	<i>I</i>	<i>c</i>	<i>E</i>
<i>a</i>	1.00	0.40	0.60	200	500	$2.85E-08$	$2.00E-02$	steel
<i>b</i>	0.70	0.20	0.40	80	850	$1.70E-08$	$1.00E-02$	steel
<i>c</i>	0.30	0.10	0.20	500	450	$4.70E-09$	$1.25E-02$	steel
<i>d</i>	0.80	0.50	0.60	65	250	$4.90E-09$	$1.10E-02$	steel
<i>e</i>	0.85	0.35	0.50	96	750	$1.80E-08$	$9.00E-03$	steel
<i>f</i>	0.50	0.18	0.40	450	950	$1.17E-08$	$1.00E-02$	steel
<i>g</i>	0.60	0.28	0.50	250	250	$3.20E-09$	$7.50E-03$	steel
<i>h</i>	0.20	0.10	0.13	400	500	$4.00E-09$	$5.00E-03$	alum
<i>i</i>	0.40	0.15	0.30	50	200	$2.75E-09$	$5.00E-03$	alum
<i>j</i>	0.20	0.10	0.15	150	80	$6.50E-10$	$5.50E-03$	alum
<i>k</i>	0.40	0.16	0.30	70	880	$4.30E-08$	$1.45E-02$	alum
<i>l</i>	0.90	0.25	0.80	90	600	$4.20E-08$	$7.50E-03$	alum
<i>m</i>	0.70	0.10	0.60	80	500	$2.10E-08$	$6.50E-03$	alum
<i>n</i>	0.85	0.15	0.70	60	120	$7.90E-09$	$1.00E-02$	alum

Problem numbers in *italics* are design problems.^{*} Note that *w* is a unit force of N/m

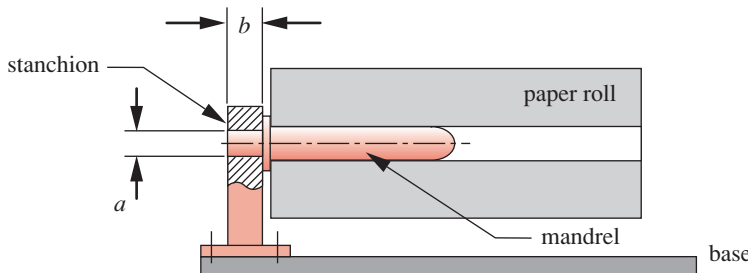


FIGURE P5-12

Problem 5-27

5

- *5-32 A part has a combined stress state and strengths (in kpsi) of: $\sigma_x = 10$, $\sigma_y = 5$, $\tau_{xy} = 4.5$, $S_{ut} = 20$, $S_{uc} = 80$, $S_y = 18$. Choose an appropriate failure theory based on the given data; find the effective stress and factor of safety against static failure.
- *5-33 For the bracket shown in Figure P5-14 and the data in the row(s) assigned from Table P5-3, determine the von Mises stresses at points A and B.
- *5-34 Calculate the safety factor for the bracket in Problem 5-33 using the distortion-energy, the maximum shear-stress, and the maximum normal-stress theories. Comment on their appropriateness. Assume a ductile material strength of $S_y = 400$ MPa (60 kpsi).
- *5-35 Calculate the safety factor for the bracket in Problem 5-33 using the Coulomb-Mohr and the modified-Mohr effective-stress theories. Comment on their appropriateness. Assume a brittle material strength of $S_{ut} = 350$ MPa (50 kpsi) and $S_{uc} = 1\,000$ MPa (150 kpsi).
- 5-36 For the bracket shown in Figure P5-14 and the data in the row(s) assigned from Table P5-3, redo Problem 5-33 considering the stress concentration at points A and B. Assume a stress-concentration factor of 2.5 in both bending and torsion.
- *5-37 A semicircular curved beam as shown in Figure P5-15 has $OD = 150$ mm, $ID = 100$ mm, and $t = 25$ mm. For a load pair $F = 14$ kN applied along the diameter, find the safety factor at the inner and outer fibers: (a) If the beam is a ductile material with $S_y = 700$ MPa, (b) If the beam is a cast-brittle material with $S_{ut} = 420$ MPa, $S_{uc} = 1\,200$ MPa.
- *5-38 Assume that the curved beam of Problem 5-37 has a crack on its inside surface of half-width $a = 2$ mm and a fracture toughness of 50 MPa-m $^{0.5}$. What is its safety factor against sudden fracture?

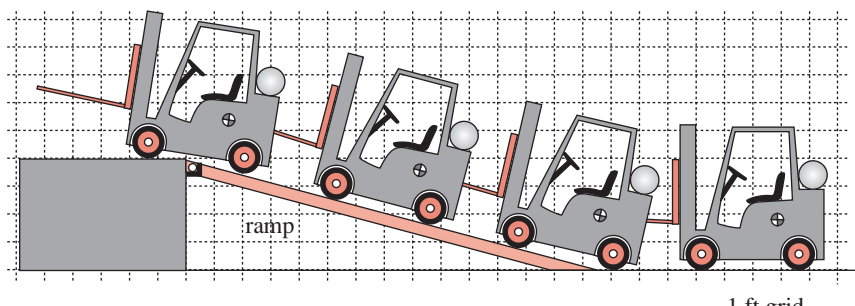


FIGURE P5-13

Problem 5-28

* Answers to these problems are provided in Appendix D. Problem numbers in *italics* are design problems. Problem numbers in **boldface** are extended from similar problems in earlier chapters with the same dash number. Problems in succeeding chapters may also continue and extend these problems.

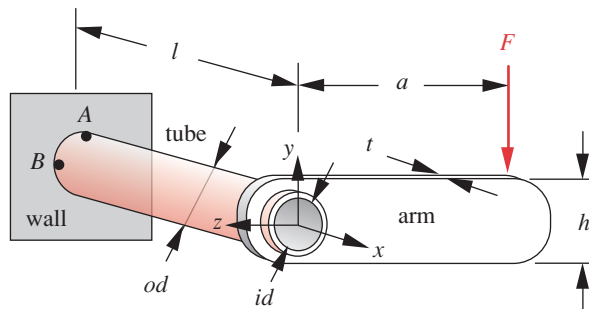


FIGURE P5-14

Problems 5-33 to 5-36 (A Solidworks model of this is on the CD)

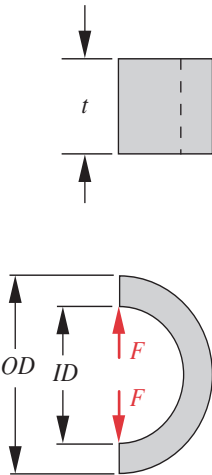


FIGURE P5-15

Problem 5-37 (A Solidworks model of this is on the CD)

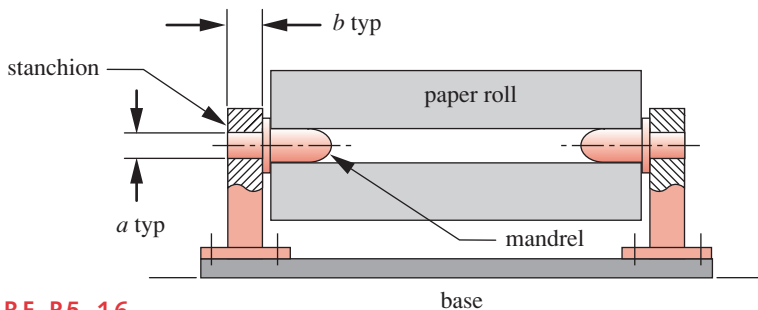
- *5-39 Consider the failed 260-in-dia by 0.73-in-wall rocket case of Figure 5-16. The steel had $S_y = 240$ kpsi and a fracture toughness $K_c = 79.6$ kpsi-in $^{0.5}$. It was designed for an internal pressure of 960 psi but failed at 542 psi. Failure was attributed to a small crack that precipitated a sudden, brittle, fracture-mechanics failure. Find the nominal stresses in the wall and the yielding safety factor at the failure conditions and estimate the size of the crack that caused it to explode. Assume $\beta = 1.0$.
- 5-40 Redesign the roll support of Problem 5-8 to be like Figure P5-16. The mandrels insert to 10% of the roll length. Design dimensions a and b for a safety factor of 2.
- (a) If the beam is a ductile material with $S_y = 300$ MPa,
(b) If the beam is a cast-brittle material with $S_{ut} = 150$ MPa, $S_{uc} = 1200$ MPa.
- *5-41 A 10-mm-ID steel tube carries liquid at 7 MPa. The steel has $S_y = 400$ MPa. Determine the safety factor for the wall if its thickness is: (a) 1 mm, (b) 5 mm.
- 5-42 A cylindrical tank with hemispherical ends is required to hold 150 psi of pressurized air at room temperature. The steel has $S_y = 400$ MPa. Determine the safety factor if the tank diameter is 0.5 m with a 1-mm wall thickness, and its length is 1 m.

Table P5-3 Data for Problems 5-33 through 5-36

Use only data that are relevant to the particular problem. Lengths in mm, forces in N.

Row	l	a	t	h	F	OD	ID	E
<i>a</i>	100	400	10	20	50	20	14	steel
<i>b</i>	70	200	6	80	85	20	6	steel
<i>c</i>	300	100	4	50	95	25	17	steel
<i>d</i>	800	500	6	65	160	46	22	alum
<i>e</i>	85	350	5	96	900	55	24	alum
<i>f</i>	50	180	4	45	950	50	30	alum
<i>g</i>	160	280	5	25	850	45	19	steel
<i>h</i>	200	100	2	10	800	40	24	steel
<i>i</i>	400	150	3	50	950	65	37	steel
<i>j</i>	200	100	3	10	600	45	32	alum
<i>k</i>	120	180	3	70	880	60	47	alum
<i>l</i>	150	250	8	90	750	52	28	alum
<i>m</i>	70	100	6	80	500	36	30	steel
<i>n</i>	85	150	7	60	820	40	15	steel

* Answers to these problems are provided in Appendix D. Problem numbers in *italics* are design problems. Problem numbers in **boldface** are extended from similar problems in earlier chapters with the same dash number. Problems in succeeding chapters may also continue and extend these problems.

**FIGURE P5-16**

Problem 5-40 (A Solidworks model of this is on the CD)

5

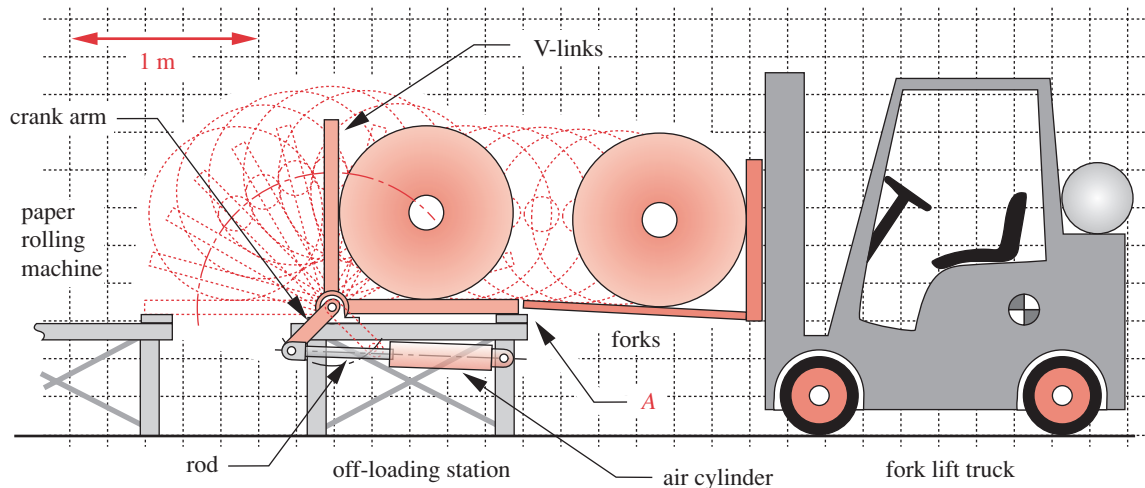
- 5-43** The paper rolls in Figure P5-17 are 0.9-m OD \times 0.22-m ID \times 3.23-m long and have a density of 984 kg/m³. The rolls are transferred from the machine conveyor (not shown) to the forklift truck by the V-linkage of the off-load station which is rotated through 90° by an air cylinder. The paper then rolls onto the waiting forks of the truck. The forks are 38-mm thick by 100-mm wide by 1.2-m long and are tipped at a 3° angle from the horizontal and have $S_y = 600$ MPa. Find the safety factor for the two forks on the truck when the paper rolls onto it under two different conditions (state all assumptions):

- (a) The two forks are unsupported at their free end.
- (b) The two forks are contacting the table at point A.

- 5-44** Determine a suitable thickness for the V-links of the off-loading station of Figure P5-17 to limit their deflections at the tips to 10 mm in any position during their rotation. Two V-links support the roll, at the 1/4 and 3/4 points along the roll's length, and each of the V arms is 10-cm wide by 1-m long. What is their safety factor against yielding when designed to limit deflection as above? $S_y = 400$ MPa. See Problem 5-43 for more information.

- 5-45** Determine the safety factor based on the critical load on the air-cylinder rod in Figure P5-17. The crank arm that it rotates is 0.3 m long and the rod has a maximum extension

Problem numbers in *italics* are design problems. Problem numbers in **boldface** are extended from similar problems in earlier chapters with the same dash number. Problems in succeeding chapters may also continue and extend these problems.

**FIGURE P5-17**

Problems 5-43 to 5-47

of 0.5 m. The 25-mm-dia rod is solid steel with a yield strength of 400 MPa. State all assumptions.

- 5-46** The V-links of Figure P5-17 are rotated by the crank arm through a shaft that is 60-mm dia by 3.23-m long. Determine the maximum torque applied to this shaft during the motion of the V-linkage and find the static safety factor against yielding for the shaft if its $S_y = 400$ MPa. See Problem 5-43 for more information.
- 5-47** Determine the maximum forces on the pins at each end of the air cylinder of Figure P5-17. Determine the safety factor for these pins if they are 30-mm dia and in single shear. $S_y = 400$ MPa.
- 5-48** Figure P5-18 shows an exerciser for a 100-kg wheelchair racer. The wheelchair has 65-cm-dia drive wheels separated by a 70-cm track width. Two free-turning rollers on bearings support the rear wheels. The lateral movement of the chair is limited by the flanges. Design the 1-m-long rollers as hollow tubes of aluminum (select alloy) to minimize the height of the platform and also limit the roller deflections to 1 mm in the worst case. Specify suitable sized steel axles to support the tubes on bearings. Calculate all significant safety factors.
- 5-49** A part made of ductile steel with $S_y = 40$ kpsi is subjected to a three-dimensional stress state of $\sigma_1 = -80$ kpsi, $\sigma_2 = -80$ kpsi, $\sigma_3 = -80$ kpsi. What is the maximum shear stress? Will the part fail?
- 5-50** A component in the shape of a large sheet is to be fabricated from 7075-T651 aluminum, which has a fracture toughness $K_c = 24.2$ MPa-m $^{0.5}$ and a tensile yield strength of 495 MPa. Determine the largest edge crack that could be tolerated in the sheet if the nominal stress does not exceed one half the yield strength.
- 5-51** A component in the shape of a large sheet is to be fabricated from 4340 steel, which has a fracture toughness $K_c = 98.9$ MPa-m $^{0.5}$ and a tensile yield strength of 860 MPa. The sheets are inspected for crack flaws after fabrication, but the inspection device cannot detect flaws smaller than 3 mm. The part is too heavy as designed. An engineer has suggested that the thickness be reduced and the material be heat-treated to increase its tensile strength to 1 515 MPa, which would result in decreasing the fracture toughness to 60.4 MPa-m $^{0.5}$. Assuming that the stress level does not exceed one half the yield strength, is the suggestion feasible? If not, why not?
- 5-52** A large plate is subjected to a nominal tensile stress of 350 MPa. The plate has a central crack that is 15.9-mm long. Calculate the stress intensity factor at the tip of the crack.
- 5-53** A movie scene calls for a stuntman to hang from a rope that is suspended 3 m above a pit of poisonous spiders. The rope is attached to a glass sheet that is 3 000 mm long by 100 mm wide and 1.27 mm thick. The stuntman knows that the glass sheet contains a central crack with total length of 16.2 mm that is oriented parallel to the ground. The fracture

Problem numbers in **boldface** are extended from similar problems in earlier chapters with the same dash number. Problems in succeeding chapters may also continue and extend these problems.

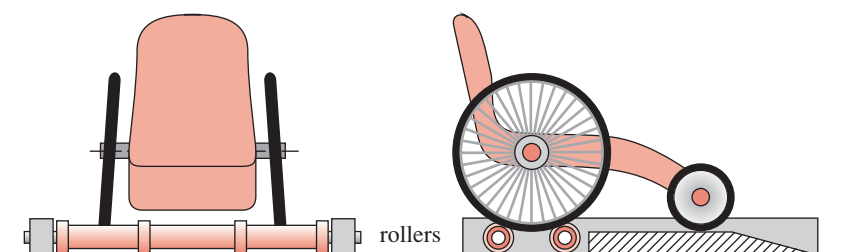
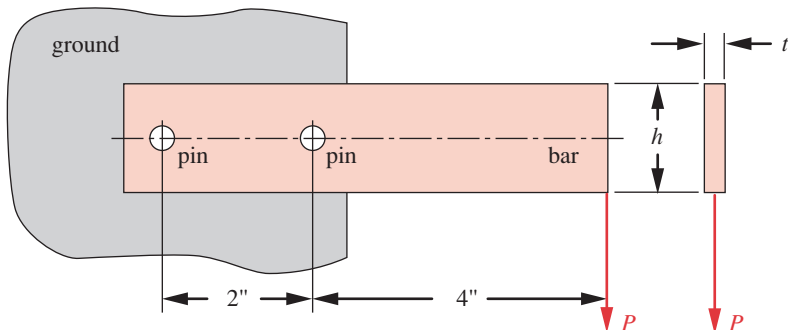


FIGURE P5-18

Problem 5-48

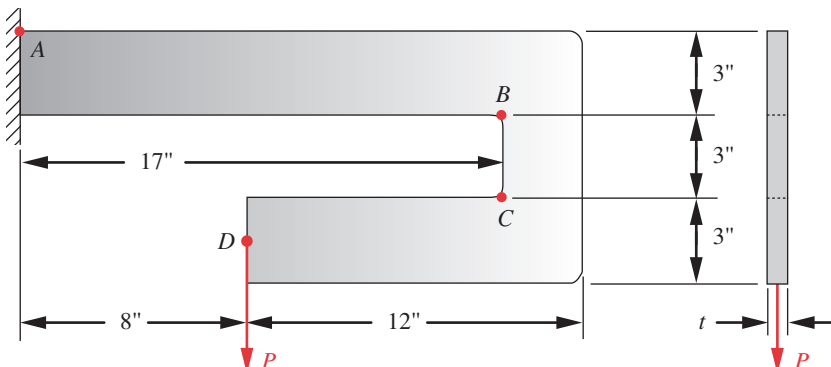
**FIGURE P5-19**

Problems 5-56 and 5-57 (A Solidworks model of this is on the CD)

5

toughness of the glass is $0.83 \text{ MPa-m}^{0.5}$. Should he do the stunt? Show all assumptions and calculations in support of your answer.

- 5-54** A material has a fracture toughness of $50 \text{ MPa-m}^{0.5}$ and a yield strength of $1\,000 \text{ MPa}$ and is to be made into a large panel. If the panel is stressed to one-half the yield stress, what is the maximum central crack size that can be tolerated without catastrophic failure?
- 5-55** A material that has a fracture toughness of $33 \text{ MPa-m}^{0.5}$ is to be made into a large panel that is 2 000 mm long by 250 mm wide and 4 mm thick. If the minimum allowable total crack length is 4 mm, what is the maximum tensile load in the long direction that can be applied without catastrophic failure with a safety factor of 2.5?
- 5-56** Figure P5-19 shows an SAE 1020 cold-rolled steel bar fastened to a rigid ground plane with two 0.25-in-dia A8 steel dowel pins, hardened to HRC52. For $P = 1\,500 \text{ lb}$ and $t = 0.25 \text{ in}$, find:
- The safety factor for each pin.
 - The safety factor for direct bearing stress in each hole.
 - The safety factor for tearout failure if $h = 1 \text{ in}$.
- 5-57** Repeat Problem 5-56 for the part made from class 50 cast iron.
- 5-58** Figure P5-20 shows a bracket machined from 0.5-in-thick SAE 1045 cold-rolled steel flat stock with 0.25-in inside-corner radii. It is rigidly attached to a support and loaded with $P = 5\,000 \text{ lb}$ at point D. Find:

**FIGURE P5-20**

Problems 5-58 and 5-59 (A Solidworks model of this is on the CD)

Problem numbers in **boldface** are extended from similar problems in earlier chapters with the same dash number. Problems in succeeding chapters may also continue and extend these problems.

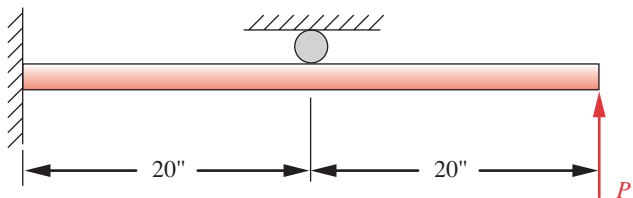


FIGURE P5-21

Problem 5-60

5

- (a) The safety factor against static failure at point *A*.
 (b) The safety factor against static failure at point *B*.

- 5-59** Repeat Problem 5-58 for the part made from 1-in-thick class 60 cast iron.
- 5-60** Figure P5-21 shows a 1-in-dia SAE 1040 hot-rolled normalized steel bar supported and subjected to the applied load $P = 500$ lb. Find the safety factor against static failure.
- 5-61** Repeat Problem 5-60 for the part made from class 60 cast iron with its diameter increased to 1.5 in.
- 5-62** Figure P5-22 shows a pivot pin that is press-fit into part *A* and a slip fit in part *B*. If $F = 100$ lb, $l = 2$ in, and $d = 0.5$ in, what is the pin's safety factor against yielding when made of SAE 1020 cold-rolled steel?
- 5-63** Figure P5-22 shows a pivot pin that is press-fit into part *A* and a slip fit in part *B*. If $F = 100$ N, $l = 50$ mm, and $d = 16$ mm, what is the pin's safety factor against fracture when made of class 50 cast iron?
- 5-64** A differential element is subjected to the stresses (in kpsi): $\sigma_x = 10$, $\sigma_y = -20$, $\tau_{xy} = -20$. The material is uneven and has strengths (in kpsi) of $S_{ut} = 50$, $S_y = 40$, and $S_{uc} = 90$. Calculate the safety factor and draw a σ_a - σ_b diagram showing the boundary for each theory with the stress state and load line using:
 (a) Coulomb-Mohr theory, and
 (b) Modified Mohr theory.
- *5-65** A differential element is subjected to the stresses (in kpsi): $\sigma_x = 10$, $\sigma_y = -5$, $\tau_{xy} = 15$. The material is uneven and has strengths (in kpsi) of $S_{ut} = 50$, $S_y = 40$, and $S_{uc} = 90$. Calculate the safety factor and draw a σ_a - σ_b diagram showing the boundary for each theory with the stress state and load line using:
 (a) Coulomb-Mohr theory, and
 (b) Modified Mohr theory.

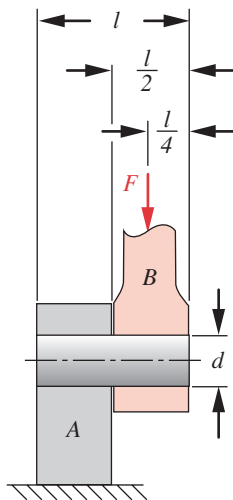


FIGURE P5-22

Problems 5-62 and 5-63

* Answers to these problems are provided in Appendix D.

Problem numbers in *italics* are design problems. Problem numbers in **boldface** are extended from similar problems in earlier chapters with the same dash number. Problems in succeeding chapters may also continue and extend these problems.

- 5-66** A differential element is subjected to the stresses (in kpsi): $\sigma_x = -20$, $\sigma_y = -15$, $\tau_{xy} = 15$. The material is uneven and has strengths (in kpsi) of $S_{ut} = 50$, $S_y = 40$, and $S_{uc} = 90$. Calculate the safety factor and draw a σ_a - σ_b diagram showing the boundary for each theory with the stress state and load line using:
 (a) Coulomb-Mohr theory, and
 (b) Modified Mohr theory.
- 5-67** Derive the Von Mises effective stress equation 5.7d for the two-dimensional case.
- *5-68** Figure P5-23 shows an oil-field pump jack. The crank drive shaft at O_2 is loaded in torsion and bending with maximum values of 6500 in-lb and 9800 in-lb, respectively. The point on the shaft with maximum stress is located away from the key that connects the shaft to the crank. Using a factor of safety of 2 against static yielding, determine a suitable diameter for the shaft if it is to be made of SAE 1040 cold-rolled steel.

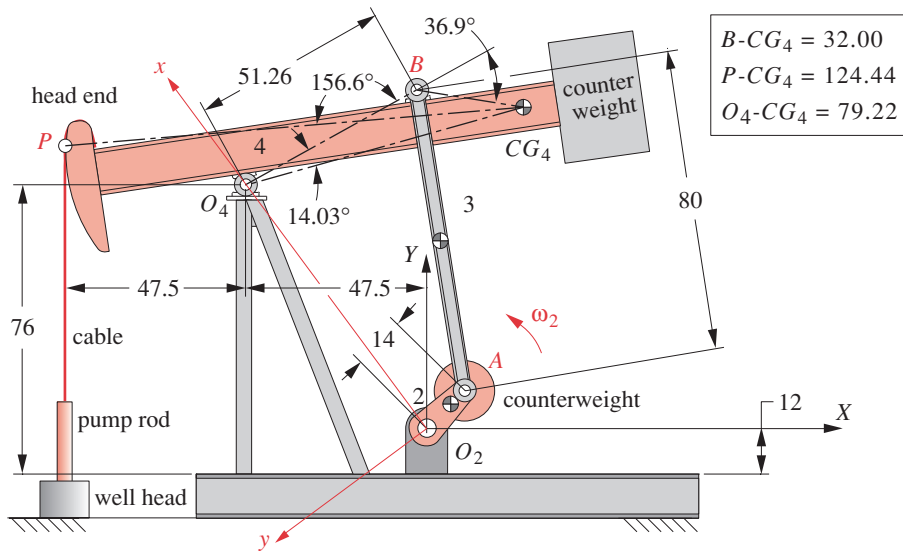


FIGURE P5-23

all linear dimensions are in inches

Problems 5-68 and 69

- 5-69** Figure P5-24a shows a C-clamp with an elliptical body dimensioned as shown. The clamp has a T-section with a uniform thickness of 3.2 mm at the throat as shown in Figure P5-24b. Find the static factor of safety if the clamping force is 2.7 kN and the material is class 40 gray cast iron.

- 5-70** A C-clamp as shown in Figure P5-24a has a rectangular cross section as in Figure P5-24c. Find the static factor of safety if the clamping force is 1.6 kN and the material is class 50 gray cast iron.

- 5-71** A C-clamp as shown in Figure P5-24a has an elliptical cross section as in Figure P5-24d. Dimensions of the major and minor axes of the ellipse are given. Find the static factor of safety if the clamping force is 1.6 kN and the material is class 60 gray cast iron.

Problem numbers in **boldface** are extended from similar problems in earlier chapters with the same dash number. Problems in succeeding chapters may also continue and extend these problems.

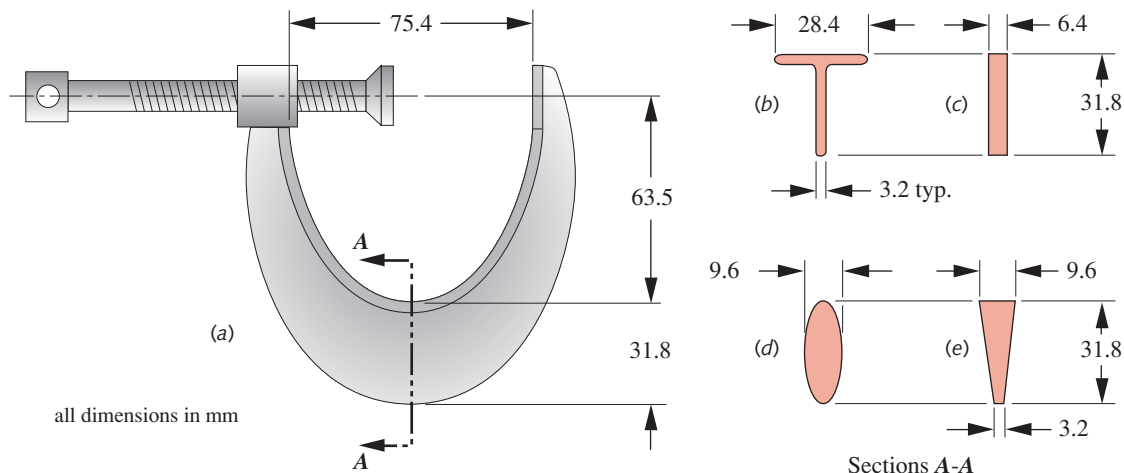


FIGURE P5-24

Problems 5-69 to 5-72 (A Solidworks model of this is on the CD)

- 5-72** A C-clamp as shown in Figure P5-24a has a trapezoidal cross section as in Figure P5-24e. Find the static factor of safety if the clamping force is 1.6 kN and the material is class 40 gray cast iron.
- 5-73** The connecting rod (3) on the oil-field pump jack shown in Figure P5-23 is, in fact, made up of two rods, one connecting on each side of the walking beam (4). Determine a suitable width of 1/2-inch-thick SAE 1020 cold-rolled bar stock to use if the maximum tensile load on the bars is 3500 lb each. Use a factor of safety of 4 against static yielding.
- 5-74** A work platform is elevated on the end of a boom that has the ability to extend its length and vary its angle with respect to ground. The platform width is large compared to the boom diameter so that it is possible to load the boom eccentrically resulting in a combination of bending, torsion, and direct compression in the base of the boom. At the base the boom is a hollow tube with an outside diameter of 8 in and a wall thickness of 0.75 in. It is made from SAE 1030 CR steel. Determine the factor of safety against static failure if the loading at a point at the base of the boom is $M = 600\,000 \text{ lb-in}$, $T = 76\,000 \text{ lb-in}$, and there is an axial compression of 4800 lb.
- 5-75** Repeat Problem 5-74 for a boom that is made from class 20 gray cast iron. At the base the boom is a hollow tube with an outside diameter of 10 in and a wall thickness of 1 in.
- 5-76** Assume that the curved beam of Problem 5-70 has a crack on its inside surface of half-width $a = 1.5 \text{ mm}$ and a fracture toughness of $35 \text{ MPa-m}^{0.5}$. What is its safety factor against sudden fracture?
- 5-77** A large aircraft panel is to be made from 7075-T651 aluminum bar. From test data it is found that the nominal tensile stress in the panel is 200 MPa. What is the average maximum central crack size that can be tolerated without catastrophic failure?
- 5-78** Design the connecting rod (link 3) of Problem 3-50 for a safety factor of 4 if the link is made from SAE 1010 hot-rolled steel sheet, the pin-hole diameter at each end is 6 mm, and the maximum applied tensile load is 2000 N. There are two links carrying the load.
- 5-79** Design the compacting ram (link 4) of Problem 3-50 for a safety factor of 4 if the ram is made from SAE 1010 hot-rolled steel bar, the pin hole diameter at the joint where link 3 attaches is 6 mm, and the applied load $F_{com} = 2000 \text{ N}$. The piston diameter is 35 mm.
- 5-80** A differential element is subjected to the stresses (in MPa): $\sigma_1 = 70$, $\sigma_2 = 0$, $\sigma_3 = -140$. A ductile material has the strengths (in MPa): $S_{ut} = 350$, $S_y = 280$, $S_{uc} = 350$. Calculate the safety factor and draw $\sigma_1 - \sigma_3$ diagrams of each theory showing the stress state using:
- Maximum shear stress theory
 - Distortion energy theory
- 5-81** A part has the combined stress state and strengths given (in MPa) of: $\sigma_x = 70$, $\sigma_y = 35$, $\tau_{xy} = 31.5$, $S_{ut} = 140$, $S_{uc} = 140$, $S_y = 126$. Using the Distortion-Energy failure theory, find the von Mises effective stress and factor of safety against static failure.
- 5-82** Repeat Problem 5-78 for the connecting rod made from class 20 cast iron.
- 5-83** Repeat Problem 5-79 for the part made from class 20 cast iron.
- 5-84** A differential element is subjected to the stresses (in MPa): $\sigma_1 = 70$, $\sigma_2 = 0$, $\sigma_3 = -140$. A brittle material has the strengths (in MPa): $S_{ut} = 350$, $S_{uc} = 630$. Calculate the safety factor and draw $\sigma_1 - \sigma_3$ diagrams of each theory showing the stress state using:
- Coulomb-Mohr theory
 - Modified-Mohr theory
- 5-85** A part has the combined stress state and strengths given (in MPa) of: $\sigma_x = 70$, $\sigma_y = 35$, $\tau_{xy} = 31.5$, $S_{ut} = 140$, $S_{uc} = 560$, $S_y = 126$. Using the Modified-Mohr failure theory, find the effective stress and factor of safety against static failure.

Problem numbers in *italics* are design problems. Problem numbers in **boldface** are extended from similar problems in earlier chapters with the same dash number. Problems in succeeding chapters may also continue and extend these problems.

6



FATIGUE FAILURE THEORIES

Science is a first-rate piece of furniture for a man's upper chamber, if he has common sense on the ground floor.

Oliver Wendell Holmes

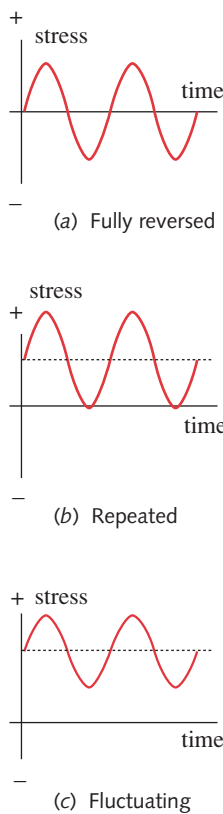
6.0 INTRODUCTION

Most failures in machinery are due to time-varying loads rather than to static loads. These failures typically occur at stress levels significantly lower than the yield strengths of the materials. Thus, using only the static failure theories of the last chapter can lead to unsafe designs when loads are dynamic.

Table 6-0 shows the variables used in this chapter and references the equations, tables, or sections in which they are used. At the end of the chapter a summary section is provided that also groups the significant equations from this chapter for easy reference and identifies the chapter section in which their discussion can be found.

History of Fatigue Failure

This phenomenon was first noticed in the 1800s when railroad-car axles began failing after only limited time in service. They were made of ductile steel but exhibited sudden, brittle-like failures. Rankine published a paper in 1843, *On the Causes of Unexpected Breakage of Journals of Railway Axles*, in which he postulated that the material had “crystallized” and become brittle due to the fluctuating stress. The axles had been designed with all the engineering expertise available at the time, which was based on experience with statically loaded structures. Dynamic loads were then a new phenomenon resulting from the introduction of steam-powered machinery. These axles were fixed to the wheels and turned with them. Thus the bending stress at any point on the surface of the axle varied cyclically from positive to negative as shown in Figure 6-1a. This loading is termed fully reversed. A German engineer, August Wohler, made the first scientific investigation (over a 12-year period) into what was known as *fatigue fail-*

**FIGURE 6-1**

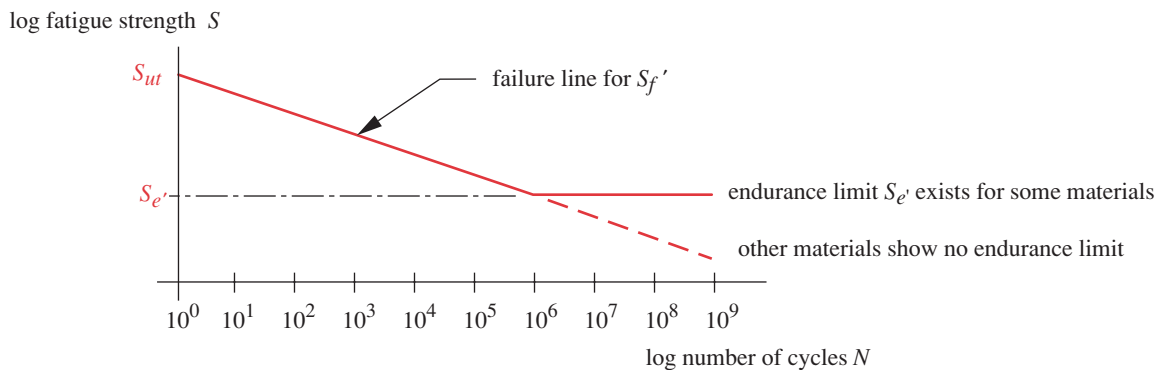
Time-Varying Stresses

Table 6-0 Variables Used in This Chapter

Symbol	Variable	ips units	SI units	See
A	amplitude ratio	none	none	Eq. 6.1d
a	half-width of crack	in	m	Eq. 6.3
A_{95}	95% stressed area	in ²	m ²	Eq. 6.7c
C_{load}	loading factor	none	none	Eq. 6.7a
C_{reliab}	reliability factor	none	none	Table 6-4
C_{size}	size factor	none	none	Eq. 6.7b
C_{surf}	surface factor	none	none	Eq. 6.7e
C_{temp}	temperature factor	none	none	Eq. 6.7f
d_{equiv}	equivalent-diameter test specimen	in	m	Eq. 6.7d
K	stress intensity	kpsi-in ^{0.5}	MPa-m ^{0.5}	Sect. 6.1
K_c	fracture toughness	kpsi-in ^{0.5}	MPa-m ^{0.5}	Sect. 6.1
ΔK	stress intensity factor range	kpsi-in ^{0.5}	MPa-m ^{0.5}	Eq. 6.3
ΔK_{th}	threshold stress intensity factor	kpsi-in ^{0.5}	MPa-m ^{0.5}	Sect. 6.5
K_f	fatigue-stress-concentration factor	none	none	Eq. 6.11
K_{fm}	mean-stress fatigue-concentration factor	none	none	Eq. 6.17
N	number of cycles	none	none	Fig. 6-2, Sect. 6.2
N_f	safety factor in fatigue	none	none	Eq. 6.14, 6.18
q	material notch sensitivity	none	none	Eq. 6.13, Fig. 6-36
R	stress ratio	none	none	Eq. 6.1d
S_e	corrected endurance limit	psi	Pa	Eq. 6.6
$S_{e'}$	uncorrected endurance limit	psi	Pa	Eq. 6.5
S_f	corrected fatigue strength	psi	Pa	Eq. 6.6
$S_{f'}$	uncorrected fatigue strength	psi	Pa	Eq. 6.5
S_m	mean strength at 10 ³ cycles	psi	Pa	Eq. 6.9
$S(N)$	fatigue strength at any N	psi	Pa	Eq. 6.10
S_{yc}	yield strength in compression	psi	Pa	Fig. 6-44, Eq. 6.16a
β	stress intensity geometry factor	none	none	Eq. 6.3
σ	normal stress	psi	Pa	
$\sigma_{1,2,3}$	principal stresses	psi	Pa	Sect. 6.10
σ_a	alternating normal stress	psi	MPa	Sect. 6.4
σ_m	mean normal stress	psi	MPa	Sect. 6.4
σ'	von Mises effective stress	psi	Pa	Sect. 6.10
σ'_a	alternating von Mises stress	psi	Pa	Sect. 6.11
σ'_m	mean von Mises stress	psi	Pa	Sect. 6.11
σ_{max}	maximum applied normal stress	psi	MPa	Sect. 6.4
σ_{min}	minimum applied normal stress	psi	MPa	Sect. 6.4

The title-page photograph is of the fractured Liberty ship *USS Schenectady*, courtesy of the Ship Structures Committee, U. S. Government.

ure by testing axles to failure in the laboratory under fully reversed loading. He published his findings in 1870, which identified the number of cycles of time-varying stress as the culprit and found the existence of an *endurance limit* for steels, i.e., a stress level

**FIGURE 6-2**Wohler Strength-Life or S - N Diagram

6

that would be tolerable for millions of cycles of fully reversed stress. The S - N , or Wohler, diagram shown in Figure 6-2 became the standard way to characterize the behavior of materials under completely reversed loading and is still in use, though other measures of material strength under dynamic loading are now also available.

The term “fatigue” was first applied to this situation by Poncelet in 1839. The mechanism of failure was not yet understood, and the brittle appearance of the failure surface in a ductile material caused speculation that the material had somehow become “tired” and embrittled from the load oscillations. Wohler later showed that the broken axle-halves were still as strong and ductile in tensile tests as was the original material. Nonetheless, the term *fatigue failure* stuck and is still used to describe any failure due to time-varying loads.

Fatigue failure constitutes a significant cost to the economy. Dowling suggests, based on data in a U.S. Government report by Reed et al.,^[1] that:

The annual cost of fatigue of materials to the U.S. economy in 1982 dollars is around \$100 billion, corresponding to about 3% of the gross national product (GNP). These costs arise from the occurrence or prevention of fatigue failure for ground vehicles, rail vehicles, aircraft of all types, bridges, cranes, power plant equipment, offshore oil well structures, and a wide variety of miscellaneous machinery and equipment including everyday household items, toys and sports equipment.^[2]

The cost can also involve human life. The first commercial passenger jet aircraft, the British *Comet*, suffered two fatal crashes in 1954 due to fatigue failure of the fuselage from the pressurization/depressurization cycles of the cabin.* More recently (1988), a Hawaiian Airlines Boeing 737 lost about one-third of its cabin top while in flight at 25 000 ft. It was landed safely with minimum loss of life. Many other recent examples of catastrophic fatigue failures exist. A great deal of work has been done over the past 150 years to determine the actual mechanism of fatigue failure. The demands placed on materials in aircraft and spacecraft applications since World War II have motivated increased investment in scientific research on this topic and it is now fairly well understood, though researchers continue to seek answers to questions about the fatigue mechanism. Table 6-1 shows a chronology of significant events in the history of fatigue-failure research.

* It is generally believed that these *Comet* failures also cost the U.K. its commercial airline industry. Britain led the field at the time, but the momentum lost in grounding and redesigning their planes gave the U.S. aircraft industry a chance to take the lead, which it holds to this day. Britain has only recently begun to achieve significant market share with the European consortium-developed Airbus.

Table 6-1 Chronology of Fatigue Failure Research Events and Accomplishments

Source: "Fracture Mechanics & Fatigue," Union College, 1992, with permission

Year	Researcher	Event or Accomplishment
1829	Albert	First to document failure due to repeated loads.
1839	Poncelet	First to use the term fatigue.
1837	Rankine	Discusses the crystallization theory of fatigue.
1849	Stephenson	Discusses the product liability associated with railway-axle fatigue failures.
1850	Braithwaite	First uses the term fatigue in an English publication and discusses the crystallization theory.
1864	Fairbairn	Reports the first experiments with repeated loads.
1871	Wohler	Publishes results of many years of investigation into axle failures, develops the rotating bending test and the $S-N$ diagram, and defines the endurance limit.
1871	Bauschinger	Develops a mirror extensometer with 10^{-6} sensitivity and studies inelastic stress-strain.
1886	Bauschinger	Proposes a cyclic "natural elastic limit" below which fatigue would not occur.
1903	Ewing/Humfrey	Discover slip lines, fatigue cracks, and crack growth to failure, disproving the crystallization theory.
1910	Bairstow	Verifies Bauschinger's theory of a natural elastic limit and Wohler's endurance limit.
1910	Basquin	Develops the exponential law of endurance tests (the Basquin equation).
1915	Smith/Wedgewood	Separate cyclic plastic strain from total plastic strain.
1921	Griffith	Develops fracture criteria and relates fatigue to crack growth.
1927	Moore/Kommers	Quantify high-cycle-fatigue data for many materials in "The Fatigue of Metals."
1930	Goodman/Soderberg	Independently determine the influence of mean stresses on fatigue.
1937	Neuber	Publishes the Neuber equation for strain concentration in notches (English translation in 1946).
1953	Peterson	Publishes "Stress Concentration Design Factors" providing an approach to account for notches.
1955	Coffin/Manson	Independently publish the strain-based low-cycle-fatigue law (Coffin-Manson law).
1961	Paris	Publishes the fracture-mechanics Paris law for fatigue-crack growth.

6.1 MECHANISM OF FATIGUE FAILURE

Fatigue failures always begin at a crack. The crack may have been present in the material since its manufacture, or it may have developed over time due to cyclic straining around stress concentrations. Fischer and Yen^[3] have shown that virtually all structural members contain discontinuities, ranging from microscopic (< 0.010 in) to macroscopic, introduced in the manufacturing or fabricating process. Fatigue cracks generally start at a notch or other stress concentration. (We will use the general term *notch* to represent any geometric contour that increases local stress.) The brittle failures of some of the World War II tankers (see Figure 5-15 on p. 266) were traced to cracks that began at an arc-strike left by a careless welder. The *Comet* airplane failures started at cracks smaller than 0.07 in long near the corners of windows that were nearly square, thus providing high stress concentrations. **Thus it is critical that dynamically loaded parts be designed to minimize stress concentrations as described in Section 4.15 (p. 186).**

There are three stages of fatigue failure: *crack initiation*, *crack propagation*, and *sudden fracture due to unstable crack growth*. The first stage can be of short duration, the second stage involves most of the life of the part, and the third stage is instantaneous.

Crack Initiation Stage

Assume that the material is a ductile metal and as manufactured has no cracks present but has the usual collection of particles, inclusions, etc., that are common to engineering materials. At a microscopic scale, metals are not homogeneous and isotropic.* As assume further that there are some regions of geometric stress concentration (notches) in locations of significant time-varying stress that contains a tensile (positive) component as shown in Figure 6-1 (p. 304). As the stresses at the notch oscillate, local yielding may occur due to the stress concentration, even though the nominal stress in the section is well below the yield strength of the material. The localized plastic yielding causes distortion and creates slip bands (regions of intense deformation due to shear motion) along the crystal boundaries of the material. As the stress cycles, additional slip bands occur and coalesce into microscopic cracks. Even in the absence of a notch (as in smooth test specimens) this mechanism still operates as long as the yield strength is exceeded somewhere in the material. Preexisting voids or inclusions will serve as stress-raisers to start the crack.

Less ductile materials do not have the same ability to yield as ductile ones and will tend to develop cracks more rapidly. They are more *notch sensitive*. Brittle (especially cast) materials which do not yield may skip this initiation stage and proceed directly to crack propagation at sites of existing voids or inclusions that serve as microcracks.

Crack Propagation Stage

Once a microcrack is established (or if present from inception), the mechanisms of fracture mechanics as described in Section 5.3 (p. 265) become operable. The sharp crack creates stress concentrations larger than those of the original notch, and a plastic zone develops at the crack tip each time a tensile stress opens the crack, blunting its tip and reducing the effective stress concentration. The crack grows a small amount. When the stress cycles to a compressive-stress regime, to zero, or to a sufficiently lower tensile stress as shown in Figure 6-1a through 6-1c (p. 304), respectively, the crack closes, the yielding momentarily ceases, and the crack again becomes sharp, but now at its longer dimension. This process continues as long as the local stress is cycling from below the tensile yield to above the tensile yield at the crack tip. Thus, **crack growth is due to tensile stress** and the crack grows along planes normal to the maximum tensile stress. It is for this reason that fatigue failures are considered to be due to tensile stress, even though shear stress starts the process in ductile materials as described above. Cyclic stresses that are always compressive will not cause crack growth, as they tend to close the crack.

The crack propagation growth rate is very small, on the order of 10^{-8} to 10^{-4} in per cycle,^[5] but this adds up over a large number of cycles. If the failed surface is viewed at high magnification, the *striations* due to each stress cycle can be seen as in Figure 6-3, which shows the crack surface of a failed aluminum specimen at 12 000x magnification along with a representation of the stress-cycle pattern that failed it. The occasional large-amplitude stress cycles show up as larger striations than the more frequent small-amplitude ones, indicating that higher stress amplitudes cause larger crack growth per cycle.

CORROSION Another mechanism for crack propagation is corrosion. **If a part containing a crack is in a corrosive environment, the crack will grow under static**

* "When viewed at a sufficiently small size scale, all materials are anisotropic and inhomogeneous. For example, engineering metals are composed of an aggregate of small crystal grains. Within each grain the behavior is anisotropic due to the crystal planes, and if a grain boundary is crossed, the orientation of these planes changes. Inhomogeneities exist not only due to the grain structure but also because of the presence of tiny voids or particles of a different chemical composition than the bulk of the material, such as hard silicate or alumina inclusions in steel."^[3]

stress. The combination of stress and corrosive environment has a synergistic effect and the material corrodes more rapidly than if unstressed. This combined condition is sometimes termed **stress-corrosion or environmentally assisted cracking.**

If the part is *cyclically stressed in a corrosive environment*, the crack will grow more rapidly than from either factor alone. This is also called **corrosion fatigue**. While the frequency of stress cycling (as opposed to the number of cycles) appears to have no detrimental effect on crack growth in a noncorrosive environment, in the presence of corrosive environments it does. Lower cyclic frequencies allow the environment more time to act on the stressed crack tip while it is held open under tensile stress, and this substantially increases the rate of crack growth per cycle.

Fracture

6

The crack will continue to grow as long as cyclical tensile stress and/or corrosion factors of sufficient severity are present. At some point, the crack size becomes large enough to raise the stress intensity factor K at the crack tip (Eq. 5.14) to the level of the material's fracture toughness K_c and sudden failure (as described in Section 5.3 (p. 265) on fracture mechanics) occurs instantaneously on the next tensile stress-cycle. This failure mechanism is the same whether the condition of $K = K_c$ was reached by reason of the crack propagating to a sufficient size (increasing a in Eq. 5.14, p. 268) or by the nominal stress being raised sufficiently (increasing σ_{nom} in Eq. 5.14). The former is commonly the case in dynamic loading while the latter is more common in static loading. The result is the same: sudden and catastrophic failure with no warning.

Examination with the naked eye of parts failed by fatigue loading show a typical pattern as seen in Figure 6-4. There is a region emanating from the site of the original microcrack that appears burnished and a separate region that appears dull and rough, looking like a brittle fracture. The burnished region was the crack and often shows *beachmarks*, so-called because they resemble ripples left on the sand by retreating waves. The beachmarks (not to be confused with the striations seen in Figure 6-3, which

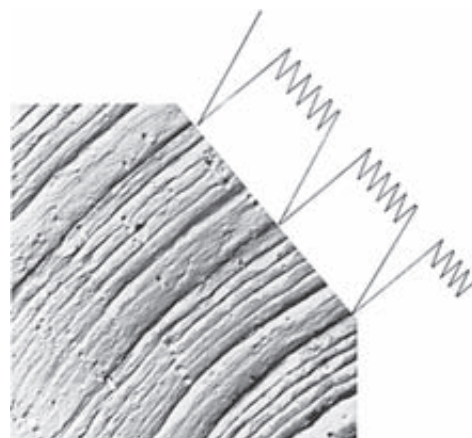


FIGURE 6-3

Fatigue Striations on the Crack Surface of an Aluminum Alloy. Spacing of the Striations Corresponds to the Cyclic Loading Pattern. (From Fig. 1.5, p. 10, in D. Broek, *The Practical Use of Fracture Mechanics*, Kluwer Publishers, Dordrecht, 1988)

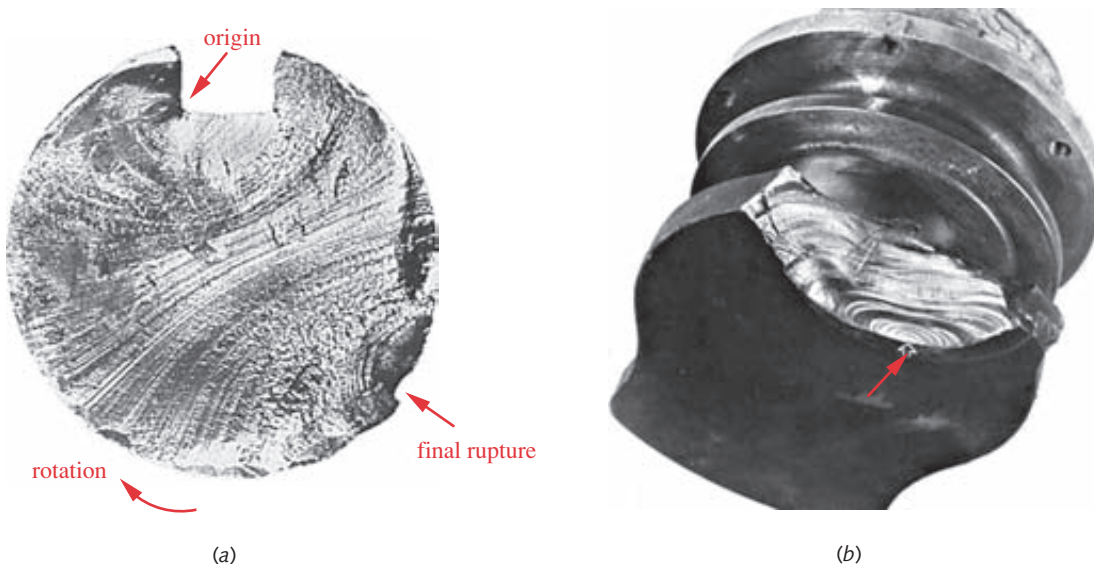


FIGURE 6-4

Two Parts That Failed in Fatigue. Note the Beachmarks: (a) 1040 Steel Keyed Shaft Failed in Rotating Bending. Crack Started at Keyway. (b) Diesel-Engine Crankshaft Failed in Combined Bending and Torsion. Crack Started at Arrow. (Source: D. J. Wulpi, *Understanding How Components Fail*. Am. Soc. for Metals: Metals Park, Ohio, 1990, Fig. 22, p. 149, and Fig. 25, p. 152.)

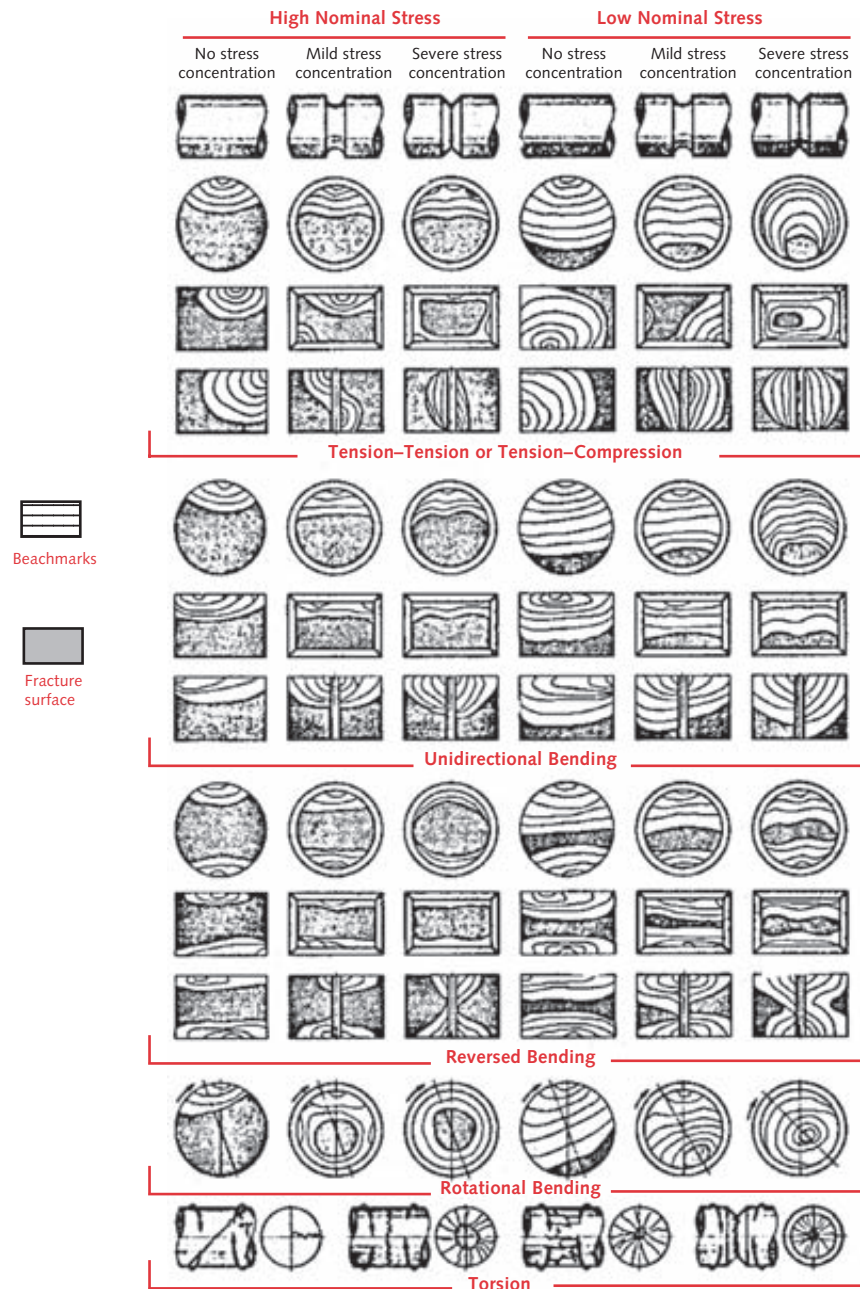
are much smaller and not discernible to the naked eye) are due to a starting and stopping of the crack growth and they surround the origin of the crack, usually at a notch or internal stress-raiser. Sometimes, if there was a lot of rubbing of the crack surfaces, the beach marks will be obscured. The brittle-failure zone is the portion that failed suddenly when the crack reached its size limit. Figure 6-5 shows drawings of failure surfaces of a variety of part geometries loaded in different ways at different levels of stress. The beachmarks can be seen in the crack zones. The brittle-fracture zone can be a small remnant of the original cross section.

6.2 FATIGUE-FAILURE MODELS

There are three fatigue failure models in current use and each has a place and a purpose. They are the *stress-life* (*S-N*) approach, the *strain-life* (ϵ -*N*) approach, and the *linear-elastic fracture-mechanics* (LEFM) approach. We will first discuss their application and their advantages and disadvantages, compare them in a general way, and then analyze some of them in more detail.

Fatigue Regimes

Based on the number of stress or strain cycles that the part is expected to undergo in its lifetime, it is relegated to either a **low-cycle fatigue (LCF)** regime or a **high-cycle fatigue (HCF)** regime. There is no sharp dividing line between the two regimes, and various investigators suggest slightly different divisions. Dowling^[6] defines HCF as starting at around 10^2 to 10^4 cycles of stress/strain variation with the number varying with the material. Juvinal^[7] and Shigley^[8] suggest 10^3 cycles and Madayag^[9] defines

**FIGURE 6-5**

Schematic Representations of Fatigue-Fracture Surfaces of Various Smooth and Notched Cross Sections Under Various Loading Conditions and Stress Levels (From *Metals Handbook*, Am. Soc. for Metals, Metals Park, Ohio, Vol. 10, 8th ed., 1975, p. 102, with permission)

10^3 to 10^4 cycles as the cutoff. In this text, we will assume that $N = 10^3$ cycles is a reasonable approximation of the divide between LCF and HCF.

The Stress-Life Approach

This is the oldest of the three models and is the most often used for high-cycle fatigue (HCF) applications where the assembly is expected to last for more than about 10^3 cycles of stress. It works best when the load amplitudes are predictable and consistent over the life of the part. It is a **stress-based model**, which seeks to determine a **fatigue strength** and/or an **endurance limit** for the material so that the cyclic stresses can be kept below that level and failure avoided for the required number of cycles. The part is then designed based on the material's fatigue strength (or endurance limit) and a safety factor. In effect, this approach attempts to keep local stresses in notches so low that the crack initiation stage *never begins*. The assumption (and design goal) is that stresses and strains everywhere remain in the elastic region and no local yielding occurs to initiate a crack.

This approach is fairly easy to implement, and large amounts of relevant strength data are available due to its longtime use. However, it is the most empirical and least accurate of the three models in terms of defining the true local stress/strain states in the part, especially for low-cycle fatigue (LCF) finite-life situations where the total number of cycles is expected to be less than about 10^3 and the stresses will be high enough to cause local yielding. On the other hand, with certain materials, the stress-life approach allows the design of parts for **infinite life** under cyclic loading.

6

The Strain-Life Approach

Because the initiation of a crack involves yielding, a stress-based approach cannot adequately model this stage of the process. A **strain-based model** gives a reasonably accurate picture of the **crack initiation stage**. It can also account for cumulative damage due to variations in the cyclic load over the life of the part, such as overloads that may introduce favorable or unfavorable residual stresses to the failure zone. Combinations of fatigue loading and high temperature are better handled by this method, because the creep effects can be included. This method is most often applied to **LCF, finite-life** problems where the cyclic stresses are high enough to cause local yielding. It is the most complicated of the three models to use and requires a computer solution. Test data are still being developed on the cyclic-strain behavior of various engineering materials.

The LEFM Approach

Fracture-mechanics theory provides the best model of the **crack propagation stage** of the process. This method is applied to **LCF, finite-life** problems where the cyclic stresses are known to be high enough to cause the formation of cracks and is most useful in predicting the remaining life of cracked parts in service. It is often used in conjunction with nondestructive testing (NDT) in a periodic service-inspection program, especially in the aircraft/aerospace industry. Its application is fairly straightforward but relies on the accuracy of the expression for the stress intensity geometry factor β (Eq. 5.14b, p. 268) and on the estimate of initial crack size a required for the computation. In the absence of a detectable crack, one approach is to assume that a crack smaller than the smallest detectable crack already exists in order to begin the calculation. It gives more accurate results when a detectable and measurable crack already exists.

6.3 MACHINE-DESIGN CONSIDERATIONS

The choice of fatigue-failure models for machine-design purposes depends on the type of machinery being designed and on its intended use. The large class of **rotating machinery** (stationary or mobile) is well served by the stress-life (*S-N*) model because the required lives are usually in the HCF range. For example, consider the number of load cycles (revolutions) required of an automobile-engine crankshaft over its useful life. Assume a desired 100 000-mi life with no failure of the crankshaft. The average rolling radius of a car tire is about 1 ft and its circumference is then 6.28 ft. The axle will then rotate $5\ 280/6.28 = 841$ rev/mi or $84E6$ rev/100 000 mi. A typical final-drive ratio for a passenger car is about 3:1, meaning that the output shaft of the transmission is turning 3x the axle speed. If we assume that most of the car's life is spent in top gear (1:1), then the engine speed also averages 3x axle speed. This means that the crankshaft and most other rotating and oscillating components in the engine will see about $2.5E8$ cycles in 100 000 miles (the valve train will see half that many). This is clearly in the HCF regime and doesn't even account for idling time. Also, the cyclic loads are reasonably predictable and consistent, so the *stress-life* approach is appropriate here.

As another example consider a typical, automated production machine as used in U.S. industry. Perhaps it is making batteries, or paper diapers, or filling soft-drink cans. Assume that its fundamental driveshaft speed is 100 rpm (a conservative estimate). Assume only one-shift operation (also conservative, since many such machines run 2 or 3 shifts). How many cycles (revolutions) will the driveshaft and all the gears, cams, etc., driven by it see in a year? In one 8-hr day, it turns $100(60)(8) = 480\ 000$ rev/shift-day. In a 260-day work-year it turns $125E6$ rev/shift-year. Again we are in the HCF regime, and the loads are usually quite predictable and consistent in amplitude.

One class of machinery that typically sees low-cycle fatigue (LCF) is that of transportation (service) machinery. The airframe of an airplane, the hull of a ship, and the chassis of a land vehicle see a load-time history that can be quite variable due to storms, gusts/waves, hard landings/dockings, etc. (for the aircraft/ship) and overloads, potholes, etc. (for the land craft). The total number of load cycles seen in its life is also less predictable due to the vagaries of its use. Even though the number of low-magnitude stress cycles may be potentially large (and in the HCF regime) over its potential lifetime, the chance of higher-than-design loads causing local yielding is always present. A series of high-stress cycles, even if less than 10^3 in number, can cause significant crack growth due to local yielding.

Manufacturers of this kind of equipment develop extensive load-time or strain-time data by instrumenting actual vehicles while operating them in regular service or under controlled-test conditions. (Look ahead to Figure 6-7 for examples.) Computer simulations are also developed and refined by comparison to experimental data. The simulated and experimental load-time histories are used, usually in conjunction with either the strain-life or LEFM models (or both), to more accurately predict failure and thus improve the design. Another example of the use of ϵ -*N* and LEFM models is in the design and analysis of gas-turbine rotor blades, which operate under high stresses at high temperatures and go through LCF thermal cycles at start-up and shutdown.

We will concentrate on the **stress-life model** in this text and also discuss the application of the **LEFM model** to cyclically loaded machine-design problems. The **strain-life model** is best at depicting the conditions of crack initiation and provides the

most complete theoretical model but is less well suited to the design of parts for HCF. A complete description of the **strain-life model** would require more space than is available in this introductory design text. The reader is directed to the references cited in the bibliography of this chapter, which provide thorough discussions of the strain-life approach (as well as of the other two approaches). The fracture-mechanics approach allows the determination of remaining life for service-cracked parts. The stress-life model is the most appropriate choice for the majority of rotating-machinery design problems due to the need for high-cycle (or infinite) life in most cases.

6.4 FATIGUE LOADS

Any loads that vary with time can potentially cause fatigue failure. The character of these loads may vary substantially from one application to another. In rotating machinery, the loads tend to be consistent in amplitude over time and repeat with some frequency. In service equipment (vehicles of all types), the loads tend to be quite variable in amplitude and frequency over time and may even be random in nature. The shape of the waveform of the load-time function seems not to have any significant effect on fatigue failure in the absence of corrosion, so we usually depict the function schematically as a sinusoidal or sawtooth wave. Also, the presence or absence of periods of quiescence in the load history is not significant as long as the environment is noncorrosive. (Corrosion will cause continuous crack growth even in the absence of any load fluctuations.) The stress-time or strain-time waveform will have the same general shape and frequency as the load-time waveform. The significant factors are the amplitude and the average value of the stress-time (or strain-time) waveform and the total number of stress/strain cycles that the part has seen.

6

Rotating Machinery Loading

The typical stress-time functions experienced by rotating machinery can be modeled as shown in Figure 6-6, which shows them schematically as sine waves. Figure 6-6a shows the **fully reversed** case for which *the mean value is zero*. Figure 6-6b shows a **repeated stress** case in which the waveform ranges from zero to a maximum with a *mean value equal to the alternating component*, and Figure 6-6c shows one version of the more general case (called **fluctuating stress**) with *all component values nonzero*. (Note that

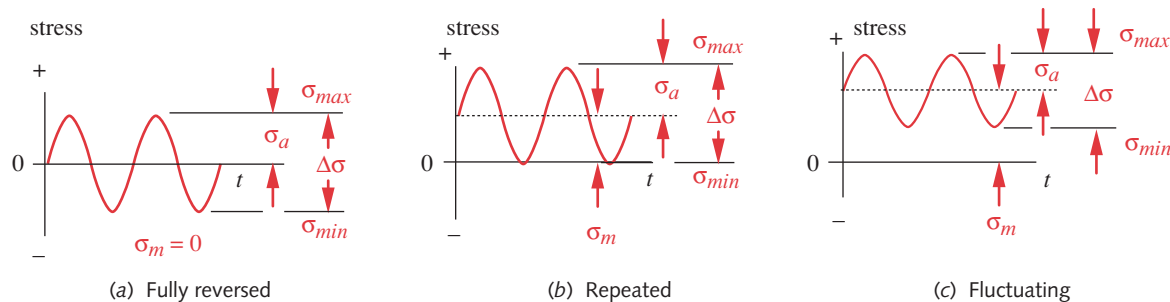


FIGURE 6-6

Alternating, Mean, and Range Values for Fully Reversed, Repeated, and Fluctuating Cyclic Stresses

any portion of the waveform could be in the compressive-stress regime as well.) Any of these waveforms can be characterized by two parameters, their mean and alternating components, their maximum and minimum values, or ratios of these values.

The **stress range** $\Delta\sigma$ is defined as

$$\Delta\sigma = \sigma_{max} - \sigma_{min} \quad (6.1a)$$

The **alternating component** σ_a is found from

$$\sigma_a = \frac{\sigma_{max} - \sigma_{min}}{2} \quad (6.1b)$$

and the **mean component** σ_m is

$$\sigma_m = \frac{\sigma_{max} + \sigma_{min}}{2} \quad (6.1c)$$

6

Two ratios can be formed:

$$R = \frac{\sigma_{min}}{\sigma_{max}} \quad A = \frac{\sigma_a}{\sigma_m} \quad (6.1d)$$

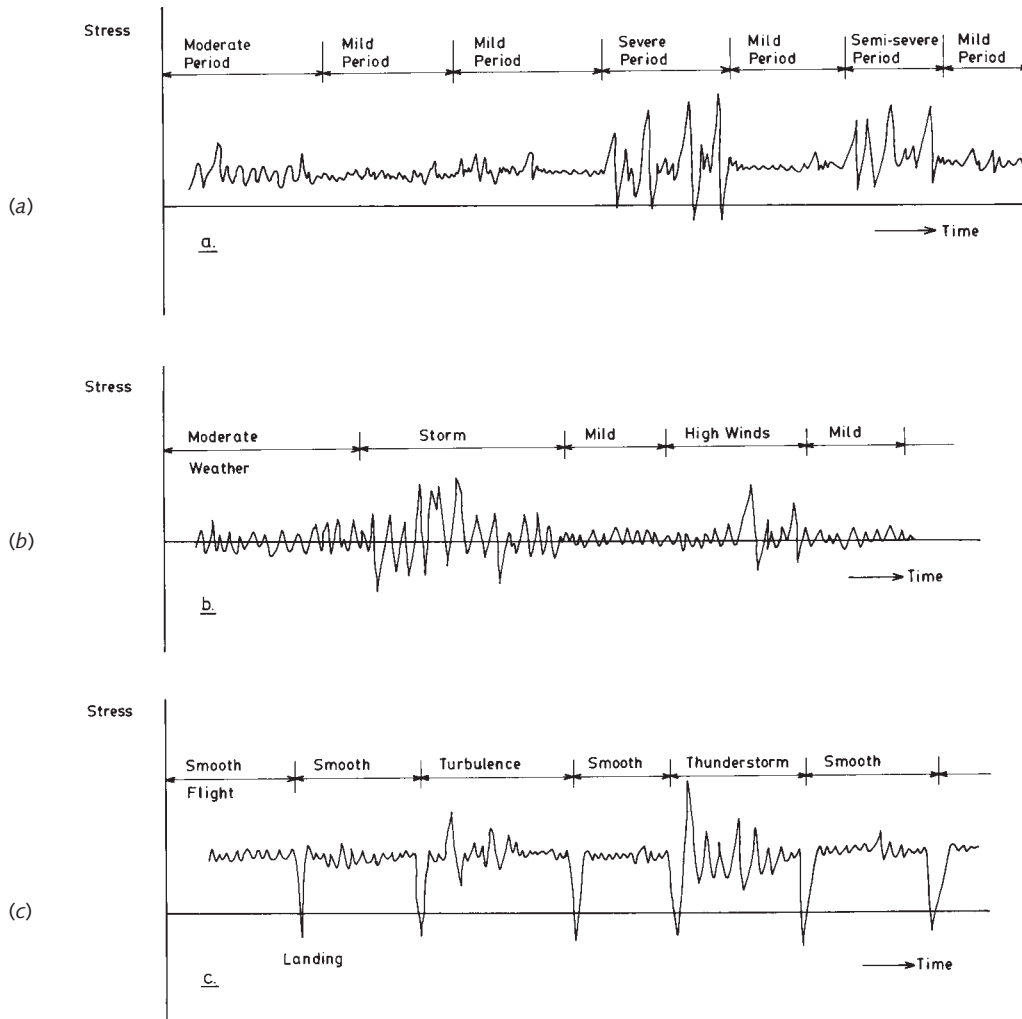
where R is the **stress ratio** and A is the **amplitude ratio**.

When the stress is fully reversed (Figure 6-6a), $R = -1$ and $A = \infty$. When the stress is repeated (Figure 6-6b), $R = 0$ and $A = 1$. When the maximum and minimum stresses have the same sign as in Figure 6-6c, both R and A are positive and $0 \leq R \leq 1$. These load patterns may result from bending, axial, torsional, or a combination of these types of stresses. We will see that the presence of a mean-stress component can have a significant effect on the fatigue life.

Service Equipment Loading

The character of the load-time function for service equipment is not so easily defined as for rotating machinery. The best data come from actual measurements made on equipment in service or operated under simulated service conditions. The automotive industry subjects prototype vehicles to test-track conditions that simulate various road surfaces and curves. The test vehicles are extensively instrumented with accelerometers, force transducers, strain gages, and other instruments that feed voluminous amounts of data to on-board computers or telemeter it to stationary computers where it is digitized and stored for later analysis. The aircraft industry also instruments test-aircraft and records in-flight force, acceleration, and strain data. The same is done with ships and offshore oil platforms, etc.

Some examples of these in-service stress-time waveforms are shown in Figure 6-7, which depicts a simulated general loading case in (a), a typical pattern for a ship or offshore platform in (b), and a pattern typical of a commercial aircraft in (c). These patterns are semirandom in nature, as the events do not repeat with any particular period. Data such as these are used in computer simulation programs that calculate the cumulative fatigue damage based on either a strain-based model, a fracture-mechanics model, or a combination of both. The stress-life model is not able to deal as effectively with this type of loading history.

**FIGURE 6-7**

Semirandom Loading in Different Periods (voyages, months, flights) for (a) General Case, (b) Ship or Offshore Structure, (c) Commercial Aircraft (From Fig. 6.10, p. 186, in D. Broek, *The Practical Use of Fracture Mechanics*, Kluwer Publishers, Dordrecht, 1988)

6.5 MEASURING FATIGUE FAILURE CRITERIA

Several different testing techniques now exist for the purpose of measuring the response of materials to time-varying stresses and strains. The oldest approach is that of Wohler who loaded a rotating cantilever beam in bending to achieve variations in stress with time. R. R. Moore later adapted this technique to a simply supported rotating beam in fully reversed, pure bending. In the last 40 years the advent of servohydraulically driven axial-testing machines has allowed much more flexibility in the patterns of either stress or strain that can be applied to a test specimen. Strain-based and fracture-mechanics data as well as stress-based data are obtained by this method. Most of the available fatigue-strength information is for a rotating beam in fully reversed bending, with less available for axial loading and less still for torsion, though this is changing as more axial fatigue data are developed. In some cases, no fatigue strength information for the de-

sired material is available at all, and we then need a means to estimate a value from available static strength data. This will be discussed in the next section.

Fully Reversed Stresses

This loading situation can be accomplished with the rotating bending, axial fatigue, cantilever bending, or torsional fatigue tests depending on the type of loading desired. The rotating bending test is a fully reversed, stress-based, HCF test that seeks to find the fatigue strength of the material under those conditions. The axial fatigue test can be used to generate similar fully reversed data to that of the rotating-beam test in a given material and it can also be used to do strain-controlled tests. The principal advantage of the axial test is its ability to apply any combination of mean and alternating stresses. The cantilever bending test subjects a nonrotating beam to oscillations in bending stress. It can provide a mean stress as well as a fully reversed stress. The torsion test alternately twists a bar in opposite directions applying pure shear stresses.

6

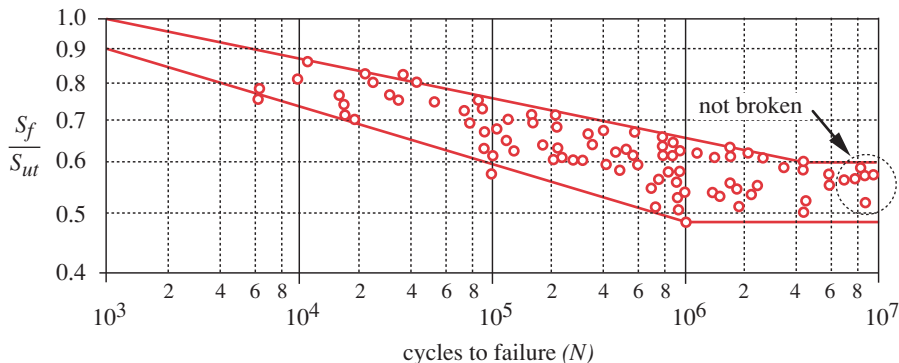
ROTATING-BEAM TEST The bulk of available fully reversed, fatigue strength data comes from the R. R. Moore rotating-beam test in which a highly polished specimen of about 0.3-in dia is mounted in a fixture which allows a constant-magnitude, pure-bending moment to be applied while the specimen is rotated at 1 725 rpm. This creates a fully reversed bending stress at any point on the circumference of the specimen as shown in Figure 6-6a (p. 313). It is run at one particular stress level until it fails, and the number of cycles to failure and the applied stress level is recorded. It takes about one-half day to reach 10^6 cycles and about 40 days to reach 10^8 cycles on one specimen. This test is repeated with multiple specimens of the same material loaded at different stress levels. The collected data are then plotted as normalized failure strength, S_f/S_{ut} against number of cycles, N , (typically on log-log coordinates) to obtain an S - N diagram.

Figure 6-8 shows the results of a number of rotating-beam tests on wrought steels of up to about 200 kpsi tensile strength. The data show that samples run at higher reversed-stress levels fail after fewer cycles. At lower stress levels, some (in the circle labeled *not broken*) do not fail at all before their tests are stopped at some number of cycles (here 10^7). Note the large amount of scatter in the data. This is typical of fatigue strength tests. Differences among the many samples of material required to generate the entire curve may account for the scatter. Some samples may have contained more, or larger, defects to serve as localized stress-raisers. (The samples are all unnotched and are polished to a fine finish to minimize the possibility of surface defects starting a crack.) The solid lines are drawn to bracket the data.

ENDURANCE LIMIT Note that the fatigue strength S falls steadily and linearly (on log-log coordinates) as a function of N until reaching a knee at about 10^6 to 10^7 cycles. This knee defines an **endurance limit** S_e' for the material, which is a stress level below which it can be cycled infinitely without failure. At the lower bound of the scatter band beyond the knee, an approximate endurance limit can be defined

$$\text{for steels : } S_e' \cong 0.5 S_{ut} \quad S_{ut} < 200 \text{ ksi} \quad (6.2a)$$

Not all materials exhibit this knee. “Many low-strength carbon and alloy steels, some stainless steels, irons, molybdenum alloys, titanium alloys and some polymers”^[10] do. Other materials, such as “aluminum, magnesium, copper, nickel alloys, some stain-

**FIGURE 6-8**

Log-Log Plot of Composite S-N Curves for Wrought Steels of $S_{ut} < 200$ ksi (From Fig. 11.7, p. 210, R. C. Juvinall, *Stress, Strain, and Strength*, McGraw-Hill, New York, 1967, with permission)

6

less steels, and high-strength carbon and alloy steels^[10] show S-N curves that continue to fall with increasing N , though the slope may become smaller beyond about 10^7 cycles. For applications requiring $< 10^6$ cycles of operation, a **fatigue strength** S_f (sometimes also called **endurance strength**) can be defined at any N from these data. The term **endurance limit** is used to represent the infinite-life strength only for those materials having one.

The data in Figure 6-8 are for steels of $S_{ut} < 200$ kpsi. Steels with higher tensile strengths do not exhibit the relationship shown in equation 6.2a. Figure 6-9 shows the endurance limit $S_{e'}$ plotted as a function of S_{ut} . There is a large scatter band but the average behavior is a line of slope 0.5 up to 200 kpsi. Beyond that level the higher-strength steels' endurance limit falls off. The usual approach is to assume that the endurance limit for steels never exceeds 50% of 200 kpsi.

$$\text{for steels : } S_{e'} \approx 100 \text{ ksi} \quad S_{ut} \geq 200 \text{ ksi} \quad (6.2b)$$

Figure 6-9 also shows scatter bands of fatigue limits for severely notched specimens and for specimens in corrosive environments. Both of these factors have a severe effect on the fatigue strength of any material. An endurance limit exists only in the absence of corrosion. Materials in corrosive environments have S-N curves that continue to fall with increasing N . We will shortly consider these factors in determining useful, corrected fatigue strengths for materials.

Figure 6-10 shows the scatter-band results of rotating-beam tests on aluminum alloys of various types including wrought alloys (with $S_{ut} < 48$ kpsi), die-cast, and sand-cast specimens. These are all unnotched and polished. Note the lack of a distinct knee, though the slope becomes smaller at around 10^7 cycles. Aluminums do not have an endurance limit, thus their **fatigue strength** S_f' is usually taken as the average failure stress at $N = 5E8$ cycles or some other value of N (which must be stated as part of the data).

Figure 6-11 shows the trend of fatigue strengths (at $N = 5E8$) for a number of aluminum alloys of varying static tensile strengths. The fatigue strength tracks the alloys' static tensile strengths at a ratio of

$$\text{for aluminums : } S_{f'} @ 5 \times 10^8 \approx 0.4 S_{ut} \quad S_{ut} < 48 \text{ kpsi} \quad (6.2c)$$

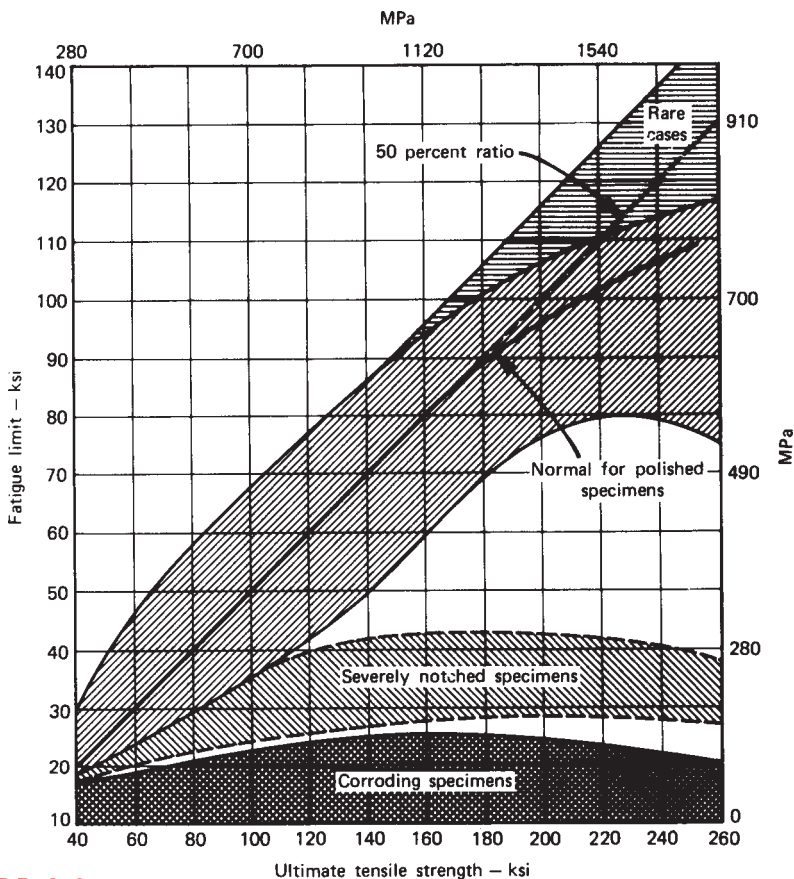


FIGURE 6-9

Relationship Between Fatigue Limit and Ultimate Strength for Steel Specimens (From *Steel and Its Heat Treatment*, by D. K. Bullens, John Wiley & Sons, New York, 1948, with permission of the publisher)

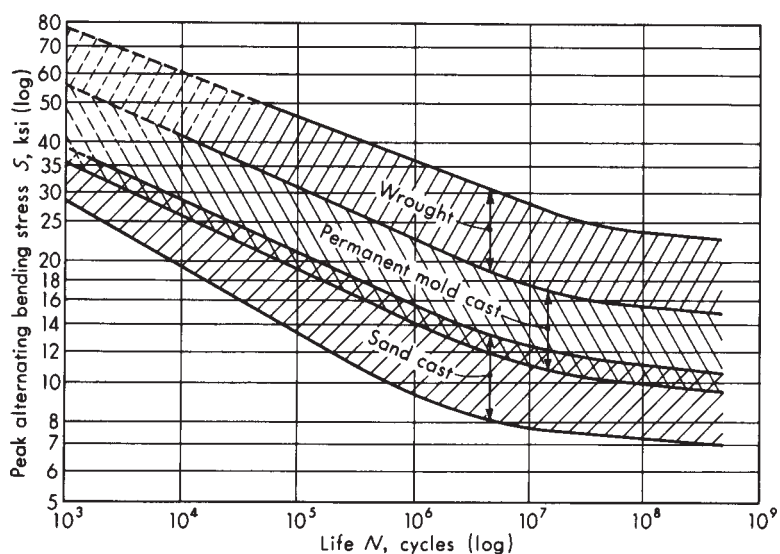
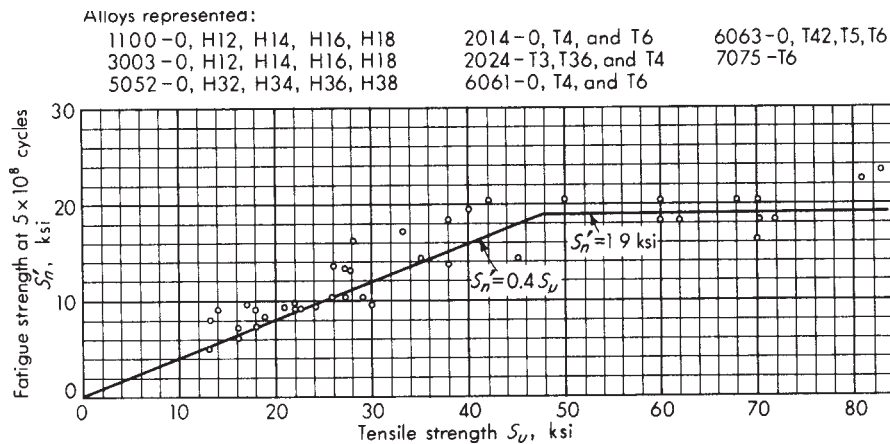


FIGURE 6-10

S-N Bands for Representative Aluminum Alloys, Excluding Wrought Alloys with $S_{ut} > 38$ ksi. (From Fig. 11.13, p. 216, R. C. Juvinall, *Stress, Strain, and Strength*, McGraw-Hill, New York, 1967, with permission)

**FIGURE 6-11**

Fatigue Strength at 5×10^8 Cycles for Common Wrought-Aluminum Alloys (From Fig. 11.12, p. 215, R. C. Juvinall, *Stress, Strain, and Strength*, McGraw-Hill, New York, 1967, with permission)

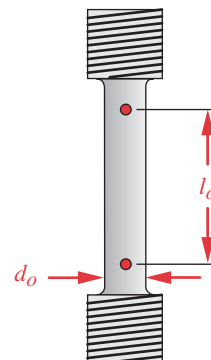
up to a plateau at around $S_f = 19$ kpsi, indicating that aluminum alloys with $S_{ut} >$ about 48 kpsi “top out” at 19 kpsi of fatigue strength. (S_n' in the figure is the same as S_f .)

$$\text{for aluminums : } S_{f'} @_{5 \times 10^8} \approx 19 \text{ ksi} \quad S_{ut} \geq 48 \text{ kpsi} \quad (6.2d)$$

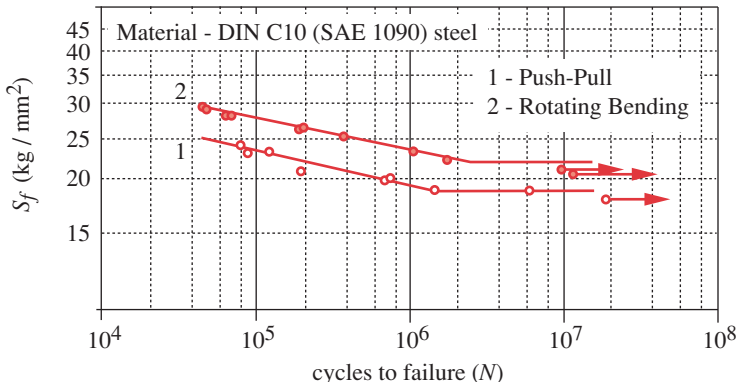
AXIAL FATIGUE TESTS The S - N diagram can also be developed for a material by using an axial fatigue test wherein a specimen similar to that shown in Figure 2-1 (repeated here) is loaded cyclically in a servohydraulic test machine. The programmability of these machines allows any combination of mean and alternating components of stress to be applied including fully reversed loading ($\sigma_m = 0$). A principal difference versus the rotating-beam test is that the entire cross section is uniformly stressed in axial tension/compression rather than having a linear stress distribution across its diameter that is maximum at the outer fiber and zero at the center. One result is that the fatigue strengths exhibited in the axial tests are typically lower than those seen in the rotating-beam test. This is thought to be due to the higher likelihood of a microcrack being present in the much larger high-stress field of the axial specimen than in the smaller-volume outer regions of the rotating specimen that are highly stressed. The fact that it is difficult to create exact axial loading with no eccentricity may also be a factor in the lower strength values, since eccentric loads will superpose bending moments on the axial loads.

Figure 6-12 shows two S - N curves for the same material (C10 steel) generated by a fully reversed axial test (labeled *push-pull*) and a rotating bending test. The axial data are seen to be at lower values than the rotating-beam data. Various authors report that the fatigue strength in reversed axial loading may be from 10%^[11] to 30%^[12] lower than the rotating-beam data for the same material. If bending is known to be present in addition to the axial loading, then the reduction may be as large as 40%.^[11]

Figure 6-13 shows the data for a fully reversed axial loading test on AISI 4130 steel, plotted on log-log coordinates. Note the slope change at around 10^3 cycles, which corresponds to the approximate transition from the LCF to the HCF region, and the change to essentially zero slope at about 10^6 cycles, corresponding to the endurance limit for infinite life. The fatigue strength is approximately 80% of the material’s static strength

**FIGURE 2-1 Repeated**

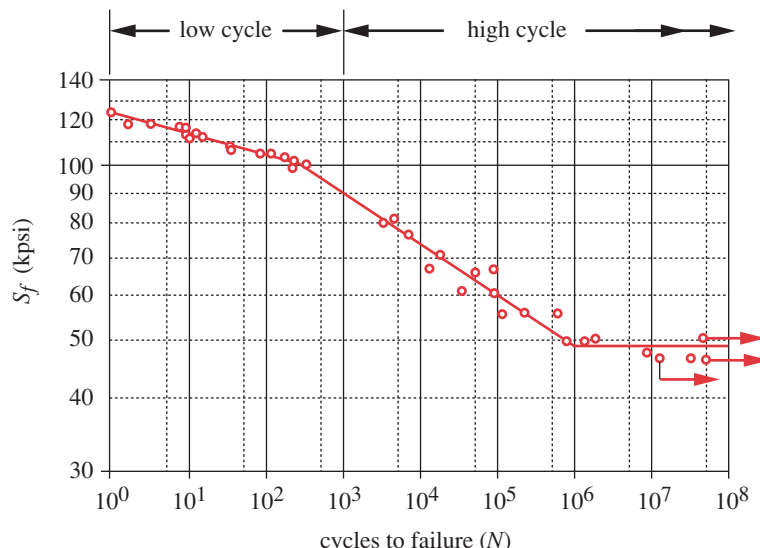
A Tensile Test Specimen

**FIGURE 6-12**

Fully Reversed Axial and Rotating-Beam S-N Curves Compared (From A. Esin, "A Method of Correlating Different Types of Fatigue Curves," *International Journal of Fatigue*, vol. 2, no. 4, pp. 153–158, 1980)

at about 10^3 cycles and about 40% of its static strength beyond 10^6 cycles, which are both 10% lower than the rotating-beam data of Figure 6-8.

CANTILEVER BENDING TESTS If a cantilever beam is oscillated at its tip by a linkage mechanism, any combination of mean and alternating stresses as shown in Figure 6-6 can be achieved. This test is not used as often as the rotating-bending or axial test but is a less expensive alternative to the latter. Some examples of data from a cantilever test are shown in Figure 6-14 for various polymers. This is a semilog plot but still shows the presence of an endurance limit for some of these nonmetallic materials.

**FIGURE 6-13**

Fully Reversed Axial S-N Curve for AISI 4130 Steel, Showing Break at LCF/HCF Transition and an Endurance Limit (From Fig. 7-3, p. 273, in Shigley and Mitchell, *Mechanical Engineering Design*, 4th ed., McGraw-Hill, New York, 1983, with permission. Data from NACA Technical Note #3866, Dec. 1966)

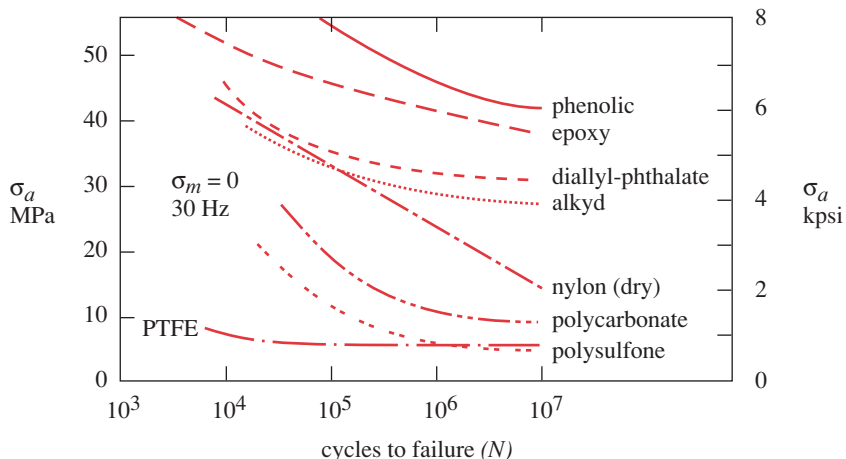


FIGURE 6-14

Stress-Life Curves from Cantilever Bending of Mineral and Glass-Filled Thermosets (Upper 4 Lines) and Unfilled Thermoplastics (Lower 4 Lines) (From Fig. 9-22, p. 362, in N. E. Dowling, *Mechanical Behavior of Materials*, Prentice-Hall, Englewood Cliffs, N.J., 1996, and based on data from M. N. Riddell, "A Guide to Better Testing of Plastics," *Plastics Engineering*, vol. 30, no. 4, pp. 71-78, with permissions)

6

TORSIONAL FATIGUE TESTS are done on a cylindrical specimen subjected to fully reversed, torsional loading. The failure points for reversed bending and reversed torsion in biaxial-stress tests are plotted on $\sigma_1-\sigma_3$ axes in Figure 6-15. Note the similarity to the distortion-energy ellipse of Figures 5-3 and 5-8 (pp. 249 and 255), which are for static loading failures. Thus the relationship between torsional strength and bending strength in cyclic loading is the same as in the static loading case. The torsional fatigue strength (or the torsional endurance limit) for a ductile material can then be expected to be about 0.577 (58%) of the bending fatigue strength (or bending endurance limit).

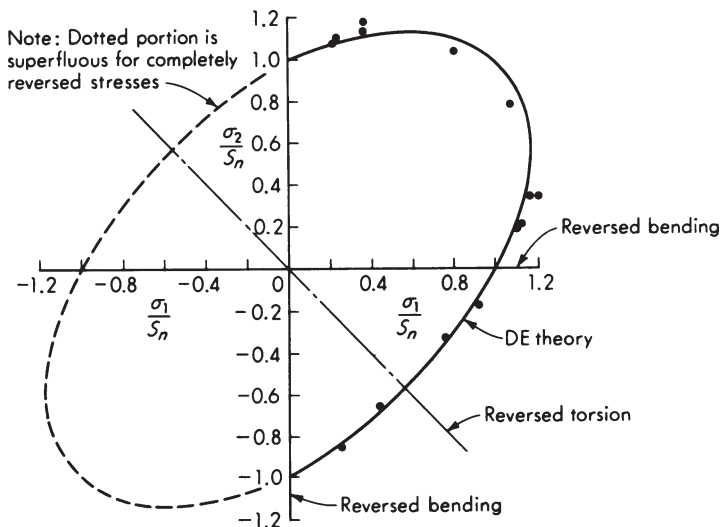


FIGURE 6-15

Fully Reversed Combined Torsional and Bending Biaxial Stress Failures Plotted on $\sigma_1-\sigma_2$ Axes (From *Behavior of Metals under Complex Static and Alternating Stresses*, ed. G. Sines in *Metal Fatigue*, by G. Sines and J. Waisman, McGraw-Hill, New York, 1959, with data from W. Savert, Germany, 1943, for annealed mild steel)

Combined Mean and Alternating Stress

The presence of a mean-stress component has a significant effect on failure. When a tensile mean component of stress is added to the alternating component as shown in Figures 6-6b and 6-6c (p. 313) the material fails at lower alternating stresses than it does under fully reversed loading. Figure 6-16 shows the results of tests made on steels at $\approx 10^7$ to 10^8 cycles (a) and aluminum alloys at $\approx 5 \times 10^8$ cycles (b) for various levels of mean and alternating stresses in combination. The plots are normalized by dividing the alternating stress σ_a by the fatigue strength S_f of the material under fully reversed stress (at the same number of cycles), and dividing the mean stress σ_m by the ultimate tensile strength S_{ut} of the material. There is a great deal of scatter in the data, but a pa-

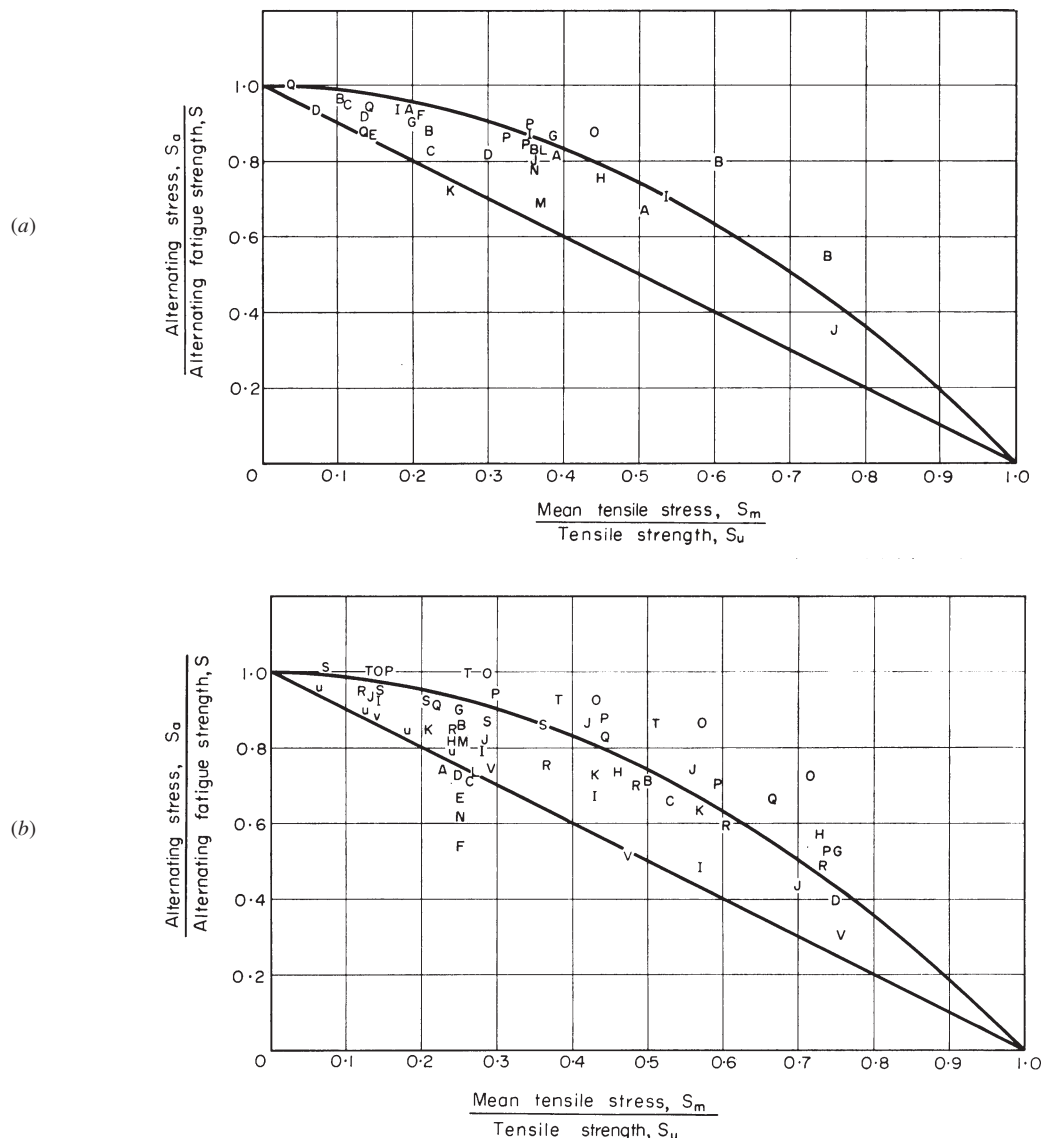


FIGURE 6-16

Effects of Mean Stress on Alternating Fatigue Strength at Long Life (a) Steels based on 10^7 to 10^8 Cycles (b) Aluminum Alloys Based on 5×10^8 Cycles. (From P. G. Forrest, *Fatigue of Metals*, Pergamon Press, London, 1962)

parabola that intercepts 1 on each axis, called the **Gerber line**, can be fitted to the data with reasonable accuracy. A straight line connecting the fatigue strength (1 on the y axis) with the ultimate strength (1 on the x axis), called the **Goodman line**, is a reasonable fit to the lower envelope of the data. The Gerber line is a measure of the average behavior of these parameters (for ductile materials) and the Goodman line is a measure of their minimum behavior. The Goodman line is often used as a design criterion, since it is safer than the Gerber line.

Figure 6-17 shows the effects of mean stresses (ranging from the compressive regime to the tensile regime) on failure when combined with alternating tensile stress for both aluminum and steel. It is clear from these data that compressive mean stresses have a beneficial effect and tensile mean stresses are detrimental. This fact provides an opportunity to mitigate the effects of alternating tensile stresses by the deliberate introduction of mean compressive stresses. One way to do this is to create **residual compressive stress** in the material in regions where large alternating components are expected. We will investigate ways to do this in later sections.

Figure 6-18 shows another view of this phenomenon by plotting the *S-N* curve (on semilog axes) for a hypothetical material with compressive mean stress, no mean stress, and tensile mean stress added. The fatigue strength or endurance limit of the material is effectively increased by the introduction of a compressive mean stress, whether applied or residual.

Fracture-Mechanics Criteria

The static fracture toughness test was described in Section 5.3 (p. 265). To develop fatigue strength data in terms of fracture-mechanics theory, a number of specimens of the same material are tested to failure at various levels of cyclical stress range $\Delta\sigma$. The test is done in an axial fatigue machine and the load pattern is usually either repeated

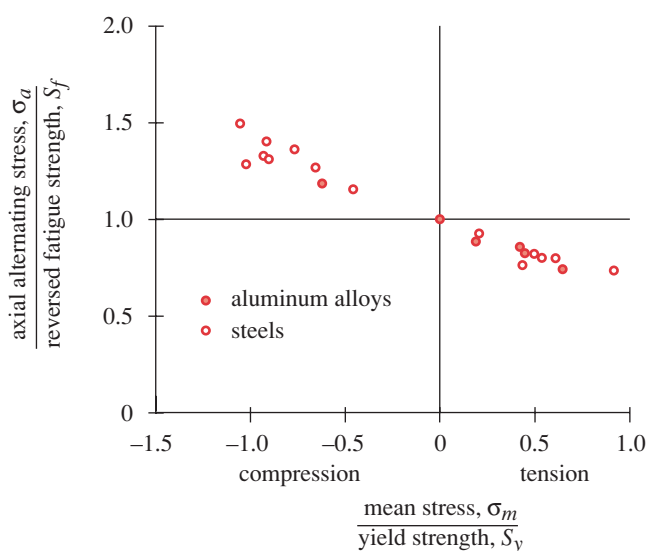
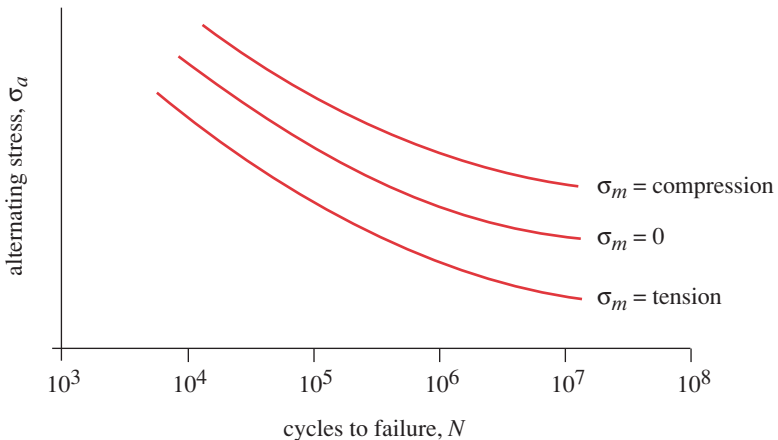


FIGURE 6-17

Compressive and Tensile Mean Stress Effect. (From G. Sines, "Failure of Materials Under Combined Repeated Stresses with Superimposed Static Stresses," NACA Technical Note #3495, 1955)

**FIGURE 6-18**

Effect of Mean Stress on Fatigue Life (From Fuchs and Stephens, *Metal Fatigue in Engineering*, New York, 1980, reprinted by permission of John Wiley & Sons, Inc.)

or fluctuating tensile stresses as shown in Figure 6-6b and 6-6c (p. 313). Reversed-stress tests are seldom done for these data, since compressive stress does not promote crack growth. The crack growth is continuously measured during the test. The applied stresses range from σ_{min} to σ_{max} . A stress intensity factor range ΔK can be calculated for each fluctuating-stress condition from

$$\Delta K = K_{max} - K_{min} : \quad \text{if } K_{min} < 0 \quad \text{then } \Delta K = K_{max} \quad (6.3a)$$

Substituting the appropriate equation 5.14 gives:

$$\begin{aligned} \Delta K &= \beta \sigma_{max} \sqrt{\pi a} - \beta \sigma_{min} \sqrt{\pi a} \\ &= \beta \sqrt{\pi a} (\sigma_{max} - \sigma_{min}) \end{aligned} \quad (6.3b)$$

The log of the rate of crack growth as a function of cycles da/dN is calculated and plotted versus the log of the stress intensity factor range ΔK as shown in Figure 6-19.

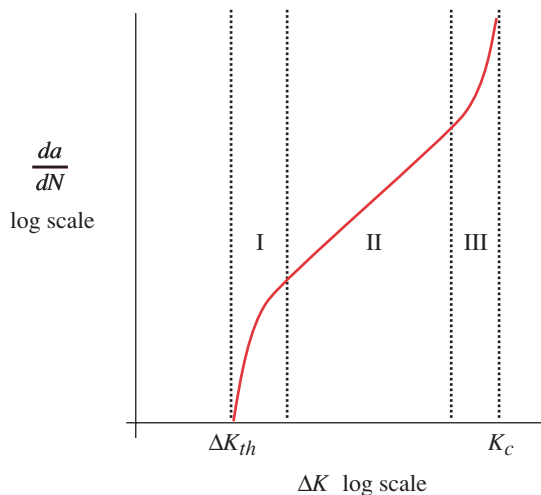
The sigmoidal curve of Figure 6-19 is divided into three regions labeled I, II, and III. Region I corresponds to the crack initiation stage, region II to the crack growth (crack propagation) stage, and region III to unstable fracture. Region II is of interest in predicting fatigue life, and that part of the curve is a straight line on log coordinates. Paris^[13] defined the relationship in region II as

$$\frac{da}{dN} = A(\Delta K)^n \quad (6.4a)$$

Barsom^[14] tested a number of steels and developed empirical values for the coefficient A and the exponent n in equation 6.4. These are shown in Table 6-2. The number of cycles N to grow a crack from an initial size a_i to a given size a_f under a known stress range cycle $\Delta\sigma$ and geometry β can be estimated from the Paris equation parameters as:^{*}

$$N = \frac{a_f^{(1-n/2)} - a_i^{(1-n/2)}}{A\beta^n \pi^{n/2} \Delta\sigma^n (1-n/2)} \quad (6.4b)$$

* See Section 5.3 for a definition of the geometry factor β .

**FIGURE 6-19**

Three Regions of the Crack Growth-Rate Curve. (From Fig. 3-12, p. 102, in Barnantime et al., *Fundamentals of Metal Fatigue Analysis*, Prentice-Hall, Englewood Cliffs, N.J., 1990, with permission)

The fatigue crack growth life is found by integrating equation 6.4 between a known or assumed initial crack length and a maximum acceptable final crack length based on the particular load, geometry, and material parameters for the application.

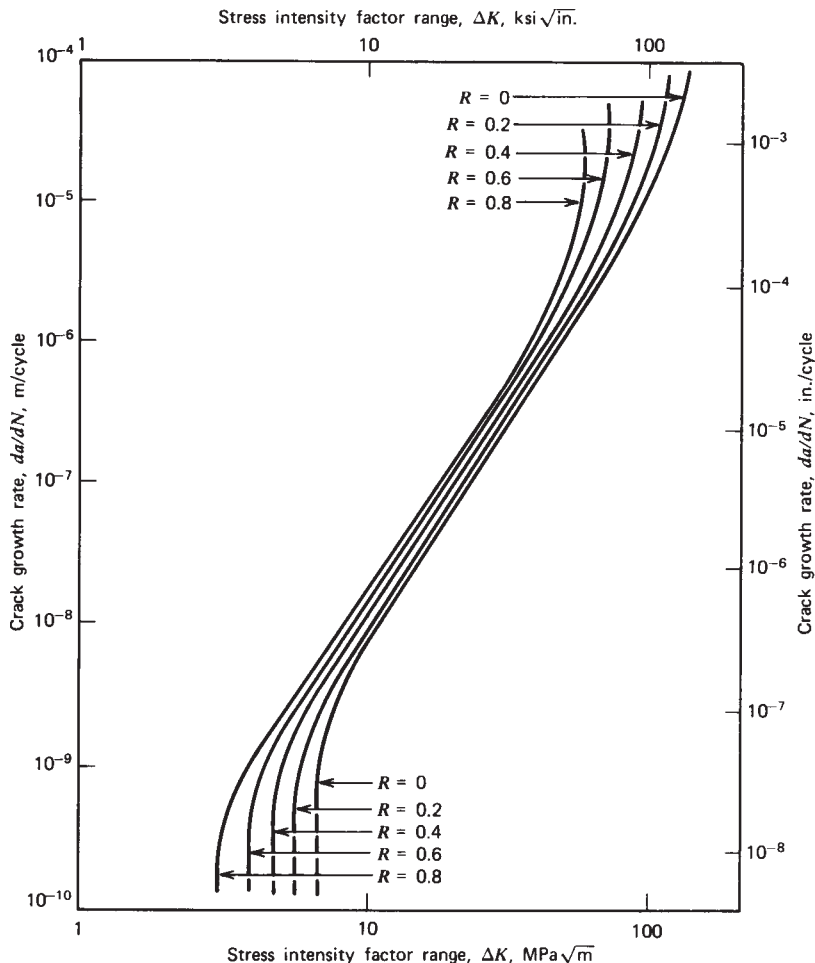
Region I in Figure 6-19 is also of interest, since it shows the existence of a minimum threshold ΔK_{th} below which no crack growth will occur. This “*threshold stress intensity factor ΔK_{th} has often been considered analogous to the unnotched fatigue limit S_e , since an applied stress intensity factor range ΔK below ΔK_{th} does not cause fatigue crack growth.*”^[15]

These axial fatigue tests have a mean stress component present, and the level of mean stress has an effect on the rate of crack propagation. Figure 6-20 shows a schematic set of da/dN curves for different levels of mean stress as defined by the stress ratio R . When $R = 0$, the stress is repeated as in Figure 6-6b (p. 313). As R approaches 1, the minimum stress approaches the maximum stress (see Eq. 6.1d, p. 314). Figure 6-20 shows little variation of the curves in Region II (crack growth), but shows significant changes with R in regions I and III. Crack initiation is thus affected by mean stress level. The threshold stress intensity factor ΔK_{th} may be reduced by a factor of 1.5 to 2.5 when R increases from 0 to 0.8^[18]. This is consistent with the effects of mean stress on the

Table 6-2 Paris-Equation Parameters for Various Steels

Source: J. M. Barsom^[14], with permission

Steel	SI units		U.S. (ips) units	
	A	n	A	n
Ferritic-Pearlitic	$6.90E-12$	3.00	$3.60E-10$	3.00
Martensitic	$1.35E-10$	2.25	$6.60E-09$	2.25
Austenitic Stainless	$5.60E-12$	3.25	$3.00E-10$	3.25

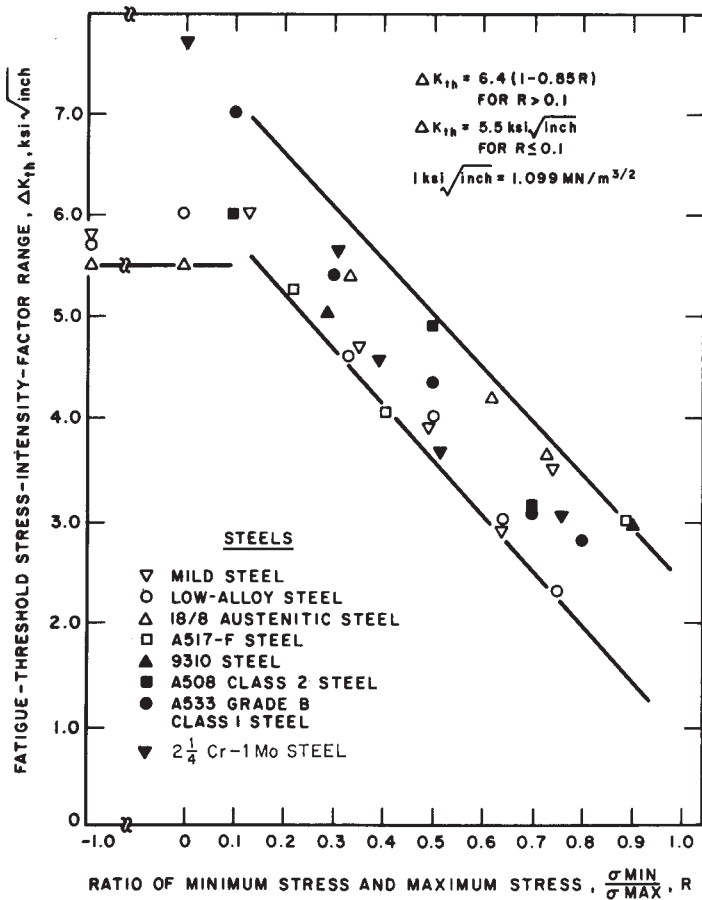
**FIGURE 6-20**

Schematic of the Effects of Mean Stress on the Crack-Growth-Rate Curve (From Fuchs and Stephens, *Metal Fatigue in Engineering*, New York, 1980, reprinted by permission of John Wiley & Sons, Inc.)

S-N data in the stress-life model discussed above (see Figure 6-16, p. 322). Figure 6-21 from reference 19 provides test data showing the effect of stress ratio R on the threshold stress intensity factor range ΔK_{th} for several steels.

Testing Actual Assemblies

While many strength data are available from test specimens, and the engineer can use these data as a starting point to estimate the strength of a particular part, the best data are obtained by testing the actual design under realistic load, temperature, and environmental conditions. This is an expensive proposition and is usually done only when the design's cost, quantity, or threat to human safety demand it. Figure 6-22 shows an elaborate test fixture built to allow fatigue testing of the wing and fuselage assemblies of the Boeing 757 aircraft during production. The entire aircraft is placed in the fixture and time-varying loads applied to various elements while measurements of strains, deflec-

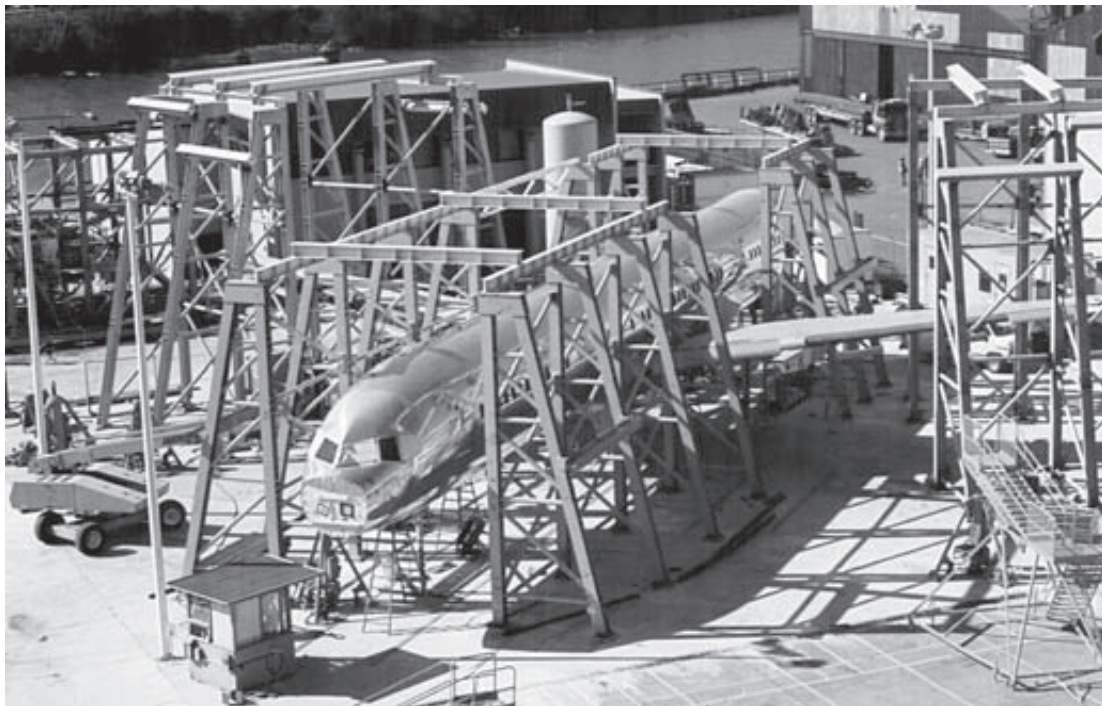
**FIGURE 6-21**

Effect of Mean Stress on Fatigue Threshold Stress Intensity Factor Range (From Fig 9.6, p. 285, in Barson and Rolfe, *Fracture and Fatigue Control in Structures*, Prentice-Hall, Englewood Cliffs, N.J., 1987, with permission)

tions, etc., are made. This is obviously a costly process but serves to provide the most realistic data possible, applying the test to actual shapes, sizes, and materials rather than to laboratory specimens.

6.6 ESTIMATING FATIGUE FAILURE CRITERIA

The best information on a material's fatigue strength at some finite life, or its endurance limit at infinite life, comes from the testing of actual or prototype assemblies of the design as described above. If this is not practical or possible, the next best information comes from fatigue tests of specimens taken from the particular material as it is manufactured for the part (i.e., as cast, forged, machined, etc.). Failing this, published fatigue strength data may be available in the literature or from the material manufacturers, but these data will be for small, polished specimens tested in controlled environ-

**FIGURE 6-22**

Boeing 757 Fatigue-Test Fixture for Wing and Fuselage Assemblies. (Courtesy of Boeing Commercial Airplane Co., Seattle, Wash.)

ments. In the absence of even these data, it will be necessary to make some estimation of the endurance limit or fatigue strength of the material based on data available from monotonic tests. This may be limited to information on the material's ultimate strength S_{ut} and yield strength S_y .

Estimating the Theoretical Fatigue Strength S_f or Endurance Limit S_e'

If published data are available for the fatigue strength S_f or endurance limit S_e' of the material, they should be used and the correction factors discussed in the next section then applied to them. Published fatigue strength data are typically from fully reversed bending or axial loading tests on small, polished specimens. If no fatigue strength data are available, an approximate S_f or S_e' can be crudely estimated from the published ultimate tensile strength of the material. Figure 6-23 shows the relationships between S_{ut} and S_f for wrought steels (a), wrought and cast irons (b), aluminum alloys (c), and wrought copper alloys (d). There is considerable scatter, and the lines are fitted approximately to the upper and lower bounds. At high tensile strengths, the fatigue strengths tend to "top out" as described above. From these data, approximate relationships can be stated between S_{ut} and S_f or S_e' . These relationships for steels and aluminum alloys were stated in the previous section as equations 6.2 and are repeated here for convenience.

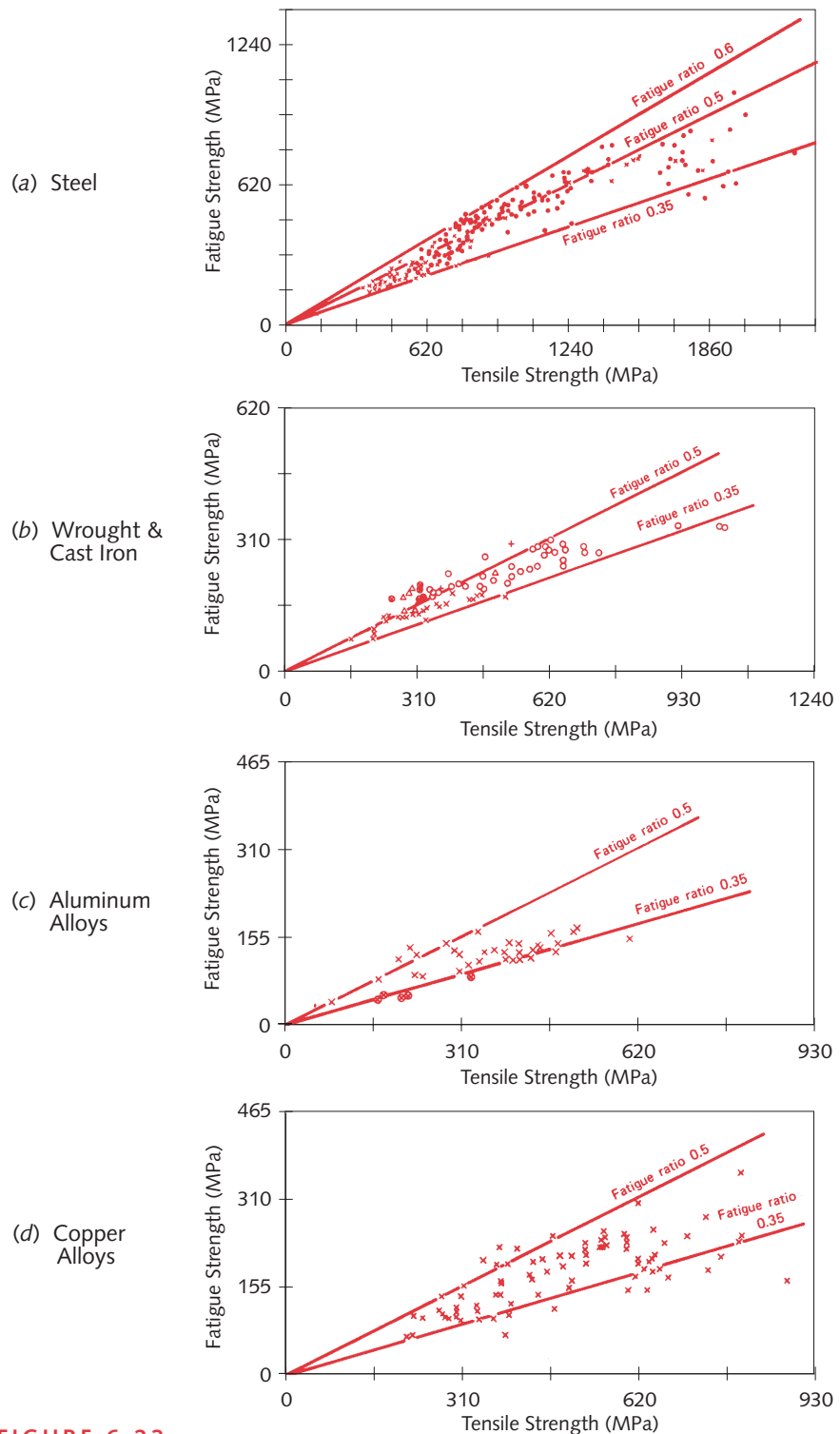


FIGURE 6-23

Relation Between Unnotched Rotating-Bending Fatigue Strength and Ultimate Strength
(From P. G. Forrest, *Fatigue of Metals*, Pergamon Press, London, 1962)

steels :
$$\begin{cases} S_{e'} \cong 0.5 S_{ut} & \text{for } S_{ut} < 200 \text{ kpsi (1400 MPa)} \\ S_{e'} \cong 100 \text{ kpsi (700 MPa)} & \text{for } S_{ut} \geq 200 \text{ kpsi (1400 MPa)} \end{cases} \quad (6.5a)$$

irons :
$$\begin{cases} S_{e'} \cong 0.4 S_{ut} & \text{for } S_{ut} < 60 \text{ kpsi (400 MPa)} \\ S_{e'} \cong 24 \text{ kpsi (160 MPa)} & \text{for } S_{ut} \geq 60 \text{ kpsi (400 MPa)} \end{cases} \quad (6.5b)$$

aluminums :
$$\begin{cases} S_{f'_{@5E8}} \cong 0.4 S_{ut} & \text{for } S_{ut} < 48 \text{ kpsi (330 MPa)} \\ S_{f'_{@5E8}} \cong 19 \text{ kpsi (130 MPa)} & \text{for } S_{ut} \geq 48 \text{ kpsi (330 MPa)} \end{cases} \quad (6.5c)$$

copper alloys :
$$\begin{cases} S_{f'_{@5E8}} \cong 0.4 S_{ut} & \text{for } S_{ut} < 40 \text{ kpsi (280 MPa)} \\ S_{f'_{@5E8}} \cong 14 \text{ kpsi (100 MPa)} & \text{for } S_{ut} \geq 40 \text{ kpsi (280 MPa)} \end{cases} \quad (6.5d)^{\ddagger}$$

Correction Factors to the Theoretical Fatigue Strength or Endurance Limit

The fatigue strengths or endurance limits obtained from standard fatigue-test specimens or from estimates based on static tests must be modified to account for physical differences between the test specimen and the actual part being designed. Environmental and temperature differences between the test conditions and the actual conditions must be taken into account. Differences in the manner of loading need to be accounted for. These and other factors are incorporated into a set of *strength-reduction factors* that are then multiplied by the theoretical estimate to obtain a corrected fatigue strength or endurance limit for the particular application.

$$\begin{aligned} S_e &= C_{load} C_{size} C_{surf} C_{temp} C_{reliab} S_e' \\ S_f &= C_{load} C_{size} C_{surf} C_{temp} C_{reliab} S_f' \end{aligned} \quad (6.6)$$

where S_e represents a corrected endurance limit for a material that exhibits a knee in its $S-N$ curve and S_f represents a corrected fatigue strength at a particular number of cycles N for a material that does not exhibit a knee. The strength reduction factors in equation 6.6 will now be defined.

LOADING EFFECTS Since the ratios described above and most published fatigue strength data are for rotating bending tests, a strength-reduction factor for axial loading must be applied. The differences between axial and rotating bending test fatigue strengths were described in the previous section. Based on that discussion of axial and bending fatigue tests, we now define a strength-reduction **load factor** C_{load} as

bending :	$C_{load} = 1$
axial loading :	$C_{load} = 0.70$

(6.7a)

* One exception to this will be the analysis and design of coil springs in Chapter 13 for which most of the available strength data are torsional shear strength values. It then makes more sense to compare torsional stresses to torsional strengths directly without conversion of the stresses to von Mises equivalents.

[†] Prof. Roger J. Hawks of Tri-State University, Angola, IN, has analyzed a large number of data for fatigue strength of copper alloys (including the data in Figure 6-23d) and finds a best fit to the data to be $S_f = 0.37 S_{ut}$ for $S_{ut} < 75$ kpsi and $S_f = 28$ kpsi for $S_{ut} > 75$ kpsi (personal communication, December 1, 2004.)

Note that a torsional fatigue test shows a strength that is 0.577 times the rotating bending fatigue strength as shown in Figure 6-15 (p. 321). For a pure-torsion fatigue case, we could compare the applied, alternating, torsional shear stress directly to the torsional fatigue strength. However, we will generally deal with the pure torsional case (and all other cases as well) by calculating the von Mises effective stress from the applied stresses.* This gives an *effective alternating tensile-stress* value that can be compared directly to a *bending-fatigue strength*. So, for pure torsion cases, use $C_{load} = 1$ with this method.

SIZE EFFECTS The rotating-beam and static test specimens are small (about 0.3-in dia). If the part is larger than that dimension, a strength-reduction **size factor** needs to be applied to account for the fact that larger parts fail at lower stresses due to the higher probability of a flaw being present in the larger stressed volume.[†] Various authors have suggested different values for the size factor. Shigley and Mitchell^[21] present a simple expression that is fairly conservative.

$$\begin{aligned} \text{for } d \leq 0.3 \text{ in (8 mm)}: \quad C_{\text{size}} &= 1 \\ \text{for } 0.3 \text{ in} < d \leq 10 \text{ in}: \quad C_{\text{size}} &= 0.869d^{-0.097} \\ \text{for } 8 \text{ mm} < d \leq 250 \text{ mm}: \quad C_{\text{size}} &= 1.189d^{-0.097} \end{aligned} \quad (6.7b)$$

For larger sizes use $C_{\text{size}} = 0.6$. (The test data on which these equations are based are for steel parts. The accuracy of equation 6.7b for nonferrous metals is questionable.)

Equation 6.7b is valid for cylindrical parts. For parts of other shapes, Kuguel^[22] suggested that equating the nonround part's cross-sectional area stressed above 95% of its maximum stress with the similarly stressed area of a rotating-beam specimen would provide an *equivalent diameter* to use in equation 6.7b. Since the stress is linearly distributed across the diameter d of a beam in rotating bending, the area A_{95} stressed above 95% of the outer-fiber stress is that which lies between $0.95d$ and $1.0d$ as shown in Figure 6-24.

$$A_{95} = \pi \left[\frac{d^2 - (0.95d)^2}{4} \right] = 0.0766d^2 \quad (6.7c)$$

The equivalent-diameter rotating-beam specimen for any cross section is then

$$d_{\text{equiv}} = \sqrt{\frac{A_{95}}{0.0766}} \quad (6.7d)$$

where A_{95} is the portion of the cross-sectional area of the nonround part that is stressed between 95% and 100% of its maximum stress. It is a simple task to compute the value of A_{95} for any cross section for which the loading is known. Shigley and Mitchell^[21] have done so for several common sections and their results are shown in Figure 6-25.

SURFACE EFFECTS The rotating-beam specimen is polished to a mirror finish to preclude surface imperfections serving as stress raisers. It is usually impractical to provide such an expensive finish on a real part. Rougher finishes will lower the fatigue strength by the introduction of stress concentrations and/or by altering the physical properties of the surface layer. A forged surface is both rough and decarburized and the reduced carbon levels weaken the surface where stresses are often highest.^[23] A strength-reduction **surface factor** C_{surf} is needed to account for these differences. Juvinal^[24] provides a chart (Figure 6-26) that gives some guidance in selecting a surface factor for a number of common finishes on steel. Note that tensile strength is also a factor, since higher-strength materials are more sensitive to the stress concentrations introduced by surface irregularities. In Figure 6-26 corrosive environments are seen to drastically reduce strength. These surface factors have been developed for steels and should only be applied to aluminum alloys and other ductile metals with the caution that testing of actual parts under realistic loading conditions be done in critical applications. Cast irons can be assigned a $C_{\text{surf}} = 1$, since their internal discontinuities dwarf the effects of a rough surface.

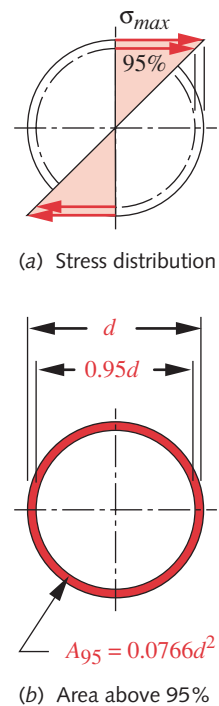
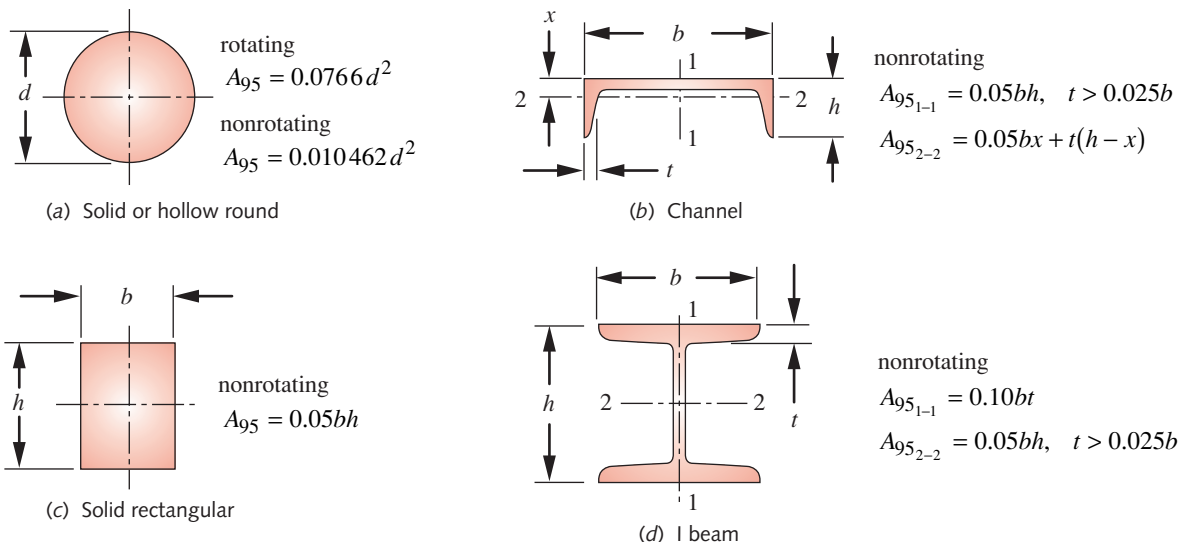


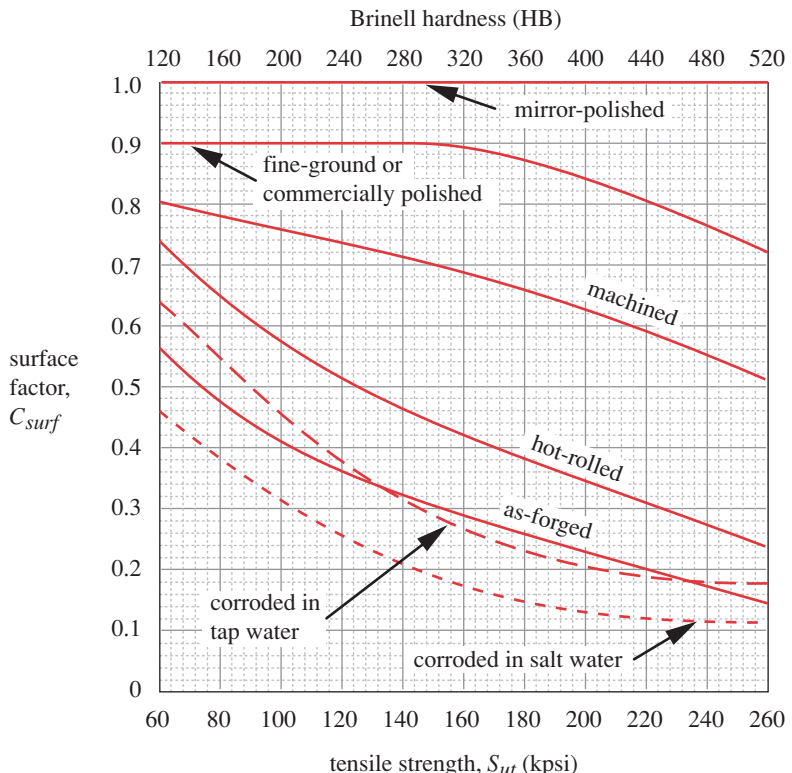
FIGURE 6-24

The Area in a Rotating Beam Specimen that is Stressed Above 95% of Maximum Stress

[†] Axially loaded sections always have $C_{\text{size}} = 1$ because failures of axially loaded test specimens evidence no sensitivity to cross-section size.

**FIGURE 6-25**

Formulas for 95% Stressed Areas of Various Sections Loaded in Bending (Adapted from: Shigley and Mitchell, *Mechanical Engineering Design*, 4th ed., McGraw-Hill, New York, 1983, with permission)

**FIGURE 6-26**

* There are many parameters used to characterize surface roughness, all of which are typically measured by passing a sharp, conical diamond stylus over the surface with controlled force and velocity. The stylus follows and encodes the microscopic contours and stores the surface profile in a computer. A number of statistical analyses are then done on the profile, such as finding the largest peak-to-peak distance (R_t), the average of the 5 highest peaks (R_{pm}), etc. The most commonly used parameter is R_a (or A_a), which is the arithmetic average of the absolute values of the peak heights and valley depths. It is this parameter that is used in Figure 6-27. See Section 7.1 for more information on surface roughness.

Surface Factors for Various Finishes on Steel (From Fig. 12.6, p. 234, R. C. Juvinall, *Stress, Strain, and Strength*, McGraw-Hill, New York, 1967, with permission)

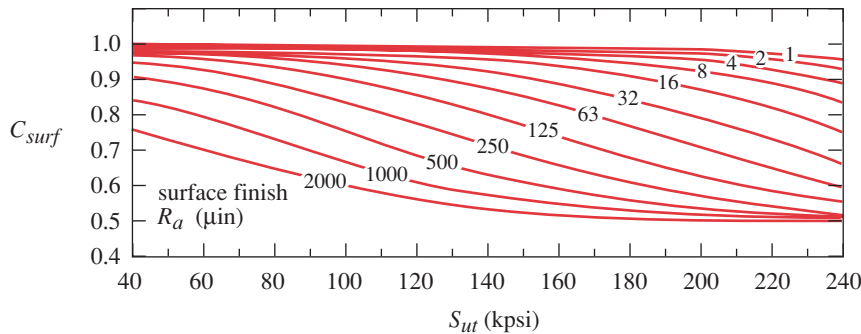


FIGURE 6-27

Surface Factor as a Function of Surface Roughness and Ultimate Tensile Strength (From R. C. Johnson, *Machine Design*, vol. 45, no. 11, 1967, p. 108, Penton Publishing, Cleveland, Ohio, with permission)

6

R. C. Johnson^[25] provides the chart shown in Figure 6-27 that gives more detail for **machined and ground surfaces** by relating C_{surf} to tensile strength based on the measured surface-average-roughness R_a in microinches.* If R_a is known for a machined or ground part, Figure 6-27 can be used to determine a suitable surface factor C_{surf} . The surface-factor curves in Figure 6-26 for hot-rolled, forged, and corroded surfaces should still be used, as they account for decarburization and pitting effects as well as surface roughness.

Shigley and Mischke^[39] suggest using an exponential equation of the form

$$C_{surf} \equiv A(S_{ut})^b \quad \text{if } C_{surf} > 1.0, \text{ set } C_{surf} = 1.0 \quad (6.7e)$$

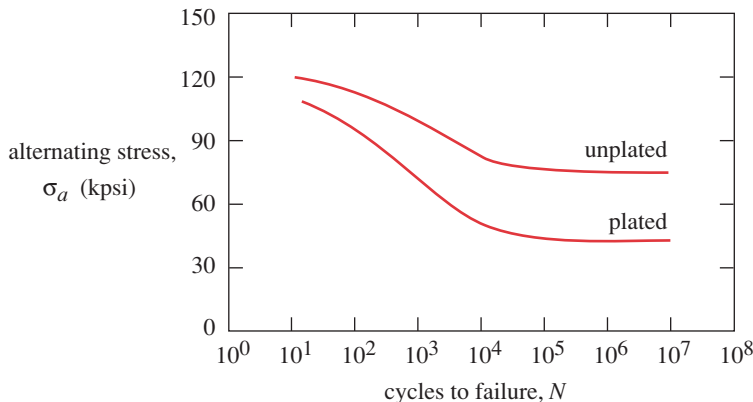
to approximate the surface factor with S_{ut} in either kpsi or MPa. The coefficients A and exponents b for various finishes were determined from data similar to those in Figure 6-26 and are shown in Table 6-3. This approach has the advantage of being computer programmable and eliminates the need to refer to charts such as Figures 6-26 and 6-27. Note that slightly different values of C_{surf} will be obtained from equation 6.7e than from the chart in Figure 6-26 due to the different data used to develop equation 6.7e and its factors in Table 6-3.

Surface treatments such as electroplating with certain metals can severely reduce the fatigue strength, as shown in Figure 6-28 for chrome plating. Plating with soft metals such as cadmium, copper, zinc, lead, and tin appears not to severely compromise

Table 6-3 Coefficients for Surface-Factor Equation 6.7e

Source: Shigley and Mischke, *Mechanical Engineering Design*, 5th ed., McGraw-Hill, New York, 1989, p. 283 with permission

Surface Finish	For S_{ut} in MPa use		For S_{ut} in kpsi (not psi) use	
	A	b	A	b
Ground	1.58	-0.085	1.34	-0.085
Machined or cold-rolled	4.51	-0.265	2.7	-0.265
Hot-rolled	57.7	-0.718	14.4	-0.718
As-forged	272	-0.995	39.9	-0.995

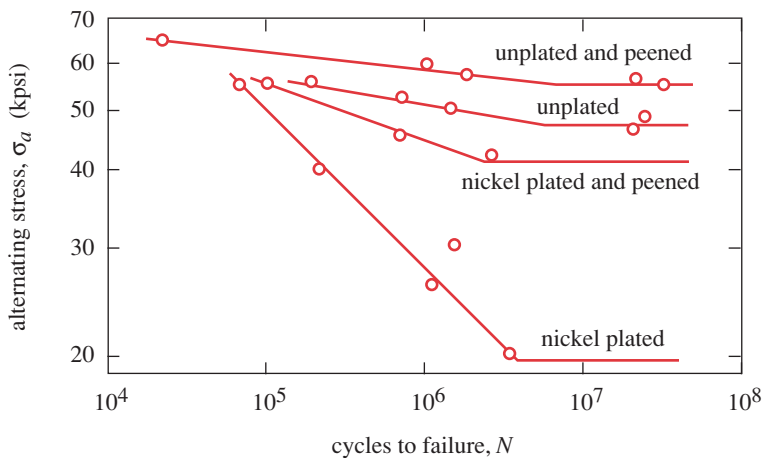
**FIGURE 6-28**

The Effect of Chrome Plating on Fatigue Strength of Steel (From C. C. Osgood, *Fatigue Design*, Pergamon Press, London, 1982, with permission)

6

fatigue strength. Electroplating with chrome and nickel is generally not recommended for parts stressed in fatigue unless additional surface treatments such as shot peening (see below) are also applied. An exception may be when the part is in a corrosive environment and the corrosion protection afforded by the plating outweighs its strength reduction. Most of the strength lost to plating can be recovered by shot-peening the surface prior to plating to introduce compressive stresses as shown in Figure 6-29. Shot peening and other means of creating residual stresses are addressed in Section 6.8 (p. 347).

TEMPERATURE Fatigue tests are most commonly done at room temperature. The fracture toughness decreases at low temperatures and increases at moderately high temperatures (up to about 350°C). But, the endurance-limit knee in the S-N diagram disappears at high temperatures, making the fatigue strength continue to decline with number of cycles, N . Also, the yield strength declines continuously with temperatures above room ambient and, in some cases, this can cause yielding before fatigue failure. At temperatures above about 50% of the material's absolute melting temperature, creep

**FIGURE 6-29**

The Effect of Nickel Plating and Shot Peening on Fatigue Strength of Steel (From Almen & Black, *Residual Stresses and Fatigue in Metals*, McGraw-Hill, New York, 1963)

becomes a significant factor and the stress-life approach is no longer valid. The strain-life approach can account for the combination of creep and fatigue under high-temperature conditions and should be used in those situations.

Several approximate formulas have been proposed to account for the reduction in endurance limit at moderately high temperatures. A **temperature factor** C_{temp} can be defined. Shigley and Mitchell^[26] suggest the following:

$$\begin{aligned} \text{for } T \leq 450^\circ\text{C (840°F)}: \quad C_{temp} &= 1 \\ \text{for } 450^\circ\text{C} < T \leq 550^\circ\text{C}: \quad C_{temp} &= 1 - 0.0058(T - 450) \\ \text{for } 840^\circ\text{F} < T \leq 1020^\circ\text{F}: \quad C_{temp} &= 1 - 0.0032(T - 840) \end{aligned} \quad (6.7f)$$

Note that these criteria are based on data for steels and should not be used for other metals such as Al, Mg, and Cu alloys.

RELIABILITY Many of the reported strength data are mean values. There is considerable scatter in multiple tests of the same material under the same test conditions. Haugen and Wirsching^[27] report that the standard deviations of endurance strengths of steels seldom exceed 8% of their mean values. Table 6-4 shows reliability factors for an assumed 8% standard deviation. Note that a 50% reliability has a factor of 1 and the factor reduces as you choose higher reliability. For example, if you wish to have 99.99% probability that your samples meet or exceed the assumed strength, multiply the mean strength value by 0.702. The values in Table 6-4 provide strength-reduction factors C_{reliab} for chosen reliability levels.

ENVIRONMENT The environment can have significant effects on fatigue strength as is evidenced by the curves for corroded surfaces in Figure 6-26 (p. 332). Figure 6-30 shows schematically the relative effects of various environments on fatigue strength. Note that even room air reduces strength compared to vacuum. The higher the relative humidity and temperature, the larger will be the reduction of strength in air. The *presoak* line represents parts soaked in a corrosive environment (water or seawater) and then tested in room air. The increased roughness of the corroded surface is thought to be the

Table 6-4
Reliability Factors
for $S_d = 0.08 \mu$

Reliability %	C_{reliab}
50	1.000
90	0.897
95	0.868
99	0.814
99.9	0.753
99.99	0.702
99.999	0.659
99.9999	0.620

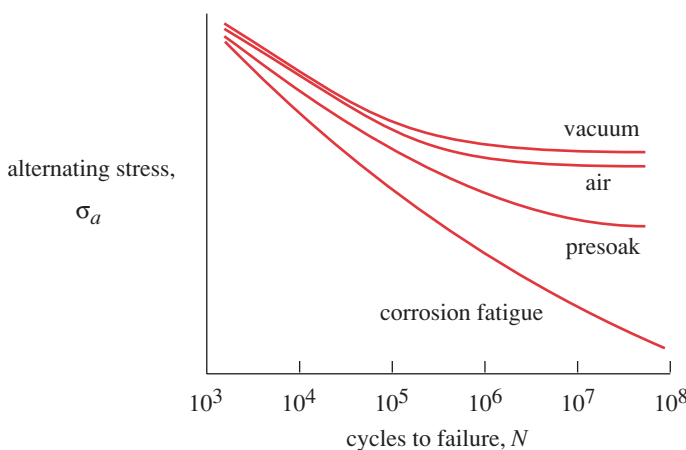
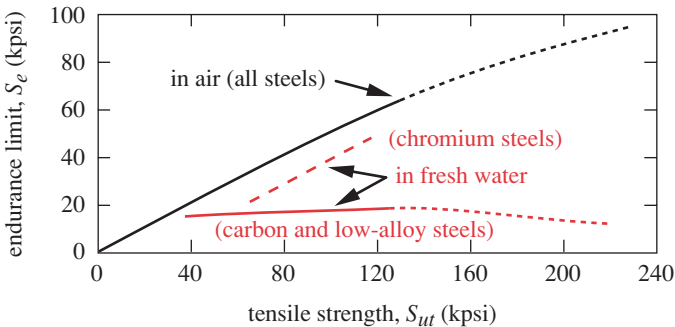


FIGURE 6-30

The Effect of Environment on Fatigue Strength of Steel. (From Fuchs and Stephens, *Metal Fatigue in Engineering*, New York, 1980, reprinted by permission of John Wiley & Sons, Inc.)

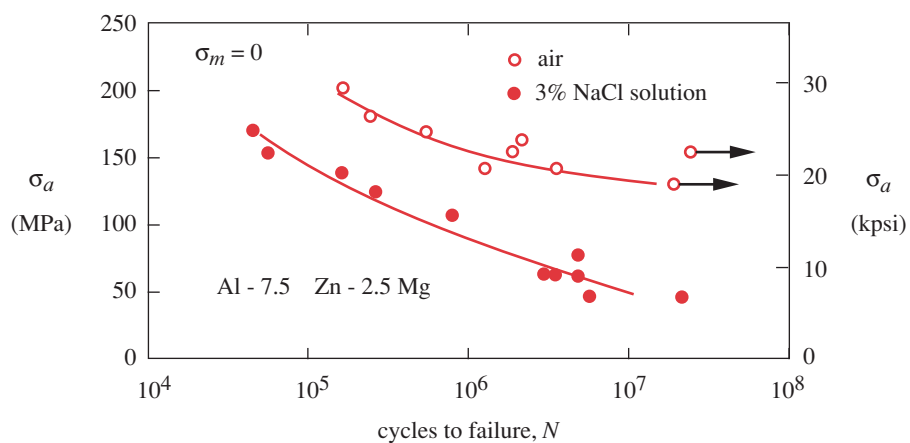
**FIGURE 6-31**

The Effect of Fresh Water on Fatigue Strength of Steel (From P. G. Forrest, *Fatigue of Metals*, Pergamon Press, Oxford, 1962)

6

reason for the loss of strength. The *corrosion fatigue* line shows a drastic reduction of strength and elimination of the endurance-limit knee.

The **corrosion-fatigue** phenomenon is not yet fully understood but empirical data such as those in Figures 6-30 and 6-31 depict its severity. Figure 6-31 shows the effect of operation in fresh water on the $S-N$ curves of carbon and low-alloy steels. The relationship between S_e and S_{ut} becomes constant at about 15 kpsi. So low-strength carbon steel is as good as high-strength carbon steel in this environment. The only steels that retain some strength in water are chromium steels (including stainless steels), since that alloying element provides some corrosion protection. Figure 6-32 shows the effects of saltwater on the fatigue strength of one alloy of aluminum. Only limited data are available for material strengths in severe environments. Thus it is difficult to define any universal strength-reduction factors for environmental conditions. The best approach is to extensively test all designs and materials in the environment that they will experience. (This is difficult to do for situations in which the long-term effects of low-frequency loading are desired because it will take an unreasonable time to obtain the

**FIGURE 6-32**

The Effect of Saltwater on the Fatigue Strength of Aluminum (From Stubbington and Forsyth, "Some Corrosion-Fatigue Observations on a High-Purity Aluminum-Zinc-Magnesium Alloy and Commercial D.T.D. 683 Alloy," *J. of the Inst. of Metals*, London, U.K., vol. 90, 1961-1962, pp. 347-354, with permission)

data.) Based on Figure 6-31, for carbon and low-alloy steels in fresh water, the relationship between S_e' and S_{ut} in equation 6.5a should be modified to

$$S_e' \approx 15 \text{ kpsi (100 MPa)} \quad \text{for carbon steel in fresh water} \quad (6.8)$$

Presumably, a saltwater environment would be even worse.

Calculating the Corrected Fatigue Strength S_f or Corrected Endurance Limit S_e

The strength-reduction factors can now be applied to the uncorrected endurance limit S_e' or to the uncorrected fatigue strength S_f' using equation 6.6 (p. 330) to obtain corrected values for design purposes.

Creating Estimated S-N Diagrams

Equations 6.6 provide information about the material's strength in the high-cycle region of the S-N diagram. With similar information for the low-cycle region, we can construct an S-N diagram for the particular material and application as shown in Figure 6-33. The bandwidth of interest is the HCF regime from 10^3 to 10^6 cycles and beyond. Let the material strength at 10^3 cycles be called S_m . Test data indicate that the following estimates of S_m are reasonable:^[28]

$$\begin{aligned} \text{bending : } & S_m = 0.9S_{ut} \\ \text{axial loading : } & S_m = 0.75S_{ut} \end{aligned} \quad (6.9)$$

The estimated S-N diagram can now be drawn on log-log axes as shown in Figure 6-33. The x axis runs from $N = 10^3$ to $N = 10^9$ cycles or beyond. The appropriate S_m from equation 6.9 for the type of loading is plotted at $N = 10^3$. Note that the correction factors from equation 6.6 are **not** applied to S_m .

If the material exhibits a knee, then the corrected S_e from equation 6.6 is plotted at $N_e = 10^6$ cycles and a straight line is drawn between S_m and S_e . The curve is continued horizontally beyond that point. If the material does not exhibit a knee, then the corrected S_f from equation 6.6 is plotted at the number of cycles for which it was generated (shown at $N_f = 5 \times 10^8$) and a straight line is drawn between S_m and S_f . This line may be extrapolated beyond that point, but its accuracy is questionable, though probably conservative (see Figure 6-10).

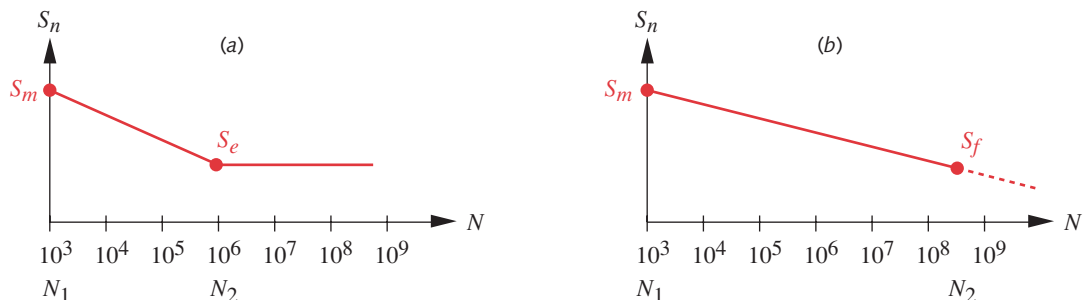


FIGURE 6-33

Estimated S-N Curves for (a) Materials with Knee, (b) Materials Without Knee

The equation of the line from S_m to S_e or S_f can be written as

$$S(N) = aN^b \quad (6.10a)$$

or

$$\log S(N) = \log a + b \log N \quad (6.10b)$$

where $S(N)$ is the fatigue strength at any N and a, b are constants defined by the boundary conditions. For all cases, the y intercept is $S(N) = S_m$ at $N = N_1 = 10^3$. For the endurance-limit case (Figure 6-33), $S(N) = S_e$ at $N = N_2 = 10^6$. For a material that does not exhibit an endurance-limit knee, the fatigue strength is taken at some number of cycles: $S(N) = S_f$ at $N = N_2$ (Figure 6-33b). Substitute the boundary conditions in equation 6.10b and solve simultaneously for a and b :

$$b = \frac{1}{z} \log \left(\frac{S_m}{S_e} \right) \quad \text{where} \quad z = \log N_1 - \log N_2 \quad (6.10c)$$

$$\log(a) = \log(S_m) - b \log(N_1) = \log(S_m) - 3b$$

Table 6-5
z-factors for Eq. 6-10c

N_2	z
$1.0E6$	-3.000
$5.0E6$	-3.699
$1.0E7$	-4.000
$5.0E7$	-4.699
$1.0E8$	-5.000
$5.0E8$	-5.699
$1.0E9$	-6.000
$5.0E9$	-6.699

Note that N_1 is always 1 000 cycles and its \log_{10} is 3. For a material with a knee at $N_2 = 10^6$, $z = (3 - 6) = -3$ as shown in Table 6-5. This curve is valid only to the knee, beyond which $S(N) = S_e$ as shown in Figure 6-33a.

For a material with no knee and $S(N) = S_f$ at $N = N_2$ (Figure 6-33b), the values of z corresponding to various values of N_2 are easily calculated. For example, the curve in Figure 6-33b shows S_f at $N_2 = 5E8$ cycles. The value for z is then

$$z_{@5E8} = \log(1000) - \log(5E8) = 3 - 8.699 = -5.699 \quad (6.10d)$$

$$b_{@5E8} = -\frac{1}{5.699} \log \left(\frac{S_m}{S_f} \right) \quad \text{for } S_f @ N_2 = 5E8 \text{ cycles}$$

The constants for any other boundary conditions are determined in the same way. Some values of z for a range of values of N_2 with N_1 set to 10^3 are shown in Table 6-5. These equations for the S - N curve allow the estimated finite life N to be found for any fully reversed fatigue strength $S(N)$, or the estimated fatigue strength $S(N)$ can be found for any N .

EXAMPLE 6-1

Determining Estimated S-N Diagrams for Ferrous Materials

Problem Create an estimated S-N diagram for a steel bar and define its equations. How many cycles of life can be expected if the alternating stress is 100 MPa?

Given The S_{ut} has been tested at 600 MPa. The bar is 150 mm square and has a hot-rolled finish. The operating temperature is 500°C maximum. The loading will be fully reversed bending.

Assumptions Infinite life is required and is obtainable since this ductile steel will have an endurance limit. A reliability factor of 99.9% will be used.

Solution

- 1 Since no endurance-limit or fatigue strength information is given, we will estimate S_e' based on the ultimate strength using equation 6.5a (p. 330).

$$S_{e'}' \cong 0.5S_{ut} = 0.5(600) = 300 \text{ MPa} \quad (a)$$

- 2 The loading is bending so the load factor from equation 6.7a is

$$C_{load} = 1.0 \quad (b)$$

- 3 The part is larger than the test specimen and is not round, so an equivalent diameter based on its 95% stressed area (A_{95}) must be determined and used to find the size factor. For a rectangular section in nonrotating bending loading, the A_{95} area is defined in Figure 6-25c (p. 332) and the equivalent diameter is found from equation 6.7d (p. 331):

$$A_{95} = 0.05bh = 0.05(150)(150) = 1125 \text{ mm}^2$$

$$d_{equiv} = \sqrt{\frac{A_{95}}{0.0766}} = \sqrt{\frac{1125 \text{ mm}^2}{0.0766}} = 121.2 \text{ mm} \quad (c)$$

and the size factor is found for this equivalent diameter from equation 6.7b (p. 331):

$$C_{size} = 1.189(121.2)^{-0.097} = 0.747 \quad (d)$$

- 4 The surface factor is found from equation 6.7e (p. 333) and the data in Table 6-3 for the specified hot-rolled finish.

$$C_{surf} = AS_{ut}^b = 57.7(600)^{-0.718} = 0.584 \quad (e)$$

- 5 The temperature factor is found from equation 6.7f (p. 335):

$$C_{temp} = 1 - 0.0058(T - 450) = 1 - 0.0058(500 - 450) = 0.71 \quad (f)$$

- 6 The reliability factor is taken from Table 6-4 (p. 335) for the desired 99.9% and is

$$C_{reliab} = 0.753 \quad (g)$$

- 7 The corrected endurance limit S_e can now be calculated from equation 6.6 (p. 330):

$$S_e = C_{load} C_{size} C_{surf} C_{temp} C_{reliab} S_{e'}$$

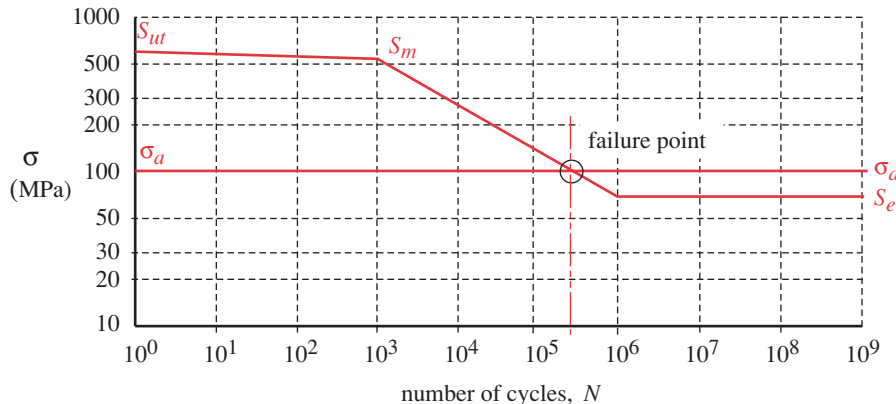
$$= 1.0(0.747)(0.584)(0.71)(0.753)(300) \quad (h)$$

$$S_e = 70 \text{ MPa}$$

- 8 To create the $S-N$ diagram, we also need a number for the estimated strength S_m at 10^3 cycles based on equation 6.9 (p. 337) for bending loading.

$$S_m = 0.90S_{ut} = 0.90(600) = 540 \text{ MPa} \quad (i)$$

- 9 The estimated $S-N$ diagram is shown in Figure 6-34 with the above values of S_m and S_e . The expressions of the two lines are found from equations 6.10a through 6.10c (p. 338) assuming that S_e begins at 10^6 cycles.

**FIGURE 6-34**

6

S-N Diagram and Alternating Stress Line Showing Failure Point for Example 6-1

$$b = -\frac{1}{3} \log\left(\frac{S_m}{S_e}\right) = -\frac{1}{3} \log\left(\frac{540}{70}\right) = -0.295765 \quad (j)$$

$$\log(a) = \log(S_m) - 3b = \log[540] - 3(-0.295765) : \quad a = 4165.707$$

$$S(N) = aN^b = 4165.707N^{-0.295765} \text{ MPa} \quad 10^3 \leq N \leq 10^6 \quad (k)$$

$$S(N) = S_e = 70 \text{ MPa} \quad N > 10^6$$

- 10 The number of cycles of life for any alternating stress level can now be found from equations (k). For the stated stress level of 100 MPa, we get

$$100 = 4165.707N^{-0.295765} \quad 10^3 \leq N \leq 10^6$$

$$\log 100 = \log 4165.707 - 0.295765 \log N$$

$$2 = 3.619689 - 0.295765 \log N \quad (l)$$

$$\log N = \frac{2 - 3.619689}{-0.295765} = 5.476270$$

$$N = 10^{5.476270} = 3.0E5 \text{ cycles}$$

Figure 6-34 shows the intersection of the alternating stress line with the failure line at $N = 3E5$ cycles.

- 11 The files EX06-01 are on the CD-ROM.

EXAMPLE 6-2**Determining Estimated S-N Diagrams for Nonferrous Materials****Problem**

Create an estimated S-N diagram for an aluminum bar and define its equations. What is the corrected fatigue strength at $2E7$ cycles?

Given

The S_{ut} for this 6061-T6 aluminum has been tested at 45 000 psi. The forged bar is 1.5 in round. The maximum operating temperature is 300°F. The loading is fully reversed torsion.

Assumptions

A reliability factor of 99.0% will be used. The uncorrected fatigue strength will be taken at 5E8 cycles.

Solution

- 1 Since no fatigue-strength information is given, we will estimate S_f' based on the ultimate strength using equation 6.5c (p. 330).

$$\begin{aligned} S_f' &\equiv 0.4S_{ut} \quad \text{for } S_{ut} < 48 \text{ ksi} \\ S_f' &\equiv 0.4(45\,000) = 18\,000 \text{ psi} \end{aligned} \quad (a)$$

This value is at $N = 5E8$ cycles. There is no knee in an aluminum S - N curve.

- 2 The loading is *pure torsion*, so the load factor from equation 6.7a (p. 330) is

$$C_{load} = 1.0 \quad (b)$$

because the applied torsional stress will be converted to an equivalent von Mises normal stress for comparison to the S - N strength.

- 3 The part size is greater than the test specimen and it is round, so the size factor can be estimated with equation 6.7b (p. 331), noting that this relationship is based on steel data:

$$C_{size} = 0.869(d_{equiv})^{-0.097} = 0.869(1.5)^{-0.097} = 0.835 \quad (c)$$

- 4 The surface factor is found from equation 6.7e (p. 333) using the data in Table 6-3 (p. 333) for the specified forged finish, again with the caveat that these relationships were developed for steels and may be less accurate for aluminum.

$$C_{surf} = A S_{ut}^b = 39.9(45)^{-0.995} = 0.904 \quad (d)$$

- 5 Equation 6.7f (p. 335) is only for steel so we will assume:

$$C_{temp} = 1 \quad (e)$$

- 6 The reliability factor is taken from Table 6-4 (p. 335) for the desired 99.0% and is

$$C_{reliab} = 0.814 \quad (f)$$

- 7 The corrected fatigue strength S_f at $N = 5E8$ can now be calculated from equation 6.6 (p. 330):

$$\begin{aligned} S_f &= C_{load} C_{size} C_{surf} C_{temp} C_{reliab} S_f' \\ &= 1.0(0.835)(0.904)(1.0)(0.814)(18\,000) = 11\,063 \text{ psi} \end{aligned} \quad (g)$$

- 8 To create the S - N diagram, we also need a number for the estimated strength S_m at 10^3 cycles based on equation 6.9 (p. 337). Note that the bending value is used for torsion.

$$S_m = 0.90S_{ut} = 0.90(45\,000) = 40\,500 \text{ psi} \quad (h)$$

- 9 The coefficient and exponent of the corrected S - N line and its equation are found using equations 6.10a through 6.10c (p. 338). The value of z is taken from Table 6-5 (p. 338) for S_f at 5E8 cycles.

$$b = -\frac{1}{5.699} \log\left(\frac{S_m}{S_f}\right) = -\frac{1}{5.699} \log\left(\frac{40\,500}{11\,063}\right) = -0.0989 \quad (i)$$

$$\log(a) = \log(S_m) - 3b = \log[40\,500] - 3(-0.0989) : \quad a = 80\,193$$

- 10 The fatigue strength at the desired life of $N = 2E7$ cycles can now be found from the equation for the corrected S - N line:

$$S(N) = aN^b = 80\,193N^{-0.0989} = 80\,193(2e7)^{-0.0989} = 15\,209 \text{ psi} \quad (j)$$

$S(N)$ is larger than S_f because it is at a shorter life than the published fatigue strength.

- 11 Note the order of operations. We first found an uncorrected fatigue strength S_f' at some “standard” cycle life ($N = 5E8$), then corrected it for the appropriate factors from equations 6.7 (pp. 330–335). Only then did we create equation 6.10a (p. 338) for the S - N line so that it passes through the **corrected** S_f at $N = 5E8$. If we had created equation 6.10a using the uncorrected S_f' , solved it for the desired cycle life ($N = 2E7$), and **then** applied the correction factors, we would get a different and incorrect result. Because these are exponential functions, superposition does not hold.

- 12 The files EX06-02 are on the CD-ROM.
-

6.7 NOTCHES AND STRESS CONCENTRATIONS

Notch is a generic term in this context and refers to any geometric contour that disrupts the “force flow” through the part as described in Section 4.15 (p. 186). A **notch** can be a *hole, a groove, a fillet, an abrupt change in cross section, or any disruption to the smooth contours of a part*. The notches of concern here are those that are deliberately introduced to obtain engineering features such as O-ring grooves, fillets on shaft steps, fastener holes, etc. It is assumed that the engineer will follow good design practice and keep the radii of these notches as large as possible and reduce stress concentrations as described in Section 4.15. Notches of extremely small radii are poor design practice and, if present, should be treated as cracks and the principles of fracture mechanics used to predict failure (see Sections 5.3 on p. 265 and 6.5 on p. 315). A notch creates a stress concentration that raises the stresses locally and may even cause local yielding. In the discussion of stress concentration in Chapters 4 and 5 where only static loads were being considered, the effects of stress concentrations were only of concern for brittle materials. It was assumed that ductile materials would yield at the local stress concentration and lower the stress to acceptable levels. With dynamic loads, the situation is different, since ductile materials behave as if brittle in fatigue failures.

The geometric (theoretical) stress-concentration factors K_t for normal stress and K_{ts} for shear stress were defined and discussed in Section 4.15. (We will refer to them both here as K_t .) These factors give an indication of the degree of stress concentration at a notch having a particular contour and are used as a multiplier on the nominal stress present in the cross section containing the notch (see equation 4.31, p. 187). Many of these *geometric or theoretical stress-concentration factors* have been determined for various loadings and part geometries and are published in various references.^{[30], [31]} For dynamic loading, we need to modify the theoretical stress-concentration factor based on the notch sensitivity of the material to obtain a **fatigue stress-concentration factor**, K_f , which can be applied to the nominal dynamic stresses.

Notch Sensitivity

Materials have different sensitivity to stress concentrations, which is referred to as the **notch sensitivity** of the material. In general, the more ductile the material, the less notch sensitive it is. Brittle materials are more notch sensitive. Since ductility and brittleness in metals are roughly related to strength and hardness, low-strength, soft materials tend to be less notch sensitive than high-strength, hard ones. Notch sensitivity is also dependent on the notch radius (which is a measure of notch sharpness). As notch radii approach zero, the notch sensitivity of materials **decreases** and also approaches zero. This is quite serendipitous, since you will recall from Section 4.15 that the theoretical stress-concentration factor K_t approaches infinity as the notch radius goes to zero. If not for the reduced notch sensitivity of materials at radii approaching zero (i.e., cracks), engineers would be at a loss to design parts able to withstand *any nominal stress level* when notches are present.

Neuber^[32] made the first thorough study of notch effects and published an equation for the fatigue stress-concentration factor in 1937. Kuhn^[33] later revised Neuber's equation and experimentally developed data for the Neuber constant (a material property) needed in his equation. Peterson^[30] subsequently refined the approach and developed the concept of notch sensitivity q defined as

$$q = \frac{K_f - 1}{K_t - 1} \quad (6.11a)$$

where K_t is the theoretical (static) stress-concentration factor for the particular geometry and K_f is the fatigue (dynamic) stress-concentration factor. The notch sensitivity q varies between 0 and 1. This equation can be rewritten to solve for K_f :

$$K_f = 1 + q(K_t - 1) \quad (6.11b)$$

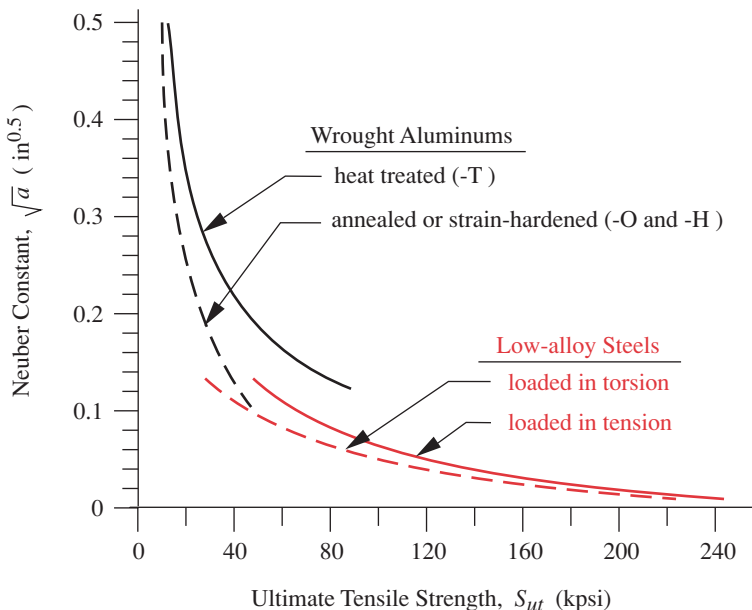
The procedure is to first determine the theoretical stress concentration K_t for the particular geometry and loading, then establish the appropriate notch sensitivity for the chosen material and use them in equation 6.11b to find the dynamic stress-concentration factor K_f . The nominal dynamic stress for any situation is then increased by the factor K_f for tensile stress (K_{fs} for shear stress) in the same manner as was done for the static case:

$$\begin{aligned} \sigma &= K_f \sigma_{nom} \\ \tau &= K_{fs} \tau_{nom} \end{aligned} \quad (6.12)$$

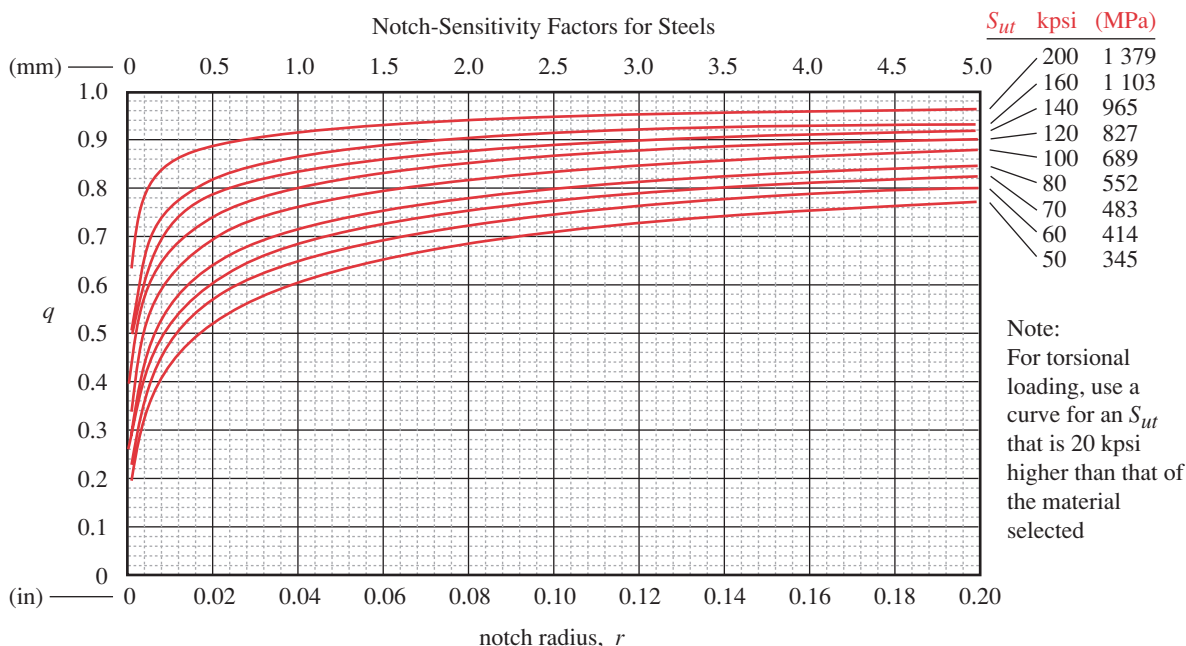
Note in equation 6.11 that when $q = 0$, $K_f = 1$ and it does not increase the nominal stress in equation 6.12. When $q = 1$, $K_f = K_t$ and the entire effect of the geometric stress-concentration factor is felt in equation 6.12.

The notch sensitivity q can also be defined from the Kuhn-Hardrath formula^[33] in terms of Neuber's constant a and the notch radius r , both expressed in inches.

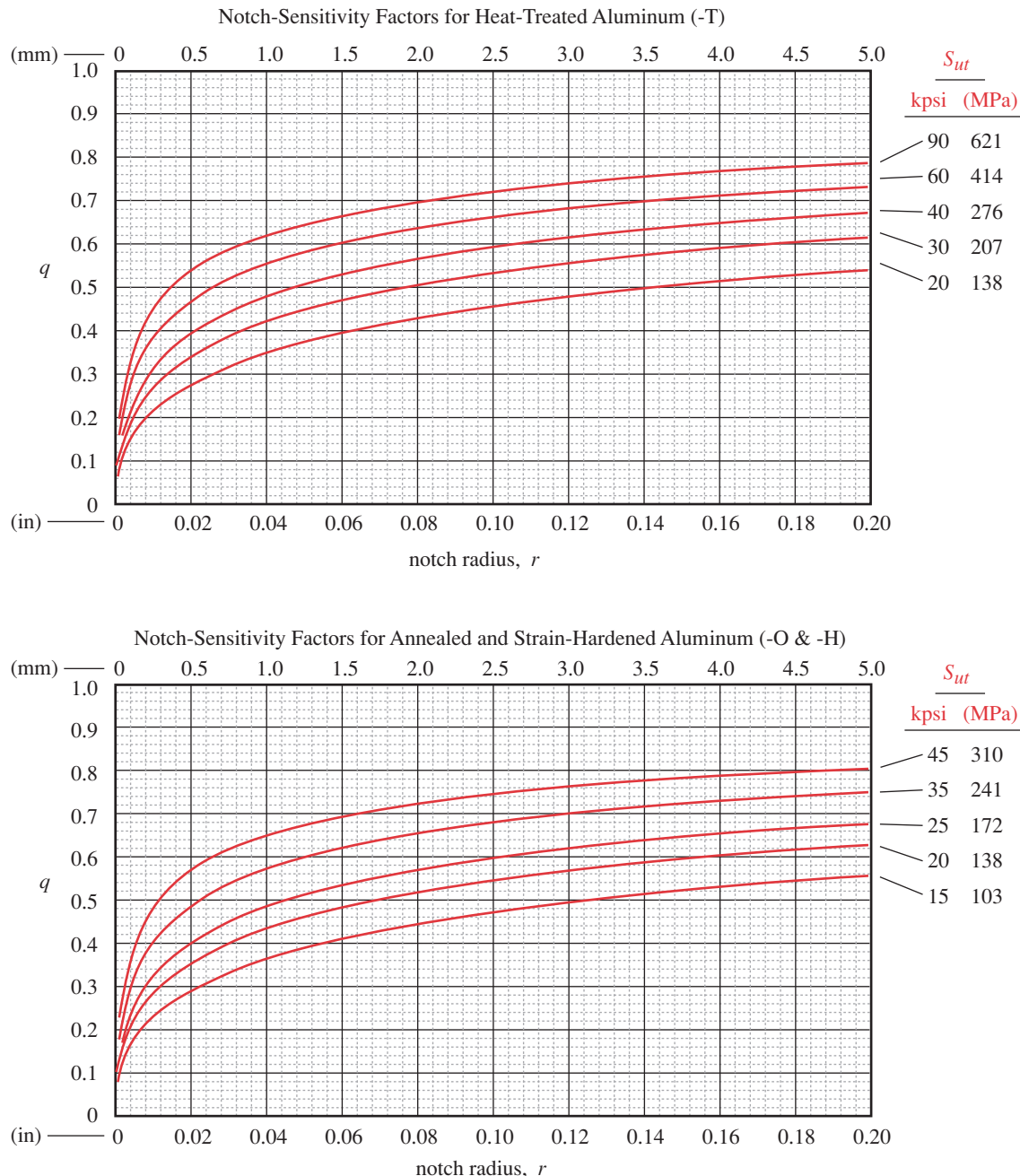
$$q = \frac{1}{1 + \frac{\sqrt{a}}{\sqrt{r}}} \quad (6.13)$$

**FIGURE 6-35**

Neuber Constants for Steel and Aluminum. (From ASME Paper 843c, "The Prediction of Notch and Crack Strength under Static or Fatigue Loading," by P. Kuhn, April 1964)

**FIGURE 6-36 Part 1**

Notch-Sensitivity Curves for Steels Calculated from Equation 6.13 Using Data from Figure 6-35 as Originally Proposed by R. E. Peterson in "Notch Sensitivity," Chapter 13 in *Metal Fatigue* by G. Sines and J. Waisman, McGraw-Hill, New York, 1959.

**FIGURE 6-36 Part 2**

Notch-Sensitivity Curves for Aluminums Calculated from Equation 6.13 Using Data from Figure 6-35 as Originally Proposed by R. E. Peterson in "Notch Sensitivity," Chapter 13 in *Metal Fatigue* by G. Sines and J. Waisman, McGraw-Hill, New York, 1959.

Table 6-6
Neuber's Constant
for Steels

S_{ut} (ksi)	\sqrt{a} (in ^{0.5})
50	0.130
55	0.118
60	0.108
70	0.093
80	0.080
90	0.070
100	0.062
110	0.055
120	0.049
130	0.044
140	0.039
160	0.031
180	0.024
200	0.018
220	0.013
240	0.009

Note that the Neuber constant is defined as the square root of a , not as a , so it is directly substituted in equation 6.13, while the value of r must have its square root taken. A plot of the Neuber constant \sqrt{a} for three types of materials is shown in Figure 6-35 (on p. 344), and Tables 6-6 to 6-8 show data taken from that figure. Note in Figure 6-35 that, for torsional loads on steel, the value of \sqrt{a} should be read for S_{ut} 20 kpsi higher than that of the material.

Figure 6-36, parts 1 and 2 (p. 344, 345) show sets of notch sensitivity curves for steels and aluminums (respectively) generated with equation 6.13 using the data in Figure 6-35. These curves are for notches whose depth is less than four times the root radius and should be used with caution for deeper notches.

The full value of the fatigue stress-concentration factor K_f applies only to the high end of the HCF regime ($N = 10^6 - 10^9$ cycles). Some authors [10], [30], [34] recommend applying a reduced portion of K_f , designated K_f' , to the alternating stress at $N = 10^3$ cycles. For high-strength or brittle materials K_f' is nearly equal to K_f , but for low-strength, ductile materials, K_f' approaches 1. Others [35] recommend applying the full value of K_f even at 10^3 cycles. The latter approach is more conservative since data indicate that the effects of stress concentration are less pronounced at lower N . We will adopt the conservative approach and apply K_f uniformly across the HCF range, since the uncertainties surrounding the estimates of fatigue strength and its collection of modifying factors encourage conservatism.

Table 6-7
Neuber's Constant
for Annealed Aluminum

S_{ut} (kpsi)	\sqrt{a} (in ^{0.5})
10	0.500
15	0.341
20	0.264
25	0.217
30	0.180
35	0.152
40	0.126
45	0.111

EXAMPLE 6-3

Determining Fatigue Stress-Concentration Factors

Problem A rectangular, stepped bar similar to that shown in Figure 4-36 (p. 190) is to be loaded in bending. Determine the fatigue stress-concentration factor for the given dimensions.

Given Using the nomenclature in Figure 4-36, $D = 2$, $d = 1.8$, and $r = 0.25$. The material has $S_{ut} = 100$ kpsi.

Solution

- 1 The geometric stress-concentration factor K_t is found from the equation in Figure 4-36:

$$K_t = A \left(\frac{r}{d} \right)^b \quad (a)$$

where A and b are given in the same figure as a function of the D/d ratio, which is $2 / 1.8 = 1.111$. For this ratio, $A = 1.0147$ and $b = -0.2179$, giving

$$K_t = 1.0147 \left(\frac{0.25}{1.8} \right)^{-0.2179} = 1.56 \quad (b)$$

- 2 The notch sensitivity q of the material can be found by using the Neuber factor \sqrt{a} from Figure 6-35 and Tables 6-6 to 6-8 in combination with equation 6.13 (p. 345), or by reading q directly from Figure 6-36. We will do the former. The Neuber factor from Table 6-6 for $S_{ut} = 100$ kpsi is 0.062. Note that this is the square root of a :

$$q = \frac{1}{1 + \frac{\sqrt{a}}{\sqrt{r}}} = \frac{1}{1 + \frac{0.062}{\sqrt{0.25}}} = 0.89 \quad (c)$$

3 The fatigue stress-concentration factor can now be found from equation 6.11b (p. 343):

$$K_f = 1 + q(K_t - 1) = 1 + 0.89(1.56 - 1) = 1.50 \quad (d)$$

4 The files EX06-03 are on the CD-ROM.

6.8 RESIDUAL STRESSES

Residual stress refers to stresses that are “built-in” to an unloaded part. Most parts will have some residual stresses from their manufacturing processes. Any procedure such as forming or heat treatment that creates localized strains above the yield point will leave stresses behind when the strain is removed. Good design requires that the engineer try to tailor the residual stresses to, at a minimum, not create negative effects on the strength and preferably to create positive effects.

Fatigue failure is a tensile-stress phenomenon. Figures 6-17 and 6-18 (pp. 323–324) show the beneficial effects of mean compressive stresses on fatigue strength. While the designer has little or no control over the presence or absence of a mean compressive stress in the loading pattern to which the part will be subjected, there are techniques that allow the introduction of **compressive residual stresses** in a part prior to its being placed in service. Properly done, these compressive residual stresses can make significant improvements in fatigue life. There are several methods for introducing compressive residual stresses: **thermal treatments**, **surface treatments**, and **mechanical prestressing treatments**. Most of them create biaxial compressive stresses at the surface, triaxial compressive stresses below the surface, and triaxial tensile stresses in the core.

Since the part is in equilibrium, the compressive stresses near the surface have to be balanced by tensile stresses in the core. If the treatment is overdone, the increased tensile core stresses can cause failure, so a balance must be struck. These treatments have the greatest value when the applied stress distribution due to loading is nonuniform and is maximally tensile at the surface, as in reversed bending. Bending in one direction will have peak tensile stress on one side only and the treatment can then be applied just to that side. Axial-tension loading is uniform across the section and so will not benefit from a nonuniform residual stress pattern, unless there are notches at the surface to cause local increases in tensile stress. Then compressive residual stresses at the surface are very helpful. In fact, regardless of loading, the net tensile stresses at notches will be reduced by adding residual compressive stresses in those locations. Since designed notches are usually at the surface, a treatment can be applied to them.

The deliberate introduction of residual compressive stresses is most effective on parts made of high-yield-strength materials. If the yield strength of the material is low, then the residual stresses may not stay long in the part due to later yielding from high applied stresses in service. Faires [36] found that steels with $S_y < 80$ kpsi showed initial increases but little long-term improvement in fatigue strength. But, Heywood [37] reports 50% improvement in the fatigue strength of rolled threads in high-strength steel.

Table 6-8
Neuber's Constant
for Hardened Aluminum

S_{ut} (kpsi)	\sqrt{a} (in $^{0.5}$)
15	0.475
20	0.380
30	0.278
40	0.219
50	0.186
60	0.162
70	0.144
80	0.131
90	0.122

THERMAL TREATMENTS Thermal stressing occurs whenever a part is heated and cooled as in hot-forming or in heat treatment. Several methods of heat treatment for steels were discussed in Chapter 2. They divide roughly into two categories, **through hardening** in which *the entire part is heated above the transition temperature then quenched*, and **case hardening** in which only *a relatively thin surface layer is heated above the transition temperature and quenched or the part is heated to a lower temperature in a special atmosphere that adds hardening elements to the surface*.

Through hardening causes *tensile residual stresses* in the surface. If the loading on the part creates high tensile stresses at the surface as in bending or torsion, or if notches at the surface of an axially loaded part cause high local tensile stress, then additional residual tensile stresses will worsen the situation. This makes through hardening a less desirable approach in these cases.

6

Case hardening by *carburizing, nitriding, flame, or induction hardening* creates *compressive residual stresses* in the surface because the volume increase associated with the material's phase change (or element additions) is localized near the surface and the unchanged core pulls the case into compression. This surface compressive stress can have a significant beneficial effect on fatigue life. A particle of the material doesn't know or care whether the stress it feels is caused by some external force or by an internal, residual one. It feels a reduced net stress that is now the algebraic sum of the positive (applied-alternating) tensile stress and the negative (residual-mean) compressive stress. If a fatigue-loaded part is to be heat treated, case hardening offers distinct advantages over through hardening. Figure 6-37 shows the effects of nitriding and carburizing on the residual-stress state near the surface, and shows the distribution of compressive and tensile residual stresses across the thickness of a carburized part.

SURFACE TREATMENTS The most common methods for introducing surface compressive stresses are **shot peening** and **cold forming**. Both involve a tensile yielding of the surface layer to some depth. Selective yielding of a portion of the material causes residual stresses of the opposite sign to be developed in that portion as the underlying, unstressed bulk of the material tries to force the yielded material back to its original size. The rule is, *to protect against later stresses in a particular direction, overstress the*

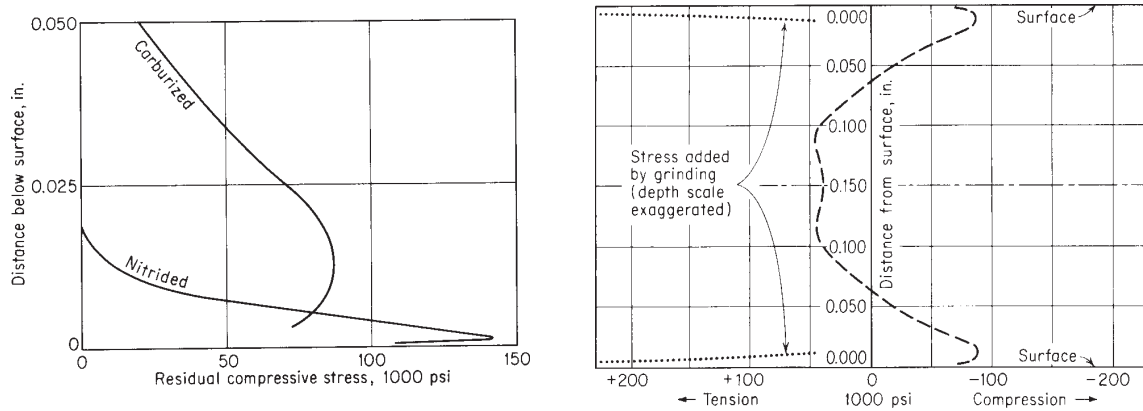


FIGURE 6-37

Distribution of Residual Stresses Due to Case Hardening (From Fig. 5.1, p. 51, and Fig. A-13, p. 202, in Almen and Black, 1963, *Residual Stresses and Fatigue in Metals*, McGraw-Hill, New York, with permission)

material (i.e., yield it) in the same direction as the applied stress will. Since we are attempting to protect against tensile stresses in fatigue loading, we want to yield the material in tension to develop compressive residual stresses. This technique of cold working the surface was known to ancient blacksmiths who hammered the surface of the sword or carriage-spring when cold as a final step to increase its strength.

Shot peening* is relatively easy to do and can be applied to parts of almost any shape. The surface of the part is impacted with a stream of shot (like buckshot) made of steel, chilled cast iron, glass, ceramic, walnut shells, or other material. The harder shot is used on steel parts and the softer shot on soft, nonferrous metals. The shot is fired at the part with high velocity either from a rotating wheel or air-blasted through a nozzle. The impacts of the shot dent the surface, yielding the material and creating a dimpled appearance. The surface is essentially stretched to a larger area, and the underlying material pulls it back into a state of compressive residual stress. There can also be some cold working of the surface material, which increases its hardness and yield strength.

Substantial levels of compressive stress can be achieved, up to about 55% of the ultimate tensile strength of the material.[†] The depth of penetration of the compressive stress can be as much as 1 mm. It is difficult to accurately determine the level of residual stress in a shot-peened part, as it must be destroyed to do so. If a slice is cut out to a depth below the peened layer, the cut will spring closed, and the amount of closure is a measure of the residual stress present. Figure 6-38 shows the distribution of residual stress resulting from the shot peening of two steels of different yield strengths. The peak compressive stress occurs just below the surface and it decays rapidly with depth.

The degree of shot peening can be measured during the treatment by including a standard Almen test strip in the shot blast. The thin test strip is held in a fixture so that only one of its sides is peened. When removed from the fixture, the strip curls up because of the compressive stresses on one side. The height of its curve is converted to an Almen number that indicates the degree of peening that the part (and it) received. If no specific data are available for the level of residual stress present after shot peening, a conservative way to account for its benefit is to set the surface factor $C_{surf} = 1$ in calculating the corrected fatigue strength with equation 6.8 (p. 337).

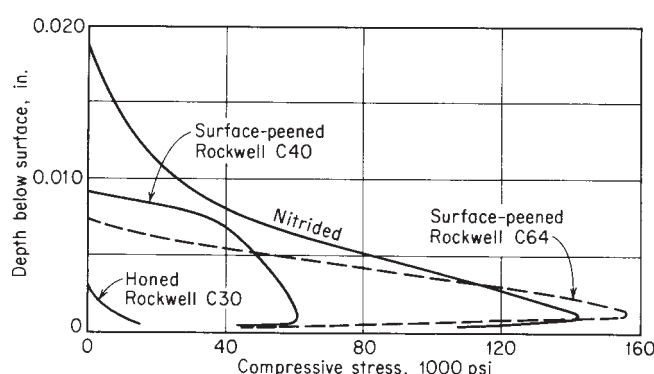


FIGURE 6-38

Distribution of Residual Stresses Due to Shot Peening (From Fig. 5.11, p. 58, in Almen and Black, 1963, *Residual Stresses and Fatigue in Metals*, McGraw-Hill, New York, with permission)

* A definitive and excellent discussion of shot peening can be found in Leghorn, G., "The Story of Shot Peening", A.S.N.E Journal, Nov. 1957, pp. 653-666, also available at: http://www.shotpeener.com/learning/story_peening.pdf. Anyone seriously interested in shot peening should read this article.

Also, the booklet "Shot Peening Applications," 8ed, by Metal Improvement Company Inc., (www.metalimprovement.com) is a valuable resource and reference on shot peening.

Another source is an online presentation at http://www.straaltechniek.net/files/straaltechniek_shot_peening_presentation.pdf

[†] American Gear Manufacturers Association Specification AGMA 938-A05

Shot peening is widely used on parts such as chain-saw blades, crankshafts, connecting rods, gears, and springs.^[38] On very large parts, **hammer peening** is sometimes done in which a hand-held air hammer is used to impact highly stressed portions of the surface (such as the roots of gear teeth) with a hardened ball. Parts of high-strength steel benefit most from peening as it can generate compressive residual stresses up to about 55% its higher S_{ut} . It is particularly beneficial on forgings and hot-rolled surfaces, which are both rough and weak from decarburization. Chrome- and nickel-plated parts can be restored to their unplated levels of fatigue strength by peening prior to plating. If peening is done before plating, not only is the negative effect of the plating blocked but the result is a higher fatigue strength than for the original unplated part, as shown in Figure 6-29 (p. 334). Properly peened helical coil springs can have their fatigue strengths increased to the point that they will fail by yielding before they will fail in fatigue.^[38] So, shot peening is obviously a useful technique for improving the fatigue life of highly stressed parts, and it does not add excessively to production costs.

6

Laser peening is a recent development that uses a pulsed laser to peen up to 1 m^2 of metal per hour. Each shock wave generated in the material by a laser pulse creates residual compressive stress 1- to 2-mm-deep over a 25-mm^2 area, deeper than some shot peening techniques and is claimed to extend fatigue life 3 to 5 times longer than conventional shot-peening techniques. Laser peening is slower and more expensive than shot peening and is sometimes used on critical areas such as the leading edges of turbine blades and the roots of gear teeth after conventional shot peening has been done to the entire part.* Unlike shot peening, laser peening does not affect the surface finish.

Cold forming can be done to surfaces of revolution such as shafts, to flat surfaces that can be passed between rollers, and to the insides of holes. For example, a hardened roller can be impressed against a shaft as it is turned in a lathe. The high forces cause local yielding under the roller that results in compressive residual stresses at the surface, which will protect it from the tensile effects of rotating-bending or reversed-torsional loading in service. Cold forming is particularly useful at fillets, grooves, or other stress-raisers.

Holes and bores can be cold formed by forcing a mandrel of slightly larger diameter through the hole to expand the inside diameter by yielding and create compressive residual stresses. This is sometimes done to gun barrels (cannon) in a process called **autofrettage**. Autofrettage is also done by filling the gun barrel with a steel mandrel that leaves a small annulus (doughnut) of space, sealing the ends, filling the annulus with gasoline,[†] and pressurizing it to over 200 000 psi. The hydrostatic pressure yields the inner surface in tension creating residual compressive stresses that protect it against fatigue failure from the cyclic tension stresses experienced when the cannon is fired.

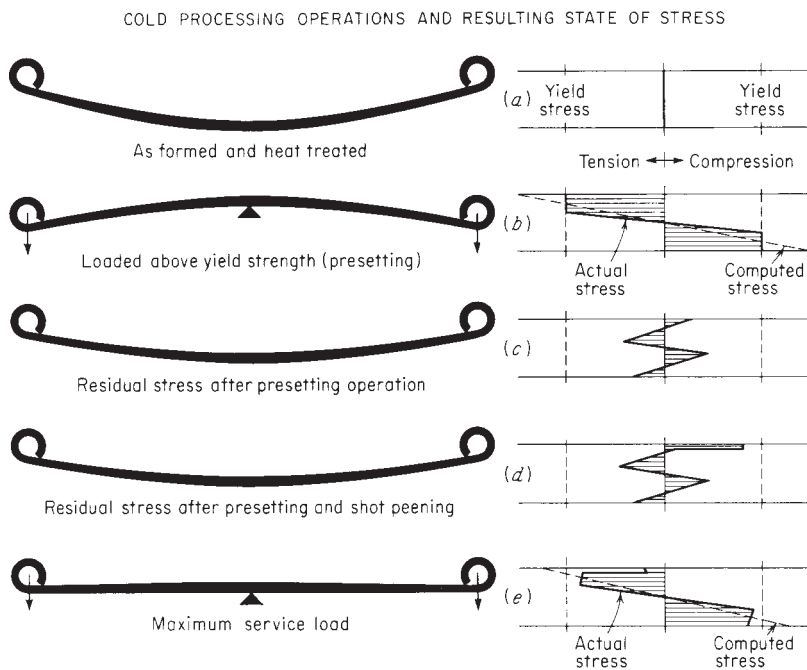
The ends of holes in any part can be **coined** by yielding their edges with a conical tool to put compressive stresses around their stress-concentration region at the surface. Reducing the dimensions of flat stock by cold rolling introduces residual compressive stress in the surface and tension in the core. Excessive rolling can cause tensile cracking by exceeding the static tensile strength at the center. The material can be annealed between successive rollings to prevent this.

MECHANICAL PRESTRESSING For parts that are dynamically loaded in service in only one direction, such as support springs for vehicles, prestressing is a useful way to create residual stresses. Prestressing refers to the deliberate overloading of the part in

* See: <http://www.llnl.gov/str/March01/Hackel301.html> and <http://www.geartechnology.com/mag/archive/rev1101.pdf> for more information.

† The ability of some liquids to transmit pressure rapidly is limited by their increase in viscosity at high pressures. Unleaded gasoline and some other liquids will withstand pressures to about 200 000 psi without serious degradation in their pressure transmissibility. Some fluids become solid at about 100 000 psi. Water will form ice-VI at about 155 000 psi and plug the tube or annulus.

Source: D. H. Newhall, Harwood Engineering Inc., Walpole, Mass., personal communication, 1994.

**FIGURE 6-39**

Residual Stresses from Prestressing and Shot Peening a Leaf Spring (From Fig. 6.2, p. 61, in Almen and Black, *Residual Stresses and Fatigue in Metals*, McGraw-Hill, New York, 1963, with permission)

the same direction as its service loading, prior to its being placed in service. The yielding that occurs during prestressing creates beneficial residual stresses.

Figure 6-39 shows an example of prestressing applied to a truck spring. The spring is initially formed with more contour than that needed at assembly. It is then placed in a fixture that loads it exactly as it will be loaded in service but at a level above its (tensile) yield strength to preset it. When the load is released, it springs back to a new shape, which is that desired for assembly. But, the elastic recovery has now placed the material that yielded into a residual-stress state, which will be in the opposite (compressive) direction from that of the applied load. Therefore this residual stress will act to protect the part against its tensile service loads. The residual stress patterns are shown in the figure and also indicate the result of shot peening the upper surface after presetting. The two treatments are additive on the upper surface in this case, affording greater protection against fluctuating tensile stresses in service. Note that if the part were reverse-loaded in service to the point of yielding the upper surface in compression, it would relieve the beneficial compressive stress and compromise the part's life. Thus, this approach is most useful for parts whose service stresses are unidirectional.

SUMMARY Residual tensile stresses can be the “fatigue designer’s best friend.” Properly configured, beneficial residual stresses can make an otherwise unworkable design safe. The designer should become thoroughly familiar with the means available for their creation. This brief description is intended to serve only as an introduction to a complicated topic and the reader is urged to consult the literature on residual stresses, some of which is noted in the bibliography of this chapter.

If quantitative data on the levels of residual stresses developed in a particular part can be obtained (usually by destructive testing) then these data can be used in the determination of safe applied-stress levels. Absent such quantitative information the designer is limited to considering the use of these treatments as providing some additional safety factor that is poorly quantified but is in the right direction.

6.9 DESIGNING FOR HIGH-CYCLE FATIGUE

We are now ready to consider how to apply all the information presented on fatigue failure *in order to avoid it* in the design of dynamically loaded parts. There are four basic categories that can be treated separately, although three of them are just special cases of the fourth, general case. As we will see, the same general approach to the solution of all four categories is both possible and desirable. However, it may aid in understanding their solutions if we deal with them separately before presenting the general solution method.

Figure 6-40 shows the four categories in a matrix. The columns define the presence or absence of a mean stress. The fully reversed case has a zero mean stress and the fluctuating-stress case has a nonzero mean value. Both have alternating components. The rows define the presence of applied-stress components on only one, or more than one axis. The uniaxial case represents simple loading cases such as pure axial loading or pure bending. The multiaxial case is general and allows applied normal-stress components on all axes in combination with applied shear stresses on any face of the stress cube. In reality, the pure loading cases are rare in practice. More often there will be some combination of multiaxial stresses on machine parts. Both the fully reversed and fluctuating stress cases are commonly encountered in practice, however.

We will first consider the simplest category (I), fully reversed uniaxial stresses. Many texts will further subdivide this category into bending loading, axial loading, and torsional loading and present separate approaches to each. We will combine them all into one category by calculating the von Mises effective stress and comparing it with the corrected bending-fatigue strength of the chosen material. This eliminates the need to consider pure torsion as a special case.

We will next consider fluctuating uniaxial stresses (Category II). This adds the complication of mean stresses, and we will employ the modified-Goodman diagram in addition to the (simpler) $S-N$ diagram. We will use the von Mises effective stress to convert pure torsional loading into an equivalent form of tensile stress.

Finally we will investigate the general categories of multiaxial stresses in both fully reversed (III) and fluctuating (IV) load cases and present a recommended “universal approach” that will work in all categories for most common loading situations. The hope is that this approach will simplify a complicated topic and provide the student with one method that can be used for HCF design in a majority of situations.

6.10 DESIGNING FOR FULLY REVERSED UNIAXIAL STRESSES

The simplest example of fatigue loading is that of category I, fully reversed uniaxial stress with a mean stress of zero (see Figure 6-6a, p. 313). Some common applications

	Fully reversed stresses ($\sigma_m = 0$)	Fluctuating stresses ($\sigma_m \neq 0$)
Uniaxial stresses	Category I	Category II
Multiaxial stresses	Category III	Category IV

FIGURE 6-40

Four Categories of Fatigue Design Situations

of this category are rotating bending of a shaft that supports a static load, or reversed torque on a shaft with large, oscillating inertia loads and a mean torque that is effectively zero compared to those oscillations. The process can be described in a set of general steps:

6

Design Steps for Fully Reversed Stresses with Uniaxial Loading:

- 1 Determine the number of cycles of loading N that the part will experience over its expected service life.
- 2 Determine the amplitude of the applied alternating loads from zero to peak (Eq. 6.1, p. 314). Note that a static load on a rotating shaft causes alternating stresses.
- 3 Create a tentative part-geometry design to withstand the applied loads based on good engineering practice. (See Chapters 3 and 4.)
- 4 Determine any appropriate geometric stress-concentration factors K_t (or K_{ts} for shear) at notches in your part's geometry. Try, of course, to minimize these through good design. (See Section 4.15 on p. 186.)
- 5 Choose a tentative material for the part and determine its properties of interest such as S_{ut} , S_y , $S_{e'}$ (or S_f' at the life required), and q , from your own test data, from the literature, or from estimates as described in this chapter.
- 6 Convert the geometric stress-concentration factors K_t (or K_{ts} for shear) to fatigue-concentration factors K_f using the material's notch sensitivity, q .
- 7 Calculate the nominal, alternating stress amplitudes σ_a (or τ_a if the load is pure shear) at critical locations in the part due to the alternating service loads based on standard stress-analysis techniques (Chapter 4) and increase them as necessary with the appropriate fatigue stress-concentration factors (Section 4.15 on p. 186 and Section 6.7 on p. 342).
- 8 Calculate the principal-stress amplitudes for the critical locations based on their states of applied stress (Chapter 4). Note that these contain the effects of stress concentrations. Calculate the von Mises effective stress for each location of interest.
- 9 Determine appropriate fatigue strength modification factors for the type of loading, size of part, surface, etc., as described in Section 6.6. Note that the loading factor C_{load} will differ based on whether there are axial or bending loads (Eq. 6.7a, p. 330). If the loading is pure torsion, then the von Mises effective-stress calculation will convert it to a pseudo-tensile stress and C_{load} should then be set to 1.

- 6
- 10 Define the corrected fatigue strength S_f at the requisite cycle life N (or the corrected endurance limit S_e for infinite life if appropriate) and a “static” strength $S_m @ N = 10^3$ cycles from equation 6.9 (p. 337). Create an S - N diagram as shown in Figure 6-33 (p. 337), and/or write equation 6.10 (p. 338) for this tentative material choice.
 - 11 Compare the alternating von Mises effective stress at the most highly stressed location with the material’s corrected fatigue strength S_n taken from the S - N curve at the desired number of life cycles N . (Note that for infinite-life situations in which the material has an S - N knee, $S_n = S_e$.)
 - 12 Calculate a safety factor for the design from the relationship,

$$N_f = \frac{S_n}{\sigma'} \quad (6.14)$$

where N_f is the safety factor in fatigue, S_n is the corrected fatigue strength at the required number of cycles of life taken from the S - N curve or equation 6.10 (p. 338), and σ' is the largest von Mises alternating stress at any location in the part, calculated to include all stress concentration effects.

- 13 Given the fact that the material was only tentatively chosen and that the design may not yet be as refined as possible, the result of the first pass through these steps will most likely be a failed design whose safety factor is either too large or too small. Iteration will be required (as it always is) to refine the design. Any subset of steps can be repeated as many times as necessary to obtain an acceptable design. The most common tactic is to return to step 3 and improve the geometry of the part to reduce stresses and stress concentrations and/or revisit step 5 to choose a more suitable material. Sometimes it will be possible to return to step 1 and redefine a shorter acceptable part life.

The design loads in step 2 may or may not be in the control of the designer. Usually they are not, unless the loading on the part is due to inertial forces; then increasing its mass to “add strength” will worsen the situation, as this will proportionately increase the loads (see Section 3.6 on p. 98). Instead, the designer may want to lighten the part without excessively compromising its strength to reduce the forces. Whatever the particular circumstances, the designer must expect to cycle through these steps several times before converging on a usable solution. Equation solvers that allow rapid recalculation of the equations are a great help in this situation.

The best way to demonstrate the use of these steps for fatigue design is with an example.

EXAMPLE 6-4

Design of a Cantilever Bracket for Fully Reversed Bending

Problem

A feed-roll assembly is to be mounted at each end on support brackets cantilevered from the machine frame as shown in Figure 6-41. The feed rolls experience a fully reversed load of 1 000-lb amplitude, split equally between the two support brackets. Design a cantilever bracket to support a fully reversed bending load of 500-lb amplitude for 10^9 cycles with no failure. Its dynamic deflection cannot exceed 0.01 in.

Given

The load-time function shape is shown in Figure 6-41a. The operating environment is room air at a maximum temperature of 120°F. The space available allows a maximum cantilever length of 6 in. Only ten of these parts are required.

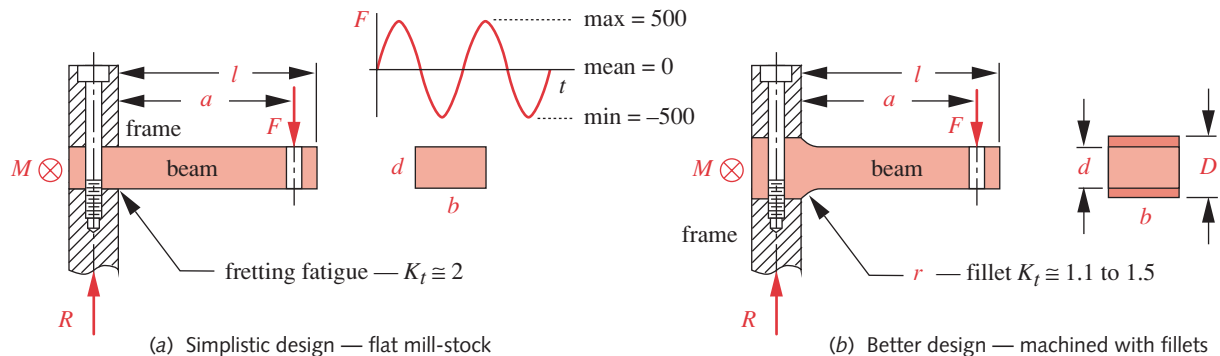


FIGURE 6-41

Design of a Cantilever Bracket for Fully Reversed Bending Loading

6

Assumptions

The bracket can be clamped between essentially rigid plates or bolted at its root. The normal load will be applied at the effective tip of the cantilever beam from a rod attached through a small hole in the beam. Since the bending moment is effectively zero at the beam tip, the stress concentration from this hole can be ignored. Given the small quantity required, machining of stock mill-shapes is the preferred manufacturing method.

Solution

See Figure 6-41 and Tables 6-9 and 6-10 (pp. 358, 359).

- 1 This is a typical design problem. Very little data are given except for the required performance of the device, some limitations on size, and the required cycle life. We will have to make some basic assumptions about part geometry, materials, and other factors as we go. Some iteration should be expected.
- 2 The first two steps of the process suggested above, finding the load amplitude and the number of cycles, are defined in the problem statement. We will begin at the third step, creating a tentative part-geometry design.
- 3 Figure 6-41a shows a tentative design configuration. A rectangular cross section is chosen to provide ease of mounting and clamping. A piece of cold-rolled bar stock from the mill could simply be cut to length and drilled to provide the needed holes, then clamped into the frame structure. This approach appears attractive in its simplicity because very little machining is required. The mill-finish on the sides could be adequate for this application. This design has some disadvantages, however. The mill tolerances on the thickness are not tight enough to give the required accuracy on thickness, so the top and bottom would have to be machined or ground flat to dimension. Also, the sharp corners at the frame where it is clamped provide stress concentrations of about $K_t = 2$ and also create a condition called **fretting fatigue** due to the slight motions that will occur between the two parts as the bracket deflects. This motion continuously breaks down the protective oxide coating, exposing new metal to oxidation and speeding up the fatigue-failure process. The fretting could be a problem even if the edges of the frame pieces were radiused.
- 4 Figure 6-41b shows a better design in which the mill stock is purchased thicker than the desired final dimension and machined top and bottom to dimension D , then machined to thickness d over the length l . A fillet radius r is provided at the clamp point to reduce fretting fatigue and achieve a lower K_t . Figure 4-36 (p. 190) shows

that with suitable control of the r/d and D/d ratios for a stepped flat bar in bending, the geometric stress-concentration factor K_t can be kept under about 1.5.

- 5 Some trial dimensions must be assumed for b , d , D , r , a , and l . We will assume (guess) values of $b = 1$ in, $d = 0.75$ in, $D = 0.94$ in, $r = 0.25$, $a = 5.0$, and $l = 6.0$ in to the applied load for our first calculation. This length will leave some material around the hole and still fit within the 6-in-length constraint.
- 6 A material must also be chosen. For infinite life, low cost, and ease of fabrication, it is desirable to use a carbon steel if possible and if environmental conditions permit. Since this is used in a controlled, indoor environment, carbon steel is acceptable on the latter point. The fact that the deflection is of concern is also a good reason to choose a material with a large E . Low- to medium-carbon, ductile steels have the requisite endurance-limit knee for the infinite life required in this case and also have low notch sensitivities. An SAE 1040 normalized steel with $S_{ut} = 80\,000$ psi is selected for the first trial.
- 7 The reaction force and reaction moment at the support are found using equations h from Example 4-5. Next the area moment of inertia of the cross section, the distance to the outer fiber, and the nominal alternating bending stress at the root are found using the alternating load's 500-lb amplitude.

$$R = F = 500 \text{ lb} \quad (a)$$

$$M = Rl - F(l - a) = 500(6) - 500(6 - 5) = 2\,500 \text{ lb-in}$$

$$I = \frac{bd^3}{12} = \frac{1(0.75)^3}{12} = 0.0352 \text{ in}^4 \quad (b)$$

$$c = \frac{d}{2} = \frac{0.75}{2} = 0.375 \text{ in}$$

$$\sigma_{a_{nom}} = \frac{Mc}{I} = \frac{2\,500(0.375)}{0.0352} = 26\,667 \text{ psi} \quad (c)$$

- 8 Two ratios must be calculated for use in Figure 4-36 (p. 190) in order to find the geometric stress-concentration factor K_t for the assumed part dimensions.

$$\frac{D}{d} = \frac{0.938}{0.75} = 1.25 \quad \frac{r}{d} = \frac{0.25}{0.75} = 0.333 \quad (d)$$

$$\text{interpolating} \quad A = 0.9658 \quad b = -0.266 \quad (e)$$

$$K_t = A \left(\frac{r}{d} \right)^b = 0.9658 (0.333)^{-0.266} = 1.29 \quad (f)$$

- 9 The notch sensitivity q of the chosen material is calculated based on its ultimate strength and the notch radius using equation 6.13 (p. 344) and the data for Neuber's constant from Table 6-6 (p. 346).

$$\text{From the Table for } S_{ut} = 80 \text{ kpsi :} \quad \sqrt{a} = 0.08 \quad (g)$$

$$q = \frac{1}{1 + \frac{\sqrt{a}}{\sqrt{r}}} = \frac{1}{1 + \frac{0.08}{\sqrt{0.25}}} = 0.862 \quad (h)$$

- 10 The values of q and K_t are used to find the fatigue stress-concentration factor K_f , which is in turn used to find the local alternating stress σ_a in the notch. Because we have the simplest case of a uniaxial tensile stress, the largest alternating principal stress σ_{1a} for this case is equal to the alternating tensile stress, as is the von Mises alternating stress σ'_a . See equations 4.6 (p. 145) and 5.7c (p. 249).

$$K_f = 1 + q(K_t - 1) = 1 + 0.862(1.29 - 1) = 1.25 \quad (i)$$

$$\sigma_a = K_f \sigma_{a_{nom}} = 1.25(26\,667) = 33\,343 \text{ psi} \quad (j)$$

$$\tau_{ab} = \pm \sqrt{\left(\frac{\sigma_x - \sigma_y}{2}\right)^2 + \tau_{xy}^2} = \sqrt{\left(\frac{33\,343 - 0}{2}\right)^2 + 0} = 16\,672 \text{ psi}$$

$$\sigma_{1a}, \sigma_{3a} = \frac{\sigma_x + \sigma_y}{2} \pm \tau_{ab} = 33\,343 \text{ psi, } 0 \text{ psi} \quad (k)$$

$$\sigma' = \sqrt{\sigma_1^2 - \sigma_1 \sigma_2 + \sigma_2^2} = \sqrt{33\,343^2 - 33\,343(0) + 0} = 33\,343 \text{ psi}$$

- 11 The uncorrected endurance limit $S_{e'}$ is found from equation 6.5a (p. 330). The size factor for this rectangular part is determined by calculating the cross-sectional area stressed above 95% of its maximum stress (see Figure 6-25c, p. 332) and using that value in equation 6.7d (p. 331) to find an equivalent diameter test specimen for use in equation 6.7b (p. 331) to find C_{size} .

$$S_{e'} = 0.5S_{ut} = 0.5(80\,000) = 40\,000 \text{ psi} \quad (l)$$

$$A_{95} = 0.05db = 0.05(0.75)(1) = 0.04 \text{ in}^2$$

$$d_{equiv} = \sqrt{\frac{A_{95}}{0.0766}} = 0.700 \text{ in} \quad (m)$$

$$C_{size} = 0.869(d_{equiv})^{-0.097} = 0.900$$

- 12 Calculation of the corrected endurance limit S_e requires that several factors be computed. C_{load} is found from equation 6.7a (p. 330). C_{surf} for a machined finish is found from equation 6.7e (p. 333). C_{temp} is found from equation 6.7f (p. 335) and C_{reliab} is chosen from Table 6-4 (p. 335) for a 99.9% reliability level.

$$C_{load} = 1 : \quad \text{for bending}$$

$$C_{surf} = A(S_{ut \text{ kpsi}})^b = 2.7(80)^{-0.265} = 0.845 : \quad \text{machined} \quad (n)$$

$$C_{temp} = 1 : \quad \text{room temperature}$$

$$C_{reliab} = 0.753 : \quad \text{for 99.9% reliab.}$$

The corrected endurance limit is found from equation 6.6 (p. 330).

$$\begin{aligned} S_e &= C_{load} C_{size} C_{surf} C_{temp} C_{reliab} S_{e'} \\ &= 1(0.900)(0.845)(1)(0.753)40\,000 = 22\,907 \text{ psi} \end{aligned} \quad (o)$$

Note that the corrected S_e is only about 29% of S_{ut} .

- 13 The safety factor is calculated using equation 6.14 (p. 354) and the beam deflection y is computed using equation (j) from Example 4-5 (p. 168).

Table 6-9 Example 6-4 - Design of a Cantilever Bracket for Reversed Bending
 First Iteration: An Unsuccessful Design (File EX06-04A)

Input	Variable	Output	Unit	Comments
500	<i>F</i>		lb	applied load amplitude at point <i>a</i>
1	<i>b</i>		in	beam width
0.75	<i>d</i>		in	beam depth over length
0.94	<i>D</i>		in	beam depth in wall
0.25	<i>r</i>		in	fillet radius
6	<i>l</i>		in	beam length
5	<i>a</i>		in	distance to load <i>F</i>
6	<i>lx</i>		in	distance for deflection calculation
3E7	<i>E</i>		psi	modulus of elasticity
80 000	<i>Sut</i>		psi	ultimate tensile strength
1	<i>Cload</i>			load factor for bending
	<i>Csurf</i>	0.85		machined finish
1	<i>Ctemp</i>			room temperature
0.753	<i>Creliab</i>			99.9% reliability factor
	<i>R</i>	500	lb	reaction force at support
	<i>M</i>	2 500	in-lb	reaction moment at support
	<i>I</i>	0.035 2	in^4	area moment of inertia
	<i>c</i>	0.38	in	dist to outer fiber
	<i>signom</i>	26 667	psi	bending stress at root
	<i>Doverd</i>	1.25		bar width ratio $1.01 < D/d < 2$
	<i>roverd</i>	0.33		ratio radius to small dimension
	<i>Kt</i>	1.29		geometric stress-concentration factor
	<i>q</i>	0.86		Peterson's notch-sensitivity factor
	<i>Kf</i>	1.25		fatigue stress-concentration factor
	<i>sigx</i>	33 343	psi	concentrated stress at root
	<i>sigI</i>	33 343	psi	largest principal alternating stress
	<i>sigvm</i>	33 343	psi	von Mises alternating stress
	<i>Seprime</i>	40 000	psi	uncorrected endurance limit
	<i>A95</i>	0.04	in^2	95% stress area
	<i>dequiv</i>	0.7	in	equivalent-diameter test specimen
	<i>Csize</i>	0.9		size factor based on 95% area
	<i>Se</i>	22 907	psi	corrected endurance limit
	<i>Nsf</i>	0.69		predicted safety factor
	<i>y</i>	-0.026	in	deflection at end of beam

Table 6-10 Example 6-4 – Design of a Cantilever Bracket for Reversed Bending

Final Iteration: A Successful Design (File EX06-04B)

Input	Variable	Output	Unit	Comments
500	<i>F</i>		lb	applied load amplitude at point <i>a</i>
2	<i>b</i>		in	beam width
1	<i>d</i>		in	beam depth over length
1.125	<i>D</i>		in	beam depth in wall
0.5	<i>r</i>		in	fillet radius
6	<i>l</i>		in	beam length
5	<i>a</i>		in	distance to load <i>F</i>
6	<i>lx</i>		in	distance for deflection calculation
3E7	<i>E</i>		psi	modulus of elasticity
80 000	<i>Sut</i>		psi	ultimate tensile strength
1	<i>Cload</i>			load factor for bending
	<i>Csurf</i>	0.85		machined finish
1	<i>Ctemp</i>			room temperature
0.753	<i>Creliab</i>			99.9% reliability factor
	<i>R</i>	500	lb	reaction force at support
	<i>M</i>	2 500	in-lb	reaction moment at support
	<i>I</i>	0.166 7	in^4	area moment of inertia
	<i>c</i>	0.5	in	dist to outer fiber
	<i>signom</i>	7 500	psi	bending stress at root
	<i>Doverd</i>	1.13		bar width ratio $1.01 < D/d < 2$
	<i>roverd</i>	0.50		ratio radius to small dimension
	<i>Kt</i>	1.18		geometric stress-concentration factor
	<i>q</i>	0.90		Peterson's notch-sensitivity factor
	<i>Kf</i>	1.16		fatigue stress-concentration factor
	<i>sigx</i>	8 688	psi	concentrated stress at root
	<i>sig1</i>	8 688	psi	largest principal alternating stress
	<i>sigym</i>	8 688	psi	von Mises alternating stress
	<i>Seprime</i>	40 000	psi	uncorrected endurance limit
	<i>A95</i>	0.10	in^2	95% stress area
	<i>dequiv</i>	1.14	in	equivalent-diameter test specimen
	<i>Csize</i>	0.86		size factor based on 95% area
	<i>Se</i>	21 843	psi	corrected endurance limit
	<i>Nsf</i>	2.5		predicted safety factor
	<i>y</i>	-0.005	in	deflection at end of beam

$$N_f = \frac{S_n}{\sigma} = \frac{22\ 907}{33\ 343} = 0.69 \quad (p)$$

$$y = \frac{F}{6EI} [x^3 - 3ax^2 - (x-a)^3] \quad (q)$$

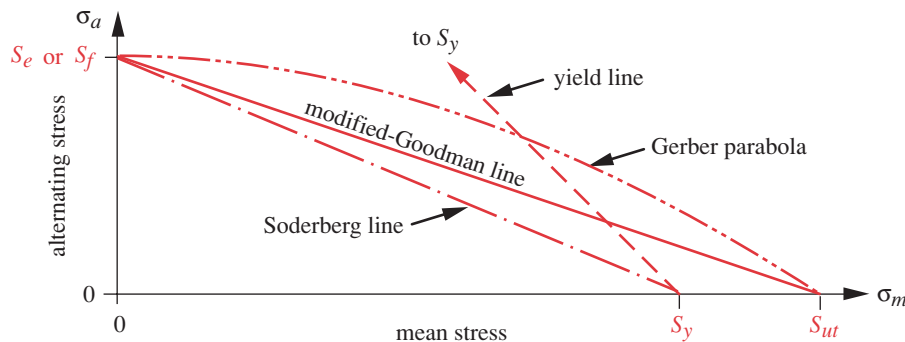
$$y_{@x=l} = \frac{500}{6(3E7)(0.0352)} [6^3 - 3(5)(6)^2 - (6-5)^3] = -0.026 \text{ in}$$

- 6**
- 14 The results of all these computations for the first assumed design are seen in Table 6-9 (p. 358). The deflection of 0.026 in is not within the stated specification, and the design fails with a safety factor of less than one. So, more iterations are needed, as was expected. Any of the dimensions can be changed, as can the material. The material was left unchanged but the beam cross-sectional dimensions and the notch radius were increased and the model rerun (this took only a few minutes) until the results shown in Table 6-10 (p. 359) were achieved.
 - 15 The final dimensions are $b = 2$ in, $d = 1$ in, $D = 1.125$ in, $r = 0.5$, $a = 5.0$, and $l = 6.0$ in. The safety factor is now 2.5 and the maximum deflection is 0.005 in. These are both satisfactory. Note how low the fatigue stress-concentration factor is at $K_f = 1.16$. The dimension D was deliberately chosen to be slightly less than a stock mill size so that material would be available for the cleanup and truing of the mounting surfaces. Also, with this design, hot-rolled steel (HRS) could be used, rather than the cold-rolled steel (CRS) initially assumed (Figure 6-41a, p. 355). Hot-rolled steel is less expensive than CRS and, if normalized, has less residual stress, but its rough, decarburized surface needs to be removed by machining all over, or to be treated with shot peening to strengthen it.
 - 16 The files EX06-04 are on the CD-ROM.

The above example should demonstrate that designing for fully reversed HCF loading is straightforward, once the principles are understood. If the design called for fully reversed-torsional, -rotating-bending, or -axial loading, the design procedure would be the same as in this example. The only differences would be in the choices of stress equations and strength modification factors as described in the previous sections. Note that calculation of the principal and von Mises stresses is somewhat redundant in this simple example, since they are both identical to the applied stress. However it is done for the sake of consistency, since these stresses will not be identical in more complicated applied stress situations. The value of using a computer and equation solver in this or any design problem cannot be overstated, as it allows rapid iteration from initial guesses to final dimensions with minimum effort.

6.11 DESIGNING FOR FLUCTUATING UNIAXIAL STRESSES

Repeating or fluctuating stresses as shown in Figure 6-6b and c (p. 313), have nonzero mean components and these must be taken into account when determining the safety factor. Figures 6-16 (p. 322), 6-17 (p. 323), 6-18 (p. 324), and 6-21 (p. 327) all show experimental evidence of the effect of mean-stress components on failure when present in combination with alternating stresses. This situation is quite common in machinery of all types.

**FIGURE 6-42**

Various Failure Lines for Fluctuating Stresses

6

Figure 6-42 shows the **modified-Goodman line**, **Gerber parabola**, **Soderberg line**, and the **yield line** plotted on σ_m - σ_a axes. The Gerber parabola best fits the experimental failure data and the modified-Goodman line fits beneath the scatter in the data as shown in Figure 6-16, which superimposes these lines on the experimental failure points. Both of these lines intersect the corrected endurance limit S_e or fatigue strength S_f on the σ_a axis with S_{ut} on the σ_m axis. A yield line connecting S_y on both axes is also shown to serve as a limit on the first cycle of stress. (If the part yields, it has failed, regardless of its safety in fatigue.) The Soderberg line connects S_e or S_f to the yield strength S_y and is thus a more conservative failure criterion, but it does eliminate the need to invoke the yield line. It also eliminates otherwise safe σ_m - σ_a combinations, as can be seen in Figure 6-16 (p. 322). Whichever lines are chosen to represent failure, safe combinations of σ_m and σ_a lie to the left and below their envelope. These failure lines are defined by

$$\text{Gerber parabola : } \sigma_a = S_e \left(1 - \frac{\sigma_m^2}{S_{ut}^2} \right) \quad (6.15a)$$

$$\text{Modified - Goodman line : } \sigma_a = S_e \left(1 - \frac{\sigma_m}{S_{ut}} \right) \quad (6.15b)$$

$$\text{Soderberg line : } \sigma_a = S_e \left(1 - \frac{\sigma_m}{S_y} \right) \quad (6.15c)$$

While the Gerber parabola is a good fit to experimental data, making it useful for the analysis of failed parts, the modified-Goodman line is a more conservative and commonly used failure criterion when designing parts subjected to mean plus alternating stresses. The Soderberg line is less often used, as it is overly conservative. We will now explore the use of the modified-Goodman line in more detail.

Creating the Modified-Goodman Diagram

Figure 6-43a shows a schematic plot of the three-dimensional surface formed by the alternating stress component σ_a , the mean stress component σ_m and the number of cycles N for a material possessing an endurance-limit knee at 10^6 cycles. If we look in at the σ_a - N plane as shown in Figure 6-43b, we see projections of lines on the surface that are S - N

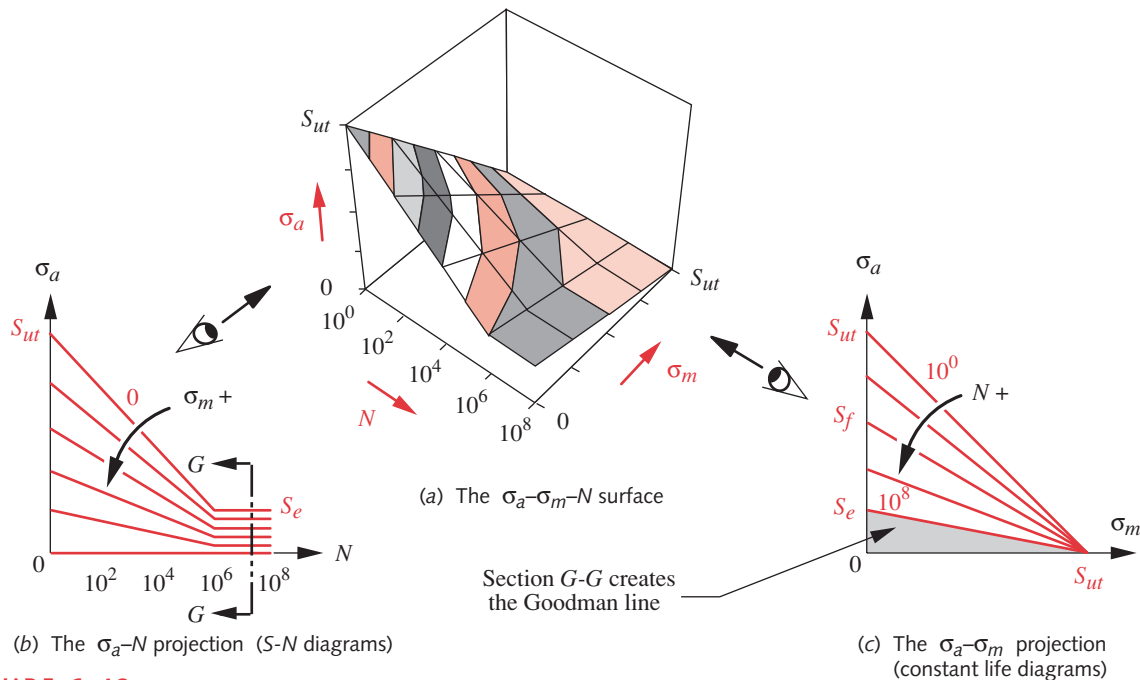


FIGURE 6-43

Effect of a Combination of Mean and Alternating Stresses

diagrams for various levels of mean stress. When $\sigma_m = 0$, the S-N diagram is the topmost line, connecting S_{ut} to S_e , as also shown in Figures 6-2 (p. 305) and 6-8 (p. 317). As σ_m increases, the σ_a intercept at $N = 1$ cycle reduces, becoming zero when $\sigma_m = S_{ut}$.

Figure 6-43c shows projections on the $\sigma_a-\sigma_m$ plane for various values of N . This is called a **constant-life diagram**, as each line on it shows the relationship between mean and alternating stress at a particular cycle life. When $N = 1$, the plot is a 45° line connecting S_{ut} on both axes. This is a static failure line. The σ_a -intercept decreases as N increases, becoming equal to the endurance limit S_e beyond about 10^6 cycles. The line connecting S_e on the σ_a axis and S_{ut} on the σ_m axis in Figure 6-43c is the **modified-
Goodman line**, taken at section G-G as shown in Figure 6-43a.

Figure 6-44 shows a plot of alternating stress σ_a versus mean stress σ_m , which we refer to as an “augmented” **modified-Goodman diagram**.^{*} This is an embellishment of the modified-Goodman line shown in Figures 6-16 (p. 322) and 6-42. The yield lines and the compressive-stress region are included. Various failure points are noted. On the mean stress (σ_m) axis, the yield strength S_y and the ultimate tensile strength S_{ut} of the particular material are defined at points A, E, and F. On the alternating stress (σ_a) axis, the corrected fatigue strength S_f at some number of cycles (or the corrected endurance limit S_e) and the yield strength S_y of the particular material are defined at points C and G. Note that this diagram usually represents a section such as G-G from the three-dimensional surface in Figure 6-43. That is, the modified-Goodman diagram is usually drawn for the infinite-life or very high-cycle case ($N > 10^6$). But, it can be drawn for any section along the N axis in Figure 6-43, representing a shorter finite-life situation.

* Goodman's original diagram plotted the relationship between mean and alternating stresses on a different set of axes than shown here and included an assumption that the fatigue limit was $1/3 S_{ut}$. Goodman's original approach is now seldom used. J. O. Smith^[46] suggested the representation of the Goodman line shown in Figure 6-42, which has become known as the modified-Goodman diagram. Smith's version did not show the yield line or the compressive region as depicted in Figure 6-44—thus the use of the term “augmented” here to note the addition of that information to the diagram. We will nevertheless refer to it as the modified-Goodman diagram or just MGD for simplicity. Also, references here to the “Goodman line” should be understood as shorthand for “modified-Goodman line,” and not as a reference to Goodman's original representation.

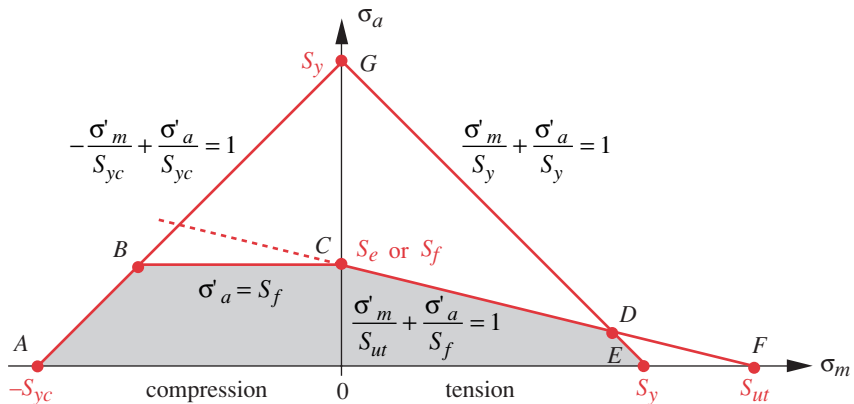


FIGURE 6-44

An "Augmented" Modified-Goodman Diagram

6

Lines defining failure can be drawn connecting various points on the diagram. The line CF is the Goodman line and can be extended into the compressive region (shown dotted) based on empirical data such as those shown in Figure 6-17 (p. 323). However, it is conventional to draw the more conservative horizontal line CB to represent a failure line in the compressive region. This in effect ignores the beneficial effects of compressive mean stress and considers that situation to be identical to the fully reversed case of the previous section.[†]

In the tensile region, the line GE defines static yielding and the failure envelope is defined as the lines CD and DE to account for the possibility of either fatigue or yield failure. If the mean component of stress were very large, and the alternating component very small, their combination could define a point in the region DEF that would be safely within the Goodman line but would yield on the first cycle. The failure envelope is defined by the lines surrounding the shaded area labeled $ABCDEA$. Any combination of alternating and mean stress that falls within that envelope (i.e., within the shaded area) will be safe. Combinations landing on those lines are at failure and if outside the envelope will have failed.

In order to determine the safety factor of any fluctuating-stress state, we will need expressions for the lines that form the failure envelope shown in Figure 6-44. The line AG defines yielding in compression and is

$$-\frac{\sigma'_m}{S_{yc}} + \frac{\sigma'_a}{S_{yc}} = 1 \quad (6.16a)$$

Line BC defines fatigue failure in combination with compressive mean stress and is

$$\sigma'_a = S_f \quad (6.16b)$$

Line CF defines fatigue failure in combination with tensile mean stress and is:

$$\frac{\sigma'_m}{S_{ut}} + \frac{\sigma'_a}{S_f} = 1 \quad (6.16c)$$

[†] A loading situation in which the mean stress σ_m is negative should be handled by assuming $\sigma_m = 0$, thus making it a fully reversed stress case solvable by the methods of Section 6.10. This is the preferred approach, because including a negative mean stress in the calculation of an effective von Mises stress will result in an overly conservative safety factor due to the squaring of the negative mean stress value in its computation. Assuming a negative mean stress to be zero is still conservative, since doing so ignores its potentially beneficial effects shown in Figure 6-17 (p. 323).

Line GE defines yielding in tension and is

$$\frac{\sigma'_m}{S_y} + \frac{\sigma'_a}{S_y} = 1 \quad (6.16d)$$

These equations are shown on Figure 6-44.

Applying Stress-Concentration Effects with Fluctuating Stresses

The alternating component of stress is treated the same way as it was for the case of fully reversed stress (see Example 6-3). That is, the geometric stress-concentration factor K_t is found, the material's notch sensitivity q is determined, and these are used in equation 6.11b (p. 343) to find a fatigue stress-concentration factor K_f . The local value of σ_a is then found from equation 6.12 (p. 343) for use in the modified-Goodman diagram.

6

The mean component of stress σ_m is treated differently depending on the ductility or brittleness of the material and, if ductile, on the amount of yielding possible at the notch. If the material is brittle, then the full value of the geometric stress concentration K_t is usually applied to the nominal mean stress $\sigma_{m,nom}$ to obtain the local mean stress σ_m at the notch using equation 4.31 (p. 187). If the material is ductile, Dowling [40] suggests one of three approaches based on Juvinal [41] depending on the relationship of the maximum local stresses to the yield strength of the ductile material.

A mean stress fatigue-concentration factor K_{fm} is defined based on the level of local mean stress σ_m at the stress concentration versus the yield strength. Figure 6-45a shows a generalized fluctuating-stress situation. Figure 6-45b depicts localized yielding that may occur around a stress concentration. For this analysis an *elastic-perfectly plastic* stress-strain relationship is assumed as shown in part (c). Three possibilities exist based on the relationship between σ_{max} and the material's yield strength S_y . If $\sigma_{max} < S_y$, no yielding occurs (see Figure 6-45d) and the full value of K_f is used for K_{fm} .

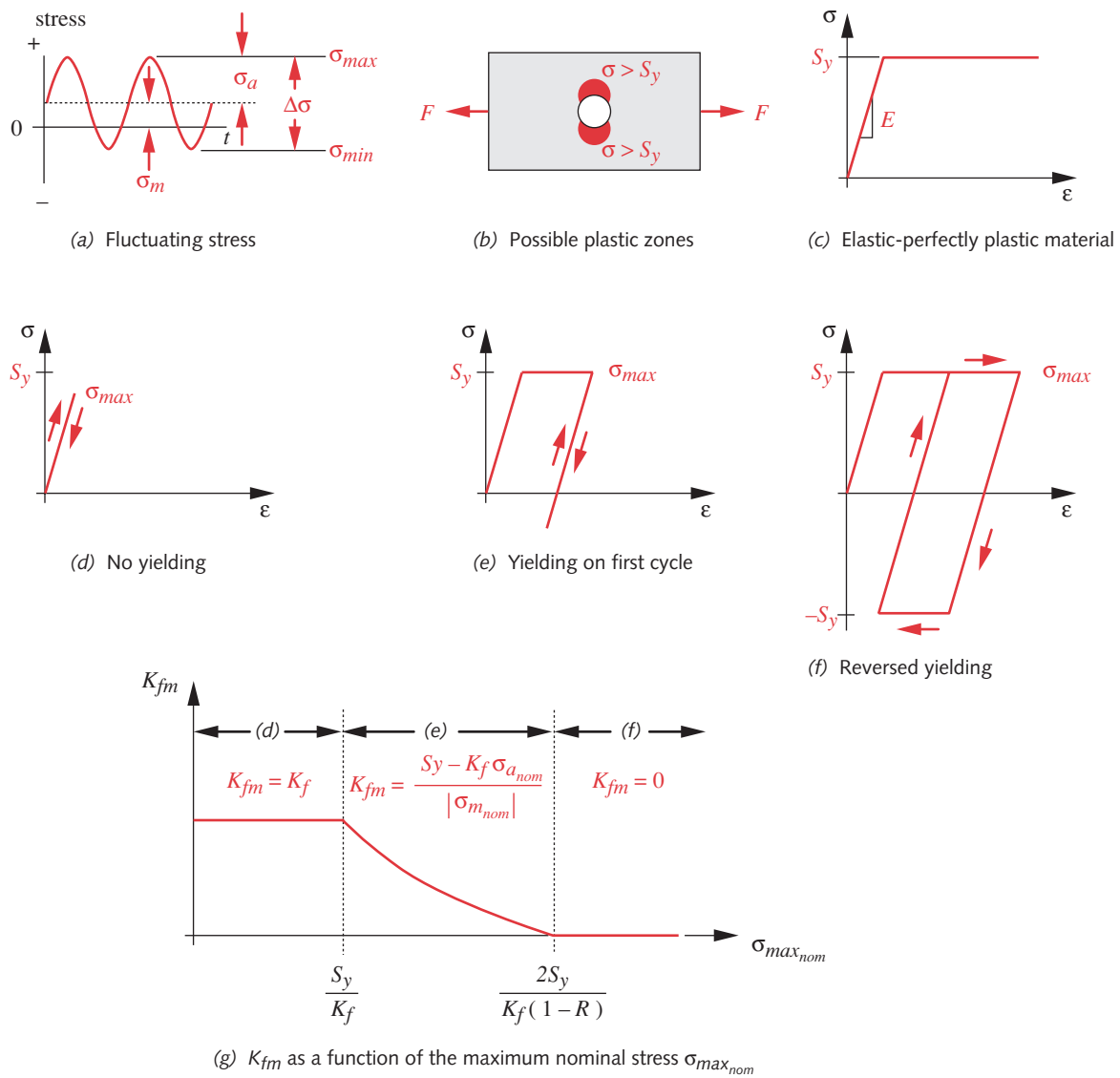
If $\sigma_{max} > S_y$ but $|\sigma_{min}| < S_y$, local yielding occurs on the first cycle (Figure 6-45e), after which the maximum stress cannot exceed S_y . The local stress at the concentration is relieved and a lower value of K_{fm} can be used as defined in Figure 6-45g, which plots the relationship between K_{fm} and σ_{max} .

The third possibility is that the stress range $\Delta\sigma$ exceeds $2S_y$ causing reversed yielding as shown in Figure 6-45f. The maximum and minimum stresses now equal $\pm S_y$ and the mean stress becomes zero (see equation 6.1c, p. 314), making $K_{fm} = 0$.

These relationships can be summarized as follows:

$$\begin{aligned} \text{if } K_f |\sigma_{max,nom}| &< S_y \text{ then :} & K_{fm} &= K_f \\ \text{if } K_f |\sigma_{max,nom}| &> S_y \text{ then :} & K_{fm} &= \frac{S_y - K_f \sigma_{a,nom}}{|\sigma_{m,nom}|} \\ \text{if } K_f |\sigma_{max,nom} - \sigma_{min,nom}| &> 2S_y \text{ then :} & K_{fm} &= 0 \end{aligned} \quad (6.17)$$

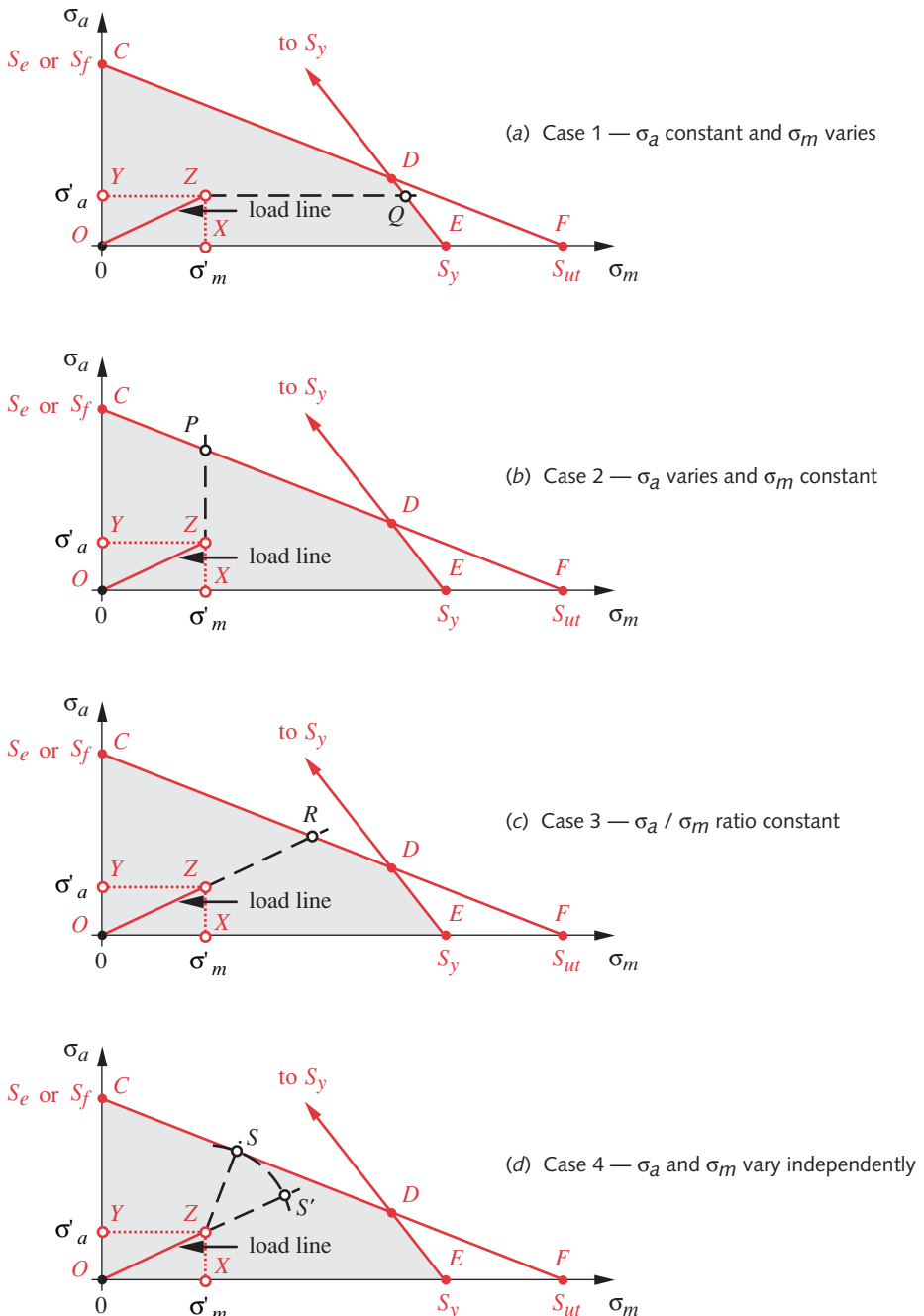
The absolute values are used to account for either compressive or tensile situations. The value of the local mean stress σ_m for use in the modified-Goodman diagram is then

**FIGURE 6-45**

Variation of Mean Stress-Concentration Factor with Maximum Stress in Ductile Materials with Possibility of Local Yielding
(Adapted from Fig. 10-14, p. 415, N. E. Dowling, *Mechanical Behavior of Materials*, Prentice-Hall, Englewood Cliffs, N.J., 1993, with permission.)

found from equation 6.12 (p. 343) with K_{fm} substituted for K_f . Note that the stress-concentration factors should be applied to the nominal applied stresses, be they normal or shear stress.

The local applied stresses (with their fatigue stress-concentration effects included) are used to calculate the alternating and mean von Mises stresses. This calculation is done separately for the alternating and mean components σ'_a and σ'_m . (See equations 6.22a and 6.22b, p. 379.) We will use these von Mises components to find the safety factor.

**FIGURE 6-46**

Safety Factors from the Modified-Goodman Diagram for Four Possible Load-Variation Scenarios

Determining the Safety Factor with Fluctuating Stresses

Figure 6-46 shows four views of the tension side of the augmented modified-Goodman diagram and also shows a combination of mean and alternating von Mises stresses at

point Z representing a part subjected to fluctuating stresses. The safety factor for any fluctuating-stress state depends on the manner in which the mean and alternating components can vary with respect to one another in service. There are four possible cases to consider, as shown in Figure 6-46.

- 1 The alternating stress will remain essentially constant over the life of the part but the mean stress can increase under service conditions. (Line YQ in Figure 6-46a.)
- 2 The mean stress will remain essentially constant over the life of the part but the alternating stress can increase under service conditions. (Line XP in Figure 6-46b.)
- 3 Both alternating and mean stress components can increase under service conditions but their ratio will remain constant. (Line OR in Figure 6-46c.)
- 4 Both alternating and mean stress components can increase under service conditions but there is no known relationship between their amounts of increase. (Line ZS in Figure 6-46d.)

The safety factor for each of these cases is calculated differently. Note that S_f will be used in the following expressions to represent either the corrected fatigue strength at some defined number of cycles or the corrected endurance limit. So, S_e can be substituted for S_f in any of these expressions if appropriate to the material used.

FOR CASE 1 Failure occurs at point Q and the safety factor is the ratio of the lines YQ/YZ. To express this mathematically, we can solve equation 6.16d (p. 363) for the value of $\sigma'_{m@Q}$ and divide that by $\sigma'_{m@Z}$.

$$\begin{aligned}\sigma'_{m@Q} &= \left(1 - \frac{\sigma'_a}{S_y}\right) S_y \\ N_f &= \frac{\sigma'_{m@Q}}{\sigma'_{m@Z}} = \frac{S_y}{\sigma'_m} \left(1 - \frac{\sigma'_a}{S_y}\right)\end{aligned}\quad (6.18a)$$

If σ'_a were so large and σ'_m so small that point Q was on line CD instead of DE, then equation 6.16c (p. 363) should be used instead to determine the value of $\sigma'_{m@Q}$.

FOR CASE 2 Failure occurs at point P and the safety factor is the ratio of the lines XP/XZ. To express this mathematically, we can solve equation 6.16c (p. 363) for the value of $\sigma'_{a@P}$ and divide that by $\sigma'_{a@Z}$.

$$\begin{aligned}\sigma'_{a@P} &= \left(1 - \frac{\sigma'_m}{S_{ut}}\right) S_f \\ N_f &= \frac{\sigma'_{a@P}}{\sigma'_{a@Z}} = \frac{S_f}{\sigma'_a} \left(1 - \frac{\sigma'_m}{S_{ut}}\right)\end{aligned}\quad (6.18b)$$

If σ'_m were so large and σ'_a so small that point P was on line DE instead of CD, then equation 6.16d (p. 364) should be used instead to determine the value of $\sigma'_{a@P}$.

FOR CASE 3 Failure occurs at point R and the safety factor is the ratio of the lines OR/OZ or by similar triangles, either of the ratios $\sigma'_{m@R} / \sigma'_{m@Z}$ or $\sigma'_{a@R} / \sigma'_{a@Z}$.

To express this mathematically, we can solve equations 6.16c (p. 363) and the equation of line OR simultaneously for the value of $\sigma'_{m@R}$ and divide that by $\sigma'_{m@Z}$.

$$\text{from equation 6.16c : } \sigma'_{a@R} = \left(1 - \frac{\sigma'_{m@R}}{S_{ut}}\right) S_f \quad (6.18c)$$

$$\text{from line } OR : \sigma'_{a@R} = \left(\frac{\sigma'_{a@Z}}{\sigma'_{m@Z}}\right) \sigma'_{m@R} = \left(\frac{\sigma'_a}{\sigma'_m}\right) \sigma'_{m@R}$$

The simultaneous solution of these gives

$$\sigma'_{m@R} = \frac{S_f}{\frac{\sigma'_a}{\sigma'_m} + \frac{S_f}{S_{ut}}} \quad (6.18d)$$

6

which after substitution and some manipulation yields

$$N_f = \frac{\sigma'_{m@R}}{\sigma'_{m@Z}} = \frac{S_f S_{ut}}{\sigma'_a S_{ut} + \sigma'_m S_f} \quad (6.18e)$$

There is also the possibility that point R may lie on line DE instead of CD , in which case equation 6.16d (p. 364) should be substituted for 6.16c in the above solution.

FOR CASE 4 In which the future relationship between the mean and alternating stress components is either random or unknown, the point S on the failure line closest to the stress state at Z can be taken as a conservative estimate of the failure point. Line ZS is normal to CD , so its equation can be written and solved simultaneously with that of the line CD to find the coordinates of point S and the length ZS , which are

$$\begin{aligned} \sigma'_{m@S} &= \frac{S_{ut}(S_f^2 - S_f \sigma'_a + S_{ut} \sigma'_m)}{S_f^2 + S_{ut}^2} \\ \sigma'_{a@S} &= -\frac{S_f}{S_{ut}} (\sigma'_{m@S}) + S_f \\ ZS &= \sqrt{(\sigma'_m - \sigma'_{m@S})^2 + (\sigma'_a - \sigma'_{a@S})^2} \end{aligned} \quad (6.18f)$$

To establish a ratio for the safety factor, swing point S about point Z to be coincident with line OZS' at point S' . The safety factor is the ratio OS'/OZ .

$$\begin{aligned} OZ &= \sqrt{(\sigma'_a)^2 + (\sigma'_m)^2} \\ N_f &= \frac{OZ + ZS}{OZ} \end{aligned} \quad (6.18g)$$

There is also the possibility that point S may lie on line DE instead of CD , in which case equation 6.16d (p. 364) should be substituted for 6.16c in the above solution.

Case 4 gives a more conservative safety factor than Case 3. The same approach can be used to obtain safety-factor expressions for stress-component combinations in

the left half-plane of the modified-Goodman diagram. Also, if the diagram is drawn to scale, rough estimates of the safety factors can be scaled from it. The file GOODMAN supplied with this text calculates all the safety factors defined in equations 6.18 (p. 366 and 367) for any supplied values of σ'_a and σ'_m , and it plots the modified-Goodman diagram and the stress line OZ extended so that the failure intercept can be seen.

Design Steps for Fluctuating Stresses

A set of design steps similar to those listed for the fully reversed case can be defined for the case of fluctuating stresses:

- 1 Determine the number of cycles of loading N that the part will experience over its expected service life.
- 2 Determine the amplitude of the applied alternating loads (mean to peak) and of the mean load. (See Chapter 3 and equations 6.1, p. 314.)
- 3 Create a tentative part-geometry design to withstand the applied loads based on good engineering practice. (See Chapters 3 and 4.)
- 4 Determine any geometric stress-concentration factors K_t at notches in the part's geometry. Try, of course, to minimize these through good design. (See Section 4.15 on p. 186.)
- 5 Convert the geometric stress-concentration factors K_t to fatigue-concentration factors K_f using the material's q .
- 6 Calculate the nominal, alternating tensile-stress amplitudes σ_a (see Figure 6-6c, p. 313) at critical locations in the part due to the alternating service loads based on standard stress-analysis techniques (Chapter 4) and increase them as necessary with the appropriate fatigue stress-concentration factors from equation 6.11 (p. 343). (See Sections 4.15 on p. 186 and 6.7 on p. 342.) Calculate the nominal mean stress amplitudes at the same critical locations and increase them as necessary with the appropriate mean fatigue stress-concentration factors K_{fm} from equation 6.17 (p. 364).
- 7 Calculate the principal stress and von Mises stress amplitudes for the critical locations based on their states of applied stress. Do this separately for the mean and alternating components. (See Chapter 4 and equations 6.22, p. 379.)
- 8 Choose a tentative material for the part and determine its properties of interest such as S_{ut} , S_y , S_e' (or S_f' at the life required), and notch sensitivity q , from your own test data, from the literature, or from estimates as described in this chapter.
- 9 Determine appropriate fatigue strength modification factors for the type of loading, size of part, surface, etc., as described in Section 6.6 (p. 327). Note that the loading factor C_{load} will differ based on whether there are axial or bending loads (Eq. 6.7a, p. 330). If the loading is pure torsion, then the von Mises effective-stress calculation will convert it to a pseudo-tensile stress and C_{load} should then be set to 1.
- 10 Define the corrected fatigue strength S_f at the requisite cycle life N (or the corrected endurance limit S_e for infinite life if appropriate). Create a modified-Goodman diagram as shown in Figure 6-44 (p. 363) using the material's corrected fatigue strength S_f taken from the S - N curve at the desired number of cycles N . (Note that for infinite life situations in which the material has an S - N knee, $S_f = S_e$). Write equations 6.16 (p. 363 and 364) for the Goodman and yield lines.

- 11 Plot the mean and alternating von Mises stresses (for the most highly stressed location) on the modified-Goodman diagram and calculate a safety factor for the design from one of the relationships shown in equations 6.18 (pp. 367–368).
- 12 Given the fact that the material was only tentatively chosen and that the design may not yet be as refined as possible, the result of the first pass through these steps will most likely be a failed design whose safety factor is either too large or too small. Iteration will be required (as it always is) to refine the design. Any subset of steps can be repeated as many times as necessary to obtain an acceptable design. The most common tactic is to return to step 3 and improve the geometry of the part to reduce stresses and stress concentrations and/or revisit step 8 to choose a more suitable material. Sometimes it will be possible to return to step 1 and redefine a shorter acceptable part life. The design loads in step 2 may or may not be in the control of the designer. Usually they are not, unless the loading on the part is due to inertial forces, in which case increasing its mass to “add strength” will worsen the situation, as this will proportionately increase the loads (see Section 3.6 on p. 98). The designer may want to lighten the part without compromising its strength excessively in order to reduce the inertial forces. Whatever the particular circumstances, the designer must expect to cycle through these steps several times before converging on a usable solution. Equation solvers that allow rapid recalculation of the equations are a great help in this situation. If the equation solver can also “backsolve,” allowing variables to be exchanged from input to output, the geometry needed to achieve a desired safety factor can be directly calculated by making the safety factor an input and the geometry variable an output.

The best way to demonstrate the use of these steps for fluctuating-stress fatigue design is with an example. We will repeat the previous example, modifying its load pattern.

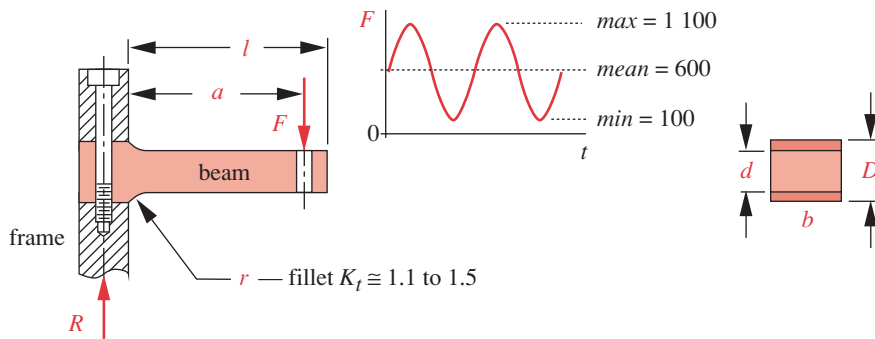
EXAMPLE 6-5

Design of a Cantilever Bracket for Fluctuating Bending

Problem A feed-roll assembly is to be mounted at its ends on support brackets cantilevered from the machine frame as shown in Figure 6-47. The feed rolls experience a total fluctuating load that varies from a minimum of 200 lb to a maximum of 2 200 lb, split equally between the two support brackets. Design a cantilever bracket to support a fluctuating bending load of 100- to 1 100-lb amplitude for 10^9 cycles with no failure. Its dynamic deflection cannot exceed 0.02 in.

Given The load-time function shape is shown in Figure 6-47. The operating environment is room air at a maximum temperature of 120°F. The space available allows a maximum cantilever length of 6 in. Only ten of these parts are required.

Assumptions The bracket can be clamped between essentially rigid plates bolted at its root. The normal load will be applied at the effective tip of the cantilever beam from a rod attached through a small hole in the beam. Since the bending moment is effectively zero at the beam tip, the stress concentration from this hole can be ignored. Given the small quantity required, machining of stock mill-shapes is the preferred manufacturing method.

**FIGURE 6-47**

Design of a Cantilever Bracket for Fluctuating-Bending Loading

6

Solution

See Figure 6-47 and Tables 6-11 and 6-12.

- 1 This is a typical design problem. Very few data are given except for the loading on the device, some limitations on size, and the required cycle life. We will have to make some basic assumptions about part geometry, materials, and other factors as we go. Some iteration should be expected.
- 2 Figure 6-47 shows the same tentative design configuration as in Figure 6-41b (p. 355). The mill stock is purchased thicker than the desired final dimension and machined top and bottom to dimension D , then machined to thickness d over the length l . A fillet radius r is provided at the clamp point to reduce fretting fatigue and achieve a lower K_t . (See Figure 4-37 on p. 191.) Figure 4-36 (p. 190) shows that with suitable control of the r/d and D/d ratios for a stepped flat bar in bending, the geometric stress-concentration factor K_t can be kept under about 1.5.
- 3 A material must be chosen. For infinite life, low cost, and ease of fabrication, it is desirable to use a carbon steel if environmental conditions permit. Since this is used in a controlled, indoor environment, carbon steel is acceptable on the latter point. The fact that the deflection is of concern is also a good reason to choose a material with a large E . Low- to medium-carbon, ductile steels have the requisite endurance-limit knee for the infinite life required in this case and also have low notch sensitivities. An SAE 1040 normalized carbon steel with $S_{ut} = 80$ ksi and $S_y = 60$ ksi is selected for the first trial.
- 4 We will assume the trial dimensions to be the same as those of the successful solution to the fully reversed case from Example 6-4. These are $b = 2$ in, $d = 1$ in, $D = 1.125$ in, $r = 0.5$ in, $a = 5$ in, and $l = 6.0$ in. This value of a will leave some material around the hole and still fit within the 6-in-length constraint.
- 5 The mean and alternating components of the load and their reaction forces can be calculated from the given maximum and minimum load.

$$F_m = \frac{F_{max} + F_{min}}{2} = \frac{1100 + 100}{2} = 600 \text{ lb} \quad (a)$$

$$F_a = \frac{F_{max} - F_{min}}{2} = \frac{1100 - 100}{2} = 500 \text{ lb}$$

$$R_a = F_a = 500 \text{ lb} \quad R_m = F_m = 600 \text{ lb} \quad R_{max} = F_{max} = 1100 \text{ lb} \quad (b)$$

- 6 From these, the mean and alternating moments, and the maximum moment acting at the root of the cantilever beam can be calculated.

$$\begin{aligned} M_a &= R_a l - F_a(l-a) = 500(6) - 500(6-5) = 2500 \text{ lb-in} \\ M_m &= R_m l - F_m(l-a) = 600(6) - 600(6-5) = 3000 \text{ lb-in} \\ M_{max} &= R_{max} l - F_{max}(l-a) = 1100(6) - 1100(6-5) = 5500 \text{ lb-in} \end{aligned} \quad (c)$$

- 7 Find the cross-section area moment of inertia and the distance to the outer fiber.

$$\begin{aligned} I &= \frac{bd^3}{12} = \frac{2.0(1.0)^3}{12} = 0.1667 \text{ in}^4 \\ c &= \frac{d}{2} = \frac{1.0}{2} = 0.5 \text{ in} \end{aligned} \quad (d)$$

6

- 8 The nominal bending stresses at the root are found for both the alternating load and the mean load from:

$$\begin{aligned} \sigma_{a_{nom}} &= \frac{M_a c}{I} = \frac{2500(0.5)}{0.1667} = 7500 \text{ psi} \\ \sigma_{m_{nom}} &= \frac{M_m c}{I} = \frac{3000(0.5)}{0.1667} = 9000 \text{ psi} \end{aligned} \quad (e)$$

- 9 Two ratios must be calculated for use in Figure 4-36 (p. 190) in order to find the geometric stress-concentration factor K_t for the assumed part dimensions.

$$\frac{D}{d} = \frac{1.125}{1.0} = 1.125 \quad \frac{r}{d} = \frac{0.5}{1.0} = 0.5 \quad (f)$$

Interpolating in the table of Figure 4-36 : $A = 1.012$ $b = -0.221$ (g)

$$K_t = A \left(\frac{r}{d} \right)^b = 1.012(0.5)^{-0.221} = 1.18 \quad (h)$$

- 10 The notch sensitivity q of the chosen material is calculated based on its ultimate strength and the notch radius using equation 6.13 (p. 345) and the data for Neuber's constant from Table 6-6 (p. 346). The values of q and K_t are used to find the fatigue stress-concentration factor K_f using equation 6.11b (p. 343). K_{fm} is calculated from equation 6.17 (p. 364).

From Table 6-6 for $S_{ut} = 80$ ksi : $\sqrt{a} = 0.08$ (i)

$$q = \frac{1}{1 + \frac{\sqrt{a}}{\sqrt{r}}} = \frac{1}{1 + \frac{0.08}{\sqrt{0.5}}} = 0.898 \quad (j)$$

$$K_f = 1 + q(K_t - 1) = 1 + 0.898(1.18 - 1) = 1.16 \quad (k)$$

$$\begin{aligned} \text{if } K_f |\sigma_{max}| < S_y \text{ then } K_{fm} &= K_f \\ K_f \left| \frac{M_{max}c}{I} \right| = 1.16 \left| \frac{5500(0.5)}{0.1667} \right| &= 19113 < 60000 : \quad K_{fm} = 1.16 \end{aligned} \quad (l)$$

- 11 Use these factors to find the local mean and alternating notch stresses.

$$\sigma_a = K_f \sigma_{a_{nom}} = 1.16(7\ 500) = 8\ 711 \text{ psi} \quad (m)$$

$$\sigma_m = K_{fm} \sigma_{m_{nom}} = 1.16(9\ 000) = 10\ 454 \text{ psi}$$

- 12 The local stresses are used to compute the von Mises alternating and mean stresses from equations 6.22b (p. 379).

$$\sigma'_a = \sqrt{\sigma_{x_a}^2 + \sigma_{y_a}^2 - \sigma_{x_a}\sigma_{y_a} + 3\tau_{xy_a}^2} = \sqrt{8\ 711^2 + 0 - 8\ 711(0) + 3(0)} = 8\ 711 \quad (n)$$

$$\sigma'_m = \sqrt{\sigma_{x_m}^2 + \sigma_{y_m}^2 - \sigma_{x_m}\sigma_{y_m} + 3\tau_{xy_m}^2} = \sqrt{10\ 454^2 + 0 - 10\ 425(0) + 3(0)} = 10\ 454$$

- 13 The uncorrected endurance limit S_e' is determined from equation 6.5a (p. 330).

$$S_e' = 0.5S_{ut} = 0.5(80\ 000) = 40\ 000 \text{ psi} \quad (o)$$

- 14 The *size factor* for this rectangular part is determined by calculating the cross-sectional area stressed above 95% of its maximum stress (see Figure 6-25 on p. 332) and using that value in equation 6.7d (p. 331) to find an equivalent-diameter test specimen.

$$A_{95} = 0.05db = 0.05(1.0)(2.0) = 0.1 \text{ in}^2$$

$$d_{equiv} = \sqrt{\frac{A_{95}}{0.076\ 6}} = \sqrt{\frac{0.1}{0.076\ 6}} = 1.143 \text{ in} \quad (p)$$

$$C_{size} = 0.869(d_{equiv})^{-0.097} = 0.859$$

- 15 Calculation of the corrected endurance limit S_e requires that several factors be computed. C_{load} is found from equation 6.7a (p. 330). C_{surf} for a machined finish is found from equation 6.7e (p. 333). C_{temp} is found from equation 6.7f (p. 335) and C_{reliab} is chosen from Table 6-4 (p. 335) for a 99.9% reliability level.

$$S_e = C_{load} C_{size} C_{surf} C_{temp} C_{reliab} S_e' \quad (q)$$

$$= 1(0.859)(0.85)(1)(0.753)40\ 000 = 21\ 883 \text{ psi}$$

- 16 The four possible safety factors are calculated from equations 6.18 (pp. 367–368). The smallest or most appropriate one can be selected from those calculated. Equation (r) shows the Case 3 safety factor, which assumes that the alternating and mean components will have a constant ratio if they vary in maximum amplitude over the life of the part.

$$N_{f_3} = \frac{S_e S_{ut}}{\sigma'_a S_{ut} + \sigma'_m S_e} = \frac{21\ 883(80\ 000)}{8\ 688(80\ 000) + 10\ 425(21\ 883)} = 1.9 \quad (r)$$

- 17 The maximum deflection is calculated using the maximum applied force F_{max} .

$$y_{@x=l} = \frac{F_{max}}{6EI} \left[x^3 - 3ax^2 - (x-a)^3 \right] \quad (s)$$

$$= \frac{1\ 100}{6(3E7)(0.1667)} \left[6^3 - 3(5)(6)^2 - (6-5)^3 \right] = -0.012 \text{ in}$$

Table 6-11 Design of a Cantilever Bracket for Fluctuating Bending

First Iteration for Example 6-5 (File EX06-05A)

Input	Variable	Output	Unit	Comments
2	<i>b</i>		in	beam width
1	<i>d</i>		in	beam depth over length
1.125	<i>D</i>		in	beam depth in wall
0.5	<i>r</i>		in	fillet radius
5	<i>a</i>		in	beam length to load <i>F</i>
80 000	<i>Sut</i>		psi	ultimate tensile strength
60 000	<i>Sy</i>		psi	yield strength
'machined	<i>finish</i>			'ground, 'machined, 'hotroll, 'forged
'bending	<i>loading</i>			'bending, 'axial, 'shear
99.9	<i>percent</i>			reliability % desired
1 100	<i>Fmax</i>		lb	maximum applied load
100	<i>Fmin</i>		lb	minimum applied load
	<i>Fa</i>	500	lb	alternating applied force
	<i>Fm</i>	600	lb	mean applied force
	<i>Kt</i>	1.18		geometric stress-conc. factor
	<i>q</i>	0.898		Peterson's notch-sensitivity factor
	<i>Kf</i>	1.16		fatigue stress-conc. factor — alter.
	<i>Kfm</i>	1.16		fatigue stress-conc. factor — mean
	<i>siganom</i>	7 500	psi	alternating nominal stress
	<i>sigia</i>	8 711	psi	alternating stress with concentration
	<i>sigavm</i>	8 711	psi	von Mises alternating stress
	<i>sigmnom</i>	9 000	psi	mean nominal stress
	<i>sigm</i>	10 454	psi	mean stress with concentration
	<i>sigmvm</i>	10 454	psi	von Mises mean stress
	<i>Seprime</i>	40 000	psi	uncorrected endurance limit
	<i>Cload</i>	1		load factor for bending
	<i>Csurf</i>	0.845		machined finish
	<i>Csize</i>	0.859		size factor based on 95% area
	<i>Ctemp</i>	1		room temperature
	<i>Creliab</i>	0.753		99.9% reliability factor
	<i>Se</i>	21 883	psi	corrected endurance limit
	<i>Nsf_1</i>	5.5		FS for sigalt = constant
	<i>Nsf_2</i>	2.2		FS for sigmean = constant
	<i>Nsf_3</i>	1.9		FS for sigalt/sigmean = constant
	<i>Nsf_4</i>	1.7		FS for closest failure line

- 18 The data for this design are shown in Table 6-11. Using the same cross-section dimensions and the same alternating load as in Example 6-4 now gives a safety factor $N_f3 = 1.9$ and maximum deflection $y_{max} = 0.012$ in for this fluctuating loading

Table 6-12 Design of a Cantilever Bracket for Fluctuating Bending

Final Iteration for Example 6-5 (File EX06-05B)

Input	Variable	Output	Unit	Comments
2	<i>b</i>		in	beam width
1.2	<i>d</i>		in	beam depth over length
1.4	<i>D</i>		in	beam depth in wall
0.5	<i>r</i>		in	fillet radius
5	<i>a</i>		in	beam length to load <i>F</i>
80 000	<i>Sut</i>		psi	ultimate tensile strength
60 000	<i>Sy</i>		psi	yield strength
'machined	<i>finish</i>			'ground, 'machined, 'hotroll, 'forged
'bending	<i>loading</i>			'bending, 'axial, 'shear
99.9	<i>percent</i>			reliability % desired
1 100	<i>Fmax</i>		lb	maximum applied load
100	<i>Fmin</i>		lb	minimum applied load
	<i>Fa</i>	500	lb	alternating applied force
	<i>Fm</i>	600	lb	mean applied force
	<i>Kt</i>	1.22		geometric stress-conc. factor
	<i>q</i>	0.898		Peterson's notch-sensitivity factor
	<i>Kf</i>	1.20		fatigue stress-conc. factor — alter.
	<i>Kfm</i>	1.20		fatigue stress-conc. factor — mean
	<i>siganom</i>	5 208	psi	alternating nominal stress
	<i>sigal</i>	6 230	psi	alternating stress with concentration
	<i>sigavm</i>	6 230	psi	von Mises alternating stress
	<i>signnom</i>	6 250	psi	mean nominal stress
	<i>sigm</i>	7 476	psi	mean stress with concentration
	<i>sigmvm</i>	7 476	psi	von Mises mean stress
	<i>Seprime</i>	40 000	psi	uncorrected endurance limit
	<i>Cload</i>	1		load factor for bending
	<i>Csurf</i>	0.85		machined finish
	<i>Csize</i>	0.85		size factor based on 95% area
	<i>Ctemp</i>	1		room temperature
	<i>Creliab</i>	0.753		99.9% reliability factor
	<i>Se</i>	21 658	psi	corrected endurance limit
	<i>Nsf_1</i>	8.6		FS for sigalt = constant
	<i>Nsf_2</i>	3.2		FS for sigmean = constant
	<i>Nsf_3</i>	2.6		FS for sigalt/sigmean = constant
	<i>Nsf_4</i>	2.3		FS for closest failure line

case, compared to $N_f = 2.5$ and $y_{max} = 0.005$ in for the fully reversed loading situation of Example 6-4. The addition of a mean stress to the previous level of alternating stress reduced the safety factor and increased the deflection, as expected.

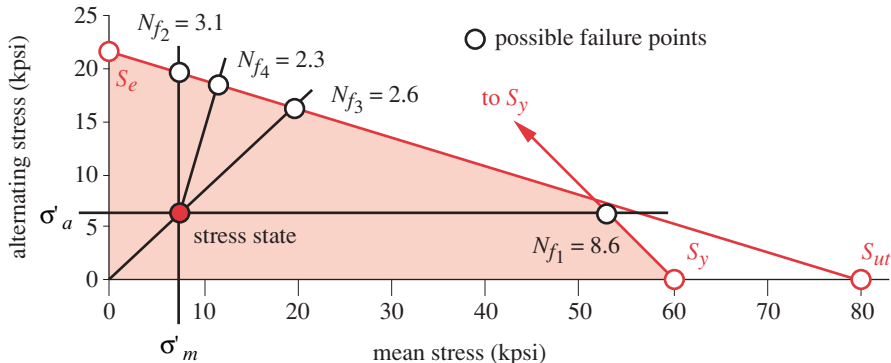


FIGURE 6-48

Modified-Goodman Diagram for Example 6-5 Showing Final Solution Data from Table 6-12

- 19 Increasing the part's cross-section dimensions slightly gives the better design shown in Table 6-12. The final dimensions are $b = 2$ in, $d = 1.2$ in, $D = 1.4$ in, $r = 0.5$ in, $a = 5$ in, and $l = 6.0$ in. N_f becomes 2.6 as shown in the Goodman diagram of Figure 6-48, and the maximum deflection becomes 0.007 in. These are both acceptable. The dimension D was deliberately chosen to be slightly less than a stock mill size so that some material would be available for machining in order to clean up and true the mounting surfaces.
- 20 The files EX06-05A and EX06-05B are on the CD-ROM.

The above example should demonstrate that designing for fluctuating HCF loads is straightforward once the principles are understood. If the design called for fluctuating torsional, bending, or axial loading, the design procedure would be the same as in this example. The only differences would be in the choices of stress equations and strength modification factors as described in the previous sections. The value of using a computer and equation solver in this or any design problem cannot be overstated, as it allows rapid iteration from initial guesses to final dimensions with minimum effort.

6.12 DESIGNING FOR MULTIAXIAL STRESSES IN FATIGUE

The previous discussions were limited to cases in which the loading produced uniaxial stresses in the part. It is quite usual in machinery to have combined loads that create simultaneous time-varying biaxial or triaxial stresses at the same point. A common example is a rotating shaft subjected to both a static bending moment and a torque. Because the shaft is turning, the static moment creates fully reversed normal stresses that are maximum at the shaft's outer fiber, and the torque creates shear stresses that are also maximum at the outer fiber. There are many possible loading combinations. The torque might be constant, fully reversed, or fluctuating. If the torque is not constant, it could be synchronous, asynchronous, in- or out-of-phase with the bending moment. These factors complicate the stress calculation. We explored the case of combined stresses under static loading in Chapter 5 and used the *von Mises stress* to convert them

to an equivalent tensile stress that could be used to predict failure in the static loading case. Similar techniques exist for handling combined stresses in dynamic loading.

Frequency and Phase Relationships

When multiple time-varying loads are present, they may be periodic, random, or some combination of the two. If periodic, they can be mutually synchronous or asynchronous. If synchronous, they may have phase relationships from in-phase to 180° out-of-phase or anything in between. The possible combinations are quite varied, and only a few such combinations have been studied to determine their effects on fatigue failure. Collins^[49] suggests that the assumption that loads are synchronous and in-phase is usually accurate for machine design and usually (but not always) conservative.

The most-studied cases are those of periodic, synchronous, in-phase loads that cause combined stresses whose principal directions do not change with time. This is referred to as **simple multiaxial stress**. Sines^[42] developed a model for this case in 1955. Pressure vessels or pipes that are subjected to time-varying internal pressures may see synchronous, in-phase multiaxial tensile stresses from a single load source. The case of a rotating shaft in combined bending and torsion can also be in this category if the torque is constant with time, since the alternating component of principal stress, due only to bending, is then in a constant direction. If the torque is time-varying, then the alternating principal stress directions are not constant. Also when stress concentrations are present, such as a transverse hole through a shaft, the local stresses at the concentration will be biaxial. These situations, in which the directions of the principal stresses vary with time or in which the stresses are asynchronous or out-of-phase, are called **complex multiaxial stress** and are still being studied. According to the SAE *Fatigue Design Handbook*,^[51] “*Analysis of this situation is, in general, beyond the current state of the technology. The design process must proceed by very approximate analyses supported by extensive experimental studies simulating the material and geometry as well as the loading.*” Analysis methods have been developed for some of these cases by Kelly,^[43] Garud,^[44] Brown,^[45] Langer,^[48] and others. Some of these approaches are fairly complicated to use. Reference 51 also “*caution(s) against direct use of these data unless the conditions examined match those being analyzed.*” We will limit our discussion to a few approaches that are useful for design purposes and that should give approximate but conservative results in most machine-design situations.

6

Fully Reversed Simple Multiaxial Stresses

Experimental data developed for simple biaxial stresses, such as those shown in Figure 6-15 (p. 321), indicate that for fully reversed, simple multiaxial stresses in ductile materials, the distortion energy theory is applicable if the von Mises stress is calculated for the alternating components using equation 5.7 (p. 249). For the three-dimensional case:

$$\sigma'_a = \sqrt{\sigma_{1_a}^2 + \sigma_{2_a}^2 + \sigma_{3_a}^2 - \sigma_{1_a}\sigma_{2_a} - \sigma_{2_a}\sigma_{3_a} - \sigma_{1_a}\sigma_{3_a}} \quad (6.19a)$$

and for the two-dimensional case:

$$\sigma'_a = \sqrt{\sigma_{1_a}^2 - \sigma_{1_a}\sigma_{2_a} + \sigma_{2_a}^2} \quad (6.19b)$$

Note that this form of the von Mises equation contains the alternating principal stresses which are computed from the alternating applied-stress components of the multiaxial stress state using equation 4.4c—for 3-D (p. 144) or 4.6—for 2-D (p. 145) after those alternating components have been increased by all applicable fatigue stress-concentration factors. This effective alternating stress σ'_a can then be used to enter an *S-N* diagram to determine a safety factor using

$$N_f = \frac{S_n}{\sigma'_a} \quad (6.20)$$

where S_n is the fatigue strength of the material at the desired life N and σ'_a is the von Mises alternating stress.

6

Fluctuating Simple Multiaxial Stresses

SINES METHOD Sines [42] developed a model for fluctuating simple multiaxial stresses which creates an equivalent mean stress as well as an equivalent alternating stress from the applied stress components. His equivalent alternating stress is, in fact, the von Mises alternating stress as defined in equation 6.19a above. However, we will present it in an alternate form that uses the applied stresses directly instead of the principal stresses. For a triaxial stress state:

$$\sigma'_a = \sqrt{\frac{(\sigma_{x_a} - \sigma_{y_a})^2 + (\sigma_{y_a} - \sigma_{z_a})^2 + (\sigma_{z_a} - \sigma_{x_a})^2 + 6(\tau_{xy_a}^2 + \tau_{yz_a}^2 + \tau_{zx_a}^2)}{2}} \quad (6.21a)$$

$$\sigma'_m = \sigma_{x_m} + \sigma_{y_m} + \sigma_{z_m}$$

and, for a biaxial stress state:

$$\sigma'_a = \sqrt{\sigma_{x_a}^2 + \sigma_{y_a}^2 - \sigma_{x_a}\sigma_{y_a} + 3\tau_{xy_a}^2} \quad (6.21b)$$

$$\sigma'_m = \sigma_{x_m} + \sigma_{y_m}$$

The applied stress components in equations 6.21 are the local stresses, increased by all applicable stress-concentration factors. The two equivalent stresses σ'_a and σ'_m are then used in a modified-Goodman diagram as described in the previous section, and the appropriate safety factor calculated from equations 6.18 (pp. 367–368).

While the individual local stresses in equations 6.19 and 6.21 each can be increased by a different stress-concentration factor, there may be some conflicts when the corrected fatigue strength or endurance limit is calculated for a combined stress state. For example, a combination of bending and axial loading would give two choices for the load factors from equations 6.7a (p. 330) and 6.9 (p. 337). Use the axial factor if axial loads are present, with or without bending loads.

Note that the Sines equivalent mean stress σ'_m of equations 6.21 contains only normal stress components (which are the hydrostatic stress) while the von Mises equivalent alternating stress σ'_a of equations 6.21 contains both normal and shear stresses. The mean components of shear stress thus do not contribute to Sines' model. This is con-

sistent with experimental data for smooth, polished, unnotched, round bars tested in combined bending and torsion.^[46] But, notched specimens under the same loading do show dependence on the value of mean torsional stress,^[46] so equations 6.21 may be nonconservative in such cases.

VON MISES METHOD Others^{[47],[49]} recommend using the von Mises effective stress for both alternating and mean components of applied stress in simple multiaxial stress loading. Appropriate (and possibly different) stress-concentration factors can be applied to the alternating and mean components of the applied stresses as described in section 6.10. Then the von Mises effective stresses for the alternating and mean components are calculated for a triaxial stress state using

$$\sigma'_a = \sqrt{\frac{(\sigma_{x_a} - \sigma_{y_a})^2 + (\sigma_{y_a} - \sigma_{z_a})^2 + (\sigma_{z_a} - \sigma_{x_a})^2 + 6(\tau_{xy_a}^2 + \tau_{yz_a}^2 + \tau_{zx_a}^2)}{2}} \quad (6.22a)$$

$$\sigma'_m = \sqrt{\frac{(\sigma_{x_m} - \sigma_{y_m})^2 + (\sigma_{y_m} - \sigma_{z_m})^2 + (\sigma_{z_m} - \sigma_{x_m})^2 + 6(\tau_{xy_m}^2 + \tau_{yz_m}^2 + \tau_{zx_m}^2)}{2}}$$

or for a biaxial stress state using:

$$\sigma'_a = \sqrt{\sigma_{x_a}^2 + \sigma_{y_a}^2 - \sigma_{x_a}\sigma_{y_a} + 3\tau_{xy_a}^2} \quad (6.22b)$$

$$\sigma'_m = \sqrt{\sigma_{x_m}^2 + \sigma_{y_m}^2 - \sigma_{x_m}\sigma_{y_m} + 3\tau_{xy_m}^2}$$

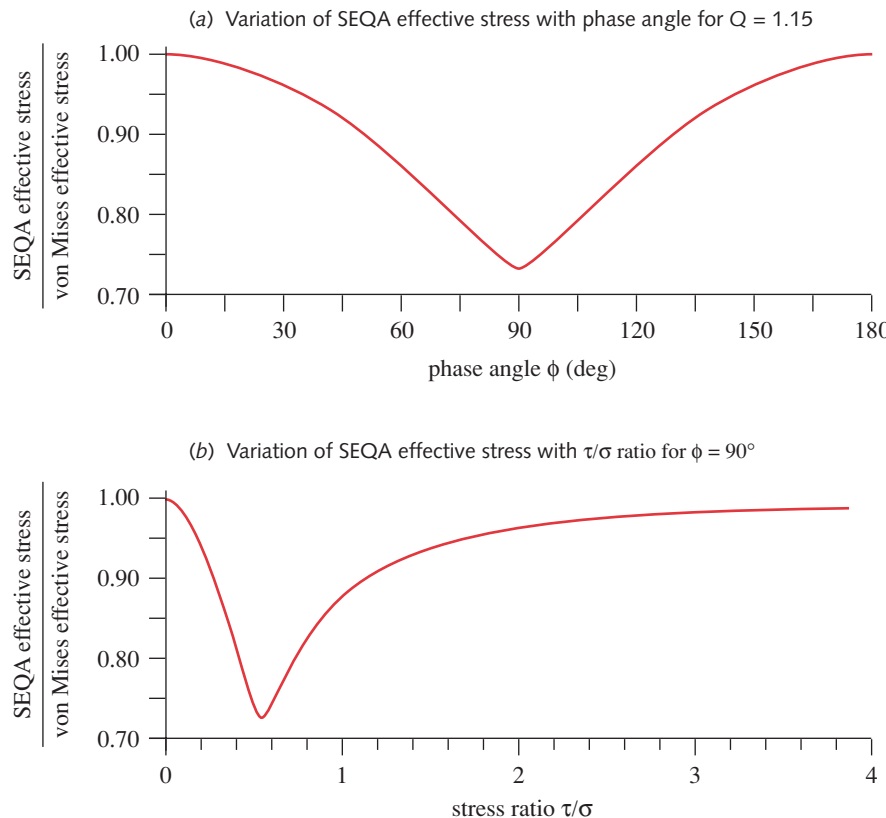
These alternating and mean von Mises effective stresses are then used in a modified-Goodman diagram to determine a safety factor using the appropriate version of equations 6.18. This approach is more conservative than the Sines method and is thus more appropriate for situations involving stress concentrations due to notches.

Complex Multiaxial Stresses

This topic is still under investigation by numerous researchers. Many specific cases of complex multiaxial stresses have been analyzed but no overall design approach applicable to all situations has yet been developed.^[50] Nishihara and Kawamoto^[52] found that the fatigue strengths of two steels, a cast iron, and an aluminum alloy tested under complex multiaxial stress were not less than their in-phase fatigue strengths at any phase angle. For the common biaxial stress case of combined bending and torsion, such as occurs in shafts, several approaches have been proposed.^[50] One of these, called SEQA, which is based on the ASME Boiler Code,* will be discussed briefly. SEQA is an equivalent or effective stress (similar in concept to the von Mises effective stress), which combines the effects of normal and shear stresses and the phase relationship between them into an effective-stress value that can be compared to a ductile material's fatigue and static strengths on a modified-Goodman diagram. It is calculated from

$$\text{SEQA} = \frac{\sigma}{\sqrt{2}} \left[1 + \frac{3}{4} Q^2 + \sqrt{1 + \frac{3}{2} Q^2 \cos 2\phi + \frac{9}{16} Q^4} \right]^{\frac{1}{2}} \quad (6.23)$$

* ASME Boiler and Pressure Vessel Code, Section III, Code Case N-47-12, American Society of Mechanical Engineers, New York, 1980.

**FIGURE 6-49**

Variation of SEQA Effective Stress with the τ / σ Ratio and the Phase Angle Between τ and σ

where σ = bending - stress amplitude including any stress - concentration effects

$$Q = 2 \frac{\tau}{\sigma}$$

τ = torsional - stress amplitude including any stress - concentration effects

ϕ = phase angle between bending and torsion

The SEQA can be computed for both mean and alternating components of stress.

Figure 6-49 shows the variation of the SEQA effective stress, expressed as a ratio to the von Mises stress for the same bending-torsion combination as a function of two variables: the phase angle ϕ and the ratio τ/σ . Note in Figure 6-49a that when the bending and torsion are either in-phase, or 180° out-of-phase, the SEQA equals the von Mises stress σ' . At $\phi = 90^\circ$, the SEQA is about 73% of σ' . The SEQA stress also varies with the relative values of τ and σ as shown in Figure 6-49b. When $\tau / \sigma = 0.575$ ($Q = 1.15$), the reduction in SEQA stress at $\phi = 90^\circ$ is maximal and it approaches σ' for large and small τ/σ ratios. This figure indicates that using the von Mises stress for combined bending and torsion fatigue gives a conservative result at any phase angle or τ/σ ratio. However, Garud has shown that this approach will be nonconservative for out-of-phase

loading if the local strain is above about 0.13%.^[44] Thus, this approach is not recommended for low-cycle fatigue situations. Tipton and Nelson^[50] show that the SEQA approach is conservative for out-of-phase high-cycle fatigue (low-strain) applications. In fact, when the stress-concentration factors K_f and K_{fs} for the notch were set to 1, the SEQA and similar approaches* gave reasonably accurate predictions of HCF failure.^[50]

The complex multiaxial fatigue analysis method presented above assumes that the applied loads are synchronous with a predictable phase relationship. If the sources of the multiple loads are decoupled and have a random or unknown time-phase relationship, then this method may not be sufficient to solve the problem. The reader should consult the literature as described in the bibliography to this chapter for more information on complex multiaxial loading cases. The best approach for unusual situations is a testing program of your own.

6.13 A GENERAL APPROACH TO HIGH-CYCLE FATIGUE DESIGN

The previous sections and examples have used a consistent approach regardless of the category of fatigue loading involved (see Figure 6-40 on p. 353). Even in the uniaxial stress cases, the von Mises stress was calculated for the alternating and mean stresses. It could be argued that this step is unnecessary with uniaxial stress, since the von Mises stress will be identical to the applied stress. Nevertheless, for a slight additional computational burden (which is irrelevant if using a computer), we gain the advantage of consistency. In addition, the appropriate individual stress-concentration factors can be applied to the various stress components before incorporating them into the von Mises stress calculation. Frequently, the geometric stress-concentration factors for the same contour on a part will vary for different loadings (axial versus bending, etc.).

Whether the loading is uniaxial or multiaxial, bending or torsion, or any combination thereof, the safety factor with this approach is found in the same manner, comparing some combination of alternating and mean von Mises stresses to a line defined by the fatigue tensile strength and a static tensile strength of the material. This eliminates the need for computing separate torsional fatigue strengths. If you accept the approach outlined in the previous section for multiaxial loadings with stress concentrations, namely using the von Mises stress for both mean and alternating stress components, the difference between uniaxial and multiaxial cases disappears. The same computational algorithm then can apply to all four categories of Figure 6-40 on p. 353.

In respect to the difference between fluctuating and fully reversed loading modes, recall that the latter is just a special case of the former. We can treat all fatigue-loading cases as fluctuating and consistently apply the modified-Goodman diagram (MGD) criteria of failure with good results. Note in Figure 6-43 (p. 362) that the MGD and the *S-N* diagram are simply different views of the same three-dimensional relationship between mean stress σ'_m , alternating stress σ'_a , and number of cycles N . Figure 6-43c shows the Goodman section taken through the 3-D surface that relates the variables. A fully reversed stress state ($\sigma'_a \neq 0, \sigma'_m = 0$) can be plotted on a Goodman diagram and its safety factor calculated easily when you realize that the resulting data point will be on the σ'_a axis. Equation 6.18b gives its safety factor and is the same as equation 6.14 (p. 354) when $\sigma'_m = 0$. For that matter, a static loading problem ($\sigma'_m \neq 0, \sigma'_a = 0$) can also be plotted on the MGD and its data point will fall on the σ'_m axis. Its safety fac-

* A similar method based on the maximum shear-stress theory is also defined in reference [50]. This method, called SALT, gives similar but even more conservative results for HCF than those shown for the SEQA method in Figure 6-49. The caveats regarding its application only to HCF loading apply, though it gives better correlation to experimental results of low-cycle, strain-based multiaxial fatigue tests than does the SEQA method.^[44]

tor can be calculated from equation 6.18a (p. 367), which is identical to equation 5.8a (p. 251) when $\sigma'_a = 0$. Thus, the modified-Goodman diagram provides a universal tool to determine a safety factor for any stress problem, whether static, fully reversed fatigue, or fluctuating fatigue.

The recommended general approach to HCF design with uniaxial or synchronous multiaxial stresses is then:

- 1 Generate a suitable modified-Goodman diagram from tensile strength information for the particular material. This can be done for any desired finite life or for infinite life by taking the Goodman section at a different point N_2 along the N axis in Figure 6-42 (p. 361). This is automatically accomplished by the choice of S_f at some number of cycles N_2 as shown in Figure 6-33 (p. 337) and equation 6.10 (p. 338). Apply the appropriate strength-reduction factors from equations 6.7 (pp. 330–335) to obtain a corrected fatigue strength.
- 2 Calculate the alternating and mean components of the applied stresses at all points of interest in the part and apply the appropriate stress-concentration factor to each applied stress component. (See Example 4-9 and the summary section of Chapter 4.)
- 3 Convert the alternating and mean components of the applied stresses at any point of interest in the loaded part to alternating and mean von Mises effective stresses using equations 6.22 (p. 379).
- 4 Plot the alternating and mean von Mises stresses on the modified-Goodman diagram and determine the appropriate safety factor from equations 6.18 (pp. 367–368).

Recall from the discussion of static failure theories in Chapter 5 that the von Mises approach was recommended only for use with ductile materials, as it accurately predicts yielding in the static loading case where shear is the failure mechanism. Here we are using it for a slightly different purpose, namely to combine the multiaxial mean and alternating applied stresses into effective (pseudo-uniaxial) mean and alternating tensile stresses that can be compared with tensile fatigue and static strengths on a modified-Goodman diagram. As such, the von Mises approach can be used for both ductile and brittle materials in HCF fatigue loading, since the (correct) assumption is that fatigue failures are tensile failures regardless of the ductility or brittleness of the material. In fact, it was long thought that ductile materials had somehow become embrittled under prolonged fatigue loading because their failure surfaces look like those of a statically failed brittle material. However, this is now known to be untrue.

The designer should nevertheless be cautioned about using cast-brittle materials in fatigue-loaded situations because their tensile strengths tend to be lower than equivalent-density wrought materials, and it is more likely that they will contain stress raisers within the material from the casting process. Many successful applications of castings under fatigue loading can be cited, such as IC engine crankshafts, camshafts, and connecting rods. These applications tend to be in smaller-size, low-power engines for lawn mowers, etc. Higher-powered automotive and truck engines will usually use (ductile) forged steel or nodular (ductile) cast iron rather than (brittle) gray cast iron for crankshafts and connecting rods, for example.

We now present an example of simple multiaxial fatigue using the same bracket that was investigated in Examples 4-9 and 5-1. This time the load is fluctuating with time.

EXAMPLE 6-6**Multiaxial Fluctuating Stresses****Problem**

Determine the safety factors for the bracket tube shown in Figure 5-9 (repeated on next page).

Given

The material is 2024-T4 aluminum with $S_y = 47\,000$ psi, and $S_{ut} = 68\,000$ psi. The tube length $l = 6$ in and arm $a = 8$ in. The tube outside diameter $OD = 2$ in and inside diameter $ID = 1.5$ in. The applied load varies sinusoidally from $F = 340$ to -200 lb.

Assumptions

The load is dynamic and the assembly is at room temperature. Consider shear due to transverse loading as well as other stresses. A finite-life design will be sought with a life of 6E7 cycles. The notch radius at the wall is 0.25 in and stress-concentration factors are for bending, $K_t = 1.7$, and for shear, $K_{ts} = 1.35$.

Solution

See Figure 5-9, repeated here. Also see Example 4-9 (p. 180) for a more complete explanation of the stress analysis for this problem.

- 1 Aluminum does not have an endurance limit. Its endurance strength at 5E8 cycles can be estimated from equation 6.5c (p. 330). Since the S_{ut} is larger than 48 kpsi, the uncorrected $S_f @ 5E8 = 19$ kpsi.
- 2 The correction factors are calculated from equations 6.7 (pp. 330–335) and Figure 6-25 (p. 332) and used to find a corrected endurance strength at the standard 5E8 cycles.

$$C_{load} = 1 : \text{ for bending}$$

$$C_{size} = 0.869 \left(d_{equiv} \right)^{-0.097} = 0.869 \left(\sqrt{\frac{0.01046d^2}{0.0766}} \right)^{-0.097} = 0.869(0.739)^{-0.097} = 0.895$$

$$C_{surf} = 2.7(S_{ut})^{-0.265} = 2.7(68)^{-0.265} = 0.883 \quad (a)$$

$$C_{temp} = 1$$

$$C_{reliab} = 0.753 : \text{ for 99.9\%}$$

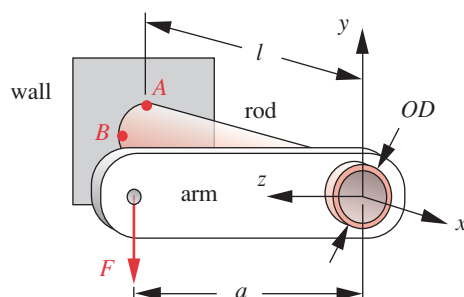


FIGURE 5-9 Repeated

Bracket for Example 6-6

$$\begin{aligned} S_{f@5e8} &= C_{load} C_{size} C_{surf} C_{temp} C_{reliab} S_f \\ &= (1)(0.895)(0.883)(1)(0.753)19\,000 = 11\,299 \text{ psi} \end{aligned} \quad (b)$$

Note that the bending value of C_{load} is used despite the fact that both bending and torsion are present. The torsional shear stress will be converted to an equivalent tensile stress with the von Mises calculation. C_{surf} is calculated from equation 6.7e (p. 333) using data from Table 6-3 (p. 333). This corrected fatigue strength is still at the tested number of cycles, $N = 5E8$.

- 3 This problem calls for a life of $6E7$ cycles, so a strength value at that life must be estimated from the $S-N$ line of Figure 6-33b (p. 337) using the corrected fatigue strength at that life. Equation 6.10a (p. 338) for this line can be solved for the desired strength after we compute the values of its coefficient a and exponent b from equation 6.10c (p. 338).

6

$$b = \frac{1}{z} \log \left(\frac{S_m}{S_f} \right) = \frac{1}{-5.699} \log \left[\frac{0.9(68\,000)}{11\,299} \right] = -0.1287$$

$$\log(a) = \log(S_m) - 3b = \log[0.9(68\,000)] - 3(-0.1287) : \quad a = 148\,929 \quad (c)$$

$$S_n = aN^b = 148\,929 N^{-0.1287} = 148\,929(6e7)^{-0.1287} = 14\,846 \text{ psi}$$

Note that S_m is calculated as 90% of S_{ut} because the loading is bending rather than axial (Eq. 6.9, p. 337). The value of z is taken from Table 6-5 (p. 338) for $N = 5E8$ cycles. This is a corrected fatigue strength for the shorter life required in this case and so is larger than the corrected test value, which was calculated at a longer life.

- 4 The notch sensitivity of the material must be found to calculate the fatigue stress-concentration factors. Table 6-8 (p. 347) shows the Neuber factors for hardened aluminum. Interpolation gives a value of 0.147 for \sqrt{a} at the material's S_{ut} . Equation 6.13 (p. 345) gives the resulting notch sensitivity for an assumed notch radius of 0.25 in.

$$q = \frac{1}{1 + \frac{\sqrt{a}}{\sqrt{r}}} = \frac{1}{1 + \frac{0.147}{\sqrt{0.25}}} = 0.773 \quad (d)$$

- 5 The fatigue stress-concentration factors are found from equation 6.11b (p. 343) using the given geometric stress-concentration factors for bending and torsion, respectively.

$$K_f = 1 + q(K_t - 1) = 1 + 0.773(1.7 - 1) = 1.541 \quad (e)$$

$$K_{fs} = 1 + q(K_{ts} - 1) = 1 + 0.773(1.35 - 1) = 1.270 \quad (f)$$

- 6 The bracket tube is loaded both in bending (as a cantilever beam) and in torsion. The shapes of the shear, moment, and torque distributions are shown in Figure 4-31 (p. 183). All are maximum at the wall. The alternating and mean components of the applied force, moment, and torque at the wall are

$$\begin{aligned} F_a &= \frac{F_{max} - F_{min}}{2} = \frac{340 - (-200)}{2} = 270 \text{ lb} \\ F_m &= \frac{F_{max} + F_{min}}{2} = \frac{340 + (-200)}{2} = 70 \text{ lb} \end{aligned} \quad (g)$$

$$M_a = F_a l = 270(6) = 1620 \text{ lb-in} \quad (h)$$

$$M_m = F_m l = 70(6) = 420 \text{ lb-in}$$

$$T_a = F_a a = 270(8) = 2160 \text{ lb-in} \quad (i)$$

$$T_m = F_m a = 70(8) = 560 \text{ lb-in}$$

- 7 The fatigue stress-concentration factor for the mean stresses depends on the relationship between the maximum local von Mises stress in the notch and the yield strength as defined in equation 6.17, a portion of which is shown here.

6

$$\text{if } K_f |\sigma_{\max}| < S_y \text{ then} \quad K_{fm} = K_f, \quad K_{fsm} = K_{fs}$$

$$\sigma_{\max} = K_f \left| \frac{M_{max}c}{I} \right| = K_f \left| \frac{F_{max}l c}{I} \right| = 1.541 \left| \frac{340(6)(1)}{0.5369} \right| = 5855$$

$$\tau_{\max} = K_{fs} \left| \frac{T_{max}r}{J} \right| = K_{fs} \left| \frac{F_{max}ar}{J} \right| = 1.270 \left| \frac{340(8)(1)}{1.074} \right| = 3216 \quad (j)$$

$$\sigma'_{\max} = \sqrt{5855^2 + (3)3216^2} = 8081 < 47000$$

$$\therefore K_{fm} = K_f = 1.541, \quad K_{fsm} = K_{fs} = 1.270$$

In this case, there is no reduction in stress-concentration factors for the mean stress because there is no yielding at the notch to relieve the stress concentration.

- 8 The largest tensile bending stress will be in the top or bottom outer fiber at points A or A'. The largest torsional shear stress will be all around the outer circumference of the tube. (See Example 4-9 on p. 180 for more details.) First take a differential element at point A or A' where both of these stresses combine. (See Figure 4-32 on p. 184.) Find the alternating and mean components of the normal bending stress and of the torsional shear stress on point A using equations 4.11b (p. 156) and 4.23b (p. 178), respectively.

$$\sigma_a = K_f \frac{M_{aC}}{I} = 1.541 \frac{1620(1)}{0.5369} = 4649 \text{ psi} \quad (k)$$

$$\tau_{a_{torsion}} = K_{fs} \frac{T_ar}{J} = 1.270 \frac{2160(1)}{1.074} = 2556 \text{ psi}$$

$$\sigma_m = K_{fm} \frac{M_{mC}}{I} = 1.541 \frac{420(1)}{0.5369} = 1205 \text{ psi} \quad (l)$$

$$\tau_{m_{torsion}} = K_{fsm} \frac{T_mr}{J} = 1.270 \frac{560(1)}{1.074} = 663 \text{ psi}$$

- 9 Find the alternating and mean von Mises stresses at point A (Eq. 6.22b, p. 379).

$$\begin{aligned} \sigma'_a &= \sqrt{\sigma_{x_a}^2 + \sigma_{y_a}^2 - \sigma_{x_a}\sigma_{y_a} + 3\tau_{xy_a}^2} \\ &= \sqrt{4649^2 + 0^2 - 4649(0) + 3(2556)^2} = 6419 \text{ psi} \end{aligned} \quad (m)$$

$$\begin{aligned} \sigma'_m &= \sqrt{\sigma_{x_m}^2 + \sigma_{y_m}^2 - \sigma_{x_m}\sigma_{y_m} + 3\tau_{xy_m}^2} \\ &= \sqrt{1205^2 + 0^2 - 1205(0) + 3(663)^2} = 1664 \text{ psi} \end{aligned}$$

- 10 Because the moment and torque are both caused by the same applied force, they are synchronous and in-phase and any changes in them will be in a constant ratio. This is a Case 3 situation and the safety factor is found using equation 6.18e (p. 368).

$$N_f = \frac{S_f S_{ut}}{\sigma'_a S_{ut} + \sigma'_m S_f} = \frac{14\ 846(68\ 000)}{6\ 419(68\ 000) + 1\ 664(14\ 846)} = 2.2 \quad (n)$$

- 11 Since the tube is a short beam, we need to check the shear due to transverse loading at point *B* on the neutral axis where the torsional shear is also maximal. The maximum transverse shear stress at the neutral axis of a hollow, thin-walled, round tube was given as equation 4.15d (p. 161).

$$\tau_{a_{transverse}} = K_{fs} \frac{2V_a}{A} = 1.270 \frac{2(270)}{1.374} = 499 \text{ psi} \quad (o)$$

$$\tau_{m_{transverse}} = K_{fsm} \frac{2V_m}{A} = 1.270 \frac{2(70)}{1.374} = 129 \text{ psi}$$

Point *B* is in pure shear. The total shear stress at point *B* is the sum of the transverse shear stress and torsional shear stress which act on the same planes of the element.

$$\begin{aligned} \tau_{a_{total}} &= \tau_{a_{transverse}} + \tau_{a_{torsion}} = 499 + 2\ 556 = 3\ 055 \text{ psi} \\ \tau_{m_{total}} &= \tau_{m_{transverse}} + \tau_{m_{torsion}} = 129 + 663 = 792 \text{ psi} \end{aligned} \quad (p)$$

- 12 Find the alternating and mean von Mises stresses for point *B* (Eq. 6.22b, p. 379).

$$\sigma' = \sqrt{\sigma_{x_a}^2 + \sigma_{y_a}^2 - \sigma_{x_a} \sigma_{y_a} + 3\tau_{xy_a}^2} = \sqrt{0 + 0 - 0 + 3(3\ 055)^2} = 5\ 291 \text{ psi} \quad (q)$$

$$\sigma' = \sqrt{\sigma_{x_m}^2 + \sigma_{y_m}^2 - \sigma_{x_m} \sigma_{y_m} + 3\tau_{xy_m}^2} = \sqrt{0 + 0 - 0 + 3(792)^2} = 1\ 372 \text{ psi}$$

- 13 The safety factor for point *B* is found using equation 6.18e (p. 368).

$$N_f = \frac{S_f S_{ut}}{\sigma'_a S_{ut} + \sigma'_m S_f} = \frac{14\ 846(68\ 000)}{5\ 291(68\ 000) + 1\ 372(14\ 846)} = 2.7 \quad (r)$$

Both points *A* and *B* are safe against fatigue failure.

- 14 The files EX06-06A and EX06-06B can be found on the CD-ROM.
-

6.14 A CASE STUDY IN FATIGUE DESIGN

The following case study contains all the elements of an HCF fatigue design problem. It is an actual design problem from the author's consulting experience and serves to illustrate many of the points of this chapter. While it is long and fairly complicated, its careful study will repay the time invested.

CASE STUDY 6**Redesign of a Failed Laybar for a Water-Jet Power Loom****Problem**

The laybars in a number of water-jet looms have begun to fail in fatigue. The owner of the weaving works had increased the speed of the looms to boost production. The original design of a painted steel laybar had lasted with no failures for 5 years of 3-shift operation at the lower speed but began failing within months of the speed increase. The owner had a local machine shop make painted steel replacements similar to the original and these failed in six months of use. The owner substituted an aluminum replacement laybar of his own design, which lasted 3 months. He then sought engineering assistance. Analyze the failures of the three existing designs and redesign the part to last for an additional 5 years at the higher speed.

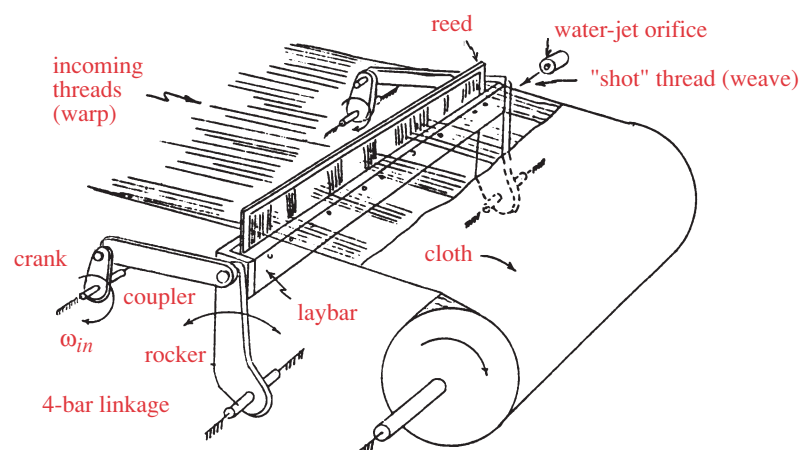
Given

The laybar is 54 in long and is carried between the rockers of two identical Grashof crank-rocker fourbar linkages that are driven synchronous and in-phase by gear trains connected through a 54-in-long transmission shaft. The loom arrangement is shown in Figure 6-50 and the linkage is shown in Figure 6-51. Details of its operation are discussed below. Cross sections of the failed designs are shown in Figure 6-53 and photographs in Figure 6-54. The new design cannot be any wider than the widest existing one (2.5 in). The original loom speed was 400 rpm and the new speed is 500 rpm. The cost of a new design should be competitive with the cost of current (failed) designs (about \$300 each in lots of 50).

Assumptions

The major fluctuating loading on the part is inertial and occurs because its own mass plus that of the reed carried on it are being accelerated and decelerated by the linkage motion. There is also a "beat-up" force on the reed when it strikes the cloth to push the latest weave thread into place. This force causes a repeated torque on the laybar that may or may not be significant in the failure. The magnitude of the beat-up force is not accurately known and will vary

6

**FIGURE 6-50**

Warp, Weave, Laybar, Reed, and Laybar Drive for a Water-Jet Loom

with the weight of the cloth being woven. It is estimated to be 10 lb/in of cloth width (540-lb total). The environment is wet with fresh water and all failed specimens show evidence of corrosion.

Solution

See Figures 6-50 to 6-56 and Table 6-13 (p. 398).

- 1 Some additional background information is needed to understand the problem before pursuing its solution. Weaving looms for the making of cloth are very old devices and were originally human-powered. The power loom was invented during the industrial revolution and presently exists in many forms. Figure 6-50 shows parts of the water-jet power loom of concern here. Perhaps the best way to understand a loom's fundamental operation is to consider a hand-powered one, which the reader may have seen in a museum, a custom-weaving shop, or a hobbyist's workroom. Its basic elements are similar to some of those in the figure.

A set of threads called the *warp* is strung across the loom. Each thread is grabbed by a device (not shown) that can pull it up or down. These devices are activated by a mechanism that, in a hand-loom, is typically operated by foot pedals. When one pedal is pushed, every other warp thread is raised up and the alternate ones pulled down to create a "tunnel" if observed from the edge of the cloth. This tunnel is called the *shed*. A *shuttle*, which looks like a miniature canoe, and contains a bobbin of thread within it, is next "thrown" through the shed by the weaver's hand. The shuttle trails a single thread called the *weave* through the warp shed. The weaver then pulls on the *laybar*, which carries a comblike device called a *reed*. The warp threads are strung through the teeth of this reed-comb. The reed pushes the new weave thread sideways into the previous ones to "beat-up" the cloth and create a tight weave. The weaver next switches pedals on the shed and the "up" threads of the warp become the "down" threads and vice versa, creating a new tunnel (shed) of crossed threads. The shuttle is again thrown through the warp (from the other side), weaving another thread to be beat-up by the reed.

The original power looms simply mechanized the manual process, replacing the weaver's hands and feet with linkages and gears. The throwing of the wooden shuttle was accomplished by literally hitting it with a stick, flying it through the shed and

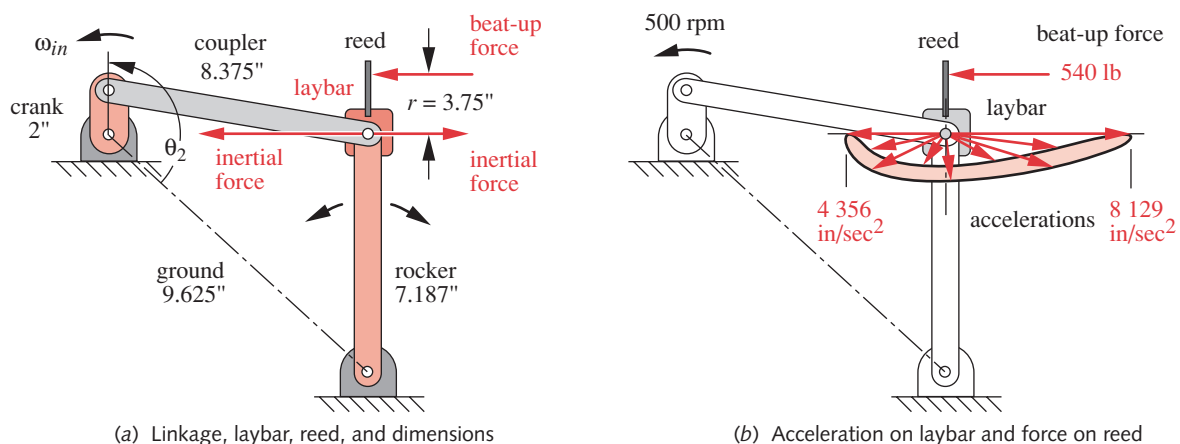


FIGURE 6-51

Fourbar Linkage for Laybar Drive, Showing Forces and Accelerations on Laybar

catching it on the other side. The dynamics of this (pre-NASA) "shuttle flight" became the limiting factor on the loom's speed. Shuttle looms can only go at about 100 picks (threads) per minute (ppm). Much effort was expended to develop faster looms, and these usually involved eliminating the shuttle, whose mass limited the speed. Both air-jet and water-jet looms were developed in the 20th century that shoot the weave thread across the shed on a jet of air or water. Figure 6-50 shows the orifice through which the thread is fed. At the right time in the cycle, a small piston pump shoots a jet of water through the orifice and surface tension pulls the thread across the shed. The water-jet loom can operate at up to about 500 ppm. The looms in question were designed to operate at 400 ppm but the owner changed their gearing to increase the speed to 500 ppm. Failures soon ensued because the dynamic loads increased with the square of the speed and exceeded the loads for which the machine was designed.

- 2 Figures 6-50 and 6-51 show the laybar, which is carried between two identical four-bar linkages that move it in an arc to push the reed into the cloth at the right point in the cycle. The laybar is bolted securely to the linkage rockers at each end and rotates with them. The linkage pivots are in self-aligning ball-bearings, which allow us to model the laybar as a simply supported beam that carries a uniformly distributed load that is equal to its total mass times its acceleration plus the beat-up force. The total mass is the sum of the laybar mass and the mass of its 10-lb payload, the reed. Figure 6-51 shows the laybar-linkage geometry, its dimensions, and a polar plot of the acceleration vectors at the mass-center of the laybar. The tangential components of acceleration are the largest and create bending moments in the directions of the inertial forces shown in the same figure. Figure 6-52 plots the tangential acceleration component of the laybar mass-center for 1 cycle and shows the beat-up force in its phase relationship with acceleration. The acceleration creates a fluctuating bending moment, and the beat-up force, being offset 3.75 in from the mass center of the laybar, creates a repeated torque on the laybar. Depending on the laybar's cross-sectional geometry, this combination of loads can create a case of synchronous, in-phase, *simple multiaxial stress* at locations of maximum stress (see Section 6.12 on p. 376). Because the loading is largely inertial, the design of the laybar should minimize its mass (to reduce the inertial loading) while simultaneously maximizing its stiffness and strength. These are conflicting constraints, making the design task more challenging.
- 3 Since this is a case of fluctuating loading, we will follow the set of design steps recommended in Section 6.11 (p. 360), the first of which is to determine the number of loading cycles expected over the service life. The owner has requested that the new design last for 5 years of 3-shift operation. Assuming 2 080 hours per shift in a standard work-year, this amounts to

$$N = 500 \frac{\text{cycles}}{\text{min}} \left(\frac{60 \text{ min}}{\text{hr}} \right) \left(\frac{2 080 \text{ hr}}{\text{yr}} \right) (3 \text{ shifts})(5 \text{ yr}) = 9.4E8 \text{ cycles} \quad (a)$$

This is clearly in the HCF regime and could benefit from the use of a material with an endurance limit.

The owner reports that his steel replacement laybar lasted about 6 months and his aluminum design lasted 3 months. (See Figures 6-53 and 6-54.) The cycle lives are:

$$6 \text{ mos : } N = 500 \frac{\text{cycles}}{\text{min}} \left(\frac{60 \text{ min}}{\text{hr}} \right) \left(\frac{2 080 \text{ hr}}{\text{yr}} \right) (3 \text{ shifts})(0.5 \text{ yr}) = 9.4E7 \text{ cycles} \quad (b)$$

$$3 \text{ mos : } N = 500 \frac{\text{cycles}}{\text{min}} \left(\frac{60 \text{ min}}{\text{hr}} \right) \left(\frac{2 080 \text{ hr}}{\text{yr}} \right) (3 \text{ shifts})(0.25 \text{ yr}) = 4.7E7 \text{ cycles}$$

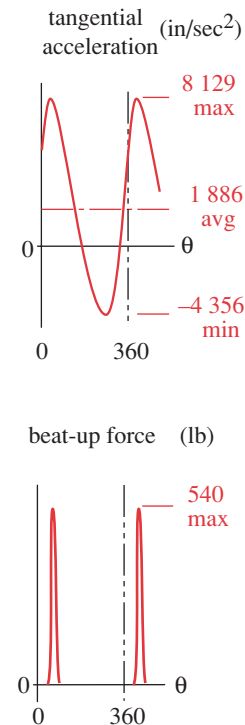
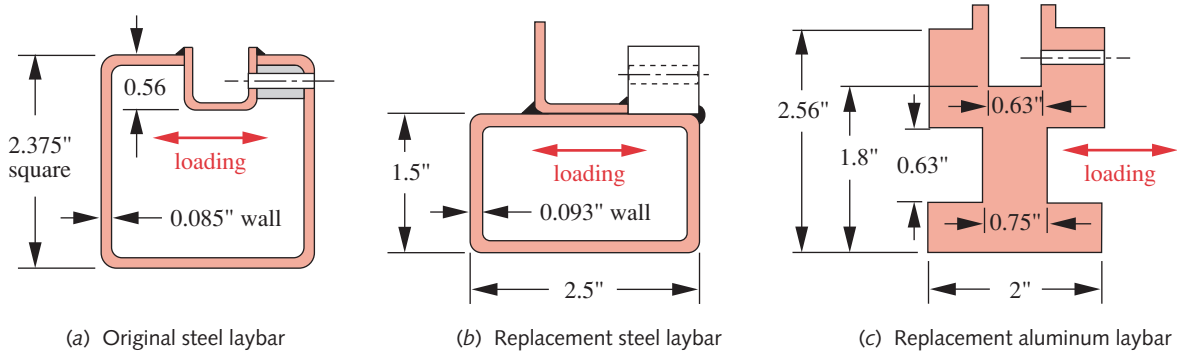


FIGURE 6-52

Time-Varying Acceleration and Load on the Laybar at 500 rpm
Showing Their Phase Relationship

**FIGURE 6-53**

Existing Laybar Designs, All of Which Failed in Fatigue

6

- 4 Since the amplitudes of the applied bending loads are a function of acceleration (which is determined) and the mass of the part (which will vary with the design), it is best to express the bending loads in terms of $F = ma$. The applied torque is assumed to be the same for any design based on the owner's estimate of a typical beat-up force. These data are shown in Figure 6-52 and the mean and alternating terms are

$$F_{mean} = ma_{mean} = m \frac{a_{max} + a_{min}}{2} = m \frac{8129 + (-4356)}{2} = 1886.5m$$

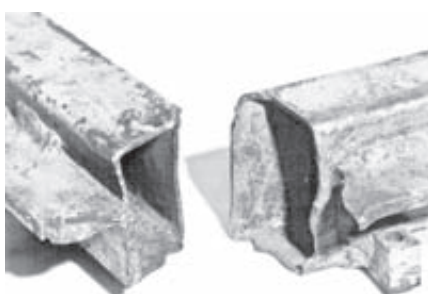
Bending :

$$F_{alt} = ma_{alt} = m \frac{a_{max} - a_{min}}{2} = m \frac{8129 - (-4356)}{2} = 6242.5m$$

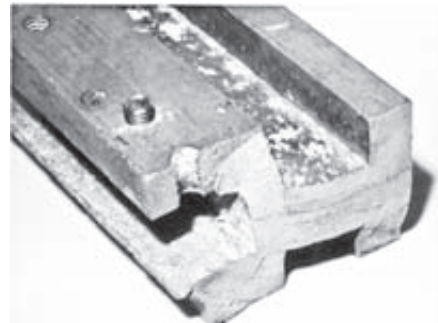
$$T_{mean} = \left(\frac{F_{beat_{max}} + F_{beat_{min}}}{2} \right) r = \left(\frac{540 + 0}{2} \right) 3.75 = 1012.5 \text{ lb-in}$$

Torque :

$$T_{alt} = \left(\frac{F_{beat_{max}} - F_{beat_{min}}}{2} \right) r = \left(\frac{540 - 0}{2} \right) 3.75 = 1012.5 \text{ lb-in}$$



(a)



(b)

FIGURE 6-54

Photographs of Failed Laybars (a) Replacement steel laybar — after 6 mos, (b) Replacement aluminum laybar — after 3 mos.

- 5 We are in the enviable position of having test data for typical parts run under actual service conditions available in the form of the failed specimens. In effect, the owner had inadvertently run a test program (to his chagrin) and had determined stress levels that caused failure in this application. Thus the first step will be to analyze the existing failed designs in order to learn more about the problem. We know that laybars of the original design (Figure 6-53a) survived for 5 years at the lower stress levels associated with 400-rpm operation. They only began to fail when he increased the speed, which increased the inertial loading.

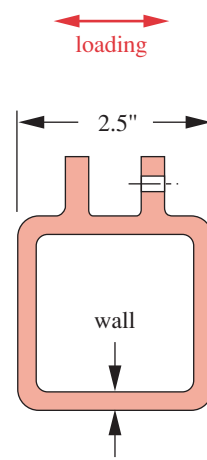
There are many factors involved in this application that are difficult to quantify. Corrosion is evident on the failed parts. The steel laybars are rusted with pitted surfaces. The unanodized aluminum part is also pitted. The designer(s) did not take great care to minimize stress concentrations, and the fatigue fractures can be seen to have started (as is typical) at stress-raiser. The failed aluminum part in Figure 6-54b shows that the crack started at a tapped hole, which is a very sharp notch. The cracks in the steel part (Figure 6-54b) appear to have started at a weld bead used to attach the reed supports. Welds are notorious stress-raiser and always leave tensile residual stresses behind. We should take these lessons into account in our redesign and attempt to reduce these negative factors. **By definition, a failed part has a safety factor of 1.** Knowing this, a model of the part's loading, stresses, and safety factor can be created and then *back-calculated with the safety factor set to 1* in order to determine various of the above factors that are difficult to quantify for a particular application.

- 6 A model was created to solve the equations for this case. Data specific to each of the three failed designs were input and the model modified as necessary to account for differences in geometry and material among the three designs. The same model was further modified to accommodate the proposed new designs shown in Figure 6-55. Eight versions of the model resulted, and their data files are included with this text. They are labeled CASE6-0 through CASE6-7. Space does not permit discussion of the contents of all eight models, so only two will be discussed in detail, and the results of the others will be compared in summary. The failed original design and the final new design will be presented. The reader may open the models in the program of his choice if desired.
- 7 The analysis of the original laybar design is contained in CASE6-1. The section geometry and the beam mass must be calculated to determine the bending stresses.

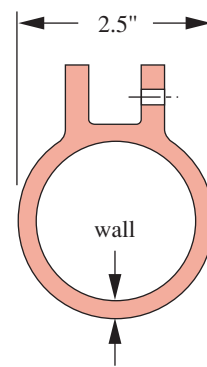
$$\begin{aligned} \text{area} &= 2.375^2 - 2.205^2 + 2(0.56)(0.085) = 0.874 \text{ in}^2 \\ \text{weight} &= \text{area}(\text{length})(\gamma) = 0.874(54)(0.286) = 13.5 \text{ lb} \\ m &= \frac{\text{weight} + \text{reed}}{386.4} = \frac{13.5 + 10}{386.4} = 0.061 \text{ blobs} \\ I &= \frac{b_{out}h_{out}^3 - b_{in}h_{in}^3}{12} = \frac{2.375^4 - 2.205^4}{12} = 0.68 \text{ in}^4 \end{aligned} \quad (e)$$

Note that the area calculation includes the reed-trough sides, since they add mass but the calculation for I ignores them since they add a negligible amount to that quantity. The specific weight γ is for steel and the mass unit is blobs or $\text{lb}\cdot\text{sec}^2/\text{in}$.

- 8 The nominal mean and alternating components of the inertial force and bending moment can now be calculated.



(a) Square design



(b) Round design

FIGURE 6-55

Two New Designs for the Water-Jet Laybar

$$F_{mean} = 1886.5m = 1886.5(0.061) = 115 \text{ lb}$$

$$F_{alt} = 6242.5m = 6242.5(0.061) = 380 \text{ lb}$$

(f)

$$M_{mean} = \frac{wl^2}{8} = \frac{(wl)l}{8} = \frac{Fl}{8} = \frac{115(54)}{8} = 775 \text{ lb-in}$$

$$M_{alt} = \frac{wl^2}{8} = \frac{(wl)l}{8} = \frac{Fl}{8} = \frac{380(54)}{8} = 2565 \text{ lb-in}$$

The moment equations are for the maximum moment in the center of a simply supported beam with uniformly distributed load (see Figure B-2 in Appendix B). The nominal bending stresses (not including any stress concentration) are then

$$\sigma_{m_{nom}} = \frac{M_{mean}(c)}{I} = \frac{775(1.188)}{0.68} = 1351 \text{ psi}$$

$$\sigma_{a_{nom}} = \frac{M_{alt}(c)}{I} = \frac{2565(1.188)}{0.68} = 4470 \text{ psi}$$
6
(g)

- 9 The nominal shear stresses due to torsion in a hollow-square section are maximum in the centers of the four sides and so occur at points of maximum bending stress. The shear stress is found from $\tau_{max} = T/Q$ (Eq. 4.26a, p. 178) where Q for the particular geometry is found in Table 4-2 (p. 172):

$$Q = 2t(a-t)^2 = 2(0.085)\left(\frac{2.375}{2} - 0.085\right)^2 = 0.207 \text{ in}^3$$
(h)

where t is the wall thickness and a is the half-width of the cross section. The nominal mean and alternating shear stresses are then

$$\tau_{m_{nom}} = \frac{T_{mean}}{Q} = \frac{1012.5}{0.207} = 4900 \text{ psi}$$

$$\tau_{a_{nom}} = \frac{T_{alt}}{Q} = \frac{1012.5}{0.207} = 4900 \text{ psi}$$
(i)

- 10 The stress-concentration factors for bending and shear need to be found or estimated. Peterson^[30] provides a chart for the case of a hollow, rectangular section in torsion, and from that a $K_{ts} = 1.08$ is found. No suitable data were found for the bending stress-concentration factor for this case. The corrosion and pitting in combination with rough welds would predict a large K_t . The approach taken here was to backsolve for K_t with the safety factor set to 1 and all other material factors and the nominal stresses specified. The result was $K_t = 4.56$ in this failed part. This result is presented at this point to provide continuity of narrative, but it must be understood that the value of K_t was found by *back-solving* the model using iteration after all other factors were defined. The local alternating and mean stresses and K_t were then solved for simultaneously with $N_f = 1$, representing a failure condition.
- 11 The material's notch sensitivity and the estimated fatigue stress-concentration factors for alternating bending and shear are found from equations 6.11b and 6.13 (p. 343) following the procedure used in Example 6-3 (p. 346). Using the value of K_t found in step 10 and $q = 0.8$, the results are: $K_f = 3.86$, and $K_{fs} = 1.06$. The corresponding fatigue stress-concentration factors for the mean stress are found from equation 6.17 (p. 364) and since the local stress is below the yield point for both bending and torsion in this case, they are identical to the factors for the alternating stress: $K_{fm} = K_f$, and $K_{fms} = K_f$.

- 12 The estimated local-stress components can now be found using the fatigue stress-concentration factors:

$$\begin{aligned}\sigma_m &= K_{fm} \sigma_{m_{nom}} = 3.86(1\,351) = 5\,212 \text{ psi} \\ \sigma_a &= K_f \sigma_{a_{nom}} = 3.86(4\,470) = 17\,247 \text{ psi}\end{aligned}\quad (j)$$

$$\begin{aligned}\tau_m &= K_{fsm} \tau_{m_{nom}} = 1.06(4\,900) = 5\,214 \text{ psi} \\ \tau_a &= K_{fsm} \tau_{a_{nom}} = 1.06(4\,900) = 5\,214 \text{ psi}\end{aligned}\quad (k)$$

- 13 Since we have a case of combined, fluctuating, biaxial stresses that are synchronous and in-phase, and that have stress concentration, the general method using von Mises effective stresses for both mean and alternating components is appropriate (equation 6.22b). These calculate equivalent alternating and mean stresses for the biaxial case.

$$\begin{aligned}\sigma'_a &= \sqrt{\sigma_{x_a}^2 + \sigma_{y_a}^2 - \sigma_{x_a} \sigma_{y_a} + 3\tau_{xy_a}^2} \\ &= \sqrt{17\,247 + 0 - 0 + 3(5\,214)} = 19\,468 \text{ psi} \\ \sigma'_m &= \sqrt{\sigma_{x_m}^2 + \sigma_{y_m}^2 - \sigma_{x_m} \sigma_{y_m} + 3\tau_{xy_m}^2} \\ &= \sqrt{5\,212 + 0 - 0 + 3(5\,214)} = 10\,428 \text{ psi}\end{aligned}\quad (l)$$

- 14 The material properties must now be determined. A laboratory test was done on a sample from the failed part, and its chemical composition matched that of an AISI 1018 cold-rolled steel. Strength values for this material were obtained from published data (see Appendix A) and are: $S_{ut} = 64\,000 \text{ psi}$ and $S_y = 50\,000 \text{ psi}$. A shear yield strength was calculated from $S_{ys} = 0.577S_y = 28\,850 \text{ psi}$. An uncorrected endurance limit was taken as $S_e' = 0.5S_{ut} = 32\,000 \text{ psi}$.
- 15 The strength modification factors were found from the equations and data in Section 6.6 (p. 327). The loading is a combination of bending and torsion. However, we have incorporated the torsion stresses into the von Mises equivalent stress, which is a normal stress, so

$$C_{load} = 1 \quad (m)$$

The equivalent-diameter test specimen is found from the 95% stress area using equations 6.7c and 6.7d (p. 331). The size factor is then found from equation 6.7b (p. 331):

$$\begin{aligned}A_{95} &= 0.05bh = 0.05(2.375)^2 = 0.282 \text{ in}^2 \\ d_{equiv} &= \sqrt{\frac{A_{95}}{0.0766}} = 1.92 \text{ in} \\ C_{size} &= 0.869(d_{equiv})^{-0.097} = 0.869(1.92)^{-0.097} = 0.82\end{aligned}\quad (n)$$

The surface factor is found from equation 6.7e (p. 333) and the data in Table 6-3 (p. 333) for machined or cold-drawn surfaces. The material of the laybar appeared to have been originally cold drawn but was corroded. Corrosion could dictate the use of a lower-valued surface factor, but it was decided to allow the geometric stress-concentration factor K_t to account for the effects of pitting in this case as described above, and the machined-surface factor was applied.

$$C_{surf} = A(S_{ut})^b = 2.7(64)^{-0.265} = 0.897 \quad (o)$$

The temperature factor and the reliability factor were both set to 1. The reliability was taken as 50% for this back-calculation in order to place all the uncertainty in the highly-variable stress-concentration factor.

- 16 A corrected endurance limit can now be calculated from

$$\begin{aligned} S_e &= C_{load} C_{size} C_{surf} C_{temp} C_{reliab} S_e \\ S_e &= (1)(0.81)(0.90)(1)(1)(32\,000) = 23\,258 \text{ psi} \end{aligned} \quad (p)$$

- 17 The safety factor is calculated from equation 6.18e (p. 368). Safety-factor case 3 is applicable here since, with inertial loading, the mean and alternating components of bending stress will maintain a constant ratio with changes in speed. Because the minimum beat-up force is always zero, that ratio is also constant regardless of the maximum force.

$$\begin{aligned} N_f &= \frac{S_e S_{ut}}{\sigma'_a S_{ut} + \sigma'_m S_e} \\ &= \frac{23\,258(64\,000)}{19\,468(64\,000) + 10\,428(23\,258)} = 1.0 \end{aligned} \quad (q)$$

The alternating and mean stresses were back-solved and can now be used to plot a modified-Goodman diagram. Since we forced the safety factor to 1 to represent the known failure of this part, the applied stress point σ'_a, σ'_m falls on the Goodman line.

- 18 The above analysis was repeated, changing the operating speed to the original design value of 400 rpm. Using the same stress-concentration factor of 4.56 that was backed out of the failed-part analysis, the safety factor at 400 rpm is 1.3, indicating why the original design survived at the design rpm (file Case6-0).
- 19 The analysis of this and the other failed parts provides some insight into the constraints of the problem and allows a better design to be created. Some of the factors that influenced the new design were the corrosive environment, which makes steel a less desirable material despite its endurance limit. The painted finishes had not protected the now rusty steel parts. The one failed aluminum sample examined also showed significant pitting in only 3 months of use. If aluminum is to be used, an anodized finish should be applied to protect it from oxidation.

Another obvious factor is the role of stress concentration, which appears to be quite high in this part. The presence of welds and tapped holes in regions of high stress clearly contributed to the failures. Any new design should reduce stress concentrations by moving the required screw holes for reed attachment to locations of lower stress. Welds in high-stress regions should be avoided if possible. Surface treatments such as shot peening should be considered in order to provide beneficial compressive residual stresses.

The poorly defined but potentially significant levels of torsional stresses are a concern. The weaving of heavier cloth will provide larger levels of torsional stress. Thus the geometry of any new design should be resistant to torsional stress as well as to bending stress. Finally, a new design should not be much heavier than the existing design since additional mass will cause the higher inertial forces to be transmitted to all other parts of the machine, possibly engendering failures of other parts.

- 20 Because the loading on the beam is primarily inertial in nature and because it carries a fixed-weight payload, there should be an optimum cross section for any design. A beam's resistance to bending is a function of its area moment of inertia I . The inertial loading is an inverse function of its area A . If the cross section were solid, its I would be the largest possible for a given outside dimension but so would its area, mass, and inertial load. If the wall were made paper-thin, its mass would be minimal but so would its I . Both A and I are nonlinear functions of its dimensions. Thus, there must be some particular wall thickness that maximizes the safety factor, all else constant.

With all the above factors in mind, two designs were considered, as shown in Figure 6-55: a square and a round cross section with integral external ears to support the reed. They both share some common features. The contours have generous radii to minimize K_t . (The round section is the ultimate in this regard.) The reed-support ears, which must contain threaded holes, are close to the neutral axis where the bending stress is lower and they are external to the basic geometric structure. There may not need to be any welds if the shape can be extruded as shown. Both are basically closed sections that can resist torques, and the round section is the optimum shape for torsional loading. The square section will have a larger I and will thus resist bending better than a round shape of the same overall dimension.

Two materials were considered, mild steel and aluminum. (Titanium would be ideal in terms of its strength-to-weight ratio (SWR) and endurance limit, but its high cost precludes consideration.) Aluminum (if anodized) has the advantage of better corrosion resistance in water, but steel has the advantage of an endurance limit if protected from corrosion. The overall weight of the new design is of concern. High-strength aluminum has a better SWR than mild steel. (High-strength steel does not show an endurance limit and is notch sensitive as well as expensive.) Aluminum can be custom extruded with integral ears for low tooling cost, thus making a short production run economically feasible. Tooling for a custom cross section in steel would require very large quantities be purchased to amortize the tooling cost. So, a steel design will be limited to stock mill-shapes and will require welding-on of the ears.

- 21 Each of the geometries in Figure 6-55 was designed separately in both steel and aluminum. The wall thickness was varied within each model as a list of values from very thin to nearly solid in order to determine the optimum dimension. The final design chosen was a round section in 6061-T6 extruded aluminum with a wall thickness of 0.5 in. This design will now be discussed, though it must be understood that a great deal of iteration was required to arrive at the result presented here. Space does not permit discussion of all the iterations.
- 22 The previous calculations of *cycle life* (equation *a*, step 3), *acceleration* and *beat-up force* (equations *c* and *d*, step 4) are still applicable. The section properties are

$$\begin{aligned} \text{area} &= \pi \left(\frac{2.5^2 - 1.5^2}{4} \right) + 2(0.5)(0.75) = 3.892 \text{ in}^2 \\ \text{weight} &= \text{area}(\text{length})(\gamma) = 3.892(54)(0.10) = 21 \text{ lb} \\ m &= \frac{\text{weight} + \text{reed}}{386} = \frac{21+10}{386} = 0.080 \text{ blobs} \\ I &= \pi \left(\frac{2.5^4 - 1.5^4}{64} \right) = 1.669 \text{ in}^4 \end{aligned} \quad (r)$$

Note that the area calculation includes the ears since they add mass but the calculation for I ignores them since they add a negligible amount to that quantity. The weight density γ for aluminum is in lb/in³ and the mass unit is blobs or lb-sec²/in.

- 23 The mean and alternating components of the inertial force and bending moment are

$$\begin{aligned} F_{mean} &= 1886.5m = 1886.5(0.08) = 152 \text{ lb} \\ F_{alt} &= 6242.5m = 6242.5(0.08) = 502 \text{ lb} \\ M_{mean} &= \frac{Fl}{8} = \frac{152(54)}{8} = 1023 \text{ lb-in} \\ M_{alt} &= \frac{Fl}{8} = \frac{502(54)}{8} = 3386 \text{ lb-in} \end{aligned} \quad (s)$$

The moment equations are for the maximum moment in the center of a simply supported beam with uniformly distributed load. The nominal bending stresses (not including stress concentration) are then

$$\begin{aligned} \sigma_{m_{nom}} &= \frac{M_{mean}(c)}{I} = \frac{1023(1.25)}{1.669} \approx 766 \text{ psi} \\ \sigma_{a_{nom}} &= \frac{M_{alt}(c)}{I} = \frac{3386(1.25)}{1.669} \approx 2536 \text{ psi} \end{aligned} \quad (t)$$

If we compare these results to those of the original design (see step 8), the forces and moments are now greater due to the heavier part but the stresses are less due to the larger I of the cross section.

- 24 The torsional shear stresses in a hollow-round section are maximum at the outer fiber and so occur at points of maximum bending stress. The nominal shear stress is found from $\tau_{max} = Tr / J$ where J for its geometry is found from equation 4.25b (p. 178):

$$J = \pi \left(\frac{d_{out}^4 - d_{in}^4}{32} \right) = \pi \left(\frac{2.5^4 - 2.0^4}{32} \right) = 3.338 \text{ in}^4 \quad (u)$$

The nominal mean and alternating shear stresses are then

$$\begin{aligned} \tau_{m_{nom}} &= \frac{T_{mean}(r)}{J} = \frac{1012.5}{3.338} = 379 \text{ psi} \\ \tau_{a_{nom}} &= \frac{T_{alt}(r)}{J} = \frac{1012.5}{3.338} = 379 \text{ psi} \end{aligned} \quad (v)$$

- 25 Because of the large radius and smooth contours of this round part, K_t and K_{ts} were taken as 1. There will be larger stress concentrations at the roots of the ears, but the bending stress is much lower there and the shear stress in this torsionally optimum shape is very low. The material's notch sensitivity is irrelevant when $K_t = 1$, making both $K_f = 1$ and $K_{fs} = 1$. The fatigue stress-concentration factors for the mean stress are also 1 with the above assumptions. The local-stress components are then the same as the nominal stress components found in equations *t* and *v*.
- 26 Since we have a case of combined, fluctuating, biaxial stresses that are synchronous and in-phase, and the notches have been designed out, the method of Sines is now appropriate (equation 6.21b, p. 378). This calculates equivalent alternating and mean stresses for the biaxial, unnotched case.

$$\begin{aligned}\sigma_a' &= \sqrt{\sigma_{x_a}^2 + \sigma_{y_a}^2 - \sigma_{x_a} \sigma_{y_a} + 3\tau_{xy_a}^2} \\ &= \sqrt{2536 + 0 - 0 + 3(379)} = 2619 \text{ psi} \\ \sigma_m' &= \sigma_{x_m} + \sigma_{y_m} = 766 + 0 = 766 \text{ psi}\end{aligned}\quad (w)$$

- 27 The material properties must now be determined. Aluminum does not have an endurance limit, but fatigue strengths at particular cycle lives are published. A search of the literature showed that of all the aluminum alloys, 7075 and 5052 offered the largest fatigue strengths S_f . However, no aluminum extruders were found locally that could extrude either of those alloys. The strongest extruded alloy available was 6061-T6 with a published $S_f = 13500$ psi at $N = 5E7$, $S_{ut} = 45000$, and $S_y = 40000$ psi.
- 28 The strength modification factors were found from the equations and data in Section 6.6. The loading is a combination of bending and torsion, which appears to create a conflict in the selection of a loading factor from equation 6.7a (p. 330). However, we have incorporated the torsion stresses into the Sines equivalent stress, which is a normal stress, so $C_{load} = 1$. The equivalent diameter for a nonrotating round part is found from Figure 6-25 and equation 6.7d (p. 331). The size factor is then found from equation 6.7b (p. 331):

$$\begin{aligned}A_{95} &= 0.010462d^2 = 0.010462(2.5)^2 = 0.065 \text{ in}^2 \\ d_{equiv} &= \sqrt{\frac{A_{95}}{0.0766}} = \sqrt{\frac{0.065}{0.0766}} = 0.924 \text{ in} \\ C_{size} &= 0.869(d_{equiv})^{-0.097} = 0.869(0.924)^{-0.097} = 0.88\end{aligned}\quad (x)$$

The surface factor is found from equation 6.7e (p. 333) and the data in Table 6-3 (p. 333) for machined or cold-drawn surfaces. Corrosion could dictate the use of a lower-valued surface factor, but since the part will be anodized for corrosion resistance, the machined-surface factor was applied.

$$C_{surf} = AS_{ut}^b = 2.7(45)^{-0.265} = 0.98 \quad (y)$$

Note that S_{ut} is in kpsi for equation 6.7e. The temperature factor was set to 1, since it operates in a room-temperature environment. C_{reliab} was set to 0.702 from Table 6-4 (p. 335) to represent a desired 99.99% reliability for the new design.

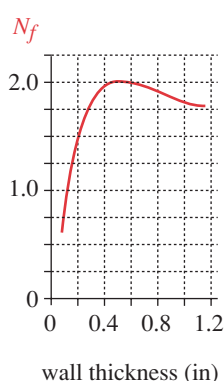
- 29 A corrected fatigue strength can now be calculated from

$$\begin{aligned}S_n &= C_{load} C_{size} C_{surf} C_{temp} C_{reliab} S_f \\ S_{n@5E7} &= 1(0.88)(0.98)(1)(0.702)(13500) \cong 8173 \text{ psi}\end{aligned}\quad (z)$$

- 30 This corrected fatigue strength $S_{n@5E7}$ is at the published test life of $N = 5E7$ cycles. Since we need a life of about $N = 9.4E8$ cycles, the equation for this material's $S-N$ curve must be written and solved for S_n at $N = 9.4E8$ cycles. To do so we need the material's strength S_m at 10^3 cycles from equation 6.9a:

$$S_m = 0.9S_{ut} = 0.9(45000) = 40500 \text{ psi} \quad (aa)$$

Use equations 6.10 to find the coefficient and exponent of the $S-N$ line. The value of -4.699 comes from Table 6-5 (p. 338) and corresponds to the number of cycles ($5E7$) at which these published test data were taken.

**FIGURE 6-56**

Safety Factor N_f as a Function of Wall Thickness for a Round Aluminum Laybar

$$b = \frac{1}{-4.699} \log\left(\frac{S_m}{S_{n@5E7}}\right) = \frac{1}{-4.699} \log\left(\frac{40500}{8173}\right) = -0.14792 \quad (ab)$$

$$\log(a) = \log(S_m) - 3b = \log(40500) - 3(-0.14792) = 5.0512; \quad a = 112\ 516$$

$$S_{n@9.4E8} = aN^b = 112\ 516(9.4E8)^{-0.14792} \approx 5\ 296 \text{ psi} \quad (ac)$$

This value will be used as a corrected S_n at the desired life.

- 31 The equivalent alternating and mean stresses can now be plotted on a modified-Goodman diagram or the safety factor can be calculated from equation 6.18e (p. 368) for a case 3 situation as described in step 17.

$$N_f = \frac{S_n S_{ut}}{\sigma'_a S_{ut} + \sigma'_m S_n} = \frac{5\ 296(45\ 000)}{2\ 536(45\ 000) + 766(5\ 296)} = 2.0 \quad (ad)$$

This safety factor is quite acceptable, but for an additional measure of safety, the finished parts were shot peened before anodizing. The variation of safety factor with wall thickness is shown in Figure 6-56. The peak occurs at a wall thickness of about 0.5 in, which was the value used in the design. Curves of safety factor versus wall thickness are plotted for all designs within the models. They are similar in shape to Figure 6-56 and all show an optimum wall thickness to maximize the safety factor.

- 32 The file names and pertinent data for the seven designs are shown in Table 6-13. The original design is shown both for the machine's design speed of 400 rpm, at which it performed successfully, and for the increased speed of 500 rpm, at which it failed. The only difference is the safety factor, which went from 1.3 to 1. The K_t factors are back-calculated for the failed designs (safety factor = 1) as described above but are estimated for the new designs. The steel designs use the back-calculated K_t from the failed original laybar to account for possible corrosion and weld concentration effects. The square aluminum design has an elevated K_t due to its internal corners.

Table 6-13 Data for Various Laybar Designs

Case Study 6: Dimensions in inches and pounds

Design	See Figure	Rpm	Material	File Name	Wall Thickness	Beam Depth	K_t	Weight Factor	Safety Factor	Comment
Original Laybar	6-53a	400	1018 Steel	CASE6-0	0.085	2.38	4.6	1	1.4	safe at design speed
Original Laybar	6-53a	500	1018 Steel	CASE6-1	0.085	2.38	4.6	1	1	failed at higher speed
Steel Replacement	6-53b	500	1020 Steel	CASE6-2	0.093	2.50	3.2	1	1	failed in 6 mos.
Aluminum Replacement	6-53c	500	6061-T6 Aluminum	CASE6-3	solid	2.00	7.2	1.4	1	failed in 3 mos.
Square Steel	6-55a	500	1020 Steel	CASE6-4	0.062	2.50	4.6	1.4	0.5	rejected design
Round Steel	6-55b	500	1020 Steel	CASE6-5	0.10	2.50	4.6	1.4	0.5	rejected design
Square Aluminum	6-55a	500	6061-T6 Aluminum	CASE6-6	0.35	2.50	2.0	1.4	1.0	rejected design
Round Aluminum	6-55b	500	6061-T6 Aluminum	CASE6-7	0.50	2.50	1.0	1.4	2.0	selected design

The weight factor is calculated as the ratio of total weight (with reed) of the new design over the total weight (with reed) of the original laybar. The values for safety factor in the table are the largest attainable without exceeding the weight factor (1.4) of the heaviest replacement laybar that operated without inflicting damage on the rest of the machine (Figure 6-53c, p. 390). Larger safety factors than those shown in Table 6-13 are achievable with some of the rejected designs, but only at a weight penalty. Thus the selected round design is seen to be the best one on a safety-factor-to-weight basis.

Other factors that entered into the decision to use the round-aluminum design were the corrosion resistance of anodized aluminum, its availability at reasonable cost in custom-extruded shapes, which eliminated all welding except at the ends, and the superior torsional resistance and lack of stress concentration of a round cross section. Approximately 100 laybars of this design were made and installed in 1971–1972. They operated without a single failure for over 7 years. The machinery was later sold and shipped overseas and the author lost track of them.

6.15 SUMMARY

Time-varying loads are more the rule than the exception in machinery. Designing to avoid failure under these conditions is more challenging than is design for static loading. The fatigue-failure mechanism is now reasonably well understood, though research continues on its many details. Two loading regimes are considered, low-cycle fatigue (LCF), where the total number of stress oscillations over the life of the part is less than about 1000, and high-cycle fatigue (HCF), which sees cycles into the millions or more. A strain-based analysis is the most accurate method for determining fatigue strengths and is preferred for LCF situations, where the local stresses may occasionally exceed the yield strength of the material on particular cycles. An example is an airframe, which sees occasionally severe overloads within a series of lower-level stress oscillations during its life as shown in Figure 6-7 (p. 315). Fracture mechanics (FM) is an increasingly useful tool for predicting incipient failure in assemblies that can be inspected for cracks. The crack growth is monitored and FM theory used to calculate a projected time to failure. The part is then replaced on a maintenance schedule that precludes its failure in service. This is regularly done in the aircraft industry. Most factory-based machinery and some land-transport vehicles see more uniform-magnitude oscillations in stress and are also expected to endure them for many millions of cycles. For these cases the more approximate, but easily applied, methods of stress-based HCF analysis are appropriate.

Rules of thumb and approximations are used to estimate material strengths under dynamic loading conditions, especially for the high-cycle fatigue case. Many of these err on the side of conservatism. If specific test data are available for the fatigue strength of the chosen material, those data should always be used in preference to a calculated estimate. Lacking specific test data, the uncorrected fatigue strength can be estimated as a percentage of the ultimate tensile strength. In either event, the uncorrected fatigue strength is then reduced with a collection of factors as defined in Section 6.6 and equations 6.7 to account for differences between the actual part and the test specimen from which the ultimate strength was measured. A modified-Goodman diagram is then constructed using estimates of the material's "static" strength at 1 000 cycles and its corrected fatigue strength at some larger number of cycles appropriate to the part's expected life. (See Section 6.11.)

A general approach to designing for HCF cases is presented in Section 6.13. The von Mises effective-stress equation is used to create effective alternating and mean components of stress for the most highly loaded points within the part. In some cases the mean stress component may be zero. All appropriate stress-concentration effects should be included in these stress calculations. The mean and alternating von Mises components are then plotted on the modified-Goodman diagram and a safety factor calculated based on an assumption about the way in which the mean and alternating stresses may vary in service. See Section 6.11 and equations 6.18 (pp. 367–368).

Important Equations Used in This Chapter

Fluctuating-Stress Components (Section 6.4):

$$\Delta\sigma = \sigma_{max} - \sigma_{min} \quad (6.1a)$$

$$\sigma_a = \frac{\sigma_{max} - \sigma_{min}}{2} \quad (6.1b)$$

$$\sigma_m = \frac{\sigma_{max} + \sigma_{min}}{2} \quad (6.1c)$$

$$R = \frac{\sigma_{min}}{\sigma_{max}} \quad A = \frac{\sigma_a}{\sigma_m} \quad (6.1d)$$

Uncorrected Fatigue Strength Estimates (Section 6.5):

$$\text{steels : } \begin{cases} S_{e'} \cong 0.5 S_{ut} & \text{for } S_{ut} < 200 \text{ kpsi (1400 MPa)} \\ S_{e'} \cong 100 \text{ kpsi (700 MPa)} & \text{for } S_{ut} \geq 200 \text{ kpsi (1400 MPa)} \end{cases} \quad (6.5a)$$

$$\text{irons : } \begin{cases} S_{e'} \cong 0.4 S_{ut} & \text{for } S_{ut} < 60 \text{ kpsi (400 MPa)} \\ S_{e'} \cong 24 \text{ kpsi (160 MPa)} & \text{for } S_{ut} \geq 60 \text{ kpsi (400 MPa)} \end{cases} \quad (6.5b)$$

$$\text{aluminums : } \begin{cases} S_{f_{@5E8}} \cong 0.4 S_{ut} & \text{for } S_{ut} < 48 \text{ kpsi (330 MPa)} \\ S_{f_{@5E8}} \cong 19 \text{ kpsi (130 MPa)} & \text{for } S_{ut} \geq 48 \text{ kpsi (330 MPa)} \end{cases} \quad (6.5c)$$

$$\text{copper alloys : } \begin{cases} S_{f_{@5E8}} \cong 0.4 S_{ut} & \text{for } S_{ut} < 40 \text{ kpsi (280 MPa)} \\ S_{f_{@5E8}} \cong 14 \text{ kpsi (100 MPa)} & \text{for } S_{ut} \geq 40 \text{ kpsi (280 MPa)} \end{cases} \quad (6.5d)$$

Correction Factors for Fatigue Strength (Section 6.6):

$$\text{bending : } C_{load} = 1 \quad (6.7a)$$

$$\text{axial loading : } C_{load} = 0.70$$

$$\text{for } d \leq 0.3 \text{ in (8 mm)} : \quad C_{size} = 1$$

$$\text{for } 0.3 \text{ in} < d \leq 10 \text{ in} : \quad C_{size} = 0.869 d^{-0.097} \quad (6.7b)$$

$$\text{for } 8 \text{ mm} < d \leq 250 \text{ mm} : \quad C_{size} = 1.189 d^{-0.097}$$

$$C_{surf} \equiv A(S_{ut})^b \quad \text{if } C_{surf} > 1.0, \text{ set } C_{surf} = 1.0 \quad (6.7e)$$

for $T \leq 450^\circ\text{C}$ (840°F): $C_{temp} = 1$

for $450^\circ\text{C} < T \leq 550^\circ\text{C}$: $C_{temp} = 1 - 0.0058(T - 450)$ (6.7f)

for $840^\circ\text{F} < T \leq 1020^\circ\text{F}$: $C_{temp} = 1 - 0.0032(T - 840)$

Corrected Fatigue Strength Estimates (Section 6.6):

$$\begin{aligned} S_e &= C_{load} C_{size} C_{surf} C_{temp} C_{reliab} S_e' \\ S_f &= C_{load} C_{size} C_{surf} C_{temp} C_{reliab} S_f' \end{aligned} \quad (6.6)$$

Approximate Strength at 1 000 Cycles (Section 6.6):

$$\begin{aligned} \text{bending : } S_m &= 0.9S_{ut} \\ \text{axial loading : } S_m &= 0.75S_{ut} \end{aligned} \quad (6.9)$$

S-N Diagram (Section 6.6):

$$\log S(N) = \log a + b \log N \quad (6.10b)$$

$$b = \frac{1}{z} \log \left(\frac{S_m}{S_e} \right) \quad \text{where} \quad z = \log N_1 - \log N_2 \quad (6.10c)$$

$$\log(a) = \log(S_m) - b \log(N_1) = \log(S_m) - 3b$$

Notch Sensitivity (Section 6.7):

$$q = \frac{1}{1 + \frac{\sqrt{a}}{\sqrt{r}}} \quad (6.13)$$

Fatigue Stress-Concentration Factors (Sections 6.7 and 6.11):

$$K_f = 1 + q(K_t - 1) \quad (6.11b)$$

if $K_f |\sigma_{max_{nom}}| < S_y$ then: $K_{fm} = K_f$

if $K_f |\sigma_{max_{nom}}| > S_y$ then: $K_{fm} = \frac{S_y - K_f \sigma_{a_{nom}}}{|\sigma_{m_{nom}}|}$ (6.17)

if $K_f |\sigma_{max_{nom}} - \sigma_{min_{nom}}| > 2S_y$ then: $K_{fm} = 0$

Safety Factor - Fully Reversed Stresses (Section 6.10):

$$N_f = \frac{S_n}{\sigma'} \quad (6.14)$$

Modified-Goodman Diagram (Section 6.11):

$$-\frac{\sigma'_m}{S_{yc}} + \frac{\sigma'_a}{S_{yc}} = 1 \quad (6.16a)$$

$$\sigma'_a = S_f \quad (6.16b)$$

$$\frac{\sigma'_m}{S_{ut}} + \frac{\sigma'_a}{S_f} = 1 \quad (6.16c)$$

$$\frac{\sigma'_m}{S_y} + \frac{\sigma'_a}{S_y} = 1 \quad (6.16d)$$

Safety Factor - Fluctuating Stresses (Section 6.11):

Case 1:

$$N_f = \frac{\sigma'_m @ Q}{\sigma'_m @ Z} = \frac{S_y}{\sigma'_m} \left(1 - \frac{\sigma'_a}{S_y} \right) \quad (6.18a)$$

Case 2:

$$N_f = \frac{\sigma'_a @ P}{\sigma'_a @ Z} = \frac{S_f}{\sigma'_a} \left(1 - \frac{\sigma'_m}{S_{ut}} \right) \quad (6.18b)$$

Case 3:

$$N_f = \frac{\sigma'_m @ R}{\sigma'_m @ Z} = \frac{S_f S_{ut}}{\sigma'_a S_{ut} + \sigma'_m S_f} \quad (6.18e)$$

$$ZS = \sqrt{(\sigma'_m - \sigma'_m @ S)^2 + (\sigma'_a - \sigma'_a @ S)^2} \quad (6.18f)$$

$$OZ = \sqrt{(\sigma'_a)^2 + (\sigma'_m)^2}$$

Case 4:

$$N_f = \frac{OZ + ZS}{OZ} \quad (6.18g)$$

Sines Method for Multiaxial Stresses in Fatigue - 3-D (Section 6.12):

$$\sigma'_a = \sqrt{\frac{(\sigma_{x_a} - \sigma_{y_a})^2 + (\sigma_{y_a} - \sigma_{z_a})^2 + (\sigma_{z_a} - \sigma_{x_a})^2 + 6(\tau_{xy_a}^2 + \tau_{yz_a}^2 + \tau_{zx_a}^2)}{2}} \quad (6.21a)$$

$$\sigma'_m = \sigma_{x_m} + \sigma_{y_m} + \sigma_{z_m}$$

Sines Method for Multiaxial Stresses in Fatigue - 2-D (Section 6.12):

$$\sigma'_a = \sqrt{\sigma_{x_a}^2 + \sigma_{y_a}^2 - \sigma_{x_a} \sigma_{y_a} + 3\tau_{xy_a}^2} \quad (6.21b)$$

$$\sigma'_m = \sigma_{x_m} + \sigma_{y_m}$$

General Multiaxial Stresses in Fatigue - 3-D (Section 6.12):

$$\sigma'_a = \sqrt{\frac{(\sigma_{x_a} - \sigma_{y_a})^2 + (\sigma_{y_a} - \sigma_{z_a})^2 + (\sigma_{z_a} - \sigma_{x_a})^2 + 6(\tau_{xy_a}^2 + \tau_{yz_a}^2 + \tau_{zx_a}^2)}{2}} \quad (6.22a)$$

$$\sigma'_m = \sqrt{\frac{(\sigma_{x_m} - \sigma_{y_m})^2 + (\sigma_{y_m} - \sigma_{z_m})^2 + (\sigma_{z_m} - \sigma_{x_m})^2 + 6(\tau_{xy_m}^2 + \tau_{yz_m}^2 + \tau_{zx_m}^2)}{2}}$$

General Multiaxial Stresses in Fatigue - 2-D (Section 6.12):

$$\sigma'_a = \sqrt{\sigma_{x_a}^2 + \sigma_{y_a}^2 - \sigma_{x_a}\sigma_{y_a} + 3\tau_{xy_a}^2} \quad (6.22b)$$

$$\sigma'_m = \sqrt{\sigma_{x_m}^2 + \sigma_{y_m}^2 - \sigma_{x_m}\sigma_{y_m} + 3\tau_{xy_m}^2}$$

SEQA Method for Complex Multiaxial Stresses in Fatigue (Section 6.12):

$$\text{SEQA} = \frac{\sigma}{\sqrt{2}} \left[1 + \frac{3}{4} Q^2 + \sqrt{1 + \frac{3}{2} Q^2 \cos 2\phi + \frac{9}{16} Q^4} \right]^{\frac{1}{2}} \quad (6.23)$$

Fracture Mechanics in Fatigue (Section 6.5):

$$\Delta K = \beta \sigma_{max} \sqrt{\pi a} - \beta \sigma_{min} \sqrt{\pi a} \\ = \beta \sqrt{\pi a} (\sigma_{max} - \sigma_{min}) \quad (6.3b)$$

$$\frac{da}{dN} = A(\Delta K)^n \quad (6.4)$$

6.16 REFERENCES

- 1 R. P. Reed, J. H. Smith, and B. W. Christ, *The Economic Effects of Fracture in the United States: Part I*, Special Pub. 647-1, U. S. Dept. of Commerce, National Bureau of Standards, Washington, D.C., 1983.
- 2 N. E. Dowling, *Mechanical Behavior of Materials*. Prentice-Hall: Englewood Cliffs, N.J., p. 340, 1993.
- 3 J. W. Fischer and B. T. Yen, *Design, Structural Details, and Discontinuities in Steel, Safety and Reliability of Metal Structures*, ASCE, Nov. 2, 1972.
- 4 N. E. Dowling, *Mechanical Behavior of Materials*. Prentice-Hall: Englewood Cliffs, N.J., p. 355, 1993.
- 5 D. Broek, *The Practical Use of Fracture Mechanics*. Kluwer Academic Publishers: Dordrecht, The Netherlands, p. 10, 1988.
- 6 N. E. Dowling, *Mechanical Behavior of Materials*. Prentice-Hall: Englewood Cliffs, N.J., p. 347, 1993.
- 7 R. C. Juvinal, *Engineering Considerations of Stress, Strain and Strength*. McGraw-Hill: New York, p. 280, 1967.
- 8 J. E. Shigley and C. R. Mischke, *Mechanical Engineering Design*. 5th ed. McGraw-Hill: New York, p. 278, 1989.
- 9 A. F. Madayag, *Metal Fatigue: Theory and Design*. John Wiley & Sons: New York, p. 117, 1969.
- 10 N. E. Dowling, *Mechanical Behavior of Materials*. Prentice-Hall: Englewood Cliffs, N.J., p. 418, 1993.
- 11 R. C. Juvinal, *Engineering Considerations of Stress, Strain and Strength*. McGraw-Hill: New York, p. 231, 1967.

- 12 **J. A. Bannantine, J. J. Comer, and J. L. Handrock**, *Fundamentals of Metal Fatigue*. Prentice-Hall: Englewood Cliffs, N. J., p. 13, 1990.
- 13 **P. C. Paris and F. Erdogan**, *A Critical Analysis of Crack Propagation Laws*. *Trans. ASME, J. Basic Eng.*, **85**(4): p. 528, 1963.
- 14 **J. M. Barsom**, *Fatigue-Crack Propagation in Steels of Various Yield Strengths*. *Trans. ASME, J. Eng. Ind., Series B*(4): p. 1190, 1971.
- 15 **H. O. Fuchs and R. I. Stephens**, *Metal Fatigue in Engineering*. John Wiley & Sons: New York, p. 88, 1980.
- 16 **J. A. Bannantine, J. J. Comer, and J. L. Handrock**, *Fundamentals of Metal Fatigue*. Prentice-Hall: Englewood Cliffs, N. J., p. 106, 1990.
- 17 **J. M. Barsom and S. T. Rolfe**, *Fracture and Fatigue Control in Structures*, 2nd ed. Prentice-Hall: Englewood Cliffs, N. J., p. 256, 1987.
- 18 **H. O. Fuchs and R. I. Stephens**, *Metal Fatigue in Engineering*. John Wiley & Sons: New York, p. 89, 1980.
- 19 **J. M. Barsom and S. T. Rolfe**, *Fracture and Fatigue Control in Structures*. 2nd ed. Prentice-Hall: Englewood Cliffs, N. J., p. 285, 1987.
- 20 **P. G. Forrest**, *Fatigue of Metals*. Pergamon Press: London, 1962.
- 21 **J. E. Shigley and L. D. Mitchell**, *Mechanical Engineering Design*. 4th ed. McGraw-Hill: New York, p. 293, 1983.
- 22 **R. Kuguel**, *A Relation Between Theoretical Stress-Concentration Factor and Fatigue Notch Factor Deduced from the Concept of Highly Stressed Volume*. *Proc. ASTM*, **61**: pp. 732-748, 1961.
- 23 **R. C. Juvinall**, *Engineering Considerations of Stress, Strain and Strength*. McGraw-Hill: New York, p. 233, 1967.
- 24 *Ibid.*, p. 234.
- 25 **R. C. Johnson**, *Machine Design*, vol. 45, p. 108, 1973.
- 26 **J. E. Shigley and L. D. Mitchell**, *Mechanical Engineering Design*. 4th ed. McGraw-Hill: New York, p. 300, 1983.
- 27 **E. B. Haugen and P. H. Wirsching**, "Probabilistic Design." *Machine Design*, vol. 47, pp. 10-14, 1975.
- 28 **R. C. Juvinall and K. M. Marshek**, *Fundamentals of Machine Component Design*. 2nd ed. John Wiley & Sons: New York, p. 270, 1967.
- 29 *Ibid.*, p. 267.
- 30 **R. E. Peterson**, *Stress-Concentration Factors*. John Wiley & Sons: New York, 1974.
- 31 **R. J. Roark and W. C. Young**, *Formulas for Stress and Strain*. 5th ed. McGraw-Hill: New York, 1975.
- 32 **H. Neuber**, *Theory of Notch Stresses*. J. W. Edwards Publisher Inc.: Ann Arbor Mich., 1946.
- 33 **P. Kuhn and H. F. Hardrath**, *An Engineering Method for Estimating Notch-size Effect in Fatigue Tests on Steel*. Technical Note 2805, NACA, Washington, D.C., Oct. 1952.

- 34 **R. B. Heywood**, *Designing Against Fatigue*. Chapman & Hall Ltd.: London, 1962.
- 35 **R. C. Juvinall**, *Engineering Considerations of Stress, Strain and Strength*. McGraw-Hill: New York, p. 280, 1967.
- 36 **V. M. Faires**, *Design of Machine Elements*. 4th ed. Macmillan: London, p. 162, 1965.
- 37 **R. B. Heywood**, *Designing Against Fatigue of Metals*. Reinhold: New York, p. 272, 1962.
- 38 **H. O. Fuchs and R. I. Stephens**, *Metal Fatigue in Engineering*. John Wiley & Sons: New York, p. 130, 1980.
- 39 **J. E. Shigley and C. R. Mischke**, *Mechanical Engineering Design*. 5th ed. McGraw-Hill: New York, p. 283, 1989.
- 40 **N. E. Dowling**, *Mechanical Behavior of Materials*. Prentice-Hall: Englewood Cliffs, N J., p. 416, 1993.
- 41 **R. C. Juvinall**, *Engineering Considerations of Stress, Strain and Strength*. McGraw-Hill: New York, p. 280, 1967.
- 42 **G. Sines**, *Failure of Materials under Combined Repeated Stresses Superimposed with Static Stresses*, Technical Note 3495, NACA, 1955.
- 43 **F. S. Kelly**, *A General Fatigue Evaluation Method*, Paper 79-PVP-77, ASME, New York, 1979.
- 44 **Y. S. Garud**, *A New Approach to the Evaluation of Fatigue Under Multiaxial Loadings*, in *Methods for Predicting Material Life in Fatigue*, W. J. Ostergren and J. R. Whitehead, ed. ASME: New York. pp. 249-263, 1979.
- 45 **M. W. Brown and K. J. Miller**, *A Theory for Fatigue Failure under Multiaxial Stress-Strain Conditions*. *Proc. Inst. Mech. Eng.*, **187**(65): pp. 745-755, 1973.
- 46 **J. O. Smith**, *The Effect of Range of Stress on the Fatigue Strength of Metals*. Univ. of Ill., *Eng. Exp. Sta. Bull.*, (334), 1942.
- 47 **J. E. Shigley and L. D. Mitchell**, *Mechanical Engineering Design*. 4th ed. McGraw-Hill: New York, p. 333, 1983.
- 48 **B. F. Langer**, *Design of Vessels Involving Fatigue*, in *Pressure Vessel Engineering*, R. W. Nichols, ed. Elsevier: Amsterdam. pp. 59-100, 1971.
- 49 **J. A. Collins**, *Failure of Materials in Mechanical Design*. 2nd ed. J. Wiley & Sons: New York, pp. 238-254, 1993.
- 50 **S. M. Tipton and D. V. Nelson**, *Fatigue Life Predictions for a Notched Shaft in Combined Bending and Torsion*, in *Multiaxial Fatigue*, K. J. Miller and M. W. Brown, Editors. ASTM: Philadelphia, PA. pp. 514-550, 1985.
- 51 **R. C. Rice**, ed. *Fatigue Design Handbook*. 2nd ed. Soc. of Automotive Engineers: Warrendale, PA. p. 260, 1988.
- 52 **T. Nishihara and M. Kawamoto**, *The Strength of Metals under Combined Alternating Bending and Torsion with Phase Difference*. Memoirs College of Engineering, Kyoto Univ., Japan, **11**(85), 1945.
- 53 *Shot Peening of Gears*. American Gear Manufacturers Association AGMA 938-A05, 2005.

Table P6-0[†]

Topic/Problem Matrix

Sect. 6.4 Fatigue Loads

6-1

Sect. 6.5 Fracture Mechanics

6-51, 6-52, 6-53

Sect. 6.6 S/N Diagrams

6-2, 6-4, 6-5, 6-54, 6-55, 6-56, 6-57

Sect. 6.7 Stress Conc.

6-15, 6-58, 6-59, 6-60, 6-63 to 6-66

Sect. 6.10 Fully Reversed

6-6, 6-7, 6-8, 6-20, 6-26, 6-29, 6-33, 6-35, 6-37, 6-46, 6-48

Sect. 6.11 Fluctuating

6-3, 6-9, 6-10, 6-11, 6-12, 6-13, 6-14, 6-16, 6-17, 6-18, 6-19, 6-21, 6-22, 6-23, 6-24, 6-25, 6-27, 6-28, 6-30, 6-31, 6-32, 6-34, 6-36, 6-38, 6-40, 6-43, 6-44, 6-45, 6-70

Sect. 6.12 Multiaxial

6-39, 6-41, 6-42, 6-61, 6-62, 6-67, 6-68, 6-69

6

6.17 BIBLIOGRAPHY**For more information on fatigue design, see:****J. A. Bannantine, J. J. Comer, and J. L. Handrock,** *Fundamentals of Metal Fatigue*. Prentice-Hall: Englewood Cliffs, N.J., 1990.**H. E. Boyer**, ed., *Atlas of Fatigue Curves*. Amer. Soc. for Metals: Metals Park, Ohio. 1986.**H. O. Fuchs and R. I. Stephens**, *Metal Fatigue in Engineering*. John Wiley & Sons: New York, 1980.**R. C. Juvinall**, *Engineering Considerations of Stress, Strain and Strength*.**A. J. McEvily**, ed. *Atlas of Stress-Corrosion and Corrosion Fatigue Curves*. Amer. Soc. for Metals: Metals Park, Ohio. 1990. McGraw-Hill: New York, 1967.**For more information on the strain-life approach to low-cycle fatigue, see:****N. E. Dowling**, *Mechanical Behavior of Materials*. Prentice-Hall: Englewood Cliffs, N.J., 1993.**R. C. Rice**, ed. *Fatigue Design Handbook*. 2nd ed. Soc. of Automotive Engineers: Warrendale, PA. 1988.**For more information on the fracture mechanics approach to fatigue, see:****J. M. Barsom and S. T. Rolfe**, *Fracture and Fatigue Control in Structures*. 2nd ed. Prentice-Hall: Englewood Cliffs, N.J., 1987.**D. Broek**, *The Practical Use of Fracture Mechanics*. Kluwer Academic Publishers: Dordrecht, The Netherlands, 1988.**For more information on residual stresses, see:****J. O. Almen and P. H. Black**, *Residual Stresses and Fatigue in Metals*. McGraw-Hill: New York, 1963.**For more information on multiaxial stresses in fatigue, see:****A. Fatemi and D. F. Socie**, *A Critical Plane Approach to Multiaxial Fatigue Damage Including Out-of-Phase Loading*. Fatigue and Fracture of Engineering Materials and Structures, **11**(3): pp. 149-165, 1988.**Y. S. Garud**, *Multiaxial Fatigue: A Survey of the State of the Art*. J. Test. Eval., **9**(3), 1981.**K. F. Kussmaul, D. L. McDiarmid and D. F. Socie**, eds. *Fatigue Under Biaxial and Multiaxial Loading*. Mechanical Engineering Publications Ltd.: London. 1991.**G. E. Leese and D. Socie**, eds. *Multiaxial Fatigue: Analysis and Experiments*. Soc. of Automotive Engineers: Warrendale, Pa., 1989.**K. J. Miller and M. W. Brown**, eds. *Multiaxial Fatigue*. Vol. STP 853. ASTM: Philadelphia, Pa., 1985.**G. Sines**, *Behavior of Metals Under Complex Static and Alternating Stresses*, in *Metal Fatigue*, G. Sines and J. L. Waisman, eds. McGraw-Hill: New York. 1959.**R. M. Wetzel**, ed., *Fatigue Under Complex Loading: Analyses and Experiments*. SAE Pub. No. AE-6, Soc. of Automotive Engineers: Warrendale, Pa., 1977.

^{*} Answers to these problems are provided in Appendix D.

[†] Problem numbers in **boldface** are extended from similar problems in earlier chapters with the same dash number. Problem numbers in *italics* are design problems.

6.18 PROBLEMS

- *6-1 For the data in the row(s) assigned in Table P6-1, find the stress range, alternating stress component, mean stress component, stress ratio, and amplitude ratio.
- 6-2 For the steel-material strength data in the row(s) assigned in Table P6-2, calculate the uncorrected endurance limit and draw a strength-life (*S-N*) diagram.
- *6-3 For the bicycle pedal arm assembly in Figure P6-1 assume a rider-applied force that ranges from 0 to 1 500 N at the pedal each cycle. Determine the fluctuating stresses in the 15-mm-dia pedal arm. Find the fatigue safety factor if $S_{ut} = 500$ MPa.
- 6-4 For the aluminum-material strength data in the row(s) assigned in Table P6-2, calculate the uncorrected fatigue strength at 5E8 cycles and draw a strength-life (*S-N*) diagram for the material.
- 6-5 For the data in the row(s) assigned in Table P6-3, find the corrected endurance strength (or limit), create equations for the *S-N* line, and draw the *S-N* diagram.
- *6-6 For the trailer hitch from Problem 3-6 on p. 127 (also see Figure P6-2 and Figure 1-5, p. 14), find the infinite-life fatigue safety factors for all modes of failure, assuming that the horizontal impact force of the trailer on the ball is fully reversed. Use steel with $S_{ut} = 600$ MPa and $S_y = 450$ MPa.
- *6-7 Design the wrist pin of Problem 3-7 (p. 127) for infinite life with a safety factor of 1.5 if the 2 500-g acceleration is fully reversed and $S_{ut} = 130$ kpsi.
- *6-8 A paper machine processes rolls of paper having a density of 984 kg/m³. The paper roll is 1.50-m outside dia (*OD*) × 0.22-m inside dia (*ID*) × 3.23 m long and is on a simply supported, hollow, steel shaft with $S_{ut} = 400$ MPa. Find the shaft *ID* needed to obtain a dynamic safety factor of 2 for a 10-year life running three 8-hour shifts per day if the shaft *OD* is 22 cm and the roll turns at 50 rpm.
- 6-9 For the ViseGrip® plier-wrench drawn to scale in Figure P6-3, and for which the forces were analyzed in Problem 3-9 (p. 127) and stresses in Problem 4-9 (p. 229),

Table P6-1

Data for Problem 6-1

Row	σ_{max}	σ_{min}
a	1 000	0
b	1 000	-1 000
c	1 500	500
d	1 500	-500
e	500	-1 000
f	2 500	-1 200
g	0	-4 500
h	2 500	1 500

6

Table P6-2

Data for Problems 6-2, 6-4

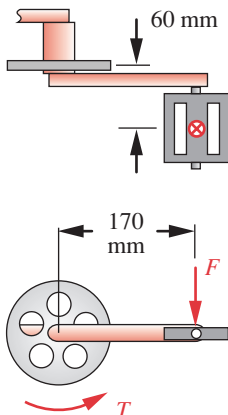
Row	S_{ut} (psi)	mat'l
a	90 000	steel
b	250 000	steel
c	120 000	steel
d	150 000	steel
e	25 000	alum.
f	70 000	alum.
g	40 000	alum.
h	35 000	alum.

Table P6-3 Data for Problem 6-5

Row	Material	S_{ut} kpsi	Shape	Size inches	Surface Finish	Loading	Temp °F	Reliability
a	steel	110	round	2	ground	torsion	room	99.9
b	steel	90	square	4	mach.	axial	600	99.0
c	steel	80	I-beam	16 x 18*	hot rolled	bending	room	99.99
d	steel	200	round	5	forged	torsion	-50	99.999
e	steel	150	square	7	cold rolled	axial	900	50
f	aluminum	70	round	9	mach.	bending	room	90
g	aluminum	50	square	9	ground	torsion	room	99.9
h	aluminum	85	I-beam	24 x 36*	cold rolled	axial	room	99.0
i	aluminum	60	round	4	ground	bending	room	99.99
j	aluminum	40	square	6	forged	torsion	room	99.999
k	ductile iron	70	round	5	cast	axial	room	50
l	ductile iron	90	square	7	cast	bending	room	90
m	bronze	60	round	9	forged	torsion	50	90
n	bronze	80	square	6	cast	axial	212	99.999

* width x height

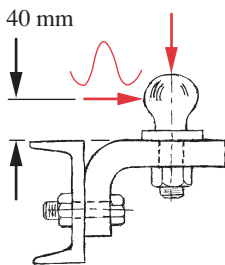
* Answers to these problems are provided in Appendix D. Problem numbers in *italics* are design problems. Problem numbers in **boldface** are extended from similar problems in earlier chapters with the same dash number. Problems in succeeding chapters may also continue and extend these problems.



6

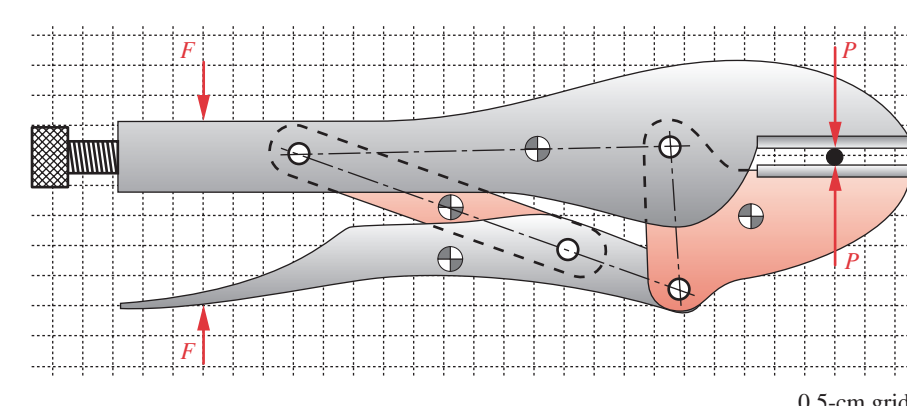
FIGURE P6-1

Problem 6-3 (A Solidworks model of this is on the CD)

**FIGURE P6-2**

Problem 6-6 (A Solidworks model of this is on the CD)

* Answers to these problems are provided in Appendix D. Problem numbers in *italics* are design problems. Problem numbers in **boldface** are extended from similar problems in earlier chapters with the same dash number. Problems in succeeding chapters may also continue and extend these problems.

**FIGURE P6-3**

Problem 6-9 (A Solidworks model of this is on the CD)

find the safety factors for each pin for an assumed clamping force of $P = 4\ 000$ N in the position shown. The steel pins are 8-mm dia with $S_y = 400$ MPa, $S_{ut} = 520$ MPa, and are all in double shear. Assume a desired finite life of $5E4$ cycles.

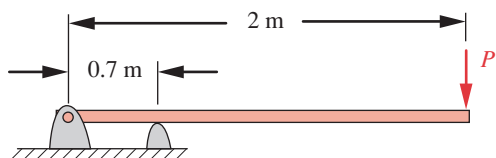
- *6-10** An overhung diving board is shown in Figure P6-4a. A 100-kg person is standing on the free end. Assume cross-sectional dimensions of 305 mm \times 32 mm. What is the fatigue safety factor for finite life if the material is brittle fiberglass with $S_f = 39$ MPa @ $N = 5E8$ cycles and $S_{ut} = 130$ MPa in the longitudinal direction?

- *6-11** Repeat Problem 6-10 assuming the 100-kg person in Problem 6-10 jumps up 25 cm and lands back on the board. Assume the board weighs 29 kg and deflects 13.1 cm statically when the person stands on it. What is the fatigue safety factor for finite life if the material is brittle fiberglass with $S_f = 39$ MPa @ $N = 5E8$ cycles and $S_{ut} = 100$ MPa in the longitudinal direction?

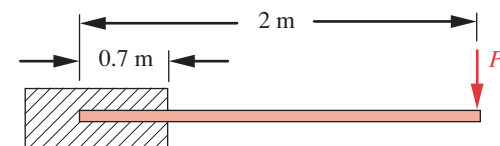
- 6-12** Repeat Problem 6-10 using the cantilevered diving board design in Figure P6-4b.

- 6-13** Repeat Problem 6-11 using the diving board design shown in Figure P6-4b. Assume the board weighs 19 kg and deflects 8.5 cm statically when the person stands on it.

- 6-14** Figure P6-5 shows a child's toy called a *pogo stick*. The child stands on the pads, applying half her weight on each side. She jumps up off the ground, holding the pads up against her feet, and bounces along with the spring cushioning the impact and storing energy to help each rebound. Assume a 60-lb child and a spring constant of 100 lb/in. The pogo stick weighs 5 lb. Design the aluminum cantilever beam sections on which she stands to survive jumping 2 in off the ground with a dynamic



(a) Overhung diving board



(b) Cantilevered diving board

FIGURE P6-4

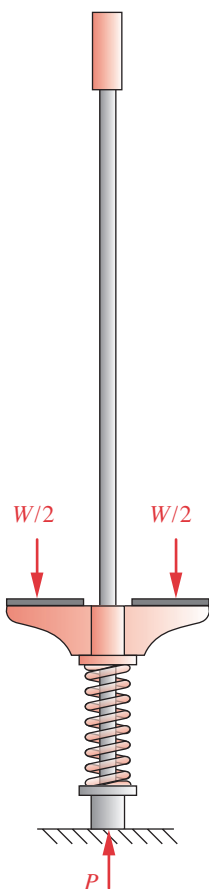
Problems 6-10 through 6-13

Table P6-4 Data For Problem 6-15

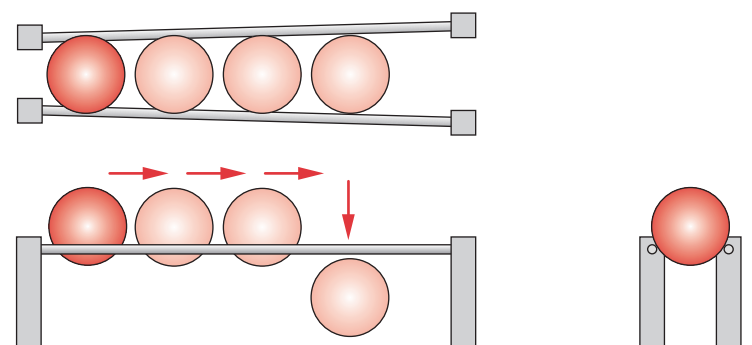
Row	S_{ut} (kpsi)	K_t	r (in)	Material	Loading
a	100	3.3	0.25	steel	bending
b	90	2.5	0.55	steel	torsion
c	150	1.8	0.75	steel	bending
d	200	2.8	1.22	steel	torsion
e	20	3.1	0.25	soft aluminum	bending
f	35	2.5	0.28	soft aluminum	bending
g	45	1.8	0.50	soft aluminum	bending
h	50	2.8	0.75	hard aluminum	bending
i	30	3.5	1.25	hard aluminum	bending
j	90	2.5	0.25	hard aluminum	bending

safety factor of 2 for a finite life of $5E4$ cycles. Use 2000 series aluminum. Define the beam shape and size.

- *6-15** For a notched part having notch dimension r , geometric stress-concentration factor K_t , material strength S_{ut} , and loading as shown in the assigned row(s) of Table P6-4, find the Neuber factor a , the material's notch sensitivity q , and the fatigue stress-concentration factor K_f .
- 6-16** A track to guide bowling balls is designed with two round rods as shown in Figure P6-6. The rods have a small angle between them. The balls roll on the rods until they fall between them and drop onto another track. Each rod's unsupported length is 30 in and the angle between them is 3.2° . The balls are 4.5-in-dia and weigh 2.5 lb. The center distance between the 1-in-dia rods is 4.2 in at the narrow end. Find the infinite-life safety factor for the 1-in-dia SAE 1010 cold-rolled steel rods.
- (a) Assume rods are simply supported at each end.
(b) Assume rods are fixed at each end.
- *6-17** A pair of ice tongs is shown in Figure P6-7. The ice weighs 50 lb and is 10-in wide across the tongs. The distance between the handles is 4 in, and the mean radius r of a steel tong is 6 in. The rectangular cross-sectional dimensions are 0.750 in \times 0.312 in. Find the safety factor for the tongs for $5E5$ cycles if their $S_{ut} = 50$ kpsi.

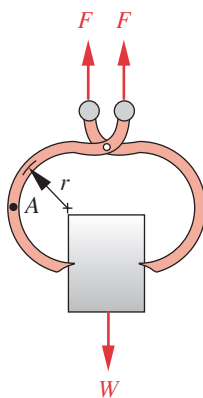
**FIGURE P6-5**

Problem 6-14

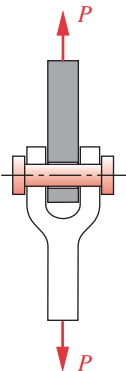
**FIGURE P6-6**

Problem 6-16

* Answers to these problems are provided in Appendix D. Problem numbers in *italics* are design problems. Problem numbers in **boldface** are extended from similar problems in earlier chapters with the same dash number. Problems in succeeding chapters may also continue and extend these problems.

**FIGURE P6-7**

Problem 6-17

**FIGURE P6-8**

Problem 6-19

**FIGURE P6-10**

Problem 6-22

* Answers to these problems are provided in Appendix D. Problem numbers in *italics* are design problems. Problem numbers in **boldface** are extended from similar problems in earlier chapters with the same dash number. Problems in succeeding chapters may also continue and extend these problems.

- 6-18** Repeat Problem 6-17 with the tongs made of Class 40 gray cast iron.

- *6-19** Determine the size of the clevis pin shown in Figure P6-8 needed to withstand an applied repeated force of 0 to 130 000 lb for infinite life. Also determine the required outside radius of the clevis end to not fail in either tearout or bearing if the clevis flanges each are 2.5 in thick. Use a safety factor of 3. Assume $S_{ut} = 140$ ksi for the pin and $S_{ut} = 80$ ksi for the clevis.

- 6-20** A ± 100 N-m torque is applied to a 1-m-long, solid, round steel shaft. Design it to limit its angular deflection to 2° and select a steel alloy to have a fatigue safety factor of 2 for infinite life.

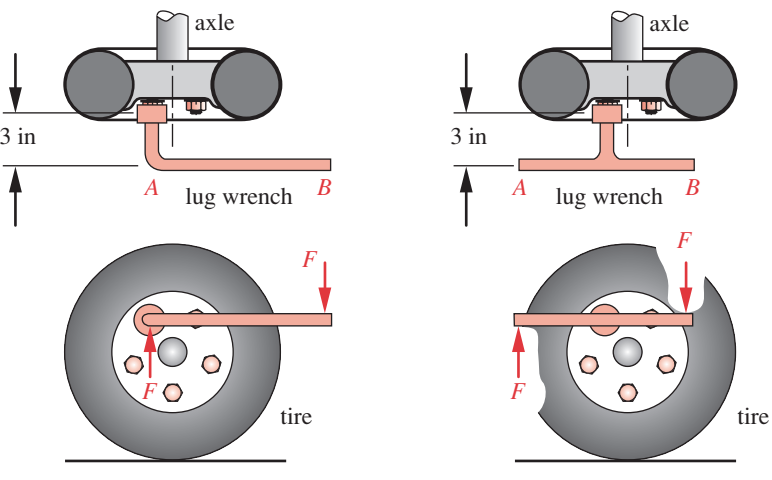
- 6-21** Figure P6-9 shows an automobile wheel with two styles of lug wrench, a single-ended wrench in (a), and a double-ended wrench in (b). The distance between points A and B is 1 ft in both cases and the handle diameter is 0.625 in. How many cycles of tightening can be expected before a fatigue failure if the average tightening torque is 100 ft-lb and the material $S_{ut} = 60$ ksi?

- *6-22** An in-line “roller-blade” skate is shown in Figure P6-10. The polyurethane wheels are 72-mm dia and spaced on 104-mm centers. The skate-boot-foot combination weighs 2 kg. The effective “spring rate” of the person-skate system is 6 000 N/m. The 10-mm-dia axle pins are in double shear and of steel with $S_{ut} = 550$ MPa. Find the infinite-life fatigue safety factor for the pins when a 100-kg person lands a 0.5-m jump on one foot.

- (a) Assume that all four wheels land simultaneously.
(b) Assume that one wheel absorbs all the landing force.

- *6-23** The beam in Figure P6-11a is subjected to a sinusoidal force time function with $F_{max} = F$ and $F_{min} = -F/2$, where F and the beam’s other data are given in the row(s) assigned from Table P6-5. Find the stress state in the beam due to this loading and choose a material specification that will give a safety factor of 3 for $N = 5E8$ cycles.

- *6-24** The beam in Figure P6-11b is subjected to a sinusoidal force time function with $F_{max} = F$ N and $F_{min} = F/2$, where F and the beam’s other data are given in the row(s) assigned from Table P6-5. Find the stress state in the beam due to this

**FIGURE P6-9**

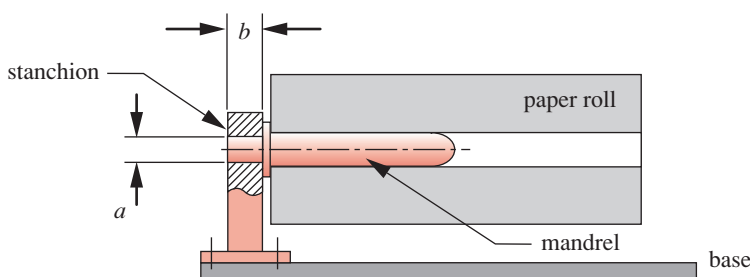
Problem 6-21

Table P6-5 Data for Problems 6-23 through 6-26Use Only Data Relevant to a Particular Problem. Lengths in m, Forces in N, I in m^4

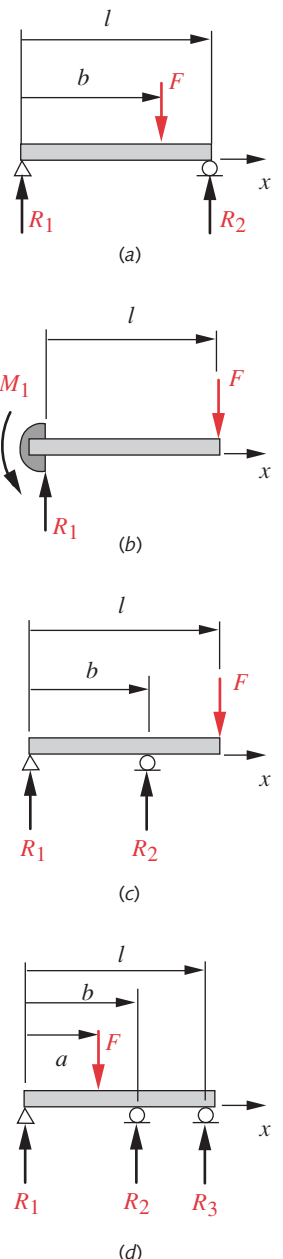
Row	l	a	b	F	I	c	E
<i>a</i>	1.00	0.40	0.60	500	$2.85E-08$	$2.00E-02$	steel
<i>b</i>	0.70	0.20	0.40	850	$1.70E-08$	$1.00E-02$	steel
<i>c</i>	0.30	0.10	0.20	450	$4.70E-09$	$1.25E-02$	steel
<i>d</i>	0.80	0.50	0.60	250	$4.90E-09$	$1.10E-02$	steel
<i>e</i>	0.85	0.35	0.50	750	$1.80E-08$	$9.00E-03$	steel
<i>f</i>	0.50	0.18	0.40	950	$1.17E-08$	$1.00E-02$	steel
<i>g</i>	0.60	0.28	0.50	250	$3.20E-09$	$7.50E-03$	steel
<i>h</i>	0.20	0.10	0.13	500	$4.00E-09$	$5.00E-03$	alum.
<i>i</i>	0.40	0.15	0.30	200	$2.75E-09$	$5.00E-03$	alum.
<i>j</i>	0.20	0.10	0.15	80	$6.50E-10$	$5.50E-03$	alum.
<i>k</i>	0.40	0.16	0.30	880	$4.30E-08$	$1.45E-02$	alum.
<i>l</i>	0.90	0.25	0.80	600	$4.20E-08$	$7.50E-03$	alum.
<i>m</i>	0.70	0.10	0.60	500	$2.10E-08$	$6.50E-03$	alum.
<i>n</i>	0.85	0.15	0.70	120	$7.90E-09$	$1.00E-02$	alum.

loading and choose a material specification that will give a safety factor of 1.5 for $N = 5E8$ cycles.

- *6-25 The beam in Figure P6-11c is subjected to a sinusoidal force time function with $F_{max} = F$ and $F_{min} = 0$, where F and the beam's other data are given in the row(s) assigned from Table P6-5. Find the stress state in the beam due to this loading and choose a material specification that will give a safety factor of 2.5 for $N = 5E8$ cycles.
- *6-26 The beam in Figure P6-11d is subjected to a sinusoidal force time function with $F_{max} = F$ lb and $F_{min} = -F$, where F and the beam's other data are given in the row(s) assigned from Table P6-5. Find the stress state in the beam due to this loading and choose a material specification that will give a safety factor of 6 for $N = 5E8$ cycles.
- *6-27 A storage rack is to be designed to hold the paper roll of Problem 6-8 as shown in Figure P6-12. Determine a suitable value for dimension a in the figure for an infinite-life fatigue safety factor of 2. Assume dimension $b = 100$ mm and that the mandrel is solid and inserts halfway into the paper roll: (more overleaf)

**FIGURE P6-12**

Problem 6-27

**FIGURE P6-11**

Beams and Beam Loadings for Problems 6-23 to 6-26: See Table P6-5 for Data

* Answers to these problems are provided in Appendix D.

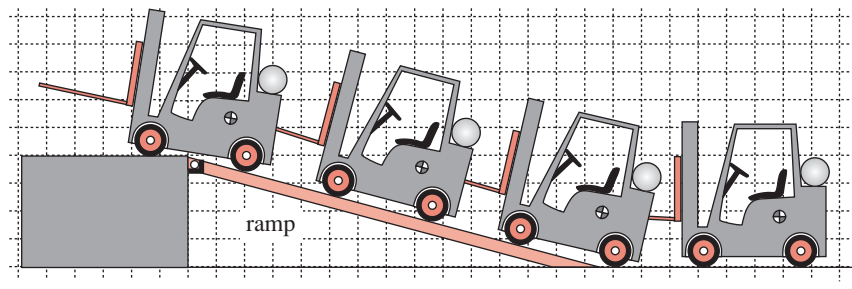


FIGURE P6-13

Problem 6-28

- (a) If the beam is a ductile material with $S_{ut} = 600 \text{ MPa}$,
(b) If the beam is a cast-brittle material with $S_{ut} = 300 \text{ MPa}$.

6-28 Figure P6-13 shows a forklift truck negotiating a 15° ramp to drive onto a 4-ft-high loading platform. The truck weighs 5 000 lb and has a 42-in wheelbase. Design two (one for each side) 1-ft-wide ramps of steel to have a safety factor of 2 for infinite life in the worst case of loading as the truck travels up them. Minimize the weight of the ramps by using a sensible cross-sectional geometry. Choose an appropriate steel or aluminum alloy.

***6-29** A bar 22 mm \times 30 mm in cross section is loaded axially in tension with $F(t) = \pm 8 \text{ kN}$. A 10-mm hole passes through the center of the 30-mm side. Find the safety factor for infinite life if the material has $S_{ut} = 500 \text{ MPa}$.

6-30 Repeat Problem 6.29 with $F_{min} = 0$, $F_{max} = 16 \text{ kN}$.

***6-31** Repeat Problem 6.29 with $F_{min} = 8 \text{ kN}$, $F_{max} = 24 \text{ kN}$.

6-32 Repeat Problem 6.29 with $F_{min} = -4 \text{ kN}$, $F_{max} = 12 \text{ kN}$.

6-33 The bracket in Figure P6-14 is subjected to a sinusoidal force time function with $F_{max} = F$ and $F_{min} = -F$, where F and the beam's other data are given in the row(s) assigned from Table P6-6. Find the stress states at points A and B due to this fully reversed loading and choose a ductile steel or aluminum material specification that will give a safety factor of 2 for infinite life if steel or $N = 5E8$ cycles if aluminum. Assume a geometric stress-concentration factor of 2.5 in bending and 2.8 in torsion.

***6-34** The bracket in Figure P6-14 is subjected to a sinusoidal force time function with $F_{max} = F$ and $F_{min} = 0$, where F and the beam's other data are given in the row(s)

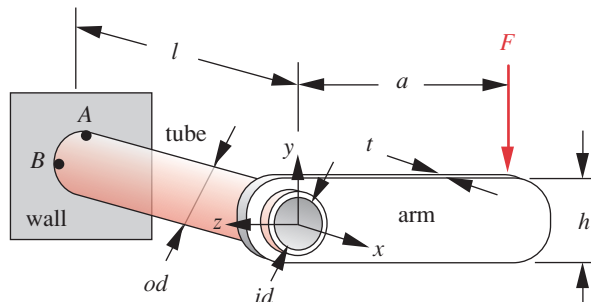


FIGURE P6-14

Problems 6-33 to 6-36 (A Solidworks model of this is on the CD)

* Answers to these problems are provided in Appendix D. Problem numbers in *italics* are design problems. Problem numbers in **boldface** are extended from similar problems in earlier chapters with the same dash number. Problems in succeeding chapters may also continue and extend these problems.

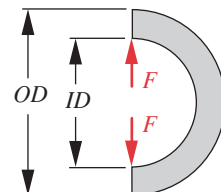
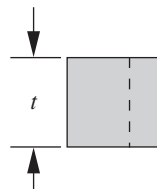
Table P6-6 Data for Problems 6-33 through 6-36

Use only data that are relevant to the particular problem. Lengths in mm, forces in N.

Row	<i>l</i>	<i>a</i>	<i>t</i>	<i>h</i>	<i>F</i>	<i>od</i>	<i>id</i>	<i>E</i>
<i>a</i>	100	400	10	20	50	20	14	steel
<i>b</i>	70	200	6	80	85	20	6	steel
<i>c</i>	300	100	4	50	95	25	17	steel
<i>d</i>	800	500	6	65	160	46	22	alum.
<i>e</i>	85	350	5	96	900	55	24	alum.
<i>f</i>	50	180	4	45	950	50	30	alum.
<i>g</i>	160	280	5	25	850	45	19	steel
<i>h</i>	200	100	2	10	800	40	24	steel
<i>i</i>	400	150	3	50	950	65	37	steel
<i>j</i>	200	100	3	10	600	45	32	alum.
<i>k</i>	120	180	3	70	880	60	47	alum.
<i>l</i>	150	250	8	90	750	52	28	alum.
<i>m</i>	70	100	6	80	500	36	30	steel
<i>n</i>	85	150	7	60	820	40	15	steel

assigned from Table P6-6. Find the stress states at points *A* and *B* due to this repeated loading and choose a ductile steel or aluminum material specification that will give a safety factor of 2 for infinite life if steel or $N = 5E8$ cycles if aluminum. Assume a geometric stress-concentration factor of 2.8 in bending and 3.2 in torsion.

- 6-35 Repeat Problem 6-33 using a cast iron material.
- 6-36 Repeat Problem 6-34 using a cast iron material.
- *6-37 A semicircular curved beam as shown in Figure P6-15 has $od = 150$ mm, $id = 100$ mm and $t = 25$ mm. For a load pair $F = \pm 3$ kN applied along the diameter, find the fatigue safety factor at the inner and outer fibers:
- if the beam is steel with $S_{ut} = 700$ MPa,
 - if the beam is cast iron with $S_{ut} = 420$ MPa.
- 6-38 A 42-mm-dia steel shaft with a 19-mm transverse hole is subjected to a sinusoidal combined loading of $\sigma = \pm 100$ MPa bending stress and a steady torsion of 110 MPa. Find its safety factor for infinite life if $S_{ut} = 1$ GPa.
- *6-39 A 42-mm-dia steel shaft with a 19-mm transverse hole is subjected to a combined loading of $\sigma = \pm 100$ MPa bending stress and an alternating torsion of ± 110 MPa which are 90° out-of-phase. Find its safety factor for infinite life if $S_{ut} = 1$ GPa.
- 6-40 Redesign the roll support of Problem 6-8 to be like Figure P6-16. The mandrels insert to 10% of the roll length. Design dimensions *a* and *b* for an infinite-life safety factor of 2.
- If the beam is steel with $S_{ut} = 600$ MPa,
 - If the beam is cast iron with $S_{ut} = 300$ MPa.
- *6-41 A 10-mm-ID steel tube carries liquid at 7 MPa. The pressure varies periodically from zero to maximum. The steel has $S_{ut} = 400$ MPa. Determine the infinite-life fatigue safety factor for the wall if its thickness is:
- 1 mm,
 - 5 mm.

**FIGURE P6-15**

Problem 6-37 (A Solidworks model of this is on the CD)

* Answers to these problems are provided in Appendix D. Problem numbers in *italics* are design problems. Problem numbers in **boldface** are extended from similar problems in earlier chapters with the same dash number. Problems in succeeding chapters may also continue and extend these problems.

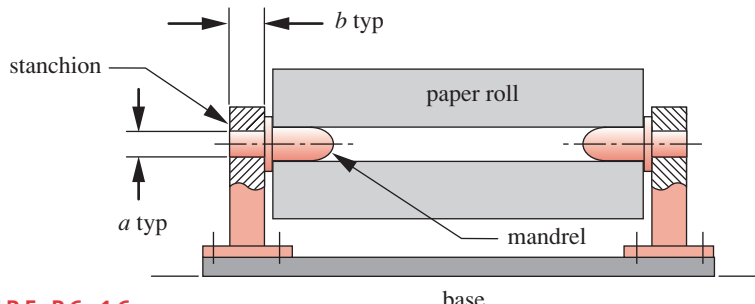


FIGURE P6-16

Problem 6-40 (A Solidworks model of this is on the CD)

6

- 6-42** A cylindrical tank with hemispherical ends is required to hold 150 psi of pressurized air at room temperature. The pressure cycles from zero to maximum. The steel has $S_{ut} = 500$ MPa. Determine the infinite-life fatigue safety factor if the tank diameter is 0.5 m, the wall thickness is 1 mm, and its length is 1 m.
- 6-43** The paper rolls in Figure P6-17 are 0.9-m-OD \times 0.22-m-ID \times 3.23 m long and have a density of 984 kg/m³. The rolls are transferred from the machine conveyor (not shown) to the forklift truck by the V-linkage of the off-load station, which is rotated through 90° by an air cylinder. The paper then rolls onto the waiting forks of the truck. The forks are 38-mm-thick by 100-mm-wide by 1.2 m long and are tipped at a 3° angle from the horizontal and have $S_{ut} = 600$ MPa. Find the infinite-life fatigue safety factor for the two forks on the truck when the paper rolls onto it under two different conditions (state all assumptions):
- The two forks are unsupported at their free end.
 - The two forks are contacting the table at point A.
- 6-44** Determine a suitable thickness for the V-links of the off-loading station of Figure P6-17 to limit their deflections at the tips to 10 mm in any position during their rotation. Two V-links support the roll, at the 1/4 and 3/4 points along the roll's length, and each of the V arms is 10 cm wide by 1 m long. What is their infinite-

* Problem numbers in *italics* are design problems. Problem numbers in **boldface** are extended from similar problems in earlier chapters with the same dash number. Problems in succeeding chapters may also continue and extend these problems.

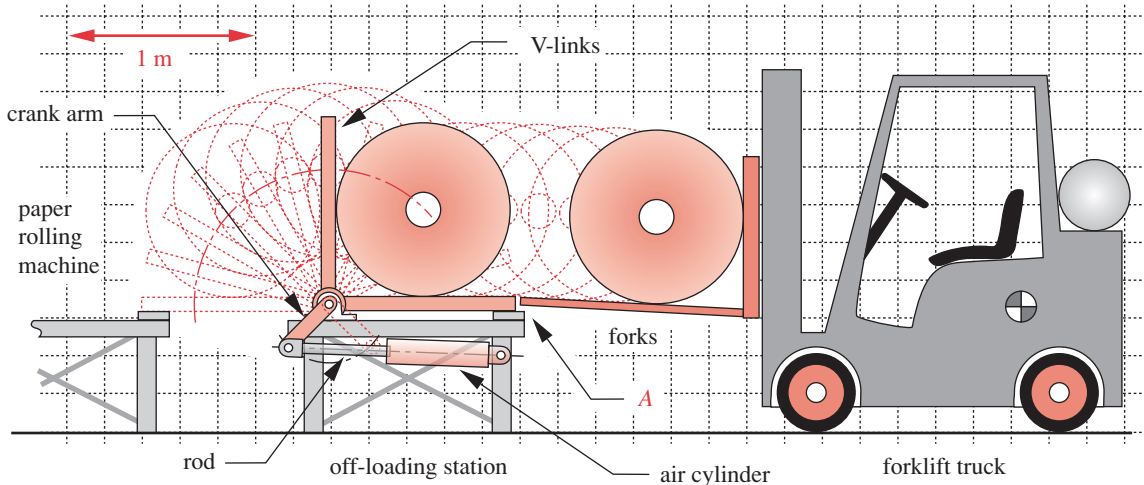


FIGURE P6-17

Problems 6-43 to 6-47

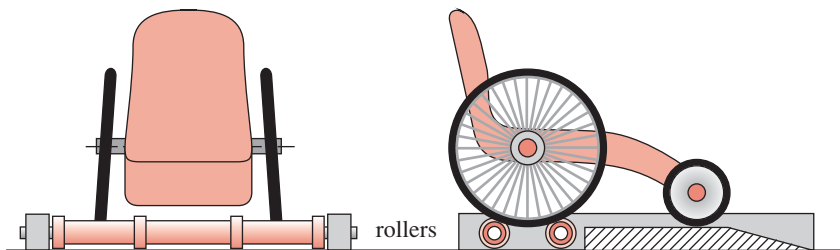


FIGURE P6-18

Problem 6-48

life fatigue safety factor when designed to limit deflection as above?

$S_{ut} = 600 \text{ MPa}$. See Problem 4-43 for more information.

- 6-45** Determine the infinite-life fatigue safety factor based on the tension load on the air-cylinder rod in Figure P6-17. The tension load cycles from zero to maximum (compression loads below the critical buckling load will not affect fatigue life). The crank arm that it rotates is 0.3 m long and the rod has a maximum extension of 0.5 m. The 25-mm-dia rod is solid steel with $S_{ut} = 600 \text{ MPa}$. State all assumptions.
- 6-46** The V-links of Figure P6-17 are rotated by the crank arm through a shaft that is 60-mm dia by 3.23-m long. Determine the maximum torque applied to this shaft during the motion of the V-linkage and find the infinite-life fatigue safety factor for the shaft if its $S_{ut} = 600 \text{ MPa}$. See Problem 6-43 for more information.
- *6-47** Determine the maximum forces on the pins at each end of the air cylinder of Figure P6-17. Determine the infinite-life fatigue safety factor for these pins if they are 30-mm dia and in single shear. $S_{ut} = 600 \text{ MPa}$. See Problem 6-43 for more information.
- 6-48** Figure P6-18 shows an exerciser for a 100-kg wheelchair racer. The wheelchair has 65-cm-dia drive wheels separated by a 70-cm track width. Two free-turning rollers on bearings support the rear wheels. The lateral movement of the chair is limited by the flanges. Design the 1-m-long rollers as hollow tubes of aluminum (select alloy) to minimize the height of the platform and also limit the roller deflections to 1 mm in the worst case. Specify suitably sized steel axles to support the tubes on bearings. Calculate the fatigue safety factors at a life of $N = 5E8$ cycles.
- 6-49** Figure P6-19 shows a machined pivot pin that is a press-fit into part A and is a slip fit in part B. If $F = 100 \text{ lb}$, $l = 2 \text{ in}$, and $d = 0.5 \text{ in}$, what is the pin's safety factor against fatigue when made of SAE 1020 cold-rolled steel? The loading is fully reversed and a reliability of 90% is desired. There is a bending stress concentration factor $K_t = 1.8$ at the section where the pin leaves part A on the right-hand side.
- 6-50** Figure P6-19 shows a machined pivot pin that is a press-fit into part A and is a slip fit in part B. If $F = 100 \text{ N}$, $l = 50 \text{ mm}$, and $d = 16 \text{ mm}$, what is the pin's safety factor against fatigue when made of class 50 cast iron? The loading is fully reversed and a reliability of 90% is desired. There is a bending stress concentration factor $K_t = 1.8$ at the section where the pin leaves part A on the right-hand side.
- 6-51** A component in the shape of a large sheet is to be fabricated from 7075-T651 aluminum, which has fracture toughness $K_c = 24.2 \text{ MPa}\cdot\text{m}^{0.5}$ and a tensile yield strength of 495 MPa. Determine the number of loading cycles that can be endured if the nominal stress varies from 0 to one-half the yield strength and the initial crack had a total length of 1.2 mm. The values of the coefficient and exponent in equation 6.4 for this material are $A = 5 \times 10^{-11} (\text{mm}/\text{cycle})$ and $n = 4$.

6

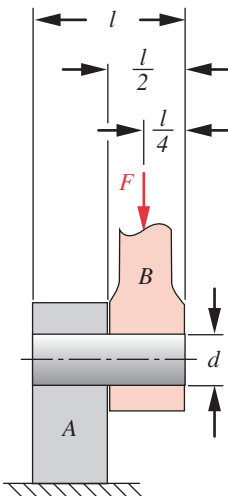


FIGURE P6-19

Problems 6-49 and 6-50

* Answers to these problems are provided in Appendix D. Problem numbers in *italics* are design problems. Problem numbers in **boldface** are extended from similar problems in earlier chapters with the same dash number. Problems in succeeding chapters may also continue and extend these problems.

- *6-52 A component in the shape of a large sheet is to be fabricated from SAE 4340 steel, which has a fracture toughness $K_c = 98.9 \text{ MPa}\cdot\text{m}^{0.5}$. The sheets are inspected for crack flaws after fabrication, but the inspection device cannot detect flaws smaller than 5 mm. Determine the minimum thickness required for the sheet to have a minimum cycle life of 10^6 cycles (using fracture-mechanics criteria) if its width is 400 mm and the load normal to the crack varies from 20 to 170 kN. The values of the coefficient and exponent in equation 6.4 for this material are $A = 4 \times 10^{-9} \text{ (mm/cycle)}$ and $n = 3$.
- 6-53 A closed, thin-wall cylinder is made from an aluminum alloy that has a fracture toughness of $38 \text{ MPa}\cdot\text{m}^{0.5}$ and has the following dimensions: length = 200 mm, $OD = 84 \text{ mm}$, and $ID = 70 \text{ mm}$. A 2.8-mm-deep semicircular crack is discovered on the inner diameter away from the ends, oriented along a line parallel to the cylinder axis. If the cylinder is repeatedly pressurized from 0 to 75 MPa, how many pressure cycles can it withstand? The values of the coefficient and exponent in equation 6.4 for this material are $A = 5 \times 10^{-12} \text{ (mm/cycle)}$ and $n = 4$. (Hint: The value of the geometry factor for a semicircular surface flaw is $b = 2/p$ and the crack grows in the radial direction.)
- 6-54 A nonrotating, hot-rolled, steel beam has a channel section with $h = 64 \text{ mm}$ and $b = 127 \text{ mm}$. It is loaded in repeated bending with the neutral axis through the web. Determine its corrected fatigue strength with 90% reliability if it is used in an environment that has a temperature that is below 450°C and has an ultimate tensile strength of 320 MPa.
- 6-55 A nonrotating, machined, steel rod has a round section with $d = 50 \text{ mm}$. It is loaded with a fluctuating axial force. Determine its corrected fatigue strength with 99% reliability if it is used in an environment that has a temperature below 450°C and has an ultimate tensile strength of 480 MPa.
- 6-56 A nonrotating, cold-drawn, steel rod has a round section with $d = 76 \text{ mm}$. It is loaded in repeated torsion. Determine its corrected fatigue strength with 99% reliability if it is used in an environment that has a temperature of 500°C and has an ultimate tensile strength of 855 MPa.
- 6-57 A nonrotating, ground, steel rod has a rectangular section with $h = 60 \text{ mm}$ and $b = 40 \text{ mm}$. It is loaded in repeated bending. Determine its corrected fatigue strength with 99.9% reliability if it is used in an environment that has a temperature that is below 450°C and has an ultimate tensile strength of 1 550 MPa.
- 6-58 A grooved steel shaft similar to that shown in Figure C-5 (Appendix C) is to be loaded in bending. Its dimensions are: $D = 57 \text{ mm}$, $d = 38 \text{ mm}$, $r = 3 \text{ mm}$. Determine the fatigue stress-concentration factor if the material $S_{ut} = 1130 \text{ MPa}$.
- 6-59 A steel shaft with a transverse hole similar to that shown in Figure C-8 (Appendix C) is to be loaded in torsion. Its dimensions are: $D = 32 \text{ mm}$, $d = 3 \text{ mm}$. Determine the fatigue stress-concentration factor if the material $S_{ut} = 808 \text{ MPa}$.
- 6-60 A hardened aluminum filleted flat bar similar to that shown in Figure C-9 (Appendix C) is to be loaded axially. Its dimensions are: $D = 1.20 \text{ in}$, $d = 1.00 \text{ in}$, $r = 0.10 \text{ in}$. Determine the fatigue stress-concentration factor if the material $S_{ut} = 76 \text{ ksi}$.
- 6-61 A rotating shaft with a shoulder fillet seated in the inner race of a rolling contact bearing with the shoulder against the edge of the bearing is shown in Figure P6-20. The bearing has a slight eccentricity that induces a fully reversed bending moment in the shaft as it rotates. Measurements indicate that the resulting alternating stress amplitude due to bending is $\sigma_a = 57 \text{ MPa}$. The torque on the shaft fluctuates from a high of 90 N·m to a low of 12 N·m and is in phase with the bending stress. The shaft is ground and its dimensions are $D = 23 \text{ mm}$, $d = 19 \text{ mm}$, and $r = 1.6 \text{ mm}$. The

* Answers to these problems are provided in Appendix D.

shaft material is SAE 1040 cold-rolled steel. Determine the infinite-life fatigue safety factor for the shaft for a reliability of 99%.

- 6-62 A tension member in a machine is filleted as shown in Figure P6-21. The member has a manufacturing defect that causes the fluctuating tension load to be applied eccentrically resulting in a fluctuating bending load as well. Measurements indicate that the maximum bending stress is 16.4 MPa and the minimum is 4.1 MPa. The tensile load fluctuates from a high of 3.6 kN to a low of 0.90 kN and is in phase with the bending stress. The member is machined and its dimensions are $D = 33$ mm, $d = 25$ mm, $h = 3$ mm and $r = 3$ mm. The material is SAE 1020 cold-rolled steel. Determine the infinite-life fatigue safety factor for the member for 90% reliability.
- 6-63 For a filleted flat bar in tension similar to that shown in Figure C-9 (Appendix C) and the data from the row(s) assigned from Table P6-7, determine the alternating and mean axial stresses as modified by the appropriate stress concentration factors in the bar.
- 6-64 For a filleted flat bar in bending similar to that shown in Figure C-10 (Appendix C) and the data from the row(s) assigned from Table P6-7, determine the alternating and mean bending stresses as modified by the appropriate stress concentration factors in the bar.
- 6-65 For a shaft, with a shoulder fillet, in tension similar to that shown in Figure E-1 (Appendix C) and the data from the row(s) assigned from Table P6-7, determine the alternating and mean axial stresses as modified by the appropriate stress concentration factors in the shaft.
- 6-66 For a shaft, with a shoulder fillet, in bending similar to that shown in Figure E-2 (Appendix C) and the data from the row(s) assigned from Table P6-7, determine the alternating and mean bending stresses as modified by the appropriate stress concentration factors in the shaft.
- 6-67 A machine part is subjected to fluctuating, simple, multiaxial stresses. The fully corrected nonzero stress ranges are: $\sigma_{xmin} = 50$ MPa, $\sigma_{xmax} = 200$ MPa, $\sigma_{ymin} = 80$ MPa, $\sigma_{ymax} = 320$ MPa, $\tau_{xzmin} = 120$ MPa, $\tau_{xymax} = 480$ MPa. The material properties are: $S_e = 525$ MPa and $S_{ut} = 1200$ MPa. Using a Case 3 load line, calculate and compare the infinite-life safety factors given by the Sines and von Mises methods.
- 6-68 A cylindrical tank with hemispherical ends has been built. It was made from hot rolled steel that has $S_{ut} = 380$ MPa. The tank outside diameter is 300 mm with 20 mm wall thickness. The pressure may fluctuate from 0 to an unknown maximum.

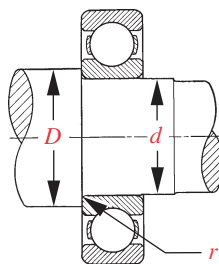


FIGURE P6-20

Problem 6-61

6

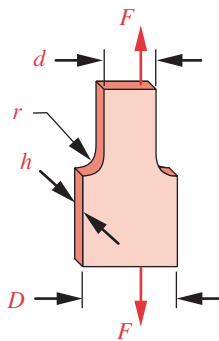


FIGURE P6-21

Problem 6-62

Table P6-7 Data for Problems 6-63 through 6-66

Use only data that are relevant to the particular problem.

Lengths in mm, forces in N, and moments in N-m.

Row	D	d	r	h	M_{min}	M_{max}	P_{min}	P_{max}	Material
a	40	20	4	10	80	320	8000	32000	SAE 1020 CR
b	26	20	1	12	100	500	9500	47500	SAE 1040 CR
c	36	30	1.5	8	60	180	6500	19500	SAE 1020 CR
d	33	30	1	8	75	300	7200	28800	SAE 1040 CR
e	21	20	1	10	50	150	5500	16500	SAE 1050 CR
f	51	50	1.5	7	80	320	8000	32000	SAE 1020 CR
g	101	100	5	8	400	800	15000	60000	SAE 1040 CR

Table P6-8

Data for Problem 6-70

Row	σ_m'	σ_a'
a	50	30
b	70	30
c	100	10
d	20	60
e	80	40
f	40	40
g	120	50
h	80	80

For an infinite-life fatigue safety factor of 4 with 99.99% reliability, what is the maximum pressure to which the tank may be subjected?

- 6-69 A rotating shaft has been designed and fabricated from SAE 1040 HR steel. It is made from tubing that has an outside diameter of 60 mm and a wall thickness of 5 mm. Strain gage measurements indicate that there is a fully reversed axial stress of 68 MPa and a torsional stress that fluctuates from 12 MPa to 52 MPa in phase with the axial stress at the critical point on the shaft. Determine the infinite-life fatigue safety factor for the shaft for a reliability of 99%.
- 6-70 For the mean and alternating stress values (in MPa) in the row(s) assigned in Table P6-8, find the safety factor for each of the four loading variation cases based on the Modified-Goodman diagram if $S_e = 100$, $S_y = 150$, and $S_{ut} = 200$ MPa.
- 6-71 A rotating shaft with a shoulder fillet, in torsion similar to that shown in Appendix C Figure C-3 is made from SAE 1020 CR steel and has dimensions $D = 40$ mm, $d = 20$ mm, and $r = 4$ mm. The shaft is ground and is subjected to a fully reversed torque of $+/- 80$ N-m. Determine the shaft's infinite-life safety factor for 99.9% reliability.

7



SURFACE FAILURE

*Use it up, wear it out;
Make it do, or do without.*

NEW ENGLAND MAXIM

7.0 INTRODUCTION

There are only three ways in which parts or systems can “fail”: *obsolescence*, *breakage*, or *wearing out*. My old computer still works well but is obsolete and no longer of any use to me. My wife’s favorite vase is now in pieces since I dropped it on the floor, and it is irrecoverable. However, my 123 000-mile automobile is still quite serviceable and useful despite showing some signs of wear. Most systems are subject to all three types of possible failure. Failure by obsolescence is somewhat arbitrary. (My grandchild is now getting good use of the old computer.) Failure by breakage is often sudden and may be permanent. Failure by “wearing out” is generally a gradual process and is sometimes repairable. Ultimately, any system that does not fall victim to one of the other two modes of failure will inevitably wear out if kept in service long enough. Wear is the final mode of failure, which nothing escapes. Thus, we should realize that we cannot design to avoid all types of wear completely, only to postpone them.

The previous chapters have dealt with failure of parts by distortion (yielding) and breakage (fracture). **Wear** is a broad term that encompasses many types of failures, all of which involve changes to the **surface** of the part. Some of these so-called *wear mechanisms* are still not completely understood, and rival theories exist in some cases. Most experts describe five general categories of wear: **adhesive wear**, **abrasive wear**, **erosion**, **corrosion wear**, and **surface fatigue**. The following sections discuss these topics in detail. In addition, there are other types of surface failure that do not fit neatly into one of the five categories or that can fit into more than one. **Corrosion fatigue** has aspects of the last two categories as does **fretting corrosion**. For simplicity, we will discuss these hybrids in concert with one of the five main categories listed above.

Failure from wear usually involves the loss of some material from the surfaces of solid parts in the system. The wear motions of interest are sliding, rolling, or some

Table 7-0 Variables Used in This Chapter

Symbol	Variable	ips units	SI units	See
a	half-width of contact patch	in	m	Sect. 7.8–7.10
A_a	apparent area of contact	in ²	m ²	Sect. 7.2
A_r	real area of contact	in ²	m ²	Eq. 7.1
B	geometry factor	1/in	1/m	Eq. 7.9b
b	half-length of contact patch	in	m	Sect. 7.8–7.10
d	depth of wear	in	m	Eq. 7.7
E	Young's modulus	psi	Pa	all
F, P	force or load	lb	N	all
f	friction force	lb	N	Eq. 7.2
f_{max}	maximum tangential force	lb	N	Eq. 7.22f
K	wear coefficient	none	none	Eq. 7.7
l	length of linear contact	in	m	Eq. 7.7
L	length of cylindrical contact	in	m	Eq. 7.14
m_1, m_2	material constants	1/psi	m ² /N	Eq. 7.9a
H	penetration hardness	psi	kg/mm ²	Eq. 7.7
N	number of cycles	none	none	Eq. 7.26
N_f	safety factor in surface fatigue	none	none	Example 7-5
p	pressure in contact patch	psi	N/m ²	Sect. 7.8–7.10
P_{avg}	avg pressure in contact patch	psi	N/m ²	Sect. 7.8–7.10
P_{max}	max pressure in contact patch	psi	N/m ²	Sect. 7.8–7.10
R_1, R_2	radii of curvature	in	m	Eq. 7.9b
S_{us}	ultimate shear strength	psi	Pa	Sect. 7.3
S_{ut}	ultimate tensile strength	psi	Pa	Sect. 7.3
S_y	yield strength	psi	Pa	Sect. 7.3
S_{yc}	yield strength in compression	psi	Pa	Sect. 7.3
V	volume	in ³	m ³	Eq. 7.7
x, y, z	generalized length variables	in	m	all
μ	coefficient of friction	none	none	Eq. 7.2–7.6
v	Poisson's ratio	none	none	all
σ	normal stress	psi	Pa	all
σ_1	principal stress	psi	Pa	Sect. 7.11
σ_2	principal stress	psi	Pa	Sect. 7.11
σ_3	principal stress	psi	Pa	Sect. 7.11
τ	shear stress	psi	Pa	all
τ_{13}	maximum shear stress	psi	Pa	Sect. 7.11
τ_{21}	principal shear stress	psi	Pa	Sect. 7.11
τ_{32}	principal shear stress	psi	Pa	Sect. 7.11

* A 1977 study sponsored by the ASME estimated that the energy cost to the U.S. economy associated with the replacement of equipment that failed from wear accounted for 1.3% of total U.S. energy consumption. This was then equivalent to about 160 million barrels of oil per year. See O. Pinkus and D. F. Wilcock, *Strategy for Energy Conservation through Tribology*, ASME, New York, 1977, p. 93.

combination of both. Wear is a serious cost to the national economy.* It only requires the loss of a very small volume of material to render the entire system nonfunctional. Rabinowicz^[1] estimated that a 4 000-lb automobile, when completely “worn out,” will

have lost only a few ounces of metal from its working surfaces. Moreover, these damaged surfaces will not be visible without extensive disassembly, so it is often difficult to monitor and anticipate the effects of wear before failure occurs.

Table 7-0 shows the variables used in this chapter and references the equations, tables, or sections in which they are used. At the end of the chapter, a summary section is provided that also groups all the significant equations from this chapter for easy reference and identifies the chapter section in which their discussion can be found.

7.1 SURFACE GEOMETRY

Before discussing the types of wear mechanisms in detail it will be useful to define the characteristics of an engineering surface that are relevant to these processes. (Material strength and hardness will also be factors in wear.) Most solid surfaces that are subject to wear in machinery will be either machined or ground, though some will be as-cast or as-forged. In any case, the surface will have some degree of roughness that is concomitant with its finishing process. Its degree of roughness or smoothness will have an effect on both the type and degree of wear that it will experience.

Even an apparently smooth surface will have microscopic irregularities. These can be measured by any of several methods. A profilometer passes a lightly loaded, hard (e.g., diamond) stylus over the surface at controlled (low) velocity and records its undulations. The stylus has a very small (about $0.5 \mu\text{m}$) radius tip that acts, in effect, as a low-pass filter, since contours smaller than its radius are not sensed. Nevertheless, it gives a reasonably accurate profile of the surface with a resolution of $0.125 \mu\text{m}$ or better. Figure 7-1 shows the profiles and SEM* photographs (100x) of both ground (a) and machined (b) surfaces of hardened steel cams. The profiles were measured with a Hom-

* Scanning Electron Microscope

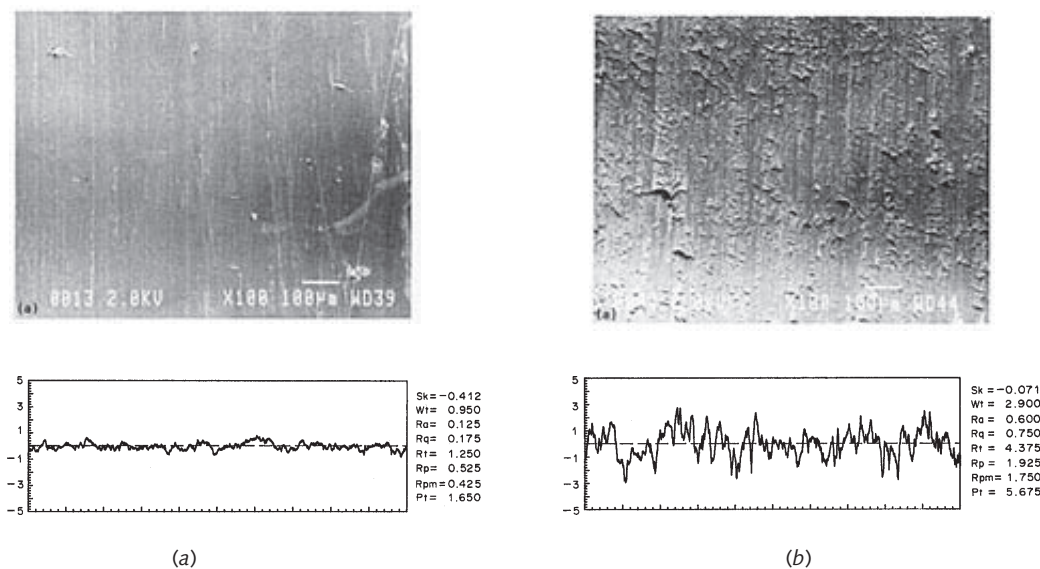


FIGURE 7-1

Scanning Electron Microscope Surface-Replica Photographs (100x) and Profiles of Ground (a) and Milled (b) Cam Surfaces

mel T-20 profilometer that digitizes 8 000 data points over the sample length (here 2.5 mm). The microscopic "mountain peaks" on the surfaces are called **asperities**.

From these profiles a number of statistical measures may be calculated. ISO defines at least 19 such parameters. Some of them are shown in Figure 7-2 along with their mathematical definitions. Perhaps the most commonly used parameters are R_a , which is the average of the absolute values of the measured points, or R_q , which is their rms average. These are very similar in both value and meaning. Unfortunately many engineers specify only one of these two parameters, neither of which tells enough about the surface. For example, the two surfaces shown in Figures 7-3a and b have the same R_a and R_q values but are clearly different in nature. One has predominantly positive, and the other predominantly negative, features. These two surfaces will react quite differently to sliding or rolling against another surface.

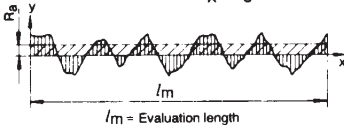
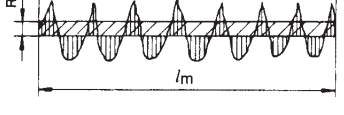
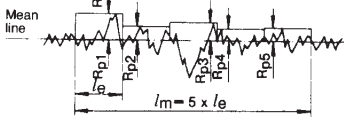
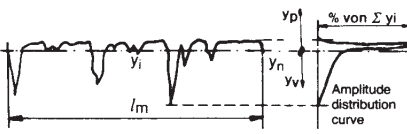
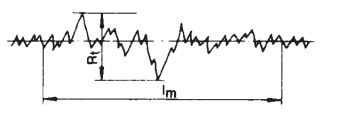
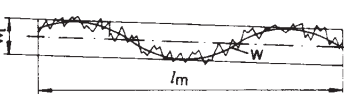
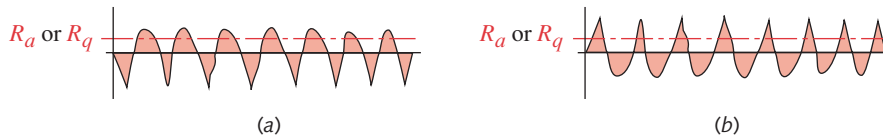
R_a (CLA) (AA)	Arithmetic mean roughness value The arithmetic average value of filtered roughness profile determined from deviations about the centre line within the evaluation length l_m . $R_a = \frac{1}{l_m} \int_{x=0}^{x=l_m} y dx$ 	R_q (RMS) The RMS value obtained from the deviations of the filtered roughness profile over the evaluation length l_m . $R_q = \sqrt{\frac{1}{l_m} \int_0^{l_m} y^2(x) dx}$ 
R_{pm} Mean peak height value above the mean line DIN 4762	The arithmetic average value of the five single highest peaks above the mean line R_{p1} – R_{p5} , similar to the R_z (DIN) definition specified in DIN 4768. The five highest peaks are determined from the "centre line" of the filtered roughness profile each from a single sampling length l_e . $R_{pm} = \frac{1}{5} \cdot (R_{p1} + R_{p2} + \dots + R_{p5})$	Sk Skewness of the profile A measure of the shape or symmetry of the amplitude distribution curve obtained from the filtered roughness profile. A negative skewness would represent good bearing properties. $Sk = \frac{1}{R_q^3} \cdot \frac{1}{n} \sum_{i=1}^{i=n} (y_i - \bar{y})^3$
R_p Single highest peak above mean line DIN 4762 ISO 4287/1	The value of the highest single peak above the centre line of the filtered profile as obtained from R_{pm} . 	Amplitude-distribution curve DIN 4762 ISO 4287/1 A graph of the frequency in % of profile amplitudes. 
R_t (R_h) (R_d) DIN 4762 (1960) since 1978 it is R_{max} .	Maximum peak-to-valley height of the filtered profile over the evaluation length l_m irrespective of the sampling lengths l_e . 	W_t Waviness depth The maximum peak-to-valley height of levelled waviness profile (roughness eliminated) within the evaluation length l_m . 

FIGURE 7-2

DIN and ISO Surface Roughness, Waviness, and Skewness Parameter Definitions (Courtesy of Hommel America Inc., New Britain, Ct.)

**FIGURE 7-3**

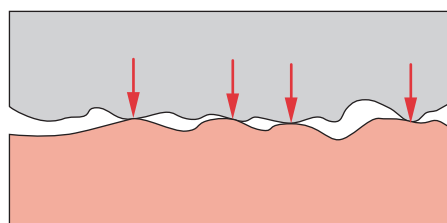
Different Surface Contours Can Have the Same R_a or R_q Values

In order to differentiate these surfaces that have identical R_a or R_q values, other parameters should be calculated. Skewness S_k is a measure of the average of the first derivative of the surface contour. A negative value of S_k indicates that the surface has a predominance of valleys (Figure 7-3a) and a positive S_k defines a predominance of peaks (Figure 7-3b). Many other parameters can be computed (see Figure 7-2). For example, R_t defines the largest peak-to-valley dimension in the sample length, R_p the largest peak height above the mean line, and R_{pm} the average of the 5 largest peak heights. All the roughness measurements are calculated from an electronically filtered measurement that zeros out any slow-changing waves in the surface. An average line is computed from which all peak/valley measurements are then made. In addition to these roughness measurements (denoted by R), the waviness W_t of the surface can also be computed. The W_t computation filters out the high-frequency contours and preserves the long-period undulations of the raw surface measurement. If you want to completely characterize the surface-finish condition, note that using only R_a or R_q is not sufficient.

7.2 MATING SURFACES

When two surfaces are pressed together under load, their apparent area of contact A_a is easily calculated from geometry but their real area of contact A_r is affected by the asperities present on their surfaces and is more difficult to accurately determine. Figure 7-4 shows two parts in contact. The tops of the asperities will initially contact the mating part and the initial area of contact will be extremely small. The resulting stresses in the asperities will be very high and can easily exceed the compressive yield strength of the material. As the mating force is increased, the asperity tips will yield and spread until their combined area is sufficient to reduce the average stress to a sustainable level, i.e., some *compressive penetration strength* of the weaker material.

We can get a measure of a material's compressive penetration strength from conventional hardness tests (Brinell, Rockwell, etc.), which force a very smooth stylus into

**FIGURE 7-4**

The Actual Contact Between Two Surfaces Is Only at the Asperity Tips

the material and deform (yield) the material to the stylus' shape. (See Section 2.4.) The penetration strength S_p is easily calculated from these test data and tends to be of the order of 3 times the compressive yield strength S_{yc} of most materials.^[2]

The real area of contact can then be estimated from

$$A_r \cong \frac{F}{S_p} \cong \frac{F}{3S_{yc}} \quad (7.1)$$

where F is the force applied normal to the surface and the strengths are as defined in the above paragraph, taken for the weaker of the two materials. *Note that the contact area for a material of particular strength under a given load will be the same regardless of the apparent area of the mating surfaces.*

7.3 FRICTION

7

Note that the real area of contact A_r (Eq. 7.1) is independent of the apparent area A_a that is defined by the geometry of the mating parts. This is the reason that Coulomb friction between two solids is also independent of the apparent area of contact A_a . The equation for Coulomb sliding friction is

$$f = \mu F \quad (7.2a)$$

where f is the force of friction, μ is the coefficient of dynamic friction, and F is the normal force.

The normal force presses the two surfaces together and creates elastic deformations and adhesions (see next section) at the asperities' tips. We can define the dynamic Coulomb friction force f as being the force necessary to shear the adhered and elastically interlocked asperities in order to allow a sliding motion. This shearing force is equal to the product of the shear strength of the weaker material and the actual contact area A_r plus a "plough force" P .

$$f = S_{us} A_r + P \quad (7.2b)$$

The plough force P is due to loose particles digging into the surfaces and is negligible compared to the shear force,^{*} so can be ignored. Recalling equation 7.1 gives

$$A_r \cong \frac{F}{3S_{yc}} \quad (7.2c)$$

Substituting equation 7.2c in 7.2b (ignoring P) gives

$$f \cong F \frac{S_{us}}{3S_{yc}} \quad (7.2d)$$

Combining equations 7.2a and 7.2d gives

$$\mu = \frac{f}{F} \cong \frac{S_{us}}{3S_{yc}} \quad (7.3)$$

which indicates that the coefficient of friction μ is a function only of a ratio of material strengths of the weaker of the two materials in contact.

* This will be true only if the two surfaces have about the same hardness. If one surface is harder and rougher than the other, there could be a significant plough force.

The ultimate shear strength can be estimated based on the ultimate tensile strength of the material.

$$\begin{aligned} \text{steels : } S_{us} &\cong 0.8S_{ut} \\ \text{other ductile metals : } S_{us} &\cong 0.75S_{ut} \end{aligned} \quad (7.4)$$

The yield strength in compression as a fraction of the ultimate tensile strength varies with the material and alloy over a fairly broad range, perhaps

$$0.5S_{ut} < S_{yc} < 0.9S_{ut} \quad (7.5)$$

Substituting equations 7.4 and 7.5 in equation 7.3 gives

$$\frac{0.75S_{ut}}{3(0.9S_{ut})} < \mu < \frac{0.8S_{ut}}{3(0.5S_{ut})}$$
$$0.28 < \mu < 0.53 \quad (7.6)$$

which is approximately the range of values of μ common for dry metals in air. Note that if the metals are thoroughly cleaned, their μ will be as much as twice these values. In vacuum, the μ for clean surfaces can approach infinity due to cold-welding. There is so much variation in coefficient of friction with contaminant levels and other factors that the engineer should develop test data for the actual materials used under realistic service conditions. It is a simple test to perform.

7

Effect of Roughness on Friction

One might expect the surface roughness to have a strong influence on the friction coefficient. Tests show only a weak relationship, however. At extremely smooth finishes, below about $10 \mu\text{in } R_a$, the coefficient of friction μ does increase by as much as a factor of 2 due to an increase in the real contact area. At very rough finishes, above about $50 \mu\text{in } R_a$, μ also increases slightly due to the energy needed to overcome asperity interferences (plowing) in addition to shearing their adhesion bonds.

Effect of Velocity on Friction

Kinetic Coulomb friction is usually modeled as being independent of sliding velocity V except for a discontinuity at $V = 0$ where a larger, static coefficient is measured. In reality, there is a continuous, nonlinear drop in μ with increasing V . This function is approximately a straight line when plotted against the log of V , and its negative slope is a few percent per decade.^[7] It is believed that some of this occurs because the increased interface temperatures resulting from the higher velocities reduces the material's shear yield strength in equation 7.3 (p. 424).

Rolling Friction

When a part rolls on another without any sliding, the coefficient of friction is much lower with μ in the range of $5E-3$ to $5E-5$. The friction force will vary as some power of the load (from 1.2 to 2.4) and inversely with the radius of curvature of the rolling elements. Surface roughness does have an effect on rolling friction, and most such joints are fin-

ished by grinding to minimize their roughness. High hardness materials are usually used to obtain the needed strengths and promote smooth ground finishes. There is little variation of rolling friction with velocity.^[7]

Effect of Lubricant on Friction

Introduction of a lubricant to a sliding interface has several beneficial effects on the friction coefficient. Lubricants may be liquid or solid, but will share the properties of low shear strength and high compressive strength. A liquid lubricant such as petroleum oil is essentially incompressible at the levels of compressive stress encountered in bearings but it readily shears. Thus, it becomes the weakest material in the interface, and its low shear strength in equation 7.3 reduces the coefficient of friction. Lubricants also act as contaminants to the metal surfaces and coat them with monolayers of molecules that inhibit adhesion even between compatible metals (see next section). Many commercial lubricant oils are mixed with various additives that react with the metals to form monolayer contaminants. So-called EP (*Extreme Pressure*) lubricants add fatty acids or other compounds to the oil that attack the metal chemically and form a contaminant layer that protects and reduces friction even when the oil film is squeezed out of the interface by high contact loads. Lubricants, especially liquids, also serve to remove heat from the interface. Lower temperatures reduce surface interactions and wear. Lubricants and lubrication phenomena will be discussed in more detail in Chapter 11. Table 7-1 shows some typical values of friction coefficients for commonly encountered pairs.

7.4 ADHESIVE WEAR

When (clean) surfaces such as those shown in Figure 7-1 (p. 421) are pressed against one another under load, some of the asperities in contact will tend to adhere to one another due to the attractive forces between the surface atoms of the two materials.^[3] As sliding between the surfaces is introduced, these adhesions are broken, either along the

Table 7-1 Coefficients of Friction for Some Material Combinations

Material 1	Material 2	Static		Dynamic	
		Dry	Lubricated	Dry	Lubricated
mild steel	mild steel	0.74		0.57	0.09
mild steel	cast iron		0.183	0.23	0.133
mild steel	aluminum	0.61		0.47	
mild steel	brass	0.51		0.44	
hard steel	hard steel	0.78	0.11–0.23	0.42	0.03–0.19
hard steel	babbitt	0.42–0.70	0.08–0.25	0.34	0.06–0.16
Teflon	Teflon	0.04			0.04
steel	Teflon	0.04			0.04
cast iron	cast iron	1.10		0.15	0.07
cast iron	bronze			0.22	0.077
aluminum	aluminum	1.05		1.4	

Source: *Mark's Mechanical Engineers' Handbook*, T. Baumeister, ed., McGraw-Hill, New York.

original interface or along a new plane through the material of the asperity peak. In the latter case, a piece of part A is transferred to part B, causing surface disruption and damage. Sometimes, a particle of one material will be broken free and become debris in the interface, which can then scratch the surface and plough furrows in both parts. This damage is sometimes called **scoring** or **scuffing*** of the surface. Figure 7-5 shows an example of a shaft failed by adhesive wear in the absence of adequate lubricant.^[6]

The original adhesion theory postulated that all asperity contacts would result in yielding and adhesion due to the high stresses present. It is now believed that in most cases of contact, especially with repeated rubbing, only a small fraction of the asperity contacts actually result in yielding and adhesion; elastic deformations of the asperities also play a significant role in the tractive forces (friction) developed at the interface.^[32]

COMPATIBILITY An important factor affecting adhesion is the metallurgical compatibility of the mating materials. **Metallurgical compatibility** between two metals is defined as *high mutual solubility or the formation of intermetallic compounds*.^[4] Davies defines two conditions for metallurgical **incompatibility**, meaning that the *metals can then slide on one another with relatively little scoring*.^[5]

- 1 *The metals must be insoluble in each other, with neither material dissolving in the other nor forming an alloy with it.*
- 2 *At least one of the materials must be from the B-subgroup, i.e., the elements to the right of the Ni-Pd-Pt column in the Periodic Table.*[†]

Unfortunately this terminology can be confusing, because the word *compatibility* usually means an ability to work together, whereas in this context it means that they do not work (slide) together well. Their metallurgical “compatibility” in this case is one of *adhering together*, which acts to prevent sliding, making them **frictionally incompatible**.

Rabinowicz^[33] groups material pairs into (metallurgically) identical, compatible, partially compatible, partially incompatible, and incompatible categories based on the above criteria. The identical and compatible combinations should not be run together in unlubricated sliding contact. The incompatible and the partial categories can be run together. Figure 7-6 shows a compatibility chart for commonly used metals based on his categories. The dotted circles indicate **metallurgically compatible** metals (i.e., not acceptable for sliding contact). A dark quarter circle indicates **partially compatible**, and a dark half circle **partially incompatible** combinations. The latter are better in slid-

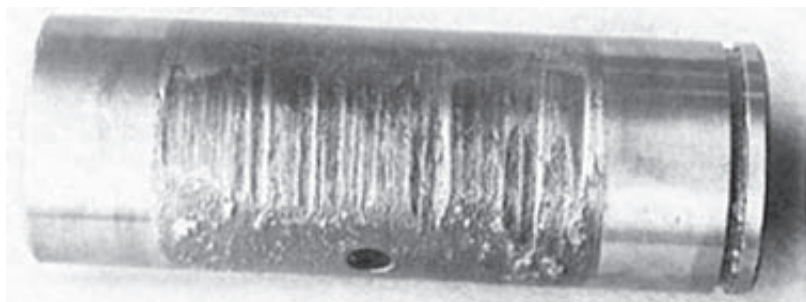
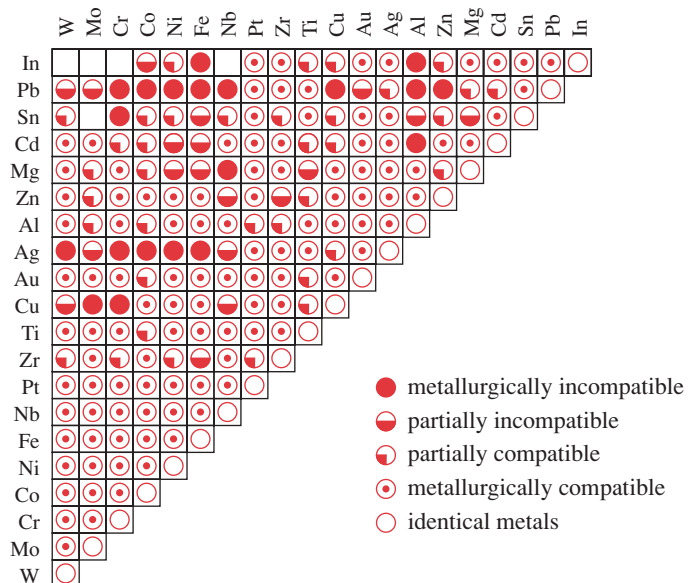


FIGURE 7-5

Adhesive Wear on a Shaft. Source: D. J. Wulpi, *Understanding How Components Fail*. Amer. Soc. for Metals: Metals Park, Ohio, 1990, with permission.

* Note that scuffing is often associated with gear teeth, which typically experience a combination of rolling and sliding. See Chapter 11 for further discussion.

† Some metals in this B-subgroup that are of possible interest for affordable bearing alloys are (in alphabetical order): Aluminum (Al), Antimony (Sb), Bismuth (Bi), Cadmium (Cd), Carbon (C), Copper (Cu), Lead (Pb), Silicon (Si), Tin (Sn), Zinc (Zn).

**FIGURE 7-6**

Compatibility Chart for Metal Pairs Based on Binary Phase Diagrams (Adapted from Figure 7, p. 491, E. Rabinowicz, *Wear Coefficients—Metals*, in *Wear Control Handbook*, M. B. Peterson and W. O. Winer, ed., ASME, New York, 1980, with permission)

ing contact than the former. The solid-color circles indicate **metallurgically incompatible** pairs that can be expected to resist adhesive wear best of any combinations shown.

CONTAMINANTS Adhesive bonding at the asperities can only occur if the material is clean and free of contaminants. Contaminants can take the form of oxides, skin oils from human handling, atmospheric moisture, etc. Contaminants in this context also include materials deliberately introduced to the interface such as coatings or lubricants. In fact, one of the chief functions of a lubricant is to prevent these adhesions and thus reduce friction and surface damage. A lubricant film effectively isolates the two materials and can prevent adhesion even between identical materials.

SURFACE FINISH It is not necessary for the surfaces to be “rough” for this adhesive-wear mechanism to operate. The fine-ground finish of the part in Figure 7-1a is seen to have as many asperities available for this process as the rougher milled surface in Figure 7-1b (p. 421).

COLD-WELDING If the mating materials are metals, are compatible, and are extremely clean, the adhesive forces will be high and the sliding friction can generate enough localized heat to weld the asperities together. If the clean metal surfaces are also finished to a low roughness value (i.e., polished), and then rubbed together (with sufficient force), they can cold-weld (seize) with a bond virtually as strong as the parent metal. This process is enhanced if done in a vacuum, as the absence of air eliminates contamination from surface oxidation. The **roll-bonding** process in which two compatible metals are cold-welded (in air) by rolling or coining them together under high normal loads is used commercially to make bimetallic strips for thermostats, and dimes and quarters for your pocket.

GALLING describes a situation of incomplete cold-welding where, for whatever reason (usually contamination), the parts do not completely weld together. But, portions of the surfaces do adhere, causing material to be transferred from one part to the other in large streaks visible to the naked eye. Galling generally ruins the surface in one pass.

These factors explain the reasons for what is common knowledge among machinists and experienced engineers: *the same material should generally not be run against itself*. There are some exceptions to this rule, notably for hardened steel on hardened steel, but other combinations such as aluminum on aluminum *must* be avoided.

The Adhesive-Wear Coefficient

In general, wear is inversely proportional to hardness. The rate of wear can be determined by running a pin against a rotating disk under controlled loading and lubrication conditions over a known sliding distance and measuring the loss in volume. The volume of wear is independent of the velocity of sliding and can be expressed as

$$V = K \frac{Fl}{H} \quad (7.7a)$$

where V = volume of wear from the softer of the two materials, F = normal force, l = length of sliding, and H is the penetration hardness in kgf / mm² or psi. H may be expressed as Brinell (HB), Vickers (HV), or other absolute hardness units. A Rockwell hardness reading can be used if it is first converted to one of the other scales having true units. (See Table 2-3, p. 44.) The factor K is the **wear coefficient** and is a dimensionless property of the sliding system. K will be a function of the materials used and also of the lubrication situation.

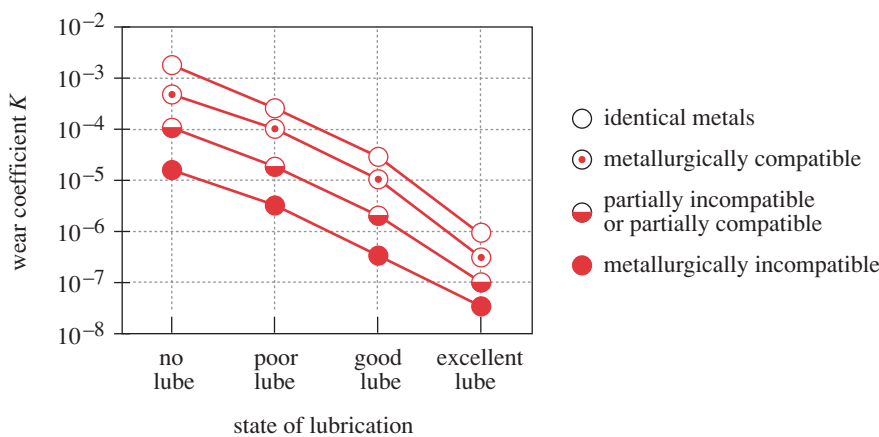
Since the depth of wear d may be of more engineering interest than the volume, equation 7.7a can be written in those terms as

$$d = K \frac{Fl}{HA_a} \quad (7.7b)$$

where A_a is the apparent area of contact of the interface.

Values of K obtained for the same materials tested under the same conditions vary by about a factor of 2 from test to test. This kind of variability is also seen in tests of friction coefficients, which typically have standard deviations of $\pm 20\%$. The reasons for these variations are not fully understood but are generally attributed to the difficulty in accurately reproducing the same surface conditions from test to test.^[33] Despite this large variation, the data obtained are nevertheless better than no data and are useful to make estimates of wear rates for situations in which testing of the actual design is not feasible.

Tables of empirical values for various combinations of material pairs and lubrication conditions have been published in the literature.^[33] While it is possible to find wear coefficient data for combinations that approximate your particular situation, the sheer number of possible permutations dictates that some design situations will not fit the available data. Figure 7-7 shows a generalized plot of the wear coefficient K as a function of both the lubrication condition and Rabinowicz's compatibility categories. An approximate value of K can be obtained from this figure for any design situation. Rec-

**FIGURE 7-7**

Adhesion-Wear Coefficient as a Function of Compatibility and Lubrication (Adapted from Figure 11, p. 495, E. Rabinowicz, "Wear Coefficients—Metals," in *Wear Control Handbook*, M. B. Peterson and W. O. Winer, ed., ASME, New York, 1980, with permission)

7

ognize that only a testing program can give reasonably accurate wear life data for a design. Note that the data in Figure 7-7 are based on the wear coefficient associated with material loss. Material is also transferred from one of the sliding materials to the other by adhesion. The wear coefficient for adhesive transfer is about three times that for material loss from the system.^[33]

7.5 ABRASIVE WEAR

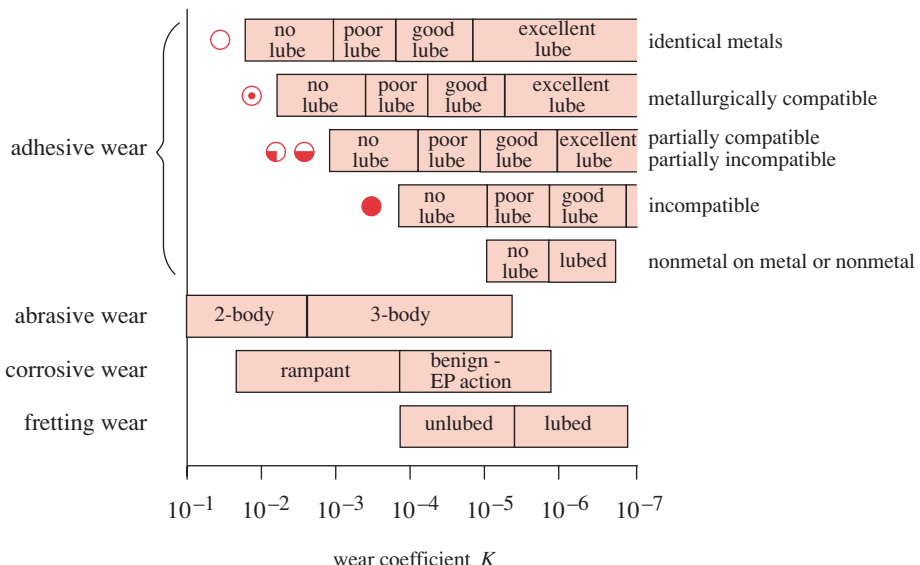
Abrasion occurs in two modes, referred to as the *two-body* and *three-body* abrasive wear processes.^[9] **Two-body abrasion** refers to a *hard rough material sliding against a softer one*. The hard surface digs into and removes material from the softer one. An example is a file used to contour a metal part. **Three-body abrasion** refers to the *introduction of hard particles between two sliding surfaces, at least one of which is softer than the particles*. The hard particles abrade material from one or both surfaces. Lapping and polishing are in this category. **Abrasives** is then *a material removal process in which the affected surfaces lose mass at some controlled or uncontrolled rate*. Abrasive wear also obeys the wear equation 7.7 (p. 429). See Figure 7-8 for an indication of wear coefficients for abrasive wear. Table 7-2 also shows typical abrasive-wear coefficients.

UNCONTROLLED ABRASION Earth-moving equipment such as backhoes, bulldozers, and mining equipment operates in a relatively uncontrolled three-body abrasion

Table 7-2 Wear Coefficient K for Abrasion

	File	Abrasive Paper, New	Loose Abrasive Grains	Coarse Polishing
Dry Surfaces	$5E-2$	$1E-2$	$1E-3$	$1E-4$
Lubricated	$1E-1$	$2E-2$	$2E-3$	$2E-4$

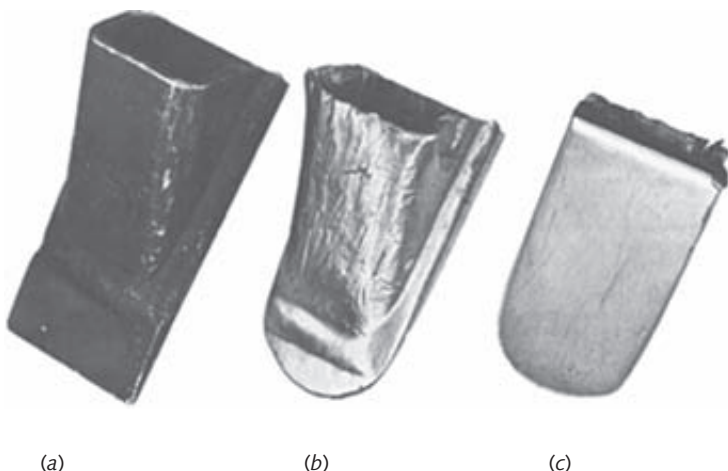
Source: E. Rabinowicz, "Wear Coefficients—Metals," in *Wear Control Handbook*, M. B. Peterson and W. O. Winer, ed., ASME, New York, 1980.

**FIGURE 7-8**

Wear Coefficients for Various Sliding Situations. Source: E. Rabinowicz, "Wear Coefficients—Metals," in *Wear Control Handbook*, M. B. Peterson and W. O. Winer, ed., ASME, New York, 1980

7

mode, since the dug earth or minerals often contain materials harder than the steel surfaces of the equipment. Silica (sand) is the most abundant solid material on the earth's surface and it is harder than most metals (absolute hardness of 800 kg/mm^2). Soft steel's absolute hardness is only about 200 kg/mm^2 , but hardened tool steels can be as high as $1\,000 \text{ kg/mm}^2$ and so can survive in these applications. Hard-steel files can thus be used to abrade softer metals, nonmetals, and even glass (which is a form of silica). Many

**FIGURE 7-9**

A Backhoe Tooth: (a) New, (b) Abrasive Wear on Soft Back Face, (c) Abrasive Wear on Hard Front Face. Source: D. J. Wulpi, *Understanding How Components Fail*, Amer. Soc. for Metals: Metals Park, Ohio, 1990

machine-design applications involve the handling of materials of production that are abrasive. The pumping of wet concrete, rock crushing, earth excavation, and the transport of ceramic parts are examples of abrasive-media handling. Figure 7-9 shows the effects of uncontrolled abrasion on the replaceable tooth of a backhoe. A new part (*a*) is contrasted with the worn back side (*b*) and front side (*c*) of a used part. The front side is made of 8640 medium-hard steel while the back side is soft 1010 steel.^[6]

Machine parts that operate in cleaner environments can be designed to minimize or eliminate abrasive wear through proper selection of materials and finishes. Smooth, hard materials will not abrade soft ones in two-body contact. Sleeve bearings and shafts are typically finished to very low roughness and made of suitable pairs of materials as indicated in Section 7.4. The smooth finishes minimize abrasion at the outset and, unless hard particulate contaminants are later introduced to the interface in service, that situation should continue. One reason for making sleeve bearings of soft materials (running against hard shafts) is to promote the embedding in the soft bearing material of any hard particles that find their way into the bearing. The particles are then trapped (buried) in the soft material and their potential damage to the shaft minimized. Particles may enter the bearing either as foreign contaminants in the lubricant or as oxidation products generated within the bearing. Iron oxides are harder than the steel that spawns them and will abrade the shaft. If hydrostatic lubrication is used (in which the lubricant is actively circulated—see Chapter 11), then filtration of the lubricant should be done to remove any particulates that enter the system. A properly designed, hydrostatically lubricated bearing should experience no abrasive wear if it has sufficient, clean lubricant.

CONTROLLED ABRASION In addition to designing systems to avoid abrasion, engineers also design them to *create* controlled abrasive wear. Controlled abrasion is widely used in manufacturing processes. Two-body **grinding** is perhaps the most common example, in which abrasive media such as silicon carbide (Carborundum) are forced against the part under high sliding velocities to remove material and control size and finish. A coolant is often used both to protect the material from an unwanted heat treatment and to enhance the abrasion process. Moisture increases the abrasion rate by about 15% over dry abrasion.^[10] Abrasive paper and cloth provide a means of applying an abrasive medium to a compound-curved surface as well. Sandblasting is an example of erosion, where one body is the sand and the other is the surface to be abraded or eroded.

A common example of controlled three-body abrasion in manufacturing is the **tumbling process** in which parts are placed in a drum along with some abrasive particles and then tumbled together. The parts rub and bounce off one another in the abrasive mix. The result is removal of burrs and sharp edges and a general polishing of all exposed surfaces. Another example is the **surface polishing** process, which involves the use of very fine, hard particulates trapped between a relatively soft and conforming material (e.g., cloth) and the surface to be polished. Relative velocities are high, and moisture is often added.

PARTICLE SIZE has an effect on the efficiency of an abrasion process. There is a threshold particle size for any situation, above which abrasion will continue rapidly but below which the wear rate slows. It is believed that the wear rate is slowed when the particles abraded from the workpiece are as large as, or larger than, the abrasive particles. In that case, they prevent the abrasives from digging into the workpiece.

Abrasive Materials

The two requirements for an abrasive are hardness and sharpness. The abrasive must be harder than the material to be abraded. Excessive hardness beyond about 150% of the workpiece hardness does not increase the wear rate but does prolong the useful “sharpness life” of the abrasive, which itself loses its cutting ability over time.^[11] Sharpness is achieved by using brittle materials that break into sharp-edged particles. The classes of materials that best meet these two criteria are ceramics and hard nonmetals. Most commercial abrasives are of these types. Table 7-3 shows some common abrasive materials and their hardness. Aluminum oxide (corundum) and silicon carbide (Carborundum) are the most used due to their favorable combination of relatively high hardness and low cost. Boron carbide and diamond are used for applications requiring the hardest materials, but both are expensive.

Abrasion-Resistant Materials

Some engineering materials are better suited to abrasive-wear applications than others based largely on their hardness. However, with hardness usually comes brittleness, and thus their resistance to impact or fatigue loads can be less than optimum. Table 7-4 shows the hardness of some materials that are suitable for abrasive-wear applications.

COATINGS Some ceramic materials can be plasma-sprayed onto metal substrates to provide a hard facing that also has high corrosion and chemical resistance. These plasma-sprayed coatings are quite rough upon application (like severely orange-peeled paint) and thus must be diamond ground to obtain a finish suitable for a sliding joint. These coatings are also very brittle and may chip from the substrate if overstressed either mechanically or thermally.

Note that aluminum oxide can be created in controlled fashion on aluminum by anodizing and will have a finish as good as the substrate. So-called hard-anodizing is merely a thicker anodized coating than used for corrosion protection and is commonly used to protect aluminum parts in abrasive-wear conditions. (See Section 2.5 on p. 48.)

Table 7-3 Materials for Use as Abrasives

Material	Composition	Hardness (kg/mm ²)
Diamond	C	8 000
Boron Carbide	B ₄ C	2 750
Carborundum (Silicon Carbide)	SiC	2 500
Titanium Carbide	TiC	2 450
Corundum (Alumina)	Al ₂ O ₃	2 100
Zirconium Carbide	ZrC	2 100
Tungsten Carbide	WC	1 900
Garnet	Al ₂ O ₃ 3FeO 3SiO ₂	1 350
Zirconia	ZrO ₂	150
Quartz, Silica, Sand	SiO ₂	800
Glass	Silicate	≤ 500

Source: E. Rabinowicz, *Friction and Wear of Materials*, 1965, reprinted by permission of John Wiley & Sons, Inc., New York

Table 7-4 Materials Resistant to Abrasion

Material	Hardness (kg/mm ²)	Relative Wear
Tungsten carbide (sintered)	1 400-1 800	0.5-5
High-chromium white cast iron		5-10
Tool steel	700-1 000	20-30
Bearing steel	700-950	
Chromium (electroplated)	900	
Carburized steel	900	20-30
Nitrided steel	900-1 250	20-30
Pearlitic white iron		25-50
Austenitic manganese steel		30-50
Pearlitic low-alloy (0.7% C) steel	480	30-60
Pearlitic unalloyed (0.7% C) steel	300	50-70
As-rolled or normalized low-carbon (0.2% C) steel		100

Source: E. Rabinowicz, *Friction and Wear of Materials*, 1965, reprinted by permission of John Wiley & Sons, Inc., New York.
T. E. Norman, *Abrasive Wear of Metals*, in *Handbook of Mechanical Wear*, C. Lipson, ed., U. Mich. Press, 1961.

7.6 CORROSION WEAR

CORROSION occurs in normal environments with virtually all materials except those termed noble, i.e., gold, platinum, etc. The most common form of corrosion is oxidation. Most metals react with the oxygen in air or water to form oxides. In some materials, such as aluminum, the oxidation is self-limiting as long as the surface is undisturbed. Aluminum in air forms an oxide layer that gradually builds to a thickness of 0.02 µm, at which point the reaction ceases because the nonporous aluminum-oxide film seals the substrate from further contact with the oxygen in the air. (This is the principle of anodizing, which creates a uniform, controlled-thickness layer of aluminum oxide on the part before it is placed in service.) Iron alloys, on the other hand, form a discontinuous and porous film of oxide that readily flakes off by itself to expose new substrate material. Oxidation will continue until all the iron is converted to oxides. Elevated temperatures greatly increase the rate of all chemical reactions.

CORROSION WEAR adds to the chemically corrosive environment a mechanical disruption of the surface layer due to a sliding or rolling contact of two bodies. This surface contact can act to break up the oxide (or other) film and expose new substrate to the reactive elements, thus increasing the rate of corrosion. If the products of the chemical reaction are hard and brittle (as with oxides), flakes of this layer can become loose particles in the interface and contribute to other forms of wear such as abrasion. See Figure 7-8 (p. 431) for an indication of wear coefficients for corrosion wear.

Some reaction products of metals such as metallic chlorides, phosphates, and sulfides are softer than the metal substrate and are also not brittle. These corrosion products can act as beneficial contaminants to reduce adhesive wear by blocking the adhesion of the metal asperities. This is the reason for adding compounds containing chlorine, sulphur, and other reactive agents to EP (extreme pressure) oils. The strategy is to trade a slow rate of corrosive wear for a more rapid and damaging rate of adhesive wear on

metal surfaces such as gear teeth and cams, which can have poor lubrication due to their nonconforming geometry.

Corrosion Fatigue

Chapter 6 discussed the mechanisms of fracture mechanics and fatigue failure in detail and made brief mention of the phenomenon variously called corrosion fatigue or stress corrosion. This mechanism is not yet fully understood, but the empirical evidence of its result is strong and unequivocal. When a part is stressed in the presence of a corrosive environment, the corrosion process is accelerated and failure occurs more rapidly than would be expected from either the stress state alone or the corrosion process alone.

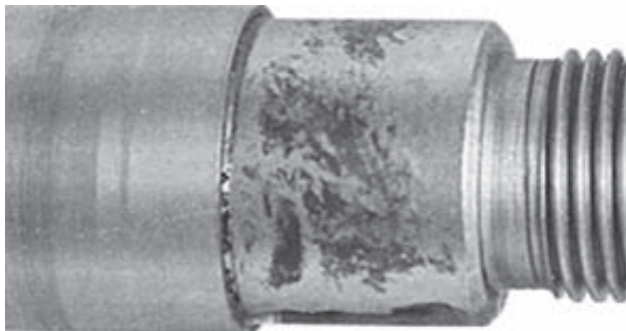
Static stresses are sufficient to accelerate the corrosion process. The combination of stress and corrosive environment has a synergistic effect and the material corrodes more rapidly than if unstressed. This combined condition of static stress and corrosion is termed **stress corrosion**. If the part is *cyclically stressed in a corrosive environment*, the crack will grow more rapidly than from either factor alone. This is called **corrosion fatigue**. While the frequency of stress cycling (as opposed to the number of cycles) appears to have no detrimental effect on crack growth in a noncorrosive environment, in the presence of corrosive environments it does. Lower cyclic frequencies allow the environment more time to act on the stressed crack tip while it is held open under tensile stress, and this substantially increases the rate of crack growth. See Figures 6-30 to 6-32 (pp. 335–336) and their discussion in Chapter 6 for more information on this phenomenon.

7

Fretting Corrosion

When two metal surfaces are in intimate contact, such as press-fit or clamped, one would expect no severe corrosion to occur at the interface, especially if in air. However, these kinds of contacts are subject to a phenomenon called **fretting corrosion** (or **fretting**) that can cause significant loss of material from the interface. Even though no gross sliding motions are possible in these situations, even small deflections (of the order of thousandths of an inch) are enough to cause fretting. Vibrations are another possible source of small fretting motions.

The fretting mechanism is believed to be some combination of abrasion, adhesion, and corrosion.^[12] Free surfaces will oxidize in air, but the rate will slow as the oxides formed on the surface gradually block the substrate from the atmosphere. As discussed above, some metals actually self-limit their oxidation if left undisturbed. The presence of vibrations or repeated mechanical deflections tends to disturb the oxide layer, scraping it loose and exposing new base metal to oxygen. This promotes adhesion of the “cleaned” metal asperities between the parts and also provides abrasive media in the form of hard oxide particles in the interface for three-body abrasion. All of these mechanisms tend to slowly reduce the solid volume of the materials and produce a “dust” or “powder” of abraded/oxidized material. Over time, significant dimensional loss can occur at the interface. In other cases, the result can be only a minor discoloration of the surfaces or adhesion similar to galling. All this from a joint that has no designed-in relative motion and was probably thought of by the designer as rigid! Of course, nothing is truly rigid, and fretting is evidence that microscopic motions are enough to

**FIGURE 7-10**

Fretting Wear on a Shaft Beneath a Press-Fit Hub Source: D. J. Wulpi, *Understanding How Components Fail*, Amer. Soc. for Metals: Metals Park, Ohio, 1990

7

cause wear. Figure 7-10 shows fretting on a shaft where a hub was press-fitted.^[6] See Figure 7-8 (p. 431) for an indication of wear coefficients for fretting wear.

Some techniques that have proven to reduce fretting are the reduction of deflections (i.e., stiffer designs or tighter clamping) and the introduction of dry or fluid lubricants to the joint to act as an oxygen barrier and friction reducer. The introduction of a gasket, especially one with substantial elasticity (such as rubber) to absorb the vibrations has been shown to help. Harder and smoother surfaces on the metal parts are more resistant to abrasion and will reduce fretting damage. Corrosion-resistant platings such as chromium are sometimes used. The best method (impractical in most instances) is to eliminate the oxygen by operating in a vacuum or inert-gas atmosphere.

7.7 SURFACE FATIGUE

All the surface-failure modes discussed above apply to situations in which the relative motions between the surfaces are essentially pure sliding. When two surfaces are in **pure rolling** contact, or are primarily rolling in combination with a small percentage of sliding, a different surface failure mechanism comes into play, called **surface fatigue**. Many applications of this condition exist such as ball and roller bearings, cams with roller followers, nip rolls, and spur or helical gear tooth contact. All except the gear teeth and nip rolls typically have essentially pure rolling with only about 1% sliding. Gear teeth have significant sliding at portions of their tooth interface and this will change the stress state significantly compared to the pure rolling cases, as we shall see. Other types of gears such as spiral bevel, hypoid, and worm sets have essentially pure sliding at their interfaces and one or more of the wear mechanisms discussed above will apply. Nip rolls (such as those used to roll sheet steel) can be run with or without sliding depending on their purpose.

The stresses introduced in two materials contacting at a rolling interface are highly dependent on the geometry of the surfaces in contact as well as on the loading and material properties. The general case allows any three-dimensional geometry on each contacting member and, as would be expected, its calculation is the most complex. Two

special-geometry cases are of practical interest and are also somewhat simpler to analyze. These are *sphere-on-sphere* and *cylinder-on-cylinder*. In all cases, the radii of curvature of the mating surfaces will be significant factors. By varying the radii of curvature of one mating surface, these special cases can be extended to include the sub-cases of *sphere-on-plane*, *sphere-in-cup*, *cylinder-on-plane*, and *cylinder-in-trough*. It is only necessary to make the radii of curvature of one element infinite to obtain a plane, and negative radii of curvature define a concave cup, or concave trough surface. For example, some ball bearings can be modeled as *sphere-on-plane* and some roller bearings as *cylinder-in-trough*.

As a ball passes over another surface, the theoretical contact patch is a point of zero dimension. A roller against a cylindrical or flat surface theoretically contacts along a line of zero width. Since the area of each of these theoretical contact geometries is zero, any applied force will then create an infinite stress. We know that this cannot be true, as the materials would instantly fail. In fact, the materials must deflect to create sufficient contact area to support the load at some finite stress. This deflection creates a semi-ellipsoidal pressure distribution over the contact patch. In the general case, the contact patch is elliptical as shown in Figure 7-11a. Spheres will have a circular contact patch, and cylinders create a rectangular contact patch as shown in Figure 7-11b.

Consider the case of a spherical ball rolling in a straight line against a flat surface with no slip, and under a constant normal load. If the load is such as to stress the material only below its yield point, the deflection in the contact patch will be elastic and the surface will return to its original curved geometry after passing through contact. The same spot on the ball will contact the surface again on each succeeding revolution. The resulting stresses in the contact patch are called **contact stresses or Hertzian stresses**. The contact stresses in this small volume of the ball are **repeated** at the ball's rotation frequency. This creates a fatigue-loading situation that eventually leads to a **surface-fatigue failure**.

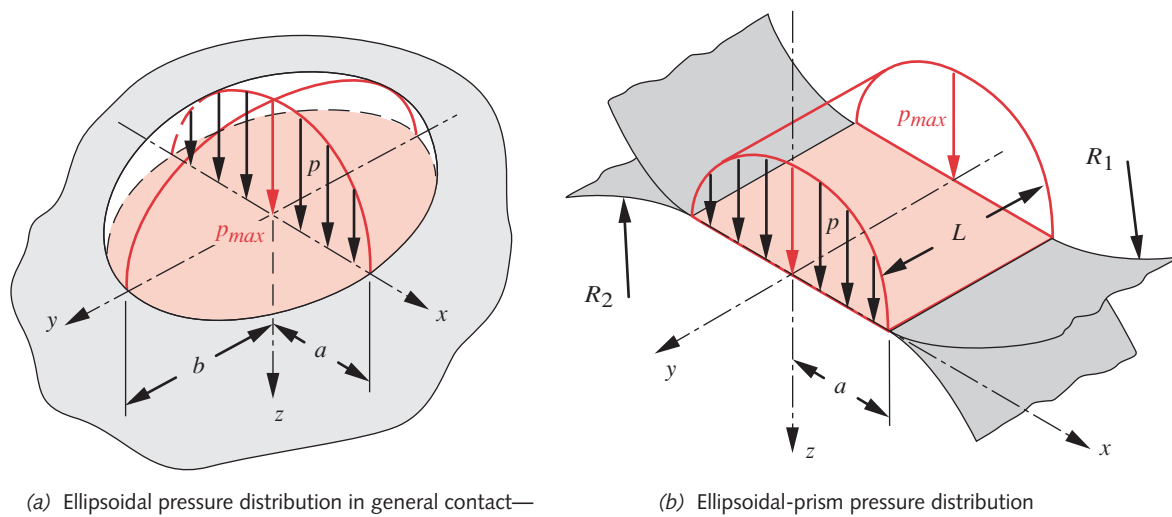


FIGURE 7-11
 Pressure Distributions and Contact Zones of Spherical, Cylindrical, and General Hertzian Contact

This repeated loading is similar to the tensile fatigue-loading case shown in Figure 6-1b (p. 304). The significant difference in this case is that the principal contact stresses at the center of the contact patch are all compressive, not tensile. Recall from Chapter 6 that fatigue failures are considered to be initiated by shear stress and continued to failure by tensile stress. There is also a shear stress associated with these compressive contact stresses, and it is believed to be the cause of crack formation after many stress-cycles. Crack growth then eventually results in failure by **pitting**—*the fracture and dislodgment of small pieces of material from the surface*. Once the surface begins to pit, its surface finish is compromised and it rapidly proceeds to failure by **spalling**—*the loss of large pieces of the surface*.* Figure 7-12 shows some examples of pitted and spalled surfaces.

If the load is large enough to raise the contact stress above the material's compressive yield strength, then the contact-patch deflection will create a permanent flat on the ball. This condition is sometimes called **false brinelling**, because it has a similar appearance to the indentation made to test a material's Brinell hardness. Such a flat on even one of its balls (or rollers) makes a ball (or roller) bearing useless.

7

We will now investigate the contact-patch geometries, pressure distributions, stresses, and deformations in rolling contacts starting with the relatively simple geometry of *sphere-on-sphere*, next dealing with the *cylinder-on-cylinder* case, and finally discussing the *general* case. Derivation of the equations for these cases are among the more complex sets of examples from the theory of elasticity. The equations for the area of contact, deformation, pressure distribution, and contact stress on the centerline of two bodies with static loading were originally derived by Hertz in 1881,^[13] an English translation of which can be found in reference 14. Many others have since added to the understanding of this problem.^{[15],[16],[17],[18]}

* According to Ding and Gear^[36],

... there has been no unified definition established in the literature to consistently distinguish pitting from spalling. Much of the literature has used the terms pitting and spalling, or sometimes micropitting, indiscriminately: while some of the literature has used pitting, micropitting, and spalling to designate the different levels of severity of surface contact fatigue. Tallian defined spalling as macro-scale contact fatigue caused by crack propagation and reserved pitting as surface damage caused by sources other than crack propagation. One of the reasons for the confusion is probably due to the fact that the physical causes of pitting and spalling have not yet been established. In order to discuss the issue on a consistent ground, Ding defined pitting (is) taken to be the formation of shallow craters [$\leq 10 \mu\text{m}$] developed mainly from surface defects; while spalling (is) considered to be the formation of deeper cavities developed mainly from subsurface defects. ...

7.8 SPHERICAL CONTACT

Cross sections of two spheres in contact are shown in Figure 7-13. The dotted lines indicate the possibilities that one is a flat plane or a concave cup. The difference is only in the magnitude or the sign of its radius of curvature (convex +, concave -). Figure 7-11a (p. 437) shows the general semi-ellipsoidal pressure distribution over the contact patch. For a sphere-on-sphere, it will be a hemisphere with a circular contact patch ($a = b$).

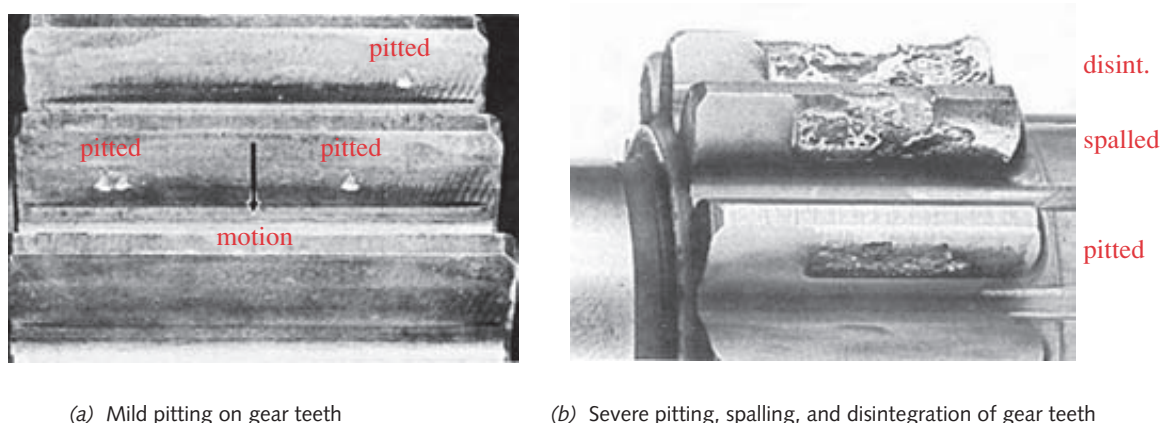
Contact Pressure and Contact Patch in Spherical Contact

The contact pressure is a maximum p_{max} at the center and zero at the edge. The total applied load F on the contact patch is equal to the volume of the hemisphere:

$$F = \frac{2}{3} \pi a^2 p_{max} \quad (7.8a)$$

where a is the half-width (radius) of the contact patch. This can be solved for the maximum pressure:

$$p_{max} = \frac{3}{2} \frac{F}{\pi a^2} \quad (7.8b)$$

**FIGURE 7-12**

Examples of Surfaces Failed by Pitting and Spalling due to Surface Fatigue Source: J. D. Graham, *Pitting of Gear Teeth*, in *Handbook of Mechanical Wear*, C. Lipson, ed., U. Mich. Press, 1961, pp. 138, 143, with permission

The average pressure on the contact patch is the applied force divided by its area:

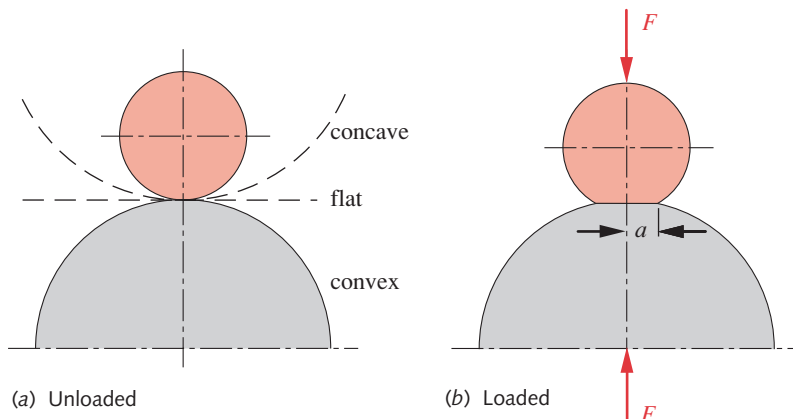
$$p_{avg} = \frac{F}{area} = \frac{F}{\pi a^2} \quad (7.8c)$$

and substituting equation 7.8c in 7.8b gives:

$$p_{max} = \frac{3}{2} p_{avg} \quad (7.8d)$$

We now define *material constants* for the two spheres

$$m_1 = \frac{1-v_1^2}{E_1} \quad m_2 = \frac{1-v_2^2}{E_2} \quad (7.9a)$$

**FIGURE 7-13**

Contact Zone of Two Spheres or Cylinders

where E_1, E_2 and ν_1, ν_2 are the Young's moduli and Poisson's ratios for the materials of sphere 1 and sphere 2, respectively.

The dimensions of the contact area are typically very small compared to the radii of curvature of the bodies, which allows the radii to be considered constant over the contact area despite the small deformations occurring there. We can define a *geometry constant* that depends only on the radii R_1 and R_2 of the two spheres,

$$B = \frac{1}{2} \left(\frac{1}{R_1} + \frac{1}{R_2} \right) \quad (7.9b)$$

To account for the case of a sphere-on-plane, R_2 becomes infinite, making $1/R_2$ zero. For a sphere-in-cup, R_2 becomes negative. (See Figure 7-13, p. 439.) Otherwise R_2 is finite and positive, as is R_1 .

The contact-patch radius a is then found from

$$a = \frac{\pi}{4} p_{max} \frac{m_1 + m_2}{B} \quad (7.9c)$$

Substitute equation 7.8b in 7.9c:

$$\begin{aligned} a &= \frac{\pi}{4} \left(\frac{3}{2} \frac{F}{\pi a^2} \right) \frac{m_1 + m_2}{B} \\ a &= \sqrt[3]{0.375 \frac{m_1 + m_2}{B} F} \end{aligned} \quad (7.9d)$$

The pressure distribution within the hemisphere is

$$p = p_{max} \sqrt{1 - \frac{x^2}{a^2} - \frac{y^2}{a^2}} \quad (7.10)$$

We can normalize the pressure p to the magnitude of p_{avg} and the patch dimension x or y to the patch radius a and then plot the normalized pressure distribution across the patch, which will be an ellipse as shown in Figure 7-14.

Static Stress Distributions in Spherical Contact

The pressure on the contact patch creates a three-dimensional stress state in the material. The three applied stresses σ_x , σ_y , and σ_z are compressive and are maximal at the sphere's surface in the center of the patch. They diminish rapidly and nonlinearly with depth and with distance from the axis of contact. They are called **Hertzian stresses** in honor of their original discoverer. A complete derivation of these equations can be found in reference 19. Note that these applied stresses in the x , y , and z directions are also the principal stresses in this case. If we look at these stresses as they vary along the z axis (with z increasing into the material) we find

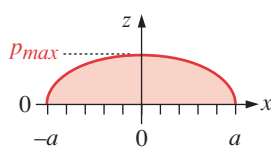


FIGURE 7-14

Pressure Distribution Across Contact Patch

$$\sigma_z = p_{max} \left[-1 + \frac{z^3}{(a^2 + z^2)^{3/2}} \right] \quad (7.11a)$$

$$\sigma_x = \sigma_y = \frac{p_{max}}{2} \left[-(1+2\nu) + 2(1+\nu) \left(\frac{z}{\sqrt{a^2+z^2}} \right) - \left(\frac{z}{\sqrt{a^2+z^2}} \right)^3 \right] \quad (7.11b)$$

Poisson's ratio is taken for the sphere of interest in this calculation. These normal (and principal) stresses are maximal at the surface, where $z = 0$:

$$\sigma_{z_{max}} = -p_{max} \quad (7.11c)$$

$$\sigma_{x_{max}} = \sigma_{y_{max}} = -\frac{1+2\nu}{2} p_{max} \quad (7.11d)$$

There is also a principal shear stress induced from these principal normal stresses:

$$\tau_{13} = \frac{p_{max}}{2} \left[\frac{(1-2\nu)}{2} + (1+\nu) \left(\frac{z}{\sqrt{a^2+z^2}} \right) - \frac{3}{2} \left(\frac{z}{\sqrt{a^2+z^2}} \right)^3 \right] \quad (7.12a)$$

which is not a maximum at the surface but rather at a small distance $z_{@}\tau_{max}$ below the surface.

$$\tau_{13_{max}} = \frac{p_{max}}{2} \left[\frac{(1-2\nu)}{2} + \frac{2}{9}(1+\nu)\sqrt{2(1+\nu)} \right] \quad (7.12b)$$

$$z_{@}\tau_{max} = a \sqrt{\frac{2+2\nu}{7-2\nu}} \quad (7.12c)$$

Figure 7-15 shows a plot of the principal normal and maximum shear stresses as a function of depth z along a radius of the sphere. The stresses are normalized to the maximum pressure p_{max} , and the depth is normalized to the half-width a of the contact patch. This plot provides a dimensionless picture of the stress distribution on the centerline under a spherical contact. Note that all the stresses have diminished to <10% of p_{max} within $z = 5a$. The subsurface location of the maximum shear stress can also be seen. If both materials are steel, it occurs at a depth of about $0.63a$ and its magnitude is about $0.34 p_{max}$. The shear stress is about $0.11 p_{max}$ at the surface on the z axis.

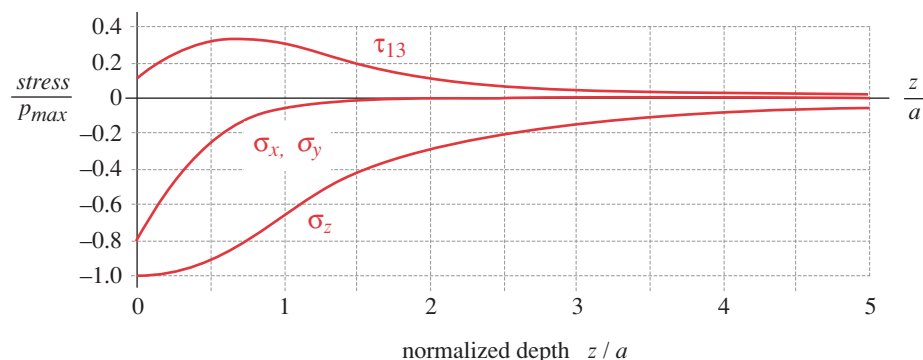


FIGURE 7-15

Normalized Stress Distribution Along the z Axis in Static Spherical Contact - xyz Stresses are Principal

The subsurface location of the maximum shear stress is believed by some to be a significant factor in surface-fatigue failure. The theory says cracks that begin below the surface eventually grow to the point that the material above the crack breaks out to form a pit as shown in Figure 7-12 (p. 439). Other evidence indicates that cracks may sometimes start at the surface.

Figure 7-16 shows a photoelastic model of the contact stresses in a cam immediately beneath a loaded roller follower.^[20] Experimental photoelastic stress analysis uses a physical model of the part to be analyzed made from a transparent plastic material (Lexan in this example) that shows fringes of constant stress magnitude when loaded and viewed in polarized light. The maximum shear stress can be clearly seen a small distance into the cam directly under the follower. While this is a cylindrical rather than a spherical contact, their stress distributions along the centerline are similar, as will be seen in the next section.

When we move off the centerline of the contact patch on the surface of the sphere, the stresses diminish. At the edge of the patch the radial stress σ_z is zero but there is a condition of pure shear stress with the magnitude:

$$\tau_{xy} = \frac{1-2v}{3} p_{max} \quad (7.13a)$$

Picture the Mohr's circle for a pure shear case. The two nonzero principal stresses will be $\pm \tau_{xy}$, which means that there is also a tensile stress at that point of

$$\sigma_{1_{edge}} = \frac{1-2v}{3} p_{max} \quad (7.13b)$$

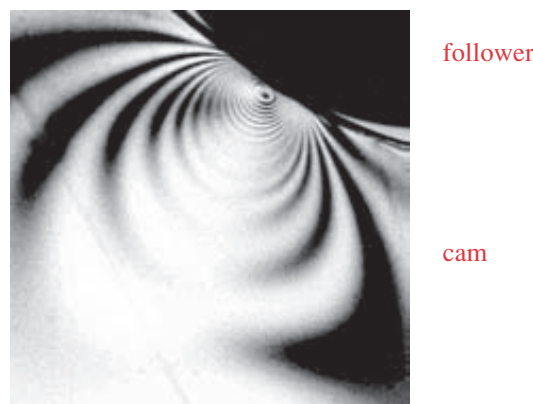


FIGURE 7-16

Photoelastic Analysis of Contact Stresses Under a Cam Follower Source: V. S. Mahkijani, *Study of Contact Stresses as Developed on a Radial Cam Using Photoelastic Model and Finite Element Analysis*. M.S. Thesis, Worcester Polytechnic Institute, 1984

EXAMPLE 7-1**Stresses in a Ball Thrust Bearing****Problem**

A ball thrust bearing with 7 balls is loaded axially across its races through the balls. What is the size of the contact patch on a race and what are the stresses developed in balls and races? What is the depth of the maximum shear stress in a ball?

Given

The 7 spherical balls are 10-mm (0.394-in) dia and the races are flat. All parts are hardened steel. The axial load is 151 lb or 21.5 lb per ball.

Assumptions

The 7 balls share the load equally. The rotational speed is sufficiently slow that this can be considered a static loading problem.

Solution

- We need to first determine the size of the contact patch, for which we need to find the geometry constant and material constants from equations 7.9a and b (pp. 439–440).

$$B = \frac{1}{2} \left(\frac{1}{R_1} + \frac{1}{R_2} \right) = \frac{1}{2} \left(\frac{1}{0.197} + \frac{1}{\infty} \right) = 2.54 \quad (a)$$

Note the infinite radius of curvature for R_2 .

$$m_1 = m_2 = \frac{1 - v_1^2}{E_1} = \frac{1 - 0.28^2}{3E7} = 3.072E - 8 \quad (b)$$

Note both materials are the same in this example. The material and geometry constants can now be used in equation 7.9d (p. 440).

$$a = \sqrt[3]{\frac{3(m_1 + m_2)}{B} F} = \sqrt[3]{0.375 \frac{2(3.072E - 8)}{2.54} 21.5} = 0.0058 \text{ in} \quad (c)$$

where a is the half-width (radius) of the contact patch. The circular contact-patch area is then

$$\text{area} = \pi a^2 = \pi (0.0058^2) = 1.057E - 4 \text{ in}^2 \quad (d)$$

- The average and maximum contact pressure can now be found from equations 7.8c and d (p. 439).

$$p_{avg} = \frac{F}{\text{area}} = \frac{21.5}{1.057E - 4} = 203\,587 \text{ psi} \quad (e)$$

$$p_{max} = \frac{3}{2} p_{avg} = \frac{3}{2} (203\,587) = 305\,381 \text{ psi} \quad (f)$$

- The maximum normal stresses in the center of the contact patch at the surface are then found using equations 7.11c and d (p. 441).

$$\sigma_{z_{max}} = -p_{max} = -305\,381 \text{ psi} \quad (g)$$

$$\sigma_{x_{max}} = \sigma_{y_{max}} = -\frac{1+2v}{2} p_{max} = -\frac{1+2(0.28)}{2} (305\,381) = -238\,197 \text{ psi} \quad (h)$$

- 4 The maximum shear stress and its location under the surface are found from equations 7.12b and c (p. 441).

$$\begin{aligned}\tau_{yz\max} &= \frac{p_{max}}{2} \left[\frac{(1-2v)}{2} + \frac{2}{9}(1+v)\sqrt{2(1+v)} \right] \\ &= \frac{305\,381}{2} \left[\frac{(1-2(0.28))}{2} + \frac{2}{9}(1+0.28)\sqrt{2(1+0.28)} \right] = 103\,083 \text{ psi} \quad (i)\end{aligned}$$

$$z_{@\tau_{max}} = a \sqrt{\frac{2+2v}{7-2v}} = 0.005\,8 \sqrt{\frac{2+2(0.28)}{7-2(0.28)}} = 0.0037 \text{ in} \quad (j)$$

- 5 All the stresses found so far exist on the centerline of the patch. At the edge of the patch, at the surface, there will be a shear stress of

$$\tau_{xy} = \frac{1-2v}{3} p_{max} = \frac{1-2(0.28)}{3} (305\,381) = 44\,789 \text{ psi} \quad (k)$$

and a tensile stress of the same magnitude.

- 6 Since both parts are the same material, all of these stresses apply to both.
7 The files EX07-01 can be found on the CD-ROM.
-

7.9 CYLINDRICAL CONTACT

Cylindrical contact is common in machinery. Contacting rollers are often used to pull web material such as paper through machinery or to change the thickness of a material in the rolling or calendering process. Roller bearings are another application. The cylinders can be both convex, one convex and one concave (cylinder-in-trough), or in the limit, a cylinder-on-plane. In all such contacts there is the possibility of sliding as well as rolling at the interface. The presence of tangential sliding forces has a significant effect on the stresses compared to pure rolling. We will first consider the case of two cylinders in pure rolling and later introduce a sliding component.

Contact Pressure and Contact Patch in Parallel Cylindrical Contact

When two cylinders roll together, their contact patch will be rectangular as shown in Figure 7-11b (p. 437). The pressure distribution will be a semi-elliptical prism of half-width a . The contact zone will look as shown in Figure 7-13 (p. 439). The contact pressure is a maximum p_{max} at the center and zero at the edges as shown in Figure 7-14 (p. 440). The applied load F on the contact patch is equal to the volume of the half-prism:

$$F = \frac{1}{2} \pi a L p_{max} \quad (7.14a)$$

where F is the total applied load and L is the length of contact along the cylinder axis. This can be solved for the maximum pressure:

$$p_{max} = \frac{2F}{\pi aL} \quad (7.14b)$$

The average pressure is the applied force divided by the contact-patch area:

$$p_{avg} = \frac{F}{area} = \frac{F}{2aL} \quad (7.14c)$$

Substituting equation 7.14c in 7.14b gives

$$p_{max} = \frac{4}{\pi} P_{avg} \cong 1.273 P_{avg} \quad (7.14d)$$

We now define a cylindrical geometry constant that depends on the radii R_1 and R_2 of the two cylinders, (Note that it is the same as equation 7.9b (p. 440) for spheres.)

$$B = \frac{1}{2} \left(\frac{1}{R_1} + \frac{1}{R_2} \right) \quad (7.15a)$$

To account for the case of a cylinder-on-plane, R_2 becomes infinite, making $1/R_2$ zero. For a cylinder-in-trough, R_2 becomes negative. Otherwise R_2 is finite and positive, as is R_1 . The contact-patch half-width a is then found from

$$a = \sqrt{\frac{2}{\pi} \frac{m_1 + m_2}{B} \frac{F}{L}} \quad (7.15b)$$

where m_1 and m_2 are material constants as defined in equation 7.9a (p. 439).

The pressure distribution within the semi-elliptical prism is

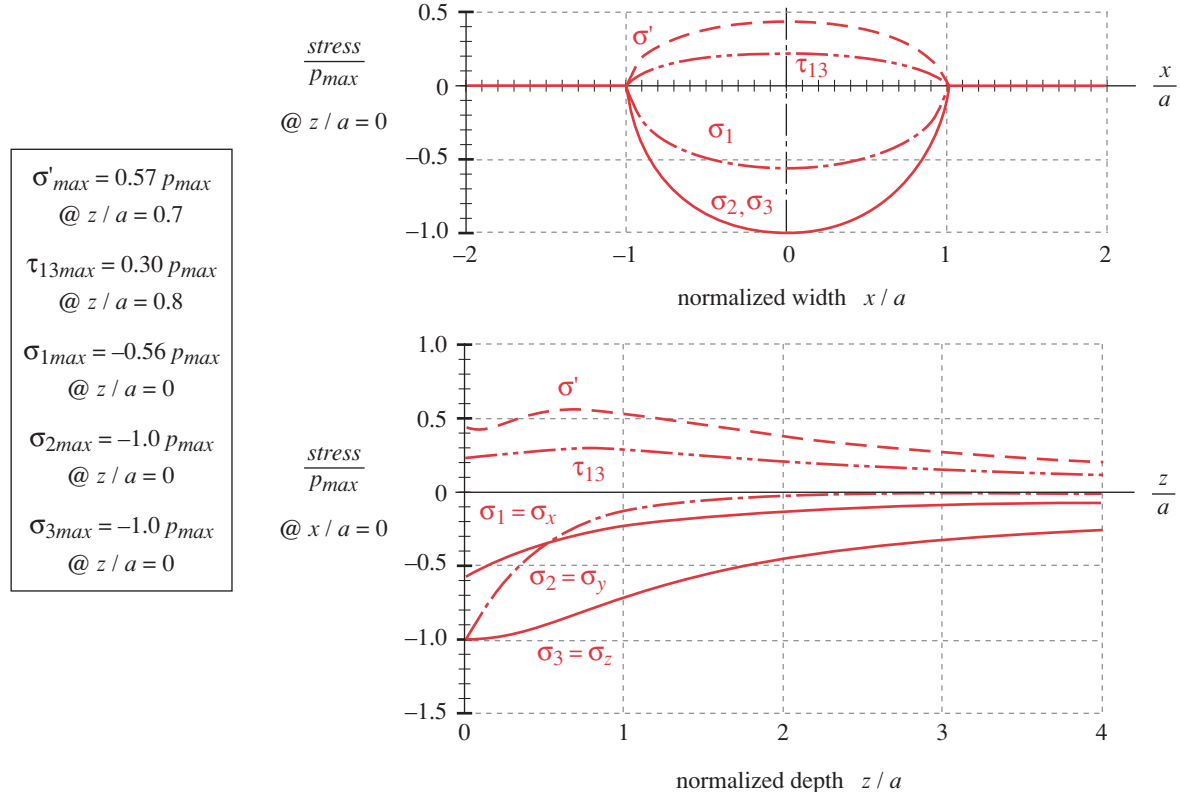
$$p = p_{max} \sqrt{1 - \frac{x^2}{a^2}} \quad (7.16)$$

which is an ellipse as shown in Figure 7-11 (p. 437).

Static Stress Distributions in Parallel Cylindrical Contact

Hertzian stress analysis is for static loading but is also applied to pure rolling contact. The stress distributions within the material are similar to those shown in Figure 7-15 (p. 441) for the sphere-on-sphere case. Two cases are possible: *plane stress*, where the cylinders are very short axially as in some cam roller-follower, and *plane strain*, where the cylinders are long axially such as in squeeze-rollers. In the plane-stress case, one of the principal stresses is zero. In plane strain, all three principal stresses may be non-zero.

Figure 7-17 shows the principal stress, maximum shear, and von Mises stress distributions across the patch width at the surface and along the z axis (where they are largest) for two cylinders in static or pure rolling contact. The normal stresses are all compressive and are maximal at the surface. They diminish rapidly with depth into the material and also diminish away from the centerline, as shown in Figure 7-17.

**FIGURE 7-17**

Principal, Maximum Shear, and von Mises Stress Distributions for Steel Cylinders in Static Loading or Pure Rolling

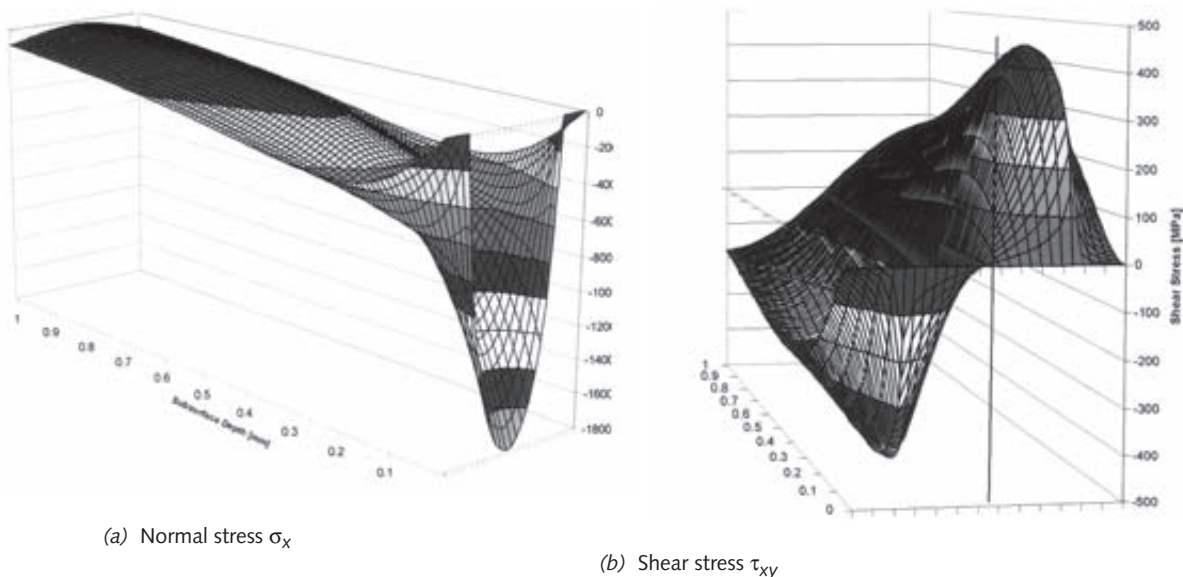
At the surface on the centerline, the maximum applied normal stresses are

$$\begin{aligned}\sigma_x &= \sigma_z = -p_{\text{max}} \\ \sigma_y &= -2\nu p_{\text{max}}\end{aligned}\tag{7.17a}$$

These stresses are principal, since there is no applied shear stress. The maximum shear stress τ_{13} on the z axis that results from the combination of stresses on the Mohr's-circle plane is beneath the surface as it was in the spherical-contact case. For two steel cylinders in static contact, the peak value and location of the maximum shear stress are^[19]

$$\begin{aligned}\tau_{13\text{max}} &= 0.304 p_{\text{max}} \\ z_{\text{@ } \tau_{\text{max}}} &= 0.786a\end{aligned}\tag{7.17b}$$

However, note in Figure 7-17 that, on the z axis, the maximum shear stress is not zero but is $0.22 p_{\text{max}}$ at the surface and does not vary greatly over the depth $0 < z < 2a$. Figure 7-18 shows the three-dimensional distribution of normal and shear subsurface stresses in cylindrical contact.^[35]

**FIGURE 7-18**

Subsurface Stress Distribution in Cylindrical Contact [35]

EXAMPLE 7-2**Stresses in Cylindrical Contact****Problem**

An overhead crane wheel runs slowly on a steel rail. What is the size of the contact patch between wheel and rail and what are the stresses? What is the depth of the maximum shear stress?

Given

The wheel is 12-in dia by 0.875-in thick and the rail is flat. Both parts are steel. The radial load is 5 000 lb.

Assumptions

The rotational speed is sufficiently slow that this can be considered a static loading problem.

Solution

- First determine the size of the contact patch, for which the geometry constant and material constants are found from equations 7.15a (p. 445) and 7.9a (p. 439).

$$B = \frac{1}{2} \left(\frac{1}{R_1} + \frac{1}{R_2} \right) = \frac{1}{2} \left(\frac{1}{6} + 0 \right) = 0.083 \quad (a)$$

Note the infinite radius of curvature for R_2 .

$$m_1 = m_2 = \frac{1 - v_1^2}{E_1} = \frac{1 - 0.28^2}{3E7} = 3.072E - 8 \quad (b)$$

Note both materials are the same in this example. The material and geometry constants can now be used in equation 7.15b (p. 445).

$$a = \sqrt{\frac{2}{\pi} \frac{m_1 + m_2}{B} \frac{F}{L}} = \sqrt{\left(\frac{2}{\pi}\right) \frac{2(3.072E-8)}{0.083} \left(\frac{5000}{0.875}\right)} = 0.0518 \text{ in} \quad (c)$$

where a is the half-width of the contact patch. The rectangular contact-patch area is

$$\text{area} = 2aL = 2(0.0518)(0.875) = 0.091 \text{ in}^2 \quad (d)$$

- 2 The average and maximum contact pressure are found from equations 7.14b and c (p. 445).

$$p_{avg} = \frac{F}{\text{area}} = \frac{5000}{0.09063} = 55169 \text{ psi} \quad (e)$$

$$p_{max} = \frac{2F}{\pi a L} = \frac{2(5000)}{\pi(0.051789)(0.875)} = 70243 \text{ psi} \quad (f)$$

- 3 The maximum normal stresses in the center of the contact patch at the surface are then found using equations 7.17a (p. 446).

$$\sigma_{z_{max}} = \sigma_{x_{max}} = -p_{max} = -70243 \text{ psi} \quad (g)$$

$$\sigma_{y_{max}} = -2vp_{max} = -2(0.28)(70243) = -39336 \text{ psi} \quad (h)$$

- 4 The maximum shear stress and its location (depth) are found from equations 7.17b (p. 446).

$$\tau_{13_{max}} = 0.304p_{max} = 0.304(70243) = 21354 \text{ psi} \quad (i)$$

$$z_{@ \tau_{max}} = 0.786a = 0.786(0.0518) = 0.041 \text{ in}$$

- 5 All the stresses found exist on the z axis and the normal stresses are principal. These stresses apply to the wheel and rail, as both are steel.

- 6 The files EX07-02 can be found on the CD-ROM.

7.10 GENERAL CONTACT

When the geometry of the two contacting bodies is allowed to have any general curvature, the contact patch is an ellipse and the pressure distribution is a semi-ellipsoid, as shown in Figure 7-11a (p. 437). Even the most general curvature can be represented as a radius of curvature over a small angle with minimal error. The size of the contact patch for most practical materials in these applications is so small that this approximation is reasonable. Thus the compound curvature of each body is represented by two mutually orthogonal radii of curvature at the contact point.

Contact Pressure and Contact Patch in General Contact

The contact pressure is a maximum p_{max} at the center and zero at the edge. The total applied load F on the contact patch is equal to the volume of the semi-ellipsoid:

$$F = \frac{2}{3} \pi ab p_{max} \quad (7.18a)$$

where a is the half-width of the major axis and b the half-width of the minor axis of the contact-patch ellipse. This can be solved for the maximum pressure:

$$p_{max} = \frac{3}{2} \frac{F}{\pi ab} \quad (7.18b)$$

The average pressure on the contact patch is the applied force divided by its area:

$$p_{avg} = \frac{F}{area} = \frac{F}{\pi ab} \quad (7.18c)$$

and substituting equation 7.18c in 7.18b gives

$$p_{max} = \frac{3}{2} P_{avg} \quad (7.18d)$$

We must define three geometry constants that depend on the radii of curvature of the two bodies,

$$A = \frac{1}{2} \left(\frac{1}{R_1} + \frac{1}{R_1'} + \frac{1}{R_2} + \frac{1}{R_2'} \right) \quad (7.19a)$$

$$B = \frac{1}{2} \left[\left(\frac{1}{R_1} - \frac{1}{R_1'} \right)^2 + \left(\frac{1}{R_2} - \frac{1}{R_2'} \right)^2 + 2 \left(\frac{1}{R_1} - \frac{1}{R_1'} \right) \left(\frac{1}{R_2} - \frac{1}{R_2'} \right) \cos 2\theta \right]^{\frac{1}{2}} \quad (7.19b)$$

$$\phi = \cos^{-1} \left(\frac{B}{A} \right) \quad (7.19c)$$

where R_1 and R_1' are the two radii of curvature* of body 1, R_2 and R_2' are the radii* of body 2, and θ is the angle between the planes containing R_1 and R_2 .

The contact-patch dimensions a and b are then found from

$$a = k_a \sqrt[3]{\frac{3F(m_1 + m_2)}{4A}} \quad b = k_b \sqrt[3]{\frac{3F(m_1 + m_2)}{4A}} \quad (7.19d)$$

where m_1 and m_2 are material constants as defined in equation 7.9a (p. 439) and the values of k_a and k_b are from Hertz's original data in Table 7-5 corresponding to the value of ϕ from equation 7.19c.

* Measured in mutually perpendicular planes.

Table 7-5 Factors For Use in Equation 7.19d

ϕ	0	10	20	30	35	40	45	50	55	60	65	70	75	80	85	90
k_a	∞	6.612	3.778	2.731	2.397	2.136	1.926	1.754	1.611	1.486	1.378	1.284	1.202	1.128	1.061	1
k_b	0	0.319	0.408	0.493	0.530	0.567	0.604	0.641	0.678	0.717	0.759	0.802	0.846	0.893	0.944	1

Sources: H. Hertz, *Contact of Elastic Solids*, in *Miscellaneous Papers*, P. Lenard, ed. Macmillan & Co. Ltd.: London, 1896, pp. 146-162.
H. L. Whittemore and S. N. Petrenko, *Natl. Bur. Std. Tech. Paper* 201, 1921.

For more accurate estimates than can be obtained by interpolation in the table, functions have been fitted to the data in Table 7-5 and can be used to calculate approximate values of k_a and k_b for any value of the angle ϕ (in deg) from:

$$\begin{aligned} k_a &= 50.192\phi^{-0.86215} & (R = 0.99927) \\ k_b &= 0.0045333 + 0.043581\phi - 0.0017292\phi^2 + 3.7374E - 5\phi^3 \\ &\quad - 3.7418E - 7\phi^4 + 1.4207E - 9\phi^5 & (R = 0.99949) \end{aligned} \quad (7.19e)$$

The pressure distribution within the semi-ellipsoid is

$$p = p_{max} \sqrt{1 - \frac{x^2}{a^2} - \frac{y^2}{b^2}} \quad (7.20)$$

which is an ellipse as shown in Figure 7-11 (p. 437).

Stress Distributions in General Contact

The stress distributions within the material are similar to those shown in Figure 7-17 for the cylinder-on-cylinder case. The normal stresses are all compressive and are maximal at the surface. They diminish rapidly with depth into the material and away from the centerline. At the surface on the centerline, the maximum normal stresses are^[19]

$$\begin{aligned} \sigma_x &= -\left[2v + (1-2v)\frac{b}{a+b}\right]p_{max} \\ \sigma_y &= -\left[2v + (1-2v)\frac{a}{a+b}\right]p_{max} \\ \sigma_z &= -p_{max} \end{aligned} \quad (7.21a)$$

$$k_3 = \frac{b}{a} \quad k_4 = \frac{1}{a} \sqrt{a^2 - b^2} \quad (7.21b)$$

These applied stresses are also the principal stresses. The maximum shear stress at the surface associated with these stresses can be found from equation 4.5. The largest shear stress occurs slightly below the surface, with that distance dependent on the ratio of the semiaxes of the contact ellipse. For $b/a = 1.0$, the largest shear stress occurs at $z = 0.63a$, and for $b/a = 0.34$ at $z = 0.24a$. Its peak magnitude is approximately 0.34 p_{max} .^[19]

At the ends of the major axis of the contact ellipse the shear stress at the surface is^[19]

$$\tau_{xz} = (1-2v) \frac{k_3}{k_4^2} \left(\frac{1}{k_4} \tanh^{-1} k_4 - 1 \right) p_{max} \quad (7.21c)$$

At the ends of the minor axis of the contact ellipse the shear stress at the surface is

$$\tau_{xz} = (1-2v) \frac{k_3}{k_4^2} \left[1 - \frac{k_3}{k_4} \tan^{-1} \left(\frac{k_4}{k_3} \right) \right] p_{max} \quad (7.21d)$$

The location of the largest surface shear stress will vary with the ellipse ratio k_3 . For some cases it is as shown in equation 7.21c, but in others it moves to the center of the ellipse and is found from the principal stresses in equation 7.21a using equation 4.5 (p. 144).

EXAMPLE 7-3

Stresses in a Crowned Cam Follower

Problem

A crowned cam roller-follower has a gentle radius transverse to its rolling direction to eliminate the need for critical alignment of its axis with that of the cam. The cam's radius of curvature and dynamic load vary around its circumference. What is the size of the contact patch between cam and follower and what are the worst-case stresses?

Given

The roller radius is 1 in with a 20-in crown radius at 90° to the roller radius. The cam's radius of curvature at the point of maximum load is 3.46 in and it is flat axially. The rotational axes of the cam and roller are parallel, which makes the angle between the two bodies zero. The force is 250 lb, normal to the contact plane.

Assumptions Materials are steel. The relative motion is rolling with <1% sliding.

Solution

1 Find the material constants from equation 7.9a.

$$m_1 = m_2 = \frac{1 - v_1^2}{E_1} = \frac{1 - 0.28^2}{3E7} = 3.072E - 8 \quad (a)$$

2 Two geometry constants are needed from equations 7.19a and b.

$$A = \frac{1}{2} \left(\frac{1}{R_1} + \frac{1}{R_1'} + \frac{1}{R_2} + \frac{1}{R_2'} \right) = \frac{1}{2} \left(\frac{1}{1} + \frac{1}{20} + \frac{1}{3.46} + \frac{1}{\infty} \right) = 0.6695 \quad (b)$$

$$B = \frac{1}{2} \left[\left(\frac{1}{R_1} - \frac{1}{R_1'} \right)^2 + \left(\frac{1}{R_2} - \frac{1}{R_2'} \right)^2 + 2 \left(\frac{1}{R_1} - \frac{1}{R_1'} \right) \left(\frac{1}{R_2} - \frac{1}{R_2'} \right) \cos 2\theta \right]^{\frac{1}{2}} \quad (c)$$

$$B = \frac{1}{2} \left[\left(\frac{1}{1} - \frac{1}{20} \right)^2 + \left(\frac{1}{3.46} - \frac{1}{\infty} \right)^2 + 2 \left(\frac{1}{1} - \frac{1}{20} \right) \left(\frac{1}{3.46} - \frac{1}{\infty} \right) \cos 2(0) \right]^{\frac{1}{2}} = 0.6195$$

The angle ϕ is found from their ratio (equation 7.19c),

$$\phi = \cos^{-1} \left(\frac{B}{A} \right) = \cos^{-1} \left(\frac{0.6195}{0.6695} \right) = 22.284^\circ \quad (d)$$

and used in equations 7.19e (p. 450) to find the factors k_a and k_b .

$$k_a = 50.192\phi^{-0.86215} = 50.192(22.284)^{-0.86215} = 3.455$$

$$k_b = 0.0045333 + 0.043581(22.284) - 0.0017292(22.284)^2 + 3.7374E - 5(22.284)^3$$

$$-3.7418E - 7(22.284)^4 + 1.4207E - 9(22.284)^5 = 0.415 \quad (e)$$

3 The material and geometry constants can now be used in equation 7.19d (p. 449).

$$a = k_a \sqrt[3]{\frac{3F(m_1 + m_2)}{4A}} = 3.455 \sqrt[3]{\frac{3(250)2(3.072E - 8)}{4(0.6695)}} = 0.0892 \quad (f)$$

$$b = k_b \sqrt[3]{\frac{3F(m_1 + m_2)}{4A}} = 0.415 \sqrt[3]{\frac{3(250)2(3.072E - 8)}{4(0.6695)}} = 0.0107$$

where a is the half-width of the major axis, and b is the half-width of the minor axis of the contact patch. The contact-patch area is then

$$\text{area} = \pi ab = \pi(0.0892)(0.0107) = 0.0030 \text{ in}^2 \quad (g)$$

4 The average and maximum contact pressure can be found from equations 7.18b and c (p. 449).

$$p_{avg} = \frac{F}{\text{area}} = \frac{250}{0.003} = 83\ 281 \text{ psi} \quad (h)$$

$$p_{max} = \frac{3}{2} p_{avg} = \frac{3}{2}(83\ 281) = 124\ 921 \text{ psi} \quad (i)$$

5 The maximum normal stresses in the center of the contact patch at the surface are then found using equations 7.21a (p. 450).

$$\begin{aligned} \sigma_x &= -\left[2v + (1-2v)\frac{b}{a+b}\right]p_{max} \\ &= -\left[2(.28) + (1-2(.28))\frac{0.0107}{0.0892+0.0107}\right]124\ 921 = -75\ 849 \text{ psi} \\ \sigma_y &= -\left[2v + (1-2v)\frac{a}{a+b}\right]p_{max} \\ &= -\left[2(.28) + (1-2(.28))\frac{0.0892}{0.0892+0.0107}\right]124\ 921 = -119\ 028 \text{ psi} \\ \sigma_z &= -p_{max} = -124\ 921 \text{ psi} \end{aligned} \quad (j)$$

These stresses are principal: $\sigma_1 = \sigma_x$, $\sigma_2 = \sigma_y$, $\sigma_3 = \sigma_z$. The maximum shear stress associated with them at the surface will be (from equation 4.5, p. 144)

$$\tau_{13} = \left| \frac{\sigma_1 - \sigma_3}{2} \right| = \left| \frac{-75\ 849 + 124\ 921}{2} \right| = 24\ 536 \text{ psi (at surface)} \quad (k)$$

6 The largest shear stress under the surface on the z axis is approximately

$$\tau_{13} \cong 0.34p_{max} = 0.34(124\ 921) \cong 42\ 168 \text{ psi (below surface)} \quad (l)$$

- 7 All the stresses found so far exist on the centerline of the patch. At the edge of the patch, at the surface, there will also be a shear stress. Two constants are found from equation 7.21b (p. 450) for this calculation.

$$k_3 = \frac{b}{a} = \frac{0.0107}{0.0892} = 0.120 \quad (m)$$

$$k_4 = \frac{1}{a} \sqrt{a^2 - b^2} = \frac{1}{0.0892} \sqrt{0.0892^2 - 0.0107^2} = 0.993$$

These constants are used in equations 7.21c and d (p. 450) to find the shear stresses on the surface at the ends of the major and minor axes.

$$\tau_{xz} = (1 - 2\nu) \frac{k_3}{k_4^2} \left(\frac{1}{k_4} \tanh^{-1} k_4 - 1 \right) p_{max} \quad (n)$$

$$\tau_{xz} = (1 - 0.56) \frac{0.120}{(0.993)^2} \left(\frac{1}{0.993} \tanh^{-1} 0.993 - 1 \right) 124\,921 = 12\,253 \text{ psi}$$

$$\tau_{xz} = (1 - 2\nu) \frac{k_3}{k_4^2} \left[1 - \frac{k_3}{k_4} \tan^{-1} \left(\frac{k_4}{k_3} \right) \right] p_{max} \quad (o)$$

$$\tau_{xz} = (1 - 0.56) \frac{0.120}{(0.993)^2} \left[1 - \frac{0.120}{0.993} \tan^{-1} \left(\frac{0.993}{0.120} \right) \right] 124\,921 = 5\,522 \text{ psi}$$

7

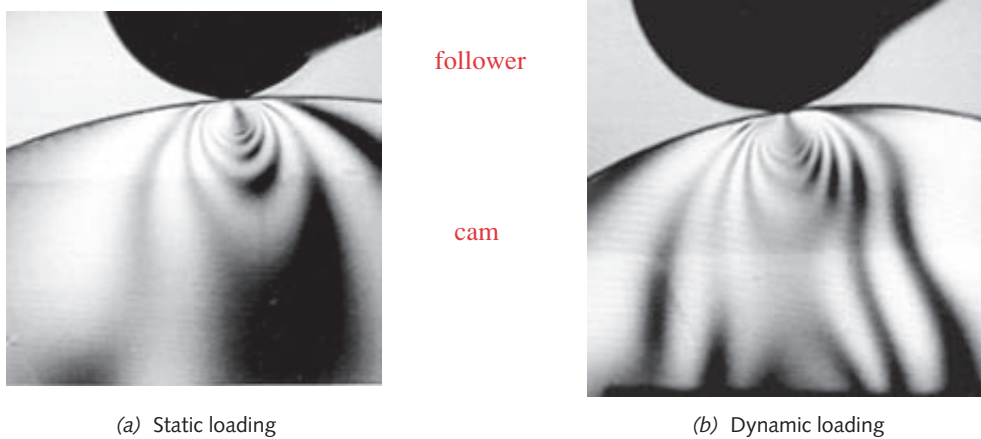
- 8 The files EX07-03 are on the CD-ROM.
-

7.11 DYNAMIC CONTACT STRESSES

The equations presented above for contact stresses assume that the load is pure rolling. When rolling and sliding are both present, the stress field is distorted by the tangential loading. Figure 7-19 shows a photoelastic study of a cam-follower pair^[20] loaded statically (a) and dynamically with sliding (b). The distortion of the stress field from the sliding motion can be seen in part b. This is a combination of rolling contact with relatively low-velocity sliding. Increased sliding causes more distortion of the stress field.

Effect of a Sliding Component on Contact Stresses

Smith and Lui^[18] analyzed the case of parallel rollers in combined rolling and sliding and developed the equations for the stress distribution beneath the contact point. The sliding (frictional) load has a significant effect on the stress field. The stresses can be expressed as separate components, one set due to the normal load on the rolls (denoted by a subscript *n*) and the other set due to the tangential friction force (denoted by a subscript *t*). These are then combined to obtain the complete stress situation. The stress field can be two-dimensional in a very short roll, such as a thin plate cam or thin gear, assumed to be in plane stress. If the rolls are long axially, then a plane strain condition will exist in regions away from the ends, giving a three-dimensional stress state.

**FIGURE 7-19**

Photoelastic Study of Stresses for Two Cylinders in Contact in Static (a) and Dynamic Pure Rolling Loading (b). Source: V. S. Mahkijani, *Study of Contact Stresses as Developed on a Radial Cam Using Photoelastic Model and Finite Element Analysis*, M.S. Thesis, WPI, 1984.

7

The contact geometry is as shown in Figure 7-11b (p. 437) with the x axis aligned to the direction of motion, the z axis radial to the rollers, and the y axis axial to the rollers. The stresses due to the normal loading p_{max} are

$$\begin{aligned}\sigma_{x_n} &= -\frac{z}{\pi} \left[\frac{a^2 + 2x^2 + 2z^2}{a} \beta - \frac{2\pi}{a} - 3x\alpha \right] p_{max} \\ \sigma_{z_n} &= -\frac{z}{\pi} [a\beta - x\alpha] p_{max} \\ \tau_{xz_n} &= -\frac{1}{\pi} z^2 \alpha p_{max}\end{aligned}\quad (7.22a)$$

and those due to the frictional unit force f_{max} are

$$\begin{aligned}\sigma_{x_t} &= -\frac{1}{\pi} \left[(2x^2 - 2a^2 - 3z^2)\alpha + 2\pi \frac{x}{a} + 2(a^2 - x^2 - z^2) \frac{x}{a} \beta \right] f_{max} \\ \sigma_{z_t} &= -\frac{1}{\pi} z^2 \alpha f_{max} \\ \tau_{xz_t} &= -\frac{1}{\pi} \left[(a^2 + 2x^2 + 2z^2) \frac{z}{a} \beta - 2\pi \frac{z}{a} - 3xz\alpha \right] f_{max}\end{aligned}\quad (7.22b)$$

where the factors α and β are given by

$$\alpha = \frac{\pi}{k_1} \frac{1 - \sqrt{\frac{k_2}{k_1}}}{\sqrt{\frac{k_2}{k_1}} \sqrt{2 \sqrt{\frac{k_2}{k_1}} + \left(\frac{k_1 + k_2 - 4a^2}{k_1} \right)}} \quad (7.22c)$$

$$\beta = \frac{\pi}{k_1} \frac{1 + \sqrt{\frac{k_2}{k_1}}}{\sqrt{\frac{k_2}{k_1}} \sqrt{2 \sqrt{\frac{k_2}{k_1}} + \left(\frac{k_1 + k_2 - 4a^2}{k_1} \right)}} \quad (7.22d)$$

$$k_1 = (a+x)^2 + z^2 \quad k_2 = (a-x)^2 + z^2 \quad (7.22e)$$

The tangential unit force f_{max} is found from the normal load and a coefficient of friction μ .

$$f_{max} = \mu p_{max} \quad (7.22f)$$

The independent variables in these equations are then the coordinates x, z in the cross section of the roller, referenced to the contact point, the half-width a of the contact patch, and the maximum normal load p_{max} at the contact point.

Equations 7.22 (pp. 454–455) define the behavior of the stress functions below the surface, but when $z = 0$, the factors α and β become infinite and these equations fail. Other forms are needed to account for the stresses on the surface of the contact patch.

$$\text{When } z = 0 : \text{ if } |x| \leq a \text{ then } \sigma_{x_n} = -p_{max} \sqrt{1 - \frac{x^2}{a^2}} \text{ else } \sigma_{x_n} = 0 \quad (7.23a)$$

$$\sigma_{z_n} = \sigma_{x_n}$$

$$\tau_{xz_n} = 0$$

$$\text{if } x \geq a \text{ then } \sigma_{x_t} = -2f_{max} \left(\frac{x}{a} - \sqrt{\frac{x^2}{a^2} - 1} \right) \quad (7.23b)$$

$$\text{if } x \leq -a \text{ then } \sigma_{x_t} = -2f_{max} \left(\frac{x}{a} + \sqrt{\frac{x^2}{a^2} - 1} \right) \quad (7.23b)$$

$$\text{if } |x| \leq a \text{ then } \sigma_{x_t} = -2f_{max} \frac{x}{a}$$

$$\sigma_{z_t} = 0$$

$$\text{if } |x| \leq a \text{ then } \tau_{xz_t} = -f_{max} \sqrt{1 - \frac{x^2}{a^2}} \text{ else } \tau_{xz_t} = 0 \quad (7.23c)$$

The total stress on each Cartesian plane is found by superposing the components due to the normal and tangential loads:

$$\begin{aligned} \sigma_x &= \sigma_{x_n} + \sigma_{x_t} \\ \sigma_z &= \sigma_{z_n} + \sigma_{z_t} \\ \tau_{xz} &= \tau_{xz_n} + \tau_{xz_t} \end{aligned} \quad (7.24a)$$

For short rollers in plane stress, σ_y is zero, but if the rollers are long axially, then a plane strain condition will exist away from the ends and the stress in the y direction will be:

$$\sigma_y = v(\sigma_x + \sigma_z) \quad (7.24b)$$

where v is Poisson's ratio.

These stresses are maximum at the surface and decrease with depth. Except at very low ratios of tangential force to normal force (< about 1/9)^{[18],[21]} the maximum shear stress occurs at the surface as well, unlike the pure rolling case. A computer program was written to evaluate equations 7.22 and 7.23 (pp. 454–455) for the conditions at the surface and plot them. (See the file CONTACT.EXE.) The stresses are all normalized to the maximum normal load p_{max} and the locations normalized to the patch half-width a . A coefficient of friction of 0.33 and steel rollers with $v = 0.28$ were assumed for the examples. The magnitudes and shapes of the stress distributions will be a function of these factors.

Figure 7-20a shows the x direction stresses at the surface, which are due to the normal and tangential loads, and also shows their sum from the first of equations 7.24a. Note that the stress component σ_{x_t} due to the tangential force is tensile from the contact point to and beyond the trailing edge of the contact patch. This should not be surprising, as one can picture that the tangential force is attempting to pile up material in front of the contact point and stretch it behind that point, just as a carpet bunches up in front of anything you try to slide across it. The stress component σ_{x_n} due to the normal force is compressive everywhere. However, the sum of the two σ_x components has a significant normalized tensile value of twice the coefficient of friction (here 0.66 p_{max}) and a compressive peak of about $-1.2 p_{max}$. Figure 7-20b shows all of the applied stresses in x , y , and z directions across the surface of the contact zone. Note that the stress fields on the surface extend beyond the contact zone when a tangential force is present, unlike the situation in pure rolling where they are within the contact zone. (See Figure 7-17 (p. 446) and program CONTACT.EXE.)

Figure 7-21 shows the principal stresses, maximum shear stress, and von Mises stress for the plane strain, applied stress state in Figure 7-20. Note that the magnitude

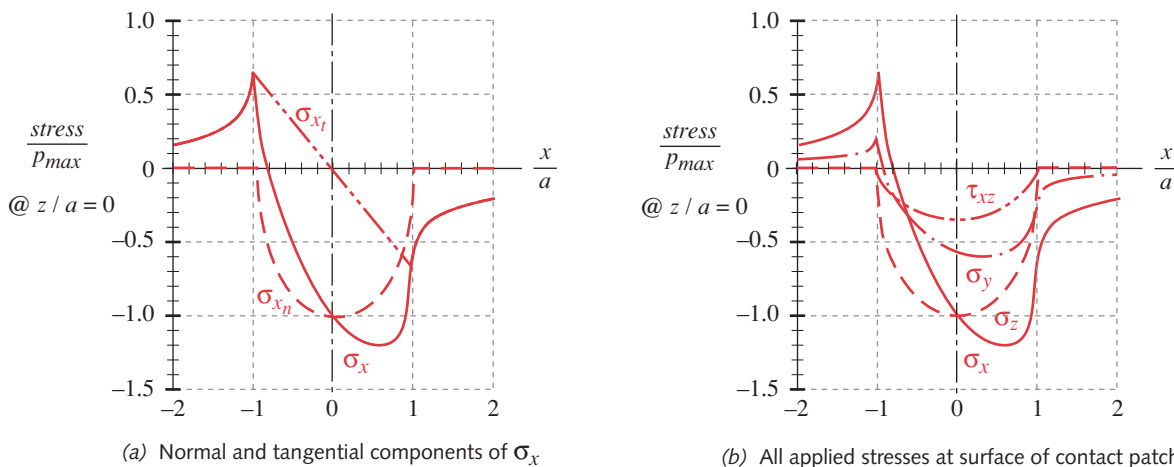
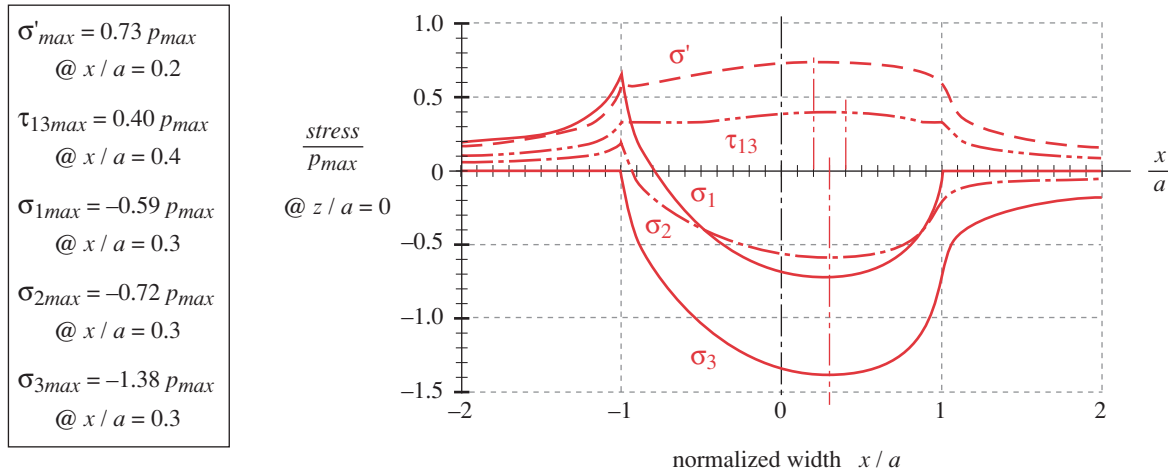


FIGURE 7-20

Applied Tangential and Normal and Shear Stresses at Surface for Cylinders in Combined Rolling and Sliding with $\mu = 0.33$

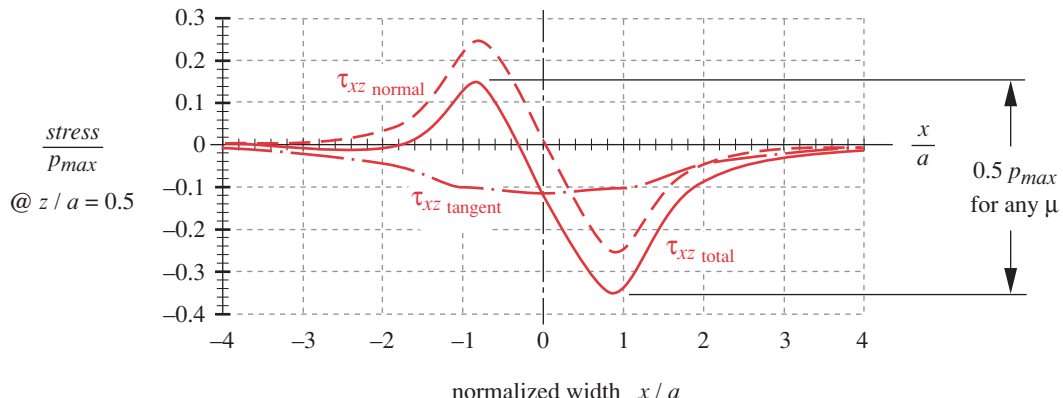
**FIGURE 7-21**

Principal and von Mises Stresses Across Contact Zone at Surface for Cylinders in Combined Rolling and Sliding with $\mu = 0.33$

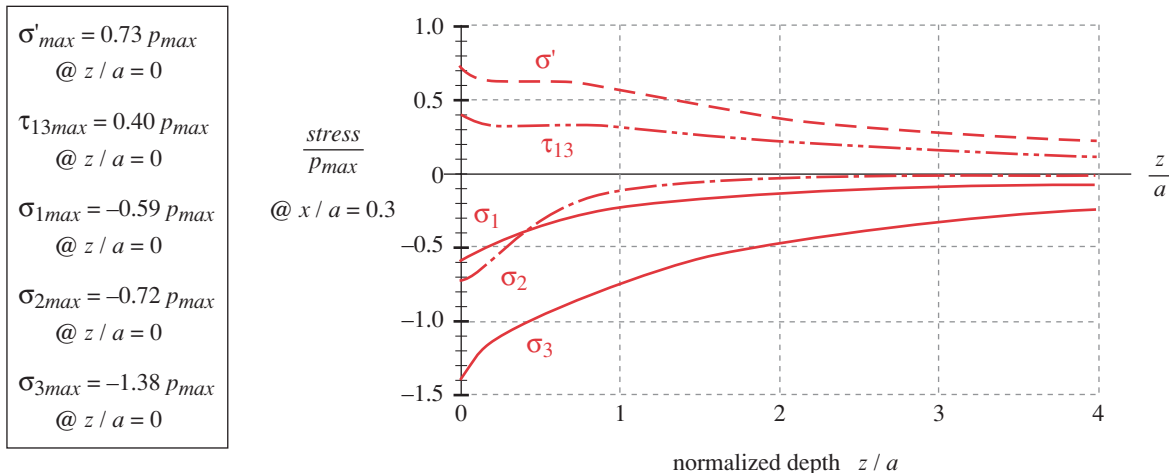
7

of the largest compressive principal stress is about $1.38 p_\text{max}$ and the largest tensile principal stress is $0.66 p_\text{max}$ at the trailing edge of the contact patch. The presence of an applied tangential shear stress in this example increases the peak compressive stress by 40% over a pure rolling case and introduces a tensile stress in the material. The principal shear stress reaches a peak value of $0.40 p_\text{max}$ at $x / a = 0.4$. All the stresses shown in Figures 7-19 and 7-20 are at the surface of the rollers.

Beneath the surface, the magnitudes of the compressive stresses due to the normal load reduce. However, the shear stress τ_{xz_n} due to the normal loading increases with depth, becoming a maximum beneath the surface at $z = 0.5a$, as shown in Figure 7-22. Note the sign reversal at the midpoint of the contact zone. There are fully reversed shear-stress components acting on each differential element of material as it passes through the contact zone. The peak-to-peak range of this fully reversed shear stress in the xz plane is greater in magnitude than the range of the maximum shear stress and is considered by some to be responsible for subsurface pitting failures.^[17]

**FIGURE 7-22**

Shear Stresses Below Surface at $z / a = 0.5$ for Cylinders in Combined Rolling and Sliding—Plotted with $\mu = 0.33$

**FIGURE 7-23**

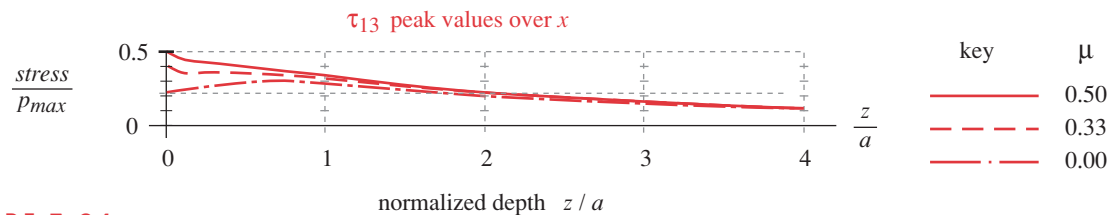
Principal and von Mises Stresses Below Surface at $x / a = 0.3$ for Cylinders in Combined Rolling and Sliding with $\mu = 0.33$

7

Figure 7-23 plots the principal stresses, maximum shear stress, and von Mises stress (calculated for $\mu = 0.33$ and a plane strain condition) versus the normalized depth z / a taken at the $x / a = 0.3$ plane (where the principal stresses are maximum as shown in Figure 7-21). All the stresses are maximum at the surface. The principal stresses diminish rapidly with depth, but the shear and von Mises stresses remain nearly constant over the first $1a$ of depth.

At the surface, the maximum shear stress is relatively uniform across the patch width with a peak of 0.4 at $x / a = 0.4$ when $\mu = 0.33$, as shown in Figure 7-21. This τ_{max} peak location moves versus the patch centerline with increasing depth, but its magnitude varies only slightly with depth. Figure 7-24 plots the largest peak value of the shear stress τ_{13} occurring at any value of x across the patch zone, and so is a composite plot of the peak shear stress value in each z plane. For $0 < \mu < 0.5$ the peak value remains within 60–80% of its largest value over the first a of depth and is still 58–70% of its peak value at $z / a = 2.0$. As the coefficient of friction is increased to 0.5 or greater, the normalized maximum shear-stress value becomes equal to μ and is constant across the contact-patch surface.

The limited variation of τ_{max} over small z depths may explain why some pitting failures appear to start at the surface and some below it. With a relatively uniform-magnitude maximum shear stress over the entire near-surface region, any inclusion in that

**FIGURE 7-24**

Peak Values of Maximum Shear Stress at All Values of x / a for Cylinders in Combined Rolling and Sliding with $0 \leq \mu \leq 0.5$

region of the material creates a stress concentration and serves as a crack initiation point. The fact that the peak value of the maximum shear stress occurs at slightly different transverse locations at different depths within the contact zone is irrelevant, since an inclusion at any particular depth will pass through that location once per revolution and be exposed to the peak stress value.

The programs CONTACT, SURFCY LZ, and SURFCY LX provided on disk solve and plot equations 7.22, 7.23, and 7.24 (pp. 455–456) for any user-specified roller geometry, materials, load, and coefficient of friction, at any specified range of locations below and along the surface.

EXAMPLE 7-4

Stresses in Combined Rolling and Sliding of Cylinders

Problem A pair of calendering rolls are run together with a combination of rolling and sliding. Find the maximum tensile, compressive, and shear stresses in the rollers.

Given The roller radii are 1.25 and 2.5 in and are each 24 in long. The force is 5000 lb, normal to the contact plane.

Assumptions Both materials are steel. The coefficient of friction is 0.33.

Solution

- 1 The contact-patch geometry is found in the same way as was done in Example 7-2. Find the material constants from equation 7.9a (p. 439).

$$m_1 = m_2 = \frac{1 - v_1^2}{E_1} = \frac{1 - 0.28^2}{3E7} = 3.072E - 8 \quad (a)$$

The geometry constant is found from equation 7.15a (p. 445)

$$B = \frac{1}{2} \left(\frac{1}{R_1} + \frac{1}{R_2} \right) = \frac{1}{2} \left(\frac{1}{1.25} + \frac{1}{2.5} \right) = 0.600 \quad (b)$$

and the patch half-width from equation 7.15b (p. 445).

$$a = \sqrt{\frac{2}{\pi} \frac{m_1 + m_2}{B} \frac{F}{L}} = \sqrt{\left(\frac{2}{\pi}\right) \frac{2(3.072E - 8)}{0.600} \left(\frac{5000}{24}\right)} = 0.003685 \text{ in} \quad (c)$$

where a is the half-width of the contact patch. The rectangular contact-patch area is then

$$\text{area} = 2aL = 2(0.003685)(24) = 0.1769 \text{ in}^2 \quad (d)$$

- 2 The average and maximum contact pressure can now be found from equations 7.14b and c (p. 445).

$$p_{avg} = \frac{F}{\text{area}} = \frac{5000}{0.1769} = 28266 \text{ psi} \quad (e)$$

$$p_{max} = \frac{2F}{\pi aL} = \frac{2(5000)}{\pi(0.0037)24} = 35\ 989 \text{ psi} \quad (f)$$

The tangential pressure is found from equation 7.22f (p. 455):

$$f_{max} = \mu p_{max} = 0.33(35\ 989) = 11\ 876 \text{ psi} \quad (g)$$

- 3 With $\mu = 0.33$, the principal stresses in the contact zone will be maximal on the surface ($z = 0$) at $x = 0.3a$ from the centerline as shown in Figures 7-20 (p. 456) and 7-22 (p. 457). The applied stress components are found from equation 7.23a (p. 454) for the normal force and equation 7.23b (p. 454) for the tangential force.

$$\sigma_{x_n} = -p_{max} \sqrt{1 - \frac{x^2}{a^2}} = -35\ 989 \sqrt{1 - 0.3^2} = -34\ 331 \text{ psi} \quad (h)$$

$$\sigma_{x_t} = -2f_{max} \frac{x}{a} = -2(11\ 876)(0.3) = -7\ 126 \text{ psi}$$

$$\sigma_{z_n} = -p_{max} \sqrt{1 - \frac{x^2}{a^2}} = -35\ 989 \sqrt{1 - 0.3^2} = -34\ 331 \text{ psi} \quad (i)$$

$$\sigma_{z_t} = 0 \qquad \tau_{xz_n} = 0$$

$$\tau_{xz_t} = -f_{max} \sqrt{1 - \frac{x^2}{a^2}} = -11\ 876 \sqrt{1 - 0.3^2} = -11\ 329 \text{ psi} \quad (j)$$

- 4 Equations 7.24a and b (p. 455-456) can now be solved for the total applied stresses along the x , y , and z axes.

$$\sigma_x = \sigma_{x_n} + \sigma_{x_t} = -34\ 331 - 7\ 126 = -41\ 457 \text{ psi} \quad (k)$$

$$\sigma_z = \sigma_{z_n} + \sigma_{z_t} = -34\ 331 + 0 = -34\ 331 \text{ psi} \quad (l)$$

$$\tau_{xz} = \tau_{xz_n} + \tau_{xz_t} = 0 - 11\ 329 = -11\ 329 \text{ psi} \quad (m)$$

- 5 Since the rollers are long, we expect a plane strain condition to exist. The stress in the third dimension is found from equation 7.24b (p. 456):

$$\sigma_y = v(\sigma_x + \sigma_z) = 0.28(-41\ 457 + 34\ 331) = -21\ 221 \text{ psi} \quad (n)$$

- 6 Unlike the pure rolling case, these stresses are not principal because of the applied shear stress. The principal stresses are found from equation 4.4 (p. 144) using a cubic root-finding solution (See program MOHR or the file STRESS3D).

$$\begin{aligned} \sigma_1 &= -21\ 221 \text{ psi} \\ \sigma_2 &= -26\ 018 \text{ psi} \\ \sigma_3 &= -49\ 771 \text{ psi} \end{aligned} \quad (o)$$

The maximum shear stress is found from the principal stresses using equation 4.5 (p. 144).

$$\tau_{13} = \frac{|\sigma_1 - \sigma_3|}{2} = \frac{|-21\ 221 + 49\ 771|}{2} = 14\ 275 \text{ psi} \quad (p)$$

- 7 The principal stresses are maximum at the surface as seen in Figures 7-20 and 7-22.
- 8 The files EX07-04 can be found on the CD-ROM.

7.12 SURFACE FATIGUE FAILURE MODELS—DYNAMIC CONTACT

There is still some disagreement among experts as to the actual mechanism of failure that results in pitting and spalling of surfaces. The possibility of having a maximum shear stress at a subsurface location (in pure rolling) has led some to conclude that pits begin at or near that location. Others have concluded that pitting begins at the surface. It is possible that both mechanisms are at work in these cases, since failure initiation usually begins at an imperfection, which may be on or below the surface. Figure 7-25 shows both surface and subsurface cracks in a case-hardened steel roll subjected to heavy rolling loads.^[22]

An extensive experimental study of pitting under rolling contact was done by Way^[23] in 1935. Over 80 tests were made with contacting, pure rolling, parallel rollers of different materials, lubricants, and loads, run for up to 18 million cycles, though most samples failed between $0.5E6$ and $1.5E6$ cycles. The samples were monitored for the appearance of minute surface cracks, which inevitably presaged a pitting failure within less than about 100 000 additional cycles in the presence of a lubricant.

Harder and smoother surfaces better resisted pitting failure. Highly polished samples did not fail in over $12E6$ cycles. Nitrided rolls with very hard cases on a soft core were longer-lived than other materials tested. **No pitting occurred on any samples in the absence of a lubricant** even though dry-running produced surface cracks. The cracked parts would continue to run dry with no failure for as many as $5E6$ cycles un-

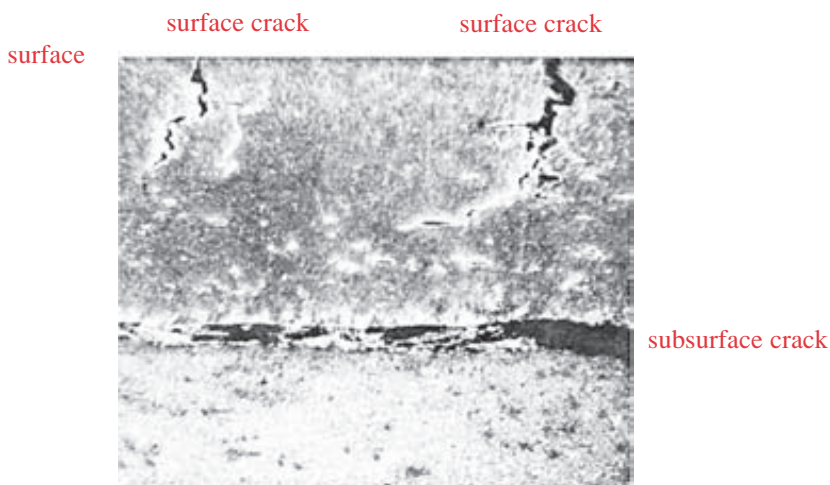


FIGURE 7-25

Photomicrograph (100x) of Surface and Subsurface Cracks in a Carburized and Hardened Roll (HRC 52-58) Subjected to a Heavy Rolling Load Source: J. D. Graham, *Pitting of Gear Teeth*, in C. Lipson, *Handbook of Mechanical Wear*, U. Mich. Press, 1961, p.137, with permission.

til some lubricant was added. Then the surface cracks would rapidly enlarge and turn to pits of a characteristic arrowhead shape within 100 000 additional cycles.

The suggested explanation for the deleterious effect of the lubricant was that once suitably oriented surface cracks form, they are pumped full of oil on approaching the roll-nip, and then are pressed closed within the roll-nip, pressurizing the fluid trapped in the crack. The fluid pressure creates tensile stress at the crack tip, causing rapid crack growth and subsequent break-out of a pit. Higher-viscosity lubricants did not eliminate metal-to-metal contact but did delay the pitting failure, indicating that the fluid must be able to readily enter the crack to do the damage.

Way reached a number of conclusions regarding how to design rollers to delay surface fatigue failure.^[23]

- 1 Use no oil (though he was quick to point out that this is not a practical solution, as it promotes other types of wear as discussed in previous sections).
- 2 Increase the viscosity of the lubricant.
- 3 Polish the surfaces (though this is expensive to do).
- 4 Increase the surface hardness (preferably on a softer, tough core).

No conclusions were drawn with respect to the reasons for the initiation of the initial cracks on the surface. Though, with pure rolling, the shear stresses are not maximal at the surface, they are nonzero there at some locations (see Figures 7-12, p. 439 and 7-17, p. 446).

Littmann and Widner^[24] performed an extensive analytical and experimental study on contact fatigue in 1966 and describe five different modes of failure in rolling contact. These are listed in Table 7-6 along with some factors that promote their occurrence. Some of these modes address the crack initiation issue and others the crack propagation issue. We will briefly discuss each in the order listed.

INCLUSION ORIGIN describes a mechanism for crack initiation and is similar to the one discussed in Section 6.1 on fatigue failure. It is assumed that the crack originates in a shear-stress field at a subsurface or surface location containing a small inclu-

Table 7-6 Modes of Surface Failure and Their Causes

Mode of Failure	Factors That Promote Occurrence
Inclusion origin	Frequency and severity of oxide or other hard inclusions.
Geometric stress concentration	End-of-contact geometry. Misalignment and deflections. Possible lubricant-film thickness effects.
Point-surface origin (PSO)	Low lubricant viscosity. Thin elastohydrodynamic film compared to asperities on contact surfaces. Tangential forces and/or gross sliding.
Peeling (superficial pitting)	Low lubricant viscosity. Frequent asperities in surface finish exceeding elastohydrodynamic-film thickness. Loss of elastohydrodynamic pressure due to side leakage or scratches in contact surface.
Subcase fatigue (on carburized components)	Low core hardness. Thin case depth relative to radius of curvature for elements in contact.

Source: W. E. Littmann and R. L. Widner, Propagation of Contact Fatigue from Surface and Subsurface Origins, *J. Basic Eng. Trans. ASME*, vol. 88, pp. 624–636, 1966.

sion of “foreign” matter. The most commonly identified inclusions are oxides of the material that formed during processing and were captured within it. These are typically hard and irregular in shape and create stress concentration. Several researchers^{[25],[26],[27]} have published photomicrographs of (or otherwise identified) subsurface cracks starting at oxide inclusions. “These oxide inclusions are often present as stringers or elongated aggregates of particles . . . , which provide a much greater chance for a point of high stress concentration to be in an unfavorable position with respect to the applied stress.”^[28] The propagation of a crack from the inclusion may remain subsurface, or break out to the surface. In the latter case it provides a site for hydraulic pressure propagation, as described above. In either case, it ultimately results in pitting or spalling.

GEOMETRIC STRESS CONCENTRATION (GSC) was discussed in Chapter 4. This mechanism can act on a surface when, for example, one contacting part is shorter axially than the other (common with cam-follower joints and roller bearings). The ends of the shorter roller create line-contact stress concentration in the mating roller as shown in Figure 7-26a, and pitting or spalling will likely occur at that location. This is one reason for using crowned rollers, which have a large crown radius of curvature in the yz plane in addition to their roller radius in the xz plane. If the contact load is predictable, the crown radius can be sized to provide a more uniform stress distribution across the axial length of the contact area due to the deflections of the rollers, as shown in Figure 7-26b. However, at lighter loads, there will be reduced contact area and thus higher stresses at the center, and at higher-than-design loads the stress concentrations at the ends will return. A partial crown can be used as shown in Figure 7-26c but may cause some stress concentration at the transition from straight to crown. Reusner^[29] has shown that a logarithmic curve on the crown as shown in Figure 7-26d will give a more uniform stress distribution under varied load levels.

POINT-SURFACE ORIGIN (PSO) is the phenomenon described by Way and discussed above. Littmann et al.^[24] consider PSO to be more a manner of crack propagation than crack initiation and suggest that an inclusion at or near the surface may be responsible for starting the crack. Handling nicks or dents can also provide a crack nucleus on the surface. Once present, and if pointing in the right direction to capture oil, the crack rapidly propagates to failure. Once spalling starts, the debris can create new nicks to serve as additional crack sites.

PEELING refers to a situation in which the fatigue cracks are at shallow depth and extend over a large area such that the surface “peels” away from the substrate. Rough surfaces exacerbate peeling if the surface asperities are larger than the lubricant film thickness.

SUBCASE FATIGUE, also called *case crushing*, occurs only on case-hardened parts and is more likely if the case is so thin that the subsurface stresses extend into the softer, weaker core material. The fatigue crack starts below the case and eventually causes the case to either collapse into the failed subsurface material or break out in pits or spalls. Talbourdet^[34] found that the depth of the case should be at least twice the depth of the point of maximum shear stress and recommends that for high unit loads it should be between 0.060 and 0.070 in.

Whatever the detailed cause of the start of a crack, once started the outcome is predictable. So, the designer needs to take all possible precautions to improve the part’s resistance to pitting as well as to all other wear modes. The summary section to this chapter will attempt to set some guidelines to this end.

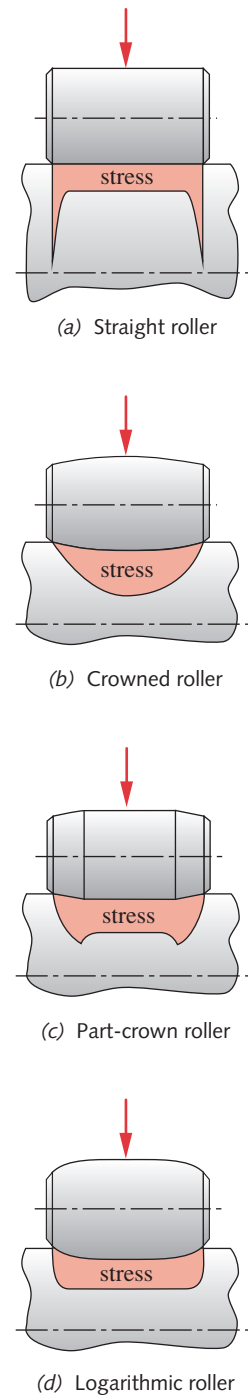


FIGURE 7-26

Stress Concentrations Beneath Variously Shaped Rollers

7.13 SURFACE FATIGUE STRENGTH

Repeated, time-varying loads tend to fail parts at lower stress levels than the material can stand in static load applications. Bending- and axial-fatigue strength were discussed extensively in Chapter 6. The concept of **surface fatigue strength** is similar except for one main difference. While steels and a few other materials loaded in bending or axial fatigue show an endurance limit, *no materials* in general show an equivalent property when loaded in surface fatigue. Thus, we should expect that our machine, though carefully designed to be safe against all other forms of failure, will eventually succumb to surface fatigue if so loaded for enough cycles.*

Morrison^[30] and Cram^[31] report separately on an experimental study of the surface-fatigue strength of materials done at USM Corp. from 1932 to 1956 by G. Talbourdet.^[34] Four wear-testing machines were operated **24 hours per day for 24 years** at about 1000 rpm to gather surface fatigue strength data on cast iron, steel, bronze, aluminum, and nonmetallic materials. Their tests included rollers in pure rolling as well as rolling plus varying percentages of sliding of the driving roll up to 75%. Most of their roll-slide data are done at 9% sliding, since that simulates the average conditions on spur and helical gear teeth. The percent sliding figure is defined as the relative sliding velocity between the rollers or gear teeth divided by the pitch-line velocity of the interface.

Previous sections have shown the complexity of the stress state that exists in the surface and subsurface regions of the contact zones of mating cylinders, spheres, or other bodies. The discussion of crack initiation mechanisms above indicates that the location of an incipient crack is quite unpredictable, given the random distribution of inclusions in the material. Therefore it is more difficult to accurately predict the condition of stress at an expected point of failure in a contact zone than was the case in designing a cantilever beam, for example. This dilemma is resolved by using one, easily calculated contact-zone stress as a *reference value* to compare to material strengths. The one chosen is the largest negative (compressive) principal contact stress. In a pure rolling case, its magnitude will be equal to the applied maximum contact pressure P_{max} . But it will be greater than that value if sliding is present.

To develop allowable surface fatigue strengths, the material is typically run under controlled loading conditions (i.e., controlled p_{max}) and the number of cycles to failure recorded and reported along with other loading factors such as percent sliding, lubrication, body geometry, etc. This “virtual strength” can be compared to the peak magnitude of compressive stress in other applications having similar loading factors. Thus the reported surface fatigue strength has only an indirect relationship to the actual stresses that may have been present in the test piece and in your similarly loaded part. While the Hertzian stress equations are only theoretically valid for static loading, Talbourdet found that the compressive stresses determined from their extensive tests were in close agreement to those predicted by the Hertz equation.^[34]

The expression for the normal, compressive Hertzian static stress in cylindrical contact is found by combining equations 7.14b (p. 445) and 7.17a (p. 446):

$$\sigma_z = -p_{max} = \frac{2F}{\pi aL} \quad (7.25a)$$

* Note, however, that recent advances in steel manufacturing have developed so-called “clean” steels, made with such low levels of impurities that they give evidence of an infinite-life endurance limit in surface fatigue. [T. A. Harris, *Rolling Bearing Analysis*. John Wiley & Sons: New York, pp. 872-888, 1991.]

Substitute the expression for a from equation 7.15b (p. 445), square both sides, and simplify:

$$\sigma_z^2 = \frac{2}{\pi} \frac{F}{L} \frac{B}{(m_1 + m_2)} \quad (7.25b)$$

Rearrange to solve for the load F ,

$$F = \sigma_z^2 \frac{\pi L(m_1 + m_2)}{2B} \quad (7.25c)$$

and collect terms in a constant K ,

$$F = \frac{KL}{2B} \quad (7.25d)$$

where

$$K = \pi(m_1 + m_2)\sigma_z^2 \quad (7.25e)$$

This factor K is termed an *experimental load factor* and is used to determine the safe endurance load F at a specified number of cycles or the number of cycles that can be expected before failure occurs at a given load.

Table 7-7 shows experimentally determined load factors K , surface fatigue strengths S_c , and strength factors λ , ζ , for a number of materials running either against themselves or against hardened tool steel.^[30] See the original reference for a complete listing, as some materials were omitted here due to lack of space. Two different loading modes are also addressed in separate sections of the table: pure rolling, and rolling with 9% sliding. The first column of the table defines the material. In each section, the next two columns give the K value and the surface fatigue strength at $1E8$ cycles as tested. The next two columns contain strength factors λ and ζ , which represent the slope and intercept of the S - N diagram (on log-log coordinates) for the surface fatigue strength of the material as determined by regression on large amounts of test data. These factors can be used in the equation of the statistically fitted S - N line to find the expected cycle life N for the applied stress level.

$$\log_{10} K = \frac{\zeta - \log_{10} N}{\lambda} \quad (7.26)$$

The K values in Table 7-7 can be used directly in equation 7.25d to calculate an allowable load F for the selected material at $1E8$ cycles of stress. For other desired design cycle lives, first calculate the largest negative (compressive) radial stress for your design from the appropriate equations as defined in the preceding sections. Then calculate K from equation 7.25e and use it and the values of λ and ζ from Table 7-7 to find the value of N for the application from equation 7.26. Since there is no endurance limit for surface fatigue loading, we can expect pitting to begin after approximately N stress cycles at the level of nominal stress contained in your calculated K factor.

Alternatively, a desired number of cycles N can be chosen and an allowable design-stress level σ_z for a chosen material computed from equations 7.25e (p. 465) and 7.26 (p. 465). A safety factor can be applied either by selecting a material with a longer cycle

life than required for the application or by sizing the parts to have a stress level below the calculated allowable stress level for a necessary number of cycles.

Table 7-7 Surface Fatigue Strength Data for Various Materials

Part 1: Materials Running Against an HRC 60-62 Tool-Steel Roller

7

#	Material	Pure Rolling				Rolling & 9% Sliding			
		K psi	S _c @ 1E8 cycles, psi	λ	ζ	K psi	S _c @ 1E8 cycles, psi	λ	ζ
1	1020 steel, carburized, 0.045 in min depth HRC 50-60	12 700	256 000	7.39	38.33	10 400	99 000	13.20	61.06
2	1020 steel, HB 130-150	—	—	—	—	1 720	94 000	4.78	23.45
3	1117 steel, HB 130-150	1 500	89 000	4.21	21.41	1 150	77 000	3.63	19.12
4	X1340 steel, induction hardened, 0.045 in min depth HRC 45-58	10 000	227 000	6.56	34.24	8 200	206 000	8.51	41.31
5	4150 steel, h-t, HB 270-300, flash-chrome plated	6 060	177 000	11.18	50.29	—	—	—	—
6	4150 steel, h-t, HB 270-300, phosphate coated	9 000	216 000	8.80	42.81	6 260	180 000	11.56	51.92
7	4150 cast steel, h-t, HB 270-300	—	—	—	—	2 850	121 000	17.86	69.72
8	4340 steel, induction hardened, 0.045 in min depth HRC 50-58	13 000	259 000	14.15	66.22	9 000	216 000	14.02	63.44
9	4340 steel, h-t, HB 270-300	—	—	—	—	5 500	169 000	18.05	75.55
10	6150 steel, HB 300-320	1 170	78 000	3.10	17.51	—	—	—	—
11	6150 steel, HB 270-300	—	—	—	—	1 820	97 000	8.30	35.06
12	18% Ni maraging tool steel, air hardened, HRC 48-50	—	—	—	—	4 300	146 000	3.90	22.18
13	Gray iron, Cl. 20, HB 140-160	790	49 000	3.83	19.09	740	47 000	4.09	19.72
14	Gray iron, Cl. 30, HB 200-220	1 120	63 000	4.24	20.92	—	—	—	—
15	Gray iron, Cl. 30, h-t (austempered) HB 255-300, phosphate-coated	2 920	102 000	5.52	27.11	2 510	94 000	6.01	28.44
16	Gray iron, Cl. 35, HB 225-255	2 000	86 000	11.62	46.35	1 900	84 000	8.39	35.51
17	Gray iron, Cl. 45, HB 220-240	—	—	—	—	1 070	65 000	3.77	19.41
18	Nodular iron, Gr. 80-60-03, h-t HB 207-241	2 100	96 000	10.09	41.53	1 960	93 000	5.56	26.31
19	Nodular iron, Gr. 100-70-03, h-t HB 240-260	—	—	—	—	3 570	122 000	13.04	54.33
20	Nickel bronze, HB 80-90	1 390	73 000	6.01	26.89	—	—	—	—
21	SAE 65 phosphor-bronze sand casting, HB 65-75	730	52 000	2.84	16.13	350	36 000	2.39	14.08
22	SAE 660 cont-cast bronze, HB 75-80	—	—	—	—	320	33 000	1.94	12.87
23	Aluminum bronze	2 500	98 000	5.87	27.97	—	—	—	—
24	Zinc die-casting, HB 70	250	28 000	3.07	15.35	220	26 000	3.11	15.29
25	Acetal resin	620	—	—	—	580	—	—	—
26	Polyurethane rubber	240	—	—	—	—	—	—	—

Table 7-7 Surface Fatigue Strength Data for Various Materials

Part 2: Materials Running Against the Same Material

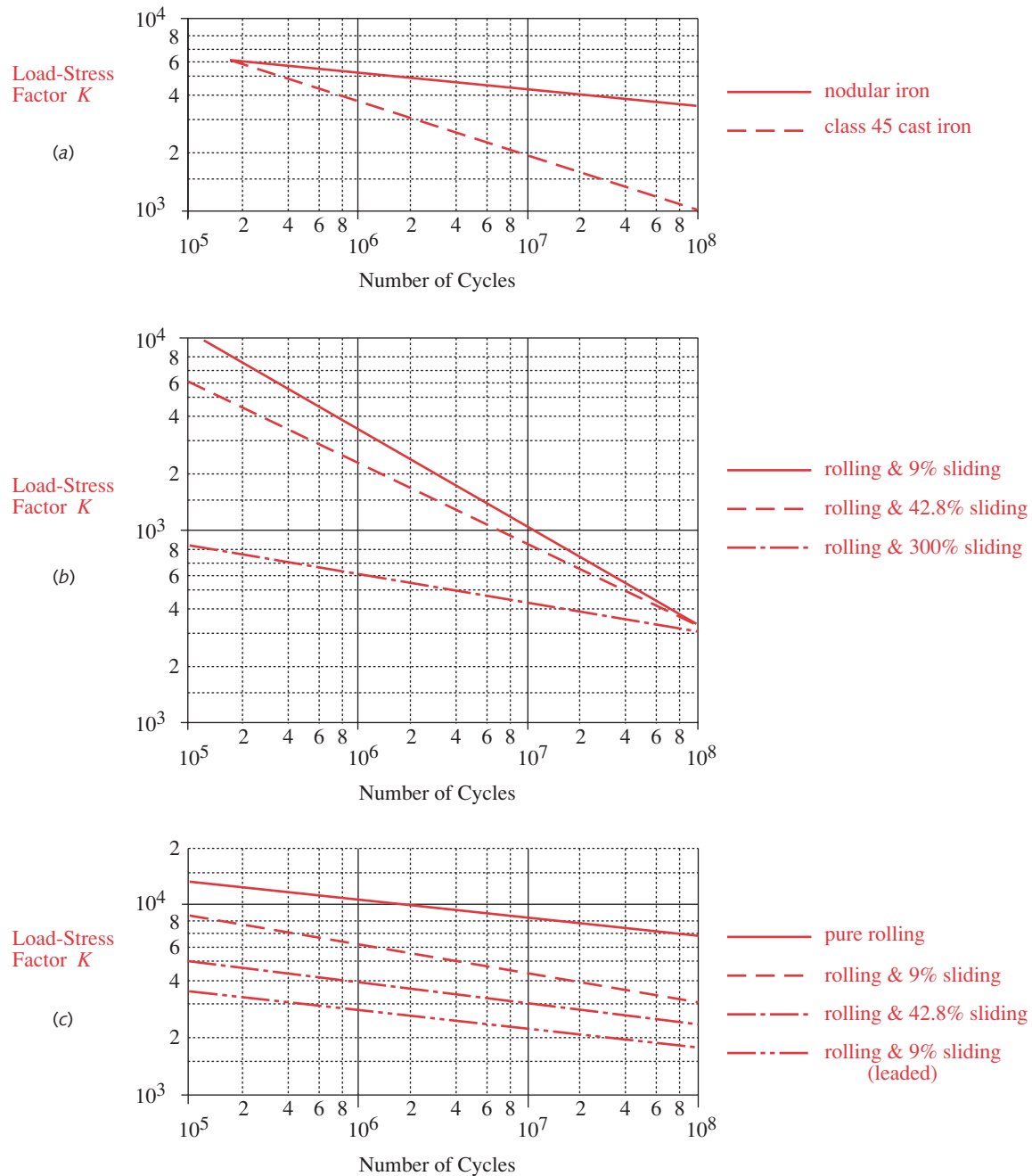
#	Material	Pure Rolling				Rolling & 9% Sliding			
		K psi	S _c @ 1E8 cycles, psi	λ	ζ	K psi	S _c @ 1E8 cycles, psi	λ	ζ
27	1020 steel, HB 130-170, and same but phosphate coated	2 900	122 000	7.84	35.17	1 450	87 000	6.38	28.23
28	1144 steel CD steel, HB 260-290, (stress-proof)	—	—	—	—	2 290	109 000	4.10	21.79
29	4150 steel, h-t, HB 270-300, and same but phosphate coated	6 770	187 000	10.46	48.09	2 320	110 000	9.58	40.24
30	4150 leaded steel, phosphate coated, h-t, HB 270-300	—	—	—	—	3 050	125 000	6.63	31.1
31	4340 steel, h-t, HB 320-340, and same but phosphate coated	10 300	230 000	18.13	80.74	5 200	164 000	26.19	105.31
32	Gray iron, Cl. 20, HB 130-180	960	45 000	3.05	17.10	920	43 900	3.55	18.52
33	Gray iron, Cl. 30, h-t (austempered) HB 270-290	3 800	102 000	7.25	33.97	3 500	97 000	7.87	35.90
34	Nodular iron, Gr. 80-60-03, h-t HB 207-241	3 500	117 000	4.69	24.65	1 750	82 000	4.18	21.56
35	Meehanite, HB 190-240	1 600	80 000	4.77	23.27	1 450	76 500	4.94	23.64
36	6061-T6 aluminum, hard anodized coating	350	—	10.27	34.15	260	—	5.02	20.12
37	HK31XA-T6 magnesium, HAE coating	175	—	6.46	22.53	275	—	11.07	35.02

Source: R. A. Morrison, "Load/Life Curves for Gear and Cam Materials," *Machine Design*, vol. 40, pp. 102–108, Aug. 1, 1968, A Penton Publication, Cleveland, Ohio, with the publisher's permission.

7

The strength values in Table 7-7 were obtained using rollers in contact, lubricated with a light mineral oil of 280-320 SSU at 100°F. The researchers report that "an orderly transition occurs from pitting fatigue to abrasive wear as percent sliding is increased." Pitting failures were observed under as high as 300% sliding on some cast irons, and abrasive wear was seen at as low as 9% sliding on hardened steels under high stress. They also note that the addition of oxide coatings, fortified (EP) lubricants, or lead as an alloying element all reduced tangential stress levels and increased fatigue life or allowable % sliding. The addition of phosphate coatings to the surfaces reduced sparking and flashing of lubricant, reduced the friction coefficient, and also increased fatigue life. They saw evidence of pitting starting both at the surface under high % sliding and below the surface in pure rolling or low-percent-sliding situations.^[30] Increased sliding percentages reduce fatigue life but not linearly. Figure 7-27 (p. 468) shows some S-N curves (from reference 30) for three materials with various percentages of sliding.

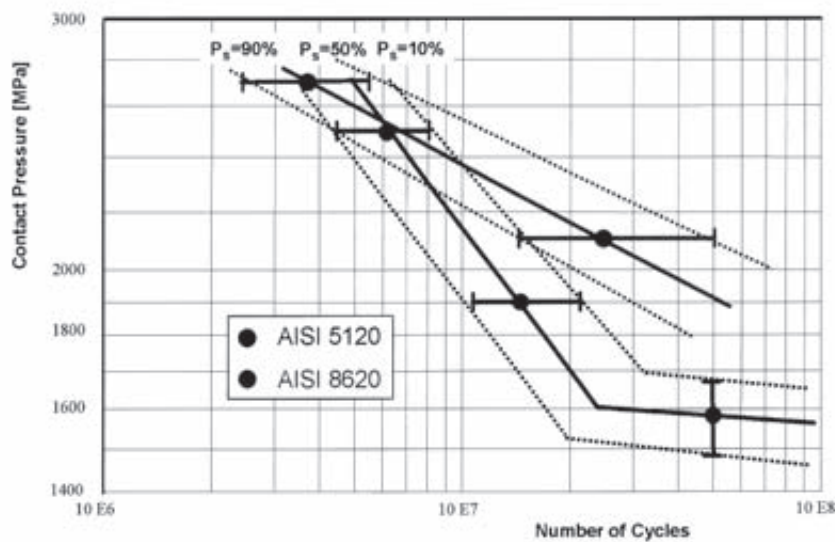
The speed of stress cycling only affected nonmetallic materials, wherein friction heat blistered or yielded the material. A material's stiffness is a factor, however. Lower-modulus materials reduce the contact stress because their larger deflections increase the contact-patch area. Cast iron on cast iron had longer life than cast iron on hardened steel. The free graphite in cast iron also makes it a good choice in contact situations, as it acts to retard adhesion as well as being a dry lubricant, though the lower grades of CI have strengths too low to be useful in this situation. Nodular iron in its harder forms may



Typical curves showing load-life relationships for common gear and cam materials. Curves in (a) are for 100-70-30 nodular iron (HB 240-260) and class 45 gray cast iron (HB 220-240), both materials running on carbon tool steels (HRC 60-62). Curves in (b) are for continuous-cast bronze running on hardened steel. Curves in (c) are for heat-treated 4150 steel running against the same material, but phosphate coated. In all charts, 9% sliding velocity is 54 fpm; 42.8% sliding velocity is 221 fpm.

FIGURE 7-27

Load-Life Curves for Some Combinations of Materials in Combined Rolling and Sliding. Source: R. A. Morrison, "Load/Life Curves for Gear and Cam Materials," *Machine Design*, vol. 40, pp. 102-108, Aug. 1, 1968, A Penton Publication, Cleveland, Ohio, with permission

**FIGURE 7-28**Surface Fatigue S-N Diagrams for Two Case-Hardened Steels^[35]

7

be a better choice. Hardness of a material was not found to correlate closely with its surface endurance. Some softer steels performed better than some harder ones.^[30]

More recent surface-fatigue test data were reported in 2007 by Hoffman and Jandeska.^[35] Several case-hardened steel alloys and powdered-metal (PM) materials commonly used in automotive transmissions were subjected to cylindrical rolling contact under controlled loading, lubrication, and percent sliding conditions. Eddy current methods were used to detect crack initiation and crack growth rate. They observed crack initiation both at and below the surface in various tests. Surface cracks can start at micropits formed by lack of sufficient lubrication or from preexisting inclusions and grow into the material at a 30° angle driven by shear stress. Subsurface cracks usually form in regions of the highest von Mises stress, first growing parallel to the surface before turning toward the surface and forming pits. A third mode of failure observed was core crushing or sub-case fatigue in the softer core, due to insufficient heat treatment. Figure 7-28 shows S-N curves with scatter bands for two case-hardened steel alloys. Note that the curves never go horizontal, though one has a smaller negative slope after a knee. This is further evidence of the lack of a true endurance limit in surface fatigue.

EXAMPLE 7-5

Finding the Safety Factor in Surface Fatigue

Problem

Choose a material to provide 10 years of life for the rollers in Example 7-4.

Given

The rollers have radii of 1.25 and 2.5 in and are each 24 in long. The principal stresses are as shown in Example 7-4. The smaller roller is turning at 4 000 rpm.

Assumptions There is 9% sliding combined with rolling. Both materials will be of the same steel. The machine will operate 3 shifts/day for 345 days/year.

Solution

- Calculate the required cycle life from the given data:

$$\text{cycles} = 4000 \frac{\text{rev}}{\text{min}} \cdot 60 \frac{\text{min}}{\text{hr}} \cdot 24 \frac{\text{hr}}{\text{day}} \cdot 345 \frac{\text{day}}{\text{yr}} \cdot 10 \text{ yr} = 2.0E10 \quad (a)$$

- The maximum normal stress calculated in Example 7-4 is 49 771 psi compressive. Its K factor can be calculated from equation 7.25d (p. 465). The previously calculated material constants m_1 and m_2 are needed:

$$m_1 = m_2 = \frac{1 - v_1^2}{E_1} = \frac{1 - 0.28^2}{3E7} = 3.072E - 8 \quad (b)$$

$$K = \pi(m_1 + m_2)\sigma_z^2 = 2\pi(3.072E - 8)(49771)^2 = 478 \quad (c)$$

7

- A trial material must be selected from Table 7-7 (pp. 466–467). With a K this low, virtually any of the steels can probably be used. We will try the HB 130-170 SAE 1020, phosphate-coated steel (#27 in part 2 of the table), since the same materials are running together. The slope and intercept factors of this steel for rolling with 9% sliding are

$$\lambda = 6.38 \quad \zeta = 28.23 \quad (d)$$

- These are used in equation 7.26 (p. 465) along with the value of K from equation c above to find the number of cycles that can be expected at this load before pitting begins.

$$\begin{aligned} \log_{10} K &= \frac{\zeta - \log_{10} N_{life}}{\lambda} \\ \log_{10} N_{life} &= \zeta - \lambda \log_{10} K = 28.23 - 6.38 \log_{10}(478) \\ N_{life} &= 10^{(28.23 - 6.38 \log_{10}(478))} = 1.4E11 \end{aligned} \quad (e)$$

- A safety factor against pitting can now be calculated from the ratio of the projected cycle life and the desired number of cycles.

$$N_f = \frac{N_{life}}{\text{cycles}} = \frac{1.4E11}{2.0E10} = 6.9 \quad (f)$$

- The files EX07-05 can be found on the CD-ROM.
-

7.14 SUMMARY

This chapter has presented a brief introduction to the very broad topic of surface wear. Wear is generally considered to be divisible into five general categories: *adhesive wear*, *abrasive wear*, *erosion*, *corrosive wear*, and *surface fatigue*. Other mechanisms such as *corrosion fatigue* and *fretting corrosion* combine elements from more than one category.

Wear usually requires some relative motion to be present between two surfaces. **Adhesive wear** occurs when the asperities of two mating surfaces adhere to one another

and then break when sliding occurs, transferring material from one part to the other, or out of the system. **Abrasive wear** involves a hard, rough surface abrading material from a softer one, or loose, hard particles trapped between two surfaces and abrading both.

Corrosion wear occurs when a corrosive atmosphere (such as oxygen) is present to attack the surface of the material in combination with sliding that breaks the oxides or other contaminants free from the surfaces. This exposes new material to the corrosive elements and also turns the often hard corrosion products into abradants. Corrosion fatigue refers to the combination of a corrosive environment with cyclic stresses. This combination is particularly deadly and greatly shortens the fatigue life of materials. Fretting corrosion occurs in tight joints (such as press fits) where no gross motion is present. Tiny vibratory motions are sufficient to set up a corrosive wear process called fretting that can remove significant volumes of material over time.

Surface fatigue occurs in pure rolling or roll-sliding contact, but not in pure sliding situations. The very high contact stresses engendered by the small areas of contact act to cause fatigue failure of the material after many thousands of cycles of repeated stress. **Pitting** is the loss of small pieces of material from the surface, leaving behind pits. Pits will grow into larger areas of flaked-off surface material, which is then called **spalling**. An audible warning is usually noticeable when the pitting process begins. If unattended, it will proceed to gross damage of the part.

High-strength, smooth materials are required in contact-stress applications. **No materials show an endurance limit against surface fatigue** and all will eventually fail by this mechanism if subjected to a sufficient number of contact-stress reversals.

Designing to Avoid Surface Failure

There are a number of precautions that a designer may take to reduce the chances of a wear failure by any of the mechanisms described in this chapter.

- 1 **Proper choice of materials:** The issues of material compatibility must be observed. Careful attention to surface finish and hardness as well as to strength is necessary to reduce abrasion and increase surface fatigue life. Corrosive environments require special materials. Coatings should be considered in some situations. Homogeneity of materials in contact-stress situations is desirable. More expensive steels processed to create more uniform and inclusion-free microstructures can give superior service in highly stressed surface fatigue cases and may be cheaper in the long run. In general, higher surface hardness reduces both adhesive and abrasive wear as well as surface fatigue.
- 2 **Proper lubricants:** It is rare that a heavily loaded joint is run dry (and then only if some overriding concern is present, such as fear of contamination of the product with escaped lubricant). Hydrodynamic or hydrostatic lubrication should be used where feasible. Boundary lubrication is less desirable, though is often unavoidable. If boundary lubrication is used, an EP lubricant may significantly reduce adhesive wear at the expense of some corrosive wear. See Chapter 11 for more on lubrication.
- 3 **Cleanliness:** Reasonable measures should be taken to ensure that no external or environmental contaminants can enter bearings or joints. Seals or other means to protect them should be provided. If particulate contamination cannot be avoided (as in dirty environments), soft materials should be chosen for bearings to allow embedment of trapped particles.

- 4 **Stress:** Avoid or minimize stress concentrations, especially in fatigue-loaded applications. Consider using a less-stiff material to increase the contact-patch area and reduce stresses in surface-fatigue cases. Be extremely wary of situations in which any kind of fatigue loading (not just surface fatigue) is present in combination with a corrosive environment, since corrosion fatigue is then a problem. A test program is probably necessary in such situations, as little data are available on this phenomenon.
- 5 **Fretting:** Consider the possibility of fretting failure if vibration or repeated deflections are present in combination with press fits or tight joints.

Important Equations Used in This Chapter

See the referenced sections for information on the proper use of these equations.

Real Area of Contact (Section 7.3):

$$A_r \equiv \frac{F}{S_p} \equiv \frac{F}{3S_{yc}} \quad (7.1)$$

Coefficient of Friction (Section 7.3):

$$\mu = \frac{f}{F} \equiv \frac{S_{us}}{3S_{yc}} \quad (7.3)$$

Volume of Wear (Section 7.4):

$$V = K \frac{Fl}{H} \quad (7.7a)$$

Maximum Pressure—Spherical Contact (Section 7.8):

$$p_{max} = \frac{3}{2} \frac{F}{\pi a^2} \quad (7.8b)$$

Material Constants (Section 7.8):

$$m_1 = \frac{1-v_1^2}{E_1} \quad m_2 = \frac{1-v_2^2}{E_2} \quad (7.9a)$$

Geometry Constant for Spherical and Cylindrical Contact (Section 7.8):

$$B = \frac{1}{2} \left(\frac{1}{R_1} + \frac{1}{R_2} \right) \quad (7.9b)$$

Radius of Contact Patch—Spherical Contact (Section 7.8):

$$a = \sqrt[3]{0.375 \frac{m_1 + m_2}{B} F} \quad (7.9d)$$

Maximum Stresses—Spherical Contact (Section 7.8):

$$\sigma_{z_{max}} = -p_{max} \quad (7.11c)$$

$$\sigma_{x_{max}} = \sigma_{y_{max}} = -\frac{1+2v}{2} p_{max} \quad (7.11d)$$

$$\tau_{13_{max}} = \frac{p_{max}}{2} \left[\frac{(1-2v)}{2} + \frac{2}{9}(1+v)\sqrt{2(1+v)} \right] \quad (7.12b)$$

$$z_{@ \tau_{max}} = a \sqrt{\frac{2+2v}{7-2v}} \quad (7.12c)$$

Maximum Pressure—Cylindrical Contact (Section 7.9):

$$p_{max} = \frac{2F}{\pi aL} \quad (7.14b)$$

Half-Width of Cylindrical Contact Patch (Section 7.9):

$$a = \sqrt{\frac{2}{\pi} \frac{m_1 + m_2}{B} \frac{F}{L}} \quad (7.15b)$$

Maximum Stresses—Cylindrical Contact (Section 7.9):

$$\begin{aligned} \sigma_x &= \sigma_z = -p_{max} \\ \sigma_y &= -2v p_{max} \end{aligned} \quad (7.17a)$$

$$\begin{aligned} \tau_{13_{max}} &= 0.304 p_{max} \\ z_{@ \tau_{max}} &= 0.786a \end{aligned} \quad (7.17b)$$

Maximum Pressure—General Contact (Section 7.10):

$$p_{max} = \frac{3}{2} \frac{F}{\pi ab} \quad (7.18b)$$

Half-Dimensions of Elliptical Contact Patch (Section 7.10—See Table 7-5 for k_a and k_b):

$$a = k_a \sqrt[3]{\frac{3F(m_1 + m_2)}{4A}} \quad b = k_b \sqrt[3]{\frac{3F(m_1 + m_2)}{4A}} \quad (7.19d)$$

$$A = \frac{1}{2} \left(\frac{1}{R_1} + \frac{1}{R_1'} + \frac{1}{R_2} + \frac{1}{R_2'} \right) \quad (7.19a)$$

Maximum Stresses—General Contact (Section 7.10):

$$\begin{aligned} \sigma_x &= -\left[2v + (1-2v) \frac{b}{a+b} \right] p_{max} \\ \sigma_y &= -\left[2v + (1-2v) \frac{a}{a+b} \right] p_{max} \\ \sigma_z &= -p_{max} \end{aligned} \quad (7.21a)$$

Friction Unit Force—Parallel Cylinders Rolling and Sliding (Section 7.11):

$$f_{max} = \mu p_{max} \quad (7.22f)$$

Maximum Stresses—Parallel Cylinders Rolling and Sliding (Section 7.11):

When $z = 0$: if $|x| \leq a$ then $\sigma_{x_n} = -p_{max} \sqrt{1 - \frac{x^2}{a^2}}$ else $\sigma_{x_n} = 0$

$$\sigma_{z_n} = \sigma_{x_n}$$

$$\tau_{xz_n} = 0$$
(7.23a)

$$\text{if } x \geq a \text{ then } \sigma_{x_t} = -2f_{max} \left(\frac{x}{a} - \sqrt{\frac{x^2}{a^2} - 1} \right)$$

$$\text{if } x \leq -a \text{ then } \sigma_{x_t} = -2f_{max} \left(\frac{x}{a} + \sqrt{\frac{x^2}{a^2} - 1} \right)$$
(7.23b)

$$\text{if } |x| \leq a \text{ then } \sigma_{x_t} = -2f_{max} \frac{x}{a}$$

$$\sigma_{z_t} = 0$$

$$\text{if } |x| \leq a \text{ then } \tau_{xz_t} = -f_{max} \sqrt{1 - \frac{x^2}{a^2}}$$
(7.23c)

$$\sigma_x = \sigma_{x_n} + \sigma_{x_t}$$
(7.24a)

$$\sigma_z = \sigma_{z_n} + \sigma_{z_t}$$
(7.24a)

$$\tau_{xz} = \tau_{xz_n} + \tau_{xz_t}$$
(7.24b)

$$\sigma_y = v(\sigma_x + \sigma_z)$$
(7.24b)

Material Surface Fatigue Strength Factor (Section 7.12):

$$K = \pi(m_1 + m_2) \sigma_z^2$$
(7.25e)

S-N Line Equation for Surface Fatigue (Section 7.12—See Table 7-7 for λ and ζ):

$$\log_{10} K = \frac{\zeta - \log_{10} N}{\lambda}$$
(7.26)

7.15 REFERENCES

- 1 E. Rabinowicz, *Friction and Wear of Materials*. John Wiley & Sons: New York, p. 110, 1965.
- 2 *Ibid.*, pp. 21, 33.
- 3 *Ibid.*, p. 125.
- 4 *Ibid.*, p. 30.
- 5 R. Davies, Compatibility of Metal Pairs, in *Handbook of Mechanical Wear*, C. Lipson, ed. Univ. of Mich. Press: Ann Arbor, p. 7, 1961.
- 6 D. J. Wulpi, *Understanding How Components Fail*. American Society for Metals: Metals Park, OH, 1990.
- 7 E. Rabinowicz, *Friction and Wear of Materials*. John Wiley & Sons: New York, p. 60, 1965.

- 8 *Ibid.*, p. 85.
- 9 **J. T. Burwell**, Survey of Possible Wear Mechanisms. *Wear*, **1**: pp. 119-141, 1957.
- 10 **E. Rabinowicz**, *Friction and Wear of Materials*. John Wiley & Sons: New York, pp. 179, 1965.
- 11 *Ibid.*, p. 180.
- 12 **J. R. McDowell**, Fretting and Fretting Corrosion, in *Handbook of Mechanical Wear*, C. Lipson and L. V. Colwell, ed. Univ. of Mich. Press: Ann Arbor, pp. 236-251, 1961.
- 13 **H. Hertz**, On the Contact of Elastic Solids. *J. Math.*, **92**: pp. 156-171, 1881 (in German).
- 14 **H. Hertz**, Contact of Elastic Solids, in *Miscellaneous Papers*, P. Lenard, ed. Macmillan & Co. Ltd.: London, pp. 146-162, 1896.
- 15 **H. L. Whittemore and S. N. Petrenko**, *Friction and Carrying Capacity of Ball and Roller Bearings*, Technical Paper 201, National Bureau of Standards, Washington, D.C., 1921.
- 16 **H. R. Thomas and V. A. Hoersch**, *Stresses Due to the Pressure of One Elastic Solid upon Another*, Bulletin 212, U. Illinois Engineering Experiment Station, Champaign, Ill., July 15, 1930.
- 17 **E. I. Radzimovsky**, *Stress Distribution and Strength Condition of Two Rolling Cylinders*, Bulletin 408, U. Illinois Engineering Experiment Station, Champaign, Ill., Feb 1953.
- 18 **J. O. Smith and C. K. Lui**, Stresses Due to Tangential and Normal Loads on an Elastic Solid with Application to Some Contact Stress Problems. *J. Appl. Mech. Trans. ASME*, **75**: pp. 157-166, 1953.
- 19 **S. P. Timoshenko and J. N. Goodier**, *Theory of Elasticity*, 3rd ed., McGraw-Hill: New York, pp. 403-419, 1970.
- 20 **V. S. Mahkijani**, *Study of Contact Stresses as Developed on a Radial Cam Using Photoelastic Model and Finite Element Analysis*. M.S. Thesis, Worcester Polytechnic Institute, 1984.
- 21 **J. Poritsky**, Stress and Deformations due to Tangential and Normal Loads on an Elastic Solid with Applications to Contact of Gears and Locomotive Wheels, *J. Appl. Mech. Trans ASME*, **72**: p. 191, 1950.
- 22 **E. Buckingham and G. J. Talbourdet**, *Recent Roll Tests on Endurance Limits of Materials*. in Mechanical Wear Symposium. ASM: 1950.
- 23 **S. Way**, Pitting Due to Rolling Contact. *J. Appl. Mech. Trans. ASME*, **57**: pp. A49-58, 1935.
- 24 **W. E. Littmann and R. L. Widner**, Propagation of Contact Fatigue from Surface and Subsurface Origins, *J. Basic Eng. Trans. ASME*, **88**: pp. 624-636, 1966.
- 25 **H. Styri**, *Fatigue Strength of Ball Bearing Races and Heat-Treated 52100 Steel Specimens*. Proceedings ASTM, **51**: p. 682, 1951.
- 26 **T. L. Carter, et al.**, Investigation of Factors Governing Fatigue Life with the Rolling Contact Fatigue Spin Rig, *Trans. ASLE*, **1**: p. 23, 1958.
- 27 **H. Hubbell and P. K. Pearson**, *Nonmetallic Inclusions and Fatigue under Very High Stress Conditions, in Quality Requirements of Super Duty Steels*. AIME Interscience Publishers: p. 143, 1959.

Table P7-0[†]

Topic/Problem Matrix

7.2 Mating Surfaces

7-1, 7-25, 7-27, 7-35, 7-37

7.3 Friction

7-2, 7-26, 7-28, 7-36, 7-38

7.4 Adhesive Wear

7-12, 7-15, 7-29, 7-39

7.5 Abrasive Wear7-13, **7-14**, 7-30, 7-46, 7-47**7.8 Spherical Contact****7-4**, **7-5**, **7-6**, 7-16, 7-17, 7-40**7.9 Cylindrical Contact**7-7, 7-8, **7-9**, **7-10**, **7-11**, 7-18, 7-19**7.10 General Contact**7-20, 7-21, **7-22**, 7-41, 7-43, 7-44**7.11 Dynamic Contact**

7-23, 7-31, 7-32, 7-42, 7-45

7.13 Fatigue Strength**7-3**, 7-24, 7-33, 7-34, 7-48, 7-49

7

- 28 **W. E. Littmann and R. L. Widner**, Propagation of Contact Fatigue from Surface and Subsurface Origins, *J. Basic Eng. Trans. ASME*, **88**: p. 626, 1966.
- 29 **H. Reusner**, The Logarithmic Roller Profile - the Key to Superior Performance of Cylindrical and Tapered Roller Bearings, *Ball Bearing Journal*, SKF, **230**, June 1987.
- 30 **R. A. Morrison**, "Load/Life Curves for Gear and Cam Materials." *Machine Design*, v. 40, pp. 102-108, Aug. 1, 1968.
- 31 **W. D. Cram**, Experimental Load-Stress Factors, in *Handbook of Mechanical Wear*, C. Lipson and L. V. Colwell, eds., Univ. of Mich. Press: Ann Arbor, pp. 56-91, 1961.
- 32 **J. F. Archard**, "Wear Theory and Mechanisms," in *Wear Control Handbook*, M. B. Peterson and W. O. Winer, eds., McGraw-Hill: New York, pp. 35-80, 1980.
- 33 **E. Rabinowicz**, "Wear Coefficients—Metals," in *Wear Control Handbook*, M. B. Peterson and W. O. Winer, eds., McGraw-Hill: New York, pp. 475-506, 1980.
- 34 **G. J. Talbourdet**, "Surface Endurance Limits of Various USMC Engineering Materials," Research Division of United Shoe Machinery Corporation, Beverly, MA, 1957.
- 35 **G. Hoffman and W. Jandeska**, "Effects on Rolling Contact Fatigue Performance," *Gear Technology*, Jan/Feb 2007, pp. 42-52.
- 36 **Y. Ding and J.A. Gear**, "Spalling Depth Prediction Model," *Wear* 267 (2009), pp. 1181-1190.

7.16 PROBLEMS

*7-1 Two 3 × 5 cm blocks of steel with machined finish $R_a = 0.6 \mu\text{m}$ are rubbed together with a normal force of 400 N. Estimate their true area of contact if their $S_y = 400 \text{ MPa}$.

*7-2 Estimate the dry coefficient of friction between the two pieces in Problem 7-1 if their $S_{ut} = 600 \text{ MPa}$.

*†7-3 For the bicycle pedal arm assembly in Figure P7-1 assume a rider-applied force that ranges from 0 to 400 N at the pedal each cycle. Determine the maximum contact stresses at one sprocket-tooth chain-roller interface. Assume that one tooth takes all the applied torque, the chain roller is 8-mm dia, the sprocket has a nominal (pitch) dia of 100 mm, and the sprocket tooth is essentially flat at the point of contact. The roller and sprocket contact over a length of 8 mm. Assuming rolling plus 9% sliding, estimate the number of cycles to failure for this particular tooth-roller combination.

*7-4 For the trailer hitch from Problem 3-4 on p. 127 (also see Figures P7-2 and 1-5, p. 14), determine the contact stresses in the ball and the ball cup (not shown). Assume that the ball is 2-in dia and the ill-fitting ball cup that surrounds it has an internal spherical surface 10% larger in diameter than the ball.

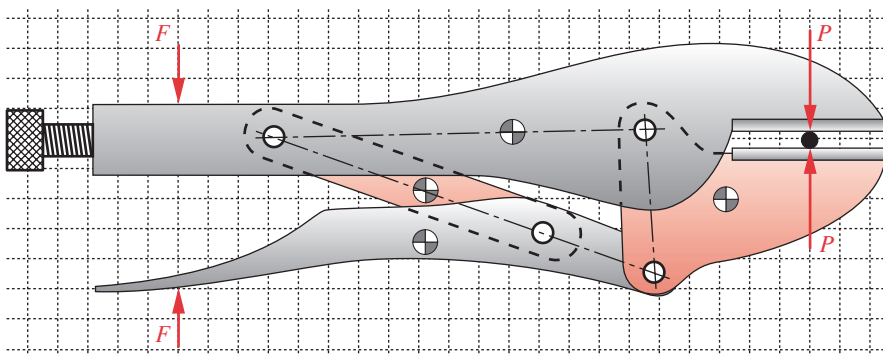
7-5 For the trailer hitch from Problem 3-5 on p. 127 (also see Figures P7-2 and 1-5, p. 14) determine the contact stresses in the ball and the ball cup (not shown). Assume that the ball is 2-in dia and the ill-fitting ball cup that surrounds it has an internal spherical surface 10% larger in diameter than the ball.

7-6 For the trailer hitch from Problem 3-6 on p. 127 (also see Figures P7-2 and 1-5, p. 14) determine the contact stresses in the ball and the ball cup (not shown). Assume that the ball is 2-in dia and the ill-fitting ball cup that surrounds it has an internal spherical surface 10% larger in diameter than the ball.

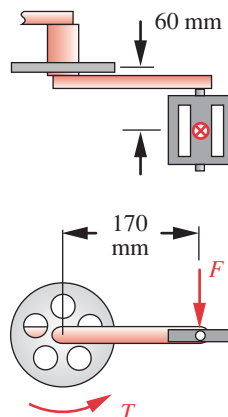
* Answers to these problems are provided in Appendix D.

[†] Problem numbers in **boldface** are extended from similar problems having the same dash number in earlier chapters.

- 7-7** For the 12-mm-dia steel wrist pin of Problem 3-7 (p. 127) find the maximum contact stress if the 2 500-g acceleration is fully reversed. The aluminum piston has a hole for the wrist pin that is 2% larger than the pin and an engagement length of 2 cm.
- *7-8** A paper machine processes rolls of paper having a density of 984 kg/m^3 . The paper roll is 1.50-m OD \times 0.22-m ID \times 3.23-m long and has an effective modulus of elasticity in compression of 14 MPa and $v = 0.3$. Determine the width of its contact patch when it sits on a flat steel surface, loaded by its own weight.
- 7-9** For the ViseGrip® plier-wrench drawn to scale in Figure P7-3, and for which the forces were analyzed in Problem 3-9, find the clamping force needed to create a 0.25-mm-wide flat on each side of a 2-mm-dia aluminum pin squeezed in its 5-mm-wide jaws.
- *7-10** An overhung diving board is shown in Figure P7-4a. A 100-kg person is standing on the free end. It sits on a fulcrum that has a cylindrical contact surface of 5-mm radius. What is the size of the contact patch between the board and the aluminum fulcrum if the board material is fiberglass with $E = 10.3 \text{ GPa}$ and $v = 0.3$?
- 7-11** Repeat Problem 7-10 assuming the 100-kg person in Problem 7-10 jumps up 25 cm and lands back on the board. Assume the board weighs 29 kg and deflects 13.1 cm statically when the person stands on it. What is the size of the contact patch between the board and the 5-mm-radius aluminum fulcrum if the board material is fiberglass with $E = 10.3 \text{ GPa}$ and $v = 0.3$?
- 7-12** Estimate the volume of adhesive wear to expect from an HB270 steel shaft of 40-mm dia rotating at 250 rpm, three 8-hour shifts per day for 10, 360-day years in a plain bronze bushing if the transverse load is 1 000 N.
 - For conditions of poor lubrication.
 - For conditions of good lubrication.
- *7-13** Estimate how much time it will take to file 1 mm off a 2-cm cube of HB150 steel if the machinist applies 100 N over a 10-cm stroke at 60 strokes/min.
 - If done dry.
 - If done lubricated.
- †7-14** Figure P7-5 shows a child's toy called a *pogo stick*. The child stands on the pads, applying half her weight on each side. She jumps up off the ground, holding the pads up against her feet, and bounces along with the spring cushioning the impact and storing energy to help each rebound. Assume a 60-lb child and a spring rate of 100 lb/in. The pogo stick weighs 5 lb. Estimate the abrasive-wear rate for the tip, which impacts the ground, assuming a condition of dry, loose abrasive grains (sand). Express the wear rate in number of jumps to remove 0.02 in from the 1-in-dia aluminum tip if its $S_{ut} = 50 \text{ ksi}$.

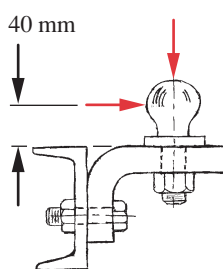
**FIGURE P7-3**

Problem 7-9 (A Solidworks model of this is on the CD)

**FIGURE P7-1**

Problem 7-3 (A Solidworks model of this is on the CD)

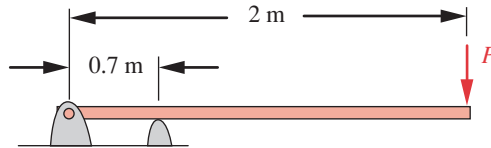
7

**FIGURE P7-2**Problems 7-4, 7-5, 7-6
(A Solidworks model of this is on the CD)

* Answers to these problems are provided in Appendix D.

† Problem numbers in boldface are extended from similar problems having the same dash number in earlier chapters.

‡ See Table 7-7 (pp. 461-462) for data on material strengths for these problems.



Overhung diving board

FIGURE P7-4

Problems 7-10 and 7-11

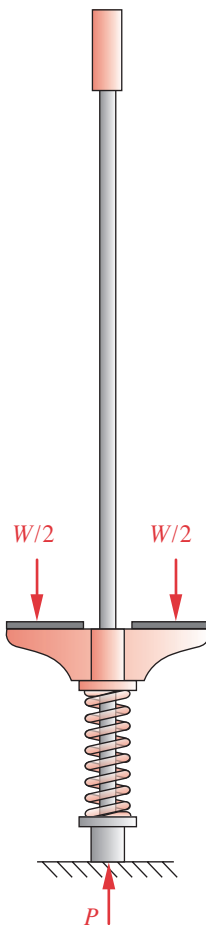


FIGURE P7-5

Problem 7-14

* Answers to these problems are provided in Appendix D. Problem numbers in **boldface** are extended from similar problems having the same dash number in earlier chapters.

[†] See Table 7-7 (pp. 466-467) for data on material strengths for these problems.

- 7-15 Create a table of acceptable materials to run against a steel shaft based on their metallurgical compatibility. Rank them as to suitability.
- *7-16** Determine the size of the contact patch and the maximum contact stresses for a 20-mm-dia steel ball rolled against a flat aluminum plate with 1 kN.
- 7-17 Determine the size of the contact patch and the maximum contact stresses for a 20-mm-dia steel ball rolled against a 30-mm dia aluminum ball with 800 N.
- *7-18** Determine the size of the contact patch and the maximum contact stresses for a 40-mm-dia steel cylinder, 25 cm long, rolled against a flat aluminum plate with 4 kN.
- 7-19 Determine the size of the contact patch and the maximum contact stresses for a 40-mm-dia steel cylinder, 25 cm long, rolled against a parallel 50-mm-dia steel cylinder with 10 kN of radial force.
- *7-20** Determine the size of the contact patch and the maximum contact stresses for a 20-mm-dia steel ball rolled against a 40-mm-dia steel cylinder, 25 cm long, with 10 kN.
- 7-21 A cam-follower system has a dynamic load of 0 to 2 kN. The cam is cylindrical with a minimum radius of curvature of 20 mm. The roller follower is crowned with radii of 15 mm in one direction and 150 mm in the other. Find the contact stresses and safety factor if the follower is 4150 steel at HB300 with $S_{fc} = 1\ 500$ MPa, and the cam is nodular iron at HB207. They run lubricated with less than 1% slip.[†]
- *7-22** Figure P7-6 shows an inline “roller-blade” skate. The polyurethane wheels are 72-mm dia by 12-mm thick with a 6 mm crown radius and are spaced on 104-mm centers. The skate-boot-foot combination weighs 2 kg. The effective “spring rate” of the person-skate system is 6 000 N/m. Find the contact stresses in the wheels when a 100-kg person lands a 0.5-m jump on one foot on concrete. Assume the polyurethane wheels have $E = 600$ MPa with $v = 0.4$ and the concrete has $E = 21E3$ MPa in compression with $v = 0.2$.
- Assume that all 4 wheels land simultaneously.
 - Assume that one wheel absorbs all the landing force.
- *7-23** A pair of 12-in-dia cylindrical steel rolls run together with 9% slip. Find their contact stresses for a radial contact force of 1 000 lb/in of length.[†]
- 7-24 Estimate the cycle life of the rolls in Problem 7-23 if they are made of class 30 gray cast iron, austempered to HB270.[†]
- 7-25 The flat end of a 12-mm-dia, class 30 gray cast iron pad is supported by a flat steel plate made from SAE 4340 steel, quenched and tempered at 800°F. The force on the pad is 3.8 kN. Estimate the real area of contact and the ratio of the real area to the apparent area of contact.
- 7-26 Estimate the dry coefficient of friction between the two materials in Problem 7-25 if the shear strength of the cast iron is $S_{us} = 310$ MPa. How does this compare to the value given in Table 7-1?

- 7-27 Two 0.5-in \times 1-in 1040 hot-rolled steel pads are in contact with a force of 900 lb. Estimate the real area of contact and the ratio of real to apparent area of contact.
- 7-28 Estimate the dry coefficient of friction between the two materials in Problem 7-27. How does this compare to the value given in Table 7-1?
- 7-29 Two materials with 10 mm² contact area have been tested to determine how much adhesive wear takes place when they are run together. Table P7-1 shows the test parameters and average depth-of-wear results for 350 tests. Find the average wear coefficient if the Brinell hardness of the softer of the two materials tested is HB 277.
- 7-30 A piece of mild steel with HB = 280 has its thickness reduced in an abrasive grinder. Both the grinding wheel and the steel part have the same width, which is 20 mm. On each pass through the grinder 0.1 mm is removed. If the abrasive-wear coefficient for this operation is 5E-1, what is the approximate normal force on the grinding wheel?
- 7-31 Two steel gears with involute tooth profiles are in mesh. At the line of contact between the gears they can be modeled as two cylinders in contact. When the contact is away from the pitch point there is a combination of rolling and sliding. Determine and plot the dynamic-contact principal stresses on the surface of the teeth for the following gears if the contact force is 500 lb and the coefficient of friction is 0.15: $R_1 = 2.0$ in, $R_2 = 6.0$ in. The thickness (face width) of both gears is 0.5 in. Also find the value of x/a for which the principal stresses have an extreme value.
- 7-32 Two steel gears with involute tooth profiles are in mesh. At the line of contact between the gears they can be modeled as two cylinders in contact. When the contact is away from the pitch point there is a combination of rolling and sliding. Determine the dynamic-contact stresses on the surface of the teeth for the following gears if the contact force is 1 500 lb and the coefficient of friction is 0.33: $R_1 = 2.5$ in, $R_2 = 5.0$ in. The thickness (face width) of both gears is 0.625 in.
- 7-33 Two contacting rollers are needed for a machine application. They run together with a combination of rolling and 9% sliding. Both are to be made from SAE 1144 cold-rolled steel. The radial contact force is 1200 N and the coefficient of friction is 0.33. The rollers are to have the same radii and are both 10-mm long. If the design life is 8E8 cycles, determine a suitable radius for the rollers.
- 7-34 Two contacting rollers are needed for a machine application. They run together with a combination of rolling and 9% sliding. Both are to be made from Meehanite. The rollers have the same radius (30 mm) and are both 45 mm long. If the design life is 1E8 cycles, determine the allowable load that may be applied to these rollers.
- 7-35 The flat end of a 25-mm-dia, Class 20 gray cast iron pad is supported by the flat side of a 30-mm-wide steel bar made from SAE 4130 steel, quenched and tempered at 800F. The force on the pad is 2800 N. Estimate the real area of contact and the ratio of the real area to the apparent area of contact between pad and bar.
- 7-36 Estimate the dry coefficient of friction between the two materials in Problem 7-35 if the shear strength of the cast iron is $S_{us} = 310$ MPa. How does this compare to the value given in Table 7-1?
- 7-37 Two 25-mm \times 40-mm SAE 1020 hot-rolled steel pads are in contact with a force of 9 kN. Estimate the real area of contact and the ratio of the real to apparent area of contact.
- 7-38 Estimate the dry coefficient of friction between the two materials in Problem 7-37. How does this compare to the value given in Table 7-1?
- *7-39 A 25-mm-diameter steel shaft of hardness HB420 rotates at 700 rpm in a 40-mm-long plain bronze bushing with an average radial load of 500 N. Estimate the time it would take to remove 0.05 mm of bushing material by adhesive wear if the lubrication were suddenly lost assuming a uniform wear rate around the bushing.



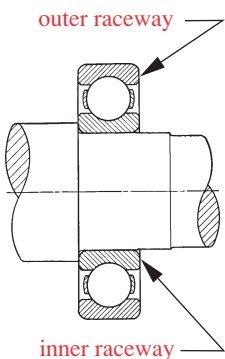
FIGURE P7-6

Problem 7-22

Table P7-1
 Data for Problem 7-29

F N	I m	d mm	No. Tests
100	5 000	0.180	100
200	5 000	0.372	75
200	7 500	0.550	75
400	10 000	1.470	100

* Answers to these problems are provided in Appendix D.

**FIGURE P7-7**

Problem 7-41

7

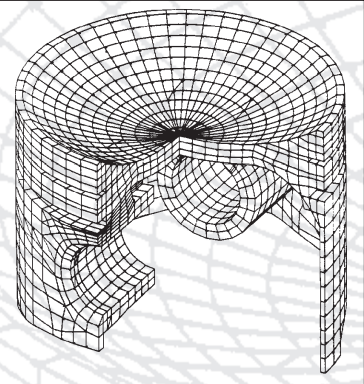
- 7-40 A machine has a tripod base that utilizes 15-mm-dia nylon 11 balls as support pads at its feet. The tripod rests on a flat steel plate. The 360N weight of the machine is distributed equally to the three legs of the tripod. Determine the size of the contact patch and the contact stresses in the nylon balls. Assume that Poisson's ratio for nylon is 0.25.
- 7-41 A ball bearing consists of a number of steel balls (separated by a ball cage) and two rings with raceways as in Figure P7-7. The raceways have compound curvature. In a plane containing the axis of the bearing the curvature is concave and conforms closely to the ball radius. In a plane perpendicular to the axis the curvature is convex for the inner raceway and is related to the bore size of the bearing. Determine the size of the contact patch and the maximum contact stresses between a ball and the inner raceway with a radial load of 5200 N in a steel bearing with dimensions: ball dia = 8 mm, raceway radius for concave surface = 4.05 mm, raceway radius for convex surface = 13 mm.
- *7-42 A pair of steel rollers used in a manufacturing process roll together with a combination of rolling and sliding. One roller has a diameter of 75 mm and the other has a diameter of 50 mm. They are both 200-mm long. The contact force, which is normal to the contact plane, is 18 500 N. Assuming that the coefficient of friction between the rollers is 0.33, determine the maximum tensile, compressive, and shear stresses in the rollers.
- 7-43 Repeat Problem 7-41 for contact between a ball and outer raceway. The outer raceway radius for the concave surface is 4.05 mm and the outer raceway radius for the convex surface is 17.02 mm.
- 7-44 A machine has two crowned, cylindrical rollers rolling against each other with a dynamic load varying from 0 to 3.5 kN. The first roller has a major radius of 14 mm with a crown radius of 80 mm. The second roller has a major radius of 75 mm and a crown radius of 100 mm. The two axes of rotation have a 30 degree angle between them. Find the contact stresses if both rollers are steel.
- 7-45 A cam-follower system has a motion with a combination of rolling and sliding. The cylindrical cam has a minimum radius of curvature of 80 mm. The roller follower is also cylindrical with a radius of 14 mm. They are both 18-mm long. The maximum contact force, which is normal to the contact plane, is 3200 N. Both cam and roller are of hardened steel. Assume a coefficient of friction between the cam and roller follower of 0.33 and determine the maximum tensile, compressive, and shear stresses in the cam.
- 7-46 Estimate how long it will take to remove $2\mu\text{m}$ of material from the 5000 mm^2 surface of a block of HB110 steel if a coarse polishing machine applies 80 N over a 400-mm stroke at 120 strokes per minute.
- If done dry.
 - If done lubricated.
- 7-47 Loose abrasive grains are introduced in error into the lubricating system of a flat bronze thrust bearing that has a hardness of 60HB and a surface area of 500 mm^2 . If a hardened steel part exerts a force of 50 N on the bearing while oscillating across it at 200 strokes/min with a stroke of 30 mm, what depth of wear occurs in an 8-hour shift?
- 7-48 Two rollers are in contact with a 9% sliding combined with rolling and the resulting maximum compressive principal stress in the contact zone is 15 500 psi. Both rollers are made from 6061-T6 hard anodized aluminum. The design life of the rollers is 4 years of 2-shift operation at 260 days/year and they each turn at 200 rpm. What is the expected safety factor against pitting for the roller pair?
- 7-49 Two contacting rollers run together in pure rolling. Both are made from Class 20 Gray iron, HB 130-180. One roller has a diameter of 2.75 in and the other has a diameter of 3.25 in. Both are 10 in long. The applied load is 5500 lbf. If the design life is $1E08$ cycles, determine the factor of safety against pitting failure.

8

FINITE ELEMENT ANALYSIS

If you put garbage in a computer nothing comes out but garbage. But this garbage, having passed through a very expensive machine, is somehow ennobled and none dare criticize it.

ANONYMOUS

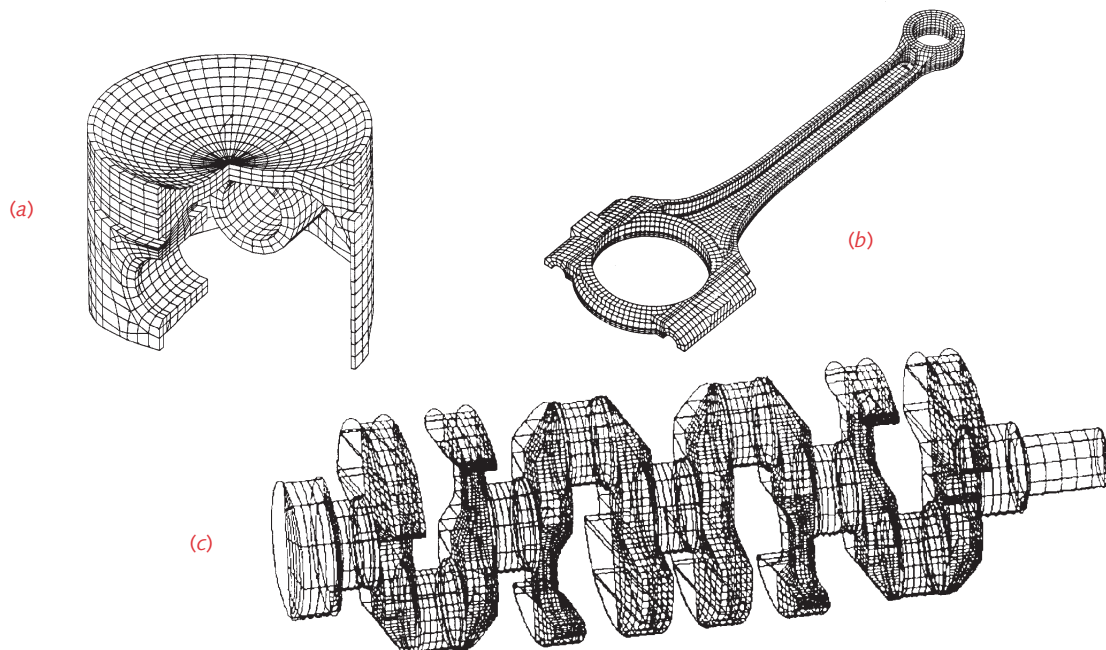


8.0 INTRODUCTION

All of the stress and deflection analysis examples presented in previous chapters have been able to be solved by classical closed-form analysis techniques, which are the main focus of this book. These techniques are primarily applicable to parts that are made up of simple geometry, such as cylinders, rectangular prisms, etc. However, many real machine parts have more complicated geometric shapes, making accurate calculation of stress and deflection difficult or even impossible with classical techniques. Consider, for example, the complex shape of an engine crankshaft as shown in Figure 2-14 (p. 48). To analyze the stress and deflection in a part of such geometric complexity, one can break its volume into a finite set of contiguous, discrete elements and solve a (large) set of simultaneous equations, each of which applies to an element and to the nodes that connect the elements. Figure 8-1 shows finite element models of a crankshaft, piston and connecting rod for an engine.

The concept of linear finite element analysis (FEA) is quite simple, but the computations to accomplish it are not. The mathematical theory behind FEA is beyond the scope of this text but is covered in a number of other books, some of which are noted in the bibliography of this chapter. Our goal here is to introduce the reader to the existence of the technique, point out some of its requirements and pitfalls, and provide some examples of its use.

It has become relatively easy to use FEA because of the availability of commercial analysis packages, many of which interface with one or more solid modeling CAD packages. Engineers entering the profession in the 21st century will most likely find that their company has and uses both solid modeling and FEA in the design of their products and machines. Using commercial FEA software, it is very easy to obtain FEA re-



8

FIGURE 8-1

Finite-element models of an engine piston (a), connecting rod (b), and crankshaft (c). Courtesy of General Motors Co.

sults that look reasonable but can be grossly in error if the user does not understand how to use the tool properly. It is recommended that the student of machine design take a course in the theory and application of FEA. Most engineering curricula now provide these.

Stress and Strain Computation

Stress varies throughout the continuum of any part. By dividing the part into a finite number of discrete *elements* connected together at their *nodes* (called a *mesh*), one can obtain an *approximation* of the stress and strain within the part for any given set of boundary conditions and loads applied at various nodes in the structure.* The approximation can be improved by using more elements of smaller size at the expense of increased computation time. With present computer speeds (which will continue to increase in future) this is less of a problem than in the early days of FEA.[†] Part of the analyst's problem is to choose an appropriate type, number and distribution of elements to optimize the trade-off between accuracy and computation time. Larger elements can be used in regions of the part where the stress gradient (slope) varies slowly. In regions where the stress gradient changes rapidly, such as near stress concentrations or applied loads and boundary conditions, a finer mesh is needed. Note in Figure 8-1c that the elements near the ends of the crankshaft where the diameter is constant are larger than those in the webs and crankpins.

* For that matter, calculations of stress by classical closed-form methods also are only approximations due to the simplifying assumptions that typically must be made to solve the problem.

[†] Though, as computer speeds increase, engineers challenge them with more complex FEA problems and these, especially if nonlinear, can result in long computation times even on powerful computers.

FEA is not limited to structural analysis. It is used also for calculation of fluid mechanics, heat transfer, acoustics, electromagnetics, and other specialized problems. We will only discuss its use for linear problems in structural mechanics. All FEA commer-

cial codes will handle this case. Others can also deal with nonlinear systems in which the deformations exceed the limits assumed for linear static analysis, the material properties are nonlinear, or surface contact must be modeled. FEA will give information on the stress, strain, deflection, natural frequencies and mode shapes (eigenvalues and eigenvectors), impact, and transient or steady-state vibration of a structure.

Several different mathematical formulations have been proposed and used since 1956 when the finite element method was first codified and named by Turner et al.^[1] The approach used for structural analysis in many commercial FEA software packages is the Direct Stiffness Method (DSM) that uses element stiffness to compute the nodal displacements and internal forces that result from a set of applied external loads and boundary conditions. Strains are computed from the displacements and stresses from the strains using Hooke's law.

8.1 FINITE ELEMENT METHOD

We will present only the simplest possible example of the mathematical process for the direct stiffness method of finite element analysis. The concept is easy to understand in this simple form. Its implementation is more mathematically complex than described here and is computationally intensive, requiring the solution of large matrices. Many books are available that explain the mathematics and implementation of FEA in detail. See the bibliography for more information.

Figure 8-2a shows a free-body diagram of the simplest possible structural finite element, a linear spring in one dimension. It possesses a stiffness characteristic (spring constant) $k_h = f/\Delta u$, so displacement creates a nodal force. Assume positive displacements u_i and u_j and sum forces at each node.

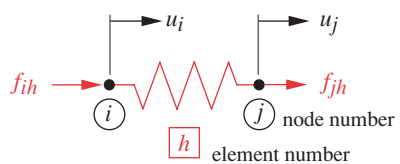
$$\begin{aligned} f_{ih} &= k_h u_i - k_h u_j \\ f_{jh} &= -k_h u_i + k_h u_j \end{aligned} \quad (8.1a)$$

Put these in matrix form:

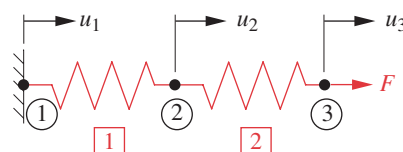
$$\begin{bmatrix} k_h & -k_h \\ -k_h & k_h \end{bmatrix} \begin{Bmatrix} u_i \\ u_j \end{Bmatrix} = \begin{Bmatrix} f_{ih} \\ f_{jh} \end{Bmatrix} \quad (8.1b)$$

which can be written in matrix notation as:

$$[k]\{d\} = \{f\} \quad (8.1c)$$



(a) Element FBD



(b) Mesh of 2 elements and 3 nodes

FIGURE 8-2

Simple Spring Element and Model

where k is the stiffness matrix, d is the element nodal displacement vector, and f is the vector of element internal forces.

Figure 8-2b shows two of these simple elements connected to one another to create a finite element mesh. Element 1 is fixed to ground, which creates a boundary condition constraint, and element 2 has an external force applied at node 3. Apply equation 8.1a to these elements.

$$\begin{bmatrix} k_1 & -k_1 \\ -k_1 & k_1 \end{bmatrix} \begin{Bmatrix} u_1 \\ u_2 \end{Bmatrix} = \begin{Bmatrix} f_{11} \\ f_{21} \end{Bmatrix} \quad (8.2a)$$

$$\begin{bmatrix} k_2 & -k_2 \\ -k_2 & k_2 \end{bmatrix} \begin{Bmatrix} u_2 \\ u_3 \end{Bmatrix} = \begin{Bmatrix} f_{22} \\ f_{32} \end{Bmatrix} \quad (8.2b)$$

The forces in equations 8.2 are internal forces in the element that act on the nodes. For equilibrium, the sum of the nodal forces must equal the applied external forces at the node. Let F_i represent the external force at each node, where i is the node number. Then summing forces at each node:

at node 1	$f_{11} = F_1$
at node 2	$f_{21} + f_{22} = F_2$
at node 3	$f_{32} = F_3$

(8.3)

Substitute the expressions for the internal node forces from equation 8.2 into 8.3.

$$\begin{aligned} k_1 u_1 &\quad -k_1 u_2 &= F_1 \\ -k_1 u_1 + (k_1 + k_2) u_2 - k_2 u_3 &= F_2 \\ -k_2 u_2 + k_2 u_3 &= F_3 \end{aligned} \quad (8.4a)$$

and put the result in matrix form:

$$\begin{bmatrix} k_1 & -k_1 & 0 \\ -k_1 & k_1 + k_2 & -k_2 \\ 0 & -k_2 & k_2 \end{bmatrix} \begin{Bmatrix} u_1 \\ u_2 \\ u_3 \end{Bmatrix} = \begin{Bmatrix} F_1 \\ F_2 \\ F_3 \end{Bmatrix} \quad (8.4b)$$

or:

$$[K]\{D\} = \{F\} \quad (8.4c)$$

The applied forces and the stiffnesses are known. The nodal displacements are to be solved for, which requires premultiplication of both sides by the inverse of $[K]$.* But, this $[K]$ has a singular inverse, so it does not have a unique solution. This is because the system of equation 8.4 has a kinematic (rigid body) degree of freedom (DOF) and can be in equilibrium at any location in its one-dimensional universe. We have not yet accounted for the rigid attachment of node 1 to ground. To solve a static FEA problem we must remove all kinematic DOF by applying appropriate boundary conditions. We can fixate this system by setting the displacement of node 1 (u_1) to zero as a boundary condition. This zeros the first column of the stiffness matrix, leaving us with 3 equations and 2 unknowns. If the reaction force F_1 is unknown, we can eliminate the first equation and use the remaining two to solve for the unknown displacements. Also, Figure 8-2b shows no external force applied to node 2, making F_2 zero. Substituting yields:

* The computer solution does not actually generate and premultiply the inverse matrix as this is too computationally intensive. Other numerical techniques that are more efficient are used to solve the matrix equations with the same result.

$$\begin{bmatrix} k_1 + k_2 & -k_2 \\ -k_2 & k_2 \end{bmatrix} \begin{Bmatrix} u_2 \\ u_3 \end{Bmatrix} = \begin{Bmatrix} 0 \\ F \end{Bmatrix} \quad (8.5)$$

The k -matrix is called the reduced stiffness matrix and has a nonsingular inverse, so the equation can be solved for the unknown displacements. After the displacements are found, the internal forces on each element can be calculated from equations 8.2. The equations involving unknown reaction forces that were removed to reduce the matrix can now be solved to determine the reaction forces. The strains are found by differentiating the displacements, and the stress is found from the strains and material properties. Most solvers will calculate and display both principal and von Mises stresses as well as strain and displacement.

This trivial example contains the essential steps in an FEA solution. In an actual problem, more complicated elements whose nodes have multiple degrees of freedom would be used, and there would be a very large number of elements, which also can have nonlinear “spring” functions.

8.2 ELEMENT TYPES

Elements can be one-, two-, or three-dimensional, also called line, surface, and volume elements, respectively.* They also may be of different “order” where that term refers to the order of the function (usually a polynomial) that defines the distribution of displacement across the element. Figure 8-3 shows some commonly used elements, grouped by dimensionality and order. In general, one would like to use the simplest elements that will give the desired information because computation time is greater for elements of higher dimension or order.

8

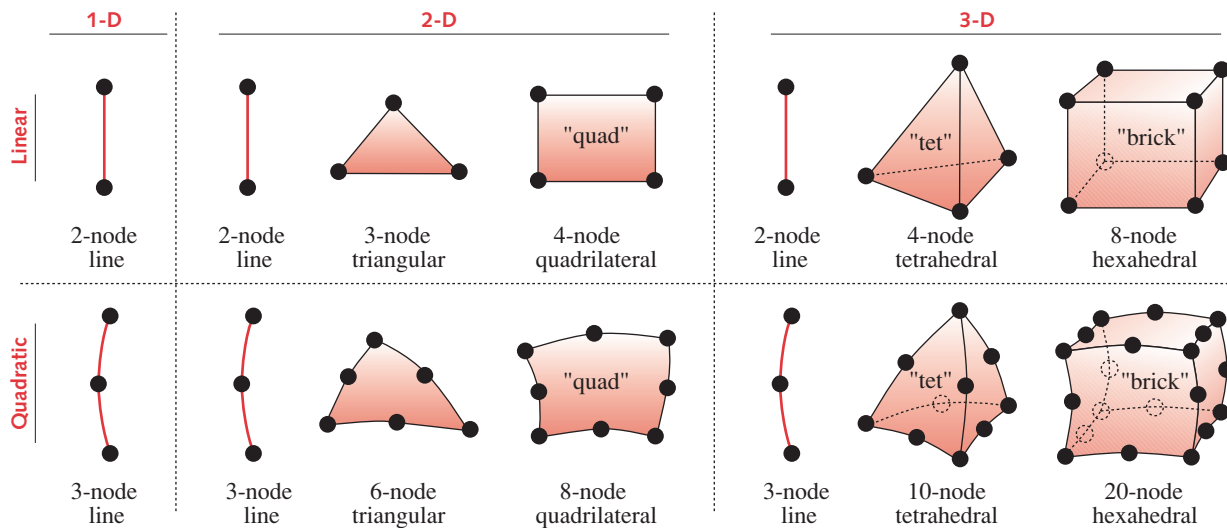
Element Dimension and Degree of Freedom (DOF)

In Figure 8-3, the elements shown are divided into one-, two-, and three-dimensional groups, labeled 1-D, 2-D, and 3-D, respectively. These dimensional groups define how many DOF each node of an element may possess.[†] Note that the line element is in all of the groups. Line elements are suitable for modeling structures such as truss members and beams of constant cross section and can have 1, 2, 3, or 6 DOF at each of their nodes. A 1-D line element has 2 DOF total, one on each node. Physically, this represents a truss element, connected by pin joints to its neighbors. It can only transmit force along its length (one dimension) and cannot support moments at its nodes. A 2-D line element has 3 DOF per node and can represent a 2-D beam that can support a moment at its nodes as well as linear forces in two directions. A 3-D line element has 6 DOF per node and can represent a 3-D shaft-beam with moments and torques at each node in addition to linear forces in three directions. Elements of more complicated geometry such as the triangle, quadrilateral, tetrahedral, and hexahedral (brick) have more DOF.

Note that a 1-D line element can give good results for a truss member loaded in axial tension but will not be able to correctly predict buckling if the axial load is compressive. Buckling must be separately checked using the appropriate Euler, Johnson, or secant formula as described in Section 4.16. Some FEA codes provide a means to calculate buckling separately.

* There are also zero-dimensional elements available that include spring elements, rigid-body elements, concentrated masses, and other special types.

[†] The “dimensional groups” in Figure 8-3 refer to the geometric dimensions of the model.

**FIGURE 8-3**

Some common finite elements

8

Two-dimensional elements can be used to model a 3-dimensional structure if its geometry and loading create a plane stress or plane strain case, which have zero magnitudes in the third dimension. A long beam with applied bending or axial loads symmetrical about its width dimension can be analyzed with 2-D elements. However, if the loads are offset, then 3-D elements will be needed. For a 2-D analysis of a beam to be valid, all longitudinal planes in the beam must remain in their original planes when the beam deflects.

If a part is axisymmetric and thin-walled and the loading is symmetrically distributed, such as in a pipe or pressure vessel subjected to internal pressure, then 2-D surface (shell) elements can be used. This assumes that the stress gradient across the thin wall is small enough to ignore. Non-axisymmetric structures can be analyzed with shell elements provided that their wall thickness is small compared to their surface area.

Many machine parts have loading and geometry that requires the use of 3-D elements. If their geometry is simple, then they may be solvable by classical closed-form methods. The examples in Figure 8-1 all have geometry too complicated to use the classic approach with any reasonable accuracy and need 3-D continuum elements for FEA.

Element Order

Higher-order elements can have curved boundaries, while linear elements must have straight boundaries. The former have better ability to conform to geometric contours of complex parts and can handle steeper stress gradients. But, increasing element order can significantly increase computation time, so many analysts will first try to model a part with linear elements.

Strain is a function of the rate of change of displacement across the element (i.e., the displacement gradient) and is computed by differentiating the displacement function in the element. For a linear triangular or tetrahedral (tet) element, the displacement

function across the element is a straight line and the strain is constant. This makes them overly stiff. Stress is computed from the strain and the material's modulus of elasticity. Thus, linear triangles and tets also have constant stress across their dimension. Quadratic triangles, tets, and bricks have parabolic displacement functions and a linear strain (and stress) distribution within the element and so give better estimates of stress.

Experts recommend against using the 3-node triangular or 4-node tet elements because they give inaccurate estimates of stress and stiffness. Better estimates of stress will result by using a 4-node quadrilateral (quad) or 8-node hexahedral (brick) element, which has linear strain across the element. Unfortunately, it is more difficult to mesh odd-shaped parts with quads or bricks than with triangles or tetrahedra. An alternative is to increase the order of the triangle or tetrahedral element to improve their ability to estimate stresses. The higher-order, 6-node triangle and 10-node tet give better stress approximations than their lower-order counterparts and have been shown to be about as good as the linear 4-node quad or 8-node brick, respectively.

Since adjacent elements (of any order) share nodes, and each element has a different stress than its neighbors, there will be at least two values of stress possible for each node. As a result, the stress field calculated by FEA has a series of discontinuous steps across the continuum of the part rather than the continuous stress field of the real part. Most FEA post-processors will create an average stress for each element in order to display a smooth stress contour plot.

H-Elements Versus P-Elements

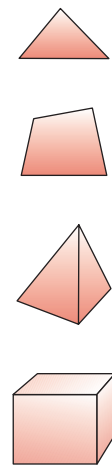
Two types of elements are used by various FEA solvers, called *h-elements* and *p-elements*, respectively. H-elements are most commonly used and their order is typically limited to quadratic. Mesh refinement (see below) must be used to increase the number and reduce the size of h-elements near regions of high stress gradient. P-elements allow the order of the element's edge (interpolation) polynomial to be increased to 9 or higher in order to capture local stress variation where needed. P-elements can then be relatively large and less numerous than h-elements for the same problem. They can also conform well to the complex shape of a part's boundaries by using a high order edge (interpolation) function.

Element Aspect Ratio

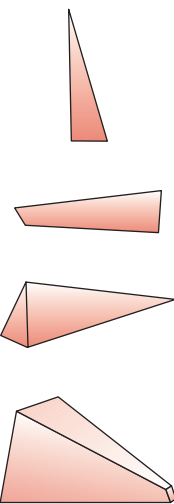
The element aspect ratio is obtained by dividing the length of the longest side of the element by that of the shortest side.^[2] An aspect ratio less than about 5:1 is preferred for h-elements, though p-elements can handle ratios up to about 20:1.^[3] If the element shape deviates excessively from its basic shape, error will be introduced. Figure 8-4 shows some examples of elements with good and poor aspect ratios. The *warp*, *skew* and *taper* of an element also play a part in its accuracy. See reference [4] for definitions.

8.3 MESHING

In the early days of FEA, meshing a part required huge effort. Now, automeshers and preprocessors in FEA packages make that task much easier. Many packages will import the part geometry from a solid modeling CAD program and automesh the part.



(a) Good aspect ratios



(b) Poor aspect ratios

FIGURE 8-4

Good and Poor Element Aspect Ratios

Most automeshers default a 2-D mesh to linear quads or a quad-dominant mesh with triangles added in regions where part shape requires. Many automeshers can only mesh 3-D models with tetrahedral elements (tets). Linear tets have been shown to be less than ideal for stress estimation, but higher-order tets are acceptable. An FEA package will also have a preprocessor that allows manual meshing of the part with your choice of elements. A better result in 3-D can be achieved by meshing with a combination of 8-node bricks and 6-node wedges, or alternatively by increasing the order of the tetrahedral elements, though this increases computation time. This is becoming less of a problem as computers become faster. For example, some of the case studies in this chapter used 16th-order tets. Manual meshing requires more effort and skill by the analyst than automeshing but may be necessary to obtain good results. Often, when designing a new part, automeshing will be used despite its accuracy limitations in order to speed the process. Even though the absolute numbers may be less accurate, one can compare alternate designs based on automeshed FEA results. Early in a design process it is better to get less accurate information rapidly in order to determine if the design is feasible before spending a lot of time to learn that the concept is not viable. When the design settles down, more time can be spent to generate a better mesh and get more accurate numbers for the final design.

Mesh Density

8

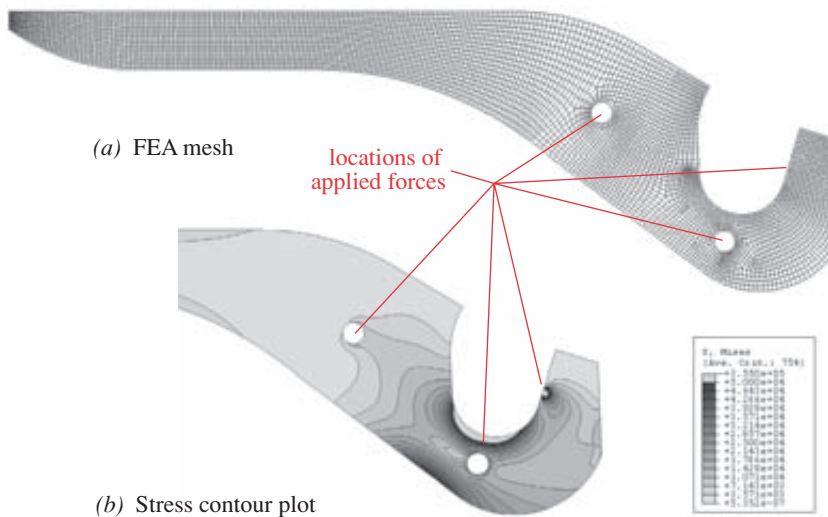
To minimize computation time a coarse mesh of larger elements is desired. In regions where the stress gradient in the part is small, a coarse mesh can give adequate results. But in regions where the stress gradient is high, such as near stress concentrations, applied loads, or boundary conditions, a finer mesh of h-elements (or the same density mesh with higher-order p-elements) is needed to capture the stress variation. For example, see the photoelastic stress distributions around stress concentrations in Figure 4-34 (p. 187), and at points of load application in Figure 7-19 (p. 454). Thus, it may be necessary to vary the mesh density over the model, a process called mesh refinement. Some engineering judgment based on an understanding of the force flow concept (see Figures 4-37 and 4-38, pp. 191–192) and stress concentration (Section 4.15, p. 186) is required to do this.

Mesh Refinement

A coarse mesh may be applied to a part initially, but the designer or analyst must use engineering judgment based on an understanding of stress distribution in loaded parts to decide what regions need to have a finer mesh applied. Figure 8-5 shows an example of mesh refinement in a 2-D model. Note in part (a) the concentration of smaller elements around the hole and around the applied force on the jaw. The stress concentration in these locations is visible in the stress contour plot of part (b). Mesh refinement is needed particularly in regions of high stress concentration.

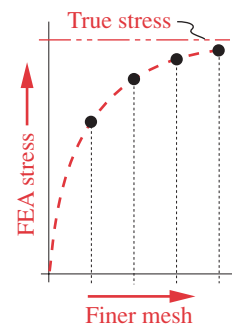
Convergence

How does one know when a mesh has been sufficiently refined? The usual approach is to apply a convergence test. Starting with a mesh of some size, the model is solved for stress. The element size is then changed by some factor in regions of anticipated high stress gradient and the model solved again. The stress values for particular locations are compared between the different mesh density solutions. If there is a signifi-

**FIGURE 8-5**

Finite Element Analysis of the Stresses in the Crimping Tool of Case Study 2B

cant difference between one solution and another, it indicates that the earlier mesh was too coarse in that region and may need further refinement. Eventually, the change in computed stress values for successively finer meshes will become small, indicating that you are converging on the true solution. If you plot the results of several successive mesh refinements for stress in a particular location, it will look like the curve in Figure 8-6. The curve exponentially approaches an asymptote that is the true stress value.*

**FIGURE 8-6**

Results of Mesh Refinement

EXAMPLE 8-1

Finite Element Analysis of a Notched Cantilever Beam

Problem:

A notched, rectangular cross-section cantilever beam is loaded in bending by a fully-reversed transverse force. Determine a reasonable finite element mesh and compare its prediction of maximum stress and deflection with a closed form solution for points at the beam end l , distance b , and the notch at a .

Given:

The beam dimensions in Figure 8-7a are: $a = 4$, $d = 7.5$, $l = 10$, $b = 0.1$, $h = 1$, and $r = 0.167$ in. The load $F = 25$ lb. The material is steel.

Assumptions:

The supporting wall is considered to be much stiffer than the beam. Beam weight is negligible compared to the applied load. The reduction in beam cross section due to the notch has a minimal effect on the total beam deflection, but a significant effect on the local stress. A 2-D FEA model is sufficient as plane stress may be assumed.

Solution:

- First do a closed-form solution to determine the theoretical values of stress and deflection. Figure 8-7b shows an FBD and the shear and moment diagrams for this

* Some FEA solvers apply a strategy to converge from above rather than from below the optimum as shown in Figure 8-6. Whatever the strategy employed, the end result should be similar.

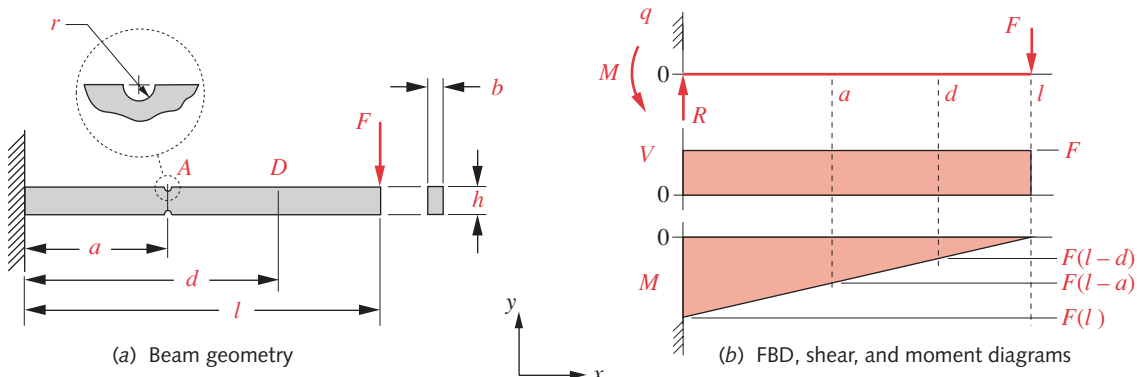


FIGURE 8-7

Cantilever Beam for Example 8-1

beam. Three locations are of interest, the beam outer fibers at the wall, also at D , and in the root of the notch at A where there is stress concentration. At the wall the moment magnitude is $Fl = 250$ in-lb and the bending stress in the outer fiber is:

$$\sigma = \frac{Mc}{I} = \frac{250(0.5)}{\frac{0.1(1)^3}{12}} = \frac{125}{0.0083} = 15\,000 \text{ psi} \quad (a)$$

Point D provides a check on a stress away from any concentrations.* At distance d from the wall the moment is $F(l-d) = 25(10-7.5) = 62.5$ in-lb and the bending stress in the outer fiber at point D is:

$$\sigma = \frac{Mc}{I} = \frac{62.5(0.5)}{\frac{0.1(1)^3}{12}} = 3750 \text{ psi} \quad (b)$$

At the notch the stress concentration factor from Figure E-12 is:

$$K_t = A \left(\frac{r}{d} \right)^b = 0.98315 \left(\frac{0.167}{1-2(0.167)} \right)^{-0.33395} = 1.56 \quad (c)$$

The moment magnitude is $F(l-a) = 25(10-4) = 150$ in-lb and the local bending stress at the notch is:

$$\sigma = K_t \frac{Mc}{I} = 1.56 \frac{150(0.5-0.167)}{\frac{0.1[1-2(0.167)^3]}{12}} = 1.56 \frac{49.950}{0.00246} = 31\,676 \text{ psi} \quad (d)$$

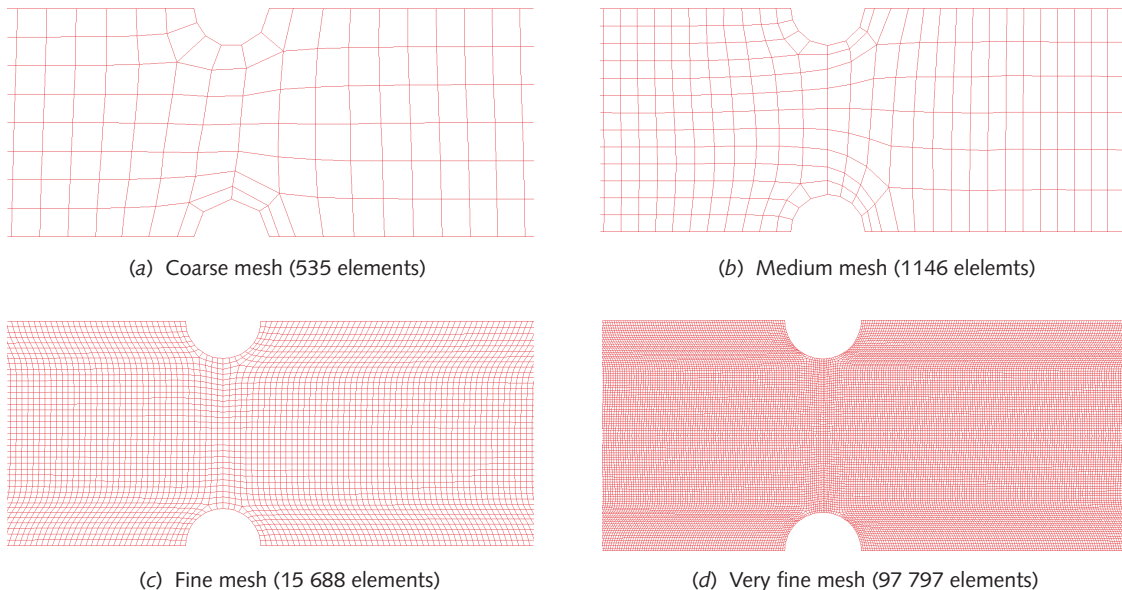
- 2 The equation for maximum deflection due to bending is found in Figure D-1:

$$y_{\max} = -\frac{Fl^3}{3EI} = \frac{25(10)^3}{3(30E)(0.0083)} = -0.0335 \text{ in} \quad (e)$$

- 3 Quad elements are preferred to triangular, so they will be used. Figure 8-8 shows four mesh conditions used. Table 8-1 shows the stresses calculated at point D and at the notch for each of these mesh conditions. Figure 8-9 plots the stresses at the notch against mesh size. Convergence to the analytically calculated value at point D is more rapid than at the notch because of the absence of stress concentration there.[†]

* By St. Venant's principle, stresses at locations away from the point of application of forces or reactions will be unaffected by the area of contact of the force.

[†] Note that it is not necessary to refine the mesh over the entire part as was done here. It would have been sufficient to refine it locally around the notch where stress concentration is present. For this example, the entire mesh was refined in order to show the effects at point D far from the notch, as well as at the notch.

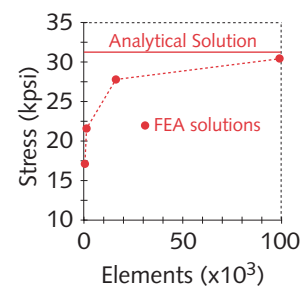
**FIGURE 8-8**

Mesh Refinement of the Beam in Example 8-1 (Partial Area Shown Only)

8

But the “very fine” mesh of Figure 8-8d is needed to get good convergence at the notch. The differences between the FEA stresses calculated at point D at various mesh sizes and the analytical value is due in part to the fact that the analytical stress is calculated at the outer fiber, but the FEA stresses shown are an average of stresses calculated at the 4 integration points for each element, and so differ depending on element size. Other options are to report the FEA stresses at the element nodes or at the integration points, giving 4 values per quad element.

- 4 Table 8-2 shows the FEA estimates of deflection on the neutral axis at the beam tip for each mesh size compared to the analytical deflection solution. Note that there is little difference between the results with these very different mesh sizes which points out that a fine mesh is not as necessary for accurate deflections as for local stresses. Also note that the FEA deflections are all larger than the analytical. This is because the FEA solution includes the effects of deflection due to transverse shear, which is not accounted for in the bending deflection equation (e) but can be significant if the beam is short. Here it adds 10% to the bending deflection.
- 5 Figure 8-10 shows the distribution of von Mises stresses in the beam as calculated by FEA. These include the transverse shear stress. Note the stress concentrations at the notches (point A) and at the tip of the beam where the load was applied (L). The analytical solution did not automatically calculate these stress concentrations. We had to recognize the need to apply a stress concentration factor to the stress calculation at the notch. Unless we also did so at the point of load application, we would not see the increased stress there. It is not as easy to see in this figure but there is also some stress concentration at the beam root (R) where the boundary condition at the wall causes a local stress increase. FEA (using 2-D or higher elements) has the advantage of automatically revealing stress concentrations, whether due to local geometry, or locally applied forces and boundary conditions. But, you need to make sure that you have a properly converged mesh especially around areas of potential stress concentration or your results may have large errors as can be seen in Table 8-1 and Figure 8-9.

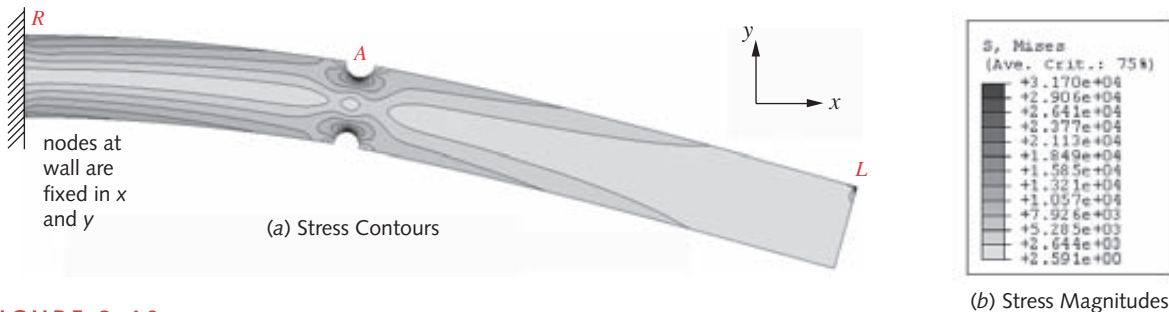
**FIGURE 8-9**

Mesh Convergence at the Notch in Example 8-1

Table 8-2

Deflection Versus Mesh Size in Example 8-1

Elements	Deflection (in)
535	0.0359
1146	0.0364
15 688	0.0368
97 797	0.0369
analytical	0.0335

**FIGURE 8-10**

Von Mises Stresses Calculated with FEA for Example 8-1

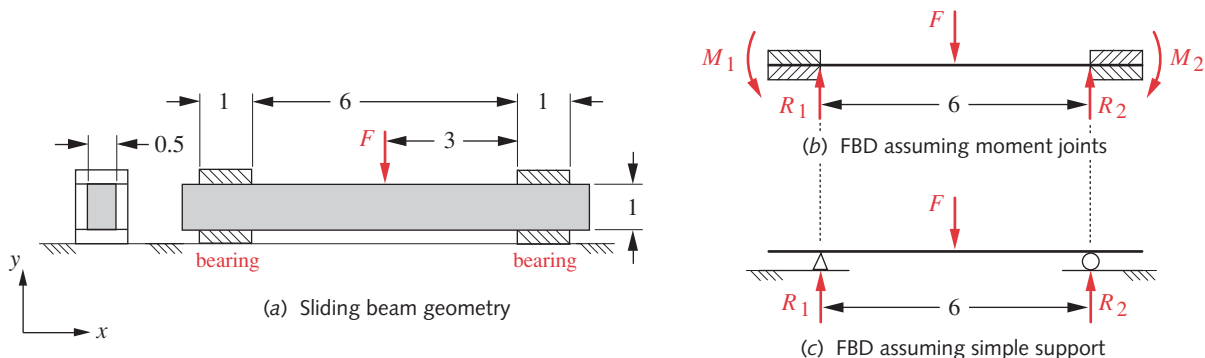
8.4 BOUNDARY CONDITIONS

Definition of boundary conditions (BC) that realistically represent the constraints on a real part is not a trivial task and can make the difference between a reasonable and ridiculous solution to the problem. Each node of an element has some number of degrees of freedom as described on p. 485. The nodes of a 2-D plane-stress quad each have 2 translational DOF, and those of a 3-D brick, 3 translational DOF. Shell or line elements can also have rotational DOF at their nodes. External constraints are applied to nodes of the model. At a minimum, enough constraints must be applied to remove all the kinematic DOF of the part and put it in static equilibrium. In addition, the physical connections of the part to its neighbors in the assembly must be modeled as closely as possible. BCs should neither restrict nor allow deformations that would not occur in actuality. A physical constraint will never have infinite stiffness, but when you specify that a node cannot move in an FEA model, it is truly fixed and becomes infinitely stiff. This tends to exaggerate the effect of the physical constraint. If too few BC are applied, the system will be underconstrained and the computation will fail. If too many BC are applied, the system is overconstrained and will be too stiff.

For example, consider the rectangular cross-section slide supported in two plain bearings with a transverse load applied as shown in Figure 8-11a.* The linear bearings are stationary and fastened to the machine frame, which sits on the floor. The floor is part of a building, which sits on the earth. If we want to determine the stresses and deflections of the slide from this applied load, how much of the system do we need to model? Can we just model the slide or do we need to include the bearings, machine frame, floor, and the swamp upon which the building sits? You would no doubt conclude that in this case we can safely ignore the compliance of the earth, building and machine frame and consider them to be infinitely stiff for our purposes, unless we happen to have a really big slide with a really big load, large enough for the building to notice.

With that assumption, we need to define how the bearings constrain the slide to support the load. The bearings appear to contact the slide over their length, which is a significant fraction of the unsupported slide length. What type of constraint do these bearings provide to the slide? If they prevent the slide from changing slope within their length, then they would function as a moment joint. If not, then they would effectively provide “simple support.”

* Note that this “sliding beam” model can be considered as a surrogate for that of a rotating shaft in plain bearings as the lessons learned regarding the effects of boundary condition choices on deflection are the same. However, a shaft model would require a 3-D FEA analysis. The sliding beam model can be analyzed in 2-D with no loss of generality.

**FIGURE 8-11**

Beam Supported in Sliding Bearings with Alternate Free Body Diagrams

Figures 8-11b and c show the free body diagrams that would result from each of these assumptions. Which is “correct”? Probably neither. Both are idealizations commonly used in closed-form analysis of mechanics problems. The moment joint assumes that the support (here the bearing) is infinitely stiff in bending and that the slide is coupled to it in a way that allows no relative motion in the plane of bending. For this to be true, there would have to be zero clearance between the slide and the bearing, which would make it a bit difficult for the slide to move. The simply supported model assumes that the slide is supported on a knife edge at one end and on a frictionless roller at the other. Even if we take this assumption, where should we place the knife edge and roller, in the centers of the bearings or at their edges, and which edge? Some thought will reveal that if the bearings are stiff and the shaft deflects downward at the center, the slide will contact the inner edges of the bearings as shown in Figure 8-11c. Let’s analyze each of these models both in closed-form and in FEA and see what happens.

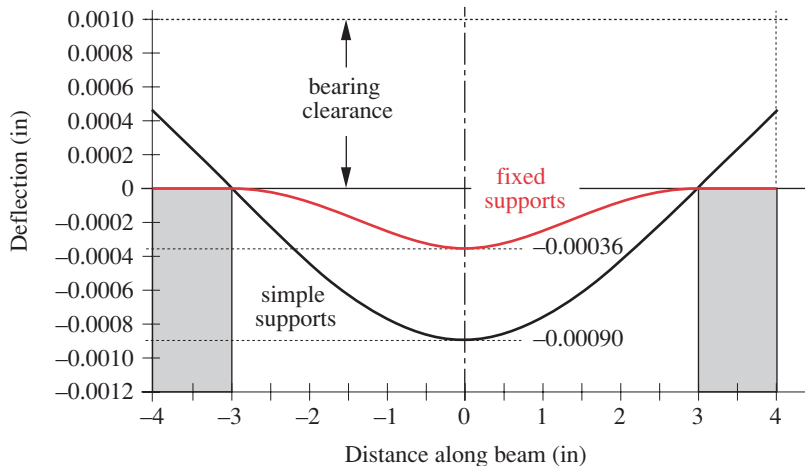
EXAMPLE 8-2**Boundary Conditions of a Sliding Beam**

Problem: A rectangular cross-section sliding beam is supported in sliding bearings and loaded in bending by a transverse force at a fixed location in x as shown in Figure 8-11a. Determine a reasonable boundary condition arrangement and compare its prediction of deflection with closed form solutions.

Given: The beam dimensions are shown in Figure 8-11a. The load $F = 250$ lb. The material is steel.

Assumptions: The supporting bearings are considered to be much stiffer than the beam. Beam weight is negligible compared to the applied load. The bearings have 0.001-inch clearance around the beam cross section to allow sliding.

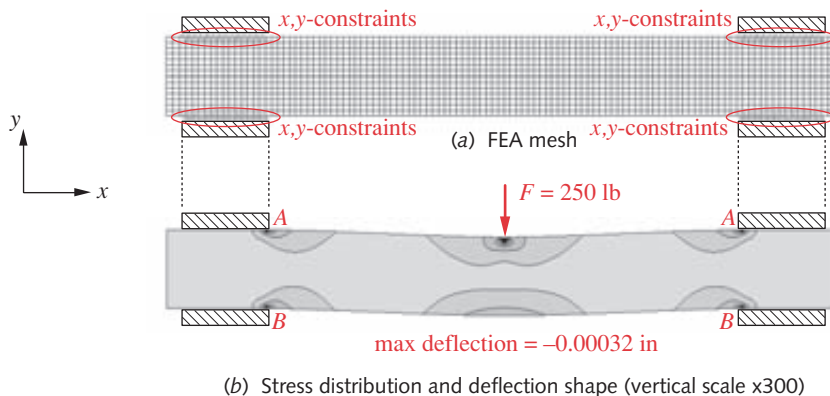
Solution:

**FIGURE 8-12**

Deflections of Two Boundary Condition Models of Example 8-2 from Closed-Form Solutions

8

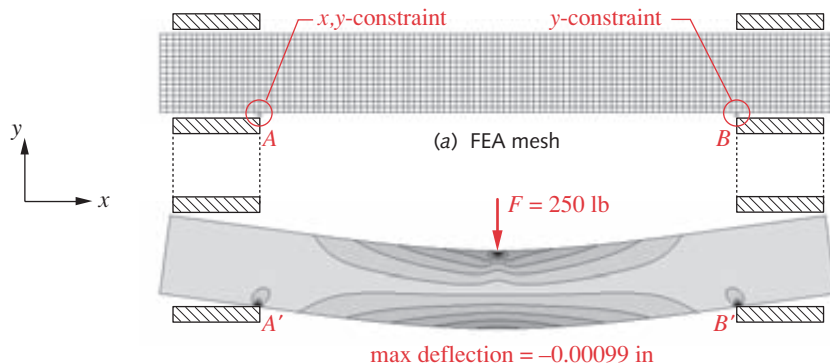
- 1 The deflection curves from closed-form solutions for the cases in Figures 8-11b and c are shown in Figure 8-12. The maximum deflection for the fixed-fixed model is -0.00036 in and is -0.00090 in for the simply-supported model. The end fixation reduces total deflection by a factor of 3. This is because the moment constraints make the beam slope zero at the bearings and effectively stiffen it.
- 2 Even though this is a 3-D system, we will first use a 2-D plane-stress FEA model with quad elements for simplicity. Because FEA is displacement based, the model's deflections provide a good means to check whether the constraints applied are reasonable. If the deflections are believable and the mesh convergence is separately proven, then one can have some confidence in the results. For this example, the load is applied in the center of the span.
- 3 Figure 8-13a shows the mesh for the fixed-fixed case with the nodes of all the elements that contact the bearings constrained in the x - and y -directions to simulate moment joints at each bearing. Figure 8-13b shows the deflected shape and the maximum deflection as found by FEA, which is -0.00032 in, close to the value found in step 1. Note the stress concentrations at the point of force application and at points A and B where the edges of the bearings contact the slide. This shows the effect of boundary conditions on local stresses.
- 4 Figure 8-14a shows the same meshed model as Figure 8-13a but the boundary conditions have been changed to simulate simple support at each end. At the left end (circled at point A) a single node at the inner edge of the bearing is fixed in x and y to represent a hinge. At the right end (circled at point B) a single node at the inner edge of the bearing is constrained only in y to represent the roller support. Figure 8-14b shows the deflected shape and the maximum deflection of the simply supported beam as found by FEA, which is -0.00099 in, close to the value found in step 1. Note the stress concentrations at the point of force application and at points A' and B' where the edges of the bearings contact the slide, showing the effect of boundary conditions on local stresses. Note also that the top edges of the beam do not contact the insides of the upper bearings, consistent with the closed-form calculation. (See Figure 8-12.)

**FIGURE 8-13**

FEA model with Fixed-Fixed Boundary Conditions for the Beam in Example 8-2

So, which one is the better boundary condition model? Is it reasonable to assume that the bearings prevent any rotation of the slide about the z axis? If the slide is to move in the bearing, then some clearance is necessary. Assume that there is a total clearance of 0.001 in. What angle can the slide assume within the length of the bearing with that clearance? A simple calculation gives 0.057 degrees. The slope of the slide at the supports in the simply supported model is 0.035 deg. Since this angle is less than the angular clearance in the bearing, the slide can achieve that slope under this applied load. The bearing cannot apply a couple to the slide until the clearance is taken up and the top and bottom of the slide contact opposite ends of the bearing. Up to that point, it is simply supported as can be seen in Figure 8-12, which shows about 0.00052-in clearance remaining at the outer bearing edges. So, we conclude that the simply-supported model is closer to reality than the fixed-fixed one in this particular case.

But, is it the best we can do? Is it reasonable to assume that the slide and bearings contact at only one node at each bearing? A node has zero dimension which would

**FIGURE 8-14**

FEM model with Simply-Supported Boundary Conditions for the Beam in Example 8-2

give infinite stress. What if the load were increased? Would the bearing clearance then be taken up? A better boundary condition model would account for the possibility of some area of contact between the two parts at both top and bottom bearing surfaces. Some FEA codes provide contact constraints that allow transmission of force in only one direction. If the force reverses sign then they separate. A better way to model the boundary between the slide and bearing in the above example would be to apply contact constraints to all the nodes along the length of both bearing-slide interfaces. With no load applied, all nodes on the bottom will be in contact, analogous to the fixed-fixed model above. As a load is applied, the elements at the bottom outside ends of the bearings will separate and allow the beam shape to move toward that of the simply-supported model. With sufficient load applied, the beam will contact the top surface of the bearing and change the effective boundary constraint. The only downside is that contact constraints are nonlinear and so require a nonlinear FEA solution, which increases computation time. Let's redo Example 8-2 using contact constraints in the FEA model.

EXAMPLE 8-3

Contact Constraints as Boundary Conditions in FEA

8

Problem: The rectangular cross-section beam of Example 8-2 is supported in sliding bearings and loaded in bending by a transverse force at a fixed location in x as shown in Figure 8-11a. Construct an FEA model using contact constraints for the boundary conditions and compare its prediction of deflection with the results from Example 8-2.

Given: The material is steel. The beam dimensions are shown in Figure 8-11a. Consider two loading cases, a load of $F = 250$ lb as in Example 8-2 and a larger load of $F = 1000$ lb.

Assumptions: The supporting bearings are considered to be much stiffer than the beam. Beam weight is negligible compared to the applied load. The bearings have 0.001-inch clearance around the beam cross section to allow sliding.

Solution:

- Figure 8-15 shows an FEA mesh with contact-constraints (boundary conditions) applied at A and B . These constraints are applied to the bearings, not to the beam. They do not allow the beam to intrude upon the bearing geometry but do allow nodes to pull away from the bearing surface. Thus they can support a compressive load between beam and bearing but not a tensile load. As the load is applied to the beam

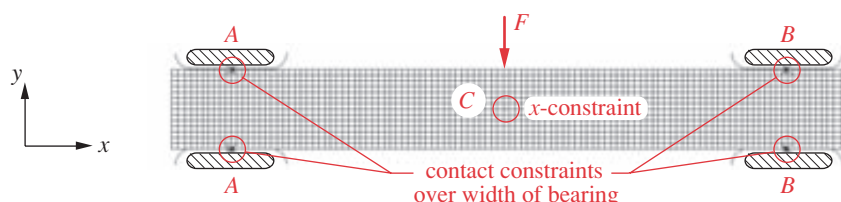


FIGURE 8-15

FEA model With Contact-Constraint Boundary Conditions for the Beam in Example 8-3

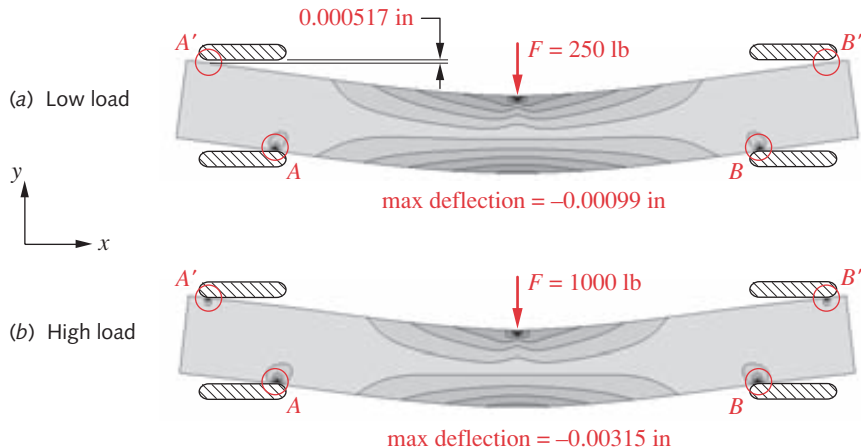


FIGURE 8-16

Stress and Deflection Using Contact-Constraint Boundary Conditions for the Beam in Example 8-3

and it deflects, the nodal contact will vary along the bearing length, just as happens with the real system. The beam is fixed against movement in the x direction by a boundary constraint at point C on the neutral axis. By placing this x -constraint at the beam center, both ends of the beam are allowed to slide along the bearings in the x direction as in the real system. The bearing geometry in the FEA model is given rounded edges to avoid creating infinite stresses that would result from point contact at the ends of the bearings as the beam deflects.

- 2 Figure 8-16a shows the stresses and deflection that result when a 250-lb transverse load is applied in the center of this beam. Note the similarity to the simply-supported case with the same load as shown in Figure 8-14. The beam contacts the bearings at their bottom inner corners (points A and B), where stress concentration can be seen. The upper surface of the beam does not contact the top surface of the bearings at points A' and B'. The clearance there is 0.000517 in, similar to that shown in Figure 8-12. The maximum deflection calculated with this model at this load is -0.00099 in, the same as that of the simply supported FEA model in Example 8-2.
- 3 Figure 8-16b shows the stresses and deflection that result when a 1000-lb transverse load is applied in the center of the beam. The increased load causes the beam to deflect sufficiently to cause the top of the beam to contact the upper bearing surfaces at points A' and B' where stress concentration can be seen. The beam is now behaving more like the fixed-fixed model of Example 8-2. Note that the deflection with a 1000 lb load is only 3.18x as large as that with a 250 lb load. If the simply-supported model were valid in both cases, then one would expect the deflection to be 4x larger, in direct proportion to the increased load. The change in boundary conditions as a function of load makes it a nonlinear system.
- 4 Figure 8-17 shows a plot of the beam deflection as a function of the fraction of maximum load applied in each case, which can be thought of as resulting from a slowly increasing application of each load from zero to its maximum value. For the 250-lb load case, the increase in (negative) deflection with increasing load is linear. For the 1000-lb load case, the deflection increases linearly until the beam ends hit the upper bearings, at which point (labeled A), the slope abruptly changes because the beam is suddenly stiffer. The curve becomes nonlinear beyond point A due to the changing points of contact as it deflects. This shows the nonlinear response of the beam to a load that "takes up" the bearing clearance, and changes the boundary conditions.*

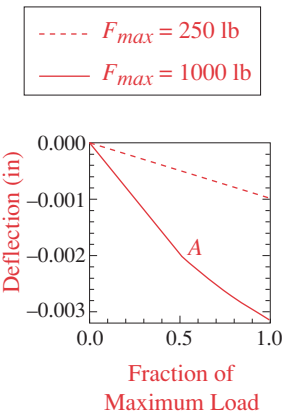
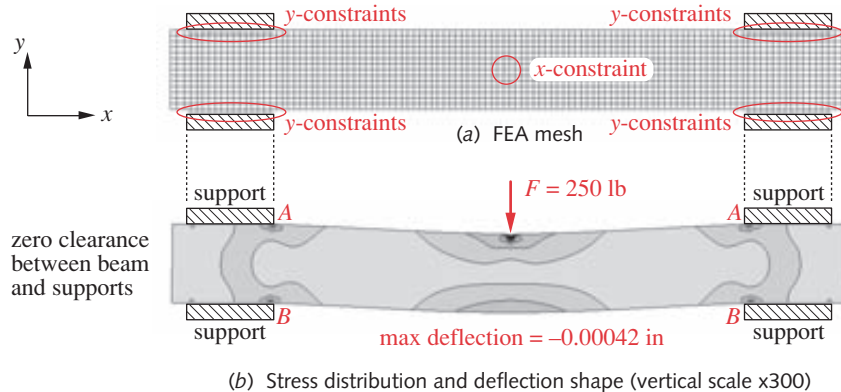


FIGURE 8-17

Deflection Change as Load is Applied for the Two Load Cases in Example 8-3

* This phenomenon is often used to obtain a desired result such as with variable rate valve springs used in automotive valve trains. Some of the spring coils are wound closer together than others (see Figure 14-2a on p. 789) so that as the spring deflects in use, the closely-spaced coils touch and become solid. This changes the spring stiffness in mid-deflection and helps reduce spring vibration.

Truck suspension systems use a similar concept by adding stiffer (helper) springs that are engaged only when suspension travel exceeds a certain level, as happens when overloading the vehicle or in hitting a large bump. When the gap is taken up, the suspension stiffness suddenly increases to limit deflection.



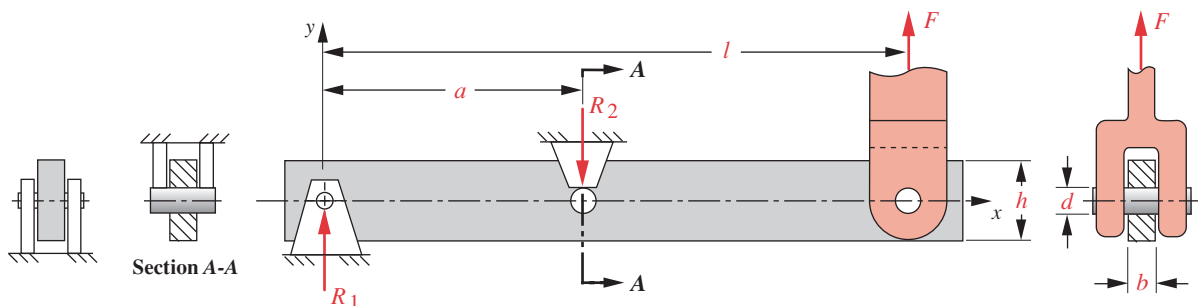
FEA Model of the Beam in Figure 8-11 Fixed Only in the y -Direction with One Node Constrained in x

8

Consider a slightly different example. Suppose the beam in Figure 8-11 (p. 493) were not required to slide and was supported at both ends with moment joints having zero clearance. In Example 8-2 we made that assumption in step 3 (p. 494). The resulting mesh boundary conditions and FEA results are shown in Figure 8-13 (p. 495). The FEA-calculated maximum deflection was -0.00032 in., which compared favorably to the closed-form solution of -0.00036 in. The boundary conditions of Figure 8-13 fix all the nodes within the supports in both x and y directions. This simulates a condition in which the beam is clamped so tightly within the supports that no relative sliding motion, even microscopic, is allowed between the beam and the supports. This could be realistic if in fact the beam were so clamped. However, another possibility is that the supports prevent any y -direction motion, but allow slight movement in x , even in the absence of any clearance. Such a situation can be simulated in FEA by a different set of boundary conditions as shown in Figure 8-18a. Here, all the nodes within the supports are fixed in the y -direction, but not in x . The x DOF is removed, as it was in Example 8-3, by fixing one node on the neutral axis at the beam center. Figure 8-18b shows the resulting stress distribution and deflection. Note that the maximum deflection is now -0.00042 in., greater than either the fixed-fixed FEA model in Figure 8-13 or the fixed-fixed closed-form result of Figure 8-12 on p. 494 (which assumes fixation in the supports in both x and y directions, like that of Figure 8-13a).

The above analyses show the sensitivity of FEA results to the choice of boundary conditions. The next discussion will reinforce that concept. The issue here has to do with the boundary constraints between a shaft (or pin) and its bearing or a bolt and its hole.

We will use a different example to investigate this. Figure 8-19 shows a lever used in a linkage system. We wish to model it to determine its stresses and deflection under a given load, and from that find its spring rate as a beam. It is supported on two pins that serve as pivots and run in bronze bearings. Both the pin and bearing have elasticity. Pins are usually made of steel and plain bearings of bronze or other softer bearing material such as babbitt (see Chapter 11), which are less stiff than steel. But the bronze or babbitt is usually made quite thin and backed up by steel. So the bearing can usually be assumed to be as stiff as the surrounding material, which in this case is also steel.

**FIGURE 8-19**

Overhung Beam in Example 8-4

In this example, the loading is vertical; there are no horizontal components of applied force. A closed-form solution using beam theory will assume the forces to act at the hole centers, but an FEA model would normally not have any elements within the holes.

If the pins were a press-fit in the holes, then they would contact all around the circumference and distribute the load accordingly. With diametral clearance, if both pin and bearing were infinitely stiff, there would be only line contact at one location. This could be simulated by constraining one node at the top or bottom of the hole in a 2-D model. The stresses and deflection will obviously be very different between these two scenarios, as one would provide a moment joint and the other simple support. As you might expect, reality lies somewhere between these two extremes.

Both parts will deflect locally under load and create a contact patch as was described in Section 7.9 (p. 444). This will result in some area of contact that extends to either side of the theoretical line contact at the bottom (or top) of the bearing. The boundary conditions need to take this into account. Changes to these contact conditions will affect the beam deflection and stress in locations away from the contact points as they did in the previous discussion. Changes to the boundary conditions will also affect the estimate of the local stress concentration in the contact region.

One choice that could be made is to fix all the elements around the circumference of the hole at each support. This, however, will overconstrain the part as compared to the real constraint that the pin provides in the hole. The question remains, if we must constrain nodes around the hole's circumference, what portion of it should we constrain?

This dilemma can be resolved quite easily if the FEA package used offers “rigid-body” elements among its choices. The strategy is to place a node at the center of the hole and connect it with rigid body elements to all of the nodes on the circumference of the hole. These will look like the spokes of a bicycle wheel. The node at the center is then constrained in the appropriate way. In this example, both hole centers will be constrained in both x and y to represent a pin joint. The load F can be handled in the same way by applying it to a node at the hole center that is connected to the circumference with rigid elements. The following example will analyze two of these approaches to the application of boundary conditions at a pivot pin and compare their results to a closed-form solution using beam theory.

EXAMPLE 8-4**Boundary Conditions Between a Pin and Hole**

Problem: An overhung beam is supported on two pins in bearings. Determine a suitable boundary condition scenario for its analysis and estimate its maximum deflection, maximum stress, and spring rate at the load point.

Given: The beam dimensions in Figure 8-19 (p. 499) are: $a = 8$, $l = 20$, $b = 0.75$, $h = 2$, and $d = 0.5$ in. The load $F = 100$ lb. The beam and pins are steel and the bearings are bronze on steel. The beam cross section is constant over its length except for the pin holes, which are all 0.5-in-dia.

Assumptions: Loading and supports reactions are coplanar. Pin supports are significantly stiffer than the beam.

Solution:

- First solve the beam by classical closed-form methods as shown in Example 4-6 (p. 169). The equations for this overhung beam case can also be found in Appendix B, Figure B3, part (a). The maximum stress will be at the right support of Figure 8-19 where the moment magnitude is at its maximum: $M = F(l - a) = 1200$ lb-in. The bending stress at the outer fiber at $x = a$ is:

$$\sigma = \frac{Mc}{I} = \frac{1200(1)}{\frac{0.75(2^3 - 0.5^3)}{12}} = \frac{1200}{0.4922} = 2438 \text{ psi} \quad (a)$$

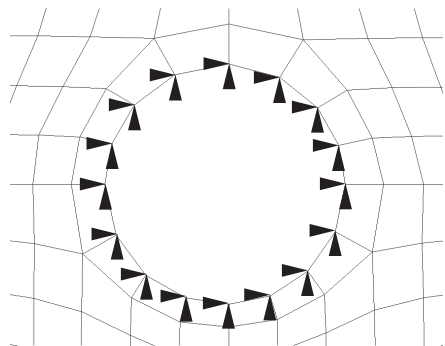
Note that the I of the cross section was reduced by the effect of the hole at $x = a$.

- The maximum deflection will be at the right end of the beam and is found from the equation in Appendix B, Figure B3, part (a) with $x = 20$, $a = 8$, $l = 20$, and $I = 0.50$ for the full cross section without any reduction for holes:

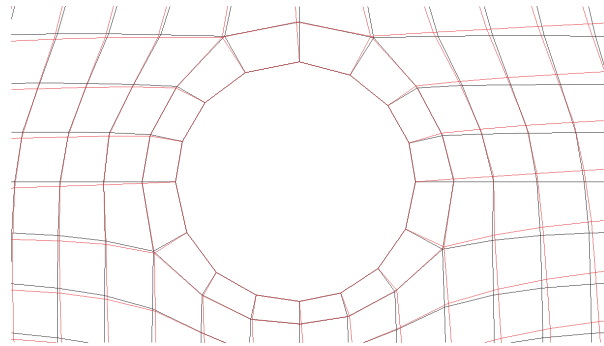
$$y = \frac{F}{6EI} \left[(a-l)x^3 - a(x-l)^3 + l(x-a)^3 + l(-l^2 + 3al - 2a^2)x \right] \\ = -0.0064 \text{ in} \quad (b)$$

- The first trial constrains all the nodes around the circumference of each hole in both x and y directions. The mesh and boundary conditions around one hole of the beam and the undeflected and deflected mesh are shown in Figure 8-20. Note that there is no movement of any of the nodes on the hole circumference.
- The second trial places a node at the hole center and connects it with rigid body elements to all the nodes on the hole circumference. These are sometimes called “kinematic couplings.” This technique effectively constrains the nodes on the circumference to have no motion in the radial direction but leaves them free to rotate about the hole center.* Figure 8-21a shows the mesh around one hole with these constraints applied. The nodes at both hole centers are fixed in x and y because the pins are on the beam’s neutral axis, which does not change length when the beam deflects. Figure 8-21b shows the undeflected and deflected meshes superposed. Note the rotation of the nodes on the hole circumference when the beam deflects, allowing the part to rotate on the “pin” as it deflects.

* If your FEA package does not provide rigid body elements, the same effect can be obtained by setting up a cylindrical coordinate system at the hole center and then constraining the radial coordinates of the nodes on the hole circumference while leaving their angles unconstrained.



(a) Mesh around hole with boundary constraints

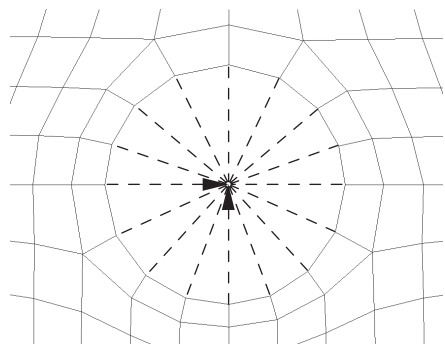


(b) Undeflected mesh (black) and deflected mesh (color) around hole

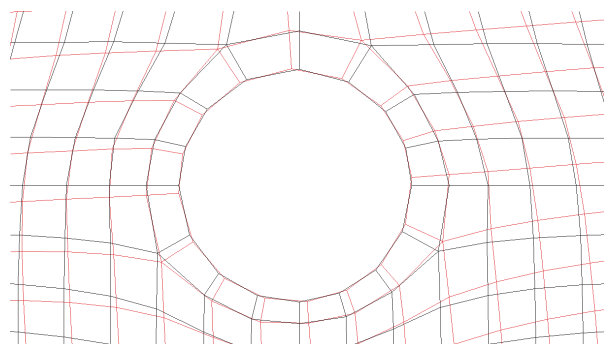
FIGURE 8-20

Mesh for Circumferential Boundary Constraints in Example 8-4 Step 3

- 5 Figure 8-22 shows the deflected shapes and maximum deflections of the two beam models and their von Mises stress distributions. The deflection calculated by the “kinematic coupling” method was 0.0066 in, very close to that calculated by beam theory in step 2.
- 6 The deflection calculated by the FEA “circumferential fixation” method was 0.0049 in, a 23% error. Constraining the entire hole circumference makes the beam much stiffer.
- 7 The spring rate for the beam is easily calculated from the deflection and applied force as $k = F / y = 100 / 0.0066 = 15\,152 \text{ lb/in}$.



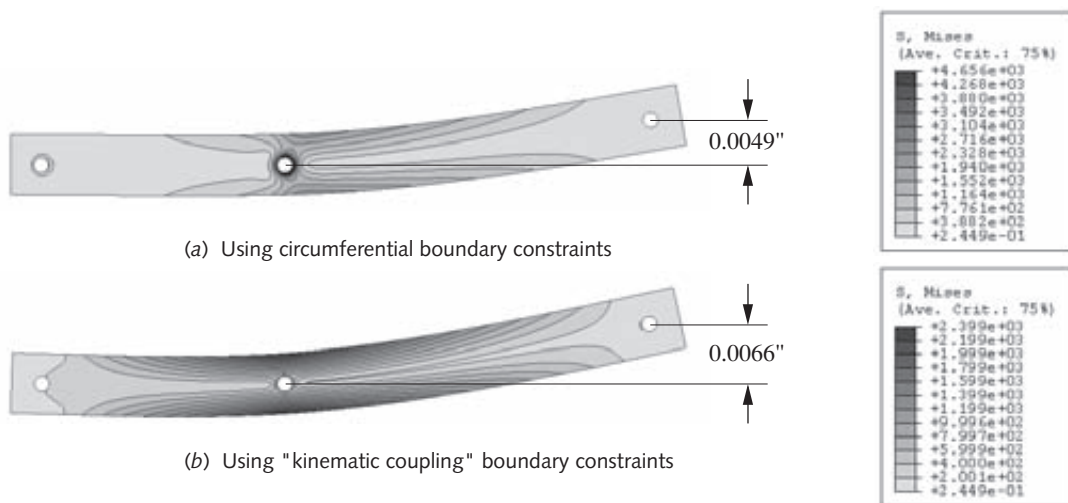
(a) Mesh around hole with boundary constraints



(b) Undeflected mesh (black) and deflected mesh (color) around hole

FIGURE 8-21

Mesh for Kinematic Coupling Boundary Constraints in Example 8-4 Step 4

**FIGURE 8-22**

Deflection and Stress Distributions for the Two Boundary Condition Cases in Example 8-4

8.5 APPLYING LOADS

Properly applying loads to a model is a similar problem to that of applying boundary conditions correctly. We often depict loads in closed-form models as if applied at a point.* This could be done in FEA as well, since a load can be applied at a single node. But, actual loads are distributed over some finite portion of a part. If we could really apply a load at a point, the local stress there would be infinite.

Most FEA packages provide a variety of loading models. They will distribute a specified load's magnitude and direction over any portion of the model you specify, apportioning the load to the nodes within the specified location according to your choice of function. The loading function can be uniform over a length or area, or follow a function you define. A pressure can be applied to a surface. An acceleration can be applied of any magnitude and direction to represent gravity or an inertial force on a dynamic system. Moment loads are a bit more difficult to apply if the elements used have only translational DOF. One common technique is to attach two rigid elements of equal length to the model perpendicular to, and on opposite sides of, the moment axis and apply a couple to the ends of the rigid elements. A good check on your model is to have the solver compute the reaction forces and moments due to your loads. If these match your calculations of $\Sigma F = 0$ and $\Sigma M = 0$ it indicates that your model setup is correct.

Be very careful of units when applying loads. Most CAD systems have a default set of units and they may not be what you want to work in. It is most important that the units of all elements and forces be in a consistent system. When doing dynamic analyses or applying acceleration loads, take note of the default density and mass units in your solid modeler. Many U.S. brands use lb_m as the default mass unit. This is not a true mass unit as it is numerically equal to lb_f and must be divided by g to put it in proper mass units. See Section 1.9 on the proper use of units. It is quite likely that more errors in engineering are traceable to units problems than any other single cause. Even rocket scientists are not immune to units errors as the footnote on p. 22 shows.

* By St. Venant's principle, stresses at locations away from the point of application of forces or reactions will be unaffected by the area of contact of the force.

8.6 TESTING THE MODEL (VERIFICATION)

The examples discussed above were all chosen to have sufficiently simple geometry and loading so as to allow the execution of at least one closed-form solution as a check for the sake of the example. Real problems that are candidates for FEA seldom have geometry simple enough to allow a closed form solution. If they did, it would usually be quicker to use the closed-form method. Nevertheless, before tackling a complicated problem, it is a good idea to set up and solve a simplified version of the problem that can be solved in closed form. Its closed-form solution can then be compared to the FEA results of the simplified model. This allows the boundary conditions to be iterated to a reasonable state and may help with mesh refinement as well. Once you have reasonable agreement between the closed form solution and your FEA result, you can reintroduce the original complicated geometry and proceed with the analysis based on the experience and understanding gained from the simplified test model and using its proven boundary constraints.

Example 8-4 was a simplification of a real problem with more complex geometry and loading for which an accurate closed form solution was unattainable. The simplified model was created to determine the proper boundary conditions for the problem. The real problem will now be presented as another example.

EXAMPLE 8-5

Analysis of a Cam-Follower Arm

Problem: A beam is supported on two pins in bearings having small clearance. Estimate its maximum deflection and spring rate at the load point.

Given: The beam dimensions in Figure 8-23 are: $a = 8$, $l = 20$, $b = 0.75$, $h = 2$, $d = 0.5$ in, $e = 0.375$ in, $f = 0.438$ in, and $g = 0.375$ in. The pin holes are all 0.5-in-dia. The load $F = 100$ lb. The beam and pins are steel and the bearings are bronze on steel. The beam cross section is tapered and pocketed to reduce its mass. The basic geometry is as in Example 8-4.

Assumptions: Loading and support reactions are parallel but out of plane. Pin supports are significantly stiffer than the beam.

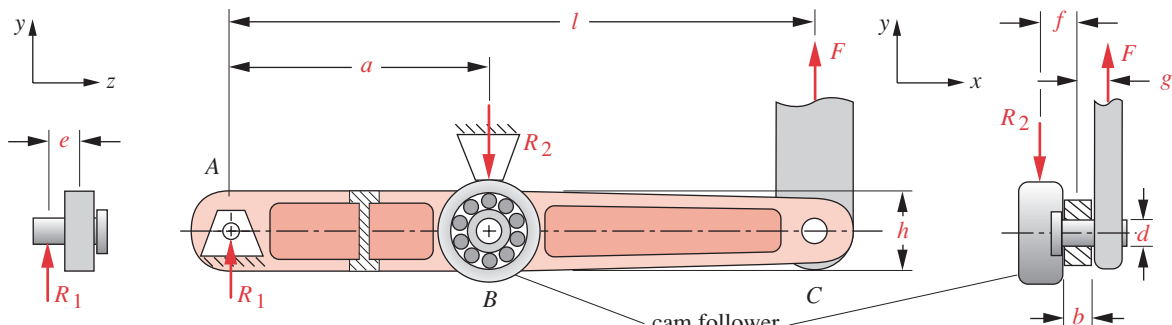
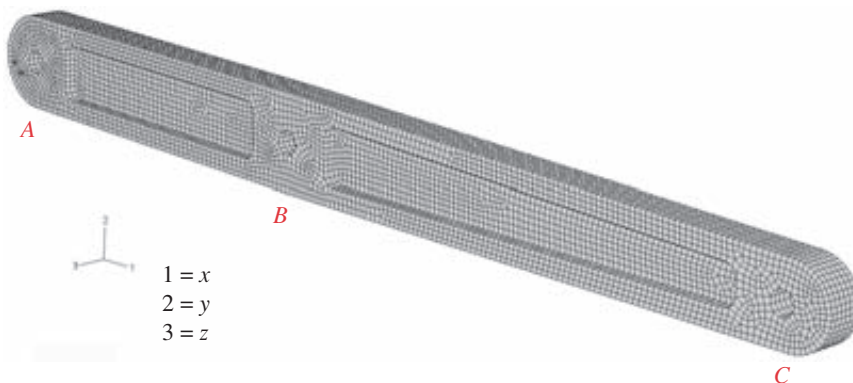


FIGURE 8-23

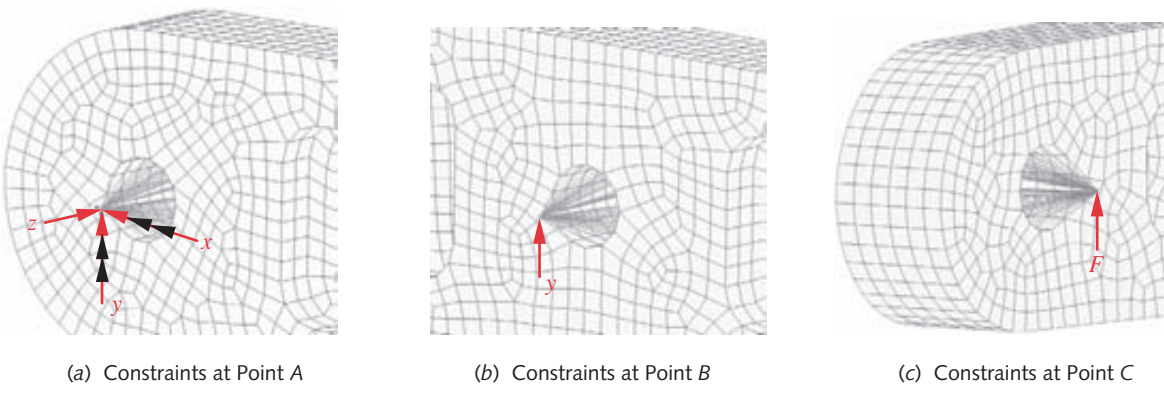
Overhung Beam in Example 8-5

Solution:

- 1 Example 8-4 analyzed a simplified version of this beam in which the loads and reactions were all assumed to be coplanar and the beam cross-section geometry was constant over the length of the beam rather than tapered and pocketed as shown in Figure 8-23. These simplifications allowed a closed form solution to be done using beam theory in order to compare it to the 2-D FEA results. This is an important step in any FEA analysis because it provides a check on the validity of your choices of mesh size and boundary conditions. Once those issues have been resolved, you will be ready to analyze the more complicated geometry of the real part with some confidence that the results will be valid.
- 2 Figure 8-24 shows a mesh of 3-D, 8-node linear hexahedral elements (bricks) applied to the tapered, pocketed beam of Figure 8-23. Since we are primarily interested in deflections in this example, mesh refinement is not as critical as it is when accurate stress estimates are also needed.
- 3 Because the applied and reaction loads on this part are not in the central plane of the beam, but are offset to either side in the z -direction, the boundary conditions and load must be applied to nodes placed at those locations. Figure 8-25 shows these boundary conditions with rigid-element “kinematic constraints” connecting a node offset the proper distance at the center of the “pin” to nodes on the physical beam. This is the same technique as was used in step 4 of Example 8-4 (see Figure 8-21, p. 501), but note that the z -offset makes these connections form a set of rigid element “cones” that attach the single node at the boundary condition (or load) to all the nodes on the inside of its pin hole. This technique effectively creates a rigid “pin” in the form of the offset node connected rigidly to the pin hole and allows the part to rotate about the z -axis of the pin.
- 4 Constraints are applied at A to fix displacement in x , y , and z , and to fix rotation about x and y . Displacement at B is fixed in y . The x and z displacements at B are left unconstrained because the roller on the cam allows motion in those directions. The 100-lb load is applied in the positive y direction at C . See Figure 8-25.
- 5 Figure 8-26 shows the deflection (exaggerated by 10x) and the von Mises stress distribution in the beam. Stress values are not shown as the mesh was not refined to give accurate results. The stress contour plots serve to show the “hot spots” of stress

**FIGURE 8-24**

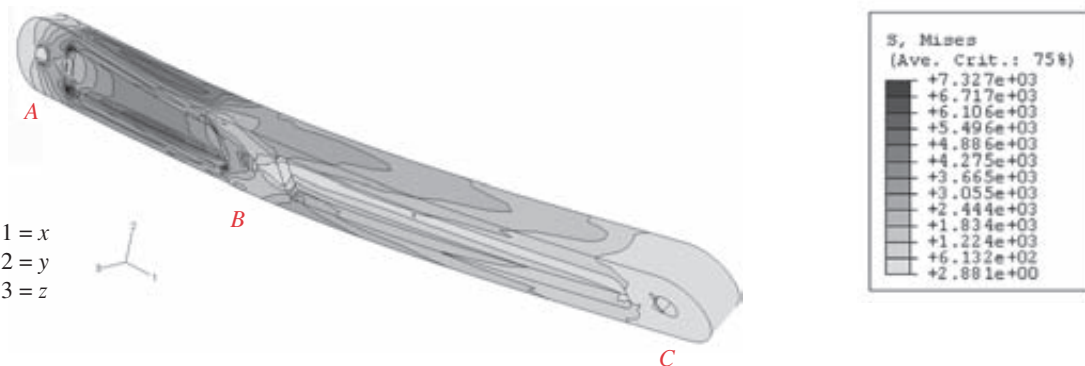
Mesh for the Pocketed Beam in Example 8-5

**FIGURE 8-25**

Boundary Conditions and Applied Load for the Beam in Example 8-5

in this case. If this estimate of stress had indicated any dangerously high levels (which it did not), then additional runs of the model with finer meshes would have been done. Note, however, that the beam shows significant torsional as well as bending deflection because of the offset loads. This should not be surprising given its out-of-plane loading. The deflection in the y -direction at the applied load (at C) is 0.0193 in.

- 6 The deflection calculated by the 2-D model of the same beam with simplified geometry and coplanar loads was 0.0066 in, about 1/3 of the above value. One should expect this 3-D model to have larger deflection since the beam has been weakened by its taper and removal of the pocket material (to reduce mass for better dynamics), and because the offset loads superpose a torsional deflection on that due to bending. Remember that the simpler model of this beam used in Example 8-4 was created for the purpose of determining the most appropriate set of boundary conditions. For that, we needed a model simple enough to check with a closed-form method. That done, we could proceed to this more complex model and have some confidence in its result.

**FIGURE 8-26**

Deflections and Stress Distributions for the Pocketed Beam in Example 8-5

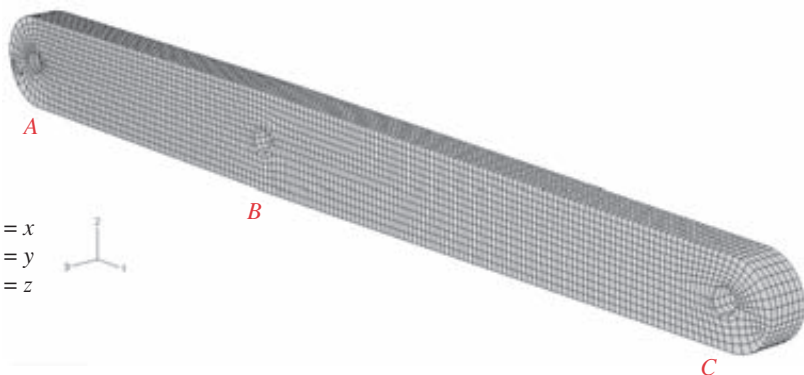


FIGURE 8-27

Mesh for the Redesigned, (Unpocketed) Solid-Tapered Beam in Example 8-5

8

- 7 In this case (which was a real cam-follower arm) the deflection of 0.0193 in (0.5 mm) was deemed too large. Thus some redesign was needed. Since the torsional deflection was of the same order as the bending deflection, the beam model was redesigned with the pockets removed to increase its torsional stiffness.* The mesh for this redesigned arm is shown in Figure 8-27. The boundary constraints and load were applied in the same way as in step 4 and Figure 8-25.
- 8 Figure 8-28 shows the deflection (exaggerated by 10x) and the von Mises stress distribution in the redesigned beam. The deflection at the load is now 0.0099 in, about half that of the pocketed beam design. This was deemed to be acceptable.
- 9 The spring rate for the beam in bending is easily calculated from the bending deflection and applied force as $k = F / y = 100 / 0.0099 = 10\,101 \text{ lb/in}$.

* Refer to Example 4-8 (p. 175) to review why open sections such as the I-beam shape of this pocketed beam are a poor choice for torsional loading situations.

8.7 MODAL ANALYSIS

All the examples shown so far involved only static analysis. FEA is also capable of modal analysis from which dynamic properties of the structure can be determined. The



FIGURE 8-28

Deflections and Stress Distributions for the Redesigned (Unpocketed) Beam in Example 8-5

natural frequencies and mode shapes (eigenvalues and eigenvectors) of a structure can be calculated with FEA. Most of the caveats regarding proper selection of element types, mesh convergence, and boundary constraint selection still apply but some are less critical for a modal analysis than for a stress analysis. For example, a reasonable estimate of the eigenvalues and eigenvectors of a structure can be obtained with a coarse mesh that might be unsuitable for accurate stress and deflection analysis. Also, mesh refinement around local changes in geometry is less critical for an eigenanalysis because the modal properties are global rather than local. However, if dynamic stress estimations for time-dependent loading conditions are required from the modal analysis then the mesh needs to be as refined as it would be for a static stress analysis problem.

EXAMPLE 8-6

Modal Analysis of a Cam-Follower Arm

Problem: Find the eigenvalues (natural frequencies) and eigenvectors (mode shapes) of the part in Example 8-5 if its pivot pins are subjected to random excitation from the machine in which it is mounted.

Given: The beam geometry is as defined in Example 8-5 and Figure 8-23.

Assumptions: Loading and support reactions are parallel but out of plane. Pin supports are significantly stiffer than the beam. The beam supports are subjected to random vibration.

Solution:

- 1 Example 8-5 analyzed this beam statically. The mesh and kinematic coupling boundary constraints that worked for the static analysis can also be used for the modal analysis, which was analyzed here with the same model.
- 2 Figure 8-29 shows the first mode shapes of both the pocketed and unpocketed beam designs of Example 8-5. The first natural frequency of the pocketed beam is 49.48 Hz. Removing the pockets more than doubles this value to 104.44 Hz.

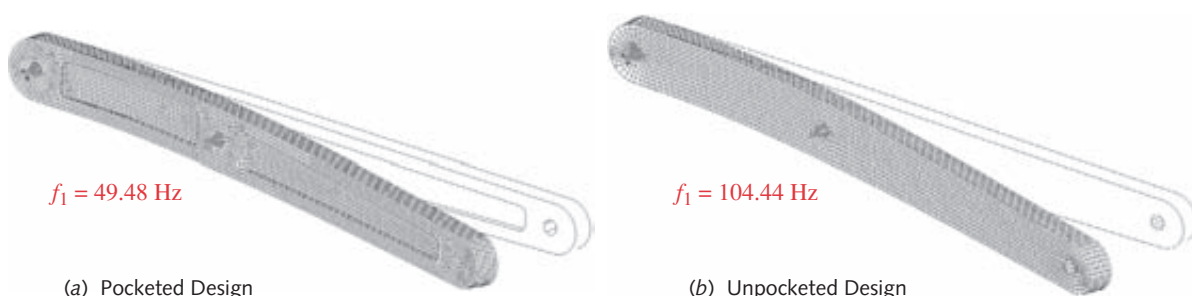
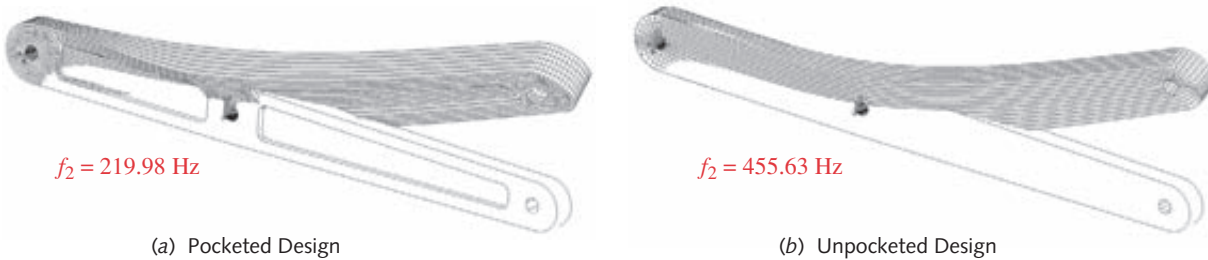
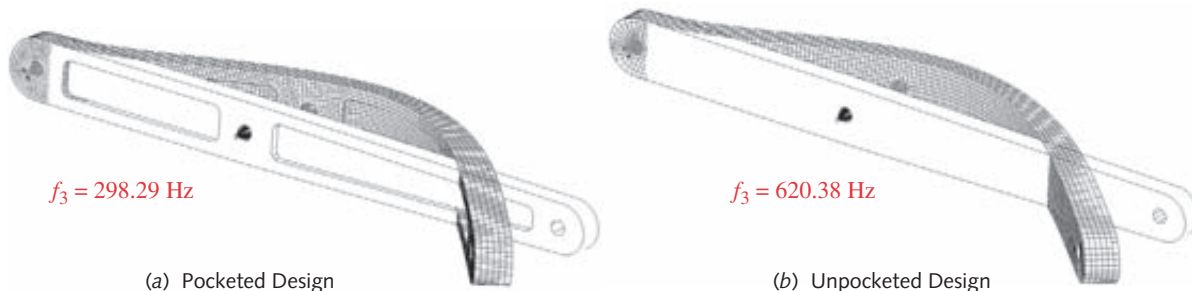


FIGURE 8-29

First Mode Shapes of the Pocketed and Unpocketed Beams in Example 8-6 (deflections greatly exaggerated)

**FIGURE 8-30**

Second Mode Shapes of the Pocketed and Unpocketed Beams in Example 8-6 (deflections greatly exaggerated)

**FIGURE 8-31**

Third Mode Shapes of the Pocketed and Unpocketed Beams in Example 8-6 (deflections greatly exaggerated)

- 8
- 3 Figure 8-30 shows the second mode shapes of both beam designs. The second natural frequency of the pocketed beam is 219.98 Hz which increases to 455.63 Hz when the pockets are removed.
 - 4 Figure 8-31 shows the third mode shapes of both beam designs. The third natural frequency of the pocketed beam is 298.29 Hz which increases to 620.38 Hz when the pockets are removed.
 - 5 It is clear from this study that the pockets are hurting this design more than helping it. The pockets doubled the static deflection and reduced the natural frequencies by more than a factor of 2. Despite the mass reduction delivered by the removal of the pocket material, the cost in stiffness probably makes it not worth doing in this case. It would have been more difficult and time consuming to reach this conclusion without the use of FEA.

8.8 CASE STUDIES

The principles developed in this chapter will now be applied to problems of more complicated geometry.

CASE STUDY 1 D

FEA Analysis of a Bicycle Brake Lever

Problem

A bicycle brake lever was analyzed for stress and deflection with classical methods and simplified geometry in Case Study 1B (p. 206). Analyze this assembly with FEA and compare the results to the earlier study.

Given

The geometry and loading are known from Case Study 1A (p. 79) and a classical stress analysis was done in Case Study 1B (p. 206). The average human's hand can develop a grip force of about 267 N (60 lb) in the lever position shown.

Assumptions

A static analysis is acceptable due to a small number of load cycles.

Solution

See Figures 8-32 to 8-33.

- Figure 3-1 shows the brake lever assembly and Figure 4-48 shows the simplified model of the lever geometry, loads, and constraints that were used for the classical solution of Case Study 1B. The complex geometry of the handle had to be ignored and it was modeled as a straight cantilever beam cut or truncated where the handle joins the pivot block. A solid model of the arm that accurately captures the geometry is easily created in CAD. Finite element analysis can then be applied.
- As a first step, a model of the truncated beam of Figure 4-48a that was analyzed in the previous study was created but with its real geometry. Figure 8-32a shows the solid model with load and boundary conditions applied as a cantilever beam. Figure 8-32b shows the mesh, and Figure 8-32c shows the stress contour plot. The mesh uses 16th-order tetrahedral elements with 16 nodes per side. The highest stress is at the point labeled P in the figure and is 69.63 MPa. This compares to a value of 70.9 MPa from the classical analysis that assumed a round cross section for the handle at that point. The FEA model has an oval cross section. These numbers agree within 2%, which points out the value of a simple model such as was used in the classical solution. The FEA solution involved more work in this case than the classical solution. That will not always be the case as parts of very complex geometry are difficult to model by classical methods. The classical method gives a deflection of 0.54 mm and this FEA model gives 0.69 mm due to the real arm geometry being less stiff than in Figure 4-48b.

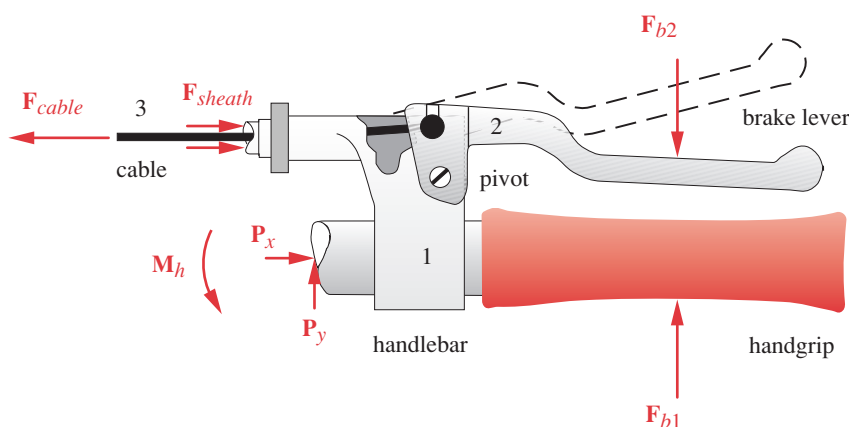
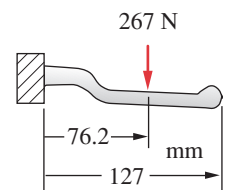
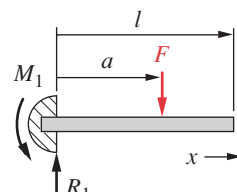


FIGURE 3-1

Bicycle Brake Lever Assembly



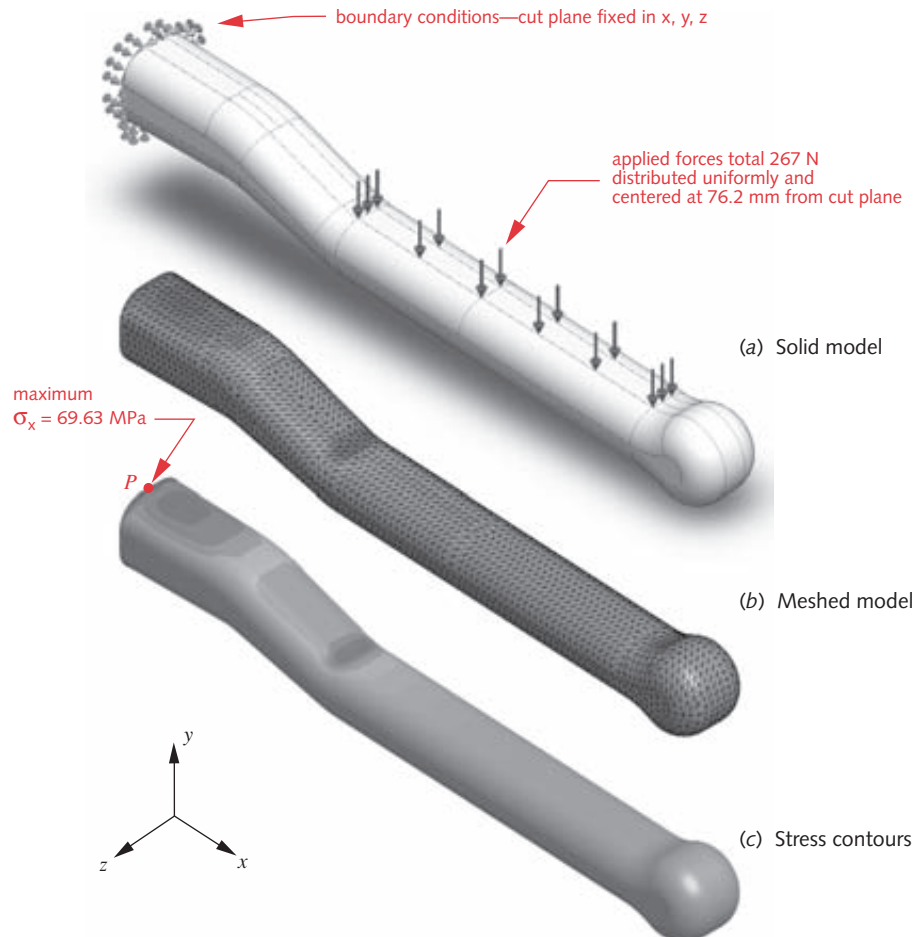
(a) The handle as a cantilever beam



(b) The cantilever-beam model

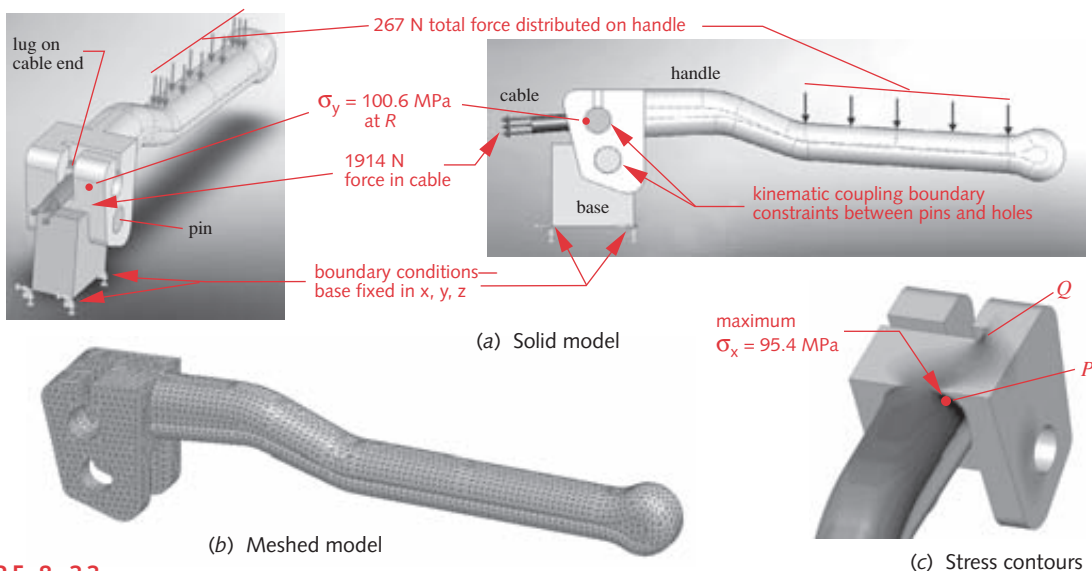
FIGURE 4-48

Cantilever-Beam Model of Handle

**FIGURE 8-32**

Solid Model, FEA mesh, and Stress Distribution in Truncated Beam Model of Case Study 1D

- 3 With the ability to model complex geometry, we can create a model in FEA that includes the parts of the assembly that were ignored in the truncated model of Figure 4-48, namely the pivot block end of the handle, pivot pin, and cable. Figure 8-33 shows a model that includes these details.
- 4 Figure 8-33a shows the complete handle attached to a base of arbitrary shape by kinematic constraints around the pin on the base that fits the hole in the handle. The cable end has a cylindrical lug that fits in the open hole of the handle and its interaction with the handle is also defined by kinematic constraints on the half of the hole surface that bears the cable-lug load. The hand load is applied to the handle and is balanced by the cable load along with reaction forces at the fixed boundary conditions at the bottom of the base. This arrangement closely mimics the actual loading on the handle.
- 5 Figure 8-33b shows the meshed model of the handle alone. Base and cable end were also meshed and the system solved as an assembly in FEA. The finest mesh available was used and the elements are all 16th-order tetrahedra. Figure 8-33c shows stress distributions in the pivot block and handle where they are greatest. The highest tensile stress is at the juncture of the handle and pivot block (labeled P) where the stress con-

**FIGURE 8-33**

Solid Model, FEA mesh, Loading, and Stress Distribution in Complete Model of Case Study 1D

centration of that corner raises the stress to 98.12 MPa. This is 1.4 times the 69.63 MPa calculated with the simpler truncated model, meaning that this corner has a stress concentration factor $K_c = 1.4$. The truncated model cannot give information on the stress concentration because the sharp corner does not exist in that model. In that sense this more complicated model is superior, but it took a lot more time and effort to do. As an alternative, the classical solution could estimate a stress concentration factor for the corner and obtain a better estimate of stress with less time and effort than needed for this FEA solution. Point Q also has elevated stress in the sharp corner. This could be improved by redesigning it to have a full radius at the end of that slot. The stress at R was estimated as 91.9 MPa in the classical model and is 100.6 MPa in this more accurate FEA model. Deflection at the end of the handle in the complete model is 0.98 mm. A Solidworks model of this study is in the folder Case 1-D on the CD-ROM.

CASE STUDY 2 D

FEA Analysis of a Crimping Tool

Problem

A crimping tool was analyzed for stress and deflection with classical methods and simplified geometry in Case Study 2B (p. 209). Analyze this assembly with FEA and compare the results to the earlier study.

Given

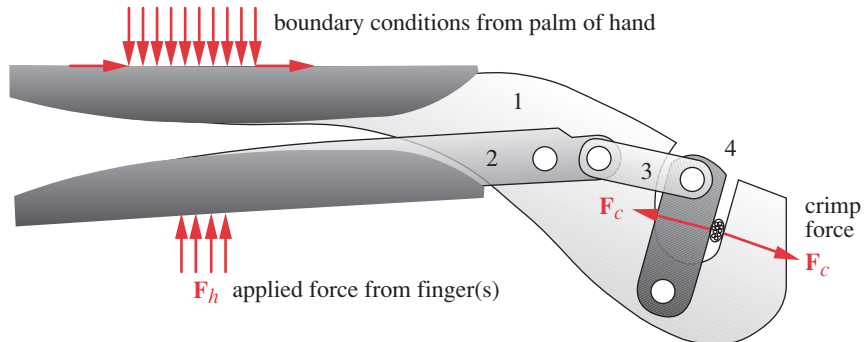
The geometry and loading are known from Case Study 2A on p. 84. The thickness of link 1 is 0.313 in, of links 2 and 3 is 0.125 in and of link 4, 0.187 in. All material is AISI 1095 steel.

Assumptions

A static analysis is acceptable due to a small number of load cycles.

Solution

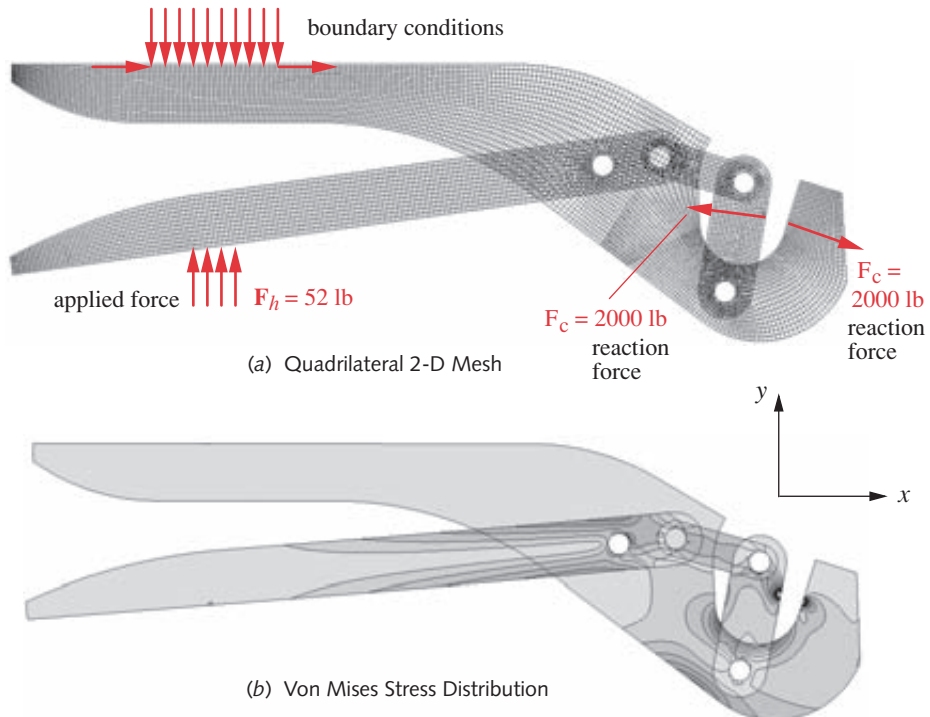
See Figures 8-34 to 8-35.

**FIGURE 8-34**

Wire Connector Crimping Tool

8

- Figure 8-34 shows the loads and constraints applied to the crimping tool assembly of Case Study 2B. The tool is supported (constrained) by the palm of the hand on the top handle and a force is applied to the bottom handle by the fingers until the required crimp force ($F_c = 2000$ lb) is applied by the jaws of the tool to the part being crimped. The geometry was defined in Case Study 2A.
- Figure 8-35a shows an FEA mesh of quadrilateral elements applied to the assembly with boundary constraints and loads applied. The links are connected with pins in the model. A set of nodes along the top surface is constrained in y and x to represent the constraint of the palm of the hand. The required finger force F_h is applied to the bottom handle.

**FIGURE 8-35**

FEA Mesh, Forces, Boundary Conditions, and Stress Distribution in the Crimping Tool Assembly

- 3 Figure 8-35b shows the stress distribution in the part with the applied boundary conditions and loads of 2000 lb at the crimp. Results of the two methods are compared in Table 8-3. Table 8-4 shows the pin forces calculated by each method.*
- 4 In Case Study 2B a simplification was made to the geometry at the right end of link 1 to make it compatible with a closed-form solution of a curved beam. We do not have to make any such geometric simplification here as the mesh can fit to the real geometry. The closed form solution gave a maximum stress of 74 kpsi at point *P*. The FEA study indicates that the largest stress in the part is 81 kpsi at point *P*. The difference is probably due to the geometric simplification made in the previous solution.

Table 8-3

Closed-Form (CF) vs. FEA
Principal Stress Results

Link	Stress (kpsi)	
	CF	FEA
1	74.0	81.2
2	N.A.	45.5
3	-50.0	-40.0
4	31.0	26.9

C A S E S T U D Y 4 D**FEA Analysis of a Bicycle Brake Arm****Problem**

A bicycle brake arm was analyzed for stress and deflection with classical methods and simplified geometry in Case Study 4B (p. 217). Analyze this assembly with FEA and compare the results to the earlier study.

Given

The geometry and loading are known from Case Study 4A (p. 94) and the arm is acted on by a cable force of 1 046 N in the position shown.

Assumptions

The accelerations are negligible. A Class 1 load model is appropriate and a static analysis is acceptable. The coefficient of friction between the brake pad and wheel rim has been measured and is 0.45 at room temperature and 0.40 at 150°F.

Solution

See Figures 8-36 to 8-37.

- 1 Figure 3-9 shows the geometry of the brake arm assembly. Symmetry allowed it to be analyzed for one side only in Case Study 4B and we will do so here as well. It was broken into two cantilever beams for the classical solution. That is not necessary here and it will be analyzed as an assembly consisting of the arm, pivot pin, and constraints to represent the wheel rim. The cross section shape had to be crudely modeled as a rectangular tee shape in the classical solution and curved beam theory was used to analyze bending stress. In the FEA model, the actual geometry is used and a general stress analysis done. We should expect some differences in the results between the two models.
- 2 Figure 8-36 shows the solid-model assembly. The arm is supported on a pin, one end face of which is fixed to ground in *x*, *y*, and *z*. The arm is kinematically constrained to the pin allowing the hole surface to turn on the outside diameter of the pin, but is unable to move in *x* or *y*. The *z*-direction of the arm is constrained by creating a “washer” detail on its hub face and this “washer” area is constrained against motion in *z*. Rotation of the arm about the *z*-axis of the pin is prevented by constraining an area “*A*” on the face of the slotted portion against motion in *x*. This represents the brake pad attached there, which is pressed against the wheel rim. The torque from the wheel and friction with the brake pad are modeled as traction forces in the *y* and *z* directions on the same area *A* and on area *B* on the back side. These traction forces appear as arrows laying on the surface both on the pad side of the arm and on the recessed surface of the slot on the back side of the arm where the bolt that holds the pad is seated. Finally, the cable force is applied at hole *C* as *x* and *y* components.

Table 8-4

Closed-Form (CF) vs. FEA Pin Force Results

Force	Magnitude (lb)	
	CF	FEA
<i>F</i> ₁₂	1560	1574
<i>F</i> ₁₄	452	456
<i>F</i> ₂₃	1548	1545
<i>F</i> ₄₃	1548	1545

* Note that the pin forces must be calculated in advance of doing a closed-form stress analysis as they are needed in the stress equations. An FEA calculation, on the other hand, needs only the applied loads and boundary conditions to calculate the stresses. The reaction forces can then be back-calculated from the stresses. It is a good idea to check the reaction forces that result from the FEA analysis and compare them to a static force analysis of the system using $\Sigma F=0$ and $\Sigma M=0$. If they agree, it verifies that your FEA model is reasonable.

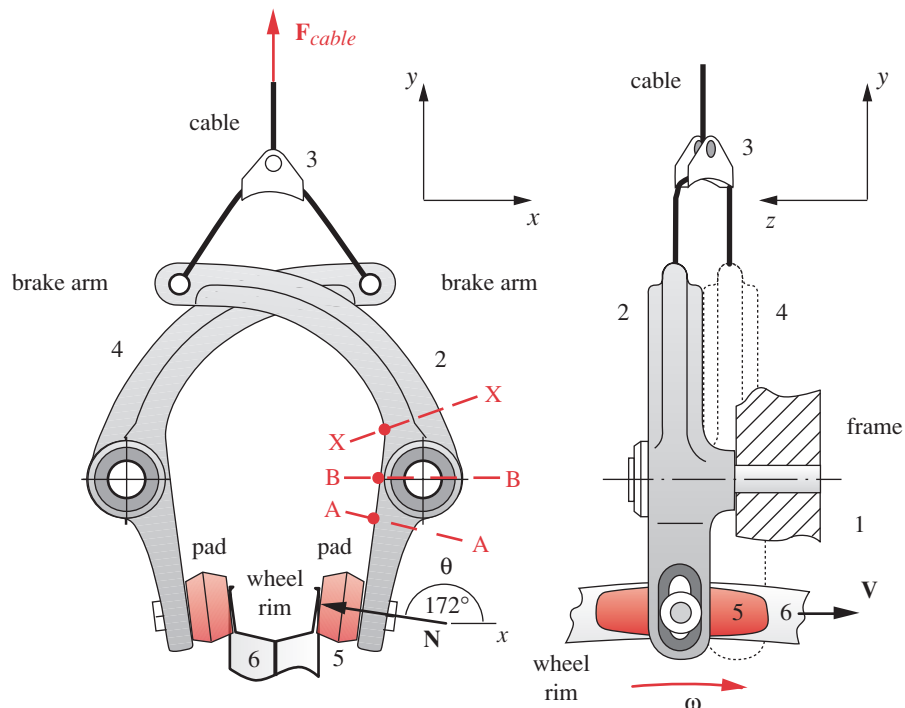


FIGURE 3-9 repeated

Center-Pull Bicycle Brake Arm Assembly

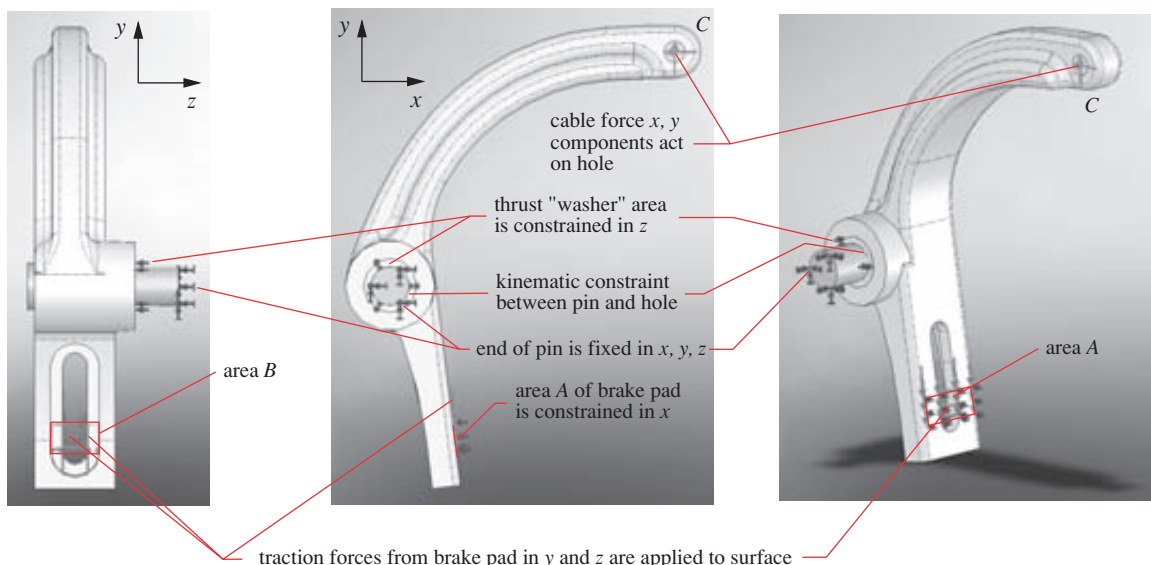
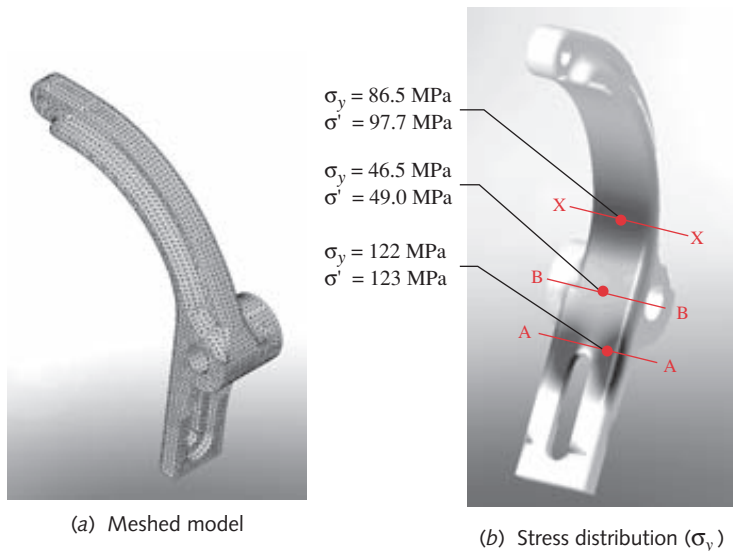


FIGURE 8-36

Boundary Conditions, Constraints, and Loads on FEA Model of Bicycle Brake Arm

**FIGURE 8-37**

Mesh and Stress Distribution on FEA Model of Bicycle Brake Arm

8

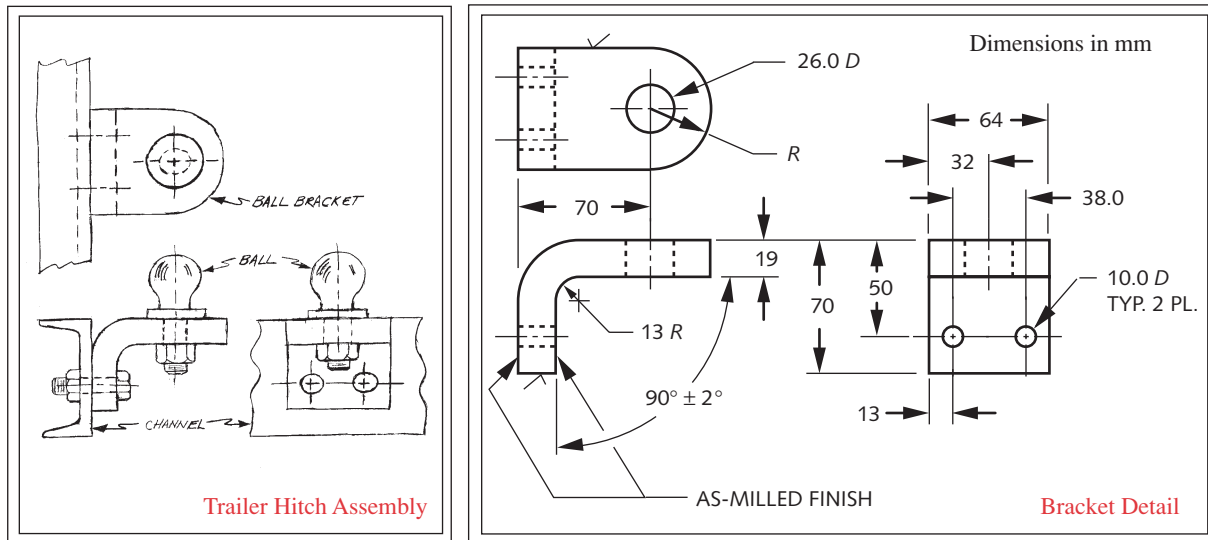
- 3 The classical stress analysis of this part done in Case Study 4B chose several locations of presumed high stress to analyze. These comprised a plane labeled X-X in Figure 3-9 through the curved beam section near its root, a plane B-B through the pivot hole, and a plane A-A cutting close to the root of the rectangular cantilever that contains the slot for mounting the brake pad. In all three planes the highest tensile stresses were at the inner surface at points shown with colored dots in Figure 3-9 (repeated) opposite.
- 4 Figure 8-37a shows the arm meshed with 54 432, 16th-order tetrahedral elements and Figure 8-37b shows a stress contour plot of the inside surface of the arm. This plots tensile normal stress σ_y , which is the component calculated for these points in Case Study 4B. Traces of the cut planes A-A, B-B, and X-X are shown at the inside surface. Hot spots of high stress are clearly visible at A-A and X-X, but not at B-B. This is because the stress at B-B is less than at the other locations. The von Mises stress is also shown and is close to the σ_y value because it is dominant at those points.
- 5 Table 8-5 compares the results from the classical stress analysis with those of this FEA for tensile stress in the y-direction at the inner fiber for the three locations. Table 8-6 compares the results from the classical stress analysis with those of this FEA for compressive stress at the outer fiber of section X-X. At the inside surface of the sections A-A and X-X the FEA results show lower stress than the classical analysis. This is most likely due to the fact that the classical analysis ignored the increase in section thickness due to the fillet radii on the outside contours of the arm and assumed that the beam depth (thickness) was constant all the way to the root on both sides of the hub. The good news is that the classical analysis gave a conservative estimate at these two locations. However, the FEA predicts nearly twice the stress at section B-B than did the classical analysis. In this case the FEA gives a better estimate of the stress.
- 6 The FEA gives a superior result in this case due to the complex geometry that had to be overly simplified for the classical analysis. The Solidworks model is on the CD-ROM in a folder labeled CASE 4-D.

Table 8-5Classical Analysis (CA) vs. FEA Results for Tensile Stress σ_y at Inside Surface

Location	Stress (MPa)	
	CF	FEA
A-A	142.2	122.0
B-B	25.4	46.5
X-X	162.0	86.5

Table 8-6Classical Analysis (CA) vs. FEA Results for Compressive Stress σ_y at Outside Surface

Location	Stress (MPa)	
	CF	FEA
X-X	-190.0	-79.3

**FIGURE 8-38**

8

Trailer Hitch Assembly and Detail

CASE STUDY 7**FEA Analysis of a Trailer Hitch****Problem**

A trailer hitch subassembly and dimensions of its bracket are shown in Figure 8-38. Loads are applied as shown in Figure 8-39. Analyze this assembly with FEA and determine its stresses.

Given

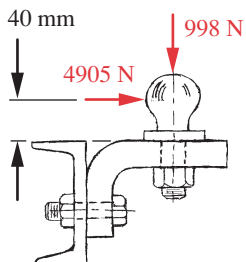
The tongue weight of 998 N acts downward, and the pull force of 4905 N acts horizontally. All material is steel.

Assumptions

The frame to which the hitch is bolted is significantly stiffer than the hitch assembly. Bolts are snug-tight with no preload.

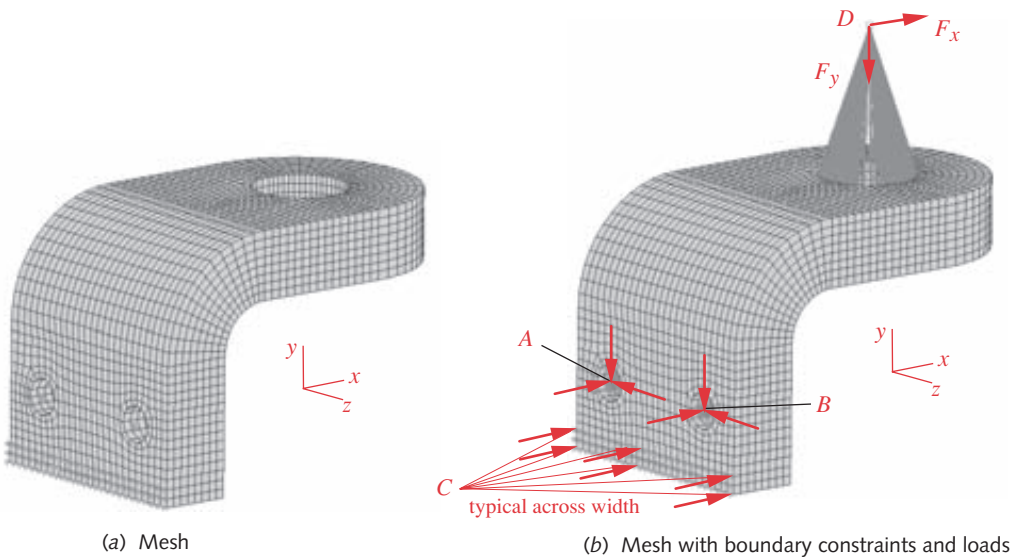
Solution

See Figures 8-38 to 8-41.

**FIGURE 8-39**

Hitch Loading

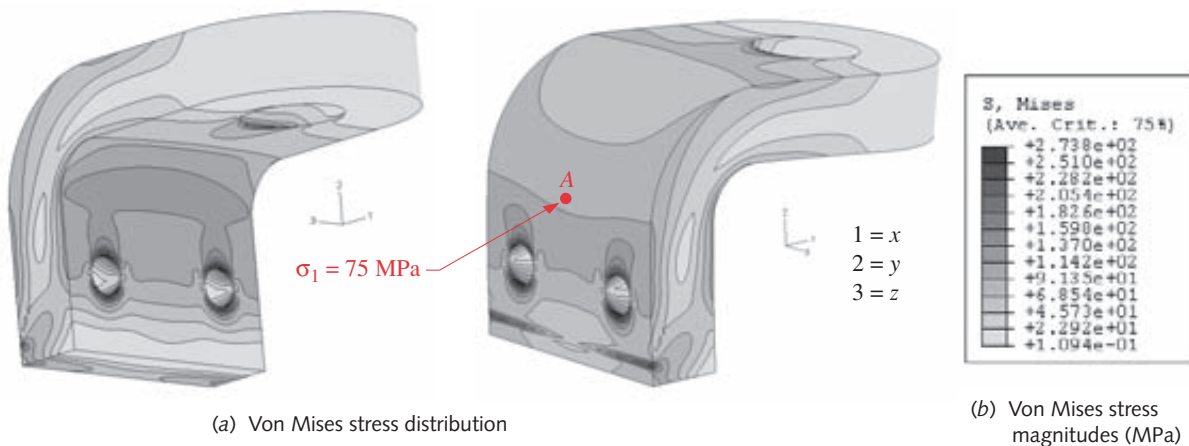
- 1 The geometry of the part requires a 3-D FEA model if information on stress concentration around the holes is needed. Figure 8-40a shows the part meshed with 8-node, linear hexahedral “brick” elements. Note the finer mesh pattern around the holes. This mesh was refined until the stresses converged to values that changed only slightly with successively finer meshes as was done in Example 8-1.
- 2 Figure 8-40b shows the boundary constraints applied. The holes at points A and B have the same type of “kinematic constraints” applied as were used in prior examples to simulate a pin or round fastener (here a bolt) in a hole. A node is placed in the center of the hole at the back surface where the bracket touches the frame (not shown) to which it is clamped. Rigid elements attach this central node to all the nodes on the inside surface of the hole. The central nodes at A and B are fixed in x, y, and z.

**FIGURE 8-40**

Mesh and Boundary Constraints for the Trailer Hitch Bracket in Case Study 7

8

- 3 The area at the bottom of the back surface labeled *C* in Figure 8-40 has all the surface nodes of the bottom two rows of elements fixed in *x* to represent contact with the frame and prevent rigid-body rotation about the *z* axis. Note that a superior way to do this would be to provide contact constraints to all the nodes on the back surface that touch the frame. This would account for a possible load reversal that could tend to separate the bottom rows of nodes from the frame. Using contact constraints would then require a nonlinear FEA analysis that would significantly increase computation time. The approach used here allows a linear FEA calculation. (Note that because this part is symmetric about the midplane and is loaded in that plane, a 2-D analysis of the part without any holes would also give good—but less complete—information and would have much shorter run time.)
- 4 Another node is placed at point *D*, 40-mm above the top surface on the axis of the hole that accepts the hitch ball. This node is connected with rigid elements to the nodes on the inner surface of the 26-mm-dia hole. Forces are applied to this offset node to represent their application at the center of the hitch ball. This approach makes the implicit assumption that the ball is much stiffer than the bracket (i.e., essentially rigid). If we had been concerned about stresses and deflections in the ball, we could have included it in the model at the expense of model generation and computation time.
- 5 Figure 8-41 shows the distribution of von Mises stresses throughout the bracket, which range from 11 to 274 MPa. Note the stress concentrations around the holes. Point *A* at the tangent between the outside radius and the back surface that is clamped to the frame has a maximum principal stress of 75 MPa. This correlates well with the value of 72.8 MPa calculated at the same point with classical cantilever-beam theory in the solution of Problem 4-4e (p. 228) as reported in Appendix D (p. 1007). Note that there are points with higher stresses than this within the part, typically at locations of stress concentration around holes.

**FIGURE 8-41**

Stress Distribution in the Trailer Hitch Bracket of Case Study 10

8.9 SUMMARY

Finite Element Analysis is a very powerful tool and one which is used extensively in engineering. It allows the solution of problems whose geometry is too complex for classical closed-form methods of stress and deflection analysis. However, as with any tool, it requires some skill to use properly, and when misused the results can be disastrous. It is important to understand enough of the theory and mathematical basis of FEA to be aware of its limitations. It is also important to test and verify any FEA model against either a closed-form solution of a test problem or experimental data rather than accepting its results at face value.

This chapter has presented only a brief introduction to the topic and has attempted to point out some of the pitfalls associated with the construction of viable FEA models. Choosing an element type that best suits the geometry and loading situation is the first step. Checking that the mesh has converged reasonably to a believable solution is also important. Perhaps the most difficult aspect of FEA modeling is setting up realistic boundary constraints on the model that fairly represent the actual boundary conditions on the physical system being modeled. Several examples in this chapter have shown how significant errors can result if these details are not properly attended to.

Before attempting to use FEA professionally, the student is urged to seek further information and/or instruction in the theory and practice of FEA, either through courses devoted to that subject or by reading in the available literature. A reasonable start toward the latter goal can be made with the books listed in the bibliography below. Their bibliographies, in turn, will lead you deeper into the world of FEA. There is also a wealth of information about FEA on the web including complete textbooks. Some sites are listed below. A web search on the topic will reveal many others.

8.10 REFERENCES

- 1 M. J. Turner, R. W. Clough, H. C. Martin, and L. J. Topp, "Stiffness and Deflection Analysis of Complex Structures," *J. Aero. Sci.*, 23, pp. 805-824, 1956.
- 2 http://www.iti-cae.com/caelabs/user_guide/plasticslab/plasticslab-291.html
- 3 V. Adams and A. Askenazi, *Building Better Products with Finite Element Analysis*. Onword Press: Santa Fe, N.M., p. 246, 1998.
- 4 D. L. Logan, *A First Course in the Finite Element Method*. 2ed. PWS Kent: Boston, p. 408, 1992.

8.11 BIBLIOGRAPHY

V. Adams and A. Askenazi, *Building Better Products with Finite Element Analysis*. Onword Press: Santa Fe, N.M., 1998.

K. J. Bathe, *Finite Element Procedures in Engineering Analysis*. Prentice-Hall: Englewood Cliffs, N.J., 1982.

D. L. Logan, *A First Course in the Finite Element Method*. 2ed. PWS Kent: Boston, 1992.

I. H. Shames and C. L. Dym, *Energy and Finite Element Methods in Structural Mechanics*. Hemisphere Publishing: New York, 1985.

E. Zahavi, *The Finite Element Method in Machine Design*. Prentice-Hall: Englewood Cliffs, N.J., 1992.

8.12 WEB RESOURCES

- <http://caswww.colorado.edu/courses.d/IFEM.d/Home.html>
- <http://www.devdept.com/fem/books.php>
- http://feaservices.com/intro_fea/intro_fea.html
- <http://www.memagazine.org/supparch/medesign/mesh/mesh.html>
- <http://caswww.colorado.edu/Felippa.d/FelippaHome.d/Publications.d/Report.CU-CAS-00-13.pdf>
- <http://campus.umr.edu/mfge/ugumrmfge/FEMwebpage/Projecta.htm>
- http://www.engr.usask.ca/~macphed/finite/fe_resources/fe_resources.html
- http://www3.sympatico.ca/peter_budgell/Modeling_issues.html
- <http://www.DermotMonaghan.com/>
- <http://www.femur.wpi.edu/>

8.13 PROBLEMS*

- 8-1 Do Problem 4-10 using FEA.
- 8-2 Do Problem 4-11 using FEA.
- 8-3 Do Problem 4-12 using FEA.
- 8-4 Do Problem 4-13 using FEA.
- 8-5 Do Problem 4-17 using FEA.
- 8-6 Do Problem 4-19 using FEA.
- 8-7 Do Problem 4-23 for the row(s) assigned using FEA.
- 8-8 Do Problem 4-24 for the row(s) assigned using FEA.
- 8-9 Do Problem 4-25 for the row(s) assigned using FEA.
- 8-10 Do Problem 4-26 for the row(s) assigned using FEA.
- [†]8-11 Do Problem 4-33 for the row(s) assigned using FEA.
- [†]8-12 Do Problem 4-34 for the row(s) assigned using FEA.
- 8-13 Do Problem 4-37 using FEA.
- 8-14 Do Problem 4-59 using FEA.
- 8-15 Do Problem 4-60 using FEA.
- 8-16 Do Problem 4-62 using FEA.
- 8-17 Do Problem 4-63 using FEA.
- 8-18 Do Problem 4-66 using FEA.
- [†]8-19 Do Problem 9-4 for the row(s) assigned using FEA.
- [†]8-20 Do Problem 9-5 for the row(s) assigned using FEA.
- [†]8-21 Do Problem 4-3 using FEA.
- [†]8-22 Do Problem 4-9 using FEA.
- [†]8-23 Do Problem 4-33 using FEA.
- [†]8-24 Do Problem 4-34 using FEA.
- [†]8-25 Do Problem 4-35 using FEA.
- [†]8-26 Do Problem 4-40 using FEA.
- [†]8-27 Do Problem 4-57 using FEA.
- [†]8-28 Do Problem 4-59 using FEA.
- [†]8-29 Do Problem 4-60 using FEA.
- [†]8-30 Do Problem 4-61 using FEA.
- [†]8-31 Do Problem 4-69 using FEA.
- [†]8-32 Do Problem 4-70 using FEA.
- [†]8-33 Do Problem 4-71 using FEA.
- [†]8-34 Do Problem 4-72 using FEA.

* Some of the referenced problems from earlier chapters have answers in Appendix D. For the others, your instructor may be willing to provide you with the closed-form solution values to the original problem from the solution manual to use as a check on your FEA results. If not, you can solve them by classical methods yourself as a check.

[†] Solidworks models of the geometry for these problems are on the CD.

Part

II

MACHINE DESIGN

9



DESIGN CASE STUDIES

*No man's knowledge here
can go beyond his experience.*

JOHN LOCKE

9.0 INTRODUCTION

This chapter will introduce and set up several design case studies that are larger in scale than those presented in the earlier chapters. These case studies will be used throughout the remainder of the book to illustrate the application of the design process for various aspects of each design problem. Subsequent chapters will each explore a different type of design element, such as shafts, gears, springs, etc., which are commonly found in machinery. This collection of elements cannot be exhaustive, but it will illustrate the way in which the principles of the first part of the book can be applied to practical design problems. The particular machine elements selected for study are chosen partly because of their common usage and partly because of their ability to exemplify some of the design and failure criteria discussed in Part I of the text. Table 9-0 shows the variables used in this chapter and references the case studies in which they are used.

Design is, by its nature, an iterative process. When presented with a design-problem statement, some simplifying assumptions are always necessary in order to get started. As the design takes shape, the results of later design choices will inevitably force the designer to revisit earlier assumptions about parts already designed and change them to suit the new conditions. A simple example of this could be the design of a set of gears mounted on shafts. Whether one starts by designing the shafts or the gears (say the shafts), when it is time to address the second of the two elements (say the gears), their requirements may force a change to some of the assumptions made regarding the shaft design done earlier. Eventually, one arrives at a compromise that satisfies all the constraints, but only after some iteration that inevitably involves the redesign of parts done earlier.

Because of the need for iteration, any time spent to set up the problem solution in a computerized tool such as a spreadsheet or equation solver will be well rewarded when

Table 9-0 Variables Used in This Chapter

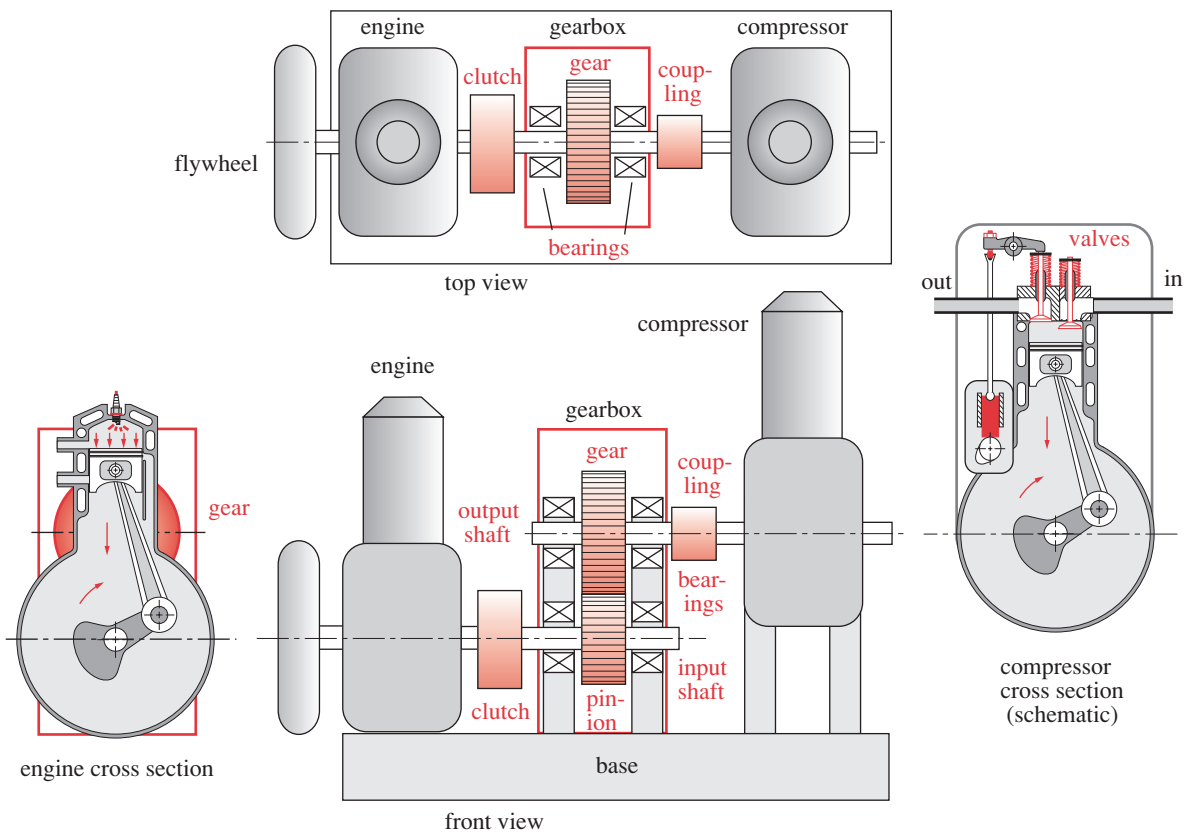
Symbol	Variable	ips units	SI units	See
A	area	in ²	m ²	Case 7A
a	acceleration	in/sec ²	m/sec ²	Case 8A
c	damping constant	lb-sec/in	N-sec/m	Case 8A, 9A
C_f	coefficient of fluctuation	none	none	Case 9A
d	diameter	in	m	Case 7A
E	energy	in-lb	joules	Case 9A
F	force or load	lb	N	all
g	gravitational acceleration	in/sec ²	m/sec ²	Case 8A
k	gas-law exponent	none	none	Case 7A
k	spring rate or spring constant	lb/in	N/m	Case 8A, 9A
l	length	in	m	Case 7A
m	mass	lb-sec ² /in	kg	all
P	power	hp	watts	Case 8A
p	pressure	psi	Pa	Case 7A
r	radius	in	m	Case 7A
T	torque	lb-in	N-m	all
v	volume	in ³	m ³	Case 7A
v	linear velocity	in/sec	m/sec	Case 8A
W	weight	lb	N	Case 8A
y	displacement	in	m	all
ω	rotational or angular velocity	rad/sec	rad/sec	all
ω_n	natural frequency	rad/sec	rad/sec	Case 9A
ζ	damping ratio	none	none	Case 9A

* The student may not have yet been exposed to all aspects of these broad-scale problems in his or her studies to date, but should nevertheless not be dismayed if some details of these case studies seem obscure. One will undoubtedly encounter more detailed explanation of these topics in other courses, in later experience, or in self-study. One of the more interesting aspects of design engineering is its breadth. One must continually learn new things in order to be able to solve real engineering problems. An engineering education only begins in college and is far from complete at graduation. One should welcome the challenge of exploring new topics throughout one's career.

you have to redesign each part several times. A CAD solid modeling program will also be a valuable design tool. Lacking a computer-based model, you will be faced with redoing your calculations from scratch for each iteration, which is not a pleasant prospect. We will make extensive use of computer-aided design tools in these case studies.

9.1 CASE STUDY 8—A PORTABLE AIR COMPRESSOR*

A building contractor needs a small, gasoline-engine powered air compressor to use for driving air hammers on remote job sites. A preliminary design concept is shown in Figure 9-1. A single-cylinder, two-stroke engine with flywheel is coupled through a clutch (that can be disengaged to start the engine) to a gearset to reduce the engine speed and boost its torque appropriately. The ratio for this gearset is to be determined. The 2.5-hp gasoline engine is governed at 3800 rpm. The gearset's output shaft drives the crankshaft of a single-cylinder Schramm (poppet valve) piston compressor through a keyed coupling. Some preliminary thermodynamic calculations (see files CASE7-A) have indi-

**FIGURE 9-1**

Preliminary Design Schematic of Gasoline-Engine-Powered Portable Air Compressor, Gearbox, Couplings, Shafts, and Bearings

cated that the desired flow rate of 9 cfm at a mean effective pressure of 26 psig can be obtained from a 25-in³ stroke-volume compressor running at 1500 rpm.

Figure 9-1 shows the engine mounted on a base (which could be on wheels) with its output shaft connected via a clutch to the input shaft of a gearbox. The gearbox contains a single gearset to reduce the high engine speed to a lower one suitable for the compressor. The required gear ratio is 1500:3800 or 0.39:1. The output shaft from the gearbox is connected via a coupling to the crankshaft of the compressor. The shafts in the gearbox housing are carried in suitable bearings. The cross section of the compressor shows the active exhaust valve driven by a cam-operated pushrod and rocker-arm train. The intake valve is passive, i.e., opened and closed by the pressure differentials and its light spring. The valve spring on the exhaust valve must be strong enough to keep the follower in contact with the cam.

There are several aspects of this device that we will investigate. We will assume that the gasoline engine will be purchased as a unit. The compressor will dictate the loads on the elements between the engine and itself, so some information is needed on the load-time characteristics of the compressor. The shafts, couplings, bearings, and gears that deliver the power from engine to compressor will be the principal elements to be designed in this case study. We will also look at a few elements within the com-

pressor such as the headbolts and valve spring since they provide excellent examples of fatigue design. Because of their complicated geometries, the design of other parts of the compressor such as the piston, connecting rod, and crankshaft is more suited to the application of *Finite Element Analysis* (FEA) and will not be addressed in this case study (see Chapter 8).

CASE STUDY 8 A

Preliminary Design of a Compressor Drive Train

Problem Determine the force-time function within the compressor's cylinder and the torque-time function acting on the input shaft of the compressor during any one cycle.

Given Compressor speed is 1 500 rpm. The compressor has a bore of 3.125 in, a stroke of 3.26 in, and a connecting-rod-to-crank ratio of 3.5. Inlet pressure is atmospheric (14.7 psia), peak cylinder pressure is 132 psig, and the mean effective pressure (mep) is 26 psig. Flow is 8.9 cfm at mep, giving 1.6 hp.

Assumptions The piston weight is 1 lb, the connecting rod weighs 2 lb with its center of mass at the 1/3 point from the big end. The crankshaft weighs 5.4 lb including a counterbalance that optimally overbalances it to minimize the shaking force. The exponent for the gas law equation is $k = 1.13$.

Solution See Figures 9-1 to 9-3 and files CASE8-A.

- 1 The force-time function in the cylinder depends on the compressed-gas pressure, which in turn depends on the slider-crank mechanism's geometry and the gas law:

$$p_1 v_1^k = p_2 v_2^k \quad (a)$$

where p_1 is atmospheric pressure (in psia), v_1 is the expanded cylinder volume at bottom dead center (BDC), and p_2, v_2 are the pressure and volume of the compressed gas at top dead center (TDC) or at any other position. The gas-law exponent k is assumed to be 1.13, since the process is neither isothermal ($k = 1$) nor adiabatic ($k = 1.4$). A compression ratio of 10.9:1 is also assumed as typical. An expression for piston displacement y referenced to BDC (assuming constant crankshaft ω) is

$$y = \left(r \cos \theta + l \sqrt{1 - \left(\frac{r}{l} \sin \theta \right)^2} \right) - l + r \quad (b)$$

where r = crank radius, l = connecting-rod length, and θ = crank angle. See reference 1 for a derivation of the expression in parentheses.

- 2 Combining these functions with the assumed pressure ranges and gas-law constant gives an approximate function for the cylinder pressure p as a function of crank angle for this particular problem's data:

$$\text{If } \pi \leq \theta \leq 2\pi \text{ then } p \equiv 924 \left(\frac{\theta - \pi}{\pi} \right)^6 - 792 \left(\frac{\theta - \pi}{\pi} \right)^7 \text{ else } p \equiv 0 \quad (c)$$

This function is shown in Figure 9-2.* The force F_g on the piston and cylinder head due to the gas pressure is then

$$F_g = pA_p = \frac{\pi}{4}pd_p^2 \quad (d)$$

where A_p is piston area and d_p is piston diameter. This is the same function as shown in Figure 9-2 multiplied by a constant. A second scale is shown on the ordinate giving gas force F_g in addition to the gas pressure p for this problem.

- 3 The torque required to drive the compressor crankshaft has two components, one from the gas force F_g and another from the inertial forces F_i due to the accelerations.^[1]

$$T = T_g + T_i$$

where

$$T_g \cong F_g r \sin \theta \left(1 + \frac{r}{l} \cos \theta \right) \quad (e)$$

and

$$T_i \cong \frac{1}{2} mr^2 \omega^2 \left(\frac{r}{2l} \sin \theta - \sin 2\theta - \frac{3r}{2l} \sin 3\theta \right)$$

The mass m is taken as that of the piston and wrist pin plus the portion of the connecting rod (about 1/3) considered to be acting at the piston.^[1] When the data for this problem are substituted into (e), the torque-time function is as shown in Figure 9-3.*

The force-time and torque-time functions shown in the Figures 9-2 and 9-3 assume that the shaft speed is essentially constant. This is a reasonable assumption for the steady-state condition, since the engine driving it is governed and has a flywheel to smooth its own speed oscillations. These force and torque functions define the time-varying loading that the shafts, couplings, and gears will feel and are thus a starting point for their design. Because of the time variation of the loads, all the parts will be subjected to fatigue loading and must be designed accordingly, using the theories outlined in Chapters 6 and 7.

9.2 CASE STUDY 9—A HAY-BALE LIFTER

A dairy farmer in Bellows Falls, Vermont, needs a small winch-hoist to use for the lifting of hay bales into the barn loft. A preliminary design concept is shown in Figure 9-4. An electric motor is coupled to a worm-wheel gearset to reduce its speed and boost the torque appropriately. The best ratio for this gearset is to be determined. The gearbox output shaft is coupled to the winch-drum shaft, and both turn in bearings to be selected. The drum serves as a capstan around which is wound a rope that has a forged hook at its end. The entire winch assembly will ultimately be suspended from the rafters in the hayloft above a central floor-hatch. Hay bales will be manually attached below and manually removed above. The electric motor is reversible, and the worm-wheel set must be designed to be self-locking in order to hold the load when the motor is unpowered.

The above problem statement is very unstructured, as it gives no information about the size and weight of a hay bale nor what number of bales should be lifted at a time for the best efficiency. These considerations in combination with the choice of winch-drum diameter will determine the torque requirements that the drive train will have to meet. The start-up load can be significantly higher than the steady-state lifting load due

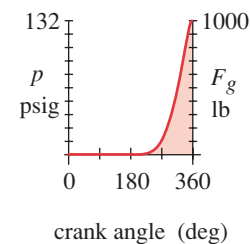
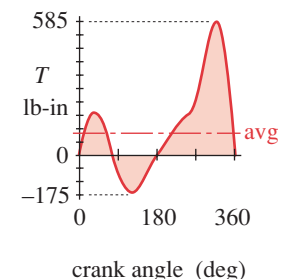


FIGURE 9-2

Pressure and Force Within Cylinder During One Cycle



9

FIGURE 9-3

Total Torque-Time Function at Crankshaft with Constant ω

* The functions in Figures 9-2 and 9-3 were generated with program ENGINE from reference 1.

to shock loading when the slack is first taken out of the line and the load lifted. The dynamic loading at start-up will be modeled using a differential-equation solver.

CASE STUDY 9A

Preliminary Design of a Winch Lift

Problem	Determine the force-time function in the lifting cable, the necessary drum diameter, and the torque-time function acting on the shaft of the winch drum during any 1 cycle. Define the gear ratio and the power and torque requirements for the motor.
Given	A hay bale's weight varies depending on its moisture content but can be assumed to average about 60 lb. The hay truck holds 100 bales and the farmer would like to unload it in 30 min. The lift height is 24 ft.
Assumptions	Nylon rope of 3/4 in dia has a minimum break strength of about 8 000 lb and a spring constant of about 50 000 lb/in per ft of length in axial tension.
Solution	See Figures 9-4 to 9-6 and files CASE9-A.

9

- 1 The nominal load depends on the number of bales to be lifted at one time and the weight of any structure used to support the bales. To unload 100 bales from the truck, one at a time in 30 min, requires that the average bale rate be $100 / 30 = 3.3$ bales/min, or an 18-sec average period per bale. Since some of this time must be used to return the empty lift to the ground, we cannot use the entire 18 sec to lift the load. We must also allow some time for manual loading and unloading of the bales at top and bottom. The portion of the total period during which the mechanism is working is called its *duty cycle*. Let's assume that 1/3 of the period is used to load/unload, 1/3 to lift,

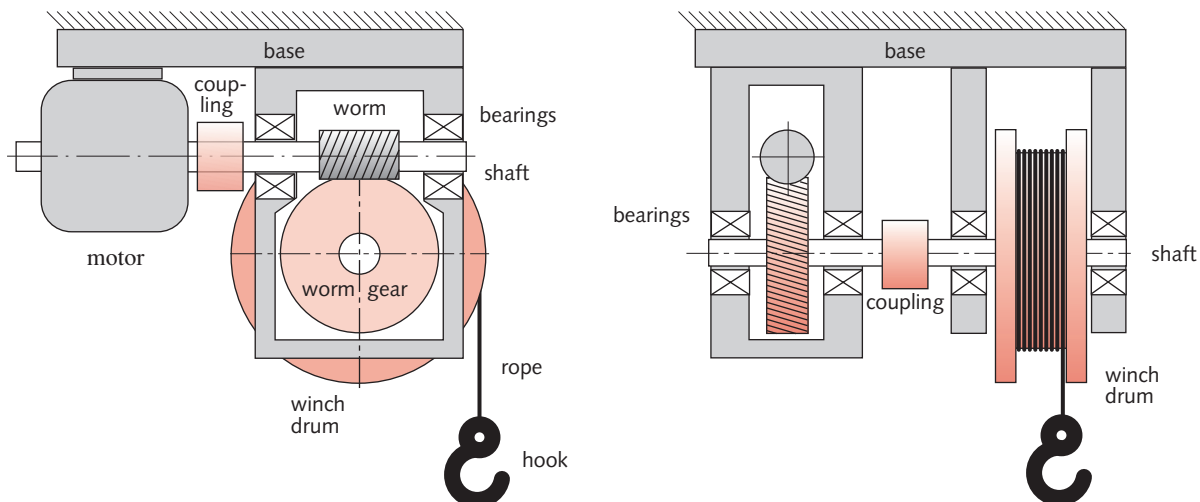


FIGURE 9-4

Motor-Driven Winch with Gear Train, Shafts, Bearings, and Couplings

and 1/3 to lower. This allows 6 sec per bale if we lift only one bale at a time. The average velocity of the lift would then have to be 24 ft. / 6 sec = 4 ft/sec. A better arrangement would seem to be to load two bales at a time on the lift. This doubles the period to 36 sec, doubles the time available for lifting to 12 sec, and halves the average velocity to 2 ft/sec, still keeping the same duty cycle.

- 2 The payload with two bales on the lift is 120 lb. The dead load will be the weight of the rope, hook, and any platform or structure used to support the bales. Since this structure has yet to be designed, its weight is unknown. We will assume that we can keep this dead weight under 50 lb. The total nominal load will then be 170 lb for the lift phase, and 50 lb for the lowering phase.
- 3 At steady state, the load on the rope should be the above number. However, at start-up, the load can be significantly higher due to the need to accelerate the load to its steady-state velocity and due also to the fact that there are both spring and mass in the system. A combination of spring and mass in a dynamic system allows oscillations to occur as the kinetic energy of the moving mass is transferred to potential energy in the elastic spring and vice versa. The rope is a spring. When the slack in the rope is suddenly taken up against the mass of the load, the rope will stretch, storing potential energy. When the force in the stretched rope becomes sufficient to move the load, it will accelerate the mass upward, increasing its velocity and transferring the spring's potential energy to kinetic energy in the mass. If the mass accelerates sufficiently, it will take the rope slack again. When the mass falls to take up the slack, the cycle repeats. Thus, as it starts up, the force in the rope can oscillate from zero to some value significantly greater than the steady-state nominal load. To calculate the dynamic loading requires writing and solving the differential equations of motion for the system.
- 4 Figure 9-5a shows a simplified schematic of the portion of the dynamic system containing the lift mass and the rope spring. Figure 9-5b shows the system modeled as a lumped mass supported by a spring and a damper. Figure 9-5c shows a free-body diagram (FBD) of the mass acted upon by its weight W , the spring force F_s , and the damper force F_d . Writing Newton's second law for this FBD gives

$$\sum F = ma$$

$$F_s + F_d - W = \frac{W}{g} \ddot{y}_2 \quad (a)$$

where

$$F_s = k(y_1 - y_2)$$

$$F_d = c(\dot{y}_1 - \dot{y}_2) \quad (b)$$

Substitute the initial conditions:

$$\text{when } t = 0 \quad y_1(0) = 0, \quad \dot{y}_1(0) = v_0, \quad y_2(0) = 0, \quad \dot{y}_2(0) = 0 \quad (c)$$

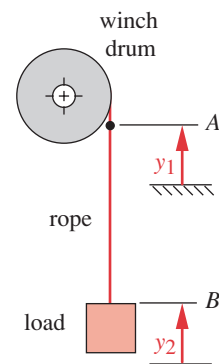
$$\text{from which} \quad F_s(0) = 0, \quad F_d(0) = 0 \quad (d)$$

$$m\ddot{y}_2 = k(y_1 - y_2) + c(\dot{y}_1 - \dot{y}_2) - W$$

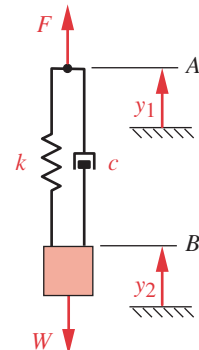
$$\ddot{y}_2 = \frac{1}{m} [k(y_1 - y_2) + c(\dot{y}_1 - \dot{y}_2) - W]$$

$$\text{Let } \dot{y}_1 = v, \quad y_1 = vt$$

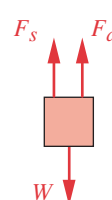
$$\text{then} \quad \ddot{y}_2 = \left[\frac{k}{m} (vt - y_2) + \frac{c}{m} (v - \dot{y}_2) - g \right] \quad (e)$$



(a) Dynamic system



(b) Lumped model



(c) Free-body diagram

FIGURE 9-5

Dynamic System, Lumped Model, and Free-Body Diagram of a Rope Hoist

5 The constants for this equation are defined as follows:

$$v = 24 \frac{\text{in}}{\text{sec}}$$

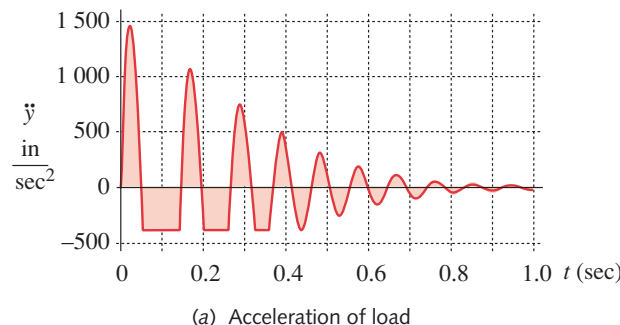
$$W = 170 \text{ lb}, \quad m = \frac{W}{g} = \frac{170}{386} = 0.44 \frac{\text{lb} \cdot \text{sec}^2}{\text{in}} \quad (f)$$

$$k = 50\,000 \frac{\text{lb/in}}{\text{ft}} / 24 \text{ ft} = 2\,083 \frac{\text{lb}}{\text{in}}$$

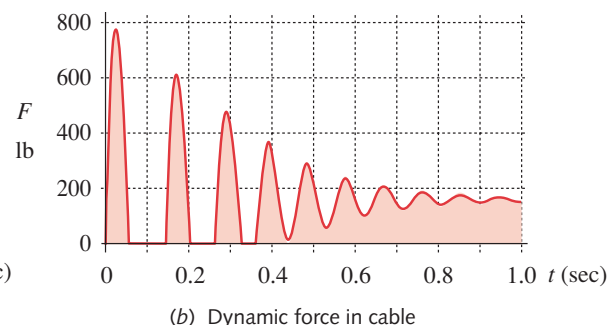
The critical damping c_c is easily calculated from the known mass and spring-constant values. This system is only lightly damped by the rope's internal friction. We will assume that its ratio of actual damping to critical damping, ζ , is about 10% (0.1) and use this to calculate a damping value for equation (e).

$$\begin{aligned} c_c &= 2m\sqrt{\frac{k}{m}} = 2(0.44)\sqrt{\frac{2\,083}{0.44}} = 61 \frac{\text{lb} \cdot \text{sec}}{\text{in}} \\ c &= \zeta c_c = 0.10(61) = 6.1 \frac{\text{lb} \cdot \text{sec}}{\text{in}} \\ \frac{c}{m} &= \frac{6.1}{0.44} = 14 \end{aligned} \quad (g)$$

- 9
- 6 Equation (e) was solved with the ASDEQ* simulation package. The acceleration of the load over the first second of operation is shown in Figure 9-6a. Downward acceleration (gravity) is taken as negative. Note the periods of negative acceleration (at a limiting value of $-g$) during which the load is in free-fall and the rope is slack with no tension. The force in the rope over the first second of operation is shown in Figure 9-6b. Note that the tension force rises to over four times the nominal load on the first oscillation and then drops to zero as the rope goes slack, since it cannot support a compressive force. This pattern repeats for 3 cycles, at which point the damping has reduced the oscillations to the point that the rope is always in tension. After about 10 cycles, it has settled down to the value of the nominal load.
- 7 The torque required to drive the drum shaft will depend on the dynamic loads just calculated and on the diameter of drum selected. Too small a diameter will cause high stresses and wear on the rope. A large drum diameter will increase the required torque and increase the package size. A 3/4-in-dia rope can wrap around a 20-in-dia sheave. Since $T = Fr$, the torque required on the shaft will then be 10 times the tension in the rope (using in-lb) and will have the same time variations as shown in Figure 9-6b.



(a) Acceleration of load



(b) Dynamic force in cable

FIGURE 9-6

Acceleration and Cable Force at Start-up of Load-Lift

* *Automatic Solution of Differential Equations*, by Maj. Abram Jack and Maj. James D. Brown, U. S. Military Academy, West Point, N.Y. Note that this package is available from the U.S.M.A. and is included with this text.

- 8 The average power required can be easily found from the change in potential energy over the time desired. To raise a 170-lb load 24 ft in 12 sec requires

$$P = \frac{170 \text{ lb} (24 \text{ ft})}{12 \text{ sec}} = 340 \frac{\text{ft} \cdot \text{lb}}{\text{sec}} = 0.62 \text{ hp} \quad (h)$$

Since there will be losses in the gear train and winch, we will need an input power larger than this, say 1 hp for a first trial. It is desirable to keep it at or below this level since larger horsepower motors will require higher voltage than 110 V.

This average power is based on the nominal load. The peak load at start-up requires more power. Rather than size the motor to accommodate the transient start-up load, another approach is to provide sufficient flywheel effect in the system to supply the transient pulse of energy to get it past the start-up phase. It is possible that the rotational inertia of the drum and worm gear will supply enough flywheel effect, assuming that the winch is up to speed before the slack is first taken out of the rope.

- 9 The average drum angular velocity is determined from the required average linear velocity of the rope, which is 2 ft/sec. At a 10-in drum radius this gives

$$\omega = \frac{v}{r} = \frac{24 \text{ in/sec}}{10 \text{ in}} = 2.4 \text{ rad/sec} \equiv 23 \text{ rpm} \quad (i)$$

- 10 Electric motors for 60-Hz AC operation are made in only a few standard rotational speeds, the most common of which are 1 725 rpm and 3 450 rpm. These speeds come about from the line-frequency-synchronous speeds of 1 800 rpm and 3 600 rpm minus some slippage in these nonsynchronous motors. To minimize the gear ratio in the wormset, we should choose the slower of the two standard speeds, or 1 725 rpm. This gives a desired gear ratio of 23:1 725 or 1:75. This ratio is obtainable in one stage of a worm-wheel combination, and so is feasible.
- 11 To summarize the parameters determined from this preliminary design study, we are looking to design a system that has a 1-hp, 1 725 rpm, 110-VAC electric motor, driving a 1:75 reduction worm-wheel set that, in turn, drives a 20-in-dia winch drum at 23 rpm. A 3/4-in rope is capstan-wound around the drum and its forged hook attached to a platform that weighs no more than 50 lb and stably supports two hay bales of up to 60 lb each. These constitute a set of task specifications for our design.

9

This formerly unstructured problem now has some structure that can be used as a starting point for more detailed design of the various components. Some of the components of this case study will be addressed in the ensuing chapters as the relevant topics such as shafts, gears, bearings, etc., are presented. Note that though the load is relatively steady with time in this device, the oscillations at start-up and the repeated cycles of use make this a fatigue-design problem, as virtually any machine will be. The parts are subjected to fatigue loading and must be designed accordingly, using the theories outlined in Chapters 6 and 7.

9.3 CASE STUDY 10—A CAM-TESTING MACHINE

A machine is needed that will allow the dynamic characteristics of cams to be measured. This machine must itself be dynamically quiet, have minimal deflections, and provide a virtually constant but adjustable rotational speed in the face of variations in torque

loading from the cams. Instrumentation will be provided to measure the dynamic forces and accelerations of the cam-follower. The mounting of the 1-in rise test cams can be custom designed to fit the test machine. The cam profiles are defined. The rotational speed is to be as high as possible without causing any follower jump. The cams must be easily and quickly replaceable on the machine. The cams will run in an oil bath that must be contained within the machine.

This is also an unstructured problem statement that allows the designer a great deal of latitude in respect to the solution. We will now attempt to further bound the problem with assumptions and preliminary calculations in order to allow a more detailed design to take place.

CASE STUDY 10A

Preliminary Design of a Cam Dynamic Test Fixture (CDTF)

Problem Define a preliminary design concept to satisfy the general constraints of the problem listed above. Determine the force-time function acting on the follower and the torque-time function on the camshaft during any one cycle. Define the drive ratio and the power and torque requirements for the motor.

Given The four-dwell cams have a minimum diameter of 6 in and a maximum diameter of 8 in. The rise is 1 in. The roller follower is 2-in dia. The cams are run at 180 rpm. The cam shape is shown in Figure 9-7.

Assumptions Plain bearings must be used throughout, since rolling-element bearings introduce too much noise. A speed-controlled DC motor will be used.

Solution See Figures 9-7 to 9-13.

- 1 A preliminary design is shown in Figure 9-8. The camshaft is tapered to receive a matching taper in the cam. This avoids the use of keyways, which can introduce vibration and noise on torque reversal. The cam will be axially clamped to the shaft for concentric location. A dowel pin at a large radius keys the cam to the hub to establish a zero position. This arrangement allows quick removal and installation when changing cams.
- 2 A flywheel is attached to the camshaft to provide modulation of the speed oscillations during torque variations. The flywheel also serves as a sheave for a flat belt from the motor's smaller driving sheave in order to reduce the camshaft speed appropriately.
- 3 The follower arm is pivoted 12 in from the camshaft and carries a commercial roller follower running in a plain bearing. A helical-coil tension spring loads the follower-arm roller against the cam. This spring must be detensioned and removed to replace a cam and then retensioned for the new cam. The cover, which is pivoted at the follower-arm pivot, applies tension to the spring when closed and releases it when opened.
- 4 Accelerometers and force transducers are fitted on and between the roller pivot and follower arm to measure the desired parameters.
- 5 The whole is mounted on a box-structure base that supports it, provides rigidity, and also contains an openable oil chamber around the cam. The base can be supported

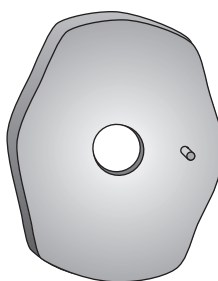
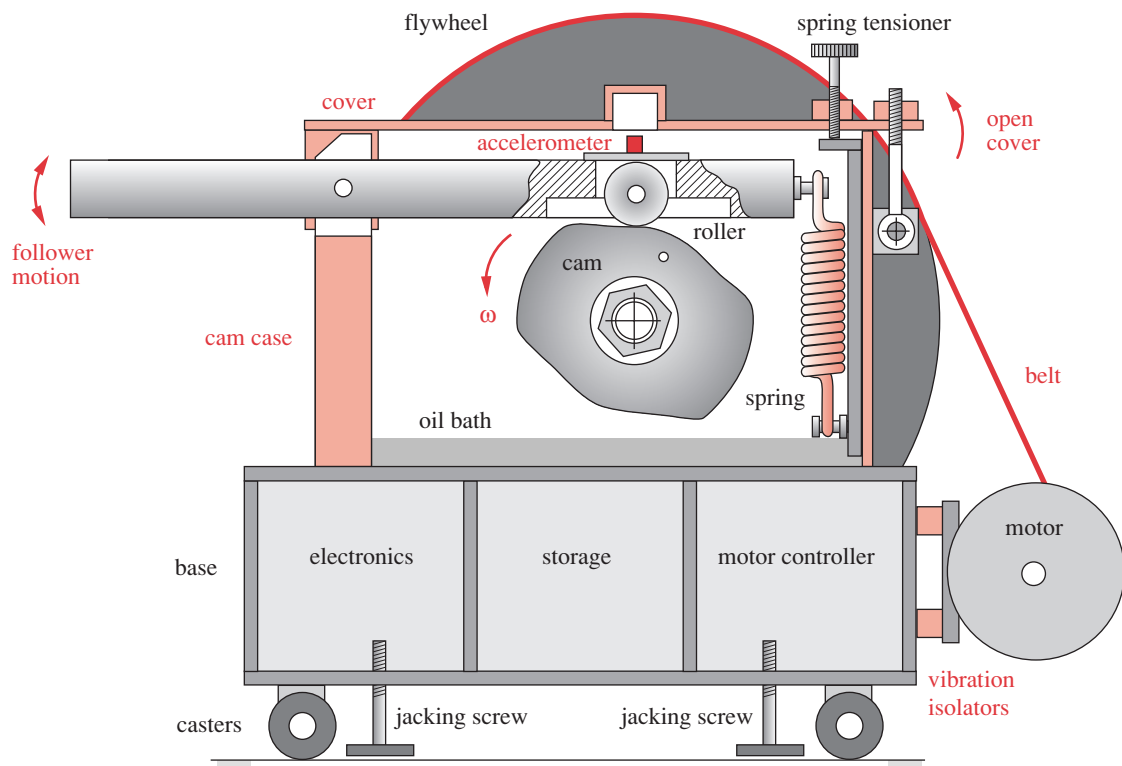


FIGURE 9-7

Four-Dwell Cam

**FIGURE 9-8**

Cam Dynamic Test Fixture—General Design Scheme

either on casters for mobility, or on jacking legs for stability. The motor is mounted to the base on rubber vibration isolators. The electronics for motor control and instrumentation are contained within the base.

- 6 The design of the cam itself along with its rotational velocity determines the magnitudes and shapes of the acceleration of the follower arm. This follower-acceleration function, generated from program DYNACAM,^[2] is shown in Figure 9-9. The acceleration function multiplied by the effective mass of the follower is one component of the dynamic force needed for stress calculations. The dynamic system of cam and follower can be modeled as a linearized, lumped-parameter, single-degree-of-freedom system as shown in Figure 9-10. The motion of the roller centerline on the rotating follower arm is actually along an arc, but that arc is quite flat in this design due to the length of the arm's radius. The error in assuming the roller's motion to be linear over its short excursion is minimal. A portion of the moving follower mass is then considered to be lumped at the roller so as to be dynamically equivalent. From Newton's second law, the differential equation for the lumped system in Figure 9-10 is^[3]

$$\sum F = ma$$

$$F(t) - F_d - F_s = m\ddot{y}$$

where $F_d = c\dot{y}$, $F_s = ky + F_{pl}$

and

$$F(t) = m\ddot{y} + c\dot{y} + (ky + F_{pl}) \quad (a)$$

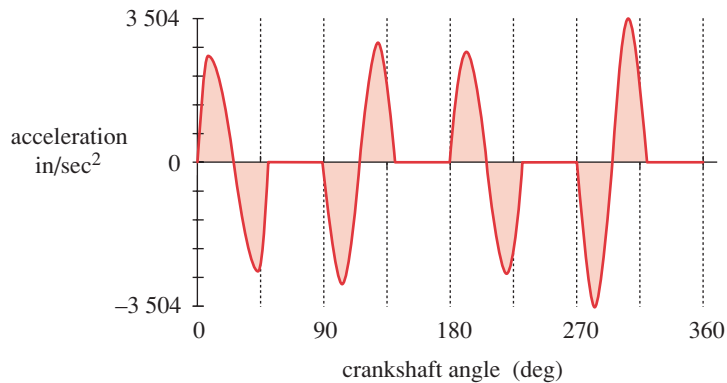


FIGURE 9-9

Acceleration Function for Cam Over 1 Cycle

The spring force F_s has two components. The spring constant k times the deflection y is added to whatever initial force F_{pl} was created by preloading the spring at installation. The damping force F_d is proportional to velocity by a damping coefficient c .

- 7 Equation (a) can be solved kinematically in this case, since we are maintaining a constant angular velocity and the displacement (y), velocity (\dot{y}), and acceleration (\ddot{y}) are defined functions of time. The value of m will depend on our design of the follower arm and anything attached to it as moving mass, such as the roller. The value of the damping factor c is sometimes difficult to predict, and the usual way to estimate its value is to define an expected damping ratio ζ for the type of system and calculate damping from

$$c = 2\zeta m \omega_n$$

where $\omega_n = \sqrt{\frac{k}{m}}$ (b)

Koster^[4] found that a typical value of ζ for cam-follower systems is about 0.06. The term ω_n is the undamped natural frequency of the system.

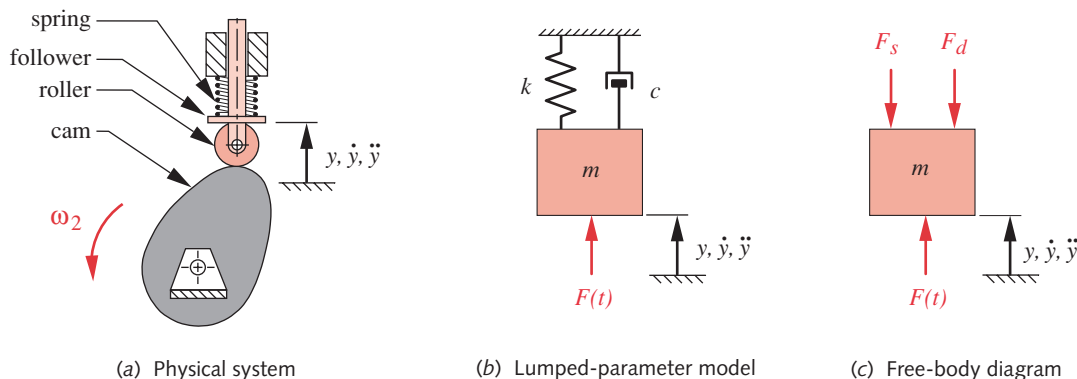
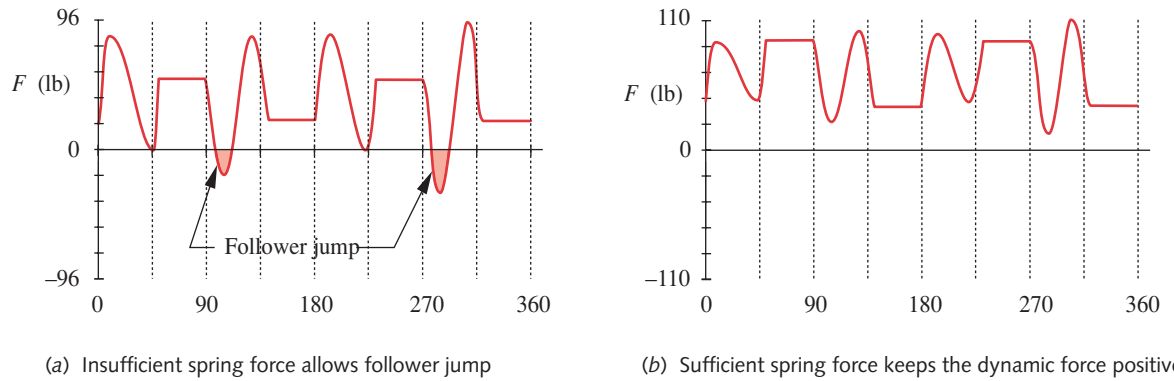


FIGURE 9-10

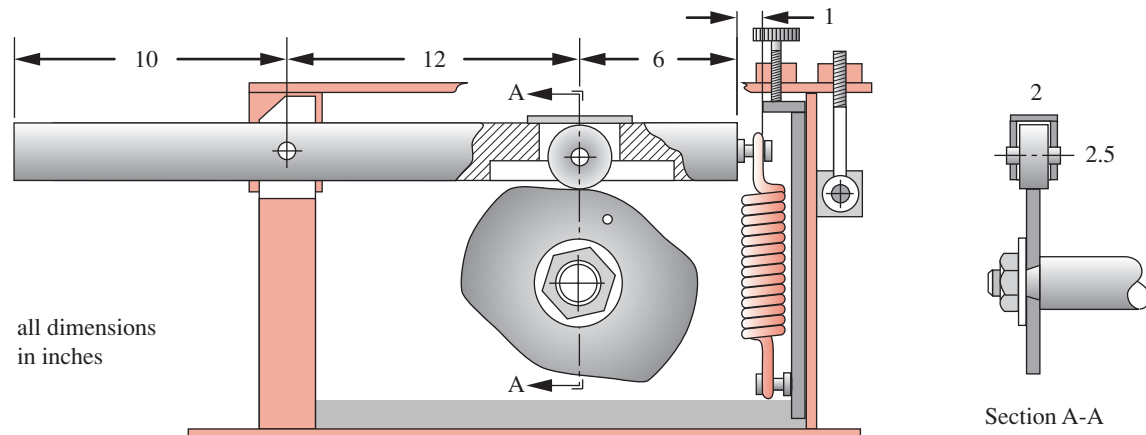
Linearized Cam-Follower System

**FIGURE 9-11**

Dynamic Force Between Cam and Cam Follower

The value of the spring constant k is under the control of the designer as is the amount of spring preload F_{pl} . We will later design a suitable spring for this system that will provide appropriate values for these variables. Note that we cannot numerically calculate the dynamic load on the system until we have preliminary designs of the moving parts in order to define their masses. At that point we can define a desired spring k and F_{pl} and then try to design a viable spring that delivers those values.

- 8 For a given mass, damping ratio, and acceleration function, the choice of k and F_{pl} determines whether the follower will jump off the cam during the fall. Figure 9-11a shows the effect on the dynamic force $F(t)$ of a too-small combination of k and F_{pl} . The shaded areas highlight portions where the dynamic force is negative. A cam-follower joint cannot deliver a negative (tension) force any more than the rope of the previous case study could support a compressive force. Thus the spring constant and preload must be increased in some combination until the dynamic-force function remains positive throughout the cycle, as shown in Figure 9-11b.
- 9 For this case study we will define the follower-arm geometry as shown in Figure 9-12. It is a solid 2 in \times 2.5 in rectangular cross section of aluminum, relieved internally

**FIGURE 9-12**

Dimensions of Cam Follower Arm

around the follower for clearance. The distance from pivot to roller follower is 12 in with a 10 in extension beyond the pivot for balance. It extends 6 in beyond the roller follower to attach the spring. The effective mass of the follower arm reflected to the roller centerline, plus the mass of roller and its pivot, is 0.02 lb-sec²/in. Using this value of effective mass and applying a spring constant at the end of the arm of $k = 25$ lb/in and a spring preload $F_{pl} = 25$ lb (which translates to effective values of $k = 56.25$ and $F_{pl} = 37.5$ lb at the follower) we achieve the dynamic force function shown in Figure 9-11b. The peak dynamic force is 110 lb and the minimum force is 13 lb **at the cam follower**. The deflection at the spring is 1.5 in.

- 10 The camshaft torque can be found from^[5]

$$T(t) = \frac{F(t)\dot{\gamma}}{\omega} \quad (c)$$

This torque function for the values assumed above is shown in Figure 9-13. The maximum torque is 176 in-lb and the minimum torque is -204 in-lb. The average torque is 7 lb-in.

- 11 The flywheel is 24-in-dia and 1.88-in-thick solid steel. Its mass moment of inertia is $I = 44$ blob-in². The coefficient of fluctuation C_f for this flywheel is found by integrating the torque-time function of Figure 9-13, pulse by pulse, to find the maximum energy oscillation E over one cycle. That integration was done numerically with program DYNACAM^[2] and gives $E = 3\,980$ in-lb of energy over one cycle. The coefficient of fluctuation is then^[6]

$$C_f = \frac{E}{I \omega^2} = \frac{3\,980}{44(18.85)^2} = 0.25 \quad (d)$$

Despite the relatively large size and weight (220 lb) of this flywheel, it gives only a 75% reduction in peak torque because its angular velocity is so low. Flywheels need either high speed or very large mass to be effective. The maximum torque with this flywheel is reduced to 47 in-lb and the minimum torque is now -48 in-lb. The average torque is unchanged at 7 lb-in. The shape of the torque function is the same as Figure 9-13 with these reduced peak values.

- 12 The average power required is very low (about 0.02 hp), but it is necessary to size the motor to handle the peak torque in order to maintain the constant speed required. Using

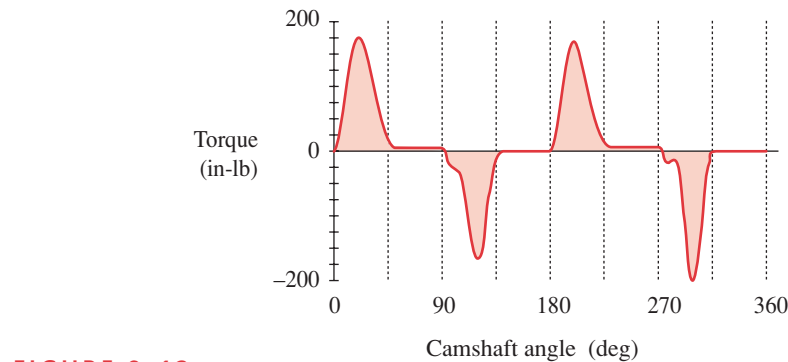


FIGURE 9-13

Camshaft Torque Without Flywheel

the peak torque value with the flywheel and the camshaft operating speed gives a minimum power level of

$$P_{peak} = T_{peak} \omega = 47 \text{ lb-in} \left(18.9 \frac{\text{rad}}{\text{sec}} \right) = 888 \frac{\text{in-lb}}{\text{sec}} = 74 \frac{\text{ft-lb}}{\text{sec}} = 0.14 \text{ hp} \quad (e)$$

Since frictional losses were only crudely estimated in this case and other cams will operate at higher speeds, a 1/2-hp speed-controlled DC motor was selected to drive the camshaft. This uses 110-V AC power to the motor's rectifier/speed controller.

- 13 We need to select a speed ratio for the belt drive from motor to flywheel. Since the motor is speed-controlled over an operating range of 0–1800 rpm, we can afford to allow a broader range of operating speeds than dictated by this particular cam, which needs 180 rpm. A range of 0–400 rpm is reasonable, since that will put the motor in the middle of its speed range for this cam and allow other cams to be run either faster or slower. The drive-pulley diameter is then

$$d_{in} = d_{out} \frac{\omega_{out}}{\omega_{in}} = 24 \frac{400}{1800} = 5.33 \text{ in} \quad (f)$$

- 14 Files for this case study are on the CD-ROM and are named CASE10.

Many details remain to be worked out to create a finished design, but these preliminary calculations indicate that the proposed design is feasible. For more detailed information on the modeling of the cam dynamics in this case study, see Chapters 8 and 15 of reference 1. Later chapters of this text will continue the study of various aspects of this case as they relate to subsequent topics such as bearing and spring design.

9

9.4 SUMMARY

This chapter has presented preliminary design calculations for some case studies of relatively simple machines. The intent is to incorporate further study of these cases in subsequent chapters that will deal with the design of elements common to a wide variety of machinery. Space will not permit a complete treatment of all the design details involved in any one of these case studies but it is hoped that their presentation will provide some insight into the way design must integrate a wide variety of often conflicting requirements to obtain a working product.

A number of open-ended design projects are also listed at the end of this chapter. These can be used as term-long project assignments for individual or group effort. Or, subsets of the suggested design projects can serve as multiweek design assignments.

9.5 REFERENCES

- 1 R. L. Norton, *Design of Machinery*, 3ed. McGraw-Hill: New York, pp. 645-661, 2004.
- 2 *Ibid.*, pp. 794-808.
- 3 *Ibid.*, pp. 742-743.
- 4 M. P. Koster, *Vibrations of Cam Mechanisms*. Macmillan: London, 1974.

5 R. L. Norton, *Design of Machinery*, 3ed. McGraw-Hill: New York, p. 750, 2004.

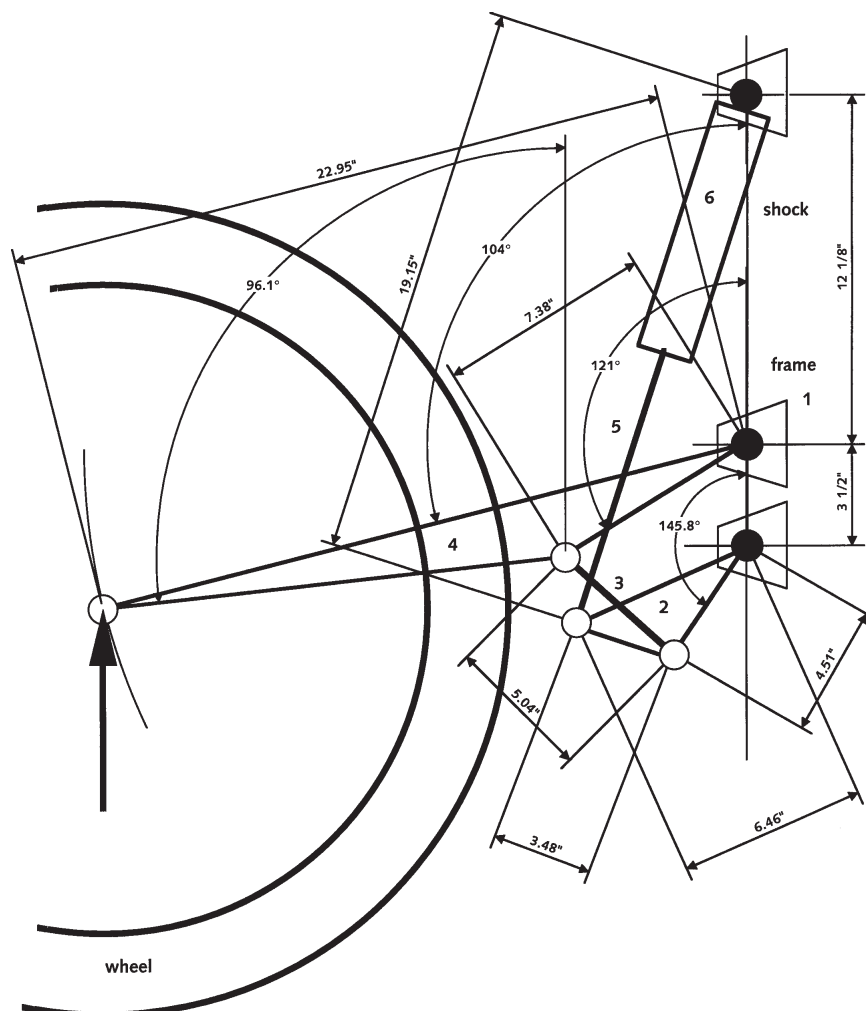
6 *Ibid.*, p. 591.

9.6 DESIGN PROJECTS

These large-scale problems are deliberately unstructured and are typical of real engineering design problems. In fact, most of them are real problems. They then have many valid solutions. While some of these project problems were “invented” for this chapter, most come either from the author’s consulting experience or from senior projects assigned to and completed by his students at Worcester Polytechnic Institute. In the latter cases, the projects were typically done by a team of 2-4 students over a three- or four-term period (21–28 weeks) and often resulted in a working prototype of the solution. The versions of such senior projects stated here have been simplified or truncated with the intention that they be tractable for solution by a team of students over a one-term course. The consulting problems have also been abridged to suit the structure and time available in a typical junior or senior design course. Some of the projects listed here have been used successfully by the author as term-long projects in the course for which this text is intended.

- 9-1 Complete the design of the portable air compressor in Case Study 8A. Note that some parts of this design are addressed in later chapters.
- 9-2 Complete the design of the winch lift in Case Study 9A. Note that some parts of this design are addressed in later chapters.
- 9-3 Complete the design of the cam-testing machine in Case Study 10A. Note that some parts of this design are addressed in later chapters.
- 9-4 Case Studies 5A and 5B in Chapter 3 describe the design of a fourbar linkage demonstrator machine. Complete its detailed design based on the information given in those case studies. Some aspects not addressed therein are the size of the gear train to reduce the motor speed, the bearings, torque coupling, flywheel, and stresses.
- 9-5 Design a safer log splitter with the following characteristics:
- Able to be towed at highway speeds behind a full-size pickup truck.
 - An 8-hp gasoline engine drives a two-stage hydraulic pump that in turn pressurizes a hydraulic cylinder to split the log.
 - Accommodates a 2-ft-long log.
 - Generates 15 tons of force on the log against a stationary splitting wedge.
 - Has a safety cage that covers the log/wedge/cylinder area during splitting to prevent injury to the operator. This cage slides (manually) out of the way to load/unload logs and is interlocked such that it must be in place before the hydraulic cylinder will move.
- 9-6 Design an inspection capsule to be lowered into an oil well to a depth of 5 000 ft. The capsule must fit in a 6-in-dia hole with at least 10% diametral clearance, have a suitable attachment for the lowering cable, and a 1.5-in-dia quartz lens port in the sidewall. A 0.5-in-dia power and communications cable passes through the top end of the cylinder. Some design concerns are the hydrostatic pressure at that depth, the abrasive nature of the rock walls of the well hole, and the hydraulic integrity of the seals around the lens port and power cable. The capsule has a dry nitrogen atmosphere inside at 800 psig. Design for a finite life of at least $1E4$ insertions/removals from a well.

- 9-7 Design a battery-powered, motorized shopping cart capable of carrying a 200-lb person plus 50 lb of groceries around the aisles of a supermarket. It should hold at least half the volume of foodstuffs of a conventional, manual shopping cart, be speed limited, safe against tipover, and require constant pressure on its control to run (i.e., a “dead-man” switch). When the power is cut, an automatic brake should stop it within 1 ft. Intended users are elderly or infirm shoppers. It should run for 1 hour between recharges.
- 9-8 Figure P9-1 shows the geometry and dimensions of a popular off-road motorcycle rear suspension system. The wheel is carried at the end of link 4, which is part of the fourbar linkage 1-2-3-4, where 1 is the frame of the cycle, 2 is the triangular rocker, and 3 is a binary coupler connecting 2 to 4. The shock strut 5 is pivoted to link 2 and slides into the shock cylinder 6. The shock cylinder 6 is pivoted to the frame 1. The total vertical travel of the rear axle is about 12 in.



9

FIGURE P9-1

Geometry of an Off-Road Motorcycle Rear-Wheel Suspension System

Figure P9-2 shows the result of a dynamic simulation of a 250-lb motorcycle, with a 200-lb rider, traveling at 18 mph, jumping 3 ft vertically and landing on the rear wheel.* The graphs in Figure P9-2 show the resulting dynamic force at the rear axle and at the pivot of link 4. Design the rear suspension system based on the given loading and geometry data. Some design concerns are the shock strut as a column, the pivot pins in shear, and the links in bending plus tension or compression in some instances. It will be of value to inspect a similar motorcycle suspension system to obtain additional information on its general design.

* This simulation was done using the software package *Working Model* by Knowledge Revolution.

- 9-9 Off-road motorcycles typically have chain-and-sprocket drives from the transmission output shaft to the rear wheel. Some road bikes use enclosed transmission

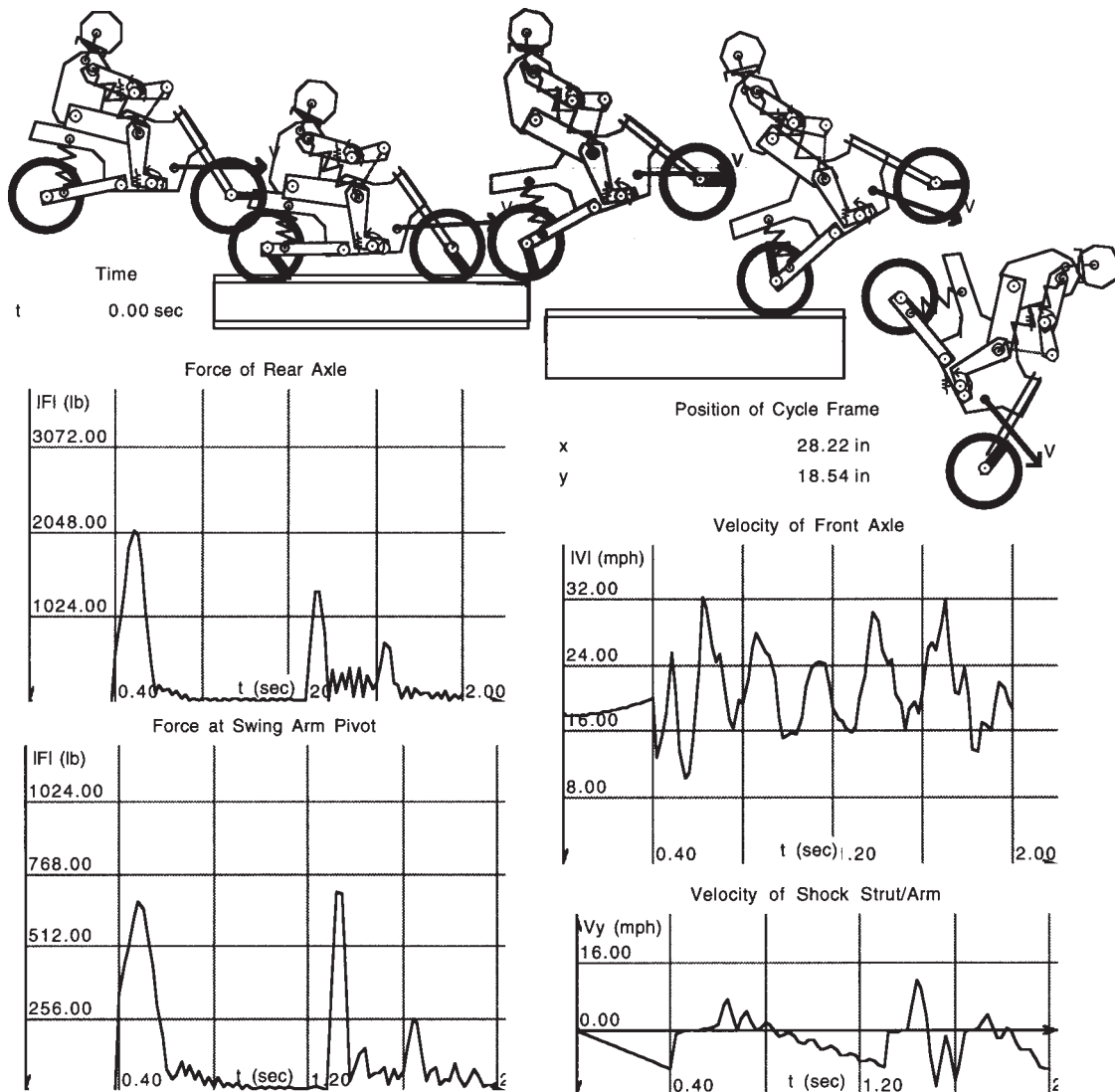


FIGURE P9-2

Simulation of Forces Generated by a Motorcycle Jumping and Landing on Its Rear Wheel

shafts and gear drives instead of a chain and sprockets. The advantage of chain drives is light weight, but exposure to the dust and mud of off-road riding reduces their reliability. Enclosed shaft drives are protected from the elements. Design a lightweight shaft-drive system for the off-road motorcycle of Figures P9-1 and P9-2. Assume an engine of 60 hp at 9 000 rpm. Low gear in the transmission has a ratio of 1:4, and the final drive ratio from transmission output shaft to rear wheel should be approximately 1:3.5. At least one universal joint will be needed in the driveshaft to accommodate the suspension motion. Some combination of spur (or helical) and bevel gears will be needed. Suitable bearings, housings, and seals should be specified. It will be of value to inspect a similar motorcycle shaft-drive system to obtain additional information on its general design.

- 9-10 The Army wants a machine to test combat boots for durability. This machine should mimic, as closely as possible, the geometry and forces of a typical soldier walking in combat boots as shown in Figure P9-3. It should repeat this motion for an unlimited number of cycles until the boot leather breaks down. The single boot will be fitted to a prosthetic foot that is attached to the test machine. Design it for infinite life.

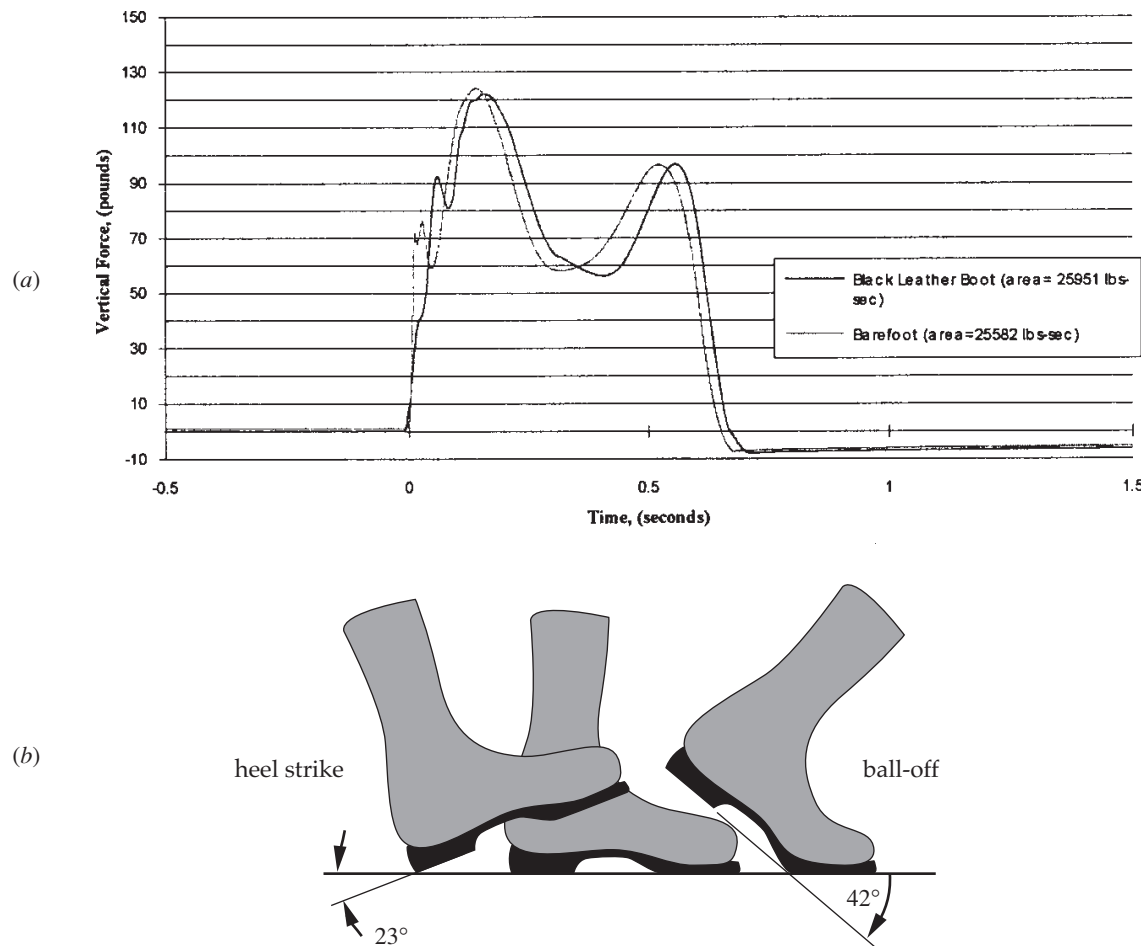
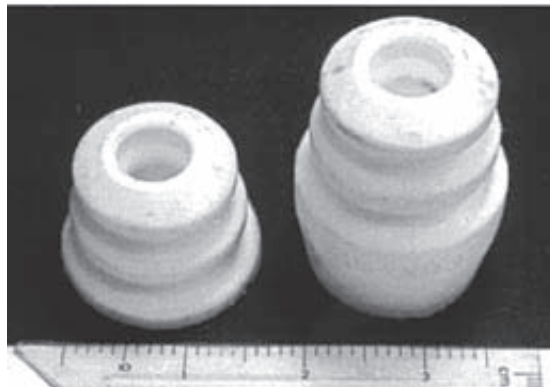


FIGURE P9-3
Typical Walking Forces (a) and Geometry (b)

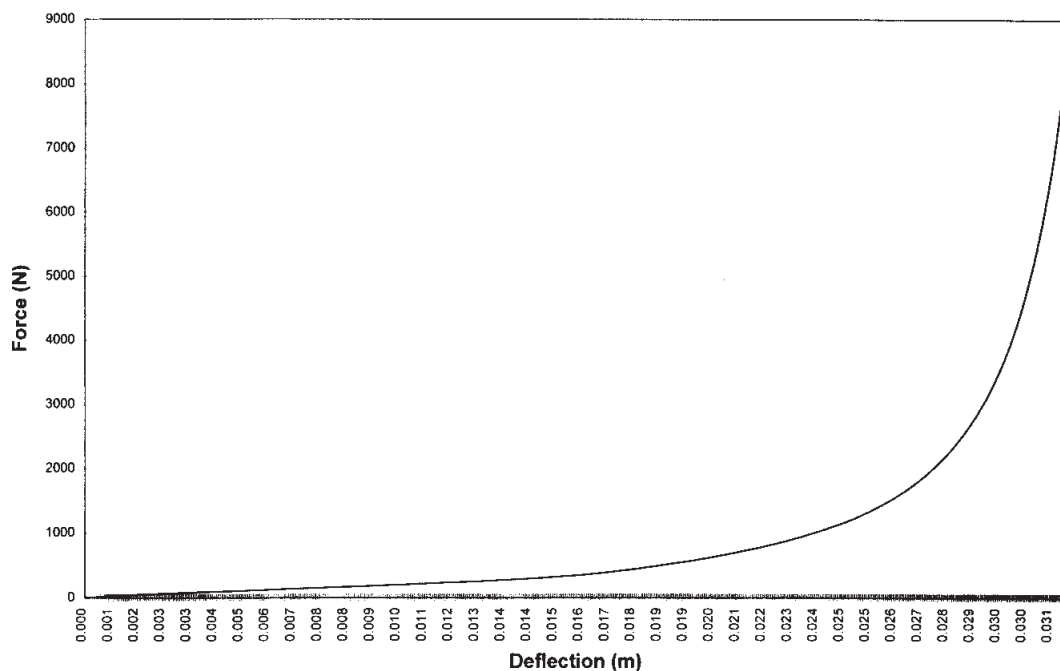
**FIGURE P9-4**

Two Sizes of Urethane Jounce Bumpers for Use in Automotive Suspension Systems

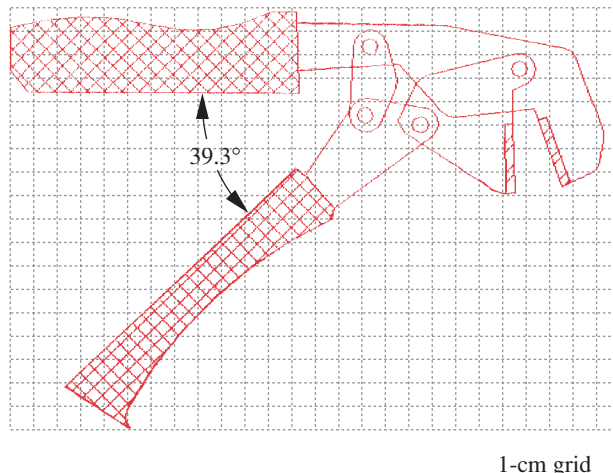
- 9-11 A company that manufactures molded urethane jounce bumpers, as shown in Figure P9-4, wants a test machine that will repeatedly impact these bumpers to determine their durability. The static force-deflection characteristic of one size bumper is shown in Figure P9-5. The suggested concept is a drop weight that will impact the bumper. A resetting mechanism to lift and repeatedly drop the weight is required. A dynamic analysis should be done to determine the size and height of weight needed to fully compress the specified bumper.

9

**Static Force vs. Deflection Curve
Small Jounce Bumper**

**FIGURE P9-5**

Static Force-Deflection Curve for One Size of Urethane Jounce Bumper



1-cm grid

FIGURE P9-6

Crimping Tool Geometry

- 9-12 The crimping tool shown in Figure P9-6 is used to crimp (yield) metal connectors onto wire. The wire is inserted into the connector (not shown), the pair then put into the crimping tool's jaws and the handles squeezed. Case Study 2 analyzed the forces, stresses, and safety factors for a similar tool of slightly different design. Figure P9-7 shows a table of data measured from the tool in Figure P9-6 while crimping the largest wire. The forces required at the handle are quite large. The

9

Angle Between Handles, Deg.	Torque, lb _f -in	Distance Between Handles, in	Force, lb _f
39.3	0	2.89	0
24.4	49.17	1.89	11.84
22.3	73.27	1.74	17.36
20.9	97.53	1.63	22.89
19.7	122.01	1.54	28.42
18.7	146.62	1.46	33.95
17.8	171.38	1.40	39.47
16.5	220.91	1.30	50.52
15.1	271.10	1.19	61.57
13.7	321.77	1.08	72.63
12.6	372.41	1.00	83.68
11.2	423.77	0.89	94.73
9.5	475.78	0.75	105.79
8.0	502.66	0.64	111.32
7.6	528.12	0.60	116.84
5.5	580.52	0.43	127.89
4.8	606.27	0.39	133.42
0.8	653.34	0.06	143.29

FIGURE P9-7

Crimping Tool Force and Torque-Displacement Data

distances between handles are measured at a 4.56-in radius. Repeated manual use of such a tool at these force levels frequently leads to physical problems such as carpal-tunnel syndrome. The manufacturer would like a device that will mechanically create the required force on the handles of this existing crimp tool to eliminate manual use and avoid such injuries. Some of the constraints placed on this device are as follows:

- (a) No larger than 12 in \times 4 in \times 6 in.
- (b) Self-contained, including a portable energy supply.
- (c) Weigh less than 10 lb.
- (d) Require only one- or two-hand operation by one person.
- (e) Perform a crimp in less than 10 sec.
- (f) Accommodate maximum handle angle of 40° and handle splay of 7 in.

- 9-13 A motorized, roll-around stand for a portable X-ray machine is needed as shown in Figure 9-8. The X-ray head weighs 65 lb and is 10 in \times 8 in \times 16 in high. The head must be motor-adjusted over a vertical range from 41 in to 82 in measured from the floor to the 18-in-long cantilevered arm from which the X-ray head is suspended. The head must traverse its maximum vertical travel in 20 sec or less and stop within 0.5 in of a desired location. Limit switches must automatically shut off the motor at each end of the head's vertical travel. The stand must be able to pass through a standard 3-ft \times 7-ft interior hospital door and operate from a 15-A, 110-V AC circuit. Certain Underwriters Laboratories (UL) specifications also must be met such as:

9

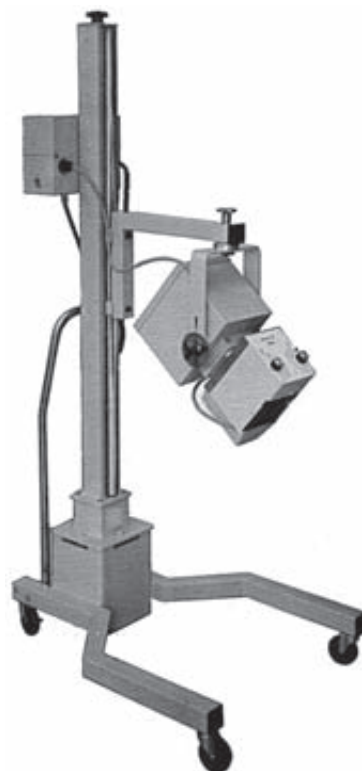


FIGURE P9-8

Motorized, Portable, Roll-Around X-ray Stand

- UL 27.4-A — must not tip on a 10° incline with the head in the lowest position.
 - UL 27.4-B — must not tip on a 5° incline with the head in the highest position.
 - UL 27.4-C — must not tip on a 0° incline when a horizontal force of 25% of its weight is applied at the transport handle.
- 9-14 Design a dumping-bed attachment to retrofit an existing full-size pickup truck. This device should require minimal modification of the truck and be capable of remote activation from the cab. It should lift and dump up to 3/4 ton of cargo. It will take its power from the truck engine and can be electrically, mechanically, or hydraulically driven, or any combination thereof.
- 9-15 Design a wheelchair lift device to operate in a residential garage. The garage floor is 1 m below the main floor of the house. The device should safely raise or lower the wheelchair and its 100-kg occupant through that vertical distance.
- 9-16 Design a device to transfer a 100-kg paraplegic patient safely from bed to wheelchair and vice versa. The patient has good upper body strength but no control of the lower extremities. Your design should be operable by the patient with minimal assistance. Safety is of paramount concern.
- 9-17 Design an indoor bicycle exerciser similar in concept to the wheelchair exerciser shown in Problem 6-48. The concept is to provide twin rollers to support the rear wheel and a single roller for the front wheel. The rear rollers will be attached in some kinematic fashion (to be designed) to a DC generator whose output is shunted through an electrical load that can be varied by the rider to provide a dynamometric resistance. Design all parts with suitable geometries and materials for infinite life.
- 9-18 Design a service stand for an off-road motorcycle that will allow the bike to be suspended at a convenient working height and rotated to allow access to all serviceable systems. Stability in all rotated positions, and with various states of partial disassembly, is of paramount importance.
- 9-19 Fluorescent light bulbs must be coated inside with tin oxide while hot. The 46-in-long, straight glass tubes are carried through a baking oven on a metal chain conveyor that travels at a constant velocity of 5 500 bulbs per hour. The bulbs are spaced 2 in apart on the chain. As they exit the oven at 550°C , a mechanism carrying two spray heads chases a pair of bulbs, accelerates to match their constant velocity, travels with them for a short distance, and sprays the tin oxide into the hot bulbs within 3/4 sec. The two spray heads mount on a 6 in \times 10 in rectangular table that is carried on linear bearings. The spray equipment bolted to the table weighs 10 lb. All elements exposed to the tin-oxide spray must be stainless steel to resist chemical attack from the hydrochloric acid by-product in the spray.

A cam drives the table to match the conveyor velocity and returns it in time to accelerate and catch the next two bulbs. A plate cam has been designed to accomplish this action and it is defined in the file SPRAY.CAM supplied on disk with this text. This disk file can be input to the program DYNACAM (also supplied on disk) to obtain the necessary dynamic data for the required design. The cam is driven from the conveyor sprocket that has an 8.931-in pitch dia.

What is required is a detailed design of the spray table, its bearings and mounting hardware for infinite life. The dynamic loads on the cam and follower will be highly dependent on the mass of this moving assembly. Once an estimate of the moving mass is available from your preliminary design, program DYNACAM can be used to quickly calculate the dynamic forces at the cam-follower interface. The stresses in the various parts of the assembly can then be estimated based on the level of dynamic forces present. See reference 2 for information on using program DYNACAM.

- 9-20 In line-shaft driven production machinery, torsional deflections and vibrations of the camshaft due to the time-varying torque of the various cams can cause synchronization problems between the various stations on the machine. We need to design a testing machine that will measure the torsional vibration effects of dynamic torque loading on a camshaft. This machine will accommodate two cams, each of which will drive its own spring-loaded translating roller follower on a slider mechanism at speeds up to 300 rpm.

These cams will be designed to give approximately opposite torque-time functions to one another. They can then be used singly or in pairs to investigate the effectiveness of the addition to a production machine of a torque-balancing cam that drives a dummy load. The cams will be split to allow removal and installation without disassembling the shaft. The torque-time and follower-force-time functions for the primary cam are provided as an Excel file P09-20 on the CD-ROM. The secondary cam will be a mirror image of the primary cam to approximately balance the torque.

The camshaft in this test fixture must be designed to have torsional deflections that are large enough to be measured by 5 000-count-per-revolution, optical shaft encoders attached at each end of the camshaft, but not so large as to fatigue-fail the shaft. At the same time, we want the camshaft to be stiff in bending and have a bending natural frequency at least 10 times its torsional natural frequency to minimize any coupling effects between bending and torsional modes. Stated another way: what should the shaft diameter be to give sufficient torsional deflections to be measurable under the designed loading conditions, but not to create undesirable bending deflections or vibrations?

Plain bearings should be used to avoid vibrations that would come from rolling-element bearings. The test machine will be driven by a speed-controlled PM DC motor through a gear-reduction unit of your design. Motor selection is also your responsibility.

What is required is a detailed design of a camshaft torsional vibration test machine including the camshaft, keys, follower trains, bearings, couplings, gearbox, frame, and mounting hardware. Infinite life is desired.

- 9-21 Our client (a Fortune 500 company) manufactures consumer products in very high quantities. These products contain molded plastic parts and assemblies, some of which are made in "two-shot" injection molding machines. A two-shot part requires a rotating die and two sets of cavities per part in that die. The first portion of the finished part is molded of material A with the die in position 1. The die is then opened and one half is rotated 180 degrees to position 2 with the molded part still in its cavity. The die closes again, placing portion I of the part against the second cavity. Material B is then injected into portion I, creating portion II of the part. The die opens again and the finished assembly is ejected.

Our task is to design the die-rotating mechanism to be fastened into the molding machine and to which any number of different dies can be bolted. The largest die to be accommodated is 910 mm high by 790 mm wide by 326 mm long along its horizontal axis of rotation. Assume the die to be a block of solid steel. The die will bolt to a round turntable of your design that is driven by a servomotor to accomplish the required rotation. It must rotate 180 degrees in 0.8 sec. It will then remain stationary for a variable length of time (0.5 to 2 sec, depending on the molding cycle of the part) after which it will again rotate 180 degrees in 0.8 sec. The cycle will then repeat. The molding machine will operate 24 hours a day, 7 days a week, 50 weeks a year. No failure of this mechanism is allowed for a period of at least 10 years.

When the die is hung on the turntable it must not deflect more than 0.001 inch (0.025 mm) in either the vertical or axial directions at any point on the die face. Vibrations of the die should be minimized on stopping to avoid delays in mold closing. The length of the assembly in the axial direction should be kept as short as is practical. The opening/closing motion of the die will be a maximum of 25 mm. A hydraulic cylinder will provide the axial motion.

The rotation will be driven by a servomotor through a gear-reduction unit of your design. Either plain or rolling-element bearings may be used. Motor torque/power specification is also your responsibility, as is specification of the size and power needed from the hydraulic cylinder to obtain the axial motion in the time specified. The dynamic torque will depend on the mass moment of inertia of the system and the assumed acceleration profile applied to the servomotor by its controller. Assume a reasonable acceleration profile based on good cam design practice.

What is required is a detailed design of a mold rotation machine including the turntable, shaft, keys, gear train, bearings, couplings, frame, and mounting hardware (fasteners).

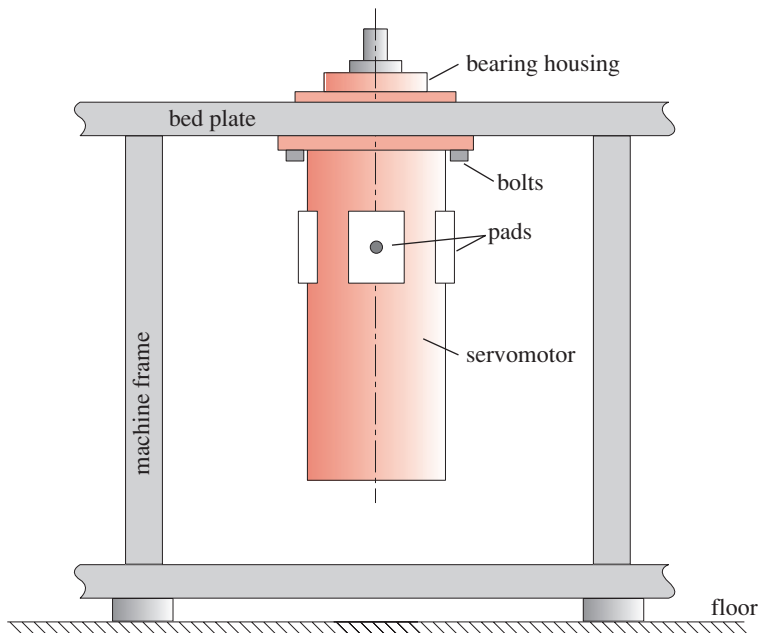
- 9-22 A motorized and instrumented gear-train test bed is needed to be used for demonstration and experimentation. The envisioned device will consist of an electric-motor-driven gear set which is in turn loaded by a brake. Faults will be deliberately introduced to the gear teeth in order to produce measurable vibrations. The device will be instrumented and an attempt made to detect and diagnose the faults from the measured vibration data.

Design a device that needs no more than 1 hp of input power and is no larger than a 3-ft cube. A single gearset of 1:2 ratio should be supported in sleeve bearings and driven by a speed-controlled electric motor that is vibration isolated from the gearset.

- 9-23 A motorized and instrumented rolling-element (ball) bearing test bed is needed to be used for demonstration and experimentation. The envisioned device will consist of an electric motor-driven shaft which is in turn loaded by a brake. Faults will be deliberately introduced to the ball bearings in order to produce measurable vibrations. The device will be instrumented and an attempt made to detect and diagnose the faults from the measured data.

Design a device that needs no more than 1 hp of input power and is no larger than a 3-ft cube. A single ball bearing of convenient size will be used. All other bearings must be sleeve bearings to avoid introducing spurious noise. The device will be driven by a speed-controlled electric motor that is vibration isolated from the bearing shaft.

- 9-24 A company that manufactures razors needs to test them for damage after dropping from a 1.5 m height onto a hard surface such as a tiled bathroom floor. The razor including head and handle weighs 20 g. When the razor is dropped it lands in a random orientation. Some orientations do more damage than others. It is difficult to repeat an experiment when manually dropping them onto the floor. They would like a machine that simulates the drop of the actual razor onto a hard surface from the 1.5-m height but which will allow the orientation of the razor at impact to be the same for each test. This must be accomplished without constraining the razor excessively in order to duplicate as closely as possible the “free-free” boundary conditions of a falling razor at impact. The impact orientation must however be adjustable to simulate different impact orientations. Adjustment through ± 40 degrees around each axis will be sufficient. Design an apparatus that will impart the same impact energy to the razor as it experiences in an actual fall, and which allows it to bounce off the impact surface but strikes it only once. This apparatus must allow the impact event to be filmed with a high speed video camera.

**FIGURE P9-9**

Servomotor Installation

9

- 9-25 A machine uses a number of large servomotors that bolt up under the bed plate of the machine as shown in Figure P9-9. The underside of the bed plate is 30 inches from the floor and the motors are 24-in-long with a 2-in-long shaft protruding from the top. The motors weigh 300 lb and are 12-in diameter. Design a mechanism that can transport a motor from the stockroom to the machine across a flat factory floor, place the motor under the machine's bed plate, lift it into place, and hold it in position while a mechanic bolts it in. The motor has a 6-in-diameter pilot flange that must enter a hole in the bed plate and a dowel pin that also enters a hole in the bed plate. There is 0.002-in clearance between the flange and hole and 0.001-in clearance between dowel pin and hole, so the motor must be aligned accurately with the holes when it is lifted into position by your mechanism. The motor has 4 pads with tapped holes at its CG that can be used to attach the motor to your mechanism.

10

SHAFTS, KEYS, AND COUPLINGS



The greater our knowledge increases, the greater our ignorance unfolds.

JOHN F. KENNEDY

10.0 INTRODUCTION

Transmission shafts, or just shafts, are used in virtually every piece of rotating machinery to transmit rotary motion and torque from one location to another. Thus, the machine designer is often faced with the task of designing shafts. This chapter will explore some of the common problems encountered in that endeavor. Table 10-0 shows the variables used in this chapter and notes the equations or sections in which they occur.

At a minimum, a shaft typically transmits torque from the driving device (motor, or engine) through the machine. Sometimes shafts will carry gears, sheaves (pulleys), or sprockets, which transmit the rotary motion via mating gears, belts, or chains from shaft to shaft. The shaft may be an integral part of the driver, such as a motor shaft or engine crankshaft, or it may be a freestanding shaft connected to its neighbor by a coupling of some design. Automated production machinery often has line shafts that extend the length of the machine (10 m or more) and carry the power to all the workstations. Shafts are carried in bearings, in a simply supported (straddle-mounted) configuration, cantilevered, or overhung, depending on the machine configuration. The pros and cons of these mounting and coupling arrangements will also be discussed.

10.1 SHAFT LOADS

The loading on rotating transmission shafts is principally one of two types: torsion due to the transmitted torque or bending from transverse loads at gears, sheaves, and sprockets. These loads often occur in combination, since, for example, the transmitted torque may be associated with forces at the teeth of gears or sprockets attached to the shafts.

Table 10-0 Variables Used in This Chapter

Symbol	Variable	ips units	SI units	See
A	area	in ²	m ²	various
c	distance to outer fiber	in	m	Sect. 10.6
C_f	coefficient of fluctuation	none	none	Eq. 10.19
d	diameter	in	m	various
e	eccentricity of a shaft or disk	in	m	Eq. 10.26
E	Young's modulus	psi	Pa	various
E_k, E_p	kinetic energy, potential energy	in-lb	joule	Eq. 10.25
F	force or load	lb	N	various
F_l	fluctuation (in speed)	rad/sec	rad/sec	Eq. 10.19
f_n	natural frequency	Hz	Hz	Eq. 10.24
g	gravitational acceleration	in/sec ²	m/sec ²	Sect. 10.13, .14
G	shear modulus, modulus of rigidity	psi	Pa	various
I, J	2nd moment, polar 2nd moment of area	in ⁴	m ⁴	Sects. 10.6, .14
I_m, I_s	mass moment of inertia about axis	lb-in-sec ²	N-m-sec ²	Sect. 10.13
k	spring rate or spring constant	lb/in	N/m	Sect. 10.14
K_f, K_{fm}	fatigue stress-concentration factors	none	none	Sects. 10.6, .10
K_t, K_{ts}	geometric stress-concentration factors	none	none	Sect. 10.10
l	length	in	m	various
m	mass	lb-sec ² /in	kg	Sect. 10.13, .14
M	moment, moment function	lb-in	N-m	various
N_f	safety factor in fatigue	none	none	Eq. 10.5–10.8
N_y	safety factor in yielding	none	none	Ex. 10-7
P	power	hp	watts	Eq. 10.1
p	pressure	psi	N/m ²	Sect. 10.12
r	radius	in	m	various
S_e, S_f	corrected endurance limit, fatigue strength	psi	Pa	Eqs. 10.5–10.8
S_{ut}, S_y	ultimate tensile strength, yield strength	psi	Pa	Eqs. 10.5–10.8
T	torque	lb-in	N-m	Eq. 10.1
W	weight	lb	N	various
α	angular acceleration	rad/sec ²	rad/sec ²	Eq. 10.18
δ	deflection	in	m	various
ν	Poisson's ratio	none	none	various
θ	angular deflection or beam slope	rad	rad	various
γ	weight density	lb/in ³	N/m ³	Eq. 10.23
σ	normal stress (with various subscripts)	psi	Pa	various
σ'	von Mises stress (with various subscripts)	psi	Pa	various
τ	shear stress (with various subscripts)	psi	Pa	various
ω	angular velocity	rad/sec	rad/sec	Eq. 10.1
ω_n	natural frequency	rad/sec	rad/sec	Sect. 10.14
ζ	damping ratio	none	none	Sect. 10.14

The character of both the torque and bending loads may be either steady (constant) or may vary with time. Steady and time-varying torque and bending loads can also occur in any combination on the same shaft.

If the shaft is stationary (nonrotating) and the sheaves or gears rotate with respect to it (on bearings), then it becomes a statically loaded member as long as the applied loads are steady with time. However, such a nonrotating shaft is not a transmission shaft, since it is not transmitting any torque. It is merely an axle, or round beam, and can be designed as such. This chapter is concerned with rotating, transmission shafts and their design for fatigue loading.

Note that a rotating shaft subjected to a steady, transverse-bending load will experience a fully reversed stress state as shown in Figure 10-1a. Any one stress element on the shaft surface goes from tension to compression each cycle as the shaft turns. Thus, even for steady bending loads, a rotating shaft must be designed against fatigue failure. If either or both the torque and transverse loads vary with time, the fatigue loading becomes more complex, but the fatigue-design principles remain the same, as outlined in Chapter 6. The torque, for example, could be repeated or fluctuating as shown in Figures 10-1b and c, as could the bending loads.

We will deal primarily with the general case, which allows for the possibility of both steady and time-varying components in both bending and torsion loads. If either load lacks a steady or time-varying component in a given case, it will merely force a term in the general equations to zero and simplify the calculation.

10.2 ATTACHMENTS AND STRESS CONCENTRATIONS

While it is sometimes possible to design useful transmission shafts that have no changes in section diameter over their length, it is most common for shafts to have a number of steps or shoulders where the diameter changes to accommodate attached elements such as bearings, sprockets, gears, etc., as shown in Figure 10-2, which also shows a collection of features commonly used to attach or locate elements on a shaft. Steps or shoulders are necessary to provide accurate and consistent axial location of the attached elements as well as to create the proper diameter to fit standard parts such as bearings.

Keys, snap rings, or cross-pins are often used to secure attached elements to the shaft in order to transmit the required torque or to capture the part axially. Keys require a groove in both shaft and part and may need a setscrew to prevent axial motion. Snap rings groove the shaft, and cross-pins create a hole through the shaft. Each of these changes in contour will contribute some stress concentration and this must be accounted for in the fatigue-stress calculations for the shaft. Use generous radii where possible, and techniques such as those shown in Figures 4-37 (p. 191), 4-38 (p. 192), and 10-2 (at the sheave and snap ring) to reduce the effects of these stress concentrations.

Keys and pins can be avoided by using friction to attach elements (gears, sprockets) to a shaft. Many designs of **clamp collars** (keyless fits*) are available, which squeeze the outside diameter (*OD*) of the shaft with high compressive force to clamp something to it, as shown on the sprocket hub in Figure 10-2 and in Figure 10-34 (p. 605). The hub has a gently tapered bore, and a matching taper on this type of clamp collar is forced into the space between hub and shaft by tightening the bolts. Axial slits in the tapered portion of the collar allow it to change diameter and squeeze the shaft, creating sufficient friction to transmit the torque. Another type of clamp collar, called a **split collar**, uses a screw to close a radial slit and clamp the collar to the shaft. **Press and shrink fits** are also used for this purpose and will be discussed in a later section of this

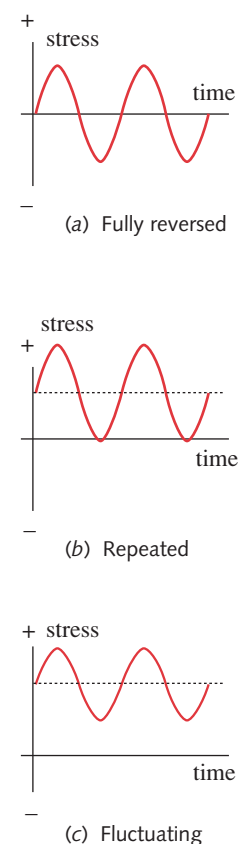
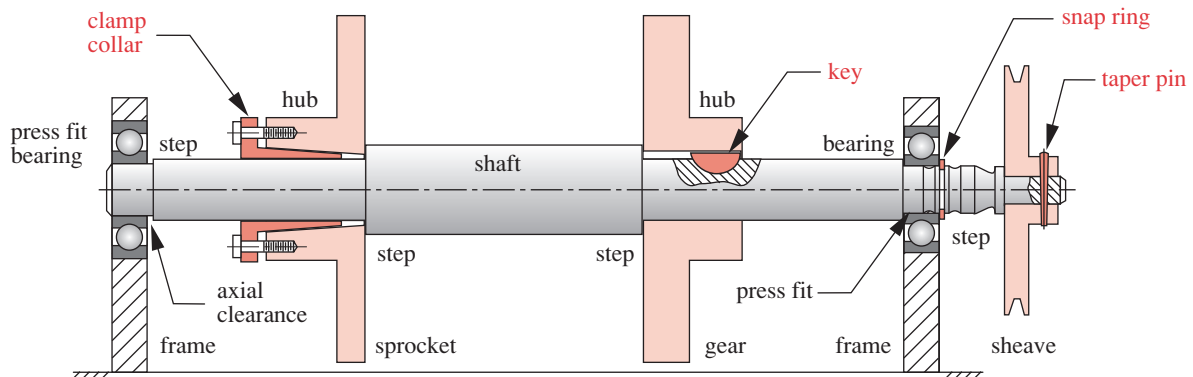


FIGURE 10-1
Time-Varying Stresses

* See the ANSI/AGMA Standard 9003-A91, *Flexible Couplings—Keyless Fits*.

**FIGURE 10-2**

Various Methods to Attach Rotating Elements to Shafts

chapter. However, as we will see, these friction couplings also create stress concentrations in the shaft and can cause fretting corrosion as described in Section 7-6 (p. 434).

A standard taper pin is sometimes used to couple elements to shafts as seen in the sheave of Figure 10-2. The hole is reamed to match the standardized pin-taper and the purchased pin is driven into place. The shallow taper locks it by friction. It must be driven out for disassembly. This technique should be used with caution in locations of large bending moment, as it weakens the shaft as well as creating stress concentration.

Rolling-element bearings as shown in Figure 10-2 are intended to have their inner and outer races be press-fitted to shaft and housing, respectively. This requires close-tolerance machining of the shaft diameter and requires a step shoulder to provide a stop for the press fit and for axial location. Thus, one must start with a larger stock shaft diameter than the bearing inside diameter (ID) and machine the shaft to fit the selected bearing whose sizes are standardized (and are metric). A snap ring is sometimes used to guarantee no axial movement of the shaft versus the bearing as shown at the sheave end of the shaft in Figure 10-2. Snap rings are commercially available in a variety of styles and require that a small, close-tolerance groove of specific dimension be machined in the shaft. Note in Figure 10-2 how the axial location of the shaft is achieved by capturing only one of the bearings (the right one) axially. The other bearing at the left-hand end has axial clearance between it and the step. This is to prevent axial stresses being generated by thermal expansion of the shaft between the two bearings.

So, it appears that we cannot escape the problems of stress concentration in practical machinery. In the case of shafts, we need to provide steps, snap rings, or other means to accurately locate components axially on the shaft, and we have to key, pin, or squeeze the shaft to transmit the torque.

Each of these methods of attachment has its own advantages and disadvantages. A key is simple to install and sizes are standardized to the shaft diameter. It provides accurate phasing* and is easily disassembled and repaired. It may have no resistance to axial movement and it does not always provide a truly tight torque coupling due to the slight clearance between key and keyway. Torque reversals can cause slight backlash.

* Phasing means the relative angular locations of the various elements attached to the shaft.

A taper pin creates a truly tight torque coupling and locates axially as well as radially with phasing but weakens the shaft. It can be disassembled with slightly more difficulty than a key. A clamp collar is easy to install but has no repeatable phasing. This is only a disadvantage if timing of the shaft rotation to other shafts in the system is required. It allows easy (though inaccurate) adjustment of phasing if desired. Press fits are semipermanent connections that require special equipment to disassemble. They do not provide repeatable phasing.

10.3 SHAFT MATERIALS

In order to minimize deflections, steel is the logical choice for a shaft material because of its high modulus of elasticity, though cast or nodular iron is sometimes also used, especially if gears or other attachments are integrally cast with the shaft. Bronze or stainless steel is sometimes used for marine or other corrosive environments. Where the shaft also serves as the journal, running against a sleeve bearing, hardness can become an issue. Through- or case-hardened steel may be the material of choice for the shaft in these cases. See Chapter 11 for a discussion of desired relative hardness and material combinations for shafts and bearings. Rolling-element bearings do not need hardened shafts.

Most machine shafts are made from low- to medium-carbon steel, either cold rolled or hot rolled, though alloy steels are also used where their higher strengths are needed. Cold-rolled steel is more often used for smaller-diameter shafts (< about 3-in dia) and hot-rolled used for larger sizes. The same alloy when cold rolled has higher mechanical properties than if hot rolled due to the cold working, but this comes at the cost of residual tensile stresses in the surface. Machining for keyways, grooves, or steps relieves these residual stresses locally and can cause warping. Hot-rolled bars must be machined all over to remove the carburized outer layer, whereas portions of a cold-rolled surface can be left as-rolled except where machining to size is needed for bearings, etc. Prehardened (30HRC) and ground precision (straight) steel shafting can be purchased in small sizes and can be machined with carbide tools. Full-hard, ground, precision shafting (60HRC) is also available but cannot be machined.

10.4 SHAFT POWER

The power transmitted through a shaft can be found from first principles. In any rotating system, instantaneous power is the product of torque and angular velocity,

$$P = T\omega \quad (10.1a)$$

where ω must be expressed in radians per unit time. Whatever the base units used for calculations, power is usually converted to units of horsepower (hp) in any English system or to kilowatts (kW) in any metric system. (See Table 1-5 on p. 24 for conversion factors.) Both torque and angular velocity can be time varying, though much of rotating machinery is designed to operate at constant or near-constant speeds for large blocks of time. In such cases, the torque will often vary with time. The average power is found from

$$P_{avg} = T_{avg}\omega_{avg} \quad (10.1b)$$

10.5 SHAFT LOADS

The most general shaft-loading case is that of a fluctuating torque and a fluctuating moment in combination. There can be axial loads as well, if the shaft axis is vertical or is fitted with helical or worm gears having an axial force component. (A shaft should be designed to minimize the portion of its length subjected to axial loads by taking them to ground through suitable thrust bearings as close to the source of the load as possible.) Both torque and moment can be time varying, as shown in Figure 10-1, and can have both mean and alternating components.

The combination of a bending moment and a torque on a rotating shaft creates multiaxial stresses. The issues discussed in Section 6.12 (p. 376) on multiaxial stresses in fatigue are then germane. If the loadings are asynchronous, random, or misphased, then it will be a *complex multiaxial* stress case. But, even if the moment and torque are in phase (or 180° out of phase), it may still be a complex multiaxial stress case. The critical factor in determining whether it has simple or complex multiaxial stresses is the direction of the principal alternating stress on a given shaft element. If its direction is constant with time, then it is considered a simple multiaxial stress case. If it varies with time, then it is a complex multiaxial stress case. Most rotating shafts loaded in both bending and torsion will be in the complex category. While the direction of the alternating bending stress component will tend to be constant, the torsional component's direction varies as the element rotates around the shaft. Combining them on the Mohr's circle will show that the result is an alternating principal stress of varying direction. One exception to this is the case of a constant torque superposed on a time-varying moment. Since the constant torque has no alternating component to change the direction of the principal alternating stress, this becomes a simple multiaxial stress case. However even this exception cannot be taken if there are stress concentrations present, such as holes or keyways in the shaft, since they will introduce local biaxial stresses and require a complex multiaxial fatigue analysis.

Assume that the bending moment function over the length of the shaft is known or is calculable from the given data and that it has both a mean component M_m and an alternating component M_a . Likewise, assume the torque on the shaft is known or calculable from given data and has both mean and alternating components, T_m and T_a . Then the general approach follows that outlined in the list labeled **Design Steps for Fluctuating Stresses** in Section 6.11 (p. 360) in combination with the multiaxial stress issues addressed in Section 6.12 (p. 376). Any locations along the length of the shaft that appear to have large moments and/or torques (especially if in combination with stress concentrations) need to be examined for possible stress failure and the cross-sectional dimensions or material properties adjusted accordingly.

10.6 SHAFT STRESSES

With the understanding that the following equations will have to be calculated for a multiplicity of points on the shaft and their combined multiaxial effects also considered, we must first find the applied stresses at all points of interest. The largest alternating and mean bending stresses are at the outside surface and are found from

$$\sigma_a = k_f \frac{M_a c}{I} \quad \sigma_m = k_{fm} \frac{M_m c}{I} \quad (10.2a)$$

where k_f and k_{fm} are the bending-fatigue stress-concentration factors for the alternating and mean components, respectively (see equations 6.11 and 6.17 on pp. 339 and 360). Since the typical shaft is a solid-round cross section,* we can substitute for c and I :

$$c = r = \frac{d}{2} \quad I = \frac{\pi d^4}{64} \quad (10.2b)$$

giving

$$\sigma_a = k_f \frac{32M_a}{\pi d^3} \quad \sigma_m = k_{fm} \frac{32M_m}{\pi d^3} \quad (10.2c)$$

where d is the local shaft diameter at the section of interest.

The alternating and mean torsional shear stresses are found from

$$\tau_a = k_{fs} \frac{T_a r}{J} \quad \tau_m = k_{fsm} \frac{T_m r}{J} \quad (10.3a)$$

where k_{fs} and k_{fsm} are the torsional fatigue stress-concentration factors for the alternating and mean components, respectively (see equation 6.11 on p. 343 for k_{fs} and use the applied shear stresses and shear yield strength in equation 6.17 on p. 364 to get k_{fsm}). For a solid-round cross section,* we can substitute for r and J :

$$r = \frac{d}{2} \quad J = \frac{\pi d^4}{32} \quad (10.3b)$$

giving

$$\tau_a = k_{fs} \frac{16T_a}{\pi d^3} \quad \tau_m = k_{fsm} \frac{16T_m}{\pi d^3} \quad (10.3c)$$

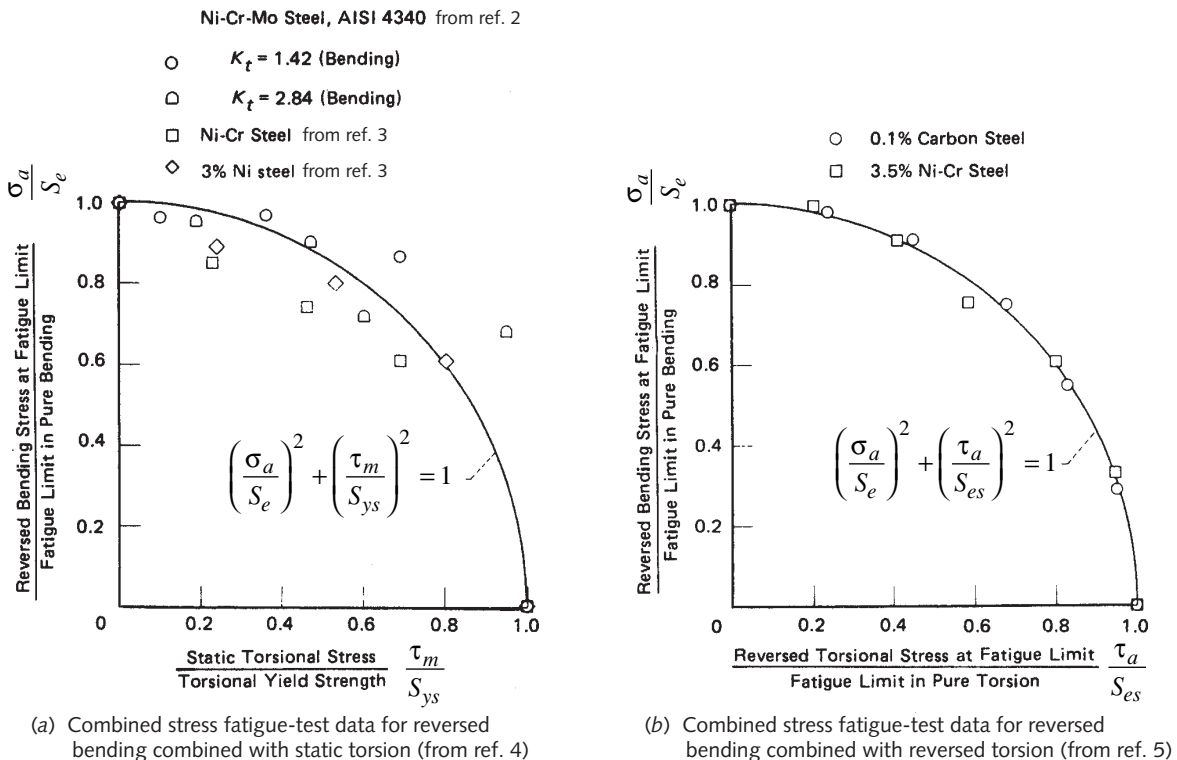
A tensile axial load F_z , if any is present, will typically have only a mean component (such as the weight of the components) and can be found from

$$\sigma_{m_{axial}} = k_{fm} \frac{F_z}{A} = k_{fm} \frac{4F_z}{\pi d^2} \quad (10.4)$$

10.7 SHAFT FAILURE IN COMBINED LOADING

Extensive studies of fatigue failure of both ductile steels and brittle cast irons in combined bending and torsion were done originally in England in the 1930s by Davies^[3] and Gough and Pollard.^[5] These early results are shown in Figure 10-3, which is taken from the ANSI/ASME Standard B106.1M-1985 on the *Design of Transmission Shafting*. Data from later research is also included on these plots.^[2, 4] The combination of torsion and bending on ductile materials in fatigue was found to generally follow the elliptical relationship as defined by the equations in the figure. Cast brittle materials (not shown) were found to fail based on the maximum principal stress. These findings are similar to those for combined torsional and bending stresses in fully reversed loading shown in Figure 6-15 (p. 321).

* For a hollow shaft, substitute the appropriate expressions for I and J .

**FIGURE 10-3**

10

Results of Fatigue Tests of Steel Specimens Subjected to Combined Bending and Torsion (From *Design of Transmission Shafts*, American Society of Mechanical Engineers, New York, ANSI/ASME Standard B106.1M-1985, with permission)

10.8 SHAFT DESIGN

Both stresses and deflections need to be considered in shaft design. Often, deflection can be the critical factor, since excessive deflections will cause rapid wear of shaft bearings. Gears, belts, or chains driven from the shaft can also suffer from misalignment introduced by shaft deflections. Note that the stresses in a shaft can be calculated locally for various points along the shaft based on known loads and assumed cross sections. But, the deflection calculations require that the entire shaft geometry be defined. So, a shaft is typically first designed using stress considerations and then the deflections calculated once the geometry is completely defined. The relationship between the shaft's natural frequencies (in both torsion and bending) and the frequency content of the force- and torque-time functions can also be critical. If the forcing functions are close in frequency to the shaft's natural frequencies, resonance can create vibrations, high stresses, and large deflections.

General Considerations

Some general rules of thumb for shaft design can be stated as follows:

- 1 To minimize both deflections and stresses, the shaft length should be kept as short as possible and overhangs minimized.
- 2 A cantilever beam will have a larger deflection than a simply supported (straddle mounted) one for the same length, load, and cross section, so straddle mounting should be used unless a cantilevered shaft is dictated by design constraints. (*Figure 10-2 shows a situation in which an overhung or cantilevered section of shaft is required for serviceability. The sheave on the right-hand end of the shaft carries an endless V-belt. If the sheave were mounted between the bearings, then the shaft assembly would have to be disassembled to change a belt, which is undesirable. In such cases, the cantilevered shaft can be the lesser of the evils.*)
- 3 A hollow shaft has a better stiffness/mass ratio (specific stiffness) and higher natural frequencies than a comparably stiff or strong solid shaft, but will be more expensive and larger in diameter.
- 4 Try to locate stress-raiser away from regions of large bending moment if possible and minimize their effects with generous radii and reliefs.
- 5 If minimizing deflection is the primary concern, then low-carbon steel may be the preferred material, since its stiffness is as high as that of more expensive steels and a shaft designed for low deflection will tend to have low stresses.
- 6 Deflections at gears carried on the shaft should not exceed about 0.005 in and the relative slope between the gear axes should be less than about 0.03° .^[1]
- 7 If plain (sleeve) bearings are used, the shaft deflection across the bearing length should be less than the oil-film thickness in the bearing.^[1]
- 8 If non-self-aligning rolling element bearings are used, the shaft's slope at the bearings should be kept to less than about 0.04° .^[1]
- 9 If axial thrust loads are present, they should be taken to ground through a single thrust bearing per load direction. Do not split axial loads between thrust bearings, as thermal expansion of the shaft can overload the bearings.
- 10 The first natural frequency of the shaft should be at least three times the highest forcing frequency expected in service, and preferably much more. (A factor of 10X or more is preferred, but this is often difficult to achieve in mechanical systems).

Design for Fully Reversed Bending and Steady Torsion

This loading case is a subset of the general case of fluctuating bending and fluctuating torsion, and, because of the absence of an alternating component of torsional stress, is considered to be a simple multiaxial fatigue case. (The presence of local stress concentrations can cause complex multiaxial stresses, however.) This simple loading case has been experimentally investigated, and data exist for failure of parts so loaded as shown in Figure 10-3. The ASME has defined an approach for the design of shafts loaded in this manner.

THE ASME METHOD An ANSI/ASME Standard for the *Design of Transmission Shafting* is published as B106.1M-1985. This standard presents a simplified approach to the design of shafts. The ASME approach *assumes that the loading is fully reversed bending (zero mean bending component) and steady torque (zero alternating torque component)* at a level that creates stresses below the torsional yield strength of the material. The standard makes the case that many machine shafts are in this category. It

uses the elliptical curve of Figure 10-3 fitted through the bending endurance strength on the σ_a axis and the **tensile yield strength** on the σ_m axis as the failure envelope. The tensile yield strength is substituted for the torsional yield strength by using the von Mises relationship of equation 5.9 (p. 251). The derivation of the ASME shaft equation is as follows.

Starting with the relationship for the failure envelope shown in Figure 10-3a:

$$\left(\frac{\sigma_a}{S_e}\right)^2 + \left(\frac{\tau_m}{S_{ys}}\right)^2 = 1 \quad (10.5a)$$

introduce a safety factor N_f

$$\left(N_f \frac{\sigma_a}{S_e}\right)^2 + \left(N_f \frac{\tau_m}{S_{ys}}\right)^2 = 1 \quad (10.5b)$$

Recall the von Mises relationship for S_{ys} from equation 5.9 (p. 251):

$$S_{ys} = S_y / \sqrt{3} \quad (10.5c)$$

and substitute it in equation 10.5b.

$$\left(N_f \frac{\sigma_a}{S_e}\right)^2 + \left(N_f \sqrt{3} \frac{\tau_m}{S_y}\right)^2 = 1 \quad (10.5d)$$

Substitute the expressions for σ_a and τ_m from equations 10.2c and 10.3c, respectively:

$$\left[\left(k_f \frac{32M_a}{\pi d^3}\right) \left(\frac{N_f}{S_e}\right)\right]^2 + \left[\left(k_{fsm} \frac{16T_m}{\pi d^3}\right) \left(\frac{N_f \sqrt{3}}{S_y}\right)\right]^2 = 1 \quad (10.5e)$$

which can be rearranged to solve for the shaft diameter d as

$$d = \left\{ \frac{32N_f}{\pi} \left[\left(k_f \frac{M_a}{S_f} \right)^2 + \frac{3}{4} \left(k_{fsm} \frac{T_m}{S_y} \right)^2 \right]^{1/2} \right\}^{1/3} \quad (10.6a)$$

The notation used in equation 10.6 is slightly different than that of the ANSI/ASME standard in order to remain consistent with the notation used in this text. The standard uses the approach of reducing the fatigue strength S_f by the fatigue-stress-concentration factor k_f rather than using k_f as a stress increaser as is done consistently in this text. In most cases (including this one) the result is the same. Also, the ASME standard assumes the stress concentration for mean stress k_{fsm} to be 1 in all cases, which gives

$$d = \left\{ \frac{32N_f}{\pi} \left[\left(k_f \frac{M_a}{S_f} \right)^2 + \frac{3}{4} \left(\frac{T_m}{S_y} \right)^2 \right]^{1/2} \right\}^{1/3} \quad (10.6b)$$

The ASME has abandoned this shaft design standard, so it has only historical value now. If used at all, equation 10.6 should be applied only to situations where the loads are as it assumes them to be, namely constant torque and fully reversed moment. **The ASME standard gives nonconservative results if either of the loading components that it assumes to be zero is in fact nonzero in a given case. We recommend using the more general approach of equation 10.8 (see below) for shaft design as it covers all loading situations.**

Figure 10-4 shows the Gough elliptical failure line of Figure 10-3 superposed on the Gerber, Soderberg, and modified-Goodman lines. Note that the elliptical line closely matches the Gerber line at the left-hand end but diverges to intersect the yield strength on the mean stress axis. The elliptical line has the advantage of accounting for possible yielding without needing to introduce an additional constraint involving the yield line. However, the Gough elliptical line, while a good fit to the failure data, is less conservative than the combination of Goodman line and yield line used as a failure envelope.

Design for Fluctuating Bending and Fluctuating Torsion

When the torque is not constant, its alternating component will create a complex multiaxial stress state in the shaft. Then the approach described in Section 6.12 (p. 376), which computes the von Mises components of the alternating and mean stresses using equations 6.22 (p. 379), can be used. A rotating shaft in combined bending and torsion has a biaxial stress state, which allows the two-dimensional version of equation 6.22b to be used.

$$\sigma'_a = \sqrt{\sigma_a^2 + 3\tau_a^2} \quad (10.7a)$$

$$\sigma'_m = \sqrt{(\sigma_m + \sigma_{m_{axial}})^2 + 3\tau_m^2}$$

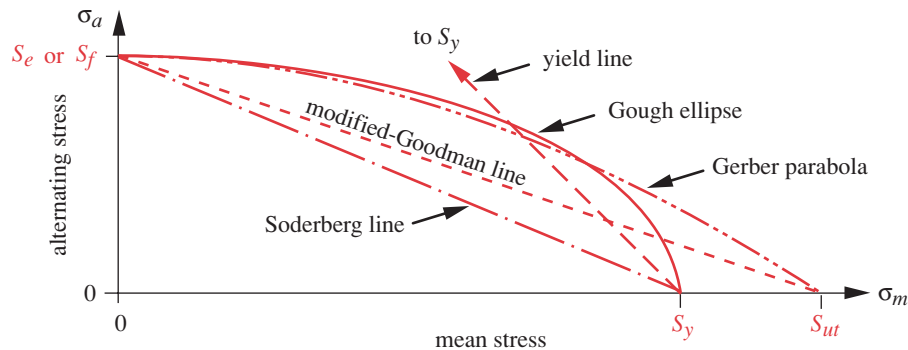
These von Mises stresses can now be entered into a modified-Goodman diagram (MGD) for a chosen material to find a safety factor, or equations 6.18 (pp. 367–368) can be applied without drawing the MGD.

For design purposes, where the diameter of the shaft is the desired quantity to be found, equations 10.2, 10.3, and 10.6 as presented require iteration to find a value for d , given some known loads and assumed material properties. This is not a great difficulty if an equation solver with iterative ability is used. However, a hand-calculator solution is cumbersome with the equations in this form. If a particular failure case is assumed for the MGD, the equations can be manipulated to provide a design equation (similar to equation 10.6) for shaft diameter d at the section of interest. If the failure model used is Case 3 from Section 6.11 (p. 360), which assumes that the mean and alternating loads maintain a constant ratio,* failure will occur at point R in Figure 6-46c (p. 368). The safety factor as defined in equation 6.18e (p. 368) is then

$$\frac{1}{N_f} = \frac{\sigma'_a}{S_f} + \frac{\sigma'_m}{S_{ut}} \quad (10.7b)$$

where N_f is the desired safety factor, S_f is the corrected fatigue strength at the selected cycle life (from equation 6.10 on p. 338), and S_{ut} is the ultimate tensile strength of the material.

* Note that this assumption is also implicit in equation 10.6 for the ASME method.

**FIGURE 10-4**

Elliptical Failure Line Using Yield Strength Shown with Other Failure Lines for Fluctuating Stresses

If we now also assume that the axial load on the shaft is zero and substitute equations 10.2c, 10.3c, and 10.7a into equation 10.7b we get

$$d = \left\{ \frac{32N_f}{\pi} \left[\frac{\sqrt{(k_f M_a)^2 + \frac{3}{4}(k_{fa} T_a)^2}}{S_f} + \frac{\sqrt{(k_{fm} M_m)^2 + \frac{3}{4}(k_{fsm} T_m)^2}}{S_{ut}} \right] \right\}^{\frac{1}{3}} \quad (10.8)$$

which can be used as a design equation to find a shaft diameter for any combination of bending and torsional loading with the assumptions noted above of zero axial load and a constant ratio between alternating and mean values of load over time.

10

EXAMPLE 10-1**Shaft Design for Steady Torsion and Fully Reversed Bending**

Problem Design a shaft to support the attachments shown in Figure 10-5 with a minimum design safety factor of 2.5.

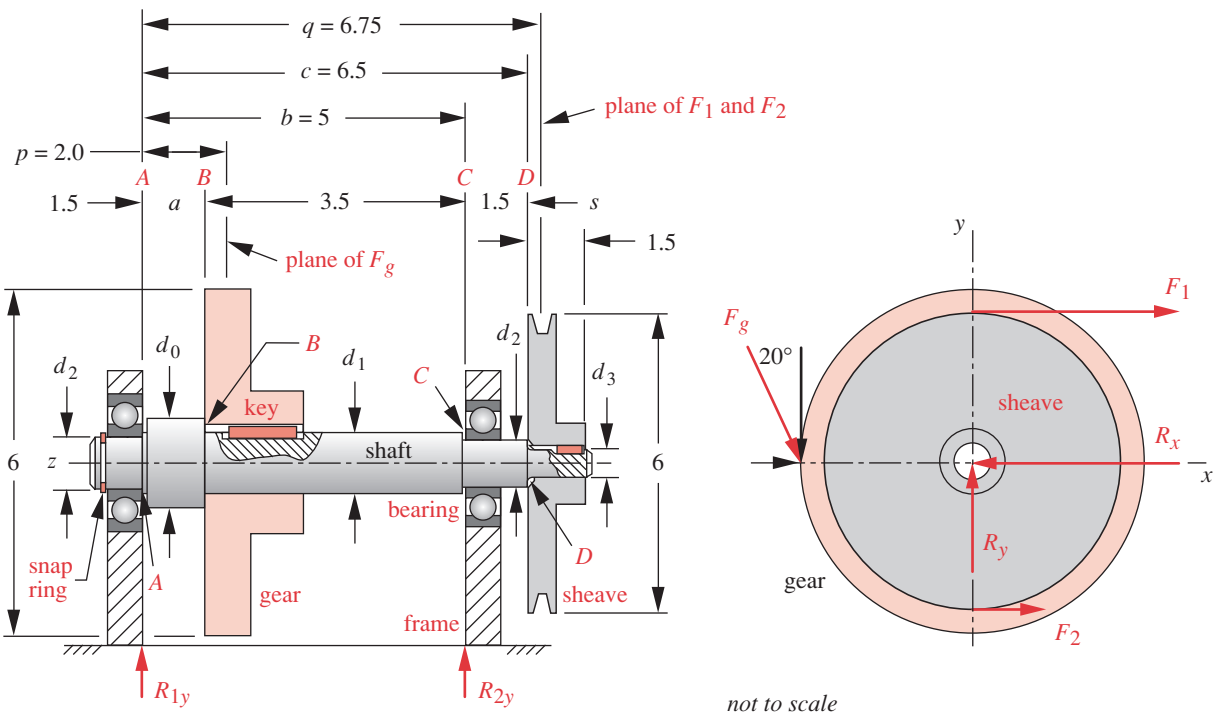
Given A preliminary design of the shaft configuration is shown in Figure 10-5. It must transmit 2 hp at 1725 rpm. The torque and the force on the gear are both constant with time.

Assumptions There are no applied axial loads. Steel will be used for infinite life. Assume a stress-concentration factor of 3.5 for the step radii in bending, 2 for step radii in torsion, and 4 at the keyways.* Since the torque is steady and the bending moment fully reversed, the ASME method of equation 10.6 can be used, and it will be compared to the general method using equation 10.8.

Solution See Figures 10-5 through 10-8.

- First determine the transmitted torque from the given power and angular velocity using equation 10.1 (p. 553).

* See R. E. Peterson, *Stress Concentration Factors*, John Wiley, 1974, Figures 72, 79, and 183, which show these numbers as approximate maxima for these contours and loadings. Since we are creating a preliminary design at this stage and have not yet defined the shaft geometry in detail, it is not fruitful to try to define these factors any more accurately. This can be done later and the design refined accordingly.

**FIGURE 10-5**

Geometry of a Preliminary Design for Examples 10-1 through 10-3

$$T = \frac{P}{\omega} = \frac{2 \text{ hp}}{1725 \text{ rpm}} \left(\frac{6600 \text{ in-lb/sec}}{\text{hp}} \right) \left(\frac{2\pi}{60} \frac{\text{rad/sec}}{\text{rpm}} \right) = 73.1 \text{ lb-in} \quad (a)$$

This torque exists only over the portion of shaft between the sheave and the gear and is uniform in magnitude over that length as shown in Figure 10-6.

- 2 The tangential forces on sheave and gear are found from the torque and their respective radii. A V-belt has tension on both sides, and the ratio between the force F_1 on the tight side and F_2 on the "slack" side is usually assumed to be about 5. The net force associated with the driving torque is $F_n = F_1 - F_2$, but the force that bends the shaft is $F_s = F_1 + F_2$. Combining these relationships gives $F_s = 1.5F_n$. Looking from the sheave end:

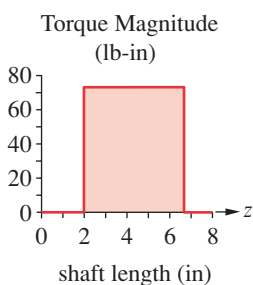
$$F_n = \frac{T}{r} = \frac{73.1 \text{ lb-in}}{3 \text{ in}} = 24.36 \hat{i} \text{ lb}$$

$$F_s = 1.5F_n = 36.54 \hat{i} \text{ lb} \quad (b)$$

- 3 The tangential force at the spur-gear tooth is

$$F_{gtangential} = \frac{T}{r} = \frac{73.1 \text{ lb-in}}{3 \text{ in}} = -24.36 \hat{j} \text{ lb} \quad (c)$$

The spur gear has a 20° pressure angle as shown, which means that there will also be a radial component of force at the gear tooth of

**FIGURE 10-6**

Torque in Example 10-1

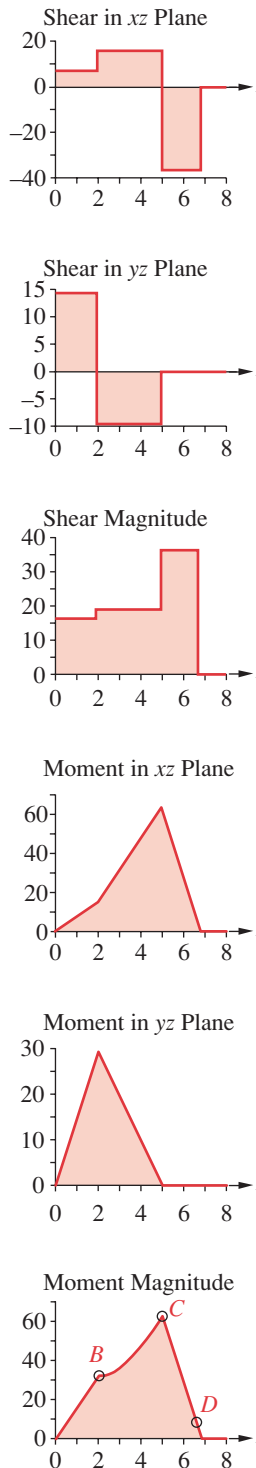


FIGURE 10-7

Loading in Example 10-1

$$F_{g_{\text{radial}}} = F_{g_{\text{tangential}}} \tan(20^\circ) = 8.87 \hat{i} \text{ lb} \quad (d)$$

- 4 We will consider the gear and sheave forces to be concentrated at their centers. Solve for the reaction forces in the xz and yz planes using $\sum F_x = 0$, $\sum M_x = 0$ and $\sum F_y = 0$, $\sum M_y = 0$ with the trial beam dimensions, $a = 1.5$, $b = 5$, and $c = 6.5$, which make $p = 2$ and $q = 6.75$.

$$\begin{aligned} \sum M_A &= R_2 b + F_g p + F_s q = 0 \\ R_2 &= -\frac{1}{b}(F_g p + F_s q) = -\frac{1}{5}(2F_g + 6.75F_s) = -0.40F_g - 1.35F_s \end{aligned} \quad (e)$$

$$\begin{aligned} \sum F &= R_1 + F_g + F_s + R_2 = 0 \\ R_1 &= -F_g - F_s - R_2 = -F_g - F_s - (-0.40F_g - 1.35F_s) = -0.60F_g + 0.35F_s \end{aligned} \quad (f)$$

Equations (e) and (f) can be solved for R_1 and R_2 in each plane, using the appropriate components of the applied loads F_g and F_s .

$$\begin{aligned} R_{1x} &= -0.60F_{gx} + 0.35F_{sx} = -0.60(8.87) + 0.35(36.54) = 7.47 \text{ lb} \\ R_{1y} &= -0.60F_{gy} + 0.35F_{sy} = -0.60(-24.36) + 0.35(0) = 14.61 \text{ lb} \end{aligned} \quad (g)$$

$$\begin{aligned} R_{2x} &= -0.40F_{gx} - 1.35F_{sx} = -0.40(8.87) - 1.35(36.54) = -52.87 \text{ lb} \\ R_{2y} &= -0.40F_{gy} - 1.35F_{sy} = -0.40(-24.36) - 1.35(0) = 9.74 \text{ lb} \end{aligned}$$

- 5 The shear load and bending moment acting on the shaft can now be found. Write an equation for the loading function q using singularity functions, integrate it to get the shear function V , and integrate again for the moment function M .

$$q = R_1(z-0)^{-1} + F_g(z-2)^{-1} + R_2(z-5)^{-1} + F_s(z-6.75)^{-1} \quad (h)$$

$$V = R_1(z-0)^0 + F_g(z-2)^0 + R_2(z-5)^0 + F_s(z-6.75)^0 \quad (i)$$

$$M = R_1(z-0)^1 + F_g(z-2)^1 + R_2(z-5)^1 + F_s(z-6.75)^1 \quad (j)$$

Recall that the integration constants C_1 and C_2 are zero when we include the reaction forces in the equation.

- 6 Substitute the values of the loads and reaction forces for each coordinate direction into equations (h), (i), and (j) and evaluate them for all values of z along the shaft axis. Then combine the moment-function components in the xz and yz planes (using the Pythagorean theorem) to find the maximum magnitude of the moment function.

The shear and moment distributions over the shaft length are shown in Figure 10-7. The applied torque is uniform over the portion of shaft between points B and D as shown in Figure 10-6. Within that length, there are three locations of concern where a moment occurs in combination with a stress concentration: point B at the step and keyway under the gear ($M_B = \pm 33$ lb-in), point C at the right bearing where there is a step with a small radius to fit the bearing ($M_C = \pm 63$ lb-in), and point D at the sheave step ($M_D = \pm 9$ lb-in). Note that because of its high stress concentration, the snap-ring groove used for axial location has been placed at the end of the shaft where the moment and torque are both zero.

- 7 A trial material needs to be selected for the computations. We will first try an inexpensive, low-carbon, cold-rolled steel such as SAE 1020 with $S_{ut} = 65$ kpsi and $S_y = 38$ kpsi. Though not exceptionally strong, this material has low notch sensitivity, which will be an advantage given the large stress concentrations. Calculate the uncorrected endurance strength using equation 6.5 (p. 330):

$$S_e' = 0.5S_{ut} = 0.5(65\,000) = 32\,500 \text{ psi} \quad (k)$$

This must be reduced by various factors to account for differences between the part and the test specimen.

$$\begin{aligned} S_e &= C_{load} C_{size} C_{surf} C_{temp} C_{reliab} S_e' \\ S_e &= (1)(1)(0.84)(1)(1)(32\,500) = 27\,300 \text{ psi} \end{aligned} \quad (l)$$

The loading is bending and torsion, so C_{load} is 1. Since we don't yet know the part size, we will temporarily assume $C_{size} = 1$ and adjust it later. C_{surf} is chosen for a machined finish from either Figure 6-26 (p. 332) or equation 6.7e (p. 333). The temperature is not elevated, so $C_{temp} = 1$, and we assume 50% reliability at this preliminary design stage with $C_{reliab} = 1$.

- 8 The material's notch sensitivity is found from either equation 6.13 (p. 345) or Figure 6-36 (pp. 344–345) and is $q = 0.5$ in bending and $q = 0.57$ in torsion, assuming a notch radius of 0.01 in.
- 9 The fatigue stress-concentration factor is found from equation 6.11b (p. 343) using the assumed geometric stress-concentration factor noted above. For the bending stress in the step at point C :

$$K_f = 1 + q(K_t - 1) = 1 + 0.5(3.5 - 1) = 2.25 \quad (m)$$

The stress concentration for a step loaded in torsion is less than for the same geometry loaded in bending:

$$K_{fs} = 1 + q(K_{ts} - 1) = 1 + 0.57(2 - 1) = 1.57 \quad (n)$$

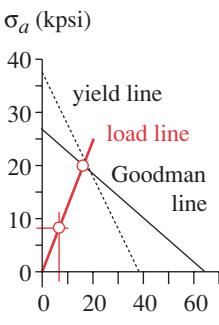
From equation 6.17 (p. 364) we find that in this case, the same factor should be used on the mean torsional stress component:

$$K_{fsm} = K_{fs} = 1.57 \quad (o)$$

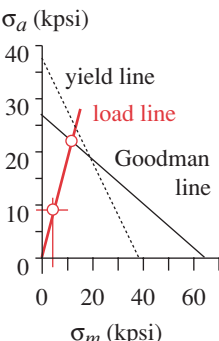
- 10 The shaft diameter at point C can now be found from equation 10.6 using the moment magnitude at that point of 63.9 in-lb.

$$\begin{aligned} d_2 &= \left\{ \frac{32N_f}{\pi} \left[\left(k_f \frac{M_a}{S_f} \right)^2 + \frac{3}{4} \left(k_{fsm} \frac{T_m}{S_y} \right)^2 \right]^{\frac{1}{2}} \right\}^{\frac{1}{3}} \\ &= \left\{ \frac{32(2.5)}{\pi} \left[\left(2.25 \frac{63.9}{27\,300} \right)^2 + \frac{3}{4} \left(1.57 \frac{73.1}{38\,000} \right)^2 \right]^{\frac{1}{2}} \right\}^{\frac{1}{3}} = 0.531 \text{ in} \quad (p) \end{aligned}$$

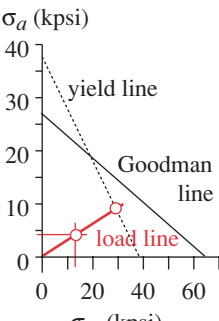
If k_{fsm} is set to 1 as ASME recommends, then equation 10.6 gives $d = 0.520$ in. If the more general equation 10.8 is used, the result is $d = 0.557$ in. Note that the ASME



(a) Stresses at point B



(b) Stresses at point C



(c) Stresses at point D

FIGURE 10-8

Modified-Goodman Diagrams for Three Points on Shaft in Example 10-1

method is less conservative than equation 10.8 as it gives smaller shaft diameters for the same safety factor. A modified-Goodman diagram for this stress element is shown in Figure 10-8b. It predicts failure from fatigue.

- 11 At point B, under the gear, the moment is less, but the fatigue stress-concentration factors K_f and K_{fs} are greater so should also be calculated. At B:

$$K_f = 1 + q(K_t - 1) = 1 + 0.5(4 - 1) = 2.50 \quad (q)$$

$$K_{fs} = 1 + q(K_t - 1) = 1 + 0.57(4 - 1) = 2.70$$

- 12 The minimum recommended diameter at point B from equation 10.6 is

$$d_1 = \left\{ \frac{32N_f}{\pi} \left[\left(k_f \frac{M_a}{S_f} \right)^2 + \frac{3}{4} \left(k_{fsm} \frac{T_m}{S_y} \right)^2 \right]^{\frac{1}{2}} \right\}^{\frac{1}{3}}$$

$$= \left\{ \frac{32(2.5)}{\pi} \left[\left(2.50 \frac{32.8}{27300} \right)^2 + \frac{3}{4} \left(2.71 \frac{73.1}{38000} \right)^2 \right]^{\frac{1}{2}} \right\}^{\frac{1}{3}} = 0.517 \text{ in} \quad (r)$$

If k_{fsm} is set to 1 as ASME recommends, then equation 10.6 gives $d = 0.444$ in. If the more general equation 10.8 is used, the result is $d = 0.524$ in. Again, the ASME method is nonconservative compared to equation 10.8. A modified-Goodman diagram for this stress element is shown in Figure 10-8a. It predicts failure from fatigue.

- 13 Another location of possible failure is the step against which the sheave seats, at point D. The moment is lower than at C, being about 9.1 lb-in. (See Figure 10-7.) However, the shaft will be stepped smaller there and will have the same order of stress concentration as at point C. (The keyway for the sheave is in a region of zero moment and so will be ignored.) Using those data in equation 10.6 (p. 558) for point D:

$$d_3 = \left\{ \frac{32N_f}{\pi} \left[\left(k_f \frac{M_a}{S_f} \right)^2 + \frac{3}{4} \left(k_{fsm} \frac{T_m}{S_y} \right)^2 \right]^{\frac{1}{2}} \right\}^{\frac{1}{3}}$$

$$= \left\{ \frac{32(2.5)}{\pi} \left[\left(2.25 \frac{9.1}{27300} \right)^2 + \frac{3}{4} \left(1.57 \frac{73.1}{38000} \right)^2 \right]^{\frac{1}{2}} \right\}^{\frac{1}{3}} = 0.411 \text{ in} \quad (s)$$

If k_{fsm} is set to 1 as ASME recommends, then equation 10.6 gives $d = 0.360$ in. If the more general equation 10.8 is used, the result is $d = 0.387$ in. A modified-Goodman diagram for this stress element is shown in Figure 10-8c. It predicts a yielding failure.

- 14 From these preliminary calculations, we can determine reasonable sizes for the four step diameters, d_0, d_1, d_2, d_3 of Figure 10-5 (p. 561). The next largest standard ball-bearing diameter to the $d_2 = 0.531$ in calculated for point C is 15 mm or 0.591 in. Selecting this value for d_2 , we set $d_3 = 0.50$ in, and $d_1 = 0.625$ in. The stock size d_0 is then 0.75 in, left as-rolled for the outside diameter at the gear flange. These dimen-

sions will give safety factors that meet or exceed the specification. The stresses and safety factors at all three points should now be recalculated using more accurate strength-reduction (e.g., C_{size}) and stress-concentration factors based on the final dimensions.*

EXAMPLE 10-2

Shaft Design for Repeated Torsion with Repeated Bending

Problem

Design a shaft to support the attachments shown in Figure 10-5 (p. 561) with a minimum design safety factor of 2.5.

Given

The torque and the moment on the shaft are both varying with time in repeated fashion, i.e., their alternating and mean components are of equal magnitude. The mean and alternating components of torque are both 73 lb-in, making the peak torque twice the mean value of Example 10-1. The mean and alternating components of moment are equal in magnitude. Figure 10-9 shows the peak moment and peak torque, which are each twice the value of their fully reversed counterparts of Figure 10-5 and Example 10-1 due to the presence of the mean moment.

Assumptions

There are no applied axial loads. Steel will be used for infinite life. Assume a stress-concentration factor of 3.5 for the step radii in bending, 2 for the step radii in torsion, and 4 at the keyways. Since the torsional load is not steady and the bending moment is not fully reversed, the ASME method of equation 10.6 (p. 558) should not be used.

Solution

See Figures 10-5 (p. 561), 10-9, 10-10 and Table 10-1.

- For comparison purposes, we will keep all factors except the loading configuration the same as in the previous example. The same low-carbon, cold-rolled steel SAE 1020, which has $S_{ut} = 65$ ksi, $S_y = 38$ ksi, and a corrected $S_e = 27.3$ ksi, is used. Its notch sensitivity is 0.5.
- There are three points of interest, labeled B , C , and D in Figure 10-5 (p. 561). The fatigue stress-concentration factors are assumed to be the same at C and D and are larger at B . See Example 10-1 (p. 560) for their calculation.
- The required shaft diameter at point C can be found from equation 10.8 (p. 560).

$$d_2 = \left\{ \frac{32N_f}{\pi} \left[\frac{\sqrt{(k_f M_a)^2 + \frac{3}{4}(k_{fs} T_a)^2}}{S_f} + \frac{\sqrt{(k_{fm} M_m)^2 + \frac{3}{4}(k_{fsm} T_m)^2}}{S_{ut}} \right] \right\}^{\frac{1}{3}}$$

$$= \left\{ \frac{32(2.5)}{\pi} \left[\frac{\sqrt{[2.25(64)]^2 + \frac{3}{4}[1.57(73.1)]^2}}{27\ 300} + \frac{\sqrt{[2.25(64)]^2 + \frac{3}{4}[1.57(73.1)]^2}}{65\ 000} \right] \right\}^{\frac{1}{3}}$$

$$d_2 = 0.614 \quad (a)$$

* Files EX10-01a, EX10-01b, EX10-01c, and EX10-01d are on the CD-ROM.

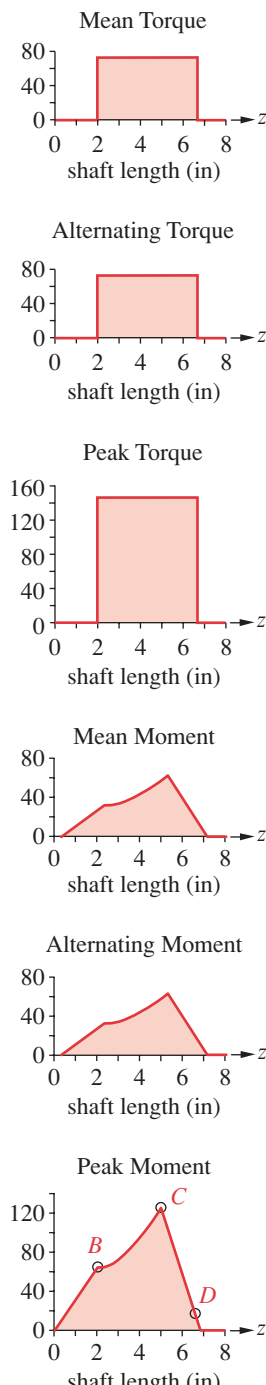
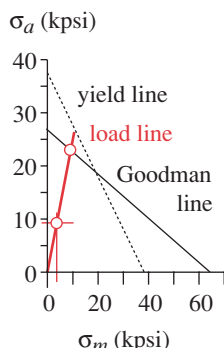
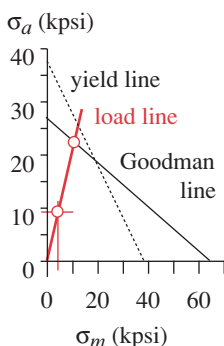


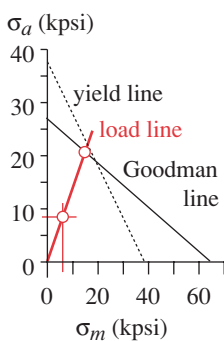
FIGURE 10-9
Torque and Moments in
Example 10-2 (lb-in)



(a) Stresses at point B



(b) Stresses at point C



(c) Stresses at point D

FIGURE 10-10

Modified-Goodman Diagrams for Three Points on Shaft in Example 10-2

Compare this to the value of 0.557 from the same equation in the prior example where the loads were steady.

- 4 At point *B* the required diameter from equation 10.8 is

$$d_1 = \left\{ \frac{32(2.5)}{\pi} \left[\frac{\sqrt{[2.5(32.8)]^2 + \frac{3}{4}[2.71(73.1)]^2}}{27\,300} + \frac{\sqrt{[2.5(32.8)]^2 + \frac{3}{4}[2.71(73.1)]^2}}{65\,000} \right] \right\}^{\frac{1}{3}}$$

$$d_1 = 0.632 \quad (b)$$

Compare this to the value of 0.517 from the same equation in the prior example where the loads were steady.

- 5 And at point *D*:

$$d_3 = \left\{ \frac{32(2.5)}{\pi} \left[\frac{\sqrt{[2.25(9.1)]^2 + \frac{3}{4}[1.57(73.1)]^2}}{27\,300} + \frac{\sqrt{[2.25(9.1)]^2 + \frac{3}{4}[1.57(73.1)]^2}}{65\,000} \right] \right\}^{\frac{1}{3}}$$

$$d_3 = 0.512 \quad (c)$$

Compare this to the value of $d_3 = 0.411$ from the same equation in the prior example where the loads were steady.

- 6 The presence of repeated stresses requires a larger shaft to maintain the same safety factor. We need the next larger standard bearing at *C*, which is a 17 mm (0.669 in) inside diameter. Selecting this value for d_2 , we try values of $d_3 = 0.531$ in, which is a smaller standard inch size, and $d_1 = 0.750$ in, which is a larger standard inch size. The stock size is now 0.875 in and is left as-rolled for the outside diameter at the gear flange. These dimensions will give safety factors that meet or exceed the specification as shown in the modified-Goodman diagrams of Figure 10-10. The stresses and safety factors at all three points should now be recalculated using more accurate strength-reduction and stress-concentration factors based on the final dimensions.
- 7 Table 10-1 compares the results from Examples 10-1 and 10-2 to show the differences in shaft diameter needed for steady loading or fluctuating loading. Note that the peak load in Example 10-1 is half that of Example 10-2. The final safety factors are larger than the design minimum due to the need to size-up the shaft to fit an available stock bearing size. Files EX10-02a, EX10-02b, EX10-02c, and EX10-02d are on the CD-ROM.

10.9 SHAFT DEFLECTION

A shaft is a beam that deflects transversely and is also a torsion bar that deflects torsionally. Both modes of deflection need to be analyzed. The principles of deflection analysis were reviewed in Chapter 4 and will not be detailed again here. Section 4.10 (p. 162) developed an approach for calculating beam deflections using singularity functions and Section 4.12 (p. 177) investigated torsional deflection.

Table 10-1 Comparison of Shaft Design Results from Examples 10-1 and 10-2Minimum Diameters Give $N_f = 2.5$ at Each Point

Design	Max Alt Torque	Max Mean Torque	Max Alt Moment	Max Mean Moment	d_0 (in) nom	d_1 (in) min / nom	d_2 (in) min / nom	d_3 (in) min / nom	S_f at C
Ex. 9-1	0	73.1	63.9	0	0.750	0.517 / 0.625	0.557 / 0.591	0.411 / 0.500	2.5 / 3.0
Ex. 9-2	73.1	73.1	63.9	63.9	0.875	0.632 / 0.750	0.614 / 0.669	0.512 / 0.531	2.5 / 3.8

Shafts as Beams

The methods of Section 4.10 are directly applicable. The only complicating factor is the usual presence of steps in a shaft that change the cross-sectional properties along its length. The integration of the M / EI function becomes much more complicated due to the fact that both I and M are now functions of the dimension along the shaft-beam. Rather than do an analytical integration as was done in Section 4.10 for the case of constant I , we will use a numerical integration technique such as Simpson's rule or the trapezoidal rule to form the slope and deflection functions from the M / EI function. This will be demonstrated in an example. If the transverse loads and moment are time varying, then the absolute maximum magnitudes should be used to calculate the deflections. The deflection function will depend on the loading and the beam boundary conditions, i.e., whether simply supported, cantilevered, or overhung.

Shafts as Torsion Bars

The methods of Section 4.12 are directly applicable, particularly equation 4.24 (p. 178), since the only practical shaft cross section is circular. The angular deflection θ (in radians) for a shaft of length l , shear modulus G , polar moment of inertia J , with torque T is

$$\theta = \frac{Tl}{GJ} \quad (10.9a)$$

from which we can form the expression for the torsional spring constant:

$$k_t = \frac{T}{\theta} = \frac{GJ}{l} \quad (10.9b)$$

If the shaft is stepped, the changing cross sections complicate the torsional deflection and spring constant calculation due to the changing polar moment of inertia J .

Any collection of adjacent, different-diameter sections of shaft can be considered as a set of springs in series since their deflections add and the torque passes through unchanged. An effective spring constant or an effective J can be computed for any segment of shaft in order to find the relative deflection between its ends. For a segment of a shaft containing three sections of differing cross sections J_1 , J_2 , and J_3 with corresponding lengths l_1 , l_2 , l_3 , the total deflection is merely the sum of the deflections of each section subjected to the same torque. We assume that the material is consistent throughout.

$$\theta = \theta_1 + \theta_2 + \theta_3 = \frac{T}{G} \left(\frac{l_1}{J_1} + \frac{l_2}{J_2} + \frac{l_3}{J_3} \right) \quad (10.9c)$$

The effective spring constant k_{eff} of a three-segment stepped shaft is

$$\frac{1}{k_{t_{eff}}} = \frac{1}{k_{t_1}} + \frac{1}{k_{t_2}} + \frac{1}{k_{t_3}} \quad (10.9d)$$

These expressions can be extended to any number of segments of a stepped shaft.

EXAMPLE 10-3

Designing a Stepped Shaft to Minimize Deflection

Problem	Design the same shaft as in Example 10-2 to have a maximum bending deflection of 0.002 in and a maximum angular deflection of 0.5° between sheave and gear.
Given	The loading is the same as in Example 10-2. The peak torque is 146 lb-in. Figure 10-9 shows the distribution of the peak moment over the shaft length. The values are 65.6 lb-in at point B, 127.9 lb-in at point C, and 18.3 lb-in at point D.
Assumptions	The lengths will remain the same as in previous example, but diameters can be changed to stiffen the shaft if necessary. The material is the same as in Example 10-2.
Solution	See Figures 10-5 (p. 561), and 10-11 to 10-13.

- 1 The torsional deflection is found from equations 10.9. The lengths of each segment are (from Figure 10-5 on p. 561): $AB = 1.5$ in, $BC = 3.5$ in, and $CD = 1.5$ in. The polar area moments of inertia are first calculated for each segment of different diameter.

$$\begin{aligned} \text{from } A \text{ to } B : \quad J &= \frac{\pi d_{AB}^4}{32} = \frac{\pi(0.875)^4}{32} = 0.0575 \text{ in}^4 \\ \text{from } B \text{ to } C : \quad J &= \frac{\pi d_{BC}^4}{32} = \frac{\pi(0.750)^4}{32} = 0.0311 \text{ in}^4 \\ \text{from } C \text{ to } D : \quad J &= \frac{\pi d_{CD}^4}{32} = \frac{\pi(0.669)^4}{32} = 0.0197 \text{ in}^4 \end{aligned} \quad (a)$$

and used in equation 10.9c (p. 568).

$$\begin{aligned} \theta &= \frac{T}{G} \left(\frac{l_1}{J_1} + \frac{l_2}{J_2} + \frac{l_3}{J_3} \right) \\ &= \frac{146}{1.2E7} \left(\frac{1.5}{0.0575} + \frac{3.5}{0.0311} + \frac{1.5}{0.0197} \right) = 0.15 \text{ deg} \end{aligned} \quad (b)$$

This deflection is within the requested specification.

- 2 The moment function for this shaft was derived using singularity functions as equation (j) in Example 10-1 (p. 560). It must now be divided by the product of E

and the area moment of inertia I at each point along the shaft axis. While E is constant, the value of I changes with each diametral change in the stepped shaft.

$$\frac{M}{EI} = \frac{1}{EI} [R_1(z-0)^1 + F_g(z-1.5)^1 + R_2(z-5)^1 + F_s(z-6.5)^1] \quad (c)$$

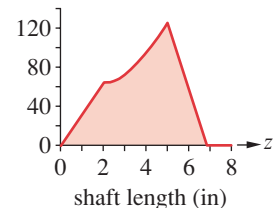
Figure 10-11a shows the moment function for this shaft as derived in the previous examples and Figure 10-11b shows the M / EI function for the section diameters defined in Example 10-2.

- 3 The bending deflection is found by integrating the moment function twice.

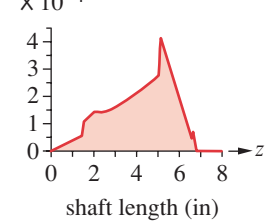
$$\theta = \int \frac{M}{EI} dz + C_3 \quad (d)$$

$$\delta = \int \int \frac{M}{EI} dz + C_3 z + C_4 \quad (e)$$

- 4 The first integration of the M / EI function from equation (c) gives the beam slope and the second integration gives the deflection function. In previous discussions of beam deflection (see Section 4.10 on p. 162 and Examples 4-4 to 4-7 on pp. 164 to 171) the cross section I of the beam was constant across its length. In a stepped shaft, I is a function of the shaft length. This makes the analytical integration of the M / EI function much more complicated. A simpler approach is to numerically integrate the function twice using a trapezoidal or Simpson's rule. This numerical integration must be done for each coordinate direction to obtain the x and y components of deflection. These are then combined vectorially to get the deflection-magnitude and phase-angle functions over the shaft length.
- 5 Since the shaft deflection is zero at $z = 0$, $C_4 = 0$. The other constant of integration C_3 can be determined numerically. Figure 10-12a shows the beam slope in the y direction as integrated by a trapezoidal rule, and also shows the corrected slope function. The integrated result is shifted up by the integration constant C_3 . However, we do not know where the proper zero crossover is for this function, so we cannot determine C_3 from the beam-slope function.
- 6 The as-integrated deflection function in Figure 10-12b does not equal zero at the second support. Since the deflection is really zero there, the error in this integrated



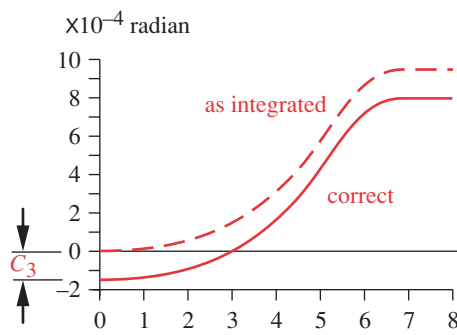
(a) Moment magnitude



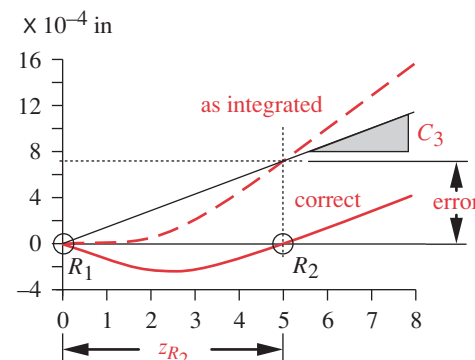
(b) Moment / EI

FIGURE 10-11

Moment and Moment / EI
Functions in Example 10-3



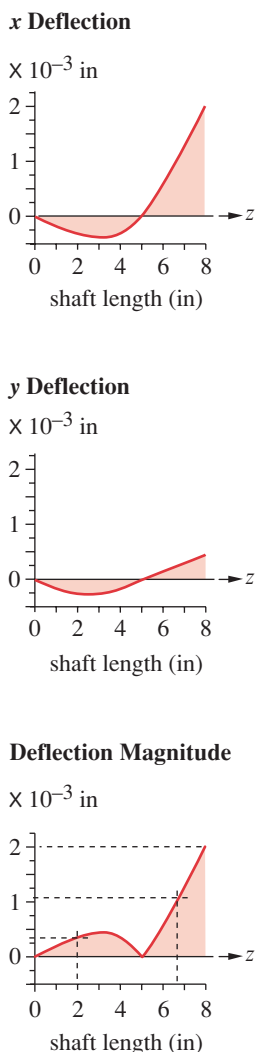
(a) Beam slope



(b) Beam deflection

FIGURE 10-12

Numerical Integration of Moment Function and Finding the Integration Constant C_3

**FIGURE 10-13**

Deflection Functions for Example 10-3

function can be used to determine the constant of integration C_3 . A line is drawn in Figure 10-12b from the origin to the point on the curve at $z = 5$ where the function should be zero. The slope of this straight line is the constant C_3 for the y direction, which is found from

$$C_{3y} = \frac{\text{error}_y}{z_{R2}} = \frac{0.0007}{5.0} = 0.00014 \text{ in} \quad (f)$$

The constant for the x direction is found in similar manner. The functions are then recalculated using the correct values of C_3 .

- 7 These deflection functions are plotted in Figure 10-13 for the shaft diameters of $d_0 = 0.875$, $d_1 = 0.750$, $d_2 = 0.669$, $d_3 = 0.531$ from Example 10-2. The magnitude of the deflection at the gear is 0.0003 in, which is well within the requested specification. At the sheave the deflection is 0.001 in, also within the specification. The deflection at the right-hand end of the shaft is 0.002 in. Files EX10-03a and EX09-02b are on the CD-ROM.

10.10 KEYS AND KEYWAYS

The ASME defines a **key** as “*a demountable machinery part which, when assembled into keyseats, provides a positive means for transmitting torque between the shaft and hub.*” Keys are standardized as to size and shape in several styles.* A **parallel key** is square or rectangular in cross section and of constant height and width over its length. (See Figure 10-14a.) A **tapered key** is of constant width but its height varies with a linear taper of 1/8 in per foot, and it is driven into a tapered slot in the hub until it locks. It may either have no head or have a **gib head** to facilitate removal. (See Figure 10-14b.) A **Woodruff key** is semicircular in plan and of constant width. It fits in a semicircular keyseat milled in the shaft with a standard circular cutter. (See Figure 10-14c.) The tapered key serves to lock the hub axially on the shaft, but the parallel or Woodruff keys require some other means for axial fixation. Retaining rings or clamp collars are sometimes used for this purpose.

Parallel Keys

Parallel keys are the most commonly used. The ANSI and ISO standards each define particular key cross-sectional sizes and keyseat depths as a function of shaft diameter at the keyseat. A partial reproduction of this information is provided in Table 10-2 for the lower range of shaft diameters. Consult the respective standards for larger shaft sizes. Square keys are recommended for shafts up to 6.5-in dia (US), or 25 mm-dia (ISO), and rectangular keys for larger diameters. The parallel key is placed with half of its height in the shaft and half in the hub, as shown in Figure 10-14a.

Parallel keys are typically made from standard cold-rolled bar stock, which is conventionally “negatively tolerated,” meaning it will never be larger than its nominal dimension, only smaller. For example, a nominal 1/4-in square bar will have a tolerance on width and height of +0.000, -0.002 in. Thus, the keyseat can be cut with a standard 1/4-in milling cutter and the bar stock key will fit with slight clearance. A special keystock is also available, which is positively tolerated (e.g., 0.250 +0.002, -0.000).

* ANSI standard B17.1-1967, *Keys and Keyseats*, and B17.2-1967, *Woodruff Keys and Keyseats*, available from the American Society of Mechanical Engineers, 345 East 47th St., New York, N.Y. 10017.

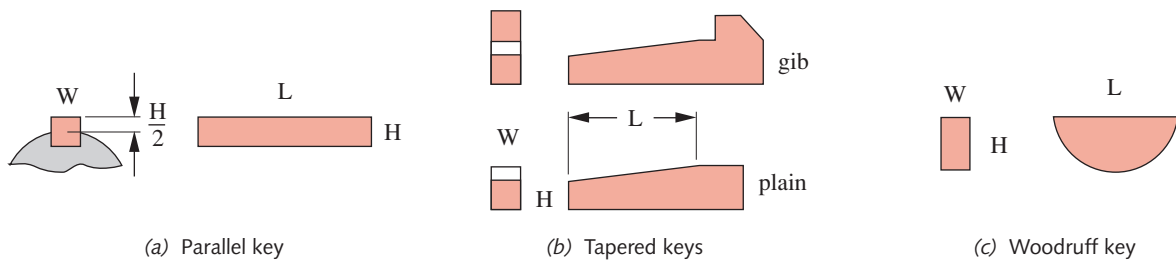


FIGURE 10-14

Various Styles of Keys

It is used when a closer fit between key and keyseat is desired and may require machining of the keystock to final dimension.

The key fit can be of concern when the torque loading is alternating from positive to negative each cycle. When the torque changes sign, any clearance between key and keyway will be suddenly taken up with resulting impact and high stresses. This is termed **backlash**. A setscrew in the hub, placed at 90° from the key, can both hold the hub axially and stabilize the key against backlash. The ANSI Standard also defines the size of setscrew to be used with each size key as shown in Table 10-2. Key length should be less than about 1.5 times the shaft diameter to avoid excessive twisting with shaft deflection. If more strength is needed, two keys can be used, oriented at 90° and 180° for example.

Tapered Keys

The width of a tapered key for a given shaft diameter is the same as for a parallel key as shown in Table 10-2. The taper and gib-head size are defined in the standard. The

Table 10-2 Standard Key and Setscrew Sizes for US and Metric Sized Shafts

Shaft Diameter (in)	Nominal Key Width (in)	Setscrew Dia. (in)	Shaft Diameter (mm)	Key Width x Height (mm)
$0.312 < d \leq 0.437$	0.093	#10	$8 < d \leq 10$	3 x 3
$0.437 < d \leq 0.562$	0.125	#10	$10 < d \leq 12$	4 x 4
$0.562 < d \leq 0.875$	0.187	0.250	$12 < d \leq 17$	5 x 5
$0.875 < d \leq 1.250$	0.250	0.312	$17 < d \leq 22$	6 x 6
$1.250 < d \leq 1.375$	0.312	0.375	$22 < d \leq 30$	8 x 7
$1.375 < d \leq 1.750$	0.375	0.375	$30 < d \leq 38$	10 x 8
$1.750 < d \leq 2.250$	0.500	0.500	$38 < d \leq 44$	12 x 8
$2.250 < d \leq 2.750$	0.625	0.500	$44 < d \leq 50$	14 x 9
$2.750 < d \leq 3.250$	0.750	0.625	$50 < d \leq 58$	16 x 10
$3.250 < d \leq 3.750$	0.875	0.750	$58 < d \leq 65$	18 x 11
$3.750 < d \leq 4.500$	1.000	0.750	$65 < d \leq 75$	20 x 12
$4.500 < d \leq 5.500$	1.250	0.875	$75 < d \leq 85$	22 x 14
$5.500 < d \leq 6.500$	1.500	1.000	$85 < d \leq 95$	25 x 14

taper is a locking one, which means that the friction force between the surfaces holds the key in place axially. The gib head is optional and provides a surface for prying the key out when the small end is not accessible. Tapered keys tend to create eccentricity between hub and shaft, as they drive all the radial clearance to one side.

Woodruff Keys

Woodruff keys are used on smaller shafts. They are self-aligning, so are preferred for tapered shafts. The penetration of a Woodruff key into the hub is the same as that of a square key, i.e., half the key width. The semicircular shape creates a deeper keyseat in the shaft, which resists key-rolling, but weakens the shaft compared to a square or tapered keyseat. Woodruff key widths as a function of shaft diameter are essentially the same as those for square keys shown in Table 10-2. The other dimensions of the Woodruff key are defined in the ANSI Standard, and keyseat cutters are readily available to match these dimensions. Table 10-3 reproduces a sample of the key-size specifications from the standard. Each key size is given a key number, which encodes its dimensions. The ANSI Standard states: "The last two digits give the nominal key diameter in eighths of an inch and the digits preceding the last two give the nominal width in thirty-second of an inch." For example, the key number 808 defines a key size of $8/32 \times 8/8$ or $1/4$ wide \times 1-in dia. See reference 6 for complete dimensional information on keys.

Stresses in Keys

There are two modes of failure in keys: shear and bearing. A shear failure occurs when the key is sheared across its width at the interface between the shaft and hub. Bearing failure occurs by crushing either side in compression.

Table 10-3 ANSI Standard Sizes of Woodruff Keys

Partial List: See the Standard for Complete Information and Figure 10-14c for Labels

Key Number	Nominal Key Size W x L	Height H
202	0.062×0.250	0.106
303	0.093×0.375	0.170
404	0.125×0.500	0.200
605	0.187×0.625	0.250
806	0.250×0.750	0.312
707	0.218×0.875	0.375
608	0.187×1.000	0.437
808	0.250×1.000	0.437
1208	0.375×1.000	0.437
610	0.187×1.250	0.545
810	0.250×1.250	0.545
1210	0.187×1.250	0.545
812	0.250×1.500	0.592
1212	0.375×1.500	0.592

SHEAR FAILURE The average stress due to direct shear was defined in equation 4.9, repeated here:

$$\tau_{xy} = \frac{F}{A_{shear}} \quad (10.10)$$

where F is the applied force and A_{shear} is the shear area being cut. In this case A_{shear} is the product of the key's width and length. The force on the key can be found from the quotient of the shaft torque and the shaft radius. If the shaft torque is constant with time, the force will be also and the safety factor can be found by comparing the shear stress to the shear yield strength of the material. If the shaft torque is time varying, then a fatigue failure of the key in shear is possible. The approach then is to compute the mean and alternating shear-stress components and use them to compute the mean and alternating von Mises stresses. These can then be used in a modified-Goodman diagram to find the safety factor as described in Section 6.13 (p. 381).

BEARING FAILURE The average bearing stress is defined as

$$\sigma_x = \frac{F}{A_{bearing}} \quad (10.11)$$

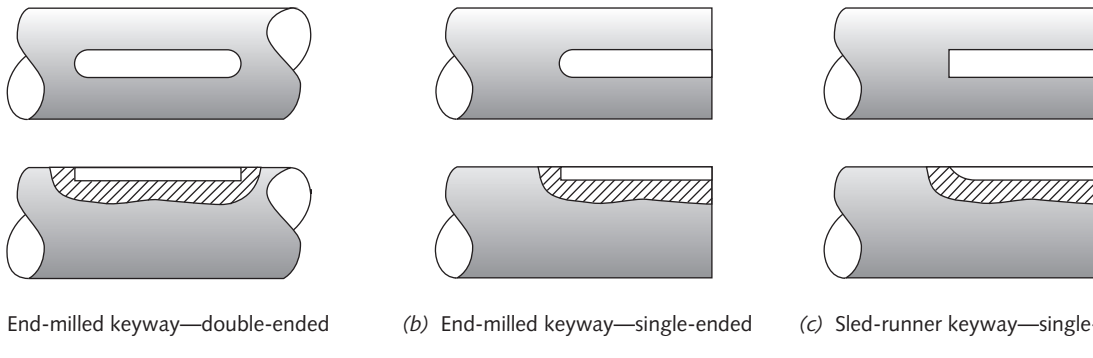
where F is the applied force and the bearing area is the area of contact between the key side and the shaft or the hub. For a square key this will be its half-height times its length. A Woodruff key has a different bearing area in the hub than in the shaft. The hub's Woodruff bearing area is much smaller and will fail first. The bearing stress should be calculated using the maximum applied force, whether constant or time varying. Since compressive stresses do not cause fatigue failures, bearing stresses can be considered static. The safety factor is found by comparing the maximum bearing stress to the material yield strength in compression.

Key Materials

Because keys are loaded in shear, ductile materials are used. Soft, low-carbon steel is the most common choice unless a corrosive environment requires a brass or stainless steel key. Square or rectangular keys are often made from cold-rolled bar stock and merely cut to length. The special keystock mentioned above is used when a closer fit is required between key and keyway. Tapered and Woodruff keys are also usually made from soft, cold-rolled steel.

Key Design

Only a few design variables are available when sizing a key. The shaft diameter at the keyseat determines the key width. The key height (or its penetration into the hub) is also determined by the key width. This leaves only the length of the key and the number of keys used per hub as design variables. A straight or tapered key can be as long as the hub allows. A Woodruff key can be had in a range of diameters for a given width, which effectively determines its length of engagement in the hub. Of course, as the Woodruff key diameter is increased, it further weakens the shaft with its deeper keyseat. If a single key cannot handle the torque at reasonable stresses, an additional key can be added, rotated 90° from the first.

**FIGURE 10-15**

Various Styles of Keyways in Shafts

It is common to size the key so that it will fail before the keyseat or other location in the shaft fails in the event of an overload. The key then acts like a shear pin in an outboard motor to protect the more expensive elements from damage. A key is inexpensive and relatively easy to replace if the keyseat is undamaged. This is one reason to use only soft, ductile materials for the key, having lower strength than that of the shaft so that a bearing failure will selectively affect the key rather than the keyway if the system sees an overload beyond its design range.

Stress Concentrations in Keyways

Since keys have relatively sharp corners ($< 0.02\text{-in}$ radius), keyseats must also. This causes significant stress concentrations. The keyway is broached in the hub and runs through its length, but the keyway must be milled into the shaft and has one or two ends. If an end-mill is used, the keyway will look like Figure 10-15a and will have sharp corners in the side view at one or both ends as well as along each side. If, instead, a sled-runner keyway is cut as shown in Figure 10-15c, the sharp corner at the end is eliminated and the stress concentration reduced. A Woodruff keyseat in the shaft also has a large radius in the side view but it (and every keyseat) suffers from sharp corners on the sides.

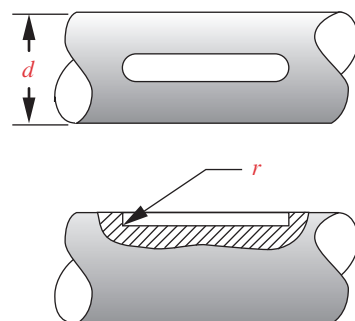
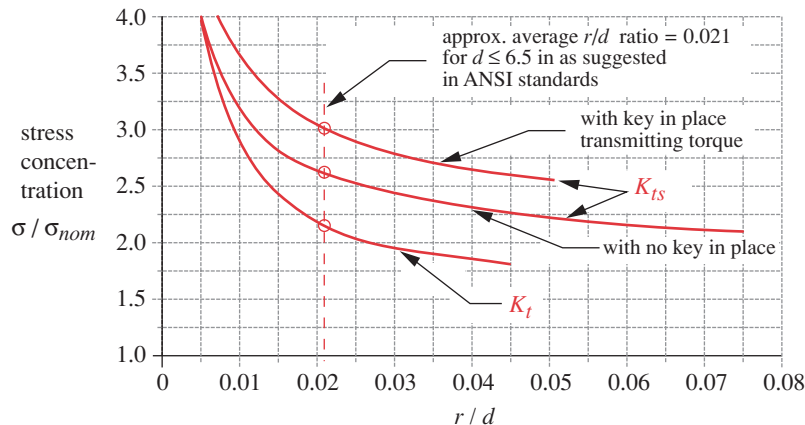
Peterson^[7] shows experimentally derived stress-concentration curves for end-milled keyseats in shafts under either bending or torsional loading. These are reproduced in Figure 10-16. These factors range from about 2 to about 4 depending on the ratio of the corner radius to the shaft diameter. Curve-fits to Figure 10-16 have been done and functions created for these curves so that the stress-concentration factor can be determined “on the fly” during a shaft-design computation. See the file SHFTDES for example. These factors should be applied to the bending and shear stresses in the shaft at the keyway location as was done in Examples 10-1 and 10-2.

EXAMPLE 10-4

Designing Shaft Keys

Problem

Design the keys for the shaft in Examples 10-2 (p. 565) and 10-3 (p. 568) and refine the estimate of the shaft’s safety factors based on the

**FIGURE 10-16**

Stress-Concentration Factors for an End-Milled Keyseat in Bending (K_t) and Torsion (K_{ts}) Source: R. E. Peterson, *Stress Concentration Factors*, 1974, Figures 182 and 183, pp. 266–267, reprinted by permission of John Wiley & Sons, Inc.

preliminary design dimensions from that earlier example in conjunction with refined stress-concentration factors.

Given

The loading is the same as in Example 10-2. The peak torque is 146 lb-in. Figure 10-9 (p. 565) shows the distribution of the peak moment over the shaft length. The values are 65.6 lb-in at point B and 18.3 lb-in at point D. The preliminary shaft diameters at the keys are $d_1 = 0.750$ in at B and $d_3 = 0.531$ in at D. See Figure 10-5 (p. 561) for labels.

Assumptions

Use square, parallel keys with end-milled keyways. The shaft material is the same as in Example 10-3. A low-carbon steel, SAE 1010, will be used for the keys. Its $S_{ut} = 53$ kpsi and $S_y = 44$ kpsi. S_e is calculated to be 22 990 psi. See Figure 10-16 for stress-concentration factors.

Solution

See Figure 10-5 (p. 561).

- 1 There are two locations with keys on this shaft, at points B and D. The design diameters chosen for these sections in Example 10-3 were $d_1 = 0.750$ at B and $d_3 = 0.531$ in at D. Table 10-2 (p. 571) shows that the standard key width for d_1 is 0.187 in and for d_3 is 0.125 in. The key length can be adjusted for each location.
- 2 At point B, the mean and alternating components of force on the key are found from the torque component divided by the shaft radius at that point.

$$F_a = \frac{T_a}{r} = \frac{73.1}{0.375} = 194.67 \text{ lb}$$

$$F_m = \frac{T_m}{r} = \frac{73.1}{0.375} = 194.67 \text{ lb} \quad (a)$$

- 3 Assume a key length of 0.5 in and calculate the alternating and mean shear stress components from

$$\tau_a = \frac{F_a}{A_{shear}} = \frac{194.67}{0.187(0.500)} = 2082 \text{ psi}$$

$$\tau_m = \frac{F_m}{A_{shear}} = \frac{194.67}{0.187(0.500)} = 2082 \text{ psi} \quad (b)$$

- 4 To find a safety factor for shear fatigue of the key, compute the von Mises equivalent stresses for each of these components from equation 5.7d (p. 249),

$$\sigma'_a = \sqrt{\sigma_x^2 + \sigma_y^2 - \sigma_x \sigma_y + 3\tau_{xy}^2} = \sqrt{3(2082)^2} = 3606 \text{ psi}$$

$$\sigma'_m = \sqrt{\sigma_x^2 + \sigma_y^2 - \sigma_x \sigma_y + 3\tau_{xy}^2} = \sqrt{3(2082)^2} = 3606 \text{ psi} \quad (c)$$

and use them in equation 6.18e (p. 368) to determine the fatigue safety factor:

$$N_f = \frac{1}{\frac{\sigma'_a}{S_e} + \frac{\sigma'_m}{S_{ut}}} = \frac{1}{\frac{3606}{22990} + \frac{3606}{53000}} = 4.4 \quad (d)$$

- 5 The bearing stress on the key is compression and thus can be considered a static load. It is calculated using the maximum force on the key:

$$\sigma_{max} = \frac{F_m + F_a}{A_{bearing}} = \frac{194.67 + 194.67}{0.0935(0.500)} = 8328 \text{ psi} \quad (e)$$

- 6 Calculate the safety factor for bearing failure from:

$$N_s = \frac{S_y}{\sigma_{max}} = \frac{44000}{4164} = 5.3 \quad (f)$$

- 7 At point D, the force on the key is

$$F_a = \frac{T_a}{r} = \frac{73.1}{0.266} = 275 \text{ lb}$$

$$F_m = \frac{T_m}{r} = \frac{73.1}{0.266} = 275 \text{ lb} \quad (g)$$

- 8 Assume a key length of 0.50 in and calculate the alternating and mean shear stress components from

$$\tau_a = \frac{F_a}{A_{shear}} = \frac{275}{0.125(0.50)} = 4400 \text{ psi}$$

$$\tau_m = \frac{F_m}{A_{shear}} = \frac{275}{0.125(0.50)} = 4400 \text{ psi} \quad (h)$$

- 9 Compute the von Mises equivalent stresses for each of these components from equation 5.7d,

$$\sigma'_a = \sqrt{\sigma_x^2 + \sigma_y^2 - \sigma_x \sigma_y + 3\tau_{xy}^2} = \sqrt{3(4399)^2} = 7620 \text{ psi}$$

$$\sigma'_m = \sqrt{\sigma_x^2 + \sigma_y^2 - \sigma_x \sigma_y + 3\tau_{xy}^2} = \sqrt{3(4399)^2} = 7620 \text{ psi} \quad (i)$$

and use them in equation 6.18e:

$$N_f = \frac{1}{\frac{\sigma'_a}{S_e} + \frac{\sigma'_m}{S_{ut}}} = \frac{1}{\frac{7620}{22990} + \frac{7620}{53000}} = 2.1 \quad (j)$$

- 10 The bearing stress on the key is calculated using the maximum force on the key:

$$\sigma_{max} = \frac{F_m + F_a}{A_{bearing}} = \frac{275 + 275}{0.0625(0.50)} = 17\,600 \text{ psi} \quad (k)$$

11 Calculate the safety factor for bearing failure from

$$N_s = \frac{S_y}{\sigma_{max}} = \frac{44\,000}{17\,600} = 2.5 \quad (l)$$

12 The safety factors for the shaft at these locations can now be recalculated using a stress-concentration factor at the keyways that takes into account the actual shaft diameter and actual notch radii. Our previous design calculation in Example 10-2 used a worst-case assumption for these values. Figure 10-16 shows the stress-concentration functions for end-milled keyways in both bending and torsion. To use these charts we must calculate the r/d ratio of the end-mill radius versus the shaft diameter. Assume a radius on the end mill of 0.010 in. The r/d ratios for the two points are then

$$\begin{aligned} \text{for point } B: \quad \frac{r}{d} &= \frac{0.010}{0.750} = 0.0133 \\ \text{for point } D: \quad \frac{r}{d} &= \frac{0.010}{0.531} = 0.0188 \end{aligned} \quad (m)$$

The corresponding stress-concentration factors are read from Figure 10-16 as

$$\begin{aligned} \text{for point } B: \quad K_t &= 2.5 & K_{ts} &= 2.9 \\ \text{for point } D: \quad K_t &= 2.2 & K_{ts} &= 2.7 \end{aligned} \quad (n)$$

13 These are used in equations (m), (n), and (o) of Example 10-1 to obtain the fatigue stress-concentration factors, which for a material notch sensitivity $q = 0.5$ are

$$\begin{aligned} \text{for point } B: \quad K_f &= 1.75 & K_{fs} &= 2.09 \\ \text{for point } D: \quad K_f &= 1.60 & K_{fs} &= 1.97 \\ \text{for both points:} \quad K_{fm} &= K_f & K_{fsm} &= K_{fs} \end{aligned} \quad (o)$$

14 The new safety factors are then calculated using equation 10.8 (p. 560) with the data from equations (b) and (c) from Example 10-2 with the design values for shaft diameter and the above stress-concentration values inserted. For point B:

$$0.75 = \left\{ \frac{32(N_f)}{\pi} \left[\frac{\sqrt{[1.75(32.8)]^2 + \frac{3}{4}[2.09(73.1)]^2}}{27\,300} + \frac{\sqrt{[1.75(32.8)]^2 + \frac{3}{4}[2.09(73.1)]^2}}{65\,000} \right] \right\}^{\frac{1}{3}}$$

$$N_f = 5.5 \quad (p)$$

for point D:

$$0.531 = \left\{ \frac{32(N_f)}{\pi} \left[\frac{\sqrt{[1.60(9.1)]^2 + \frac{3}{4}[1.97(73.1)]^2}}{27\,100} + \frac{\sqrt{[1.60(9.1)]^2 + \frac{3}{4}[1.97(73.1)]^2}}{65\,000} \right] \right\}^{\frac{1}{3}}$$

$$N_f = 2.2 \quad (q)$$

At point *B* the safety factor is greater than the specified value of 2.5. At point *D* it is lower. Increasing the diameter at *D* to 0.562 in gives a safety factor of 2.7. Then the safety factors for key failure (4.4 at *B* and 2.1 at *D*) are lower than those for shaft failure, which is desirable, since the keys will then fail before the shafts in an overload situation. This is now a viable and acceptable design.*

10.11 SPLINES

When more torque must be transmitted than can be handled by keys, splines can be used instead. Splines are essentially “built-in keys” formed by contouring the outside of the shaft and inside of the hub with toothlike forms. Early splines had teeth of square cross section but these have been supplanted by involute spline teeth, as shown in Figure 10-17. The involute tooth form is universally used on gears, and the same cutting techniques are used to manufacture splines. In addition to its manufacturing advantage, the involute tooth has less stress concentration than a square tooth and is stronger. The SAE defines standards for both square and involute spline tooth forms and ANSI publishes involute spline standards.[†] The standard involute spline has a pressure angle of 30° and half the depth of a standard gear tooth. The tooth size is defined by a fraction whose numerator is the diametral pitch (which defines tooth width—see Chapter 12 for more information on these terms) and whose denominator controls tooth depth (and is always double the numerator). Standard diametral pitches are 2.5, 3, 4, 5, 6, 8, 10, 12, 16, 20, 24, 32, 40, and 48. Standard splines can have from 6 to 50 teeth. Splines may have either a flat root or a filleted root, both shapes being shown in Figure 10-17. See reference 8 for complete dimensional information on standard splines.

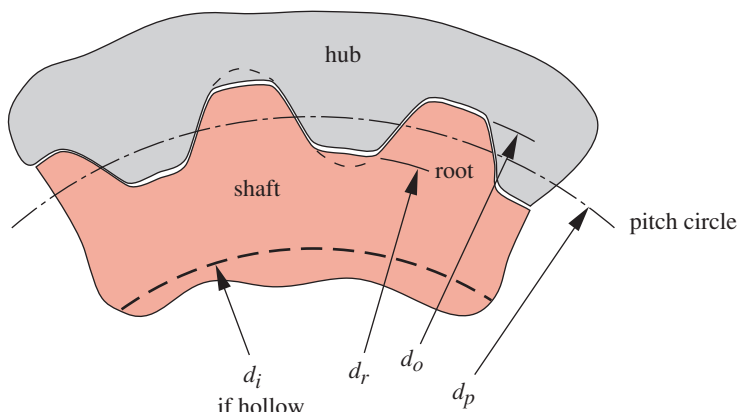
Some advantages of splines are maximum strength at the root of the tooth, accuracy of tooth form due to the use of standard cutters, and good machined surface finish from the standard gear-cutting (hobbing) process, which eliminates the need for grinding. A major advantage of splines over keys is their ability (with proper clearances) to accommodate large axial movements between shaft and hub while simultaneously transmitting torque. They are used to connect the transmission output shaft to the driveshaft

* Files EX10-04A, EX10-04B, EX10-04C, and EX10-04D are on the CD-ROM.

[†] ANSI Standard B92.1 and B92.2M, American National Standards Institute, 11 West 42nd St., New York, N.Y. 10036

FIGURE 10-17

Involute Spline Geometry



in automobiles and trucks where the suspension movement causes axial motion between the members. They are also used within nonautomatic, nonsynchromesh truck transmissions to couple the axially shiftable gears to their shafts. In addition, engine torque is usually passed into the transmission through a spline that connects the engine clutch to the transmission input shaft and allows the axial motion necessary to disengage the clutch from the flywheel.

The loading on a spline is typically pure torsion, either steady or fluctuating. While it is possible to have bending loads superposed, good design practice will minimize the bending moments by proper placement of bearings and by keeping a cantilevered spline as short as possible. As with keys, two failure modes are possible, bearing or shear. Shear failure is usually the limiting mode. Unlike keys, many teeth are available to share the load to some degree. Ideally, the spline length l needs to be only as long as is required to develop a combined tooth shear strength equal to the torsional shear strength of the shaft itself. If the spline were made perfectly with no variation in either tooth thickness or spacing, all teeth would share the load equally. However, the realities of manufacturing tolerances prohibit this ideal condition. The SAE states that “actual practice has shown that due to inaccuracies in spacing and tooth form, the equivalent of about 25% of teeth are in contact, so that a good approximate formula for a splined shaft (length) is”

$$l \equiv \frac{d_r^3(1 - d_i^4/d_r^4)}{d_p^2} \quad (10.12)$$

where d_r is the root diameter of the external spline, d_i is the internal diameter (if any) of a hollow shaft, and d_p is the pitch diameter of the spline, which is approximately at mid-tooth. The variable l represents the actual engaged length of the spline teeth with one another and should be considered as the minimum value needed to develop the strength in the teeth of an equivalent-diameter shaft.

The shear stress is calculated at the pitch diameter of the splines, where the shear area is

$$A_{\text{shear}} = \frac{\pi d_p l}{2} \quad (10.13a)$$

The shear stress can be calculated using the SAE assumption that only 25% of the teeth are actually sharing the load at any one time by considering only 1/4 of the shear area to be stressed:

$$\tau \equiv \frac{4F}{A_{\text{shear}}} = \frac{4T}{r_p A_{\text{shear}}} = \frac{8T}{d_p A_{\text{shear}}} = \frac{16T}{\pi d_p^2 l} \quad (10.13b)$$

where T is the torque on the shaft. Any bending stresses on the spline must also be calculated and properly combined with this shear stress. If the loading is pure torsion and static, then the shear stress of equation 10.13b is compared to the shear yield strength of the material to obtain a safety factor. If the loads are fluctuating or if bending is present, then the applied stresses should be converted to equivalent von Mises tensile stresses and compared to the appropriate strength criteria using the modified-Goodman diagram.

10.12 INTERFERENCE FITS

Another common means of coupling a hub to a shaft is to use a **press or shrink fit**, also called an **interference fit**. A press fit is obtained by machining the hole in the hub to a slightly smaller diameter than that of the shaft as shown in Figure 10-18. The two parts are then forced together slowly in a press, preferably with oil lubricant applied to the joint. The elastic deflection of both shaft and hub act to create large normal and frictional forces between the parts. The friction force transmits the shaft torque to the hub and resists axial motion as well. The American Gear Manufacturers Association (AGMA) publishes a standard AGMA 9003-A91, *Flexible Couplings—Keyless Fits* which defines formulas for the calculation of interference fits.

Only relatively small parts can be press-fitted without exceeding the force capacity of a typical shop press. For larger parts, a **shrink fit** can be made by heating the hub to expand its inside diameter and/or an **expansion fit** can be made by cooling the shaft to reduce its diameter. The hot and cold parts can be slipped together with little axial force, and when they equilibrate to room temperature, their dimensional change creates the desired interference for frictional contact. Another method is to hydraulically expand the hub with pressurized oil delivered through passageways in the shaft or hub. This technique can be used to remove a hub as well.

The amount of interference needed to create a tight joint varies with the diameter of the shaft. Approximately 0.001 to 0.002 units of diametral interference per unit of shaft diameter is typical (the rule of thousandths), the smaller amount being used with larger shaft diameters. For example, the interference for a diameter of 2 in would be about 0.004 in, but a diameter of 8 in would receive only about 0.009 to 0.010 in of interference. Another (and simpler) machinist's rule of thumb is to use 0.001 in of interference for diameters up to 1 in, and 0.002 in for diameters from 1 to 4 in.

Stresses in Interference Fits

An interference fit creates the same stress state in the shaft as would a uniform external pressure on its surface. The hub experiences the same stresses as a thick-walled cylinder subjected to internal pressure. The equations for stresses in a thick-walled cylinder were presented in Section 4.17 (p. 203) and depend on the applied pressures and the radii of the elements. The pressure p created by the press fit can be found from the deformation of the materials caused by the interference.

$$p = \frac{0.5\delta}{\frac{r}{E_o} \left(\frac{r_o^2 + r^2}{r_o^2 - r^2} + v_o \right) + \frac{r}{E_i} \left(\frac{r^2 + r_i^2}{r^2 - r_i^2} - v_i \right)} \quad (10.14a)$$

where $\delta = 2\Delta r$ is the total diametral interference between the two parts, r is the nominal radius of the interface between the parts, r_i is the inside radius (if any) of a hollow shaft, and r_o is the outside radius of the hub as shown in Figure 10-18. E and v are the Young's moduli and Poisson's ratios of the two parts, respectively.

The torque that can be transmitted by the interference fit can be defined in terms of the pressure p at the interface, which creates a friction force at the shaft radius.

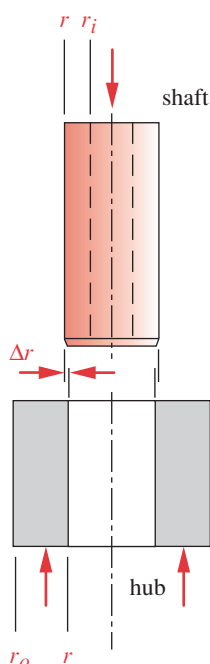


FIGURE 10-18

An Interference Fit

$$T = 2\pi r^2 \mu pl \quad (10.14b)$$

where l is the length of the hub engagement, r is the shaft radius, and μ is the coefficient of friction between shaft and hub. The AGMA standard suggests a value of $0.12 \leq \mu \leq 0.15$ for hydraulically expanded hubs and $0.15 \leq \mu \leq 0.20$ for shrink or press-fit hubs. AGMA assumes (and recommends) a surface finish of $32 \mu\text{in rms}$ ($1.6 \mu\text{m } R_a$), which requires a ground finish on both diameters. Equations 10.14a and 10.14b can be combined to give an expression that defines the torque obtainable from a particular deformation, coefficient of friction, and geometry.

$$T = \frac{\pi lr \mu \delta}{\frac{1}{E_o} \left(\frac{r_o^2 + r^2}{r_o^2 - r^2} + v_o \right) + \frac{1}{E_i} \left(\frac{r^2 + r_i^2}{r^2 - r_i^2} - v_i \right)} \quad (10.14c)$$

The pressure p is used in equations 4.47 (p. 204) to find the radial and tangential stresses in each part. For the shaft:

$$\sigma_{t_{\text{shaft}}} = -p \frac{r^2 + r_i^2}{r^2 - r_i^2} \quad (10.15a)$$

$$\sigma_{r_{\text{shaft}}} = -p \quad (10.15b)$$

where r_i is the inside radius of a hollow shaft. If the shaft is solid, r_i will be zero.

For the hub:

$$\sigma_{t_{\text{hub}}} = p \frac{r_o^2 + r^2}{r_o^2 - r^2} \quad (10.16a)$$

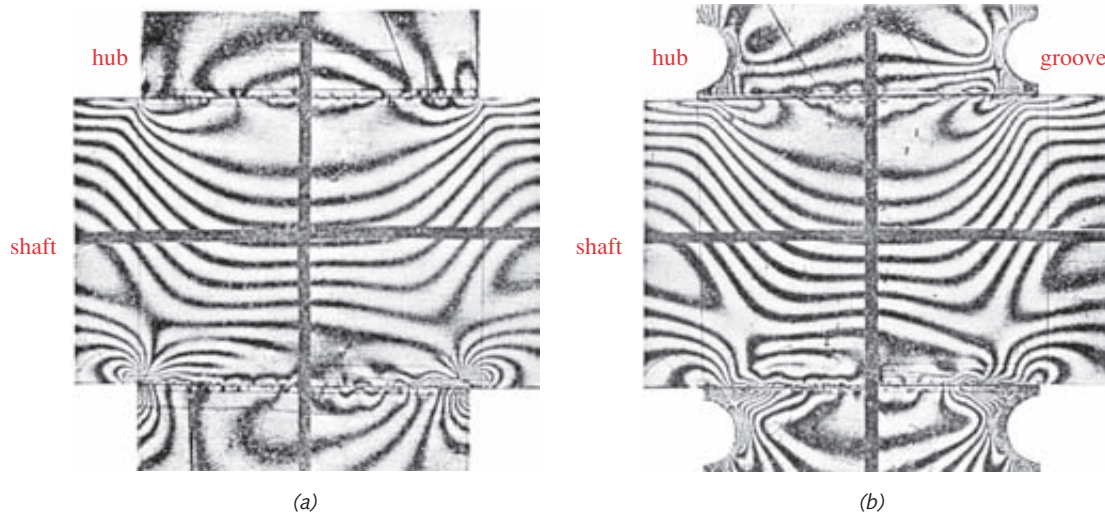
$$\sigma_{r_{\text{hub}}} = -p \quad (10.16b)$$

These stresses need to be kept below the yield strengths of the materials to maintain the fit. If the materials yield, the hub will become loose on the shaft.

Stress Concentration in Interference Fits

Even though there may be no disruption of the smooth surface of the press-fit shaft by shoulders or keyways, an interference fit nevertheless creates stress concentrations in the shaft and hub at the ends of the hub due to the abrupt transition from uncompressed to compressed material. Figure 10-19a shows a photoelastic study of a press-fit hub on a shaft. The fringes show stress concentration at the corners. Figure 10-19b shows how the stress concentration can be reduced by providing circumferential relief grooves in the faces of the hub close to the shaft diameter. These grooves make the material at the edge of the hub more compliant enabling it to deflect away from the shaft and reduce the stress locally. This approach is similar to the techniques for stress-concentration reduction shown in Figure 4-38 (p. 192).

Figure 10-20 shows curves of stress-concentration factors for interference fits between hubs and shafts developed from the photoelastic study of Figure 10-19a. The values on the abscissa are ratios of hub length to shaft diameter. These geometric stress-concentration

**FIGURE 10-19**

Photoelastic Stress Analysis of (a) A Plain Press-fit Assembly and (b) A Grooved-Hub Press-fit Assembly. Source: R. E. Peterson and A. M. Wahl, "Fatigue of Shafts at Fitted Members, with a Related Photoelastic Analysis," *ASME J. App. Mech.*, vol. 57, p. A1, 1935.

factors are applied in the same manner as before. For static loading they need to be used to determine whether local yielding will compromise the interference fit. For dynamic loading, they are modified by the material's notch sensitivity to get a fatigue stress-concentration factor to use in equation 10.8 (p. 560) for shaft design.

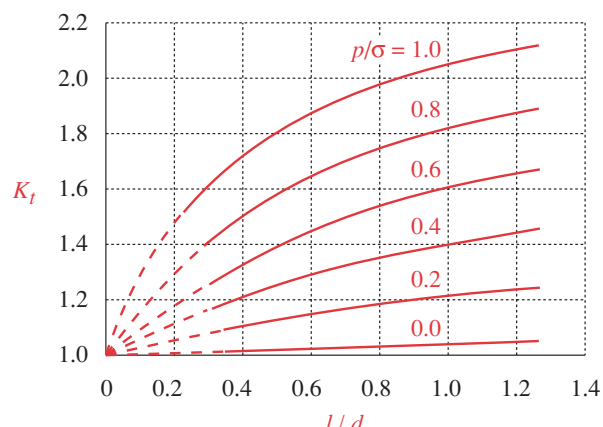
10

Fretting Corrosion

This problem was discussed in Chapter 7. Interference fits are the primary victims of fretting problems. Though the fretting mechanism is not yet fully understood, certain precautions are known to help reduce its severity. See Section 7.6 (p. 434) for more details.

$$p/\sigma = \frac{\text{nominal press-fit pressure}}{\text{nominal bending stress}}$$

$$l/d = \frac{\text{length of hub}}{\text{diameter of shaft}}$$

**FIGURE 10-20**

Stress Concentration in a Press-Fit or Shrink-Fit Hub on a Shaft. Source: R. E. Peterson and A. M. Wahl, "Fatigue of Shafts at Fitted Members, with a Related Photoelastic Analysis," *ASME J. App. Mech.*, vol. 57, p. A73, 1935.

EXAMPLE 10-5**Designing an Interference Fit****Problem**

Redesign the attachment of the gear to the shaft in Figure 10-5 (p. 561) to make it an interference fit rather than a keyed connection. Define the shaft and gear hole dimensions and their tolerances for a press fit.

Given

The loading is the same as in Example 10-2 (p. 565). The peak torque at the gear (point *B*) is 146 lb-in. Use the nominal shaft diameters of $d_0 = 0.875$ in, $d_1 = 0.750$ in. See Figure 10-5 for labels. The gear hub diameter is 3 in and its length is 1.5 in.

Assumptions

The shaft material is the same as in Example 10-2. Class 40 gray cast iron is used for the gear with $S_{ut} = 42$ kpsi and $E = 14$ Mpsi. See Figure 10-20 for stress-concentration factors. The 0.750 shaft diameter will be increased slightly to 0.780 nominal, where it press fits into the gear hub to allow the gear to slip over the rest of the shaft at assembly.

Solution

See Figure 10-5 and Table 10-4.

- 1 The nominal diameter of the shaft at the gear hub is 0.780 in. Based on the rule of thousandths, a reasonable diametral interference would be 0.0015 in. From this assumption, the bearing pressure after pressing can be found from equation 10.14 (pp. 580–581).

$$\begin{aligned} p &= \frac{0.5\delta}{\frac{r}{E_o}\left(\frac{r_o^2 + r^2}{r_o^2 - r^2} + v_o\right) + \frac{r}{E_i}\left(\frac{r^2 + r_i^2}{r^2 - r_i^2} - v_i\right)} \\ &= \frac{0.5(0.0015)}{\frac{0.390}{1.4E7}\left(\frac{1.5^2 + 0.390^2}{1.5^2 - 0.390^2} + 0.28\right) + \frac{0.390}{3.0E7}\left(\frac{0.390^2 + 0}{0.390^2 - 0} - 0.28\right)} \quad (a) \\ p &= 15\,288 \text{ psi} \end{aligned}$$

- 2 The stresses in the shaft after pressing are found from equations 10.15 (p. 581).

$$\sigma_{t_{shaft}} = -p \frac{r^2 + r_i^2}{r^2 - r_i^2} = -15\,288 \frac{0.390^2 + 0}{0.390^2 - 0} = -15\,288 \text{ psi} \quad (b)$$

$$\sigma_{r_{shaft}} = -p = -15\,288 \text{ psi} \quad (c)$$

- 3 The stresses in the hub after pressing are found from equations 10.16 (p. 581).

$$\sigma_{t_{hub}} = p \frac{r_o^2 + r^2}{r_o^2 - r^2} = 15\,288 \frac{1.5^2 + 0.390^2}{1.5^2 - 0.390^2} = 17\,505 \text{ psi} \quad (d)$$

$$\sigma_{r_{hub}} = -p = -15\,288 \text{ psi} \quad (e)$$

- 4 To find the stress-concentration factor we need the hub-length to shaft-diameter ratio, l/d :

$$\frac{l}{d} = \frac{1.500}{0.780} = 1.923 \quad (f)$$

and the ratio of press-fit pressure to nominal bending stress:

$$\sigma = \frac{Mc}{I} = \frac{65.6(0.390)64}{\pi(0.780^4)} = 1408 \text{ psi} \quad (g)$$

$$\frac{p}{\sigma} = \frac{15288}{1408} = 10.9 \quad (h)$$

- 5 Taking these values to Figure 10-20, we find that they are off the chart. We will assume an approximate value for the stress-concentration factor of:

$$K_t \approx 2.4 \quad (i)$$

- 6 The safety factors against failure during press fitting can now be found:

$$N_{s_{\text{shaft}}} = \frac{S_y}{K_t \sigma_{t_{\text{shaft}}}} = \frac{-38000}{2.4(-15288)} = 1.0 \quad (j)$$

$$N_{s_{\text{hub}}} = \frac{S_{ut}}{K_t \sigma_{t_{\text{hub}}}} = \frac{42000}{2.4(17505)} = 1.0 \quad (k)$$

- 7 Both parts are at failure with this much interference. The computations were repeated for a range of interference values from 0.0008 to 0.0015 in, and those results are shown in Table 10-4. The safety factors range from 2.0 to 1.0.
- 8 We would like a tolerance range of at least 0.0002 in on each part or a total variation in interference of at least 0.0004 in for a set of mass-produced parts. So we choose to set the range of interference from 0.0008 to 0.0013 in, a total range of 0.0005 in.
- 9 The part dimensions are then established as

$$\begin{aligned} \text{hub dia} &= 0.7799 + 0.0003 / -0.0000 = \frac{0.7802}{0.7799} \text{ in} \\ \text{shaft dia} &= 0.7812 + 0.0000 / -0.0002 = \frac{0.7812}{0.7810} \text{ in} \end{aligned} \quad (l)$$

giving a range of interference of

$$\begin{aligned} \text{min interference} &= 0.7810 - 0.7802 = 0.0008 \text{ in} \\ \text{max interference} &= 0.7812 - 0.7799 = 0.0013 \text{ in} \end{aligned} \quad (m)$$

- 10 What torque will this pressed joint transmit at its minimum interference, assuming $\mu = 0.15$? From equation 10.14c (p. 581):

$$\begin{aligned} T &= \frac{\pi l r \mu \delta}{\frac{1}{E_o} \left(\frac{r_o^2 + r^2}{r_o^2 - r^2} + v_o \right) + \frac{1}{E_i} \left(\frac{r^2 + r_i^2}{r^2 - r_i^2} - v_i \right)} \\ T &= \frac{\pi(1.5)(0.375)(0.15)(0.0008)}{0.375 \left(\frac{1.5^2 + 0.390^2}{1.5^2 - 0.390^2} + 0.28 \right) + \frac{0.375}{3.0 E 7} \left(\frac{0.390^2 + 0}{0.390^2 - 0} - 0.28 \right)} \quad (n) \\ T &= 1753 \text{ in-lb} \end{aligned}$$

* See file EX10-05 on the CD-ROM.

This is well in excess of the peak operating torque of 146 in-lb, so it will work.*

Table 10-4 Safety Factors for Various Interferences in Example 10-5

Interference (in)	p (psi)	p/σ	K_t	$N_{s_{\text{shaft}}}$	$N_{s_{\text{hub}}}$
0.000 8	8 154	5.8	2.3	2.0	1.9
0.000 9	9 173	6.5	2.4	1.8	1.7
0.001 0	10 192	7.2	2.4	1.6	1.5
0.001 1	11 212	8.0	2.4	1.4	1.4
0.001 2	12 231	8.7	2.4	1.3	1.3
0.001 3	13 250	9.4	2.4	1.2	1.2
0.001 4	14 269	10.1	2.4	1.1	1.1
0.001 5	15 288	10.9	2.4	1.0	1.0

10.13 FLYWHEEL DESIGN*

A flywheel is used to smooth out variations in the speed of a shaft caused by torque fluctuations. Many machines have load patterns that cause the torque-time function to vary over the cycle. Piston compressors, punch presses, rock crushers, etc., all have time-varying loads. The prime mover can also introduce torque oscillations to the transmission shaft. Internal-combustion engines with one or two cylinders are an example. Other systems may have both smooth torque sources and smooth loads, such as an electrical generator driven by a steam turbine. These smooth-acting devices have no need for a flywheel. If the source of the driving torque or the load torque has a fluctuating nature, then a flywheel is usually called for.

A flywheel is an energy-storage device. It absorbs and stores kinetic energy when speeded up and returns energy to the system when needed by slowing its rotational speed. The kinetic energy E_k in a rotating system is

$$E_k = \frac{1}{2} I_m \omega^2 \quad (10.17a)$$

where I_m is the mass moment of inertia of all rotating mass on the shaft about the axis of rotation and ω is the rotational velocity. This includes the I_m of the motor rotor and anything else rotating with the shaft plus that of the flywheel.

Flywheels may be as simple as a cylindrical disk of solid material, or may be of spoked construction with a hub and rim. The latter arrangement is more efficient of material, especially for large flywheels, as it concentrates the bulk of its mass in the rim, which is at the largest radius. Since the mass moment of inertia I_m of a flywheel is proportional to mr^2 , mass at larger radius contributes much more. If we assume a solid-disk geometry with inside radius r_i and outside radius r_o , the mass moment of inertia is

$$I_m = \frac{m}{2} (r_o^2 + r_i^2) \quad (10.17b)$$

The mass of a solid circular disk of constant thickness t and having a central hole is

$$m = \frac{W}{g} = \pi \frac{\gamma}{g} (r_o^2 - r_i^2) t \quad (10.17c)$$

* Portions of this section are adapted from R. L. Norton, *Design of Machinery*, 4th ed, McGraw-Hill, 2008, pp. 596–602, with the publisher's permission.

Substituting in equation 10.17b gives an expression for I_m in terms of the disk geometry:

$$I_m = \frac{\pi \gamma}{2g} (r_o^4 - r_i^4) t \quad (10.17d)$$

where γ is the material's weight density and g is the gravitational constant.

There are two stages to the design of a flywheel. First, the amount of energy required for the desired degree of smoothing must be found and the moment of inertia needed to absorb that energy determined. Then a flywheel geometry must be defined that both supplies that mass moment of inertia in a reasonably sized package and is safe against failure at design speeds.

Energy Variation in a Rotating System

Figure 10-21 shows a flywheel, designed as a flat circular disk, attached to a motor shaft. The motor supplies a torque magnitude T_m , which we would like to be as constant as possible, i.e., to be equal to the average torque T_{avg} . Assume that the load on the other side of the flywheel demands a torque T_l , which is time varying, as shown in Figure 10-22. This torque variation can cause the shaft speed to vary depending on the torque-speed characteristic of the driving motor. We need to determine how much I_m to add in the form of a flywheel to reduce the speed variation of the shaft to an acceptable level. Write Newton's law for the free-body diagram in Figure 10-21.

$$\sum T = I_m \alpha$$

$$T_l - T_m = I_m \alpha \quad (10.18a)$$

but we want

$$T_m = T_{avg}$$

so

$$T_l - T_{avg} = I_m \alpha \quad (10.18b)$$

Substituting

$$\alpha = \frac{d\omega}{dt} = \frac{d\omega}{dt} \left(\frac{d\theta}{d\theta} \right) = \omega \frac{d\omega}{d\theta}$$

gives

$$T_l - T_{avg} = I_m \omega \frac{d\omega}{d\theta}$$

$$(T_l - T_{avg}) d\theta = I_m \omega d\omega \quad (10.18c)$$

Integrating

$$\int_{\theta @ \omega_{min}}^{\theta @ \omega_{max}} (T_l - T_{avg}) d\theta = \int_{\omega_{min}}^{\omega_{max}} I_m \omega d\omega$$

$$\int_{\theta @ \omega_{min}}^{\theta @ \omega_{max}} (T_l - T_{avg}) d\theta = \frac{1}{2} I_m (\omega_{max}^2 - \omega_{min}^2) \quad (10.18d)$$

The left-hand side of this expression represents the change in kinetic energy E_k between the maximum and minimum shaft ω 's and is equal to the area under the torque-time diagram of Figure 10-22 between those extreme values of ω . The right-hand side of equation 10.18c is the change in kinetic energy stored in the flywheel. The only way

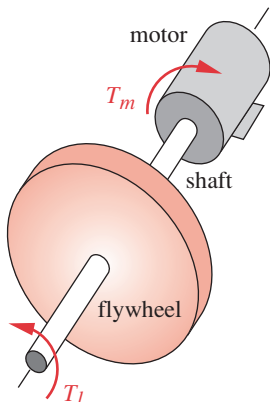


FIGURE 10-21

A Flywheel on a Transmission Shaft

to extract kinetic energy from the flywheel is to slow it down, as shown in equation 10.17a. Adding kinetic energy speeds it up. It is impossible to obtain exactly constant shaft velocity in the face of changing energy demands by the load. The best we can do is to minimize the speed variation ($\omega_{max} - \omega_{min}$) by providing a flywheel with sufficiently large I_m .

EXAMPLE 10-6

Determining the Energy Variation in a Torque-Time Function

Problem Find the energy variation per cycle in a torque-time function that needs to be absorbed by a flywheel for smooth operation.

Given A torque-time function that varies over its cycle as shown in Figure 10-22. The torque varies during the 360° cycle about its average value.

Assumptions The one cycle of torque variation shown is representative of the steady-state condition. Energy delivered from the source to the load will be considered positive and energy returned from load to source, negative.

Solution

- 1 Calculate the average value of the torque-time function over one cycle using numerical integration. In this case it is 7 020 lb-in. (Note that in some cases the average value may be zero.)
- 2 Note that the integration on the left-hand side of equation 10.18c is done with respect to the average line of the torque function, not with respect to the θ axis. (From the definition of the average, the sum of positive area above an average line is

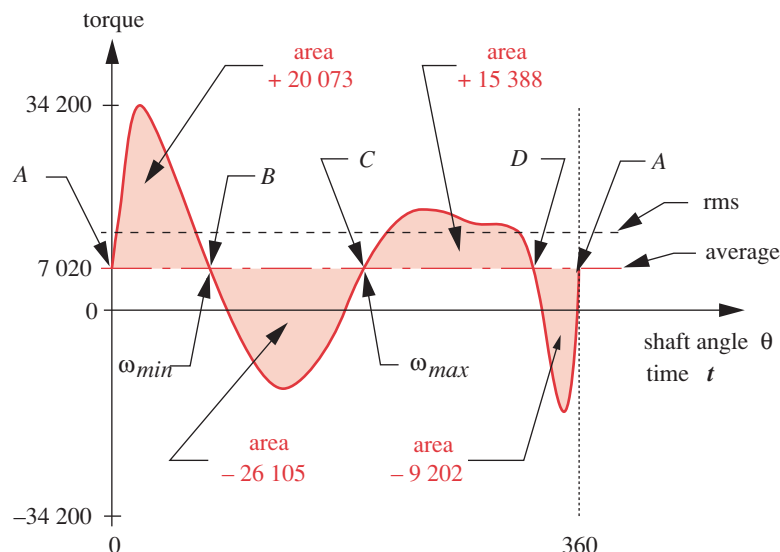


FIGURE 10-22

Integrating the Pulses Above and Below the Average Value in the Torque-Time Function

Table 10-5 Accumulation of Energy Pulses Under a Torque-Time Curve

From	$\Delta\text{Area} = \Delta E$	Accumulated Sum = E	Min & Max
A to B	+20 073	+20 073	$\omega_{min} @ B$
B to C	-26 105	-6 032	$\omega_{max} @ C$
C to D	+15 388	+9 356	
D to A	-9 202	+154	
$\text{Total } \Delta E = E @ \omega_{max} - E @ \omega_{min}$ $= (-6 032) - (+20 073) = -26 105 \text{ in-lb}$			

equal to the sum of negative area below that line.) The integration limits in equation 10.18 are from the shaft angle θ , at which the shaft ω is a minimum to the shaft angle θ , at which ω is a maximum.

- 3 The minimum ω will occur after the maximum positive energy has been delivered from the motor to the load, i.e., at a point θ where the summation of positive energy (area) in the torque pulses is at its largest positive value.
- 4 The maximum ω will occur after the maximum negative energy has been returned to the load, i.e., at a point θ where the summation of energy (area) in the torque pulses is at its largest negative value.
- 5 To find these locations in θ corresponding to the maximum and minimum ω 's and thus find the amount of energy needed to be stored in the flywheel, we need to numerically integrate each pulse of this function from crossover to crossover with the average line. The crossover points have been labeled A, B, C, and D and the areas between them are shown in Figure 10-22.
- 6 The remaining task is to accumulate these pulse areas beginning at an arbitrary crossover (in this case point A) and proceeding pulse by pulse across the cycle. Table 10-5 shows this process and the result.
- 7 Note in Table 10-5 that the minimum shaft speed occurs after the largest accumulated positive energy pulse (+20 073 in-lb) has been delivered from the driveshaft to the system. This delivery of energy slows the motor down. The maximum shaft speed occurs after the largest accumulated negative energy pulse (-6 032 in-lb) has been received back from the load by the shaft. This return of stored energy will tend to speed up the motor. The total energy variation is the algebraic difference between these two extreme values, which in this example is -26 105 in-lb. This energy coming back from the load needs to be absorbed by the flywheel and later returned to the system within each cycle to smooth the variations in shaft speed. See files EX09-07a and EX09-07b that also contain the calculations for Example 10-6.

Determining the Flywheel Inertia

We must now determine how large a flywheel is needed to absorb this energy with an acceptable change in speed. The change in shaft speed during a cycle is called its fluctuation F_l and is equal to

$$F_l = \omega_{max} - \omega_{min} \quad (10.19a)$$

We can normalize this to a dimensionless ratio by dividing it by the average shaft speed. This ratio is called the coefficient of fluctuation C_f .

$$C_f = \frac{(\omega_{max} - \omega_{min})}{\omega_{avg}} \quad (10.19b)$$

This coefficient of fluctuation is a design parameter to be chosen by the designer. It is typically set to a value between 0.01 and 0.05 for precision machinery, and as high as 0.20 for crushing or hammering machinery, which correspond to a 1 to 5% fluctuation in shaft speed. The smaller this chosen value, the larger the flywheel will have to be. This presents a design trade-off. A larger flywheel will add more cost and weight to the system, which are factors that have to be considered against the smoothness of operation desired.

We found the required change in kinetic energy E_k by integrating the torque curve,

$$\int_{\theta @ \omega_{min}}^{\theta @ \omega_{max}} (T_l - T_{avg}) d\theta = E_k \quad (10.20a)$$

and can now set it equal to the right-hand side of equation 10.18c:

$$E_k = \frac{1}{2} I_m (\omega_{max}^2 - \omega_{min}^2) \quad (10.20b)$$

Factoring this expression:

$$E_k = \frac{1}{2} I_m (\omega_{max} + \omega_{min})(\omega_{max} - \omega_{min}) \quad (10.20c)$$

If the torque-time function were a pure harmonic, then its average value could be expressed exactly as

$$\omega_{avg} = \frac{(\omega_{max} + \omega_{min})}{2} \quad (10.21)$$

Our torque functions will seldom be pure harmonics, but the error introduced by using this expression as an approximation of the average is acceptable. We can now substitute equations 10.19b and 10.21 into equation 10.20c to get an expression for the mass moment of inertia I_s needed in the entire rotating system in order to obtain the selected coefficient of fluctuation.

$$E_k = \frac{1}{2} I_s (2\omega_{avg})(C_f \omega_{avg})$$

$$I_s = \frac{E_k}{C_f \omega_{avg}^2} \quad (10.22)$$

Equation 10.22 can be used to design the physical flywheel by choosing a desired coefficient of fluctuation C_f , and using the value of E_k from the numerical integration of the torque curve (see Table 10-5 for an example) and the average shaft ω to compute the needed system I_s . The physical flywheel's mass moment of inertia I_m is then set equal to the required system I_s . But, if the moments of inertia of the other rotating elements on the same shaft (such as the motor) are known, the physical flywheel's required I_m can be reduced by those amounts.

The most efficient flywheel design in terms of maximizing I_m for minimum material used is one in which the mass is concentrated in its rim and its hub is supported on spokes, like a carriage wheel. This puts the majority of the mass at the largest radius possible and minimizes the weight for a given I_m . Even if a flat, solid circular disk flywheel design is chosen, either for simplicity of manufacture or to obtain a flat surface for other functions (such as an automobile clutch), the design should be done with an eye to reducing weight and thus cost. Since, in general, $I_m = mr^2$, a thin disk of large diameter will need fewer pounds of material to obtain a given I_m than will a thicker disk of smaller diameter. Dense materials such as cast iron and steel are the obvious choices for a flywheel. Aluminum is seldom used. Though many metals (lead, gold, silver, platinum) are more dense than iron and steel, one can seldom get the accounting department's approval to use them in a flywheel.

Figure 10-23 shows the change in the torque of Figure 10-22 after the addition of a flywheel sized to provide a coefficient of fluctuation of 0.05. The oscillation in torque about the unchanged average value is now 5%, much less than what it was without the flywheel. Note that the peak value is now 87 instead of 372 lb-in. A much smaller-horsepower motor can now be used because the flywheel is available to absorb the energy returned from the load during the cycle.

Stresses in Flywheels

As a flywheel spins, the centrifugal force acts upon its distributed mass and attempts to pull it apart. These centrifugal forces are similar to those caused by an internal pressure in a cylinder. Thus, the stress state in a spinning flywheel is analogous to a thick-walled cylinder under internal pressure (see Section 4.17 on p. 203). The tangential stress of a solid-disk flywheel as a function of its radius r is

$$\sigma_t = \frac{\gamma}{g} \omega^2 \left(\frac{3+\nu}{8} \right) \left(r_i^2 + r_o^2 + \frac{r_i^2 r_o^2}{r^2} - \frac{1+3\nu}{3+\nu} r^2 \right) \quad (10.23a)$$

and the radial stress is

$$\sigma_r = \frac{\gamma}{g} \omega^2 \left(\frac{3+\nu}{8} \right) \left(r_i^2 + r_o^2 - \frac{r_i^2 r_o^2}{r^2} - r^2 \right) \quad (10.23b)$$

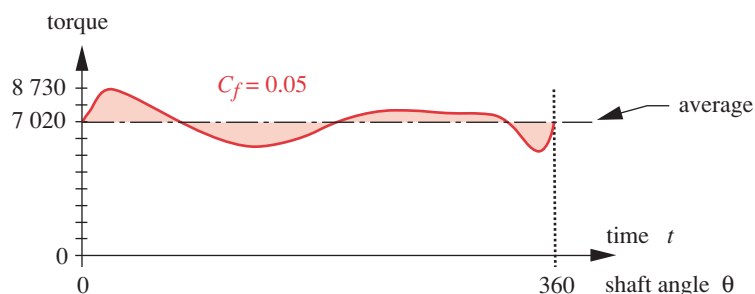


FIGURE 10-23

Torque-Time Function of Figure 9-22 After Adding a Flywheel with $C_f = 0.05$

where γ = material weight density, ω = angular velocity in rad/sec, v = Poisson's ratio, r is the radius to a point of interest, and r_i, r_o are inside and outside radii of the solid-disk flywheel.

Figure 10-24 shows how these stresses vary over the radius of the flywheel. The tangential stress is a maximum at the inner radius. The radial stress is zero at inside and outside radii and peaks at an interior point but is everywhere less than the tangential stress. The point of most interest is then at the inside radius. The tangential tensile stress at that point is what fails a flywheel, and when it fractures at that point, it typically fragments and explodes with extremely dangerous results. Since the forces causing the stress are a function of rotational speed, there will always be some speed that will fail the flywheel. A maximum safe operating speed should be calculated for a flywheel and some means taken to preclude its operation at higher speeds, such as a speed control or governor. A safety factor against overspeeding can be determined as the quotient of the speed that will cause yielding over the operating speed, $N_{os} = \omega / \omega_{yield}$.

Failure Criteria

If the flywheel spends most of its life operating at essentially constant speed, then it can be considered to be statically loaded and the yield strength used as a failure criterion. The number of start-stop cycles in its operating regime will determine whether a fatigue-loading situation needs to be considered. Each runup to operational speed and rundown to zero constitutes a fluctuating stress cycle. If the number of these start-stop cycles is large enough over the projected life of the system, then fatigue-failure criteria should be applied. A low-cycle fatigue regime may require a strain-based fatigue failure analysis rather than a stress-based one, particularly if there exists the possibility of any transient overloads that may cause the local stresses to exceed the yield stress at stress concentrations.

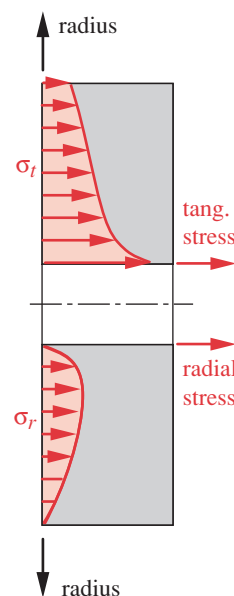


FIGURE 10-24

Stress Distributions Along the Radius of a Spinning Flywheel

EXAMPLE 10-7

Designing a Solid-Disk Flywheel

Problem Design a suitable flywheel for the system of Example 10-6. An overspeed safety factor of at least 2 is desired.

Given An input torque-time function which varies over its cycle as shown in Figure 10-22 (p. 587). The torque is varying during the 360° cycle about its average value, and the energy variation per cycle is 26 105 in-lb as shown in Table 10-5 (p. 588). The shaft $\omega = 800$ rad/sec.

Assumptions The one cycle of torque variation shown is representative of the steady-state condition. The desired coefficient of fluctuation is 0.05. The system is in continuous operation with minimal start-stop cycles. A steel of 62 kpsi yield strength will be used. No keyway will be used in order to reduce stress concentrations. Instead, a tapered locking hub will frictionally couple it to the shaft and the hub will be axially bolted to the flywheel.

Solution

See Figure 10-25 and Table 10-6.

- 1 We know the amount of energy needed from the torque-time diagram from Example 10-6 and have defined the shaft ω and a desired coefficient of fluctuation. From these data we can determine a required mass moment of inertia for the system I_s using equation 10.22 (p. 589).

$$I_s = \frac{E}{C_f \omega_{avg}^2} = \frac{26105}{0.05(800)^2} = 0.816 \text{ lb-in sec}^2 \quad (a)$$

The flywheel need only supply a portion of this amount if other rotating masses such as the motor armature are present. However, we will assume in this example that the flywheel will provide all of the required inertia, making $I_m = I_s$.

- 2 The flywheel dimensions for this moment of inertia can be defined from equation 10.17d. We will assume a steel material with $\gamma = 0.28 \text{ lb/in}^3$ and an inside radius $r_i = 1 \text{ in}$.

$$\begin{aligned} I_m &= \frac{\pi \gamma}{2g} (r_o^4 - r_i^4) t = 0.816 \\ 0.816 &= \frac{\pi}{2} \left(\frac{0.28}{386} \right) (r_o^4 - 1^4) t \\ 716.14 &= (r_o^4 - 1)t \end{aligned} \quad (b)$$

So, the required I_m can be obtained with an infinity of combinations of flywheel radius r_o and thickness t for the assumed data.

- 3 The best solution to equation (b) will be one that balances the conflicting factors of flywheel size, weight, stresses, and safety factor. Consider two possible designs, one with a small thickness t and the other with a large t . The thin flywheel will be larger in diameter but considerably lighter than the thick one due to the nonlinearity of the terms involving r_o . But, as r_o increases, so will the stresses, because the mass at larger radius exerts more centrifugal force on the material.
- 4 To get a value of r_o that is consistent with any desired safety factor, the tangential stress equation 10.23a can be back-solved with assumed values of $\sigma_t = S_y / N_y$, r_i , and material parameters ν and γ ,

$$\begin{aligned} \sigma_t &= \frac{\gamma \omega^2}{g} \left(\frac{3+\nu}{8} \right) \left(r_i^2 + r_o^2 + \frac{r_i^2 r_o^2}{r^2} - \frac{1+3\nu}{3+\nu} r^2 \right) = \frac{S_y}{N_y} \\ \frac{62\,000}{N_y} &= \frac{0.28}{386} (800)^2 \left(\frac{3+0.28}{8} \right) \left(1 + r_o^2 + \frac{r_o^2}{1} - \frac{1+3(0.28)}{3+0.28} (1) \right) \\ r_o^2 &= \frac{162.9}{N_y} - 0.535 \end{aligned} \quad (c)$$

That value of r_o can then be used in equation (b) to find the flywheel thickness. For a design safety factor against yielding of 2.5 and the values assumed in equation (c), we get $r_o = 8.06 \text{ in}$ and $t = 0.172 \text{ in}$.

- 5 With the flywheel geometry now defined, the rotational speed at which yielding will begin can be computed from equation 10.17d using the yield strength for the stress value.

Table 10-6 Data for Example 10-7 with $I_m = 0.816 \text{ lb-in-sec}^2$

Thickness (in)	Diameter (in)	r/t ratio	Weight (lb)	Stress (psi)	Safety Factor Yielding	Safety Factor Overspeed
0.125	17.40	69.6	8.20	28 896	2.1	1.5
0.250	14.63	29.3	11.60	20 459	3.0	1.7
0.375	13.22	17.6	14.10	16 722	3.7	1.9
0.500	12.31	12.3	16.20	14 494	4.3	2.1
0.625	11.64	9.3	18.10	12 974	4.8	2.2
0.750	11.12	7.4	19.70	11 852	5.2	2.3
0.875	10.70	6.1	21.30	10 980	5.6	2.4
1.000	10.35	5.2	22.70	10 277	6.0	2.5
1.125	10.05	4.5	24.00	9 695	6.4	2.5
1.250	9.79	3.9	25.20	9 202	6.7	2.6

$$\sigma_t = S_y = \frac{\gamma}{g} \omega^2 \left(\frac{3+v}{8} \right) \left(r_i^2 + r_o^2 + \frac{r_i^2 r_o^2}{r^2} - \frac{1+3v}{3+v} r^2 \right)$$

$$62\ 000 = \frac{0.28}{g} \omega_{yield}^2 \left(\frac{3+0.28}{8} \right) \left(1 + 8.06^2 + \frac{8.06^2}{1} - \frac{1+3(0.28)}{3+0.28}(1) \right) \quad (d)$$

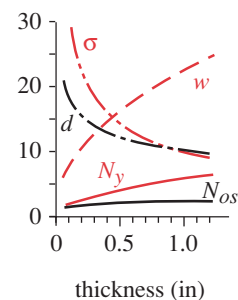
$$\omega_{yield} = 1\ 265 \text{ rad/sec}$$

Since this operating speed causes failure, a safety factor against overspeeding can be computed from

$$N_{os} = \frac{\omega_{yield}}{\omega} = \frac{1\ 265 \text{ rad/sec}}{800 \text{ rad/sec}} = 1.6 \quad (e)$$

- 6 To show the variation of parameters with flywheel geometry, this set of equations was solved for a list of possible thicknesses t chosen over a reasonable design range of 0.125 to 1.25 in. Table 10-6 shows the resulting data and Figure 10-25 plots the trends. Note that the weight increases as the outside diameter decreases and the thickness increases. The maximum tangential stress at the inside radius decreases with decreasing r_o , the safety factor against yielding increases from 2.1 to 6.7, and the safety factor for overspeed varies from 1.5 to 2.6 over this range of thicknesses.
- 7 The final design chosen is $t = 0.438$ in and $r_o = 6.36$ in because it has a reasonable mix of parameter values (size, weight) and provides a safety factor of 2 against overspeeding. In other words, the flywheel could be run at up to twice its design speed before it would yield. The safety factor against yielding at the lower design speed will then always be higher and is now 4. Choosing larger safety factors will exact a weight penalty, as can be seen in Figure 10-25. See files EX10-07a and EX10-07b that also contain the calculations for Example 10-6.

— weight (lb)
— stress (ksi)
— diameter (in)
— N_y
— N_{os}

**FIGURE 10-25**

Variation of Weight, Stress, Safety Factors, and Diameter with Flywheel Thickness in Example 10-7

10.14 CRITICAL SPEEDS OF SHAFTS

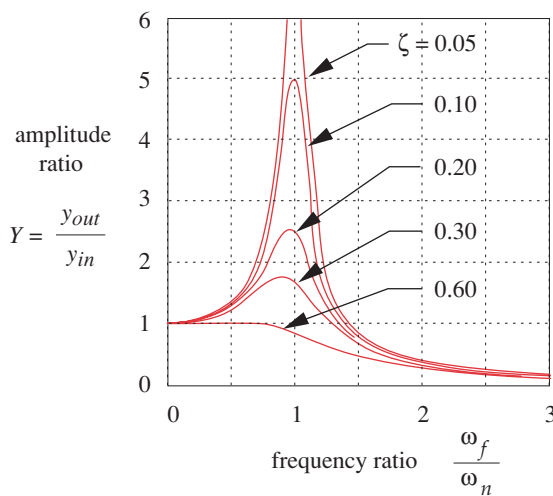
All systems containing energy-storage elements will possess a set of natural frequencies at which the system will vibrate with potentially large amplitudes. Any moving

mass stores kinetic energy and any spring stores potential energy. All machine elements are made of elastic materials and thus can act as springs. All elements have mass, and if they also have a velocity, they will store kinetic energy. When a dynamic system vibrates, a transfer of energy from potential to kinetic to potential, etc., repeatedly takes place within the system. Shafts meet these criteria, rotating with some velocity and deflecting both in torsion and in bending.

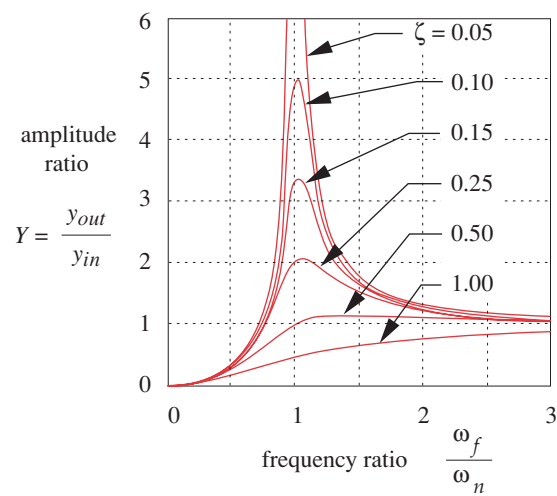
If a shaft, or any element for that matter, is subjected to a time-varying load, it will vibrate. Even if it receives only a transient load, such as a hammer blow, it will vibrate at its natural frequencies, just as a bell rings when struck. This is called a **free vibration**. Such a transient or free vibration will eventually die out due to the damping present in the system. If the time-varying loading is sustained, as, for example, in a sinusoidal manner, the shaft or other element will continue to vibrate at the driving function's **forcing frequency**. If the forcing frequency happens to coincide with one of the element's natural frequencies, then the amplitude of the vibratory response will be much larger than the amplitude of the driving function. The element is then said to be in **resonance**.

Figure 10-26a shows the amplitude response of a forced vibration, and Figure 10-26b a self-excited vibration, as a function of the ratio of the forcing frequency to the system's natural frequency ω_f / ω_n . When this ratio is 1, the system is in resonance and the amplitude of the response approaches infinity in the absence of damping. The amplitude responses in Figure 10-26 are shown as a dimensionless ratio of the output to input amplitudes. Any damping, shown as a damping ratio ζ , reduces the amplitude ratio at resonance. A natural frequency is also called a **critical frequency** or **critical speed**. *Exciting a system at or near its critical (resonant) frequencies must be avoided, since the resulting deflections will often cause stresses large enough to quickly fail the part.*

A system consisting of discrete lumps of mass connected with discrete spring elements can be considered to have a finite number of natural frequencies equivalent to its number of kinematic degrees of freedom. But a continuous system such as a beam



(a) Externally forced vibration response



(b) Self-excited vibration response

FIGURE 10-26

Response of a Single-Degree-of-Freedom System to Varying Forcing or Self-Excitation Frequencies

or shaft has an infinite number of particles, each of which is capable of elastic motion versus its neighboring particles. Thus a continuous system has an infinity of natural frequencies. In either case, the lowest, or fundamental, natural frequency is usually of most interest.

The natural frequencies of vibration of a system can be expressed either as a circular frequency ω_n with units of rad/sec or rpm, or as a linear frequency f_n with units of hertz (Hz). They are the same frequencies expressed in different units. The general expression for the fundamental natural frequency is

$$\omega_n = \sqrt{\frac{k}{m}} \quad \text{rad/sec} \quad (10.24a)$$

$$f_n = \frac{1}{2\pi} \sqrt{\frac{k}{m}} \quad \text{Hz} \quad (10.24b)$$

where k is the spring constant of the system and m is its mass. The natural frequencies are a physical property of the system; once built, it retains them essentially unchanged unless it loses or gains mass or stiffness during its useful life. Equations 10.24 define the undamped natural frequency. Damping reduces the natural frequency slightly. Shafts, beams, and most machine parts tend to be lightly damped, so the undamped value can be used with little error.

The usual design strategy is to keep all forcing, or self-exciting, frequencies below the first critical frequency by some comfort margin. The larger this margin, the better, but a factor of at least 3 or 4 is desirable. This keeps the amplitude-response ratio close to one or zero, as shown in Figures 10-26a and 10-26b. In some cases, the fundamental frequency of a shaft system cannot be made higher than the required rotating frequency. If the system can be accelerated rapidly enough through resonance, before the vibrations have a chance to build up amplitude, then the system can be run at a speed higher than resonance. Stationary power plants are in this category. The massiveness of the turbines and generators gives a low fundamental frequency (see equation 10.24), but they must be run at a high speed to generate the proper line frequency of AC current. Thus they operate to the right of the peak in Figure 10-14b where the amplitude ratio approaches one at high ratios of ω_f / ω_n . Their start-ups and shutdowns may be infrequent but must always be accomplished rapidly to get through the resonance peak before any damage is caused by excessive deflections. Also, sufficient driving power must be available to provide the energy absorbed at resonance by the oscillations in addition to accelerating the rotating mass. If the driver lacks sufficient power, then the system may stall in resonance, unable to increase its speed in the face of the potentially destructive vibrations. This is called the Sommerfeld effect.^[9]

There are three types of shaft vibration of concern:

- 1 Lateral vibration
- 2 Shaft whirl
- 3 Torsional vibration

The first two involve bending deflections and the last torsional deflection of the shaft.

Lateral Vibration of Shafts and Beams—Rayleigh's Method

A complete analysis of the natural frequencies of a shaft or beam is a complicated problem, especially if the geometry is complex, and is best solved with the aid of *Finite Element Analysis* software. A so-called **modal analysis** can be done on a finite element model of even complex geometries and will yield a large number of natural frequencies (in three dimensions) from the fundamental up. This is the preferred and frequently used approach when analyzing a completed or mature design in detail. However, in the early stages of design, when the part geometries are still not fully defined, a quick and easily applied method for finding at least an approximate fundamental frequency for a proposed design is very useful. **Rayleigh's method** serves that purpose. It is an energy method that gives results within a few percent of the true ω_n . It can be applied to a continuous system or to a lumped-parameter model of the system. The latter approach is usually preferred for simplicity.

RAYLEIGH'S METHOD equates the potential and kinetic energies in the system. The potential energy is in the form of strain energy in the deflected shaft and is maximum at the largest deflection. The kinetic energy is a maximum when the vibrating shaft passes through the undeflected position with maximum velocity. This method assumes that the lateral vibrating motion of the shaft is sinusoidal and that some external excitation is present to force the lateral vibration (Figure 10-26a).

To illustrate the application of this method, consider a simply-supported shaft with three disks (gears, sheaves, etc.) on it as shown in Figure 10-27. We will model this as three discrete lumps of known mass on a massless shaft. The shaft's geometry will define the bending spring constant, thus lumping all the “spring” into the shaft. The total potential energy stored at maximum deflection is the sum of the potential energies of each lumped mass:

$$E_p = \frac{g}{2} (m_1\delta_1 + m_2\delta_2 + m_3\delta_3) \quad (10.25a)$$

where the deflections are all taken as positive regardless of the local shape of the deflection curve because the strain energy is not affected by the external coordinate system. The energy of the deflected shaft is ignored as small compared to the disk energy.

The total kinetic energy is the sum of the individual kinetic energies:

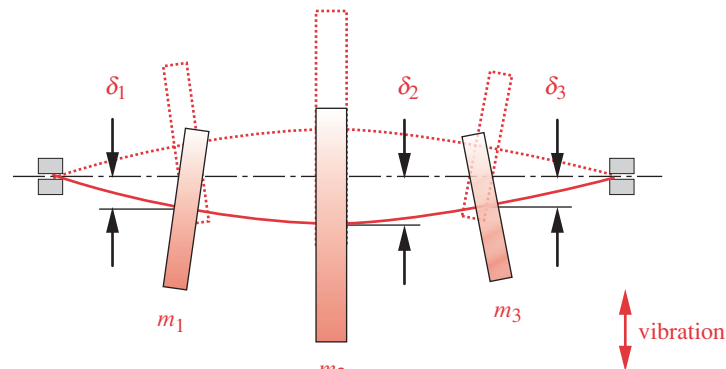
$$E_k = \frac{\omega_n^2}{2} (m_1\delta_1^2 + m_2\delta_2^2 + m_3\delta_3^2) \quad (10.25b)$$

where the velocities are taken as positive.

Equating these gives

$$\omega_n = \sqrt{g \frac{\sum_{i=1}^n m_i \delta_i}{\sum_{i=1}^n m_i \delta_i^2}} = \sqrt{g \frac{\sum_{i=1}^n (W_i/g) \delta_i}{\sum_{i=1}^n (W_i/g) \delta_i^2}} = \sqrt{g \frac{\sum_{i=1}^n W_i \delta_i}{\sum_{i=1}^n W_i \delta_i^2}} \quad (10.25c)$$

the second version resulting from substituting $m = W/g$, where the W_i are the weight forces of the discrete lumps into which we divided the system and the δ_i are the dynamic deflections at the locations of the weights due to their vibration. The weight forces and their deflections are all taken as positive to represent the maximum stored energies.

**FIGURE 10-27**

A Shaft in Lateral Vibration (amplitude greatly exaggerated)

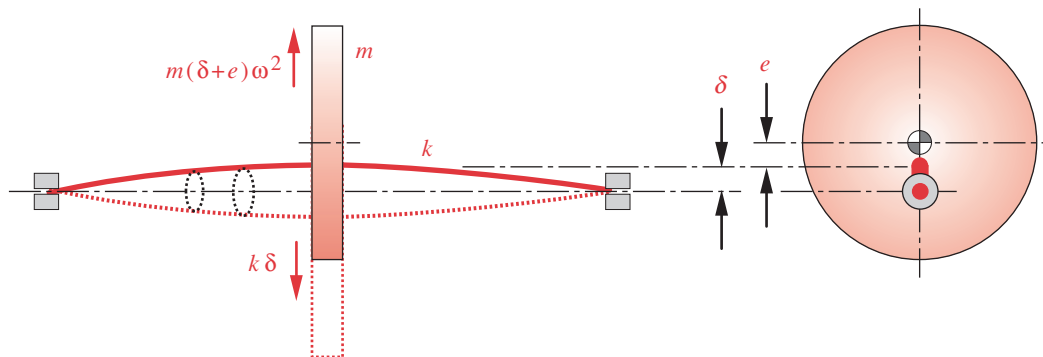
The problem is that we typically do not know the dynamic deflections of the system *a priori*. Rayleigh showed that virtually any estimate of the deflection curve, provided that it reasonably represents the maximum deflection and the boundary conditions of the actual dynamic curve, will suffice. The static deflection curve due to the weights of the assumed lumps (including the weight of the shaft or not as desired) is a very suitable estimate. Note that any applied external loads are not included in this deflection calculation, only the gravitational forces. The resulting approximate ω_n will always be higher than the true fundamental frequency by a few percent regardless of the assumed deflection-curve shape. If more than one estimated deflection curve is tried, the one yielding the lowest value of ω_n should be used, as it will be the closest approximation.

Equation 10.25c can be applied to a system of any complexity by breaking it into a large number of lumps. If gears, pulleys, etc., are on the shaft, they make logical lumped masses. If the shaft mass is significant or dominant, it can be broken into discrete elements along its length with each piece providing a term in the summation.

Rayleigh's method can theoretically be used to find higher frequencies than the fundamental but to do so is difficult without a good estimate of the shape of the higher-order deflection curve. More accurate methods for approximating both the fundamental frequency and the higher frequencies exist but are somewhat more complicated to implement. Ritz modified Rayleigh's method (Rayleigh-Ritz) to allow iteration to the higher frequencies. Holzer's method is more accurate and can find multiple frequencies. See reference 10 for more information.

Shaft Whirl

Shaft whirl is a self-excited vibratory phenomenon to which all shafts are potentially subject. While it is common and recommended practice to dynamically balance all rotating elements in machinery (especially if operated at high speeds), it is not possible to achieve exact dynamic balance except by chance. (See reference 12 for a discussion of dynamic balancing.) Any residual unbalance of a rotating element causes its true mass center to be eccentric from the axis of shaft rotation. This eccentricity creates a centrifugal force that tends to deflect the shaft in the direction of the eccentricity, increasing it and thus further increasing the centrifugal force. The only resistance to this force

**FIGURE 10-28**

Shaft Whirl (amplitude greatly exaggerated)

comes from the elastic stiffness of the shaft as shown in Figure 10-28. The initial shaft eccentricity is labeled e and the dynamic deflection is δ . A free-body diagram shows the forces acting to be

$$k\delta = m(\delta + e)\omega^2 \quad (10.26a)$$

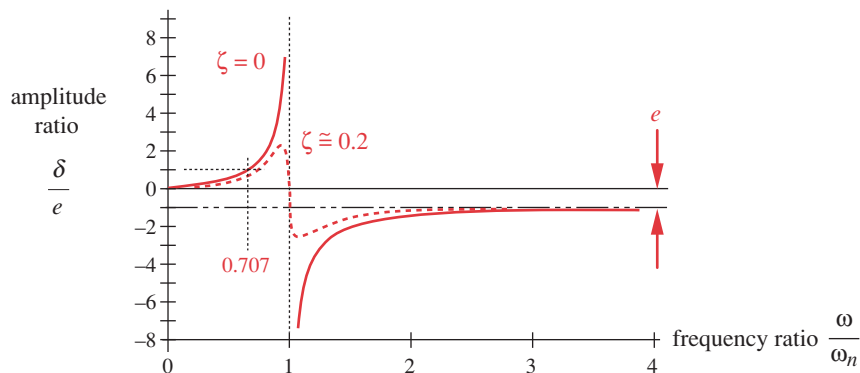
$$\delta = \frac{e\omega^2}{(k/m) - \omega^2} \quad (10.26b)$$

The dynamic deflection of the shaft from this centrifugal force causes it to whirl about its axis of rotation with points at the center of the deflected shaft describing circles about the axis. Note in equation 10.26b that the deflection becomes infinite when $\omega^2 = k/m$. As the rotational speed of the shaft approaches the fundamental natural (or critical) speed of lateral vibration, a similar resonance phenomenon to that of lateral vibration occurs. Note in equation 10.26b that when $\omega^2 = k/m$, $\delta = \infty$. Equation 10.26b can be normalized to a nondimensional form, which clearly shows the relationship:

$$\frac{\delta}{e} = \frac{(\omega/\omega_n)^2}{1 - (\omega/\omega_n)^2} \quad (10.26c)$$

Equation 10.26c and Figure 10-29 show the amplitude of shaft deflection normalized to the original eccentricity (δ/e) as a function of the ratio between the rotational frequency and critical frequency ω/ω_n . Note that at $\omega/\omega_n = 0$, there is no response, unlike the forced vibration of the previous section. This is because no centrifugal force exists unless the shaft is rotating. As the shaft speed increases, the deflection rapidly increases. If no damping is present ($\zeta = 0$), at $\omega/\omega_n = 0.707$, the deflection of the shaft is equal to the eccentricity and it becomes theoretically infinite at resonance ($\omega/\omega_n = 1$). Of course, there will always be some damping present, but if ζ is small, the deflections will be very large at resonance and can cause stresses large enough to fail the shaft.

Note what happens when the shaft speed passes through ω_n . The phase shifts 180° , which means that the deflection switches sides abruptly at resonance. At higher ratios of ω/ω_n , the deflection approaches $-e$, which means that the system is then rotating about the mass center of the eccentric mass, and the shaft centerline is eccentric. Conservation of energy makes the system want to rotate about its true mass center. In any

**FIGURE 10-29**

Amplitude Response of a Self-Excited Shaft-Whirl System as a Function of Frequency Ratio

system where the rotating elements are eccentric and large compared to the shaft this will occur. Perhaps you have observed a pivoted ceiling fan rotating with its motor center orbiting about the axis of rotation. The fan blades are usually not in perfect balance and the assembly rotates about the mass center of the blade assembly rather than about the motor/shaft centerline.

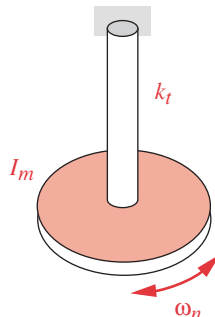
It should be clear that rotation of a system at or near its critical frequency is to be strictly avoided. The critical frequency for shaft whirl is the same as for lateral vibration and can be found using Rayleigh's method or any other suitable technique. Because this shaft-whirl vibration amplitude ratio starts at zero rather than at one (as with forced vibrations) the forcing frequency can be closer to the critical frequency than for the lateral vibration case. Keeping the operating speed below about half the shaft-whirl critical frequency will usually provide good results unless the initial eccentricity is excessive (which should not be allowed anyway).

Note the difference between shaft *lateral vibration* and *shaft whirl*. **Lateral vibration** is a *forced vibration*, requiring some outside source of energy such as vibrations from other parts of the machine to precipitate it, and the shaft then vibrates in one or more lateral planes whether or not it is rotating. **Shaft whirl** is a *self-excited vibration* caused by the shaft rotation acting on an eccentric mass. It will *always* occur when both rotation and eccentricity are present. The shaft assumes a deflected shape, which then rotates or whirls about the axis much like a jump-rope being swung by children.

Torsional Vibration

Just as a shaft can vibrate laterally, it can also vibrate torsionally and will have one or more torsional natural frequencies. The same equations that describe lateral vibrations can be used for torsional ones. The systems are analogous. Force becomes torque, mass becomes mass moment of inertia, and linear spring constant becomes torsional spring constant. Equation 10.24 (p. 595) for the circular natural frequency becomes, for a single-degree-of-freedom rotating system:

$$\omega_n = \sqrt{\frac{k_t}{I_m}} \quad \text{rad/sec} \quad (10.27a)$$

**FIGURE 10-30**

Disk on Axle in Torsional Vibration

The torsional spring constant k_t for a solid circular shaft is

$$k_t = \frac{GJ}{l} \quad \text{lb-in/rad or N-m/rad} \quad (10.27b)$$

where G is the material's modulus of rigidity, and l is the shaft length. The polar second moment of area J of a solid circular shaft is

$$J = \frac{\pi d^4}{32} \quad \text{in}^4 \text{ or m}^4 \quad (10.27c)$$

If the shaft is stepped, then an equivalent polar second moment of area J_{eff} is found from

$$J_{eff} = \frac{l}{\sum_{i=1}^n \frac{l_i}{J_i}} \quad (10.27d)$$

where l is total shaft length, and J_i , and l_i are the polar moments and lengths of the sub-sections of shaft of differing diameters, respectively.

The mass moment of inertia of a solid circular disk about its axis of rotation is:

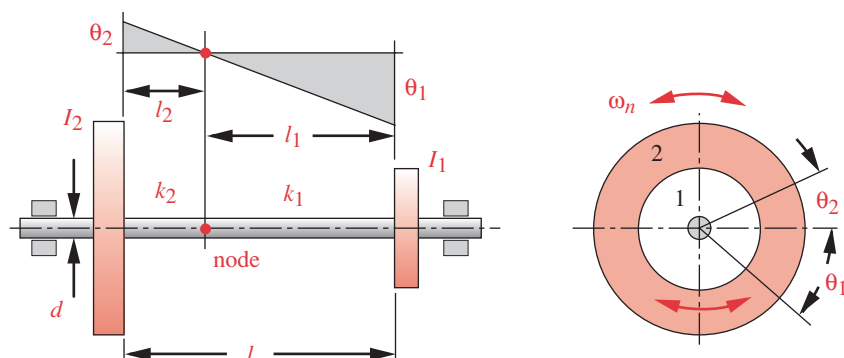
$$I_m = \frac{mr^2}{2} \quad \text{in-lb-sec}^2 \text{ or kg-m}^2 \quad (10.27e)$$

where r is the disk radius and m is its mass.

These equations are sufficient to find the critical frequency of a single disk mounted on a fixed axle, as shown in Figure 10-30.

Two Disks on a Common Shaft

A more interesting problem is that of two (or more) disks displaced on a common shaft as shown in Figure 10-31. The two disks shown will oscillate torsionally at the same natural frequency, 180° out of phase. There will be a point, called a node, somewhere on the shaft, at which there will be no angular deflection. On either side of the node,

**FIGURE 10-31**

Torsional Vibration of Two Disks on a Common Shaft

points on the shaft rotate in opposite angular directions when vibrating. The system can be modeled as two separate, single-mass systems coupled at this stationary node. One has mass moment and spring constant I_1, k_1 and the other I_2, k_2 . Their common natural frequency is then

$$\omega_n = \sqrt{\frac{k_1}{I_1}} = \sqrt{\frac{k_2}{I_2}} \quad (10.28a)$$

The spring constants of the shaft segments are each found from $k_t = JG / l$ assuming that the J is constant across the node.

$$\sqrt{\frac{JG}{l_1 I_1}} = \sqrt{\frac{JG}{l_2 I_2}}$$

and

$$l_1 I_1 = l_2 I_2 = I_2(l - l_1)$$

so

$$l_1 = \frac{I_2 l}{I_1 + I_2} \quad (10.28b)$$

Equation 10.28b allows the location of the node to be found. Substituting this expression into equation 10.28a gives

$$\begin{aligned} \omega_n &= \sqrt{\frac{k_1}{I_1}} = \sqrt{\frac{JG}{l_1 I_1}} = \sqrt{\frac{JG}{l} \frac{I_1 + I_2}{I_1 I_2}} \\ \omega_n &= \sqrt{k_t \frac{I_1 + I_2}{I_1 I_2}} \quad \text{or} \quad \omega_n^2 = k_t \frac{I_1 + I_2}{I_1 I_2} \end{aligned} \quad (10.28c)$$

which defines the critical speed for torsional vibration in terms of the known mass properties of the two disks and the overall spring constant of the shaft.

The critical frequency needs to be avoided in any forcing functions applied to the shaft in order to avoid torsional resonance that will overload it. Devices attached to the shaft, such as piston engines or piston pumps, will have frequencies in their torque-time functions that correspond to the pulses of their operation multiplied by their rotational frequency. For example, a four-cylinder engine will have a strong forcing frequency component at four times its rpm. If this fourth harmonic coincides with the shaft's critical frequency, there could be a problem. When designing a shaft, the frequency characteristics of the driving and driven rotating devices attached to it must be taken into account along with their primary rotational frequency.

Multiple Disks on a Common Shaft

Two disks on a common shaft have one node and one torsional natural frequency. Three disks will have two nodes and two natural frequencies. This pattern will hold for any number of disks, assuming in all cases that the masses of the disks dominate the shaft mass, allowing it to be ignored. N disks will have $N - 1$ nodes and natural frequencies. The degree of the equation for the natural frequencies will also be $N - 1$ if we consider the variable to be ω_n^2 rather than ω_n . Note that equation 10.28c for two masses is linear with this assumption. The equation for three masses is quadratic in ω_n^2 and for four masses is a cubic in ω_n^2 .

For the three-mass case, the squares of the natural frequencies are the two roots of

$$I_1 I_2 I_3 (\omega_n^2)^2 - [k_2(I_1 I_2 + I_1 I_3) + k_1(I_2 I_3 + I_1 I_3)] \omega_n^2 + k_1 k_2 (I_1 + I_2 + I_3) = 0 \quad (10.29)$$

Higher-order polynomials can be derived for additional masses and an iterative root-finding method can be used to solve them.

Approximate methods are also available to solve for the torsional natural frequencies with any number of masses. These allow the shaft mass to be easily accounted for if desired by breaking it into discrete masses. Holzer's method is commonly used for torsional as well as for lateral vibration of shafts. See reference 10 or any vibrations text for a derivation and discussion of these methods. Space does not allow a complete treatment of them here.

Controlling Torsional Vibrations

When shafts are long and/or have a number of masses distributed along their length, torsional vibrations can be a serious design problem. Internal-combustion engine crankshafts are an example. The crank-throw geometry severely reduces the torsional stiffness, which lowers their natural frequency. This, in combination with the presence of strong higher harmonics from the cylinder explosions in the torque, can lead to early failure from torsional fatigue. The straight-eight engine popular in the 1930s through 1940s was less successful than its straight-six cousin, due in part to the problems of torsional vibrations in the long, eight-throw crankshaft. The V-8 engine with its shorter, stiffer, four-throw crankshaft has completely supplanted the straight-eight. Even in these shorter engines, torsional crankshaft vibrations can be a problem.

Several methods can be used to counter the effects of an unwanted correspondence between the forcing frequencies and the system natural frequencies. The first line of defense is to redesign the mass and stiffness properties of the system to get the critical frequencies as far above the highest forcing frequency as possible. This usually involves increasing stiffness while removing mass, something not always easy to do. Effective use of geometry to obtain the maximum stiffness with a minimum of material is required. The term **specific stiffness** refers to the *stiffness-to-mass ratio* of an object. We want to maximize the specific stiffness to increase the natural frequencies. Finite element analysis can be very useful in refining a design's geometry to alter its natural frequencies because of the detailed information obtainable from that analysis.

Another approach is the addition of a **tuned absorber** to the system. A tuned absorber is a mass-spring combination added to the system whose presence alters the set of natural frequencies away from any dominant forcing frequencies. The system is effectively tuned away from the undesired frequencies. This approach can be quite effective in some cases and is used in linear-motion as well as in torsional systems.

A **torsional damper** is usually added to the end of an engine crankshaft to reduce its oscillations. This device, also called a Lanchester damper after its inventor, is a disk coupled to the shaft through an energy-absorbent medium such as rubber or oil. The oil-coupling provides viscous damping and the rubber has significant internal hysteresis damping. Its effect is to reduce the peak amplitude at resonance, as can be seen in Figure 10-26 (p. 594) for larger values of ζ . The reader is referred to reference 11 for more information on all of these methods.

EXAMPLE 10-8**Determining the Critical Frequencies of a Shaft****Problem**

Find the shaft whirl and torsional critical frequencies of the shaft in Example 10-2 and compare them to its forcing frequency.

Given

The steel shaft dimensions are 0.875-in dia for 1.5 in, 0.750-in dia for 3.5 in, 0.669-in dia for 1.5 in, and 0.531-in dia for 1.5 in. Its rotational speed is 1 725 rpm. Shaft supports are at 0 and 5 in on an 8-in-long shaft. The steel gear weighs 10 lb and acts at $z = 2$ in. It has a mass moment of inertia of 0.23 lb-in-sec². The aluminum sheave weighs 3 lb and acts at $z = 6.75$ in. It has a mass moment of inertia of 0.07 lb-in-sec².

Assumptions

The static deflection of the shaft due to the weights of gear and sheave will be used as an estimate for Rayleigh's method, but the gear and sheave weights will be applied in the directions that give the largest static deflection. The shaft weight will be ignored.

Solution

See Figures 10-5 (p. 561) and 10-32.

- 1 The deflection of the stepped shaft is found by the same technique used in Example 10-3 (p. 568). In this instance, the loads are taken as just the weights of the two disks. But, we will consider the gear weight-force to act downward and the sheave weight-force to act upward, since that arrangement better represents the dynamic situation where the inertia forces act outward from the axis in whatever direction increases the deflection. If we directed both weight forces downward in this case, we would get a smaller maximum deflection and a different curve shape than that of the dynamic deflection. Figure 10-32 shows the applied weight forces and the deflection curve for this shaft. The magnitude of the deflection at the gear is $6.0E-5$ in and at the sheave is $1.25E-4$ in. These values are needed in equation 10.25c (p. 596).

- 2 Calculate the critical frequency for shaft whirl from equation 10.25c:

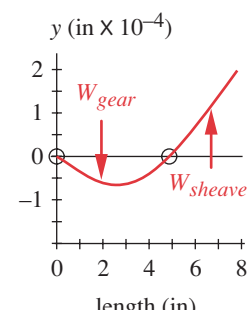
$$\omega_n = \sqrt{g \frac{\sum_{i=1}^n W_i \delta_i}{\sum_{i=1}^n W_i \delta_i^2}} = \sqrt{386 \frac{10(6.0E-5) + 3(1.25E-4)}{10(6.0E-5)^2 + 3(1.25E-4)^2}} = 2131 \text{ rad/sec} \quad (a)$$

Note that the magnitudes of the weight forces and their corresponding deflections are all taken as positive regardless of their vector directions in the static deflection case.

- 3 Compare the critical whirl frequency to the forcing frequency.

$$\frac{\omega_n}{\omega_f} = \frac{30/\pi(2131 \text{ rad/sec})}{1725 \text{ rpm}} = \frac{20350 \text{ rpm}}{1725 \text{ rpm}} = 11.8 \quad (b)$$

This is a very comfortable margin. If, in this example, the shaft weight is included in both the deflection calculation and the critical-frequency calculation, the critical frequency becomes 20 849 rpm, which is 12.1 times the forcing frequency. Even with the relatively light disks on this shaft, ignoring the shaft weight does not introduce a large error. Both of these values from Rayleigh's method are higher than the actual natural frequency. The reader can examine their differences in the models supplied by simply changing the density of the shaft material from 0.28 lb/in³ (for

**FIGURE 10-32**

Static Deflection Due to Weight Forces of Disks on Shaft Oriented to Give the Maximum Deflection of a Shape Similar to the Dynamic Deflection

steel) to zero to eliminate the shaft's effect from the computation. The models include the shaft weight in the computation by dividing it into 50 increments over its length.

- 4 To find the torsional critical frequency of a stepped shaft requires that an effective spring constant for the combined stepped sections be found. The shaft portion of interest is between the sheave and gear. The spring constant of any one section is

$$k_t = \frac{GJ}{l} = \frac{G\pi d^4}{32l} \text{ lb-in/rad}$$

$$k_{t_1} = \pi \frac{11.5E6(0.75)^4}{32(3.5)} = 102\ 065 \text{ lb-in/rad} \quad (c)$$

$$k_{t_2} = \pi \frac{11.5E6(0.669)^4}{32(1.5)} = 150\ 769 \text{ lb-in/rad}$$

Since the shaft sections all have the same torque but different deflections (which sum to the total deflection as shown in equation 10.9b on p. 567), they act as springs in series. The effective spring constant k_{teff} of the portion of stepped shaft between the two torque loads is found from equation 10.9d:

$$\frac{1}{k_{teff}} = \frac{1}{k_{t_1}} + \frac{1}{k_{t_2}} = \frac{1}{102\ 065} + \frac{1}{150\ 769}$$

$$k_{teff} = 60\ 863 \text{ lb-in/rad} \quad (d)$$

- 5 The critical torsional frequency is found from equation 10.28c (p. 601).

$$\omega_n = \sqrt{k_{teff} \frac{I_1 + I_2}{I_1 I_2}} = \sqrt{60\ 863 \frac{0.23 + 0.07}{(0.23)(0.07)}} = 1\ 065 \text{ rad/sec} \quad (e)$$

- 6 Compare the critical torsional frequency to the forcing frequency.

$$\frac{\omega_n}{\omega_f} = \frac{30/\pi(1\ 065 \text{ rad/sec})}{1\ 725 \text{ rpm}} = \frac{10\ 170 \text{ rpm}}{1\ 725 \text{ rpm}} = 5.9 \quad (f)$$

This is an acceptable margin.

- 7 The files EX10-08 can be found on the CD-ROM.

10.15 COUPLINGS

A wide variety of commercial shaft couplings are available, ranging from simple keyed, rigid couplings to elaborate designs that utilize gears, elastomers, or fluids to transmit the torque from one shaft to another or to other devices in the presence of various types of misalignment. Couplings can be roughly divided into two categories, rigid and compliant. Compliant in this context means that the coupling can absorb some misalignment between the two shafts and rigid implies that no misalignment is allowed between the connected shafts.

**FIGURE 10-33**

Various Types and Sizes of Rigid Shaft Couplings Courtesy of Ruland Manufacturing Inc., Watertown, Mass.

Rigid Couplings

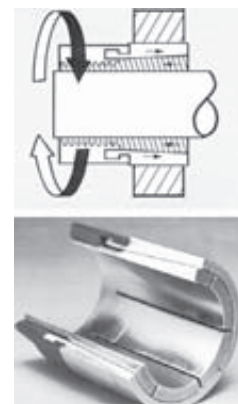
Rigid couplings lock the two shafts together allowing no relative motion between them, though some axial adjustment is possible at assembly. These are used when accuracy and fidelity of torque transmission are of paramount importance, as, for example, when the phase relationship between driver and driven device must be accurately maintained. Automated production machinery driven by long line-shafts often uses rigid couplings between shaft sections for this reason. Servomechanisms also need zero backlash connections in the drive train. The trade-off is that the alignment of the coupled shaft axes must be adjusted with precision to avoid introducing large side forces and moments when the coupling is clamped in place.

Figure 10-33 shows some examples of commercial rigid couplings. There are three general types: setscrew couplings, keyed couplings, and clamp couplings.

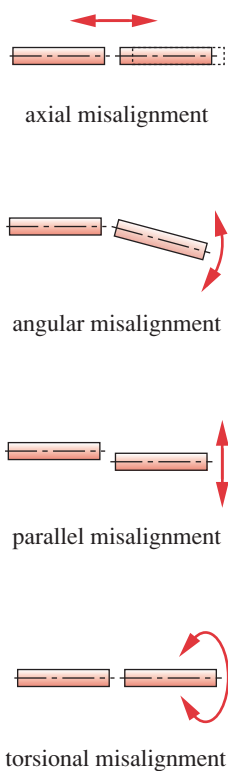
SETSCREW COUPLINGS use a hard setscrew that digs into the shaft to transmit both torque and axial loads. These are not recommended for any but light-load applications and can loosen with vibration.

KEYED COUPLINGS use standard keys as discussed in an earlier section and can transmit substantial torque. Setscrews are often used in combination with a key, the screw being located 90° from the key. For proper holding against vibration, a cup-point setscrew is used to dig into the shaft. For better security, the shaft should be dimpled with a shallow drilled hole under the setscrew to provide a mechanical interference against axial slip rather than relying on friction.

CLAMP COUPLINGS are made in several designs, the most common being one- or two-piece split couplings that clamp around both shafts and transmit torque through friction as shown in Figure 10-33. A taper-lock coupling uses a split-tapered collet which is squeezed between shaft and the tapered coupling housing to clamp the shaft as shown in Figure 10-34.

**FIGURE 10-34**

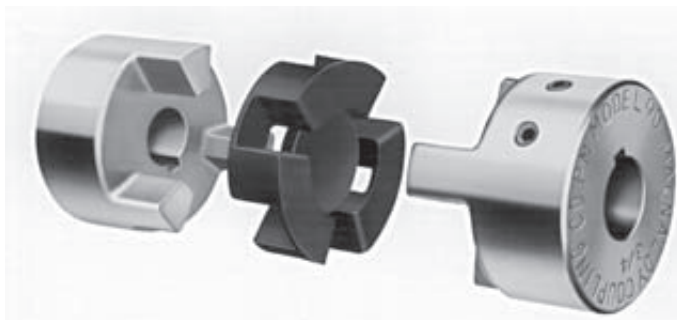
A Trantorque Taper-Lock Coupling - Courtesy of Fenner Manheim, Manheim, Pa. 17545



10

FIGURE 10-35

Types of Shaft Misalignment

**FIGURE 10-36**

Exploded View of a Jaw Coupling Showing Jaws and Elastomer Insert Courtesy of Magnaloy Coupling Company, Alpena, Mich. 49707

Compliant Couplings

A shaft as a rigid body has six potential degrees of freedom (DOF) with respect to a second shaft. However, due to symmetry only four of these DOF are of concern. They are **axial**, **angular**, **parallel**, and **torsional** misalignment, as shown in Figure 10-35. These can occur singly or in combination and may be present at assembly due to manufacturing tolerances or may occur during operation due to the relative motions of the two shafts. The final driveline of an automobile has relative motion between the ends of the driveshaft. The drive end is affixed to the frame and the driven end is on the road. The frame and road are separated by the car's suspension, so the driveshaft couplings must absorb both angular and axial misalignment as the car traverses bumps.

Unless care is taken to align two adjacent shafts, there can be axial, angular, and parallel misalignment in any machinery. Torsional misalignment occurs dynamically when a driven load attempts to lead or lag the driver. If the coupling allows any torsional clearance, there will be backlash when the torque reverses sign. This is undesirable if accurate phasing is needed, as in servomechanisms. Torsional compliance in a coupling may be desirable if large shock loads or torsional vibrations must be isolated from the driver.

Numerous designs of compliant couplings are manufactured and each offers a different combination of features. The designer can usually find a suitable coupling available commercially for any application. Compliant couplings can be roughly divided into several subcategories, which are listed in Table 10-7 along with some of their characteristics. The torque ratings are not shown, as these vary widely with size and materials. Various size couplings can handle power levels from subfractional horsepower to thousands of horsepower.

JAW COUPLINGS have two (often identical) hubs with protruding jaws, as shown in Figure 10-36. These jaws overlap axially and interlock torsionally through a compliant insert of rubber or soft-metal material. The clearances allow some axial, angular, and parallel misalignment, but can also allow some undesirable backlash.

FLEXIBLE-DISK COUPLINGS are similar to jaw couplings in that their two hubs are connected by a compliant member (disk) of elastomeric or metallic-spring material, as shown in Figure 10-37. These allow axial, angular, and parallel misalignment, with some torsional compliance but little or no backlash.

**FIGURE 10-37**

A Flexible Disk Coupling
Courtesy of Zero-Max,
Minneapolis, Minn. 55441

GEAR AND SPLINE COUPLINGS use straight or curved external gear teeth in mesh with internal teeth, as shown in Figure 10-38. These can allow substantial axial movement between shafts and, depending on the tooth shapes and clearances, can absorb small angular and parallel misalignment as well. They have high torque capacity due to the number of teeth in mesh.

HELICAL AND BELLOWS COUPLINGS are one-piece designs that use their elastic deflections to allow axial, angular, and parallel misalignment with little or no backlash. Helical couplings (Figure 10-39 and Chapter 10 title page photograph) are made from a solid metal cylinder cut with a helical slit to increase its compliance. Metal-bellows couplings (Figure 10-40) are made of thin sheet metal by welding a series of cupped washers together, by hydraulically forming a tube into the shape, or by electroplating a thick coating on a mandrel. These couplings have limited torque capability compared to other designs but offer zero backlash and high torsional stiffness in combination with axial, angular, and parallel misalignment.

LINKAGE COUPLINGS or Schmidt couplings (Figure 10-41) connect two shafts through a network of links that allow significant parallel misalignment with no side loads or torque losses and no backlash. Some designs allow small amounts of angular and axial misalignment as well. These couplings are often used where large parallel adjustments or dynamic motions are needed between shafts.

UNIVERSAL JOINTS are of two common types, the Hooke coupling (Figure 10-42), which does not have constant velocity (CV), and the Rzeppa coupling, which does. Hooke couplings are generally used in pairs to cancel their velocity error. Both types can handle very large angular misalignment, and in pairs provide large parallel offsets



FIGURE 10-38

A Flexible Gear Coupling
Courtesy of Amerigear/Zurn Industries, Inc., Erie, Pa. 16514

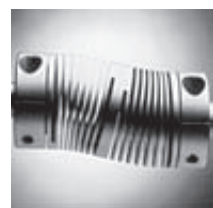


FIGURE 10-39

A Helical Coupling Courtesy of Helical Products Co., Inc., Santa Maria, Calif. 93456



FIGURE 10-40

Metal-Bellows Coupling
Courtesy of Senior Flexonics Inc., Metal Bellows Division, Sharon, Mass. 02067



FIGURE 10-41

Schmidt Offset Coupling
Courtesy of Zero-Max/Holland Co., Minneapolis, Minn. 55441

Table 10-7 Characteristics of Various Types of Couplings

Class	Misalignment Tolerated					Comments
	Axial	Angular	Parallel	Torsional		
Rigid	large	none	none	none		requires accurate alignment
Jaw	slight	slight ($< 2^\circ$)	slight ($3\% d$)	moderate		shock absorption—significant backlash
Gear	large	slight ($< 5^\circ$)	slight ($< 1/2\% d$)	none		slight backlash—large torque capacity
Spline	large	none	none	none		slight backlash—large torque capacity
Helical	slight	large (20°)	slight ($< 1\% d$)	none		one piece - compact—no backlash
Bellows	slight	large (17°)	moderate ($20\% d$)	none		subject to fatigue failure
Flexible disk	slight	slight (3°)	slight ($2\% d$)	slight to none		shock absorption—no backlash
Linkage (Schmidt)	none	slight (5°)	large ($200\% d$)	none		no backlash—no side loads on shaft
Hooke	none	large	large (in pairs)	none		slight backlash—speed variation unless used in pairs
Rzeppa	none	large	none	none		constant velocity

**FIGURE 10-42**

A Hooke's Coupling Courtesy of Lovejoy, Inc., Downers Grove, Ill. 60515

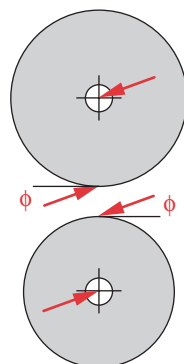
10.16 CASE STUDY

We will now address the design of shafts in one of the Case Study assemblies that were defined in Chapter 9.

Designing Driveshafts for a Portable Air Compressor

The preliminary design of this device is shown in Figure 9-1 (repeated opposite). There are two shafts, input and output. The output shaft will have the larger torque in this case since it is at the slower speed of 1 500 rpm. The torque on that shaft was defined in the earlier Case Study 8A in Chapter 9 and is shown in Figure 9-3 (repeated opposite). Since this is a time-varying torque, the shaft must be designed for fatigue loading. In addition to the torque on the shafts, there will be side loads from the gears that apply bending moments, making a combined-loading situation. Note in Figure 9-1 that the shafts are shown as short, being only long enough to accommodate the gear and bearings. This is done to minimize the bending moments from the gear forces.

Since the gears are yet to be designed, we will have to make some assumptions about their diameters and thicknesses to do a preliminary design of the shafts. Later selection of bearings may also dictate some changes to our shaft design. This is typical of design problems, since all of their elements interact. Iteration is necessary to refine all the elements' designs.

**FIGURE 10-43**

Forces on a Gearset

CASE STUDY 8B

Preliminary Design of Shafts for a Compressor Drive Train

Problem

Determine reasonable sizes for the input and output shafts of the gearbox in Figure 9-1 (opposite) based on the loadings defined in Case Study 8A and specify a suitable type of coupling.

Given

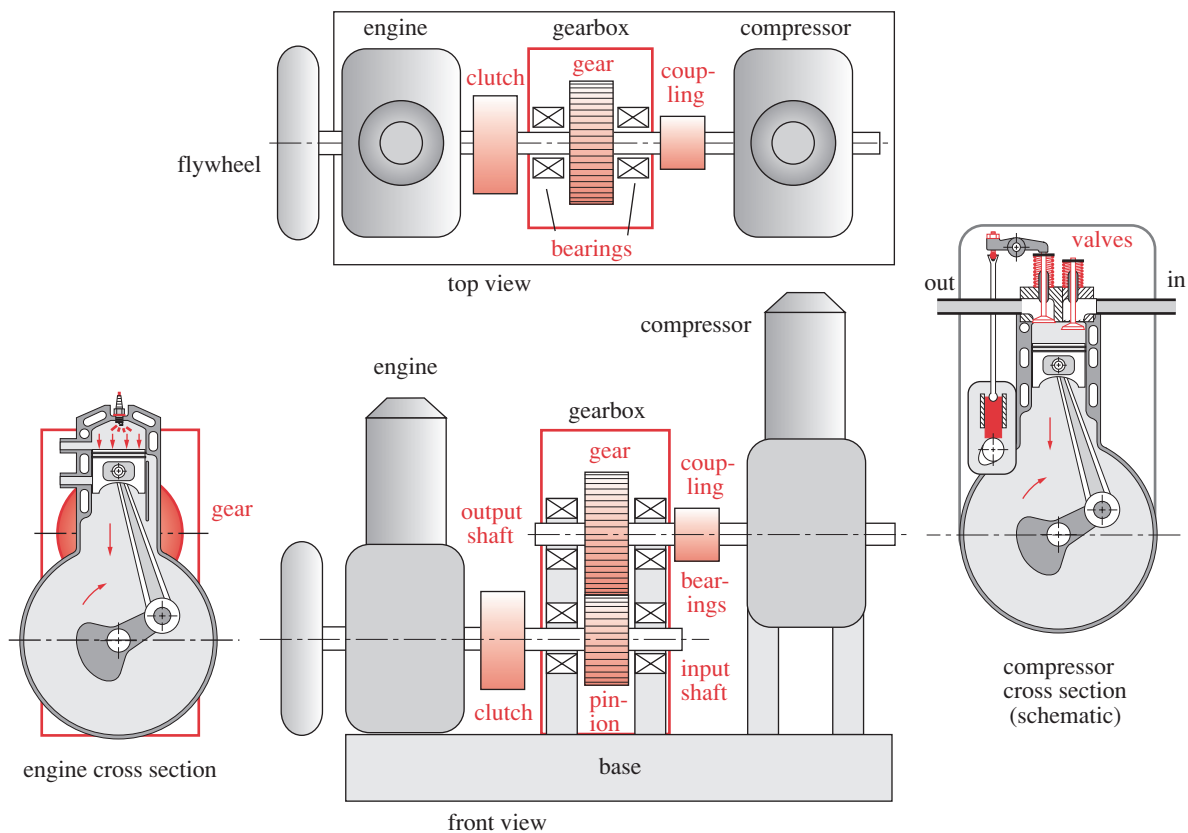
The torque-time function on the output shaft is as shown in Figure 9-3. The required gear ratio is a 2.5:1 reduction in velocity from the input to the output shaft.

Assumptions

Try an input gear (pinion) diameter of 4 in and output gear diameter of 10 in, both of 2 in thickness and 20° pressure angle. Ball bearings of standard diameters will be used on all shafts.

Solution

See Figures 9-1, 9-3, and 10-43.

**FIGURE 9-1 Repeated**

Preliminary Design Schematic of Gasoline-Engine-Powered Portable Air Compressor, Gearbox, Couplings, Shafts, and Bearings

- The time-varying torque on the output shaft is defined in Figure 9-3 (repeated below) as varying between -175 and $+585$ lb-in. From these data and the assumed gear diameters, we can determine the forces at the gear mesh that are felt by the shaft. Figure 10-43 shows a free-body diagram of a gearset. Because of the pressure angle ϕ between the gears, there are both radial and tangential components of force at the gear mesh. The tangential component is found from the known torque and the assumed gear radius:

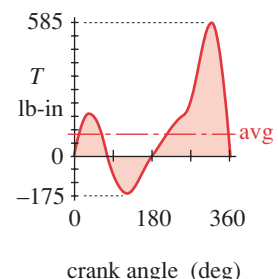
$$F_{t_{max}} = \frac{T_{max}}{r_g} = \frac{585 \text{ lb-in}}{5 \text{ in}} = 117 \text{ lb}$$

$$F_{t_{min}} = \frac{T_{min}}{r_g} = \frac{-175 \text{ lb-in}}{5 \text{ in}} = -35 \text{ lb} \quad (a)$$

- The maximum and minimum resultant forces are found from:

$$F_{\max} = \frac{F_{t_{\max}}}{\cos \phi} = \frac{117 \text{ lb}}{\cos 20^\circ} = 124.5 \text{ lb}$$

$$F_{\min} = \frac{F_{t_{\min}}}{\cos \phi} = \frac{-35 \text{ lb}}{\cos 20^\circ} = -37.25 \text{ lb} \quad (b)$$

**FIGURE 9-3 Repeated**

Total Torque-Time Function at Crankshaft with Constant ω

Note that these forces will be the same on the input shaft, whose torque is 0.4 times that of the output shaft because of the 1:2.5 gear ratio.

- 3 The maximum and minimum moments on the shaft can now be found. We will assume that the gears will be centered between the simply supported bearings that are set 4 in apart. The bearing reaction forces are then half of the gear forces and the bending moments peak in the center with a magnitude of

$$M_{max} = F_{max} \frac{l}{4} = 124.5 \frac{4}{4} = 124.5 \text{ lb-in}$$

$$M_{min} = F_{min} \frac{l}{4} = -37.25 \frac{4}{4} = -37.25 \text{ lb-in} \quad (c)$$

- 4 The shafts will ultimately need to be stepped for the bearings at each end and either stepped or snap-ringed to provide axial location for the gears. At this stage of the design, we will assume a constant-diameter shaft in order to get an approximate size for the torque and moment loading.

Since a keyway will probably be needed at the gear, assume a stress-concentration factor of 3 for both bending and torsion at that critical location where both moment and torque components are largest. (See Figure 10-16, p. 575.) After the gears are designed and the bearings selected, we can refine the design, including stepped shoulders and using more accurate stress-concentration factors.

- 5 The loading is a combination of a fluctuating moment and a fluctuating torque that are synchronous. The mean and alternating components of both moment and torque are needed for the stress calculations.

10

$$M_m = \frac{M_{max} + M_{min}}{2} = \frac{124.5 - 37.25}{2} = 43.6 \text{ lb-in}$$

$$M_a = \frac{M_{max} - M_{min}}{2} = \frac{124.5 + 37.25}{2} = 80.9 \text{ lb-in} \quad (d)$$

$$T_m = \frac{T_{max} + T_{min}}{2} = \frac{585 - 175}{2} = 205 \text{ lb-in}$$

$$T_a = \frac{T_{max} - T_{min}}{2} = \frac{585 + 175}{2} = 380 \text{ lb-in} \quad (e)$$

- 6 A trial material needs to be selected for the computations. We will first try an inexpensive, low-carbon, cold-rolled steel such as SAE 1018 with $S_{ut} = 64 \text{ ksi}$ and $S_y = 54 \text{ ksi}$. Though not exceptionally strong, this material has low notch sensitivity, which will be an advantage given the stress concentrations. Calculate the uncorrected endurance strength using equation 6.5 (p. 330):

$$S_e' = 0.5S_{ut} = 0.5(64\,000) = 32\,000 \text{ psi} \quad (f)$$

This must be reduced by various factors to account for differences between the part and the test specimen.

$$S_e = C_{load} C_{size} C_{surf} C_{temp} C_{reliab} S_e'$$

$$S_e = (1)(1)(0.84)(1)(1)(32\,000) \approx 27\,000 \text{ psi} \quad (g)$$

The loading is bending and torsion, so C_{load} is 1. Since we don't yet know the part size, we will temporarily assume $C_{size} = 1$ and adjust it later. C_{surf} is chosen for a machined finish from either Figure 6-26 (p. 332) or equation 6.7e (p. 333). The temperature is not elevated, so $C_{temp} = 1$, and we assume 50% reliability with $C_{reliab} = 1$.

- 7 The notch sensitivity of the material is found from either equation 6.13 (p. 345) or Figure 6-36 (pp. 344–345) and for bending is $q = 0.50$, and for torsion is $q = 0.57$, both for an assumed notch radius of 0.01 in.
- 8 The bending-fatigue stress-concentration factor is found from equation 6.11b (p. 343) using the assumed geometric stress-concentration factor.

For bending stress in the keyway:

$$K_f = 1 + q(K_t - 1) = 1 + 0.50(3.0 - 1) = 2.00 \quad (h)$$

For torsional stress in the keyway:

$$K_f = 1 + q(K_t - 1) = 1 + 0.57(3.0 - 1) = 2.15 \quad (i)$$

- 9 From equation 6.17 (p. 364) we find that in this case, the same factor should be used on the mean stress components:

$$\begin{aligned} K_{fm} &= K_f = 2.00 \\ K_{fsm} &= K_{fs} = 2.15 \end{aligned} \quad (j)$$

- 10 The shaft diameter can now be found from equation 10.8 (p. 560) using an assumed safety factor of 3 to account for the uncertainties in this preliminary design. Note that the ASME equation (10.6) on p. 558 cannot be safely used in this case since it assumes constant torque. The more general, modified-Goodman line approach of equation 10.8 must be used.

$$\begin{aligned} d_{output} &= \left\{ \frac{32N_{sf}}{\pi} \left[\frac{\sqrt{(k_f M_a)^2 + \frac{3}{4}(k_{fs} T_a)^2}}{S_f} + \frac{\sqrt{(k_{fm} M_m)^2 + \frac{3}{4}(k_{fsm} T_m)^2}}{S_{ut}} \right] \right\}^{\frac{1}{3}} \\ &= \left\{ \frac{32(3)}{\pi} \left[\frac{\sqrt{[2.00(80.9)]^2 + \frac{3}{4}[2.15(380)]^2}}{27\,000} + \frac{\sqrt{[2.00(43.6)]^2 + \frac{3}{4}[2.15(205)]^2}}{64\,000} \right] \right\}^{\frac{1}{3}} \\ d_{output} &= 1.00 \text{ in} \end{aligned} \quad (k)$$

So a 1-in nominal shaft diameter seems acceptable for the output shaft.

- 11 The input shaft has the same mean and alternating bending moments as the output shaft, but its torque is only 40% of the output shaft's. The mean and alternating torques on it are 82 and 152 lb-in. When these are put in equation 10.8 with all other factors the same, a smaller shaft diameter results.

$$\begin{aligned} d_{input} &= \left\{ \frac{32(3)}{\pi} \left[\frac{\sqrt{[2.00(80.9)]^2 + \frac{3}{4}[2.15(152)]^2}}{27\,000} + \frac{\sqrt{[2.00(43.6)]^2 + \frac{3}{4}[2.15(82)]^2}}{64\,000} \right] \right\}^{\frac{1}{3}} \\ d_{input} &= 0.768 \text{ in} \end{aligned} \quad (l)$$

The input shaft can then be a nominal 0.781-in diameter, which is a stock size.

- 12 The couplings between the engine and input shaft and between the output shaft and compressor must be able to accommodate some angular and parallel misalignment due to tolerances in the mounting of the three subassemblies of engine, gearbox, and compressor. Torsional compliance in the couplings would also serve to absorb some of the shock associated with the torque reversal seen in Figure 9-3 (p. 609).

With these constraints, a jaw-type coupling with an elastomer insert might be a good choice for both couplings. The backlash inherent in these couplings would not be a problem, since the phasing of the three subassemblies is not critical in this application. A flexible-disk coupling could also be used. A rigid coupling would require more accurate mounting of the subassemblies than is otherwise warranted. See Table 10-7 (p. 607) for information on coupling characteristics.

- 13 The files CASE8B-1 and CASE8B-2 are on the CD-ROM.

10.17 SUMMARY

Shafts are used in all rotating machinery. Steel is the usual choice of material to obtain high stiffness for low deflections. Shafts may be of soft, low-carbon steel or of medium- to high-carbon steel for higher strength or if a hard surface finish is needed for wear resistance. Machine shafts usually have stepped shoulders for axial location of attached elements such as bearings, gears, or sprockets (sheaves). These shoulders create stress concentrations that must be considered in the stress analysis. Keyways or interference fits also create stress concentrations.

The loading on shafts is usually a combination of torsion and bending, either or both of which can be time varying. The general loading case of fluctuating torque combined with fluctuating bending requires a modified-Goodman diagram approach to its failure analysis. For the common case of the torque and bending moment being related through common forces, the modified-Goodman approach is captured in equation 10.8 (p. 560) which provides a design tool to determine a shaft diameter for known fluctuating loads, stress concentrations, material strengths, and a chosen safety factor. The ASME shaft design equation 10.6 (p. 558) only applies to cases of constant torque with a constant applied bending moment that is fully reversed due to shaft rotation. Equation 10.6 can be used only in situations that match this loading limitation. It is always better to use the general design equation 10.8 (p. 560) that accounts for fluctuating moments and torques if they are present.

Several techniques or devices such as keys, splines, and interference fits are commonly used to attach elements to shafts. Keys are standardized to the shaft diameter. Consult the ANSI standard or reference 3 for data on size ranges not reproduced in this chapter. Splines provide greater torque capacity than keys. Interference fits may be by direct press fit or by thermally expanding or shrinking one or both members. Very high stresses can be created by these techniques, possibly failing the part during assembly.

Flywheels are used when some torque or velocity smoothing is needed. The flywheel must be sized to give the desired coefficient of speed fluctuation and then checked for stress at the operating speed. The maximum stresses in a flywheel occur at the in-

side diameter. A maximum safe speed must be determined, as the stresses increase with the square of the rotational speed. When a flywheel fails while spinning, it typically flies apart and can cause serious injury.

All spinning shafts will have critical frequencies at which they will resonate with large deflections, causing failure. The fundamental lateral and torsional frequencies will be different and both must be avoided in operation by keeping the rotational speed well below the lowest critical frequency of the shaft.

A wide variety of shaft couplings are commercially available. Some types and their characteristics are briefly discussed in this chapter. The manufacturers should be consulted for more complete and definitive information.

Important Equations Used in This Chapter

See the referenced sections for information on the proper use of these equations.

Power-Torque Relationship (Section 10.4):

$$P = T\omega \quad (10.1a)$$

ASME Shaft-Design Equation (Section 10.8):

$$d = \left\{ \frac{32N_f}{\pi} \left[\left(k_f \frac{M_a}{S_f} \right)^2 + \frac{3}{4} \left(\frac{T_m}{S_y} \right)^2 \right]^{\frac{1}{2}} \right\}^{\frac{1}{3}} \quad (10.6b)$$

General Shaft-Design Equation (Section 10.8):

$$d = \left\{ \frac{32N_f}{\pi} \left[\frac{\sqrt{\left(k_f M_a \right)^2 + \frac{3}{4} \left(k_{fs} T_a \right)^2}}{S_f} + \frac{\sqrt{\left(k_{fm} M_m \right)^2 + \frac{3}{4} \left(k_{fsm} T_m \right)^2}}{S_{ut}} \right] \right\}^{\frac{1}{3}} \quad (10.8)$$

Shaft Torsional Deflection (Section 10.9):

$$\theta = \frac{Tl}{GJ} \quad (10.9a)$$

Pressure Generated by an Interference Fit (Section 10.11):

$$p = \frac{0.5\delta}{\frac{r}{E_o} \left(\frac{r_o^2 + r^2}{r_o^2 - r^2} + v_o \right) + \frac{r}{E_i} \left(\frac{r^2 + r_i^2}{r^2 - r_i^2} - v_i \right)} \quad (10.14a)$$

Tangential Stresses in Shaft and Hub of an Interference Fit (Section 10.11):

$$\sigma_{t_{shaft}} = -p \frac{r^2 + r_i^2}{r^2 - r_i^2} \quad (10.15a)$$

$$\sigma_{t_{hub}} = p \frac{r_o^2 + r^2}{r_o^2 - r^2} \quad (10.16a)$$

Energy Stored in a Spinning Flywheel (Section 10.13):

$$E_k = \frac{1}{2} I_m \omega^2 \quad (10.17a)$$

Mass Moment of Inertia of a Solid-Disk Flywheel (Section 10.13):

$$I_m = \frac{\pi}{2} \frac{\gamma}{g} (r_o^4 - r_i^4) \quad (10.17d)$$

Flywheel Inertia Needed for a Chosen Coefficient of Fluctuation (Section 10.13):

$$\begin{aligned} E_k &= \frac{1}{2} I_s (2\omega_{avg}) (C_f \omega_{avg}) \\ I_s &= \frac{E_k}{C_f \omega_{avg}^2} \end{aligned} \quad (10.22)$$

Tangential Stress in a Spinning Flywheel (Section 10.13):

$$\sigma_t = \frac{\gamma}{g} \omega^2 \left(\frac{3+v}{8} \left(r_i^2 + r_o^2 + \frac{r_i^2 r_o^2}{r^2} - \frac{1+3v}{3+v} r^2 \right) \right) \quad (10.23a)$$

Natural Frequency of Single-Degree-of-Freedom System (Section 10.14):

$$\omega_n = \sqrt{\frac{k}{m}} \text{ rad/sec} \quad (10.24a)$$

$$f_n = \frac{1}{2\pi} \sqrt{\frac{k}{m}} \text{ Hz} \quad (10.24b)$$

First Lateral Critical Frequency (Approximate) (Section 10.14):

$$\omega_n = \sqrt{g \frac{\sum_{i=1}^n m_i \delta_i}{\sum_{i=1}^n m_i \delta_i^2}} = \sqrt{g \frac{\sum_{i=1}^n (W_i/g) \delta_i}{\sum_{i=1}^n (W_i/g) \delta_i^2}} = \sqrt{g \frac{\sum_{i=1}^n W_i \delta_i}{\sum_{i=1}^n W_i \delta_i^2}} \quad (10.25c)$$

First Torsional Critical Frequency for Two Masses on Weightless Shaft (Section 10.14):

$$\omega_n = \sqrt{k_t \frac{I_1 + I_2}{I_1 I_2}} \quad \text{or} \quad \omega_n^2 = k_t \frac{I_1 + I_2}{I_1 I_2} \quad (10.28c)$$

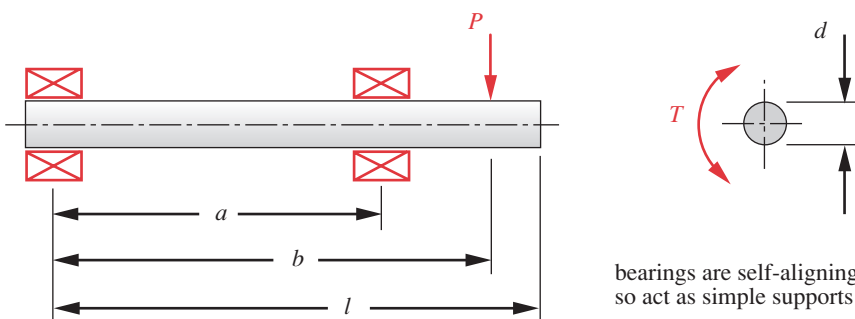
10.18 REFERENCES

- 1 R. C. Juvinall and K. M. Marshek, *Fundamentals of Machine Component Design*, 2ed. John Wiley & Sons: New York, p. 656, 1991.
- 2 D. B. Kececioglu and V. R. Lalli, "Reliability Approach to Rotating Component Design," *Technical Note TN D-7846*, NASA, 1975.

- 3 **V. C. Davies, H. J. Gough, and H. V. Pollard**, "Discussion to The Strength of Metals Under Combined Alternating Stresses," *Proc. of the Inst. Mech Eng.*, **131**(3): pp. 66–69, 1935.
- 4 **S. H. Loewenthal**, Proposed Design Procedure for Transmission Shafting Under Fatigue Loading, *Technical Note TM-78927*, NASA, 1978.
- 5 **H. J. Gough and H. V. Pollard**, The Strength of Metals Under Combined Alternating Stresses. *Proc. of the Inst. Mech Eng.*, **131**(3): pp. 3–103, 1935.
- 6 **E. Oberg and F. D. Jones**, eds. *Machinery's Handbook*, 17th ed., Industrial Press Inc.: New York, pp. 867–883, 1966.
- 7 **R. C. Peterson**, *Stress-concentration factors*. John Wiley & Sons: New York, pp. 266–267, 1974.
- 8 **E. Oberg et al**, *Machinery's Handbook*, 25th ed., Industrial Press Inc.: New York, pp. 2042–2070, 1996.
- 9 **M. Dimentberg et al.**, "Passage Through Critical Speed with Limited Power by Switching System Stiffness," AMD-Vol. 192 / DE-Vol. 78, *Nonlinear and Stochastic Dynamics*, ASME 1994.
- 10 **C. R. Mischke**, *Elements of Mechanical Analysis*. Addison Wesley: Reading, Mass., pp. 317–320, 1963.
- 11 **R. M. Phelan**, *Dynamics of Machinery*. McGraw-Hill: New York, pp. 178–196, 1967.
- 12 **R. L. Norton**, *Design of Machinery*. 3ed, McGraw-Hill: New York, p. 608, 2004.

10.19 PROBLEMS

- ***10-1** A simply supported shaft is shown in Figure P10-1. A constant-magnitude transverse load P is applied as the shaft rotates subject to a time-varying torque that varies from T_{min} to T_{max} . For the data in the row(s) assigned from Table P10-1, find the diameter of shaft required to obtain a safety factor of 2 in fatigue loading if the shaft is steel of $S_{ut} = 108$ ksi and $S_y = 62$ ksi. The dimensions are in inches, the force in pounds, and the torque in lb-in. Assume no stress concentrations are present.
- 10-2** A simply supported shaft is shown in Figure P10-2. A constant magnitude distributed unit load p is applied as the shaft rotates subject to a time-varying torque that varies from



bearings are self-aligning
so act as simple supports

FIGURE P10-1

Shaft Design for Problems 10-1, 10-4, and 10-15

Table P10-0[†]

Topic/Problem Matrix

10.4 Shaft Power

10-15, 10-16, 10-41, 10-42

10.8 Shaft Design

10-1, 10-2, 10-3, 10-8, 10-31,
9-32,
10-33, 10-34. 10-35

10.9 Shaft Deflection

10-4, 10-5, 10-17b, 10-18, 10-21

10.10 Keys and Keyways

10-6, 10-7, 10-9, 10-10, 10-17a,
10-19, 10-20, 10-28, 10-29,
9-30, 10-36

10.12 Interference Fits

10-11, 10-37, 10-40, 10-43, 10-44

10.13 Flywheel Design

10-12, 10-38, 10-39, 10-45, 10-46

10.14 Critical Speeds

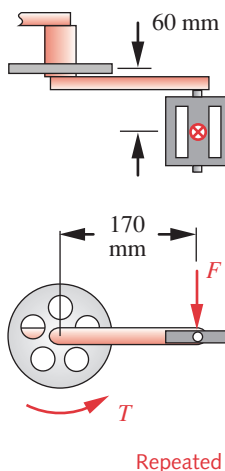
10-13, 10-14, 10-17c, 10-22,
9-23,
10-24, 10-25, 10-26, 10-27

* Answers to these problems are provided in Appendix D.

[†] Problem numbers in *italics* are design problems. Problem numbers in **boldface** are extended from similar problems in earlier chapters with the same dash number.

Table P9-1 Data for Problems

Row	<i>l</i>	<i>a</i>	<i>b</i>	<i>P</i> or <i>p</i>	<i>T</i> _{min}	<i>T</i> _{max}
<i>a</i>	20	16	18	1 000	0	2 000
<i>b</i>	12	2	7	500	-100	600
<i>c</i>	14	4	12	750	-200	400
<i>d</i>	8	4	8	1 000	0	2 000
<i>e</i>	17	6	12	1 500	-200	500
<i>f</i>	24	16	22	750	1 000	2 000



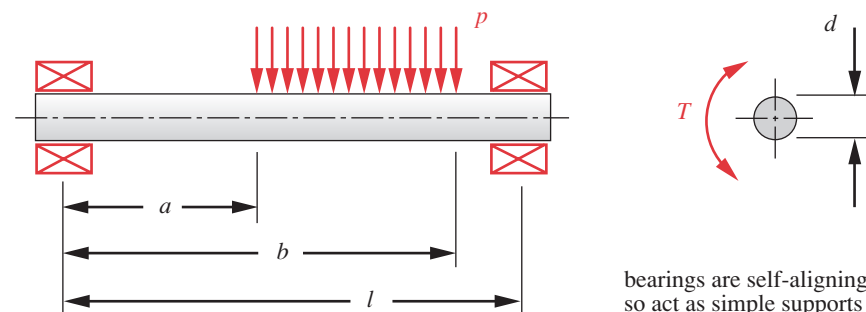
10

FIGURE P6-1

Problem 10-3

*T*_{min} to *T*_{max}. For the data in the row(s) assigned from Table P10-1, find the diameter of shaft required to obtain a safety factor of 2 in fatigue loading if the shaft is steel of $S_{ut} = 745$ MPa and $S_y = 427$ MPa. The dimensions are in cm, the distributed force in N/cm, and the torque in N-m. Assume no stress concentrations are present.

- 10-3** For the bicycle pedal arm assembly in Figure P6-1 (repeated here) assume a rider-applied force that ranges from 0 to 1500 N at each pedal each cycle. Design a suitable shaft to connect the two pedal arms and carry the sprocket against a step. Use the fatigue safety factor of 2 and a material with $S_{ut} = 500$ MPa. The shaft has a square detail on each end where it inserts into the pedal arms.
- ***10-4** Determine the maximum deflections in torsion and in bending of the shaft shown in Figure P10-1 for the data in the row(s) assigned in Table P10-1 if the steel shaft diameter is 1.75 in.
- ***10-5** Determine the maximum deflections in torsion and in bending of the shaft shown in Figure P10-2 for the data in the row(s) assigned in Table P10-1 if the steel shaft diameter is 4 cm.
- ***10-6** Determine the size of key necessary to give a safety factor of at least 2 against both shear and bearing failure for the design shown in Figure P10-3 using the data from the row(s) assigned in Table P10-1. Assume a shaft diameter of 1.75 in. The shaft is steel of $S_{ut} = 108$ kpsi and $S_y = 62$ kpsi. The key is steel of $S_{ut} = 88$ kpsi and $S_y = 52$ kpsi.
- 10-7** Determine the size of key necessary to give a safety factor of at least 2 against both shear and bearing failure for the design shown in Figure P10-4 using the data from the row(s) assigned in Table P10-1. Assume a shaft diameter of 4 cm. The shaft is steel of $S_{ut} = 745$ MPa and $S_y = 427$ MPa. The key is steel of $S_{ut} = 600$ MPa and $S_y = 360$ MPa.

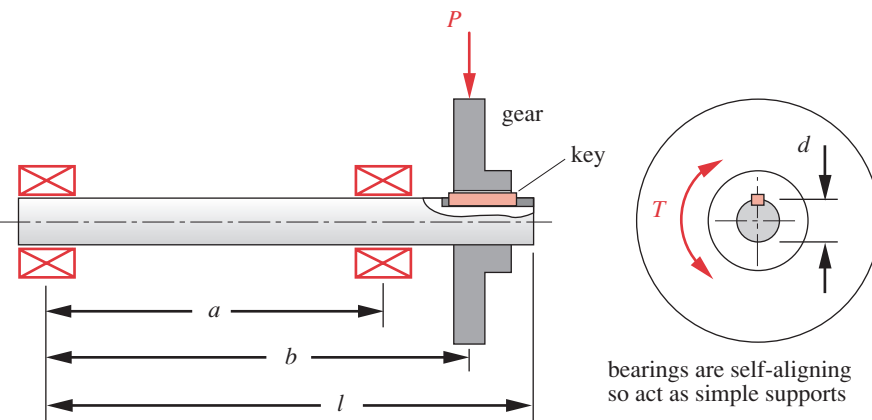


bearings are self-aligning
so act as simple supports

FIGURE P10-2

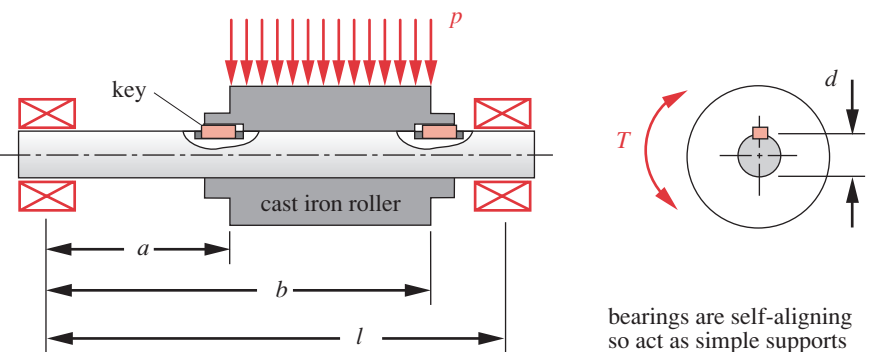
Shaft Design for Problems 10-2, 10-5, and 10-16 (A Solidworks model of this is on the CD)

* Answers to these problems are provided in Appendix D. Problem numbers in *italics* are design problems. Problem numbers in **boldface** are extended from similar problems in earlier chapters with the same dash number.

**FIGURE P10-3**

Shaft Design for Problems 10-6, 10-9, 10-11, and 10-12 (A Solidworks model of this is on the CD)

- *10-8** A paper machine processes rolls of paper having a density of 984 kg/m^3 . The paper roll is 1.50-m outside dia. (OD) \times 22-cm inside diameter (ID) \times 3.23-m long and is on a simply supported, hollow, steel shaft with $S_{ut} = 400 \text{ MPa}$. Find the shaft ID needed to obtain a dynamic safety factor of 2 for a 10-year life if the shaft OD is 22 cm and the roll turns at 50 rpm with 1.2 hp absorbed.
- *10-9** Repeat Problem 10-1 taking the stress concentration at the keyway shown in Figure P10-3 into account.
- 10-10** Repeat Problem 10-2 taking the stress concentrations at the keyways shown in Figure P10-4 into account.
- *10-11** Determine the amount of diametral interference needed to provide a suitable interference fit for the 6-in-dia by 1-in-thick gear of Figure P10-3 using a shaft dia of 1.75 in, such that the stresses in the hub and shaft will be safe and the torque from the assigned row(s) in Table P10-1 can be transmitted through the interference fit. Assume that $S_{ut} = 108 \text{ ksi}$ and $S_y = 62 \text{ ksi}$.
- 10-12** Assume that the device shown keyed to the shaft of Figure P10-3 is a Class 50, cast iron flywheel of 20-in outside diameter and 1-in thickness. The hub is 4-in dia and 3-in thick.

**FIGURE P10-4**

Shaft Design for Problems 10-7, 10-10, and 10-14 (A Solidworks model of this is on the CD)

* Answers to these problems are provided in Appendix D. Problem numbers in *italics* are design problems. Problem numbers in **boldface** are extended from similar problems in earlier chapters with the same dash number.

Determine the maximum speed at which it can safely be run using a safety factor of 2. Use the dimensions and other appropriate data from Problem 10-6 using the data from the row(s) assigned in Table P10-1. Consider the transverse force P to be zero in this case.

- *10-13 Determine the critical frequency of shaft whirl for the assembly shown in Figure P9-3 using the dimensions from the assigned row(s) of Table P10-1 and a steel shaft diameter of 2 in. Use the flywheel dimensions of Problem 10-12.
- 10-14 Determine the critical frequency of shaft whirl for the assembly shown in Figure P9-4 using the dimensions from the assigned row(s) of Table P10-1 and a steel shaft diameter of 4 cm. The cast iron roller diameter is 3 times the shaft diameter.
- *10-15 What are the maximum, minimum, and average power values for the shaft shown in Figure P10-1 for the data in the row(s) assigned in Table P10-1 if the shaft speed is 750 rpm?
- *10-16 What are the maximum, minimum, and average power values for the shaft shown in Figure P10-2 for the data in the row(s) assigned in Table P10-1 if the shaft speed is 50 rpm?
- *10-17 Figure P10-5 shows a roller assembly driven by a gear. The roller extends over 80% of length a and is centered in that dimension. The roller occupies 95% of the exposed shaft length between the bearing faces. The shaft is steel with $S_y = 427$ MPa and $S_{ut} = 745$ MPa. For the data in the assigned row(s) of Table P10-1, find:
 - (a) The safety factor against fatigue failure for a shaft diameter of 40 mm.
 - (b) The maximum torsional deflection between gear and roller.
 - (c) The torsional natural frequency of the shaft.
- *10-18 Figure P10-5 shows a roller assembly driven by a gear. The roller extends over 80% of length a and is centered in that dimension. The roller occupies 95% of the exposed shaft length between the bearing faces. For the data in the assigned row(s) of Table P10-1, find the maximum bending deflection of the 40-mm-dia shaft.
- *10-19 Figure P10-6 shows two gears on a common shaft. Assume that the constant radial force P_1 is 40% of P_2 . For the data in the row(s) assigned from Table P10-1, find the diameter of shaft required to obtain a safety factor of 2 in fatigue loading if the shaft is steel of $S_{ut} = 108$ ksi and $S_y = 62$ ksi. The dimensions are inches, the force lb, and torque is lb-in.

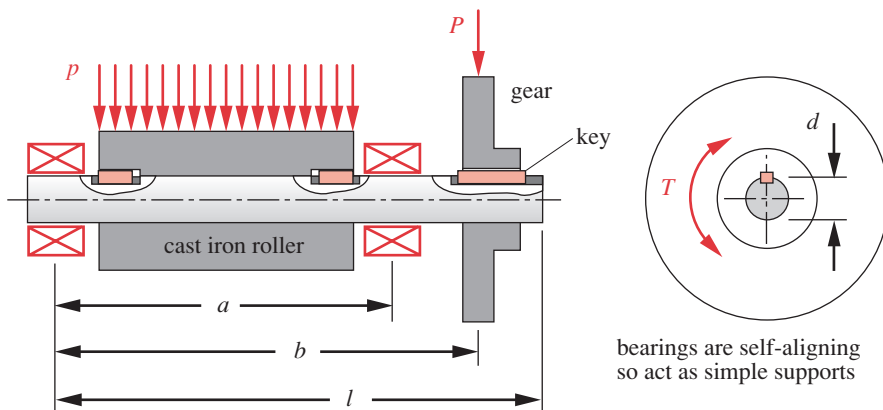
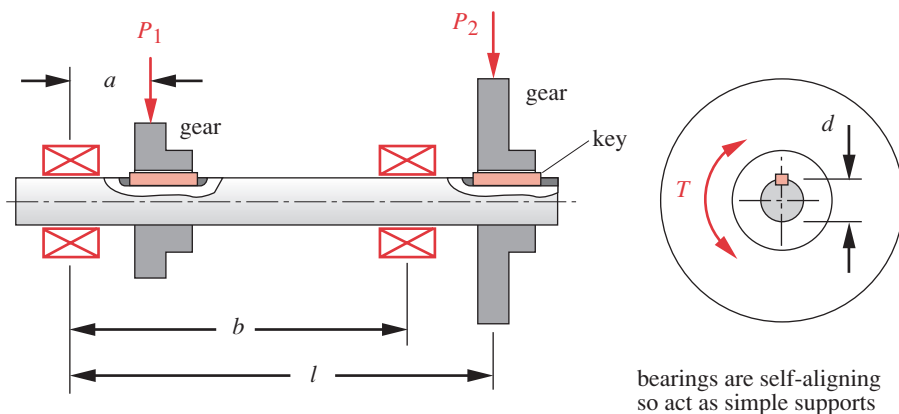


FIGURE P10-5

Shaft Design for Problems 10-17 and 10-18 (A Solidworks model of this is on the CD)

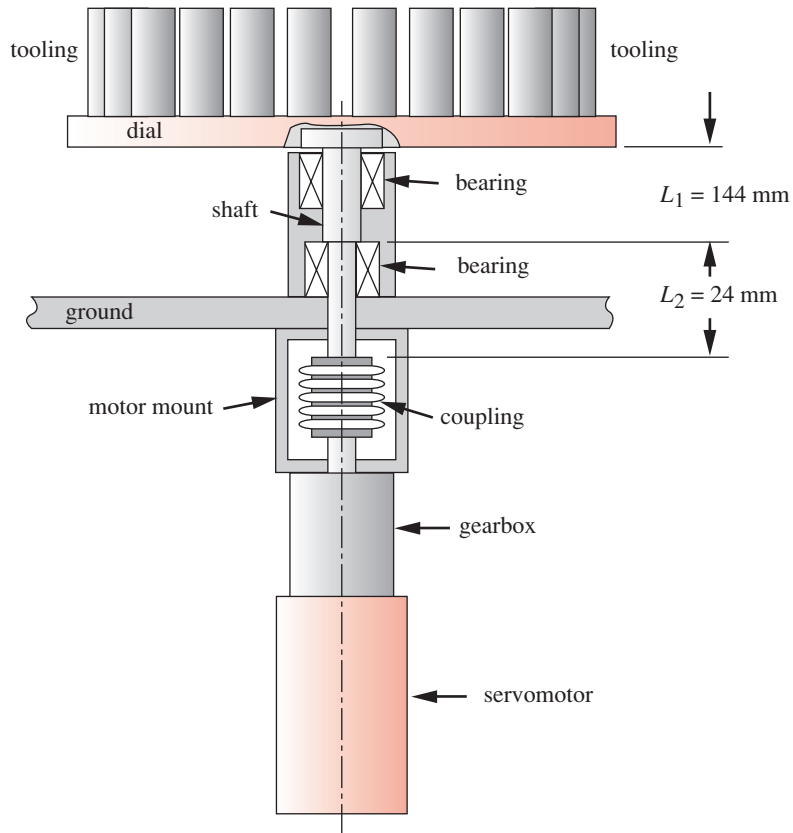
* Answers to these problems are provided in Appendix D.

**FIGURE P10-6**

Shaft Design for Problem 10-19 (A Solidworks model of this is on the CD)

- 10-20 A 300-mm-long, solid, straight shaft is supported in self-aligning bearings at each end. A gear is attached at the middle of the shaft with a 10-mm square steel key in a slot. The geometric stress-concentration factor in the keyslot is 2.5 and its corner radius is 0.5 mm. The gear drives a fluctuating load which creates a bending moment that varies from +10 N-m to +100 N-m and a torque that varies from -35 N-m to +170 N-m each cycle. The material chosen is cold-drawn 4140 steel, hardened and tempered to Rockwell C45 ($S_{ut} = 1250$ MPa). Design the shaft for infinite life and determine the diameter needed for a safety factor of 1.5.
- 10-21 Figure P10-7 shows a dial assembly. The dial is 500-mm-dia by 16-mm-thick solid steel and is bolted to the top flange of the shaft. The shaft is 70 mm dia over length L_1 and 40 mm dia over length L_2 and is carried on tapered roller bearings. All shaft fillet radii are 0.5 mm. A 5-kw motor drives the shaft through a 20:1 reduction gearbox and a commercial bellows coupling. The maximum rated torque from the motor is 17.75 N-m and its stall torque is 3 \times its rated torque. Find the maximum stress and angular deflection in the shaft under conditions of dial locked and motor at stall.
- 10-22 For the dial assembly of Problem 10-21 and Figure P10-7, find the first torsional natural frequency of the shaft-dial assembly as felt at the motor shaft. The gearbox has a torsional stiffness of $1.56E5$ N-m/rad and the coupling has a torsional stiffness of $5.1E5$ N-m/rad. Assume the dial is empty of tooling and all ground support is infinitely stiff.
- 10-23 Repeat Problem 10-22 when the dial is fitted with 20 sets of tooling bolted to its top surface, equispaced on a 416-mm bolt circle. Each tooling assembly weighs 75.62 N. Assume all ground support is infinitely stiff.
- 10-24 Repeat Problem 10-22 when the dial assembly has a motor mount with a torsional stiffness of $2.44E5$ N-m/rad.
- 10-25 The tooling on the dial assembly of Problem 10-21 and Figure P10-7 imparts a time-varying torque to the dial that ranges from a peak of 30% of the motor's rated torque (at the motor) to zero, 20 times per dial revolution. If the motor speed is 600 rpm, find the worst-case stress-time and deflection-time functions for the shaft. Choose a shaft material to give a safety factor of at least 3 against failure. Disregard the response of the system to the forced vibration.

* Answers to these problems are provided in Appendix D. Problem numbers in *italics* are design problems.

**FIGURE P10-7**

Shaft Design for Problems 10-21 to 10-28

- 10-26 Combining the data from Problems 10-23 and 10-25 (a) find the ratio between the torsional forcing frequency and the first torsional natural frequency of the dial assembly; (b) using the frequency ratio calculated in part (a), repeat Problem 10-25 taking into account the forced vibration response of the system if the damping ratio $\zeta = 0.20$.
- 10-27 Repeat Problem 10-25 for an impulsive impact loading of 500 N applied tangentially to the dial rim 20 times per revolution, equispaced in time.
- 10-28 For the dial assembly of Problem 10-21 and Figure P10-7, size a square key to couple the 40-mm-dia dial shaft to the coupling.
- 10-29 Repeat Problem 10-28 for the loading of Problem 10-25.
- 10-30 Repeat Problem 10-28 for the loading of Problem 10-27.

- [†]10-31 A simply supported shaft with overhanging load is shown in Figure P10-1. A constant-magnitude transverse force P is applied as the shaft rotates. The shaft is also subject to a constant torque of T_{max} . For the data in the row(s) assigned from Table P10-1 (ignoring T_{min}), find the diameter of shaft required to obtain a safety factor of 2.5 in fatigue loading if the shaft is steel of $S_{ut} = 118 \text{ kpsi}$ and $S_y = 102 \text{ kpsi}$. The dimensions are in inches, the force in pounds, and the torque in lb-in. Assume no stress concentrations are present, the shaft is machined, the required reliability is 90%, and the shaft operates at room temperature.

[†] Problem numbers in *italics* are design problems.

- 10-32 Repeat Problem 10-31 taking the stress concentration at the keyway shown in Figure P10-3 into account.
- 10-33 A simply supported shaft is shown in Figure P10-2. A constant-magnitude distributed unit load p is applied as the shaft rotates. The shaft is also subject to a steady torque of T_{max} . For the data in the row(s) assigned from Table P10-1 (ignoring T_{min}), find the diameter of shaft required to obtain a safety factor of 2.5 in fatigue loading if the shaft is steel of $S_{ut} = 814$ MPa and $S_y = 703$ MPa. The dimensions are in cm, the distributed force in N/cm, and the torque in N-m. Assume no stress concentrations are present, the shaft is machined, the required reliability is 90%, and the shaft operates at room temperature.
- 10-34 Repeat Problem 10-33 taking the stress concentration at the keyways shown in Figure P10-4 into account.
- 10-35 Figure P10-8 shows the last stage in a gearbox with dual output. The gear is manufactured integrally with the shaft. The shaft is supported by two self-aligning ball bearings. Crank arms are connected to each end of the shaft. The load on the cranks produces equal fluctuating transverse forces on the shaft ends as well as equal fluctuating torques. The torque is transmitted through end-milled keyways in the crank and shaft and a parallel key that fits snugly in each keyway. The crank is located axially by a shoulder that is $L = 50$ -mm from the plane in which the transverse load acts. The fillet radius to shaft diameter is $r/d = 0.05$ and the shoulder to shaft diameter ratio is $D/d = 1.2$. The shaft/gear material is SAE 4130 steel Q&T @ 1200F. The transverse force fluctuates from 8 kN to 16.5 kN and the torque fluctuates from 1.1 kN-m to 2.2 kN-m. For a factor of safety of 2.5 against an infinite-life fatigue failure, determine a suitable shaft diameter, d .
- 10-36 Determine the size of key necessary to give a safety factor of at least 2 against both shear and bearing failure for the crank/shaft connection of Problem 10-35. Assume a shaft diameter of 58 mm and a key made from SAE 1040 CR steel.
- *10-37 As an alternative to the keyed connection in Problem 10-35 determine the amount of diametral interference needed to provide a suitable interference fit for the crank of Figure P10-8 using a shaft diameter of 58 mm, such that the stresses in the hub and shaft will be safe and the maximum torque can be transmitted through the interference fit. The crank material is the same as the shaft and its length along the shaft is 64 mm. The effective outside diameter of the crank is 150 mm.

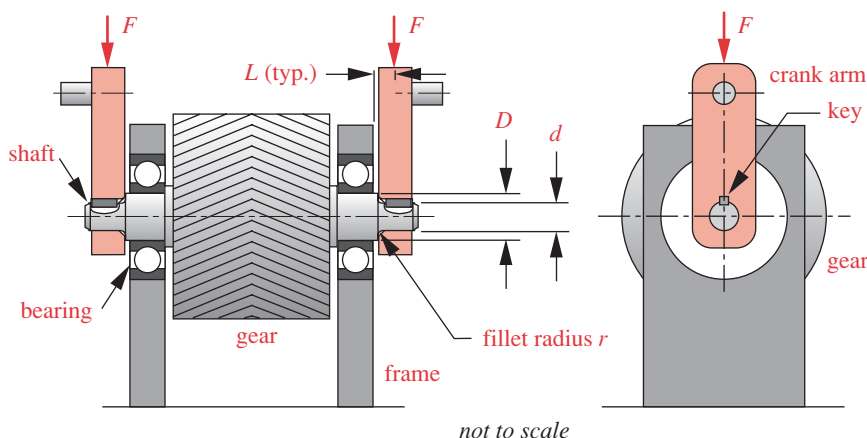


FIGURE P10-8

Problems 10-35 through 10-37

* Answers to these problems are provided in Appendix D. Problem numbers in *italics* are design problems.

- *10-38 An electric motor-driven shaft that has a fluctuating load torque turns at an average speed of 1600 rpm. The load torque varies sinusoidally once per revolution of the shaft with a peak torque of 29 500 in-lb. The shaft diameter is 2.0 in. Design a suitable flywheel for this system that will provide a coefficient of fluctuation of 0.05 and an overspeed safety factor of at least 4. The flywheel is to be a solid circular disc of constant thickness made from SAE 1020 CR steel.
- 10-39 Repeat Problem 10-38 for a peak load torque of 40 500 in-lb and a torque vs. shaft position function of $T_l = T_{peak} (\sin \theta + \sin 2\theta)$.
- 10-40 As an alternative to the keyed connection in Problem 10-6 determine the amount of diametral interference needed to provide a suitable interference fit for the gear of Figure P10-3 using the data of Problem 10-6 and the row(s) assigned in Table P10-1. The gear hub diameter is 3.50 in, its length along the shaft is 2.00 in, and it has the same properties as the shaft material.
- 10-41 Figure P10-6 shows a shaft, running at 400 rpm, with two attached gears. The right-hand gear (2) furnishes the load torque and the left-hand gear (1) furnishes an equal but opposite direction input torque. The torque varies between 2.2 kN-m and 6.2 kN-m. Determine the minimum, maximum, and average power transmitted by the shaft.
- 10-42 Figure P10-6 shows a shaft, running at 750 rpm, with two attached gears. The right-hand gear (2) furnishes the load torque and the left-hand gear (1) furnishes an equal but opposite direction input torque. The forces on a gear act at the pitch diameter and have a radial (P in the figure) and a tangential component (not shown). If the pitch diameter of gear 1 is 250 mm and the tangential force varies between 15 kN and 60 kN, determine the minimum, maximum, and average power transmitted by the shaft.
- 10-43 Determine the amount of diametral interference needed to provide a suitable interference fit (instead of the keyed attachment shown) for the 5-in diameter by 1.5-in thick gear (1) of Figure P10-6 using a shaft diameter of 1.5 in, such that the stresses in the hub and shaft will be safe and the input torque of 1500 lbf-in can be transmitted through the interference fit. Both parts are SAE 4130 steel normalized @ 1650F.
- 10-44 Determine the amount of diametral interference needed to provide a suitable interference fit (instead of the keyed attachment shown) for the 125-mm diameter by 75-mm thick gear (1) of Figure P10-6 using a shaft diameter of 80 mm, such that the stresses in the hub and shaft will be safe and the input torque of 170 N-m can be transmitted through the interference fit. Both parts are SAE 4140 steel normalized @ 1650F.
- 10-45 Table P10-2 shows the energy pulses delivered to (positive) and from (negative) a rotating system along with the shaft angles at which the torque function crosses the average torque line in a torque-time function. Using this data, determine the shaft angles at which minimum and maximum shaft speed occur and the total change in energy from the shaft position at which maximum speed occurs to the position at which minimum speed occurs.
- 10-46 An electric motor-driven shaft that has a fluctuating load torque turns at an average speed of 1950 rpm. The energy pulses to (positive) and from (negative) the driven system are given in Table P10-2. The shaft diameter is 50 mm. Design a suitable flywheel for this system that will provide a coefficient of fluctuation of 0.05 and an overspeed safety factor of at least 5. The flywheel is to be a hollow circular disc of constant thickness made from SAE 1040 CR steel.

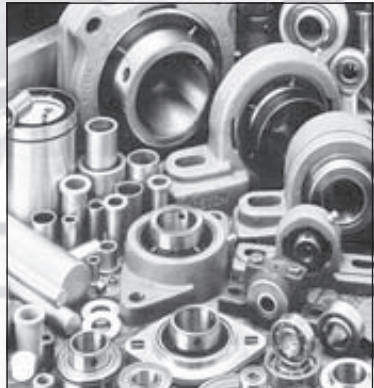
Table P-10-2

Data for Problem 10-45

Shaft Angles	Delta Energy
0° to 75°	-1040 N-m
75° to 195°	+2260 N-m
195° to 330°	-2950 N-m
330° to 360°	+1740 N-m

* Answers to these problems are provided in Appendix D. Problem numbers in *italics* are design problems.

11



BEARINGS AND LUBRICATION

*The knowledge of man is as the waters,
some descending from above,
and some springing from beneath.*

Francis Bacon

11.0 INTRODUCTION

We use the term **bearing** here in its most general sense. Whenever two parts have relative motion, they constitute a bearing by definition, regardless of their shape or configuration. Usually, lubrication is needed in any bearing to reduce friction and remove heat. Bearings may roll or slide or do both simultaneously.

A *plain bearing* is formed by any two materials rubbing on one another, whether a sleeve around a shaft or a flat surface under a slider. In a plain bearing, one of the moving parts usually will be steel or cast iron or some other structural material in order to achieve the required strength and hardness. For example, transmission shafts, links, and pins are in this category. The parts that they move against will usually be made of a “bearing” material such as bronze, babbitt, or a nonmetallic polymer. A radial plain bearing may be split axially to assemble it to the shaft, or may be a complete circle called a **bushing**. A **thrust bearing** supports axial loads.

Alternatively, a rolling-element bearing, which has hardened steel balls or rollers captured between hardened steel raceways, may be used to provide very low friction. Plain bearings are typically custom designed for the application, while rolling-element bearings are typically selected from manufacturers’ catalogs to suit the loads, speeds, and desired life of the particular application. Rolling-element bearings can support radial, thrust, or combinations of those loads depending on their design.

This chapter will discuss bearings in general, both the sliding (or plain) variety and also rolling-element bearings. Lubrication theory also will be discussed as it applies to these types of bearings. Table 11-0 shows the variables used in this chapter and notes the equations or sections in which they first occur.

Table 11-0 Variables Used in This Chapter

Symbol	Variable	ips units	SI units	See
<i>A</i>	area	in ²	m ²	Sect. 11.5
<i>a, b</i>	half-width, length of contact patch	in	m	Eq. 11.18
<i>C</i>	basic dynamic load rating	lb	N	Sect. 11.10
<i>C</i> ₀	basic static load rating	lb	N	Sect. 11.10
<i>c</i> _{d, r}	diametral and radial clearance	in	m	Sect. 11.5
<i>d</i>	diameter	in	m	various
<i>E'</i>	effective Young's modulus	psi	Pa	Eq. 11.16
<i>F</i>	force (with various subscripts)	lb	N	Eq. 11.22
<i>f</i>	friction force	lb	N	Eq. 11.11
<i>h</i>	lubricant film thickness	in	m	Sect. 11.5
<i>K</i> _E	dimensionless parameter	none	none	Sect. 11.5
<i>l</i>	length	in	m	Sect. 11.5
<i>L</i>	fatigue life of rolling bearings	10 ⁶ revs	10 ⁶ revs	Eq. 11.19
<i>n'</i>	angular velocity	rps	rps	Sect. 11.5
<i>O</i> _N	Ocvirk number	none	none	Eq. 11.12
<i>P</i>	force or load	lb	N	Sect. 11.5
<i>p</i>	pressure	psi	N/m ²	Sect. 11.5
<i>r</i>	radius	in	m	Sect. 11.5
<i>R'</i>	effective radius	in	m	Eq. 11.16
<i>S</i>	Sommerfeld number	none	none	Sect. 11.5
<i>T</i>	torque	lb-in	N-m	Sect. 11.5
<i>U</i>	linear velocity	in/sec	m/sec	Sect. 11.5
<i>X, Y</i>	radial and axial force factors	none	none	Eq. 11.22
α	pressure-viscosity exponent	in ² /lb	m ² /N	Eq. 11.15
ϵ	eccentricity ratio	none	none	Eq. 11.3
ϵ_x	empirical eccentricity ratio	none	none	Eq. 11.13
ϕ	angle to resultant force	rad	rad	Sect. 11.5
Φ	power	hp	watts	Eq. 11.10
η	absolute viscosity	reyn	cP	Eq. 11.1
Λ	specific film thickness	none	none	Eq. 11.14
μ	coefficient of friction	none	none	Eq. 11.11
ν	Poisson's ratio	none	none	Eq. 11.17
θ_{max}	angle to maximum pressure	rad	rad	Sect. 11.5
ρ	mass density	blob/in ³	kg/mm ³	Eq. 11.1
τ	shear stress (with various subscripts)	psi	Pa	Sect. 11.5
ν	kinematic viscosity	in ² /sec	cS	Eq. 11.1
ω	angular velocity	rad/sec	rad/sec	Eq. 11.10

To the machine designer all bearings are of course only necessary evils, contributing nothing to the product or function of the machine; and any virtues they can have are only of a negative order. Their merits consist in absorbing as little power as possible, wearing out as slowly as possible, occupying as little space as possible, and costing as little as possible.^[1]

A Caveat

Lubrication theory for surfaces in relative motion is extremely complex mathematically. Solutions to the partial differential equations that govern the behavior are based on simplifying assumptions that yield only approximate solutions. This chapter does not attempt to present a complete discussion or explanation of all the complicated phenomena of dynamic lubrication, as that is far beyond the scope of this text. Rather an introductory discussion of a few of the common cases encountered in machine design is presented. Boundary, hydrostatic, hydrodynamic, and elastohydrodynamic lubrication are introduced and described, and the theory for the last two conditions is discussed without presentation of complete derivations of the governing equations due to space limitations.

Such topics as squeeze-film theory and oil whirl are not addressed at all, nor are the issues of lubricant supply to, and heat transfer from, the bearing. Entire books have been written on these topics and the reader is directed to those sources for more complete information. Derivations of the governing equations are presented in most of the referenced works. Reference 2 provides an excellent introduction to lubrication theory with minimal mathematics, and reference 3 is a very complete, up-to-date, and mathematically rigorous treatment of the subject.

In this chapter, we present a simple and reasonably accurate approach to the design of short journal bearings that will allow them to be designed for the loads and speeds required in most common machinery. We also address the lubrication of nonconforming contacts such as gear teeth and cam-follower joints. Finally, a discussion of rolling-element bearing selection from manufacturers' information is provided. Rolling-element bearings are a topic that is again as complicated as that of journal bearings, and books have been written on this subject as well. The reader is directed to references 3 and 4 for up-to-date and complete treatments of rolling-contact bearing theory and lubrication. The references to this chapter identify additional readings on the complex subject of lubrication and bearing design. We will barely "wet the surface" of this complicated subject here. We hope that it "whets your appetite" to learn more about the subject.

11.1 LUBRICANTS

Introduction of a lubricant to a sliding interface has several beneficial effects on the friction coefficient. Lubricants may be gaseous, liquid, or solid. Liquid or solid lubricants share the properties of low shear strength and high compressive strength. A liquid lubricant such as petroleum oil is essentially incompressible at the levels of compressive stress encountered in bearings, but it readily shears. Thus, it becomes the weakest material in the interface, and its low shear strength reduces the coefficient of friction (see equation 7.3 on p. 424). Lubricants can also act as contaminants to the

metal surfaces and coat them with monolayers of molecules that inhibit adhesion even between compatible metals.

Liquid lubricants are the most commonly used and mineral oils the most common liquid. Greases are oils mixed with soaps to form a thicker, stickier lubricant used where liquids cannot be supplied to or retained on the surfaces. Solid lubricants are used in situations where liquids either cannot be kept on the surfaces or lack some required property such as high-temperature resistance. Gaseous lubricants are used in special situations such as air bearings to obtain extremely low friction. Lubricants, especially liquids, also remove heat from the interface. Lower bearing temperatures reduce surface interactions and wear.

LIQUID LUBRICANTS are largely petroleum-based or synthetic oils, though water is sometimes used as a lubricant in aqueous environments. Many commercial lubricant oils are mixed with various additives that react with the metals to form monolayer contaminants. So-called EP (*Extreme Pressure*) lubricants add fatty acids or other compounds to the oil that attack the metal chemically and form a contaminant layer that protects and reduces friction even when the oil film is squeezed out of the interface by high contact loads. Oils are classified by their viscosity as well as by the presence of additives for EP applications. Table 11-1 shows some common liquid lubricants, their properties, and typical uses. Lubricant manufacturers should be consulted for particular applications.

SOLID-FILM LUBRICANTS are of two types: materials that exhibit low shear stress, such as graphite and molybdenum disulfide, which are added to the interface, and coatings such as phosphates, oxides, or sulfides that are caused to form on the material surfaces. The graphite and MoS₂ materials are typically supplied in powder form and can

Table 11-1 Types of Liquid Lubricants

Type	Properties	Typical Uses
Petroleum oils (mineral oils)	Basic lubrication ability fair, but additives produce great improvement. Poor lubrication action at high temperatures	Very wide and general
Polyglycols	Quite good lubricants, do not form sludge on oxidizing	Brake fluid
Silicones	Poor lubrication ability, especially against steel. Good thermal stability	Rubber seals. Mechanical dampers
Chlorofluorocarbons	Good lubricants, good thermal stability	Oxygen compressors. Chemical processing equipment
Polyphenyl ethers	Very wide liquid range. Excellent thermal stability. Fair lubricating ability	High-temperature sliding systems
Phosphate esters	Good lubricants—EP action	Hydraulic fluid + lubricant
Dibasic esters	Good lubricating properties. Can stand higher temperatures than mineral oils.	Jet engines

be carried to the interface in a binder of petroleum grease or other material. These dry lubricants have the advantage of low friction and high-temperature resistance, though the latter may be limited by the choice of binder. Coatings such as phosphates or oxides can be chemically or electrochemically deposited. These coatings are thin and tend to wear through in a short time. The EP additives in some oils provide a continuous renewal of sulfide or other chemically induced coatings. Table 11-2 shows some common solid-film lubricants, their properties, and typical uses.

11.2 VISCOSITY

Viscosity is a measure of a fluid's resistance to shear. Viscosity varies inversely with temperature and directly with pressure, both in a nonlinear fashion. It can be expressed either as an **absolute viscosity** η or as **kinematic viscosity** v . They are related as

$$\eta = \nu \rho \quad (11.1)$$

where ρ is the mass density of the fluid. The units of absolute viscosity η are either lb-sec/in² (reyn) in the English system or Pa-s in SI units. These are often expressed as μ reyn and mPa-s to better suit their typical magnitudes. A centipoise (cP) is 1 mPa-s. Typical absolute viscosity values at 20°C (68°F) are 0.0179 cP (0.0026 μ reyn) for air, 1.0 cP (0.145 μ reyn) for water, and 393 cP (57 μ reyn) for SAE 30 engine oil. Oils operating in hot bearings typically have viscosities in the 1 to 5 μ reyn range. The term viscosity used without modifiers implies absolute viscosity.

KINEMATIC VISCOSITY is measured in a *viscometer*, which may be either rotational or capillary. A capillary viscometer measures the rate of flow of the fluid through a capillary tube at a particular temperature, typically 40 or 100°C. A rotational viscometer measures the torque and speed of rotation of a vertical shaft or cone running inside a

Table 11-2 Types of Solid Film Lubricants

Type	Properties	Typical Uses
Graphite and/or MoS ₂ + binder	Best general-purpose lubricants. Low friction (0.12–0.06) reasonably long life ($\approx 10^4$ – 10^6 cycles)	Locks and other intermittent mechanisms
Teflon + binder	Life not quite as long as previous type, but resistance to some liquids better	As above
Rubbed graphite or MoS ₂ film	Friction very low (0.10–0.04), but life quite short (10^2 – 10^4 cycles)	Deep drawing and other metalworking
Soft metal (lead, indium, cadmium)	Friction higher (0.30–0.15) and life not as long as resin-bonded types	Running-in protection (temporary)
Phosphate, anodized film. Other chemical coatings	Friction high (≈ 0.20). Galling preventatives leave "spongy" surface layer.	Undercoating for resin-bonded film

Source: E. Rabinowicz, *Friction and Wear of Materials*, 1965, reprinted by permission of John Wiley & Sons, Inc.

bearing with its concentric annulus filled with the test fluid at the test temperature. The SI units of kinematic viscosity are cm^2/sec (stoke) and the English units are in^2/sec . Strokes are quite large, so centistokes (cS) are often used.

ABSOLUTE VISCOSITY is needed for calculation of lubricant pressures and flows within bearings. It is determined from the measured kinematic viscosity and the density of the fluid at the test temperature. Figure 11-1 shows a plot of the variation of absolute viscosity with temperature for a number of common petroleum oils, designated by their ISO numbers and by SAE numbers on both the engine-oil and gear-oil scales.

11.3 TYPES OF LUBRICATION

Three general types of lubrication can occur in bearings: **full-film**, **mixed film**, and **boundary lubrication**. Full-film lubrication describes a situation in which the bearing surfaces are fully separated by a film of lubricant, eliminating any contact. Full-film lubrication can be **hydrostatic**, **hydrodynamic**, or **elastohydrodynamic**, each discussed below. Boundary lubrication describes a situation where, for reasons of geometry, surface roughness, excessive load, or lack of sufficient lubricant, the bearing surfaces physically contact and adhesive or abrasive wear may occur. Mixed-film lubrication describes a combination of partial lubricant film plus some asperity contact between the surfaces.

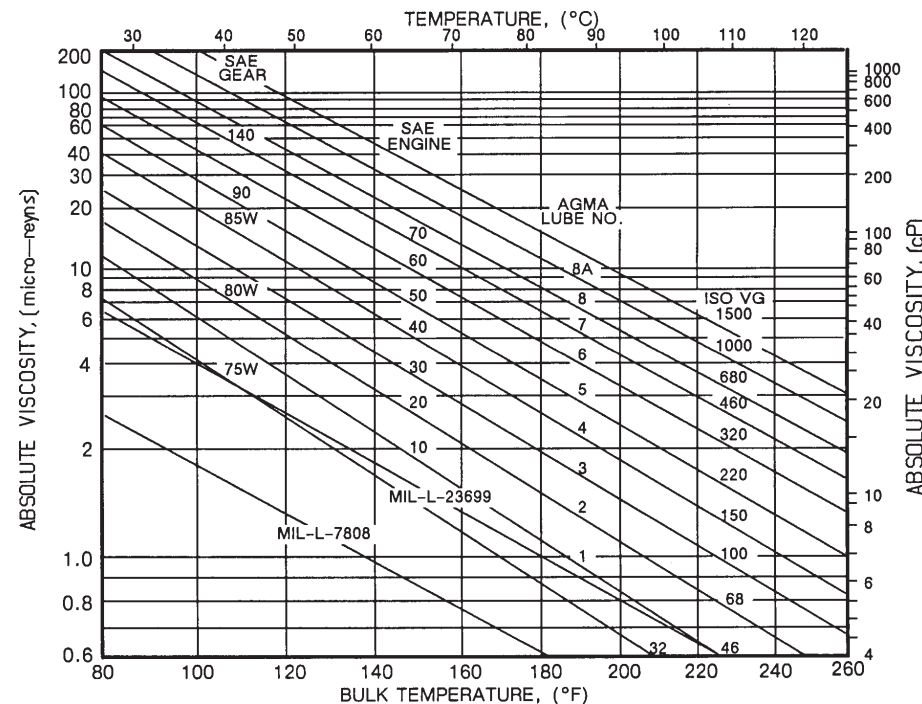


FIGURE 11-1

Absolute Viscosity Versus Temperature of Petroleum Lubricating Oils in ISO Viscosity Grades Source: Extracted from AGMA Standard 2001-B88, *Fundamental Rating Factors and Calculation Methods for Involute Spur and Helical Gear Teeth* with the permission of the publisher, American Gear Manufacturers Association, 1500 King St., Suite 201, Alexandria, Va., 22314.

Figure 11-2 shows a curve depicting the relationship between friction and the relative sliding speed in a bearing. At slow speeds, boundary lubrication occurs with concomitant high friction. As the sliding speed is increased beyond point A, a hydrodynamic fluid film begins to form, reducing asperity contact and friction in the mixed-film regime. At higher speeds, a full film is formed at point B, separating the surfaces completely with reduced friction. (This is the same phenomenon that causes automobile tires to *aquaplane* on wet roads. If the relative velocity of the tire versus the wet road exceeds a certain value, the tire motion pumps a film of water into the interface, lifting the tire off the road. The tire's coefficient of friction is drastically reduced, and the sudden loss of traction can cause a dangerous skid.) At still higher speeds the viscous losses in the sheared lubricant increase friction.

In rotating journal (sleeve) bearings, all three of these regimes will be experienced during start-up and shutdown. As the shaft begins to turn, it will be in boundary lubrication. If its top speed is sufficient, it will pass through the mixed regime and reach the desired full-film regime where wear is reduced virtually to zero if the lubricant is kept clean and not overheated. We will briefly discuss the conditions that determine these lubrication states, and then explore a few of them in somewhat greater detail.

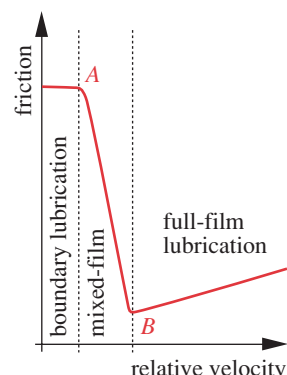


FIGURE 11-2

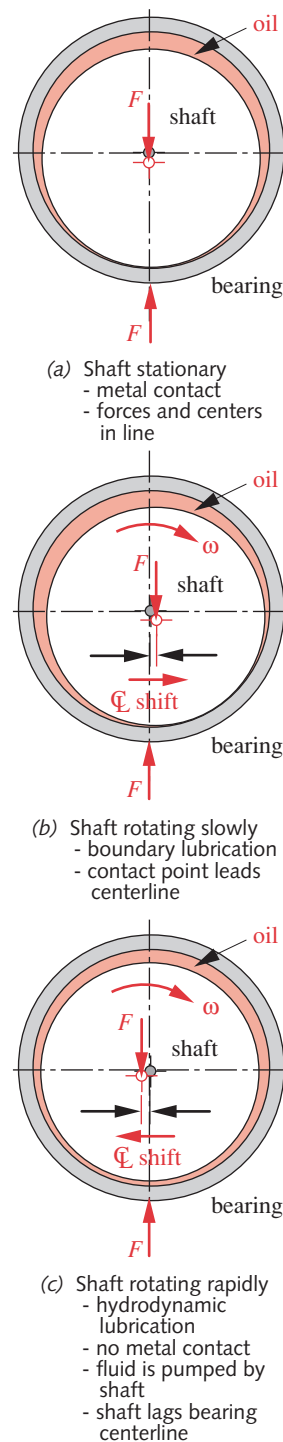
Change in Friction with Relative Velocity in a Sliding Bearing

Full-Film Lubrication

Three mechanisms can create full-film lubrication: **hydrostatic**, **hydrodynamic**, and **elastohydrodynamic** lubrication.

HYDROSTATIC LUBRICATION refers to the continuous supply of a flow of lubricant (typically an oil) to the sliding interface at some elevated hydrostatic pressure ($\approx 10^2$ – 10^4 psi). This requires a reservoir (sump) to store, a pump to pressurize, and plumbing to distribute the lubricant. When properly done, with appropriate bearing clearances, this approach can eliminate all metal-to-metal contact at the interface during sliding. The surfaces are separated by a film of lubricant, which, if kept clean and free of contaminants, reduces wear rates to virtually zero. At zero relative velocity, the friction is essentially zero. With relative velocity, the coefficient of friction in a hydrostatically lubricated interface is about 0.002 to 0.010. This is also the principle of a so-called air bearing, used on “air pallets” to lift (thrust) a load from a surface, allowing it to be moved sideways with very little effort. Hovercraft operate on a similar principle. Water is sometimes used in hydrostatic bearings. Denver’s Mile High Stadium has a 21 000-seat grandstand that slides back on hydrostatic water films to convert the stadium from baseball to football.^[5] Hydrostatic thrust bearings are more common than radial ones.

HYDRODYNAMIC LUBRICATION refers to the supply of sufficient lubricant (typically an oil) to the sliding interface to allow the relative velocity of the mating surfaces to pump the lubricant within the gap and separate the surfaces on a dynamic film of liquid. This technique is most effective in journal bearings, where the shaft and bearing create a thin annulus within their clearance that traps the lubricant so the shaft can pump it around the annulus. A leakage path exists at the ends, so a continuous supply of oil must be provided to replace the losses. This supply may be fed by gravity or pressure. This is the system used to lubricate the crankshaft and camshaft bearings in an internal-combustion engine. Filtered oil is pumped to the bearings under relatively low pressure to replenish the oil lost through the bearing ends, but the condition within the bearing is hydrodynamic, creating much higher pressures to support the bearing loads.

**FIGURE 11-3**

Boundary and Hydrodynamic Lubrication Conditions in a Sleeve Bearing—Clearance and Motions Exaggerated

In a hydrodynamic sleeve bearing at rest, the shaft or journal sits in contact with the bottom of the bearing, as shown in Figure 11-3a and is in boundary lubrication. As it begins to rotate, the shaft centerline shifts eccentrically within the bearing and the shaft acts as a pump to pull the film of oil clinging to its surface around with it, as shown in Figure 11-3b, putting it into the mixed film regime of Figure 11-2. (The “outer side” of the oil film is stuck to the stationary bearing.) A flow is set up within the small thickness of the oil film. With sufficient relative velocity, the shaft “climbs up” on a wedge of pumped oil and ceases to have metal-to-metal contact with the bearing, as shown in Figure 11-3c. It is now in the hydrodynamic regime of Figure 11-2.

Thus, a hydrodynamically lubricated bearing touches its surfaces together only when stopped or when rotating below its “aquaplane speed.” This means that adhesive wear can occur only during the transients of start-up and shutdown. As long as sufficient, clean lubricant and velocity are present to allow hydrodynamic lifting of the shaft off the bearing at its operating speed, there is essentially no adhesive wear. This greatly increases wear life over that of a continuous-contact situation. As with hydrostatic lubrication, the oil must be kept free of contaminants to preclude other forms of wear such as abrasion. The coefficient of friction in a hydrodynamically lubricated interface is about 0.002 to 0.010.

ELASTOHYDRODYNAMIC LUBRICATION When the contacting surfaces are nonconforming, as with the gear teeth or cam and follower shown in Figure 11-4, then it is more difficult to form a full film of lubricant, since the nonconforming surfaces tend to expel rather than entrap the fluid. At low speeds these joints will be in boundary lubrication, and high wear rates can result with possible scuffing and scoring. The load creates a contact patch from the elastic deflections of the surfaces, as discussed in Chapter 7. This small contact patch can provide enough of a flat surface to allow a full hydrodynamic film to form if the relative sliding velocity is high enough (see Figure 11-2). This condition is termed **elastohydrodynamic lubrication** (EHD), as it depends on the elastic deflections of the surfaces and the fact that the high pressures (100 to 500 kpsi) within the contact zone greatly increase the viscosity of the fluid. (In contrast, the film pressure in conforming bearings is only several thousand psi and the change in viscosity due to this pressure is small enough to ignore.)

Gear teeth can operate in any of the three conditions depicted in Figure 11-2. Boundary lubrication occurs in start-stop operation and if prolonged will cause severe wear. Cam-follower joints can also experience any of the regimes in Figure 11-2 but are more likely to be in a boundary-lubricated mode at locations of small radius of curvature on the cam. Rolling-element bearings can see any of the three regimes as well.

The most important parameter that determines which situation occurs in nonconforming contacts is the ratio of the oil-film thickness to the surface roughness. To get full-film lubrication and avoid asperity contact, the rms average surface roughness (R_q) needs to be no more than about 1/2 to 1/3 of the oil-film thickness. An EHD full-film thickness is normally of the order of 1 μm . At very high loads, or low speeds, the EHD film thickness may become too small to separate the surface asperities and mixed-film or boundary lubrication conditions may recur. Factors that have the most effect in creating EHD conditions are increased relative velocity, increased lubricant viscosity, and increased radius of curvature at the contact. Reduction in unit load and reduced stiffness of the material have less effect.^[6]

Boundary Lubrication

Boundary lubrication refers to situations in which some combination of the geometry of the interface, high load levels, low velocity, or insufficient lubricant quantity preclude the initiation of a hydrodynamic condition. The properties of the contacting surfaces and lubricant properties other than its bulk viscosity determine friction and wear in this situation. Viscosity of the lubricant is not a factor. Note in Figure 11-2 that friction is independent of velocity in boundary lubrication. This is consistent with the definition of Coulomb friction in Section 7.3 (p. 424). See Table 7-1 on p. 426.

Boundary lubrication implies that there is always some metal-to-metal contact in the interface. If the lubricant film is not thick enough to “bury” the asperities on the surfaces, this will be true. Rough surfaces could cause this condition. If the relative velocity or the supply of lubricant to a hydrodynamic interface is reduced, it will revert to a boundary-lubrication condition. Surfaces such as gear teeth and cam/follower interfaces (see Figure 11-4) that do not envelop each other can be in a boundary-lubrication mode if EHD conditions do not prevail. Ball and roller bearings can also operate in boundary-lubrication mode if the combination of speeds and loads does not allow EHD to occur.

Boundary lubrication is a less desirable condition than the other types described above because it allows the surface asperities to contact and wear rapidly. It is sometimes unavoidable as in the examples of cams, gears, and rolling-element bearings cited. The EP lubricants mentioned above were created for these boundary-lubrication applications, especially for hypoid gears, which experience both high sliding velocities and high loads. The coefficient of friction in a boundary-lubricated sliding interface depends on the materials used as well as on the lubricant but ranges from about 0.05 to 0.15, with most being about 0.10.

11.4 MATERIAL COMBINATIONS IN SLIDING BEARINGS

Figure 7-6 (p. 428) shows material combinations and their predicted sliding ability based on their mutual insolubility and other factors. This section will discuss some combinations of materials that have proven either successful or unsuccessful in engineering applications of bearings and sliders.

Some properties sought in a bearing material are relative softness (to absorb foreign particles), reasonable strength, machinability (to maintain tolerances), lubricity, temperature and corrosion resistance, and, in some cases, porosity (to absorb lubricant). A bearing material should be less than one-third as hard as the material running against it in order to provide embedability of abrasive particles.^[7] In addition, the compatibility issues addressed in Section 7.4 (p. 426) on adhesive wear are of concern and these also depend on the mating material. Several different classes of materials can be useful as bearings, typically those based on lead, tin, or copper. Aluminum, alone, is not a good bearing material, although it is used as an alloying element in some bearing materials.

BABBITS A whole family of alloys based on lead and tin in combination with other elements are very effective, especially when electroplated in thin films on a stronger substrate such as steel. Babbitt is probably the most common example of this family and is used for crankshaft and camshaft bearings in internal-combustion engines. Its

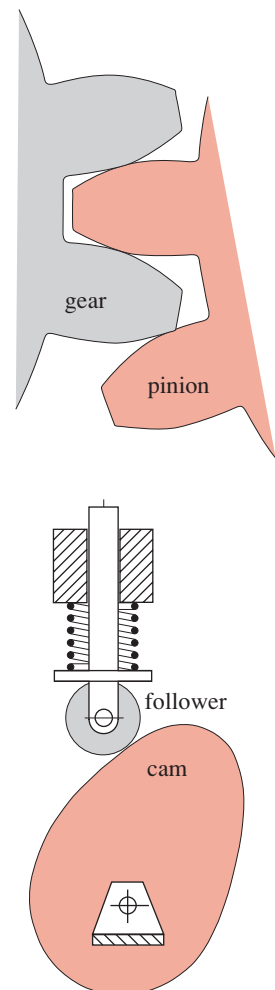


FIGURE 11-4

Open Joints That Can Have EHD, Mixed, or Boundary Lubrication

softness allows particulate embedment and it can be finished to low roughness. A thin electroplated babbitt layer has better fatigue resistance than a thick babbitt bushing, but cannot embed particles as well. Good hydrodynamic or hydrostatic lubrication is required, as babbitt has a low melt temperature and will quickly fail under boundary-lubricated conditions. Shafts for babbitt bearings should have a minimum hardness of 150–200HB and a ground surface finish* of $R_a = 0.25$ to $0.30 \mu\text{m}$ (10 to 12 μin).^[8]

BRONZES The copper-alloy family, principally bronzes, are an excellent choice for running against steel or cast iron. Bronze is softer than ferrous materials but has good strength, machinability, and corrosion resistance and runs well against ferrous alloys when lubricated. There are five common copper alloys used in bearings: copper-lead, leaded bronze, tin bronze, aluminum bronze, and beryllium copper. They have a range of hardness from that of babbitts to close to that of steel.^[8] Bronze bushings can withstand boundary lubrication and can support high loads and high temperatures. Bronze bushings and flat stock are available commercially in a variety of sizes, both solid and sintered (see below).

GRAY CAST IRON AND STEEL are reasonable bearing materials when run against each other at low velocities. The free graphite in the cast iron adds lubricity but liquid lubricant is needed as well. Steel can also be run against steel if both parts are hardened and lubricated. This is a common choice in rolling-contact as in rolling-element bearings. In fact, hardened steel will run against almost any material with proper lubrication. Hardness seems to protect against adhesion in general.

SINTERED MATERIALS are formed from powder and remain microscopically porous after heat treatment. Their porosity allows them to take up significant amounts of lubricant and hold it by capillary action, releasing it into the bearing when hot. Sintered bronze is widely used for running against steel or cast iron.

NONMETALLIC MATERIALS of some types offer the possibility of dry running if they have sufficient lubricity. Graphite is one example. Some thermoplastics such as nylon, acetal, and filled Teflon offer a low coefficient of friction μ against any metal but have low strengths and low melt temperatures, which when combined with their poor heat conduction severely limits the loads and speeds of operation that they can sustain. Teflon has a very low μ (approaching rolling values) but requires fillers to raise its strength to usable levels. Inorganic fillers such as talc or glass fiber add significant strength and stiffness to any of the thermoplastics but at the cost of a higher μ and increased abrasiveness. Graphite and MoS_2 powder are also used as fillers and these add lubricity as well as strength and temperature resistance. Some mixtures of polymers such as acetal-Teflon are also offered. Thermoplastic bearings are usually only practical where loads and temperatures are low. The practical combinations of shaft and bearing materials are really quite limited. Table 11-3 shows some usable combinations of metallic bearing materials and indicates their hardness ratios versus typical shaft-steel.^[9]

11.5 HYDRODYNAMIC LUBRICATION THEORY

Consider the sleeve bearing shown in Figure 11-3. Figure 11-5a shows a similar journal and bearing, but concentric and with the axis vertical. The diametral clearance c_d between journal and bearing is very small, typically about one-thousandth of the diameter. We can model this as two flat plates because the gap h is so small compared to

* See Section 7.1 and Figure 7-2 on p. 418 for a discussion of surface finish and a definition of R_a .

Table 11-3 Recommended Bearing Materials for Sliding Against Steel or Cast Iron

Bearing Material	Hardness kg/mm ²	Minimum Shaft Hardness kg/mm ²	Hardness Ratio
Lead-base babbitt	15-20	150	8
Tin-base babbitt	20-30	150	6
Alkali-hardened lead	22-26	200-250	9
Copper-lead	20-23	300	14
Silver (overplated)	25-50	300	8
Cadmium base	30-40	200-250	6
Aluminum alloy	45-50	300	6
Lead bronze	40-80	300	5
Tin bronze	60-80	300-400	5

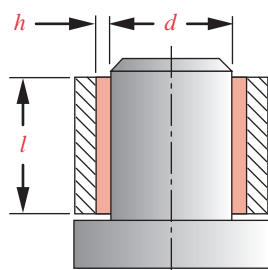
Source: Wilcock and Booser, *Bearing Design and Application*, McGraw-Hill, 1957.

the radius of curvature. Figure 11-5b shows two such plates separated by an oil film with a gap of dimension h . If the plates are parallel, the oil film will not support a transverse load. This is also true of a concentric journal and bearing. A concentric horizontal journal will become eccentric from the weight of the shaft, as in Figure 11-3. If the axis is vertical, as in Figure 11-5a, the journal can spin concentric with the bearing, since there is no transverse gravity force.

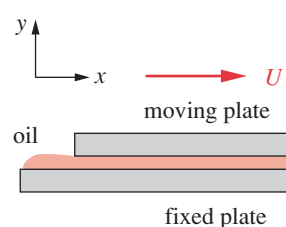
Petroff's Equation for No-Load Torque

If we hold the lower plate of Figure 11-5b stationary and move the upper plate to the right with a velocity U , the fluid between the plates will be sheared in the same manner as in the concentric gap of Figure 11-5a. The fluid wets and adheres to both plates, making its velocity zero at the stationary plate and U at the moving plate. Figure 11-5c shows a differential element of fluid in the gap. The velocity gradient causes the angular distortion β . In the limit, $\beta = dx / dy$. The shear stress τ_x acting on a differential element of fluid in the gap is proportional to the shear rate:

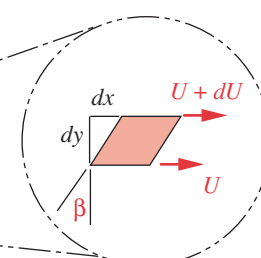
$$\tau_x = \eta \frac{d\beta}{dt} = \eta \frac{d}{dt} \frac{dx}{dy} = \eta \frac{d}{dy} \frac{dx}{dt} = \eta \frac{du}{dy} \quad (11.2a)$$



(a) Concentric journal in a bearing



(b) Parallel plates shearing an oil film



(c) Differential element in shear

FIGURE 11-5

An Oil Film Sheared Between Two Parallel Surfaces Cannot Support a Transverse Load (clearances greatly exaggerated)

* The amount of angle needed to create a supporting force is surprisingly small. For example, in a bearing of about 32-mm dia, the circumference is 100 mm. A typical entrance gap h_{max} might be 25 μm (0.0010 in), and the exit gap h_{min} , 12.5 μm (0.0005 in). The slope is then 0.0125 / 100 or about 7 / 1000 of a degree (26 seconds of arc). This is equivalent to about a 1-cm rise over a 100-yard-long football field.

† In England, in the 1880s, Beauchamp Tower was experimentally investigating the friction in hydrodynamically lubricated bearings for the railroad industry (though the term hydrodynamic and its theory were only then about to be discovered). His results showed much lower friction coefficients than expected. He drilled a radial hole through the bearing in order to add oil while running but was surprised to find that oil flowed out of the hole when the shaft turned. He corked the hole but the cork was expelled. He plugged the hole with wood but that also popped out. When he put a pressure gage in the hole he measured pressures well above the average pressure expected from a calculation of load / area. He then mapped the pressure distribution over 180° of the bearing and discovered the now familiar pressure distribution (see Figure 11-8) whose average value is load / area. On learning of this discovery, Osborne Reynolds set out to develop the mathematical theory to explain it, publishing the results in 1886.^[12]

and the constant of proportionality is the viscosity η . In a film of constant thickness h , the velocity gradient $du / dy = U / h$ and is constant. The force to shear the entire film is

$$F = A\tau_x = \eta A \frac{U}{h} \quad (11.2b)$$

where A is the area of the plate.

For the concentric journal and bearing of Figure 11-5a, let the gap $h = c_d / 2$ where c_d is the diametral clearance. The velocity is $U = \pi dn'$ where n' is revolutions per second, and the shear area is $A = \pi dl$. The torque T_0 required to shear the film is then

$$T_0 = \frac{d}{2} F = \frac{d}{2} \eta A \frac{U}{h} = \frac{d}{2} \eta \pi dl \frac{\pi dn'}{c_d/2}$$

$$T_0 = \eta \frac{\pi^2 d^3 l n'}{c_d} \quad (11.2c)$$

This is *Petroff's equation* for the no-load torque in a fluid film.

Reynolds' Equation for Eccentric Journal Bearings

To support a transverse load, the plates of Figure 11-5b must be nonparallel. If we rotate the lower plate of Figure 11-5b slightly counterclockwise and move the upper plate to the right with a velocity U , the fluid between the plates will be carried into the decreasing gap as shown in Figure 11-6a, developing a pressure that will support a transverse load P . The angle between the plates is analogous to the varying clearance due to the eccentricity e of the journal and bearing in Figure 11-6b.* When a transverse load is applied to a journal, it must assume an eccentricity with respect to the bearing in order to form a changing gap to support the load by developing pressure in the film.[†]

Figure 11-6b shows a greatly exaggerated eccentricity e and gap h for a journal bearing. The eccentricity e is measured from the center of the bearing O_b to the center of

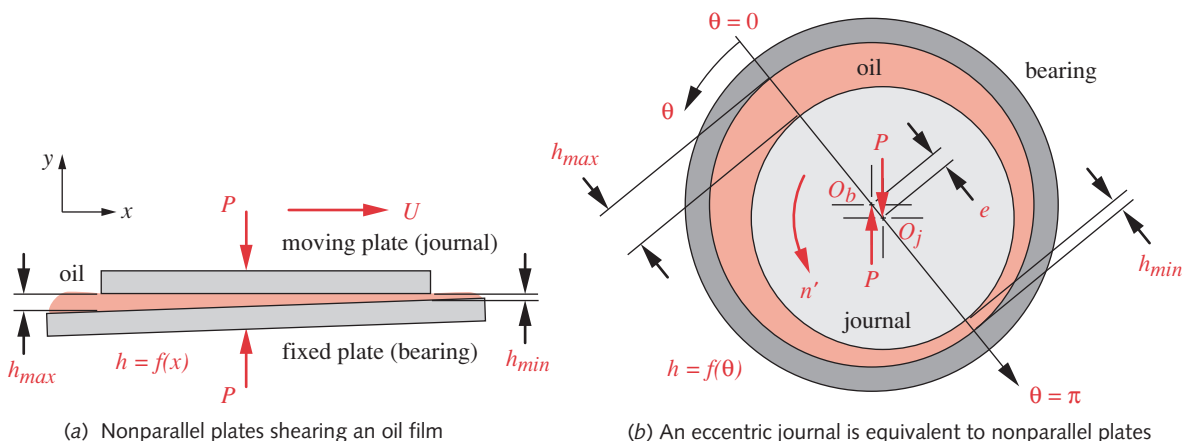


FIGURE 11-6

An Oil Film Sheared Between Nonparallel Surfaces Can Support a Transverse Load

the journal O_j . The zero-to- π axis for the independent variable θ is established along the line O_bO_j as shown in Figure 11-6b. The maximum possible value of e is $c_r = c_d / 2$, where c_r is the radial clearance. The eccentricity can be converted to a dimensionless eccentricity ratio ε :

$$\varepsilon = \frac{e}{c_r} \quad (11.3)$$

which varies from 0 at no load to 1 at maximum load when the journal contacts the bearing. An approximate expression for the film thickness h as a function of θ is

$$h = c_r(1 + \varepsilon \cos \theta) \quad (11.4a)$$

The film thickness h is maximum at $\theta = 0$ and minimum at $\theta = \pi$, found from

$$h_{min} = c_r(1 - \varepsilon) \quad h_{max} = c_r(1 + \varepsilon) \quad (11.4b)$$

Consider the journal bearing shown in Figure 11-7. In the analysis that follows, the gap is given by equation 11.4a. We can take the origin of an xy coordinate system at any point on the circumference of the bearing such as O . The x axis is tangent to the bearing, the y axis is through the bearing center O_b , and the z axis (not shown) is parallel to the axis of the bearing. Generally, the bearing is stationary and only the journal rotates, but in some cases the reverse may be true, or both may rotate as in the planet shaft of an epicyclic gear train. Thus we show a tangential velocity U_1 for the bearing as well as a tangential velocity T_2 for the journal. Note that their directions (angles) are not the same due to the eccentricity. The tangential velocity T_2 of the journal can be resolved into components in the x and y directions as U_2 and V_2 , respectively. The angle between T_2 and U_2 is so small that its cosine is essentially 1 and we can set $U_2 \equiv T_2$. The component V_2 in the y direction is due to the closing (or opening) of the gap h as it rotates and is $V_2 = U_2 \partial h / \partial x$.

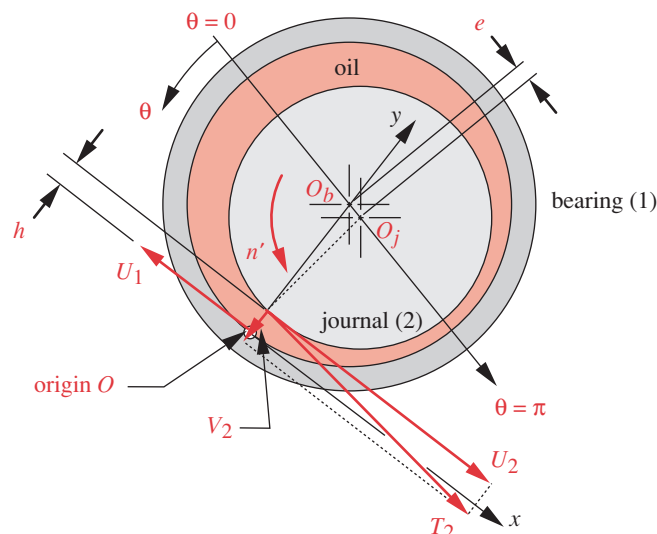


FIGURE 11-7

Velocity Components in an Eccentric Journal Bearing

Using the above assumptions, we can write Reynolds' equation* relating the changing gap thickness h , the relative velocities between the journal and bearing V_2 and $U_1 - U_2$, and the pressure in the fluid p as a function of the two dimensions x and z , assuming that the journal and bearing are parallel in the z direction and the viscosity η is constant,

$$\begin{aligned} \frac{1}{6\eta} \left[\frac{\partial}{\partial x} \left(h^3 \frac{\partial p}{\partial x} \right) + \frac{\partial}{\partial z} \left(h^3 \frac{\partial p}{\partial z} \right) \right] &= (U_1 - U_2) \frac{\partial h}{\partial x} + 2V_2 \\ &= (U_1 - U_2) \frac{\partial h}{\partial x} + 2U_2 \frac{\partial h}{\partial x} = (U_1 + U_2) \frac{\partial h}{\partial x} = U \frac{\partial h}{\partial x} \end{aligned} \quad (11.5a)$$

where $U = U_1 + U_2$.

LONG BEARING SOLUTION Equation 11.5a does not have a closed-form solution but can be solved numerically. Raimondi and Boyd did so in 1958 and provide a large number of design charts for its application to finite-length bearings.^[11] Reynolds solved a simplified version in series form (in 1886)^[12] by assuming that the bearing is infinitely long in the z direction, which makes the flow zero and the pressure distribution over that direction constant, and thus makes the term $\partial p / \partial z = 0$. With this simplification, the Reynolds' equation becomes

$$\frac{\partial}{\partial x} \left(h^3 \frac{\partial p}{\partial x} \right) = 6\eta U \frac{\partial h}{\partial x} \quad (11.5b)$$

In 1904, A. Sommerfeld found a closed-form solution for the infinitely long-bearing equation 11.5b as

$$p = \frac{\eta Ur}{c_r^2} \left[\frac{6\varepsilon(\sin \theta)(2 + \varepsilon \cos \theta)}{(2 + \varepsilon^2)(1 + \varepsilon \cos \theta)^2} \right] + p_0 \quad (11.6a)$$

which gives the pressure p in the lubricant film as a function of angular position θ around the bearing for particular dimensions of journal radius r , radial clearance c_r , eccentricity ratio ε , surface velocity U , and viscosity η . The term p_0 accounts for any supply pressure at the otherwise zero-pressure position at $\theta = 0$. Equation 11.6a is referred to as the *Sommerfeld solution* or the *long-bearing solution*.

If p is computed from this equation over $\theta = 0$ to 2π , it will predict negative pressures from $\theta = \pi$ to 2π with absolute magnitudes equal to the positive pressures from 0 to π . Since a fluid cannot withstand large negative pressure without cavitation, the equation is typically evaluated only from 0 to π and the pressure assumed to be p_0 over the other half of the circumference. This is referred to as the *half-Sommerfeld solution*.

Sommerfeld also determined an equation for the total load P on a long bearing as

$$P = \frac{\eta Ulr^2}{c_r^2} \frac{12\pi\varepsilon}{(2 + \varepsilon^2)(1 + \varepsilon^2)^{1/2}} \quad (11.6b)$$

This equation can be rearranged in nondimensional form to provide a characteristic bearing number called the **Sommerfeld number** S . First rearrange terms:

$$\frac{(2 + \varepsilon^2)(1 + \varepsilon^2)^{1/2}}{12\pi\varepsilon} = \eta \frac{Ul}{P} \left(\frac{r}{c_r} \right)^2 \quad (11.6c)$$

* For a derivation of Reynolds' equation, see reference 2, 3, 4, or 10.

The average pressure p_{avg} on the bearing is

$$p_{avg} = \frac{P}{A} = \frac{P}{ld} \quad (11.6d)$$

The velocity $U = \pi dn'$ where n' is revolutions per second, and $c_r = c_d / 2$. Substituting gives

$$\frac{(2 + \varepsilon^2)(1 + \varepsilon^2)^{1/2}}{12\pi\varepsilon} = \eta \frac{(\pi dn')l}{dl p_{avg}} \left(\frac{d}{c_d} \right)^2 = \eta \left(\frac{\pi n'}{p_{avg}} \right) \left(\frac{d}{c_d} \right)^2 = S \quad (11.6e)$$

Note that S is a function only of the eccentricity ratio ε but can also be expressed in terms of geometry, pressure, velocity, and viscosity.

SHORT-BEARING SOLUTION Long bearings are not often used in modern machinery for several reasons. Small shaft deflections or misalignment can reduce the radial clearance to zero in a long bearing, and packaging considerations often require short bearings. Typical l/d ratios of modern bearings are in the range of 1/4 to 2. The long-bearing (Sommerfeld) solution assumes no end leakage of oil from the bearing, but at these small l/d ratios, end leakage can be a significant factor. Ocvirk and DuBois^[13]–[16] solved a form of Reynolds' equation that includes the end-leakage term.

$$\frac{\partial}{\partial z} \left(h^3 \frac{\partial p}{\partial z} \right) = 6\eta U \frac{\partial h}{\partial x} \quad (11.7a)$$

This form neglects the term that accounts for the circumferential flow of oil around the bearing on the premise that it will be small in comparison to the flow in the z direction (leakage) in a short bearing. Equation 11.7a can be integrated to give an expression for pressure in the oil film as a function of both θ and z :

$$p = \frac{\eta U}{rc_r^2} \left(\frac{l^2}{4} - z^2 \right) \frac{3\varepsilon \sin \theta}{(1 + \varepsilon \cos \theta)^3} \quad (11.7b)$$

Equation 11.7b is known as the *Ocvirk solution* or the *short-bearing solution*. It is typically evaluated for $\theta = 0$ to π , with the pressure assumed to be zero over the other half of the circumference.

Figure 11-8 shows typical pressure distributions over θ and z . The $\theta = 0$ position is taken at $h = h_{max}$, and the θ axis goes through O_b and O_j . The pressure distribution p with respect to z is parabolic and peaks at the center of the bearing length l and is zero at $z = \pm l/2$. Pressure p varies nonlinearly over θ and peaks in its second quadrant. The value of θ_{max} at p_{max} can be found from

$$\theta_{max} = \cos^{-1} \left(\frac{1 - \sqrt{1 + 24\varepsilon^2}}{4\varepsilon} \right) \quad (11.7c)$$

and the value of p_{max} can be found by substituting $z = 0$ and $\theta = \theta_{max}$ in equation 11.7b.

Figure 11-9 compares the variation of pressure p in the film over $\theta = 0$ to π for the Sommerfeld long-bearing solution (taken as the reference at 100%) and the Ocvirk short-bearing solution at several l/d ratios from 1/4 to 1. Note the large error that would occur

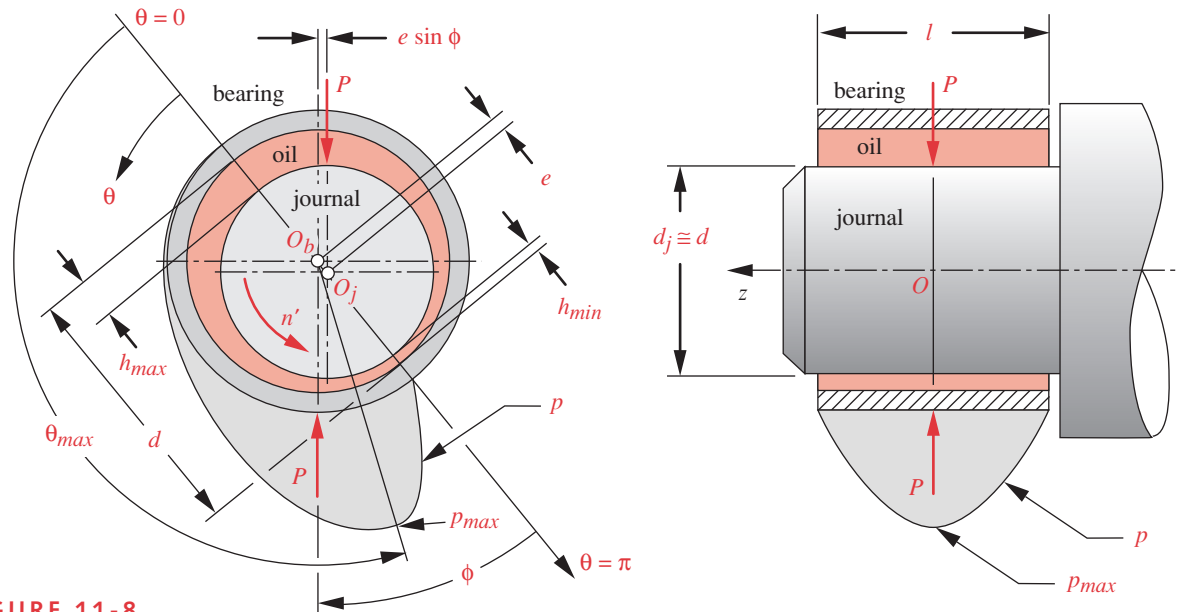


FIGURE 11-8

Pressure Distribution in a Short Journal Bearing—Film Thickness Greatly Exaggerated

11

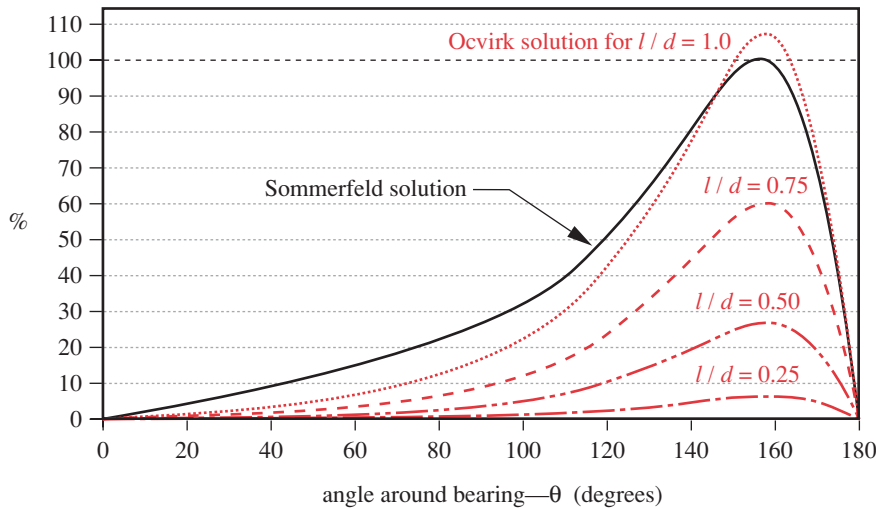
if the long-bearing solution were used for ratios < 1 . At $l/d = 1$, the two solutions give similar results with the Ocvirk solution predicting slightly higher peak pressure than the Sommerfeld solution. DuBois and Ocvirk found in tests^{[13],[14]} that the short-bearing solution gave results that closely matched experimental measurements for l/d ratios from $1/4$ to 1 and also matched experimental data up to $l/d = 2$ if that ratio was kept at 1 for the computation of bearings with actual ratios between 1 and 2 . Because most modern bearings tend to have l/d ratios between $1/4$ and 2 , the Ocvirk solution provides a convenient and reasonably accurate method to use. The Sommerfeld solution gives accurate results for l/d ratios above about 4 . Boyd and Raimondi's method^[11] gives more accurate results for intermediate l/d ratios but is more cumbersome to use.

Note in Figure 11-8 that the peak pressure occurs at an angle θ_{max} as defined in equation 11.7c. This angle is measured from the zero θ axis, which lies along the line of centers of the bearing and journal. But what determines the angle of this eccentricity line between the centers O_b and O_j ? Typically, the line of action of the force P applied to the journal is defined by external factors. This force P is shown vertical in the figure and the angle between this force and the $\theta = \pi$ axis is shown as ϕ . (Angle ϕ is used rather than the angle θ_P measured from $\theta = 0$ because ϕ will always be an acute angle.) Angle ϕ can be found from

$$\phi = \tan^{-1} \left(\frac{\pi \sqrt{1 - \epsilon^2}}{4\epsilon} \right) \quad (11.8a)$$

and the magnitude of the resultant force P is related to the bearing parameters as

$$P = K_\epsilon \frac{\eta U l^3}{c_r^2} \quad (11.8b)$$

**FIGURE 11-9**

Comparison of the Ocvirk Short-Bearing Approximation for Various l/d ratios with the Sommerfeld Long-Bearing Approximation of Pressure in the Oil Film from 0 to 180°

where K_ϵ is a dimensionless parameter that is a function of the eccentricity ratio ϵ :

$$K_\epsilon = \frac{\epsilon [\pi^2(1-\epsilon^2) + 16\epsilon^2]^{\frac{1}{2}}}{4(1-\epsilon^2)^2} \quad (11.8c)$$

The linear velocity U can be expressed as

$$U = \pi d n' \quad (11.8d)$$

and substituted in equation 11.8b along with $c_r = c_d / 2$ to get

$$P = K_\epsilon \frac{\eta U l^3}{c_r^2} = K_\epsilon \frac{4\pi\eta d n' l^3}{c_d^2} \quad (11.8e)$$

Torque and Power Losses in Journal Bearings

Figure 11-8 shows the fluid film being sheared between the journal and the bearing. The shear force acting on each member creates opposite-direction torques, T_r on the rotating member and T_s on the stationary member. However, these torques T_r and T_s are not equal because of the eccentricity. The force pair P , in Figure 11-8, one member of which acts at the journal center O_j and the other at the bearing center O_b , form a couple of magnitude $P e \sin \phi$, which adds to the stationary torque to form the rotating torque.

$$T_r = T_s + P e \sin \phi \quad (11.9a)$$

The stationary torque T_s can be found from

$$T_s = \eta \frac{d^2 l (U_2 - U_1)}{c_d} \frac{\pi}{(1 - \epsilon^2)^{1/2}} \quad (11.9b)$$

Substitute equation 11.8d in 11.9b to put it in terms of the rotational velocities of journal and bearing:

$$T_s = \eta \frac{d^3 l (n'_2 - n'_1)}{c_d} \frac{\pi^2}{(1 - \varepsilon^2)^{1/2}} \quad (11.9c)$$

Note the similarity of equation 11.9c to the Petroff equation 11.2c for the concentric-journal, no-load torque T_0 . We can form a ratio of the stationary torque in an eccentric bearing to the no-load torque as

$$\frac{T_s}{T_0} = \frac{1}{(1 - \varepsilon^2)^{1/2}} \quad (11.9d)$$

which, not surprisingly, is a function of only the eccentricity ratio ε . A similar ratio between rotating torque T_r and the Petroff no-load torque can also be formed.

The power Φ lost in the bearing can be found from the rotating torque T_r and the rotational velocity n' .

$$\Phi = T_r \omega = 2\pi T_r (n'_2 - n'_1) \quad \text{N-m/s or in-lb/s} \quad (11.10)$$

This can be converted to watts or horsepower as appropriate to the units system used.

COEFFICIENT OF FRICTION The coefficient of friction in the bearing can be determined as the ratio between the tangential shear force and the applied normal force P .

$$\mu = \frac{f}{P} = \frac{T_r / r}{P} = \frac{2T_r}{Pd} \quad (11.11)$$

11.6 DESIGN OF HYDRODYNAMIC BEARINGS

Usually the applied force P that the bearing is expected to support and the speed of rotation n' are known. The bearing diameter may or may not be known, but often will have been defined by stress, deflection, or other considerations. The design of the bearing requires finding a suitable combination of bearing diameter and/or length that will operate with a suitable viscosity of fluid, have reasonable and manufacturable clearance, and have an eccentricity ratio that will not allow metal-to-metal contact under load or any expected overload conditions.

Design Load Factor—The Ocvirk Number

A convenient way to approach this problem is to define a dimensionless load factor against which various bearing parameters can be computed, plotted, and compared. Equation 11.8e can be rearranged to provide such a factor. Solve equation 11.8e for K_e :

$$K_e = \frac{P c_d^2}{4 \eta \pi d n' l^3} \quad (11.12a)$$

Substitute equation 11.6d for the load P to introduce the average film pressure p_{avg} .

$$K_\varepsilon = \frac{p_{avg} l d c_d^2}{4 \eta \pi d n' l^3} \frac{d}{d} = \frac{1}{4\pi} \left[\left(\frac{p_{avg}}{\eta n'} \right) \left(\frac{d}{l} \right)^2 \left(\frac{c_d}{d} \right)^2 \right] = \frac{1}{4\pi} O_N \quad (11.12b)$$

The term in brackets is the desired dimensionless **load factor** or **Ocvirk number** O_N .

$$O_N = \left(\frac{p_{avg}}{\eta n'} \right) \left(\frac{d}{l} \right)^2 \left(\frac{c_d}{d} \right)^2 = 4\pi K_\varepsilon \quad (11.12c)$$

This expression contains the parameters over which the designer has control and shows that any combination of those parameters that yields the same Ocvirk number will have the same eccentricity ratio ε . The eccentricity ratio gives an indication of how close to failure the oil film is, since $h_{min} = c_r(1 - \varepsilon)$. Compare the Ocvirk number to the Sommerfeld number of equation 11.6e. The concept is the same.

Figure 11-10 shows a plot of eccentricity ratio ε as a function of Ocvirk number O_N and also shows experimental data from reference 13 for the same parameters. The theoretical curve is defined by combining equations 11.12c and 11.8c.

$$O_N = \frac{\pi \varepsilon \left[\pi^2 (1 - \varepsilon^2) + 16 \varepsilon^2 \right]^{\frac{1}{2}}}{(1 - \varepsilon^2)^2} \quad (11.13a)$$

An empirical curve is fitted through the data which shows that the theory understates the magnitude of the eccentricity ratio. The empirical curve can be approximated by

$$\varepsilon_x \approx 0.21394 + 0.38517 \log O_N - 0.0008(O_N - 60) \quad (11.13b)$$

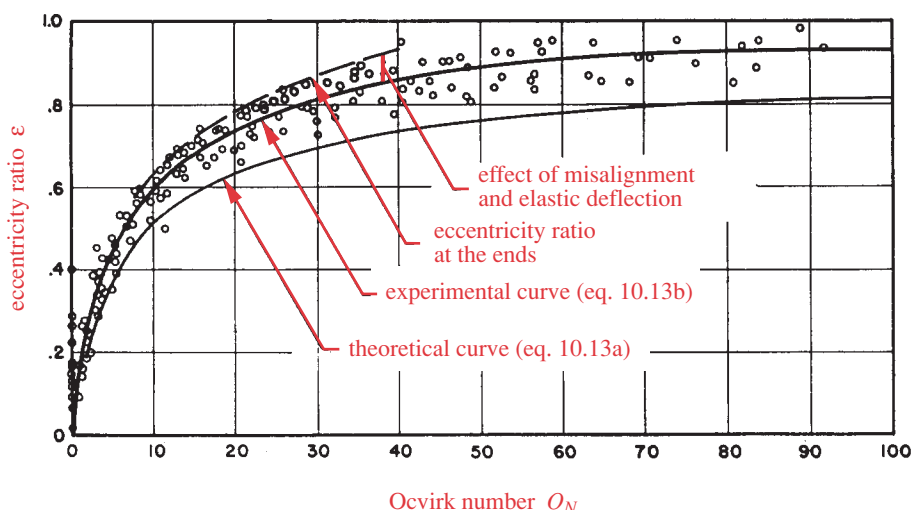
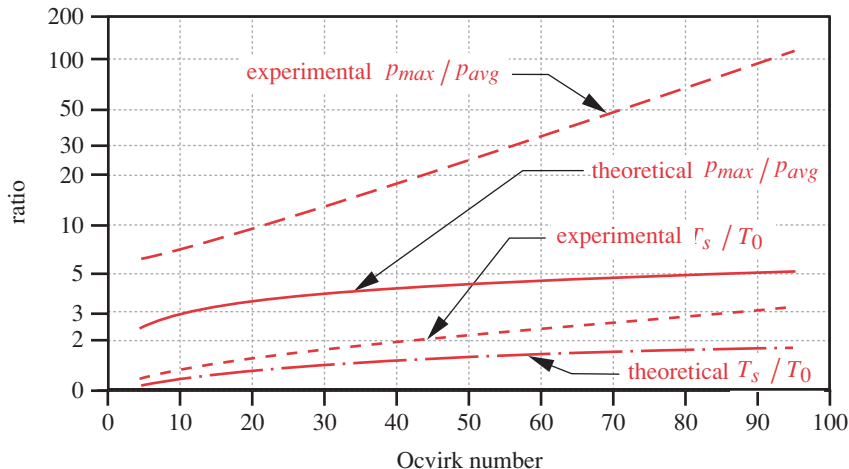


FIGURE 11-10

Analytical and Experimental Relationship Between Eccentricity Ratio ε and Ocvirk Number O_N
Source: G. B. DuBois and F. W. Ocvirk, "The Short Bearing Approximation for Plain Journal Bearings," *Trans. ASME*, vol. 77, pp. 1173–1178, 1955.

**FIGURE 11-11**

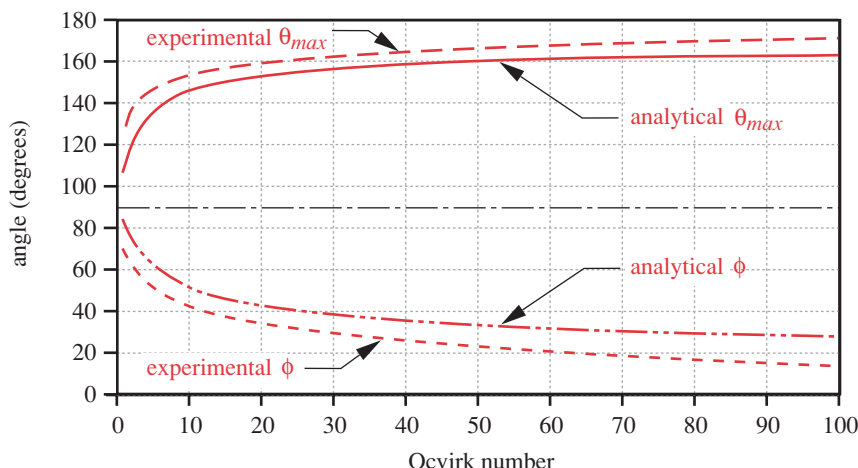
Pressure Ratios and Torque Ratios for Short Bearings as a Function of Ocvirk Number

The calculation of load, torque, average and maximum pressures in the oil film, and other bearing parameters can be done using this empirical value of ϵ in equations 11.7 to 11.11 and the minimum film thickness calculated from equation 11.4b.

Other dimensionless ratios can be formed from equations 11.7 to 11.11 for use as design aids. Figure 11-11 shows ratios of p_{max} / p_{avg} , and T_s / T_0 as a function of Ocvirk number for both theoretical and experimental values of ϵ . Figure 11-12 shows the theoretical and experimental variation in the angles θ_{max} and ϕ with the Ocvirk number.

Design Procedures

Load and speed are typically known. If the shaft has been designed for stress or deflection its diameter will be known. A bearing length or l / d ratio should be chosen based

**FIGURE 11-12**Angles θ_{max} and ϕ as a Function of the Ocvirk Number

on packaging considerations. Larger l / d ratios will give lower film pressures, all else equal. The clearance ratio is defined as c_d / d . Clearance ratios are typically in the range of 0.001 to 0.002 and sometimes as high as 0.003. Larger clearance ratios will rapidly increase the load number O_N as c_d / d is squared in equation 11.12c. Higher Ocvirk numbers give larger eccentricity, pressure, and torque as can be seen in Figures 11-10 and 11-11, but these factors increase more slowly at higher O_N . An advantage of larger clearance ratios is higher lubricant flow, which promotes cooler running. Large l / d ratios may require greater clearance ratios to accommodate shaft deflection.* An Ocvirk number can be chosen and the required viscosity of the lubricant found from equations 11.7 to 11.11. Some iteration will usually be required to obtain a balanced design.

If the dimensions of the shaft are not yet determined, a diameter and length of bearing can be found from iteration of the bearing equations with an assumed Ocvirk number. A trial lubricant must be chosen and its viscosity found for the assumed operating temperatures from charts such as Figure 11-1. After the bearing is designed, a fluid flow and heat transfer analysis can be done to determine its required oil flow rates and predicted operating temperatures. These aspects are not addressed here due to lack of space but can be found in many references, such as 3 and 10.

The choice of Ocvirk number has a significant effect on the design. G. B DuBois has offered some guidance by suggesting that a load number of $O_N = 30$ ($\epsilon = 0.82$) be considered an upper limit for “moderate” loading, $O_N = 60$ ($\epsilon = 0.90$) an upper limit for “heavy” loading, and $O_N = 90$ ($\epsilon = 0.93$) a limit for “severe” loading. At load numbers above about 30, care should be taken to carefully control manufacturing tolerances, surface finishes, and deflections. For general bearing applications it is probably better to stay below an O_N of about 30. The design procedure is best shown with an example.

EXAMPLE 11-1

Sleeve Bearing Design for a Defined Shaft Diameter

11

Problem

Design sleeve bearings to replace the rolling-element bearings on the shaft shown in Figure 10-5 (repeated overleaf). The shaft was designed in Example 10-1 (p. 560).

Given

The maximum transverse loads on the shaft at the bearings are 16 lb at R_1 and 54 lb at R_2 . Since the load at R_2 is 4x that at R_1 , one design can be created for R_2 and used also at R_1 . Shaft diameters at R_1 and R_2 are 0.591 in. The shaft speed is 1 725 rpm. The bearings are stationary.

Assumptions

Use a clearance ratio of 0.0017 and an l / d ratio of 0.75. Keep the Ocvirk number at 30 or below, preferably about 20.

Find

The bearing eccentricity ratio, maximum pressure and its location, minimum film thickness, coefficient of friction, torque, and power lost in bearing. Choose a suitable lubricant to operate at 190°F.

Solution

See Figure 10-5 on next page.

- Convert the speed given in rpm to rps and find the tangential velocity U .

* Note that if the bearing is short enough to prevent any metal contact at its ends due to shaft slope or deflection, then the bearing can be considered to give simple support to the shaft.

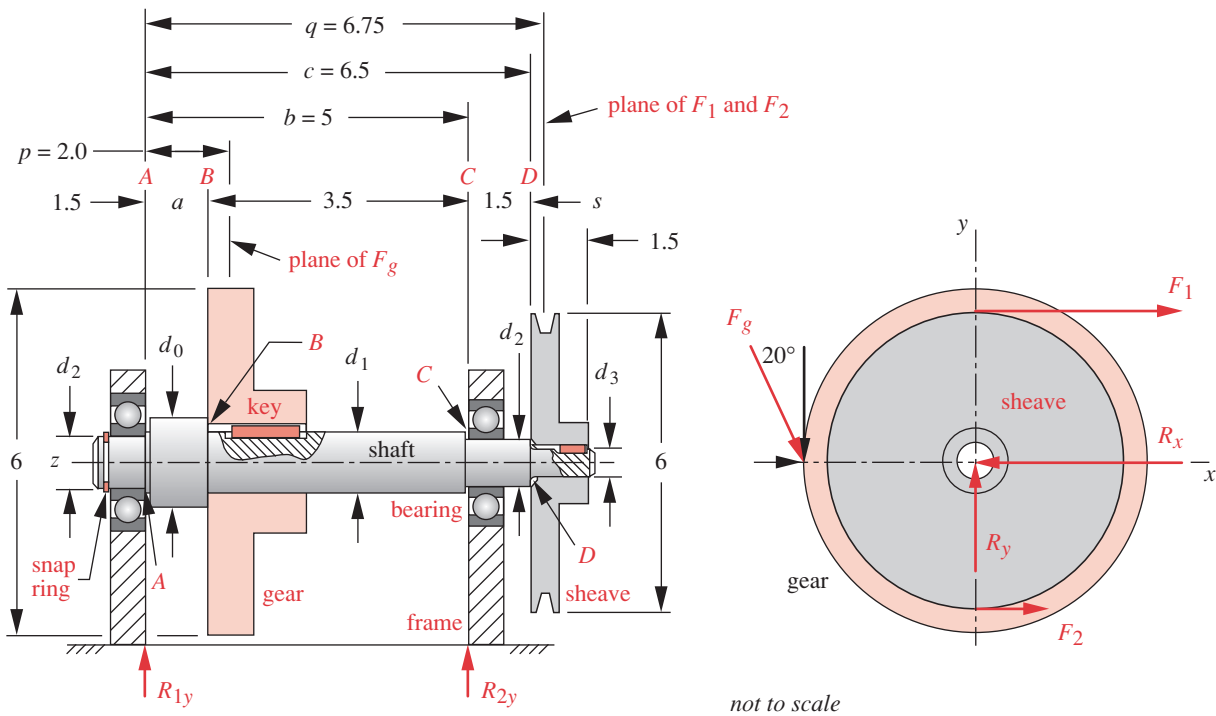


FIGURE 10-5 Repeated

Geometry of a Preliminary Design for Examples 10-1 through 10-3

11

$$n' = 1725 \frac{\text{rev}}{\text{min}} \left(\frac{1 \text{ min}}{60 \text{ sec}} \right) = 28.75 \text{ rps}$$

$$U = \pi d n' = \pi(0.591)(28.75) = 53.38 \text{ in/sec} \quad (a)$$

- 2 The diametral and radial clearances are found from the given diameter and the assumed clearance ratio:

$$c_d = 0.0017(0.591) = 0.0010 \text{ in}$$

$$c_r = c_d/2 = 0.0005 \text{ in } (b)$$

- 3 The bearing length is found from the assumed l / d ratio of 0.75.

$$l = 0.75(0.591) = 0.443 \text{ in} \quad (c)$$

- 4 Find the experimental eccentricity ratio from equation 11.13b (p. 641) or from Figure 11-10 (p. 640) using the suggested value of $O_N = 20$.

$$\begin{aligned}\epsilon_x &\equiv 0.21394 + 0.38517 \log O_N - 0.0008(O_N - 60) \\ &\equiv 0.21394 + 0.38517 \log 20 - 0.0008(20 - 60) = 0.747\end{aligned}\quad (d)$$

- 5 Find the dimensionless parameter K_ε from equation 11.12c (p. 641).

$$K_\varepsilon = \frac{O_N}{4\pi} = \frac{20}{4\pi} = 1.592 \quad (e)$$

- 6 The viscosity η of lubricant required to support the design load P can now be found by rearranging equation 11.8b:

$$\eta = \frac{P c_r^2}{K_e U l^3} = \frac{54(0.0005)^2}{1.592(53.38)(0.443)^3} = 1.825E - 6 \text{ reyn} = 1.825 \mu\text{reyn} \quad (f)$$

Enter Figure 11-1 (p. 628) to find that an oil of about ISO VG 100 will provide this value at 190°F. This oil is equivalent to an SAE 30W engine oil.

- 7 The average pressure in the oil film is found from equation 11.6d (p. 637).

$$p_{avg} = \frac{P}{l d} = \frac{54}{0.443(0.591)} = 206 \text{ psi} \quad (g)$$

- 8 The angle θ_{max} at which the pressure is maximum can be found from either equation 11.7c using the experimental value of $\varepsilon = 0.747$,

$$\theta_{max} = \cos^{-1} \left(\frac{1 - \sqrt{1 + 24\varepsilon^2}}{4\varepsilon} \right) = \cos^{-1} \left(\frac{1 - \sqrt{1 + 24(0.747)^2}}{4(0.747)} \right) = 159.2^\circ \quad (h)$$

or it can be read from the experimental curve in Figure 11-12 (p. 642) for $O_N = 20$ as 159°.

- 9 The maximum pressure can be found by substituting θ_{max} in equation 11.7b with $z = 0$, since it is maximum at the center of the bearing length l .

$$\begin{aligned} p &= \frac{\eta U}{r c_r^2} \left(\frac{l^2}{4} - z^2 \right) \frac{3\varepsilon \sin \theta}{(1 + \varepsilon \cos \theta)^3} \\ &= \frac{(1.825E - 6)(53.38)}{0.296(0.0005)^2} \left(\frac{(0.443)^2}{4} - 0^2 \right) \frac{3(0.747) \sin(159.2^\circ)}{(1 + 0.747 \cos(159.2^\circ))^3} = 1878 \text{ psi} \quad (i) \end{aligned}$$

or the ratio of p_{max}/p_{avg} can be read from the experimental curve in Figure 11-11 (p. 642) for $O_N = 20$ as 9.1 and multiplied by p_{avg} from step (g) above to get the same result.

- 10 Find the angle ϕ , which locates the $\theta = 0$ to π axis with respect to the applied load P from equation 11.8a (p. 638).

$$\phi = \tan^{-1} \left(\frac{\pi \sqrt{1 - \varepsilon^2}}{4\varepsilon} \right) = \tan^{-1} \left(\frac{\pi \sqrt{1 - (0.747)^2}}{4(0.747)} \right) = 34.95^\circ \quad (j)$$

- 11 The stationary and rotating torques can now be found from equations 11.9a and 11.9b (pp. 639) using the angle ϕ .

$$\begin{aligned} T_s &= \eta \frac{d^3 l (n'_2 - n'_1)}{c_d} \frac{\pi^2}{(1 - \varepsilon^2)^{1/2}} \\ &= (1.825E - 6) \frac{(0.591)^3 (0.443)(28.75 - 0)}{0.001} \frac{\pi^2}{(1 - (0.747)^2)^{1/2}} = 0.0713 \text{ lb-in} \quad (k) \end{aligned}$$

$$T_r = T_s + P e \sin \phi = 0.0713 + 54(0.00037) \sin 34.95^\circ = 0.0828 \text{ lb-in} \quad (l)$$

- 12 The power loss in the bearing is found from equation 11.10 (p. 640).

$$\Phi = 2\pi T_r (n'_2 - n'_1) = 2\pi(0.0828)(28.75 - 0) = 14.96 \frac{\text{in} \cdot \text{lb}}{\text{sec}} = 0.002 \text{ hp} \quad (m)$$

- 13 The coefficient of friction in the bearing can be found from the ratio of the shear force to the normal force using equation 11.11 (p. 640).

$$\mu = \frac{2T_r}{Pd} = \frac{2(0.0828)}{54(0.591)} = 0.005 \quad (n)$$

- 14 The minimum film thickness is found from equation 11.4b (p. 635).

$$h_{min} = c_r (1 - \varepsilon) = 0.0005(1 - 0.747) = 0.000126 \text{ in } (126 \mu\text{in}) \quad (o)$$

This is a reasonable value, since the composite rms surface roughness (equation 11.14a on p. 647) needs to be no more than about a third to a fourth of the minimum film thickness to avoid asperity contact (see Figure 11-13 on p. 647) and a 30–40 μin R_q finish or better is easily obtainable by precision milling, grinding, or honing.

15. A safety factor against asperity contact can be estimated by back-solving the model using a minimum film thickness equal to the assumed average surface finish of, say, 40 μin , and determining what Ocvirk number and load P would be required to reduce the minimum oil-film thickness to that value. This was easily done in the model by switching h_{min} and η to input status, P and O_N to output status, providing a guess value for O_N , and iterating to a solution. The result is:

$$\begin{aligned} \text{when } h_{min} &= 40 \mu\text{in}, & O_N &= 72.2, & \varepsilon &= 0.92, & P &= 195 \text{ lb} \\ \text{and} & & N &= \frac{195 \text{ lb}}{54 \text{ lb}} = 3.6 & & & & \end{aligned} \quad (p)$$

which is an acceptable reserve for overloads.

- 16 If this safety-factor calculation had indicated that a small overload could put the bearing in trouble, redesigning the bearing for a lower Ocvirk number would give more margin against failure under overloads. Equation 11.12c, repeated below as (q), shows what could be changed to reduce O_N :

$$O_N = \left(\frac{p_{avg}}{\eta n'} \right) \left(\frac{d}{l} \right)^2 \left(\frac{c_d}{d} \right)^2 \quad (q)$$

It would require some combination of: decreasing the clearance ratio, decreasing the d/l ratio, or using a higher-viscosity oil. Assuming the rotational speed, load, and shaft diameter remain unchanged, the bearing length could be increased or the diametral clearance reduced as well as η increased to improve the design.

- 17 The models EX11-01A (example solution) and EX11-01B (overload safety factor calculation) are on the CD-ROM.

11.7 NONCONFORMING CONTACTS

Nonconforming contacts such as gear teeth, cam-follower joints, and rolling-element bearings (balls, rollers) can operate in boundary, mixed, or elastohydrodynamic (EHD)

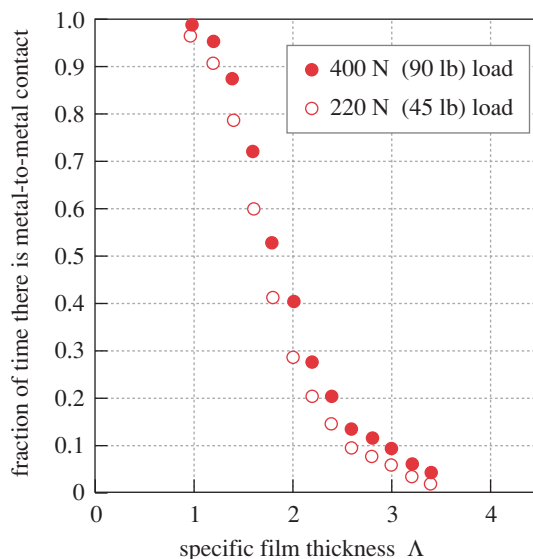
modes of lubrication. The principal factor that determines which of these situations will occur is the specific film thickness Λ , which is defined as the minimum film thickness at the patch center divided by the composite rms surface roughness of the two surfaces.

$$\Lambda = h_c / \sqrt{R_{q1}^2 + R_{q2}^2} \quad (11.14a)$$

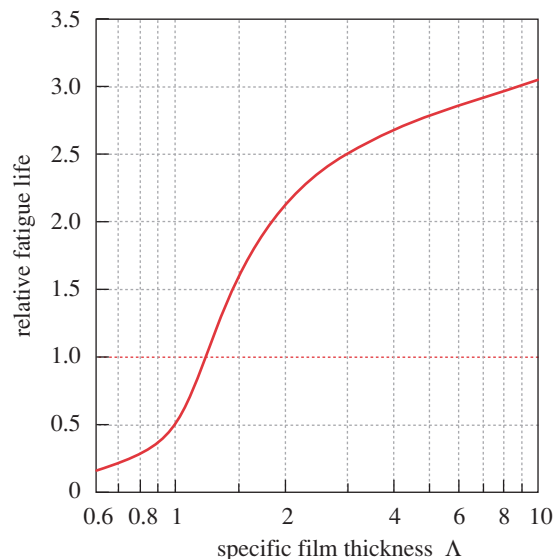
where h_c is the film thickness of the lubricant at the center of the contact patch and R_{q1} and R_{q2} are the rms average roughnesses of the two contacting surfaces. The denominator of equation 11.14a is termed the composite surface roughness. (See Section 7.1 on p. 421 for a discussion of surface roughness.) The film thickness at the center of the contact patch can be related to the minimum film thickness h_{min} at the trailing edge of contact by

$$h_c \approx \frac{4}{3} h_{min} \quad (11.14b)$$

Figure 11-13a shows the experimentally measured frequency of asperity contact within an EHD gap as a function of specific film thickness.^[28] When $\Lambda < 1$, the surfaces are in continuous metal-to-metal contact, i.e., in boundary lubrication. When $\Lambda > 3$ to 4, there is essentially no asperity contact. Between these values there is some combination of partial EHD and boundary-lubrication conditions. A majority of Hertzian contacts in gears, cams and rolling-element bearings operate in this partial EHD (mixed lubrication) region of Figure 11-2 (p. 629).^[17] From Figure 11-13a we can conclude that Λ needs to be > 1 for partial EHD to begin^[17] and > 3 to 4 for full-film EHD.^{[6], [17]} Effective partial EHD conditions begin at about $\Lambda = 2$ and if $\Lambda < 1.5$, it indicates an effective boundary-lubrication condition in which significant asperity contact occurs.^[17]



(a) Penetration of EHD film by surface asperities (ref. 28)



(b) Effect of film thickness on fatigue life (ref. 29)

FIGURE 11-13

Effect of Specific Film Thickness Λ on the Asperity Contacts and Fatigue Life

Figure 11-13b shows the effect of specific film thickness on fatigue life of a rolling bearing.^[29] The ordinate defines a ratio of expected life over the predicted catalog life for a bearing. This plot also shows the desirability of maintaining $\Lambda > 1.5$ in order to obtain the catalog life. A small increase in Λ from 1.5 to about 2 can double the fatigue life. Further increases in Λ have less dramatic effect on life and may cause higher friction due to viscous-drag losses if a heavier oil is used to obtain the greater Λ .

Surface roughness is fairly easy to measure and control. The lubricant film thickness is more difficult to predict. Chapter 7 discusses calculation of the Hertzian pressure in surface contact and shows that the pressures in the contact zone between stiff materials in nonconforming (theoretical point or line) contact are extremely high, commonly as much as 80 to 500 ksi (0.5 to 3 GPa) if both materials are steel. It was once believed that lubricants could not withstand these pressures and thus could not separate the metal surfaces. It is now known that viscosity is an exponential function of pressure, and at typical contact pressures, oil can become essentially as stiff as the metals it separates. Figure 11-14 shows the viscosity-pressure relationship for several common lubricants on a semilog plot. The curve for mineral oils can be approximated by

$$\eta = \eta_0 e^{\alpha p} \quad (11.15a)$$

where η_0 is the absolute viscosity (reyn [Pa-s]) at atmospheric pressure and p is the pressure (psi [Pa]). An approximate expression for the pressure-viscosity exponent α for

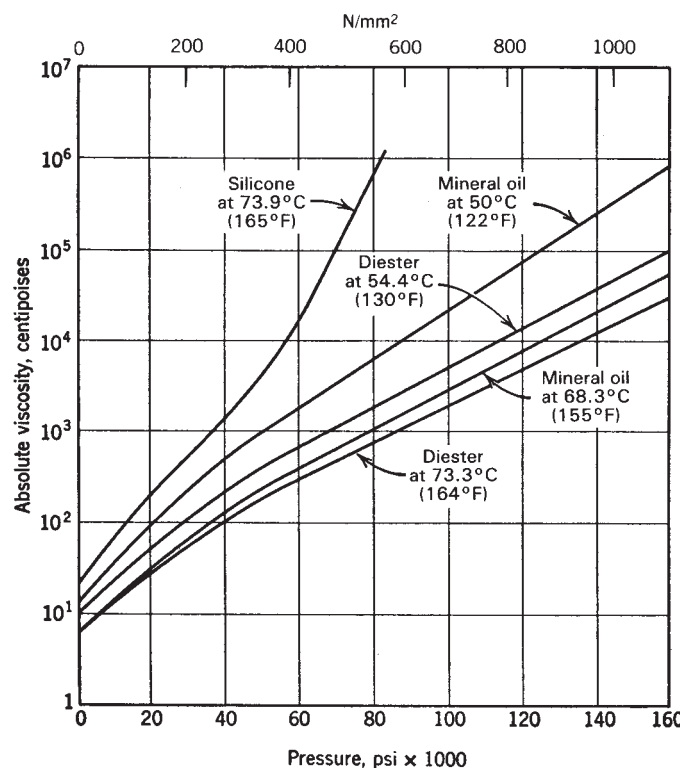


FIGURE 11-14

Absolute Viscosity Versus Pressure of Various Lubricating Oils. Source: ASME Research Committee on Lubrication, "Pressure Viscosity Report-Vol. 11," 1953.

mineral oils is (with units of $v_0 = \text{in}^2/\text{s}$ [m^2/s], $\eta_0 = \text{reyn}$ [$\text{Pa}\cdot\text{s}$], and $\rho = \text{lb}\cdot\text{s}^2/\text{in}^4$ [$\text{N}\cdot\text{s}^2/\text{m}^4$]):^[27]

$$\alpha \equiv 7.74E - 4\left(\frac{v_0}{10^4}\right)^{0.163} \cong 7.74E - 4\left(\frac{\eta_0}{\rho(10^4)}\right)^{0.163} \quad (11.15b)$$

CYLINDRICAL CONTACT Dowson and Higginson^{[18],[19]} determined a formula for the minimum film thickness in an EHD contact between cylindrical rollers as

$$h_{min} = 2.65R'(\alpha E')^{0.54}\left(\frac{\eta_0 U}{E'R'}\right)^{0.7}\left(\frac{P}{IE'R'}\right)^{-0.13} \quad (11.16)$$

where P is the transverse load (lb [N]), l is the length of axial contact (in [m]), U = average velocity ($(U_1 + U_2)/2$ (in/s [m/s])), η_0 is the absolute lubricant viscosity (reyn [$\text{Pa}\cdot\text{s}$]) at atmospheric pressure and operating temperature, and α is the pressure-viscosity exponent for the particular lubricant from equation 11.15b. The expressions in parentheses in equation 11.16 are dimensionless ratios provided that the units of their constituents are in consistent ips or SI units as indicated. The resulting film thickness is then in units of either inches or meters.

The effective radius R' is defined as

$$\frac{1}{R'} = \frac{1}{R_{1x}} + \frac{1}{R_{2x}} \quad (11.17a)$$

where R_{1x} and R_{2x} are the radii of the contacting surfaces in the direction of rolling. The effective modulus is defined as

$$E' = \frac{2}{m_1 + m_2} = \frac{2}{\frac{1-v_1^2}{E_1} + \frac{1-v_2^2}{E_2}} \quad (11.17b)$$

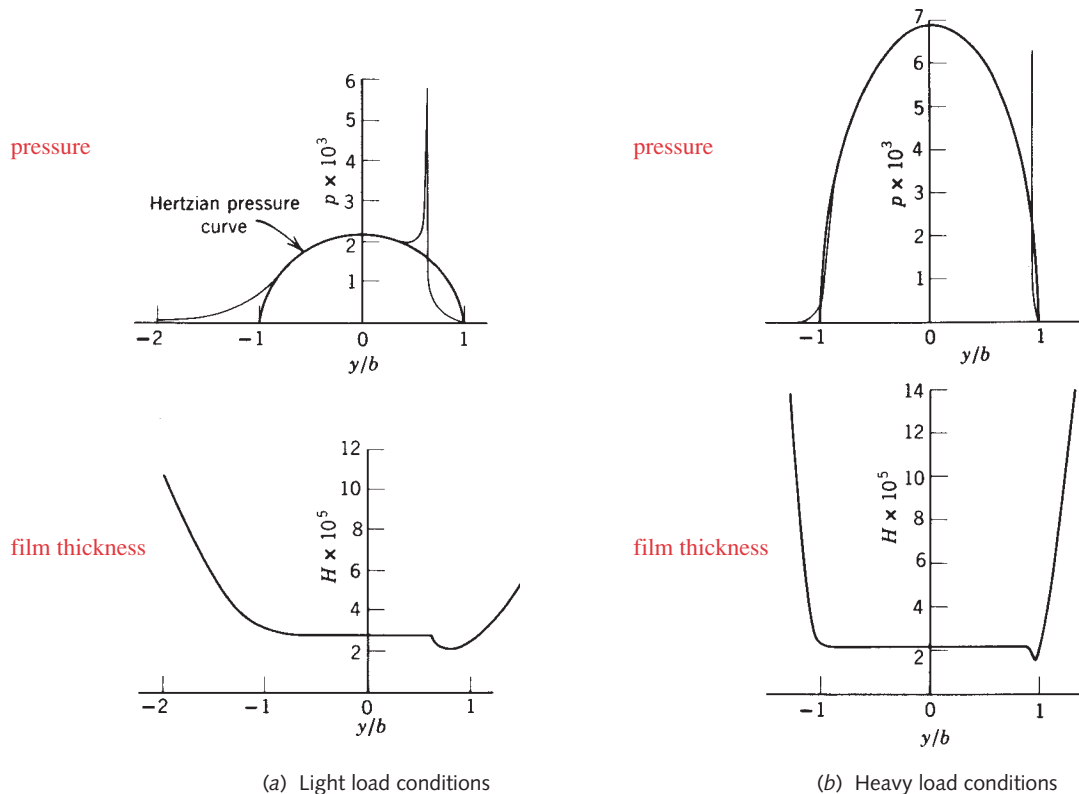
where E_1, E_2 are Young's moduli, and v_1, v_2 are Poisson's ratio for each material.

GENERAL CONTACT In general point contact, the contact patch is an ellipse as discussed in Chapter 7. The contact ellipse is defined by its major and minor half-axis dimensions, a and b , respectively. Contact between two spheres, or between a sphere and a flat plate, will have a circular contact patch, which is a special case of elliptical contact wherein $a = b$. Hamrock and Dowson^[21] developed an equation for the minimum film thickness in generalized point contact as

$$h_{min} = 3.63R'(\alpha E')^{0.49}\left(\frac{\eta_0 U}{E'R'}\right)^{0.68}\left(1 - e^{-0.68\psi}\right)\left[\frac{P}{E'(R')^2}\right]^{-0.073} \quad (11.18)$$

where ψ is the ellipticity ratio of the contact patch a/b (see Section 7.10 on p. 448).

In all these equations the film thickness is most dependent on speed and lubricant viscosity, but is relatively insensitive to load. Figure 11-15 shows pressure-distribution and film-thickness plots for light and heavy load conditions in an EHD contact between steel rollers lubricated with mineral oil.^[22] Note that the fluid pressure is the same as

**FIGURE 11-15**

Pressure Distribution and Film Thickness in an EHD Joint. Source: D. Dowson and G. Higginson, "The Effect of Material Properties on the Lubrication of Elastic Rollers," *J. Mech. Eng. Sci.*, vol. 2, no. 3, 1960, with permission

the dry Hertzian contact pressure except for the pressure spike that occurs as the film thickness contracts near the exit. Except for that local contraction, the film thickness is essentially constant throughout the contact patch.

Equations 11.16, 11.17, and 11.18 allow a minimum film thickness to be calculated for a nonconforming contact joint such as a pair of gear teeth, cam-follower, or rolling-element bearing. The specific film thickness from equation 11.14 will indicate whether EHD or boundary lubrication can be expected in the contact. An oil with EP additives is needed if EHD is not present.

EXAMPLE 11-2

Lubrication in a Crowned Cam-Follower Interface

Problem

A cam-follower system was analyzed for contact-patch geometry and contact stresses in Example 7-3 (p. 451). Determine the film-thickness parameter and the lubrication condition for a ground roller running against both a ground cam and a milled cam.

Given

The roller follower radius is 1 in with a 20-in crown radius at 90° to the roller radius with an rms surface roughness of $R_q = 7 \mu\text{in}$. The cam's minimum radius of curvature is 1.72 inches, in the direction of rolling. It is flat axially. It forms an elliptical contact patch with the cam. The half-dimensions of this ellipse are $a = 0.0889$ in and $b = 0.0110$ in. The cam angular velocity is 18.85 rad/sec and the radius to its surface at the point of minimum radius of curvature is 3.92 in. The bulk oil temperature is 180°F. The ground cam has an rms surface roughness of $R_q = 7 \mu\text{in}$ and the milled cam has $R_q = 30 \mu\text{in}$.

Assumptions

Try an ISO VG 460 oil with an assumed specific gravity of 0.9. The roller has 1% slip versus the cam.

Find

The specific film thickness and lubrication condition for the assumed lubricant and the viscosity of lubricant required to obtain effective partial or full EHD conditions for each cam, if possible.

Solution

See Figure 11-16.

- 1 Figure 11-1 (p. 628) gives the viscosity of an ISO VG 460 oil as about 6.5 μreyn at 180°F.
- 2 Find the mass density ρ of the oil from the given specific gravity SG of the oil and the weight density of water.

$$\rho = SG \frac{\gamma}{g} = 0.9 \left(0.03611 \frac{\text{lb}}{\text{in}^3} / 386 \frac{\text{in}}{\text{sec}^2} \right) = 84.2E - 6 \frac{\text{lb} - \text{sec}^2}{\text{in}^4} \text{ or } \frac{\text{blob}}{\text{in}^3} \quad (a)$$

- 3 Find the approximate pressure-viscosity exponent α from equation 11.15b (p. 649).

$$\alpha \approx 7.74E - 4 \left(\frac{\eta_0}{\rho(10^4)} \right)^{0.163} \approx 7.74E - 4 \left(\frac{6.5E - 6}{84.2E - 6(10^4)} \right)^{0.163} = 1.136E - 4 \quad (b)$$

- 4 Find the effective radius from equation 11.17a (p. 649).

$$\frac{1}{R'} = \frac{1}{R_{1_x}} + \frac{1}{R_{2_x}} = \frac{1}{1} + \frac{1}{1.720} \quad R' = 0.632 \text{ in} \quad (c)$$

- 5 Find the effective modulus of elasticity from equation 11.17b (p. 649).

$$E' = \frac{2}{\frac{1-v_1^2}{E_1} + \frac{1-v_2^2}{E_2}} = \frac{2}{\frac{1-0.28^2}{3E7} + \frac{1-0.28^2}{3E7}} = 3.255E7 \quad (d)$$

- 6 Find the average velocity U . The roller has 99% of the velocity of the cam.

$$U_2 = r\omega = 3.92 \text{ in} (18.85 \text{ rad/sec}) = 73.892 \text{ in/sec}$$

$$U_1 = 0.99U_2 = 0.99(73.892) = 73.153 \text{ in/sec}$$

$$U = (U_1 + U_2)/2 = (73.892 + 73.153)/2 = 73.523 \text{ in/sec} \quad (e)$$

- 7 Find the ellipticity ratio = major / minor axis. The minor axis is in the direction of rolling in this case.

$$\psi = a/b = 0.0889/0.0110 = 8.082 \quad (f)$$

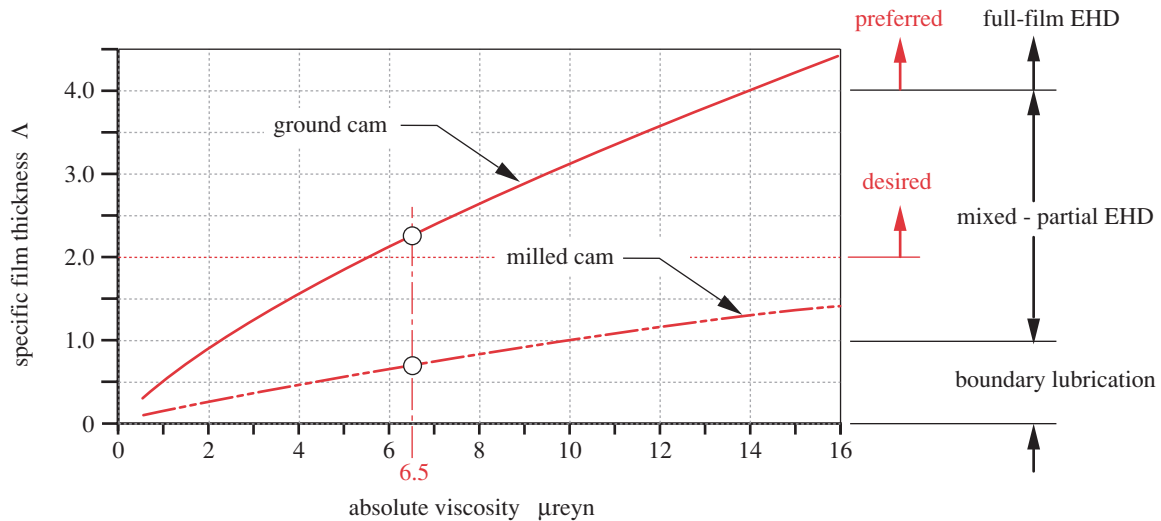


FIGURE 11-16

Variation of Specific Film Thickness Λ with Lubricant Viscosity η_0 in Example 10-2

- 8 Find the minimum film thickness from equation 11.18 (p. 649).

$$\begin{aligned}
 h_{min} &= 3.63R'(\alpha E')^{0.49} \left(\frac{\eta_0 U}{E' R'} \right)^{0.68} \left(1 - e^{-0.68\psi} \right) \left[\frac{P}{E'(R')^2} \right]^{-0.073} \\
 &= 3.63(0.632) [1.136E - 4(3.255E7)]^{0.49} \left[\frac{(6.5E - 6)(73.523)}{(3.255E7)(0.632)} \right]^{0.68} \\
 &\quad \cdot \left[1 - e^{-0.68(8.082)} \right] \left[\frac{250}{3.255E7(0.632)^2} \right]^{-0.073} = 16.6 \text{ } \mu\text{in} \quad (g)
 \end{aligned}$$

11

- 9 Convert this minimum value at the exit to an approximate thickness at the center of the contact patch with equation 11.14b (p. 647).

$$h_c \equiv \frac{4}{3} h_{min} = \frac{4}{3}(16.6) = 22.2 \text{ } \mu\text{in} \quad (h)$$

- 10 The specific film thickness values for each cam can now be found from equation 11.14a (p. 647).

$$\text{ground cam : } \Lambda = h_c / \sqrt{R_{q1}^2 + R_{q2}^2} = 22.2 / \sqrt{7^2 + 7^2} = 2.24 \quad (i)$$

$$\text{milled cam : } \Lambda = h_c / \sqrt{R_{q1}^2 + R_{q2}^2} = 22.2 / \sqrt{7^2 + 30^2} = 0.72$$

which indicates that the milled cam is in boundary lubrication and the ground cam is in partial EHD with the specified oil. These are common conditions for ground or milled cams, respectively, running against a ground roller-follower.

- 11 To determine what viscosity of oil would be needed to put each system into partial or full EHD condition, the model was solved for a range of possible η_0 values from 0.5 to 16 μreyn as shown in Figure 11-1 (p. 628) for 180°F. A plot of the results in

Figure 11-16 (p. 652) shows that an oil with $\eta_0 \geq 14 \mu\text{reyn}$ is needed to put this ground cam into full EHD lubrication, and that an oil with $\eta_0 > 10 \mu\text{reyn}$ will get this milled cam to $\Lambda > 1$ and into the low end of the mixed-partial EHD lubrication regime. But, none of the oils shown in Figure 11-1 (p. 628) can provide $\Lambda > 4$ for full-film EHD with the milled cam.

- 12 The files EX11-02 can be found on the CD-ROM.
-

11.8 ROLLING-ELEMENT BEARINGS

Rollers have been known as a means to move heavy objects since ancient times, and there is evidence of the use of ball-thrust bearings in the first century B.C.; but it was only in the 20th century that improved materials and manufacturing technology allowed precision rolling-element bearings to be made. The need for higher-speed, higher-temperature-resistant low-friction bearings was engendered by the development of aircraft gas turbines. Considerable research effort since World War II has resulted in high-quality, high-precision, rolling-element bearings (REB) being available at quite reasonable cost.

It is interesting to note that from their earliest designs around 1900, ball and roller bearings have been standardized worldwide in metric sizes. It is possible to remove a REB from the wheel assembly of an antique automobile made in almost any country in the 1920s, for example, and find a replacement in a current bearing manufacturer's catalog which will fit. The new bearing will be much improved over the original in terms of design, quality, and reliability, but it will have the same external dimensions.

MATERIALS A majority of modern ball bearings are made from AISI 5210 steel and hardened to a high degree, either throughout or on the surface. This chromium-steel alloy is through-hardenable to HRC 61-65. Roller bearings are often made from case-hardened AISI 3310, 4620, and 8620 steel alloys. Recent improvements in steel manufacturing processes have resulted in bearing steels with reduced levels of impurities. Bearings made with these "clean" steels show significantly improved life and reliability. Though rolling bearings have always been considered to have finite fatigue lives and "standard" ones still do, REB made of "clean" steels have recently given evidence of an infinite-life endurance limit in surface fatigue.^[23]

MANUFACTURING Rolling-element bearings are made by all major bearing manufacturers worldwide to standard dimensions defined by the Anti-Friction Bearing Manufacturers Association (AFBMA) and/or the International Standards Organization (ISO), and they are interchangeable. One can be reasonably assured that selecting any manufacturer's bearing made to these standards will not result in an unrepairable assembly in the future, even if that manufacturer goes out of the bearing business. The AFBMA Standards for bearing design have been adopted by the American National Standards Institute (ANSI). Some of the information in this section is taken from ANSI/AFBMA Standard 9-1990 for ball bearings^[24] and Standard 11-1990 for rolling bearings.^[25] The standards also define tolerance classes for bearings. Radial bearings are classed by ANSI into ABEC-1 through -9 tolerance classes, precision increasing with class number. ISO defines Class 6 through Class 2, precision varying inversely with class number. Cost increases with increased precision.

Table 11-4

Typical Coefficients of Friction for Rolling Element Bearings*

Type	μ
Ball, self-aligning	0.0010
Roller, cylindrical	0.0011
Ball, thrust	0.0013
Ball, deep-groove	0.0015
Roller, spherical	0.0018
Roller, tapered	0.0018
Roller, needle	0.0045

* Source: Palmgren, A., *Ball and Roller Bearing Engineering*, 2ed., S. H. Burbank Co., Phila., 1946

Comparison of Rolling and Sliding Bearings

Rolling-element bearings have a number of advantages over sliding-contact bearings and vice versa. Hamrock^[26] lists the following advantages of rolling over sliding bearings:

- 1 low starting and operating friction, $\mu_{\text{static}} \equiv \mu_{\text{dynamic}}$ in range of 0.001 to 0.005
- 2 can support combined radial and thrust loads
- 3 less sensitive to interruptions of lubrication
- 4 no self-excited instabilities
- 5 good low-temperature starting
- 6 can seal lubricant within bearing and “lifetime-lubricate”
- 7 typically require less space in axial direction

The following are disadvantages of rolling bearings compared to hydrodynamic conformal sliding bearings:^[26]

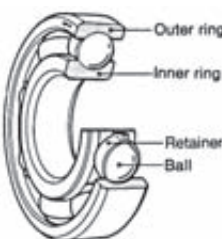
- 1 rolling bearings may eventually fail from fatigue
- 2 require more space in radial direction
- 3 poor damping ability
- 4 higher noise level
- 5 some have more severe alignment requirements
- 6 higher cost

Types of Rolling-Element Bearings

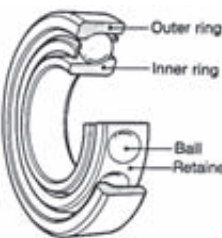
Rolling-element bearings can be grouped into two broad categories, ball and roller bearings, both of which have many variants within these divisions. Ball bearings are most suitable for small, high-speed applications. For large, heavily-loaded systems, roller bearings are preferred. If misalignments can occur between shaft and housing, then self-aligning bearings are needed. Tapered roller bearings can handle heavy loads in both radial and thrust directions at moderate speeds. For situations with radial and heavy thrust loads at high speeds, deep-groove ball bearings are best. The friction coefficients of various types of bearings are shown in Table 11-4.

BALL BEARINGS capture a number of hardened and ground steel spheres between two raceways, an inner and outer race for radial bearings, or top and bottom races for thrust bearings. A retainer (also called a cage or separator) is used to keep the balls properly spaced around the raceways, as shown in Figure 11-17. Ball bearings can support combined radial and thrust loads to varying degrees depending on their design and construction. Figure 11-17a shows a deep-groove or Conrad-type ball bearing that will support both radial and moderate thrust loads. Figure 11-17b shows an angular contact ball bearing designed to handle larger thrust loads in one direction as well as radial loads. Some ball bearings are available with shields to keep out foreign matter and seals to retain factory-applied lubricant. Ball bearings are most suitable for smaller sizes, high speeds, and lighter loads.

ROLLER BEARINGS use straight, tapered, or contoured rollers running between raceways as shown in Figure 11-18. In general, roller bearings can support larger static and



(a) Deep-groove (Conrad) ball bearing



(b) Angular-contact ball bearing

FIGURE 11-17

Ball Bearings. Courtesy of NTN Corporation

dynamic (shock) loads than ball bearings because of their line contact and are less expensive for larger sizes and heavier loads. Unless the rollers are tapered or contoured, they can support a load in only one direction, either radial or thrust according to the bearing design.

Figure 11-18a shows a straight, cylindrical roller bearing designed to support only radial loads. It has very low friction and floats axially, which can be an advantage on long shafts where thermal expansion can load-up a ball-bearing pair in the axial direction if not properly mounted. Figure 11-18b shows a needle bearing that uses small-diameter rollers and may or may not have an inner race or cage. Its advantages are higher load capacity due to the full complement of rollers and its compact radial dimension, especially if used without an inner race. In such cases the shaft against which the rollers run must be hardened and ground. Though the full-complement needle bearing has higher load capacity, it also has a higher wear rate than one with fewer rollers separated by a cage to prevent them rubbing on each other.

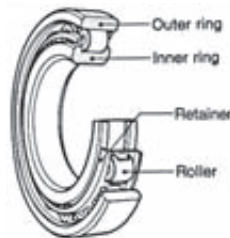
Figure 11-18c shows a tapered roller bearing designed to support large thrust and radial loads. These are often used as wheel bearings in automobiles and trucks. Tapered (and other) roller bearings can be split apart axially, which makes assembly easier than with ball bearings that are usually permanently assembled. Figure 11-18d shows a spherical roller bearing that is self aligning, allowing no moment to be supported at the bearing.

THRUST BEARINGS Ball and roller bearings are also made for pure thrust loads as shown in Figure 11-19. Cylindrical-roller-thrust bearings have higher friction than ball-thrust bearings due to the sliding that occurs between roller and raceways (because only one point on the roller can match the varying linear velocity over the raceways' radii) and should not be used in high-speed applications.

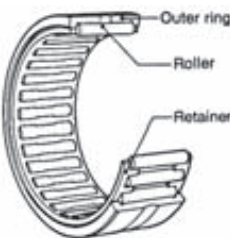
BEARING CLASSIFICATIONS Figure 11-20 shows a classification of REB types. Each of the main categories of ball and roller divides into radial and thrust subcategories. Within these divisions, much variety is possible. Single- or double-row configurations are offered, with the latter giving higher load capacity. Unidirectional or angular contact is another choice, the former accepting "pure" radial or thrust loading, and the latter accepting a combination of both. Deep-groove ball bearings are capable of handling both large radial loads and limited thrust loads in both directions, and are the most commonly used.

The angular-contact ball bearing can stand larger thrust loads than the deep-groove ball bearing, but only in one direction. They are often used in pairs to absorb axial loads in both directions. The maximum-capacity ball bearings have a filling slot to allow more balls to be inserted than can be accommodated by eccentric displacement of the races at assembly as is done with the deep-groove (Conrad-type) ball bearing, but the filling slot limits its axial load capacity.

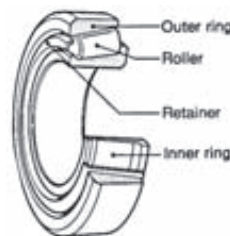
Self-aligning designs have the advantage of accommodating some shaft misalignment and also create simple support for the shaft. They also have very low friction. If non-self-aligning bearings are used on a shaft, the bearing mounts must be carefully aligned for colinearity and angularity to avoid creating residual loads on the bearings at assembly, which will severely shorten their life.



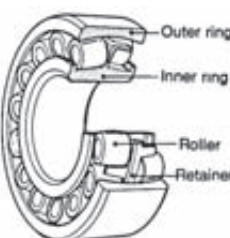
(a) Cylindrical roller bearing



(b) Needle roller bearing



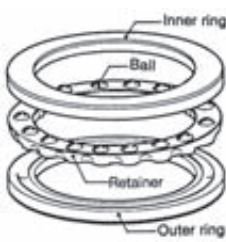
(c) Tapered roller bearing



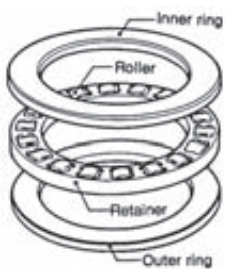
(d) Spherical roller bearing

FIGURE 11-18

Roller-Type Bearings
Courtesy of NTN Corporation



(a) Ball thrust bearing



(b) Roller thrust bearing

FIGURE 11-19

Thrust Bearings Courtesy of NTN Corporation

Figure 11-21 shows size ranges and one bearing manufacturer's ratings and recommendations regarding the use of various types of bearings as an example. Note that a few types are available in inch sizes, but most are available only in metric dimensions. The columns labeled *Capacity* indicate relative ability to accommodate radial and thrust

Radial ball bearings		Single row deep groove ball bearings
		Maximum capacity type ball bearings
		Single row angular contact ball bearings
		Duplex angular contact ball bearings
		Double row angular contact ball bearings
		Four-point contact ball bearings
		Self-aligning ball bearings
		Single direction thrust ball bearings with flat back face
		Single direction thrust ball bearings with seating ring
		Double direction thrust ball bearings with flat back face
Thrust ball bearings		Double direction thrust ball bearings with seating rings
		Double direction angular contact thrust ball bearings
Radial roller bearings		Single row cylindrical roller bearings
		Double row cylindrical roller bearings
		Needle roller bearings
		Single row tapered roller bearings
		Double row tapered roller bearings
		Spherical roller bearings
Thrust roller bearings		Cylindrical roller thrust bearings
		Needle roller thrust bearings
		Tapered roller thrust bearings
		Spherical roller thrust bearings

FIGURE 11-20

Classification of Rolling-Element Bearings Courtesy of NTN Corporation

loads for each type. The *Limiting Speed* column uses the Conrad-type bearing as the standard of comparison, since it has one of the best high-speed capabilities. Consult the bearing manufacturers' catalogs for additional information on other types and series of bearings. Many more are available than are shown in these few figures.

	TYPE	SIZE RANGE IN INCHES		AVERAGE RELATIVE RATINGS			AVAILABLE WITH			DIMENSIONS		
				Capacity		Limiting Speed	Permit- able Misalign- ment	Shields	Seals	Snap Rings	Metric	
		Bore	O.D.	Radial	Thrust						Inch	
Ball	CONRAD TYPE		.1181 to 41.7323	.3750 to 55.1181	Good	Fair 	Conrad is basis for comparison 1.00					
	MAXIMUM TYPE		.6693 to 4.3307	1.5748 to 8.4646	Excellent	Poor 	1.00					
	ANGULAR CONTACT 15°/40°		.3937 to 7.4803	1.0236 to 15.7480	Good	Good (15°) Excellent (40°) 	1.00 0.70					
	ANGULAR CONTACT 35°		.3937 to 4.3307	1.1811 to 9.4488	Excellent	Good 	0.70					
	SELF-ALIGNING		.1969 to 4.7244	.7480 to 9.4488	Fair	Fair 	1.00					
CYLINDRICAL ROLLER BEARINGS	SEPARABLE INNER RING NON-LOCATING		.4724 to 19.6850	1.2598 to 28.3465	Excellent	0	1.00					
	SEPARABLE INNER RING ONE DIR. LOCATING		.4724 to 12.5984	1.2598 to 22.8346	Excellent	Poor 	1.00					
	SELF-CONTAINED TWO DIR. LOCATING		.4724 to 3.9370	1.4567 to 8.4646	Excellent	Poor 	1.00					
TAPERED ROLLER BEARINGS	SEPARABLE		.6205 to 6.0000	1.5700 to 10.0000	Good	Good 	0.60					
SPHERICAL ROLLER BEARINGS	SELF-ALIGNING		.9843 to 12.5984	2.0472 to 22.8346	Good	Fair 	0.50					
	SELF-ALIGNING		.9843 to 35.4331	2.0472 to 46.4567	Excellent	Good 	0.75					
Roller	COMPLETE BEARINGS with or without locating rings & lubricating groove		.2362 to 14.1732	.6299 to 17.3228	Good	0	0.60					
	DRAWN CUP		.1575 to 2.3622	.3150 to 2.6772	Good	0	0.30					
THRUST BEARINGS	SINGLE DIRECTION BALL GROOVED RACE		.2540 to 46.4567	.8130 to 57.0866	Poor	Excellent 	0.30					
	SINGLE DIRECTION CYL. ROLLER		1.1811 to 23.6220	1.8504 to 31.4960	0	Excellent 	0.20					
	SELF-ALIGNING SPHERICAL ROLLER		3.3622 to 14.1732	4.3307 to 22.0472	Poor	Excellent 	0.50					

FIGURE 11-21

Relative Performance, Size, and Availability Information for Rolling-Element Bearings Courtesy of FAG Bearings Corp., Stamford, Conn.

11.9 FAILURE OF ROLLING-ELEMENT BEARINGS

If sufficient, clean lubricant is provided, failure in rolling bearings will be by surface fatigue, as described in Chapter 7. Failure is considered to occur when either raceway or balls (rollers) exhibit the first pit. Typically the raceway will fail first. The bearing will give an audible indication that pitting has begun by emitting noise and vibration. It can be run beyond this point, but as the surface continues to deteriorate, the noise and vibration will increase, eventually resulting in spalling or fracture of the rolling elements and possible jamming and damage to other connected elements. If you have ever had a wheel bearing fail on your automobile, you know the growling sound of a pitted or spalled rolling-element bearing *in extremis*.

Any large sample of bearings will exhibit wide variations in life among its members. The failures do not distribute statistically in a symmetrical Gaussian manner, but rather according to a Weibull distribution, which is skewed. Bearings are typically rated based on the life, stated in revolutions (or in hours of operation at the design speed), that 90% of a random sample of bearings of that size can be expected to reach or exceed at their design load. In other words, 10% of the batch can be expected to fail at that load before the design life is reached. This is called the L_{10} life.* For critical applications, a smaller failure percentage can be designed for, but most manufacturers have standardized on the L_{10} life as a means of defining the load-life characteristic of a bearing. The rolling-bearing selection process largely involves using this parameter to obtain whatever life is desired under the anticipated loading or overloading conditions expected in service.

Figure 11-22 shows a curve of bearing failure and survival percentages as a function of relative fatigue life. The L_{10} life is taken as the reference. The curve is relatively linear to 50% failure, which occurs at a life 5 times that of the reference. In other words, it should take 5 times as long for 50% of the bearings to fail as it does for 10% to do so. After that point the curve becomes quite nonlinear, showing that it will take about 10 times as long to fail 80% of the bearings as to fail 10%, and at 20 times the L_{10} life there are still a few percent of the original bearings running.

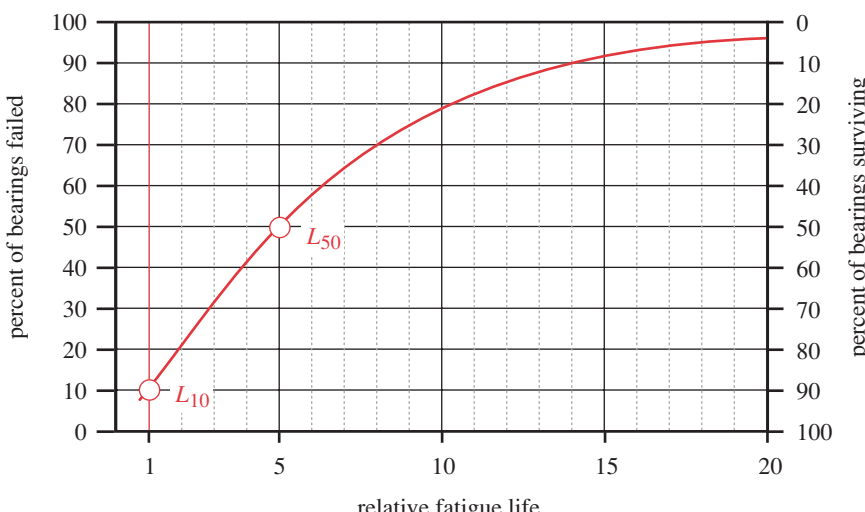


FIGURE 11-22

Typical Life Distribution in Rolling-Element Bearings *Adapted from SKF USA Inc.*

* Some bearing manufacturers refer to this as the B_{90} or C_{90} life, referring to the survival of 90% of the bearings rather than the failure of 10%.

The life L for other failure percentages than the standard 10% can be calculated by multiplying the L_{10} life by a reliability factor K_R taken from the Weibull distribution curve that it obeys.

$$L_P = K_R L_{10} \quad (11.19)$$

where L is fatigue life expressed in millions of revolutions. The Weibull factors K_R for various failure percentages are shown in Table 11-5.

Table 11-5

Reliability Factors R
for a Weibull Distribution
Corresponding to the
Probability of Failure P

P%	R%	K _R
50	50	5.0
10	90	1.0
5	95	0.62
4	96	0.53
3	97	0.44
2	98	0.33
1	99	0.21

11.10 SELECTION OF ROLLING-ELEMENT BEARINGS

Once a bearing type suited to the application is chosen based on considerations discussed above and outlined in Figure 11-21, selection of an appropriate-size bearing depends on the magnitudes of applied static and dynamic loads and the desired fatigue life.

Basic Dynamic Load Rating C

Extensive testing by bearing manufacturers, based on well-established theory, has shown that the L_{10} fatigue life of rolling bearings is inversely proportional to the third power of the load for ball bearings, and to the $10/3$ power for roller bearings. These relationships can be expressed as

ball bearings :
$$L_{10} = \left(\frac{C}{P}\right)^3 \quad (11.20a)$$

roller bearings :
$$L_{10} = \left(\frac{C}{P}\right)^{10/3} \quad (11.20b)$$

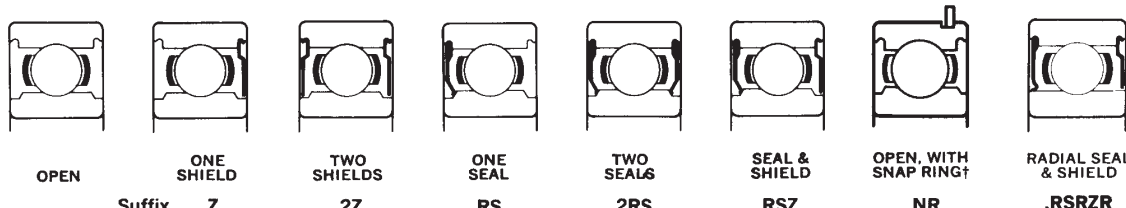
where L_{10} is fatigue life expressed in millions of revolutions, P is the constant applied load,* and C is the *basic dynamic load rating* for the particular bearing that is defined by the manufacturer and published for each bearing in the bearing catalogs. The **basic dynamic load rating** C is defined as *the load that will give a life of 1 million revolutions of the inner race*. This load C is typically larger than any practical load that one would subject the particular bearing to, because the desired life is usually much higher than 1 million revolutions. In fact some bearings will fail statically if actually subjected to a load equal to C . It is simply a reference value that allows bearing life to be predicted at any level of actual applied load. Figure 11-23 shows a page from a bearing manufacturer's catalog that specifies the value of C for each bearing. Each bearing's maximum limiting speed is also defined.

Combine equations 11.20a and 11.20b with equation 11.19 to obtain expressions for a bearing life at any selected failure rate.

ball bearings :
$$L_P = K_R \left(\frac{C}{P}\right)^3 \quad (11.20c)$$

roller bearings :
$$L_P = K_R \left(\frac{C}{P}\right)^{10/3} \quad (11.20d)$$

* Note that a constant external load applied to a rotating bearing creates dynamic loads in the bearing elements in the same manner that a constant moment on a rotating shaft causes dynamic stresses, because any one point on a ball, roller, or raceway sees the load come and go as the bearing rotates.



This configuration only shown to illustrate new standard enclosures. Some bearings are now being converted.

BEARING NUMBER*	BOUNDARY DIMENSIONS					SNAP RING DIMENSIONS			MAX. FILLET RADIUS Shaft & Hsg. Inch	APPROX. WEIGHT lb.	S_L LIMITING SPEED ± rpm	C DYNAMIC LOAD RATING lb.	C _o STATIC LOAD RATING lb.	
	BORE mm	BORE inch	O. DIAM. mm	O. DIAM. inch	WIDTH mm	WIDTH inch	H	S						
6300	10	.3937	35	1.3780	11	.4331	.125	1.562	.044	.025	.13	22000	1400	850
6301	12	.4724	37	1.4567	12	.4724	.125	1.625	.044	.040	.15	20000	1700	1040
6302	15	.5906	42	1.6535	13	.5118	.125	1.821	.044	.040	.20	18000	1930	1200
6303	17	.6693	47	1.8504	14	.5512	.141	2.074	.044	.040	.25	16000	2320	1460
6304	20	.7874	52	2.0472	15	.5906	.141	2.276	.044	.040	.34	14000	3000	1930
6305	25	.9843	62	2.4409	17	.6693	.195	2.665	.067	.040	.58	11000	3800	2550
6306	30	1.1811	72	2.8346	19	.7480	.195	3.091	.067	.040	.83	9500	5000	3400
6307	35	1.3780	80	3.1496	21	.8268	.195	3.406	.067	.060	1.07	8500	5700	4000
6308	40	1.5748	90	3.5433	23	.9055	.226	3.799	.097	.060	1.41	7500	7350	5300
6309	45	1.7717	100	3.9370	25	.9843	.226	4.193	.097	.060	1.95	6700	9150	6700
6310	50	1.9685	110	4.3307	27	1.0630	.226	4.587	.097	.080	2.50	6000	10600	8150
6311	55	2.1654	120	4.7244	29	1.1417	.271	5.104	.111	.080	3.30	5300	12900	10000
6312	60	2.3622	130	5.1181	31	1.2205	.271	5.498	.111	.080	3.81	5000	14000	10800
6313	65	2.5591	140	5.5118	33	1.2992	.304	5.892	.111	.080	4.64	4500	16000	12500
6314	70	2.7559	150	5.9055	35	1.3780	.304	6.286	.111	.080	5.68	4300	18000	14000
6315	75	2.9528	160	6.2992	37	1.4567	.304	6.679	.111	.080	6.60	4000	19300	16300
6316	80	3.1496	170	6.6929	39	1.5354	.346	7.198	.122	.080	9.53	3800	21200	18000
6317	85	3.3465	180	7.0866	41	1.6142	.346	7.593	.122	.100	11.00	3400	21600	18600
6318	90	3.5433	190	7.4803	43	1.6929	.346	7.986	.122	.100	11.60	3400	23200	20000
6319	95	3.7402	200	7.8740	45	1.7717	.346	8.380	.122	.100	13.38	3200	24500	22400
6320	100	3.9370	215	8.4646	47	1.8504	—	—	—	.100	16.34	3000	28500	27000
6321	105	4.1338	225	8.8582	49	1.9291	—	—	—	.100	17.8	2800	30500	30000
6322	110	4.3307	240	9.4488	50	1.9685	—	—	—	.100	21.0	2600	32500	32500
6324	120	4.7244	260	10.2362	55	2.1654	—	—	—	.100	32.3	2400	36000	38000
6326	130	5.1181	280	11.0236	58	2.2835	—	—	—	.12	40.1	2200	39000	43000
6328	140	5.5118	300	11.8110	62	2.4409	—	—	—	.12	48.1	2000	44000	50000
6330	150	5.9055	320	12.5984	65	2.5590	—	—	—	.12	57.8	1900	49000	60000

*Bearing numbers listed are for open bearings only. For shields, seals and snap rings, add suffix or prefix indicated below bearing diagram. Eg. 6300.Z, 6300.RS, 6300.NR, etc. Check availability of closures for larger sizes.

†Snap ring bearings available with shields or seals. Add both suffixes. Eg. 6300.ZNR, etc.

For grease lubricated bearings without seals. For other conditions, see Page 114.

For mounting data, shaft and housing fits and shoulder diameters, see Pages 124-132.

FIGURE 11-23

Dimensions and Load Ratings for 6300 Series, Medium, Metric, Deep-Groove (Conrad-type) Ball Bearings Courtesy of FAG Bearings Corporation, Stamford, Conn.

Modified Bearing Life Rating

The ASME and ISO have recently adopted a new standard (ISO 281/2) for the calculation of rolling bearing life. Equation 11.20 is based only on Hertzian contact stresses. The new standard also includes the effects of a number of factors such as friction, hoop

stress from press fits, lubrication condition and cleanliness, centrifugal loading, and others. This approach uses a von Mises stress criterion in order to include stresses due to these factors. It also makes use of the latest empirical data on the surface fatigue strength of bearing steels. All of these effects are combined into a stress-life factor A_{sl} which is then applied to the traditional L_{10} value from equation 11.20.

$$L_{ASME} = A_{sl}L_{10} \quad (11.21)$$

Test data has shown that equation 11.21 gives a more accurate calculation of bearing life than equations 11.20. Calculation of the factor A_{sl} is explained in reference [30] and is quite complicated. That reference comes with a computer program called *ASMELife* that will calculate the projected L_{ASME} life of a bearing of any design for any set of loading and environmental parameters. While the algorithm for its calculation is fully explained in the reference, space prohibits its inclusion here. Moreover, the user-friendly and inexpensive software provided for its calculation make further exposition unnecessary. The reader is directed to the ASME publication for further information. For the purpose of examples in this chapter, we will assume $A_{sl} = 1.0$.

Basic Static Load Rating C_0

Permanent deformations on rollers or balls can occur at even light loads because of the very high stresses within the small contact area. The limit on static loading in a bearing is defined as the load that will produce a total permanent deformation in the raceway and rolling element at any contact point of 0.0001 times the diameter d of the rolling element. Larger deformations will cause increased vibration and noise, and can lead to premature fatigue failure. The stresses required to cause this $0.0001d$ static deformation in bearing steel are quite high, ranging from about 4 GPa (580 kpsi) in roller bearings to 4.6 GPa (667 kpsi) in ball bearings. Bearing manufacturers publish a basic static load rating C_0 for each bearing, calculated according to AFBMA standards. This loading can sometimes be exceeded without failure, especially if rotating speeds are low, which avoids vibration problems. It usually takes a load of $8C_0$ or larger to fracture a bearing. Figure 11-23 (previous page) shows a page from a bearing manufacturer's catalog that specifies the value of C_0 for each bearing.

EXAMPLE 11-3

Selection of Ball Bearings for a Designed Shaft

Problem Select radial ball bearings for the shaft shown in Figure 11-5 (p. 633). The shaft was designed in Example 10-1 (p. 560).

Given The maximum transverse loads on the shaft at the bearings are 16 lb at R_1 and 54 lb at R_2 . Since the load at R_2 is 4X that at R_1 , one design can be created for R_2 and used also at R_1 . Shaft diameter at both R_1 and R_2 is 0.591 in, based on the tentative choice of a 15-mm-ID bearing in Example 10-1. The shaft speed is 1 725 rpm.

Assumptions Thrust loads are negligible. A 5% failure rate is desired.

Find The bearing fatigue lives at both shaft locations.

Solution

- 1 From Figure 11-23 (p. 660), choose a #6302 bearing with 15-mm inside diameter. Its dynamic load rating factor is $C = 1\ 930$ lb. The static load rating $C_0 = 1\ 200$ lb. The static applied load of 54 lb is obviously well below the bearing's static rating.
- 2 From Table 11-5 (p. 659), choose the factor for a 5% failure rate: $K_R = 0.62$.
- 3 Calculate the projected life with equations 11.20a and 11.19 or their combination, equation 11.20c (all on p. 659). Note that the equivalent load in this case is simply the applied radial load due to the absence of any thrust load. For the larger reaction load of 54 lb at R_2 :

$$L_{10} = \left(\frac{C}{P} \right)^3 = \left(\frac{1\ 930}{54} \right)^3 = 45E3 \text{ millions of revs} = 45E9 \text{ revs}$$

$$L_P = K_R L_{10} = 0.62(45E9) = 27.9E9 \text{ revs} \quad (a)$$

- 4 For the smaller reaction load of 16 lb at R_1 :

$$L_{10} = \left(\frac{C}{P} \right)^3 = \left(\frac{1\ 930}{16} \right)^3 = 1.75E6 \text{ millions of revs} = 1.75E12 \text{ revs}$$

$$L_P = K_R L_{10} = 0.62(1.75E12) = 1.09E12 \text{ revs} \quad (b)$$

This shows the nonlinear relationship between load and life. A 3.5X reduction in load results in a 38X increase in fatigue life. These bearings are obviously very lightly loaded, but their size was dictated by considerations of stresses in the shaft that defined the shaft diameters.

- 5 From Figure 11-23, this bearing's limiting speed is 18 000 rpm, well above the operating speed of 1 725 rpm.

Combined Radial and Thrust Loads

If both radial and thrust loads are applied to a bearing, an equivalent load must be calculated for use in equation 11.20. The AFBMA recommends the following equation:

$$P = XVF_r + YF_a \quad (11.22a)$$

where P = equivalent load

F_r = applied constant radial load

F_a = applied constant thrust load

V = a rotation factor (see Figure 11-24)

X = a radial factor (see Figure 11-24)

Y = a thrust factor (see Figure 11-24)

The rotation factor V is 1 for a bearing with a rotating inner ring. If the outer ring rotates, V is increased to 1.2 for certain types of bearings. The factors X and Y vary with bearing type and relate to that type's ability to accommodate thrust as well as radial loads. Values of V , X , and Y are defined by bearing manufacturers in tables such as the one reproduced in Figure 11-24. Bearing types, such as cylindrical roller, that cannot support thrust loads are not included in this table. A factor e is also specified for the

bearing types in Figure 11-24 and defines a minimum ratio between the axial and radial forces below which the axial force can be ignored (set to zero) in equation 11.22b.

$$\text{if } \frac{F_a}{VF_r} \leq \epsilon \quad \text{then } X = 1 \text{ and } Y = 0 \quad (11.22b)$$

Calculation Procedures

Equations 11.20 and 11.22 can be solved together for any situation in which either the applied load or a desired fatigue life is known. Usually, the radial and thrust loads act-

Factors V, X, and Y for Radial Bearings

Bearing Type			In Relation to the Load the Inner Ring is		Single Row Bearings 1)		Double Row Bearings 2)				ϵ	
			Rotating	Stationary	$\frac{F_a}{VF_r} > \epsilon$		$\frac{F_a}{VF_r} \leq \epsilon$		$\frac{F_a}{VF_r} > \epsilon$			
					V	V	X	Y	X	Y		
3)	4)	5)										
Radial Contact Groove Ball Bearings	$\frac{F_a}{C_0}$	$\frac{F_a}{i Z D_w^2}$										
Groove Ball Bearings	0.014 0.028 0.056	25 50 100					2.30 1.99 1.71					
	0.084 0.11 0.17	150 200 300	↑ 1 ↓	↑ 1.2 ↓	↑ 0.56 ↓	↑ 1.55 1.45 1.31	↑ 1 ↓	↑ 0 ↓	↑ 0.56 ↓	↑ 2.30 1.99 1.71 ↓	0.19 0.22 0.26	
	0.28 0.42 0.56	500 750 1000					1.15 1.04 1.00					
20° 25° 30° 35° 40°			↑ 1 ↓	↑ 1.2 ↓	0.43 0.41 0.39 0.37 0.35	1.00 0.87 0.76 0.66 0.57	↑ 1 ↓	1.09 0.92 0.78 0.66 0.55	0.70 0.67 0.63 0.60 0.57	1.63 1.44 1.24 1.07 0.93	0.57 0.68 0.80 0.95 1.14	
Self-Aligned Ball Bearings			1	1	0.40	$0.4 \cot \alpha$	1	$0.42 \cot \alpha$	0.65	$0.65 \cot \alpha$	$1.5 \tan \alpha$	
Self-Aligned and Tapered Roller Bearings			1	1.2	0.40	$0.4 \cot \alpha$	1	$0.45 \cot \alpha$	0.67	$0.67 \cot \alpha$	$1.5 \tan \alpha$	

- 1) For single row bearings, when $\frac{F_a}{VF_r} \leq \epsilon$ use $X = 1$ and $Y = 0$.

For two single row angular contact ball or roller bearings mounted "face-to-face" or "back-to-back" the values of X and Y which apply to double row bearings. For two or more single row bearings mounted "in tandem" use the values of X and Y which apply to single row bearings.

- 2) Double row bearings are presumed to be symmetrical.

- 3) Permissible maximum value of $\frac{F_a}{C_0}$ depends on the bearing design.

- 4) C_0 is the basic static load rating.

- 5) Units are pounds and inches.

Values of X , Y and ϵ for a load or contact angle other than shown in the table are obtained by linear interpolation.

FIGURE 11-24

V, X, and Y Factors for Radial Bearings Courtesy of SKF USA Inc.

ing on each bearing location will be known from a load analysis of the design. Often an approximate shaft size will be known from stress or deflection calculations. A bearing catalog should then be consulted, a trial bearing (or bearings) selected, and the values of C , C_0 , V , X , and Y extracted. The effective load P can be found from equation 11.22 and used in equation 11.20 with C to find the predicted fatigue life L .

Alternatively, since V , X , and Y depend only on the type but not the size of a bearing, they can be determined first and equations 11.20 and 11.22 solved simultaneously for the value of dynamic load factor C required to achieve a desired life L . The bearing catalogs can then be consulted to find a suitably sized bearing with the necessary C value. In either case, the static load should also be compared to the static load factor C_0 for the chosen bearing to guard against excessive deformations.

EXAMPLE 11-4

Selection of Ball Bearings for Combined Radial and Thrust Loads

Problem Select a deep-groove ball bearing for specified loading and desired life.

Given The radial load $F_r = 1\,686$ lb (7 500 N) and the axial load $F_a = 1\,012$ lb (4 500 N). The shaft speed is 2 000 rpm.

Assumptions Use a Conrad-type deep-groove ball bearing. The inner ring rotates.

Find A suitable size bearing to give an L_{10} life of 5E8 revolutions.

Solution

11

1 Try a #6316 bearing from Figure 11-23 (p. 660) and extract its data as: $C = 21\,200$ lb (94 300 N), $C_0 = 18\,000$ lb (80 000 N), and maximum rpm = 3 800.

2 Calculate the ratio F_a / C_0 :

$$\frac{F_a}{C_0} = \frac{1\,012}{18\,000} = 0.056 \quad (a)$$

and take this value to Figure 11-24 to find the corresponding value of $e = 0.26$ for radial-contact groove ball bearings.

3 Form the ratio $F_a / (V F_r)$ and compare it to the value of e .

$$\frac{F_a}{V F_r} = \frac{1\,012}{1(1\,686)} = 0.6 > e = 0.26 \quad (b)$$

Note that $V = 1$ because the inner ring is rotating.

4 Since the ratio in step 3 is $> e$, extract the X and Y factors from Figure 11-24 as $X = 0.56$ and $Y = 1.71$, and use them to calculate the equivalent load from equations 11.22 (pp. 662–663).

$$P = X V F_r + Y F_a = 0.56(1)(1\,686) + 1.71(1\,012) = 2\,675 \text{ lb} \quad (c)$$

5 Use the equivalent load in equation 11.21 (p. 661) to find the L_{10} life for this bearing.

$$L_{10} = \left(\frac{C}{P} \right)^3 = \left(\frac{21200}{2675} \right)^3 = 5.0E2 \text{ millions of revs} = 5.0E8 \text{ revs} \quad (d)$$

This result actually required some iteration, trying several bearing numbers before finding that this one would give the desired life.

- 6 Models called EX11-04 are on the CD-ROM. The Mathcad model provides an alternate approach for the solution of this example.
-

11.11 BEARING MOUNTING DETAILS

Rolling bearings are made with close tolerances on their inside and outside diameters to allow press-fitting on the shaft or in the housing. The bearing races (rings) should be tightly coupled to the shaft and housing to guarantee that motion only occurs inside the low-friction bearing. Press-fitting both rings can make for a difficult assembly or disassembly in some cases. Various clamping arrangements are commonly used to capture either the inner or outer ring without a press fit, the other being secured by pressing. The inner ring is usually located against a shoulder on the shaft. Bearing catalog tables provide recommended shaft shoulder diameters, which should be observed to avoid interference with seals or shields. Maximum allowable fillet radii to clear the rings' corners are also defined by the manufacturers.

Figure 11-25a shows a nut and lock-washer arrangement used to clamp the inner ring to the shaft to avoid a press fit. Bearing manufacturers supply special nuts and washers standardized to fit their bearings. Figure 11-25b shows a snap ring used to axially locate the inner ring, which would be pressed to the shaft. Figure 11-25c shows the outer ring clamped axially to the housing and the inner ring located by a sleeve spacer between the inner ring and an external accessory flange on the same shaft.

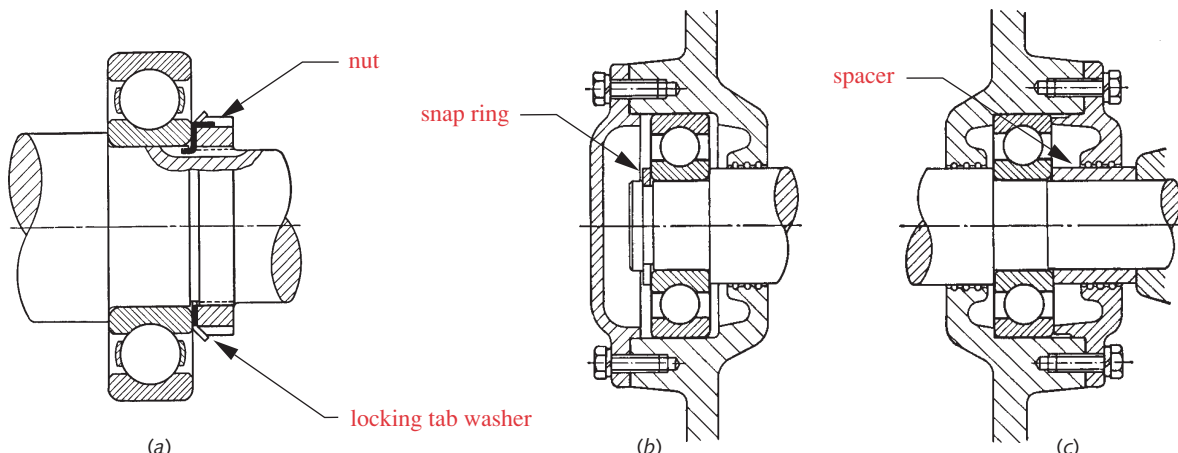
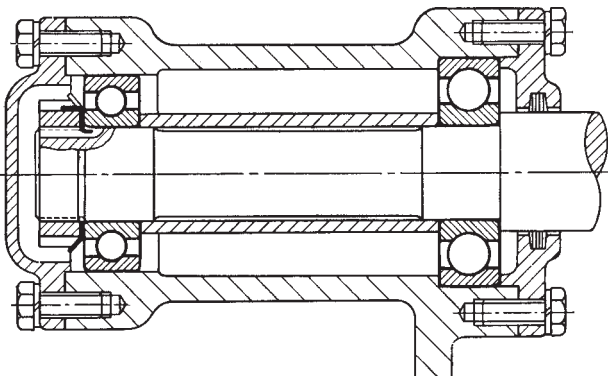


FIGURE 11-25

Bearing Mounting Methods Source: SKF Engineering Data, SKF USA Inc., 1968

**FIGURE 11-26**

Bearings on Shaft, One Fixed Axially and One Floating Axially *Source: SKF Engineering Data, SKF USA Inc., 1968*

Pairs of bearings on the same shaft are commonly needed to provide moment support. Figure 11-26 shows one possible arrangement to axially capture the assembly without risking the introduction of axial forces to the bearings from thermal expansion of the parts. The inner races of both bearings are clamped axially with a nut on the left and a spacer between them. The outer race of the bearing on the right is captured (clamped) axially to the housing, but the outer race of the one on the left is “floating” axially in the housing to allow for thermal expansion. It might be tempting to capture both right and left bearings axially, but this would be unwise. It is considered good practice to capture a long assembly axially at only one location to avoid expansion-induced axial forces on the bearings, which would seriously shorten their life. Another way to accomplish this is to use only one bearing that can support an axial load (e.g., a ball bearing) and use a cylindrical roller or other type bearing that cannot support axial load across its rolling elements at the other end of the shaft.

11

11.12 SPECIAL BEARINGS

Many other types and arrangements of rolling-element bearings are available. Pillow blocks and flange-units package standard ball or roller bearings in cast-iron housings that make it easy to attach bearings to horizontal or vertical surfaces. Figure 11-27 shows a pillow block and a flange-unit bearing.

Cam followers, as shown in Figure 11-28, are made with ball or roller bearings and a special outer race that can be run directly against a cam surface. They are available with integral mounting studs as shown) or with a hole to mount on a rod or stud. Rod ends are typically a single spherical ball in a socket designed to attach to rods and provide a self-aligning, low-friction connection between links in a mechanism as shown in Figure 11-29.

Linear motion is easily guided on plain bushings, but will have moderate friction levels. For lower friction in linear motion, ball bushings are available as shown in Figure 11-30. These require special hardened and ground shafts made to close tolerances. Alignment of parallel shafts must be done very precisely to obtain the low-friction ad-

vantages of linear ball bearings. They are not as able to absorb shock loads as a plain bushing, however.

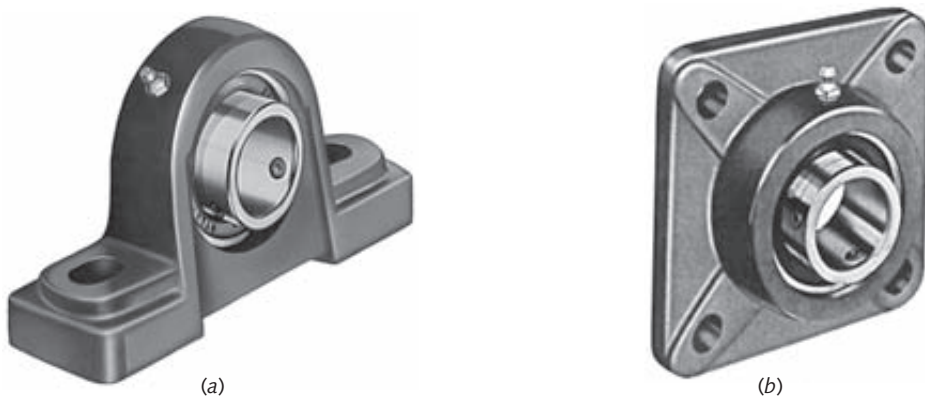


FIGURE 11-27

Pillow Block (a) and Flange-Mount Bearing Units (b) Courtesy of McGill Manufacturing Co. Inc., Bearing Division, Valparaiso, Ind.

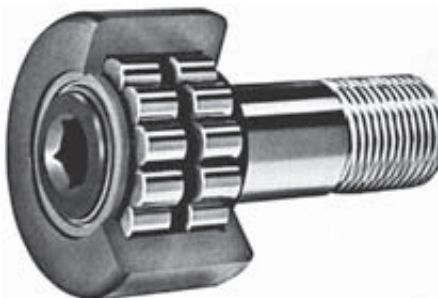


FIGURE 11-28

Roller-Bearing Cam Follower Courtesy of Roller Bearing Company of America, Newtown Pa.

11

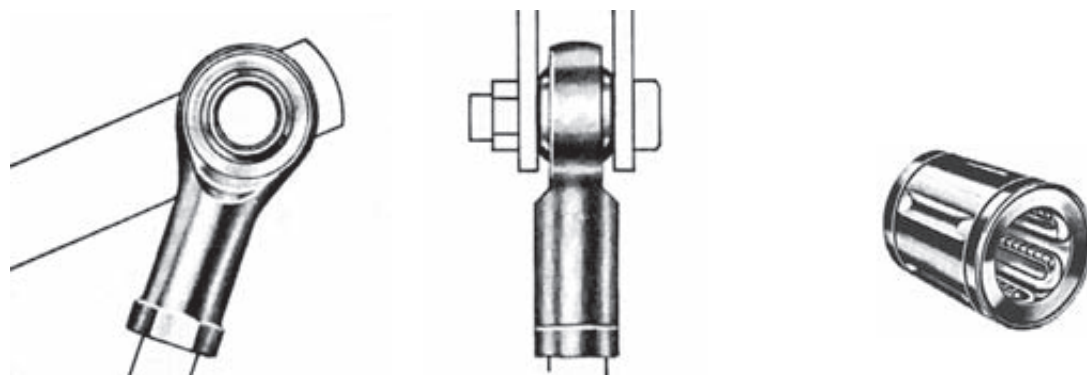


FIGURE 11-29

Spherical Rod End Courtesy of Morse Chain, Division of Borg-Warner Corp., Aurora, Ill.

FIGURE 11-30

Linear Ball Bushing Courtesy of Thompson Industries, Inc., Manhasset, N.Y.

11.13 CASE STUDY

Case Study 10A, which was set up in Chapter 9, describes the design of a test fixture for the dynamic measurement of cam-follower accelerations and forces. The sensitive nature of these measurements requires that only sliding bearings be used throughout, because the vibrations and noise from rolling-element bearings would contaminate the measurements. We will now continue that case study for the design of its main cam-shaft bearings.

CASE STUDY 10B

Design of Hydrodynamic Bearings for a Cam Test Fixture

Problem	Determine the hydrodynamic conditions in the proposed bearings for the camshaft in the Cam Dynamic Test Fixture (CDTF).
Given	The cam generates a peak dynamic force of 110 lb at a maximum speed of 180 rpm (3 rps), as defined in Case Study 10A (p. 532). The flywheel weighs 220 lb and is located midway between the two bearings. Bulk oil temperature is controlled to 200°F. The camshaft is 2-in dia and the preliminary design of the bearings allows up to 2 in of length each.
Assumptions	Plain bearings must be used throughout, since rolling-element bearings introduce too much noise. Porous bronze bushings are proposed. Use a clearance ratio of 0.001. Try a mineral oil of SAE 30W (ISO VG 100). Gravity oilers will be provided at each bearing.
Solution	See Figures 9-8 (p. 533) and 11-31.

11

- Find the reaction forces acting on each bearing from the applied forces and dimensions defined in Figure 11-31. Sum moments about R_1 and assume upward forces positive.

$$\sum M = 0 = -110(-4.5) + [-220(3.125)] + 6.25R_2 \\ R_2 = 30.8 \text{ lb} \quad (a)$$

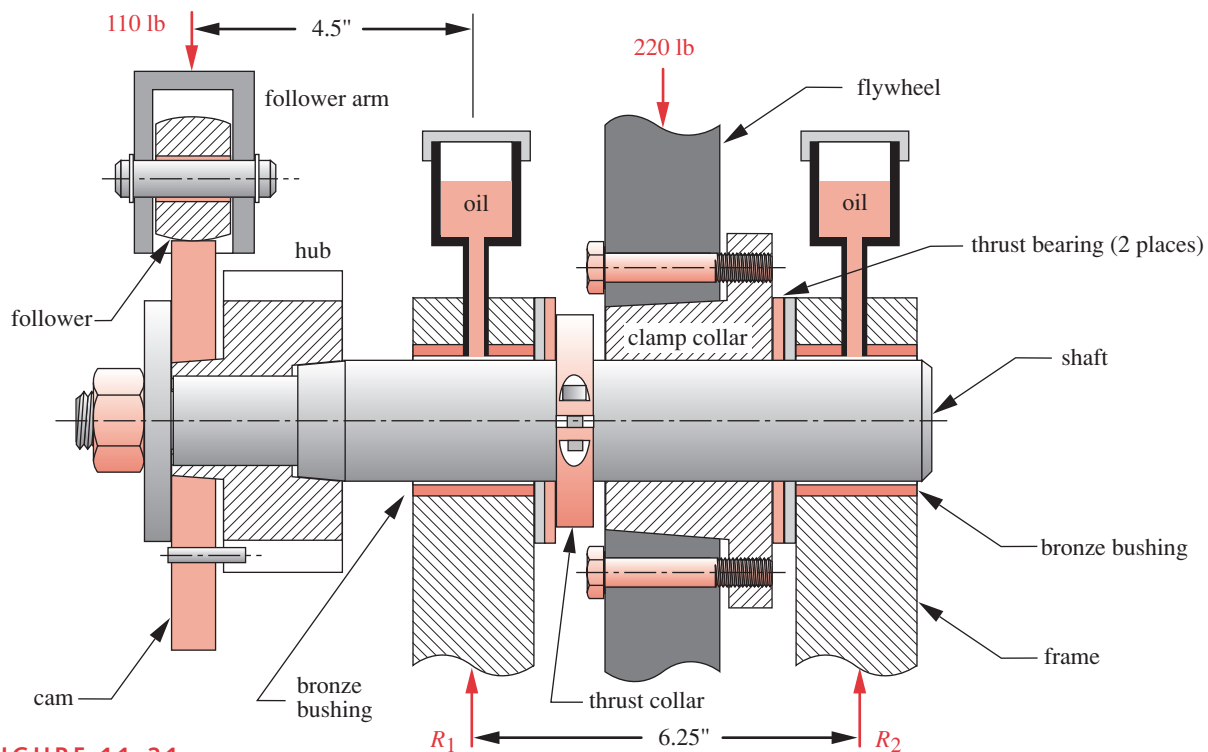
$$\sum F = 0 = -110 - 220 + 30.8 + R_1 \\ R_1 = 299.2 \text{ lb} \quad (b)$$

The bearing at R_1 takes most of the load, so we will design for that force.

- An ISO VG100 oil was suggested. Figure 11-1 (p. 628) gives a viscosity for this oil at 200°F of about 1.5 μ reyn.
- Find the average pressure in the bearing for an assumed length of 2 in.

$$P_{avg} = \frac{P}{ld} = \frac{299.2}{2(2)} = 74.8 \text{ psi} \quad (c)$$

- Find the diametral clearance in the bearing for the assumed clearance ratio.

**FIGURE 11-31**

Cross-Section of the Camshaft for the Cam Dynamic Test Fixture of Case Study 10

$$c_d = 0.001(2) = 0.002 \text{ in}$$

$$c_r = c_d/2 = 0.001 \text{ in} \quad (d)$$

11

- 5 Find the surface velocity of the shaft in the bearing.

$$U = \pi d n' = \pi(2)(3) = 18.85 \text{ in/sec} \quad (e)$$

- 6 Since the load and speed are known and the bearing dimensions are assumed, as is the viscosity, equation 11.8b (p. 638) can be solved for the dimensionless parameter K_e .

$$K_e = \frac{P c_r^2}{\eta U l^3} = \frac{299.2(0.001)^2}{(1.5E-6)(18.85)(2)^3} = 1.323 \quad (f)$$

- 7 The Ocvirk number can now be found from equation 11.12c.

$$O_N = 4\pi K_e = 4\pi(1.323) = 16.6 \quad (g)$$

The bearing design is viable based on this acceptable Ocvirk number.

- 8 The eccentricity ratio can be found from equation 11.13b (p. 641), which fits actual experimental data better than the theoretical equation.

$$\begin{aligned} \epsilon &\approx 0.21394 + 0.38517 \log O_N - 0.0008(O_N - 60) \\ &\approx 0.21394 + 0.38517 \log(16.6) - 0.0008(16.6 - 60) = 0.719 \end{aligned} \quad (h)$$

9 The minimum film thickness is found from equation 11.4b (p. 635).

$$h_{min} = c_r(1 - \varepsilon) = 0.001(1 - 0.719) = 0.000\ 281 \text{ in } (281 \mu\text{in}) \quad (i)$$

This is an ample film to protect even a poorly finished bearing, which this is not.

10 The files Case10B can be found on the CD-ROM.

11.14 SUMMARY

Low friction in sliding or rotating joints can be obtained either with hydrostatically or hydrodynamically lubricated plain bearings or with rolling-element bearings. Each has its own set of advantages and disadvantages.

HYDROSTATIC BEARINGS use a high-pressure source of fluid to separate the surfaces even when no relative motion is present. Air, water, or oil can be used as the fluid. Air bearings have essentially zero friction and wear. A Hovercraft is supported on an “air bearing,” for example.

HYDRODYNAMIC BEARINGS use the relative motion of the surfaces to pump the entrained lubricant (usually an oil) around the annulus between shaft and bearing. A properly designed hydrodynamic bearing separates the two parts on a film of oil when in motion and has no metal-to-metal contact except at start-up and shutdown. If the oil is kept clean and plentiful, essentially zero wear and very low friction are possible. Two surfaces that “conform” geometrically, such as a shaft in a hole, entrap the lubricant and thus readily form the supporting oil film.

Geometrically nonconforming joints, such as cam-follower contacts, gear teeth, and rolling bearings, tend to expel the fluid rather than entrap it, making it more difficult to achieve full-film separation of the surfaces. **Elastohydrodynamic lubrication** (EHD) refers to the combination of elastic deflection of a contact patch between two nonconforming surfaces (analogous to the contact patch between your tire and the road) and the pumping of fluid between the “flattened” surfaces to create at least a partial hydrodynamic film. These joints often have some combination of fluid film and metal-to-metal contact at the surface asperities. Thus wear can be higher than in a conforming hydrodynamic joint. The minimum fluid-film thickness between the surfaces in comparison to their composite surface roughness determines how much asperity contact occurs. In the absence of sufficient lubricant, speed, or geometry to form a separating fluid film, a bearing will revert to **boundary lubrication**, in which significant metal contact and wear occurs.

ROLLING BEARINGS are commercially available in a variety of configurations that use either balls or rollers of hardened steel captured between hardened steel raceways or rings. Since the contact is rolling, with little or no sliding, the friction is low both statically and dynamically. Start-up torque is significantly lower for rolling bearings than for hydrodynamic ones* (which require a relative velocity to establish the low-friction fluid film). Rolling bearings are available that can accommodate radial, thrust, or a combination of both types of loads. The lubrication state in rolling bearings will be either elastohydrodynamic, boundary, or some combination of the two referred to as

* When railroad cars were converted from hydrodynamic plain bearings to rolling-element bearings over a century ago, long freight trains that had required two engines to start them moving (but only one to keep them moving) could be started moving with only one engine.

partial EHD. Designing with rolling bearings largely involves the proper selection of a bearing from those commercially available. The manufacturers define a load-life parameter based on the load at which 90% of a batch of bearings can be expected to survive for 1 million revolutions of the inner race. This and other manufacturer-supplied data are used to calculate a projected life for a particular bearing under the given load and speed conditions of the application. Bearing companies will provide assistance in selecting the proper bearing for any application.

Important Equations Used in This Chapter

Absolute Viscosity Versus Kinematic Viscosity (Section 11.2):

$$\eta = \nu \rho \quad (11.1)$$

Petroff's Equation for No-Load Torque (Section 11.5):

$$T_0 = \eta \frac{\pi^2 d^3 l n'}{c_d} \quad (11.2c)$$

Eccentricity Ratio (Section 11.5):

$$\epsilon = \frac{e}{c_r} \quad (11.3)$$

Lubricant Film Thickness in a Hydrodynamic Bearing (Section 11.5):

$$h = c_r (1 + \epsilon \cos \theta) \quad (11.4a)$$

$$h_{min} = c_r (1 - \epsilon) \quad h_{max} = c_r (1 + \epsilon) \quad (11.4b)$$

Average Pressure in a Hydrodynamic Bearing (Section 11.5):

$$p_{avg} = \frac{P}{A} = \frac{P}{ld} \quad (11.6d)$$

Sommerfeld's Equations for Pressure and Load in an Infinite Bearing (Section 11.5):

$$p = \frac{\eta Ur}{c_r^2} \left[\frac{6\epsilon(\sin \theta)(2 + \epsilon \cos \theta)}{(2 + \epsilon^2)(1 + \epsilon \cos \theta)^2} \right] + p_0 \quad (11.6a)$$

$$P = \frac{\eta Ul r^2}{c_r^2} \frac{12\pi\epsilon}{(2 + \epsilon^2)(1 + \epsilon^2)^{1/2}} \quad (11.6b)$$

Ocvirk's Equations for Pressure and Load in a Short Bearing (Section 11.5):

$$p = \frac{\eta U}{rc_r^2} \left(\frac{l^2}{4} - z^2 \right) \frac{3\epsilon \sin \theta}{(1 + \epsilon \cos \theta)^3} \quad (11.7b)$$

$$P = K_\epsilon \frac{\eta Ul^3}{c_r^2} \quad (11.8b)$$

$$K_\varepsilon = \frac{\varepsilon [\pi^2(1-\varepsilon^2) + 16\varepsilon^2]^{\frac{1}{2}}}{4(1-\varepsilon^2)^2} \quad (11.8c)$$

Location of Maximum Pressure in a Short Bearing (Section 11.5):

$$\theta_{max} = \cos^{-1} \left(\frac{1 - \sqrt{1 + 24\varepsilon^2}}{4\varepsilon} \right) \quad (11.7c)$$

Location of Resultant Load in a Short Bearing (Section 11.5):

$$\phi = \tan^{-1} \left(\frac{\pi\sqrt{1-\varepsilon^2}}{4\varepsilon} \right) \quad (11.8a)$$

Torque in a Hydrodynamic Bearing (Section 11.5):

$$T_s = \eta \frac{d^3 l (n'_2 - n'_1)}{c_d} \frac{\pi^2}{(1-\varepsilon^2)^{1/2}} \quad (11.9c)$$

$$T_r = T_s + P e \sin \phi \quad (11.9a)$$

Power Loss in a Hydrodynamic Bearing (Section 11.5):

$$\Phi = T_r \omega = 2\pi T_r (n'_2 - n'_1) \quad \text{N-m/s or in-lb/s} \quad (11.10)$$

Coefficient of Friction in a Hydrodynamic Bearing (Section 11.5):

$$\mu = \frac{f}{P} = \frac{T_r/r}{P} = \frac{2T_r}{Pd} \quad (11.11)$$

The Ocvirk Number for a Short Hydrodynamic Bearing (Section 11.6):

$$O_N = \left(\frac{P_{avg}}{\eta n'} \right) \left(\frac{d}{l} \right)^2 \left(\frac{c_d}{d} \right)^2 = 4\pi K_\varepsilon \quad (11.12c)$$

Theoretical Relationship Between Ocvirk Number and Eccentricity Ratio (Section 11.6):

$$O_N = \frac{\pi \varepsilon [\pi^2(1-\varepsilon^2) + 16\varepsilon^2]^{\frac{1}{2}}}{(1-\varepsilon^2)^2} \quad (11.13a)$$

Empirical Relationship Between Ocvirk Number and Eccentricity Ratio (Section 11.6):

$$\varepsilon_x \cong 0.21394 + 0.38517 \log O_N - 0.0008(O_N - 60) \quad (11.13b)$$

Specific Film Thickness (Section 11.7):

$$\Lambda = h_c / \sqrt{R_{q_1}^2 + R_{q_2}^2} \quad (11.14a)$$

$$h_c \cong \frac{4}{3} h_{min} \quad (11.14b)$$

Minimum Film Thickness for EHD Cylindrical Contact (Section 11.7):

$$h_{min} = 2.65R'(\alpha E')^{0.54} \left(\frac{\eta_0 U}{E'R'} \right)^{0.7} \left(\frac{P}{lE'R'} \right)^{-0.13} \quad (11.16)$$

$$E' = \frac{2}{m_1 + m_2} = \frac{2}{\frac{1-v_1^2}{E_1} + \frac{1-v_2^2}{E_2}} \quad (11.17b)$$

Minimum Film Thickness for EHD General (Elliptical) Contact (Section 11.7):

$$h_{min} = 3.63R'(\alpha E')^{0.49} \left(\frac{\eta_0 U}{E'R'} \right)^{0.68} \left(1 - e^{-0.68\psi} \right) \left[\frac{P}{E'(R')^2} \right]^{-0.073} \quad (11.18)$$

Load-Life Relationship for Rolling-Element Bearings (Section 11.10):

ball bearings : $L_{10} = \left(\frac{C}{P} \right)^3$ (11.20a)

roller bearings : $L_{10} = \left(\frac{C}{P} \right)^{10/3}$ (11.20b)

Equivalent Load for Rolling-Element Bearings (Section 11.10):

$$P = XVF_r + YF_a \quad (11.22a)$$

11.15 REFERENCES

- 1 A. G. M. Michell, "Progress of Fluid-Film Lubrication", *Trans. ASME*, 51: pp. 153-163, 1929.
- 2 A. Cameron, *Basic Lubrication Theory*. John Wiley & Sons: New York, 1976.
- 3 B. J. Hamrock, *Fundamentals of Fluid Film Lubrication*. McGraw-Hill: New York, 1994.
- 4 T. A. Harris, *Rolling Bearing Analysis*. John Wiley & Sons: New York, 1991.
- 5 R. C. Elwell, "Hydrostatic Lubrication," in *Handbook of Lubrication*, E. R. Booser, ed., CRC Press: Boca Raton, Fla., p. 105, 1983.
- 6 J. L. Radovich, "Gears," in *Handbook of Lubrication*, E. R. Booser, ed., CRC Press: Boca Raton, Fla., p. 544, 1983.
- 7 E. Rabinowicz, *Friction and Wear of Materials*. John Wiley & Sons: New York, p. 182, 1965.
- 8 W. Glaeser, "Bushings," in *Wear Control Handbook*, M. B. Peterson and W. O. Winer, Editor. ASME: Wear Control Handbook, p. 598, 1980.
- 9 D. F. Wilcock and E. R. Booser, *Bearing Design and Application*. McGraw-Hill: New York, 1957.
- 10 A. H. Burr and J. B. Cheatham, *Mechanical Analysis and Design*, 2nd ed. Prentice-Hall: Englewood Cliffs, N.J., pp. 31-51, 1995.

- 11 **A. A. Raimondi and J. Boyd**, "A Solution for the Finite Journal Bearing and its Application to Analysis and Design—Parts I, II, and III," *Trans. Am. Soc. Lubrication Engineers*, 1(1): pp. 159-209, 1958.
- 12 **O. Reynolds**, "On the Theory of Lubrication and its Application to Mr. Beauchamp Tower's Experiments". *Phil. Trans. Roy. Soc. (London)*, 177: pp. 157-234, 1886.
- 13 **G. B. DuBois and F. W. Ocvirk**, "The Short Bearing Approximation for Full Journal Bearings," *Trans. ASME*, 77: pp. 1173-1178, 1955.
- 14 **G. B. DuBois, F. W. Ocvirk, and R. L. Wehe**, *Experimental Investigation of Eccentricity Ratio, Friction, and Oil Flow of Long and Short Journal Bearings—With Load Number Charts*, TN3491, NACA, 1955.
- 15 **F. W. Ocvirk**, *Short Bearing Approximation for Full Journal Bearings*, TN2808, NACA, 1952.
- 16 **G. B. DuBois and F. W. Ocvirk**, *Analytical Derivation and Experimental Evaluation of Short Bearing Approximation for Full Journal Bearings*, TN1157, NACA, 1953.
- 17 **H. S. Cheng**, "Elastohydrodynamic Lubrication," in *Handbook of Lubrication*, E. R. Booser, ed., CRC Press: Boca Raton, Fla., pp. 155-160, 1983.
- 18 **D. Dowson and G. Higginson**, "A Numerical Solution to the Elastohydrodynamic Problem," *J. Mech. Eng. Sci.*, 1(1): p. 6, 1959.
- 19 **D. Dowson and G. Higginson**, "New Roller Bearing Lubrication Formula," *Engineering*, 192: pp. 158-159, 1961.
- 20 **G. Archard and M. Kirk**, "Lubrication at Point Contacts," *Proc. Roy. Soc. (London)* Ser. A261, pp. 532-550, 1961.
- 21 **B. Hamrock and D. Dowson**, "Isothermal Elastohydrodynamic Lubrication of Point Contacts—Part III—Fully Flooded Results," *ASME J. Lubr. Technol.*, 99: pp. 264-276, 1977.
- 22 **D. Dowson and G. Higginson**, *Proceedings of Institution of Mechanical Engineers*, 182 (Part 3A): pp. 151-167, 1968.
- 23 **T. A. Harris**, *Rolling Bearing Analysis*. John Wiley & Sons: New York, pp. 872-888, 1991.
- 24 *Load Ratings and Fatigue Life for Ball Bearings*, ANSI/AFBMA Standard 9-1990, American National Standards Institute, New York, 1990.
- 25 *Load Ratings and Fatigue Life for Roller Bearings*, ANSI/AFBMA Standard 11-1990, American National Standards Institute, New York, 1990.
- 26 **B. J. Hamrock**, *Fundamentals of Fluid Film Lubrication*. McGraw-Hill: New York, p. 16, 1994.
- 27 ASME Research Committee on Lubrication "Pressure-Viscosity Report—Vol. 11," *ASME*, 1953.
- 28 **T. E. Tallian**, "Lubricant Films in Rolling Contact of Rough Surfaces," *ASLE Trans.*, 7(2): pp. 109-126, 1964.
- 29 **E. N. Bamberger, et al.**, "Life Adjustment Factors for Ball and Roller Bearings," *ASME Engineering Design Guide*, 1971.
- 30 **R. Barnsby, et al.**, "Life Ratings for Modern Rolling Bearings," *ASME International*, 2003.

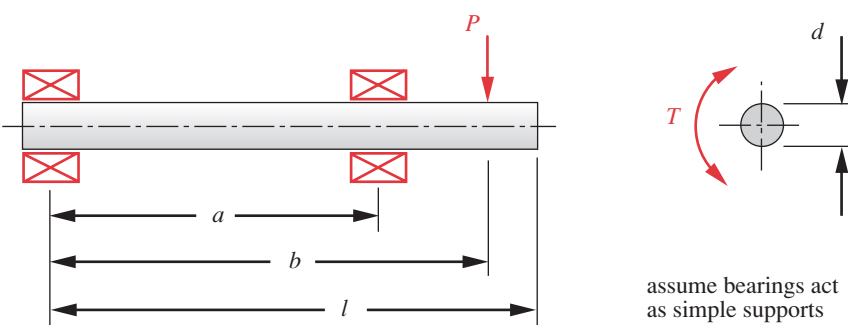


FIGURE P11-1

Shaft Design for Problem 11-1

11.16 PROBLEMS

***11-1** The shaft shown in Figure P11-1 was designed in Problem 10-1. For the data in the row(s) assigned from Table P11-1, and the corresponding diameter of shaft found in Problem 10-1, design suitable bearings to support the load for at least 7E7 cycles at 1 500 rpm. State all assumptions.

- (a) Using hydrodynamically lubricated bronze sleeve bearings with $O_N = 20$, $l/d = 1.25$, and a clearance ratio of 0.0015.
- (b) Using deep-groove ball bearings for a 10% failure rate.

11-2 The shaft shown in Figure P11-2 was designed in Problem 10-2. For the data in the row(s) assigned from Table P11-1, and the corresponding diameter of shaft found in Problem 10-2, design suitable bearings to support the load for at least 3E8 cycles at 2 500 rpm. State all assumptions.

- (a) Using hydrodynamically lubricated bronze sleeve bearings with $O_N = 30$, $l/d = 1.0$, and a clearance ratio of 0.002.
- (b) Using deep-groove ball bearings for a 10% failure rate.

***11-3** An oil has a kinematic viscosity of 300 centistokes. Find its absolute viscosity in centipoise (cP). Assume a specific gravity of 0.89.

11-4 An oil has an absolute viscosity of $2 \mu\text{rey}$. Find its kinematic viscosity in in^2/sec . Assume a specific gravity of 0.87.

***11-5** Find the Petroff no-load torque for the journal bearing designed in Case Study 10B.

***11-6** Find the minimum film thickness for a long bearing with: 45-mm dia, 200 mm long, $\epsilon = 0.55$, clearance ratio = 0.001, 2500 rpm, ISO VG 46 oil at 150°F.

Table P11-0[†]

Topic/Problem Matrix

11.2 Viscosity

11-3, 11-4, 11-23, 11-24

11.5 Lubrication Theory

11-5, 11-6, 11-7, 11-9, 11-10,
11-11, **11-12**, 11-13, 11-14,
11-15, 11-25, 11-39 to 11-42

11.6 Hydrodynamic Bearings

11-1a, **11-2a**, **11-8**, **11-17a**,
11-19a

11.7 EHD Contact

11-16, 11-18, 11-20, 11-21,
11-43

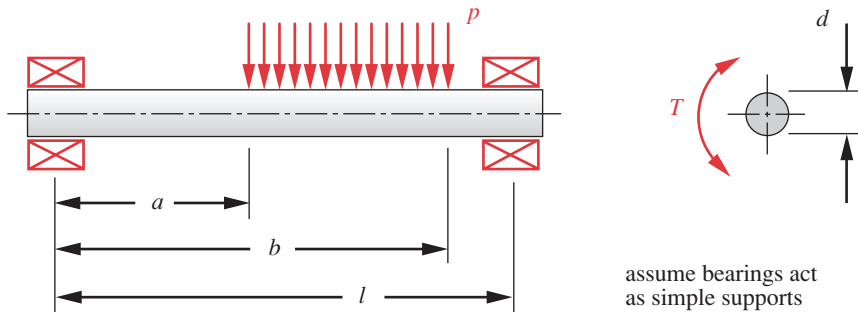
11.10 Rolling Contact

11-1b, **11-2b**, **11-17b**, **11-19b**,
11-22, 11-26, 11-27, 11-28,
11-29, 11-30, 11-31, 11-32,
11-33, 11-34, 11-35, 11-36,
11-37, 11-38, 11-44, 11-45**Table P11-1 Data for Problems**

Row	<i>l</i>	<i>a</i>	<i>b</i>	<i>P</i> or <i>p</i>	<i>T</i> _{min}	<i>T</i> _{max}
<i>a</i>	20	16	18	1000	0	2000
<i>b</i>	12	2	7	500	-100	600
<i>c</i>	14	4	12	750	-200	400
<i>d</i>	8	4	8	1000	0	2000
<i>e</i>	17	6	12	1500	-200	500
<i>f</i>	24	16	22	750	1000	2000

* Answers to these problems are provided in Appendix D.

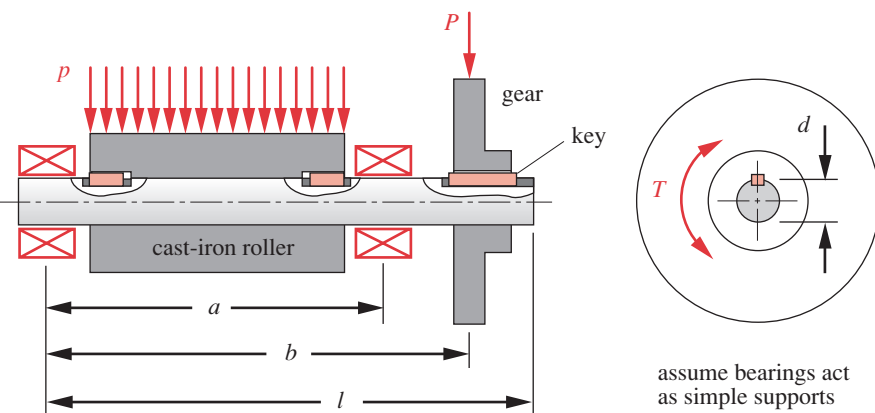
[†] Problem numbers in *italics* are design problems. Problem numbers in **boldface** are extended from similar problems in earlier chapters with the same dash number.

**FIGURE P11-2**

Shaft Design for Problem 11-2

- *11-7 Find the torques and power lost in the bearing of Problem 11-6.
- *11-8** A paper machine processes rolls of paper having a density of 984 kg/m^3 . The paper roll is 1.50-m *OD* \times 22-cm *ID* \times 3.23-m long and is on a simply supported, 22-cm *OD*, steel shaft. The roll turns at 50 rpm. Design suitable hydrodynamically lubricated full-film bronze short bearings of $l/d = 0.75$ to support the shaft at each end. Specify the viscosity of lubricant needed at 180°F . State all assumptions.
- 11-9 Find the minimum film thickness for a long bearing with the following data: 30-mm dia, 130 mm long, 0.0015 clearance ratio, 1 500 rpm, ISO VG 100 oil at 200°F , and supporting a load of 7 kN.
- *11-10 Find the minimum film thickness for a bearing with these data: 45-mm dia, 30 mm long, 0.001 clearance ratio, 2 500 rpm, $O_N = 25$, ISO VG 46 oil at 150°F .
- 11-11 Find the minimum film thickness for a bearing with these data: 30-mm dia, 25 mm long, 0.0015 clearance ratio, 1 500 rpm, $O_N = 30$, ISO VG 220 oil at 200°F .
- 11-12** Problem 7-12 estimated the volume of adhesive wear to expect from a steel shaft of 40 mm dia rotating at 250 rpm for 10 years in a plain bronze bushing with a transverse load of 1 000 N for conditions of both poor and good lubrication. If the bushing has $l/d = 0.5$ and a clearance ratio of 0.001, define the lubricant viscosity in microreyn (μreyn) needed to obtain good lubrication.
- 11-13 Find the torques and power lost in the bearing of Problem 11-9.
- *11-14 Find the torques and power lost in the bearing of Problem 11-10.
- 11-15 Find the torques and power lost in the bearing of Problem 11-11.
- 11-16** Problem 7-16 determined the half-width of the contact patch for a 0.787-in-dia steel ball rolled against a flat aluminum plate with 224.81 lb of force to be 0.020 in. Assuming the ball rolls at 1 200 rpm, determine its lubrication condition with ISO VG 68 oil at 150°F . Assume $R_q = 16 \mu\text{in}$ (ball), $R_q = 64 \mu\text{in}$ (plate).
- *11-17** The shaft shown in Figure P11-3 was designed in Problem 10-17. For the data in the row(s) assigned from Table P11-1, and the corresponding diameter of shaft found in Problem 10-17, design suitable bearings to support the load for at least $1E8$ cycles at 1800 rpm. State all assumptions.
- Using hydrodynamically lubricated bronze sleeve bearings with $O_N = 15$, $l/d = 0.75$, and a clearance ratio of 0.001.
 - Using deep-groove ball bearings for a 10% failure rate.

* Answers to these problems are provided in Appendix D. Problem numbers in *italics* are design problems. Problem numbers in **boldface** are extended from similar problems in earlier chapters with the same dash number.

**FIGURE P11-3**

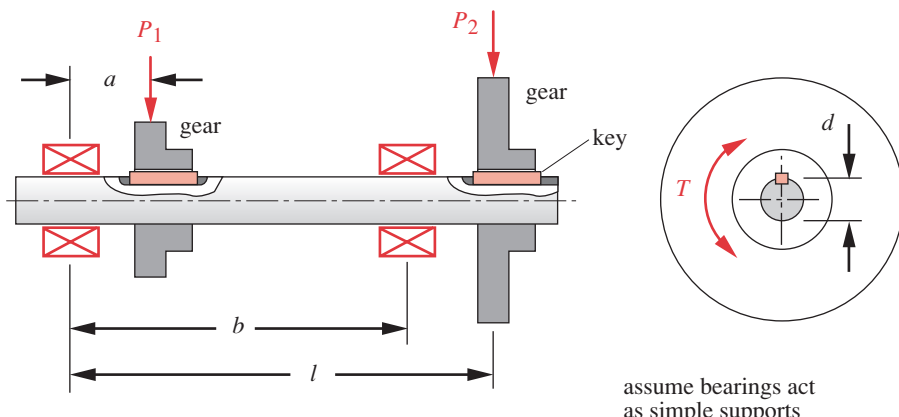
Shaft Design for Problems 11-17

- 11-18** Problem 7-18 determined the half-width of the contact patch for a 1.575-in-dia steel cylinder, 9.843 in long, rolled against a flat aluminum plate with 900 lb of force to be 0.0064 in. If the cylinder rolls at 800 rpm, determine its lubrication condition with ISO VG 1000 oil at 200°F. $R_q = 64 \mu\text{in}$ (cylinder); $R_q = 32 \mu\text{in}$ (plate).

- 11-19** The shaft shown in Figure P11-4 was designed in Problem 10-19. For the data in the row(s) assigned from Table P11-1, and the corresponding diameter of shaft found in Problem 10-19, design suitable bearings to support the load for at least $5E8$ cycles at 1200 rpm. State all assumptions.

- Using hydrodynamically lubricated bronze sleeve bearings with $O_N = 40$, $l/d = 0.80$, and a clearance ratio of 0.0025.
- Using deep-groove ball bearings for a 10% failure rate.

- *11-20** Problem 7-20 determined the half-dimensions of the contact patch for a 0.787-in-dia steel ball rolled against a 1.575-in-dia steel cylinder with 2 248 lb force to be $a = 0.037$ in and $b = 0.028$ in. The ball rolls at 1 800 rpm. Determine its lubrication condition with ISO VG 460 oil at 120°F. Assume $R_q = 32 \mu\text{in}$ for both.

**FIGURE P11-4**

Shaft Design for Problems 11-19 and 11-22

* Answers to these problems are provided in Appendix D. Problem numbers in *italics* are design problems. Problem numbers in **boldface** are extended from similar problems in earlier chapters with the same dash number.

- 11-21** Problem 7-21 determined the half-dimensions of the contact patch for a cam-follower system with a dynamic load of 0 to 450 lb to be $a = 0.080$ in and $b = 0.013$ in. The cam is cylindrical with a minimum radius of curvature of 0.787 in. The 1-in-dia roller follower is crowned with a 6-in radius in the other direction. Find the specific film thickness and lubrication condition between cam and follower if lubricated with an ISO VG 1500 oil at 200°F. Assume $R_q = 8 \mu\text{in}$ (follower), $R_q = 32 \mu\text{in}$ (cam). Follower rpm = 300.
- 11-22** The shaft shown in Figure P11-4 was designed in Problem 10-19. For the data in row (a) of Table P11-1, and the corresponding diameter of shaft found in Problem 10-19, design suitable bearings to support the load for at least $5E8$ cycles at 1 200 rpm using deep-groove ball bearings. In addition to the radial loads found in Problem 10-19, the right bearing supports an axial load that is 120% of the concentrated transverse load P . The shaft diameter is 1.153 in, the L_{10} design life is $500E6$ revolutions, and the concentrated transverse load is 1 000 lb. Assume an axial-force factor = 1.2 and a shaft-rotation factor = 1.0. Also assume that the shaft diameter can be reduced at the left bearing where the moment is zero.
- 11-23** An ISO VG 100 oil has a bulk temperature of 80°C. Find its absolute viscosity in centipoise (cP) and its kinematic viscosity in centistokes (cS). Assume a specific gravity of 0.91.
- 11-24** An ISO VG 68 oil has a bulk temperature of 175°F. Find its absolute viscosity in microreyn (μreyn) and its kinematic viscosity in in^2/sec . Assume a specific gravity of 0.90.
- 11-25** A journal and bearing are to be designed for a shaft that turns at 200 rpm. Oil that has a viscosity of $2 \mu\text{reyn}$ is to be used and the bearing length is to be equal to the diameter. If the no-load power loss is not to exceed $2E-04$ horsepower and the diametral clearance is 0.004 times the diameter, estimate the maximum diameter that can be used for the journal.
- 11-26** Figure P11-5 shows a stepped shaft supported by two 6300-series bearings. Two gears with equal and opposite torque are keyed to the shaft as shown. The load on each gear consists of a radial component and a tangential component, which acts at diameter D . The radial component on each gear is 0.466 times the tangential component on that gear. Note that the gear loads are 90 degrees out of phase from gear 1 to gear 2. For the data in the row(s) assigned from Table P11-2, select a suitable bearing (from Figure 11-23 for a 10% failure rate) for bearing 1. Choose the bearing that has the least bore diameter and meets the load-rating requirement. Specify bearing number, bore, OD , width (all in mm) and the basic dynamic load rating of the bearing. Ignore the axial load given in the table.
- 11-27** Figure P11-5 shows a stepped shaft supported by two 6300-series bearings. Two gears with equal and opposite torque are keyed to the shaft as shown. The load on each gear consists of a radial component and a tangential component, which acts at diameter D . The radial component on each gear is 0.466 times the tangential component on that gear. Note that the gear loads are 90 degrees out of phase from gear 1 to gear 2. For the data in the row(s) assigned from Table P11-2, select a suitable bearing (from Figure 11-23 for a 10% failure rate) for bearing 2. Choose the bearing that has the least bore diameter and meets the load-rating requirement. Specify bearing number, bore, OD , width (all in mm) and the basic dynamic load rating of the bearing. Ignore the axial load given in the table.
- 11-28** Repeat Problem 11-26 with the axial force F_a given in the row(s) assigned in Table P10-2 acting on gear 1.
- 11-29** Repeat Problem 11-27 with the axial force F_a given in the row(s) assigned in Table P10-2 acting on gear 2.

Problem numbers in *italics* are design problems. Problem numbers in **boldface** are extended from similar problems in earlier chapters with the same dash number.

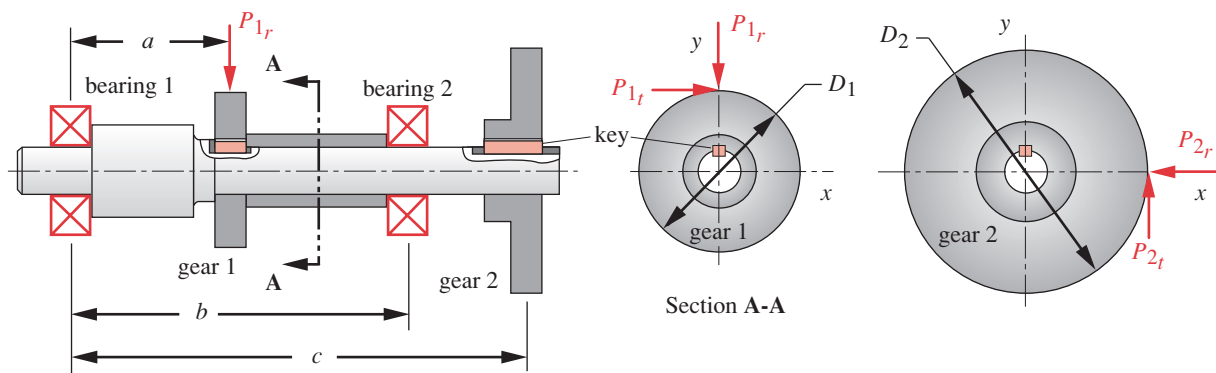
Table P11-2 Data for Problems 11-26 through 11-29

Row	a in	b in	c in	P_{It} lb	D_I in	D_2 in	Design L_{10}^*	F_a lb
a	4.0	8.0	12.0	2000	2.00	4.00	80	800
b	2.0	6.0	10.0	1800	1.80	2.50	60	900
c	3.0	5.0	8.0	2500	2.25	3.50	75	1200
d	2.0	5.0	10.0	2100	2.00	3.80	70	1000
e	1.5	4.5	7.5	2800	1.50	3.00	65	1200
f	2.5	5.0	8.0	1500	1.75	2.75	50	850

* millions of revolutions

- 11-30 Repeat Problem 11-1(b) using a failure rate of 5%.
- 11-31 Repeat Problem 11-2(b) using a failure rate of 4%.
- 11-32 Repeat Problem 11-17(b) using a failure rate of 3%.
- *11-33 Repeat Problem 11-19(b) using a failure rate of 2%.
- 11-34 Repeat Problem 11-26 using a failure rate of 5%.
- 11-35 Repeat Problem 11-27 using a failure rate of 4%.
- *11-36 Repeat Problem 11-22 using a failure rate of 5%.
- 11-37 Repeat Problem 11-28 using a failure rate of 4%.
- 11-38 Repeat Problem 11-29 using a failure rate of 3%.
- 11-39 A short journal bearing has the following characteristics: $d = 48.6$ mm, $l = 50$ mm, diametral clearance ratio = 0.002. While running under load with a velocity of $U = 6.36$ m/s and a lubricant of viscosity of $\eta = 2.30$ cP the eccentricity ratio is $\varepsilon = 0.807$. Plot the pressure distribution in the bearing as a function of θ for $z = 0$, and as a function of z for $\theta = \theta_{max}$.

* Answers to these problems are provided in Appendix D. Problem numbers in *italics* are design problems. Problem numbers in **boldface** are extended from similar problems in earlier chapters with the same dash number.



assume bearings act as simple supports

FIGURE P11-5

Gear and Bearing Arrangement for Problems 11-26 through 11-29

- 11-40 A short journal bearing has the following characteristics: $d = 40.0$ mm, $l = 30$ mm, diametral clearance ratio = 0.001. While running under load with a velocity of $U = 3.77$ m/s and a lubricant of viscosity of $\eta = 20.66$ cP the eccentricity ratio is $\epsilon = 0.703$. Plot the pressure distribution in the bearing as a function of θ for $z = 0$, and as a function of z for $\theta = \theta_{max}$.
- 11-41 For the bearing and conditions of Problem 11-39, determine
- the angle ϕ of the line of centers with respect to the direction of the applied load
 - the dimensionless parameter, K_e
 - the magnitude of the applied load, P
 - the rotating torque, T_r .
- 11-42 For the bearing and conditions of Problem 11-40, determine
- the angle ϕ of the line of centers with respect to the direction of the applied load
 - the dimensionless parameter, K_e
 - the magnitude of the applied load, P
 - the rotating torque, T_r .
- 11-43 Problem 7-32 determined the half-dimensions of the contact patch for two steel gears in mesh with a contact force of 1500 lb to be $a = 0.0177$ in and $b = 0.3125$ in (half-width of a tooth face). The gears are modeled as two cylinders in contact with radii of 2.500 in (driver) and 5.000 in (driven gear). Find the specific film thickness and lubrication condition between the two teeth in contact if lubricated with an ISO VG 1000 oil at 120F. Assume both teeth have $R_q = 4 \mu\text{in}$. The tangential velocities of the gear teeth are 55.6 in/sec (driver) and 57.8 in/sec (driven).
- 11-44 Select a deep-groove ball bearing from Figure 11-23 for a radial load of 1500 lb, an axial load of 450 lb, and outer race rotation. An L_5 life of 500 million revolutions is desired.
- 11-45 Select a deep-groove ball bearing from Figure 11-23 for a radial load of 600 lb, an axial load of 150 lb, and inner race rotation. An L_{10} life of 180 million revolutions is desired.

12

SPUR GEARS

The beginning of wisdom is to call things by their right names.

CHINESE PROVERB

Tim was so learned that he could name a horse in nine languages: so ignorant that he bought a cow to ride on.

BENJAMIN FRANKLIN



12.0 INTRODUCTION

Gears are used to transmit torque and angular velocity in a wide variety of applications. There is also a wide variety of gear types to choose from. This chapter will deal with the simplest type of gear, the spur gear, designed to operate on parallel shafts and having teeth parallel to the shaft axis. Other gear types such as helical, bevel, and worm can accommodate nonparallel shafts. These will be dealt with in the next chapter.

Gears are now highly standardized as to tooth shape and size. The *American Gear Manufacturers Association* (AGMA) supports research in gear design, materials, and manufacturing and publishes standards for their design, manufacture, and assembly.^[1, 2, 3] We will follow the AGMA methods and recommendations as defined in those standards.

Gears have a long history. The ancient Chinese *South-Pointing Chariot*, supposedly used to navigate across the Gobi desert in pre-Biblical times, contained gears. Leonardo DaVinci shows many gear arrangements in his drawings. Early gears were most likely made crudely of wood and other easily worked materials, their teeth merely being pegs inserted in a disk or wheel. It was not until the industrial revolution that machines demanded, and manufacturing techniques allowed, the creation of gears as we now know them with specially shaped teeth formed or cut into a metal disk.

There is a great deal of specialized terminology for gears, and it is necessary that the reader become familiar with these terms. As indicated in the above epigraphs, calling things by their correct names is important but is not sufficient to ensure complete understanding of the topic. The variables used in this chapter are listed in Table 12-0.

Table 12-0 Variables Used in This Chapter

Part 1 of 2

Symbol	Variable	ips units	SI units	See
a	addendum	in	m	Fig. 12-8
b	dedendum	in	m	Fig. 12-8
C	center distance	in	m	Eq. 12.22b
C_f	surface-finish factor	none	none	Sect. 12.8
C_H	hardness factor	none	none	Eq. 12.26, -27
C_p	elastic coefficient	none	none	Eq. 12.23
d	pitch diameter	in	m	various
F	face width	in	m	Eq. 12.14
HB	Brinell hardness	none	none	Sect. 12.8
I	AGMA surface-geometry factor	none	none	Eq. 12.22a
J	AGMA bending-geometry factor	none	none	Sect. 12.8
K_a, C_a	application factor	none	none	Sect. 12.8
K_B	rim-bending factor	none	none	Sect. 12.8
K_I	idler factor	none	none	Eq. 12.15
K_L, C_L	life factor	none	none	Fig. 12-24, -26
K_m, C_m	load-distribution factor	none	none	Sect. 12.8
K_R, C_R	reliability factor	none	none	Table 12-19
K_s, C_s	size factor	none	none	Sect. 12.8
K_T, C_T	temperature factor	none	none	Eq. 12.24a
K_v, C_v	dynamic factor	none	none	Sect. 12.8
m	module	—	mm	Eq. 12.4c
M	moment, moment function	lb-in	N-m	Fig. 12-21
m_A	mechanical advantage	none	none	Eq. 12.1b
m_G	gear ratio	none	none	Eq. 12.1c
m_p	contact ratio	none	none	Eq. 12.7a
m_V	angular velocity ratio	none	none	Eq. 12.1a
N	number of cycles or number of teeth	none	none	Fig. 12.24
N_b, N_c	factors of safety—bending and contact	none	none	various
p_b	base pitch	in	m	Eq. 12.3b
p_c	circular pitch	in	m	Eq. 12.3a
p_d	diametral pitch	1/in	—	Eq. 12.4a
Q_v	gear-quality index	none	none	Fig. 12-22
r	pitch radius	in	m	various
S_{fb}	corrected bending-endurance strength	psi	Pa	Eq. 12.24
$S_{fb'}$	uncorrected bending-endurance strength	psi	Pa	Eq. 12.24
S_{fc}	corrected surface-endurance strength	psi	Pa	Eq. 12.25
$S_{fc'}$	uncorrected surface-endurance strength	psi	Pa	Eq. 12.25
T	torque	lb-in	N-m	Eq. 12.13a
V_t	pitch-line velocity	in/sec	m/sec	Eq. 12.16

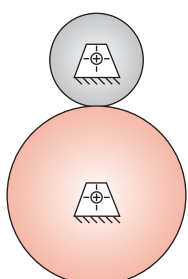
Title page photograph courtesy of Boston Gear, Division of IMO Industries, Quincy, Mass.

Portions of this chapter including Figures 12-1 through 12-8, 12-11, 12-13 through 12-16 and their discussions are adapted from R. L. Norton, *Design of Machinery*, 4ed. McGraw-Hill, 2008, Chapter 10, with the publisher's permission.

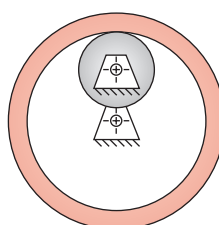
Table 12-0 Variables Used in This Chapter

Part 2 of 2

Symbol	Variable	ips units	SI units	See
W	total force on gear teeth	lb	N	Eq. 12.13c
W_r	radial force on gear teeth	lb	N	Eq. 12.13b
W_t	tangential force on gear teeth	lb	N	Eq. 12.13a
x_1, x_2	addendum modification coefficients	none	none	Sect. 12.3
Y	Lewis form factor	none	none	Eq. 12.14
Z	length of action	in	m	Eq. 12.2
ϕ	pressure angle	deg	deg	various
ρ	radius of curvature	in	m	Eq. 12.22b
σ_b	bending stress	psi	Pa	Eq. 12.15
σ_c	surface stress	psi	Pa	Eq. 12.21
ω	angular velocity	rad/sec	rad/sec	Eq. 12.1a



(a) External set



(b) Internal set

12.1 GEAR TOOTH THEORY

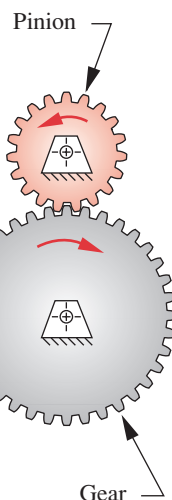
The simplest means of transferring rotary motion from one shaft to another is a pair of rolling cylinders. They may be an external set of rolling cylinders, as shown in Figure 12-1a, or an internal set, as in Figure 12-1b. If sufficient friction is available at the rolling interface, this mechanism will work quite well. There will be no slip between the cylinders until the maximum available frictional force at the joint is exceeded by the demands of torque transfer.

The principal drawbacks to the rolling-cylinder drive mechanism are its relatively low torque capability and the possibility of slip. Some drives require absolute phasing of the input and output shafts for timing purposes. This requires adding some meshing teeth to the rolling cylinders. They then become gears, as shown in Figure 12-2, and are together called a *gearset*. When two gears are placed in mesh to form a gearset such as this one, it is conventional to refer to the *smaller of the two gears as the pinion* and to the other as the *gear*.

The Fundamental Law of Gearing

Conceptually, teeth of any shape will prevent gross slip. Old water-powered mills and windmills used wooden gears whose teeth were merely round wooden pegs stuck into the rims of the cylinders. Even ignoring the crudity of construction of these early examples of gearsets, there was no possibility of smooth velocity transmission because the geometry of the tooth "pegs" violated the **fundamental law of gearing**, which states that *the angular velocity ratio between the gears of a gearset must remain constant throughout the mesh*. The angular velocity ratio m_V is equal to the ratio of the pitch radius of the input gear to that of the output gear.

$$m_V = \frac{\omega_{out}}{\omega_{in}} = \pm \frac{r_{in}}{r_{out}} \quad (12.1a)$$

**FIGURE 12-2**

An External Gearset

FIGURE 12-1

Rolling Cylinders

The pitch radii in equation 12.1a are those of the rolling cylinders to which we are adding the teeth. The positive or negative sign accounts for internal or external cylinder sets as shown in Figure 12-1. An external set reverses the direction of rotation between the cylinders and requires the negative sign. An internal gearset (and a belt or chain drive) will have the same direction of rotation on input and output shafts and require the positive sign in equation 12.1a. The surfaces of the rolling cylinders will become the **pitch circles**, and their diameters the **pitch diameters** of the gears. The contact point between the cylinders lies on the line of centers, as shown in Figure 12-4, and this point is called the **pitch point**.

Torque ratio or mechanical advantage m_A is the reciprocal of the velocity ratio m_V :

$$m_A = \frac{1}{m_V} = \frac{\omega_{in}}{\omega_{out}} = \pm \frac{r_{out}}{r_{in}} \quad (12.1b)$$

Thus a gearset is essentially a device to exchange torque for velocity or vice versa. A common gearset application reduces velocity and increases torque to drive heavy loads, as in your automobile transmission. Other applications require an increase in velocity, for which a reduction in torque must be accepted. In either case, it is usually desirable to maintain a constant ratio between the gears as they rotate. Any variation in ratio will show up as oscillation in the output velocity and torque, even if the input is constant with time.

For calculation purposes, the **gear ratio** m_G is taken as the magnitude of either the velocity ratio or the torque ratio, whichever is > 1 .

$$m_G = |m_V| \text{ or } m_G = |m_A|, \text{ for } m_G \geq 1 \quad (12.1c)$$

In other words, the gear ratio is always a positive number > 1 regardless of the direction in which the power flows through the gearset.

In order for the fundamental law of gearing to be true, the gear tooth contours on mating teeth must be conjugates of one another. There is an infinite number of possible conjugate pairs that could be used, but only a few curves have seen practical application as gear teeth. The **cycloid** is still used as a tooth form in some watches and clocks, but most gears use the **involute** of a circle for their shape.

The Involute Tooth Form

The involute of a circle is a curve that can be generated by unwrapping a taut string from a cylinder, as shown in Figure 12-3. Note the following about this involute curve:

- 1 The string is always tangent to the base circle.
- 2 The center of curvature of the involute is always at the point of tangency of the string with the base circle.
- 3 A tangent to the involute is always normal to the string, which is the instantaneous radius of curvature of the involute curve.

Figure 12-4 shows two involutes on separate cylinders in contact or “in mesh.” These represent gear teeth. The cylinders from which the strings are unwrapped are called the **base circles** of the respective gears. Note that the base circles are necessar-

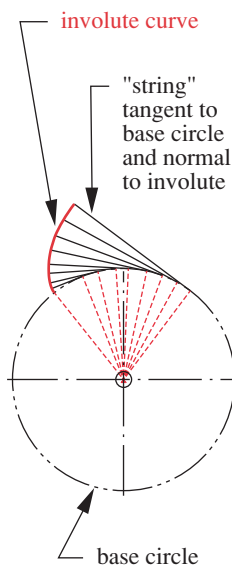
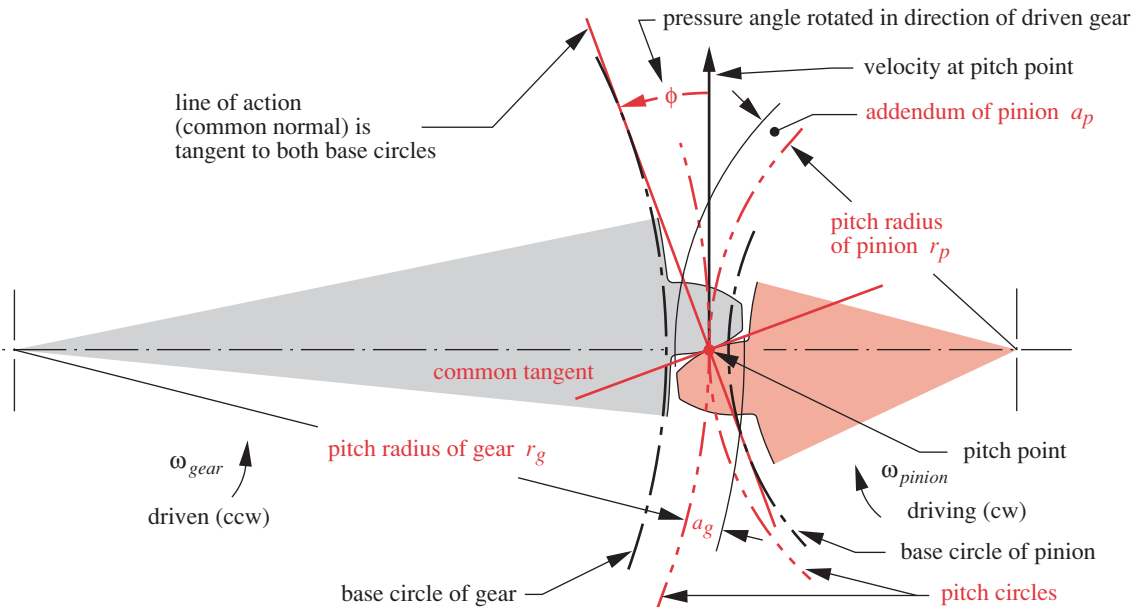


FIGURE 12-3

Development of the Involute of a Circle

**FIGURE 12-4**

Contact Geometry and Pressure Angle of Involute Gear Teeth

ily smaller than the pitch circles, which are at the radii of the original rolling cylinders, r_p and r_g . The gear tooth must project both below and above the rolling-cylinder surface (pitch circle), and the *involute only exists outside of the base circle*. The amount of tooth that sticks out above the pitch circle is the **addendum**, shown as a_p and a_g for pinion and gear, respectively. These are equal for standard, full-depth gear teeth.

There is a **common tangent** to both involute tooth curves at the contact point, and a common normal, perpendicular to the common tangent. Note that the common normal is, in fact, the “strings” of both involutes, which are colinear. Thus the **common normal**, which is also the **line of action**, always passes through the **pitch point** regardless of where in the mesh the two teeth are contacting. The pitch point has the same linear velocity in both pinion and gear, called the **pitch-line velocity**. The angle between the line of action and the velocity vector is the **pressure angle** ϕ .

Pressure Angle

The **pressure angle** ϕ in a gearset is defined as the angle between the line of action (common normal) and the direction of velocity at the pitch point such that the line of action is rotated ϕ degrees in the direction of rotation of the driven gear, as shown in Figures 12-4 and 12-5. Pressure angles of gearsets are standardized at a few values by the gear manufacturers. These are defined at the nominal center distance for the gearset as cut. The standard values are 14.5, 20, and 25°, with 20° being the most commonly used and 14.5° now being obsolete. Any custom pressure angle can be made, but its expense over the available stock gears with standard pressure angles would be hard to justify. Special cutters would have to be made. Gears to be run together must be cut to the same nominal pressure angle.

Gear Mesh Geometry

Figure 12-5 shows a pair of involute tooth forms in two positions, just beginning contact and about to leave contact. The common normals of both these contact points still pass through the same pitch point. It is this property of the involute that causes it to obey the fundamental law of gearing. The ratio of the driving-gear radius to the driven-gear radius remains constant as the teeth move into and out of mesh.

From this observation of the behavior of the involute we can restate the **fundamental law of gearing** in a more kinematically formal way as: *the common normal of the tooth profiles, at all contact points within the mesh, must always pass through a fixed point on the line of centers, called the pitch point*. The gearset's velocity ratio will then be a constant defined by the ratio of the respective radii of the gears to the pitch point.

The points of beginning and leaving contact define the **mesh** of the pinion and gear. The distance along the line of action between these points within the mesh is called the **length of action** Z , defined by the intersections of the respective addendum circles with the line of action, as shown in Figure 12-5. The distance along the pitch circle within the mesh is the **arc of action**, and the angles subtended by these points and the line of centers are the **angle of approach** and **angle of recess**. These are shown only on the gear in Figure 12-5 for clarity, but similar angles exist for the pinion. The arc of action on both pinion and gear pitch circles must be the same length for zero slip between the theoretical rolling cylinders. The length of action Z can be calculated from the gear and pinion geometry:

$$Z = \sqrt{(r_p + a_p)^2 - (r_p \cos \phi)^2} + \sqrt{(r_g + a_g)^2 - (r_g \cos \phi)^2} - C \sin \phi \quad (12.2)$$

where r_p and r_g are the pitch circle radii, and a_p and a_g the addenda of pinion and gear, respectively. C is the center distance and ϕ is the pressure angle.

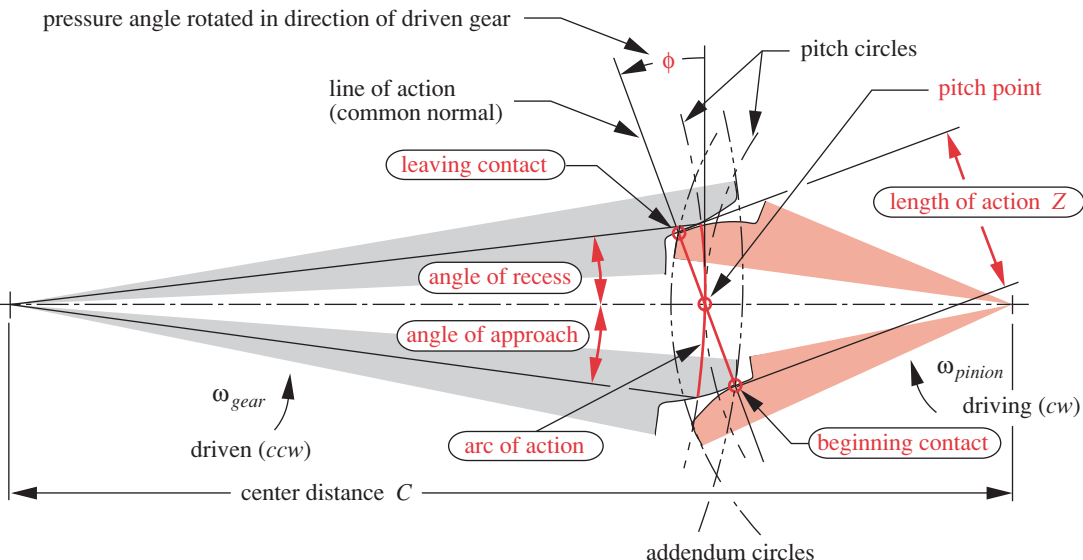


FIGURE 12-5

Length of Action, Arc of Action, and Angles of Approach and Recess During the Meshing of a Gear and Pinion

Rack and Pinion

If the diameter of the base circle of a gear is increased without limit, the base circle will become a straight line. If the “string” wrapped around this base circle to generate the involute were still in place after the base circle’s enlargement to an infinite radius, the string would be pivoted at infinity and would generate an involute that is a straight line. This linear gear is called a **rack**. Figure 12-6 shows a rack and pinion and the geometry of a standard, full-depth rack. Its teeth are trapezoids, yet are true involutes. This fact makes it easy to create a cutting tool to generate involute teeth on circular gears, by accurately machining a rack and hardening it to cut teeth in other gears. This is another advantage of the involute tooth form. Rotating the gear blank with respect to the rack cutter while moving the cutter axially back and forth across the gear blank will shape, or develop, a true involute tooth on the circular gear.

The most common application of the rack and pinion is in rotary-to-linear motion conversion or vice versa. It can be backdriven, so it requires a brake if used to hold a load. An example of its use is in rack-and-pinion steering in automobiles. The pinion is attached to the bottom end of the steering column and turns with the steering wheel. The rack meshes with the pinion and is free to move left and right in response to your angular input at the steering wheel. The rack is also one link in a multibar linkage, which converts the linear translation of the rack to the proper amount of angular motion of a rocker link attached to the front-wheel assembly in order to steer the car.

Changing Center Distance

When involute teeth (or any teeth) have been cut into a cylinder with respect to a particular base circle to create a single gear, we do not yet have a pitch circle. The pitch circle comes into being only when we mate this gear with another to create a *pair of gears*, or **gearsset**. There will be some range of center-to-center distances over which we can achieve a mesh between the gears. There will also be an ideal center distance that will give us the nominal pitch diameters for which the gears were designed. However, the limitations of the manufacturing process give a low probability that we will be able to exactly achieve this ideal center distance in every case. More likely, there will be some error in the center distance, even if small.

If the gear tooth form is **not** an involute, then an error in center distance will cause variation, or “ripple,” in the output velocity. The output angular velocity will then not

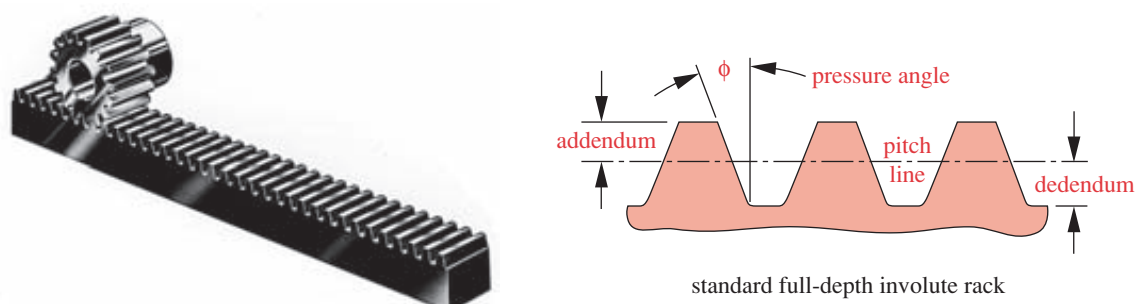
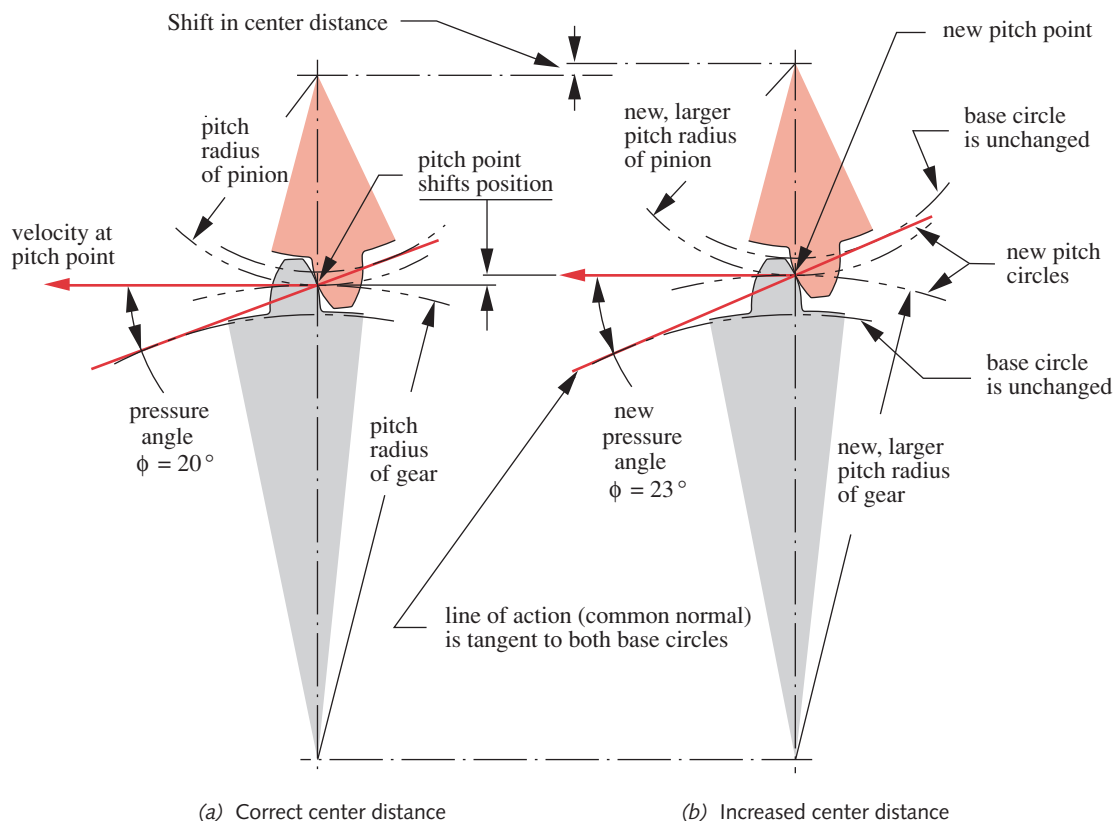


FIGURE 12-6

A Rack and Pinion *Photo Courtesy of Martin Sprocket and Gear Co., Austin, Tex.*

be constant for a constant input velocity, violating the fundamental law of gearing. However, with an **involute tooth form**, *center-distance errors do not affect the velocity ratio*. This is the principal advantage of the involute over all other possible tooth forms and is the reason why it is nearly universally used for gear teeth. Figure 12-7 shows what happens when the center distance is varied on an involute gearset. Note that the common normal still goes through the pitch point, and also through all contact points within the mesh. Only the pressure angle is affected by the change in center distance.

Figure 12-7 also shows the pressure angles for two different center distances. As the center distance increases, so will the pressure angle and vice versa. This is one result of a change, or error, in center distance when using involute teeth. Note that the fundamental law of gearing still holds in the modified center distance case. The common normal is still tangent to the two base circles and still goes through the pitch point. The pitch point has moved in proportion to the shifts of the center distance and the pitch radii. The velocity ratio is unchanged despite the shift in center distance. In fact, the velocity ratio of involute gears is fixed by the ratio of their base-circle diameters, which are unchanging once the gear is cut.

**FIGURE 12-7**

Changing Center Distance of Involute Gears Changes Only the Pressure Angle and Pitch Diameters

Backlash

Another factor affected by changing center distance C is backlash. Increasing C will increase the backlash and vice versa. **Backlash** is defined as *the gap between mating teeth measured along the circumference of the pitch circle*. Manufacturing tolerances preclude a zero backlash, as all teeth cannot be exactly the same dimensions, and all must mesh without jamming. So, there must be some small difference between the tooth thickness and the space width, (see Figure 12-8 overleaf). As long as the gearset is run with a nonreversing torque, the backlash should not be a problem. However, whenever the torque changes sign, the teeth will move from contact on one side to the other. The backlash gap will be traversed and the teeth will impact with noticeable noise and vibration. As well as increasing stresses and wear, backlash can cause undesirable positional error in some applications.

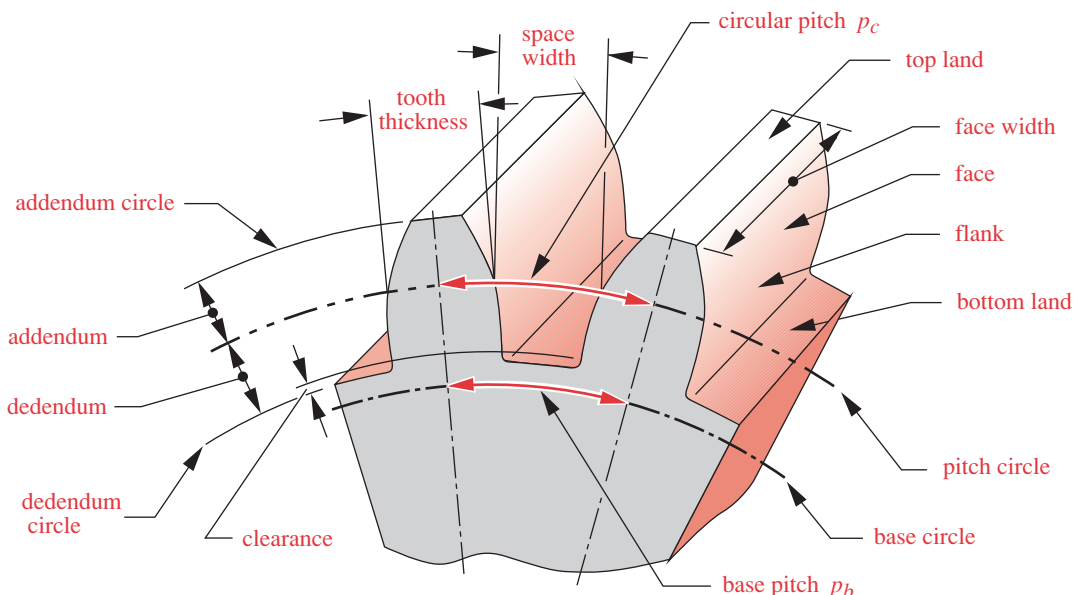
In servomechanisms, where motors are driving, for example, the control surfaces on an aircraft, backlash can cause potentially destructive “hunting” in which the control system tries in vain to correct the positional errors due to the backlash “slop” in the mechanical drive system. Such applications need **antibacklash gears**, which are really two gears back-to-back on the same shaft that can be rotated slightly at assembly (or by springs) with respect to one another, so as to take up the backlash. In less critical applications, such as the propeller drive on a boat, backlash on torque reversal will not even be noticed.

Relative Tooth Motion

The relative motion between involute teeth is pure rolling at the pitch point. At points on the tooth away from the pitch point, some sliding occurs in combination with rolling. The average amount of sliding in an involute-tooth mesh is about 9%, as discussed in Section 7.13 (p. 464). The surface stresses are increased by the sliding component, as discussed in Section 7.11 (p. 453). Table 7-7 (p. 466-467) shows surface fatigue-strength data developed from extensive testing of rolling plus 9% sliding between various material combinations.

12.2 GEAR TOOTH NOMENCLATURE

Figure 12-8 shows two teeth of a gear with the standard nomenclature defined. **Pitch circle** and **base circle** have been defined above. The tooth height is defined by the **addendum** (*added on*) and the **dedendum** (*subtracted from*), which are referenced to the nominal pitch circle. The dedendum is slightly larger than the addendum to provide a small amount of **clearance** between the tip of one mating tooth (**addendum circle**) and the bottom of the tooth space of the other (**dedendum circle**). The **working depth** of the tooth is twice the addendum and the **whole depth** is the sum of addendum and dedendum. The **tooth thickness** is measured at the pitch circle, and the tooth **space width** is slightly larger than the tooth thickness. The difference between these two dimensions is the **backlash**. The **face width** of the tooth is measured along the axis of the gear. The **circular pitch** is the arc length along the pitch circle circumference measured from a point on one tooth to the same point on the next. The circular pitch defines the tooth size. The definition of **circular pitch** p_c is

**FIGURE 12-8**

Gear Tooth Nomenclature

$$p_c = \frac{\pi d}{N} \quad (12.3a)$$

where d = pitch diameter and N = number of teeth. The tooth pitch can also be measured along the base circle circumference and then is called the **base pitch** p_b .

$$p_b = p_c \cos \phi \quad (12.3b)$$

The units of p_c are inches or millimeters. A more convenient way to define tooth size is to relate it directly to the diameter d of the pitch circle rather than to its circumference. The **diametral pitch** p_d is

$$p_d = \frac{N}{d} \quad (12.4a)$$

The units of p_d are reciprocal inches, or number of teeth per inch. This measure is used only in U.S. specification gears. Combining equations 12.3a and 12.4a gives the relationship between circular pitch and diametral pitch.

$$p_d = \frac{\pi}{p_c} \quad (12.4b)$$

The SI system, used for metric gears, defines a parameter called the **module**, which is the reciprocal of diametral pitch with pitch diameter d measured in millimeters.

$$m = \frac{d}{N} \quad (12.4c)$$

The units of the module are millimeters. Unfortunately, metric gears are not interchangeable with U.S. gears, despite both being involute tooth forms, as their standards

Table 12-1 AGMA Full-Depth Gear Tooth Specifications

Parameter	Coarse Pitch ($p_d < 20$)	Fine Pitch ($p_d \geq 20$)
Pressure angle ϕ	20° or 25°	20°
Addendum a	$1.000 / p_d$	$1.000 / p_d$
Dedendum b	$1.250 / p_d$	$1.250 / p_d$
Working depth	$2.000 / p_d$	$2.000 / p_d$
Whole depth	$2.250 / p_d$	$2.200 / p_d + 0.002$ in
Circular tooth thickness	$1.571 / p_d$	$1.571 / p_d$
Fillet radius—basic rack	$0.300 / p_d$	not standardized
minimum basic clearance	$0.250 / p_d$	$0.200 / p_d + 0.002$ in
minimum width of top land	$0.250 / p_d$	not standardized
Clearance (shaved or ground teeth)	$0.350 / p_d$	$0.350 / p_d + 0.002$ in

for tooth sizes are different (see Table 12-3). In the United States, gear tooth sizes are specified by diametral pitch. The conversion from one standard to the other is

$$m = \frac{25.4}{p_d} \quad (12.4d)$$

The velocity ratio m_V of the gearset can be put into a more convenient form by substituting equation 12.4a into equation 12.1 (p. 683), noting that the diametral pitch of meshing gears must be the same.

$$m_V = \pm \frac{r_{in}}{r_{out}} = \pm \frac{d_{in}}{d_{out}} = \pm \frac{N_{in}}{N_{out}} \quad (12.5a)$$

Thus the **velocity ratio** can be computed from the number of teeth on the meshing gears, which are integers. Note that a minus sign implies an external gearset and a positive sign an internal gearset, as shown in Figure 12-1. The gear ratio, m_G , can be expressed as the number of teeth on the gear N_g over the number of teeth on the pinion N_p .

$$m_G = \frac{N_g}{N_p} \quad (12.5b)$$

STANDARD GEAR TEETH Standard, full-depth gear teeth have equal addenda on pinion and gear, with the dedendum being slightly larger for clearance. The standard tooth dimensions are defined in terms of the diametral pitch. Table 12-1 shows the dimensions of standard, full-depth gear teeth as defined by the AGMA, and Figure 12-9 shows their shapes for three standard pressure angles. Figure 12-10 shows the actual sizes of 20° -pressure-angle, standard, full-depth teeth from $p_d = 4$ to $p_d = 80$. Note the inverse relationship between p_d and tooth size.

While there are no theoretical restrictions on the possible values of diametral pitch, a set of standard values is defined based on available gear-cutting tools. These standard tooth sizes are shown in Table 12-2 in terms of diametral pitch and in Table 12-3 in terms of metric module.

Table 12-2

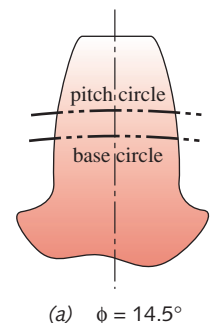
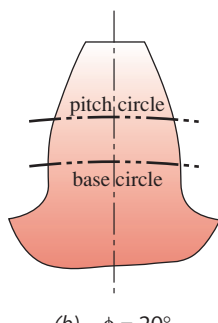
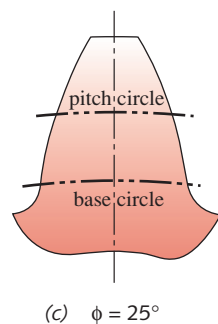
Standard Diametral Pitches

Coarse ($p_d < 20$)	Fine ($p_d \geq 20$)
1	20
1.25	24
1.5	32
1.75	48
2	64
2.5	72
3	80
4	96
5	120
6	
8	
10	
12	
14	
16	
18	

Table 12-3

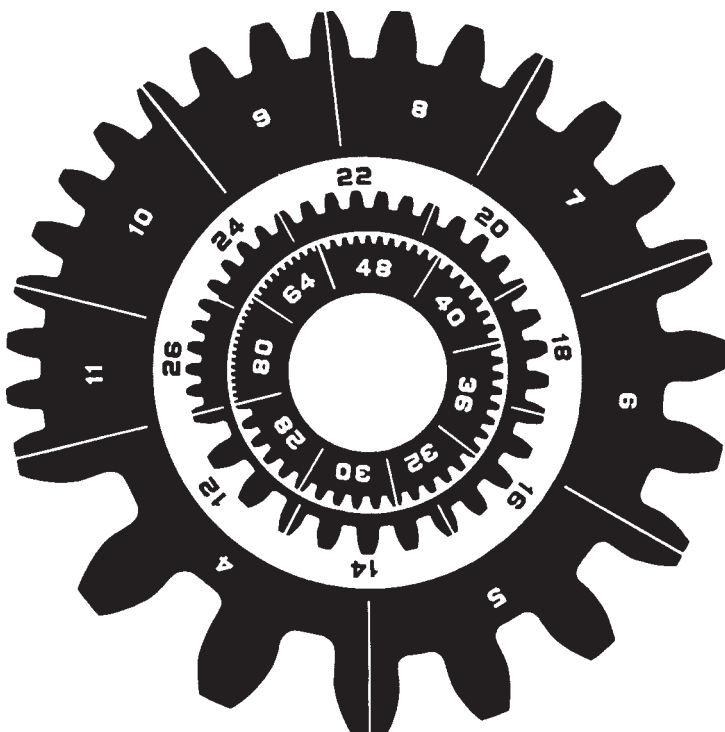
Standard Metric Modules

Metric Module (mm)	Equivalent p_d (in $^{-1}$)
0.3	84.67
0.4	63.50
0.5	50.80
0.8	31.75
1	25.40
1.25	20.32
1.5	16.93
2	12.70
3	8.47
4	6.35
5	5.08
6	4.23
8	3.18
10	2.54
12	2.12
16	1.59
20	1.27
25	1.02

(a) $\phi = 14.5^\circ$ (b) $\phi = 20^\circ$ (c) $\phi = 25^\circ$ **FIGURE 12-9**

AGMA Full-Depth Tooth Profiles for Three Pressure Angles

12

**FIGURE 12-10**

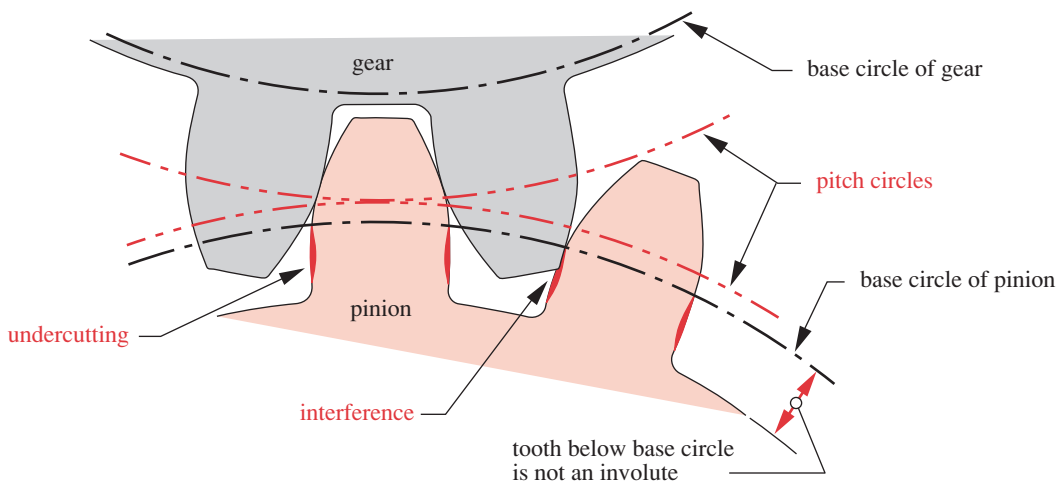
Actual Gear Tooth Sizes for Various Diametral Pitches Courtesy of Barber-Colman Co., Loves Park, Ill.

12.3 INTERFERENCE AND UNDERCUTTING

The involute tooth form is only defined outside of the base circle. In some cases, the dedendum will be large enough to extend below the base circle. If so, then the portion of tooth below the base circle will not be an involute and will interfere with the tip of the tooth on the mating gear, which is an involute. If the gear is cut with a standard gear shaper or a "hob," the cutting tool will also interfere with the portion of tooth below the base circle and will cut away the interfering material. This results in an undercut tooth, as shown in Figure 12-11. Undercutting weakens the tooth by removing material at its root. The maximum moment and maximum shear from the tooth loaded as a cantilever beam both occur in this region. Severe undercutting will cause early tooth failure.

Interference and its attendant undercutting can be prevented simply by avoiding gears with too few teeth. If a pinion has a large number of teeth, they will be small compared to its diameter. As the number of teeth is reduced for a fixed diameter pinion, the teeth must become larger. At some point, the dedendum will exceed the radial distance between the base circle and the pitch circle, and interference will occur. The minimum number of full-depth teeth required to avoid interference on a pinion running against a standard rack can be calculated from:

$$N_{min} = \frac{2}{\sin^2 \phi} \quad (12.6)$$

**FIGURE 12-11**

Interference and Undercutting of Teeth Below the Base Circle

Table 12-4 shows the minimum number of teeth required to avoid undercutting against a standard rack as a function of pressure angle. Table 12-5 shows the minimum number of full-depth pinion teeth that can be used against a selection of full-depth gears of various sizes (for $\phi = 20^\circ$). As the mating gear gets smaller, the pinion can have fewer teeth and still avoid interference.

Unequal-Addendum Tooth Forms

In order to avoid interference on small pinions, the tooth form can be changed from the standard, full-depth shapes of Figure 12-9 that have equal addenda on both pinion and gear to an involute shape with a longer addendum on the pinion and a shorter one on the gear. These are called **profile-shifted gears**. The AGMA defines addendum modification coefficients, x_1 and x_2 , which always sum to zero, being equal in magnitude and opposite in sign. The positive coefficient x_1 is applied to increase the pinion addendum and the negative x_2 decreases the gear addendum by the same amount. The total tooth depth remains the same. The net effect is to shift the pitch circles away from the pinion's base circle and eliminate that noninvolute portion of pinion tooth below the base circle. The standard coefficients are ± 0.25 and ± 0.50 , which add/subtract 25% or 50% of the standard addendum, respectively. The limit of this approach occurs when the pinion tooth becomes pointed.

There are some secondary benefits to this technique. The pinion tooth becomes thicker at its base and thus stronger. The gear tooth is correspondingly weakened, but since a full-depth gear tooth is stronger than a full-depth pinion tooth, this shift brings them to nearly equal strength. A disadvantage of unequal-addendum tooth forms is an increase in the sliding velocity at the tooth tip. The percent of sliding between the teeth is then greater than with equal addendum teeth. This increases the tooth-surface stresses, as discussed in Section 7.11 (p. 453). The friction losses in the gear mesh are also increased by higher sliding velocities. Dudley^[10] recommends avoiding more than 25%-long-addendum pinion teeth in spur or helical gears because of the disadvantages

Table 12-4

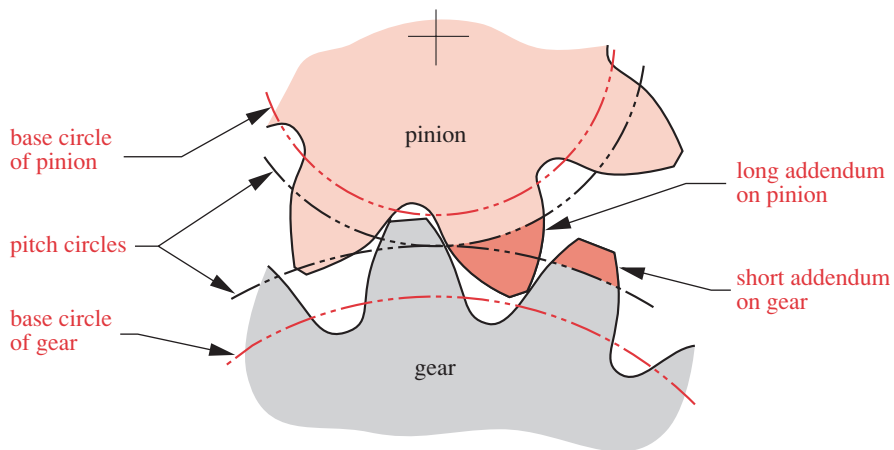
Minimum Number of Pinion Teeth to Avoid Interference Between a Full-Depth Pinion and a Full-Depth Rack

Pressure Angle (deg)	Minimum Number of Teeth
14.5	32
20	18
25	12

Table 12-5

Minimum Number of Pinion Teeth to Avoid Interference Between a 20° Full-Depth Pinion and Full-Depth Gears of Various Sizes

Minimum Pinion Teeth	Maximum Gear Teeth
17	1 309
16	101
15	45
14	26
13	16

**FIGURE 12-12**

Profile-Shifted Gear Teeth with Long and Short Addenda to Avoid Interference and Undercutting

associated with their high sliding velocities. Figure 12-12 shows the contours of profile-shifted involute teeth. Compare these to the standard tooth shapes in Figure 12-9.

12.4 CONTACT RATIO

The contact ratio m_p defines the average number of teeth in contact at any one time. It is calculated from

$$m_p = \frac{Z}{p_b} \quad (12.7a)$$

where Z is the length of action from equation 12.2 (p. 686) and p_b is the base pitch from equation 12.3b (p. 690). Substituting equations 12.3b and 12.4b into 12.7a defines m_p in terms of diametral pitch:

$$m_p = \frac{p_d Z}{\pi \cos \phi} \quad (12.7b)$$

If the contact ratio is 1, then one tooth is leaving contact just as the next is beginning contact. This is undesirable, because slight errors in the tooth spacing will cause oscillations in the velocity, vibration, and noise. In addition, the load will be applied at the tip of the tooth, creating the largest possible bending moment. At larger contact ratios than 1, there is the possibility of load sharing among the teeth. For contact ratios between 1 and 2, which are common for spur gears, there will still be times during the mesh when one pair of teeth will be taking the entire load. However, these will occur toward the center of the mesh region where the load is applied at a lower position on the tooth, rather than at its tip. This point is called the **highest point of single-tooth contact** or HPSTC. The minimum acceptable contact ratio for smooth operation is 1.2. A minimum contact ratio of 1.4 is preferred, and larger is better. Most spur gearsets will have contact ratios between 1.4 and 2. Equation 12.7b shows that for smaller teeth (larger p_d) and larger pressure angle, the contact ratio will be larger.

EXAMPLE 12-1**Determining Gear Tooth and Gear Mesh Parameters****Problem**

Find the gear ratio, circular pitch, base pitch, pitch diameters, pitch radii, center distance, addendum, dedendum, whole depth, clearance, outside diameters, and contact ratio of a gearset with the given parameters. If the center distance is increased 2% what is the new pressure angle?

Given

A $6p_d$, 20° -pressure-angle, 19-tooth pinion and a 37-tooth gear.

Assumptions

The tooth forms are standard AGMA full-depth involute profiles.

Solution

- 1 The gear ratio is easily found from the given tooth numbers on pinion and gear using equation 12.5b (p. 691).

$$m_G = \frac{N_g}{N_p} = \frac{37}{19} = 1.947 \quad (a)$$

- 2 The circular pitch can be found from either equation 12.3a or 12.4b (p. 690).

$$p_c = \frac{\pi}{p_d} = \frac{\pi}{6} = 0.524 \text{ in} \quad (b)$$

- 3 The base pitch measured on the base circle is (from equation 12.3b on p. 690):

$$p_b = p_c \cos\phi = 0.524 \cos(20^\circ) = 0.492 \text{ in} \quad (c)$$

- 4 The pitch diameters and pitch radii of pinion and gear are found from equation 12.4a.

$$d_p = \frac{N_p}{p_d} = \frac{19}{6} = 3.167 \text{ in}, \quad r_p = \frac{d_p}{2} = 1.583 \text{ in} \quad (d)$$

$$d_g = \frac{N_g}{p_d} = \frac{37}{6} = 6.167 \text{ in}, \quad r_g = \frac{d_g}{2} = 3.083 \text{ in} \quad (e)$$

- 5 The nominal center distance C is the sum of the pitch radii:

$$C = r_p + r_g = 4.667 \text{ in} \quad (f)$$

- 6 The addendum and dedendum are found from the equations in Table 12-1 (p. 691):

$$a = \frac{1.0}{p_d} = \frac{1}{6} = 0.167 \text{ in}, \quad b = \frac{1.25}{p_d} = \frac{1.25}{6} = 0.208 \text{ in} \quad (g)$$

- 7 The whole depth h_t is the sum of the addendum and dedendum.

$$h_t = a + b = 0.167 + 0.208 = 0.375 \text{ in} \quad (h)$$

- 8 The clearance is the difference between dedendum and addendum.

$$c = b - a = 0.208 - 0.167 = 0.042 \text{ in} \quad (i)$$

9 The outside diameter of each gear is the pitch diameter plus two addenda:

$$D_{o_p} = d_p + 2a = 3.500 \text{ in}, \quad D_{o_g} = d_g + 2a = 6.500 \text{ in} \quad (j)$$

10 The contact ratio is found from equations 12.2 and 12.7 (pp. 686 and 694).

$$\begin{aligned} Z &= \sqrt{(r_p + a_p)^2 - (r_p \cos \phi)^2} + \sqrt{(r_g + a_g)^2 - (r_g \cos \phi)^2} - C \sin \phi \\ &= \sqrt{(1.583 + 0.167)^2 - (1.583 \cos 20)^2} \\ &\quad + \sqrt{(3.083 + 0.167)^2 - (3.083 \cos 20)^2} - 4.667 \sin 20 = 0.798 \text{ in} \\ m_p &= \frac{Z}{p_b} = \frac{0.798}{0.492} = 1.62 \end{aligned} \quad (k)$$

11 If the center distance is increased from the nominal value due to assembly errors or other factors, the effective pitch radii will change by the same percentage. The gears' base radii will remain the same. The new pressure angle can be found from the changed geometry. For a 2% increase in center distance (1.02x):

$$\phi_{new} = \cos^{-1} \left(\frac{r_{base\ circle\ p}}{1.02r_p} \right) = \cos^{-1} \left(\frac{r_p \cos \phi}{1.02r_p} \right) = \cos^{-1} \left(\frac{\cos 20^\circ}{1.02} \right) = 22.89^\circ \quad (l)$$

12 The files EX12-01 can be found on the book's CD-ROM.

12.5 GEAR TRAINS

A **gear train** is any collection of two or more meshing gears. A pair of gears, or gear-set, is then the simplest form of gear train and *is usually limited to a ratio of about 10:1*. The gearset will become large and hard to package beyond that ratio if the pinion is kept above the minimum numbers of teeth shown in Tables 12-4 and 12-5 (p. 693). Gear trains may be **simple**, **compound**, or **epicyclic**. What follows is a brief review of the kinematic design of gear trains. For more complete information, see reference 4.

Simple Gear Trains

A simple gear train is one in which each shaft carries only one gear, the most basic two-gear example of which is shown in Figure 12-2 (p. 683). The *velocity ratio* (also called *train ratio*) of a gearset is given by equation 12.5a (p. 691). Figure 12-13 shows a simple gear train with five gears in series. Equation 12.8 shows the expression for this train's velocity ratio:

$$m_V = \left(-\frac{N_2}{N_3} \right) \left(-\frac{N_3}{N_4} \right) \left(-\frac{N_4}{N_5} \right) \left(-\frac{N_5}{N_6} \right) = +\frac{N_2}{N_6} \quad (12.8)$$

Each gearset potentially contributes to the overall train ratio, but in the case of a simple (series) train, the numerical effects of all gears except the first and last cancel out. The train ratio of a simple train is always just the ratio of the first gear over the

last. Only the sign of the overall train ratio is affected by the intermediate gears, which are called *idle*s, because no power is typically taken from their shafts. If all gears in the train are external and there is an even number of gears in the train, the output direction will be opposite to that of the input. If there are an odd number of external gears in the train, the output will be in the same direction as the input. Thus a single, external, idler gear of *any diameter* can be used to change the direction of the output gear without affecting its velocity magnitude.

It is common practice to insert a single idler gear to change direction, but more than one idler is superfluous. There is little justification for designing a gear train as is shown in Figure 12-13. If the need is to connect two shafts that are far apart, a simple train of many gears could be used but will be much more expensive than a chain or belt drive for the same application. If the need is to get a larger train ratio than can be obtained with a single gearset, it is clear from equation 12.8 that the simple gear train will be of no help.

Compound Gear Trains

To get a train ratio of greater than about 10:1 with gears it is necessary to **compound the train** (unless an epicyclic train is used—see next section). A **compound train** is one in which at least one shaft carries more than one gear. This will be a parallel or series-parallel arrangement, rather than the pure series connections of the simple gear train. Figure 12-14a shows a compound train of four gears, two of which, gears 3 and 4, are attached to the same shaft and thus have the same angular velocity. The train ratio is now

$$m_V = \left(-\frac{N_2}{N_3} \right) \left(-\frac{N_4}{N_5} \right) \quad (12.9a)$$

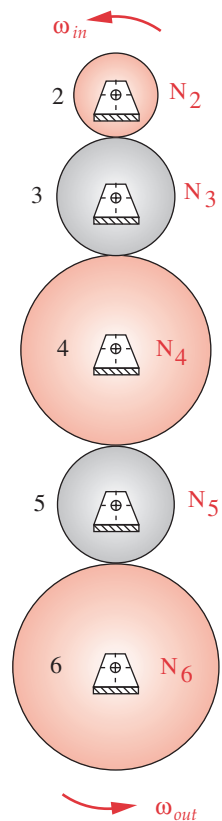


FIGURE 12-13
A Simple Gear Train

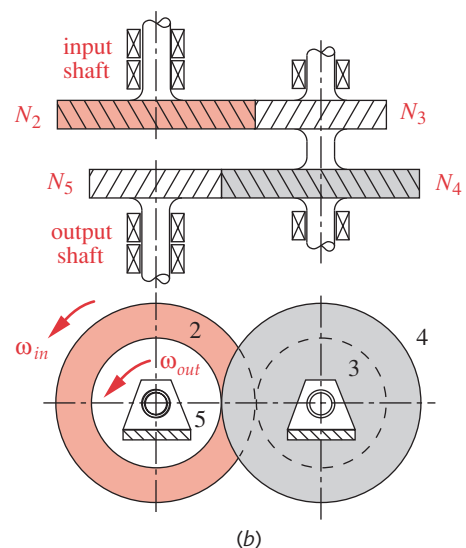
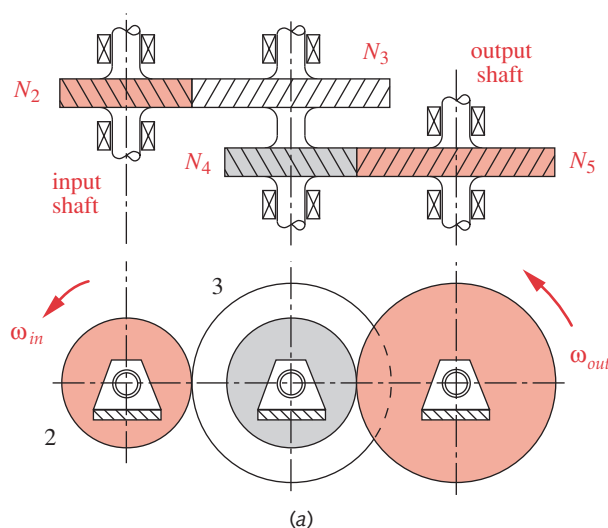


FIGURE 12-14

Two-Stage Compound Gear Trains: (a) Nonreverted, (b) Reverted

This can be generalized for any number of gears in the train as

$$m_V = \pm \frac{\text{product of number of teeth on driver gears}}{\text{product of number of teeth on driven gears}} \quad (12.9b)$$

Note that these intermediate ratios do not cancel and the overall train ratio is the product of the ratios of parallel gearsets. Thus a larger ratio can be obtained in a compound gear train despite the approximately 10:1 limitation on individual gearset ratios. The plus or minus sign in equation 12.9b depends on the number and type of meshes in the train, whether external or internal. Writing the expression in the form of equation 12.9a and carefully noting the sign of each mesh ratio in the expression will result in the correct algebraic sign for the overall train ratio.

Reverted Compound Trains

In Figure 12-14a the input and output shaft are in different locations. This may well be acceptable or even desirable in some cases, depending on other packaging constraints in the overall machine design. Such a gear train, whose *input and output shafts are not coincident*, is called a **nonreverted compound train**. In some cases, such as in automobile transmissions, it is desirable or even necessary to have the *output shaft concentric with the input shaft*, as shown in Figure 12-14b. This is referred to as “reverting the train” or “bringing it back onto itself.” The design of a **reverted compound train** is more complicated because of the additional constraint that the center distances of the stages must be equal. See reference 4 for more information.

EXAMPLE 12-2

Designing a Compound Gear Train

12

Problem Design a compound, spur-gear train for an overall train ratio of 29:1.

Given Use 25° -pressure-angle gears with a module of 3 mm in all stages.

Assumptions The largest ratio in any one gearset should be limited to about 10:1.
The minimum number of teeth on any pinion is 12 (Table 12-4, p. 693).

Solution

- 1 The required ratio is too large for one stage (one gearset), but two will each be within the 10:1 limitation. We can get an idea of the gearset ratios needed by taking the square root of the desired train ratio: $(29)^{0.5} = 5.385$. Thus, two gearsets with this ratio will do it.
- 2 Since the number of teeth on each gear must be an integer, see how close we can come to the 5.385:1 gearset ratio with integer combinations of teeth, starting with the smallest possible pinion:

$$\begin{aligned} 12(5.385) &= 64.622 \\ 13(5.385) &= 70.007 \\ 14(5.385) &= 75.392 \end{aligned} \quad (a)$$

The second of these will be very close to the correct ratio when rounded to an integer.

- 3 Try two gearsets of 13t and 70t. What will be the train ratio?

$$\left(\frac{70}{13}\right)\left(\frac{70}{13}\right) = 28.994 \quad (b)$$

- 4 If this is close enough for the application, the problem is solved. The only situation in which it might not be acceptable would be where an exact ratio was required to provide a timing function.
- 5 Note that using two identical gearsets in a compound train automatically reverts it, allowing the input and output shafts to be concentric.

Epicyclic or Planetary Gear Trains

The conventional gear trains described in the previous sections are all one-degree-of-freedom (1-DOF) devices. Another class of gear train, the **epicyclic or planetary train**, has wide application. This is a 2-DOF device. Two inputs are needed to obtain a predictable output. In some cases, such as the automotive differential, one input is provided (the driveshaft) and two frictionally coupled outputs are obtained (the two driving wheels).

Epicyclic or planetary trains have several advantages over conventional trains, among which are higher train ratios obtainable in smaller packages, reversion by default, and simultaneous, concentric, bidirectional outputs available from a single unidirectional input. These features make planetary trains popular as automatic transmissions in automobiles and trucks, etc.

Figure 12-15a shows a conventional, 1-DOF gearset in which link 1 is immobilized as the ground link. Figure 12-15b shows the same gearset with link 1 now free to rotate as an **arm** that connects the two gears. Now only the pinion pivot is grounded and the system DOF = 2. This has become an **epicyclic train** with a **sun gear** and a **planet gear** orbiting around the sun, held in orbit by the **arm**. Two inputs are required. Typi-

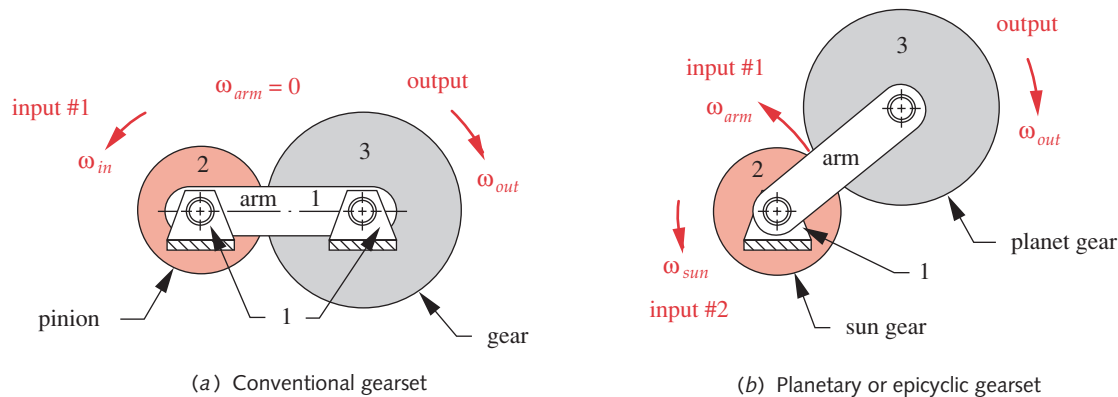


FIGURE 12-15

Conventional Gearsets are Special Cases of Planetary or Epicyclic Gearsets

cally, the arm and the sun gear will each be driven in some direction at some velocities. In many cases, one of these inputs will be zero velocity, i.e., a brake applied to either the arm or the sun gear. Note that a zero-velocity input to the arm merely makes a conventional gear train out of the epicyclic train, as shown in Figure 12-15a. Thus the conventional gear train is simply a special case of the more complex epicyclic train, in which the arm is held stationary.

In the simple example of an epicyclic train in Figure 12-15, the only gear left to act as output, after putting inputs to sun and arm, is the planet. It is a bit difficult to get a usable output from this orbiting planet gear, because its pivot is moving. A more useful configuration is shown in Figure 12-16, to which a ring gear has been added. This **ring gear** meshes with the planet and pivots concentric with the pinion, so it can be easily tapped as the output member. Most planetary trains will be arranged with ring gears to bring the planetary motion back to a grounded pivot. Note how the sun gear, ring gear, and arm are all brought out as concentric hollow shafts so that each can be accessed to tap its angular velocity and torque as either an input or an output.

While it is relatively easy to visualize the power flow through a conventional gear train and observe the directions of motion for its member gears, it is very difficult to determine the behavior of a planetary train by observation. We must do the necessary calculations to determine its behavior and may be surprised at the often counterintuitive results. Since the gears are rotating with respect to the arm, and the arm itself has motion, the velocity-difference equation must be used:

$$\omega_{gear} = \omega_{arm} + \omega_{gear}/arm \quad (12.10)$$

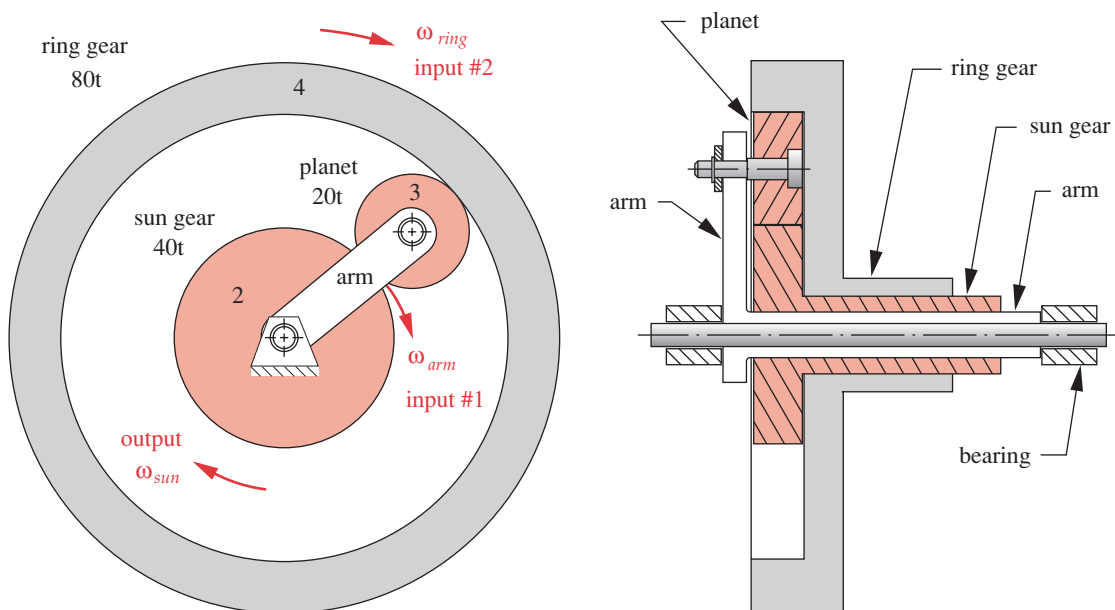


FIGURE 12-16

Planetary Gear Train with Ring Gear Used as Output

Equations 12.10 and 12.5a (p. 691) are all that are needed to solve for the velocities in an epicyclic train, provided that the tooth numbers and two input conditions are known. Rearrange equation 12.10 to solve for the velocity-difference term. Then, let ω_F represent the angular velocity of the first gear in the train (chosen at either end), and ω_L represent the angular velocity of the last gear in the train (at the other end).

For the first gear in the system:

$$\omega_{F/ \text{arm}} = \omega_F - \omega_{\text{arm}} \quad (12.11a)$$

For the last gear in the system:

$$\omega_{L/ \text{arm}} = \omega_L - \omega_{\text{arm}} \quad (12.11b)$$

Dividing the last by the first:

$$\frac{\omega_{L/ \text{arm}}}{\omega_{F/ \text{arm}}} = \frac{\omega_L - \omega_{\text{arm}}}{\omega_F - \omega_{\text{arm}}} = m_V \quad (12.11c)$$

This gives an expression for the overall train ratio m_V . The leftmost side of equation 12.11c involves only the velocity-difference terms, which are relative to the arm. This fraction is equal to the ratio of the products of tooth numbers of the gears from first to last in the train (as defined in equation 12.9b), which can be substituted for the leftmost side of equation 12.11c.

$$+ \frac{\text{product of number of teeth on driver gears}}{\text{product of number of teeth on driven gears}} = \frac{\omega_L - \omega_{\text{arm}}}{\omega_F - \omega_{\text{arm}}} \quad (12.12)$$

Equation 12.12 can be solved for any one of the three variables on the right-hand side provided that the other two are defined as inputs to this 2-DOF gear train. Either the velocities of the arm and one gear must be known or the velocities of two gears, the first and last (as so designated), must be known. Another limitation of this method is that both the first and last gears chosen must be pivoted to ground (not orbiting), and there must be a path of meshes connecting them, which may include orbiting planet gears.

EXAMPLE 12-3

Analyzing an Epicyclic Gear Train

Problem Determine the train ratio between sun gear and arm for the epicyclic train shown in Figure 12-16.

Given The sun has 40 teeth, the planet 20 teeth, and the ring gear 80 teeth. The arm is the input and the sun is the output. The ring gear is held stationary.

Assumptions The sun gear is the first gear in the train and the ring gear is the last. Let the arm have an ω of 1 rpm. The train ratio desired is sun/arm.

Solution

- 1 Equation 12.12 defines the kinematics of an epicyclic train:

$$\left(-\frac{N_2}{N_3} \right) \left(+\frac{N_3}{N_4} \right) = \frac{\omega_L - \omega_{arm}}{\omega_F - \omega_{arm}}$$

$$\left(-\frac{40}{20} \right) \left(+\frac{20}{80} \right) = \frac{0 - 1}{\omega_F - 1} \quad (a)$$

$$\omega_F = 3$$

which defines the train ratio as +3. The sun gear rotates three times as fast and in the same direction as the arm. Note the signs on the gearset ratios. One is an external set (−) and one an internal set (+).

- 2 The files EX12-03 can be found on the CD-ROM.
-

12.6 GEAR MANUFACTURING

Several methods are used to manufacture gears. They can be divided into two categories, forming and machining. Machining further divides into roughing and finishing operations. Forming refers to the direct casting, molding, drawing, or extrusion of tooth forms in molten, powdered, or heat-softened materials. Roughing and finishing are material removal techniques used to cut or grind the tooth shape into a solid blank at room temperature. Roughing methods are often used alone without any subsequent finishing operation for nonprecision gears. Despite their name, the roughing processes actually create a smooth and accurate gear tooth. Only when high precision and quiet running are required is the added cost of secondary finishing operations justified.

Forming Gear Teeth

12

In all tooth-forming operations, the teeth on the gear are formed all at once from a mold or die into which the tooth shapes have been machined. The accuracy of the teeth is entirely dependent on the quality of the die or mold and in general is much less than can be obtained from roughing or finishing methods. Most of these methods have high tooling costs, making them suitable only for high production quantities. See Chapter 2 for a more general discussion of these manufacturing processes.

CASTING Teeth can be sand cast or die cast in various metals. The advantage is low cost, as the tooth shape is built into the mold. No finishing operations on the teeth are typically done after casting, though they could be. The resulting teeth are of low precision and are used only in noncritical applications such as toys and small appliances or cement-mixer barrels, where noise and excessive backlash are not detrimental to operation. Sand casting is an economical way to obtain low-quality gear teeth in small quantities, since the tooling costs are reasonable, but surface finish and dimensional accuracy are very poor. Die casting provides a better surface finish and accuracy than sand casting but has high tooling costs, requiring large production volume to justify its use.

INVESTMENT CASTING also known as lost-wax casting, can provide reasonably accurate gears in a wide variety of materials. The mold is made of a refractory material that allows high melt-temperature materials to be cast. Accuracy is a function of the original master pattern used to make the mold.

SINTERING Powdered metals (PM) are pressed into a gear-shaped metal mold cavity, removed, and heat-treated (sintered) to increase their strength. These PM gears have similar accuracy to die-cast gears but their material properties can be controlled by mixing various metal powders. This technique is typically used for small-sized gears.

INJECTION MOLDING is used to make nonmetallic gears in various thermoplastics such as nylon and acetal. These are low-precision gears in small sizes but they have the advantages of low cost and the ability to be run without lubricant at light loads.

EXTRUDING is used to form teeth on long rods, which are then cut into usable lengths and machined for bores and keyways, etc. Nonferrous materials such as aluminum and copper alloys are commonly extruded rather than steels.

COLD DRAWING forms teeth on steel rods by drawing them through hardened dies. The cold working increases strength and reduces ductility. The rods are then cut into usable lengths and machined for bores and keyways, etc.

STAMPING Sheet metal can be stamped with tooth shapes to form low-precision gears at low cost in high quantities. Surface finish and accuracy are poor.

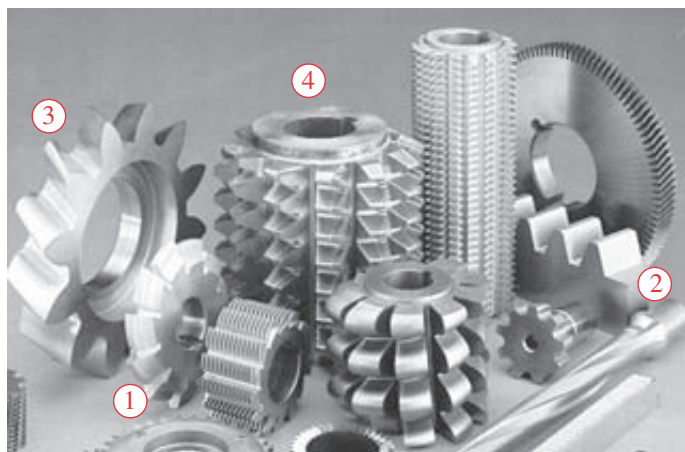
Machining

The bulk of metal gears used to transmit power in machinery are made by a machining process from cast, forged, or hot-rolled blanks. Roughing processes include milling the tooth shape with formed cutters or generating the shape with a rack cutter, a shaper cutter, or a hob. Finishing processes include shaving, burnishing, lapping, honing, or grinding. Each of these methods will be briefly described.

Roughing Processes

FORM MILLING requires a shaped milling cutter, as shown in Figure 12-17 (labeled 1). The cutter must be made to the shape of the gear tooth space for the tooth geometry and number of teeth of each particular gear. The rotating cutter is plunged into the blank to cut one tooth at a time. The gear blank is then rotated through one circular pitch and the next tooth cut. Because a different shape cutter is needed for each gear size to be made, the tooling cost becomes high. To reduce costs, the same cutter is often used for multiple-sized gears, resulting in profile errors for all but one number of teeth. This method is the least accurate of the roughing methods.

RACK GENERATION A rack cutter for any involute pitch can be easily made, since its tooth shape is a trapezoid (see Figure 12-6 on p. 687). The hardened and sharpened rack (see 2 in Figure 12-17) is then reciprocated along the axis of the gear blank and fed into it while being rotated around the gear blank so as to generate the involute tooth on the gear. The rack and gear blank must be periodically repositioned to complete the circumference. This repositioning can introduce errors in the tooth geometry, making this method less accurate than others still to be discussed.

**FIGURE 12-17**

A Collection of Gear-Cutting Tools: 1—Milling Cutter, 2—Rack Cutter, 3—Shaper Cutter, 4—Hob *Courtesy of Pfauter-Maag Cutting Tools Limited Partnership, Loves Park, Ill.*

GEAR SHAPING uses a cutting tool in the shape of a gear (see 3 in Figure 12-17), which is reciprocated axially across the gear blank to cut the teeth while the blank rotates around the shaper tool as shown in Figure 12-18. It is a true shape-generation process in that the gear-shaped tool cuts itself into mesh with the gear blank. The accuracy is good, but any errors in even one tooth of the shaper cutter will be directly transferred to the gear. Internal gears can be cut with this method as well.

HOBBLING A hob, labeled 4 in Figure 12-17, is analogous to a thread tap. Its teeth are shaped to match the tooth space and are interrupted with grooves to provide cutting surfaces. It rotates about an axis perpendicular to that of the gear blank, cutting into the rotating blank to generate the teeth. It is the most accurate of the roughing processes since no repositioning of tool or blank is required and each tooth is cut by multiple hob-teeth, averaging out any tool errors. Excellent surface finish can be achieved by this method, and it is one of the most widely used for production gears.

12

**FIGURE 12-18**

A Gear Shaper Cutting a Helical Gear *Courtesy of Pfauter-Maag Cutting Tools, Ltd Prtship, Loves Park, Ill.*

Finishing Processes

When high precision is required, secondary operations can be done to gears made by any of the above roughing methods. Finishing operations typically remove little or no material but improve dimensional accuracy, surface finish, and/or hardness.

SHAVING is similar to gear shaping, but uses accurate shaving tools to remove small amounts of material from a roughed gear to correct profile errors and improve finish.

GRINDING uses a contoured grinding wheel that is passed over the machined surface of the gear teeth, typically computer-controlled, to remove small amounts of material and improve surface finish. It can be used on gears that have been hardened after roughing to correct the heat-treatment distortion, as well as to achieve the other advantages listed above.

BURNISHING runs the rough-machined gear against a specially hardened gear. The high forces at the tooth interface cause plastic yielding of the gear tooth surface, which both improves finish and work-hardens the surface, creating beneficial compressive residual stresses.

LAPPING AND HONING both employ an abrasive-impregnated gear or gear-shaped tool that is run against the gear to abrade the surface. In both cases, the abrasive tool drives the gear in what amounts to an accelerated and controlled run-in to improve surface finish and accuracy.

Gear Quality

The AGMA Standard 2000-A88 defines dimensional tolerances for gear teeth and a quality index Q_v that ranges from the lowest quality (3) to the highest precision (16). The manufacturing method essentially determines the quality index Q_v of the gear.

Formed gears will typically have quality indices of 3–4. Gears made by the roughing methods listed above generally fall within a Q_v range of 5–7. If the gears are finished by shaving or grinding, Q_v can be in the 8–11 range. Lapping and honing can achieve higher-quality indices. Obviously, the cost of the gear will be a function of Q_v .

Table 12-6 shows the quality indices recommended by AGMA for a number of common applications of gears. Another way to select a suitable quality index is based on the linear velocity of the gear teeth at the pitch point, called the pitch-line velocity. Inaccuracies in tooth spacing will cause impacts between teeth, and impact forces are increased at higher velocities. Table 12-7 shows recommended gear-quality indices Q_v as a function of the pitch-line velocity of the gear mesh. Spur gears are seldom used with pitch-line velocities greater than 10 000 ft/min (50 m/s) due to excessive noise and vibration. Helical gears (discussed in the next chapter) are preferred in such applications.

Gear quality can have a significant effect on the load sharing between teeth. If the tooth spacings are not accurate and uniform, the teeth in the mesh will not all be in simultaneous contact. This will obviate the advantage of a large contact ratio. Figure 12-19 shows two gears with large contact ratio but low accuracy. Only one pair of teeth are in contact and taking load in the same direction. The others in the mesh are taking

Table 12-6

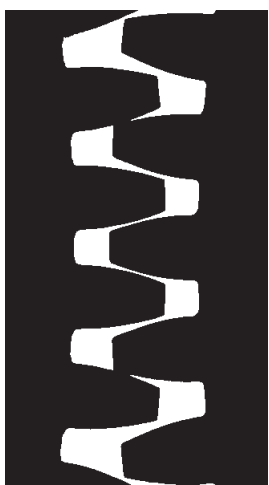
Recommended AGMA Gear Quality Numbers for Various Applications

Application	Q_v
Cement mixer	
drum drive	3–5
Cement kiln	5–6
Steel mill drives	5–6
Corn picker	5–7
Cranes	5–7
Punch press	5–7
Mining conveyor	5–7
Paper-box making machine	6–8
Gas meter mechanism	7–9
Small power drill	7–9
Clothes washing machine	8–10
Printing press	9–11
Computing mechanism	10–11
Automotive transmission	10–11
Radar antenna drive	10–12
Marine propulsion drive	10–12
Aircraft engine drive	10–13
Gyroscope	12–14

Table 12-7

Recommended Gear Quality Numbers versus Pitch Line Velocity

Pitch Velocity	Q_v
0–800 fpm	6–8
800–2000 fpm	8–10
2000–4000 fpm	10–12
Over 4000 fpm	12–14

**FIGURE 12-19**

Actual Spur-Gear Teeth in Mesh Showing Poor Load Sharing Due to Tooth Inaccuracy. Source: R. L. Thoen, "Minimizing Backlash in Spur Gears," *Gear Technology*, May/June 1994, p. 27, with permission.

no load. Despite an apparent contact ratio of about 5, the actual contact ratio at this point in the mesh is only 1.

12.7 LOADING ON SPUR GEARS

The analysis of loading on meshing gear teeth can be done by the standard methods of load analysis, as discussed in Chapter 3 using equations 3.2 or 3.3 (p. 78) as appropriate. We will only briefly discuss their application to gear teeth. Figure 12-20 shows a pair of gear teeth. The teeth are actually meshed (in contact) at the pitch point, but are shown separated for clarity. A torque T_p is being delivered by the pinion to the gear. Both are shown as free-body diagrams. At the pitch point, the only force that can be transmitted from one tooth to the other, neglecting friction, is the force W acting along the line of action at the pressure angle. This force can be resolved into two components, W_r acting in the radial direction and W_t in the tangential direction. The magnitude of the tangential component W_t can be found from

$$W_t = \frac{T_p}{r_p} = \frac{2T_p}{d_p} = \frac{2p_d T_p}{N_p} \quad (12.13a)$$

where T_p is the torque on the pinion shaft, r_p is the pitch radius, d_p the pitch diameter, N_p the number of teeth, and p_d the diametral pitch of the pinion.

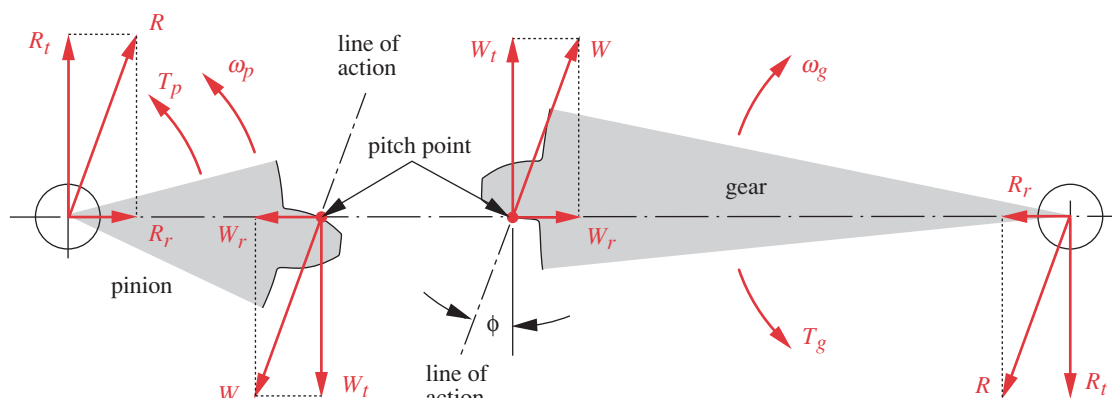
The radial component W_r is

$$W_r = W_t \tan \phi \quad (12.13b)$$

and the resultant force W is

$$W = \frac{W_t}{\cos \phi} \quad (12.13c)$$

Note that equation 12.13a could as well have been written for the gear rather than for the pinion since the force W is equal and opposite on gear and pinion.

**FIGURE 12-20**

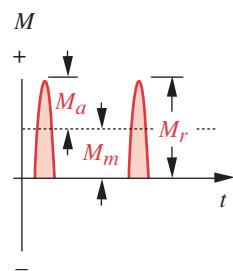
Forces on the Pinion and Gear in a Gearset (Gears Separated for Illustration—Pitch Points are Actually in Contact)

The reaction force R , and its components R_t and R_r at the pivots, are equal and opposite to the corresponding forces acting at the pitch point of the respective gear or pinion. The pinion forces are equal and opposite to those acting on the gear.

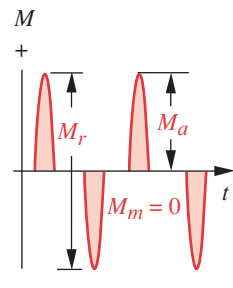
Depending on the contact ratio, the teeth can take all or part of the load W at any location from the tip of the tooth to a point near the dedendum circle as it rotates through the mesh. Obviously, the worst loading condition is when W acts at the tooth tips. Then, its tangential component W_t has the largest possible moment arm acting on the tooth as a cantilever beam. The bending moment and the transverse shear force due to bending will both be maximum at the root of the tooth. For contact ratios > 1 , there will be a highest point of single-tooth contact (HPSTC) somewhere below the tip, and this will create the maximum bending moment on any one tooth, provided that the gears' accuracies are good enough to allow load sharing. If the teeth are of low quality, as shown in Figure 12-19, then tip loading with the full value of W will occur regardless of the contact ratio.

Even if the torque T_p is constant with time, each tooth will experience repeated loading as it comes through the mesh, creating a fatigue-loading situation. The bending moment-time function for a gearset will be as shown in Figure 12-21a. There are equal mean (M_m) and alternating (M_a) components of bending moment. There is some advantage in avoiding integer values of gear ratio m_G for gearsets in order to prevent the same teeth from contacting one another every m_G revolutions. Noninteger ratios will distribute the contact more evenly among all the teeth.

If an idler gear is inserted between the pinion and gear to change the output direction, each of the idler's teeth will experience a fully reversed moment, as shown in Figure 12-21b, because the force W acts on opposite sides of each idler tooth in alternate meshes. Note that the range M_r of the moment magnitude on the idler is twice that of the nonidler gears, making it a more heavily loaded gear even though its mean moment is zero. The same is true for planet gears, as shown in Figure 12-16 (p. 700).



(a) Repeated moment on nonidler tooth



(b) Reversed moment on idler tooth

FIGURE 12-21

Time-Varying Bending Moments on Gear Teeth

EXAMPLE 12-4

Load Analysis of a Spur-Gear Train

Problem

Determine the torques and transmitted loads on the gear teeth in a 3-gear train containing a pinion, an idler gear, and a gear. Find the gear diameters and the mean and alternating components of transmitted load on each gear.

Given

The pinion shaft passes 20 hp at 2 500 rpm. The train ratio is 3.5:1. The pinion has 14 teeth, a 25° pressure angle, and $p_d = 6$. The idler has 17 teeth.

Assumptions

The pinion meshes with the idler and the idler meshes with the gear.

Solution

- Find the number of gear teeth from the given information:

$$N_g = m_G N_p = 3.5(14) = 49 \text{ teeth} \quad (a)$$

2 The torque on the pinion shaft is found from equation 10.1 (p. 553):

$$T_p = \frac{P}{\omega_p} = \frac{20 \text{ hp} \left(6600 \frac{\text{in-lb}}{\text{sec}} / \text{hp} \right)}{2500 \text{ rpm} (2\pi/60) \frac{\text{rad}}{\text{sec}} / \text{rpm}} = 504 \text{ lb-in} \quad (b)$$

3 The output torque is

$$T_g = m_G T_p = 3.5(504) = 1765 \text{ lb-in} \quad (c)$$

4 The pitch diameters are

$$d_p = \frac{N_p}{p_d} = \frac{14}{6} = 2.33 \text{ in}, \quad d_i = \frac{17}{6} = 2.83 \text{ in}, \quad d_g = \frac{49}{6} = 8.17 \text{ in} \quad (d)$$

5 The transmitted load is the same on all three gears and can be found from the torque and radius of any one of the gears:

$$W_t = \frac{T_p}{d_p/2} = \frac{504}{2.33/2} = 432 \text{ lb} \quad (e)$$

6 The radial component of load is

$$W_r = W_t \tan \phi = 432 \tan 25^\circ = 202 \text{ lb} \quad (f)$$

7 The total load is

$$W = \frac{W_t}{\cos \phi} = \frac{432}{\cos 25^\circ} = 477 \text{ lb} \quad (g)$$

8 The repeated loads on any pinion or gear tooth are

$$W_{t_{alternating}} = \frac{W_t}{2} = 216 \text{ lb} \quad W_{t_{mean}} = \frac{W_t}{2} = 216 \text{ lb} \quad (h)$$

9 The fully reversed loads on the idler are

$$W_{t_{alternating}} = W_t = 432 \text{ lb} \quad W_{t_{mean}} = 0 \text{ lb} \quad (i)$$

10 The files EX12-04 can be found on the CD-ROM.

12.8 STRESSES IN SPUR GEARS

There are two modes of failure that affect gear teeth: **fatigue fracture** due to fluctuating bending stresses at the root of the tooth and **surface fatigue** (pitting) of the tooth surfaces. Both failure modes must be checked when designing gears. Fatigue fracture due to bending can be prevented with proper design by keeping the stress state within the modified-Goodman line for the material, as discussed in Chapter 6. Since most heavily loaded gears are made of ferrous materials that do have a bending endurance limit, infinite life can be obtained for the bending loads. However, as was discussed in Chapter 7, materials do not exhibit an endurance limit for repeated surface-contact

stresses. Therefore, it is not possible to design gears for infinite life against surface failure. Properly designed gearsets should never fracture a tooth in normal service (barring overloads greater than they were designed for) but must be expected to eventually fail by one of the wear mechanisms discussed in Chapter 7. Pitting is the most common mode of failure, though abrasive or adhesive wear (scuffing or scoring) may occur, especially if the gears are not properly lubricated in service. We will address each of the two principal failure modes in turn, using the AGMA recommended procedures.

Bending Stresses

THE LEWIS EQUATION The first useful equation for the bending stress in a gear tooth was developed by W. Lewis in 1892. He recognized that the tooth is a cantilever beam with its critical section at the root. Starting with the equation for bending stress in a cantilever beam, he derived what is now known as the Lewis equation:

$$\sigma_b = \frac{W_t p_d}{F Y} \quad (12.14)$$

where W_t is the tangential force on the tooth, p_d the diametral pitch, F the face width, and Y is a dimensionless geometry factor, defined by him, and now called the Lewis form factor. His form factor took the tooth geometry into account to determine its effective strength at the root fillet. He published a table of Y values for gears of different pressure angles and numbers of teeth.^[5] Note that the radial component W_r is ignored, as it puts the tooth in compression and acts to reduce the dangerous tensile bending stress. Ignoring the radial stress is thus conservative and also simplifies the analysis.

The Lewis equation is no longer used in its original form, but it serves as the basis for a more modern version as defined by the AGMA and based on the work of Lewis and many others. The principles of Lewis' equation are still valid, but it has been augmented with additional factors to account for failure mechanisms only later understood. His form factor Y has been supplanted by a new geometry factor J , which includes the effects of stress concentration at the root fillet.^[3] Stress concentration was still waiting to be discovered in Lewis's day.

THE AGMA BENDING STRESS EQUATION as defined in AGMA Standard 2001-B88 is valid only for certain assumptions about the tooth and gear-mesh geometry:

- 1 The contact ratio is between 1 and 2.
- 2 There is no interference between the tips and root fillets of mating teeth and no undercutting of teeth above the theoretical start of the active profile.
- 3 No teeth are pointed.
- 4 There is nonzero backlash.
- 5 The root fillets are standard, assumed smooth, and produced by a generating process.
- 6 The friction forces are neglected.

The first assumption comes about in spite of the theoretical desirability of high contact ratios because the actual load sharing between teeth in such situations is subject to factors of tooth accuracy and stiffness that are difficult to predict, making the problem indeterminate. Assumption 1 is then conservative with larger contact ratios. Assumption 2 limits the analysis to pinion-gear combinations that obey the minimum-

tooth limitations described in Tables 12-4 and 12-5 (p. 693). If smaller numbers of teeth are needed for packaging purposes, then unequal-addendum teeth should be used and the AGMA method applied with the appropriate geometry factor J used in the equation. Assumption 3 deals with the limits of unequal-addendum pinions. Assumption 4 recognizes that gears with zero backlash will not run freely together due to excessive friction. Assumption 5 accounts for the use of stress-concentration factors for root fillets based on work by Dolan and Broghammer.^[6] Assumption 6 is self-explanatory. Also, this method is valid only for external gear teeth. The geometry of internal gear teeth is sufficiently different to require another approach to the calculation of bending stresses. See the AGMA standard for more information.

The AGMA bending stress equation differs slightly for U.S. and SI specification gears due to the reciprocal relationship between diametral pitch and module. We will list both versions with suffixes of *us* or *si* on the equation numbers where applicable.

$$\sigma_b = \frac{W_t p_d}{FJ} \frac{K_a K_m}{K_v} K_s K_B K_I \quad (12.15\textit{us})$$

$$\sigma_b = \frac{W_t}{FmJ} \frac{K_a K_m}{K_v} K_s K_B K_I \quad (12.15\textit{si})$$

The core of this equation is Lewis's formula with the updated geometry factor J substituted for his form factor Y . W_t , F , and p_d have the same meanings as in equation 12.14 and m is the metric module. The K factors are modifiers to account for various conditions. We will now discuss each of the empirical terms in equation 12.15.

BENDING STRENGTH GEOMETRY FACTOR J The geometry factor J can be calculated from a complicated algorithm defined in AGMA Standard 908-B89. The same standard also provides tables of J factors for standard, full-depth teeth and for 25% and 50% unequal-addendum teeth, all with 14.5, 20, and 25° pressure angles. These J factors vary with the numbers of teeth on the pinion and gear and are given only for a range of combinations which obey assumption 2 above. The AGMA recommends that tooth-number combinations that create interference be avoided.

Tables 12-8 through 12-15* replicate the AGMA geometry factors J for a subset of the gear-tooth combinations covered in the standard. In these eight tables, two gear-tooth designs are covered (the full-depth tooth, and the 25%-long-addendum tooth), each for two pressure angles (20 and 25°), and both for tip loading and for loading at the highest point of single-tooth contact (HPSTC). See the standard for other combinations.

Note in these tables that the J factors are different for the pinion and gear (labeled P and G) in each mesh combination. This results in different bending stress levels in the pinion teeth than in the gear teeth. The letter U in the tables indicates that undercutting occurs with that combination due to interference between the tip of the gear tooth and the root-flank of the pinion. The choice between tip-loaded or HPSTC J factors should be based on the manufacturing precision of the gearset. If the manufacturing tolerances are small (high-precision gears), then load sharing between the teeth can be assumed and the HPSTC tables used. If not, then it is likely that only one pair of teeth will take all the load at the tip in the worst case, as seen in Figure 12-19 (p. 706). See the AGMA Standard 908-B89 for more information on acceptable manufacturing variations in base pitch to ensure HPSTC.

* Extracted from AGMA Standard 908-B89, INFORMATION SHEET, *Geometry Factors for Determining the Pitting Resistance and Bending Strength of Spur, Helical, and Herringbone Gear Teeth*, with the permission of the publisher, American Gear Manufacturers Association, 1500 King St., Suite 201, Alexandria, Va., 22314.

DYNAMIC FACTOR K_v The dynamic factor K_v attempts to account for internally generated vibration loads from tooth-tooth impacts induced by nonconjugate meshing of the gear teeth. These vibration loads are called **transmission error** and will be worse with low-accuracy gears. Precision gears will more closely approach the ideal of smooth, constant-velocity-ratio torque transmission. In the absence of test data that define the level of transmission error to be expected in a particular gear design, the designer must estimate the dynamic factor. The AGMA provides empirical curves for K_v as a function of pitch-line velocity V_t . Figure 12-22* shows a family of these curves, which vary with the quality index Q_v of the gearset. Empirical equations for the curves numbered 6 through 11 in Figure 12-22 are

$$K_v = \left(\frac{A}{A + \sqrt{V_t}} \right)^B \quad (12.16us)$$

$$K_v = \left(\frac{A}{A + \sqrt{200V_t}} \right)^B \quad (12.16si)$$

where V_t is the pitch-line velocity of the gear mesh in units of ft/min (U.S.) or m/s (SI). The factors A and B are defined as

$$A = 50 + 56(1 - B) \quad (12.17a)$$

$$B = \frac{(12 - Q_v)^{2/3}}{4} \quad \text{for } 6 \leq Q_v \leq 11 \quad (12.17b)$$

* Extracted from AGMA Standard 2001-B88, *Fundamental Rating Factors and Calculation Methods for Involute Spur and Helical Gear Teeth*, with the permission of the publisher, American Gear Manufacturers Association, 1500 King St., Suite 201, Alexandria, Va., 22314.

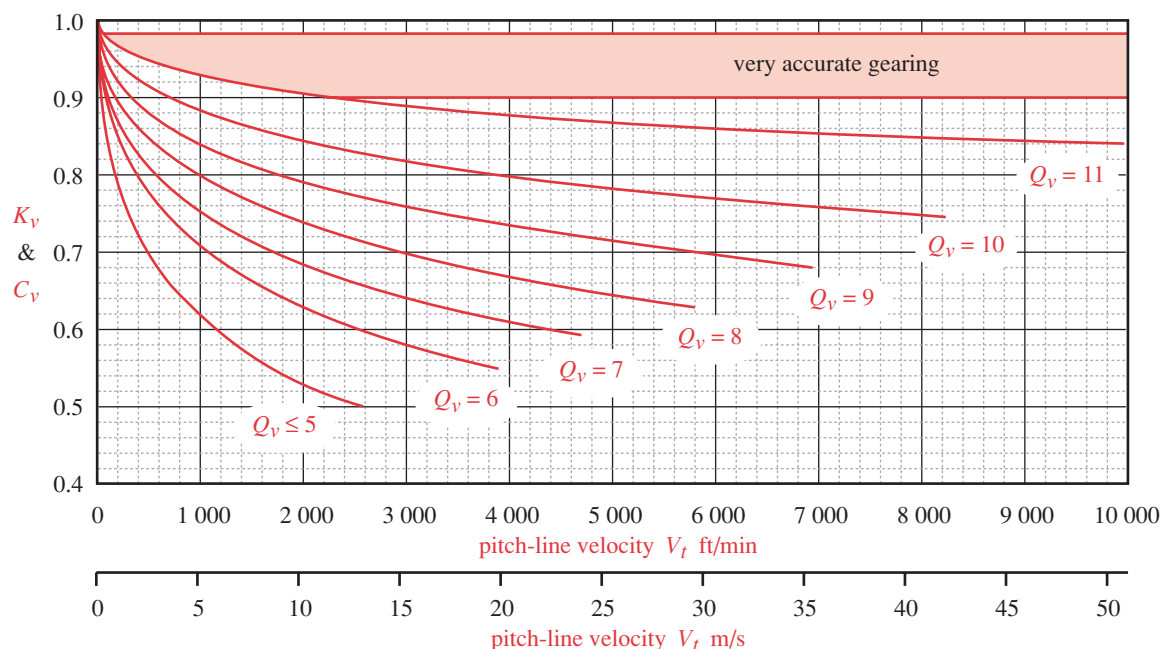


FIGURE 12-22

AGMA Dynamic Factors K_v and C_v

Table 12-8 AGMA Bending Geometry Factor J for 20°, Full-Depth Teeth with Tip Loading

Gear teeth	Pinion teeth															
	12		14		17		21		26		35		55		135	
	P	G	P	G	P	G	P	G	P	G	P	G	P	G	P	G
12	U	U														
14	U	U	U	U												
17	U	U	U	U	U	U										
21	U	U	U	U	U	U	0.24	0.24								
26	U	U	U	U	U	U	0.24	0.25	0.25	0.25						
35	U	U	U	U	U	U	0.24	0.26	0.25	0.26	0.26	0.26				
55	U	U	U	U	U	U	0.24	0.28	0.25	0.28	0.26	0.28	0.28	0.28		
135	U	U	U	U	U	U	0.24	0.29	0.25	0.29	0.26	0.29	0.28	0.29	0.29	0.29

Table 12-9 AGMA Bending Geometry Factor J for 20°, Full-Depth Teeth with HPSTC Loading

Gear teeth	Pinion teeth															
	12		14		17		21		26		35		55		135	
	P	G	P	G	P	G	P	G	P	G	P	G	P	G	P	G
12	U	U														
14	U	U	U	U												
17	U	U	U	U	U	U										
21	U	U	U	U	U	U	0.33	0.33								
26	U	U	U	U	U	U	0.33	0.35	0.35	0.35						
35	U	U	U	U	U	U	0.34	0.37	0.36	0.38	0.39	0.39				
55	U	U	U	U	U	U	0.34	0.40	0.37	0.41	0.40	0.42	0.43	0.43		
135	U	U	U	U	U	U	0.35	0.43	0.38	0.44	0.41	0.45	0.45	0.47	0.49	0.49

Table 12-10 AGMA Bending Geometry Factor J for 20°, 25%-Long-Addendum Teeth with Tip Loading

Gear teeth	Pinion teeth															
	12		14		17		21		26		35		55		135	
	P	G	P	G	P	G	P	G	P	G	P	G	P	G	P	G
12	U	U														
14	U	U	U	U												
17	U	U	U	U	0.27	0.19										
21	U	U	U	U	0.27	0.21	0.27	0.21								
26	U	U	U	U	0.27	0.22	0.27	0.22	0.28	0.22						
35	U	U	U	U	0.27	0.24	0.27	0.24	0.28	0.24	0.28	0.24				
55	U	U	U	U	0.27	0.26	0.27	0.26	0.28	0.26	0.28	0.26	0.29	0.26		
135	U	U	U	U	0.27	0.28	0.27	0.28	0.28	0.28	0.28	0.28	0.29	0.28	0.30	0.28

Table 12-11 AGMA Bending Geometry Factor J for 20°, 25%-Long-Addendum Teeth with HPSTC Loading

Gear teeth	Pinion teeth															
	12		14		17		21		26		35		55		135	
	P	G	P	G	P	G	P	G	P	G	P	G	P	G	P	G
12	U	U														
14	U	U	U	U												
17	U	U	U	U	0.36	0.24										
21	U	U	U	U	0.37	0.26	0.39	0.27								
26	U	U	U	U	0.37	0.29	0.39	0.29	0.41	0.30						
35	U	U	U	U	0.37	0.32	0.40	0.32	0.41	0.33	0.43	0.34				
55	U	U	U	U	0.38	0.35	0.40	0.36	0.42	0.36	0.44	0.37	0.47	0.39		
135	U	U	U	U	0.39	0.39	0.41	0.40	0.43	0.41	0.45	0.42	0.48	0.44	0.51	0.46

Table 12-12 AGMA Bending Geometry Factor J for 25°, Full-Depth Teeth with Tip Loading

Gear teeth	Pinion teeth															
	12		14		17		21		26		35		55		135	
	P	G	P	G	P	G	P	G	P	G	P	G	P	G	P	G
12	U	U														
14	U	U	0.28	0.28												
17	U	U	0.28	0.30	0.30	0.30										
21	U	U	0.28	0.31	0.30	0.31	0.31	0.31								
26	U	U	0.28	0.33	0.30	0.33	0.31	0.33	0.33	0.33						
35	U	U	0.28	0.34	0.30	0.34	0.31	0.34	0.33	0.34	0.34	0.34				
55	U	U	0.28	0.36	0.30	0.36	0.31	0.36	0.33	0.36	0.34	0.36	0.36	0.36		
135	U	U	0.28	0.38	0.30	0.38	0.31	0.38	0.33	0.38	0.34	0.38	0.36	0.38	0.38	0.38

12

Table 12-13 AGMA Bending Geometry Factor J for 25°, Full-Depth Teeth with HPSTC Loading

Gear teeth	Pinion teeth															
	12		14		17		21		26		35		55		135	
	P	G	P	G	P	G	P	G	P	G	P	G	P	G	P	G
12	U	U														
14	U	U	0.33	0.33												
17	U	U	0.33	0.36	0.36	0.36										
21	U	U	0.33	0.39	0.36	0.39	0.39	0.39								
26	U	U	0.33	0.41	0.37	0.42	0.40	0.42	0.43	0.43						
35	U	U	0.34	0.44	0.37	0.45	0.40	0.45	0.43	0.46	0.46	0.46				
55	U	U	0.34	0.47	0.38	0.48	0.41	0.49	0.44	0.49	0.47	0.50	0.51	0.51		
135	U	U	0.35	0.51	0.38	0.52	0.42	0.53	0.45	0.53	0.48	0.54	0.53	0.56	0.57	0.57

Table 12-14 AGMA Bending Geometry Factor J for 25°, 25%-Long-Addendum Teeth with Tip Loading

Gear teeth	Pinion teeth															
	12		14		17		21		26		35		55		135	
	P	G	P	G	P	G	P	G	P	G	P	G	P	G	P	G
12	0.32	0.20														
14	0.32	0.22	0.33	0.22												
17	0.32	0.25	0.33	0.25	0.34	0.25										
21	0.32	0.27	0.33	0.27	0.34	0.27	0.36	0.27								
26	0.32	0.29	0.33	0.29	0.34	0.29	0.36	0.29	0.36	0.29						
35	0.32	0.31	0.33	0.31	0.34	0.31	0.36	0.31	0.36	0.31	0.37	0.31				
55	0.32	0.34	0.33	0.34	0.34	0.34	0.36	0.34	0.36	0.34	0.37	0.34	0.38	0.34		
135	0.32	0.37	0.33	0.37	0.34	0.37	0.36	0.37	0.36	0.37	0.37	0.37	0.38	0.37	0.39	0.37

Table 12-15 AGMA Bending Geometry Factor J for 25°, 25%-Long-Addendum Teeth with HPSTC Loading

Gear teeth	Pinion teeth															
	12		14		17		21		26		35		55		135	
	P	G	P	G	P	G	P	G	P	G	P	G	P	G	P	G
12	0.38	0.22														
14	0.38	0.25	0.40	0.25												
17	0.38	0.29	0.40	0.29	0.43	0.29										
21	0.38	0.32	0.41	0.32	0.43	0.33	0.46	0.33								
26	0.39	0.35	0.41	0.35	0.44	0.36	0.46	0.36	0.48	0.37						
35	0.39	0.38	0.41	0.39	0.44	0.39	0.47	0.40	0.49	0.41	0.51	0.41				
55	0.39	0.42	0.42	0.43	0.44	0.44	0.47	0.44	0.49	0.45	0.52	0.46	0.55	0.47		
135	0.40	0.47	0.42	0.48	0.45	0.49	0.48	0.49	0.50	0.50	0.53	0.51	0.56	0.53	0.59	0.55

in which Q_v is the quality index of the lower-quality gear in the mesh.

Note in Figure 12-22 that these empirical curves each end abruptly at particular values of V_t . They can be extrapolated beyond those points, but the experimental data from which they were generated did not extend beyond those limits. The terminal values of V_t for each curve can be calculated from

$$V_{t_{max}} = [A + (Q_v - 3)]^2 \text{ ft/min} \quad (12.18us)$$

$$V_{t_{max}} = \frac{[A + (Q_v - 3)]^2}{200} \text{ m/s} \quad (12.18si)$$

For gears with $Q_v \leq 5$, a different equation is used:

$$K_v = \frac{50}{50 + \sqrt{V_t}} \quad (12.19us)$$

$$K_v = \frac{50}{50 + \sqrt{200V_t}} \quad (12.19si)$$

This relationship is valid only for $V_t \leq 2500$ ft/min (13 m/s), as can be seen from the $Q_v = 5$ line in Figure 12-22. Above that velocity gears of higher Q_v should be used. See Table 12-7.

Mark^[7] derives a method for computing the transmission error in parallel-axis gears that takes into account bearing misalignment, dynamic shaft misalignment, variations in tooth spacing, tooth profile modifications, and the stiffness of the structures supporting the bearings. If the actual dynamic loading due to transmission errors is known and is taken into account by increasing the applied load W_t , then the dynamic factor K_v can be set to 1.

LOAD DISTRIBUTION FACTOR K_m Any axial misalignment or axial deviation in tooth form will cause the transmitted load W_t to be unevenly distributed over the face width of the gear teeth. This problem becomes more pronounced with larger face widths. An approximate and conservative way to account for less than uniform load distribution is to apply the factor K_m to increase the stresses for larger face widths. Some suggested values are shown in Table 12-16. A useful rule of thumb is to keep the face width F of a spur gear within the limits $8/p_d < F < 16/p_d$, with a nominal value of $12/p_d$. This ratio is referred to as the **face width factor**.

APPLICATION FACTOR K_a The loading model discussed in Section 12-7 assumed that the transmitted load W_t was uniform with time. The fluctuating moments on the teeth described in that section are due to the teeth coming into and out of mesh under a uniform or average load. If either the driving or driven machine has time-varying torques or forces, then these will increase the loading felt by the gear teeth above the average values.

In the absence of definitive information about the dynamic loads in the driving and driven machines, an application factor K_a can be applied to increase the tooth stress based on the “shockiness” of the machinery connected to the gear train. For example, if the gear train connects an electric motor to a centrifugal water pump (both of which are smooth-running devices), there is no need to increase the average loads and $K_a = 1$. But, if a single-cylinder, internal-combustion engine drives a rock crusher through a gear train, both the power source and the driven device deliver shock loads to the gear teeth and $K_a > 1$. Table 12-17 shows some AGMA-suggested values for K_a based on the assumed level of shock loading in driving and driven devices.

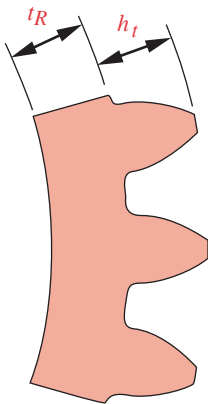
SIZE FACTOR K_s can be used in the same way as the size factor described in Chapter 6 for general fatigue loading. The test specimens used to develop fatigue strength data are relatively small (about 0.3 in dia). If the part being designed is larger than that, it may be weaker than indicated by the test data. The K_s factor allows a modification

Table 12-16Load Distribution Factors K_m

Face Width in (mm)	K_m
<2 (50)	1.6
6 (150)	1.7
9 (250)	1.8
≥ 20 (500)	2.0

Table 12-17 Application Factors K_a

Driving Machine	Driven Machine		
	Uniform	Moderate Shock	Heavy Shock
Uniform (Electric motor, turbine)	1.00	1.25	1.75 or higher
Light Shock (Multicylinder engine)	1.25	1.50	2.00 or higher
Medium Shock (Single-cylinder engine)	1.50	1.75	2.25 or higher

**FIGURE 12-23**

Parameters for AGMA Rim Thickness Factor K_B

of the tooth stress to account for such situations. However, many of the available gear strength data have been developed from tests of actual gear teeth and thus better represent reality than the general strength data of Chapter 6. The AGMA has not yet established standards for size factors and recommends that K_s be set to 1 unless the designer wishes to raise its value to account for particular situations, such as very large teeth. A value of 1.25 to 1.5 would be a conservative assumption in such cases.

RIM THICKNESS FACTOR K_B This factor was recently introduced by the AGMA to account for situations in which a large-diameter gear, made with a rim and spokes rather than as a solid disk, has a thin rim depth in comparison to the tooth depth. Such designs can fail with a radial fracture across the rim rather than through a tooth root. The AGMA defines a **backup ratio** m_B as

$$m_B = \frac{t_R}{h_t} \quad (12.20a)$$

where t_R is the rim thickness from the tooth root diameter to the rim's inside diameter and h_t is the whole depth of the tooth (the sum of addendum and dedendum) as shown in Figure 12-23.* This ratio is used to define the rim thickness factor from

$$\begin{aligned} K_B &= -2m_B + 3.4 & 0.5 \leq m_B \leq 1.2 \\ K_B &= 1.0 & m_B > 1.2 \end{aligned} \quad (12.20b)$$

Backup ratios < 0.5 are not recommended. Solid-disk gears will always have $K_B = 1$.

IDLER FACTOR K_I An idler gear is subjected both to more cycles of stress per unit time and to larger-magnitude alternating loads than its nonidler cousins. To account for this situation, the factor K_I is set to 1.42 for an idler gear or 1.0 for a nonidler gear. The AGMA uses the reciprocal of this factor to reduce the apparent strength of the material for an idler gear, but that is not consistent with the approach used in this text of applying factors that affect the stress state of a part to the stress equation, not to the material's strength.

EXAMPLE 12-5

Bending Stress Analysis of a Spur-Gear Train

Problem Determine a suitable face width and the bending stresses in the gear teeth of the 3-gear train from Example 12-4.

Given The transmitted load on the teeth is 432 lb. The pinion has 14 teeth, a 25° pressure angle, and $p_d = 6$. The idler has 17 teeth and the gear 49 teeth. Pinion speed is 2 500 rpm. See Example 12-3 for other dimensional information.

Assumptions The teeth are standard AGMA full-depth profiles. The load and source are both uniform in nature. A gear-quality index of 6 will be used.

* Extracted from AGMA Standard 2001-B88, *Fundamental Rating Factors and Calculation Methods for Involute Spur and Helical Gear Teeth*, with the permission of the publisher, American Gear Manufacturers Association, 1500 King St., Suite 201, Alexandria, Va., 22314.

Solution

- 1 Even though the transmitted load is the same, the bending stress in the teeth of each size gear will be different because of its slightly different tooth geometry. The general formula for tooth-bending stress is equation 12.15 (p. 710):

$$\sigma_b = \frac{W_t p_d}{FJ} \frac{K_a K_m}{K_v} K_s K_B K_I \quad (a)$$

W_t , p_d , F , K_a , K_m , K_v , and K_s are common to all gears in the set and J , K_B , and K_I are potentially different for each gear.

- 2 A first approximation of the face width can be estimated as a function of the diametral pitch. Take the middle of the recommended face-width-factor range $8 / p_d < F < 16 / p_d$ for a first calculation:

$$F \approx \frac{12}{p_d} = \frac{12}{6} = 2 \text{ in} \quad (b)$$

- 3 Based on the assumption of uniform load and source, the application factor K_a can be set to 1.
- 4 The load distribution factor can be estimated from Table 12-16 (p. 715) based on the assumed face width: $K_m = 1.6$.
- 5 The velocity factor K_v can be calculated from equations 12.16 and 12.17 (p. 711) based on the assumed gear-quality index Q_v and the pitch-line velocity V_t .

$$V_t = \frac{d_p}{2} \omega_p = \frac{2.33 \text{ in}}{2(12)} (2500 \text{ rpm})(2\pi) = 1527 \frac{\text{ft}}{\text{min}} \quad (c)$$

$$B = \frac{(12 - Q_v)^{2/3}}{4} = \frac{(12 - 6)^{2/3}}{4} = 0.826 \quad (d)$$

$$A = 50 + 56(1 - B) = 50 + 56(1 - 0.826) = 59.745 \quad (e)$$

$$K_v = \left(\frac{A}{A + \sqrt{V_t}} \right)^B = \left(\frac{59.745}{59.745 + \sqrt{1527}} \right)^{0.826} = 0.660 \quad (f)$$

- 6 The size factor $K_s = 1$ for all three gears.
- 7 These gears are all too small to have a rim and spokes, so $K_B = 1$.
- 8 The idler factor $K_I = 1$ for the pinion and gear and $K_I = 1.42$ for the idler gear.
- 9 The bending geometry factor J for the 25° , 14-tooth pinion in mesh with the 17-tooth idler is found from Table 12-13 (p. 713) to be $J_{pinion} = 0.33$. The pinion-tooth bending stress is then
- 12
- $$\sigma_{b_p} = \frac{W_t p_d}{FJ} \frac{K_a K_m}{K_v} K_s K_B K_I = \frac{432(6)}{2(0.33)} \frac{1(1.6)}{0.66} (1)(1)(1) = 9526 \text{ psi} \quad (g)$$
- 10 The bending geometry factor J for the 25° , 17-tooth idler in mesh with the 14-tooth pinion is found from Table 12-13 to be $J_{idler} = 0.36$. The idler-tooth bending stress is then

$$\sigma_{b_i} = \frac{W_t P_d}{FJ} \frac{K_a K_m}{K_v} K_s K_B K_I = \frac{432(6)}{2(0.36)} \frac{1(1.6)}{0.66} (1)(1)(1.42) = 12\,400 \text{ psi} \quad (h)$$

Note in Table 12-13 that the idler has a different J factor when considered to be the “gear” in mesh with the smaller pinion (0.36) than when considered to be the “pinion” in mesh with the larger gear (0.37). The smaller value of the two is used because it gives the higher stress.

- 11 The bending geometry factor J for the 25° , 49-tooth gear in mesh with the 17-tooth idler is found (by interpolation) from Table 12-13 to be $J_{gear} = 0.46$. The gear tooth bending stress is then

$$\sigma_{b_g} = \frac{W_t P_d}{FJ} \frac{K_a K_m}{K_v} K_s K_B K_I \approx \frac{432(6)}{2(0.46)} \frac{1(1.6)}{0.66} (1)(1)(1) \approx 6\,834 \text{ psi} \quad (i)$$

- 12 If this is an acceptable stress level, then the assumed face width can be used. This issue will be revisited for this design in a later example.
- 13 The files EX12-05 can be found on the CD-ROM.
-

Surface Stresses

Mating gear teeth have a combination of rolling and sliding at their interface. At the pitch point, their relative motion is pure rolling. The percentage of sliding increases with distance from the pitch point. An average value of 9% sliding is sometimes taken to represent the combined roll-slide motion between the teeth.^[8] The stresses at the tooth surface are dynamic Hertzian contact stresses in combined rolling and sliding, as defined in Section 7.11 (p. 453). These stresses are three-dimensional and have peak values either at the surface or slightly below it, depending on the amount of sliding present in combination with rolling. Depending on the surface velocity, tooth radii of curvature, and lubricant viscosity, a condition of full or partial elastohydrodynamic (EHD) lubrication or of boundary lubrication may exist in the interface as described in Chapter 11. If sufficient, clean lubricant of an appropriate type is provided in order to create at least partial EHD lubrication (specific film thickness $\Lambda > 2$) and prevent surface failure by the adhesive, abrasive, or corrosive mechanisms described in Chapter 7, the ultimate failure mode will be pitting and spalling due to surface fatigue. See Section 7.7 (p. 436) for a discussion of this mechanism and Figure 7-12 (p. 439) for examples of gear tooth surface failure.

The surface stresses in gear teeth were first investigated in a systematic way by Buckingham^[9] who recognized that two cylinders having the same radius of curvature as the gear teeth at the pitch point, and radially loaded in rolling contact, could be used to simulate gear tooth contact while controlling the necessary variables. His work led to the development of an equation for surface stresses in gear teeth that is now known as the Buckingham equation. It serves as the basis for the AGMA pitting resistance formula,^[2] which is

$$\sigma_c = C_p \sqrt{\frac{W_t}{FId} \frac{C_a C_m}{C_v} C_s C_f} \quad (12.21)$$

where W_t is the tangential force on the tooth, d the pitch diameter of the smaller of the two gears in mesh, F the face width, and I is a dimensionless **surface geometry factor** for pitting resistance. C_p is an **elastic coefficient** that accounts for differences in the gear and pinion material constants. The factors C_a , C_m , C_v , and C_s are equal, respectively, to K_a , K_m , K_v , and K_s as defined for the bending stress equation 12.15 (p. 710). The new factors I , C_p , and C_f will now be defined.

SURFACE GEOMETRY FACTOR I This factor takes into account the radii of curvature of the gear teeth and the pressure angle. AGMA defines an equation for I :

$$I = \frac{\cos \phi}{\left(\frac{1}{\rho_p} \pm \frac{1}{\rho_g} \right) d_p} \quad (12.22a)$$

where ρ_p and ρ_g are the radii of curvature of the pinion and gear teeth, respectively, ϕ is the pressure angle, and d_p is the pitch diameter of the pinion. The \pm sign accounts for external and internal gearsets. Use the upper sign for external gearsets in all related expressions. The radii of curvature of the teeth are calculated from the mesh geometry:

$$\begin{aligned} \rho_p &= \sqrt{\left(r_p + \frac{1+x_p}{p_d} \right)^2 - \left(r_p \cos \phi \right)^2} - \frac{\pi}{p_d} \cos \phi \\ \rho_g &= C \sin \phi \mp \rho_p \end{aligned} \quad (12.22b)$$

where p_d is the diametral pitch, r_p is the pitch radius of the pinion, ϕ is the pressure angle, C is the center distance between pinion and gear, and x_p is the pinion addendum coefficient, which is equal to the decimal percentage of addendum elongation for unequal addendum teeth. For standard, full-depth teeth, $x_p = 0$. For 25%-long-addendum teeth, $x_p = 0.25$, etc. Note the choice of sign in the second equation of 12.22b. Use the upper sign for an external gearset and the lower one for an internal gearset.

ELASTIC COEFFICIENT C_p The elastic coefficient accounts for differences in tooth materials and is found from

$$C_p = \sqrt{\frac{1}{\pi \left[\left(\frac{1-v_p^2}{E_p} \right) + \left(\frac{1-v_g^2}{E_g} \right) \right]}} \quad (12.23)$$

where E_p and E_g are, respectively, the moduli of elasticity for pinion and gear, and v_p and v_g are their respective Poisson's ratios. The units of C_p are either $(\text{psi})^{0.5}$ or $(\text{MPa})^{0.5}$. Table 12-18* shows values of C_p for various combinations of common gear and pinion materials based on an assumed $v = 0.3$ for all the materials.

SURFACE FINISH FACTOR C_f is used to account for unusually rough surface finishes on gear teeth. The AGMA has not yet established standards for surface-finish factors and recommends that C_f be set to 1 for gears made by conventional methods. Its value can be increased to account for unusually rough surface finishes or for the known presence of detrimental residual stresses.

* Extracted from AGMA Standard 2001-B88, *Fundamental Rating Factors and Calculation Methods for Involute Spur and Helical Gear Teeth*, with the permission of the publisher, American Gear Manufacturers Association, 1500 King St., Suite 201, Alexandria, Va., 22314.

Table 12-18 AGMA Elastic Coefficient C_p in Units of $[\text{psi}]^{0.5}$ ($[\text{MPa}]^{0.5}$)^{*†}

Pinion Material	E_p psi (MPa)	Gear Material					
		Steel	Malleable Iron	Nodular Iron	Cast Iron	Aluminum Bronze	Tin Bronze
Steel	$30E6$ ($2E5$)	2 300 (191)	2 180 (181)	2 160 (179)	2 100 (174)	1 950 (162)	1 900 (158)
Malleable Iron	$25E6$ ($1.7E5$)	2 180 (181)	2 090 (174)	2 070 (172)	2 020 (168)	1 900 (158)	1 850 (154)
Nodular Iron	$24E6$ ($1.7E5$)	2 160 (179)	2 070 (172)	2 050 (170)	2 000 (166)	1 880 (156)	1 830 (152)
Cast Iron	$22E6$ ($1.5E5$)	2 100 (174)	2 020 (168)	2 000 (166)	1 960 (163)	1 850 (154)	1 800 (149)
Aluminum Bronze	$17.5E6$ ($1.2E5$)	1 950 (162)	1 900 (158)	1 880 (156)	1 850 (154)	1 750 (145)	1 700 (141)
Tin Bronze	$16E6$ ($1.1E5$)	1 900 (158)	1 850 (154)	1 830 (152)	1 800 (149)	1 700 (141)	1 650 (137)

^{*}The values of E_p in this table are approximate and $\nu = 0.3$ was used as an approximation of Poisson's ratio for all materials. If more accurate numbers are available for E_p and ν , they should be used in equation 11.23 to obtain C_p .

EXAMPLE 12-6

Surface Stress Analysis of a Spur-Gear Train

Problem Determine the surface stresses in the gear teeth of the 3-gear train from Examples 12-4 and 12-5.

Given The transmitted load on the teeth is 432 lb. The pinion has 14 teeth, a 25° pressure angle, and $p_d = 6$. The idler has 17 teeth and the gear 49 teeth. Pinion speed is 2 500 rpm. Face width is 2 in. See Example 12-3 for other dimensional information.

Assumptions The teeth are standard AGMA full-depth profiles. The load and source are both uniform in nature. A gear-quality index of 6 will be used. All gears are steel with $\nu = 0.28$.

Solution

- 1 The general formula for tooth-surface stress is equation 12.21 (p. 718):

$$\sigma_c = C_p \sqrt{\frac{W_t}{FId} \frac{C_a C_m}{C_v} C_s C_f} \quad (a)$$

W_t , F , C_a , C_m , C_v , and C_s are common to all gears in the set. C_p , d , C_f , and I are potentially different for each pair in mesh. Use the smaller d of the pair in mesh.

- 2 The face width can be estimated as a function of the diametral pitch. Take the middle of the recommended range $8/p_d < F < 16/p_d$ for a first calculation:

$$F \cong \frac{12}{p_d} = \frac{12}{6} = 2 \text{ in} \quad (b)$$

* Extracted from AGMA Standard 2001-B88, *Fundamental Rating Factors and Calculation Methods for Involute Spur and Helical Gear Teeth*, with the permission of the publisher, American Gear Manufacturers Association, 1500 King St., Suite 201, Alexandria, Va., 22314.

- 3 Given a uniform load and source, the application factor C_a can be set to 1.
- 4 The load distribution factor can be estimated from Table 12-16 (p. 715) based on the assumed face width: $C_m = K_m = 1.6$.
- 5 The velocity factor C_v can be calculated from equations 12.16 and 12.17 (p. 711) based on the assumed gear-quality index Q_v and the pitch-line velocity V_t .

$$V_t = \frac{d_p}{2} \omega_p = \frac{2.33 \text{ in}}{2(12)} (2500 \text{ rpm})(2\pi) = 1527 \frac{\text{ft}}{\text{min}} \quad (c)$$

$$B = \frac{(12 - Q_v)^{2/3}}{4} = \frac{(12 - 6)^{2/3}}{4} = 0.826 \quad (d)$$

$$A = 50 + 56(1 - B) = 50 + 56(1 - 0.826) = 59.745 \quad (e)$$

$$C_v = \left(\frac{A}{A + \sqrt{V_t}} \right)^B = \left(\frac{59.745}{59.745 + \sqrt{1527}} \right)^{0.826} = 0.660 \quad (f)$$

- 6 The size factor $C_s = 1$ for all three gears.
- 7 The surface factor $C_f = 1$ for well-finished gears made by conventional methods.
- 8 The elastic coefficient C_p is found from equation 12.23 (p. 719).

$$C_p = \sqrt{\frac{1}{\pi \left[\left(\frac{1 - v_p^2}{E_p} \right) + \left(\frac{1 - v_g^2}{E_g} \right) \right]}} = \sqrt{\frac{1}{\pi \left[\left(\frac{1 - 0.28^2}{30E6} \right) + \left(\frac{1 - 0.28^2}{30E6} \right) \right]}} = 2276 \quad (g)$$

- 9 The pitting geometry factor I is calculated for a pair of gears in mesh. Since we have two meshes (pinion/idler and idler/gear), there will be two different values of I to be calculated using equations 12.22 (p. 719). We will need the pitch diameter and pitch radius of each gear for this calculation. From the data in Example 12-4:

$$\begin{aligned} d_p &= 2.333 & d_i &= 2.833 & d_g &= 8.167 \\ r_p &= 1.167 & r_i &= 1.417 & r_g &= 4.083 \end{aligned} \quad (h)$$

- 10 For the pinion/idler pair, let $I_{pi} = I$, $d_1 = d_p$, $r_1 = r_p$, and $r_2 = r_i$; then

$$\begin{aligned} \rho_1 &= \sqrt{\left(r_1 + \frac{1}{p_d} \right)^2 - (r_1 \cos \phi)^2} - \frac{\pi}{p_d} \cos \phi \\ &= \sqrt{\left(1.167 + \frac{1}{6} \right)^2 - (1.167 \cos 25^\circ)^2} - \frac{\pi}{6} \cos 25^\circ = 0.338 \text{ in} \end{aligned} \quad (i)$$

$$\begin{aligned} \rho_2 &= C \sin \phi - \rho_1 = (r_1 + r_2) \sin \phi - \rho_1 \\ &= (1.167 + 1.417) \sin 25^\circ - 0.338 = 0.754 \text{ in} \end{aligned} \quad (j)$$

$$I_{pi} = \frac{\cos \phi}{\left(\frac{1}{\rho_1} \pm \frac{1}{\rho_2} \right) d_1} = \frac{\cos 25^\circ}{\left(\frac{1}{0.338} + \frac{1}{0.754} \right) 2.33} = 0.091 \quad (k)$$

11 For the idler/gear pair, let $I_{ig} = I$, $d_1 = d_i$, $r_1 = r_i$, and $r_2 = r_g$, then

$$\begin{aligned}\rho_1 &= \sqrt{\left(r_1 + \frac{1}{p_d}\right)^2 - (r_1 \cos\phi)^2} - \frac{\pi}{p_d} \cos\phi \\ &= \sqrt{\left(1.417 + \frac{1}{6}\right)^2 - (1.417 \cos 25^\circ)^2} - \frac{\pi}{6} \cos 25^\circ = 0.452 \text{ in} \quad (l)\end{aligned}$$

$$\begin{aligned}\rho_2 &= C \sin\phi - \rho_1 = (r_1 + r_2) \sin\phi - \rho_1 \\ &= (1.417 + 4.083) \sin 25^\circ - 0.452 = 1.872 \text{ in} \quad (m)\end{aligned}$$

$$I_{ig} = \frac{\cos\phi}{\left(\frac{1}{\rho_1} \pm \frac{1}{\rho_2}\right)d_1} = \frac{\cos 25^\circ}{\left(\frac{1}{0.452} + \frac{1}{1.872}\right)2.83} = 0.116 \quad (n)$$

12 The surface stress for the pinion-idler mesh is then

$$\begin{aligned}\sigma_{c_p} &= C_p \sqrt{\frac{W_t}{FI_{pi}d_p} \frac{C_a C_m}{C_v} C_s C_f} \\ &= 2276 \sqrt{\frac{432}{2(0.091)(2.33)} \frac{1(1.6)}{0.66}(1)(1)} = 113 \text{ kpsi} \quad (o)\end{aligned}$$

13 The surface stress for the idler-gear mesh is then

$$\begin{aligned}\sigma_{c_i} &= C_p \sqrt{\frac{W_t}{FI_{ig}d_i} \frac{C_a C_m}{C_v} C_s C_f} \\ &= 2276 \sqrt{\frac{432}{2(0.116)(2.83)} \frac{1(1.6)}{0.66}(1)(1)} = 91 \text{ kpsi} \quad (p)\end{aligned}$$

14 The files EX12-06 can be found on the CD-ROM.

12.9 GEAR MATERIALS

Only a limited number of metals and alloys are suitable for gears that transmit significant power. Table 12-18 (p. 720) shows some of them. Steels, cast irons, and malleable and nodular irons are the most common choices for gears. Surface or through hardening is recommended (on those alloys that allow it) to obtain sufficient strength and wear resistance. Where high corrosion resistance is needed, such as in marine environments, bronzes are often used. The combination of a bronze gear and a steel pinion has advantages in terms of material compatibility and conformity, as discussed in Chapter 7, and this combination is often used in nonmarine applications as well.

CAST IRONS are commonly used for gears. The gray cast irons (CI) have advantages of low cost, ease of machining, high wear resistance, and internal damping (due to the graphite inclusions), which makes them acoustically quieter than steel gears. However, they have low tensile strength, which requires larger teeth than steel gears to

obtain sufficient bending strength. Nodular irons have higher tensile strength than gray CI and retain the other advantages of machinability, wear resistance, and internal damping, but are more costly. The combination of a steel pinion (for strength in the higher-stressed member) and a cast iron gear is often used.

STEELS are also commonly used for gears. They have superior tensile strength to cast iron and are cost competitive in their low-alloy forms. They need heat treatment to get a surface hardness that will resist wear, but soft steel gears are sometimes used in low-load, low-speed applications or where long life may not be a prime concern. For heat treatment, either a medium-to-high carbon (0.35 to 0.60% C) plain or alloy steel is needed. Small gears are typically through-hardened and larger gears flame or induction hardened to minimize distortion. Lower-carbon steels can be case hardened by carburizing or nitriding. A case-hardened gear has the advantage of a tough core and a hard surface, but if the case is not deep enough, the teeth may fail in bending fatigue beneath the case in the soft, weaker core material. It is often necessary to use secondary finishing methods such as grinding, lapping, and honing to remove the heat-treatment distortion from hardened gears if high accuracy is needed.

BRONZES are the most common nonferrous metals used for gears. The lower modulus of elasticity of these copper alloys provides greater tooth deflection and improves load sharing between the teeth. Since bronze and steel run well together, the combination of a steel pinion and a bronze gear is often used.

NONMETALLIC GEARS are often made of injection-molded thermoplastics such as nylon and acetal, sometimes filled with inorganics such as glass or talc. Teflon is sometimes added to nylon or acetal to lower the coefficient of friction. Dry lubricants such as graphite and molybdenum disulphide (MoS_2) can be added to the plastic to allow dry running. Composite gears of cloth-reinforced thermosetting phenolic have long been used for applications such as the camshaft-drive (timing) gear driven by a steel pinion in some gasoline engines. Nonmetallic gears have very low noise but are limited in torque capacity by their low material strengths.

Material Strengths

Since both of the gear-failure modes involve fatigue loading, material fatigue strength data are needed, both for bending stresses and for surface contact stresses. The methods for estimating fatigue strength outlined in Chapter 6 could be used for gear applications, since the principles involved are the same. However, better data are available on the fatigue strengths of gear alloys because of the extensive testing programs that have been done for this application over the past century. Test data for fatigue strengths of most gear materials have been compiled by the AGMA. As stated in Section 6.6 (p. 327) of this text:

The best information on a material's fatigue strength at some finite life, or its endurance limit at infinite life, comes from the testing of actual or prototype assemblies of the design . . . If published data are available for the fatigue strength S_f' or endurance limit S_e' of the material, they should be used . . .

So, it would not make sense to start by assuming an uncorrected fatigue strength as a fraction of the static ultimate tensile strength and then reducing it by the collection of correction factors outlined in Section 6.6 (p. 327), if we have more nearly correct fatigue-strength data available.

AGMA Bending-Fatigue Strengths for Gear Materials

The published AGMA data for both bending- and surface-fatigue strengths are, in effect, partially corrected fatigue strengths, since they are generated with appropriately sized parts having the same geometry, surface finish, etc., as the gears to be designed. The AGMA refers to material strengths as *allowable stresses*, which is not consistent with our procedure of reserving the term *stress* for the results of applied loading and using the term *strength* to refer to material properties. For internal consistency within this text we will designate the published AGMA bending-fatigue strength data as S_{fb}' to differentiate it from the completely uncorrected fatigue strength S_f' of Chapter 6. There are still three correction factors that need to be applied to the published AGMA bending-fatigue strength data in order to obtain what we will designate as the corrected bending-fatigue strength for gears S_{fb} .

The AGMA bending-fatigue strength data are all stated at $1E7$ cycles of repeated stress (rather than the $1E6$ or $5E8$ cycles sometimes used for other materials), and for a 99% reliability level (rather than the 50% reliability common for general fatigue and static strength data). These strengths are compared to the peak stress σ_b calculated from equation 12.15 (p. 710) using the load W_t . The Goodman-line analysis is encapsulated in this direct comparison, because the strength data are obtained from a test that provides a fluctuating stress state identical to that of the actual gear loading.

The correction formula for the bending-fatigue strength of gears is

$$S_{fb} = \frac{K_L}{K_T K_R} S_{fb}' \quad (12.24)$$

where S_{fb}' is the published AGMA bending-fatigue strength as defined above, S_{fb} is the corrected strength, and the K factors are modifiers to account for various conditions. These modifiers will now be defined and briefly discussed.

LIFE FACTOR K_L Since the test data are for a life of $1E7$ cycles, a shorter or longer cycle life will require modification of the bending-fatigue strength based on the S - N relationship for the material. The number of load cycles in this case is defined as the number of mesh contacts, under load, of the gear tooth being analyzed. Figure 12-24* shows S - N curves for the bending-fatigue strength of steels having several different tensile strengths as defined by their Brinell hardness numbers. Curve-fitted equations are also shown in the figure for each S - N line. These equations can be used to compute the appropriate K_L factor for a required number of load cycles N . The AGMA suggests that:

The upper portion of the shaded zone can be used for commercial applications. The lower portion of the shaded zone is typically used for critical service applications where little pitting and tooth wear is permissible and where smoothness of operation and low vibration levels are required.

Unfortunately, similar data have not yet been developed for gear materials other than these steels.

TEMPERATURE FACTOR K_T The lubricant temperature is a reasonable measure of gear temperature. For steel materials in oil temperatures up to about 250°F , K_T can be set to 1. For higher temperatures, K_T can be estimated from

$$K_T = \frac{460 + T_F}{620} \quad (12.24a)$$

* Extracted from AGMA Standard 2001-B88, *Fundamental Rating Factors and Calculation Methods for Involute Spur and Helical Gear Teeth*, with the permission of the publisher, American Gear Manufacturers Association, 1500 King St., Suite 201, Alexandria, VA 22314.

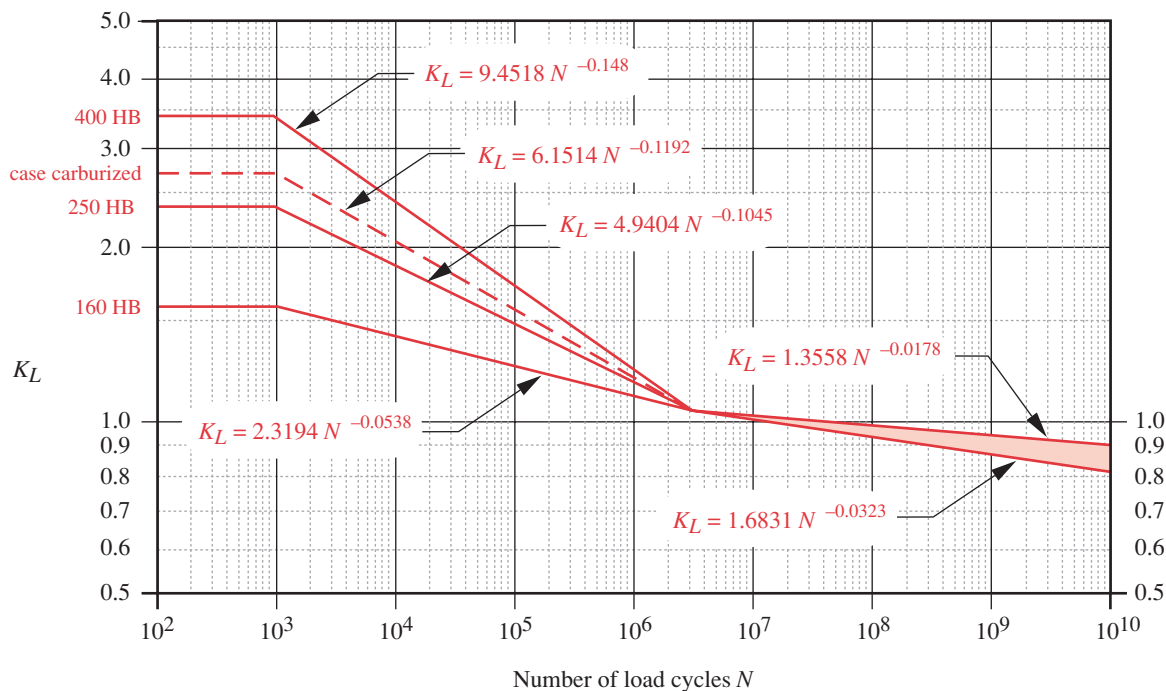


FIGURE 12-24*

AGMA Bending Strength Life Factor K_L

where T_F is the oil temperature in °F. Do not use this relationship for materials other than steel.

RELIABILITY FACTOR K_R The AGMA strength data are based on a statistical probability of 1 failure in 100 samples, or a 99% reliability. If this is satisfactory, set $K_R = 1$. If either a higher or lower reliability factor is desired, K_R can be set to one of the values in Table 12-19.*

BENDING-FATIGUE STRENGTH DATA Table 12-20 shows AGMA bending-fatigue strengths for a number of commonly used gear materials. The AGMA standard also defines heat-treatment specifications where applicable. A plot showing ranges of AGMA bending-fatigue strengths for steels as a function of their Brinell hardness is shown in Figure 12-25.* See the referenced standard for the metallurgical properties required for AGMA grades of steels. To achieve the strength values in Table 12-20 and Figure 12-25, the material should be specified to comply with that standard.

AGMA Surface-Fatigue Strengths for Gear Materials

We will designate the published AGMA surface-fatigue strength data as S_{fc}' . There are four correction factors that need to be applied to the published AGMA data in order to obtain what we will designate as the corrected surface-fatigue strength for gears S_{fc} ,

$$S_{fc} = \frac{C_L C_H}{C_T C_R} S_{fc}' \quad (12.25)$$

Table 12-19
AGMA Factor K_R

Reliability %	K_R
90	0.85
99	1.00
99.9	1.25
99.99	1.50

* Extracted from AGMA Standard 2001-B88, *Fundamental Rating Factors and Calculation Methods for Involute Spur and Helical Gear Teeth*, with the permission of the publisher, American Gear Manufacturers Association, 1500 King St., Suite 201, Alexandria, Va., 22314.

Table 12-20 AGMA Bending-Fatigue Strengths S_{fb}' for a Selection of Gear Materials*

Material	AGMA Class	Material Designation	Heat Treatment	Minimum Surface Hardness	Bending-Fatigue Strength	
					psi $\times 10^3$	MPa
Steel	A1-A5		Through hardened	≤ 180 HB	25-33	170-230
			Through hardened	240 HB	31-41	210-280
			Through hardened	300 HB	36-47	250-325
			Through hardened	360 HB	40-52	280-360
			Through hardened	400 HB	42-56	290-390
			Flame or induction hardened	Type A pattern 50-54 HRC	45-55	310-380
			Flame or induction hardened	Type B pattern	22	150
			Carburized and case hardened	55-64 HRC	55-75	380-520
		AISI 4140	Nitrided	84.6 HR15N [†]	34-45	230-310
		AISI 4340	Nitrided	83.5 HR15N	36-47	250-325
		Nitr alloy 135M	Nitrided	90.0 HR15N	38-48	260-330
		Nitr alloy N	Nitrided	90.0 HR15N	40-50	280-345
		2.5% Chrome	Nitrided	87.5-90.0 15N	55-65	380-450
Cast iron	20	Class 20	As cast		5	35
	30	Class 30	As cast	175 HB	8	69
	40	Class 40	As cast	200 HB	13	90
Nodular (ductile) iron	A-7-a	60-40-18	Annealed	140 HB	22-33	150-230
	A-7-c	80-55-06	Quenched and tempered	180 HB	22-33	150-230
	A-7-d	100-70-03	Quenched and tempered	230 HB	27-40	180-280
	A-7-e	120-90-02	Quenched and tempered	230 HB	27-40	180-280
Malleable iron (pearlitic)	A-8-c	45007		165 HB	10	70
	A-8-e	50005		180 HB	13	90
	A-8-f	53007		195 HB	16	110
	A-8-i	80002		240 HB	21	145
Bronze	Bronze 2	AGMA 2C	Sand cast	40 ksi min tensile strength	5.7	40
	Al/Br 3	ASTM B-148 78 alloy 954	Heat treated	90 ksi min tensile strength	23.6	160

[†] Rockwell 15N scale used for case-hardened materials—see Section 2-4

where S_{fc}' is the published surface-fatigue strength as defined in Table 12-21 (p. 728) and Figure 12-26, S_{fc} is the corrected strength and the C factors are modifiers to account for various conditions. The factors C_T and C_R are identical, respectively, to K_T and K_R and can be chosen as described in the previous section. The life factor C_L has the same purpose as K_L in equation 12.24 but references a different $S-N$ diagram. C_H is a hardness-ratio factor for pitting resistance. These two different factors will now be defined.

* Extracted from AGMA Standard 2001-B88, *Fundamental Rating Factors and Calculation Methods for Involute Spur and Helical Gear Teeth*, with the permission of the publisher, American Gear Manufacturers Association, 1500 King St., Suite 201, Alexandria, Va., 22314.

SURFACE-LIFE FACTOR C_L Since the published surface-fatigue test data are for a life of $1E7$ cycles, a shorter or longer cycle life will require modification of the surface-fatigue strength based on the $S-N$ relationship for the material. The number of load cycles is defined as the number of mesh contacts, under load, of the gear tooth being analyzed. Figure 12-26* shows $S-N$ curves for the surface-fatigue strength of steels. Curve-fitted equations are also shown in the figure for the $S-N$ lines. These equations

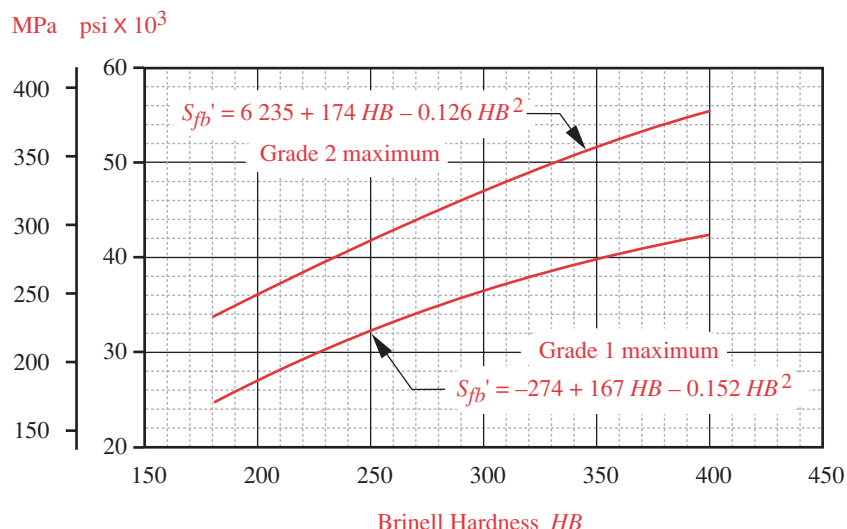


FIGURE 12-25

AGMA Bending-Fatigue Strengths S_{fb}' for Steels *

can be used to compute the appropriate C_L factor for a required number of load cycles N . The AGMA suggests that: “The upper portion of the shaded zone can be used for commercial applications. The lower portion of the shaded zone is typically used for critical service applications where little pitting and tooth wear is permissible and where smoothness of operation and low vibration levels are required.” Unfortunately, similar data have not yet been developed for gear materials other than these steels.

HARDNESS RATIO FACTOR C_H This factor is a function of the gear ratio and the relative hardness of pinion and gear. C_H is in the numerator of equation 12.25 and is always ≥ 1.0 , so it acts to increase the apparent strength of the gear. It accounts for situations in which the pinion teeth are harder than the gear teeth and thus act to work-harden the gear-tooth surfaces when run-in. C_H is only applied to the gear-tooth strength, not

* Extracted from AGMA Standard 2001-B88, *Fundamental Rating Factors and Calculation Methods for Involute Spur and Helical Gear Teeth*, with the permission of the publisher, American Gear Manufacturers Association, 1500 King St., Suite 201, Alexandria, Va., 22314.

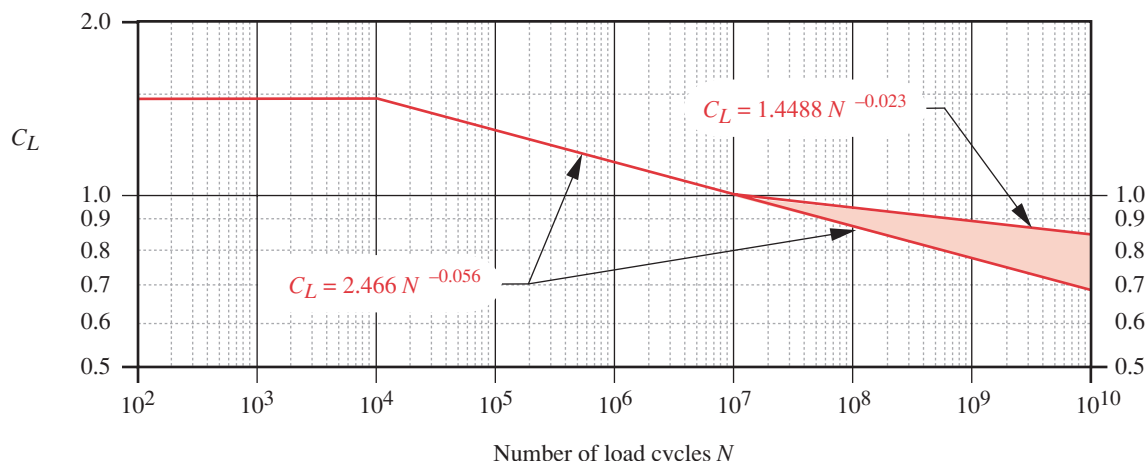


FIGURE 12-26 *

AGMA Surface-Fatigue Strength Life Factor C_L

Table 12-21 AGMA Surface-Fatigue Strengths S_{fc} ' for a Selection of Gear Materials*

Material	AGMA Class	Material Designation	Heat Treatment	Minimum Surface Hardness	Surface-Fatigue Strength	
					psi $\times 10^3$	MPa
Steel	A1-A5		Through hardened	≤ 180 HB	85-95	590-660
			Through hardened	240 HB	105-115	720-790
			Through hardened	300 HB	120-135	830-930
			Through hardened	360 HB	145-160	1000-1100
			Through hardened	400 HB	155-170	1100-1200
			Flame or induction hardened	50 HRC	170-190	1200-1300
			Flame or induction hardened	54 HRC	175-195	1200-1300
			Carburized and case hardened	55-64 HRC	180-225	1250-1300
		AISI 4140	Nitrided	84.6 HR15N [†]	155-180	1100-1250
		AISI 4340	Nitrided	83.5 HR15N	150-175	1050-1200
		Nitralloy 135M	Nitrided	90.0 HR15N	170-195	1170-1350
		Nitralloy N	Nitrided	90.0 HR15N	195-205	1340-1410
Cast iron	20	Class 20	As cast		50-60	340-410
	30	Class 30	As cast	175 HB	65-70	450-520
Nodular (ductile) iron	40	Class 40	As cast	200 HB	75-85	520-590
	A-7-a	60-40-18	Annealed	140 HB	77-92	530-630
	A-7-c	80-55-06	Quenched and tempered	180 HB	77-92	530-630
	A-7-d	100-70-03	Quenched and tempered	230 HB	92-112	630-770
Malleable iron (pearlitic)	A-7-e	120-90-02	Quenched and tempered	230 HB	103-126	710-870
	A-8-c	45007		165 HB	72	500
	A-8-e	50005		180 HB	78	540
	A-8-f	53007		195 HB	83	570
Bronze	A-8-i	80002		240 HB	94	650
	Bronze 2	AGMA 2C	Sand cast	40 ksi min tensile strength	30	450
	Al/Br 3	ASTM B-148 78 alloy 954	Heat-treated	90 ksi min tensile strength	65	450

[†] Rockwell 15N scale used for case-hardened materials—see Section 2-4

to the pinion. Two formulas for its calculation are suggested in the standard. The choice of one versus the other depends on the relative hardness of pinion and gear teeth.

For through-hardened pinions running against through-hardened gears:

$$C_H = 1 + A(m_G - 1) \quad (12.26a)$$

where m_G is the gear ratio and A is found from

$$\text{if } \frac{HB_p}{HB_g} < 1.2 \text{ then } A = 0 \quad (12.26b)$$

* Extracted from AGMA Standard 2001-B88, *Fundamental Rating Factors and Calculation Methods for Involute Spur and Helical Gear Teeth*, with the permission of the publisher, American Gear Manufacturers Association, 1500 King St., Suite 201, Alexandria, VA 22314.

$$\text{if } 1.2 \leq \frac{HB_p}{HB_g} \leq 1.7 \text{ then } A = 0.00898 \frac{HB_p}{HB_g} - 0.00829 \quad (12.26c)$$

$$\text{if } \frac{HB_p}{HB_g} > 1.7 \text{ then } A = 0.00698 \quad (12.26d)$$

where HB_p and HB_g are the Brinell hardnesses of pinion and gear, respectively.

For surface-hardened pinions (> 48 HRC) run against through-hardened gears, C_H is found from

$$C_H = 1 + B(450 - HB_g) \quad (12.27)$$

$$B = 0.00075 e^{-0.0112R_q} \quad (12.28us)$$

$$B = 0.00075 e^{-0.052R_q} \quad (12.28si)$$

where R_q is the rms surface roughness of the pinion teeth in μin rms (see Section 7.1 on p. 421).

Table 12-21* shows AGMA surface-fatigue strengths for a number of commonly used gear materials. The AGMA standard defines the heat-treatment specifications for the case-hardened steels. A plot showing ranges of AGMA surface-fatigue strengths for steels as a function of their Brinell hardness is shown in Figure 12-27.* See the referenced standard for the metallurgical properties required for AGMA Grades 1, 2, and 3 steels. To achieve the strength values in Table 12-21 and Figure 12-27, the material should be specified to comply with that standard.

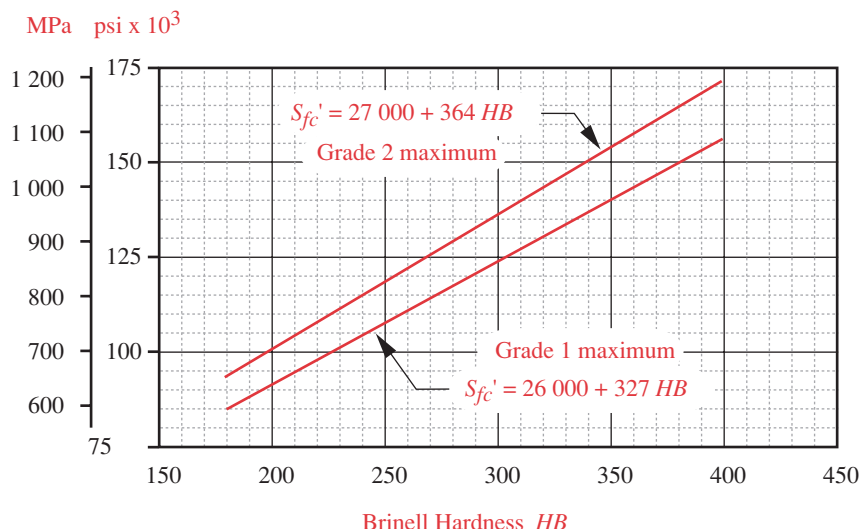


FIGURE 12-27

AGMA Surface-Fatigue Strengths S_{fc}' for Steels*

* Extracted from AGMA Standard 2001-B88, *Fundamental Rating Factors and Calculation Methods for Involute Spur and Helical Gear Teeth*, with the permission of the publisher, American Gear Manufacturers Association, 1500 King St., Suite 201, Alexandria, VA 22314.

EXAMPLE 12-7**Material Selection and Safety Factor for Spur Gears**

Problem Select suitable materials and calculate the safety factors for both bending and surface stresses in the 3-gear train from Examples 12-4, 12-5, and 12-6.

Given The stresses are as calculated in Examples 12-5 and 12-6.

Assumptions The service life required is 5 years of one-shift operation. All gears are steel. Operating temperature is 200 °F.

Solution

- 1 An estimate of the uncorrected bending-fatigue strength can be made from the curves of Figure 12-25. We will try an AGMA Grade 2 steel, through hardened to 250 HB. The uncorrected fatigue strength in bending is found from the upper curve of the figure

$$\begin{aligned} S_{fb'} &= 6235 + 174HB - 0.126HB^2 \\ &= 6235 + 174(250) - 0.126(250)^2 = 41860 \text{ psi} \end{aligned} \quad (a)$$

- 2 This value needs to be corrected for certain factors using equation 12.24.
- 3 The life factor K_L is found from the appropriate equation in Figure 12-24 based on the required number of cycles in the life of the gears. The pinion sees the largest number of repeated tooth-loadings, so we calculate the life based on it. First, calculate the number of cycles N for the required life of 5 years, one shift.

$$N = 2500 \text{ rpm} \left(\frac{60 \text{ min}}{\text{hr}} \right) \left(\frac{2080 \text{ hr}}{\text{shift - yr}} \right) (5 \text{ yr})(1 \text{ shift}) = 1.56E9 \text{ cycles} \quad (b)$$

The value of K_L is found from

$$K_L = 1.3558 N^{-0.0178} = 1.3558(1.56E9)^{-0.0178} = 0.9302 \quad (c)$$

- 4 At the specified operating temperature, $K_T = 1$.
- 5 The gear-material data are all taken at a reliability level of 99%. This is satisfactory in this case, making $K_R = 1$.
- 6 The corrected bending-fatigue strength is then

$$S_{fb} = \frac{K_L}{K_T K_R} S_{fb'} = \frac{0.9302}{1(1)} 41860 = 38937 \text{ psi} \quad (d)$$

- 7 An estimate of the uncorrected surface fatigue strength can be made from the curves of Figure 12-27. For an AGMA Grade 2 steel, through hardened to 250 HB, the strength is found from the upper curve of the figure to be

$$S_{fc'} = 27000 + 364HB = 27000 + 364(250) = 118000 \text{ psi} \quad (e)$$

- 8 This value needs to be corrected for certain factors using equation 12.25:

$$S_{fc} = \frac{C_L C_H}{C_T C_R} S_{fc'} \quad (f)$$

- 9 The life factor C_L is found from the appropriate equation in Figure 12-26 based on the required number of cycles N found above.

$$C_L = 1.4488N^{-0.023} = 1.4488(1.56E9)^{-0.023} = 0.8904 \quad (g)$$

- 10 $C_T = K_T = 1$ and $C_R = K_R = 1$.

- 11 Since the gears and pinion are of the same hardness material in this case, $C_H = 1$.

- 12 The corrected surface-fatigue strength is then

$$S_{fc} = \frac{C_L C_H}{C_T C_R} S_{fc'} = \frac{0.8904(1)}{1(1)} 118\,000 = 105\,063 \text{ psi} \quad (h)$$

- 13 The safety factor against bending failure is found by comparing the corrected bending strength to the bending stress for each gear in the mesh:

$$N_{b_{pinion}} = \frac{S_{fb}}{\sigma_{b_{pinion}}} = \frac{38\,937}{9\,526} = 4.1 \quad (i)$$

$$N_{b_{idler}} = \frac{S_{fb}}{\sigma_{b_{idler}}} = \frac{38\,937}{12\,400} = 3.1 \quad (j)$$

$$N_{b_{gear}} = \frac{S_{fb}}{\sigma_{b_{gear}}} = \frac{38\,937}{6\,834} = 5.7 \quad (k)$$

which are acceptable.

- 14 The safety factor against surface failure should be found by comparing the actual load to the load that would produce a stress equal to the material's corrected surface strength. Because surface stress is related to the square root of the load, the surface-fatigue safety factor can be calculated as the quotient of the square of the corrected surface strength divided by the square of the surface stress for each gear in the mesh:

$$N_{c_{pinion-idler}} = \left(\frac{S_{fc}}{\sigma_{c_{pinion}}} \right)^2 = \left(\frac{105\,063}{113\,315} \right)^2 = 0.86 \quad (l)$$

$$N_{c_{idler-gear}} = \left(\frac{S_{fc}}{\sigma_{c_{idler}}} \right)^2 = \left(\frac{105\,063}{90\,696} \right)^2 = 1.34 \quad (m)$$

which is too low for the pinion-idler mesh.

- 15 A small change to the design will improve these. Increasing the face width of the gears from the current 2.0 to 2.5 in ($15 / p_d$) reduces all stresses and gives new safety factors of

$$\begin{aligned} N_{b_{pinion}} &= 5.1 & N_{b_{idler}} &= 3.9 & N_{b_{gear}} &= 7.1 \\ N_{c_{pinion-idler}} &= 1.1 & N_{c_{idler-gear}} &= 1.7 \end{aligned} \quad (n)$$

- 16 These gears are very safe against tooth breakage and based on the assumptions and calculations, should have a 99% probability of lasting the required 5 years before pitting of the pinion or idler begins.
 - 17 The files EX12-07a and EX12-07b can be found on the CD-ROM.
-

12.10 LUBRICATION OF GEARING

With the exception of lightly loaded plastic gears, all gearsets must be lubricated to avoid premature failure from one of the surface-failure modes discussed in Chapter 7, such as adhesive or abrasive wear. Controlling temperature at the mesh interface is important in reducing scuffing and scoring of the teeth. Lubricants remove heat as well as separate the metal surfaces to reduce friction and wear. Sufficient lubricant must be provided to transfer the heat of friction to the environment without allowing excessive local temperatures in the mesh.

The usual and preferred approach is to provide an oil bath by housing the gears in an oil-tight box, called a gearbox. The gearbox is partially filled with an appropriate lubricant such that at least one member of each gearset is partially submerged. (The box is never completely filled with oil.) Gear rotation will carry the lubricant to the meshes and keep the unsubmerged gears oiled. The oil must be kept clean and free of contaminants and should be changed periodically. A much less desirable arrangement, sometimes used for situations in which a gearbox is not practical, is to periodically apply grease lubricant to the gears when they are stopped for servicing. Grease is merely petroleum oil suspended in a soap emulsion. This topical, grease lubrication does little for heat removal and is recommended only for low-velocity, lightly loaded gears.

Gear lubricants are typically petroleum-based oils of differing viscosity depending on the application. Light oils (10-30W) are sometimes used for gears with velocities high enough and/or loads low enough to promote elastohydrodynamic lubrication (see Chapter 11). In highly loaded and/or low-velocity gearsets, or ones with large sliding components, extreme pressure (EP) lubricants are often used. These are typically 80-90W gear oils with fatty-acid type additives that provide some protection against scuffing under boundary-lubricated conditions. See Section 7.3 (pp. 424) and Chapter 11 for more information on lubrication and lubricants. The AGMA provides extensive data in its standards on the proper selection of gear lubricants. The reader is referred to that source and to other sources such as lubricant vendors for more detailed information on lubricants.

12.11 DESIGN OF SPUR GEARS

The design of gears usually requires some iteration. Not enough information typically exists in the problem statement to directly solve for the unknowns. The values of some parameters must be assumed and a trial solution done. Many approaches are possible.

Usually, the gear ratio and either the power and speed, or the torque and speed, of one shaft are defined. The parameters to be determined are the pinion and gear pitch diameters, the diametral pitch, the face width, the material(s), and the safety factors. Some design decisions regarding the mesh accuracy required, the number of cycles, the pressure angle, the tooth form (standard or long-addendum), the gear manufacturing method (for surface finish considerations), operating-temperature range, and desired reliability must be made. With at least preliminary information on these factors, the design process can begin.

We ultimately will need to calculate safety factors for both bending-fatigue and surface-fatigue failures. These can be investigated in either order, but the better strategy is to calculate the bending stresses first, because increasing the surface hardness of the material has a greater effect on wear life than on bending strength. Thus, if the chosen material will survive the bending stresses, its hardness can be adjusted to improve its wear life with no other design change. Also, increasing tooth size has a greater effect on bending strength than on wear life, and tooth size is the primary variable in the calculations.

Before any stress calculations can be done, the loads must be determined. The tangential load on the gear teeth can be found from the known torque on the shaft and an assumed pitch radius for its pinion or gear (see equation 12.13a, p. 706). Note that a larger pitch radius reduces the tooth load but increases the pitch-line velocity. A reasonable compromise between these factors must be determined. Also, too small a pitch radius may result in a pinion with too few teeth to avoid interference, depending on the diametral pitch or module selected. Once a trial diametral pitch has been selected, its smallest acceptable pinion diameter can be used as the first choice in order to keep the package size small. The first design attempt should use a standard tooth form to keep costs low. If the design needs to be smaller than the standard tooth form allows, a long-addendum form can be investigated.

Since the bending strength of the gear tooth is directly related to tooth size as defined by its diametral pitch or module, a common starting point for the stress calculation is to assume values for diametral pitch or module and also for face width, then solve for the bending stress using equation 12.15 (p. 710). (Note that face width can also be roughly expressed as a range-function of diametral pitch ($8 / p_d < F < 16 / p_d$). See the discussion of the factor K_m above.

A trial material is then chosen and its corrected bending-fatigue strength calculated from equation 12.24 (p. 724). If the resulting safety factor is either too large or too small, the assumed values are adjusted and the calculation repeated until it converges to an acceptable solution.

The surface stress and surface-fatigue strength are then calculated from equations 12.21 and 12.25 (p. 718, 725) and a safety factor against wear determined. Material hardness can be adjusted at this point if necessary or the whole process can be repeated with adjusted values of either pitch or face width or both.

One useful strategy is to tailor the safety factors for bending failure to be higher than those for surface failure. Bending failure is sudden and catastrophic, resulting in tooth breakage and a disabling of the machine. Surface failure gives audible warning and the gears can be run for some time after the noise begins before having to be replaced. Thus, surface failure is the more desirable design limit on gear life.

12.12 CASE STUDY

We will now address the design of spur gears in one of the case-study assemblies that were defined in Chapter 9.

CASE STUDY 8C

Design of Spur Gears for a Compressor Drive Train

Problem Design a spur gearset for the compressor gearbox in Figure 9-1 based on the loadings defined in Case Study 8A and specify suitable materials and heat treatments.

Given The torque-time function on the output shaft is as shown in Figure 9-3 (repeated on next page). The required gear ratio is a 2.5:1 reduction in velocity from the input to the output shaft. Output shaft velocity is 1 500 rpm.

Assumptions A 10-year life of 1-shift operation is desired. AGMA standard full-depth teeth will be used. Based on the data in Tables 12-6 and 12-7 (p. 705), set $Q_v = 10$. Both pinion and gear will be through hardened steel.

Solution See Figures 9-1 and 9-3.

- The time-varying torque on the output shaft is defined in Figure 9-3 as varying between -175 and +585 lb-in. In Case Study 8B, in which the shafts for this same machine were designed, we assumed a 4-in pitch diameter, 20° pinion, and a 10-in gear. For a first attempt at the gearset design we will retain those assumptions. From these data we can determine the forces at the gear mesh. The tangential component is found from the known output torque and the assumed gear radius:

$$W_{t_{max}} = \frac{T_{max}}{r_g} = \frac{585 \text{ lb-in}}{5 \text{ in}} = 117 \text{ lb}$$

$$W_{t_{min}} = \frac{T_{min}}{r_g} = \frac{-175 \text{ lb-in}}{5 \text{ in}} = -35 \text{ lb} \quad (a)$$

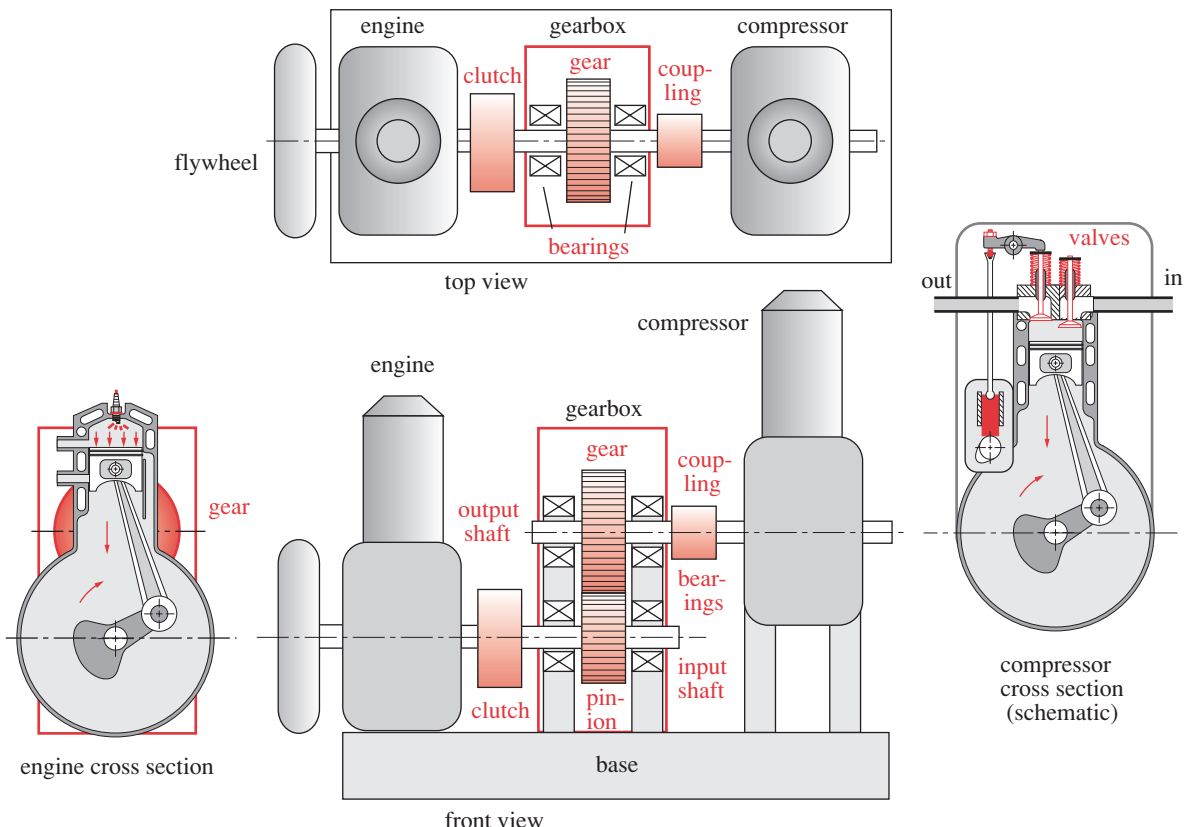
- We will take the positive peak value as the transmitted load, $W_t = 117$ lb. The -35-lb peak force acts on the opposite sides of the teeth, loading both gear and pinion similar to an idler gear. We will take that aspect of the loading into account with the application factor K_a .
- Assume a pinion with $N_p = 20$ teeth. The gear then has $2.5 N_p = 50$ teeth. The diametral pitch for that combination is

$$p_d = \frac{N}{d} = \frac{20}{4} = 5 \quad (b)$$

which is a standard pitch (Table 12-2, p. 691).

- The bending geometry factors J for this combination are found in Table 12-9 (p. 712) for loading at the highest point of single-tooth contact (HPSTC) and are approximately:

$$J_p = 0.34 \quad J_g = 0.40 \quad (c)$$

**FIGURE 9-1** Repeated

Preliminary Design Schematic of Gasoline-Engine-Powered Portable Air Compressor, Gearbox, Couplings, Shafts, and Bearings

- 5 The velocity factor K_v (C_v) is calculated from equations 12.16 and 12.17 (p. 711) based on the assumed gear-quality index Q_v and the pitch-line velocity V_t .

$$V_t = \frac{d_p}{2} \omega_p = \frac{4.0 \text{ in}}{2(12)} (3750 \text{ rpm})(2\pi) = 3927 \frac{\text{ft}}{\text{min}} \quad (d)$$

$$B = \frac{(12 - Q_v)^{2/3}}{4} = \frac{(12 - 10)^{2/3}}{4} = 0.397 \quad (e)$$

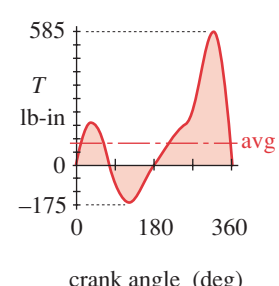
$$A = 50 + 56(1 - B) = 50 + 56(1 - 0.397) = 83.77 \quad (f)$$

$$K_v = C_v = \left(\frac{A}{A + \sqrt{V_t}} \right)^B = \left(\frac{83.77}{83.77 + \sqrt{3927}} \right)^{0.397} = 0.801 \quad (g)$$

- 6 V_t should be checked against the maximum allowable pitch-line velocity for this quality gear using equation 12.18 (p. 714):

$$V_{t_{max}} = [A + (Q_v - 3)]^2 = [83.77 + (10 - 3)]^2 = 8239 \text{ ft/min} \quad (h)$$

which is larger than V_t , so is acceptable.

**FIGURE 9-3** RepeatedTotal Torque-Time Function at Crankshaft with Constant ω

7 Assuming a face width factor of 12 the face width can be estimated as

$$F \cong \frac{12}{p_d} = \frac{12}{5} = 2.4 \text{ in} \quad (i)$$

8 This value is used to interpolate in Table 12-16 (p. 715) for K_m (C_m).

$$K_m = C_m \cong 1.61 \quad (j)$$

9 The application factor K_a is intended to account for shockiness in the driving and driven machinery. This machine has both, since it is driven by a single-cylinder engine and drives a single-cylinder compressor. In many such cases, only an average value of the transmitted torque is known, based on the average transmitted power. In this case, we have computed (in Case Study 8A) a fairly accurate torque-time function for the compressor, which in effect defines the “overloads” in the driven part of the system. We used the peak torque rather than the average torque to define the transmitted load. So, the full value of the application factor recommended in Table 12-17 (p. 715) may not be needed here. We will use it to account for the partially reversed loading on the gear teeth (Figure 9-3) as well as the shock loading associated with the driver (engine) and estimate it at $K_a = C_a = 2$.

10 The size factor K_s (C_s), and the rim bending factor K_B are all 1 for these small gears.

11 The bending stresses in pinion and gear can now be computed.

$$\sigma_{b_p} = \frac{W_t p_d}{FJ} \frac{K_a K_m}{K_v} K_s K_B K_I = \frac{117(5)}{2.4(0.34)} \frac{1(1.61)}{0.801} (1)(1)(1) = 2881 \text{ psi} \quad (k)$$

$$\sigma_{b_g} = \frac{W_t p_d}{FJ} \frac{K_a K_m}{K_v} K_s K_B K_I = \frac{117(5)}{2.4(0.40)} \frac{1(1.61)}{0.801} (1)(1)(1) = 2449 \text{ psi} \quad (l)$$

12 Additional factors are needed for the surface stress calculation. Table 12-18 (p. 720) shows an approximate elastic coefficient of 2300 for steel on steel. In Example 12-6, we computed a more accurate value of $C_p = 2276$. The surface finish factor C_f is 1.

13 The surface geometry factor I is calculated from equations 12.22 (p. 719):

$$\begin{aligned} \rho_1 &= \sqrt{\left(r_p + \frac{1}{p_d}\right)^2 - (r_p \cos\phi)^2} - \frac{\pi}{p_d} \cos\phi \\ &= \sqrt{\left(2.0 + \frac{1}{5}\right)^2 - (2.0 \cos 20^\circ)^2} - \frac{\pi}{5} \cos 20^\circ = 0.553 \text{ in} \end{aligned} \quad (m)$$

$$\begin{aligned} \rho_2 &= C \sin\phi - \rho_1 = (r_p + r_g) \sin\phi - \rho_1 \\ &= (2.0 + 5.0) \sin 20^\circ - 0.553 = 1.841 \text{ in} \end{aligned} \quad (n)$$

$$I = \frac{\cos\phi}{\left(\frac{1}{\rho_p} \pm \frac{1}{\rho_g}\right) d_p} = \frac{\cos 20^\circ}{\left(\frac{1}{0.553} + \frac{1}{1.841}\right) 2.0} = 0.100 \quad (o)$$

14 The surface stresses in the pinion-gear mesh can now be computed.

$$\begin{aligned}\sigma_{c_{pg}} &= C_p \sqrt{\frac{W_t}{FId_p} \frac{C_a C_m}{C_v} C_s C_f} \\ &= 2276 \sqrt{\frac{117}{2.4(0.100)(4.0)} \frac{1(1.61)}{0.801}(1)(1)} = 50393 \text{ psi} \quad (p)\end{aligned}$$

- 15 An estimate of the uncorrected bending-fatigue strength can be made from the curves of Figure 12-25 (p. 727). We will try an AGMA Grade 1 steel, through hardened to 250 HB. The uncorrected bending-fatigue strength is found from the lower curve of the figure:

$$\begin{aligned}S_{fb} &= -274 + 167HB - 0.152HB^2 \\ &= -274 + 167(250) - 0.152(250)^2 = 31976 \text{ psi} \quad (q)\end{aligned}$$

- 16 This value needs to be corrected for certain factors using equation 12.24 (p. 724). The life factor K_L is found from the appropriate equation in Figure 12-24 (p. 725) based on the required number of cycles in the life of the gears. The pinion sees the largest number of repeated tooth-loadings, so we calculate the life based on it. First, calculate the number of cycles N for the required life of 10 years, one shift.

$$N = 3750 \text{ rpm} \left(\frac{60 \text{ min}}{\text{hr}} \right) \left(\frac{2080 \text{ hr}}{\text{shift - yr}} \right) (10 \text{ yr})(1 \text{ shift}) = 4.7E9 \text{ cycles} \quad (r)$$

The value of K_L is found from

$$K_L = 1.3558 N^{-0.0178} = 1.3558(4.7E9)^{-0.0178} = 0.9121 \quad (s)$$

- 17 At the specified operating temperature, $K_T = 1$.
- 18 The gear-material data are all taken at a reliability level of 99%. This is satisfactory in this case, making $K_R = 1$.
- 19 The corrected bending-fatigue strength is then

$$S_{fb} = \frac{K_L}{K_T K_R} S_{fb} = \frac{0.9121}{1(1)} 31976 = 29167 \text{ psi} \quad (t)$$

- 20 An estimate of the uncorrected surface fatigue strength can be made from the curves of Figure 12-27 (p. 729). For an AGMA Grade 1 steel, through hardened to 250 HB, the strength is found from the lower curve of the figure:

$$S_{fc} = 26000 + 327HB = 26000 + 327(250) = 107750 \text{ psi} \quad (u)$$

- 21 This value needs to be corrected for certain factors using equation 12.25 (p. 725). The life factor C_L is found from the appropriate equation in Figure 12-26 (p. 727) based on the required number of cycles N found above.

$$C_L = 1.4488 N^{-0.023} = 1.4488(4.7E9)^{-0.023} = 0.8681 \quad (v)$$

- 22 $C_T = K_T = 1$ and $C_R = K_R = 1$.
- 23 Since the gears and pinion are of the same hardness material in this case, $C_H = 1$.
- 24 The corrected surface-fatigue strength is then

$$S_{fc} = \frac{C_L C_H}{C_T C_R} S_{fc'} = \frac{0.8681(1)}{1(1)} 107\,750 = 93\,543 \text{ psi} \quad (w)$$

- 25 The safety factors against bending failure are found by comparing the corrected bending strength to the bending stress for each gear in the mesh:

$$N_{b_{pinion}} = \frac{S_{fb}}{\sigma_{b_{pinion}}} = \frac{29\,167}{2\,881} = 10.1 \quad (x)$$

$$N_{b_{gear}} = \frac{S_{fb}}{\sigma_{b_{gear}}} = \frac{29\,167}{2\,449} = 11.9$$

which are too high, causing the package to be larger than necessary.

- 26 The safety factor against surface failure is found by comparing the actual load to the load that would produce a stress equal to the material's corrected surface strength. Because surface stress is related to the square root of the load, the surface-fatigue safety factor can be calculated as the quotient of the square of the corrected surface strength divided by the square of the surface stress for each gear in the mesh:

$$N_{c_{pinion-gear}} = \left(\frac{S_{fc}}{\sigma_{c_{pinion}}} \right)^2 = \left(\frac{93\,543}{50\,393} \right)^2 = 3.4 \quad (y)$$

- 27 These are higher than needed. The diametral pitch was increased from the current 5 to 8 (decreasing the tooth size) in order to reduce the pitch diameters, increase the stresses, and lower the safety factors. The face width becomes 1.5 in for the same face width factor of 12. The pinion was increased to 22 teeth, giving 55 teeth on the gear with the new p_d . The computations were redone with the results shown in Table 12-22. The new safety factors are

$$N_{b_{pinion}} = 2.8 \quad N_{b_{gear}} = 3.3 \quad N_{c_{pinion-gear}} = 1.1 \quad (z)$$

12

- 28 These gears are still safe against tooth breakage. Based on the assumptions and calculations and, if properly lubricated, they should have a 99% probability of lasting the required 10 years before pitting of the pinion begins.
- 29 Note that the change of gear pitch diameters over those assumed in Case Study 8B for the shaft design also increases the transverse gear loads on the shaft by 45%. This will require another iteration of that shaft design.
- 30 The files Case8C-1 (first design) and Case8C-2 (final design) are on the CD-ROM.

12.13 SUMMARY

There are two principal types of gear failure: tooth breakage from bending stresses and pitting from surface (Hertzian) stresses. Of the two, bending failure is more catastrophic, since tooth breakage usually disables the machine. Pitting failure comes on gradually and gives audible and visible warning (if the teeth can be inspected). Gears can run for some time after pitting begins before having to be replaced.

Table 12-22 Case Study 8C – Spur Gear Train Final Design

Input	Variable	Output	Unit	Comments
2.50	<i>ratio</i>			gear ratio
8	p_d		1/in	diametral pitch
20	ϕ		deg	pressure angle
170	W_t		lb	tangential force
22	N_{pinion}			no. of teeth on pinion
	N_{gear}	55		no. of teeth on gear
	d_{pinion}	2.75	in	pitch dia of pinion
	d_{gear}	6.88	in	pitch dia of gear
1.50	$face$		in	face width
0.34	J_{pinion}			geometry factor—pinion
0.40	J_{gear}			geometry factor—gear
	I	0.10		<i>I</i> factor for pinion/gear mesh
2.0	K_a			application factor
1.6	K_m			load distribution factor
2 276	C_p			elastic coefficient
10	Q_v			gear-quality index
	V_t	2 700	ft/min	pitch-line velocity
	V_{tmax}	8 239	ft/min	max allowable pitch-line velocity
	K_v	0.826		dynamic factor
	$\sigma_{bpinion}$	10 346	psi	bending stress—pinion tooth
	σ_{bgear}	8 794	psi	bending stress—gear tooth
	$\sigma_{cpinion}$	90 026	psi	surface stress in pinion and gear
	Sf_{bprime}	31 976	psi	uncorrected bending strength
	Sf_b	29 167	psi	corrected bending strength
	Sf_{cprime}	107 750	psi	uncorrected surface strength
	Sf_c	93 543	psi	corrected surface strength
	K_R	1.00		reliability factor
	$cycles$	4.7E+9		number of repeated pinion cycles
	K_L	0.91		life factor—bending fatigue
	C_L	0.87		life factor—surface fatigue
	N_{bp}	2.8		bending safety factor for pinion
	N_{bg}	3.3		bending safety factor for gear
	N_{cp}	1.1		surface safety factor for mesh

Both modes of failure are fatigue failures due to the repeated stressing of individual teeth as they come in and out of mesh. The principles of fatigue analysis (Chapter 6) apply and a modified-Goodman analysis is needed. However, the similar nature of the loading on all gear teeth allows the Goodman analysis to be captured in a standardized approach as defined by the AGMA.

Proper involute tooth geometry is crucial to the operation and life of gears. The AGMA defines a standard tooth profile plus several modifications to that standard for special situations. Geometry factors necessary for proper stress calculations are defined for these geometries. Extensive testing of gear materials under realistic loading conditions in combination with years of experience by gear manufacturers has resulted in a set of proven equations for the calculation of both stresses and corrected endurance strengths in bending and surface fatigue for gears.

This chapter summarizes the AGMA approach to spur-gear design and presents a number of charts and empirical formulas for calculation. The reader is directed to the AGMA standards for more complete information.

Important Equations Used in This Chapter

Circular Pitch (Section 12.2):

$$p_c = \frac{\pi d}{N} \quad (12.3a)$$

Diametral Pitch (Section 12.2):

$$p_d = \frac{N}{d} \quad (12.4a)$$

Metric Module (Section 12.2):

$$m = \frac{d}{N} \quad (12.4c)$$

Gear Ratio (Section 12.2):

$$m_G = \frac{N_g}{N_p} \quad (12.5b)$$

Contact Ratio (Section 12.4):

$$m_p = \frac{p_d Z}{\pi \cos \phi} \quad (12.7b)$$

$$Z = \sqrt{(r_p + a_p)^2 - (r_p \cos \phi)^2} + \sqrt{(r_g + a_g)^2 - (r_g \cos \phi)^2} - C \sin \phi \quad (12.2)$$

Tangential Load on Gear Teeth (Section 12.5):

$$W_t = \frac{T_p}{r_p} = \frac{2T_p}{d_p} = \frac{2p_d T_p}{N_p} \quad (12.13a)$$

AGMA Bending Stress Equations (Section 12.8):

$$\sigma_b = \frac{W_t p_d}{FJ} \frac{K_a K_m}{K_v} K_s K_B K_I \quad (12.15us)$$

$$\sigma_b = \frac{W_t}{FmJ} \frac{K_a K_m}{K_v} K_s K_B K_I \quad (12.15si)$$

AGMA Surface Stress Equation (Section 12.8):

$$\sigma_c = C_p \sqrt{\frac{W_t}{FId} \frac{C_a C_m}{C_v} C_s C_f} \quad (12.21)$$

AGMA Bending-Fatigue Strength Equation (Section 12.9):

$$S_{fb} = \frac{K_L}{K_T K_R} S_{fb} \quad (12.24)$$

AGMA Surface-Fatigue Strength Equation (Section 12.9):

$$S_{fc} = \frac{C_L C_H}{C_T C_R} S_{fc} \quad (12.25)$$

12.14 REFERENCES

- 1 **AGMA**, *Gear Nomenclature, Definitions of Terms with Symbols*. ANSI/AGMA Standard 1012-F90. American Gear Manufacturers Association, 1500 King St., Suite 201, Alexandria, Va., 22314, 1990.
- 2 **AGMA**, *Fundamental Rating Factors and Calculation Methods for Involute Spur and Helical Gear Teeth*. ANSI/AGMA Standard 2001-B88. American Gear Manufacturers Association, 1500 King St., Suite 201, Alexandria, Va., 22314, 1988.
- 3 **AGMA**, *Geometry Factors for Determining the Pitting Resistance and Bending Strength of Spur, Helical, and Herringbone Gear Teeth*. ANSI/AGMA Standard 908-B89. American Gear Manufacturers Association, 1500 King St., Suite 201, Alexandria, Va., 22314, 1989.
- 4 **R. L. Norton**, *Design of Machinery: An Introduction to the Synthesis and Analysis of Mechanisms and Machines*, 3ed. McGraw-Hill: New York, pp. 462-521, 2004.
- 5 **W. Lewis**, “Investigation of the Strength of Gear Teeth, an address to the Engineer’s Club of Philadelphia, October 15, 1892.” reprinted in *Gear Technology*, vol. 9, no. 6, p. 19, Nov./Dec. 1992.
- 6 **T. J. Dolan and E. L. Broghammer**, *A Photoelastic Study of the Stresses in Gear Tooth Fillets*. Bulletin 335, U. Illinois Engineering Experiment Station, 1942.
- 7 **W. D. Mark**, The Generalized Transmission Error of Parallel-Axis Gears. *Journal of Mechanisms, Transmissions, and Automation in Design*. **111**: pp. 414-423, 1989.
- 8 **R. A. Morrison** “Load/Life Curves for Gear and Cam Materials.” *Machine Design*, pp. 102-108, Aug. 1, 1968.
- 9 **E. Buckingham**, *Analytical Mechanics of Gears*, McGraw-Hill: New York, 1949.
- 10 **D. W. Dudley**, Gear Wear, in *Wear Control Handbook*, M. B. Peterson and W. O. Winer, ed. ASME: New York, p. 764, 1980.

Table P12-0[†]

Topic/Problem Matrix

12.1 Gear Tooth Theory12-5, 12-6, 12-37, 12-38, 12-41,
12-42, **12-59, 12-65****12.2 Nomenclature**12-1, 12-2, 12-44, 12-45, *12-60*,
12-66**12.4 Contact Ratio**12-3, 12-4, 12-39, 12-40, 12-61,
12-67**12.5 Compound Trains**12-7, 12-9, *12-10*, 12-29, 12-30,
12-31, 12-43, 12-46, 12-47**12.5 Epicyclic Trains**12-11, 12-12, 12-13, *12-48*,
12-49, 12-62, 12-68**12.7 Loading**12-14, 12-15, 12-20, 12-21,
12-22, 12-27, 12-52, 12-55**12.8, .9 Bending Stress**12-16, *12-17*, 12-23, 12-24,
12-50, 12-63**12.8, .9 Surface Stress**12-18, *12-19*, 12-25, 12-26,
12-51, 12-64**12.11 Gear Design***12-8, 12-28, 12-29, 12-30*,
12-31, 12-32, 12-33, 12-34,
12-53, 12-54, 12-56, 12-57,
12-58**12.15 PROBLEMS**

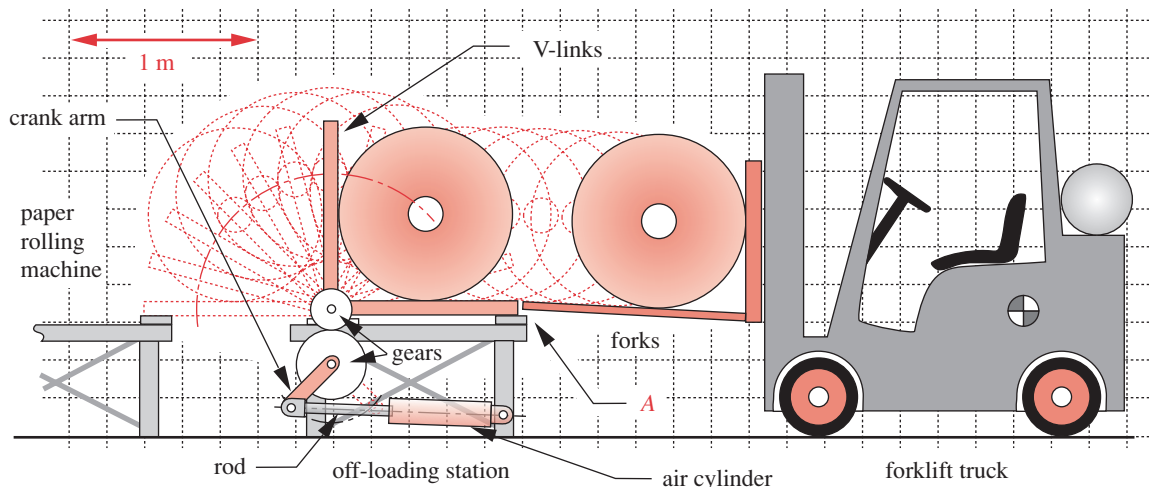
- *12-1 A 20°-pressure-angle, 27-tooth spur gear has a diametral pitch $p_d = 5$. Find the pitch dia. addendum, dedendum, outside dia, and circular pitch.
- 12-2 A 25°-pressure-angle, 43-tooth spur gear has a diametral pitch $p_d = 8$. Find the pitch dia. addendum, dedendum, outside dia, and circular pitch.
- *12-3 A 57-tooth spur gear is in mesh with a 23-tooth pinion. The $p_d = 6$ and $\phi = 25^\circ$. Find the contact ratio.
- 12-4 A 78-tooth spur gear is in mesh with a 27-tooth pinion. The $p_d = 6$ and $\phi = 20^\circ$. Find the contact ratio.
- *12-5 What will the pressure angle be if the center distance of the spur gearset in Problem 12-3 is increased by 5%?
- 12-6 What will the pressure angle be if the center distance of the spur gearset in Problem 12-4 is increased by 7%?
- *12-7 If the spur gearsets in Problems 12-3 and 12-4 are compounded as shown in Figure 12-14 (p. 697), what will the overall train ratio be?
- [†]12-8 A paper machine processes rolls of paper having a density of 984 kg/m^3 . The paper roll is 1.50-m outside dia (*OD*) \times 0.22-m inside dia (*ID*) \times 3.23 m long and is on a simply supported, hollow, steel shaft with $S_{ut} = 400 \text{ MPa}$. Design a 2.5:1 reduction spur gearset to drive this roll shaft to obtain a minimum dynamic safety factor of 2 for a 10-year life if the shaft *OD* is 22 cm and the roll turns at 50 rpm with 1.2 hp absorbed.
- *12-9 Design a two-stage compound spur gear train for an overall ratio of approximately 47:1. Specify tooth numbers for each gear in the train.
- [†]12-10 Design a three-stage compound spur gear train for an overall ratio of approximately 656:1. Specify tooth numbers for each gear in the train.
- *12-11 An epicyclic spur gear train as shown in Figure 12-16 (p. 700) has a sun gear of 33 teeth and a planet gear of 21 teeth. Find the required number of teeth in the ring gear and determine the ratio between the arm and sun gear if the ring gear is held stationary. Hint: Consider the arm to rotate at 1 rpm.
- 12-12 An epicyclic spur gear train as shown in Figure 12-16 (p. 700) has a sun gear of 23 teeth and a planet gear of 31 teeth. Find the required number of teeth in the ring gear and determine the ratio between the arm and ring gear if the sun is held stationary. Hint: Consider the arm to rotate at 1 rpm.
- 12-13 An epicyclic spur gear train as shown in Figure 12-16 (p. 700) has a sun gear of 23 teeth and a planet gear of 31 teeth. Find the required number of teeth in the ring gear and determine the ratio between the sun and ring gear if the arm is held stationary. Hint: Consider the sun to rotate at 1 rpm.
- *12-14 If the gearset in Problem 12-3 transmits 125 hp at 1 000 pinion rpm, find the torque on each shaft.
- 12-15 If the gearset in Problem 12-4 transmits 33 kW at 1 600 pinion rpm, find the torque on each shaft.
- *12-16 Size the spur gears in Problem 12-14 for a bending failure safety factor of at least 2 assuming a steady torque, 25° pressure angle, full-depth teeth, $Q_v = 9$, an AISI 4140 steel pinion, and a class 40 cast iron gear.

* Answers to these problems are provided in Appendix D.

[†] Problem numbers in *italics* are design problems. Problem numbers in **boldface** are extended from similar problems in earlier chapters with the same dash number.

- 12-17* Size the spur gears in Problem 12-15 for a bending failure safety factor of 2.5 assuming a steady torque, 20° pressure angle, full-depth teeth, $Q_v = 11$, an AISI 4340 steel pinion, and an A-7-d nodular iron gear.
- **12-18* Size the spur gears in Problem 12-14 for a surface failure safety factor of at least 2 assuming a steady torque, 25° pressure angle, full-depth teeth, $Q_v = 9$, an AISI 4140 steel pinion, and a class 40 cast-iron gear.
- 12-19* Size the spur gears in Problem 12-15 for a surface failure safety factor of 1.2, assuming a steady torque, 20° pressure angle, full-depth teeth, $Q_v = 11$, an AISI 4340 steel pinion, and an A-7-d nodular-iron gear.
- **12-20* If the gearset in Problem 12-11 transmits 83 kW at 1 200 arm rpm, find the torque on each shaft.
- 12-21* If the gearset in Problem 12-12 transmits 39 hp at 2 600 arm rpm, find the torque on each shaft.
- 12-22* If the gearset in Problem 12-13 transmits 23 kW at 4 800 sun rpm, find the torque on each shaft.
- **12-23* Size the spur gears in Problem 12-20 for a bending safety factor of at least 2.8, assuming a steady torque, 25° pressure angle, full-depth teeth, $Q_v = 9$, an AISI 4140 steel pinion and a class 40 cast iron gear.
- 12-24* Size the spur gears in Problem 12-21 for a bending safety factor of at least 2.4, assuming a steady torque, 20° pressure angle, full-depth teeth, $Q_v = 11$, an AISI 4340 steel pinion and an A-7-d nodular iron gear.
- **12-25* Size the spur gears in Problem 12-20 for a surface safety factor of at least 1.7, assuming a steady torque, 25° pressure angle, full-depth teeth, $Q_v = 9$, an AISI 4140 steel pinion and a class 40 cast-iron gear.
- 12-26* Size the spur gears in Problem 12-21 for a surface safety factor of at least 1.3, assuming a steady torque, 20° pressure angle, full-depth teeth, $Q_v = 11$, an AISI 4340 steel pinion and an A-7-d nodular iron gear.
- **12-27* If the gearset in Problem 12-10 transmits 190 kW at 1 800 input pinion rpm, find the torque on each of the four shafts.
- **12-28* Size the first-stage spur gears in Problem 12-27 for a bending safety factor of at least 3.0 and a surface safety factor of at least 1.7, assuming a steady torque, 25° pressure angle, full-depth teeth, $Q_v = 8$, and AISI 4140 steel for all gears.
- **12-29* Size the second-stage spur gears in Problem 12-27 for a bending safety factor of at least 3.0 and a surface safety factor of at least 1.7 assuming a steady torque, 25° pressure angle, full-depth teeth, $Q_v = 8$, and AISI 4140 steel for all gears.
- **12-30* Size the third-stage spur gears in Problem 12-27 for a bending safety factor of at least 3.0 and a surface safety factor of at least 1.7 assuming a steady torque, 25° pressure angle, full-depth teeth, $Q_v = 8$, and AISI 4140 steel for all gears.
- **12-31* Design a two-stage compound spur-gear train for an overall ratio of approximately 78:1. Specify tooth numbers for each spur gear in the train.
- 12-32** Figure P12-1 shows the same paper machine that was analyzed in Problem 6-46 and in other problems from previous chapters. The paper rolls in Figure P12-1 are 0.9-m OD \times 0.22-m ID \times 3.23 m long and have a density of 984 kg/m^3 . The rolls are transferred from the machine conveyor (not shown) to the forklift truck by the V-linkage of the off-load station, which is rotated through 90° by an air cylinder. The paper then rolls onto the waiting forks of the truck. The machine makes 30 rolls

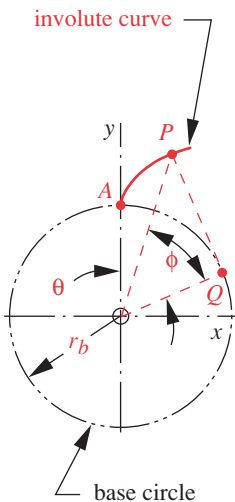
* Answers to these problems are provided in Appendix D. Problem numbers in *italics* are design problems. Problem numbers in **boldface** are extended from similar problems in earlier chapters with the same dash number.

**FIGURE P12-1**

Problem 12-32

per hour and runs 2 shifts. The V-links are rotated by the crank arm through a shaft that is 60-mm dia by 3.23 m long. A redesign of the V-link rotating mechanism is desired in order to introduce a gearset between the crank arm and the V-link shaft with a 2:1 ratio. This will reduce the required stroke of the air cylinder by 50% and improve its geometry. Design a suitable spur-gear set for this application for a 10-year life against surface failure. State all assumptions.

- 12**
- 12-33 Design a nonreverted compound transmission based on the arrangement shown in Figure 12-14a for an overall train ratio of approximately 90:1. It should be capable of transmitting 50 hp at 1 000 rpm input shaft speed. State all assumptions.
- 12-34 Design a reverted compound transmission based on the arrangement shown in Figure 12-14b for an overall train ratio of approximately 80:1. It should be capable of transmitting 30 hp at 1 500 rpm input shaft speed. State all assumptions.
- 12-35 If the 23-tooth pinion in the gearset in Problem 12-3 is on the input shaft, find the velocity ratio, torque ratio, and gear ratio for the gearset.
- 12-36 If the 78-tooth gear in the gearset in Problem 12-4 is on the input shaft, find the velocity ratio, torque ratio, and gear ratio for the gearset.
- 12-37 Figure P12-2 shows an involute of a circle that starts at point A ($0, r_b$) and continues to point P (x, y). The angle θ is known as the roll angle and ϕ is the involute pressure angle. Derive expressions for the x and y coordinates of P in terms of the base circle radius r_b and the involute pressure angle only. Plot y vs. x over the range $0^\circ < \phi < 40^\circ$ for $r_b = 2$ in.
- 12-38 Derive equation 12.2 using Figure 12-5.
- 12-39 A 39-tooth spur gear is in mesh with an 18-tooth pinion. The $p_d = 8$ and $\phi = 25^\circ$. Find the contact ratio.
- 12-40 A 79-tooth spur gear is in mesh with a 20-tooth pinion. The $p_d = 8$ and $\phi = 20^\circ$. Find the contact ratio.
- 12-41 What will the pressure angle be if the center distance of the spur gearset in Problem 12-39 is increased by 6%?

**FIGURE P12-2**

Problem 12-37

- 12-42 What will the pressure angle be if the center distance of the spur gearset in Problem 12-40 is increased by 5%?
- 12-43 If the spur gearsets in Problems 12-39 and 12-40 are compounded as shown in Figure 12-14, what will the overall train ratio be?
- 12-44 A 20° pressure angle, 23-tooth spur gear has a diametral pitch of 6. Find the pitch diameter, addendum, dedendum, outside diameter, and circular pitch.
- 12-45 A 25° pressure angle, 32-tooth spur gear has a diametral pitch of 4. Find the pitch diameter, addendum, dedendum, outside diameter, and circular pitch.
- 12-46 Design a two-stage compound spur gear train for an overall ratio of approximately 53:1. Specify tooth numbers for each gear in the train.
- 12-47 Design a three-stage compound spur gear train for an overall ratio of approximately 592:1. Specify tooth numbers for each gear in the train.
- 12-48 Design a planetary gear train similar to that shown in Figure 12-16 for an overall velocity ratio of exactly 0.2 if the sun gear is the input, the arm is the output, and the ring gear is stationary. Specify tooth numbers for each gear in the train.
- 12-49 Design a planetary gear train similar to that shown in Figure 12-16 for an overall velocity ratio of exactly $4/3$ if the sun gear is stationary, the arm is the input, and the ring gear is the output. Specify tooth numbers for each gear in the train.
- 12-50 A 21-tooth pinion rotating at 1800 rpm meshes with a 33-tooth gear in a spur gear reducer. Both pinion and gear are manufactured to a quality level of 9. A reliability of 0.9 has been specified, and the transmitted tangential load is 2800 lb. Conditions are such that $K_m = 1.7$. It is proposed that standard 25° , full-depth teeth be used, with both pinion and gear hobbed from an AISI 4140 nitrided steel. The diametral pitch is 6, and the face width 2.000 in. Estimate the number of cycles of bending stress (using the AGMA equations) that the gearset can withstand.
- 12-51 A 21-tooth pinion rotating at 1800 rpm meshes with a 33-tooth gear in a spur-gear reducer. Both pinion and gear are manufactured to a quality level of 9. A reliability of 0.9 has been specified, and the transmitted tangential load is 2800 lb. Conditions are such that $C_m = 1.7$. It is proposed that standard 25° , full-depth teeth be used, with both pinion and gear hobbed from an AISI 4140 nitrided steel. The diametral pitch is 6, and the face width 2.0 in. Estimate the number of cycles of contact (surface) stress (using the AGMA equations) that the gearset can withstand.
- *12-52 If the gearset in Problem 12-46 transmits 7.5 kW at 1750 input pinion rpm, find the torque on each of the three shafts.
- *12-53 Size the first-stage spur gears in Problem 12-52 for a bending factor of safety of at least 2.8 and a surface factor of safety of at least 1.8 assuming a steady torque, 25° pressure angle, full depth teeth, $Q_v = 9$, and AISI 4340 steel for all gears.
- 12-54 Size the second-stage spur gears in Problem 12-52 for a bending factor of safety of at least 2.8 and a surface factor of safety of at least 1.8 assuming a steady torque, 25° pressure angle, full depth teeth, $Q_v = 9$, and AISI 4340 steel for all gears.
- 12-55 If the gearset in Problem 12-47 transmits 18.8 kW at 1184 input pinion rpm, find the torque on each of the four shafts.
- 12-56 Size the first-stage spur gears in Problem 12-55 for a bending factor of safety of at least 2.4 and a surface factor of safety of at least 2.0 assuming a steady torque, 25° pressure angle, full depth teeth, $Q_v = 10$, and AISI 4140 steel for all gears.

* Answers to these problems are provided in Appendix D. Problem numbers in *italics* are design problems.

- [†]12-57 Size the second-stage spur gears in Problem 12-55 for a bending factor of safety of at least 2.4 and a surface factor of safety of at least 2.0 assuming a steady torque, 25° pressure angle, full depth teeth, $Q_v = 10$, and AISI 4140 steel for all gears.
- 12-58 Size the third-stage spur gears in Problem 12-55 for a bending factor of safety of at least 2.4 and a surface factor of safety of at least 2.0 assuming a steady torque, 25° pressure angle, full depth teeth, $Q_v = 10$, and AISI 4140 steel for all gears.
- 12-59 The pinion of an external gearset has pitch radius $r_p = 40$ mm and the gear has pitch radius $r_g = 160$ mm. If the pinion is the input member of the set, determine the velocity ratio, the torque ratio, and the gear ratio of the set.
- 12-60 A pinion having 20 teeth and a diametral pitch of 8 (in-1) is in mesh with a rack. If the pinion rotates one revolution, how far will the rack move?
- 12-61 A gearset with full-depth teeth is designed to have a pinion with 24 teeth, a gear with 54 teeth, and a diametral pitch of 6. Compare the contact ratio for this set for pressure angles of 14.5° , 20° , and 25° .
- 12-62 Design a planetary gear train similar to that shown in Figure 12-16 for an overall velocity ratio of exactly 5 if the ring gear is stationary, the arm is the input, and the sun gear is the output. Specify tooth numbers for each gear in the train.
- 12-63 A 22-tooth pinion rotating at 1650 rpm meshes with a 66-tooth gear in a spur gear reducer. Both pinion and gear are manufactured to a quality level of 10. A reliability of 0.9 has been specified, and the transmitted tangential load is 5000 lb. Conditions are such that $K_m = 1.7$. It is proposed that standard 25° , full-depth teeth be used, with both pinion and gear hobbed from an AISI 4340 nitrided steel. The diametral pitch is 5, and the face width 2.500 in. Estimate the number of cycles of bending stress (using the AGMA equations) that the gearset can withstand.
- 12-64 A 22-tooth pinion rotating at 1650 rpm meshes with a 66-tooth gear in a spur gear reducer. Both pinion and gear are manufactured to a quality level of 10. A reliability of 0.9 has been specified, and the transmitted tangential load is 5000 lb. Conditions are such that $K_m = 1.7$. It is proposed that standard 25° , full-depth teeth be used, with both pinion and gear hobbed from an AISI 4340 nitrided steel. The diametral pitch is 5, and the face width 2.500 in. Estimate the number of cycles of contact (surface) stress (using the AGMA equations) that the gearset can withstand.
- 12-65 The pinion of an internal gearset has pitch radius $r_p = 30$ mm and the gear has pitch radius $r_g = 150$ mm. If the pinion is the input member of the set, determine the velocity ratio, the torque ratio, and the gear ratio of the set.
- 12-66 A pinion having 18 teeth and a diametral pitch of 10 (in-1) is in mesh with a rack. If the rack moves 1 in, how many degrees will the pinion rotate?
- 12-67 A gearset with 25° , full-depth teeth is designed to have a pinion with 24 teeth, a gear with 54 teeth, and a diametral pitch of 6. Compare the contact ratio for this set for a range of center distances from $0.90C$ to $1.10C$.
- 12-68 Design a planetary gear train similar to that shown in Figure 12-16 for an overall velocity ratio of exactly 1.25 if the sun gear is stationary, the arm is the input, and the ring gear is the output. Specify tooth numbers for each gear in the train.

[†] Problem numbers in *italics* are design problems.

13



HELICAL, BEVEL, AND WORM GEARS

Cycle and Epicycle, Orb in Orb . . .

JOHN MILTON, PARADISE LOST

13.0 INTRODUCTION

Chapter 12 explored the topic of straight-toothed or spur gears in some detail. Gears are available in many other tooth configurations for particular applications. This chapter will present a brief introduction to designing with helical, bevel, and worm gears. The complexity of the design problem increases significantly when these more complicated gear tooth shapes are used. The *American Gear Manufacturers Association* (AGMA) presents detailed data and algorithms for their calculation. We will base this presentation on the AGMA recommendations, but cannot give a complete treatment of this complex subject in the space available here. The reader is encouraged to consult the AGMA standards for more information when faced with a real design problem involving gearing. Table 13-0 lists the variables used in this chapter and indicates the section or equation in which they appear. A summary and list of important equations appears at the end of the chapter.

13.1 HELICAL GEARS

Helical gears are very similar to spur gears. Their teeth are involutes. The difference is that their teeth are angled with respect to the axis of rotation at a helix angle ψ , as shown in Figure 13-1. The helix angle may typically range from about 10 to 45°. If the gear were long enough axially, any one tooth would wrap around the circumference 360°. The teeth form a helix, which may be either right- or left-handed. A pair of opposite-hand helical gears mesh with their axes parallel as shown in Figure 13-1a. Same-hand helical gears can be meshed with their axes skewed and are then called crossed-axis or just crossed helical gears as shown in Figure 13-1b.

Table 13-0 Variables Used in This Chapter

Part 1 of 2

Symbol	Variable	ips units	SI units	See
a	addendum	in	m	Eq. 13.18
b	dedendum	in	m	Eq. 13.18
C	center distance	none	none	Eq. 13.16
C_f	surface finish factor	none	none	Eq. 13.10
C_H	hardness factor	none	none	Eq. 13.11
C_{md}	mounting factor	none	none	Eq. 13.11
C_p	elastic coefficient	none	none	Eq. 13.10
C_R	reliability factor	none	none	Eq. 13.11
C_s	materials factor	none	none	Eq. 13.24
C_T	temperature factor	none	none	Eq. 13.11
C_{xc}	crowning factor	none	none	Eq. 13.10
d	pitch diameter (with various subscripts)	in	m	various
e	efficiency	none	none	Eq. 13.30
F	face width	in	m	Eq. 13.9, .19
I	AGMA surface geometry factor	none	none	Eq. 13.10
J	AGMA bending geometry factor	none	none	Eq. 13.9
K_a, C_a	application factor	none	none	Eq. 13.9
K_B	rim bending factor	none	none	Eq. 12.15
K_I	idler factor	none	none	Eq. 12.15
K_m, C_m	load distribution factor	none	none	Eq. 13.9, .10
K_s, C_s	size factor	none	none	Eq. 13.9, .10
K_v, C_v	dynamic factor, velocity factor	none	none	Eq. 13.9, .26
K_x	curvature factor	none	none	Eq. 13.9
L	length, lead	in	m	Eq. 13.6, .7
m	module	not used	mm	Eq. 13.9
m_F	axial contact ratio	none	none	Eq. 13.5
m_G	gear ratio	none	none	Eq. 13.15
m_N	load sharing ratio	none	none	Eq. 13.6
m_p	transverse contact ratio	none	none	Eq. 13.6
N	number of teeth (with various subscripts)	none	none	various
N_b, N_c	factors of safety—bending and contact	none	none	various
P_c	circular pitch	in	mm	Eq. 13.1c
P_d	diametral pitch	1/in	not used	Eq. 13.1c
P_t	transverse pitch	in	m	Eq. 13.1a
P_x	axial pitch	in	mm	Eq. 13.1b
S_{fb}	corrected bending-endurance strength	psi	Pa	Ex. 13-2
S_{fc}	corrected surface-endurance strength	psi	Pa	Ex. 13-2
S'_{fc}	uncorrected surface-endurance strength	psi	Pa	Eq. 13.11
T	torque (with various subscripts)	lb-in	N-m	various
V_t	pitch-line velocity	in/sec	m/sec	Eq. 13.27
W	total force on gear teeth	lb	N	Eq. 13.3
W_a	axial force on gear teeth	lb	N	Eq. 13.3

Table 13-0 Variables Used in This Chapter

Part 2 of 2

Symbol	Variable	ips units	SI units	See
W_f	friction force on gear teeth	lb	N	Eq. 13.28
W_r	radial force on gear teeth	lb	N	Eq. 13.3
W_t	tangential force on gear teeth	lb	N	Eq. 13.3
α	pitch cone angle	deg	deg	Eq. 13.7
ϕ	pressure angle	deg	deg	various
ψ	helix angle or spiral angle	deg	deg	various
λ	lead angle	deg	deg	Eq. 13.12
μ	coefficient of friction	none	none	Eq. 13.28
ω	angular velocity	rad/sec	rad/sec	Ex. 13-2
ρ	radius of curvature	in	m	Eq. 13.6
Φ	power	hp	W	Eq. 13.20
σ_b	bending stress	psi	Pa	Eq. 13.9
σ_c	surface stress	psi	Pa	Eq. 13.10



(a) Opposite-hand pair meshed on parallel axes



(b) Same-hand pair meshed on crossed axes

PARALLEL HELICAL GEARS (Figure 13-1a) mesh with a combination of rolling and sliding with contact starting at one end of the tooth and “wiping” across its face width. This is quite different than spur gear tooth contact, which occurs all at once along a line across the tooth face at the instant of tooth contact. One result of this difference is that helical gears run quieter and with less vibration than spur gears because of the gradual tooth contact. Automotive transmissions use helical gears almost exclusively in order to obtain quiet operation. One common exception is in the reverse-gear mesh of a non-automatic transmission, which often uses spur gears to enable shifting them in and out of engagement. In such a transmission, a noticeable “gear whine” can be heard when backing up the vehicle, due to the resonances of the spur-gear teeth being excited by the sudden impacts of tooth-tooth line contact. The helical forward-gear meshes are essentially silent. Parallel helical gears are also capable of transmitting high power levels.

CROSSED HELICAL GEARS (Figure 13-1b) mesh differently than parallel helical gears; their teeth slide without rolling and are in theoretical point contact rather than the line contact of parallel gears. This severely reduces their load-carrying capacity. Crossed helical gears are not recommended for applications that must transmit large torque or power. They are nevertheless frequently used in light-load applications, such as distributor and speedometer drives of automobiles.

Helical Gear Geometry

Figure 13-2 shows the geometry of a basic helical rack. The teeth form the helix angle ψ with the “axis” of the rack. The teeth are cut at this angle and the tooth form is then in the **normal plane**. The **normal pitch** p_n and the **normal pressure angle** ϕ_n are measured in this plane. The **transverse pitch** p_t and the **transverse pressure angle** ϕ_t are measured in the **transverse plane**. These dimensions are related to one another by the helix angle. The transverse pitch is the hypotenuse of the right triangle ABC.

$$p_t = p_n / \cos \psi \quad (13.1a)$$

FIGURE 13-1

Helical Gears Courtesy of Boston Gear, Division of IMO Industries, Quincy, MA

An axial pitch p_x can also be defined as the hypotenuse of the right triangle BCD .

$$p_x = p_n / \sin \psi \quad (13.1b)$$

p_t corresponds to circular pitch p_c , measured in the pitch plane of a circular gear. Diametral pitch is more commonly used to define tooth size and is related to circular pitch by

$$p_d = \frac{N}{d} = \frac{\pi}{p_c} = \frac{\pi}{p_t} \quad (13.1c)$$

where N is number of teeth and d is pitch diameter.

The diametral pitch in the normal plane is

$$p_{nd} = p_d / \cos \psi \quad (13.1d)$$

The pressure angles in the two planes are related by

$$\tan \phi_t = \tan \phi = \tan \phi_n / \cos \psi \quad (13.2)$$

Helical-Gear Forces

A set of forces acting on a tooth is shown schematically in Figure 13-2. The resultant force W is at a compound angle defined by the pressure angle and the helix angle in combination. The tangential force component W_t at the mesh can be found from the torque applied either to gear or pinion, as defined in equation 12.13a for the pinion.

$$W_t = \frac{T_p}{r_p} = \frac{2T_p}{d_p} = \frac{2p_d T_p}{N_p} \quad (12.13a)$$

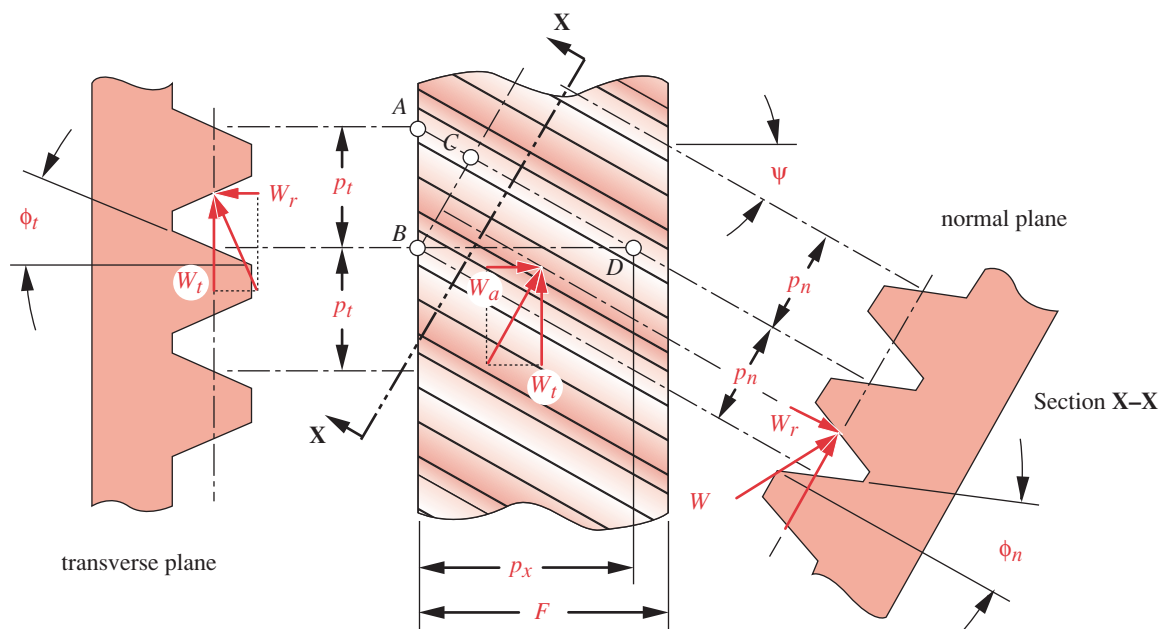


FIGURE 13-2

Basic Helical Rack Showing Normal and Transverse Planes and Resolution of Forces

In addition to the radial component W_r due to the pressure angle, there is now also a component of force W_a , which tends to separate the gears axially. Bearings with axial thrust capability must be used with helical gears to resist this force component, unless helical gears are mounted in opposite-hand pairs on the same shaft to cancel the axial force component. Sometimes for this purpose, both left- and right-hand sets of teeth are cut side by side on the same gear blank with a groove between them to clear the cutter. These are called **double helical gears**. If the clearance groove is eliminated and the opposite-hand teeth cut to run into one another, it is called a **herringbone gear**.

The components of force in a helical garmesh are

$$W_r = W_t \tan \phi \quad (13.3a)$$

$$W_a = W_t \tan \psi \quad (13.3b)$$

$$W = \frac{W_t}{\cos \psi \cos \phi_n} \quad (13.3c)$$

Virtual Number of Teeth

Another advantage of helical gears over spur gears besides quiet operation is their relatively stronger teeth for a gear with the same normal pitch, pitch diameter, and number of teeth. The reason for this can be seen in Figure 13-2. The component of force that transmits the torque is W_t , which lies in the transverse plane. The tooth size (normal pitch) is defined in the normal plane. The thickness of the tooth in the transverse plane is $1 / \cos \psi$ times that of a spur gear of equal normal pitch. Another way to visualize this is to consider the fact that the intersection of the normal plane and the pitch cylinder of diameter d is an ellipse whose radius is $r_e = (d / 2) / \cos^2 \psi$. We can then define a virtual number of teeth N_e as the quotient of the circumference of a virtual pitch circle of radius r_e and the normal pitch p_c :

$$N_e = \frac{2\pi r_e}{p_n} = \frac{\pi d}{p_n \cos^2 \psi} \quad (13.4a)$$

Substitute equation 13.1a for p_n :

$$N_e = \frac{\pi d}{p_t \cos^3 \psi} \quad (13.4b)$$

and substitute $p_t = \pi d / N$ from equation 13.1c to get

$$N_e = \frac{N}{\cos^3 \psi} \quad (13.4c)$$

This defines a **virtual gear** that is equivalent to a spur gear with N_e teeth thus giving a stronger tooth in both bending and surface fatigue than a spur gear with the same physical number of teeth as the helical gear. The larger number of virtual teeth also reduces undercutting in small pinions, allowing a lower minimum number of teeth for helical gears than for spur gears.

Contact Ratios

The **transverse contact ratio** m_p was defined for spur gears in equation 12.7 (p. 694) and is the same for helical gears. The helix angle introduces another ratio called the **axial contact ratio** m_F , which is defined as the quotient of face width F and axial pitch p_x :

$$m_F = \frac{F}{p_x} = \frac{F p_d \tan \psi}{\pi} \quad (13.5)$$

This ratio should be at least 1.15 and indicates the degree of **helical overlap** in the mesh.

Just as a larger transverse contact ratio allows multiple teeth to share the load, a wider face width for a given helix angle will increase the overlapping of teeth and also promote load sharing. However, effective load sharing will still be limited by the accuracy with which the gears are made (see Figure 12-19 on p. 706). Note that larger helix angles will increase the axial contact ratio, allowing narrower-width gears to be used, but this will be at the expense of larger axial force components.

If m_F is kept above 1 as desired, the gears are considered conventional helicals. If $m_F < 1$, then they are called **low axial contact ratio (LACR) gears** and their calculation involves additional steps. Consult the AGMA standards^[1, 2, 3] for more information on LACR gears. We will consider only conventional helical gears here.

Stresses in Helical Gears

The AGMA equations for bending stress and surface stress in spur gears are also used for helical gears. These equations were presented in Chapter 12 with extensive explanation and definition of terms that will not be repeated here. The equations from that chapter are, for bending stress:

$$\sigma_b = \frac{W_t p_d}{FJ} \frac{K_a K_m}{K_v} K_s K_B K_I \quad (12.15us)$$

$$\sigma_b = \frac{W_t}{FmJ} \frac{K_a K_m}{K_v} K_s K_B K_I \quad (12.15si)$$

and for surface stress:

$$\sigma_c = C_p \sqrt{\frac{W_t}{FId} \frac{C_a C_m}{C_v} C_s C_f} \quad (12.21)$$

The only significant differences in their application to helical gears involves the geometry factors I and J . The values of J for various combinations of helix angle (10, 15, 20, 25, 30°), pressure angle (14.5, 20, 25°), and addendum ratio (0, 0.25, 0.5) are presented in reference 3. A few examples are reproduced here as Tables 13-1 to 13-6.* Consider the AGMA standard for more complete information.

The calculation of I for conventional helical gear pairs requires the inclusion of one additional term in equation 12.22a (p. 719), which becomes:[†]

* Extracted from AGMA 908-B89, *Geometry Factors for Determining the Pitting Resistance and Bending Strength of Spur, Helical, and Herringbone Gear Teeth*, with the permission of the American Gear Manufacturers Association, 1500 King St., Suite 201, Alexandria, VA 22314.

[†] A second additional term is required for LACR helical gears but these will not be addressed here as previously noted.

$$I = \frac{\cos \phi}{\left(\frac{1}{\rho_p} \pm \frac{1}{\rho_g} \right) d_p m_N} \quad (13.6a)$$

where ρ_p and ρ_g are the radii of curvature of the pinion and gear teeth, respectively, ϕ is the pressure angle, and d_p is the pitch diameter of the pinion. The \pm sign accounts for external and internal gearsets. Use the upper sign for external gearsets in all related expressions. The term m_N is a **load-sharing ratio** defined as

$$m_N = \frac{F}{L_{min}} \quad (13.6b)$$

where F is the face width. Calculation of the **minimum length of the lines of contact** L_{min} requires several steps. First, two factors must be formed from the residuals of the transverse contact ratio m_p and the axial contact ratio m_F .

$$\begin{aligned} n_r &= \text{fractional part of } m_p \\ n_a &= \text{fractional part of } m_F \end{aligned} \quad (13.6c)$$

and

$$\text{if } n_a \leq 1 - n_r \text{ then } L_{min} = \frac{m_p F - n_a n_r p_x}{\cos \psi_b} \quad (13.6d)$$

$$\text{if } n_a > 1 - n_r \text{ then } L_{min} = \frac{m_p F - (1 - n_a)(1 - n_r)p_x}{\cos \psi_b} \quad (13.6e)$$

All the factors in these equations are defined either in this section or in Chapter 12 except for ψ_b , the base helix angle, which is

$$\psi_b = \cos^{-1} \left(\cos \psi \frac{\cos \phi_n}{\cos \phi} \right) \quad (13.6f)$$

Also, the radius of curvature of a helical pinion for equation 13.6a is calculated with a different formula than that used for spur gears. Instead of equation 12.22b, use

$$\begin{aligned} \rho_p &= \sqrt{\left\{ 0.5 \left[(r_p + a_p) \pm (C - r_g - a_g) \right] \right\}^2 - (r_p \cos \phi)^2} \\ \rho_g &= C \sin \phi \mp \rho_p \end{aligned} \quad (13.6g)$$

where (r_p, a_p) and (r_g, a_g) are the (pitch radius, addendum) of the pinion and gear, respectively, and C is the actual (operating) center distance.

The bending and surface stresses can be calculated from the above equations using the data in Tables 13-1 to 13-6. The material strengths can be found in Chapter 12 and safety factors calculated in the same manner as described there for spur gears.

Table 13-1 AGMA Bending Geometry Factor J for $\phi = 20^\circ$, $\psi = 10^\circ$ Full-Depth Teeth with Tip Loading

Gear teeth	Pinion teeth															
	12		14		17		21		26		35		55		135	
	P	G	P	G	P	G	P	G	P	G	P	G	P	G	P	G
12	U	U														
14	U	U	U	U												
17	U	U	U	U	U	U										
21	U	U	U	U	U	U	0.46	0.46								
26	U	U	U	U	U	U	0.47	0.49	0.49	0.49						
35	U	U	U	U	U	U	0.48	0.52	0.50	0.53	0.54	0.54				
55	U	U	U	U	U	U	0.49	0.55	0.52	0.56	0.55	0.57	0.59	0.59		
135	U	U	U	U	U	U	0.50	0.60	0.53	0.61	0.57	0.62	0.60	0.63	0.65	0.65

Table 13-2 AGMA Bending Geometry Factor J for $\phi = 20^\circ$, $\psi = 20^\circ$ Full-Depth Teeth with Tip Loading

Gear teeth	Pinion teeth															
	12		14		17		21		26		35		55		135	
	P	G	P	G	P	G	P	G	P	G	P	G	P	G	P	G
12	U	U														
14	U	U	U	U												
17	U	U	U	U	0.44	0.44										
21	U	U	U	U	0.45	0.46	0.47	0.47								
26	U	U	U	U	0.45	0.49	0.48	0.49	0.50	0.50						
35	U	U	U	U	0.46	0.51	0.49	0.52	0.51	0.53	0.54	0.54				
55	U	U	U	U	0.47	0.54	0.50	0.55	0.52	0.56	0.55	0.57	0.58	0.58		
135	U	U	U	U	0.48	0.58	0.51	0.59	0.54	0.60	0.57	0.61	0.60	0.62	0.64	0.64

Table 13-3 AGMA Bending Geometry Factor J for $\phi = 20^\circ$, $\psi = 30^\circ$ Full-Depth Teeth with Tip Loading

Gear teeth	Pinion teeth															
	12		14		17		21		26		35		55		135	
	P	G	P	G	P	G	P	G	P	G	P	G	P	G	P	G
12	U	U														
14	U	U	0.39	0.39												
17	U	U	0.39	0.41	0.41	0.41										
21	U	U	0.40	0.43	0.42	0.43	0.44	0.44								
26	U	U	0.41	0.44	0.43	0.45	0.45	0.46	0.46	0.46						
35	U	U	0.41	0.46	0.43	0.47	0.45	0.48	0.47	0.48	0.49	0.49				
55	U	U	0.42	0.49	0.44	0.49	0.46	0.50	0.48	0.50	0.50	0.51	0.52	0.52		
135	U	U	0.43	0.51	0.45	0.52	0.47	0.53	0.49	0.53	0.51	0.54	0.53	0.55	0.56	0.56

Table 13-4 AGMA Bending Geometry Factor J for $\phi = 25^\circ$, $\psi = 10^\circ$ Full-Depth Teeth with Tip Loading

Gear teeth	Pinion teeth															
	12		14		17		21		26		35		55		135	
	P	G	P	G	P	G	P	G	P	G	P	G	P	G	P	G
12	U	U														
14	U	U	0.47	0.47												
17	U	U	0.48	0.51	0.52	0.52										
21	U	U	0.48	0.55	0.52	0.55	0.56	0.56								
26	U	U	0.49	0.58	0.53	0.58	0.57	0.59	0.60	0.60						
35	U	U	0.50	0.61	0.54	0.62	0.57	0.63	0.61	0.64	0.64	0.64				
55	U	U	0.51	0.65	0.55	0.66	0.58	0.67	0.62	0.68	0.65	0.69	0.70	0.70		
135	U	U	0.52	0.70	0.56	0.71	0.60	0.72	0.63	0.73	0.67	0.74	0.71	0.75	0.76	0.76

Table 13-5 AGMA Bending Geometry Factor J for $\phi = 25^\circ$, $\psi = 20^\circ$ Full-Depth Teeth with Tip Loading

Gear teeth	Pinion teeth															
	12		14		17		21		26		35		55		135	
	P	G	P	G	P	G	P	G	P	G	P	G	P	G	P	G
12	0.47	0.47														
14	0.47	0.50	0.50	0.50												
17	0.48	0.53	0.51	0.54	0.54	0.54										
21	0.48	0.56	0.51	0.57	0.55	0.58	0.58	0.58								
26	0.49	0.59	0.52	0.60	0.55	0.60	0.69	0.61	0.62	0.62						
35	0.49	0.62	0.53	0.63	0.56	0.64	0.60	0.64	0.62	0.65	0.66	0.66				
55	0.50	0.66	0.53	0.67	0.57	0.67	0.60	0.68	0.63	0.69	0.67	0.70	0.71	0.71		
135	0.51	0.70	0.54	0.71	0.58	0.72	0.62	0.72	0.65	0.73	0.68	0.74	0.72	0.75	0.76	0.76

13

Table 13-6 AGMA Bending Geometry Factor J for $\phi = 25^\circ$, $\psi = 30^\circ$ Full-Depth Teeth with Tip Loading

Gear teeth	Pinion teeth															
	12		14		17		21		26		35		55		135	
	P	G	P	G	P	G	P	G	P	G	P	G	P	G	P	G
12	0.46	0.46														
14	0.47	0.49	0.49	0.49												
17	0.47	0.51	0.50	0.52	0.52	0.52										
21	0.48	0.54	0.50	0.54	0.53	0.55	0.55	0.55								
26	0.48	0.56	0.51	0.56	0.53	0.57	0.56	0.57	0.58	0.58						
35	0.49	0.58	0.51	0.59	0.54	0.59	0.56	0.60	0.58	0.60	0.61	0.61				
55	0.49	0.61	0.52	0.61	0.54	0.62	0.57	0.62	0.59	0.63	0.62	0.64	0.64	0.64		
135	0.50	0.64	0.53	0.64	0.55	0.65	0.58	0.66	0.60	0.66	0.62	0.67	0.65	0.68	0.68	0.68

EXAMPLE 13-1**Stress Analysis of a Helical-Gear Train**

Problem Redesign the spur-gear train of Examples 12-4 through 12-7 (pp. 707 to 730) using helical gears and compare their safety factors.

Given The referenced examples address, respectively, the kinematics, bending stresses, surface stresses, and safety factors for a 3-gear train with the following data: $W_t = 432.17 \text{ lb}$, $N_p = 14$, $N_{idler} = 17$, $N_g = 49$, $\phi = 25^\circ$, $p_d = 6$, $F = 2.667 \text{ in}$, pinion speed = 2 500 rpm, and 20 hp. The velocity factor $K_v = 0.66$ from previous calculations.

Assumptions The teeth are standard AGMA full-depth profiles. The load and source are both uniform in nature. A gear-quality index of 6 will be used. All gears are steel with $v = 0.28$. The service life required is 5 years of one-shift operation. Operating temperature is 200°F. Based on the assumption of uniform load and source, the application factor K_a can be set to 1. The load distribution factor can be estimated from Table 12-16 (p. 715) based on the assumed face width: $K_m = 1.6$. The idler factor $K_I = 1$ for the pinion and gear and $K_I = 1.42$ for the idler gear. The size factor $K_s = 1$ for all three gears. $C_f = 1$. $K_B = 1$. Keep the same ϕ and p_d as the previous examples' spur gears and try a 20° helix angle.

Solution

- 1 The bending geometry factor J for a 25° pressure angle, 20° helix-angle, 14-tooth pinion in mesh with the 17-tooth idler is found from Table 13-5 to be $J_{pinion} = 0.51$. The pinion-tooth bending stress is then

$$\sigma_{b_p} = \frac{W_t p_d}{FJ} \frac{K_a K_m}{K_v} K_s K_B K_I \cong \frac{432.17(6)}{2.667(0.51)} \frac{1(1.6)}{0.66} (1)(1)(1) \cong 4620 \text{ psi} \quad (a)$$

- 2 The bending geometry factor J for the 25° pressure angle, 20° helix angle, 17-tooth idler in mesh with the 14-tooth pinion from Table 13-5 is $J_{idler} = 0.54$. The idler-tooth bending stress is then

$$\sigma_{b_i} = \frac{W_t p_d}{FJ} \frac{K_a K_m}{K_v} K_s K_B K_I \cong \frac{432.17(6)}{2.667(0.54)} \frac{1(1.6)}{0.66} (1)(1)(1.42) \cong 6200 \text{ psi} \quad (b)$$

Note in Table 13-5 that the idler has a different J factor when considered to be the "gear" in mesh with the smaller pinion than when considered to be the "pinion" in mesh with the larger gear. The smaller value of the two is used because it gives the higher stress.

- 3 The bending geometry factor J for the 25° pressure angle, 20° helix angle, 49-tooth gear in mesh with the 17-tooth idler is found from Table 13-5 as $J_{gear} = 0.66$. The gear-tooth bending stress is then

$$\sigma_{b_g} = \frac{W_t p_d}{FJ} \frac{K_a K_m}{K_v} K_s K_B K_I \cong \frac{432.17(6)}{2.667(0.66)} \frac{1(1.6)}{0.66} (1)(1)(1) \cong 3570 \text{ psi} \quad (c)$$

- 4 We will need the pitch diameter and pitch radius of each gear for this calculation. From the data in Example 12-4 (p. 707):

$$\begin{array}{lll} d_p = 2.333 & d_i = 2.833 & d_g = 8.167 \\ r_p = 1.167 & r_i = 1.417 & r_g = 4.083 \end{array} \quad (d)$$

5 The addenda, dedenda, and center distances of the meshes are:

$$\begin{aligned} a_p = a_i = a_g &= \frac{1.0}{p_d} = \frac{1}{6} = 0.167 \text{ in} \\ C_{pi} &= \frac{d_p + d_i}{2} = \frac{2.333 + 2.833}{2} = 2.58 \text{ in} \\ C_{id} &= \frac{d_i + d_g}{2} = \frac{2.833 + 8.167}{2} = 5.50 \text{ in} \end{aligned} \quad (e)$$

6 Find the lengths of action Z_{pi} and Z_{ig} for the two meshes using equation 12.2 (p. 686).

$$\begin{aligned} Z_{pi} &= \sqrt{(r_p + a_p)^2 - (r_p \cos \phi)^2} + \sqrt{(r_i + a_i)^2 - (r_i \cos \phi)^2} - C_{pi} \sin \phi \\ &= \sqrt{(1.167 + 0.167)^2 - (1.167 \cos 25^\circ)^2} \\ &\quad + \sqrt{(1.417 + 0.167)^2 - (1.417 \cos 25^\circ)^2} - 2.58 \sin 25^\circ = 0.647 \end{aligned} \quad (f)$$

$$\begin{aligned} Z_{ig} &= \sqrt{(r_p + a_p)^2 - (r_p \cos \phi)^2} + \sqrt{(r_g + a_g)^2 - (r_g \cos \phi)^2} - C_{ig} \sin \phi \\ &= \sqrt{(1.167 + 0.167)^2 - (1.167 \cos 25^\circ)^2} \\ &\quad + \sqrt{(4.083 + 0.167)^2 - (4.083 \cos 25^\circ)^2} - 5.50 \sin 25^\circ = 0.692 \end{aligned}$$

7 The transverse contact ratios for the two meshes are found from equation 12.7b (p. 694).

$$\begin{aligned} \text{for the pinion - idler mesh : } m_{p_{pi}} &= \frac{p_d Z_{pi}}{\pi \cos \phi} = \frac{6(0.647)}{\pi \cos 25^\circ} = 1.36 \\ \text{for the idler - gear mesh : } m_{p_{ig}} &= \frac{p_d Z_{ig}}{\pi \cos \phi} = \frac{6(0.692)}{\pi \cos 25^\circ} = 1.46 \end{aligned} \quad (g)$$

8 The axial contact ratio m_F is found from equation 13.5 (p. 752) and the axial pitch p_x from equations 13.1a, b, and c (pp. 749–750).

$$\begin{aligned} m_F &= \frac{F p_d \tan \psi}{\pi} = \frac{2.667(6) \tan 20^\circ}{\pi} = 1.85 \\ p_x &= p_n / \sin \psi = p_t \cos \psi / \sin \psi = \frac{\pi \cos \psi}{p_d \sin \psi} = \frac{\pi \cos 20^\circ}{6 \sin 20^\circ} = 1.44 \text{ in} \end{aligned} \quad (h)$$

9 Find the normal pressure angle ϕ_n and the base helix angle ψ_b from equations 13.2 and 13.6f (pp. 750 and 753), respectively.

$$\begin{aligned} \phi_n &= \tan^{-1}(\cos \psi \tan \phi) = \tan^{-1}(\cos 20^\circ \tan 25^\circ) = 23.66^\circ \\ \psi_b &= \cos^{-1} \left(\cos \psi \frac{\cos \phi_n}{\cos \phi} \right) = \cos^{-1} \left(\cos 20^\circ \frac{\cos 23.66^\circ}{\cos 25^\circ} \right) = 18.25^\circ \end{aligned} \quad (i)$$

- 10 Find the minimum length of the lines of contact for each mesh using equations 13.6c and 13.6d or e (p. 753) and use it to find the load sharing ratio m_N from equation 13.6b (p. 753).

for the pinion - idler mesh : $n_{r_{pi}} = \text{fractional part of } m_{p_{pi}} = 0.36$

for the idler - gear mesh : $n_{r_{ig}} = \text{fractional part of } m_{p_{ig}} = 0.46$ (j)

for both meshes : $n_a = \text{fractional part of } m_F = 0.85$

for the pinion-idler mesh (equation 13.6e):

$$\text{if } n_a > 1 - n_{r_{pi}} \text{ then : } L_{min_{pi}} = \frac{m_{p_{pi}} F - (1 - n_a)(1 - n_{r_{pi}})p_x}{\cos \psi_b}$$

$$L_{min_{pi}} = \frac{1.36(2.667) - (1 - 0.85)(1 - 0.36)(1.44)}{\cos(18.25^\circ)} = 3.674 \quad (k)$$

$$m_{N_{pi}} = \frac{F}{L_{min_{pi}}} = \frac{2.667}{3.674} = 0.726 \quad (l)$$

for the idler-gear mesh (equation 13.6e):

$$\text{if } n_a > 1 - n_{r_{ig}} \text{ then : } L_{min_{ig}} = \frac{m_{p_{ig}} F - (1 - n_a)(1 - n_{r_{ig}})p_x}{\cos \psi_b}$$

$$L_{min_{ig}} = \frac{1.46(2.667) - (1 - 0.85)(1 - 0.46)(1.44)}{\cos(18.25^\circ)} = 3.977 \quad (m)$$

$$m_{N_{ig}} = \frac{F}{L_{min_{ig}}} = \frac{2.667}{3.977} = 0.671 \quad (n)$$

- 11 The radii of curvature of the gear teeth are:

$$\begin{aligned} \rho_p &= \sqrt{\left\{0.5[(r_p + a_p) \pm (C_{pi} - r_i - a_i)]\right\}^2 - (r_p \cos \phi)^2} \\ &= \sqrt{\left\{0.5[(1.167 + 0.0167) + (2.58 - 1.417 - 0.0167)]\right\}^2 - (1.167 \cos 25^\circ)^2} \\ &= 0.4931 \text{ in} \end{aligned} \quad (o)$$

$$\rho_i = C_{pi} \sin \phi - \rho_p = 2.58 \sin 25^\circ - 0.4931 = 0.5987 \text{ in}$$

$$\rho_g = C_{ig} \sin \phi - \rho_i = 5.5 \sin 25^\circ - 0.5987 = 1.726 \text{ in}$$

- 12 The pitting geometry factor I is calculated for a pair of gears in mesh. Since we have two meshes (pinion/idler and idler/gear), there will be two different values of I to be calculated using equations 13.6.

$$I_{pi} = \frac{\cos\phi}{\left(\frac{1}{\rho_p} + \frac{1}{\rho_i}\right)d_p m_{N_{pi}}} = \frac{\cos 25^\circ}{\left(\frac{1}{0.4931} + \frac{1}{0.5987}\right)(2.333)(0.726)} = 0.14 \quad (p)$$

$$I_{ig} = \frac{\cos\phi}{\left(\frac{1}{\rho_i} + \frac{1}{\rho_g}\right)d_i m_{N_{ig}}} = \frac{\cos 25^\circ}{\left(\frac{1}{0.5987} + \frac{1}{1.726}\right)(2.833)(0.671)} = 0.21$$

- 13 The elastic coefficient C_p is found from equation 12.23 (p. 719) and, as before, is 2 276.

- 14 The surface stress for the pinion-idler mesh is

$$\begin{aligned} \sigma_{c_p} &= C_p \sqrt{\frac{W_t}{FI_{pi}d_p} \frac{C_a C_m}{C_v} C_s C_f} \\ &\equiv 2 276 \sqrt{\frac{432.17}{2.667(0.14)(2.33)} \frac{1(1.6)}{0.66}(1)(1)} \equiv 79 \text{ kpsi} \end{aligned} \quad (q)$$

- 15 The surface stress for the idler-gear mesh is

$$\begin{aligned} \sigma_{c_i} &= C_p \sqrt{\frac{W_t}{FI_{ig}d_i} \frac{C_a C_m}{C_v} C_s C_f} \\ &\equiv 2 276 \sqrt{\frac{432.17}{2.667(0.21)(2.83)} \frac{1(1.6)}{0.66}(1)(1)} \equiv 59 \text{ kpsi} \end{aligned} \quad (r)$$

- 16 The corrected bending-fatigue strength of the steel from Example 12-7 (p. 730) is 39 kpsi, and its corrected surface-fatigue strength is 105 kpsi. The safety factors against bending failure are found by comparing the corrected bending strength to the bending stress for each gear in the mesh:

$$N_{b_{pinion}} = \frac{S_{fb}}{\sigma_{b_{pinion}}} = \frac{39}{4.6} \equiv 8.5 \quad (s)$$

$$N_{b_{idler}} = \frac{S_{fb}}{\sigma_{b_{idler}}} = \frac{39}{6.2} = 6.3 \quad (t)$$

$$N_{b_{gear}} = \frac{S_{fb}}{\sigma_{b_{gear}}} = \frac{39}{3.6} = 10.8 \quad (u)$$

- 17 The safety factors against surface failure are found by comparing the corrected surface strength to the surface stress for each gear in the mesh:^{*}

$$N_{c_{pinion-idler}} = \left(\frac{S_{fc}}{\sigma_{c_{pinion-idler}}} \right)^2 = \left(\frac{105}{79} \right)^2 \equiv 1.8 \quad (v)$$

$$N_{c_{idler-gear}} = \left(\frac{S_{fc}}{\sigma_{c_{idler-gear}}} \right)^2 = \left(\frac{105}{59} \right)^2 \equiv 3.2 \quad (w)$$

* The safety factor against surface failure should be found by comparing the actual load to the load that would produce a stress equal to the material's corrected surface strength. Because surface stress is related to the square root of the load, the surface-fatigue safety factor can be calculated as the quotient of the square of the corrected surface strength divided by the square of the surface stress for each gear in the mesh.

- 18 Compare these results to the safety factors for the spur-gear train in Example 12-7 (p. 730). The helical gears have significantly larger safety factors than same-pitch spur gears.

$$\begin{aligned} N_{b_{pinion}} &= 8.5 & N_{b_{idler}} &= 6.3 & N_{b_{gear}} &= 10.8 \\ &&&&& (x) \\ N_{c_{pinion-idler}} &= 1.8 & N_{c_{idler-gear}} &= 3.2 \end{aligned}$$

- 19 The files EX13-01 can be found on the CD-ROM.
-

13.2 BEVEL GEARS

Bevel gears are cut on mating cones rather than the mating cylinders of spur or helical gears. Their axes are nonparallel and intersect at the apices of the mating cones. The angle between their axes can be any value and is often 90° . If the teeth are cut parallel to the cone axis, they are **straight bevel gears**, analogous to spur gears. If the teeth are cut at a spiral angle ψ to the cone axis, they are **spiral bevel gears**, analogous to helical gears. Contact between the teeth of straight or spiral bevel gears has the same attributes as their analogous cylindrical counterparts, with the result that spiral bevels run quieter and smoother than straight bevels, and spirals can be smaller in diameter for the same load capacity.

Figure 13-3a shows a pair of straight bevel gears and Figure 13-3b a pair of spiral bevels. Another form is the *ZEROL®* gear (not shown), which has curved teeth like a spiral gear but has a zero spiral angle like a straight bevel gear. Zerol gears have some of the quietness and smooth-running characteristics of spiral gears. Spirals are the ultimate in smoothness and quiet running and are recommended for speeds up to 8 000 fpm (40 m/sec). Higher speeds require precision-finished gears. Straight helicals are

13



FIGURE 13-3

(a) Straight Bevel Gears Courtesy of Martin Sprocket and Gear Co., Arlington, Tex. and (b) Spiral Bevel Gears Courtesy of the Boston Gear Division of IMO Industries, Quincy, Mass.

limited to speeds of about 1 000 fpm (10 m/sec). *ZEROL* gears can run as fast as spirals. As with spur and helical gears, a maximum reduction of 10:1 is recommended for any one bevel or spiral gear set. A 5:1 limit is recommended when used as a speed increaser. The torque on the pinion is used as a rating parameter. The most common pressure angle for bevels or spirals is $\phi = 20^\circ$. Spirals most often have a 35° spiral angle ψ . Bevel gears in general are not interchangeable. They are made and replaced as matched sets of pinion and gear.

Bevel-Gear Geometry and Nomenclature

Figure 13-4 shows a cross section of two bevel gears in mesh. Their pitch cone angles are denoted by α_p and α_g for pinion and gear, respectively. The pitch diameters are defined at the large end, on the back cones. The tooth size and shape are defined on the back cone and are similar to a spur-gear tooth with a long addendum pinion to minimize interference and undercutting. The addendum ratio varies with the gear ratio from equal addenda (full-depth teeth) at a 1:1 gear ratio to about a 50% longer pinion addendum at gear ratios above 6:1. The face width F is generally limited to $L / 3$ with L as defined in Figure 13-4. From geometry:

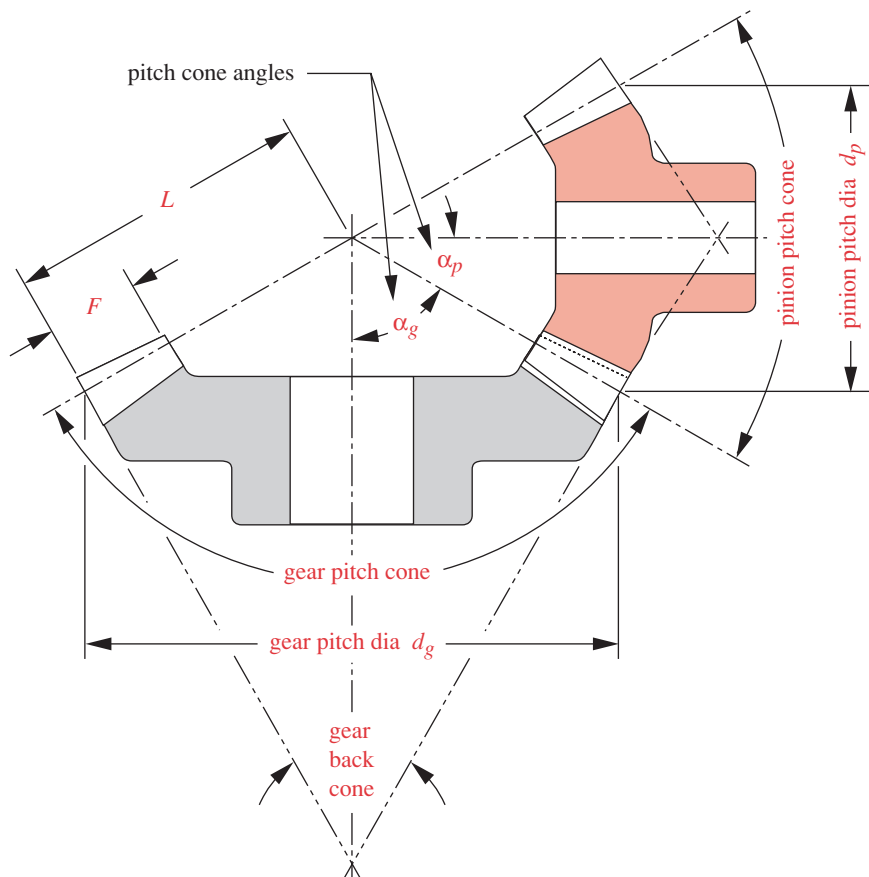


FIGURE 13-4

Bevel-Gear Geometry and Nomenclature Source: Extracted from AGMA Standard 2005-B88, *Design Manual for Bevel Gears*, with the permission of the publisher, the American Gear Manufacturers Association, 1500 King St., Suite 201, Alexandria, Va. 22314.

$$L = \frac{r_p}{\sin \alpha_p} = \frac{d_p}{2 \sin \alpha_p} = \frac{d_g}{2 \sin \alpha_g} \quad (13.7a)$$

The gear ratio m_G for a 90° bevel set can be defined in terms of the pitch cone angles as

$$m_G = \frac{\omega_p}{\omega_g} = \frac{N_g}{N_p} = \frac{d_g}{d_p} = \tan \alpha_g = \cot \alpha_p \quad (13.7b)$$

See also equations 12.1a through 12.1c (pp. 683–684).

Bevel-Gear Mounting

Straddle mounting (bearings on both sides of the tooth plane) is preferred for best support but is difficult to achieve on both pinion and gear with intersecting shafts. The gear is usually straddle mounted and the pinion cantilevered unless there is room enough to provide a bearing on the inside of the pinion to straddle mount it as well.

Forces on Bevel Gears

As in helical gears, there are tangential, radial, and axial force components acting on a bevel or spiral gear. For a straight bevel gear:

$$\begin{aligned} W_a &= W_t \tan \phi \sin \alpha \\ W_r &= W_t \tan \phi \cos \alpha \\ W &= W_t / \cos \phi \end{aligned} \quad (13.8a)$$

For a spiral bevel gear:

$$\begin{aligned} W_a &= \frac{W_t}{\cos \psi} (\tan \phi_n \sin \alpha \mp \sin \psi \cos \alpha) \\ W_r &= \frac{W_t}{\cos \psi} (\tan \phi_n \cos \alpha \pm \sin \psi \sin \alpha) \end{aligned} \quad (13.8b)$$

where the upper signs of the \pm and \mp are used for a driving pinion with a RH spiral rotating *cw* viewed from its large end, or a driving pinion with a LH spiral rotating *ccw* viewed from its large end, and the lower signs used for the opposite conditions.

In equations 13.8a and 13.8b, use the appropriate pitch cone angle α_p for the pinion or α_g for the gear in place of α to obtain the forces on each member. The tangential load W_t can be found from the torque applied to either member in combination with its mean pitch diameter d_m .

$$W_t = \frac{2T}{d_m} \quad (13.8c)$$

where the torque acting on, and the diameter of, the same element (gear or pinion) are used to find the common transmitted force.*

* See the AGMA standard 2005-B88 for the method to calculate d_m , or estimate it from a layout of the gearmesh (similar to Figure 13-4). The model files for Example 13-2 also contain the calculation for mean pitch diameter.

Stresses in Bevel Gears

The calculation of stresses and life estimates for bevel gears is more complicated than for spur or helical gears. The AGMA standards^{[4],[5]} provide more complete information than can be presented here and should be consulted for any actual design applications. We will present only a brief summary of the approach to bevel-gear design as an introduction to the subject, suitable for a basic understanding of the factors involved and for the execution of some exercises.*

BENDING STRESS IN BEVEL GEARS The bending stress in straight or spiral bevel gears is found with essentially the same equation as used for spur or helical gears. The principal difference is accounted for with the value of the J factor.

$$\sigma_b = \frac{2T_p}{d} \frac{p_d}{FJ} \frac{K_a K_m K_s}{K_v K_x} \quad \text{psi} \quad (13.9us)$$

$$\sigma_b = \frac{2000T_p}{d} \frac{1}{FmJ} \frac{K_a K_m K_s}{K_v K_x} \quad \text{MPa} \quad (13.9si)$$

Note that the applied load is expressed in terms of the pinion torque T_p by substituting equation 13.8c rather than using W_t as in equation 12.15 (p. 710). The pitch diameter d in equation 13.9 is that of the pinion. (The SI formula has lengths expressed in mm.) For our purposes, the factors K_a , K_m , K_s , and K_v can be taken to be the same as were defined in Chapter 12 for spur gears. However, some of these factors have slightly different definitions for bevel gears in the AGMA standard,^{[4],[5]} and it should be consulted for the most accurate formulas in any actual design application. The factor $K_x = 1$ for straight bevel gears and is a function of the cutter radius for spiral or Zerol gears. Use $K_x = 1.15$ as an approximation in the latter two cases.

SURFACE STRESS IN BEVEL GEARS The surface stress in straight or spiral bevel gears is calculated in similar fashion to that of spur or helical gears, but with some additional adjustment factors included. As with the bending stress for bevel gears, the applied load is expressed as pinion torque rather than as a tangential load.

$$\sigma_c = C_p C_b \sqrt{\frac{2T_D}{FId^2} \left(\frac{T_p}{T_D} \right)^z \frac{C_a C_m}{C_v} C_s C_f C_{xc}} \quad (13.10)$$

For our purposes, the factors C_p , C_a , C_m , C_v , C_s , and C_f can be taken to be the same as those defined in Chapter 12. However, some of these factors have slightly different definitions for bevel gears in the AGMA standard,^[5] and it should be consulted for the most accurate formulas in any actual design application. The adjustment factors new to this version of the surface-stress equation versus equation 12.21 (p. 718) are C_b , which is a **stress adjustment constant**, defined as 0.634 by the current AGMA standard,^[5] and C_{xc} , a **crowning factor** defined as 1.0 for uncrowned teeth and 1.5 for crowned teeth.[†] The exponent z is 0.667 when $T_p < T_D$ and 1.0 otherwise.

The two torque terms T_D and T_p require some explanation. T_p is the **operating pinion torque**, defined by the applied loads, the applied torque, or the power and speed and may be time varying. T_D is the **design pinion torque**, which is the minimum value needed to produce the full (optimum) contact patch on the gear teeth. In most cases T_D

* Extracted from AGMA Standard 2005-B88, *Design Manual for Bevel Gears*, and/or AGMA 2003-A86, *Rating the Pitting Resistance and Bending Strength of Generated Straight Bevel, ZEROL® Bevel, and Spiral Bevel Gear Teeth*, with the permission of the American Gear Manufacturers Association, 1500 King St., Suite 201, Alexandria, Va., 22314.

† Crowned teeth have surfaces modified to have convex curvature in the lengthwise direction (along the face-width) to produce localized contact and/or to prevent contact at the ends of the tooth. Crowning can be applied to all types of teeth. Crowned teeth reduce the need to accurately align the axes of the mating gears to be exactly parallel.

is the torque necessary to create a contact stress equal to the allowable contact stress for the material as defined in Table 12-21 (p. 728). T_D can be estimated from

$$T_D = \frac{F}{2} \frac{IC_v}{C_s C_{md} C_f C_a C_{xc}} \left(\frac{S'_{fc} d}{C_p C_b} \frac{0.774 C_H}{C_T C_R} \right)^2 \text{ lb-in} \quad (13.11us)$$

$$T_D = \frac{F}{2000} \frac{IC_v}{C_s C_{md} C_f C_a C_{xc}} \left(\frac{S'_{fc} d}{C_p C_b} \frac{0.774 C_H}{C_T C_R} \right)^2 \text{ N.m} \quad (13.11si)$$

where S'_{fc} is the material's surface fatigue strength from Table 12-21 and the C -factors are as defined above or in Chapter 12. (See equation 12.25 (p. 725) for C_H , C_T , and C_R .) C_{md} is a **mounting factor** to account for cantilever or straddle mounting of one or both gears. If the gear teeth are crowned, C_{md} varies from 1.2 for both members straddle mounted to 1.8 if both are cantilevered. Use a value between these two numbers if one member is cantilevered and the other straddle mounted. For uncrowned teeth, double these numbers. See the AGMA standard^[5] for more detailed information.

GEOMETRY FACTORS I AND J The geometry factors for straight and spiral bevel gears are different than those for either spur or helical gears. The AGMA standard provides charts of these factors for straight, Zerol, and spiral gears. A few of these charts are reproduced here as Figures 13-5 through 13-8.*

SAFETY FACTORS The safety factors against bending or pitting failure are calculated in the same manner as outlined for spur gears in Chapter 12.

EXAMPLE 13-2

Stress Analysis of a Bevel-Gear Train

Problem Determine the bending and surface stresses and safety factors in a straight bevel gearset made of the same steel materials, and operating under the same conditions for the same 5-year life as in Example 12-7 (p. 730).

Given $N_p = 20$, $N_g = 35$, $\phi = 25^\circ$, and $p_d = 8$, passing 10 hp at 2 500 rpm. From Example 12-7: the corrected bending strength is 38 937 psi, and the surface strength is 118 000 psi uncorrected and 105 063 psi corrected.

Assumptions From Example 12-7: $K_a = C_a = K_s = C_s = C_f = C_H = C_R = C_T = 1$, $K_m = C_m = 1.6$, $K_v = C_v = 0.652$, $C_L = 0.890$, and $C_p = 2.276$. From this section assume: $C_{xc} = K_x = 1$, $C_b = 0.634$, and $C_{md} = 1.5$.

Solution

- Determine the pinion torque from the given power and speed.

$$T_p = \frac{P}{\omega_p} = \frac{10 \text{ hp} \left(6600 \frac{\text{in-lb}}{\text{sec}} / \text{hp} \right)}{2500 \text{ rpm} (2\pi/60) \frac{\text{rad}}{\text{sec}} / \text{rpm}} = 252.1 \text{ lb-in} \quad (a)$$

* Extracted from AGMA Standard 2005-B88, *Design Manual for Bevel Gears*, and/or AGMA 2003-A86, *Rating the Pitting Resistance and Bending Strength of Generated Straight Bevel, ZEROL® Bevel, and Spiral Bevel Gear Teeth*, with the permission of the American Gear Manufacturers Association, 1500 King St., Suite 201, Alexandria, Va., 22314.

- 2 Find the pitch diameters of pinion and gear.

$$d_p = \frac{N_p}{p_d} = \frac{20}{8} = 2.50 \text{ in}, \quad d_g = \frac{35}{8} = 4.375 \text{ in} \quad (b)$$

- 3 Find the pitch cone angles from equation 13.7b (p. 762):

$$\alpha_g = \tan^{-1}\left(\frac{N_g}{N_p}\right) = \tan^{-1}\left(\frac{35}{20}\right) = 60.26^\circ$$

$$\alpha_p = 90 - \alpha_g = 90 - 60.26 = 29.74^\circ \quad (c)$$

- 4 Find the pitch cone length L from equation 13.7a (p. 762):

$$L = \frac{d_p}{2\sin\alpha_p} = \frac{2.50}{2\sin 29.74} = 2.519 \text{ in} \quad (d)$$

- 5 Use the pitch cone length L to find a suitable face width, set to the maximum recommended value.

$$F = \frac{L}{3} = \frac{2.519}{3} = 0.840 \text{ in} \quad (e)$$

- 6 Look up the bending geometry factors for pinion and gear in Figure 13-5 (p. 752) to find $J_p = 0.237$ and $J_g = 0.201$.

- 7 Find the bending stress in the pinion from equation 13.9 (p. 763) using J_p .

$$\sigma_{b_{pinion}} = \frac{2T_p}{d} \frac{p_d}{FJ} \frac{K_a K_m K_s}{K_v K_x} = \frac{2(252.1)}{2.5} \frac{8}{0.840(0.237)} \frac{1(1.6)(1)}{0.652(1)} \cong 19\,880 \text{ psi} \quad (f)$$

- 8 Find the bending stress in the gear from equation 13.9 using J_g .

$$\sigma_{b_{gear}} = \frac{2T_p}{d} \frac{p_d}{FJ} \frac{K_a K_m K_s}{K_v K_x} = \frac{2(252.1)}{2.5} \frac{8}{0.840(0.201)} \frac{1(1.6)(1)}{0.652(1)} \cong 23\,440 \text{ psi} \quad (g)$$

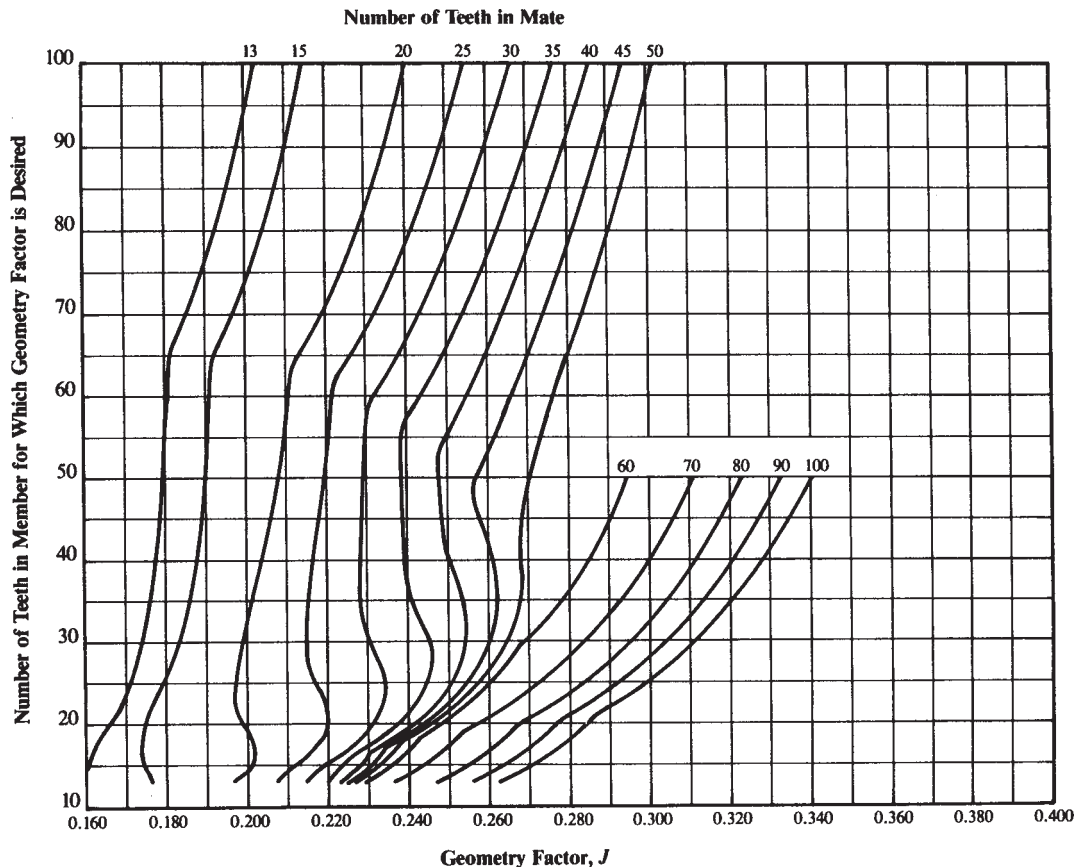
Note that the gear tooth is more highly stressed than the pinion tooth, because the long addendum on the pinion makes it stronger at the expense of the short-addendum gear tooth.

- 9 Look up the surface geometry factor for this combination of pinion and gear in Figure 13-6 (p. 767) to find $I = 0.076$. Use this in equation 13.11 (p. 764) to find T_D .

$$T_D = \frac{F}{2} \frac{IC_v}{C_s C_{md} C_f C_a C_{xc}} \left(\frac{S'_{fc} d}{C_p C_b} \frac{0.774 C_H}{C_T C_R} \right)^2$$

$$= \frac{0.840}{2} \frac{0.076(0.652)}{1(1.5)(1)(1)(1)} \left(\frac{118\,000(2.5)}{2\,276(0.634)} \frac{0.774(1)}{1(1)} \right)^2 \cong 347.5 \text{ lb-in} \quad (h)$$

- 10 Since $T_D > T_p$, $z = 0.667$. Use these data to find the surface stress with equation 13.10.

**FIGURE 13-5**

Geometry Factor J for Straight Bevel Gears with $\phi = 20^\circ$ and $0.120/p_d$ Tool-Edge Radius Source: Extracted from AGMA Standard 2003-A86, *Rating the Pitting Resistance and Bending Strength of Generated Straight Bevel, ZEROL® Bevel, and Spiral Bevel Gear Teeth*, with the permission of the publisher, the American Gear Manufacturers Association, 1500 King St., Suite 201, Alexandria, Va. 22314

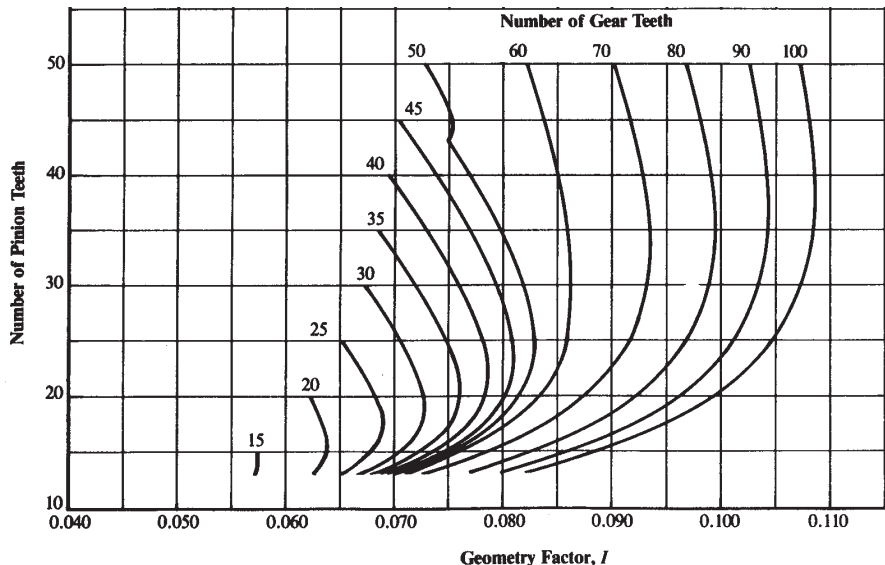
13

$$\begin{aligned} \sigma_c &= C_p C_b \sqrt{\frac{2T_D}{FId^2} \left(\frac{T_p}{T_D}\right)^2 \frac{C_a C_m}{C_v} C_s C_f C_{xc}} \\ &= 2276(0.634) \sqrt{\frac{2(347.5)}{0.840(0.076)(2.5)^2} \left(\frac{252.1}{347.5}\right)^{0.667} \frac{1(1.6)}{0.652}(1)(1)(1)} \\ &\approx 84753 \text{ psi} \end{aligned} \quad (i)$$

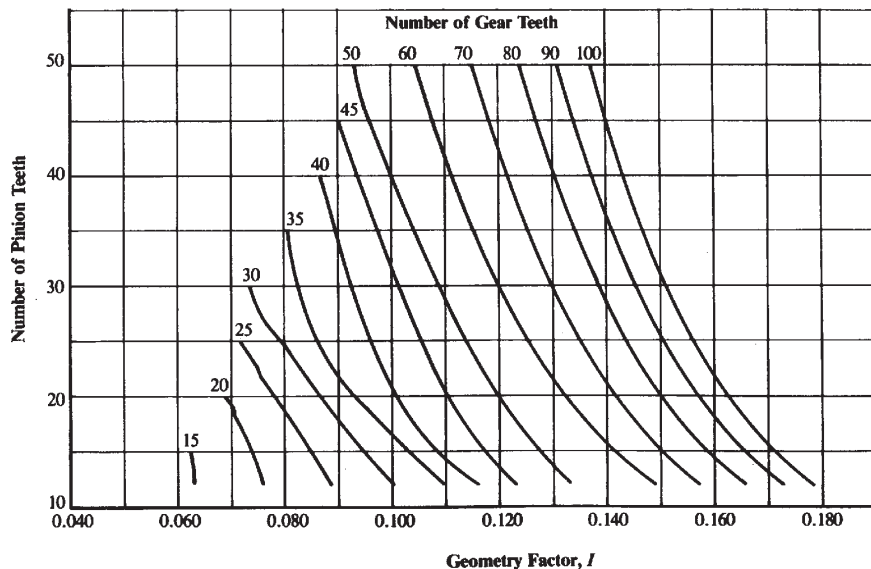
11 The safety factors can now be found as

$$N_{b_{pinion}} = \frac{S_{fb}}{\sigma_{b_{pinion}}} = \frac{38937}{19880} \approx 2.0 \quad (j)$$

$$N_{b_{gear}} = \frac{S_{fb}}{\sigma_{b_{gear}}} = \frac{38937}{23440} \approx 1.7 \quad (k)$$

**FIGURE 13-6**

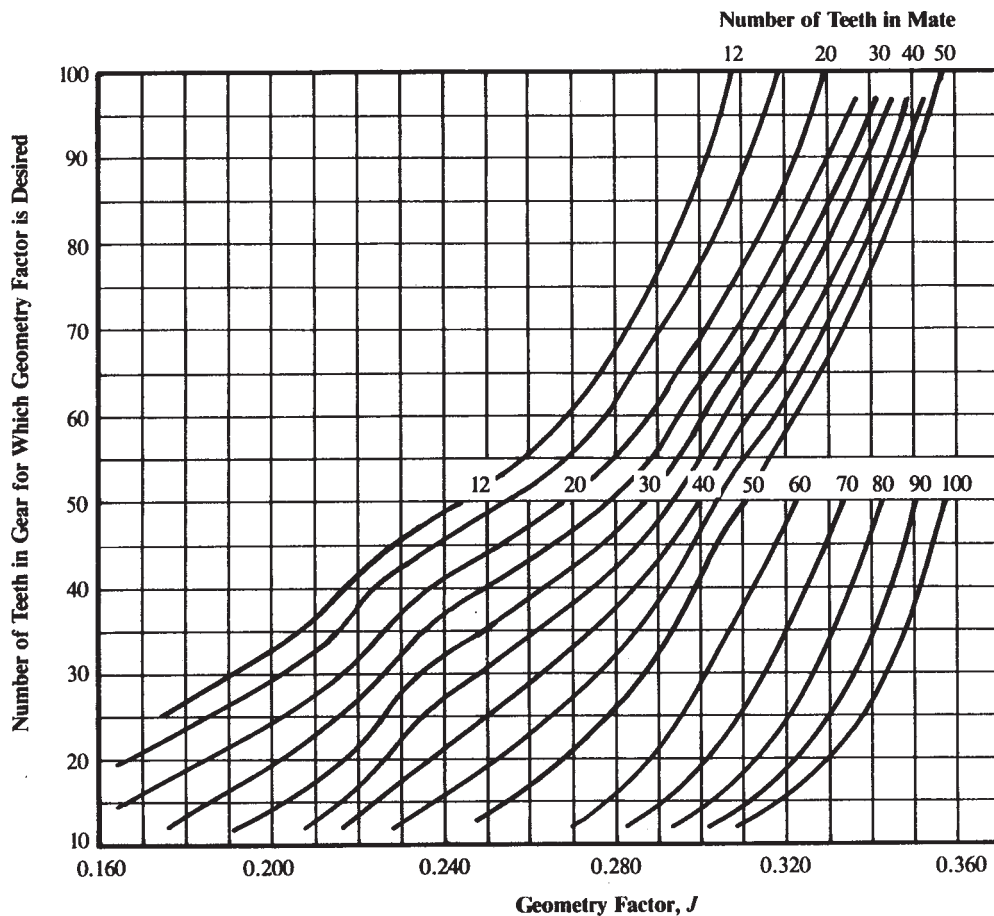
Geometry Factor I for Straight Bevel Gears with $\phi = 20^\circ$ and $0.120/p_d$ Tool-Edge Radius. Source: Extracted from AGMA Standard 2003-A86, *Rating the Pitting Resistance and Bending Strength of Generated Straight Bevel, ZEROL® Bevel, and Spiral Bevel Gear Teeth*, with the permission of the publisher, the American Gear Manufacturers Association, 1500 King St., Suite 201, Alexandria, Va. 22314

**FIGURE 13-7**

Geometry Factor I for Spiral Bevel Gears with $\phi = 20^\circ$, Spiral Angle $\psi = 35^\circ$, and $0.240/p_d$ Tool-Edge Radius. Source: Extracted from AGMA Standard 2003-A86, *Rating the Pitting Resistance and Bending Strength of Generated Straight Bevel, ZEROL® Bevel, and Spiral Bevel Gear Teeth*, with the permission of the publisher, the American Gear Manufacturers Association, 1500 King St., Suite 201, Alexandria, Va. 22314

$$N_c = \left(\frac{S_{fc}}{\sigma_c} \right)^2 = \left(\frac{105\,063}{84\,753} \right)^2 \cong 1.5 \quad (I)$$

12 These are acceptable safety factors. The files EX13-02 are on the CD-ROM.

**FIGURE 13-8**

Geometry Factor J for Spiral Bevel Gears with $\phi = 20^\circ$, Spiral Angle $\psi = 35^\circ$, and $0.240/p_d$ Tool-Edge Radius. Source: Extracted from AGMA 2003-A86, *Rating the Pitting Resistance and Bending Strength of Generated Straight Bevel, ZEROL® Bevel, and Spiral Bevel Gear Teeth*, with the permission of the publisher, the American Gear Manufacturers Association, 1500 King St., Suite 201, Alexandria, Va. 22314

13.3 WORMSETS

Worm gearing is more complicated to design than conventional gearing. We present only a brief look at the process here as an introduction to the topic. The AGMA standards contain much more information. For any real applications, the reader is encouraged to consult the AGMA documents.^[6, 7] They contain many tables of data needed for a complete design. Most of the relevant equations have been excerpted from the standard, but its tabular data are not presented here. Instead, empirical equations from the AGMA standard's appendix^[7] are included for calculation of the tabular data.*

A wormset consists of a worm and a worm gear (also called a worm wheel) as shown in Figure 13-9. They connect nonparallel, nonintersecting shafts, typically at right angles to one another. The worm is, in effect, a helical gear with a helix angle so large that a single tooth wraps continuously around its circumference. The worm is analogous to a screw thread and the worm gear is analogous to its nut. The distance that a point on the mating gear (nut) moves axially in one revolution of the worm is

* Extracted from AGMA Standard 6022-C93, *Design Manual for Cylindrical Wormgearing*, and/or AGMA Standard 6034-B92, *Practice for Enclosed Cylindrical Wormgear Speed Reducers and Gearmotors*, with the permission of the American Gear Manufacturers Association, 1500 King St., Suite 201, Alexandria, Va. 22314.

called the **lead** L and the lead divided by the pitch circumference πd of the worm is the tangent of its **lead angle** λ .

$$\tan \lambda = \frac{L}{\pi d} \quad (13.12)$$

Worms commonly have only one tooth (or thread) and thus can create ratios as large as the number of teeth on the worm gear. This ability to provide high ratios in a compact package is one of the principal advantages of a wormset over other possible gearing configurations, most of which are limited to about a 10:1 ratio per pair of gears. Wormsets can be produced with ratios ranging from 1:1 to 360:1, though the usual range available from catalogs is 3:1 to 100:1. Ratios above 30:1 usually have a single-thread worm, and ratios below that value often use multiple-thread worms. The number of threads on the worm is also referred to as its number of *starts*. A 2- or 3-start worm might be used for a low-ratio wormset, for example. The axial pitch p_x of the worm equals the circular pitch p_c of the worm gear and is related to the lead L by the chosen number of starts or number of teeth on the worm N_w .

$$p_x = \frac{L}{N_w} = p_c = \frac{\pi d_g}{N_g} \quad (13.13)$$

where d_g is the pitch diameter and N_g is the number of teeth on the worm gear. The number of starts N_w is typically between 1 and 10 for commercial wormsets, though more starts may be used on large wormsets.

Another advantage of wormsets over other types of gearsets is their ability to self-lock. If the wormset is self-locking, it will not backdrive, i.e., a torque applied to the worm gear will not rotate the worm. A self-locking wormset can only be driven “forward” from worm to worm gear. Thus it can be used to hold a load as, for example, in jacking up a car. Whether or not a particular wormset will be self-locking depends on a number of factors, including the ratio of $\tan \lambda$ to the coefficient of friction μ , the surface finish, lubrication, and vibration. Generally, self-locking occurs at lead angles below 6° and may occur at lead angles as high as 10° .^[8] (See Section 15.2 (p. 865) for a complete discussion of self-locking as it applies to power screws, the principles of which are equally applicable to wormsets.)

Standard pressure angles for wormsets are 14.5, 17.5, 20, 22.5, 25, 27.5, or 30°. Higher pressure angles give higher tooth strengths at the expense of higher friction, larger bearing loads, and higher bending stresses in the worm. For high-power applications at high speed, a relatively fine-pitch worm gear should be used. High torques at low speeds need coarse pitch and larger worm diameters.

The tooth forms for worms and worm gears are not involutes, and there are large sliding-velocity components in the mesh. Worms and worm gears are not interchangeable but are made and replaced as matched sets. To increase contact area between the teeth, either single-enveloping or double-enveloping tooth forms are used. A single-enveloping set (as shown in Figure 13-9) wraps the worm-gear teeth partially around the worm. A double-enveloping set also wraps the worm partially around the gear, making the worm an hourglass shape instead of a cylinder. These configurations increase manufacturing complexity and cost, but also increase load capacity. Both types are available commercially.

worm gear



worm

FIGURE 13-9

A Single-Enveloping Wormset, Consisting of a Worm and an Enveloping Worm Gear
Courtesy of Martin Sprocket and Gear Co., Arlington, Tex.

Materials for Wormsets

Only a few materials are suitable for wormsets. The worm is highly stressed and requires a hardened steel. Low-carbon steels such as AISI 1020, 1117, 8620, or 4320 are used and case hardened to HRC 58-62. Medium-carbon steels such as AISI 4140 or 4150 are also used, induction or flame hardened to a case of HRC 58-62. They need to be ground or polished to a finish of $16 \mu\text{in}$ ($0.4 \mu\text{m}$) R_a or better. The worm gear needs to be made from a material soft and compliant enough to run-in and conform to the hard worm under the high-sliding conditions. Sand-cast, chill-cast, centrifugal-cast, or forged bronze is typically used for the worm gear. Phosphor or tin bronze is used for high-power applications and manganese bronze for small, slower-speed worms. Cast iron, soft steel, and plastics are sometimes used for lightly loaded, low-speed applications.

Lubrication in Wormsets

The lubrication condition in a wormset can range from boundary lubrication to partial or full EHD depending on loads, velocities, temperatures, and lubricant viscosity as discussed in Chapter 12. The lubrication situation is more like that of sliding bearings than rolling bearings in this instance because of the dominant sliding velocities. Their high percentage of sliding makes wormsets less efficient than conventional gears. Lubricants containing extreme-pressure (EP) additives are sometimes used in wormsets.

Forces in Wormsets

A three-dimensional loading condition exists at the mesh of a wormset. Tangential, radial, and axial components act on each member. With a (typical) 90° angle between the axes of worm and worm gear, the magnitude of the tangential component on the worm gear W_{tg} equals the axial component on the worm W_{aw} and vice versa. These components can be defined as

$$W_{tg} = W_{aw} = \frac{2T_g}{d_g} \quad (13.14a)$$

where T_g and d_g are the torque on, and the pitch diameter of, the worm gear. The axial force W_{ag} on the worm gear and the tangential force on the worm W_{tw} are

$$W_{ag} = W_{tw} = \frac{2T_w}{d} \quad (13.14b)$$

where T_w is the torque on, and d is the pitch diameter of, the worm. The radial force W_r separating the two elements is

$$W_r = \frac{W_{tg} \tan \phi}{\cos \lambda} \quad (13.14c)$$

where ϕ is the pressure angle and λ is the lead angle.

Wormset Geometry

The pitch diameters and numbers of teeth of nonworm gearsets have a unique relationship but this is not so in wormsets. Once the decision is made regarding the number of

starts or teeth N_w desired on the worm, the number of teeth on the worm gear N_g is defined by the required gear ratio m_G :

$$N_g = m_G N_w \quad (13.15)$$

However, the pitch diameter of the worm is not tied to these tooth numbers as with other gearsets. The worm can theoretically be any diameter as long as its tooth cross section (axial pitch) matches the circular pitch of the worm gear. (This is analogous to different diameter machine screws having the same thread pitch as with #6-32, 8-32, and 10-32 sizes). Thus the worm's pitch diameter d can be selected independent of the worm-gear diameter d_g and, for any given d_g , changes in d will just vary the center distance C between worm and worm gear but will not affect the gear ratio. The AGMA recommends minimum and maximum values for the worm pitch diameter as

$$\frac{C^{0.875}}{3} \leq d \leq \frac{C^{0.875}}{1.6} \quad (13.16a)$$

and Dudley^[9] recommends using

$$d \approx \frac{C^{0.875}}{2.2} \quad (13.16b)$$

which is about midway between the AGMA limits.

The pitch diameter of the worm gear d_g can be related to that of the worm through the center distance C .

$$d_g = 2C - d \quad (13.17)$$

The addendum a and dedendum b of the teeth are found from

$$a = 0.3183p_x \quad b = 0.3683p_x \quad (13.18)$$

The face width of the worm gear is limited by the diameter of the worm. The AGMA recommends a maximum value for face width F as

$$F_{max} \leq 0.67d \quad (13.19)$$

Table 13-7 shows AGMA recommended minimum numbers of wormgear teeth as a function of pressure angle.

Rating Methods

Unlike helical and bevel gearsets, in which calculations are made separately for the bending and surface stresses in the gear teeth and compared to material properties, wormsets are rated by their ability to handle a level of input power. The **AGMA power rating** is based on their pitting and wear resistance, because experience has shown that to be the usual failure mode. Because of the high sliding velocities in wormsets, the temperature of the oil film separating the gear teeth becomes an important factor, and this is taken into account in the AGMA standard.^[6, 7] These standards are based on a duty cycle of 10 continuous hours per day of service under uniform load, defined as a service factor of 1.0. Materials for worm and worm gear are assumed to be as defined above.

Table 13-7

AGMA Suggested Minimum Numbers of Teeth for Worm Gears
Source: Reference 6.

ϕ	N_{min}
14.5	40
17.5	27
20	21
22.5	17
25	14
27.5	12
30	10

The rating of a wormset can be expressed as the allowable input power Φ , output power Φ_o , or the allowable torque T at a given speed at either the input or output shaft, these being related by the general power-torque-speed relationship (Eq. 10.1a, p. 553). The AGMA defines an input-power rating formula as

$$\Phi = \Phi_o + \Phi_l \quad (13.20)$$

where Φ_l is the power lost to friction in the mesh. Output power Φ_o is defined as

$$\Phi_o = \frac{nW_{tg}d_g}{126\,000m_G} \text{ hp} \quad (13.21us)$$

$$\Phi_o = \frac{nW_{tg}d_g}{1.91E7m_G} \text{ kW} \quad (13.21si)$$

and the power lost Φ_l is defined as

$$\Phi_l = \frac{V_t W_f}{33\,000} \text{ hp} \quad (13.22us)$$

$$\Phi_l = \frac{V_t W_f}{1\,000} \text{ kW} \quad (13.22si)$$

These are mixed-unit equations. The rotational speed n is in rpm. The tangential sliding velocity V_t is in fpm (m/s) and is taken at the worm diameter d in inches (mm). The loads W_{tg} and W_f are in lb (N). The power is in hp (kW).

The tangential load W_{tg} on the worm gear in lb (N) is found from

$$W_{tg} = C_s C_m C_v d_g^{0.8} F \quad (13.23us)$$

$$W_{tg} = C_s C_m C_v d_g^{0.8} F / 75.948 \quad (13.23si)$$

where C_s is a materials factor defined by AGMA for chill-cast bronze* as

if $C < 8$ in	$C_s = 1\,000$
if $C \geq 8$ in	$C_s = 1\,411.6518 - 455.8259 \log_{10} d_g$

(13.24)

and C_m is a ratio-correction factor defined by AGMA as

if $3 < m_G \leq 20$	$C_m = 0.0200 \sqrt{-m_G^2 + 40m_G - 76} + 0.46$
if $20 < m_G \leq 76$	$C_m = 0.0107 \sqrt{-m_G^2 + 56m_G + 5\,145}$
if $76 < m_G$	$C_m = 1.1483 - 0.00658m_G$

(13.25)

C_v is a velocity factor defined by AGMA as

if $0 < V_t \leq 700$ fpm	$C_v = 0.659e^{-0.0011V_t}$
if $700 < V_t \leq 3\,000$ fpm	$C_v = 13.31V_t^{-0.571}$
if $3\,000 < V_t$ fpm	$C_v = 65.52V_t^{-0.774}$

(13.26)

* Note that AGMA defines material factors for other bronzes as well. Consult the standard for more information [6, 7].

The tangential velocity at the worm pitch diameter is

$$V_t = \frac{\pi n d}{12 \cos \lambda} \text{ fpm} \quad (13.27)$$

The friction force W_f on the gear is

$$W_f = \frac{\mu W_{tg}}{\cos \lambda \cos \phi_h} \quad (13.28)$$

The coefficient of friction in a wormgear mesh is not constant. It is a function of velocity. The AGMA suggests the following relationships:

$$\begin{aligned} \text{if } V_t = 0 \text{ fpm} \quad & \mu = 0.15 \\ \text{if } 0 < V_t \leq 10 \text{ fpm} \quad & \mu = 0.124 e^{(-0.074 V_t^{0.645})} \\ \text{if } 10 < V_t \text{ fpm} \quad & \mu = 0.103 e^{(-0.110 V_t^{0.450})} + 0.012 \end{aligned} \quad (13.29)$$

The efficiency of the wormset alone (exclusive of bearings, oil churn, etc.) is

$$\eta = \frac{\Phi_o}{\Phi} \quad (13.30)$$

The rated output torque can be found from equations 13.14 (p. 770) and 13.23:

$$T_g = W_{tg} \frac{d_g}{2} \quad (13.31)$$

A Design Procedure for Wormsets

A common design specification for a wormset will define the desired input (or output) speed and gear ratio. Some information on the output loading, in terms either of force or torque, or of the required output power, will usually be known. There may also be some package size limits specified. One approach (of many possible) is to assume a number of starts for the worm and calculate the kinematic data for the worm and worm gear. Then assume a trial center distance C and use it to find a trial pitch diameter d for the worm from equation 13.16 (p. 771). Find a suitable face width F for the gear that obeys equation 13.19 (p. 771). The pitch diameter of the gear can then be found from equation 13.17 (p. 771) and used in equations 13.23 and 13.28 to find the tangential forces in the mesh. From these data, the rated (allowable) power and torque levels for a wormset of the assumed size can be found from equations 13.20 to 13.22 (p. 772) and 13.31. If these power and torque values are large enough to satisfy the design requirement with suitable safety margins, the design is done. If not (which is likely) the original assumptions regarding the number of starts, worm diameter, center distance, etc., must be revised and the calculation repeated until an acceptable combination is found. The center distance can be adjusted further to obtain a diametral pitch or module that matches available hobs. An equation solver can make this task much easier by allowing rapid iteration of the equations.

13.4 CASE STUDY

Case Study 9A in Chapter 9 set up a design problem involving a winch to hoist hay bales into a barn. The proposed device is to be powered by an electric motor connected to a winch with a 75:1 reduction gearset that needs to be self-locking to hold the load. A wormset is a reasonable solution in this application. We will now address the design of that gear train.

CASE STUDY 9B

Design of a Wormset Speed Reducer for a Winch Lift

Problem Size the worm and worm gear for the winch lift defined in Case Study 9A (p. 528) as shown in Figure 9-4 repeated here.

Given The force-time function was estimated in the previous study to be as shown in Figure 9-6b (repeated here). For an assumed winch-drum radius of 10 in, the peak torque will be about 7800 lb-in. The average output power required was calculated to be about 0.6 hp. A 75:1 reduction is required. Input speed to the worm is 1725 rpm. Output speed is 23 rpm.

Assumptions A single-start worm with a 20° pressure angle will be tried. The worm will be of steel case hardened to 58 HRC and the worm gear of chill-cast phosphor bronze. A self-locking wormset is needed.

Solution See Figures 9-4 and 9-6.

- 1 A single-start worm will require a 75-tooth worm for the desired 75:1 ratio. This number of worm-gear teeth is well above the minimum recommended in Table 13-7 (p. 771).

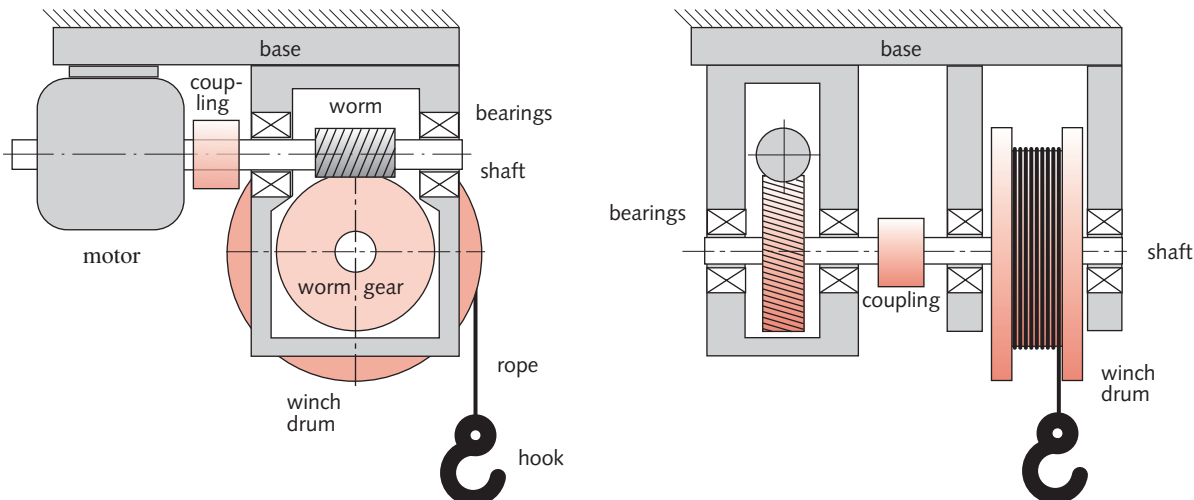
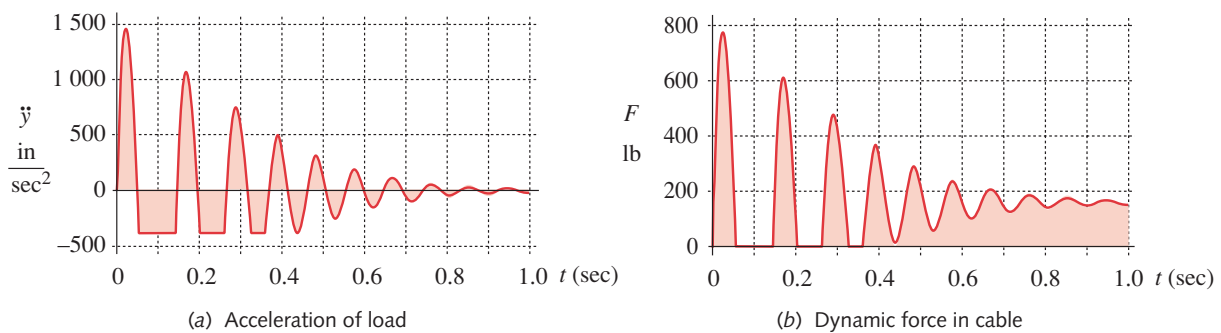


FIGURE 9-4 Repeated

Motor-Driven Winch with Gear Train, Shafts, Bearings, and Couplings

**FIGURE 9-6 Repeated**

Acceleration and Cable Force at Start-up of Load-Lift

- 2 Assume a center distance of 5.5 in for a trial calculation and find a suitable worm diameter based on that assumption from equation 13.16b (p. 771).

$$d \cong \frac{C^{0.875}}{2.2} \cong \frac{5.5^{0.875}}{2.2} = 2.02 \text{ in} \quad (a)$$

- 3 Find a suitable worm-gear diameter from equation 13.17 (p. 771).

$$d_g = 2C - d = 2(5.5) - 2.02 = 8.98 \text{ in} \quad (b)$$

- 4 Find the lead from equation 13.13 (p. 769).

$$L = \pi d_g \frac{N_w}{N_g} = \pi(8.98) \frac{1}{75} = 0.376 \text{ in} \quad (c)$$

- 5 Find the lead angle from equation 13.12 (p. 769).

$$\lambda = \tan^{-1} \frac{L}{\pi d} = \tan^{-1} \frac{0.376}{\pi(2.02)} = 3.39^\circ \quad (d)$$

This is less than 6° , so the wormset will be self-locking, as required.

- 6 Find the maximum recommended face width from equation 13.19 (p. 771).

$$F_{max} \cong 0.67d = 0.67(2.02) = 1.354 \text{ in} \quad (e)$$

- 7 Find the materials factor C_s from equation 13.24 (p. 772). Since $C < 8$ in, $C_s = 1000$.

- 8 Find the ratio-correction factor C_m from equations 13.25 (p. 772). Based on $m_G = 75$, the second of the expressions in that equation set will be used.

$$C_m = 0.0107 \sqrt{-m_G^2 + 56m_G + 5145} = 0.0107 \sqrt{-75^2 + 56(75) + 5145} = 0.653 \quad (f)$$

- 9 Find the tangential velocity V_t from equation 13.27 (p. 773).

$$V_t = \frac{\pi n d}{12 \cos \lambda} = \frac{\pi(1725)(2.02)}{12 \cos(3.392^\circ)} = 913.9 \text{ fpm} \quad (g)$$

- 10 Use this velocity to find the velocity factor C_v from equations 13.26 (p. 772). For this value of V_t , the second of these equations is appropriate.

$$C_v = 13.31(913.9)^{-0.571} = 0.271 \quad (h)$$

- 11 Find the tangential load W_t from equation 13.23 (p. 772).

$$W_{tg} = C_s C_m C_v d_g^{0.8} F = 1\,000(0.653)(0.271)(8.98)^{0.8}(1.354) = 1\,388 \text{ lb} \quad (i)$$

- 12 Find the coefficient of friction from the third expression in equation 13.29 (p. 773).

$$\mu = 0.103e^{(-0.110V_i^{0.450})} + 0.012 = 0.103e^{(-0.110[913.9]^{0.450})} + 0.012 = 0.022 \quad (j)$$

- 13 Find the friction force W_f from equation 13.28 (p. 773).

$$W_f = \frac{\mu W_{tg}}{\cos\lambda \cos\phi} = \frac{0.022(1\,388)}{\cos 3.392^\circ \cos 20^\circ} = 32 \text{ lb} \quad (k)$$

- 14 Find the rated output power from equation 13.21 (p. 772).

$$\Phi_o = \frac{nW_{tg}d_g}{126\,000m_G} = \frac{1\,725(1\,388)(8.98)}{126\,000(75)} = 2.274 \text{ hp} \quad (l)$$

- 15 Find the power lost in the mesh from equation 13.22 (p. 772).

$$\Phi_l = \frac{V_l W_f}{33\,000} = \frac{913.9(32)}{33\,000} = 0.888 \text{ hp} \quad (m)$$

- 16 Find the rated input power from equation 13.20 (p. 772).

$$\Phi = \Phi_o + \Phi_l = 2.274 + 0.888 = 3.162 \text{ hp} \quad (n)$$

- 17 The efficiency of the gearset is

$$\eta = \frac{\Phi_o}{\Phi} = \frac{2.274}{3.162} = 71.9\% \quad (o)$$

- 18 Find the rated output torque from equation 13.31 (p. 773).

$$T_g = W_{tg} \frac{d_g}{2} = 1\,388 \frac{8.98}{2} = 6\,230 \text{ lb-in} \quad (p)$$

- 13
19 While the power rating appears to be adequate for this application, the output torque rating falls short of the projected peak torque of 7 800 lb-in modeled in Case Study 9A; thus some redesign is in order.
- 20 The original assumption for center distance was increased to 6.531 in and the model recalculated. The center distance was also adjusted slightly to give an integer diametral pitch of 7 in⁻¹. This increased the worm-gear diameter to 10.714 in and the output torque rating to 9 131 lb-in. The new input power rating is 4.52 hp and the power loss is 1.18 hp for an efficiency of 73.8%. The output power rating is 3.33 hp. The new lead angle is 3.48°, so the wormset is still self-locking.
- 21 While this new design appears feasible based on the loading calculations done in the previous case study, one of the original assumptions regarding the electric motor size will need to be revised. The average net power required was estimated to be 0.62 hp. It was hoped that a 1- to 1.25-hp motor would be adequate, which would allow 110-V operation. This now appears impossible due to the 1.18-hp loss in the wormset, which would leave too little power available to lift the load even if a 1.25-hp motor were used.

The flywheel effect of the rotating winch drum can supply bursts of energy to get past the peaks of load oscillation shown in Figure 9-6, but cannot provide a sustained increase in power above the average available. So a 220-V motor of about 2 or 2.25 hp appears to be necessary for this design. The input power rating of the gearset should easily accommodate that level of power with no overheating problems.

- 22 The files CASE9B-1 and CASE9B-2, respectively, contain the first (unsuccessful) and second (successful) solutions to this problem and are on the CD-ROM.
-

13.5 SUMMARY

Several specialized forms of gears exist. This chapter has presented a brief introduction to the application and design of three types: helical, bevel, and worm gearsets.

HELICAL GEARS are formed from rolling cylinders and can perform essentially the same function as spur gears, connecting parallel shafts for speed reduction/increase and torque multiplication/division. The teeth of helical gears are angled with respect to the axis at a helix angle, which can be a few degrees or as much as 45° . Their helix is either right or left handed. Opposite-hand helical gears with the same helix angle mesh with their axes parallel. Same-hand helical gears mesh with their (nonintersecting) axes skewed or crossed and have theoretical point contact between the teeth. This limits their load-carrying capacity compared to parallel-axis helicals, which mate with a roll-slide motion similar to spur gears, but engage their teeth in a smooth, wiping action across the face width.

The principal advantages of helical over spur gearsets is their quieter running and greater strength for the same size gear. The disadvantage is greater cost than spur gears and the introduction of an axial component of force that requires thrust bearings on the shaft. Parallel-axis helical gears are used extensively in vehicle transmissions, both manual and automatic-shifting, principally because of their quiet running.

The design of helical gears is very similar to that of spur gears. The same bending and surface stress equations apply, but with different values for the geometry factors I and J . Some additional factors are also introduced to the equations. These factors are obtained from the AGMA standards, which contain tables of data for helical gears of various pressure angles, helix angles, and addendum ratios. A few of these tables are reproduced here. Consult the AGMA standards for more complete information. The materials used are the same as for spur gears. A helical gear will have lower stresses and higher safety factors than a spur gear of the same pitch and diameter, because its angled tooth is thicker in the direction of the applied load.

BEVEL GEARS are formed from rolling cones and thus connect intersecting axes. They are used principally to take motion and torque “around a corner.” Their teeth taper with the changing cone diameter and they are specified by the diameter and tooth size at their large end. Their teeth may be straight and parallel to the axis (analogous to spur gears), in which case they are called **straight bevel gears**, or the teeth may be angled with respect to the axis at a spiral angle (analogous to the helix angle of helical gears), in which case they are called **spiral bevel** or just spiral gears. Spiral bevel gears have advantages over straight bevels similar to those of helicals over spur gears. Because

their angled teeth engage gradually, spirals run smoother and quieter than straight bevels and have less vibration. Because a spiral's tooth is thicker in the direction of loading, it is stronger than a straight bevel gear of the same diameter and pitch. A spiral-type gear with curved teeth but zero spiral angle, called a ZEROL® gear, is also made to obtain the smooth running of a spiral without the additional tooth load introduced by the spiral angle.

Bevel gears are seldom made with equal addenda on pinion and gear. A long-addendum pinion is used, with the percent increase varying from zero at a 1:1 ratio to over 50% at large gear ratios. This makes the pinion tooth stronger and the gear tooth weaker to balance the design, as discussed in Chapter 12 for spur gears.

The design of bevel gears is very similar to that of spur or helical gears. The same bending and surface stress equations apply, but they use different values for the geometry factors I and J . Some additional factors are also introduced to the equations. These factors are obtained from the AGMA standards, which contain charts plotting I and J for bevel and spiral gears of various pressure angles, spiral angles, and addendum ratios. A few of these charts are reproduced here. Consult the AGMA standards for more complete information. The materials used for bevel gears are the same as for spur or helical gears.

WORMS AND WORM GEARS connect nonparallel, nonintersecting axes. The worm is similar to a screw thread, having one or a few teeth wrapped around it at what is, in effect, a very large helix angle. The worm mates with a special gear called a worm gear or worm wheel that is analogous to a nut being advanced by the thread of the worm. Their axes are typically at 90° to one another. The wormset can give very large gear ratios (up to about 360:1) in a compact package because of the small number of teeth on the worm. If the lead angle of the worm is small enough (< about 6°), the wormset can be self-locking, meaning that it cannot be backdriven from the worm gear, i.e., it will hold a load. Its main disadvantage is its relatively low efficiency compared to other gearsets. The relative motion at the teeth is sliding rather than rolling, which generates significant heat. Heat transfer from the gearbox, rather than the stresses in the teeth, can limit a wormset's life. The oil temperature in the mesh should be kept below about 200° F for long tooth life.

The design of wormsets is different than for other gearsets. The AGMA defines an **input-power rating** equation for wormsets. This equation, in combination with a number of AGMA-defined empirical factors, allows the wormset to be sized for a given power or torque-speed combination. Consult the AGMA standards for more complete information. The materials used for wormsets are quite limited. The worm is usually a steel, case hardened to 58 HRC, and the worm gear is a bronze alloy. The soft gear runs in against the hard worm in the first few hours of operation and conforms to its particular contours. If properly run-in without overloading or overheating, a properly sized (rated) wormset can be expected to give a very long cycle life before succumbing to its ultimate demise by pitting in surface fatigue. Bending failure of the teeth in wormsets is rare. A wormset's load capacity can be increased by designing it as a single- or double-enveloping configuration. A single-enveloping set wraps the gear partially around the worm to gain surface-contact area. A double-enveloping set does the above and also wraps the worm partially around the gear in an hourglass shape to obtain even more contact area.

Important Equations Used in This Chapter

Helical-Gear Geometry (Section 13.1):

$$p_t = p_n / \cos \psi \quad (13.1a)$$

$$p_x = p_n / \sin \psi \quad (13.1b)$$

$$p_d = \frac{N}{d} = \frac{\pi}{p_c} = \frac{\pi}{p_t} \quad (13.1c)$$

Helical-Gear Forces (Section 13.1):

$$W_r = W_t \tan \phi \quad (13.3a)$$

$$W_a = W_t \tan \psi \quad (13.3b)$$

$$W = \frac{W_t}{\cos \psi \cos \phi_n} \quad (13.3c)$$

Stresses in Helical Gears (Section 13.1):

$$\sigma_b = \frac{W_t p_d}{FJ} \frac{K_a K_m}{K_v} K_s K_B K_I \quad (12.15us)$$

$$\sigma_b = \frac{W_t}{FmJ} \frac{K_a K_m}{K_v} K_s K_B K_I \quad (12.15si)$$

$$\sigma_c = C_p \sqrt{\frac{W_t}{FId} \frac{C_a C_m}{C_v} C_s C_f} \quad (12.21)$$

Surface Geometry Factor for Helical Gears (Section 13.1):

$$I = \frac{\cos \phi}{\left(\frac{1}{\rho_p} \pm \frac{1}{\rho_g} \right) d_p m_N} \quad (13.6a)$$

Gear Ratio for a Bevel-Gear Set (Section 13.2):

$$m_G = \frac{\omega_p}{\omega_g} = \frac{N_g}{N_p} = \frac{d_g}{d_p} = \tan \alpha_g = \cot \alpha_p \quad (13.7b)$$

Forces on Straight Bevel Gears (Section 13.2):

$$W_a = W_t \tan \phi \sin \alpha \quad (13.8a)$$

$$W_r = W_t \tan \phi \cos \alpha \quad (13.8a)$$

$$W = W_t / \cos \phi$$

Stresses in Bevel Gears (Section 13.2):

$$\sigma_b = \frac{2T_p}{d} \frac{p_d}{FJ} \frac{K_a K_m K_s}{K_v K_x} \quad \text{psi} \quad (13.9us)$$

$$\sigma_b = \frac{2000T_p}{d} \frac{1}{FmJ} \frac{K_a K_m K_s}{K_v K_x} \quad \text{MPa} \quad (13.9si)$$

$$\sigma_c = C_p C_b \sqrt{\frac{2T_D}{FId^2} \left(\frac{T_p}{T_D} \right)^z \frac{C_a C_m}{C_v} C_s C_f C_{xc}} \quad (13.10)$$

Design Torque for Bevel Gears (Section 13.2):

$$T_D = \frac{F}{2} \frac{IC_v}{C_s C_{md} C_f C_a C_{xc}} \left(\frac{S'_{fc} d}{C_p C_b} \frac{0.774 C_H}{C_T C_R} \right)^2 \text{ lb-in} \quad (13.11us)$$

$$T_D = \frac{F}{2000} \frac{IC_v}{C_s C_{md} C_f C_a C_{xc}} \left(\frac{S'_{fc} d}{C_p C_b} \frac{0.774 C_H}{C_T C_R} \right)^2 \text{ N·m} \quad (13.11si)$$

Lead and Lead angle of a Worm (Section 13.3):

$$\tan \lambda = \frac{L}{\pi d} \quad (13.12)$$

Forces in Wormsets (Section 13.3):

$$W_{tg} = W_{aw} = \frac{2T_g}{d_g} \quad (13.14a)$$

$$W_{ag} = W_{tw} = \frac{2T_w}{d} \quad (13.14b)$$

$$W_r = \frac{W_{tg} \tan \phi}{\cos \lambda} \quad (13.14c)$$

Recommended Worm Pitch Diameter (Section 13.3):

$$d \equiv \frac{C^{0.875}}{2.2} \quad (13.16b)$$

Worm-Gear Pitch Diameter (Section 13.3):

$$d_g = 2C - d \quad (13.17)$$

Recommended Maximum Face Width of Worm Gear (Section 13.3):

$$F_{max} \leq 0.67d \quad (13.19)$$

Rated Power for a Wormset (Section 13.3):

$$\Phi_o = \frac{nW_{tg}d_g}{126\,000 m_G} \text{ hp} \quad (13.21us)$$

$$\Phi_o = \frac{nW_{tg}d_g}{1.91E7 m_G} \text{ kW} \quad (13.21si)$$

$$\Phi_l = \frac{V_t W_f}{33\,000} \text{ hp} \quad (13.22us)$$

$$\Phi_l = \frac{V_t W_f}{1\,000} \text{ kW} \quad (13.22si)$$

$$\Phi = \Phi_o + \Phi_l \quad (13.20)$$

Tangential Force on a Worm Gear (Section 13.3):

$$W_{tg} = C_s C_m C_v d_g^{0.8} F \quad (13.23us)$$

$$W_{tg} = C_s C_m C_v d_g^{0.8} F / 75.948 \quad (13.23si)$$

Friction Force on a Worm Gear (Section 13.3):

$$W_f = \frac{\mu W_{tg}}{\cos \lambda \cos \phi_n} \quad (13.28)$$

Rated Output Torque of a Worm Gear (Section 13.3):

$$T_g = W_{tg} \frac{d_g}{2} \quad (13.31)$$

Efficiency of a Wormset (Section 13.3):

$$\eta = \frac{\Phi_o}{\Phi} \quad (13.30)$$

13.6 REFERENCES

- 1 AGMA, *Gear Nomenclature, Definitions of Terms with Symbols*. ANSI/AGMA 1012-F90. American Gear Manufacturers Association, 1500 King St., Suite 201, Alexandria, Va. 22314, 1990.
- 2 AGMA, *Fundamental Rating Factors and Calculation Methods for Involute Spur and Helical Gear Teeth*. ANSI/AGMA Standard 2001-B88. American Gear Manufacturers Association, 1500 King St., Suite 201, Alexandria, Va. 22314, 1988.
- 3 AGMA, *Geometry Factors for Determining the Pitting Resistance and Bending Strength of Spur, Helical, and Herringbone Gear Teeth*. ANSI/AGMA Standard 908-B89. American Gear Manufacturers Association, 1500 King St., Suite 201, Alexandria, Va. 22314, 1989.
- 4 AGMA, *Design Manual for Bevel Gears*. ANSI/AGMA Standard 2005-B88. American Gear Manufacturers Association, 1500 King St., Suite 201, Alexandria, Va. 22314, 1988.
- 5 AGMA, *Rating the Pitting Resistance and Bending Strength of Generated Straight Bevel, ZEROL® Bevel, and Spiral Bevel Gear Teeth*. ANSI/AGMA Standard 2003-A86. American Gear Manufacturers Association, 1500 King St., Suite 201, Alexandria, Va. 22314, 1986.
- 6 AGMA, *Design Manual for Cylindrical Wormgearing*. ANSI/AGMA Standard 6022-C93. American Gear Manufacturers Association, 1500 King St., Suite 201, Alexandria, Va. 22314, 1993.
- 7 AGMA, *Practice for Enclosed Cylindrical Wormgear Speed Reducers and Gearmotors*. ANSI/AGMA Standard 6034-B92. American Gear Manufacturers Association, 1500 King St., Suite 201, Alexandria, Va. 22314, 1992.
- 8 D. W. Dudley, *Handbook of Practical Gear Design*. McGraw-Hill: New York, p. 3.66, 1984.
- 9 *Ibid.*, p. 3.67.

Table P13-0[†]

Topic/Problem Matrix

13.1 Helical Gears**Geometry**13-1, 13-2, 13-3, 13-4, 13-29,
13-30, 13-31, 13-32**Loads**

13-14, 13-15, 13-33, 13-34

Design13-8, 13-16, 13-17, 13-18,
13-19, 13-35, 13-36**13.2 Bevel Gears****Geometry and Loads**13-5, 13-6, 13-7, 13-39, 13-40,
13-41**Design**13-20, 13-21, 13-22, 13-23,
13-24, 13-25, 13-49, 13-50,
13-51**13.3 Wormsets****Geometry**13-9, 13-10, 13-11, 13-42,
13-43, 13-44, 13-47, 13-48**Loads**13-12, 13-13, 13-26, 13-27,
13-28, 13-45, 13-46**13.7 PROBLEMS**

- *13-1 A 20°-pressure-angle, 30°-helix-angle, 27-tooth helical gear has a diametral pitch $p_d = 5$. Find the pitch diameter, addendum, dedendum, outside diameter, normal, transverse, and axial pitch.
- 13-2 A 25°-pressure-angle, 20°-helix-angle, 43-tooth helical gear has a diametral pitch $p_d = 8$. Find the pitch diameter, addendum, dedendum, outside diameter, normal, transverse, and axial pitch.
- *13-3 A 57-tooth, 10°-helix-angle, helical gear is in mesh with a 23-tooth pinion. The $p_d = 6$ and $\phi = 25^\circ$. Find the transverse and axial contact ratios.
- 13-4 A 78-tooth, 30°-helix-angle, helical gear is in mesh with a 27-tooth pinion. The $p_d = 6$ and $\phi = 20^\circ$. Find the transverse and axial contact ratios.
- *13-5 A 90° straight-bevel gearset is needed to give a 9:1 reduction. Determine the pitch cone angles, pitch diameters, and gear forces if the 25°-pressure-angle pinion has 14 teeth of $p_d = 6$, and the transmitted power is 746 W at 1 000 pinion rpm.
- 13-6 A 90° straight-bevel gearset is needed to give a 4.5:1 reduction. Determine the pitch cone angles, pitch diameters, and gear forces if the 20°-pressure-angle pinion has 18 teeth of $p_d = 5$, and the transmitted power is 7 460 W at 800 pinion rpm.
- *13-7 A 90° spiral-bevel gearset is needed to give a 5:1 reduction. Determine the pitch cone angles, pitch diameters, and gear forces if the 20°-pressure-angle pinion has 16 teeth of $p_d = 7$, and the transmitted power is 3 hp at 600 pinion rpm.
- [†]13-8 A paper machine processes rolls of paper having a density of 984 kg/m³. The paper roll is 1.50-m outside dia (*OD*) × 0.22-m inside dia (*ID*) × 3.23 m long and is on a simply supported, hollow, steel shaft with $S_{ut} = 400$ MPa. Design a 2.5:1 reduction helical gearset to drive this roll shaft to obtain a minimum dynamic safety factor of 2 for a 10-year life if the shaft *OD* is 0.22 m and the roll turns at 50 rpm with 1.2 hp absorbed.
- *13-9 A 2-start wormset has $d = 50$ mm, $p_x = 10$ mm, $m_G = 22:1$. Find the lead, lead angle, worm-gear diameter, and center distance. Will it self-lock? The input speed is 2 200 rpm.
- 13-10 A 3-start wormset has $d = 1.75$ in, $p_x = 0.2$ in, $m_G = 17:1$. Find the lead, lead angle, worm gear diameter, and center distance. Will it self-lock? The input speed is 1 400 rpm.
- *13-11 A 1-start wormset has $d = 40$ mm, $p_x = 5$ mm, $m_G = 82:1$. Find the lead, lead angle, worm gear diameter, and center distance. Will it self-lock? The input speed is 4 500 rpm.
- *13-12 Determine the power transmitted and the torques and forces in the mesh for the wormset in Problem 13-9 if it runs at 1 000 worm rpm.
- 13-13 Determine the power transmitted and the torques and forces in the mesh for the wormset in Problem 13-10 if it runs at 500 worm rpm.
- *13-14 If the gearset in Problem 13-3 transmits 125 hp at 1 000 pinion rpm, find the torque on each shaft.
- 13-15 If the gearset in Problem 13-4 transmits 33 kW at 1 600 pinion rpm, find the torque on each shaft.
- *13-16 Size the helical gears in Problem 13-14 for a bending safety factor of at least 2 assuming a steady torque, 25° pressure angle, full-depth teeth, a face width factor of 10, $Q_v = 9$, an AISI 4140 steel pinion, and a class 40 cast iron gear.

* Answers to these problems are provided in Appendix D.

[†] Problem numbers in *italics* are design problems. Problem numbers in **boldface** are extended from similar problems in earlier chapters with the same dash number.

- 13-17 Size the helical gears in Problem 13-15 for a bending safety factor of 2.5, assuming a steady torque, 20° pressure angle, full-depth teeth, a face width factor of 12, $Q_v = 11$, an AISI 4340 steel pinion, and an A-7-d nodular iron gear.
- *13-18 Size the helical gears in Problem 13-14 for a surface safety factor of at least 1.6 assuming a steady torque, 25° pressure angle, full-depth teeth, a face width factor of 10, $Q_v = 9$, an AISI 4140 steel pinion, and a class 40 cast iron gear.
- 13-19 Size the helical gears in Problem 13-15 for a surface safety factor of 1.2 assuming a steady torque, 20° pressure angle, full-depth teeth, a face width factor of 12, $Q_v = 11$, an AISI 4340 steel pinion, and an A-7-d nodular iron gear.
- *13-20 Size the bevel gears in Problem 13-5 for a bending safety factor of 2, assuming a 5-year, 1-shift life, steady torque, $Q_v = 9$, and an AISI 4140 steel pinion and gear.
- 13-21 Size the bevel gears in Problem 13-6 for a bending safety factor of 2.5, assuming a 15-year, 3-shift life, steady torque, $Q_v = 11$, and an AISI 4340 steel pinion and gear.
- 13-22 Size the bevel gears in Problem 13-7 for a bending safety factor of 2.2, assuming a 10-year, 3-shift life, steady torque, $Q_v = 8$, and an AISI 4340 steel pinion and gear.
- *13-23 Size the bevel gears in Problem 13-5 for a minimum safety factor of 1.4 for any mode of failure of pinion or gear, assuming a 5-year, 1-shift life, steady torque, $Q_v = 9$, and an AISI 4140 steel pinion and gear.
- 13-24 Size the bevel gears in Problem 13-6 for a surface safety factor of 1.3, assuming a 15-year, 3-shift life, steady torque, $Q_v = 11$, and an AISI 4340 steel pinion and gear.
- 13-25 Size the bevel gears in Problem 13-7 for a surface safety factor of 1.4, assuming a 10-year, 3-shift life, steady torque, $Q_v = 8$, and an AISI 4340 steel pinion and gear.
- 13-26 Find the rated power and rated output torque of the wormset in Problem 13-9 with an input speed of 2 200 rpm.
- *13-27 Find the rated power and rated output torque of the wormset in Problem 13-10 with an input speed of 1 400 rpm.
- 13-28 Find the rated power and rated output torque of the wormset in Problem 13-11 with an input speed of 4 500 rpm.
- 13-29 A 23-tooth helical gear is cut with a 20° pressure-angle hob at a helix angle of 25° . The hob has a standard diametral pitch of 5. The resulting teeth have standard spur-gear dimensions in the normal plane. Find the pitch diameter, addendum, dedendum, outside diameter, normal, transverse, and axial pitch, and the transverse pressure angle.
- 13-30 A 38-tooth helical gear is cut with a 25° pressure-angle hob at a helix angle of 30° . The hob has a standard diametral pitch of 4. The resulting teeth have standard spur-gear dimensions in the normal plane. Find the pitch diameter, addendum, dedendum, outside diameter, normal, transverse, and axial pitch, and the transverse pressure angle.
- 13-31 A 39-tooth, 20° helix angle, helical gear is in mesh with an 18-tooth pinion. The $p_d = 8$ and $\phi = 25^\circ$. Find the transverse and axial contact ratios.
- 13-32 A 79-tooth, 30° helix angle, helical gear is in mesh with a 20-tooth pinion. The $p_d = 6$ and $\phi = 20^\circ$. Find the transverse and axial contact ratios.
- 13-33 If the gearset in Problem 13-31 transmits 135 HP at 1200 pinion rpm, find the torque on each shaft.
- 13-34 If the gearset in Problem 13-32 transmits 30 kW at 1200 pinion rpm, find the torque on each shaft.

* Answers to these problems are provided in Appendix D. Problem numbers in *italics* are design problems.

- 13-35 Size the helical gears in Problem 13-33 for a bending factor of safety of at least 2 assuming a steady torque, 25° pressure angle, full depth teeth, quality index of 9, an AISI 4140 steel pinion, and a class 40 cast iron gear.
- 13-36 Size the helical gears in Problem 13-34 for a bending factor of safety of at least 2.5 assuming a steady torque, 20° pressure angle, full depth teeth, quality index of 11, an AISI 4340 steel pinion, and an A-7-d nodular iron gear.
- 13-37 Size the helical gears in Problem 13-33 for a surface factor of safety of at least 1.6 assuming a steady torque, 25° pressure angle, full depth teeth, quality index of 9, an AISI 4140 steel pinion, and a class 40 cast iron gear.
- 13-38 Size the helical gears in Problem 13-34 for a surface factor of safety of at least 1.2 assuming a steady torque, 20° pressure angle, full depth teeth, quality index of 11, an AISI 4340 steel pinion, and an A-7-d nodular iron gear.
- 13-39 A 90° straight bevel gearset is needed to give a 3:1 reduction. Determine the pitch cone angles, pitch diameters, and gear forces if the 25° pressure angle pinion has 15 teeth of $p_d = 4$, and the transmitted power is 8 hp at 550 pinion rpm.
- 13-40 A 90° straight bevel gearset is needed to give a 6:1 reduction. Determine the pitch cone angles, pitch diameters, and gear forces if the 20° pressure angle pinion has 20 teeth of $p_d = 8$, and the transmitted power is 3 kW at 900 pinion rpm.
- 13-41 A 90° spiral bevel gearset is needed to give an 8:1 reduction. Determine the pitch cone angles, pitch diameters, and gear forces if the 20° pressure angle pinion has 21 teeth of $p_d = 10$, and the transmitted power is 2.5 kW at 1100 pinion rpm.
- 13-42 A 1-start wormset has $d = 2.00$ in, $p_x = 0.25$ in, $m_G = 40$. Find the lead, lead angle, worm gear diameter, and center distance. Will it self-lock? The input speed is 1100 rpm.
- 13-43 A 2-start wormset has $d = 2.50$ in, $p_x = 0.30$ in, $m_G = 50$. Find the lead, lead angle, worm gear diameter, and center distance. Will it self-lock? The input speed is 1800 rpm.
- 13-44 A 3-start wormset has $d = 60$ mm, $p_x = 12$ mm, $m_G = 60$. Find the lead, lead angle, worm gear diameter, and center distance. Will it self-lock? The input speed is 2500 rpm.
- 13-45 Determine the power transmitted and the torques and forces in the mesh for the wormset in Problem 13-42 if it runs at 800 worm rpm.
- 13-46 Determine the power transmitted and the torques and forces in the mesh for the wormset in Problem 13-43 if it runs at 1200 worm rpm.
- 13-47 A 2-start wormset has $L = 2.00$ in, $C = 9.00$ in, $m_G = 20$, and the angle between the shafts is 90° . Find the pitch diameters of the worm and worm gear, the lead angle, and the axial pitch.
- 13-48 A 5-start wormset has $l = 20^\circ$, $C = 2.75$ in, $N_g = 33$, and the angle between the shafts is 90° . Find the pitch diameters of the worm and worm gear, the lead, and the axial pitch.
- *13-49 Size the bevel gears in Problem 13-40 for a bending factor of safety of at least 2.5 assuming a 5-year, 2-shift life, steady torque, quality index of 8, and an AISI 4140 steel pinion and gear.
- 13-50 Size the bevel gears in Problem 13-40 for a minimum safety factor of 1.8 for any mode of failure of pinion or gear assuming a 5-year, 2-shift life, steady torque, quality index of 8, and an AISI 4140 steel pinion and gear.
- 13-51 Size the spiral gears in Problem 13-41 for a bending factor of safety of at least 2.0 assuming a 7-year, 3-shift life, steady torque, quality index of 8, and an AISI 4340 steel pinion and gear.

* Answers to these problems are provided in Appendix D. Problem numbers in *italics* are design problems.

14

SPRING DESIGN



*Not to know is bad;
not to wish to know is worse.*

NIGERIAN PROVERB

14.0 INTRODUCTION

Virtually any part made from an elastic material has some “spring” to it. The term *spring* in the context of this chapter refers to parts made in particular configurations to provide a range of force over a significant deflection and/or to store potential energy. Springs are designed to provide a *push*, a *pull*, or a *twist* force (torque), or to primarily store energy, and can be divided into those four general categories. Within each category, many configurations of springs are possible. Springs may be made of round or rectangular wire bent into a suitable form such as a coil, or made of flat stock loaded as a beam. This chapter’s opening photograph shows a few such spring configurations. Many standard spring configurations are available as stock catalog items from spring manufacturers. It is usually more economical for the designer to use a stock spring if possible. Sometimes the task requires a custom spring design. Custom springs may perform secondary functions, such as the location or mounting of other parts. In any case, the designer must understand, and properly use, spring-design theory in order to specify or design the part. Table 14-0 defines the variables used in this chapter and references the section or equation(s) in which they are used.

14.1 SPRING RATE

Regardless of the spring configuration, it will possess a **spring rate** k , defined as the slope of its force-deflection curve. If that slope is constant, it is a linear spring and k can be defined as

$$k = \frac{F}{y} \quad (14.1)$$

Title page photograph courtesy of
Associated Spring, Barnes Group
Inc.

Table 14-0 Variables Used in This Chapter

Part 1 of 2

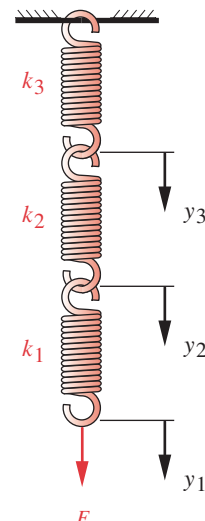
Symbol	Variable	ips units	SI units	See
A	area	in ²	m ²	Eq. 14.8a
C	spring index	none	none	Eq. 14.5
d	wire diameter	in	m	various
D	mean coil diameter	in	m	various
D_i	inside diameter	in	m	various
D_o	outside diameter	in	m	various
E	Young's modulus	psi	Pa	various
F	force or load	lb	N	various
F_a	alternating load	lb	N	Eq. 14.15
F_i	initial tension—extension spring	lb	N	Eq. 14.20
F_m	mean load	lb	N	Eq. 14.15
F_{max}	maximum fluctuating load	lb	N	Eq. 14.15
F_{min}	minimum fluctuating load	lb	N	Eq. 14.15
f_n	natural frequency	Hz	Hz	Eq. 14.11
g	gravitational acceleration	in/sec ²	m/sec ²	various
G	shear modulus, modulus of rigidity	psi	Pa	various
h	height of cone	in	m	Eq. 14.35
k	spring rate or spring constant	lb/in	N/m	Eq. 14.1
K_b	Wahl factor—bending	none	none	Eq. 14.23b
K_c	curvature factor	none	none	Eq. 14.10
K_s	direct shear factor	none	none	Eq. 14.8b
K_{rw}	shear factor for rectangular wire	none	none	Eq. 14.11a
K_w	Wahl factor—torsion	none	none	Eq. 14.9b
L_b	body length—extension spring	in	m	Eq. 14.19
L_f	free length—compression spring	in	m	various
L_{max}	coil length—torsion spring	in	m	Ex. 14.3
L_s	shut height—compression spring	in	m	Ex. 14-3
M	moment	lb-in	N-m	Eq. 14.27
N	number of cycles	none	none	various
N_a	number of active coils	none	none	various
N_{fs}	safety factor in fatigue—torsion	none	none	Eq. 14.16a
N_{fb}	safety factor in fatigue—bending	none	none	Eq. 14.34b
N_t	number of total coils	none	none	various
N_s	safety factor—static yielding	none	none	Eq. 14.14
r	radius	in	m	various
R	stress ratio	none	none	various
R_d	diameter ratio	none	none	Eq. 14.35b
R_F	force ratio	none	none	Eq. 14.15b
s	natural log of the spring index C	none	none	Eq. 14-11

The author wishes to express his appreciation to **Associated Spring, Barnes Group Inc.**, 10 Main St., Bristol, Conn., for permission to use material from their *Design Handbook: Engineering Guide to Spring Design*, 1987 edition.

Table 14-0 Variables Used in This Chapter

Part 2 of 2

Symbol	Variable	ips units	SI units	See
S_f, S_e	bending fatigue, endurance strengths— $R = -1$	psi	Pa	Eq. 14.34
S_{fs}, S_{es}	torsional fatigue, endurance strengths— $R = -1$	psi	Pa	Eq. 14.17b
S_{fw}, S_{ew}	wire torsional fatigue strengths— $R = 0$	psi	Pa	Eq. 14.12
S_{fwb}, S_{ewb}	wire bending fatigue strengths— $R = 0$	psi	Pa	Eq. 14.33
S_{sys}, S_y	shear, tensile yield strengths	psi	Pa	Tables 14-6, -13
S_{ms}	mean torsional strength at 10^3 cycles	psi	Pa	Eq. 14.13
S_{us}	ultimate shear strength	psi	Pa	Eq. 14.4
S_{ut}	ultimate tensile strength	psi	Pa	Eq. 14.3
t	thickness	in	m	Eq. 14.35
T	torque	lb-in	N-m	Eq. 14.8a
W	weight	lb	N	Eq. 14.11b
y	deflection	in	m	various
v	Poisson's ratio	none	none	Eq. 14.35
θ	angular deflection—torsion	rad	rad	Eq. 14.27
γ	weight density	lb/in ³	N/m ³	Eq. 14.11
σ	normal (bending) stress	psi	Pa	Eq. 14.23a
τ	shear stress	psi	Pa	various
ω_n	natural frequency	rad/sec	rad/sec	Eq. 14.11a



(a) Series

where F is the applied force and y the deflection. Since the deflection function can always be determined for any known geometry and loading, and because the deflection function expresses a relationship between the applied load and the deflection, it can simply be rearranged algebraically to express k as equation 14.1.

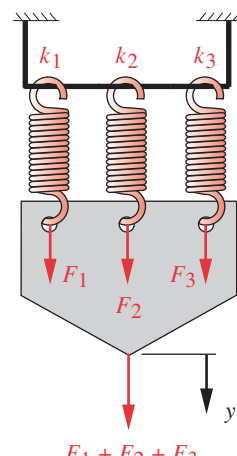
The spring rate may be a constant value (linear spring) or may vary with deflection (nonlinear spring). Both have their applications, but we often want a linear spring to control loading. Many spring configurations have constant spring rates and a few have zero rate (constant force).

When multiple springs are combined, the resulting spring rate depends on whether they are combined in series or parallel. Series combinations have the same force passing through all springs and each contributes a part of the total deflection, as shown in Figure 14-1a. Parallel springs all have the same deflection and the total force splits among the individual springs, as shown in Figure 14-1b. For springs in parallel, the individual spring rates add directly:

$$k_{total} = k_1 + k_2 + k_3 + \dots + k_n \quad (14.2a)$$

For springs in series the spring rates add reciprocally:

$$\frac{1}{k_{total}} = \frac{1}{k_1} + \frac{1}{k_2} + \frac{1}{k_3} + \dots + \frac{1}{k_n} \quad (14.2b)$$



(b) Parallel

FIGURE 14-1

Springs in Series and Parallel

14.2 SPRING CONFIGURATIONS

Springs can be categorized in different ways. The four load types mentioned in Section 14.0 are one way. Another is by the spring's physical configuration. We will use the latter approach. Figure 14-2 shows a selection of spring configurations. Additional examples can be found in reference 1. Wire-form springs come in **helical compression**, **helical tension**, **helical torsion**, and custom forms. Flat springs are typically **cantilever** or **simply supported beams** and can have many shapes. Spring washers come in a variety of styles: **curved**, **wave**, **finger**, and **Belleville**. Flat-wound springs can be **motor** (clock) springs, **volute**, or **constant-force** springs. We will discuss all of these configurations briefly and the design of some of them in detail.

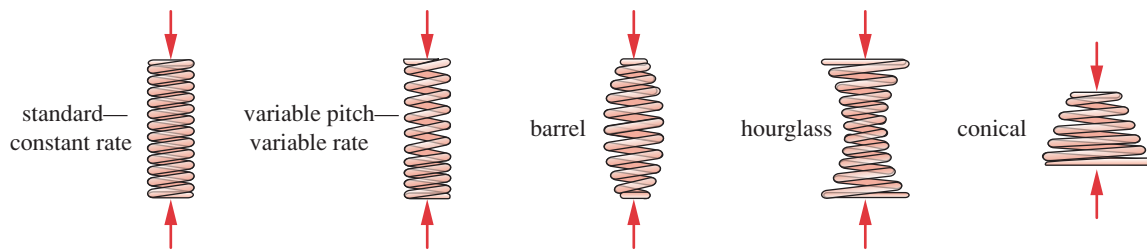
Figure 14-2a shows five forms of **helical compression spring**. All provide a push force and are capable of large deflections. Common applications are valve-return springs in engines, die springs, etc. The standard form has a constant coil diameter, constant pitch (axial distance between coils), and constant spring rate. It is the most common spring configuration, and many sizes are available off-the-shelf. Most are made of round wire, but they can be made from rectangular wire as well. The pitch can be varied to create a **variable-rate spring**. The low-rate coils will shut first, increasing the effective rate when they touch one another or "bottom."

Conical springs can be made with either a constant rate or an increasing one. Their spring rate is usually nonlinear, increasing with deflection, because the smaller diameter coils have greater resistance to deflection and the larger coils deflect first. By varying the coil pitch, a nearly constant spring rate can be obtained. Their main advantage is the ability to close to a height as small as one wire diameter if the coils nest. Barrel and hourglass springs can be thought of as two conical springs back to back, also having a nonlinear spring rate. The **barrel** and **hourglass** shapes are used primarily to change the natural frequency of the spring from that of a standard form.

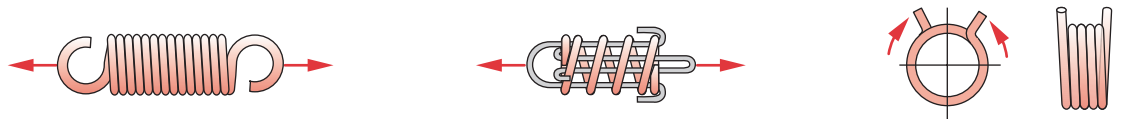
Figure 14-2b shows a **helical extension spring** with hooks on each end. It provides a pull force and is capable of large deflections. These springs are commonly used in door-closers and counterbalancers. The hook is more highly stressed than the coils and usually fails first. Anything suspended from the hook will fall when the extension spring breaks, making it a potentially unsafe design. Figure 14-2c shows a **drawbar spring**, which overcomes this problem by using a helical compression spring in a pull mode. The drawbars compress the spring and, if it breaks, will still support the load safely. Figure 14-2d shows a helical torsion spring, which is wound similar to the helical extension spring but is loaded in twist (torque). Common applications are garage-door counterbalancers, mousetraps, etc. Many different shapes and details on its "legs" are possible.

Figure 14-2e shows five common varieties of **spring washer**. All provide a push force and are commonly used to load something axially, such as to take up end play on a bearing. They typically have small deflections and, except for the Belleville, can only supply light loads. The **volute spring** in Figure 14-2f provides a push force but has significant friction and hysteresis.

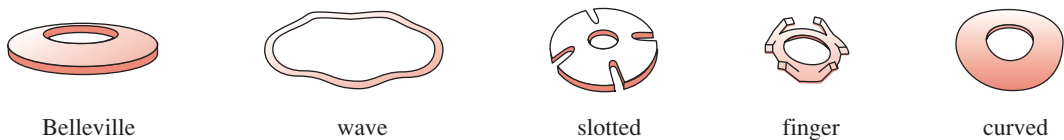
Figure 14-2g shows three varieties of **beam springs**. Any beam type can serve as a spring. Cantilever and simply supported beams are the most common. A beam spring can be constant width or shaped as in the trapezoidal example shown. The spring rate



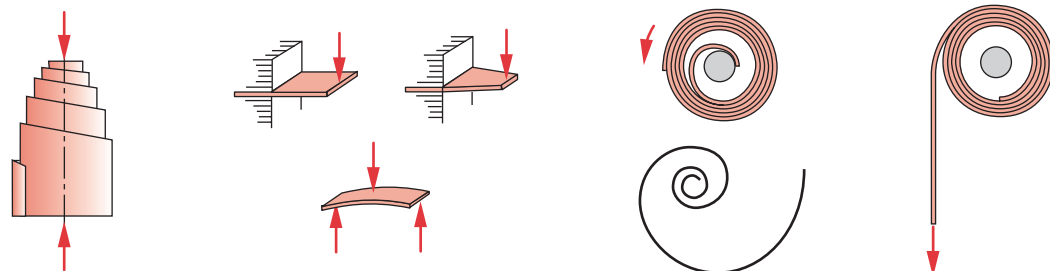
- (a) Helical compression springs. *Push*—wide load and deflection range—round or rectangular wire. Standard has constant coil diameter, pitch, and rate. Barrel, hourglass, and variable-pitch springs are used to minimize resonant surging and vibration. Conical springs can be made with minimum solid height and with constant or increasing rate.



- (b) Helical extension springs. *Pull*—wide load and deflection range—round or rectangular wire, constant rate.
- (c) Drawbar springs. *Pull*—uses compression spring and drawbars to provide extension pull with fail-safe, positive stop.
- (d) Torsion springs. *Twist*—round or rectangular wire—constant rate.



- (e) Spring washers. *Push*—Belleville has high loads and low deflections—choice of rates (constant, increasing, or decreasing). Wave has light loads, low deflection, uses limited radial space. Slotted has higher deflections than Belleville. Finger is used for axial loading of bearings. Curved is used to absorb axial end play.



- (f) Volute spring. *Push*—may have an inherently high friction damping.
- (g) Beam springs. *Push or Pull*—wide load but low deflection range—rectangular or shaped cantilever, or simply supported.
- (h) Power or motor springs. *Twist*—exerts torque over many turns. Shown in, and removed from, retainer.
- (i) Constant Force. *Pull*—long deflection at low or zero rate.

FIGURE 14-2

Spring Configurations (Adapted from: *Design Handbook: Engineering Guide to Spring Design*, 1987, Associated Spring, Barnes Group Inc., 10 Main St., Bristol, Conn., with permission)

and stress distribution can be controlled with changes in beam width or depth along its length. Loads can be high but deflections are limited.

Figure 14-2*h* shows one type of **power spring**, also called a **motor or clock spring**. It is used primarily to store energy and provide twist. Windup clocks and toys make use of this type of spring. Figure 14-2*i* shows a constant-force (Neg'ator) spring used for counterbalancing loads, returning typewriter carriages, and to make constant-torque spring motors. It provides very large deflection strokes at a nearly constant pull force (zero spring rate).

We will discuss the design of some of these spring types. For more information on the others, see reference 1.

14.3 SPRING MATERIALS

A limited number of materials and alloys are suitable for use as springs. The ideal spring material would have a high ultimate strength, high yield point, and low modulus of elasticity in order to provide maximum energy storage (area under the elastic portion of the stress-strain curve). For dynamically loaded springs, the fatigue strength properties of the material are of primary importance. High strengths and yield points are attainable from medium- to high-carbon and alloy steels, and these are the most common spring materials, despite their high modulus of elasticity. A few stainless-steel alloys are suitable for springs, as are beryllium copper and phosphor bronze, among the copper alloys.

Most light-duty springs are made of cold-drawn, round or rectangular wire or of thin, cold-rolled, flat-strip stock. Heavy-duty springs, such as vehicle-suspension parts, are typically made from hot-rolled or forged forms. Spring materials are typically hardened in order to obtain the required strength. Small cross sections are work hardened in the cold-drawing process. Large sections are typically heat treated. Low-temperature heat treatments (175 to 510°C) are used after forming to relieve residual stresses and stabilize dimensions,^[1] even in small-section parts. High-temperature quenching and tempering is used to harden larger springs that must be formed in the annealed condition.

Spring Wire

Round wire is by far the most common spring material. It is available in a selection of alloys and a wide range of sizes. Rectangular wire is available only in limited sizes. Some common wire alloys and their descriptions are shown in Table 14-1, identified by both ASTM and SAE designations. Commonly available stock wire sizes are shown in Table 14-2, along with an indication of the size ranges available for the common steel alloys, identified by ASTM number. The designer should try to use these sizes for best cost and availability, though other sizes not shown are also made. Table 14-3 shows the relative costs of a selection of common round steel spring-wire materials.

TENSILE STRENGTH The relationship between wire size and tensile strength shown in Figure 14-3 is a serendipitous situation. As discussed in Section 2.7 and Table 2-8 (p. 62), when materials are made very small in cross section, they begin to approach the very high theoretical strengths of their atomic bonds. Thus, the tensile strengths of fine steel wire become quite high. The same steel that may break at 200 000 psi in a 0.3-in

Table 14-1 Common Spring Wire Materials

Source: Reference 2

ASTM #	Material	SAE #	Description
A227	Cold-drawn wire ("hard-drawn")	1066	Least expensive general-purpose spring wire. Suitable for static loading but not good for fatigue or impact. Temperature range 0°C to 120°C (250°F).
A228	Music wire	1085	Toughest, most widely used material for small coil springs. Highest tensile and fatigue strength of all spring wire. Temperature range 0°C to 120°C (250°F).
A229	Oil-tempered wire	1065	General-purpose spring steel. Less expensive and available in larger sizes than music wire. Suitable for static loading but not good for fatigue or impact. Temperature range 0°C to 180°C (350°F).
A230	Oil-tempered wire	1070	Valve-spring quality—suitable for fatigue loading.
A232	Chrome vanadium	6150	Most popular alloy spring steel. Valve-spring quality—suitable for fatigue loading. Also good for shock and impact loads. For temperatures to 220°C (425°F). Available annealed or pretempered.
A313 (302)	Stainless steel	30302	Suitable for fatigue applications.
A401	Chrome silicon	9254	Valve-spring quality—suitable for fatigue loading. Second highest strength to music wire and has higher temperature resistance to 220°C (425°F).
B134, #260	Spring brass	CA-260	Low strength—good corrosion resistance.
B159	Phosphor bronze	CA-510	Higher strength than brass—better fatigue resistance—good corrosion resistance. Cannot be heat treated or bent along the grain.
B197	Beryllium copper	CA-172	Higher strength than brass—better fatigue resistance—good corrosion resistance. Can be heat treated and bent along the grain.
-	Inconel X-750	-	Corrosion resistance.

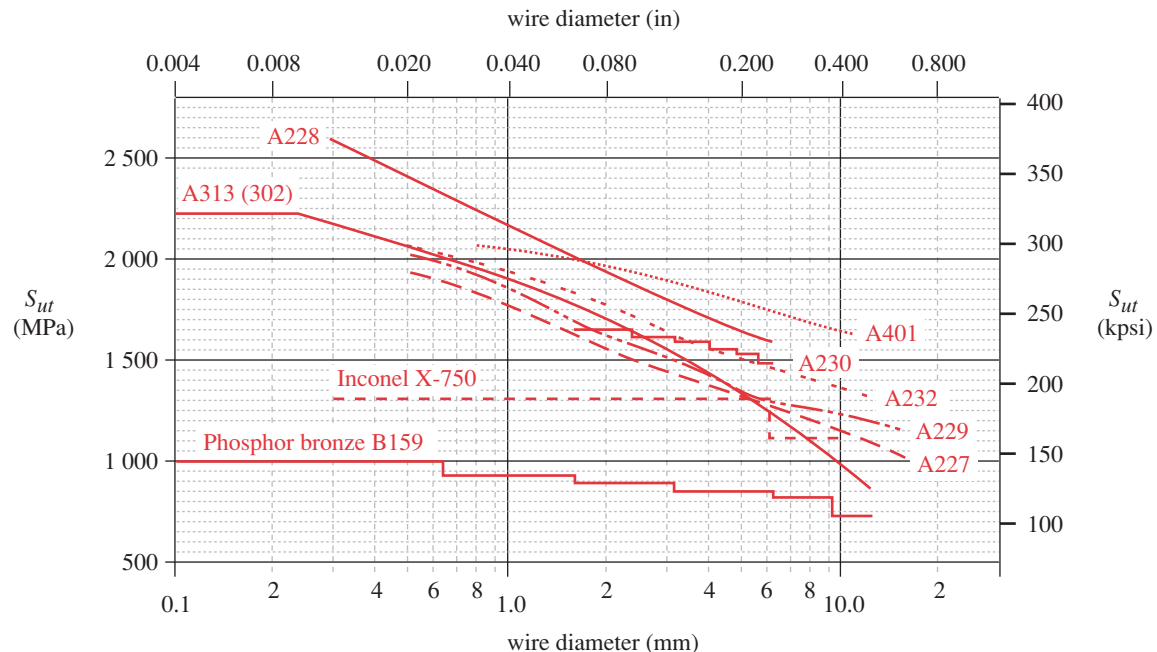
Table 14-3 Relative Costs of Common Spring Wires

Source: Reference 1

ASTM #	Material	Relative Cost of 2-mm (0.08-in) Dia Wire	
		Mill Quantities	Warehouse Lots
A227	Cold-drawn wire	1.0	1.0
A229	Oil-tempered wire	1.3	1.3
A228	Music wire	2.6	1.4
A230	Oil-tempered wire	3.1	1.9
A401	Chrome silicon	4.0	3.9
A313 (302)	302 Stainless steel	7.6	4.7
B159	Phosphor bronze	8.0	6.7
A313 (631)	17-7ph Stainless steel	11.0	8.7
B197	Beryllium copper	27.0	17.0
-	Inconel X-750	44.0	31.0

Table 14-2 Preferred Wire Diameters

U.S. (in)	SI (mm)
0.004	0.10
0.005	0.12
0.006	0.16
0.008	0.20
0.010	0.25
0.012	0.30
0.014	0.35
0.016	0.40
0.018	0.45
0.020	0.50
0.022	0.55
0.024	0.60
0.026	0.65
0.028	0.70
0.030	0.80
0.035	0.90
0.038	1.00
0.042	1.10
0.045	1.20
0.048	1.40
0.051	1.60
0.055	1.80
0.059	2.00
0.063	2.20
0.067	2.50
0.072	2.80
0.076	3.00
0.081	3.50
0.085	4.00
0.092	4.50
0.098	5.00
0.105	5.50
0.112	6.00
0.125	6.50
0.135	7.00
0.148	8.00
0.162	8.50
0.177	9.00
0.192	10.0
0.207	11.0
0.225	12.0
0.250	13.0
0.281	14.0
0.312	15.0
0.343	16.0
0.362	
0.375	
0.406	
0.437	
0.469	
0.500	
0.531	
0.562	
0.625	

**FIGURE 14-3**

Minimum Tensile Strengths of Spring Wire—Identified by ASTM Number—See Table 14-1 Source: *Design Handbook: Engineering Guide to Spring Design*, 1987, Associated Spring, Barnes Group Inc., Bristol, Conn.

(7.4-mm) diameter test-specimen can have nearly twice that strength after being cold drawn down to 0.010 in (0.25 mm). The cold-drawing process is responsible for hardening and strengthening the material at the expense of much of its ductility.

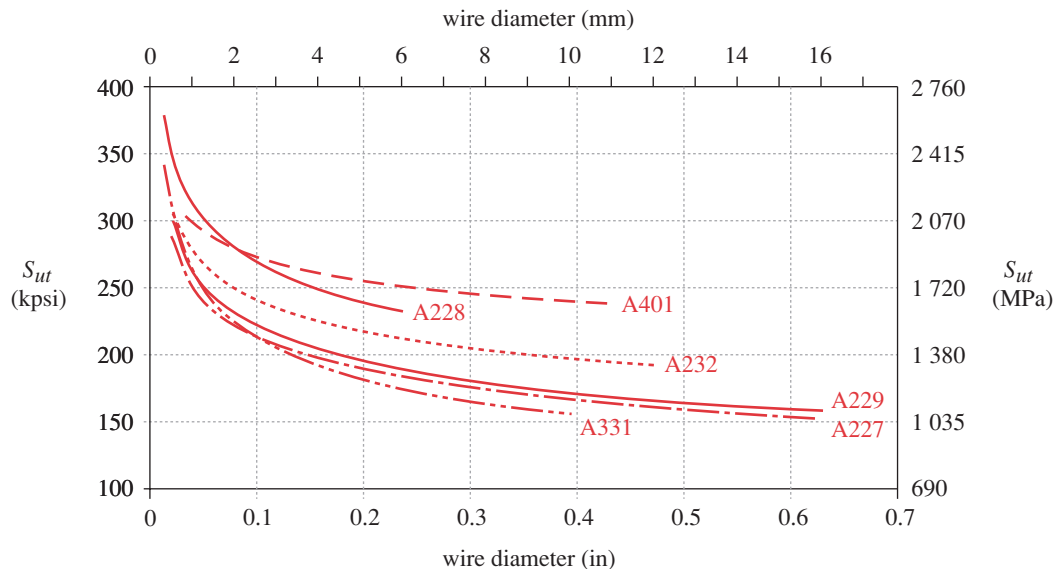
Figure 14-3 is a semilog plot of wire strength versus diameter based on extensive testing by Associated Spring, Barnes Group Inc. The data for five of the materials shown in the figure can be fitted quite closely with an exponential function of the form

$$S_{ut} \cong Ad^b \quad (14.3)$$

Table 14-4 Coefficients and Exponents for Equation 14.3

Source: Reference 1

ASTM #	Material	Range		Exponent <i>b</i>	Coefficient A		Correlation Factor
		mm	in		MPa	psi	
A227	Cold drawn	0.5–16	0.020–0.625	-0.182 2	1 753.3	141 040	0.998
A228	Music wire	0.3–6	0.010–0.250	-0.1625	2 153.5	184 649	0.9997
A229	Oil tempered	0.5–16	0.020–0.625	-0.183 3	1 831.2	146 780	0.999
A232	Chrome-v.	0.5–12	0.020–0.500	-0.145 3	1 909.9	173 128	0.998
A401	Chrome-s.	0.8–11	0.031–0.437	-0.093 4	2 059.2	220 779	0.991

**FIGURE 14-4**

Minimum Tensile Strengths of Spring-Steel Wire as Generated from Equation 14.3 and Table 14-4

where A and b are defined in Table 14-4 for these wire materials over the specified ranges of diameters. These empirical functions provide a convenient means to calculate steel-wire tensile strengths within a spring-design computer program and allow rapid iterating to a suitable design solution. Figure 14-4 plots these empirical strength functions to show, on linear axes, the change in strength with reduction of diameter.

SHEAR STRENGTH Extensive testing has determined that a reasonable estimate of the ultimate strength in torsion^{*} of common spring materials is 67% of the ultimate tensile strength.^{†[1]}

$$S_{us} \approx 0.67S_{ut} \quad (14.4)$$

Flat Spring Stock

Medium- to high-carbon steel strip stock is the most commonly used material for flat (beam) springs, volutes, clock and power springs, spring washers, etc. When corrosion resistance is needed, stainless-steel alloys 301, 302, and 17-7ph, beryllium copper, or phosphor bronze are also used for flat springs.

Cold-rolled AISI 1050, 1065, 1074, and 1095 steel are the usual flat-stock alloys used. These are available in annealed or pretempered conditions referred to as 1/4-hard, 1/2-hard, 3/4-hard, and full-hard. The two softer tempers can be readily formed (bent) into shapes, but the harder tempers have less formability. Full-hard steel can be formed with gentle contours, but not bent with small radii. The advantage of forming prehardened steel strip is to avoid heat-treatment distortion of the formed part. If sharp bends are required, annealed material will have to be used and then hardened after forming.

* Note that this relates the ultimate strength in shear to the ultimate strength in tension. It is a different relationship than the distortion-energy (Von Mises) criterion, which relates the material's yield strengths in shear and tension as $S_{ys} = 0.577S_y$.

† The factor in equation 14.4 differs from the factors suggested in equation 2.5b (p. 37) that gives general ratios of ultimate shear strength to ultimate tensile strength. The factor in equation 14.4 is based on extensive testing of spring wire materials that have been cold-worked by their drawing process. This may account for the difference in shear strength. In any event, the differences in the published numbers indicate the uncertainties involved in estimating material strengths without testing under realistic loading conditions. Equation 14.4 is derived from extensive test data on a particular type of element and material under controlled loading. As such it should be regarded as a good estimate for this situation. It may not however, be directly applicable to different materials or applications.

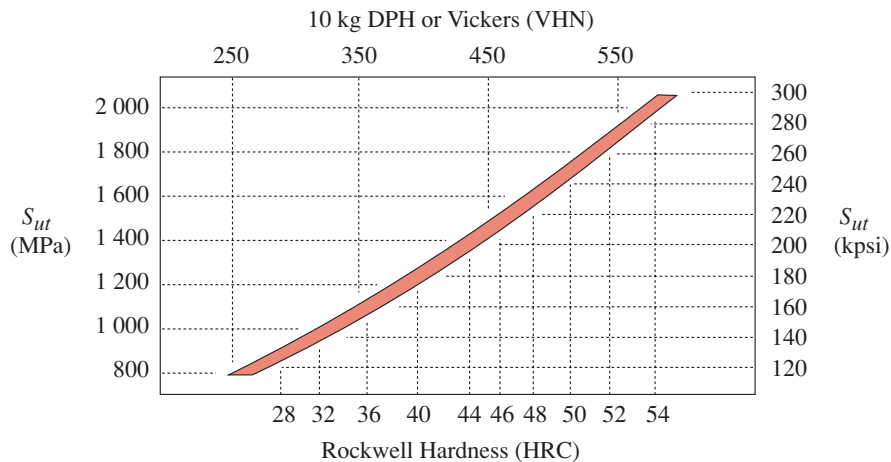


FIGURE 14-5

Tensile Strength Versus Hardness of Quenched and Tempered Spring-Steel Strip Source: Reference 1

The cold-rolling process creates a “grain” in the material analogous to (but much less pronounced than) the grain in wood. Just as wood will readily crack if bent along the grain, metal will not allow bends of small radius along its “grain” without cracking. The grain runs in the direction of rolling, which for strip stock is along the long axis. Thus, formed sheet-metal parts with sharp contours should be bent across the grain. If orthogonal bends are required, the grain should be oriented at 45° to the bends. A dimensionless bend factor $2r / t$ (where r is the bend radius and t the stock thickness) is defined to indicate the relative formability of strip stock. Low values of $2r / t$ indicate greater formability. Full- and 3/4-hard steel strip will fracture if bent along the grain.

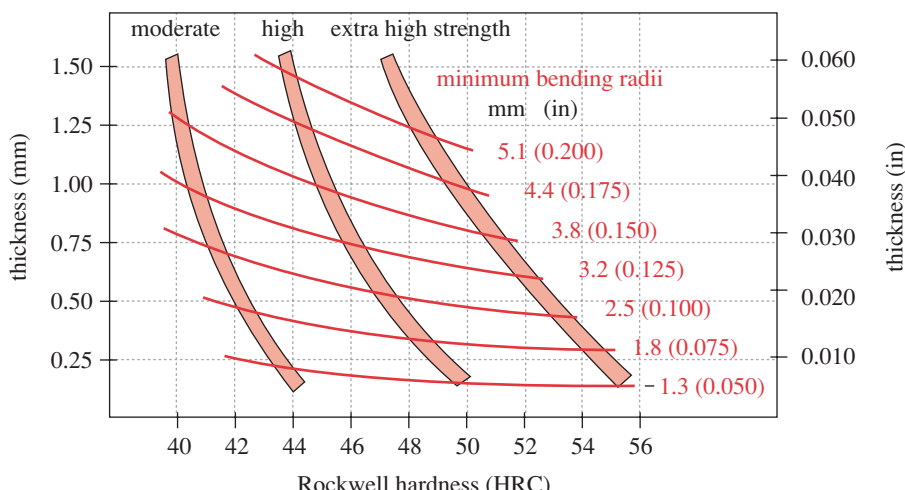


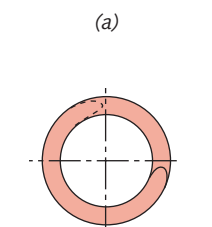
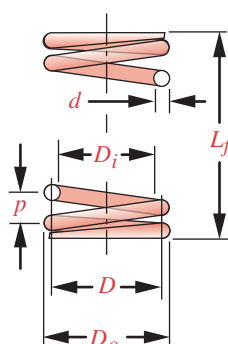
FIGURE 14-6

Minimum Transverse (across grain) Bending Radii for Various Tempers and Thicknesses of Tempered Spring Steel Source: Reference 1

Table 14-5 Typical Properties of Spring Temper Alloy Strip

Source: Reference 1

Material	Sut MPa (ksi)	Rockwell Hardness	Elongation %	Bend Factor	E GPa (Mpsi)	Poisson's Ratio
Spring steel	1 700 (246)	C50	2	5	207 (30)	0.30
Stainless 301	1 300 (189)	C40	8	3	193 (28)	0.31
Stainless 302	1 300 (189)	C40	5	4	193 (28)	0.31
Monel 400	690 (100)	B95	2	5	179 (26)	0.32
Monel K500	1 200 (174)	C34	40	5	17.9 (26)	0.29
Inconel 600	1 040 (151)	C30	2	2	214 (31)	0.29
Inconel X-750	1 050 (152)	C35	20	3	214 (31)	0.29
Beryllium copper	1 300 (189)	C40	2	5	128 (18.5)	0.33
Ni-Span-C	1 400 (203)	C42	6	2	186 (27)	—
Brass CA 260	620 (90)	B90	3	3	11 (16)	0.33
Phosphor bronze	690 (100)	B90	3	2.5	103 (15)	0.20
17-7PH RH950	1 450 (210)	C44	6	flat	203 (29.5)	0.34
17-7PH Cond. C	1 650 (239)	C46	1	2.5	203 (29.5)	0.34

number of coils = N_t 

14.4 HELICAL COMPRESSION SPRINGS

The most common helical compression spring is a constant coil diameter, constant pitch, round-wire spring, as shown in Figure 14-2a (p. 789). We will refer to this as the standard helical compression spring (HCS). Other arrangements are possible, such as conical, barrel, hourglass, and variable pitch, also shown in Figure 14-2a. All provide a push force. A helical spring may be coiled either left handed or right handed.

Sample springs and dimensional parameters for a standard helical compression spring are shown in Figure 14-7. The **wire diameter** is d , the **mean coil diameter** is D , and these two dimensions along with the **free length** L_f and the **number of coils** N_t or the **coil pitch** p are used to define the spring geometry for calculation and manufacturing purposes. The outside diameter D_o and the inside diameter D_i are of interest mainly to define the minimum hole in which it will fit or the maximum pin over which it can be placed. They are found by adding or subtracting the wire diameter d to or from

FIGURE 14-7

- (a) Sample Springs and
(b) Dimensional Parameters for Helical Compression Springs

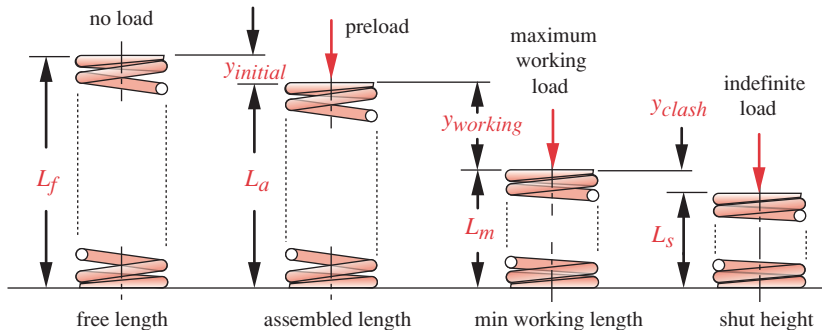
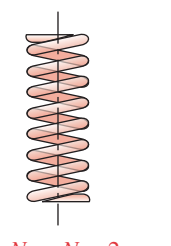
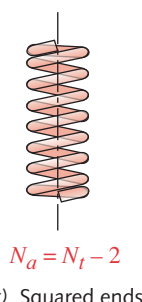
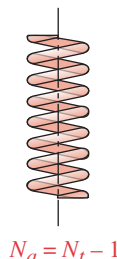
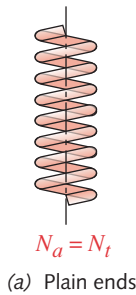


FIGURE 14-8

Various Lengths of a Helical Compression Spring in Use

the mean coil diameter D . The minimum recommended diametral clearances between the D_o and a hole or between D_i and a pin are $0.10D$ for $D < 0.5$ in (13 mm) or $0.05D$ for $D > 0.5$ in (13mm).^[1]

Spring Lengths

Compression springs have several lengths and deflections of interest, as shown in Figure 14-8. **Free length** L_f is the overall spring length in the unloaded condition, i.e., as manufactured. **Assembled length** L_a is the length after installation to its initial deflection $y_{initial}$. This initial deflection in combination with the spring rate k determines the amount of **preload** force at assembly. The **working load** is applied to further compress the spring through its **working deflection** $y_{working}$. The **minimum working length** L_m is the shortest dimension to which it is compressed in service. The **shut height** or **solid height** L_s is its length when compressed such that all coils are in contact. Once shut, the spring can support much larger “indefinite” loads up to the compressive strength of the wire. The **clash allowance** y_{clash} is the difference between the minimum working length and the shut height, expressed as a percentage of the working deflection. A minimum clash allowance of 10–15% is recommended to avoid reaching the shut height in service with out-of-tolerance springs, or with excessive deflections.

End Details

Four types of end details are available on helical compression springs: *plain*, *plain-ground*, *squared*, and *squared-ground* as shown in Figure 14-9. Plain ends result from simply cutting the coils and leaving the ends with the same pitch as the rest of the spring. This is the least expensive end detail, but provides poor alignment to the surface against which the spring is pressed. The end coils can be ground flat and perpendicular to the spring axis to provide normal surfaces for load application. Squaring the ends involves yielding the end coils to flatten them and remove their pitch. This improves the alignment. A flat surface on the end coil of at least 270° is recommended for proper operation.^[1] Squaring and grinding combined provides a 270–330° flat surface for load application. It is the most expensive end treatment but is nevertheless recommended for machinery springs unless the wire diameter is very small (< 0.02 in or 0.5 mm), in which case they should be squared but not ground.^[1]

FIGURE 14-9

Four Styles of End-Coil Treatments for Helical Compression Springs

* Some modern, servo-controlled spring winding machines can maintain 1/10 coil accuracy.

Active Coils

The total number of coils N_t may or may not contribute actively to the spring's deflection, depending on the end treatment. The number of active coils N_a is needed for calculation purposes. Squared ends effectively remove two coils from active deflection. Grinding by itself removes 1 active coil. Figure 14-9 shows the relationships between total coils N_t and active coils N_a for each of the four end-coil conditions. The calculated number of active coils is usually rounded to the nearest 1/4 coil, as the manufacturing process cannot always achieve better than that accuracy.*

Spring Index

The spring index C is the ratio of coil diameter D to wire diameter d .

$$C = \frac{D}{d} \quad (14.5)$$

The preferred range of C is from 4 to 12.^[1] At $C < 4$, the spring is difficult to manufacture, and at $C > 12$ it is prone to buckling and also tangles easily when handled in bulk.

Spring Deflection

Figure 14-10 shows a portion of a helical coil spring with compressive axial loads applied. Note that even though the load on the spring is compression, the spring wire is in *torsion*, as the load on any coil tends to twist the wire about its axis. A simplified model of this loading, neglecting the curvature of the wire, is a torsion bar as shown in Figure 4-28 (p. 177). A helical compression spring is, in fact, a torsion bar wrapped into a helical form, which packages better. The deflection of a round-wire helical compression spring is

$$y = \frac{8FD^3N_a}{d^4G} \quad (14.6)$$

where F is the applied axial load on the spring, D is mean coil diameter, d is wire diameter, N_a is number of active coils, and G is the shear modulus of the material.

Spring Rate

The equation for spring rate is found by rearranging the deflection equation:

$$k = \frac{F}{y} = \frac{d^4G}{8D^3N_a} \quad (14.7)$$

The standard, constant-pitch helical compression spring has a spring rate k that is essentially linear over most of its operating range, as shown in Figure 14-11. The first and last few percent of its deflection have a nonlinear rate. When it reaches its **shut height** L_s , all the coils are in contact and the spring rate becomes the stiffness of the solid coils in compression. The spring rate should be defined between about 15% and 85% of its total deflection^[1] and its working deflection range $L_a - L_m$ kept in that region (see Figure 14-8). Note that springs wound with varying coil pitch or diameter over their

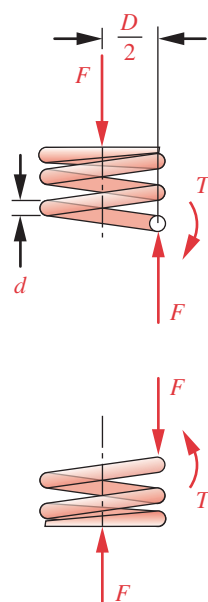


FIGURE 14-10

Forces and Torques on the Coils of a Helical Compression Spring

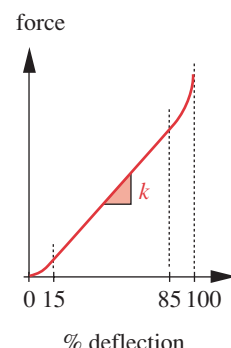


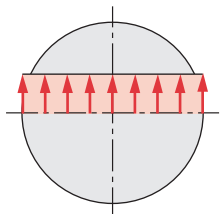
FIGURE 14-11

Force-Deflection Curve for a Standard Helical Compression Spring
(Adapted from reference 1)

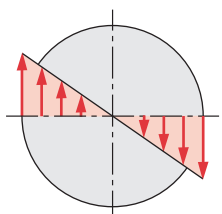
length such as those shown in Figure 14-2a (p. 789) can have a nonconstant spring rate with deflection.

Stresses in Helical Compression Spring Coils

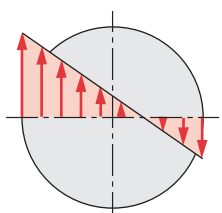
The free-body diagram in Figure 14-10 shows that there will be two components of stress on any cross section of a coil: a torsional shear stress from the torque T and a direct shear stress due to the force F . These two shear stresses have the distributions across the section shown in Figure 14-12a and b. They add directly, and the maximum shear stress τ_{max} occurs at the inner fiber of the wire's cross section, as seen in Figure 14-12c.



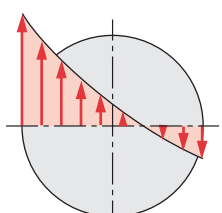
(a) Direct shear stress distribution across section



(b) Torsional shear stress distribution across section



(c) Combined direct shear and torsional stress



(d) Effects of stress concentration at inside edge

$$\begin{aligned}\tau_{max} &= \frac{Tr}{J} + \frac{F}{A} = \frac{F(D/2)(d/2)}{\pi d^4/32} + \frac{F}{\pi d^2/4} \\ &= \frac{8FD}{\pi d^3} + \frac{4F}{\pi d^2}\end{aligned}\quad (14.8a)$$

We can substitute the expression for spring index C from equation 14.5 in equation 14.8a.

$$\begin{aligned}\tau_{max} &= \frac{8FC}{\pi d^2} + \frac{4F}{\pi d^2} = \frac{8FC + 4F}{\pi d^2} \\ &= \frac{8FC}{\pi d^2} \left(1 + \frac{1}{2C}\right) = \frac{8FD}{\pi d^3} \left(1 + \frac{0.5}{C}\right) \\ \tau_{max} &= K_s \frac{8FD}{\pi d^3} \quad \text{where } K_s = \left(1 + \frac{0.5}{C}\right)\end{aligned}\quad (14.8b)$$

This manipulation has put the direct shear term of equation 14.8a into a **direct shear factor** K_s . The two equations are identical in value, but the second version (equation 14.8b) is preferred.

If the wire were straight and were subjected to the combination of direct shear force F and torque T shown in Figure 14-10, equation 14.8 would be the exact solution. However, this wire is curved into a coil. We learned in Section 4.9 (p. 154) that curved beams have a stress concentration on the inner surface of curvature. While our spring is not loaded as a beam, the same principle applies, and there is higher stress at the inner surface of the coil. Wahl^[3] determined the stress-concentration factor for round wire and defined a factor K_w , which includes both the direct shear effects and the stress concentration due to curvature, which is valid for round wire with $C \geq 1.2$.^[5]

$$K_w = \frac{4C-1}{4C-4} + \frac{0.615}{C} \quad (14.9a)$$

$$\tau_{max} = K_w \frac{8FD}{\pi d^3} \quad (14.9b)$$

This combined stress is shown in Figure 14-12d.

Since Wahl's factor K_w includes both effects, we can separate them into a curvature factor K_c and the direct shear factor K_s using

$$K_w = K_s K_c ; \quad K_c = \frac{K_w}{K_s} \quad (14.10)$$

FIGURE 14-12

Stress Distributions Across Wire in a Helical Compression Spring

If a spring is statically loaded, then yielding is the failure criterion. If the material yields locally, it will relieve the local stress concentration that is due to the curvature factor K_c , and equation 14.8b can be used to account just for the direct shear. But, if the spring is dynamically loaded, then failure will be by fatigue at stresses well below the yield point, and equation 14.9b should be used to incorporate both the direct shear and curvature effects. In a fatigue-loading case with both mean and alternating loads, equation 14.8b can be used to compute the mean stress component and equation 14.9b used for the alternating stress component.

Helical Coil Springs of Nonround Wire

Round wire is by far the most common material for helical coil springs. Nevertheless, square or rectangular wire is sometimes used when more load capacity is needed than can be obtained with round wire in a limited space. This is because, for a given cross-section dimension, a square cross-section has larger area moment of inertia, which for the same material strength can sustain a higher load at the same stress level. One disadvantage is that square or rectangular wire will have higher stress concentration from the coil curvature than round wire and Wahl's equation 14.9a does not apply.

The *Handbook of Spring Design*^[6] provides stress concentration factors for some nonround sections. Cornwell^[5] has developed expressions for stress concentration factors in both rectangular and arbitrary cross-section wire as a curved member subjected to combined torsion and direct shear loading. Finite element analysis (FEA) was done on solid and hollow rectangular shapes, I-beams, C-and Z-channels, and tees with spring index values over the range $1.2 \leq C \leq 10$. Stress concentration factors for round shapes calculated by this method match Wahl's equation, verifying the method.

While the stress concentration in a circular section is always greatest at the inside edge of the coil, this is not always true for rectangular cross sections. If they are wound "on the flat" the largest stress concentration will be at the inside edge, but if "wound on edge," it can occur within the section depth. This is also true for sections with re-entrant corners such as tees. The FEA generated stress concentration data for solid rectangular sections were curve-fitted to give an equation for a ratio between the maximum local shear stress in the section to the nominal stress:

$$K_{rw} = e^{\left(S_0 - S_1 s + S_2 s^2 - S_3 s^3 + S_4 s^4\right)} \quad (14.11a)$$

where $s = \ln(C)$ and values for S_i can be found in Table 14-6 in which b and h are the dimensions of the rectangular cross section with h being parallel to the axis of the coil. This equation reproduces and extends the tabular results presented in reference [6].

The stress in a rectangular wire helical compression spring can be found from

$$\tau = \frac{K_{rw} K_2 F D}{b h^2} \quad (14.11b)$$

The deflection is

$$y = \frac{F D^3 N_a}{K_1 b h^3 G} \quad (14.11c)$$

Table 14-6 Curve-fit Parameters for Stress Concentration in Rectangular Cross Sections in Shear^[5]

<i>b/h</i>	<i>S₀</i>	<i>S₁</i>	<i>S₂</i>	<i>S₃</i>	<i>S₄</i>
1/20	1.9128	3.5104	3.1247	1.3315	0.2123
1/10	1.8908	3.4673	3.0834	1.3129	0.2093
1/8	1.8762	3.4879	3.1492	1.3592	0.2192
1/6	1.8555	3.4495	3.1234	1.3517	0.2184
1/4	1.7984	3.4031	3.1335	1.3760	0.2253
1/3.5	1.7812	3.3661	3.1067	1.3684	0.2246
1/3	1.7737	3.2849	2.9623	1.2741	0.2045
1/2.5	1.7340	3.2187	2.9178	1.2607	0.2031
1/2	1.7090	3.1197	2.8074	1.2111	0.1951
1/1.5	1.6862	2.9657	2.6014	1.1029	0.1752
1/1	1.6844	2.8219	2.4577	1.0591	0.1721
1.5/1	1.5381	2.6479	2.2312	0.9670	0.1614
2/1	1.4268	2.3349	1.7867	0.7321	0.1220
2.5/1	1.3610	2.0761	1.3481	0.4480	0.0628
3/1	1.3350	2.0087	1.2315	0.3597	0.0421
3.5/1	1.3053	1.8913	1.0961	0.2831	0.0261
4/1	1.2941	1.8802	1.1094	0.2869	0.0250
6/1	1.3089	2.2639	1.9437	0.8026	0.1240
8/1	1.2465	2.2094	2.1381	0.9873	0.1660
10/1	1.1545	1.8620	1.8344	0.8908	0.1568
20/1	0.7530	-0.2210	-0.8708	-0.4760	-0.0822

and the spring rate is:

$$k = \frac{F}{y} = K_1 \frac{bh^3 G}{D^3 N_a} \quad (14.11d)$$

where F is spring force, D is mean coil diameter, G is the shear modulus, and K_{rw} is from equation 14.11a. K_1 and K_2 are found from Table 14-7.

Residual Stresses

When a wire is coiled into a helix, tensile residual stresses are developed at the inner surface and compressive residual stresses occur at the outer surface. Neither of these residual stresses is beneficial. They can be removed by stress relieving (annealing) the spring.

SETTING Beneficial residual stresses can be introduced by a process confusingly called both “set removal” and “setting the spring” by the manufacturers. Setting can increase the static load capacity by 45–65% and double the spring’s energy-storage capacity per lb of material.^[1] Setting is done by compressing the spring to its shut height and yielding the material to introduce beneficial residual stresses. Recall from Section 6.8 (p. 347) that the rule for introducing beneficial residual stresses is to *overstress (yield) the material in the same direction as the stresses applied in service will*. The “set” spring loses some free length but gains the benefits described above. In order to achieve the advantages of setting, the initial free length must be made longer than the desired (postset) length and should be designed to give a stress at shut height about 10 to 30% greater than the yield strength of the material. Less than that amount of overload will not create sufficient residual stress. More than 30% overstress adds little benefit and increases distortion.^[1]

Table 14-7

Shape Factors for Rectangular Wire Springs

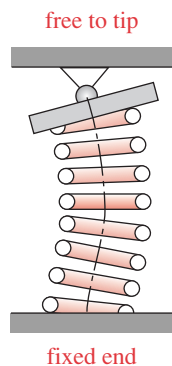
<i>b/h</i>	<i>K₁</i>	<i>K₂</i>
1.00	0.180	2.41
1.50	0.250	2.16
1.75	0.272	2.09
2.00	0.292	2.04
2.50	0.317	1.94
3.00	0.335	1.87
4.00	0.358	1.77
6.00	0.381	1.67

The allowable stress (i.e., the strength) of a spring that has been “set” is significantly higher than that of an as-wound spring. In addition, equation 14.8b with its smaller K_s factor can be used rather than equation 14.9b to calculate the stress in a “set” spring, since, for static loading, the yielding during setting relieves the curvature stress concentration. Setting is of greatest value for statically loaded springs but also has value in cyclic loading.

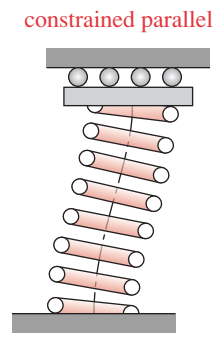
Not all commercial springs are set, as this increases their cost. The designer should specify setting if it is desired. Do not assume it will be done as a matter of course. Sometimes a setting operation is specified as part of the assembly process rather than as part of the spring-manufacturing process. If convenient, a spring can be deliberately cycled once to its shut height prior to, or when assembled into, its final location in a machine.

LOAD REVERSAL Whether set or not, coil springs typically will have some residual stresses in them. For this reason it is not acceptable to apply reversed loads to them. Assuming that the residual stresses have been arranged to be beneficial against the expected direction of loading, reversed loading will obviously exacerbate the residual stresses and cause early failure. A compression spring should never be loaded in tension nor a tension spring in compression. Even torsion springs, as we shall see, need to have a unidirectional torque applied to avoid premature failure.

SHOT PEENING is another way to obtain beneficial residual stresses in springs and is most effective against cyclic loading in fatigue. It has little benefit for statically loaded springs. The shot-peening process was discussed in Section 6.8 (p. 347). For wire springs, shot diameters of 0.008 in (0.2 mm) to 0.055 in (1.4 mm) are typically used. Springs of very small wire diameter will not benefit from shot peening as much as will ones of larger-diameter wire. Also, if the coil pitch is small (i.e., a tightly wound spring), the shot cannot effectively impact the inner surfaces of the coils.



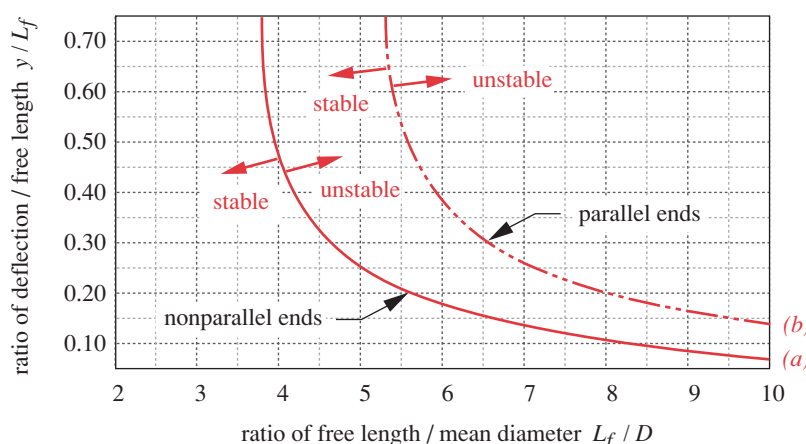
(a) Nonparallel ends



(b) Parallel ends

FIGURE 14-13

End Conditions Determine Critical Buckling Situation
Adapted from Reference 1

**FIGURE 14-14**

Critical Buckling Condition Curves Adapted from Reference 1

Buckling of Compression Springs

A compression spring is loaded as a column and can buckle if it is too slender. A slenderness ratio was developed for solid columns in Chapter 4. That measure is not directly applicable to springs due to their much different geometry. A similar slenderness factor is created as the aspect ratio of free length to mean coil diameter L_f / D . If this factor is > 4 the spring may buckle. Gross buckling can be prevented by placing the spring in a hole or over a rod. However, rubbing of the coils on these guides will take some of the spring force to ground through friction and reduce the load delivered at the spring end.

Just as with solid columns, the end constraints of the spring affect its tendency to buckle. If one end is free to tip as shown in Figure 14-13a, the spring will buckle with a smaller aspect ratio than if it is held against parallel plates at each end as shown in Figure 14-13b.

The ratio of the spring's deflection to its free length also affects its tendency to buckle. Figure 14-14 shows a plot of two lines that depict the stability of the two end-constraint cases of Figure 14-13. Springs with aspect ratio-deflection ratio combinations to the left of these lines are stable against buckling.

Compression-Spring Surge

Any device with both mass and elasticity will have one or more natural frequencies, as was discussed in Chapter 10 relative to shaft vibrations. Springs are no exception to this rule and can vibrate both laterally and longitudinally when dynamically excited near their natural frequencies. If allowed to go into resonance, the waves of longitudinal vibrations, called surging, cause the coils to impact one another. The large forces from both the excessive coil deflections and impacts will fail the spring. To avoid this condition, the spring should not be cycled at a frequency close to its natural frequency. Ideally, the natural frequency of the spring should be greater than about 13 times that of any applied forcing frequency.

The natural frequency ω_n or f_n of a helical compression spring depends on its boundary conditions. Fixing both ends is the more common and desirable arrangement, as its f_n will be twice that of a spring with one end fixed and the other free. For the fixed-fixed case:

$$\omega_n = \pi \sqrt{\frac{kg}{W_a}} \text{ rad/sec} \quad f_n = \frac{1}{2} \sqrt{\frac{kg}{W_a}} \text{ Hz} \quad (14.12a)$$

where k is the spring rate, W_a is the weight of the spring's active coils, and g is the gravitational constant. It can be expressed either as angular frequency ω_n or linear frequency f_n . The weight of the active coils can be found from

$$W_a = \frac{\pi^2 d^2 D N_a \gamma}{4} \quad (14.12b)$$

where γ is the material's weight density. For total spring weight substitute N_t for N_a .

Substituting equations 14.7 (p. 797) and 14.11a into 14.11b gives

Table 14-8 Maximum Torsional Yield Strength S_{ys} for Helical Compression Springs in Static Applications

Bending or Buckling Stresses Not Included. Source: Adapted from Ref. 1

Material	Maximum Percent of Ultimate Tensile Strength	
	Before Set Removed (Use Eq. 13.10b)	After Set Removed (Use Eq. 13.9b)
Cold-drawn carbon steel (e.g., A227, A228)	45%	60–70%
Hardened and tempered carbon and low-alloy steel (e.g., A229, A230, A232, A401)	50	65–75
Austenitic stainless steel (e.g., A313)	35	55–65
Nonferrous alloys (e.g., B134, B159, B197)	35	55–65

$$f_n = \frac{2}{\pi N_a} \frac{d}{D^2} \sqrt{\frac{Gg}{32\gamma}} \text{ Hz} \quad (14.12c)$$

for the natural frequency of a fixed-fixed helical coil spring. If one end of the spring is fixed and the other free, it acts like a fixed-fixed spring of twice its length. Its natural frequency can be found by using a number for N_a in equation 14.12c that is twice the actual number of active coils present in the fixed-free spring.

Allowable Strengths for Compression Springs

Extensive test data are available on the failure strengths of round-wire helical compression springs, both statically and dynamically loaded. The relationships of ultimate tensile strength to wire diameter were discussed in Section 14.3 (p. 790). For spring design, additional strength data are needed for yield and fatigue strengths.

TORSIONAL YIELD STRENGTH The torsional yield strengths of spring wire vary, depending on the material and whether the spring has been set or not. Table 14-8 shows recommended torsional yield-strength factors for several common spring wires as a percentage of the wire's ultimate tensile strength. These factors should be used to determine an estimated strength for a helical compression spring in static loading.*

Table 14-9 Maximum Torsional Fatigue Strength S_{fw}' for Round-Wire Helical Compression Springs in Cyclic Applications (Stress Ratio, $R = 0$)

No Surging, Room Temperature, and Noncorrosive Environment. Source: Ref. 1

Fatigue Life (cycles)	Percent of Ultimate Tensile Strength			
	ASTM 228, Austenitic Stainless Steel and Nonferrous		ASTM A230 and A232	
	Unpeened	Peened	Unpeened	Peened
10^5	36%	42%	42%	49%
10^6	33	39	40	47
10^7	30	36	38	46

* Note in Table 14-8 that Associated Spring Inc. [1] recommends using the Wahl factor (equation 14.10) to calculate the stress in a statically loaded spring if it has not had its "set" removed to introduce beneficial residual stresses, and using the lower direct shear factor (equation 14.9) if it has had "set" removal. This is in contradiction to the rule (first paragraph on p. 799) that is generally expressed about ignoring stress concentration in statically loaded situations, since their approach applies the Wahl stress concentration factor to an unset, statically loaded spring. Theirs is a more conservative approach than the general rule and one based on much experience in the manufacture of springs. N.B.

TORSIONAL FATIGUE STRENGTH over the $10^3 \leq N \leq 10^7$ cycles range varies with the material and whether it is shot peened or not. Table 14-8 shows recommended values for several wire materials in the peened and unpeened conditions at three points on their S - N diagrams, 10^5 , 10^6 , and 10^7 cycles. Note that these are torsional fatigue strengths and are determined from test springs loaded with equal mean and alternating stress components (stress ratio $R = \tau_{min}/\tau_{max} = 0$). So, they are not directly comparable to any of the fully reversed fatigue strengths generated from rotating-bending specimens discussed in Chapter 6 because of both the torsional loading and the presence of a mean stress component. We will use the designation S_{fw}' for these wire fatigue strengths to differentiate them from the fully reversed fatigue strengths of Chapter 6. These fatigue strengths S_{fw}' are nonetheless very useful in that they represent an actual (and typical) spring-fatigue-loading situation and are generated from spring samples, not test specimens, so the geometry and size are correct. Note that the fatigue strengths in Table 14-8 are declining with increasing numbers of cycles, even above 10^6 cycles, where steels usually display an endurance limit.

TORSIONAL ENDURANCE LIMIT Steel can have an endurance limit for infinite life. High-strength materials tend to show a “topping out” of their endurance limits with increasing ultimate strength. Figures 6-9 (p. 318) and 6-11 (p. 319) show this trend and equation 6.5a (p. 330) defines an uncorrected tensile endurance limit for fully reversed bending of steels with $S_{ut} > 200$ kpsi that remains constant with increasing tensile strength above that value. Note in Figure 14-3 (p. 792) that most spring wires smaller than about 10-mm diameter are in this ultimate-strength category. This would imply that these spring-wire materials should have a torsional endurance limit that is independent of size or of their particular alloy composition. Other research bears this out. Zimmerli^[4] reports that all spring-steel wire of < 10-mm diameter exhibits a torsional endurance limit for infinite life with stress ratio $R = 0$ (which, to differentiate from the fully reversed endurance limit, we will call S_{ew}').

$$\begin{aligned} S_{ew}' &\approx 45.0 \text{ kpsi (310 MPa)} \quad \text{for unpeened springs} \\ S_{ew}' &\approx 67.5 \text{ kpsi (465 MPa)} \quad \text{for peened springs} \end{aligned} \tag{14.13}$$

There is no need in this case to apply surface-, size-, or loading-correction factors to either S_{fw}' or S_{ew}' , since the test data were developed with actual conditions for those aspects of the wire materials. Table 14-9 notes that the fatigue strength data are taken at room temperature, in a noncorrosive environment, with no surging present. This is also true of Zimmerli’s data. If the spring is to operate at elevated temperature or in a corrosive environment, the fatigue strength or endurance limit can be downrated accordingly as in equation 6.8 (p. 337). Figure 6-31 (p. 336) also gives some information regarding corrosive environments. A temperature factor K_{temp} and/or a reliability factor K_{reliab} can still be applied as in equation 6.7f and Table 6-4 (p. 335). We will use the uncorrected values of S_{fw}' for S_{fw} and S_{ew}' for S_{ew} in our discussion here, assuming room temperature, no corrosion, and 50% reliability.

The Torsional-Shear S-N Diagram for Spring Wire

A torsional-shear S - N diagram for a particular wire material and size can be constructed from the information in Tables 14-4 and 14-7 (pp. 792 and 800) using the method described in Section 6.6 (p. 327) for creating estimated S - N diagrams. The region of in-

terest for high-cycle fatigue is from $N = 1\ 000$ cycles to $N = 1E7$ cycles and beyond. The endurance limit for infinite life of spring wire is defined in equation 14.13. The tensile strength S_{ut} at 1 000 cycles is typically taken as 90% of the ultimate strength S_{ut} at 1 cycle (the static strength). Since this is a torsional-loading situation, the wire tensile strengths shown in Figure 14-3 (p. 792) and defined by equation 14.3 and Table 14-4 (p. 792) must be converted to torsional strengths with equation 14.4 (p. 793). This makes the torsional strength S_{ms} at 1 000 cycles equal to

$$S_{ms} \approx 0.9S_{us} \approx 0.9(0.67S_{ut}) \approx 0.6S_{ut} \quad (14.14)$$

EXAMPLE 14-1

Constructing the S-N Diagram for a Spring-Wire Material

Problem Create the torsional-shear S-N diagrams for a range of spring-wire sizes.

Given ASTM A228 music wire, unpeened.

Assumptions Three diameters will be used: 0.010 in (0.25 mm), 0.042 in (1.1 mm), and 0.250 in (6.5 mm).

Solution See Figure 14-15.

- 1 The tensile strength of each wire size is found from equation 14.3 in combination with the coefficient and exponent from Table 14-4 for this material.

$$\begin{aligned} S_{ut} &\approx 184\ 649 d^{-0.1625} \\ &= 184\ 649(0.010)^{-0.1625} = 390\ 239 \text{ psi} \\ &= 184\ 649(0.042)^{-0.1625} = 309\ 071 \text{ psi} \quad (a) \\ &= 184\ 649(0.250)^{-0.1625} = 231\ 301 \text{ psi} \end{aligned}$$

- 2 These values are converted to shear strengths at 1 000 cycles using equation 14.14:

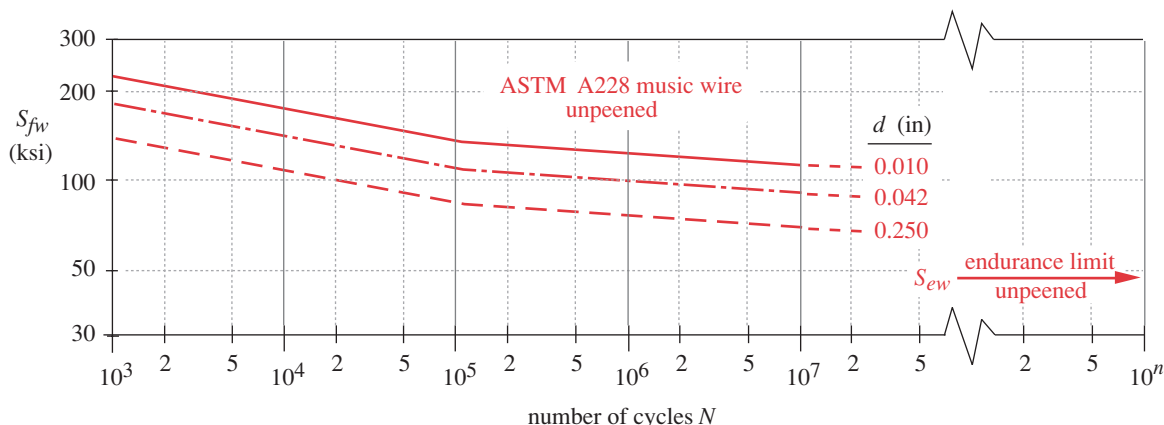


FIGURE 14-15

Torsional-Fatigue S-N Diagrams for Music Wire of Various Diameters

$$\begin{aligned}
 S_{ms} &\cong 0.6S_{ut} \\
 d = 0.010 : \quad S_{ms} &\cong 0.6(390\ 239) = 234\ 143 \text{ psi} \\
 d = 0.042 : \quad S_{ms} &\cong 0.6(309\ 071) = 185\ 443 \text{ psi} \\
 d = 0.250 : \quad S_{ms} &\cong 0.6(231\ 301) = 138\ 781 \text{ psi}
 \end{aligned} \tag{b}$$

- 3 The torsional fatigue strengths S_{fw} at three values of N are provided as percentages of the tensile strength in Table 14-9 for unpeened A228 music wire.

$$\begin{aligned}
 d = 0.010 @ N = 1E5 : S_{fw} &\cong 0.36(390\ 239) = 140\ 486 \text{ psi} \\
 d = 0.010 @ N = 1E6 : S_{fw} &\cong 0.33(390\ 239) = 128\ 779 \text{ psi} \\
 d = 0.010 @ N = 1E7 : S_{fw} &\cong 0.30(390\ 239) = 117\ 072 \text{ psi}
 \end{aligned} \tag{c}$$

These values are plotted in combination with the result from equation 14.14 to generate the S - N curves.

- 4 Figure 14-15 shows the S - N curves. There are two separate portions to each S - N curve: the $1E3 \leq N < 1E5$ segment and the segment for $N \geq 1E5$. The unpeened wire endurance limit for infinite life S_{ew} is also shown at 45 000 psi (equation 14.13).
- 5 If desired, any of these S - N curves can be fitted to an exponential equation (equations 6.10 on p. 338) by the method shown in Section 6-6. Evaluating the coefficients and exponents separately for the two pieces of the S - N curve allows the estimated wire fatigue strength S_{fw} to be easily found for any number of cycles.
- 6 It is important to remember that the S_{fw} data in Table 14-9 are for a repeated-stress state, not a fully reversed stress condition, which means that this S - N diagram is taken at some point along the σ_m axis in Figure 6-43 (p. 362).

The Modified-Goodman Diagram for Spring Wire

A modified-Goodman diagram can be constructed for any spring-loading situation. In Section 6.13 (p. 381) we presented a general approach to fatigue design that involved finding the von Mises effective stresses for any combined loading case in order to simplify the procedure. It was noted there that a pure-torsional loading situation can be solved in that manner as well, converting the shear stresses to von Mises stresses and comparing them to the material's tensile strengths. However, in the case of helical compression spring design, it makes little sense to use the von Mises approach because the empirically developed fatigue strengths for wire are expressed as torsional strengths. Thus it will be easier to construct a Goodman diagram using torsional strengths and apply the calculated torsional stresses to it directly. The results will be the same regardless of which approach is used.

EXAMPLE 14-2

Creating the Modified-Goodman Diagram for a Helical Spring

Problem Construct the Goodman line for the spring wire of Example 14-1.

Given

The required cycle life is $N = 1E6$ cycles. Wire is 0.042-in (1.1-mm) dia.

Assumptions

The torsional strengths and torsional shear stresses will be used on the Goodman diagram.

Solution

See Figure 14-16.

- 1 The material's ultimate tensile strength from Figure 14-3 or equation 14.3 (p. 792), converted to ultimate torsional strength with equation 14.4 (p. 793) using data from Table 14-4 (p. 792) allows one point on the Goodman line to be determined.

$$S_{ut} \approx 184\,649(0.042)^{-0.1625} = 309\,071 \text{ psi} \quad (a)$$

$$\begin{aligned} S_{us} &\approx 0.67S_{ut} \\ &= 0.67(309\,071) = 207\,078 \text{ psi} \end{aligned} \quad (b)$$

This value is plotted as point A on the diagram in Figure 14-16.

- 2 The $S-N$ diagrams each provide one data point (S_{fw} or S_{ew} , depending on whether for finite or infinite life) on the modified-Goodman line for a material/size combination in pure torsional loading. The fatigue strength S_{fw} for that wire material and condition is taken from the $S-N$ line of Figure 14-15 or calculated from the data in Table 14-9 (p. 813) as

$$@N = 1E6 : \quad S_{fw} \approx 0.33(309\,071) = 101\,993 \text{ psi} \quad (c)$$

The x and y intercepts are $0.5S_{fw} = 50\,996$ psi. This is plotted as point B on the diagram in Figure 14-16. Note that for infinite life the value of S_{ew} from equation 14.13 would be plotted at B instead of this value of S_{fw} for a finite life.

- 3 Note in Figure 14-16 that the wire fatigue strength S_{fw} is plotted at point B ($\tau_a = \tau_m = 0.5 S_{fw}$) corresponding to the test conditions of equal mean and alternating stress components (stress ratio $R = \tau_{min}/\tau_{max} = 0$). Point B is then connected with the ultimate shear strength S_{us} on the mean-stress axis at point A to draw the Goodman line, which is extended to point C.
- 4 We can now find the value of the fully reversed fatigue strength ($R = -1$), which is point C on the diagram. This value can be found from the equation for the Goodman line, defined in terms of its two known points, A and B:

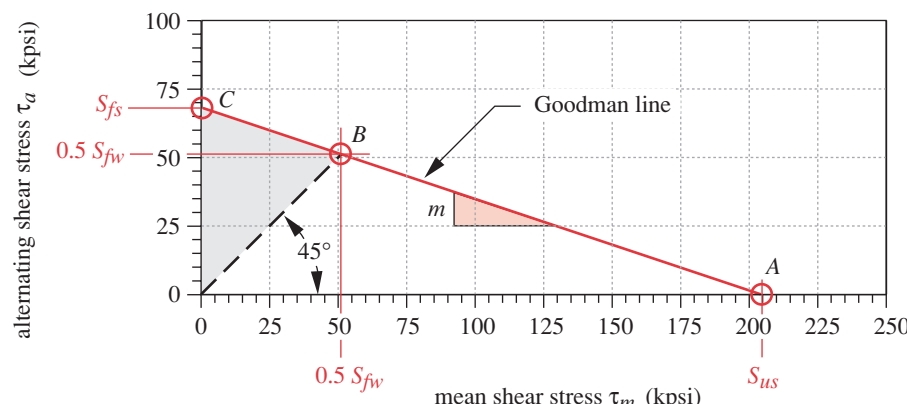


FIGURE 14-16

Torsional-Stress Modified-Goodman Diagram for 0.045-in Dia ASTM A228 Wire at $N = 1E6$ Cycles

$$\begin{aligned}
 m &= -\frac{0.5S_{fw}}{S_{us} - 0.5S_{fw}} \\
 S_{fs} &= -mS_{us} \\
 S_{fs} &= 0.5 \frac{S_{fw}S_{us}}{S_{us} - 0.5S_{fw}} \\
 &= 0.5 \frac{101\,993(207\,078)}{207\,078 - 0.5(101\,993)} = 67\,658 \text{ psi}
 \end{aligned} \tag{d}$$

- 5 This use of the Goodman line is conservative for stress ratios $R \geq 0$, and its use is justified in this case because springs should always be loaded in the same direction. Helical compression springs tend to have stress ratios between 0 and 0.8, which puts their stress coordinates to the right of the 45° line in the figure, where the Goodman line is more conservative than the Gerber line.
 - 6 Any other combination of mean and alternating stress with a stress ratio $R \geq 0$ for this material and number of cycles can now be plotted on this diagram to obtain a safety factor.
-

14.5 DESIGNING HELICAL COMPRESSION SPRINGS FOR STATIC LOADING

The functional requirements for a spring design can be quite varied. There may be a requirement for a particular force at some deflection, or the spring rate may be defined for a range of deflection. In some cases there are limitations on the outside diameter, inside diameter, or working length. The approach to design will vary depending on these requirements. In any case, spring design is inherently an iterative problem. Some assumptions must be made to establish the values of enough variables to calculate the stresses, deflections, and spring rate. Because wire size appears to the third or fourth power in the stress and deflection equations, and because material strength is dependent on wire size, the safety of the design is very sensitive to this parameter.

Many approaches may be taken to spring design, and more than one combination of spring parameters can satisfy any set of functional requirements. It is possible to optimize parameters such as spring weight for a given set of performance specifications. To minimize weight and cost, the stress levels should be made as high as possible without causing static yielding in service.

A trial wire diameter d should be assumed and a reasonable spring index C chosen, from which the coil diameter D can be calculated using equation 14.5 (p. 797). A trial spring material is chosen and the relevant material strengths calculated for the trial wire diameter. It is convenient to calculate the stress before computing the deflection because, while both involve d and D , only the deflection depends on N_a . If a required force F is defined, the stress at that force can be computed with equation 14.8 or 14.9 (p. 798) as appropriate. If two operating forces are defined with a specified deflection between them, they will define the spring rate.

The stress state is compared to the yield strength for static loading. The safety factor for static loading is

$$N_s = \frac{S_{ys}}{\tau} \quad (14.15)$$

If the calculated stress is too high compared to the material strength, the wire diameter, spring index, or material can be changed to improve the result. When the calculated stress at the required operating force seems reasonable compared to the material strength, a trial number of coils and a clash allowance can be assumed and further calculations for spring rate, deflection, and free length done using equations 14.6 and 14.7 (p. 797). Unreasonable values of any of these parameters will require further iteration with changed assumptions.

After several iterations, a reasonable combination of parameters can usually be found. Some of the things that need to be checked before the design is complete will be the stress at shut height, and the D_i , D_o , and free length of the coil with respect to packaging considerations. In addition, the possibility of buckling needs to be checked.

If the above process seems complicated, the reader should appreciate the value of making a computer do the “dirty work.” Spring design, like any iterative design procedure, is an obvious task for a computer solution. Equation solvers that allow automatic iteration are extremely well suited to these kinds of tasks since they solve all aspects of the problem simultaneously. We will now present some examples of spring design problems and show how an equation solver can be used to expedite their solutions.

EXAMPLE 14-3

Design of a Helical Compression Spring for Static Loading

Problem Design a compression spring for a static load over a known deflection.

Given The spring must give a minimum force of 100 lb and a maximum force of 150 lb over an adjustment range of 0.75-in deflection.

Assumptions Use the least expensive, unpeened, cold-drawn spring wire (ASTM A227) since the loads are static.

Solution See Table 14-10.

- 1 Assume a trial wire diameter of 0.162 in from the available sizes in Table 14-2 (p. 791).
- 2 Assume a spring index of 8, which is in the middle of the recommended range, and calculate the mean coil diameter D from equation 14.5 (p. 797).

$$D = Cd = 8(0.162) = 1.30 \text{ in} \quad (a)$$

- 3 Find the direct shear factor K_s and use it to calculate the shear stress in the coil at the larger force.

$$K_s = 1 + \frac{0.5}{C} = 1 + \frac{0.5}{8} = 1.06 \quad (b)$$

$$\tau = K_s \frac{8FD}{\pi d^3} = 1.06 \frac{8(150)(1.30)}{\pi(0.162)^3} = 123\,714 \text{ psi} \quad (c)$$

- 4 Find the ultimate tensile strength of this wire material from equation 14.3 and Table 14-4 (p. 792) and use it to find the torsional yield strength from Table 14-8 (p. 803), assuming that the set has been removed and using the low end of the recommended range.

$$S_{ut} = Ad^b = 141\,040(0.162)^{-0.182^2} = 196\,503 \text{ psi} \quad (d)$$

$$S_{ys} = 0.60S_{ut} = 0.60(196\,503) = 117\,902 \text{ psi} \quad (e)$$

- 5 Find the safety factor against yielding at this working deflection from equation 14.15 (p. 809).

$$N_s = \frac{S_{ys}}{\tau} = \frac{117\,902 \text{ psi}}{123\,714 \text{ psi}} = 0.95 \quad (f)$$

This is obviously not acceptable, so the design must be iterated with some parameters changed.

- 6 Try increasing the wire diameter slightly, perhaps to 0.192 in, keeping the same spring index. Recalculate the coil diameter, stress, strength, and safety factor.

$$D = Cd = 8(0.192) = 1.54 \text{ in} \quad (g)$$

$$\tau = K_s \frac{8FD}{\pi d^3} = 1.06 \frac{8(150)(1.54)}{\pi(0.192)^3} = 88\,074 \text{ psi} \quad (h)$$

$$S_{ut} = Ad^b = 141\,040(0.192)^{-0.182^2} = 190\,513 \text{ psi} \quad (i)$$

$$S_{ys} = 0.60S_{ut} = 0.60(190\,513) = 114\,308 \text{ psi} \quad (j)$$

$$N_s = \frac{S_{ys}}{\tau} = \frac{114\,308 \text{ psi}}{88\,074 \text{ psi}} = 1.30 \quad (k)$$

This appears to be acceptable, so we can go on to design the other spring parameters.

- 7 The spring rate is defined in this problem because of the two specified forces at a particular relative deflection.

$$k = \frac{\Delta F}{y} = \frac{150 - 100}{0.75} = 66.7 \text{ lb/in} \quad (l)$$

- 8 To achieve this spring rate, the number of active coils must satisfy equation 14.7 (p. 797):

$$k = \frac{d^4 G}{8D^3 N_a} \quad \text{or} \quad N_a = \frac{d^4 G}{8D^3 k} = \frac{(0.192)^4 11.5E6}{8(1.54)^3 66.7} = 8.09 \cong 8 \quad (m)$$

Note that we round it to the nearest 1/4 coil, as the manufacturing tolerance cannot achieve better than that accuracy. This makes the spring rate $k = 67.4 \text{ lb/in}$.

- 9 Assume squared and ground ends, making the total number of coils from Figure 14-9 (p. 796):

$$N_t = N_a + 2 = 8 + 2 = 10 \quad (n)$$

- 10 The shut height can now be determined.

$$L_s = dN_t = 0.192(10) = 1.92 \text{ in} \quad (o)$$

11 The initial deflection to reach the smaller of the two specified loads is

$$y_{initial} = \frac{F_{initial}}{k} = \frac{100}{67.4} = 1.48 \text{ in} \quad (p)$$

12 Assume a clash allowance of 15% of the working deflection:

$$y_{clash} = 0.15y = 0.15(0.75) = 0.113 \text{ in} \quad (q)$$

13 The free length (see Figure 14-8, p. 796) can now be found from

$$L_f = L_s + y_{clash} + y_{working} + y_{initial} = 1.92 + 0.113 + 0.75 + 1.48 = 4.26 \text{ in} \quad (r)$$

14 The deflection to the shut height is

$$y_{shut} = L_f - L_s = 4.26 - 1.92 = 2.34 \text{ in} \quad (s)$$

15 The force at this shut-height deflection is

$$F_{shut} = k y_{shut} = 67.4(2.34) = 158 \text{ lb} \quad (t)$$

16 The shut-height stress and safety factor are

$$\tau_{shut} = K_s \frac{8FD}{\pi d^3} = 1.06 \frac{8(158)(1.54)}{\pi(0.192)^3} = 92\ 794 \text{ psi} \quad (u)$$

$$N_{s_{shut}} = \frac{S_{sy}}{\tau_{shut}} = \frac{114\ 308 \text{ psi}}{92\ 794 \text{ psi}} = 1.2 \quad (v)$$

which is acceptable.

17 To check for buckling, two ratios need to be calculated, L_f / D and y_{max} / L_f .

$$\frac{L_f}{D} = \frac{4.26}{1.54} = 2.77 \quad (w)$$

$$\frac{y_{max}}{L_f} = \frac{y_{initial} + y_{working}}{L_f} = \frac{1.48 + 0.75}{4.26} = 0.52$$

Take these two values to Figure 14-14 (p. 801) and find that their coordinates are safely within the zones that are stable against buckling for either end-condition case.

18 The inside and outside coil diameters are

$$D_o = D + d = 1.54 + 0.192 = 1.73 \text{ in}$$

$$D_i = D - d = 1.54 - 0.192 = 1.34 \text{ in} \quad (x)$$

19 The smallest hole and largest pin that should be used with this spring are

$$hole_{min} = D_o + 0.05D = 1.73 + 0.05(1.54) = 1.81 \equiv 1\frac{13}{16} \text{ in}$$

$$pin_{max} = D_i - 0.05D = 1.34 - 0.05(1.54) = 1.26 \equiv 1\frac{1}{4} \text{ in} \quad (y)$$

20 The total weight of the spring is

$$W_t = \frac{\pi^2 d^2 D N_t \rho}{4} = \frac{\pi^2 (0.192)^2 (1.54)(10)(0.28)}{4} = 0.40 \text{ lb} \quad (z)$$

21 We now have a complete design specification for this A227 wire spring:

$$d = 0.192 \text{ in} \quad OD = 1.73 \text{ in} \quad N_t = 10, \text{ sq \& g} \quad L_f = 4.26 \text{ in} \quad (aa)$$

Other calculated spring parameters for this example are shown in Table 14-10.

- 22 Models for this example are on the CD-ROM as EX14-03. There are also alternate approaches to the solution of this example shown in separate Mathcad and TK Solver files on the CD-ROM with a letter added to their name.
-

14.6 DESIGNING HELICAL COMPRESSION SPRINGS FOR FATIGUE LOADING

When the spring loads are dynamic (time-varying), a fatigue-stress situation exists in the spring. The design process for dynamic loading is similar to that for static loading with some significant differences. A dynamically loaded spring will operate between two force levels, F_{min} and F_{max} . From these values, the alternating and mean components of force can be calculated from

$$F_a = \frac{F_{max} - F_{min}}{2} \quad (14.16a)$$

$$F_m = \frac{F_{max} + F_{min}}{2}$$

A **force ratio** R_F can also be defined as:

$$R_F = \frac{F_{min}}{F_{max}} \quad (14.16b)$$

In the most common spring-loading cases F_{min} and F_{max} are both positive, with the force ratio about $0 < R_F < 0.8$. As described in the earlier discussion of residual stresses, bi-directional loading of coil springs is to be avoided, as it causes early failure.

The fatigue-design procedure is essentially as outlined in the previous section for static loading. It is still an iterative problem. A trial wire diameter d should be assumed and a reasonable spring index C chosen, from which the coil diameter D can be calculated using equation 14.5 (p. 797). A trial spring material is chosen and the relevant material strengths calculated for the trial wire diameter. The ultimate shear strength, shear yield strength, and the endurance limit (or fatigue strength at some number of cycles) are all needed. The problem statement usually contains sufficient information to estimate the number of life-cycles required. For dynamic loading, the alternating and mean stresses are calculated separately (using F_{min} and F_{max} from equation 14.16a).

Unidirectional loading, also called fluctuating or repeated loading in Chapter 6, has nonzero mean stress and thus requires a Goodman-diagram failure analysis. Since all significant stresses in this spring are torsional-shear stresses and most spring-wire material-strength data are for torsional loading, we will use a **torsional Goodman diagram**, as discussed earlier. The modified-Goodman diagram is constructed as shown in Figures 14-16 (p. 807) and 14-17 (p. 815) with the torsional wire-fatigue strength S_{fw} or

Table 14-10 Example 14-3 – Helical Compression Spring Design for Static Loading

Input	Variable	Output	Unit	Comments
8	C			trial spring index
0.192	dia			trial wire diameter
0.750	y		in	deflection of spring
15	$clash$		%	% of deflect for clash allowance
'hdrawn	$matl$			'music, 'oiltemp, 'hdrawn, 'chromev, etc.
'sqgrnd	end			one of 'plain, 'pgrnd, 'square, 'sqgrnd
'unpeen	$surface$			one of 'unpeen or 'peen
'set	$setflag$			one of 'set or 'unset
150	F_{max}		lb	maximum applied force
100	F_{min}		lb	minimum applied force
	F_{shut}	158	lb	force at shut height
	k	67.4	lb/in	spring rate with N_a rounded
	N_a	8		no. of active coils—to nearest 1/4 coil
	N_{tot}	10		no. of total coils
	D	1.54	in	mean coil diameter
	D_{out}	1.73	in	outside coil diameter
	D_{in}	1.34	in	inside coil diameter
	K_s	1.06		static factor—direct shear - Eq. 13.8
	K_w	1.18		Wahl Factor—Eq. 13.9
	τ_{auinit}	58 716	psi	shear stress at installed length
	τ_{austat}	88 074	psi	shear stress at F_{max} for static loading
	τ_{aushut}	92 478	psi	stress at shut height
	S_{ut}	190 513	psi	tensile strength—Eq. 13.3 & Table 13-4
	S_{us}	127 644	psi	ultimate shear strength—Eq. 13.4
	S_{ys}	114 308	psi	shear yield based on Table 13-6
	N_{s_static}	1.30		safety factor—static loading at F_{max}
	N_{s_shut}	1.23		safety factor—shut height (yielding)
	L_f	4.26	in	free length
	L_{instal}	2.78	in	installed length
	L_{comp}	2.03	in	compressed length
	L_{shut}	1.92	in	shut height
	y_{init}	1.48	in	initial deflection at assembly
	y_{max}	2.23	in	max working deflection
	y_{clash}	0.113	in	coil clash allowance
	y_{shut}	2.34	in	deflection to shut height

wire-endurance strength S_{ew} defined along a 45° line from the origin to represent the test data that was generated at $R_F = 0$. Figure 14-17 uses the value of torsional wire-endurance limit S_{ew} for infinite life of peened steel wire in combination with the torsional ultimate strength S_{us} to create the torsional Goodman line.

The load line, which represents the applied stress state, is not drawn from the origin in this case, but rather from a point on the τ_m axis representing the initial stress τ_i in the coils at assembly, as shown in Figure 14-17. This assumes that some spring preload is applied, which is usually the case. We do not want $F_{min} = 0$ in a dynamic loading situation as that will create impact loads on the coils (see Section 3.8 on p. 106). If $F_{min} = 0$, the load line would start at the origin. The safety factor for torsional fatigue N_{fs} can be expressed as the ratio of the alternating strength S_a at the intersection of the load line and the Goodman line (point D) to the applied alternating stress τ_a at point E.

$$N_{fs} = S_a / \tau_a \quad (14.17a)$$

This ratio can be derived from the geometry of the two lines. Let x represent the independent variable on the mean stress axis, m represent the slope of a line and b its y intercept. Let the value on the load line for any x be y_{load} . The load-line equation is

$$\begin{aligned} y_{load} &= m_{load}x + b_{load} \\ \text{From geometry} \quad m_{load} &= \frac{\tau_a}{\tau_m - \tau_i} \quad \text{and} \quad b_{load} = -m_{load}\tau_i \\ y_{load} &= \frac{\tau_a}{\tau_m - \tau_i}(x - \tau_i) \end{aligned} \quad (14.17b)$$

Let the value on the Goodman line for any x be y_{Good} . Then its equation is:

$$\begin{aligned} y_{Good} &= m_{Good}x + b_{Good} \\ \text{From geometry} \quad m_{Good} &= -\frac{S_{es}}{S_{us}} \quad \text{and} \quad b_{Good} = S_{es} \\ y_{Good} &= -\frac{S_{es}}{S_{us}}x + S_{es} = S_{es} \left(1 - \frac{x}{S_{us}}\right) \end{aligned} \quad (14.17c)$$

At the failure point, $y_{load} = y_{Good}$. Setting 14.16b and c equal and solving for x gives

$$\begin{aligned} S_{es} \left(1 - \frac{x}{S_{us}}\right) &= \frac{\tau_a}{\tau_m - \tau_i}(x - \tau_i) \\ x &= \frac{S_{us}[S_{es}(\tau_i - \tau_m) - \tau_a\tau_i]}{S_{es}(\tau_i - \tau_m) - S_{us}\tau_a} \end{aligned} \quad (14.17d)$$

Substitute equation 14.17c in 14.16a:

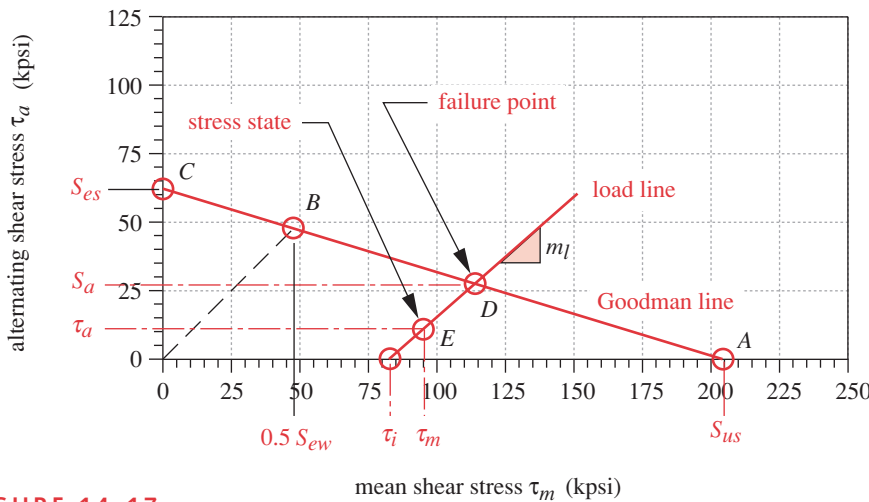
$$N_{fs} = S_a / \tau_a = y_{Good} / \tau_a = S_{es} \left(1 - \frac{x}{S_{us}}\right) / \tau_a \quad (14.17e)$$

Substitute equation 14.17d in 14.16e and simplify to get the safety factor as

$$N_{fs} = \frac{S_{es}(S_{us} - \tau_i)}{S_{es}(\tau_m - \tau_i) + S_{us}\tau_a} \quad (14.18a)$$

where the fully reversed endurance limit (point C) from Example 14-3 is

$$S_{es} = 0.5 \frac{S_{ew}S_{us}}{S_{us} - 0.5S_{ew}} \quad (14.18b)$$

**FIGURE 14-17**

Modified-Goodman Diagram Showing Load Line and Data Needed for Safety-Factor Calculation of a Dynamically Loaded Compression Spring

This approach assumes that the initial preload will not vary significantly over the life of the part and also that any increase in the loading will be such as to maintain a constant ratio between the alternating and mean components of stress. This corresponds to Case 3 of Figure 6-46 (p. 366). If this is not the situation, then one of the other cases of Section 6.11 should be used to find the safety factor by the method of equations 14.16. The stress at the initial preload must still be accounted for, and itself may vary under service conditions.

If the safety factor is too low, the wire diameter, spring index, or the material can be changed to improve the result. When the fatigue safety factor is acceptable, a trial number of coils and a clash allowance can be assumed and further calculations for spring rate, deflection and free length done using equations 14.6 and 14.7 (p. 797). Unreasonable values of any of these parameters will require further iteration with changed assumptions.

After several iterations, a reasonable combination of parameters can usually be found. Some of the things that need to be checked before the design is complete will be the stress at shut height versus the yield stress, and the D_i , D_o , and free length of the coil with respect to packaging considerations. In addition, the possibility of buckling needs to be checked, and for dynamic loading, the natural frequency of the spring must be compared to any forcing frequencies in the system to guard against surging.

Spring design for fatigue loading benefits greatly from a computer solution. Equation solvers that allow automatic iteration are extremely well suited to these kinds of tasks since they solve all aspects of the problem simultaneously. We will now present an example of spring design for fatigue loading.

EXAMPLE 14-4**Design of a Helical Compression Spring for Cyclic Loading**

Problem Design a compression spring for a dynamic load over a given deflection.

Given The spring must give a minimum force of 60 lb and a maximum force of 150 lb over a dynamic deflection of 1.00 in. The forcing frequency is 1 000 rpm. A 10-year life of 1-shift operation is desired.

Assumptions Music wire (ASTM A228) will be used, since the loads are dynamic. Peening will be used to obtain a higher endurance strength.

Solution See Figures 14-18, 14-19 and Table 14-11.

- Find the number of cycles that the spring will see over its design life.

$$N_{life} = 1\,000 \frac{\text{rev}}{\text{min}} \left(\frac{60 \text{ min}}{\text{hr}} \right) \left(\frac{2\,080 \text{ hr}}{\text{shift - yr}} \right) (10 \text{ yr}) = 1.2E9 \text{ cycles} \quad (a)$$

This large a number requires that an endurance limit for infinite life be used.

- Find the mean and alternating forces from equation 14.16a:

$$\begin{aligned} F_a &= \frac{F_{max} - F_{min}}{2} = \frac{150 - 60}{2} = 45 \text{ lb} \\ F_m &= \frac{F_{max} + F_{min}}{2} = \frac{150 + 60}{2} = 105 \text{ lb} \end{aligned} \quad (b)$$

- Assume a 0.207-in wire diameter from the available sizes in Table 14-2 (p. 791). Assume a spring index of 9 and calculate the mean coil diameter D from equation 14.5 (p. 797).

$$D = Cd = 9(0.207) = 1.863 \text{ in} \quad (c)$$

- Find the direct shear factor K_s and use it to calculate the stress τ_i at the initial deflection (lowest defined force), and the mean stress τ_m :

$$K_s = 1 + \frac{0.5}{C} = 1 + \frac{0.5}{9} = 1.056 \quad (d)$$

$$\tau_i = K_s \frac{8F_i D}{\pi d^3} = 1.056 \frac{8(60)(1.863)}{\pi(0.207)^3} = 33\,875 \text{ psi} \quad (e)$$

$$\tau_m = K_s \frac{8F_m D}{\pi d^3} = 1.056 \frac{8(105)(1.863)}{\pi(0.207)^3} = 59\,281 \text{ psi} \quad (f)$$

- Find the Wahl factor K_w and use it to calculate the alternating shear stress τ_a in the coil.

$$K_w = \frac{4C - 1}{4C - 4} + \frac{0.615}{C} = \frac{4(9) - 1}{4(9) - 4} + \frac{0.615}{9} = 1.162 \quad (g)$$

$$\tau_a = K_w \frac{8F_a D}{\pi d^3} = 1.162 \frac{8(45)(1.863)}{\pi(0.207)^3} = 27\,970 \text{ psi} \quad (h)$$

- 6 Find the ultimate tensile strength of this music-wire material from equation 14.3 and Table 14-4 (p. 792) and use it to find the ultimate shear strength from equation 14.4 and the torsional yield strength from Table 14-8 (p. 803), assuming that the set has been removed and using the low end of the recommended range.

$$S_{ut} = Ad^b = 184\,649(0.207)^{-0.1625} = 238\,507 \text{ psi}$$

$$S_{us} = 0.67S_{ut} = 159\,800 \text{ psi} \quad (i)$$

$$S_{ys} = 0.60S_{ut} = 0.60(238\,507) = 143\,104 \text{ psi} \quad (j)$$

- 7 Find the wire endurance limit for peened springs in repeated loading from equation 14.13 (p. 804) and convert it to a fully reversed endurance strength with equation 14.18b (p. 814).

$$S_{ew} = 67\,500 \text{ psi} \quad (k)$$

$$S_{es} = 0.5 \frac{S_{ew} S_{us}}{S_{us} - 0.5S_{ew}} = 0.5 \frac{67\,500(159\,800)}{159\,800 - 0.5(67\,500)} = 42\,787 \text{ psi} \quad (l)$$

- 8 The safety factor is calculated from equation 14.18a (p. 814).

$$N_{fs} = \frac{S_{es}(S_{us} - \tau_i)}{S_{es}(\tau_m - \tau_i) + S_{us}\tau_a}$$

$$= \frac{42\,787(159\,800 - 33\,875)}{42\,787(59\,281 - 33\,875) + 159\,800(27\,970)} = 1.0 \quad (m)$$

This is obviously not an acceptable design. To get some idea of what to change to improve it, the model was solved for a list of values of the spring index C from 4 to 14, keeping all other parameters as defined above. The resulting values of coil diameter, free length, spring weight, and torsional fatigue safety factor are plotted in Figure 14-18. Note that the wire diameter was held constant to develop the variation of parameters with spring index as shown in Figure 14-18. If another parameter such

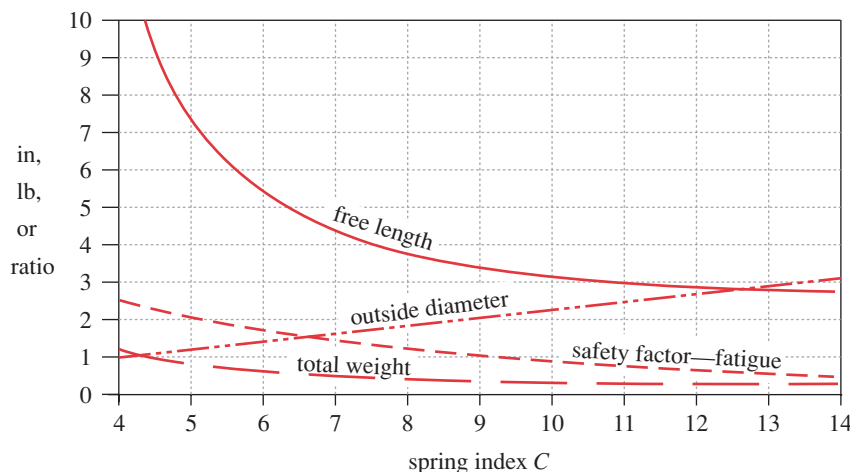
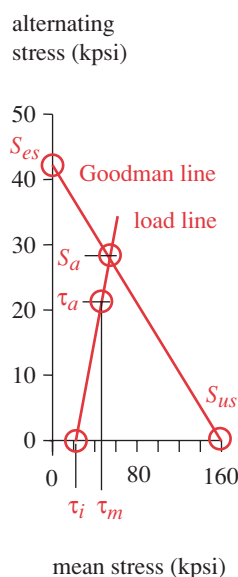


FIGURE 14-18

Variation of Helical Compression Spring Parameters with Spring Index—Constant Wire Diameter

**FIGURE 14-19**

Torsional Stress
Goodman Diagram for
Example 14-4

as mean coil diameter D were held constant instead, a different set of functions would result for the free length, weight, safety factor, etc.

The safety factor increases with decreasing spring index, so a reduction in our assumed value for C will improve the safety factor even with no change in wire diameter. Note, however, that the free length increases exponentially with decreasing spring index. If package size is limited, we may not want to decrease the spring index too much in order to avoid excessive spring length. The coil diameter increases linearly with the spring index for a constant wire diameter. Spring weight decreases slowly with increasing spring index.

If we decrease the spring index from 9 to 7, keeping all other parameters the same, we will obtain an acceptable design in this case with $N_f = 1.3$. Table 14-11 shows the results of this new calculation and of the calculations outlined below needed to complete the design. Figure 14-19 shows the modified-Goodman diagram for the final design. A summary of the changed values is

$$\begin{aligned} C &= 7 & D &= 1.45 \text{ in} & K_w &= 1.21 & K_s &= 1.07 \\ \tau_i &= 26\,743 \text{ psi} & \tau_a &= 22\,705 \text{ psi} & \tau_m &= 46\,800 \text{ psi} & N_{f_s} &= 1.3 \end{aligned} \quad (n)$$

- 9 The spring rate is defined from the two specified forces at their relative deflection.

$$k = \frac{\Delta F}{y} = \frac{150 - 60}{1.0} = 90 \text{ lb/in} \quad (o)$$

- 10 To get the defined spring rate, the number of active coils must satisfy equation 14.7 (p. 797):

$$k = \frac{d^4 G}{8D^3 N_a} \quad \text{or} \quad N_a = \frac{d^4 G}{8D^3 k} = \frac{(0.207)^4 11.5E6}{8(1.45)^3 (90)} = 9.64 \approx 9\frac{3}{4} \quad (p)$$

Note that we round it to the nearest 1/4 coil, as the manufacturing tolerance cannot achieve better than that accuracy. This makes the spring rate $k = 89 \text{ lb/in}$.

- 11 Assume squared and ground ends, making the total number of coils from Figure 14-9 (p. 796):

$$N_t = N_a + 2 = 9.75 + 2 = 11.75 \quad (q)$$

- 12 The shut height can now be determined.

$$L_s = dN_t = 0.207(11.75) = 2.43 \text{ in} \quad (r)$$

- 13 The initial deflection to reach the smaller of the two specified loads is

$$y_{initial} = \frac{F_{initial}}{k} = \frac{60}{89} = 0.674 \text{ in} \quad (s)$$

- 14 Assume a clash allowance of 15% of the working deflection:

$$y_{clash} = 0.15y = 0.15(1.0) = 0.15 \text{ in} \quad (t)$$

- 15 The free length (see Figure 14-8, p. 796) can now be found from

$$L_f = L_s + y_{clash} + y_{working} + y_{initial} = 1.82 + 0.15 + 1.0 + 0.674 = 4.25 \text{ in} \quad (u)$$

- 16 The deflection to the shut height is

$$y_{shut} = L_f - L_s = 4.25 - 2.43 = 1.82 \text{ in} \quad (v)$$

- 17 The force at this shut-height deflection is

$$F_{shut} = k y_{shut} = 89(1.82) = 162 \text{ lb} \quad (w)$$

- 18 The shut-height stress and safety factor are

$$\tau_{shut} = K_s \frac{8F_{shut}D}{\pi d^3} = 1.07 \frac{8(164)(1.45)}{\pi(0.207)^3} = 72\,875 \text{ psi} \quad (x)$$

$$N_{s_{shut}} = \frac{S_{ys}}{\tau_{shut}} = \frac{143\,104 \text{ psi}}{72\,875 \text{ psi}} = 2.0 \quad (y)$$

which is acceptable.

- 19 To check for buckling, two ratios need to be calculated, L_f / D and y_{max} / L_f .

$$\frac{L_f}{D} = \frac{4.25}{1.45} = 2.93 \quad (z)$$

$$\frac{y_{max}}{L_f} = \frac{y_{initial} + y_{working}}{L_f} = \frac{0.674 + 1.0}{4.25} = 0.39$$

Take these two values to Figure 14-14 (p. 801) and find that their coordinates are safely within the zones that are stable against buckling for either end-condition case.

- 20 The weight of the spring's active coils from equation 14.12b (p. 802) is

$$W_a = \frac{\pi^2 d^2 D N_a \gamma}{4} = \frac{\pi^2 (0.207)^2 (1.45)(9.75)(0.285)}{4} = 0.426 \text{ lb} \quad (aa)$$

- 21 The natural frequency of this spring is found from equation 14.12a (p. 802) and is

$$f_n = \frac{1}{2} \sqrt{\frac{kg}{W}} = \frac{1}{2} \sqrt{\frac{89(386)}{0.426}} = 142 \text{ Hz} = 8\,521 \frac{\text{cycles}}{\text{min}} \quad (ab)$$

The ratio between the natural frequency and the forcing frequency is

$$\frac{8\,520}{1\,000} = 8.5 \quad (ac)$$

which is sufficiently high.

- 22 The design specification for this A228 wire spring is

$$d = 0.207 \text{ in} \quad D_o = 1.66 \text{ in} \quad N_t = 11.75, \text{ sq \& g} \quad L_f = 4.25 \quad (ad)$$

- 23 Detailed results are shown in Table 14-11. The files EX14-04 are on the CD-ROM. There are also alternate approaches to the solution of this example shown in separate Mathcad and TK Solver files on the CD-ROM with a letter added to their name.

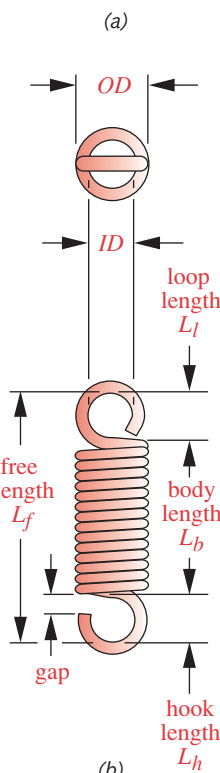
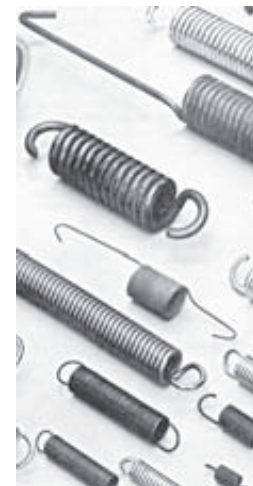


FIGURE 14-20

(a) Sample Springs and
(b) Dimensions of an Extension Spring

Table 14-11 Example 14-4 Helical Compression Spring for Dynamic Loading

Input	Variable	Output	Unit	Comments
1 000	<i>rpm</i>		rpm	excitation frequency
7	<i>C</i>			trial spring index
0.207	<i>d</i>		in	available wire diameter (List Function)
1	<i>y</i>		in	deflection of spring
'music	<i>matl</i>			one of 'music, 'oiltemp, 'hdrawn, etc.
'sqrnd	<i>end</i>			one of 'plain, 'pgrnd, 'square, 'sqrnd
'peen	<i>surface</i>			one of 'unpeen or 'peen
'set	<i>setflag</i>			set for a set spring—unset otherwise
150	<i>Fmax</i>		lb	maximum applied force
60	<i>Fmin</i>		lb	minimum applied force
	<i>Falt</i>	45	lb	alternating force
	<i>Fmean</i>	105	lb	mean force
	<i>Fshut</i>	164	lb	force at shut height
	<i>k</i>	89	lb/in	spring rate with <i>N_a</i> rounded
	<i>N_a</i>	9.75		no. of active coils—rounded to 1/4 coil
	<i>N_t</i>	11.75		no. of total coils
	<i>D</i>	1.45	in	mean coil diameter
	<i>D_{out}</i>	1.66	in	outside coil diameter
	<i>D_{in}</i>	1.24	in	inside coil diameter
	<i>K_s</i>	1.07		static factor—direct shear—Eq. 13.8
	<i>K_w</i>	1.21		Wahl Factor—Eq. 13.9
	<i>tauinit</i>	26 743	psi	shear stress at installed length
	<i>taushut</i>	72 875	psi	stress at shut height
	<i>taualt</i>	22 705	psi	alternating shear stress for fatigue
	<i>taumean</i>	46 800	psi	mean shear stress for fatigue
	<i>S_{ut}</i>	238 507	psi	tensile strength—Eq. 13.3 & Table 13-4
	<i>S_{us}</i>	159 800	psi	ultimate shear strength—Eq. 13.4
	<i>S_{ys}</i>	143 104	psi	shear yield based on Table 13-6
	<i>S_{ew}</i>	67 500	psi	wire endurance limit—Eq. 13.12
	<i>S_{es}</i>	42 787	psi	fully reversed endurance limit—Eq. 13.16b
	<i>N_f</i>	1.3		safety factor—fatigue—Eq. 13.14
	<i>N_{shut}</i>	2.0		safety factor—shut height (yielding)
	<i>L_f</i>	4.25	in	free length
	<i>L_{shut}</i>	2.43	in	shut height
	<i>y_{init}</i>	0.67	in	initial deflection at assembly
	<i>y_{shut}</i>	1.82	in	deflection to shut height
	<i>nf</i>	142	Hz	natural frequency in Hz
	<i>FreqFac</i>	8.5		ratio of nat. freq to excitation freq.

14.7 HELICAL EXTENSION SPRINGS

Helical extension springs are similar to helical compression springs, but are loaded in tension, as shown in Figure 14-2b. Figure 14-20 shows the significant dimensions of

an extension spring. Hooks or loops are provided to allow a pull force to be applied. A standard loop and standard hook are shown in the figure, but many variations are possible. See reference 1 for descriptions of other possible hook and loop configurations. The standard ends are formed simply by bending the last coil at 90° to the coil body. The hooks and loops can have higher stresses than the coil body and these may limit the safety of the design. Setting of the coils is not done with extension springs and shot-peening is impractical, since the tightly wound coils shield one another from the shot.

Active Coils in Extension Springs

All coils in the body are considered active coils, but one coil is typically added to the number of active coils to obtain the body length L_b .

$$N_t = N_a + 1 \quad (14.19)$$

$$L_b = dN_t \quad (14.20)$$

The free length is measured from the inside of one end loop (or hook) to the other and can be varied by changing the end configuration without changing the number of coils.

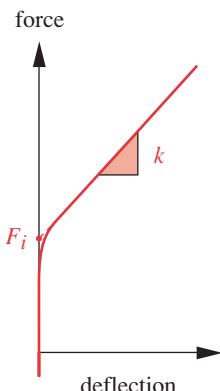


FIGURE 14-21

Force-Deflection Curve of a
Helical Extension Spring
Showing Its Initial Tension

Spring Rate of Extension Springs

Extension-spring coils are wound tightly together, and the wire is twisted as it is wound, creating a preload in the coils that must be overcome to separate them. Figure 14-21 shows a typical load-deflection curve for a helical extension spring. The spring rate k is linear except for the initial portion. The preload F_i is measured by extrapolating the linear portion of the curve back to the force axis. The spring rate can be expressed as

$$k = \frac{F - F_i}{y} = \frac{d^4 G}{8D^3 N_a} \quad (14.21)$$

Note that no deflection occurs until the applied force exceeds the preload force F_i that is built into the spring.

Spring Index of Extension Springs

The spring index is found from equation 14.5 and should be kept in the same range of about 4 to 12, as is recommended for compression springs.

Coil Preload in Extension Springs

The preload F_i can be controlled to some degree in the manufacturing process and should be designed to keep the initial coil stress within the preferred range shown in Figure 14-22.^[1] This shows desired ranges for initial coil stress as a function of spring index. Values outside the range are possible but are difficult to manufacture. Cubic functions have been fitted to the curves of Figure 14-22 to allow their use in a computer program. The approximate cubic expressions are shown on the figure and are

$$\tau_i \approx -4.231C^3 + 181.5C^2 - 3387C + 28640 \quad (14.22a)$$

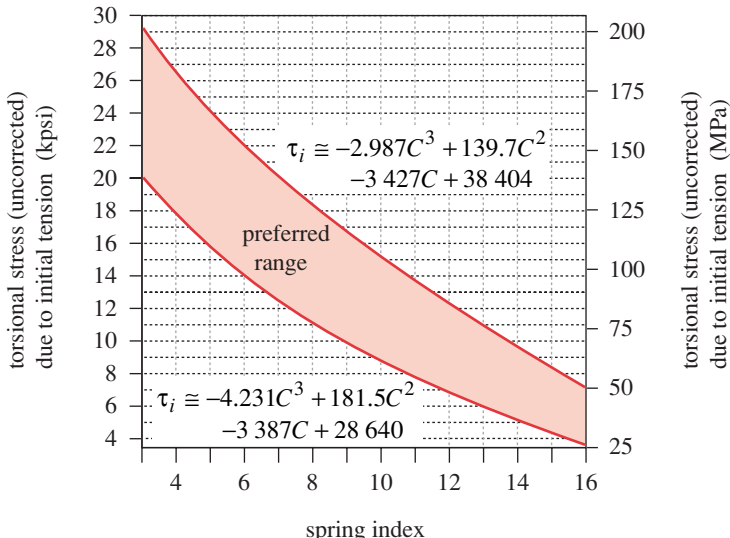


FIGURE 14-22

Preferred Range of Initial Stress in Extension Springs as a Function of Spring Index

$$\tau_i \approx -2.987C^3 + 139.7C^2 - 3427C + 38404 \quad (14.22b)$$

where τ_i is in psi. The average of the two values computed from these functions can be taken as a good starting value for initial coil stress.

Deflection of Extension Springs

Coil deflection is found from the same equation as used for the compression spring with a modification for the preload.

$$y = \frac{8(F - F_i)D^3N_a}{d^4G} \quad (14.23)$$

Coil Stresses in Extension Springs

The stresses in the coils are found from the same formulas used for compression springs. See equations 14.8 and 14.9 (p. 798). The factors K_s and K_w are used as before.

End Stresses in Extension Springs

The standard hooks or loops have two locations of high stress, as shown in Figure 14-23. The maximum torsional stress occurs at point B , where the bend radius is smallest. There is also a bending stress in the hook or loop at point A , since the end is loaded as a curved beam. Wahl also defines a stress-concentration factor K_b for bending in a curved wire.

The bending stress at point A is found from

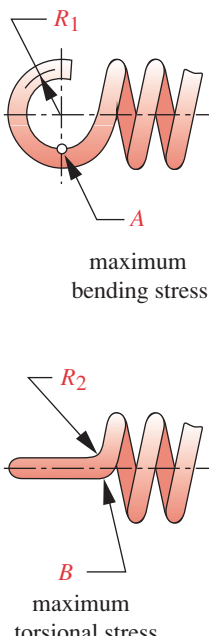


FIGURE 14-23

Points of Maximum Stress in Hook or Loop of an Extension Spring

$$\sigma_A = K_b \frac{16DF}{\pi d^3} + \frac{4F}{\pi d^2} \quad (14.24a)$$

where $K_b = \frac{4C_1^2 - C_1 - 1}{4C_1(C_1 - 1)}$ (14.24b)

and $C_1 = \frac{2R_1}{d}$ (14.24c)

R_1 is the mean loop radius, as shown in Figure 14-23. Note that for a standard end, the mean loop radius is the same as the mean coil radius.

The torsional stress at point B is found from

$$\tau_B = K_{w_2} \frac{8DF}{\pi d^3} \quad (14.25a)$$

where $K_{w_2} = \frac{4C_2 - 1}{4C_2 - 4}$ (14.25b)

and $C_2 = \frac{2R_2}{d}$ (14.25c)

R_2 is the side-bend radius, as shown in Figure 14-23. C_2 should be greater than 4.^[1]

Surging in Extension Springs

The natural frequency of a helical extension spring with both ends fixed against axial deflection is the same as that for a helical spring in compression (see equation 14.12a):

$$f_n = \frac{2}{\pi N_a} \frac{d}{D^2} \sqrt{\frac{Gg}{32\gamma}} \quad \text{Hz} \quad (14.26)$$

Material Strengths for Extension Springs

The same wire materials are used for both extension and compression springs. Some of the strength data developed for compression springs are applicable to extension springs as well. Table 14-12 shows recommended strengths for static yielding of the coil body and the ends in both torsion and bending. Note that the wire torsion strengths are the same as those for compression springs in Tables 14-8 and 14-9 (p. 803). Table 14-13 shows recommended fatigue strengths for two materials at several cycle lives, giving separate data for the body coils and the ends. The endurance limits of equation 14.13 (p. 804) are valid for extension springs and should be converted to fully reversed values with equation 14.18b (p. 814) to use in the Goodman-line safety-factor expression of equation 14.18a (p. 814).

Table 14-12 Maximum Torsional and Bending Yield Strengths S_{ys} and S_y for Helical Extension Springs in Static Applications

No Set Removal and Low-Temperature Heat Treatment Applied. Source: Ref. 1

Material	Maximum Percent of Ultimate Tensile Strength		
	S_{ys} in Torsion		S_y in Bending
	Body	End	End
Cold-drawn carbon steel (e.g., A227, A228)	45%	40%	75%
Hardened and tempered carbon and low-alloy steel (e.g., A229, A230, A232, A401)	50	40	75
Austenitic stainless steel and nonferrous alloys (e.g., A313, B134, B159, B197)	35	30	55

Design of Helical Extension Springs

The design procedure for extension springs is essentially the same as for compression springs with the additional complication of the end details. Assumptions must be made for sufficient design parameters to allow a trial computation. The assumed values are adjusted based on the result and the design iterated to an acceptable solution.

It is often convenient in extension-spring design problems to assume a spring index and a wire diameter as was done for the compression springs. The mean coil diameter can then be found from equation 14.5 (p. 797). The assumed spring index can be used with equations 14.21 (p. 821) to obtain an approximate initial coil-winding stress. Using that initial-stress value, the coil preload F_i can be computed from the stress equation 14.8 (p. 798). The coil stresses and end stresses can be found next and appropriate adjustments made to the assumed values to get acceptable safety factors.

The deflection or number of coils can be found from equation 14.23 with the other one assumed or specified. The spring rate can then be found using the maximum design force and the preload in combination with the assumed or calculated deflection using equation 14.21. Buckling is not an issue with extension springs, but the natural frequency should be compared to the forcing frequency in dynamic situations.

Table 14-13 Maximum Torsional and Bending Fatigue Strength S_{fw}' and S_{fwb}' for ASTM A228 and Type 302 Stainless Steel Wire Helical Extension Springs in Cyclic Applications (Stress Ratio, $R = 0$)

No Surging, No Shot Peening, Room Temperature, and Low Temperature Heat Treatment Applied. Source: Ref. 1

Fatigue Life (cycles)	Percent of Ultimate Tensile Strength		
	S_{fw}' in Torsion		S_{fwb}' in Bending
	Body	End	End
10^5	36%	34%	51%
10^6	33	30	47
10^7	30	28	45

The safety factors are found from equations 14.14 and 14.17 (pp. 805 and 814), being careful to use the appropriate material strength for torsion in the coils and for bending or shear in the ends. A Goodman-line analysis is needed for cyclically loaded springs, and is encapsulated in equation 14.18. A fatigue analysis is needed for the ends as well as for the coils.

EXAMPLE 14-5

Design of a Helical Extension Spring for Cyclic Loading

Problem Design an extension spring for a dynamic load over a given deflection.

Given The spring must give a minimum force of 50 lb and a maximum force of 85 lb over a dynamic deflection of 0.50 in. The forcing frequency is 500 rpm. An infinite life is desired.

Assumptions Standard hooks will be used at each end. Music wire (ASTM A228) will be used since the loads are dynamic. Setting and peening cannot be used to obtain a higher endurance strength in an extension spring.

Solution See Figure 14-24 (p. 828) and Table 14-14 (pp. 829-830).

- 1 Assume an 0.177 in trial wire diameter from the available sizes in Table 14-2 (p. 791). Assume a spring index of $C = 9$ and use it to calculate the mean coil diameter D from equation 14.5 (p. 797).

$$D = Cd = 9(0.177) = 1.59 \text{ in} \quad (a)$$

- 2 Use the assumed value of C to find an appropriate value of initial coil stress τ_i from equations 14.21 (p. 821):

$$\begin{aligned} \tau_{i_1} &\equiv -4.231C^3 + 181.5C^2 - 3387C + 28\,640 \\ &= -4.231(9)^3 + 181.5(9)^2 - 3387(9) + 28\,640 = 9\,774 \text{ psi} \end{aligned} \quad (b)$$

$$\begin{aligned} \tau_{i_2} &\equiv -2.987C^3 + 139.7C^2 - 3427C + 38\,404 \\ &= -2.987(9)^3 + 139.7(9)^2 - 3427(9) + 38\,404 = 16\,699 \text{ psi} \end{aligned} \quad (c)$$

$$\tau_i \equiv \frac{\tau_{i_1} + \tau_{i_2}}{2} = \frac{9\,774 + 16\,699}{2} = 13\,237 \text{ psi} \quad (d)$$

- 3 Find the direct shear factor:

$$K_s = 1 + \frac{0.5}{C} = 1 + \frac{0.5}{9} = 1.06 \quad (e)$$

- 4 Substitute K_s from step 3 and the value of τ_i from equation (d) of step 2 for τ_{max} in equation 14.8b (p. 798) to find the corresponding initial coil-tension force F_i :

$$F_i = \frac{\pi d^3 \tau_i}{8K_s D} = \frac{\pi(0.177)^3(13\,237)}{8(1.06)(1.59)} = 17.1 \text{ lb} \quad (f)$$

Check that this force is less than the required minimum applied force F_{min} , which in this case, it is. Any applied force smaller than F_i will not deflect the spring.

- 5 Find the mean and alternating forces from equation 14.16a (p. 812):

$$F_a = \frac{F_{max} - F_{min}}{2} = \frac{85 - 50}{2} = 17.5 \text{ lb} \quad (g)$$

$$F_m = \frac{F_{max} + F_{min}}{2} = \frac{85 + 50}{2} = 67.5 \text{ lb}$$

- 6 Use the direct shear factor K_s and previously assumed values to find the mean stress* τ_m :

$$\tau_m = K_s \frac{8F_m D}{\pi d^3} = 1.06 \frac{8(67.5)(1.59)}{\pi(0.177)^3} = 52\,122 \text{ psi} \quad (h)$$

- 7 Find the Wahl factor K_w and use it to calculate the alternating shear stress τ_a in the coil.

$$K_w = \frac{4C - 1}{4C - 4} + \frac{0.615}{C} = \frac{4(9) - 1}{4(9) - 4} + \frac{0.615}{9} = 1.16 \quad (i)$$

$$\tau_a = K_w \frac{8F_a D}{\pi d^3} = 1.16 \frac{8(17.5)(1.59)}{\pi(0.177)^3} = 14\,877 \text{ psi} \quad (j)$$

- 8 Find the ultimate tensile strength of this music-wire material from equation 14.3 and Table 14-4 (p. 792). Use it to find the ultimate shear strength from equation 14.4 and the torsional yield strength for the coil body from Table 14-12, assuming no set removal.

$$S_{ut} = Ad^b = 184\,649(0.177)^{-0.1625} = 244\,633 \text{ psi}$$

$$S_{us} = 0.667S_{ut} = 163\,918 \text{ psi} \quad (k)$$

$$S_{ys} = 0.45S_{ut} = 0.45(244\,633) = 110\,094 \text{ psi} \quad (l)$$

- 9 Find the wire endurance limit for unpeened springs from equation 14.14 (p. 805) and convert it to a fully reversed endurance strength with equation 14.18b (p. 814).

$$S_{ew} = 45\,000 \text{ psi} \quad (m)$$

$$S_{es} = 0.5 \frac{S_{ew} S_{us}}{S_{us} - 0.5S_{ew}} = 0.5 \frac{45\,000(163\,918)}{163\,918 - 0.5(45\,000)} = 26\,080 \text{ psi} \quad (n)$$

- 10 The fatigue safety factor for the coils in torsion is calculated from equation 14.18a (p. 814).

$$C_1 = \frac{2R_1}{d} = \frac{2D}{2d} = C = 9$$

$$K_b = \frac{4C_1^2 - C_1 - 1}{4C_1(C_1 - 1)} = \frac{4(9)^2 - (9) - 1}{4(9)(9 - 1)} = 1.09 \quad (p)$$

Note that the minimum stress due to force F_{min} is used in this calculation, **not** the coil-winding stress from equation (d).

* The direct shear factor K_s is used rather than the Wahl factor for the mean stress calculation because the stress-concentration factor is considered to be 1.0 for mean stress.

- 11 The stresses in the end hooks also need to be determined. The bending stresses in the hook are found from equation 14.24 (p. 823):

$$C_1 = \frac{2R_1}{d} = \frac{2D}{2d} = C = 9$$

$$K_b = \frac{4C_1^2 - C_1 - 1}{4C_1(C_1 - 1)} = \frac{4(9)^2 - (9) - 1}{4(9)(9 - 1)} = 1.09 \quad (p)$$

$$\sigma_a = K_b \frac{16DF_a}{\pi d^3} + \frac{4F_a}{\pi d^2} = 1.09 \frac{16(1.59)(17.5)}{\pi(0.177)^3} + \frac{4(17.5)}{\pi(0.177)^2} = 28\,626 \text{ psi} \quad (q)$$

$$\sigma_m = K_b \frac{16DF_m}{\pi d^3} + \frac{4F_m}{\pi d^2} = 1.09 \frac{16(1.59)(67.5)}{\pi(0.177)^3} + \frac{4(67.5)}{\pi(0.177)^2} = 110\,416 \text{ psi}$$

$$\sigma_{min} = K_b \frac{16DF_{min}}{\pi d^3} + \frac{4F_{min}}{\pi d^2} = 1.09 \frac{16(1.59)(50)}{\pi(0.177)^3} + \frac{4(50)}{\pi(0.177)^2} = 81\,790 \text{ psi} \quad (r)$$

- 12 Convert the torsional endurance strength to a tensile endurance strength with equation 14.4 (p. 793) and use it and the ultimate tensile strength from step 8 in equation 14.18 (p. 814) to find a fatigue safety factor for the hook in bending:

$$S_e = \frac{S_{es}}{0.67} = \frac{26\,080}{0.67} = 38\,925 \text{ psi}$$

$$N_{f_b} = \frac{S_e(S_{ut} - \sigma_{min})}{S_e(\sigma_{mean} - \sigma_{min}) + S_{ut}\sigma_{alt}}$$

$$= \frac{38\,925(244\,633 - 81\,790)}{38\,925(110\,416 - 81\,790) + 244\,633(28\,626)} = 0.78 \quad (s)$$

- 13 The torsional stresses in the hook are found from equation 14.25 (p. 823) using an assumed value of $C_2 = 5$.

$$R_2 = \frac{C_2 d}{2} = \frac{5(0.177)}{2} = 0.44 \text{ in}$$

$$K_{w_2} = \frac{4C_2 - 1}{4C_2 - 4} = \frac{4(5) - 1}{4(5) - 4} = 1.2 \quad (t)$$

$$\tau_{B_a} = K_{w_2} \frac{8DF_a}{\pi d^3} = 1.19 \frac{8(1.59)17.5}{\pi(0.177)^3} = 15\,202 \text{ psi}$$

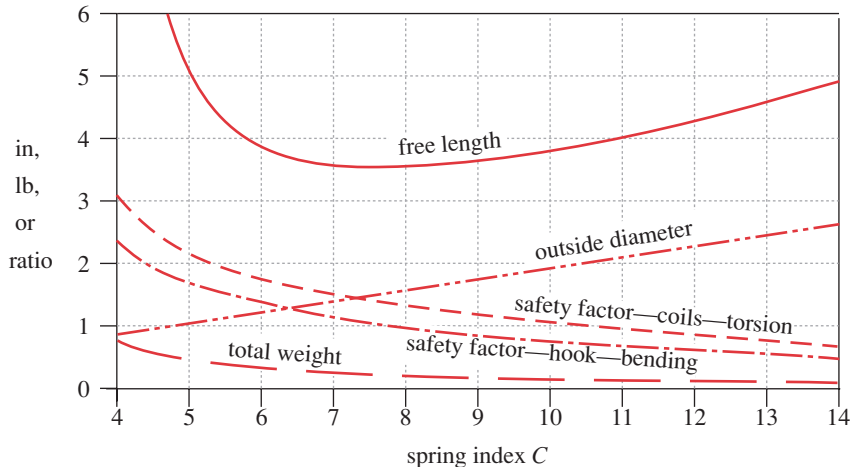
$$\tau_{B_m} = K_{w_2} \frac{8DF_m}{\pi d^3} = 1.19 \frac{8(1.59)67.5}{\pi(0.177)^3} = 58\,637 \text{ psi} \quad (u)$$

$$\tau_{B_{min}} = K_{w_2} \frac{8DF_{min}}{\pi d^3} = 1.19 \frac{8(1.59)50}{\pi(0.177)^3} = 43\,435 \text{ psi}$$

- 14 The hook's fatigue safety factor in torsion is calculated from equation 14.18a (p. 814).

$$N_{f_s} = \frac{S_{es}(S_{us} - \tau_{min})}{S_{es}(\tau_m - \tau_{min}) + S_{us}\tau_a}$$

$$= \frac{26\,080(163\,918 - 43\,435)}{26\,080(58\,637 - 43\,435) + 163\,918(15\,202)} = 1.1 \quad (v)$$

**FIGURE 14-24**

Variation of Helical Extension-Spring Parameters with Spring Index—Constant Wire Diameter

- 15 One of these safety factors is less than 1, making this an unacceptable design. To get some idea of what to change to improve it, the model was solved for a list of values of the spring index from 4 to 14, keeping all other parameters as defined above. The resulting values of coil diameter, free length, spring weight, and fatigue safety factor are plotted in Figure 14-24.

The safety factors decrease with increasing spring index, so a reduction in our assumed value for C will improve the design even with no change in wire diameter. Note, however, that the spring free length shows a minimum value at a spring index of about 7.5. The coil diameter increases linearly with the spring index for a constant wire diameter. Spring weight decreases with increasing spring index.

If we decrease the spring index from 9 to 7.5, and increase the wire diameter one size to 0.192 in, keeping all other parameters the same, we will obtain an acceptable design in this case with the smallest $N_f = 1.2$ for the hook in bending.

- 16 Table 14-14 shows the complete results for this new design. A summary of the new design is

$$\begin{array}{llll} C = 7.5 & D = 1.44 \text{ in} & K_w = 1.20 & K_s = 1.07 \\ \tau_i = 15\,481 \text{ psi} & \tau_{min} = 27\,631 \text{ psi} & \tau_a = 10\,856 \text{ psi} & \tau_m = 37\,302 \text{ psi } (w) \\ N_{s_{coil}} = 2.3 & N_{f_{s_{coil}}} = 1.8 & N_{f_{s_{hook}}} = 1.7 & N_{f_{b_{hook}}} = 1.2 \end{array}$$

The spring design can now be completed based on the new wire diameter and spring index from step 15.

- 17 The spring rate is defined from the two specified forces at their relative deflection.

$$k = \frac{\Delta F}{y} = \frac{85 - 50}{0.5} = 70 \text{ lb/in} \quad (x)$$

- 18 To get the defined spring rate, the number of active coils must satisfy equation 14.7 (p. 797):

Table 14-14a Example 14-5—Design of a Helical Extension Spring for Cyclic Loads

Part 1 of 2

Input	Variable	Output	Unit	Comments
500	<i>fn</i>		rpm	excitation frequency
7.50	<i>C</i>			trial spring index
0.192	<i>d</i>		in	trial wire diameter (List Function)
0.50	<i>y</i>		in	deflection bet Fmin & Fmax
	<i>ymax</i>	0.81	in	maximum deflection at Fmax
	<i>ymin</i>	0.31	in	minimum deflection at Fmin
'music	<i>matl</i>			'music, 'oiltemp, 'hdrawn, etc.
85	<i>Fmax</i>		lb	maximum applied force
50	<i>Fmin</i>		lb	minimum applied force
	<i>Finit</i>	28.01	lb	force from initial tension
	<i>Flow</i>	50.00	lb	lowest applied force on spring
	<i>Falt</i>	17.50	lb	alternating force
	<i>Fmean</i>	67.50	lb	mean force
	<i>k</i>	70.70	lb/in	spring rate with <i>N_a</i> rounded
	<i>N</i>	9.35		no. of active coils—exact
	<i>Na</i>	9.25		no. of active coils—nearest 1/4 coil
	<i>Ntot</i>	10.25		no. of total coils
	<i>D</i>	1.44	in	mean coil diameter
	<i>Dout</i>	1.63	in	outside coil diameter
	<i>Din</i>	1.25	in	inside coil diameter
	<i>Ks</i>	1.07		static factor—Eq. 13.8
	<i>Kw</i>	1.20		Wahl factor—Eq. 13.9
	<i>tauinit</i>	15 481	psi	shear stress from initial tension
	<i>taumin</i>	27 631	psi	shear stress at Fmin
	<i>taumax</i>	46 973	psi	shear stress at Fmax
	<i>taualt</i>	10 856	psi	alternating shear stress for fatigue
	<i>taumean</i>	37 302	psi	mean shear stress for fatigue
	<i>Sut</i>	241 441	psi	tensile strength—Eq. 13.3 & Table 13-4
	<i>Sus</i>	161 765	psi	ultimate shear strength—Eq. 13.4
	<i>Ssy</i>	108 648	psi	shear yield based on Table 13-10
	<i>Ssyh</i>	96 576	psi	shear yield in hook—Table 13-10
	<i>Sew</i>	45 000	psi	wire endurance limit—Eq. 13.12
	<i>Ses</i>	26 135	psi	fully reversed endr. limit—Eq. 13.16b
	<i>Sy</i>	181 081	psi	yield strength in bending
	<i>Se</i>	39 008	psi	endurance limit in tension

$$k = \frac{d^4 G}{8D^3 N_a} \quad \text{or} \quad N_a = \frac{d^4 G}{8D^3 k} = \frac{(0.192)^4 11.5E6}{8(1.44)^3 (70)} = 9.35 \equiv 9\frac{1}{4} \quad (\text{y})$$

Table 14-14b Example 14-5—Design of a Helical Extension Spring for Cyclic Loads

Part 2 of 2

Input	Variable	Output	Unit	Comments
	N_f	1.8		SF coils—fatigue—Eq. 13.14
	N_s	2.3		SF coils—static loading at Fmax
	N_{fht}	1.7		SF hook—torsion fatigue
	N_{sht}	1.8		SF hook—torsional yielding
	N_{fhs}	1.2		SF hook—bending fatigue
	N_{shs}	1.8		SF hook—bending yielding
	L_{body}	1.97	in	length of coil body
	$hook1$	1.25	in	length of hook on one end
	$hook2$	1.25	in	length of hook on other end
	L_f	4.46	in	free length inside hooks
	W_{total}	0.38	lb	weight of total coils—Eq. 13-11b
	n_f	140.7	Hz	natural frequency in Hz
	c_{rpm}	8 440	rpm	natural frequency in rpm
	$FreqFac$	16.9		ratio—nat. freq. to forcing freq.
5.00	C_2			should be set > 4
	R_2	0.48	in	side bend radius at hook root
	K_{hook}	1.19		K factor for hook in torsion
	$t_{maxhook}$	52 294	psi	maximum torsional stress in hook
	$t_{minhook}$	30 761	psi	minimum torsional stress in hook
	$t_{althook}$	10 766	psi	alternating torsional stress in hook
	t_{mnhook}	41 528	psi	mean torsional stress in hook
	C_1	7.50		spring index for hook

Note that we round it to the nearest 1/4 coil, as the manufacturing tolerance cannot achieve better than that accuracy. This makes the spring rate $k = 70.7 \text{ lb/in}$.

- 19 The total number of coils in the body and the body length are

$$N_t = N_a + 1 = 9.25 + 1 = 10.25 \quad (z)$$

$$L_b = N_t d = 10.25(0.192) = 1.97 \text{ in}$$

- 20 The free length can now be determined. The length of a standard hook is equal to the coil inside diameter:

$$L_f = L_b + 2L_{hook} = 1.97 + 2(1.25) = 4.46 \text{ in} \quad (aa)$$

- 21 The deflection to reach the larger of the two specified loads is

$$y_{max} = \frac{F_{max} - F_{initial}}{k} = \frac{85 - 28}{70.7} = 0.81 \text{ in} \quad (ab)$$

- 22 The natural frequency of this spring is found from equation 14.26 (p. 823) and is

$$f_n = \frac{2}{\pi N_a} \frac{d}{D^2} \sqrt{\frac{Gg}{32\gamma}} = \frac{2(0.192)}{\pi(9.25)(1.44)^2} \sqrt{\frac{11.5E6(386)}{32(0.285)}} = 140.6 \text{ Hz} = 8436 \text{ rpm} \quad (ac)$$

The ratio between the natural frequency and the forcing frequency is

$$\frac{8440}{500} = 16.9 \quad (ad)$$

which is sufficiently high.

- 23 The design specification for this A228 wire spring is

$$d = 0.192 \text{ in} \quad OD = 1.63 \text{ in} \quad N_t = 10.25 \quad L_f = 4.46 \quad (ae)$$

- 24 The results are shown in Table 14-14. The files EX14-05 are on the CD-ROM. There are also alternate approaches to the solution of this example shown in separate Mathcad and TK Solver files on the CD-ROM with a letter added to their name.
-

14.8 HELICAL TORSION SPRINGS

A helical coil spring can be loaded in torsion instead of compression or tension and is then called a **torsion spring**. The ends of the coil are extended tangentially to provide lever arms on which to apply the moment load, as shown in Figure 14-25. These coil ends can have a variety of shapes to suit the application. The coils are usually close-wound like an extension spring but do not have any initial tension. The coils can also be wound with spacing like a compression spring and this will avoid friction between the coils. However, most torsion springs are close-wound.

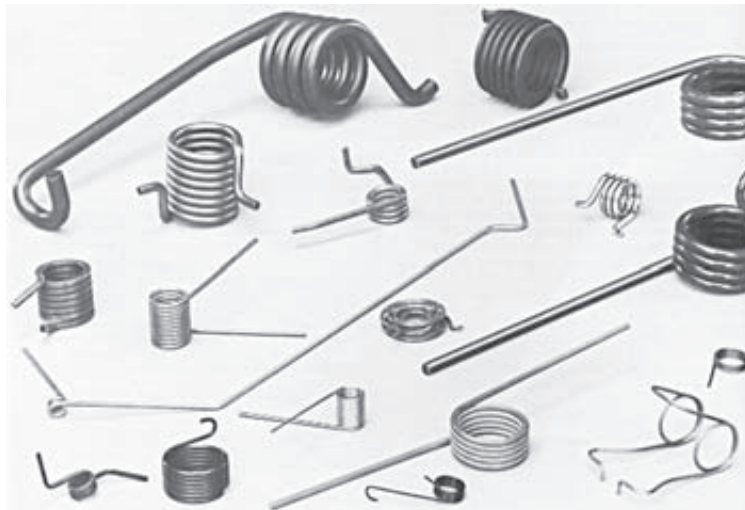
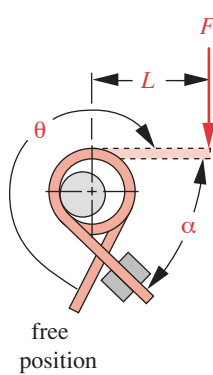
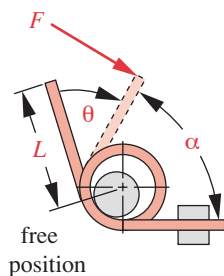


FIGURE 14-25

A Variety of End Details Is Possible on Helical Torsion Springs Courtesy of Associated Spring, Barnes Group Inc., Bristol, Conn.


specify:

- α —angle between ends
- F —load on ends at α
- L —moment arm
- θ —angular deflection from free position

FIGURE 14-26

Specifying Load and Deflection Requirements for Torsion Springs.
Source: Reference 1

The applied moment on the coils puts the wire in bending as a curved beam, as shown in Figure 14-26. The applied moment should always be arranged to close the coils rather than open them because the residual stresses from coil-winding are favorable against a closing moment. The applied moment should never be reversed in service. Dynamic loading should be repeated or fluctuating with the stress ratio $R \geq 0$.

Radial support must be provided at three or more points on the coil diameter to take the reaction forces. This support is usually accomplished by means of a rod placed inside the coil. The rod should be no larger in diameter than about 90% of the coil's smallest inside diameter when "wound-up" under load in order to avoid binding.

The manufacturing specifications of a torsion spring should define the parameters indicated in Figure 14-26 as well as wire diameter, outside coil diameter, number of coils, and spring rate. The load should be defined at an angle α between the tangent ends in the loaded position rather than at a deflection from the free position.

Because the load is bending, rectangular wire is more efficient in terms of stiffness per unit volume (larger I for same dimension). Nevertheless, most helical torsion springs are made from round wire simply because of its lower cost and the greater variety of available sizes and materials.

Terminology for Torsion Springs

The following parameters have the same meaning for torsion springs as for helical compression springs: mean coil diameter D , wire diameter d , spring index C , outside diameter D_o , inside diameter D_i , and number of active coils N_a . The spring rate k is expressed as moment per unit of angular deflection.

Number of Coils in Torsion Springs

The active coils are equal to the number of body turns N_b plus some contribution from the ends, which also bend. For straight ends, the contribution can be expressed as an equivalent number of coils N_e :

$$N_e = \frac{L_1 + L_2}{3\pi D} \quad (14.27a)$$

where L_1 and L_2 are the respective lengths of the tangent-ends of the coil. The number of active coils is then

$$N_a = N_b + N_e \quad (14.27b)$$

where N_b is the number of coils in the spring body.

Deflection of Torsion Springs

The angular deflection of the coil-end is normally expressed in radians but is often converted to revolutions. We will use revolutions. Since it is essentially a beam in bending, the (angular) deflection can be expressed as

$$\theta_{rev} = \frac{1}{2\pi} \theta_{rad} = \frac{1}{2\pi} \frac{ML_w}{EI} \quad (14.28a)$$

where M is the applied moment, L_w is the length of wire, E is Young's modulus for the material, and I is the second moment of area for the wire cross section about the neutral axis.

For torsion springs of round wire, we can substitute the appropriate geometry to get

$$\begin{aligned}\theta_{rev} &= \frac{ML_w}{EI} = \frac{1}{2\pi} \frac{M(\pi DN_a)}{E(\pi d^4/64)} \\ &= \frac{64}{2\pi} \frac{MDN_a}{d^4 E} \\ \theta_{rev} &\cong 10.2 \frac{MDN_a}{d^4 E}\end{aligned}\quad (14.28b)$$

The factor 10.2 is usually increased to 10.8 to account for the friction between coils, based on experience, and the equation becomes^[1]

$$\theta_{rev} \cong 10.8 \frac{MDN_a}{d^4 E} \quad (14.28c)$$

Spring Rate of Torsion Springs

The spring rate can always be obtained from the deflection formula:

$$k = \frac{M}{\theta_{rev}} \cong \frac{d^4 E}{10.8 DN_a} \quad (14.29)$$

Coil Closure

When a torsion spring is loaded to close the coils (as it should be), the coil diameter decreases and its length increases as the coil is “wound up.” The minimum inside coil diameter at full deflection is

$$D_{i_{min}} = \frac{DN_b}{N_b + \theta_{rev}} - d \quad (14.30)$$

where D is the unloaded mean coil diameter. Any pin that the coil works over should be limited to about 90% of this minimum inside diameter.

The maximum coil-body length at full “windup” is:

$$L_{max} = d(N_b + 1 + \theta) \quad (14.31)$$

Coil Stresses in Torsion Springs

The stress in the outer fiber of a straight beam is $M c / I$, but this is a curved beam, and we learned in Section 4.9 (p. 154) that stress is concentrated at the inside of a curved beam. Wahl^[3] derived the stress-concentration factor for the inside of a coiled round wire in bending as

$$K_{b_i} = \frac{4C^2 - C - 1}{4C(C - 1)} \quad (14.32a)$$

and at the outside of the coil

$$K_{b_o} = \frac{4C^2 + C - 1}{4C(C + 1)} \quad (14.32b)$$

where C is the spring index.

The maximum compressive bending stress at the inside coil diameter of a round-wire helical torsion spring (loaded to close its coils) is then

$$\sigma_{i_{max}} = K_{b_i} \frac{M_{max}c}{I} = K_{b_i} \frac{M_{max}(d/2)}{\pi d^4/64} = K_{b_i} \frac{32M_{max}}{\pi d^3} \quad (14.33a)$$

and the tensile bending stress components at the outside coil diameter are

$$\sigma_{o_{min}} = K_{b_o} \frac{32M_{min}}{\pi d^3}; \quad \sigma_{o_{max}} = K_{b_o} \frac{32M_{max}}{\pi d^3} \quad (14.33b)$$

$$\sigma_{o_{mean}} = \frac{\sigma_{o_{max}} + \sigma_{o_{min}}}{2}; \quad \sigma_{o_{alt}} = \frac{\sigma_{o_{max}} - \sigma_{o_{min}}}{2} \quad (14.33c)$$

Note that for static failure (yielding) of a torsion spring loaded to close its coils, the higher-magnitude compressive stress $\sigma_{i_{max}}$ at the inside of the coil is of most concern, but for fatigue failure, which is a tensile-stress phenomenon, the slightly lower maximum tensile stress at the outside of the coils is the concern. Thus the alternating and mean stress components are calculated at the outside of the coil. If the spring is loaded to open the coils (which is not recommended), it must be stress relieved to eliminate the residual stresses from coiling, and then the inside coil stress should be used to calculate the components for the fatigue safety-factor calculation.

Material Parameters for Torsion Springs

Yield and endurance strengths in bending are needed in this instance. Table 14-15 shows suggested yield strengths for several wire materials as a percentage of their ultimate tensile strength. Note that favorable residual stresses allow the material's ultimate strength to be used as a yield criterion in some cases. Table 14-16 shows bending-fatigue-strength percentages for several wires at 10^5 and 10^6 cycles in both peened and unpeened states. The same limitations on effective shot peening apply to close-wound torsion springs as to extension springs, since the closely spaced coils prevent the shot from impacting the inside diameter of the coil. Shot peening may not be effective in many torsion springs.

The torsional-endurance limit data for helical compression springs shown in equation 14.13 (p. 804) can be adapted for bending by using the von Mises relationship between torsion and tension loading.

$$S_{ew_b} = \frac{S_{ew}}{0.577} \quad (14.34a)$$

Table 14-15 Maximum Recommended Bending Yield Strength S_y for Helical Torsion Springs in Static Applications

Source: Adapted from Reference 1

Material	Maximum Percent of Ultimate Tensile Strength	
	Stress Relieved	Favorable Residual Stress
Cold-drawn carbon steel (e.g., A227, A228)	80%	100%
Hardened and tempered carbon and low-alloy steel (e.g., A229, A230, A232, A401)	85	100
Austenitic stainless steel and nonferrous alloys (e.g., A313, B134, B159, B197)	60	80

which gives

$$S_{ew_b} \equiv \frac{45.0}{0.577} = 78 \text{ kpsi (537 MPa)} \quad \text{for unpeened springs} \quad (14.34b)$$

$$S_{ew_b} \equiv \frac{67.5}{0.577} = 117 \text{ kpsi (806 MPa)} \quad \text{for peened springs}$$

Safety Factors for Torsion Springs

Failure in yielding is anticipated at the inside coil surface, and the safety factor can be found from

$$N_y = \frac{S_y}{\sigma_{i_{max}}} \quad (14.35a)$$

Note that the available fatigue and endurance data are for a repeated-stress situation (equal mean and alternating components) and so must be converted to fully reversed values before being used to calculate the safety factor in fatigue with equations 14.17. Because the bending notation is slightly different, we repeat equations 14.17 here with the appropriate substitutions of variables for the torsion spring case.

$$N_{f_b} = \frac{S_e(S_{ut} - \sigma_{o_{min}})}{S_e(\sigma_{o_{mean}} - \sigma_{o_{min}}) + S_{ut}\sigma_{o_{alt}}} \quad (14.35b)$$

Table 14-16 Maximum Recommended Bending Fatigue Strength S_{fw} ' for Helical Torsion Springs in Cyclic Applications (Stress Ratio, R = 0)

Stress Relieved, No Surging—Shot Peening May Not be Possible in All Cases.
Source: Reference 1

Fatigue Life (cycles)	Percent of Ultimate Tensile Strength			
	ASTM A228 or 302 Stainless		ASTM A230 and A232	
	Unpeened	Shot peened	Unpeened	Shot peened
10^5	53%	62%	55%	64%
10^6	50	60	53	62

$$S_e = 0.5 \frac{S_{ew_b} S_{ut}}{S_{ut} - 0.5 S_{ew_b}} \quad (14.35c)$$

Designing Helical Torsion Springs

The process for designing helical torsion springs is very similar to that for helical compression springs. The best way to illustrate it is with an example.

EXAMPLE 14-6

Design of a Helical Torsion Spring for Cyclic Loading

Problem Design a torsion spring for a dynamic load over a given deflection.

Given The spring must give a minimum moment of 50 lb-in and a maximum moment of 80 lb-in over a dynamic deflection of 0.25 revolutions (90°). An infinite life is desired.

Assumptions Use unpeened music wire (ASTM A228). Use 2-in-long straight tangent ends. The coil is loaded to close it.

Solution See Figure 14-27.

- 1 Assume a 0.192-in trial wire diameter from the available sizes in Table 14-2 (p. 791). Assume a spring index of $C = 9$ and use it to calculate the mean coil diameter D from equation 14.5 (p. 797).

$$D = Cd = 9(0.192) = 1.73 \text{ in} \quad (a)$$

- 2 Find the mean and alternating moments:

$$M_m = \frac{M_{max} + M_{min}}{2} = \frac{80 + 50}{2} = 65 \text{ lb} \quad (b)$$

$$M_a = \frac{M_{max} - M_{min}}{2} = \frac{80 - 50}{2} = 15 \text{ lb}$$

- 3 Find the Wahl bending factor for the inside surface K_{bi} and use it to calculate the maximum compressive stress in the coil at the inner surface.

$$K_{bi} = \frac{4C^2 - C - 1}{4C(C - 1)} = \frac{4(9)^2 - 9 - 1}{4(9)(9 - 1)} = 1.090 \quad (c)$$

$$\sigma_{i_{max}} = K_{bi} \frac{32M_{max}}{\pi d^3} = 1.09 \frac{32(80)}{\pi(0.192)^3} = 125,523 \text{ psi} \quad (d)$$

- 4 Find the Wahl bending factor K_{bo} for the outside surface and calculate the maximum, minimum, alternating, and mean tensile stresses in the coil at the outer surface.

$$K_{bo} = \frac{4C^2 + C - 1}{4C(C + 1)} = \frac{4(9)^2 + 9 - 1}{4(9)(9 + 1)} = 0.9222 \quad (e)$$

$$\sigma_{o_{min}} = K_{b_o} \frac{32M_{min}}{\pi d^3} = 0.9222 \frac{32(50)}{\pi(0.192)^3} = 66\ 359 \text{ psi} \quad (f)$$

$$\sigma_{o_{max}} = K_{b_o} \frac{32M_{max}}{\pi d^3} = 0.9222 \frac{32(80)}{\pi(0.192)^3} = 106\ 175 \text{ psi}$$

$$\sigma_{o_{mean}} = \frac{\sigma_{o_{max}} + \sigma_{o_{min}}}{2} = \frac{66\ 359 + 106\ 175}{2} = 86\ 267 \quad (g)$$

$$\sigma_{o_{alt}} = \frac{\sigma_{o_{max}} - \sigma_{o_{min}}}{2} = \frac{66\ 359 - 106\ 175}{2} = 19\ 908$$

- 5 Find the ultimate tensile strength of this music-wire material from equation 14.3 and Table 14-4 (p. 792) and use it to find the bending yield strength for the coil body from Table 14-15, assuming no stress relieving.

$$S_{ut} = Ad^b = 184\ 649(0.192)^{-0.1625} = 241\ 441 \text{ psi} \quad (h)$$

$$S_y = 1.0S_{ut} = 241\ 441 \text{ psi} \quad (i)$$

- 6 Find the wire bending endurance limit for unpeened springs from equation 14.34 and convert it to a fully reversed bending endurance strength with equation 14.35b.

$$S_{ew_b} \approx \frac{45\ 000}{0.577} = 77\ 990 \text{ psi} \quad (j)$$

$$S_e = 0.5 \frac{S_{ew_b} S_{ut}}{S_{ut} - 0.5S_{ew_b}} = 0.5 \frac{77\ 990(241\ 441)}{241\ 441 - 0.5(77\ 990)} = 46\ 506 \text{ psi} \quad (k)$$

- 7 The fatigue safety factor for the coils in bending is calculated from equation 14.35a.

$$\begin{aligned} N_{f_b} &= \frac{S_e(S_{ut} - \sigma_{o_{min}})}{S_e(\sigma_{o_{mean}} - \sigma_{o_{min}}) + S_{ut}\sigma_{o_{alt}}} \\ &= \frac{46\ 506(241\ 441 - 66\ 359)}{46\ 506(86\ 267 - 66\ 359) + 241\ 441(19\ 908)} = 1.4 \end{aligned} \quad (l)$$

- 8 The static safety factor against yielding is

$$N_{y_b} = \frac{S_y}{\sigma_{i_{max}}} = \frac{241\ 441}{125\ 523} = 1.9 \quad (m)$$

These are both acceptable safety factors.

- 9 The spring rate is defined from the two specified moments at their relative deflection.

$$k = \frac{\Delta M}{\theta} = \frac{80 - 50}{0.25} = 120 \text{ lb-in/rev} \quad (n)$$

- 10 To get the defined spring rate, the number of active coils must satisfy equation 14.29:

$$k = \frac{d^4 E}{10.8DN_a} \quad \text{or} \quad N_a = \frac{d^4 E}{10.8Dk} = \frac{(0.192)^4 30E6}{10.8(1.73)(120)} = 18.2 \quad (o)$$

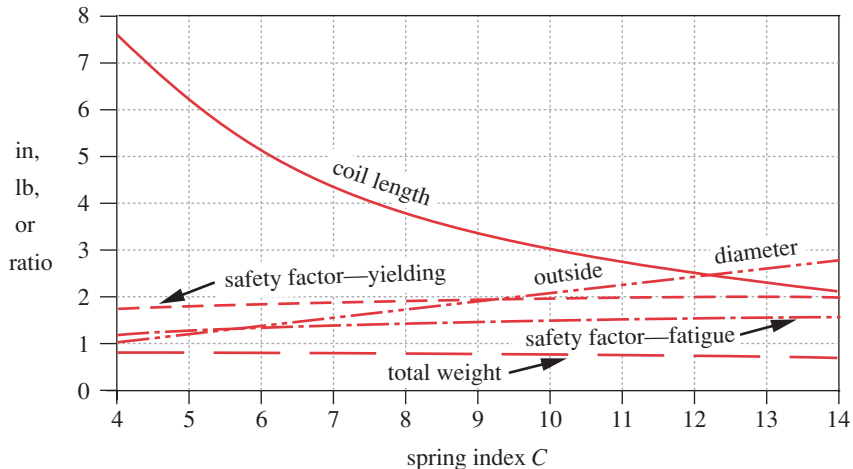


FIGURE 14-27

Variation of Helical Torsion Spring Parameters with Spring Index - Constant Wire Diameter

The ends contribute to the active coils as

$$N_e = \frac{L_1 + L_2}{3\pi D} = \frac{2+2}{3\pi(1.73)} = 0.25 \quad (p)$$

and the number of body coils in the spring is

$$N_b = N_a - N_e = 18.2 - 0.25 \approx 18 \quad (q)$$

11 The angular deflections at the specified loads from equation 14.28c are

$$\theta_{min} \approx 10.8 \frac{M_{min} DN_a}{d^4 E} = 10.8 \frac{50(1.73)(18.2)}{(0.192)^4 (30E6)} = 0.417 \text{ rev} = 150 \text{ deg} \quad (r)$$

$$\theta_{max} \approx 10.8 \frac{M_{max} DN_a}{d^4 E} = 10.8 \frac{80(1.73)(18.2)}{(0.192)^4 (30E6)} = 0.667 \text{ rev} = 240 \text{ deg} \quad (s)$$

12 The files EX14-06 can be found on the CD-ROM.

In the interest of brevity, only a single successful solution to the above example is shown. However, just as in the preceding examples, it was necessary to iterate through some unsuccessful ones to get to it. The trends in coil length, outside diameter, static and fatigue safety factors, and spring weight of a torsion spring as a function of its spring index are shown in Figure 14-27. Unlike compression and extension springs, safety factors for torsion springs increase with the spring index.

14.9 BELLEVILLE SPRING WASHERS*

* Additional design information on Belleville washers can be found at <http://spiro.com>

Belleville washers (also called disc springs), patented in France by J. F. Belleville in 1867, have a nonlinear force-deflection characteristic which makes them very useful in

**FIGURE 14-28**

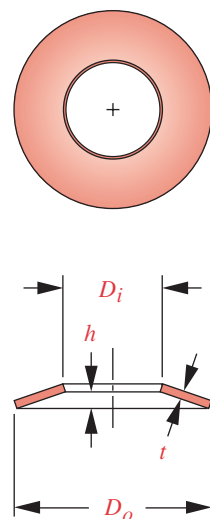
Commercially Available Belleville Washers Courtesy of Associated Spring, Barnes Group Inc., Bristol, Conn.

certain applications. A selection of commercial Belleville washers is shown in Figure 14-28. Their cross section is a coned shape with a material thickness t and inside height of cone h , as shown in Figure 14-29. They are extremely compact and are capable of large push forces, but their deflections are limited. If they are placed on a flat surface, their maximum deflection is h , which puts them in the “flat” condition, and they should be operated only between about 15% and 85% of the deflection to flat. We will later show how they can be deflected beyond the flat position to achieve some interesting effects. These springs are used where high loads over small deflections are needed in compact spaces such as metal-forming die-stripper pins, gun recoil mechanisms, etc. In their zero-spring-rate (constant force) form, they are used to load clutches and seals, which need a uniform load over a small deflection.

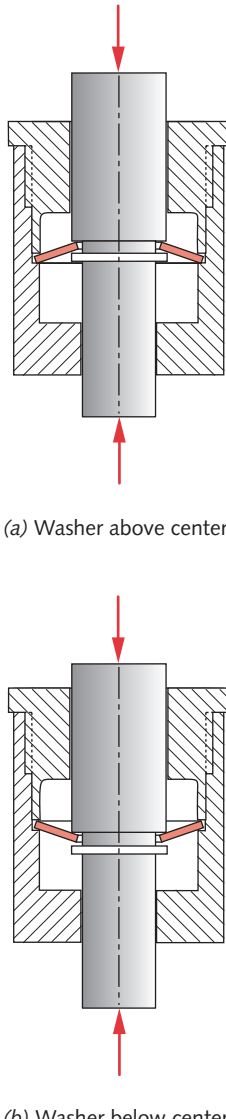
The ratio of D_o to D_i , called R_d , affects their behavior. At about $R_d = 2$ the spring has maximum energy-storage capacity. Depending on the h / t ratio, the spring rate can be essentially linear, can increase or decrease with increasing deflection, or can be essentially constant over a portion of the deflection.

Figure 14-30 shows force-deflection curves for Belleville washers with h / t ratios ranging from 0.4 to 2.8. These curves are normalized on both axes to the spring’s condition when compressed flat. Zero deflection and force are taken at the free position as shown in Figure 14-29. One hundred percent deflection represents the flat condition, and 100% force represents the force of that spring at the flat condition. The absolute values of force and deflection will vary with the h / t ratio, thickness t , and material.

At $h / t = 0.4$, the spring rate is close to linear and resembles a helical spring’s curve. As h / t is increased above 0.4, the rate becomes increasingly nonlinear, and at $h / t = 1.414$ the curve has a portion of nearly constant value, centered around the flat position. Its force deviates less than $\pm 1\%$ of the force value at 100% deflection over the range of 80% to 120% of the deflection-to-flat and is within $\pm 10\%$ over 55% to 145% of deflection-to-flat, as shown in Figure 14-31.

**FIGURE 14-29**

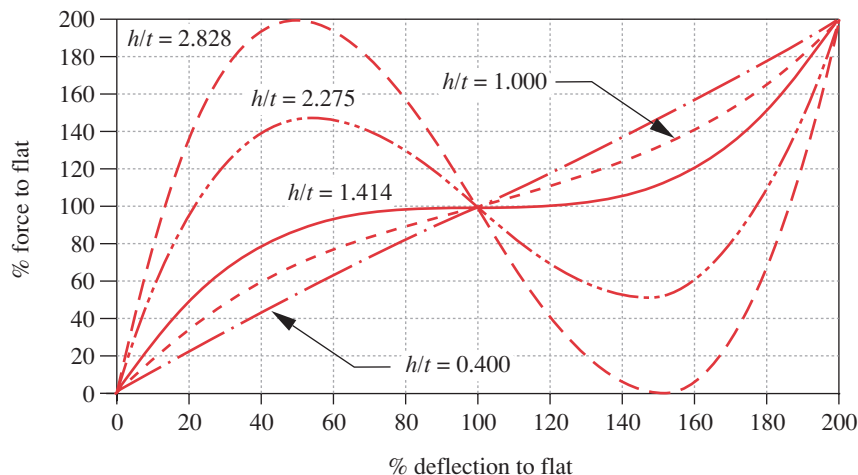
A Belleville Spring Washer



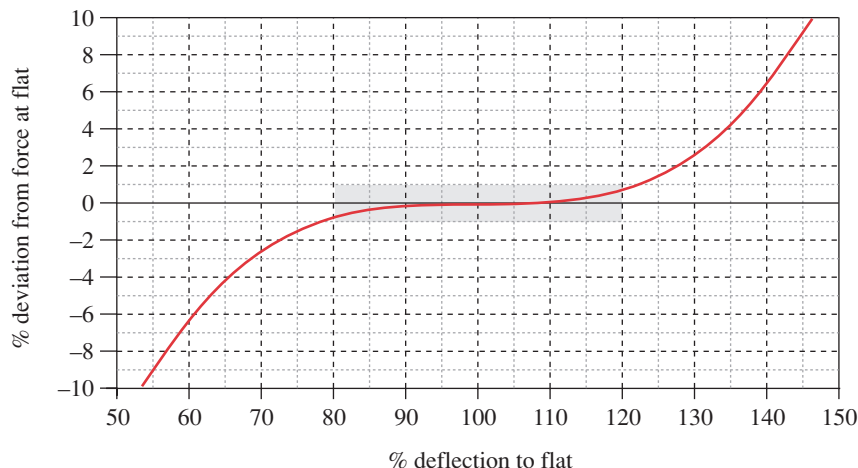
14

FIGURE 14-32

Mounting a Belleville Spring Washer to Allow Deflection Past the Flat Position

**FIGURE 14-30**

Normalized Force-Deflection Characteristics of Belleville Springs for Various h / t Ratios.

**FIGURE 14-31**

Percent Error in a Constant-Force Belleville Spring Around Its Flat Position ($R_d = 2.0$, $h / t = 1.414$)

At h / t ratios above 1.414, the curve becomes bimodal. A given applied force corresponds to more than one possible deflection. If such a spring is mounted to allow it to go beyond the flat condition as shown in Figure 14-32, it will be bistable, requiring a force in either direction to trip it past center. The mounting technique shown in Figure 14-32 is also useful for springs of smaller h / t ratios, as it allows twice the potential deflection and can use the entire constant-force section of a 1.414 h / t ratio spring.

Load-Deflection Function for Belleville Washers

The load-deflection relationship is nonlinear, so we cannot state it as a spring rate. It can be calculated from

$$F = \frac{4Ey}{K_1 D_o^2 (1 - v^2)} \left[(h - y) \left(h - \frac{y}{2} \right) t + t^3 \right] \quad (14.36a)$$

where $K_1 = \frac{6}{\pi \ln R_d} \left[\frac{(R_d - 1)^2}{R_d^2} \right]$ and $R_d = \frac{D_o}{D_i}$ (14.36b)

The load at the flat position ($y = h$) is

$$F_{flat} = \frac{4Eht^3}{K_1 D_o^2 (1 - v^2)} \quad (14.36c)$$

The curves in Figure 14-30 were generated with these equations.

Stresses in Belleville Washers

The stresses are not uniformly distributed in the washer but are concentrated at the edges of inside and outside diameters, as shown in Figure 14-33. The largest stress σ_c occurs at the inside radius on the convex side and is compressive. The edges on the concave side have tensile stresses, with the outside edge stress σ_{t_o} usually larger than the inside edge stress σ_{t_i} . The expressions for stresses at the locations defined in Figure 14-33 are

$$\sigma_c = -\frac{4Ey}{K_1 D_o^2 (1 - v^2)} \left[K_2 \left(h - \frac{y}{2} \right) + K_3 t \right] \quad (14.37a)$$

$$\sigma_{t_i} = \frac{4Ey}{K_1 D_o^2 (1 - v^2)} \left[-K_2 \left(h - \frac{y}{2} \right) + K_3 t \right] \quad (14.37b)$$

$$\sigma_{t_o} = \frac{4Ey}{K_1 D_o^2 (1 - v^2)} \left[K_4 \left(h - \frac{y}{2} \right) + K_5 t \right] \quad (14.37c)$$

where $K_2 = \frac{6}{\pi \ln R_d} \left(\frac{R_d - 1}{\ln R_d} - 1 \right)$ and $R_d = \frac{D_o}{D_i}$ (14.37d)

$$K_3 = \frac{6}{\pi \ln R_d} \left(\frac{R_d - 1}{2} \right) \quad (14.37e)$$

$$K_4 = \left[\frac{R_d \ln R_d - (R_d - 1)}{\ln R_d} \right] \left[\frac{R_d}{(R_d - 1)^2} \right] \quad (14.37f)$$

$$K_5 = \frac{R_d}{2(R_d - 1)} \quad (14.37g)$$

See equation 14.36b for K_1 . A typical variation of these stresses with deflection is shown in Figure 14-34. The steel spring dimensions in this case are $t = 0.012$ in, $h = 0.017$ in, $h/t = 1.414$, $D_o = 1$ in, $D_i = 0.5$ in.

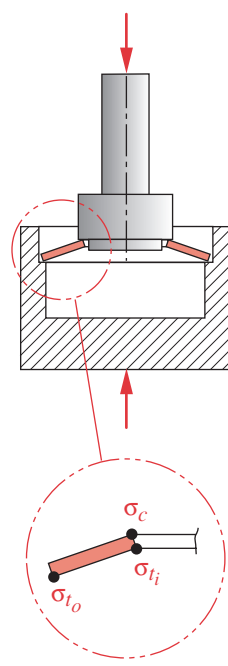
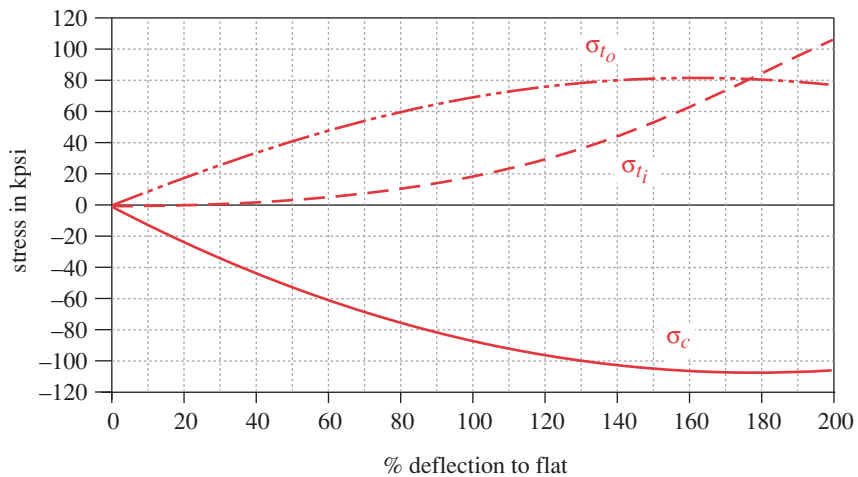


FIGURE 14-33

Points of Highest Stress in a Belleville Spring Washer

**FIGURE 14-34**

Stresses in a Carbon Steel Belleville Spring (with $R_d = 2.0$, $h/t = 1.414$, $t = 0.012$, $h = 0.017$ in)

Static Loading of Belleville Washers

The compressive stress σ_c usually controls the design in static loading, but because the stress is highly concentrated at the edges, local yielding will occur to relieve it and the stress throughout the spring will be less. Because the local σ_c is higher than the average stress, it can be compared to a strength value larger than the ultimate compressive strength S_{uc} . Since even materials are typically used for springs, $S_{uc} = S_{ut}$. Table 14-15 shows some recommended percentages of S_{ut} for comparison to σ_c in static loading. Recognize that the material in general cannot withstand these stress levels. They are just a means to predict failure based on the localized stress σ_c . Setting (set removal) can be used to introduce favorable residual stresses, and the allowable stress increases substantially, as shown in Table 14-17.

Dynamic Loading

If the spring is dynamically loaded, the maximum and minimum tensile stresses σ_{t_o} and σ_{t_i} at the extremes of its deflection range should be calculated from equations 14.36 and the alternating and mean components determined from them. A Goodman-diagram analysis can then be done and the safety factor found from equation 14.35b. The endurance limit for the material can be found using the methods of Chapter 6. Shot peening can be used to increase fatigue life.

Stacking Springs

The maximum deflection of a Belleville spring tends to be small. To get more deflection, they can be stacked in series as shown in Figure 14-35b. The total force will be the same as for one spring but the deflections will add. They can also be stacked in parallel, as shown in Figure 14-35a, in which case the total deflection will be the same as for one spring and the forces will add. Series-parallel combinations are also possible.

Table 14-17 Maximum Recommended Compressive Stress Levels σ_c for Belleville Washers in Static Applications, Assuming $S_{uc} = S_{ut}$

Source: Reference 1

Material	Maximum Percent of Ultimate Tensile Strength	
	Before Set Removed	After Set Removed
Carbon or alloy steel	120%	275%
Nonferrous and austenitic stainless steel	95	160

Note, however, that series or series-parallel stacks are inherently unstable and must be guided over a hardened pin or in a hardened hole, in which case friction will reduce the available load. Interleaf friction can also be substantial in parallel stacks, creating hysteresis. Recommended stacking arrangements and diametral clearances can be found at <http://spirol.com>.

Designing Belleville Springs

The design of Belleville springs requires iteration. Trial values of the diameter ratio R_d and the h/t ratio must be chosen. The type of force-deflection curve desired will suggest an appropriate h/t ratio (see Figure 14-30). If a force or range of forces is specified, the associated deflection can be calculated from equations 14.35 once an outside diameter and thickness are assumed. It is possible to estimate the thickness required to obtain a particular force at the flat position from

$$t = \sqrt[4]{\frac{F_{flat}}{19.2E7} \frac{D_o^2}{h/t}} \quad (14.38us)$$

$$t = \frac{1}{10} \sqrt[4]{\frac{F_{flat}}{132.4} \frac{D_o^2}{h/t}} \quad (14.38si)$$

The result from either the U.S. or the SI units* version of equation 14.38, in combination with other assumed values, can be used in equations 14.35 and 14.36 to find deflections and stresses. The best way to illustrate this process is with an example.

EXAMPLE 14-7

Design of a Belleville Spring for Static Loading

Problem

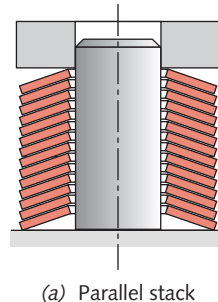
Design a Belleville spring to give a constant load over a given deflection.

Given

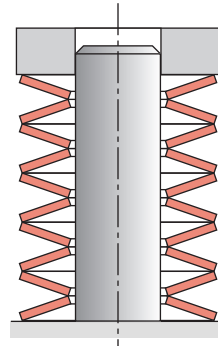
An end seal on a shaft requires a nearly constant load over small motions associated with temperature change. The spring must apply a nominal force of $10 \text{ lb} \pm 5\%$ over a range of $\pm 0.006 \text{ in}$ at any convenient nominal deflection. The spring must fit in a 1.25-in-diameter hole.

Assumptions

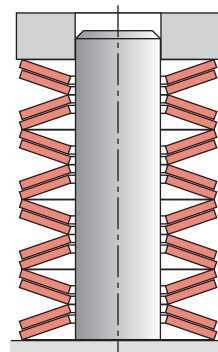
Assume a diameter ratio $R_d = 2$. Use unset carbon spring steel 50HRC.



(a) Parallel stack



(b) Series stack



(c) Series-parallel stack

FIGURE 14-35

Belleville Washers Can Be Combined in Series, Parallel, or Series-Parallel

* Equations 14.38us and 14.38si each contain constants that require particular units to be used. In the US version use inches and pounds. In the SI version use mm and newtons.

Solution

- 1 Assume an outside diameter D_o of 1.2 in to allow some clearance in the hole.
- 2 Since a constant-force spring is needed, the h / t ratio is 1.414 (see Figure 14-30).
- 3 The required force variation of not more than $\pm 5\%$ can be met by choosing an appropriate deflection range to operate in from Figure 14-31. If the deflection is kept between about 65% and 135% of the flat deflection, this tolerance will be achieved. The nominal force will then occur at the flat position and the spring must operate on both sides, so it must be mounted in similar fashion to that shown in Figure 14-33.
- 4 Use the above assumptions and the specified nominal force in equation 14.38us to find an appropriate spring thickness t :

$$t = \sqrt[4]{\frac{F_{flat}}{19.2E7} \frac{D_o^2}{h/t}} = \sqrt[4]{\frac{10}{19.2E7} \frac{(1.2)^2}{1.414}} = 0.015 \text{ in} \quad (a)$$

- 5 The height h can now be found:

$$h = 1.414t = 1.414(0.015) = 0.021 \text{ in} \quad (b)$$

- 6 Based on the choices in step 3 above, find the minimum and maximum deflections:

$$\begin{aligned} y_{min} &= 0.65h = 0.65(0.021) = 0.014 \text{ in} \\ y_{max} &= 1.35h = 1.35(0.021) = 0.029 \text{ in} \end{aligned} \quad (c)$$

The difference between these distances is greater than the required deflection range, so the force tolerance can be met over that range.

- 7 Figure 14-34 shows that the worst stress state will occur at the largest deflection y_{max} , so solve equations 14.36b and 14.37 for stresses at that deflection:

$$K_1 = \frac{6}{\pi \ln R_d} \left[\frac{(R_d - 1)^2}{R_d^2} \right] = \frac{6}{\pi \ln 2} \left[\frac{(2 - 1)^2}{2^2} \right] = 0.689 \quad (d)$$

$$K_2 = \frac{6}{\pi \ln R_d} \left(\frac{R_d - 1}{\ln R_d} - 1 \right) = \frac{6}{\pi \ln 2} \left(\frac{2 - 1}{\ln 2} - 1 \right) = 1.220 \quad (e)$$

$$K_3 = \frac{6}{\pi \ln R_d} \left(\frac{R_d - 1}{2} \right) = \frac{2}{\pi \ln 2} \left(\frac{2 - 1}{2} \right) = 1.378 \quad (f)$$

$$K_4 = \left[\frac{R_d \ln R_d - (R_d - 1)}{\ln R_d} \right] \left[\frac{R_d}{(R_d - 1)^2} \right] = \left[\frac{2 \ln 2 - (2 - 1)}{\ln 2} \right] \left[\frac{2}{(2 - 1)^2} \right] = 1.115 \quad (g)$$

$$K_5 = \frac{R_d}{2(R_d - 1)} = \frac{2}{2(2 - 1)} = 1 \quad (h)$$

$$\begin{aligned}\sigma_c &= -\frac{4Ey}{K_1 D_o^2 (1-v^2)} \left[K_2 \left(h - \frac{y}{2} \right) + K_3 t \right] \\ &= -\frac{4(30E6)(0.029)}{0.689(1.2)^2(1-0.3^2)} \left[1.220 \left(0.021 - \frac{0.029}{2} \right) + 1.378(0.015) \right] \quad (i) \\ \sigma_c &= -112\ 227 \text{ psi}\end{aligned}$$

$$\begin{aligned}\sigma_{t_i} &= \frac{4Ey}{K_1 D_o^2 (1-v^2)} \left[-K_2 \left(h - \frac{y}{2} \right) + K_3 t \right] \\ &= \frac{4(30E6)(0.029)}{0.689(1.2)^2(1-0.3^2)} \left[-1.220 \left(0.021 - \frac{0.029}{2} \right) + 1.378(0.015) \right] \quad (j) \\ \sigma_{t_i} &= 46\ 600 \text{ psi}\end{aligned}$$

$$\begin{aligned}\sigma_{t_o} &= \frac{4Ey}{K_1 D_o^2 (1-v^2)} \left[K_4 \left(h - \frac{y}{2} \right) + K_5 t \right] \\ &= \frac{4(30E6)(0.029)}{0.689(1.2)^2(1-0.3^2)} \left[1.115 \left(0.021 - \frac{0.029}{2} \right) + (1)(0.015) \right] \quad (k) \\ \sigma_{t_o} &= 87\ 628 \text{ psi}\end{aligned}$$

- 8 Table 14-5 (p. 795) gives $S_{ut} = 246$ kpsi for this material. Table 14-17 indicates that 120% of this value can be used for an unset spring. The safety factor for static loading is then

$$N_s = \frac{1.2S_{ut}}{\sigma_c} = \frac{1.2(246\ 000)}{112\ 227} = 2.6 \quad (l)$$

which is acceptable.

- 9 A summary of this spring design is

$$D_o = 1.2 \quad D_i = 0.6 \quad t = 0.015 \quad h = 0.021 \quad (m)$$

- 10 The files EX14-07 can be found on the CD-ROM.
-

14.10 CASE STUDIES

We will now address the design of a spring in one of the Case Study assemblies that were defined in Chapter 9.

Designing a Return Spring for a Cam-Testing Machine

The preliminary design of this device is shown in Figure 14-36. The follower arm is loaded against the cam by an extension spring with loops at each end. The calculations done in Case Study 10A indicate that a spring constant of 25 lb/in and a preload of 25 lb will keep the follower force positive between values of 13 and 110 lb at the design

speed of 180 rpm. The length of the spring should be suitable to the package as shown in Figure 14-36, i.e., of the same order as the cam diameter, which is 8 in. The attachment point of spring to ground is adjustable.

CASE STUDY 10C

Design of a Return Spring for a Cam-Follower Arm

Problem Design an extension spring for the cam-follower arm in Figure 14-36 based on the loadings defined in Case Study 10A (p. 532).

Given The spring rate is 25 lb/in with a preload of 25 lb. The spring's dynamic deflection is 1.5 in.

Assumptions The spring operates in an oil bath whose temperature is below 250°F. Infinite life is required. Use ASTM A228 music wire and standard loops on each end.

Solution See Figure 14-36.

- 1 Assume an 0.177-in trial wire diameter from the available sizes in Table 14-2 (p. 791). Assume a spring index of $C = 8$ and calculate the mean coil diameter D from equation 14.5 (p. 797).

$$D = Cd = 8(0.177) = 1.42 \text{ in} \quad (a)$$

- 2 Use the assumed value of C to find an appropriate value of initial coil stress τ_i from equations 14.21 (p. 821) as the average value of the functions that bracket the acceptable range of spring preloads in Figure 14-22 (p. 822):

$$\begin{aligned} \tau_{i_1} &\equiv -4.231C^3 + 181.5C^2 - 3387C + 28\,640 \\ &= -4.231(8)^3 + 181.5(8)^2 - 3387(8) + 28\,640 = 10\,994 \text{ psi} \end{aligned} \quad (b)$$

$$\begin{aligned} \tau_{i_2} &\equiv -2.987C^3 + 139.7C^2 - 3427C + 38\,404 \\ &= -2.987(8)^3 + 139.7(8)^2 - 3427(8) + 38\,404 = 18\,399 \text{ psi} \end{aligned} \quad (c)$$

$$\tau_i \equiv \frac{\tau_{i_1} + \tau_{i_2}}{2} = \frac{10\,994 + 18\,399}{2} = 14\,697 \text{ psi} \quad (d)$$

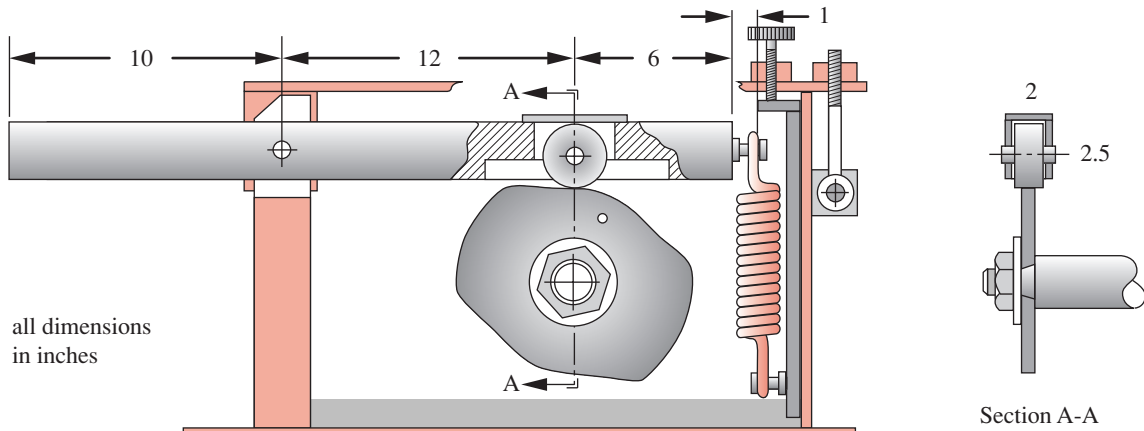
- 3 Find the direct shear factor:

$$K_s = 1 + \frac{0.5}{C} = 1 + \frac{0.5}{8} = 1.0625 \quad (e)$$

- 4 Substitute K_s from step 3 and the value of τ_i from equation (d) of step 2 for τ_{max} in equation 14.8b (p. 798) to find the corresponding initial coil-tension force F_i :

$$F_i = \frac{\pi d^3 \tau_i}{8 K_s D} = \frac{\pi (0.177)^3 (14\,697)}{8(1.0625)(1.416)} = 21.272 \text{ lb} \quad (f)$$

Check that this force is less than the required 25-lb minimum applied force F_{min} , which in this case, it is. Any force smaller than F_i in the spring will not deflect it.

**FIGURE 14-36**

Cam-Follower Arm with Helical Extension Spring

- 5 Find the maximum force from the given rate and deflection and use them to find the mean and alternating forces from equation 14.16a (p. 812):

$$\begin{aligned} F_{max} &= F_{min} + ky = 25 + 25(1.5) = 62.5 \text{ lb} \\ F_a &= \frac{F_{max} - F_{min}}{2} = \frac{62.5 - 25}{2} = 18.75 \text{ lb} \\ F_m &= \frac{F_{max} + F_{min}}{2} = \frac{62.5 + 25}{2} = 43.75 \text{ lb} \end{aligned} \quad (g)$$

- 6 Use the direct shear factor K_s and previously assumed values to find the minimum stress τ_{min} and the mean stress τ_m :

$$\begin{aligned} \tau_{min} &= K_s \frac{8F_{min}D}{\pi d^3} = 1.0625 \frac{8(25)(1.416)}{\pi(0.177)^3} = 17272 \text{ psi} \\ \tau_m &= K_s \frac{8F_m D}{\pi d^3} = 1.0625 \frac{8(43.75)(1.416)}{\pi(0.177)^3} = 30227 \text{ psi} \end{aligned} \quad (h)$$

- 7 Find the Wahl factor K_w and use it to calculate the alternating shear stress in the coil.

$$K_w = \frac{4C-1}{4C-4} + \frac{0.615}{C} = \frac{4(8)-1}{4(8)-4} + \frac{0.615}{8} = 1.184 \quad (i)$$

$$\tau_a = K_w \frac{8F_a D}{\pi d^3} = 1.184 \frac{8(18.75)(1.416)}{\pi(0.177)^3} = 14436 \text{ psi} \quad (j)$$

- 8 Find the ultimate tensile strength of this music-wire material from equation 14.3 and Table 14-4 (p. 792) and use it to find the ultimate shear strength from equation 14.4 (p. 793) and the torsional yield strength for the coil body from Table 14-12 (p. 824), assuming no set removal.

$$S_{ut} = Ad^b = 184\ 649(0.177)^{-0.1625} = 244\ 653 \text{ psi}$$

$$S_{us} = 0.67S_{ut} = 163\ 918 \text{ psi} \quad (k)$$

$$S_{ys} = 0.45S_{ut} = 0.45(244\ 653) = 110\ 094 \text{ psi} \quad (l)$$

- 9 Find the wire endurance limit for unpeened springs from equation 14.13 (p. 804) and convert it to a fully reversed endurance strength with equation 14.18b (p. 814).

$$S_{ew} = 45\ 000 \text{ psi} \quad (m)$$

$$S_{es} = 0.5 \frac{S_{ew} S_{us}}{S_{us} - 0.5 S_{ew}} = 0.5 \frac{45\ 000(163\ 918)}{163\ 918 - 0.5(45\ 000)} = 26\ 080 \text{ psi} \quad (n)$$

- 10 The fatigue safety factor for the coils in torsion is calculated from equation 14.18a (p. 814).

$$\begin{aligned} N_{f_s} &= \frac{S_{es}(S_{us} - \tau_{min})}{S_{es}(\tau_m - \tau_{min}) + S_{us}\tau_a} \\ &= \frac{26\ 080(163\ 918 - 17\ 272)}{26\ 080(30\ 227 - 17\ 272) + 163\ 918(14\ 436)} = 1.4 \end{aligned} \quad (o)$$

Note that the minimum stress due to force F_{min} is used in this calculation, **not** the coil-winding stress from equation (d).

- 11 The stresses in the end hooks also need to be determined. The bending stresses in the hook at point A in Figure 14-23 (repeated here) are found from equation 14.24 (p. 823):

$$C_1 = \frac{2R_1}{d} = \frac{2D}{2d} = C = 8$$

$$K_b = \frac{4C_1^2 - C_1 - 1}{4C_1(C_1 - 1)} = \frac{4(8)^2 - 8 - 1}{4(8)(8 - 1)} = 1.103 \quad (p)$$

$$\sigma_a = K_b \frac{16DF_a}{\pi d^3} + \frac{4F_a}{\pi d^2} = 1.103 \frac{16(1.416)(18.75)}{\pi(0.177)^3} + \frac{4(18.75)}{\pi(0.177)^2} = 27\ 650 \text{ psi} \quad (q)$$

$$\sigma_m = K_b \frac{16DF_m}{\pi d^3} + \frac{4F_m}{\pi d^2} = 1.103 \frac{16(1.416)(43.75)}{\pi(0.177)^3} + \frac{4(43.75)}{\pi(0.177)^2} = 64\ 517 \text{ psi}$$

$$\sigma_{min} = K_b \frac{16DF_{min}}{\pi d^3} + \frac{4F_{min}}{\pi d^2} = 1.103 \frac{16(1.416)(25)}{\pi(0.177)^3} + \frac{4(25)}{\pi(0.177)^2} = 36\ 867 \text{ psi} \quad (r)$$

- 12 Convert the torsional endurance strength to a tensile endurance strength with equation 14.4 (p. 793) and use it and the ultimate tensile strength in equation 14.18 (p. 814) to find a fatigue safety factor for the hook in bending:

$$S_e = \frac{S_{es}}{0.67} = \frac{26\ 080}{0.67} = 38\ 925 \text{ psi}$$

$$\begin{aligned} N_{fb} &= \frac{S_e(S_{ut} - \sigma_{min})}{S_e(\sigma_m - \sigma_{min}) + S_{ut}\sigma_a} \\ &= \frac{38\ 925(244\ 633 - 38\ 867)}{38\ 925(64\ 517 - 38\ 867) + 244\ 633(27\ 650)} = 1.0 \end{aligned} \quad (s)$$

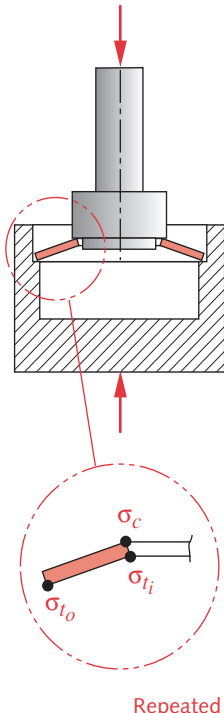


FIGURE 14-33

Points of Highest Stress in a Belleville Spring Washer

- 13 Find the torsional stresses at point *B* of the hook in Figure 14-23 using equation 14.25 (p. 823) and an assumed value of $C_2 = 5$.

$$R_2 = \frac{C_2 d}{2} = \frac{5(0.177)}{2} = 0.443 \text{ in}$$

$$K_{w_2} = \frac{4C_2 - 1}{4C_2 - 4} = \frac{4(5) - 1}{4(5) - 4} = 1.188 \quad (t)$$

$$\tau_{B_a} = K_{w_2} \frac{8DF_a}{\pi d^3} = 1.188 \frac{8(1.416)18.75}{\pi(0.177)^3} = 14,478 \text{ psi}$$

$$\tau_{B_m} = K_{w_2} \frac{8DF_m}{\pi d^3} = 1.188 \frac{8(1.416)43.75}{\pi(0.177)^3} = 33,783 \text{ psi} \quad (u)$$

$$\tau_{B_{min}} = K_{w_2} \frac{8DF_{min}}{\pi d^3} = 1.188 \frac{8(1.416)25}{\pi(0.177)^3} = 19,304 \text{ psi}$$

- 14 The fatigue safety factor for the hook in torsion is calculated from equation 14.18a (p. 814).

$$N_{f_s} = \frac{S_{es}(S_{us} - \tau_{min})}{S_{es}(\tau_m - \tau_{min}) + S_{us}\tau_a}$$

$$= \frac{26,080(163,918 - 19,304)}{26,080(33,783 - 19,304) + 163,918(14,478)} = 1.4 \quad (v)$$

Two of these safety factors are acceptable. The safety of the hook in bending is low.

- 15 To get the specified spring rate, the number of active coils must satisfy equation 14.7 (p. 797):

$$k = \frac{d^4 G}{8D^3 N_a} \quad \text{or} \quad N_a = \frac{d^4 G}{8D^3 k} = \frac{(0.177)^4 11.5E6}{8(1.416)^3 (25)} = 19.88 \cong 20 \quad (w)$$

Note that we round it to the nearest 1/4 coil, as the manufacturing tolerance cannot achieve better than that accuracy. This makes the actual spring rate $k = 24.8 \text{ lb/in}$.

- 16 The total number of coils in the body and the body length are

$$N_t = N_a + 1 = 20 + 1 = 21 \quad (x)$$

$$L_b = N_t d = 21(0.177) = 3.72 \text{ in}$$

- 17 The length of a standard loop is equal to the coil inside diameter. The free length is

$$L_f = L_b + 2L_{hook} = 3.72 + 2(1.24) = 6.2 \text{ in} \quad (y)$$

- 18 The maximum deflection and spring length at that deflection are

$$y_{max} = \frac{F_{max} - F_{initial}}{k} = \frac{62.5 - 21.27}{25} = 1.65 \text{ in}$$

$$L_{max} = L_f + y_{max} = 6.2 + 1.65 = 7.85 \text{ in} \quad (z)$$

This length is within the maximum cam diameter so is acceptable.

- 19 The natural frequency of this spring is found from equation 14.26 (p. 823) and is

$$f_n = \frac{2}{\pi N_a} \frac{d}{D^2} \sqrt{\frac{Gg}{32\gamma}} = \frac{2(0.177)}{\pi(20)(1.416)^2} \sqrt{\frac{11.5E6(386)}{32(0.285)}} = 62 \text{ Hz} = 3720 \text{ rpm} \quad (aa)$$

The ratio between the natural frequency and the forcing frequency is

$$\frac{3720}{180} = 20.7 \quad (ab)$$

which is sufficiently high.

- 20 The design specification for this A228 wire spring is

$$d = 0.177 \text{ in} \quad OD = 1.593 \text{ in} \quad N_t = 21 \quad L_f = 6.2 \text{ in} \quad (ac)$$

- 21 This design is marginal, as the hook is predicted to be at failure in bending fatigue after about a million cycles of operation. If that is too short a life, then the design should be iterated again to improve it. Increasing the wire size to 0.192 in and the spring index to 8.5 will raise all the safety factors, with the hook in bending the lowest at 1.2.
- 22 Models CASE10C-1 and CASE10C-2 are on the CD-ROM. The -1 model is as shown in this example. The -2 model uses the changed parameters of step 21 to improve the design.
-

14.11 SUMMARY

Springs are widely used in machinery of all types to provide push, pull, or twist forces, or to store potential energy. This chapter has discussed the uses of a variety of springs and the design of a few types of commonly used springs: the helical compression, helical extension, helical torsion, and Belleville. The names of the first three define the type of external load applied, not the type of stress present. It is easy to confuse these two aspects. A helical compression or extension spring has torsional stress in its coils, and a helical torsion spring has tensile and compressive stress in its coils. These three types of springs are made of coiled wire. The wire is usually round, though rectangular wire is sometimes used. Belleville spring washers are made of flat stock formed into a cone shape. The helical springs typically have an essentially linear force-deflection characteristic (constant spring rate). Belleville springs have a highly nonlinear characteristic, which can be used to advantage to obtain a near-zero rate or a bistable action.

Extensive data have been developed on the strength characteristics of spring wire and flat spring stock. Much of this literature is reproduced in this chapter. Material strength generally increases as the wire cross-section size is reduced, with the result that fine wire has very high break strength under static loads. The endurance strength of high-static-strength materials tends to saturate (“top-out”) at reasonably high levels rather than be a function of static strength. Estimates of the fatigue strength of various spring materials are also quoted from the literature in this chapter.

The design of springs, whether for static or dynamic loading, is an inherently iterative exercise. Assumptions must be made for the values of several parameters in order to do the calculations. Usually, the first result is an unsuccessful design, requiring changes to the assumed values and recalculation. A computer is an indispensable

aid in this process. Many fully worked-out examples of spring design are provided in the chapter, and the reader is encouraged to study them along with their accompanying files, which provide more information than can be presented in tables.

Important Equations Used in This Chapter

Spring Rate (Section 14.1):

$$k = \frac{F}{y} \quad (14.1)$$

Combining Springs in Parallel (Section 14.1):

$$k_{total} = k_1 + k_2 + k_3 + \dots + k_n \quad (14.2a)$$

Combining Springs in Series (Section 14.1):

$$\frac{1}{k_{total}} = \frac{1}{k_1} + \frac{1}{k_2} + \frac{1}{k_3} + \dots + \frac{1}{k_n} \quad (14.2b)$$

Spring Index (Section 14.4):

$$C = \frac{D}{d} \quad (14.5)$$

Deflection of Helical Compression Spring (Section 14.4):

$$y = \frac{8FD^3N_a}{d^4G} \quad (14.6)$$

Deflection of Helical Extension Spring (Section 14.7):

$$y = \frac{8(F - F_i)D^3N_a}{d^4G} \quad (14.23)$$

Deflection of Round-Wire Helical Torsion Spring (Section 14.8):

$$\theta_{rev} \cong 10.8 \frac{MDN_a}{d^4E} \quad (14.28c)$$

Spring Rate of Helical Compression Spring (Section 14.4):

$$k = \frac{F}{y} = \frac{d^4G}{8D^3N_a} \quad (14.7)$$

Spring Rate of Helical Extension Spring (Section 14.7):

$$k = \frac{F - F_i}{y} = \frac{d^4G}{8D^3N_a} \quad (14.21)$$

Spring Rate of Round-Wire Helical Torsion Spring (Section 14.8):

$$k = \frac{M}{\theta_{rev}} \cong \frac{d^4E}{10.8DN_a} \quad (14.29)$$

Static Stress in Helical Compression or Extension Spring (Section 14.7):

$$\tau_{max} = K_s \frac{8FD}{\pi d^3} \quad \text{where } K_s = \left(1 + \frac{0.5}{C}\right) \quad (14.8b)$$

Dynamic Stress in Helical Compression or Extension Spring (Section 14.7):

$$K_w = \frac{4C-1}{4C-4} + \frac{0.615}{C} \quad (14.9a)$$

$$\tau_{max} = K_w \frac{8FD}{\pi d^3} \quad (14.9b)$$

Stress in Helical Torsion Spring at Inside Diameter (Section 14.8):

$$K_{b_i} = \frac{4C^2 - C - 1}{4C(C-1)} \quad (14.32a)$$

$$\sigma_{i_{max}} = K_{b_i} \frac{M_{max}c}{I} = K_{b_i} \frac{M_{max}(d/2)}{\pi d^4/64} = K_{b_i} \frac{32M_{max}}{\pi d^3} \quad (14.33a)$$

Stress in Helical Torsion Spring at Outside Diameter (Section 14.8):

$$K_{b_o} = \frac{4C^2 + C - 1}{4C(C+1)} \quad (14.32b)$$

$$\sigma_{o_{min}} = K_{b_o} \frac{32M_{min}}{\pi d^3}; \quad \sigma_{o_{max}} = K_{b_o} \frac{32M_{max}}{\pi d^3} \quad (14.33b)$$

Ultimate Tensile Strength of Steel Wire—See Table 14-4 for Constants (Section 14.4):

$$S_{ut} \cong Ad^b \quad (14.3)$$

Ultimate Shear Strength of Wire (Section 14.4):

$$S_{us} \cong 0.67S_{ut} \quad (14.4)$$

Torsional Endurance Limits for Spring-Steel Wire for Stress Ratio R = 0 (Section 14.4):

$$S_{ew} \cong 45.0 \text{ kpsi (310 MPa)} \quad \text{for unpeened springs} \quad (14.13)$$

$$S_{ew} \cong 67.5 \text{ kpsi (465 MPa)} \quad \text{for peened springs}$$

Torsional Endurance Limits for Spring-Steel Wire for Stress Ratio R = -1 (Section 14.4):

$$S_{es} = 0.5 \frac{S_{ew} S_{us}}{S_{us} - 0.5S_{ew}} \quad (14.18b)$$

Bending Endurance Limits for Spring-Steel Wire for Stress Ratio R = 0 (Section 14.4):

$$S_{ew_b} = \frac{S_{ew}}{0.577} \quad (14.34a)$$

Bending Endurance Limits for Spring-Steel Wire for Stress Ratio R = -1 (Section 14.4):

$$S_e = 0.5 \frac{S_{ew_b} S_{ut}}{S_{ut} - 0.5 S_{ew_b}} \quad (14.35c)$$

Static Safety Factor for Helical Compression or Extension Spring (Section 14.5):

$$N_s = \frac{S_{ys}}{\tau} \quad (14.15)$$

Dynamic Safety Factor for Helical Compression or Extension Spring (Section 14.4):

$$N_{f_s} = \frac{S_{es}(S_{us} - \tau_i)}{S_{es}(\tau_m - \tau_i) + S_{us}\tau_a} \quad (14.18a)$$

Dynamic Safety Factor for Helical Torsion Spring (Section 14.8):

$$N_{f_b} = \frac{S_e(S_{ut} - \sigma_{o_{min}})}{S_e(\sigma_{o_{mean}} - \sigma_{o_{min}}) + S_{ut}\sigma_{o_{alt}}} \quad (14.35b)$$

Load-Deflection Function for a Belleville Washer (Section 14.9):

$$F = \frac{4Ey}{K_1 D_o^2 (1 - v^2)} \left[(h - y) \left(h - \frac{y}{2} \right) t + t^3 \right] \quad (14.36a)$$

where $K_1 = \frac{6}{\pi \ln R_d} \left[\frac{(R_d - 1)^2}{R_d^2} \right]$ and $R_d = \frac{D_o}{D_i}$ (14.36b)

Maximum Compressive Stress in a Belleville Washer (Section 14.9):

$$\sigma_c = -\frac{4Ey}{K_1 D_o^2 (1 - v^2)} \left[K_2 \left(h - \frac{y}{2} \right) + K_3 t \right] \quad (14.37a)$$

where $K_2 = \frac{6}{\pi \ln R_d} \left(\frac{R_d - 1}{\ln R_d} - 1 \right)$ and $R_d = \frac{D_o}{D_i}$ (14.37d)

$$K_3 = \frac{6}{\pi \ln R_d} \left(\frac{R_d - 1}{2} \right) \quad (14.37e)$$

Required Thickness of a Belleville Spring for Force at Flat (Section 14.9):

$$t = \sqrt[4]{\frac{F_{flat}}{19.2E7} \frac{D_o^2}{h/t}} \quad (14.38us)$$

14.12 REFERENCES

- Associated Spring, *Design Handbook: Engineering Guide to Spring Design*. Associated Spring, Barnes Group Inc., Bristol, Conn., 1987.

Table P14-0[†]

Topic/Problem Matrix

14.1 Spring Rate14-1, **14-8, 14-10, 14-12**, 14-46,
14-47, 14-53**14.3 Spring Materials**

14-9, 14-33, 14-34, 14-35, 14-36

14.4 Compression Springs14-2, 14-3, 14-4, 14-5, 14-6,
14-7, 14-49, 14-52**14.5 Static Loading**14-11, 14-21, 14-44, 14-45,
14-48, 14-54**14.6 Fatigue Loading****14-14, 14-14**, 14-15, **14-16**,
14-19, 14-20, 14-28, 14-31,
14-32**14.7 Extension Springs**14-17, 14-18, 14-29, 14-37,
14-38, 14-50**14.8 Torsion Springs****Static Design**

14-22, 14-23, 14-39, 14-40

Fatigue Design

14-24, 14-25, 14-30, 14-41

14.9 Belleville Springs**Static Design**

14-26, 14-42, 14-43, 14-51

Fatigue Design

14-27

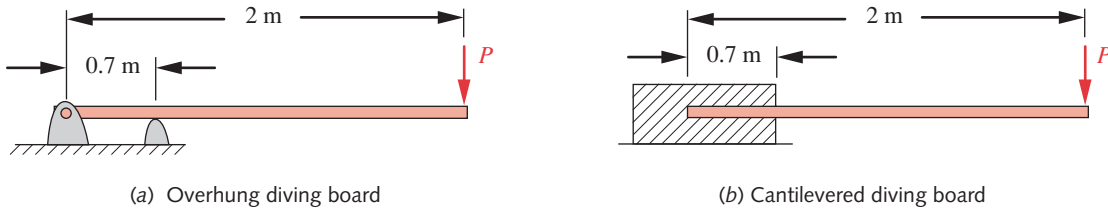
- 2 **H. C. R. Carlson**, Selection and Application of Spring Material. *Mechanical Engineering*, **78**: pp. 331-334, 1956.
- 3 **A. M. Wahl**, *Mechanical Springs*. McGraw-Hill: New York, 1963.
- 4 **F. P. Zimmerli**, "Human Failures in Spring Design." *The Mainspring, Associated Spring Corp.*, Aug.-Sept. 1957.
- 5 **R. E. Cornwell**, "Stress Concentration Factors for the Torsion of Curved Beams of Arbitrary Cross Section." *Proc. Inst. Mechanical Engineers — Part C — Journal of Mechanical Engineering Science*; Dec2006, Vol. 220 Issue 12, pp.1709-1726.
- 6 *Handbook of Spring Design*. Spring Manufacturers Institute, Oak Brook, IL, 2002.

14.13 PROBLEMS

- *14-1 A linear spring is to give 200 N at its maximum deflection of 150 mm and 40 N at its minimum deflection of 50 mm. What is its spring rate?
- 14-2 Find the ultimate tensile strength, the ultimate shear strength, and the torsional yield strength of a 1.8-mm-dia, A229 oil-tempered steel wire.
- *14-3 Find the torsional yield and ultimate shear strength of an 0.105-in-dia, unset A229 wire to be used in a helical compression spring.
- *14-4 What is the torsional fatigue strength of the wire in Problem 14-3 at $N = 5E6$ cycles?
- 14-5 Draw the modified-Goodman diagram for the wire of Problem 14-3.
- *14-6 What are the spring rate and spring index of a squared and ground compression spring with $d = 1$ mm, $D = 10$ mm, and 12 total coils?
- *14-7 Find the natural frequency of the spring in Problem 14-6.
- [†]14-8 A paper machine processes rolls of paper having a density of 984 kg/m^3 . The paper roll is 1.50-m outside dia (OD) \times 0.22-m inside dia (ID) \times 3.23 m long and is on a simply supported, hollow, steel shaft with 22-cm $OD \times$ 20-cm ID and as long as the paper roll. Find the spring rate of the shaft and the fundamental natural frequency of the shaft-roll assembly.
- 14-9 Determine the minimum allowable bending radius for a 50HRC strip-steel spring of 1-mm thickness.
- *14-10 An overhung diving board is shown in Figure P14-1a. A 100-kg person is standing on the free end in the center of its width. Assume cross-sectional dimensions of 305 mm \times 32 mm and a material $E = 10.3 \text{ GPa}$. What are the spring rate and fundamental natural frequency of the diver-board combination?
- *†14-11 Design a helical compression spring for a static load of 45 lb at a deflection of 1.25 in with a safety factor of 2.5. Use $C = 7.5$. Specify all parameters necessary to manufacture the spring.
- 14-12 Repeat Problem 14-10 using the cantilevered diving-board design in Figure P14-1b.
- *14-13 Given $d = 0.312$ in, $y_{working} = 0.75$ in, 15% clash allowance, unpeened chrome-vanadium wire, squared ends, $F_{max} = 250$ lb, and $F_{min} = 50$ lb, find N_a , D , L_f , L_{shut} , k , $y_{initial}$, and the minimum hole diameter for the spring. Infinite life is desired with a safety factor of 1.4. Choose an acceptable spring index. Setting will be done.

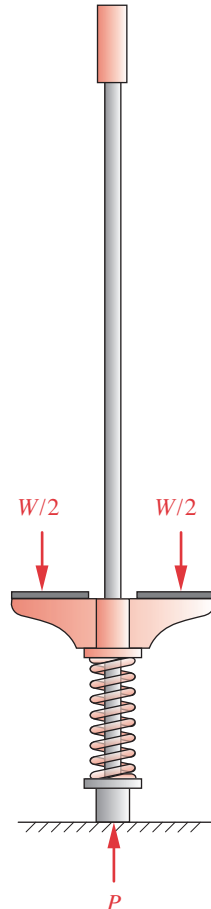
* Answers to these problems are provided in Appendix D.

[†] Problem numbers in *italics* are design problems. Problem numbers in **boldface** are extended from similar problems in earlier chapters with the same dash number.

**FIGURE P14-1**

Problems 14-10 and 14-12

- 14-14** Figure P14-2 shows a child's toy called a *pogo stick*. The child stands on the pads, applying half her weight on each side. She jumps up off the ground, holding the pads up against her feet, and bounces along with the spring cushioning the impact and storing energy to help each rebound. Assume a 60-lb child and a spring constant of 100 lb/in. The pogo stick weighs 5 lb. Design the helical compression spring to survive jumping 2 in off the ground with a dynamic safety factor of 1 for a finite life of 5E4 cycles. Determine the fundamental natural frequency of the system.
- 14-15** Draw the modified-Goodman diagram for the following spring design and find its safety factor: $S_{fw} = 40 \text{ kpsi}$, $S_{us} = 200 \text{ kpsi}$, $\tau_a = 12 \text{ kpsi}$, $\tau_m = 95 \text{ kpsi}$, $\tau_i = 75 \text{ kpsi}$.
- 14-16** Problem 6-16 describes a track for bowling balls that are 4.5-in dia and 2.5-lb weight. Design a spring-loaded launcher that will allow quadriplegic bowlers to launch the balls down the bowling alley from the point where the track of Problem 6-16 drops them with only a switch closure that releases the launcher. The launcher's plunger will be cocked by an assistant, and the energy stored in the helical compression spring, which you will design, will drive the plunger into the ball and roll it down the bowling alley. You will have to determine appropriate constraints and make many assumptions about such things as the size of the alley, the friction losses, and the energy needed to knock over the pins.
- *14-17** Design a helical extension spring to handle a dynamic load that varies from 175 N to 225 N over a 0.85-cm working deflection. Use music wire and standard hooks. The forcing frequency is 1 500 rpm. Infinite life is desired. Minimize the package size. Choose appropriate safety factors against fatigue, yielding, and surging.
- 14-18** Design a helical extension spring with standard hooks to handle a dynamic load that varies from 300 lb to 500 lb over a 2-in working deflection. Use chrome-vanadium wire. The forcing frequency is 1 000 rpm. Infinite life is desired. Minimize the package size. Choose appropriate safety factors against fatigue, yielding, and surging.
- *14-19** Design a helical compression spring to handle a dynamic load that varies from 780 N to 1000 N over a 22-mm working deflection. Use squared and ground, unpeened music wire and a 10% clash allowance. The forcing frequency is 500 rpm. Infinite life is desired. Minimize the package size. Choose appropriate safety factors against fatigue, yielding, and surging.
- 14-20** Design a helical compression spring to handle a dynamic load that varies from 135 N to 220 N over a 32-mm working deflection. Use squared, peened chrome-vanadium wire and a 15% clash allowance. The forcing frequency is 250 rpm. Infinite life is desired. Minimize the package size. Choose appropriate safety factors against fatigue, yielding, and surging.

**FIGURE P14-2**

Problem 14-14

* Answers to these problems are provided in Appendix D. Problem numbers in *italics* are design problems.

- *14-21 Design a helical compression spring for a static load of 400 N at a deflection of 45 mm with a safety factor of 2.5. Use $C = 8$. Specify all parameters necessary to manufacture the spring. State all assumptions.
- *14-22 Design a straight-ended helical torsion spring for a static load of 200 N-m at a deflection of 45° with a safety factor of 1.8. Specify all parameters necessary to manufacture the spring. State all assumptions.
- 14-23 Design a straight-ended helical torsion spring for a static load of 300 in-lb at a deflection of 75° with a safety factor of 2. Specify all parameters necessary to manufacture the spring. State all assumptions.
- *14-24 Design a straight-ended helical torsion spring for a dynamic load of 50–105 N-m over a deflection of 80° with a safety factor of 2.5. Specify all parameters necessary to manufacture the spring. State all assumptions.
- 14-25 Design a straight-ended helical torsion spring for a dynamic load of 150–350 in-lb over a deflection of 50° with a safety factor of 1.4. Specify all parameters necessary to manufacture the spring. State all assumptions.
- *14-26 Design a Belleville spring to give a constant $400 \text{ N} \pm 10\%$ static force over a 1-mm deflection.
- 14-27 Design a Belleville spring for bimodal operation between $\pm 50 \text{ N}$.
- 14-28 Given the following data for a helical compression spring loaded in fatigue, design the spring for infinite life. State all assumptions and sources of empirical data used. $C = 8.5$, $d = 8 \text{ mm}$, 625 rpm, working deflection = 20 mm, 15% clash allowance, unpeened music wire, squared ends, preset, $F_{max} = 450 \text{ N}$, $F_{min} = 225 \text{ N}$.
- 14-29 A helical extension spring, loaded in fatigue, has been designed for infinite life with the following data. $C = 9$, $d = 8 \text{ mm}$, working deflection = 50 mm, unpeened chrome-silicon wire, $F_{max} = 935 \text{ N}$, $F_{min} = 665 \text{ N}$, $F_{init} = 235 \text{ N}$, 13.75 active coils. Find the safety factors for failure in the standard hooks. State all assumptions and sources of empirical data used.
- 14-30 Given the following data for a helical torsion spring loaded in fatigue, find the spring index, unloaded coil dia, minimum loaded coil dia, and safety factor in fatigue. State all assumptions and sources of empirical data used. Deflection at assembly = 0.25 rev, working deflection = 0.5 rev, $k = 60 \text{ lb-in/rev}$, $N_a = 20$, 0.192 in music wire, unpeened.
- 14-31 A helical compression spring is required to provide a minimum force of 150 lb at installation and have a working deflection of 1 in. The spring rate is 75 lb/in. The coil must fit in a 2.1-in-dia hole with 0.1 in clearance. Use 0.25-in diameter unpeened music wire and squared/ground ends. Using a 15% clash allowance, find:
- The stresses and safety factor for infinite life in fatigue
 - The shut height
 - The stress and safety factor at shut height
 - The total number of coils
 - The free length
 - The natural frequency in Hz.
 - Draw a Goodman diagram and show the safety factor from (a) on it.
- 14-32 A helical compression coil spring is needed to provide a time-varying force that ranges from a minimum of 100 lb to a maximum of 300 lb over a deflection of 1 in. It needs to work free over a shaft of 1.25-in dia. Use a cold-drawn carbon steel wire having an $S_{ut} = 250\,000 \text{ psi}$. A spring index of 6, a clash allowance of 15%, and squared and ground ends are desired.

* Answers to these problems are provided in Appendix D. Problem numbers in *italics* are design problems.

- 14-33 Find the ultimate tensile strength and the ultimate shear strength of ASTM A228 music wire in the following preferred diameters: 0.5 mm, 1.0 mm, 2.0 mm, 4.0 mm, and 6.0 mm.
- 14-34 Find the ultimate tensile strength and the ultimate shear strength of ASTM A228 music wire in the following preferred diameters: 0.020 in, 0.038 in, 0.081 in, 0.162 in, and 0.250 in.
- 14-35 Select the preferred diameter for an ASTM A227 cold-drawn wire that will have an ultimate tensile strength as close to, but not less than, 180 kpsi.
- 14-36 Select the preferred diameter for an ASTM A229 oil-tempered wire that will have an ultimate tensile strength as close to, but not less than, 1 430 MPa.
- 14-37 Design a helical extension spring to handle a dynamic load that varies from 275 N to 325 N over 10-mm working deflection. Use chrome silicon wire and standard hooks. The forcing frequency is 800 rpm. Infinite life is desired. Minimize the package size. Choose appropriate safety factors against fatigue, yielding, and surging.
- 14-38 Design a helical extension spring to handle a dynamic load that varies from 60 lb to 75 lb over 0.5-in working deflection. Use music wire and standard hooks. The forcing frequency is 1 200 rpm. Infinite life is desired. Minimize the package size. Choose appropriate safety factors against fatigue, yielding, and surging.
- 14-39 Design a straight-ended helical torsion spring for a static load of 50 N-m at a deflection of 60° with a safety factor of 2. Specify all parameters necessary to manufacture the spring. State all assumptions.
- 14-40 Design a straight-ended helical torsion spring for a static load of 430 in-lb at a deflection of 55° with a safety factor of 2. Specify all parameters necessary to manufacture the spring. State all assumptions.
- 14-41 Given the following data for a helical torsion spring, loaded in fatigue, find the spring index, unloaded coil diameter, minimum loaded coil diameter, and safety factor in fatigue. State all assumptions and sources of empirical data used. Deflection at assembly = 0.15 rev, working deflection = 0.35 rev, $k = 10 \text{ N-m/rev}$, $N_a = 25$, 4.50 mm oil-tempered wire, unpeened.
- *14-42 Design a Belleville spring to give a static force of approximately 2000 lb at a maximum deflection of 0.05 in with a nearly constant spring rate.
- 14-43 Design a Belleville spring to give a static force of 400 lb at 50% deflection-to-flat and 200 lb at flat.
- *14-44 Design a helical compression spring for a static load of 60 lb at a deflection of 1.50 in with a safety factor of 2.0 to work in a 1.06-in-dia hole. Specify all parameters necessary to manufacture the spring.
- 14-45 Design a helical compression spring for a static load of 200 N at a deflection of 40 mm with a safety factor of 1.8 to work in a 25-mm hole. Specify all parameters necessary to manufacture the spring.
- 14-46 Three springs are arranged in series similar to the configuration shown in Figure 3-1(a). They have spring rates $k_1 = 50 \text{ N/mm}$, $k_2 = 150 \text{ N/mm}$, and $k_3 = 500 \text{ N/mm}$, respectively. Determine the total spring rate, the deflection of each spring, and the overall deflection if a load of $F = 600 \text{ N}$ is applied.

* Answers to these problems are provided in Appendix D. Problem numbers in *italics* are design problems.

- 14-47 Three springs are arranged in parallel like the configuration shown in Figure 3-1(b). They have spring rates $k_1 = 50 \text{ N/mm}$, $k_2 = 150 \text{ N/mm}$, and $k_3 = 500 \text{ N/mm}$, respectively. Determine the total spring rate, the force carried by each spring, and the overall deflection if a load of $F = 600 \text{ N}$ is applied.
- 14-48 A spring made from ASTM A228 wire with ends squared and ground, wire diameter $d = 3 \text{ mm}$, outside diameter $D_o = 27 \text{ mm}$, 14 total coils, and free length $L_f = 80 \text{ mm}$ has been chosen for an application. Determine the static safety factor if the spring is subjected to a static load of 175 N.
- 14-49 A spring with ends squared and ground, wire diameter $d = 4 \text{ mm}$, outside diameter $D_o = 40 \text{ mm}$, 18 total coils, and free length $L_f = 140 \text{ mm}$ has been chosen for an application where the initial deflection is 15 mm and the working deflection is 50 mm. Determine minimum working length, shut height, clash allowance, spring index, and spring rate for this spring.
- 14-50 An extension spring has wire diameter $d = 3 \text{ mm}$ and outside diameter $D_o = 27 \text{ mm}$. Determine the preferred preload for this spring.
- 14-51 A series-stack of Belleville springs is required for more deflection in a design. The stack will be guided by an internal pin as shown in Figure 14-35(b). The minimum inside diameter of the individual springs in the stack is $D_i = 25 \text{ mm}$. Determine the recommended surface conditions for the pin and the maximum pin diameter. (Hint: go to www.spirol.com on the internet and look up disc springs, stacking).
- 14-52 Equation 14.9a defines a combined direct shear and stress concentration factor K_w for use with round-wire helical springs. Equation 14.11a defines a similar factor K_{rw} for calculating shear stress in rectangular-wire coil springs. Find and plot the ratio K_{rw}/K_w for square wire with values of spring index C ranging from 1.2 to 10.
- 14-53 Repeat Problem 14-6 with 1-mm square wire instead of round wire.
- 14-54 A helical compression spring is required to provide a minimum force of 650 N at installation and have a working deflection of 25 mm. The spring rate is 13 N/mm. The coil must fit in a 53-mm-dia hole with 3-mm clearance. Use 6-mm square, music wire with squared/ground ends. Using a 15% clash allowance, find:
- The stress at the working deflection.
 - The shut height.
 - The stress at the shut height.
 - The total number of coils.
 - The free length.
 - The natural frequency in Hz.

15



SCREWS AND FASTENERS

*For want of a nail the shoe is lost;
For want of a shoe the horse is lost;
And, for want of a horse the rider is lost.*
GEORGE HERBERT

15.0 INTRODUCTION

The “nuts and bolts” of a design might seem to be one of its least interesting aspects, but in fact is one of the most fascinating. The success or failure of a design can hinge on proper selection and use of its fasteners. Moreover, the design and manufacture of fasteners is very big business and is a significant part of our economy. Literally thousands of different designs of fasteners are offered by vendors, and thousands to millions of fasteners are used in a single complex assembly such as an automobile or aircraft. The Boeing 747 uses about 2.5 million fasteners, some of which cost several dollars each.^[1]

There is a tremendous variety of fasteners available commercially, ranging from the mundane nuts and bolts to multipiece devices for quick-release of panels or for hidden-fastener applications. Figure 15-1 shows a small sample of the variety available. We cannot cover all of these varieties in one chapter. Whole books have been written on fasteners, and some of them are noted in the bibliography of this chapter. We will limit our discussion to the design and selection of conventional fasteners such as bolts, screws, nuts, etc., used for machine-design applications in which significant loads and stresses are encountered.

Screws are used both to hold things together as fasteners and to move loads as so-called power screws or lead screws. We will investigate both of these applications. Screws as fasteners can be arranged to take tensile loads, shear loads, or both. We will explore the application of preloads to screw fasteners, which can have significant benefit to their load-carrying abilities. Table 15-0 shows the variables used in this chapter and indicates the equations or sections in which they can be found.

Table 15-0 Variables Used in This Chapter

Part 1 of 2

Symbol	Variable	ips units	SI units	See
A	area (with various subscripts)	in ²	m ²	various
A_b	total area of bolt	in ²	m ²	Eq. 15.11a
A_m	effective stiffness of material in clamp zone	in ²	m ²	Eq. 15.18-22
A_t	tensile-stress area of bolt	in ²	m ²	Sect. 15.1
C	joint stiffness constant	none	none	Eq. 15.13
C_{load}	loading factor	none	none	Ex. 15-3
C_{reliab}	reliability factor	none	none	Ex. 15-3
C_{size}	size factor	none	none	Ex. 15-3
C_{surf}	surface factor	none	none	Ex. 15-3
C_{temp}	temperature factor	none	none	Ex. 15-3
d	diameter (with various subscripts)	in	m	various
D	diameter (with various subscripts)	in	m	various
e	efficiency	none	none	Eq. 15.7
E	Young's modulus	psi	Pa	various
F	force (with various subscripts)	lb	N	various
f	friction force	lb	N	Eq. 15.4
F_b	maximum force in bolt	lb	N	Sect. 15.7
F_i	preload force	lb	N	Sect. 15.7
F_m	minimum force in material	lb	N	Sect. 15.7
HRC	Rockwell C hardness	none	none	various
J	polar second moment of area	in ⁴	m ⁴	Eq. 15.9
k	spring rate (with various subscripts)	lb/in	N/m	Sect. 15.7
k_b	bolt stiffness (spring rate)	lb/in	N/m	Sect. 15.7
k_m	material stiffness (spring rate)	lb/in	N/m	Sect. 15.7
K_f	fatigue-stress concentration factor	none	none	Eq. 15.15b
K_{fm}	mean-stress fatigue-concentration factor	none	none	Eq. 15.15b
l	length (with various subscripts)	in	m	various
L	lead of thread	in	mm	Sect. 15.2
n	number of fasteners	none	none	Sect. 15.10
N	number of threads per unit length	none	none	Sect. 15.2
N_f	safety factor in fatigue	none	none	Eq. 15.16
N_{leak}	safety factor—leakage	none	none	Case St. 7D
N_y	safety factor—static yielding	none	none	Ex. 15-2
N_{sep}	safety factor—separation	none	none	Eq. 15.14d
p	thread pitch	in	mm	various
P	load (with various subscripts)	lb	N	various
P_b	portion of load felt by preloaded bolt	lb	N	Eq. 15.13
P_m	portion of load felt by preloaded material	lb	N	Eq. 15.13
r	radius	in	m	Sect. 15.10

The opening epigraph on the previous page is often erroneously attributed to Benjamin Franklin, who popularized Herbert's maxim as a prefix to his *Poor Richard's Almanac* over a century later. In any event, the truth of this maxim is borne out by contemporary experience. The *Boston Sunday Globe* of October 16, 1994, reported that in the summer of 1994, three radioactive fuel assemblies at the Seabrook, N.H., nuclear power plant were damaged when a foot-long, 5-pound bolt was swept into the reactor by cooling water after it vibrated loose from the pump it was attached to. The shutdown for repairs would cost consumers millions of dollars for replacement electricity. The accident was attributed to poor fastener design. For want of a bolt ..., etc.

Table 15-0 Variables Used in This Chapter

Part 2 of 2

Symbol	Variable	ips units	SI units	See
S_e	corrected endurance limit	psi	Pa	various
$S_{e'}$	uncorrected endurance limit	psi	Pa	various
S_p	bolt proof strength	psi	Pa	Sect. 15.6
S_{us}	ultimate shear strength	psi	Pa	various
S_{ut}	ultimate tensile strength	psi	Pa	various
S_y	yield strength	psi	Pa	various
S_{ys}	shear yield strength	psi	Pa	Ex. 15-6
T	torque	lb-in	N-m	Eq. 15.5
w_i, w_o	thread-geometry factors	none	none	Table 15-5
W	work	in-lb	joules	Eq. 15.7
x, y	generalized length variables	in	m	
α	radial angle of thread	deg	deg	Eq. 15.5
δ	deflection	in	m	Sect. 15.7
λ	lead angle	deg	deg	Sect. 15.2
μ	coefficient of friction	none	none	Sect. 15.2
σ	normal stress (with various subscripts)	psi	Pa	various
τ	shear stress (with various subscripts)	psi	Pa	Sect. 15.3

**FIGURE 15-1**

A Sample of the Variety of Commercially Available Fasteners Courtesy of Bolt Products Inc., City of Industry, Calif., 91745

15.1 STANDARD THREAD FORMS

The common element among screw fasteners is their thread. In general terms, the thread is a helix that causes the screw to advance into the workpiece or nut when rotated. Threads may be external (screw) or internal (nut or threaded hole). Thread forms originally differed in each major manufacturing country but after World War II were standardized in Great Britain, Canada, and the United States to what is now called the Unified National Standard (UNS) series, as shown in Figure 15-2. A European standard is also defined by ISO and has essentially the same thread cross-sectional shape, but uses metric dimensions, so is not interchangeable with UNS threads. Both UNS and ISO threads are in general use in the United States. Both use a 60° included angle and define thread size by the nominal outside (major) diameter d of an external thread. The thread pitch p is the distance between adjacent threads. The crests and roots are defined as flats to reduce the stress concentration from that of a sharp corner. The specifications allow for rounding of these flats due to tool wear. The pitch diameter d_p and the root diameter d_r are defined in terms of the thread pitch p with slightly different ratios used for UNS and ISO threads.

The lead L of the thread is the distance that a mating thread (nut) will advance axially with one revolution of the nut. If it is a **single thread**, as shown in Figure 15-2, the lead will equal the pitch. Screws can also be made with **multiple threads**, also called **multiple-start threads**. A **double thread** (2-start) has two parallel grooves wrapped around the diameter, like a pair of helical “railroad tracks.” In this case the lead will be twice the pitch. A **triple thread** (3-start) will have a lead of three times the pitch, etc. The advantages of multiple threads are smaller thread height and the increased lead for fast advance of the nut. Some automotive power-steering screws use 5-start threads. However, most screws are made with only a single thread (1-start).

Three standard series of thread-pitch families are defined in UNS threads: coarse-pitch (UNC), fine-pitch (UNF), and extra-fine-pitch (UNEF). ISO also defines coarse and fine series of threads. The **coarse series** is most common and is recommended for ordinary applications, especially where repeated insertions and removals of the screw are required or where the screw is threaded into a softer material. Coarse threads are less likely to cross or strip the soft material on insertion. **Fine threads** are more resistant to loosening from vibrations than coarse threads because of their smaller helix angle

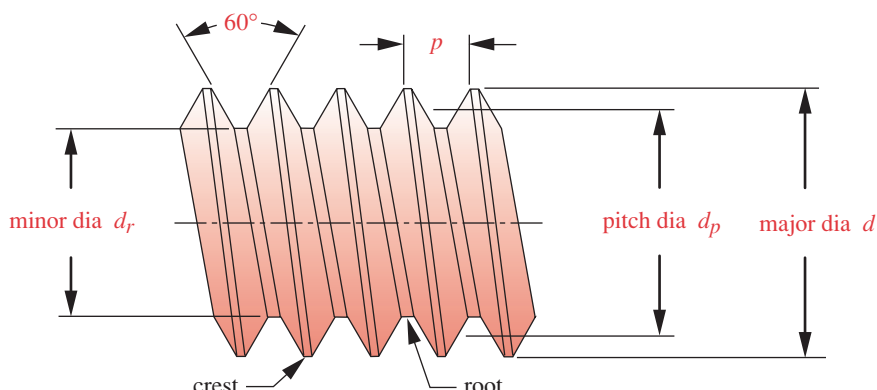


FIGURE 15-2

Unified National and ISO Standard Thread Form

and so are used in automobiles, aircraft, and other applications that are subject to vibration. **Extra-fine-series** threads are used where wall thickness is limited and their short threads are an advantage.

The Unified National and ISO standards define tolerance ranges for both internal and external threads to control their fit. The UNS defines three fit classes, labeled class 1, 2, and 3. Class 1 has the broadest tolerances and is used for “hardware-quality” (i.e., inexpensive) fasteners intended for casual use around the home, etc. Class 2 defines closer tolerances for a better-quality fit between mating threads and is suitable for general machine-design applications. Class 3 is the highest precision and can be specified where closer fits are needed. Cost increases with higher class of fit. A letter designator indicates an external (A) or internal (B) thread.

A thread is specified with a code that defines its series, diameter, pitch, and class of fit. The pitch of UNS threads is defined reciprocally as the number of threads per inch, while metric (ISO) thread pitch is specified by the pitch dimension in mm. An example of a UNS thread specification is

1/4-20 UNC-2A

which defines a 0.250-in-diameter by 20-threads-per-inch, coarse-series, class-2-fit, external thread. An example of a metric thread specification is

M8 × 1.25

which defines an 8-mm-diameter by 1.25-mm-pitch thread in the ISO coarse series. All standard threads are right-hand (RH) by default unless specified as left-hand by adding the letters LH to the specification.* A right-hand thread will advance the nut (or screw) away from you when either is turned clockwise.

Tensile Stress Area

If a threaded rod as shown in Figure 15-2 is subjected to pure tensile loading, one might expect its strength to be limited by the area of its minor (root) diameter, d_r . However, testing of threaded rods in tension shows that their tensile strength is better defined by the average of the minor and pitch diameters. A *tensile-stress area* A_t is defined as

$$A_t = \frac{\pi}{4} \left(\frac{d_p + d_r}{2} \right)^2 \quad (15.1a)$$

where, for UNS threads:

$$d_p = d - 0.649\ 519/N \quad d_r = d - 1.299\ 038/N \quad (15.1b)$$

and for ISO threads:

$$d_p = d - 0.649\ 519p \quad d_r = d - 1.226\ 869p \quad (15.1c)$$

with d = outside diameter, N = number of threads per inch, and p = pitch in mm.

The stress in a threaded rod due to a pure axial tensile load F is then

$$\sigma_t = \frac{F}{A_t} \quad (15.2)$$

* A left-hand-threaded nut often has a circumferential groove cut around its hex flats to identify it as a left-hand (LH) nut.

Standard Thread Dimensions

Table 15-1 shows the principal dimensions of UNS threads and Table 15-2 shows the same for ISO threads. UNS threads smaller than 0.25-in diameter are designated by a gage number. A useful algorithm for determining the diameter of numbered threads is

Table 15-1 Principal Dimensions of Unified National Standard Screw Threads

Data Calculated from Equations 15.1—See Reference 3 for More Information

Size	Major Diameter d (in)	Coarse Threads—UNC			Fine Threads—UNF		
		Threads per inch	Minor Diameter d_r (in)	Tensile Stress Area A_t (in^2)	Threads per inch	Minor Diameter d_r (in)	Tensile Stress Area A_t (in^2)
0	0.0600	—	—	—	80	0.0438	0.0018
1	0.0730	64	0.0527	0.0026	72	0.0550	0.0028
2	0.0860	56	0.0628	0.0037	64	0.0657	0.0039
3	0.0990	48	0.0719	0.0049	56	0.0758	0.0052
4	0.1120	40	0.0795	0.0060	48	0.0849	0.0066
5	0.1250	40	0.0925	0.0080	44	0.0955	0.0083
6	0.1380	32	0.0974	0.0091	40	0.1055	0.0101
8	0.1640	32	0.1234	0.0140	36	0.1279	0.0147
10	0.1900	24	0.1359	0.0175	32	0.1494	0.0200
12	0.2160	24	0.1619	0.0242	28	0.1696	0.0258
1/4	0.2500	20	0.1850	0.0318	28	0.2036	0.0364
5/16	0.3125	18	0.2403	0.0524	24	0.2584	0.0581
3/8	0.3750	16	0.2938	0.0775	24	0.3209	0.0878
7/16	0.4375	14	0.3447	0.1063	20	0.3725	0.1187
1/2	0.5000	13	0.4001	0.1419	20	0.4350	0.1600
9/16	0.5625	12	0.4542	0.1819	18	0.4903	0.2030
5/8	0.6250	11	0.5069	0.2260	18	0.5528	0.2560
3/4	0.7500	10	0.6201	0.3345	16	0.6688	0.3730
7/8	0.8750	9	0.7307	0.4617	14	0.7822	0.5095
1	1.0000	8	0.8376	0.6057	12	0.8917	0.6630
1 1/8	1.1250	7	0.9394	0.7633	12	1.0167	0.8557
1 1/4	1.2500	7	1.0644	0.9691	12	1.1417	1.0729
1 3/8	1.3750	6	1.1585	1.1549	12	1.2667	1.3147
1 1/2	1.5000	6	1.2835	1.4053	12	1.3917	1.5810
1 3/4	1.7500	5	1.4902	1.8995			
2	2.0000	4.5	1.7113	2.4982			
2 1/4	2.2500	4.5	1.9613	3.2477			
2 1/2	2.5000	4	2.1752	3.9988			
2 3/4	2.7500	4	2.4252	4.9340			
3	3.0000	4	2.6752	5.9674			
3 1/4	3.2500	4	2.9252	7.0989			
3 1/2	3.5000	4	3.1752	8.3286			
3 3/4	3.7500	4	3.4252	9.6565			
4	4.0000	4	3.6752	11.0826			

Table 15-2 Principal Dimensions of ISO Metric Standard Screw Threads

Data Calculated from Equations 15.1—See Reference 4 for More Information

Major Diameter d (mm)	Coarse Threads			Fine Threads		
	Pitch p mm	Minor Diameter d_r (mm)	Tensile Stress Area A_t (mm ²)	Pitch p mm	Minor Diameter d_r (mm)	Tensile Stress Area A_t (mm ²)
3.0	0.50	2.39	5.03			
3.5	0.60	2.76	6.78			
4.0	0.70	3.14	8.78			
5.0	0.80	4.02	14.18			
6.0	1.00	4.77	20.12			
7.0	1.00	5.77	28.86			
8.0	1.25	6.47	36.61	1.00	6.77	39.17
10.0	1.50	8.16	57.99	1.25	8.47	61.20
12.0	1.75	9.85	84.27	1.25	10.47	92.07
14.0	2.00	11.55	115.44	1.50	12.16	124.55
16.0	2.00	13.55	156.67	1.50	14.16	167.25
18.0	2.50	14.93	192.47	1.50	16.16	216.23
20.0	2.50	16.93	244.79	1.50	18.16	271.50
22.0	2.50	18.93	303.40	1.50	20.16	333.06
24.0	3.00	20.32	352.50	2.00	21.55	384.42
27.0	3.00	23.32	459.41	2.00	24.55	495.74
30.0	3.50	25.71	560.59	2.00	27.55	621.20
33.0	3.50	28.71	693.55	2.00	30.55	760.80
36.0	4.00	31.09	816.72	3.00	32.32	864.94
39.0	4.00	34.09	975.75	3.00	35.32	1028.39

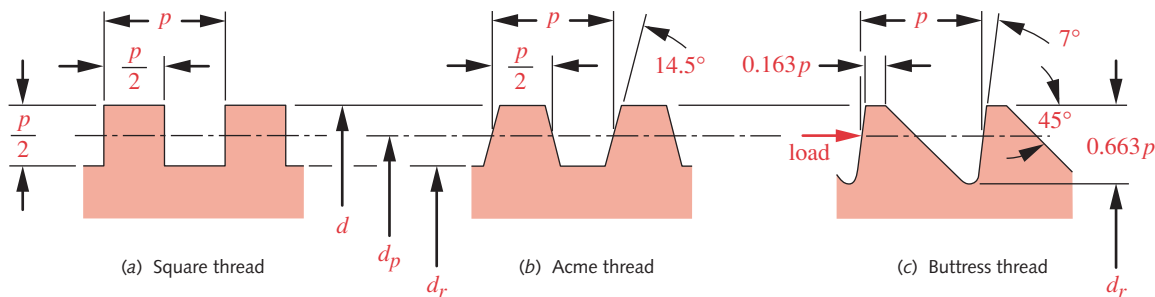
to multiply the gage number by 13 and add 60. The result is its approximate major diameter in thousandths of an inch. The minor diameter = major diameter – pitch. See references 2, 3, and 4 for more detailed dimensional information on standard threads, including tolerances for the different classes of fit.

15.2 POWER SCREWS

Power screws, also called lead screws, are used to convert rotation to linear motion in actuators, production machines, and jacks, among many other applications. They are capable of very large mechanical advantages and so can lift or move large loads. In such cases, a very strong thread form is needed. While the standard thread forms described above are well suited to use in fasteners, they may not be strong enough for all power-screw applications. Other thread profiles have been standardized for such applications.

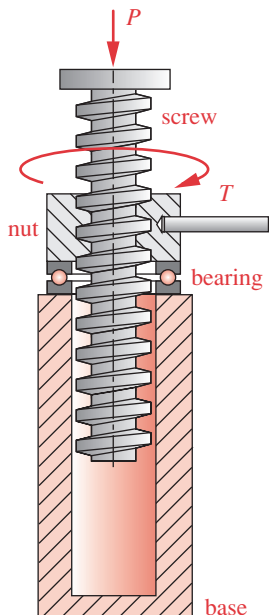
Square, Acme, and Buttress Threads

The square thread shown in Figure 15-3a provides the greatest strength and efficiency and also eliminates any radial component of force between the screw and nut. How-

**FIGURE 15-3**

Square, Acme, and Buttress Threads

ever, it is more difficult to cut because of its perpendicular face. A modified square thread (not shown) is made with a 10° included angle to improve its manufacturability. The Acme thread of Figure 15-3b has a 29° included angle, making it easier to manufacture and also allowing the use of a split nut that can be squeezed radially against the screw to take up wear. An Acme stub thread (not shown) is also available, with teeth $0.3 p$ high instead of the standard $0.5 p$. Its advantage is more uniform heat-treatability. The Acme thread is a common choice for power screws that must take loads in both directions. If the axial load on the screw is unidirectional, the buttress thread (Figure 15-3c) can be used to obtain greater strength at the root than either of the others shown. Table 15-3 shows some principal dimensions for standard Acme threads.



Power Screw Application

Figure 15-4 shows one possible arrangement of a power screw used as a jack to lift a load. The nut is turned by an applied torque T and the screw translates up to lift the load P or down to lower it. There needs to be some friction at the load surface to prevent the screw from turning with the nut. Once the load P is engaged, this is not a problem. Alternatively, the screw could be turned against a fixed nut to lift the load. In either case there will be significant friction between the screw and the nut as well as friction between the nut and base, requiring that a thrust bearing be provided as shown. If a plain (i.e., nonrolling) thrust bearing is used, it is possible for the bearing interface to generate larger friction torque than the threads. Ball-thrust bearings are often used in this application to reduce these losses.

Other applications for power screws are in linear actuators, which operate on the same principle as shown in Figure 15-4, but either motorize the nut rotation to translate the screw or motorize the screw rotation to translate the nut, as shown in Figure 15-5. These devices are used in machine tools to move the table and workpiece under the cutting tool, in assembly machines to position parts, and in aircraft to move the control surfaces, as well as in many other applications. If the rotating input is provided by a servomotor or stepping motor in combination with a precision lead screw, very accurate positioning can be obtained.

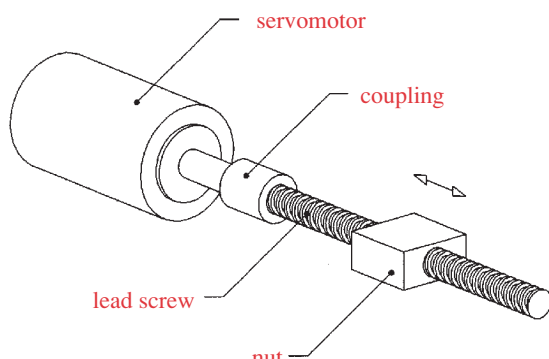
FIGURE 15-4

An Acme-Thread Power-Screw Jack

Table 15-3 Principal Dimensions of American Standard Acme Threads

See Reference 2 for More Complete Dimensional and Tolerance Information

Major Diameter (in)	Threads per inch	Thread Pitch (in)	Pitch Diameter (in)	Minor Diameter (in)	Tensile Stress Area (in ²)
0.250	16	0.063	0.219	0.188	0.032
0.313	14	0.071	0.277	0.241	0.053
0.375	12	0.083	0.333	0.292	0.077
0.438	12	0.083	0.396	0.354	0.110
0.500	10	0.100	0.450	0.400	0.142
0.625	8	0.125	0.563	0.500	0.222
0.750	6	0.167	0.667	0.583	0.307
0.875	6	0.167	0.792	0.708	0.442
1.000	5	0.200	0.900	0.800	0.568
1.125	5	0.200	1.025	0.925	0.747
1.250	5	0.200	1.150	1.050	0.950
1.375	4	0.250	1.250	1.125	1.108
1.500	4	0.250	1.375	1.250	1.353
1.750	4	0.250	1.625	1.500	1.918
2.000	4	0.250	1.875	1.750	2.580
2.250	3	0.333	2.083	1.917	3.142
2.500	3	0.333	2.333	2.167	3.976
2.750	3	0.333	2.583	2.417	4.909
3.000	2	0.500	2.750	2.500	5.412
3.500	2	0.500	3.250	3.000	7.670
4.000	2	0.500	3.750	3.500	10.321
4.500	2	0.500	4.250	4.000	13.364
5.000	2	0.500	4.750	4.500	16.800

**FIGURE 15-5**Servomotor-Driven Lead Screw for Use as a Positioning Device *Courtesy of J. Karsberg, Gillette Co. Inc.*

Power Screw Force and Torque Analysis

SQUARE THREADS A screw thread is essentially an inclined plane that has been wrapped around a cylinder to create a helix. If we unwrapped one revolution of the helix, it would look like Figure 15-6a, which shows a block representing the nut being slid up the inclined plane of a square thread. The forces acting on the nut as a free-body diagram are also shown. Figure 15-6b shows the free-body diagram of the same nut as it slides down the plane. The friction force, of course, always opposes motion. The inclination of the plane is called the lead angle λ .

$$\tan \lambda = \frac{L}{\pi d_p} \quad (15.3)$$

For the load-lifting case in Figure 15-6a, sum forces in x and y directions:

$$\begin{aligned} \sum F_x &= 0 = F - f \cos \lambda - N \sin \lambda = F - \mu N \cos \lambda - N \sin \lambda \\ F &= N(\mu \cos \lambda + \sin \lambda) \end{aligned} \quad (15.4a)$$

$$\begin{aligned} \sum F_y &= 0 = N \cos \lambda - f \sin \lambda - P = N \cos \lambda - \mu N \sin \lambda - P \\ N &= \frac{P}{(\cos \lambda - \mu \sin \lambda)} \end{aligned} \quad (15.4b)$$

where μ is the coefficient of friction between screw and nut and the other variables are defined in Figure 15-6. Combine these equations to get an expression for the force F :

$$F = P \frac{(\mu \cos \lambda + \sin \lambda)}{(\cos \lambda - \mu \sin \lambda)} \quad (15.4c)$$

The screw torque T_{s_u} required to lift the load is

$$T_{s_u} = F \frac{d_p}{2} = \frac{P d_p}{2} \frac{(\mu \cos \lambda + \sin \lambda)}{(\cos \lambda - \mu \sin \lambda)} \quad (15.4d)$$

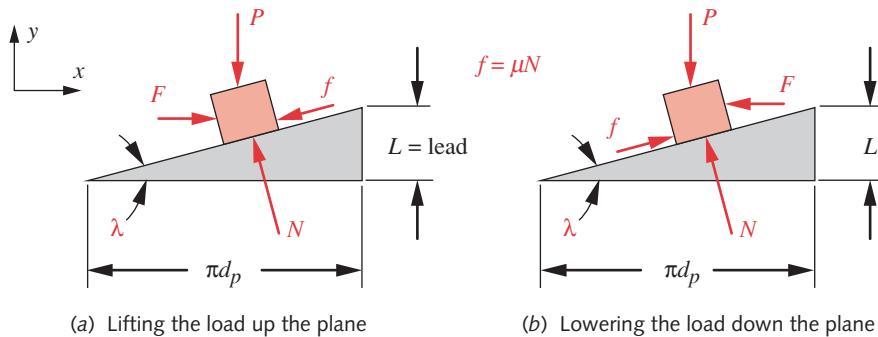
It is sometimes more convenient to express this as a function of lead L rather than lead angle λ , so divide the numerator and denominator of in equation 15.4d by $\cos \lambda$ and substitute the right-hand side of equation 15.3 for $\tan \lambda$:

$$T_{s_u} = \frac{P d_p}{2} \frac{(\mu \pi d_p + L)}{(\pi d_p - \mu L)} \quad (15.4e)$$

This expression accounts for the screw-nut interface of a square thread, but the thrust collar also contributes a friction torque, which must be added. The torque required to turn the thrust collar is

$$T_c = \mu_c P \frac{d_c}{2} \quad (15.4f)$$

where d_c is the mean diameter of the thrust collar and μ_c is the coefficient of friction in the thrust bearing. Note that the torque needed to overcome collar friction can equal

**FIGURE 15-6**

Force Analysis at the Screw-Nut Interface

or exceed the screw torque unless rolling-element bearings are used in the thrust collar. Smaller collar diameters will also reduce the collar torque.

The **total torque** T_u to **lift the load** with a square thread is then

$$T_u = T_{s_u} + T_c = \frac{Pd_p}{2} \frac{(\mu\pi d_p + L)}{(\pi d_p - \mu L)} + \mu_c P \frac{d_c}{2} \quad (15.4g)$$

The same analysis can be done for the case of lowering the load, as shown in Figure 15-6b. The applied- and friction-force signs change, and the **torque** T_d to **lower the load** is

$$T_d = T_{s_d} + T_c = \frac{Pd_p}{2} \frac{(\mu\pi d_p - L)}{(\pi d_p + \mu L)} + \mu_c P \frac{d_c}{2} \quad (15.4h)$$

ACME THREADS The radial angle of an Acme (or other) thread introduces an additional factor in the torque equations. The normal force between screw and nut is angled in two planes, at the lead angle λ as shown in Figure 15-6, and also at the $\alpha = 14.5^\circ$ angle of the Acme thread as shown in Figure 15-7. A similar derivation as done for the square thread will give expressions for lifting and lowering torques of

$$T_u = T_{s_u} + T_c = \frac{Pd_p}{2} \frac{(\mu\pi d_p + L \cos \alpha)}{(\pi d_p \cos \alpha - \mu L)} + \mu_c P \frac{d_c}{2} \quad (15.5a)$$

$$T_d = T_{s_d} + T_c = \frac{Pd_p}{2} \frac{(\mu\pi d_p - L \cos \alpha)}{(\pi d_p \cos \alpha + \mu L)} + \mu_c P \frac{d_c}{2} \quad (15.5b)$$

These equations reduce to those for the square thread when angle $\alpha = 0$.

Friction Coefficients

Experiments indicate that the coefficient of friction in an oil-lubricated thread-nut combination is about 0.15 ± 0.05 .^[5] The friction in a plain (nonrolling) thrust bearing is

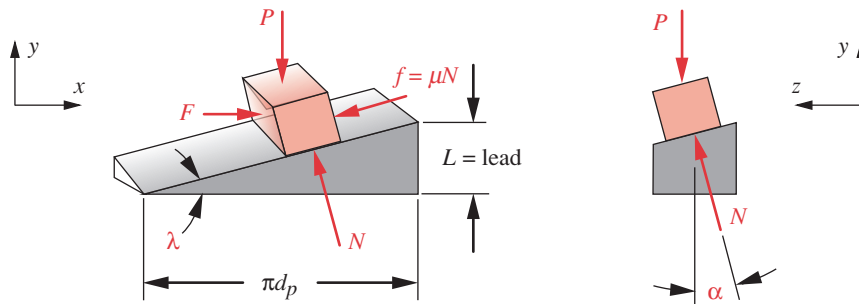


FIGURE 15-7

Force Analysis for an Acme-Thread Screw-Nut Interface

about the same as in the threads. Steel on bronze or steel on cast iron are common plain-bearing combinations. If a rolling-element bearing is used for the thrust washer, its coefficient of friction will be about 1/10 of the plain bearing values (i.e., 0.01 to 0.02).

Self-Locking and Back-Driving of Power Screws

Self-locking refers to a condition in which the screw cannot be turned by the application of any magnitude of force applied axially (not as a torque) to the nut. In other words, a self-locking screw will hold the load in place without any application of torque. It does not need a brake to hold the load. This is a very useful situation. For example, if you jacked up your car with a screw jack that was not self-locking, as soon as you let go of the jack handle the car would run the jack back down. You would have to be pretty fast with the lug wrench to change a tire in that case.

The opposite situation to self-locking is a screw that can be back driven, which means that pushing axially on the nut will cause the screw to turn. While of no value for a jack application, this is a useful feature in other situations. One example is a so-called *Yankee screwdriver*, which has a high-lead thread on its barrel that is attached to the blade. The handle is the nut. As you push down axially on the handle, the barrel turns, driving the wood screw into place. Any application in which you want to convert linear motion to rotary motion is a candidate for a back-drivable lead screw.

The condition of self-locking for a power or lead screw is easily predicted if the coefficient of friction in the screw-nut joint is known. The relationship between the friction coefficient and the screw's lead angle determines its self-locking condition. A screw will self-lock if

$$\mu \geq \frac{L}{\pi d_p} \cos \alpha \quad \text{or} \quad \mu \geq \tan \lambda \cos \alpha \quad (15.6a)$$

If it is a square thread, $\cos \alpha = 1$, and this reduces to

$$\mu \geq \frac{L}{\pi d_p} \quad \text{or} \quad \mu \geq \tan \lambda \quad (15.6b)$$

Note that these relationships presume a static loading situation. The presence of any vibration from dynamic loading or other sources can cause an otherwise self-locking screw to back down. Any vibrations that cause relative motion between screw and nut will inevitably cause slippage down the thread's incline.

Screw Efficiency

The efficiency of any system is defined as *work out / work in*. The work done on a power screw is the product of torque and angular displacement (in radians), which for one revolution of the screw is

$$W_{in} = 2\pi T \quad (15.7a)$$

The work delivered over one revolution is the load-force times the lead:

$$W_{out} = PL \quad (15.7b)$$

The efficiency is then

$$e = \frac{W_{out}}{W_{in}} = \frac{PL}{2\pi T} \quad (15.7c)$$

Substituting equation 15.5a (neglecting the collar-friction term) gives

$$e = \frac{L}{\pi d_p} \frac{\pi d_p \cos \alpha - \mu L}{\pi \mu d_p + L \cos \alpha} \quad (15.7d)$$

This can be simplified by substituting equation 15.3:

$$e = \frac{\cos \alpha - \mu \tan \lambda}{\cos \alpha + \mu \cot \lambda} \quad (15.7e)$$

Note that efficiency is a function only of the screw geometry and the coefficient of friction. For a square thread, $\alpha = 0$ and

$$e = \frac{1 - \mu \tan \lambda}{1 + \mu \cot \lambda} \quad (15.7f)$$

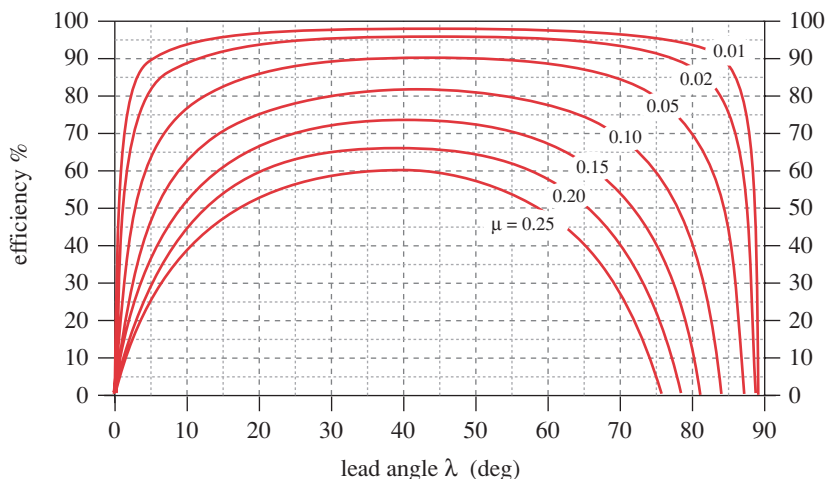
Figure 15-8 shows plots of the efficiency function for an Acme thread over a range of coefficients of friction, neglecting collar friction. Higher coefficients of friction reduce efficiency, as should be expected. Note that the efficiency is zero when the lead angle $\lambda = 0$, because no useful work is being done to raise the load, but friction is still present. The efficiency also approaches zero at high lead angles, because the torque is simply increasing the normal force (and thus friction) without any useful component to rotate the nut. The total efficiency including collar friction will be lower than is shown in Figure 15-8.

Figure 15-8 points out the major drawback of conventional power screws: their potentially low efficiency. Standard Acme screws have lead angles that vary between about 2 and 5°, as shown in Table 15-4. This puts them at the extreme left of the set of curves in Figure 15-8. The efficiencies of standard Acme screws for an assumed coefficient of friction of 0.15 are seen in Table 15-4 to vary between 18 and 36%. If the thread friction can be reduced, significant efficiency increases can be realized.

Table 15-4

Lead Angle and Efficiency for Standard Acme Threads with Coefficient of Friction $\mu = 0.15$

Size	Lead Angle (deg)	Efficiency %
1/4 - 16	5.2	36
5/16 - 14	4.7	34
3/8 - 12	4.5	34
7/16 - 12	3.8	30
1/2 - 10	4.0	31
5/8 - 8	4.0	31
3/4 - 6	4.5	34
7/8 - 6	3.8	30
1 - 5	4.0	31
1 1/8 - 5	3.6	28
1 1/4 - 5	3.2	26
1 3/8 - 4	3.6	29
1 1/2 - 4	3.3	27
1 3/4 - 4	2.8	24
2 - 4	2.4	21
2 1/4 - 3	2.9	25
2 1/2 - 3	2.6	23
2 3/4 - 3	2.4	21
3 - 2	3.3	27
3 1/2 - 2	2.8	24
4 - 2	2.4	21
4 1/2 - 2	2.1	19
5 - 2	1.9	18

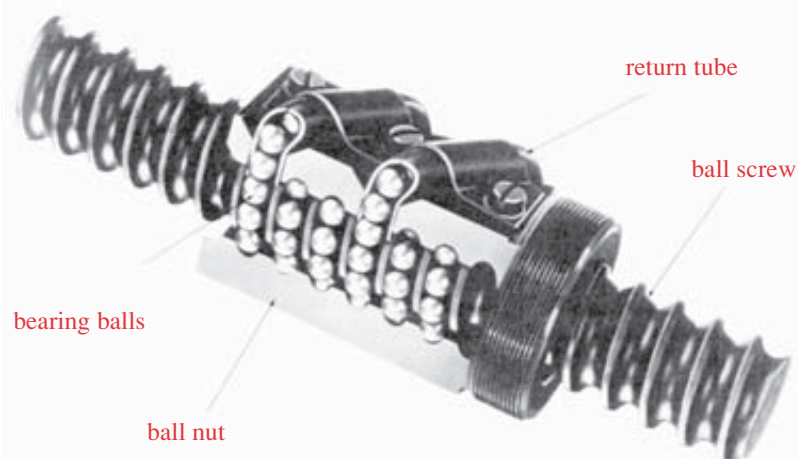
**FIGURE 15-8**

Efficiency for an Acme-Thread Power Screw (Neglecting Thrust-Collar Friction)

Ball Screws

A significant reduction in thread friction can be obtained with the use of ball screws, which use a train of ball bearings in the nut to create an approximate rolling contact with the screw threads, as shown in Figure 15-9. The thread form is shaped to fit the spherical balls and is usually hardened and ground for long life. The friction coefficient is similar to that of conventional ball bearings, putting them in the range of the top two curves in Figure 15-8, with correspondingly higher efficiency.

The low friction of ball screws makes them back-drivable and thus **not** self-locking. Thus a brake must be used to hold a load driven by a ball screw. So, ball screws can be used to convert linear to rotary motion. They have very high load capacity, typi-

**FIGURE 15-9**

A Ball Screw and Ball Nut Courtesy of Thompson-Saginaw Ball Screw Co., Saginaw, Mich.

cally larger than a conventional screw of the same diameter, and they do not suffer from the stick-slip characteristics of sliding joints.

Ball screws are used in many applications from aircraft control-surface and landing-gear actuators to machine-tool controls, automotive steering mechanisms, and hospital-bed mechanisms. Many manufacturers supply ball-screw assemblies, and they should be consulted for technical information regarding their proper application.

EXAMPLE 15-1

Torque and Efficiency of a Power Screw

Problem Determine the lifting and lowering torques and the efficiency of the power screw shown in Figure 15-4 (p. 866) using an Acme screw and nut. Is it self-locking? What is the contribution of collar friction versus screw friction if the collar has (a) sliding friction, (b) rolling friction?

Given The screw is a single-start Acme 1.25–5. The axial load is 1 000 lb. The mean collar diameter is 1.75 in.

Assumptions The screw and nut are lubricated with oil. Sliding friction $\mu = 0.15$, rolling friction $\mu = 0.02$.

Solution

- There are several aspects to this problem. We need to compute the lifting and lowering torques for two cases, one with a sliding-friction collar and one with a ball-bearing collar. In both cases we will calculate the screw and collar contributions to torque and efficiency separately for comparison and also combine them. First do the case of the sliding collar.
- Since it is a single-start thread, the lead L equals the pitch p , which is $1/N = 0.2$. The pitch diameter of the thread d_p is found in Table 15-3 (p. 867). The torque to lift the load is found from equation 15.5a (p. 869):

$$\begin{aligned} T_u &= T_{s_u} + T_c = \frac{Pd_p}{2} \frac{(\mu\pi d_p + L \cos\alpha)}{(\pi d_p \cos\alpha - \mu L)} + \mu_c P \frac{d_c}{2} \\ &= \frac{1000(1.15)}{2} \frac{(0.15\pi(1.15) + 0.2 \cos 14.5)}{(\pi(1.15)\cos 14.5 - 0.15(0.2))} + 0.15(1000) \frac{1.75}{2} \end{aligned} \quad (a)$$

$$T_u = 122.0 + 131.2 = 253.2 \text{ lb-in}$$

Note that the collar friction exceeds the screw friction.

- The torque to lower the load is found from equation 15.5b:

$$\begin{aligned} T_d &= T_{s_d} + T_c = \frac{Pd_p}{2} \frac{(\mu\pi d_p - L \cos\alpha)}{(\pi d_p \cos\alpha + \mu L)} + \mu_c P \frac{d_c}{2} \\ &= \frac{1000(1.15)}{2} \frac{(0.15\pi(1.15) - 0.2 \cos 14.5)}{(\pi(1.15)\cos 14.5 - 0.15(0.2))} + 0.15(1000) \frac{1.75}{2} \end{aligned} \quad (b)$$

$$T_d = 56.8 + 131.2 = 188.0 \text{ lb-in}$$

- 4 The efficiency in the lifting mode will be less than for lowering and is found from equations 15.7 (p. 871). We choose the version shown as equation 15.7c in order to account for both screw and collar components.

$$e = \frac{PL}{2\pi T}$$

For the screw $e_{screw} = \frac{1000(0.2)}{2\pi(122.0)} = 0.26$ (c)

For both combined $e = \frac{1000(0.2)}{2\pi(253.2)} = 0.13$

- 5 Now recalculate the collar torque and total torque to lift the load with a ball-bearing thrust washer, using equation 15.4f.

$$T_c = \mu_c P \frac{d_c}{2} = 0.02(1000) \frac{1.75}{2} = 17.5 \text{ lb-in} \quad (d)$$

$$T_u = T_{s_u} + T_c = 122.0 + 17.5 = 139.5 \text{ lb-in} \quad (e)$$

- 6 The efficiency with the ball-bearing thrust washer is now:

$$e = \frac{PL}{2\pi T} = \frac{1000(0.2)}{2\pi(139.5)} = 0.23 \quad (f)$$

The improvement in efficiency is significant and shows why it is poor practice to use anything but a rolling-element bearing as a thrust washer on a power screw.

- 7 The self-locking aspects of the screw are independent of the thrust-collar friction and can be found from equation 15.6a (p. 870).

$$\begin{aligned} \mu &\geq \frac{L}{\pi d_p} \cos \alpha \\ 0.15 &\geq \frac{0.2}{\pi(1.15)} \cos(14.5^\circ) \end{aligned} \quad (g)$$

$0.15 \geq 0.06$ so it self-locks

Note that the positive lowering torque in step 3 also indicates that the screw is self-locking. A negative lowering torque means that a braking torque of opposite sense to the lift torque must be applied to hold the load. The files EX15-01A and EX15-01B are on the CD-ROM.

15.3 STRESSES IN THREADS

A similar situation exists in mating threads as in mating gear teeth. Section 12.4 (p. 694) discusses the desirability of having multiple gear teeth in contact in a garmesh (contact ratio > 1), and Figure 12-19 (p. 706) shows a garmesh in which two teeth are taking all the load due to inaccuracies in tooth spacing despite an apparently large contact ratio. When a nut engages a thread, theoretically all the threads in engagement should share the load. In actuality, inaccuracies in thread spacing cause virtually all the load to be taken by the first pair of threads. Thus, the conservative approach in calculating

thread stresses is to assume the worst case of one thread-pair taking the entire load. The other extreme is to assume that all the engaged threads share the load equally. Both of these assumptions can be used to calculate estimated thread stresses. The true stress will be between these extremes, but most likely closer to the one-thread assumption. Power screws and fasteners for high-load applications are usually made of high-strength steel and are often hardened. Power-screw nuts may also be of hardened material for strength and wear resistance. Fastener nuts, on the other hand, are often made of soft material and are thus typically weaker than the screw. This promotes local yielding in the nut threads when the fastener is tightened, which can improve the thread fit and promote load-sharing between threads. Hardened nuts are used on high-strength, hardened bolts.

Axial Stress

A power screw can see axial loads of either tension or compression. A threaded fastener typically sees only axial tension. The tensile stress area of a screw thread was discussed earlier and is defined in equation 15.1 (p. 863) and Tables 15-1, 15-2, and 15-3 (pp. 864–867) for various types of threads. Equation 15.2 (p. 863) can be used to compute the axial tension stress in a screw. For power screws loaded in compression, the possibility of column buckling must be investigated using the methods outlined in Section 4.16 (p. 193). Use the screw's minor diameter to compute the slenderness ratio.

Shear Stress

One possible shear-failure mode involves stripping of the threads either out of the nut or off the screw. Which, if either, of these scenarios occurs is dependent on the relative strengths of the nut and screw materials. If the nut material is weaker (as is often the case), it may strip its threads at its major diameter. If the screw is weaker, it may strip its threads at its minor diameter. If both materials are of equal strength, the assembly may strip along the pitch diameter. In any event, we must assume some degree of load sharing among the threads in order to calculate a stress. One approach is to consider that, since complete failure requires all threads to strip, all can be considered to share the load equally. This is probably a good assumption as long as the nut or screw (or both) is ductile to allow each thread to yield as the assembly begins to fail. However, if both parts are brittle (e.g., high-hardness steels or cast iron) and the thread fit is poor, one can envision each thread taking the entire load in turn until it fractures and passes the job to the next thread. Reality is again somewhere between these extremes. If we express the shear area in terms of number of threads in engagement, a judgment can be made in each case as to what degree of load sharing is appropriate.

The stripping-shear area A_s for one screw thread is the area of the cylinder of its minor diameter d_r :

$$A_s = \pi d_r w_i p \quad (15.8a)$$

where p is the thread pitch and w_i is a factor that defines the percentage of the pitch occupied by metal at the minor diameter. Values of w_i for several common thread forms are shown in Table 15-5. The area for one thread pitch from equation 15.8a can be multiplied by all, one, or some fraction of the total number of threads in engagement based on the designer's judgment of the factors discussed above for the particular case.

Table 15-5

Area Factors for Thread-Stripping Shear Area

Thread Type	w_i (minor)	w_o (major)
UNS/ISO	0.80	0.88
Square	0.50	0.50
Acme	0.77	0.63
Buttress	0.90	0.83

For the nut stripping at its major diameter, the shear area for one screw thread is

$$A_s = \pi d w_o p \quad (15.8b)$$

where the value for w_o at the major diameter is found in Table 15-5.

The shear stress for thread stripping τ_s is then found from:

$$\tau_s = \frac{F}{A_s} \quad (15.8c)$$

MINIMUM NUT LENGTH If the nut is long enough, the load required to strip the threads will exceed the load needed to fail the screw in tension. The equations for both modes of failure can be combined and a minimum nut length computed for any particular screw size. For any UNS/ISO threads or Acme threads of $d \leq 1$ in, a nut length of at least $0.5 d$ will have a strip strength in excess of the screw's tensile strength. For larger-diameter Acme threads, the strip-strength of a nut with length $\geq 0.6 d$ will exceed the screw's tensile strength. These figures are valid only if the screw and nut are of the same material, which is usually the case.

MINIMUM TAPPED-HOLE ENGAGEMENT When a screw is threaded into a tapped hole rather than a nut, a longer thread engagement is needed. For same-material combinations, a thread-engagement length at least equal to the nominal thread diameter d is recommended. For a steel screw in cast iron, brass, or bronze, use $1.5d$. For steel screws in aluminum, use $2d$ of minimum thread-engagement length.

Torsional Stress

When a nut is tightened on a screw, or when a torque is transmitted through a power-screw nut, a torsional stress can be developed in the screw. The torque that twists the screw is dependent on the friction at the screw-nut interface. If the screw and nut are well lubricated, less of the applied torque is transmitted to the screw and more is absorbed between the nut and the clamped surface. If the nut is rusted to the screw, all the applied torque will twist the screw, which is why rusty bolts usually shear even when you attempt to loosen the nut. In a power screw, if the thrust collar has low friction, all the applied torque at the nut will create torsional stress in the screw (since little torque is taken to ground through the low-friction collar). Thus, to accommodate the worst case of high thread friction, use the total applied torque in the equation for torsional stress in a round section (see Section 4.12 on p. 177):

$$\tau = \frac{Tr}{J} = \frac{16T}{\pi d_r^3} \quad (15.9)$$

The minor diameter d_r of the thread should be used in this calculation.

15.4 TYPES OF SCREW FASTENERS*

There is a wide variety of screw styles available, many of which are for specialized applications. Conventional bolts and nuts typically use standard threads as defined in Section 15.1. Variations in the standard thread are possible among certain varieties of

* Complete descriptions and size information for a large variety of standard fasteners can be found in reference [2].

screws, especially those intended for self-tapping applications. Fasteners can be classified in different ways: by their intended use, by thread type, by head style, and by their strength. Fasteners of all types are available in a variety of materials including steel, stainless steel, aluminum, brass, bronze, and plastics.

Classification by Intended Use

BOLTS AND MACHINE SCREWS The same fastener may take on a different name when used in a particular manner. For example, a **bolt** is a fastener with a head and a straight, threaded shank intended to be used with a **nut** to clamp an assembly together. However, the same fastener is called a **machine screw** or **cap screw** when it is threaded into a tapped hole rather than used with a nut. This is only a semantic distinction, but one in which some purists take great stock. The ANSI standards distinguish between a bolt and a screw by noting that a bolt is intended to be held stationary while a nut is torqued onto it to make the joint, whereas a screw is intended to be turned into its receptacle, be that a tapped or untapped hole, by torquing its head. (Nevertheless, it is not yet illegal in most states to place a nut on a machine screw, but be forewarned—you will change it instantly into a bolt by doing so!)

STUDS A **stud** is a headless fastener, threaded on both ends and intended to be semipermanently threaded into one-half of an assembly. A hole in the mating part then drops over the protruding stud and is secured with a nut. Each end of the stud can have either the same or different pitch thread. The permanent end sometimes has a higher-class thread fit to grip the tapped hole and resist loosening when the nut is removed from the top half.

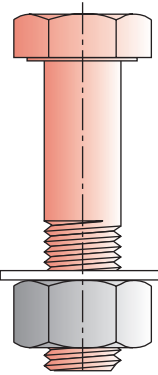
Figure 15-10 shows a bolt (with nut and washer), a machine screw, and a stud. Another distinction between screws and bolts is that a bolt has only straight, uniform threads whereas a screw can have any thread form, including tapered or interrupted as shown in Figure 15-11. Thus, there are **wood screws** but not “wood bolts” (though *carriage bolts* are used to fasten wood assemblies).

Classification by Thread Type

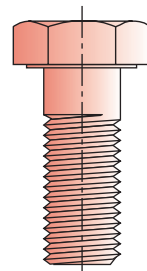
TAPPING SCREWS All fasteners intended to make their own hole or make their own threads are called **tapping screws**, as in *self-tapping*, *thread-forming*, *thread-cutting*, and *self-drilling screws*. Figure 15-11 shows a selection of the many thread types available in tapping screws. Tapping-screw threads are similar to the standard form but are often spaced further apart (i.e., larger pitch) for use in sheet metal or plastic to allow the displaced material a place to go as the screw forces its way into a small pilot hole while forming the threads. Thread-cutting screws have a standard thread form but are relieved with axial grooves and hardened to provide a cutting edge to tap the part as the screw is inserted. Self-drilling screws (not shown) have a drill-bit shape at their tip to make the pilot hole. They also form the threads as they are driven in.

Classification by Head Style

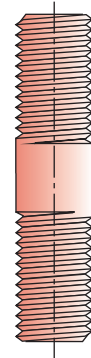
SLOTTED SCREWS Many different head styles are made, including straight-slot, cross-slot (Phillips), hexagonal, hexagonal socket, and others. Head shape can be round, flat



(a) Bolt, washer, and nut



(b) Machine (cap) screw



(c) Stud

FIGURE 15-10

Bolt and Nut, Machine Screw and Stud



(a) Socket head



(b) Socket flat head



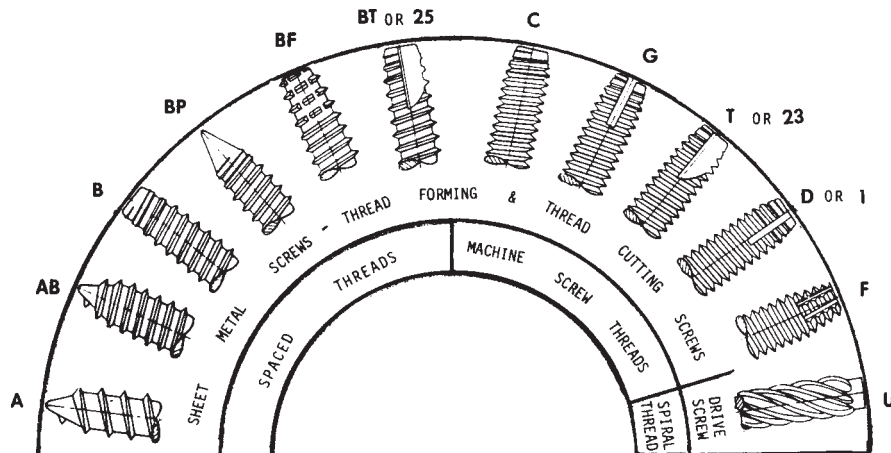
(c) Socket button head



(d) Shoulder screw



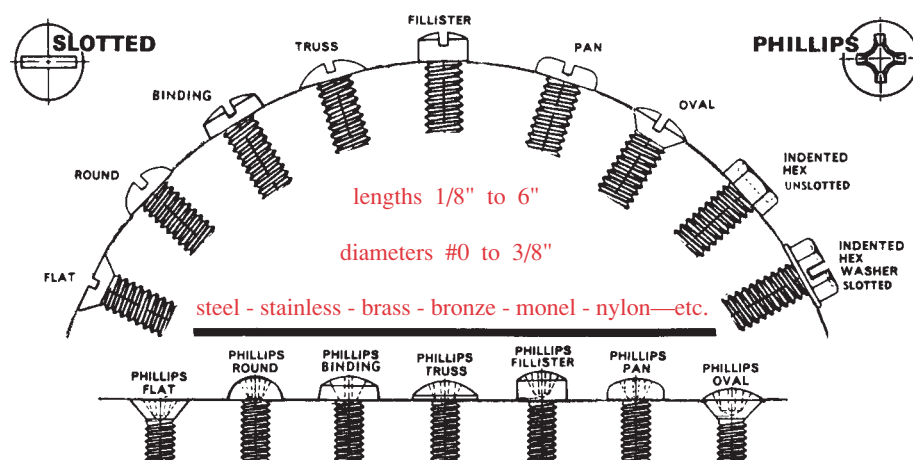
(e) Socket set screw

**FIGURE 15-11**

Various Styles of Threads Used on Tapping Screws Courtesy of Cordova Bolt Inc., Buena Park, Calif. 90621

(recessed), filister, pan, etc., as shown in Figure 15-12. These head styles in combination with slotted or Phillips grooves are typically used only on smaller machine or tapping screws, as the maximum torque obtainable with these slots is limited. The torques needed with larger screws are more readily obtained with hexagonal heads or hexagonal-socket heads, as shown in Figures 15-10 and 15-13. Hex heads are the most popular style for larger bolts and machine screws that require substantial torque unless space is limited, in which case the socket-head cap screw is a better choice.

SOCKET-HEAD CAP SCREWS as shown in Figure 15-13 are typically made of high-strength, hardened steel, stainless steel, or other metals, and are used extensively in ma-

**FIGURE 15-12**

Various Styles of Heads Used on Small Machine Screws Courtesy of Cordova Bolt Inc., Buena Park, Calif.

FIGURE 15-13

Various Styles of Socket-Head Cap Screws Courtesy of Cordova Bolt Inc., Buena Park, Calif.

chinery. The hex socket allows sufficient torque to be applied with special hexagonal Allen wrenches. The standard socket head style (Figure 15-13a) is designed to be placed in a counterbore so that the head is flush-to-below the surface. The flat-head cap screw (Figure 15-13b) is countersunk flush. The shoulder screw (Figure 15-13d) has a close-tolerance, ground-finish shank that can be used as a pivot or to accurately locate a part. The screw is torqued tightly against its shoulder, and yet a properly sized part can be free to pivot between its head and the surface into which it is screwed. Set screws (Figure 15-13e) are used to lock collars and hubs to shafts, as described in Chapter 10.

Nuts and Washers

NUTS Figure 15-14 shows a sample of the large variety of nuts available. The jam nut is a thinner version of the standard hex nut and is used in combination with a standard nut to lock the standard nut to the bolt. The castle nut has grooves for insertion of a cotter pin through a cross-hole in the bolt to prevent the nut from working loose. An acorn nut is used for decorative purposes and a wing nut allows removal without tools.

LOCK NUTS A universal concern is the prevention of spontaneous loosening of nuts due to vibration. Two nuts jammed together on the bolt or a castle nut with cotter pin both reliably achieve this goal. Many other proprietary designs of lock nuts are offered by manufacturers. A few are shown in Figure 15-15. The elliptical lock nut has its top few threads upset into an elliptical shape after the nut is made. These threads provide interference with those on the bolt and, when forced on, grip the thread and resist loosening. Nuts are also made with nylon inserts in the threads that deform when forced onto the bolt. The nylon flows into the thread clearances and grips the bolt. A pin lock nut has a steel pin that allows tightening, but digs into the bolt threads to prevent loosening. Nuts are also made with serrations on one face that act to dig into the clamped part and resist loosening.

WASHERS A plain washer is simply a flat, doughnut-shaped part that serves to increase the area of contact between the bolt head or nut and the clamped part (see Figure 15-10). Hardened-steel washers are used where the bolt compression load on the clamped part needs to be distributed over a larger area than the bolt head or nut provides. A soft washer will yield in bending rather than effectively distribute the load. Any plain washer also prevents marring of the part surface by the nut when it is tightened. Nonmetallic washers are used when electrical insulation of the bolt from the part is required. Flat-washer sizes are standardized to bolt size (see reference 2). If washers larger than the standard diameter are needed, **fender washers** (which have larger outside diameter) can be used. **Belleville washers** (see Section 14.9 on p. 838) are sometimes used under nuts or screw heads to provide a controlled axial force over changes in bolt length.

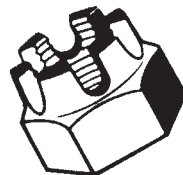
LOCK WASHERS To help prevent spontaneous loosening of standard nuts (as opposed to lock nuts) lock washers can be used under the nut of a bolt or under the head of a machine screw. Figure 15-16 shows several of the many styles of lock washers available. The split washer is hardened steel and acts as a spring under the nut. Its sharp corners also tend to dig into the clamped surfaces. Various styles of toothed washers are also offered. Their turned-up teeth are compressed when clamped, and dig into the nut and part surfaces. Lock washers are generally considered to be less effective in preventing loosening than lock nuts, which are preferred.



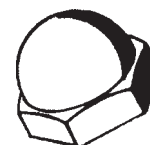
(a) Standard hex nut



(b) Hex jam nut



(c) Hex castle nut



(d) Hex acorn nut



(e) Wing nut

FIGURE 15-14

Some Styles of Standard Nuts
Courtesy of Cordova Bolt Inc.,
Buena Park, Calif. 90621



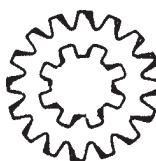
(a) Split lock washer



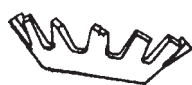
(b) Internal-tooth washer



(c) External-tooth washer



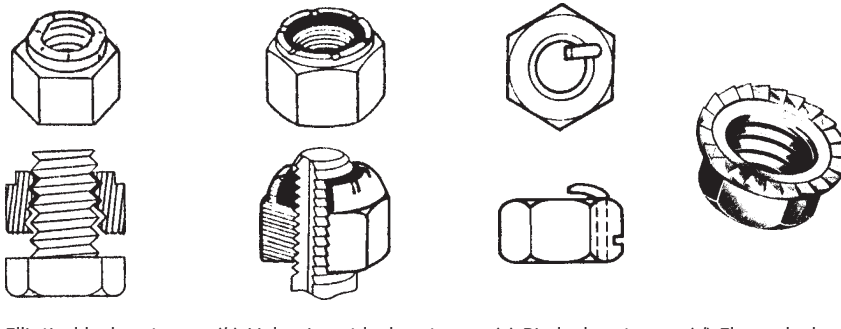
(d) Internal-external tooth



(e) Countersunk tooth

FIGURE 15-16

Types of Lock Washers
Courtesy of Cordova Bolt Inc., Buena Park, Calif.

**FIGURE 15-15**

A Small Sample of the Types of Lock Nuts Available Courtesy of Cordova Bolt Inc., Buena Park, Calif.

SEMS are combinations of nuts and captive lock washers that remain with the nut. Many styles are made, one of which is shown in Figure 15-17. Their main advantage is to ensure that the lock washer will not be left out at assembly or reassembly.

15.5 MANUFACTURING FASTENERS

THREAD CUTTING Several techniques are available for making threads. Internal threads are usually cut with a special tool called a **tap** that has the desired thread form and looks like a screw. A tap is made of hardened tool steel and has axial grooves that interrupt its threads to provide cutting edges in the shape of the threads. A pilot hole is drilled with a proper-size tap drill and the lubricated tap is turned slowly into the hole while being advanced at a suitable rate. Nuts too large to tap are threaded in a lathe with a thread-shaped, single-point tool that is advanced axially through the hole by a lead screw to control its lead and pitch. External threads can also be cut with a single-point tool in a lathe or alternatively with a **die**, which is the external-thread equivalent of a tap. The rod to be threaded is the same size as the outside diameter of the thread. Specialized machines called *screw machines* are used to produce screws, bolts, and nuts (as well as other turned parts) in high quantity at low cost. All threads made by the methods described above are classified as **cut threads**.

THREAD ROLLING Another, and superior, method for making external threads is by **thread rolling**, also called **thread forming**. Hardened-steel dies in the form of threads are forced into the surface of the rod being threaded. The dies cold-flow the material into the thread shape. The final outside diameter of the thread is larger than the initial diameter of the rod, because material is forced out of the roots and into the crests of the threads.

There are several advantages of rolling versus cutting threads. The cold forming work-hardens and strengthens the material, creates radii at root and crest, and introduces favorable compressive residual stresses at the thread roots. The disruption of the material's shape into the thread form causes a reorientation of the material's grain to the thread shape. In contrast, thread cutting interrupts the grain. All of these factors contribute to a significant increase in the strength of rolled threads compared to cut threads.

In addition to their better strength, rolled threads have less waste than cut threads, as no material is removed, and the blank is consequently smaller in volume. High-strength fasteners are usually hardened steel. Thread rolling should be done after hardening the bolt, if possible, as the thermal hardening process will relieve the desirable residual stresses introduced by rolling.

Figure 15-18 shows the profiles and grain structure of cut and rolled threads. In any application where the loads on fasteners are high or where fatigue loads are present, rolled threads should always be used. In noncritical or lightly loaded applications, the weaker and less-expensive cut threads may be used.

HEAD FORMING The heads of bolts and screws are typically cold formed in an *upsetting* process. To picture this process, imagine taking a rod of modeling clay in your hand, leaving a short length sticking up above your fist. Smack the top of the clay rod axially with your other hand while tightly gripping the rod in your fist and you will mushroom the rod-end into a shorter but larger-diameter head. In similar fashion, the shank of the *bolt-to-be* is gripped tightly in the cold-heading machine with the appropriate length sticking out. A die of the desired head diameter surrounds this exposed end. When the hammer comes down, it cold-flows the material into a round head. Similar improvements in grain orientation in the head are achieved as were described above for thread rolling. Bolts over about 3/4-in diameter must be heated before being headed. Hexagonal sockets and Phillips slots are formed in the cold (or hot) heading process. Hexagonal flats or screw slots are later machined into the head.

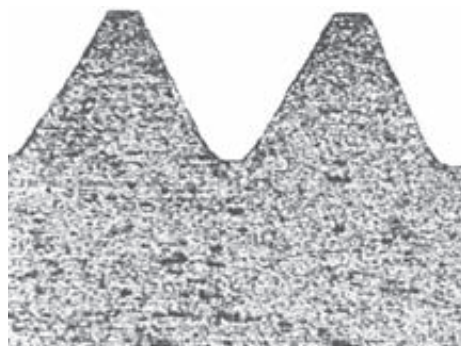


FIGURE 15-17

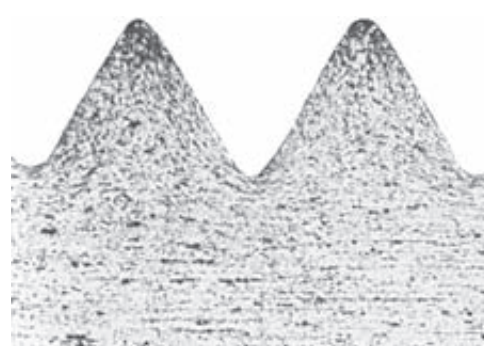
Nut with Captive Lock Washer
(SEM) Courtesy of Cordova Bolt Inc., Buena Park, Calif. 90621

15.6 STRENGTHS OF STANDARD BOLTS AND MACHINE SCREWS

Bolts and screws for structural or heavily loaded applications should be selected based on their proof strength S_p as defined in SAE, ASTM, or ISO specifications. These organizations define bolt grades or classes that specify material, heat treatment, and a **minimum proof strength** for the bolt or screw. **Proof strength** S_p is the stress at which the bolt begins to take a permanent set, and is close to, but lower than, the yield strength of the material. The grade or class of each bolt is indicated by marks (or their absence)



(a) Cut threads



(b) Rolled threads

FIGURE 15-18

Grain Structure of Cut and Rolled Threads Source: R. D. Barer and B. F. Peters, *Why Metals Fail*, Gordon and Breach, New York, 1970, p. 23

Table 15-6 SAE Specifications and Strengths for Steel Bolts

SAE Grade Number	Size Range Outside Diameter (in)	Minimum Proof Strength (kpsi)	Minimum Yield Strength (kpsi)	Minimum Tensile Strength (kpsi)	Material
1	0.25–1.5	33	36	60	low or medium carbon
2	0.25–0.75	55	57	74	low or medium carbon
2	0.875–1.5	33	36	60	low or medium carbon
4	0.25–1.5	65	100	115	medium carbon, cold drawn
5	0.25–1.0	85	92	120	medium carbon, Q&T*
5	1.125–1.5	74	81	105	medium carbon, Q&T
5.2	0.25–1.0	85	92	120	low-carbon martensite, Q&T
7	0.25–1.5	105	115	133	medium-carbon alloy, Q&T
8	0.25–1.5	120	130	150	medium-carbon alloy, Q&T
8.2	0.25–1.0	120	130	150	low-carbon martensite, Q&T

* Quenched and Tempered.

SAE Grade



1



2



4



5



5.2



7



8



8.2

on the head. Table 15-6 shows strength information for several SAE grades of bolts and Table 15-7 shows similar information for metric bolts. The head markings for each grade or class are shown in Figures 15-19 and 15-20.

15.7 PRELOADED FASTENERS IN TENSION

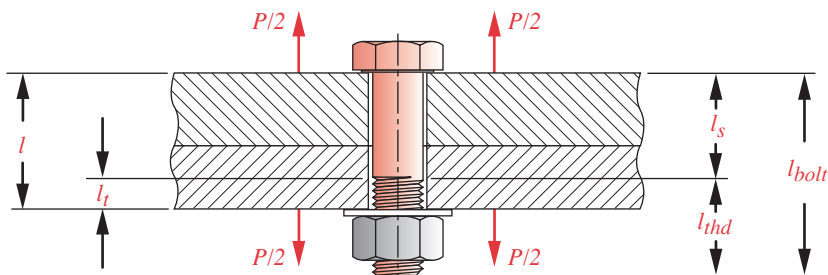
One of the primary applications of bolts and nuts is clamping parts together in situations where the applied loads put the bolt(s) in tension, as shown in Figure 15-21. It is common practice to preload the joint by tightening the bolt(s) with sufficient torque to create tensile loads that approach their proof strength. For statically loaded assemblies, a preload that generates bolt stress as high as 90% of the proof strength is sometimes used. For dynamically loaded assemblies (fatigue loading) a preload of 75% or more of proof strength is commonly used. Assuming that the bolts are suitably sized for the applied loads, these high preloads make it very unlikely that the bolts will break in ser-

Table 15-7 Metric Specifications and Strengths for Steel Bolts

Class Number	Size Range Outside Diameter (mm)	Minimum Proof Strength (MPa)	Minimum Yield Strength (MPa)	Minimum Tensile Strength (MPa)	Material
4.6	M5–M36	225	240	400	low or medium carbon
4.8	M1.6–M16	310	340	420	low or medium carbon
5.8	M5–M24	380	420	520	low or medium carbon
8.8	M3–M36	600	660	830	medium carbon, Q&T
9.8	M1.6–M16	650	720	900	medium carbon, Q&T
10.9	M5–M36	830	940	1 040	low-carbon martensite, Q&T
12.9	M1.6–M36	970	1 100	1 220	alloy, quenched & tempered

FIGURE 15-19

Head Marks for SAE Bolts

**FIGURE 15-21**

A Bolted Assembly in Tension

vice if they do not break while being tensioned (tightened). The reasons for this are subtle and require an understanding of how the elasticities of the bolt and the clamped members interact when the bolt is tightened and when the external load is later applied.

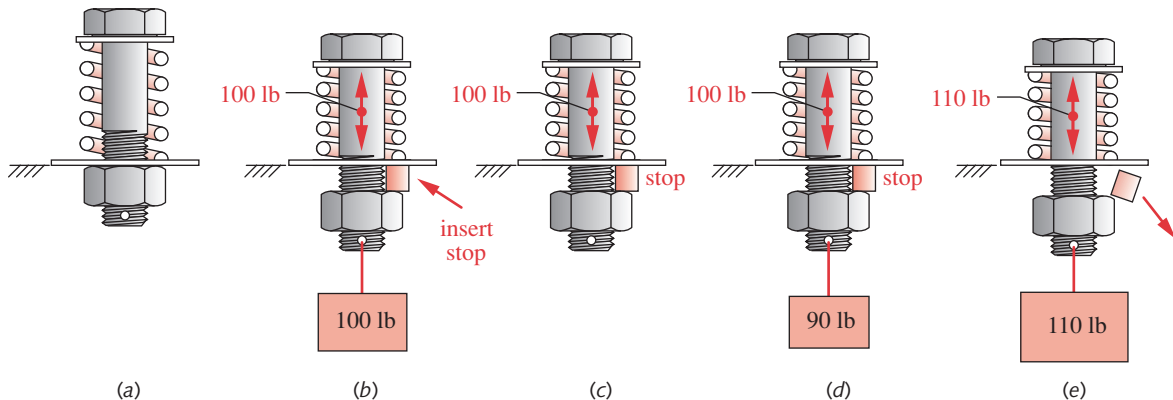
Figure 15-22 shows a bolt clamping a spring, which is the analogue of the clamped material in Figure 15-21. Whatever material is clamped, it will have a spring constant and will compress when the bolt is tightened. (The bolt, also being elastic, will stretch when tightened.) We show a spring as the clamped material in Figure 15-22a in order to exaggerate its compression for illustration purposes. For the same reason, we also postulate an unusual method for tensioning this particular bolt. It seems that we misplaced our wrench, and so had to ask Crusher Casey to grab that nut and pull it down with 100 lb of force while we stuck a scrap of steel between the nut and the ground plane to serve as a stop as shown in (b). The bolt now has 100 lb of tensile preload in it and the spring (i.e., the material) has 100 lb of compressive preload. This preload remains in the assembly even after Crusher has let go (c). The situation depicted in (c) is identical to that which would result if the nut had been tightened conventionally to compress the spring the same amount.

Figure 15-22d shows a new load of 90 lb applied to the bolt. Note that the tension in the bolt is still 100 lb and will be so regardless of the external load applied until that

Metric Class	Head Marks—Metric Bolts
4.6	
4.8	
5.8	
8.8	
9.8	
10.9	
12.9	

FIGURE 15-20

Head Marks—Metric Bolts

**FIGURE 15-22**

Preloading a Bolted Assembly

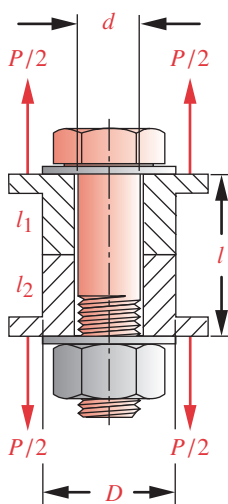


FIGURE 15-23

A Preloaded Bolt Compressing a Cylinder to Which External Loads Are Applied

load exceeds the preload of 100 lb in this case. Figure 15-22e shows that a load larger than the preload further compresses the spring, breaking the contact between nut and ground plane, and the bolt tension is now equal to the new applied load of 110 lb. When the bolt and the material separate as in (e), the bolt takes the full amount of the applied load. This diagram hints at why the presence of a preload is advantageous, especially when the applied loads are varying with time. To fully understand why requires further examination of the joint's elastic behavior under loading.

Figure 15-23 shows a bolt clamping a cylinder of known cross section and length. We wish to examine the loads, deflections, and stresses in both bolt and cylinder under preload and after an external load is applied. The spring constant of a bar in tension is found from the equation for the deflection of a tension bar:

$$\delta = \frac{Fl}{AE} \quad (15.10a)$$

and

$$k = \frac{F}{\delta} = \frac{AE}{l} \quad (15.10b)$$

The clamped material typically contains two or more pieces and they may be of different materials. Also, a long bolt will have threads over only a portion of its length and thus have two different cross-sectional areas. These different-stiffness sections act as springs in series that combine according to equation 14.2b, repeated here:

$$\frac{1}{k_{total}} = \frac{1}{k_1} + \frac{1}{k_2} + \frac{1}{k_3} + \dots + \frac{1}{k_n} \quad (14.2b)$$

For a round bolt of diameter d and axially loaded thread length l_t within its clamped zone of length l as shown in Figure 15-21, the theoretical spring constant is

$$\frac{1}{k_b} = \frac{l_t}{A_t E_b} + \frac{l - l_t}{A_b E_b} = \frac{l_t}{A_t E_b} + \frac{l_s}{A_b E_b} \quad \therefore \quad k_b = \frac{A_t A_b}{A_b l_t + A_t l_s} E_b \quad (15.11a)$$

where A_b is the total cross-sectional area and A_t is the tensile-stress area of the bolt, and $l_s = (l - l_t)$ is the length of the unthreaded shank. The length of the threaded portion is standardized as twice the bolt diameter plus 1/4 in for U.S. bolts (plus 6 mm for metric bolts) up to 6 in (150 mm) long. An additional 1/4 in of thread is provided on longer bolts. Bolts shorter than the standard thread length are threaded as close to the head as possible.^[2]

For the cylindrical material geometry in Figure 15-23 (ignoring the flanges), the material spring constant becomes

$$\frac{1}{k_m} = \frac{l_1}{A_{m1} E_1} + \frac{l_2}{A_{m2} E_2} = \frac{4l_1}{\pi D_{eff1}^2 E_1} + \frac{4l_2}{\pi D_{eff2}^2 E_2} \quad (15.11b)$$

where the A_m are the effective areas of the clamped materials and the D_{eff} are the effective diameters of those areas.

If both clamped materials are the same

$$k_m = \frac{A_m E_m}{l} \quad (15.11c)$$

where A_m is the effective area of the clamped material (also see Section 15.8). If A_m can be defined as a solid cylinder with an effective diameter D_{eff} , equation 15.11c becomes

$$k_m = \frac{\pi D_{eff}^2}{4} \frac{E_m}{l} \quad (15.11d)$$

Preloaded Bolts Under Static Loading

Figure 15-24a plots the load-deflection behavior of both bolt and material on common axes with their initial length taken as zero deflection δ . Note that the slope of the bolt line is positive, because its length increases with increased force. The slope of the material line is negative, as its length decreases with increasing force. The material is shown stiffer than the bolt, since its area is typically larger and we are assuming the same material for both. The force in both bolt and material is the same as long as they remain in contact. As a preload force F_i is introduced by tightening the bolt, the deflections of bolt δ_b and material δ_m are controlled by their spring rates and reach points A and B on their respective load-deflection curves, as shown in Figure 15-24a. With our assumptions for the relative magnitudes of k_b and k_m , the bolt stretches more (δ_b) than the material compresses (δ_m).

When an external load P is applied to the joint of Figure 15-23, there is an additional deflection $\Delta\delta$ introduced to both bolt and material as shown in Figure 15-24b. This deflection must be the same in both the bolt and the material unless the applied load is large enough to separate the joint (i.e., $P_m > F_i$ as shown in Figure 15-22e). The additional deflection $\Delta\delta$ creates a new load situation in both the bolt and material as shown in Figure 15-24b. The load in the material is reduced by P_m and moves down the material stiffness line to point D with a new value F_m . The load in the bolt is increased by P_b and moves up the bolt stiffness line to point C with a new value F_b . Note that the applied load P is split into two components, one (P_m) taken by the material and one (P_b) taken by the bolt.

$$P = P_m + P_b \quad (15.12a)$$

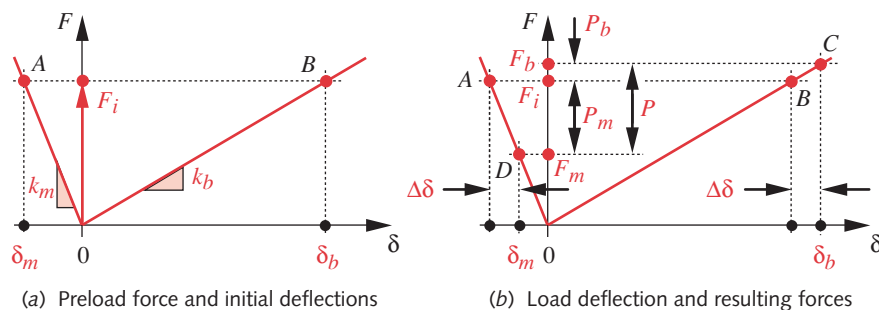


FIGURE 15-24

Effects on Bolt and Material from Preload: (a) Preload and (b) Applied Load

The compressive load F_m in the material is now

$$F_m = F_i - P_m : \quad F_m \geq 0^* \quad (15.12b)$$

and the tensile load F_b in the bolt becomes

$$F_b = F_i + P_b \quad (15.12c)$$

Note what has happened as a result of the preload force F_i . The “spring” of the material was “wound up” under preloading. Any applied loads are partially supported by the “unwinding” of this spring. If the relative stiffness of bolt and material are as shown in Figure 15-24 (i.e., material stiffer than bolt), the material supports the majority of the applied load and the bolt feels little additional load above that of the initial preload. This is one aspect of the justification for the earlier statement that “if the bolt doesn’t fail when preloaded, it probably won’t fail in service.” There is also another reason for this being true, which will be discussed in a later section.

Note, however, that if the applied load P is large enough to cause the component P_m to exceed the preload force F_i , then the joint will separate, F_m will be zero, and the bolt will feel the full value of the applied load P . The material can no longer contribute to supporting the load if the joint is separated. This is one reason for the very large recommended preloads as a percentage of bolt proof strength. In order to get the full benefit of material load sharing, the preload should be high.

We can summarize the information in Figure 15-24 in the following way. The common change in deflection $\Delta\delta$ due to the applied load P is

$$\Delta\delta = \frac{P_b}{k_b} = \frac{P_m}{k_m} \quad (15.13a)$$

$$\text{or : } P_b = \frac{k_b}{k_m} P_m \quad (15.13b)$$

Substitute equation 15.12a to get

$$\begin{aligned} P_b &= \frac{k_b}{k_m + k_b} P \\ \text{or} \end{aligned} \quad (15.13c)$$

$$P_b = CP \quad \text{where } C = \frac{k_b}{k_m + k_b}$$

The term C is called the joint’s *stiffness constant* or just the **joint constant**. Note that C is typically < 1 , and if k_b is small compared to k_m , C will be a small fraction. This confirms that the bolt will see only a portion of the applied load P .

In like fashion,

$$P_m = \frac{k_m}{k_b + k_m} P = (1 - C)P \quad (15.13d)$$

These expressions for P_b and P_m can be substituted into equations 15.12b and 15.12c to get expressions for the bolt and material loads in terms of the applied load P :

* If F_m has a negative value, set $F_m = 0$, because the material cannot support a tensile force—it will separate.

$$F_m = F_i - (1 - C)P \quad (15.14a)$$

$$F_b = F_i + CP \quad (15.14b)$$

Equation 15.14b can be solved for the preload F_i needed for any given combination of applied load P and maximum allowable bolt (proof) load F_b , provided that the joint constant C is known.

The load P_0 required to separate the joint can be found from equation 15.14a by setting F_m to zero.

$$P_0 = \frac{F_i}{(1 - C)} \quad (15.14c)$$

A safety factor against joint separation can be found from

$$N_{separation} = \frac{P_0}{P} = \frac{F_i}{P(1 - C)} \quad (15.14d)$$

EXAMPLE 15-2

Preloaded Fasteners in Static Loading

Problem Determine a suitable bolt size and preload for the joint shown in Figure 15-23 (repeated here). Find its safety factor against yielding and separation. Determine the optimum preload as a percentage of proof strength to maximize the safety factors.

Given The joint dimensions are $D = 1$ in and $l = 2$ in. The applied load $P = 2000$ lb.

Assumptions Both of the clamped parts are steel. The effects of the flanges on the joint stiffness will be ignored. A preload of 90% of the bolt's proof strength will be applied as a first trial.

Solution See Figure 15-25.

- 1 As with most design problems, there are too many unknown variables to solve the necessary equations in one pass. Trial values must be chosen for various parameters and iteration used to find a good solution. We actually made several iterations to solve this problem, but will only present two in the interest of brevity. Thus the trial values used here have already been massaged to reasonable values.
- 2 The bolt diameter is the principal trial value to be chosen along with a thread series and a bolt class to define the proof strength. We choose a 5/16-18 UNC-2A steel bolt of SAE class 5.2. (This was actually our third trial choice.) For a clamp length of 2 in, assume a bolt length of 2.5 in to allow sufficient protrusion for the nut. The preload is taken at 90% of proof strength as assumed above.
- 3 Table 15-6 (p. 882) shows the proof strength of this bolt to be 85 kpsi. The tensile-stress area from equation 15-1a (p. 863) is 0.052 431 in². The preload is then

$$F_i = 0.9S_p A_t = 0.9(85\ 000)(0.052431) = 4\ 011 \text{ lb} \quad (a)$$

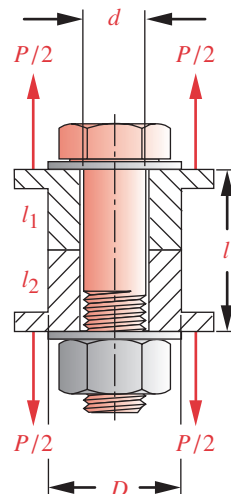


FIGURE 15-23 Repeated

A Preloaded Bolt Compressing a Cylinder to Which External Loads Are Applied

- 4 Find the lengths of thread l_{thd} and shank l_s of the bolt as shown in Figure 15-21 (p. 883):

$$\begin{aligned} l_{thd} &= 2d + 0.25 = 2(0.3125) + 0.25 = 0.875 \text{ in} \\ l_s &= l_{bolt} - l_{thd} = 2.5 - 0.875 = 1.625 \text{ in} \end{aligned} \quad (b)$$

from which we can find the length of thread l_t that is in the clamp zone:

$$l_t = l - l_s = 2.0 - 1.625 = 0.375 \text{ in} \quad (c)$$

- 5 Find the stiffness of the bolt from equation 15.11a (p. 884).

$$\begin{aligned} \frac{1}{k_b} &= \frac{l_t}{A_t E} + \frac{l_s}{A_b E} = \frac{0.375}{0.05243(30E6)} + \frac{1.625(4)}{\pi(0.3125)^2(30E6)} \\ k_b &= 1.059E6 \text{ lb/in} \end{aligned} \quad (d)$$

- 6 The calculation for the stiffness of the clamped material is simplified in this example by its relatively small diameter. We can assume in this case that the entire cylinder of material is compressed by the bolt force. (We will soon address the problem of finding the clamped area in a continuum of material.) The material stiffness from equation 15.11d is

$$k_m = \frac{\pi(D^2 - d^2)}{4} \frac{E_m}{l} = \frac{\pi(1.0^2 - 0.312^2)}{4} \frac{(30E6)}{2.0} = 1.063E7 \text{ lb/in} \quad (e)$$

- 7 The joint stiffness factor from equation 15.13c (p. 886) is

$$C = \frac{k_b}{k_m + k_b} = \frac{1.059E6}{1.063E7 + 1.059E6} = 0.09056 \quad (f)$$

- 8 The portions of the applied load P felt by the bolt and the material can now be found from equations 15.13.

$$\begin{aligned} P_b &= CP = 0.09056(2\ 000) = 181 \text{ lb} \\ P_m &= (1 - C)P = (1 - 0.09056)(2\ 000) = 1\ 819 \text{ lb} \end{aligned} \quad (g)$$

- 9 Find the resulting loads in bolt and material after the load P is applied.

$$\begin{aligned} F_b &= F_i + P_b = 4\ 011 + 181 = 4\ 192 \text{ lb} \\ F_m &= F_i - P_m = 4\ 011 - 1\ 819 = 2\ 192 \text{ lb} \end{aligned} \quad (h)$$

Note how little the applied load adds to the preload in the bolt.

- 10 The maximum tensile stress in the bolt is

$$\sigma_b = \frac{F_b}{A_t} = \frac{4\ 192}{0.052\ 431} = 79\ 953 \text{ psi} \quad (i)$$

Note that no stress-concentration factor is used because it is static loading.

- 11 This is a uniaxial stress situation, so the principal stress and von Mises stress are identical to the applied tensile stress. The safety factor against yielding is then

$$N_y = \frac{S_y}{\sigma_b} = \frac{92\ 000}{79\ 953} = 1.15 \quad (j)$$

The yield strength is found from Tables 15-6 and 15-7 (p. 882).

- 12 The load required to separate the joint and the safety factor against joint separation are found from equations 15.14c and 15.14d.

$$P_0 = \frac{F_i}{(1-C)} = \frac{4\ 011}{(1-0.09056)} = 4\ 410 \text{ lb} \quad (k)$$

$$N_{separation} = \frac{P_0}{P} = \frac{4\ 410}{2\ 000} = 2.2 \quad (l)$$

- 13 The safety factor against separation is acceptable. The yielding safety factor is low but this is to be expected, since the bolt is deliberately preloaded to a level close to its yield strength.
- 14 The model was solved for the range of possible preloads from zero to 100 percent of proof strength and the safety factors plotted versus preload percentage. The results are shown in Figure 15-25. The separation safety factor rises linearly with increasing preload, but is < 1 until the preload exceeds about 40% of the proof strength. At least that much preload is needed to keep the joint together under the applied load. The yielding safety factor is high at low preloads and decreases nonlinearly with increasing preload. The two lines cross at a preload of about 65% of proof strength at point A. That preload would balance the safety factors against both modes of failure at a value of 1.6. However, if the goal is to protect the joint against possible overloads, then a larger preload is better. At point B, the safety factor against overloading is 2.2, and there is still a 15% reserve against yielding during preloading as shown in the equations above.
- 14 The recommended design is then a 5/16-18 UNC-2A, grade 5.2 bolt, 2.5 in long, preloaded to 90% of proof strength with a preload force of

$$F_i = 0.90S_pA_t = 0.90(85\ 000)(0.052431) \approx 4\ 011 \text{ lb} \quad (m)$$

- 15 The files EX15-02 can be found on the CD-ROM.

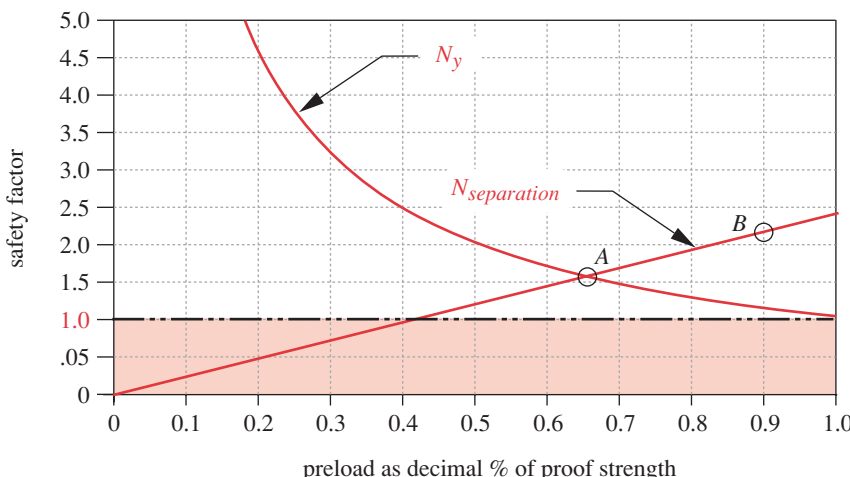


FIGURE 15-25

Safety Factors Versus Preload for the Statically Loaded Bolt in Example 15-2

Preloaded Bolts Under Dynamic Loading

The value of preloading is even greater for dynamically loaded joints than for statically loaded ones. Consider again the joint shown in Figure 15-23 but let the applied force P be a function of time, varying between some minimum and maximum values P_{min} and P_{max} , both positive. A very common situation is that of a fluctuating load ($P_{min} = 0$) such as in a bolted pressure vessel that is cycled from zero to maximum pressure.

Figure 15-26 shows the load deflection diagram of a bolted assembly subjected to a fluctuating load. When the fluctuating load drops to zero, the diagram looks like Figure 15-26a, i.e., with only the static preload F_i present. When the load rises to a maximum, the diagram looks like Figure 15-26b. P_{max} is split between the bolt and the material in the same manner as in the static loading case of Figure 15-24 (p. 885). The bolt feels only a portion of the fluctuating load due to the presence of the preload, which causes the material to absorb the bulk of the load's oscillations. This drastically reduces the dangerous alternating tensile stress in the bolt from what it would be with no preload. The compressive-stress oscillations in the material are of no concern with respect to fatigue failure, which is always due to tensile stress.

The mean and alternating forces felt by the bolt are

$$F_{alt} = \frac{F_b - F_i}{2}, \quad F_{mean} = \frac{F_b + F_i}{2} \quad (15.15a)$$

where F_b is found from equation 15.14b (p. 887) with $P = P_{max}$.

The mean and alternating stresses in the bolt are

$$\sigma_a = K_f \frac{F_{alt}}{A_t}, \quad \sigma_m = K_{fm} \frac{F_{mean}}{A_t} \quad (15.15b)$$

where A_t is the bolt's tensile-stress area from Table 15-1 or 15-2 (pp. 864–865), K_f is the fatigue stress-concentration factor for the bolt which can be estimated from:^{*}

$$\begin{aligned} K_f &= 5.7 + 0.6812d & d \text{ in inches} \\ \text{or} \\ K_f &= 5.7 + 0.02682d & d \text{ in mm} \end{aligned} \quad (15.15c)$$

15

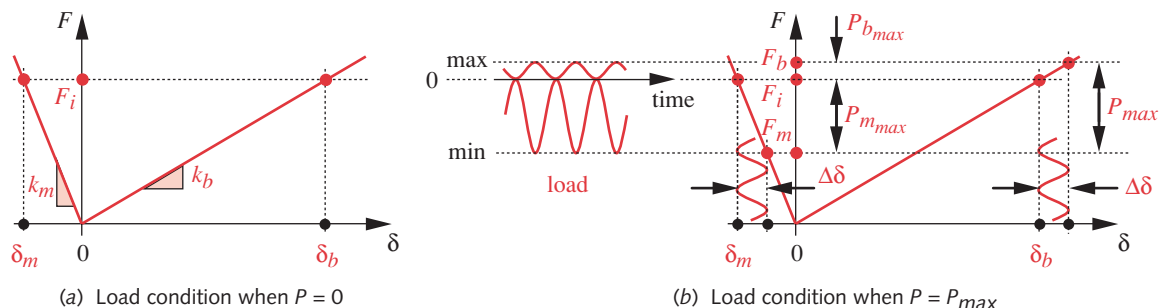


FIGURE 15-26

Effects on Bolt and Material of a Load Fluctuating from Zero to P_{max}

* Equation 15.15c was fitted to the stress concentration data in reference [16] by linear regression. The correlation coefficient is $r^2 = 0.91$.

where d is the nominal thread diameter. This relationship is based on fatigue test data of both cut and rolled threads that shows stress concentration in threads varies with bolt diameter from about 5.7 for a 0.25-in-diameter thread to about 9 for a 5-in-diameter thread.^[16] K_{fm} is the mean-stress-concentration factor from equation 6.17 (p. 364). Note that K_{fm} typically will be close to 1.0 for preloaded bolts.

The stress due to the preload force F_i is

$$\sigma_i = K_{fm} \frac{F_i}{A_t} \quad (15.15d)$$

Peterson^[6] reports that about 15% of bolt failures occur at the fillet under the head, 20% at the end of the threads on the shank, and about 65% in the thread at the nut face. Rolled threads have significantly higher fatigue strength due to their favorable grain orientation.^[16, 17] High-strength bolts usually have rolled threads.

The stresses calculated from equations 15.15 need to be compared to a suitable set of material strength parameters on a modified-Goodman diagram, as discussed in Section 6.11 (p. 360). The endurance strength can be calculated by the methods of Section 6.6 (p. 327) using a machined-finish factor for either rolled or cut threads. This will be demonstrated in an example. The fatigue safety factor can be calculated without drawing the Goodman diagram by employing equation 14.34b (p. 835), using notation consistent with this section.

$$N_f = \frac{S_e(S_{ut} - \sigma_i)}{S_e(\sigma_m - \sigma_i) + S_{ut}\sigma_a} \quad (15.16)$$

The value of high preloads in reducing the effects of fatigue loading should be clear from the previous discussion. If no preload were applied to the joint, the mean and alternating loads and stresses felt by the bolt would increase by the factor $1/C$, which is potentially a large number, as C is typically small and always less than 1.

EXAMPLE 15-3

Preloaded Fasteners in Dynamic Loading

Problem

Repeat Example 15-2 with a fluctuating load applied to the joint. Determine a suitable bolt size and preload for the joint shown in Figure 15-23 (repeated). Find its safety factors against fatigue, yielding, and separation. Determine the optimum preload as a percentage of proof strength to maximize the fatigue, yielding, and separation safety factors.

Given

The joint dimensions are $D = 1$ in and $l = 2$ in. The applied load fluctuates between $P = 0$ and $P = 1000$ lb.

Assumptions

The bolt has rolled threads. Both of the clamped parts are steel. The effects of the flanges on the joint stiffness will be ignored. A preload of 90% of the bolt's proof strength will be applied as a first trial. Use 99% reliability and an operating temperature of 300°F.

Solution

See Figures 15-27 to 15-29.

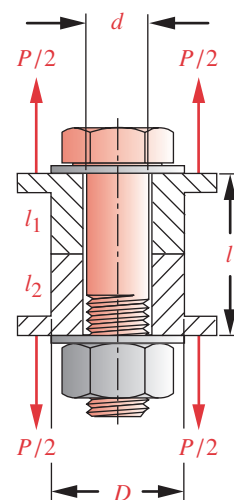


FIGURE 15-23 Repeated

A Preloaded Bolt Compressing a Cylinder to Which External Loads Are Applied

- Again, there are too many unknown variables to solve the necessary equations in one pass. Trial values must be chosen for various parameters and iteration used to find a good solution. We actually made several iterations to solve this problem but will present only one in the interest of brevity. The trial values used here have already been massaged to reasonable values.
- The bolt diameter is the principal trial value to be chosen along with a thread series and a bolt class to define the proof strength. We choose a 5/16-18 UNC-2A steel bolt of SAE class 5.2 based on its successful use in the static loading problem of Example 15-2 (p. 887) which is similar. For a clamp length of 2 in, assume a bolt length of 2.5 in to allow sufficient protrusion for the nut. The preload is taken at 90% of proof strength as assumed above.
- The proof strength, tensile-stress area, preload force, bolt stiffness, material stiffness, and joint constant are all the same as were found in Example 15-2 for the 90% preload factor. See that example for details. In summary they are

$$\begin{aligned} S_p &= 85 \text{ kpsi} & A_t &= 0.052431 \text{ in}^2 & F_i &= 4011 \text{ lb} \\ k_b &= 1.059E6 \text{ lb/in} & k_m &= 1.063E7 \text{ lb/in} & C &= 0.09056 \end{aligned} \quad (a)$$

- The portions of the peak fluctuating load P felt by the bolt and the material and the resulting loads in bolt and material after the load is applied are found the same way as in the previous example, but the peak load here is smaller:

$$\begin{aligned} P_b &= 91 \text{ lb} & P_m &= 909 \text{ lb} \\ F_b &= 4102 \text{ lb} & F_m &= 3102 \text{ lb} \end{aligned} \quad (b)$$

- Because these loads are fluctuating, we need to calculate the mean and alternating components of the force felt in the bolt. Figure 15-27 shows the load-deflection diagram for this problem, drawn to scale with the above forces applied. The shallow sine wave between the initial force line A and the maximum bolt force line B is the only fluctuating load felt by the bolt. The mean and alternating forces are then

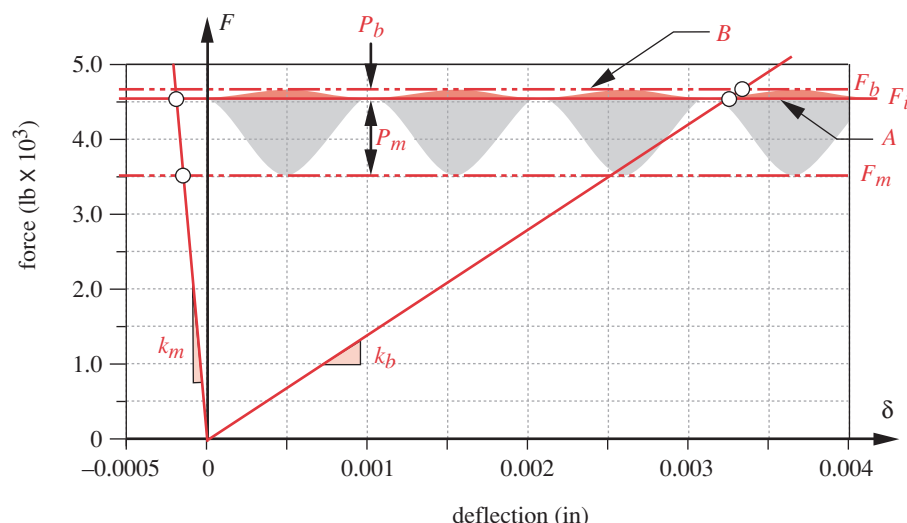


FIGURE 15-27

Dynamic Forces in Bolt and Material for Example 15-3, Drawn to Scale

$$F_{alt} = \frac{F_b - F_i}{2} = \frac{4\ 102 - 4\ 011}{2} = 45.3 \text{ lb} \quad (c)$$

$$F_{mean} = \frac{F_b + F_i}{2} = \frac{4\ 102 + 4\ 011}{2} = 4056.2 \text{ lb}$$

Note how little of the 0–1000-lb fluctuating force is felt by the bolt.

- 6 The nominal mean and alternating stresses in the bolt are:

$$\sigma_{a_{nom}} = \frac{F_{alt}}{A_t} = \frac{45.3}{0.052431} = 864 \text{ psi} \quad (d)$$

$$\sigma_{m_{nom}} = \frac{F_{mean}}{A_t} = \frac{4\ 056.2}{0.052431} = 77\ 364 \text{ psi}$$

- 7 The fatigue stress-concentration factor for this diameter thread is found from equation 15.15c and the mean stress-concentration factor K_{fm} is found from equation 6.17 (p. 364).

$$K_f = 5.7 + 0.6812d = 5.7 + 0.6812(0.3125) = 5.9$$

$$\text{if } K_f |\sigma_{max_{nom}}| > S_y \text{ then:} \quad K_{fm} = \frac{S_y - K_f \sigma_{a_{nom}}}{|\sigma_{m_{nom}}|}$$

$$K_f |\sigma_{max_{nom}}| = K_f |\sigma_{a_{nom}} + \sigma_{m_{nom}}| = 5.9 |864 + 77\ 364| = 462\ 548 \text{ psi}$$

$$462\ 548 \text{ psi} > S_y = 92\ 000 \text{ psi}$$

$$K_{fm} = \frac{S_y - K_f \sigma_{a_{nom}}}{|\sigma_{m_{nom}}|} = \frac{92\ 000 - 5.9(864)}{77\ 364} = 1.12 \quad (e)$$

- 8 The local mean and alternating stresses in the bolt are then:

$$\sigma_a = K_f \sigma_{a_{nom}} = 5.9(864) = 5\ 107 \text{ psi} \quad (f)$$

$$\sigma_m = K_{fm} \sigma_{m_{nom}} = 1.12(77\ 364) = 86\ 893 \text{ psi}$$

- 9 The stress at the initial preload is

$$\sigma_i = K_{fm} \frac{F_i}{A_t} = 1.12 \frac{4\ 011}{0.052431} = 85\ 923 \text{ psi} \quad (g)$$

- 10 An endurance strength must be found for this material. Using the methods of Section 6.6 (p. 327) we find

$$S_e = 0.5S_{ut} = 0.5(120\ 000) = 60\ 000 \text{ psi} \quad (h)$$

$$\begin{aligned} S_e &= C_{load} C_{size} C_{surf} C_{temp} C_{reliab} S_e \\ &= 0.70(0.995)(0.76)(1)(0.81)(60\ 000) = 25\ 726 \text{ psi} \end{aligned} \quad (i)$$

where the strength reduction factors are taken from the tables and formulas in Section 6.6 (p. 327) for, respectively, axial loading, the bolt size, a machined finish, room temperature, and 99% reliability.

- 11 The corrected endurance strength and the ultimate tensile strength are used in equation 15.16 (p. 891) to find the safety factor from the Goodman line.

$$N_f = \frac{S_e(S_{ut} - \sigma_i)}{S_e(\sigma_m - \sigma_i) + S_{ut}\sigma_a}$$

$$= \frac{25\ 837(120\ 000 - 85\ 923)}{25\ 726(86\ 893 - 85\ 923) + 120\ 000(5\ 107)} = 1.38 \quad (j)$$

The modified-Goodman diagram for this stress state is shown in Figure 15-28.

- 12 The static bolt stress after initial local yielding and the yielding safety factor are:

$$\sigma_s = \frac{F_{bolt}}{A_t} = \frac{4\ 102}{0.045\ 36} = 78\ 227 \text{ psi} \quad N_y = \frac{S_y}{\sigma_b} = \frac{92\ 000}{78\ 227} = 1.18 \quad (k)$$

- 13 The preload required to obtain these safety factors is

$$F_i = 0.90S_pA_t = 0.90(85\ 000)(0.052\ 431) \approx 4\ 011 \text{ lb} \quad (l)$$

- 14 The safety factor against joint separation is found from equation 15.14d (p. 887).

$$N_{separation} = \frac{F_i}{P(1-C)} = \frac{4\ 011}{1\ 000(1-0.09056)} = 4.4 \quad (m)$$

- 15 The fatigue and separation safety factors are acceptable. The yielding safety factor is low but is nevertheless acceptable, since the bolt is being deliberately preloaded to a level close to its yield strength.
- 16 The model was solved for the range of possible preloads from zero to 100 percent of proof strength and the safety factors plotted versus percent preload. The results are shown in Figure 15-29. The fatigue and separation safety factors are < 1 below 40% preload, at which point the preload becomes effective at keeping the joint closed. The fatigue safety factor remains essentially constant as preload is increased above the 40% threshold, but the safety factor against joint separation increases linearly with increasing preload. To protect the bolted joint against possible overloads, it is

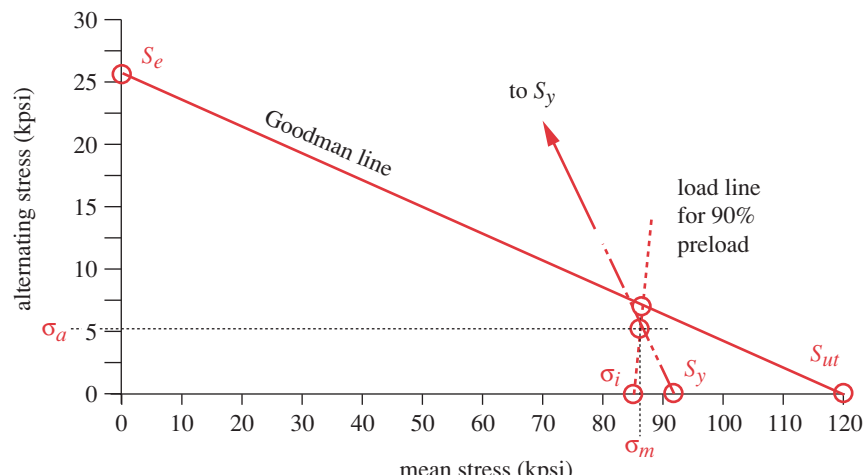
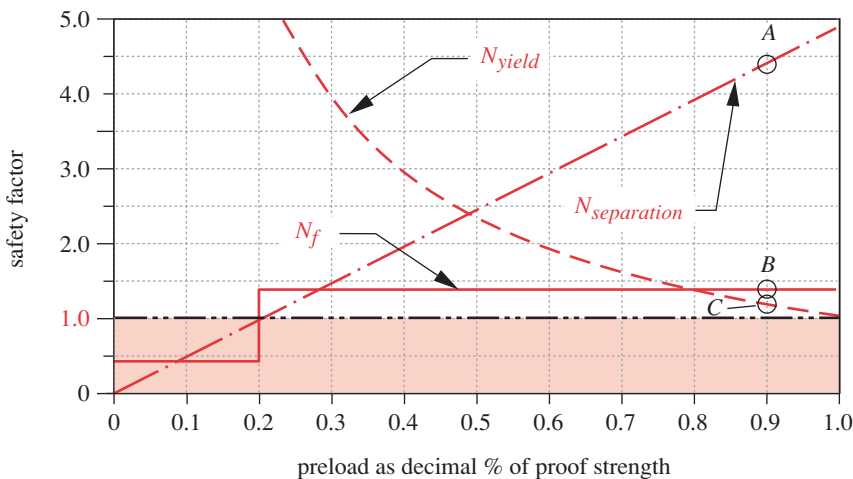


FIGURE 15-28

Modified-Goodman Diagram for Example 15-3

**FIGURE 15-29**

Safety Factors Versus Preload for Dynamically Loaded Bolt in Example 15-3

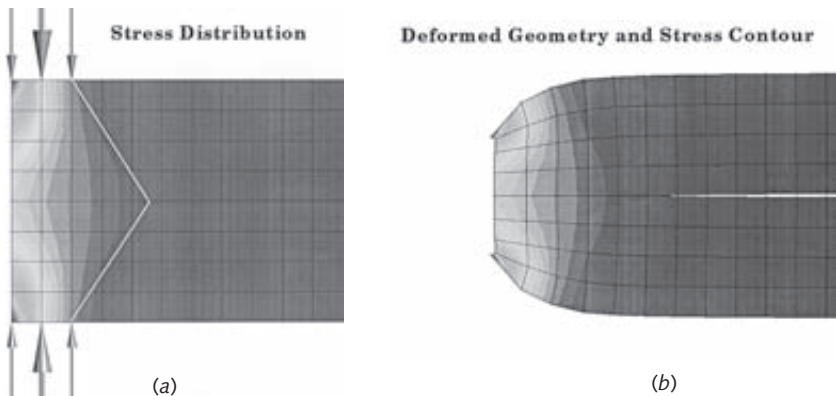
desirable to use the largest preload that will not yield the bolt when tightened. In this example, preloading to 90% of the bolt's proof strength gives an overload margin of $N_{separation} = 4.4$ at A, with an 18% reserve against yielding during preloading ($N_y = 1.18$ at C), along with a safety factor against fatigue failure of $N_f = 1.38$ at B.

- 17 The recommended design is then a 5/16-18 UNC-2A, grade 5.2 bolt, 2.5 in long, preloaded to 90% of proof strength with a force of 4 011 lb. Note that this one, small, preloaded bolt will support a half-ton of fluctuating load! The files EX15-03 can be found on the CD-ROM.

15.8 DETERMINING THE JOINT STIFFNESS FACTOR

In the previous discussion, for simplicity, the clamped materials' cross section was assumed to be a small-diameter cylinder, as shown in Figure 15-23 (p. 884). A more realistic situation is depicted in Figure 15-21 (p. 883), in which the clamped materials are a continuum extending well beyond the region of the bolt's influence. In fact, most assemblies will have a number of bolts distributed in a pattern over the clamped surface. (When the bolt pattern is circular, the *circumference on which the bolt centerlines lie* is called the **bolt circle**.) The question then becomes, what amount of clamped material should be included in a calculation of the material stiffness k_m whose value is needed to find the joint stiffness factor C ?

The stress distribution within the material under the bolt has a complex geometry. This problem has been studied by a number of investigators^[7, 8, 9] and an accurate computation of the distribution of the stressed volume is quite complicated and best done with FEA. The compressive stress in the material is (not surprisingly) highest directly under the bolt and falls off as you move laterally away from the bolt centerline (CL). At some lateral distance from the CL, the compressive stress at the joint interface goes to zero, and beyond that point the joint tends to separate, since it cannot sustain a tensile stress.

**FIGURE 15-30**

Finite-Element Analysis of the Stress Distribution and Deformation Within the Clamp Zone of a Bolted Connection [10]

Figure 15-30 shows the results of a finite element analysis (FEA) study of the stress distribution in a two-part joint-sandwich clamped together with a single, preloaded bolt.^[10, 11] Only one-half of the sandwich is analyzed because of its axisymmetry. The vertical bolt centerline is to the left of the left-hand edge of each diagram. The stress distribution around the bolt is sometimes modeled as a truncated-cone (or cone-frusta) barrel shape^[12], as seen in Figure 15-30a. Figure 15-30b shows the deformed geometry and greatly exaggerates the vertical dimension in order to show the very small deflections in the clamp zone and the joint separation in the right-hand half of the clamped assembly. Some studies proposed that a cone angle of $\phi = 30^\circ$ gives a reasonable approximation of the stressed volume.^[12, 13] The material spring constant for a machine screw or cap screw can be estimated in similar fashion. These approaches give only approximate results and will not be used here. Others^[13, 14, 15] have done FEA studies of the bolted joint that provide better estimates of its behavior. We present one of them.

Cornwell^[15] did an extensive FEA study of bolt and joint stiffness of 4424 unique combinations of four joint parameters: bolt diameter, joint thickness, individual plate thicknesses, and various plate material combinations. This study also included the effects of deflection of the bolt head which can be much greater than the theoretical bolt stiffness predicted by equation 15.11a. The head deflection can be included by using the following equation for bolt stiffness instead of equation 15.11a.

$$k_{b'} = \left(1 + \frac{d}{l}\right)^{-1} k_b \quad \approx \quad \left(1 + \frac{d}{l}\right)^{-1} \frac{A_t A_b}{A_b l_t + A_t l_s} E_b \quad (15.17)$$

Cornwell fitted empirical equations to his FEA data that taken together calculate the joint stiffness constant C as a function of bolt diameter d , clamped length l , relative plate thickness of the two parts clamped, and the two clamped materials' moduli of elasticity E . The empirical equations match the FEA data of all models with an average error of 0.6% and have a correlation coefficient with the data of 0.9998. This approach avoids the need to estimate the material stiffness k_m in the clamp zone to determine C as was done in the two preceding examples and in all the other methods referenced here. The value of C can be used directly in equations 15.14 to determine the loads in bolt and material and the joint's safety factor against separation. His equations are valid for any combinations of materials whose Young's moduli are between those of steel and aluminum.

Cornwell defines a joint aspect ratio j as bolt diameter d over clamped length l ,

$$j = \frac{d}{l} \quad (15.18a)$$

a plate to bolt modulus ratio r as

$$r = \frac{E_{material}}{E_{bolt}} \quad (15.18b)$$

and a plate thickness ratio t

$$t = \frac{T_L}{T_L + T_H} \quad (15.18c)$$

where T_L is the thickness of the plate of lower Young's modulus and T_H is the thickness of the plate of higher Young's modulus.

Joints With Two Plates of the Same Material

Cornwell's study investigated joints with joint aspect ratios j ranging from 0.1 to 2.0 and plate to bolt modulus ratios r ranging from 0.35 for aluminum plates and steel bolts to 1.0 for both of steel. The effect of variation in plate to bolt modulus ratio r on joint factor C was analyzed. The resulting FEA data were curve fit to yield an expression for C versus r over the ranges noted above for the case of like materials in the joint.

$$C_r = p_3 r^3 + p_2 r^2 + p_1 r + p_0 \quad (15.19)$$

where the coefficients p_i are given in Table 15-8 as a function of j .

For a joint of the same materials, $C = C_r$. For a joint of two different materials, the C_r factor must be separately computed for each material. C_H and C_L represent joint factors for the same connection made entirely of the high or low modulus material, respectively.

Table 15-8 Parameters for Equation 15.19 [15]

<i>j</i>	<i>p₀</i>	<i>p₁</i>	<i>p₂</i>	<i>p₃</i>
0.10	0.4389	-0.9197	0.8901	-0.3187
0.20	0.6118	-1.1715	1.0875	-0.3806
0.30	0.6932	-1.2426	1.1177	-0.3845
0.40	0.7351	-1.2612	1.1111	-0.3779
0.50	0.7580	-1.2632	1.0979	-0.3708
0.60	0.7709	-1.2600	1.0851	-0.3647
0.70	0.7773	-1.2543	1.0735	-0.3595
0.80	0.7800	-1.2503	1.0672	-0.3571
0.90	0.7797	-1.2458	1.0620	-0.3552
1.00	0.7774	-1.2413	1.0577	-0.3537
1.25	0.7667	-1.2333	1.0548	-0.3535
1.50	0.7518	-1.2264	1.0554	-0.3550
1.75	0.7350	-1.2202	1.0581	-0.3574
2.00	0.7175	-1.2133	1.0604	-0.3596

Joints With Two Plates of Different Materials

Figure 15-31 shows a representative sample of data from FEA computations of the relationship between joint constant C and the plate thickness ratio t . A family of polynomial curves are fitted to the data for each of several values of joint aspect ratio j . These curves are defined by the expressions:

$$C_t = q_5 t^5 + q_4 t^4 + q_3 t^3 + q_2 t^2 + q_1 t + q_0 \quad (15.20a)$$

$$C_t = q_3 t^3 + q_2 t^2 + q_1 t + q_0 \quad (15.20b)$$

where equation 15.20a is used only for the case of joint aspect ratio $j = 0.1$ and equation 15.20b applies to all other values of j . The values for the coefficients q_i for various joint aspect ratios are shown in Table 15-9.

These are nonlinear functions but the relationship with respect to j among the members of the curve family in Figure 15-31 is also quite nonlinear as evidenced by the different shapes of the curves of C versus t for different j . To make it simple to use these data in a computation of C for various values of j , Cornwell creates a correction factor that accounts for both the shape and magnitude of the deviation of the actual joint stiffness factor from the straight line between C_H and C_L in Figure 15-31. The shape of the correction factor is given by equations 15.20 and the amplitude by equation 15.21.

$$a = e^{0.0598(\ln j)^3 + 0.1385(\ln j)^2 - 0.4350(\ln j) - 2.3516} \quad (15.21)$$

The linearized functions are shown only for two curves ($j = 0.1$ and $j = 0.5$) to reduce clutter in the figure. The parameter a is shown on each of those two curves and represents the maximum deviation between the actual curve and the straight line between its endpoints. Those endpoints are labeled C_H and C_L and represent, respectively, the

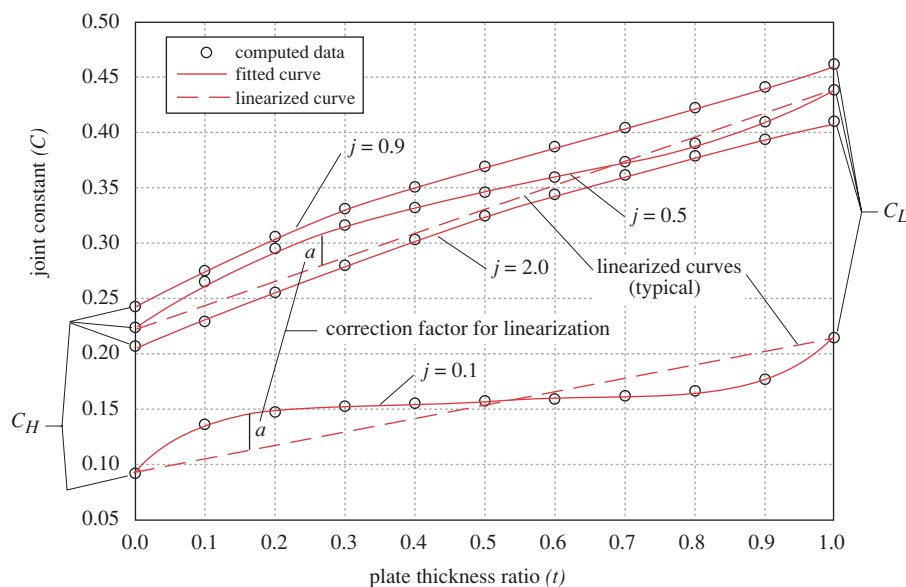


FIGURE 15-31

Family of Curves of Joint Constant C Versus Plate Thickness Ratio t and Joint Aspect Ratio j [15]

Table 15-9 Parameters for Equation 15.20 [15]

<i>j</i>	<i>q</i> ₀	<i>q</i> ₁	<i>q</i> ₂	<i>q</i> ₃	<i>q</i> ₄	<i>q</i> ₅
0.10	0.0079	17.040	-92.832	202.44	-209.38	82.726
0.20	0.1010	8.5465	-24.166	15.497		
0.30	0.0861	8.2344	-22.274	13.963		
0.40	0.0695	8.0297	-20.727	12.646		
0.50	0.0533	7.8676	-19.357	11.457		
0.60	0.0372	7.6705	-17.951	10.262		
0.70	0.0197	7.3030	-16.235	8.9273		
0.80	0.0029	6.9893	-14.737	7.7545		
0.90	-0.0123	6.7006	-13.363	6.6784		
1.00	-0.0265	6.4643	-12.188	5.7481		
1.25	-0.0524	5.7363	-9.3326	3.6348		
1.50	-0.0678	5.0674	-7.0322	2.0107		
1.75	-0.0763	4.5187	-5.1590	0.6861		
2.00	-0.0784	3.9617	-3.5248	-0.3956		

case of 100% high modulus material and 100% low modulus material in the joint. These values are needed for the final computation as they define the slope and intercept of each linearized curve. The values of C_H and C_L are calculated with equation 15.19 using the plate to bolt modulus ratios from equation 15.18b for the high and low modulus plate materials, respectively.

Once the values of C_H , C_L , C_t , and a are found, the joint constant C is found as a function of those parameters and the plate thickness ratio t from:

$$C = C_H + (t + aC_t)(C_L - C_H) \quad (15.22)$$

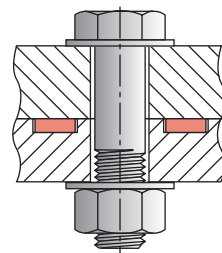
The value of C can then be used in equations 15.14. The material stiffness k_m can be found from equation 15.13c knowing C and using k_b from equation 15.17.

Gasketed Joints

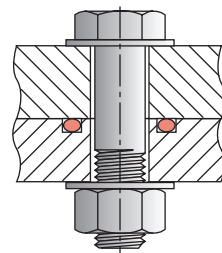
Gaskets are often used in joints where pressure seals are needed. There are different styles of gaskets, which can be divided into two general classes: **confined** and **unconfined**. Figures 15-32a and 15-32b show two variations of confined gaskets, one being an O-ring. All confined gaskets allow the hard faces of the mating parts to contact and this makes the joint behave as an ungasketed one in terms of its spring constant k_m . The approaches described above can be used to estimate k_m for confined gaskets.

Unconfined-gasket joints as shown in Figure 15-32c have the relatively soft gasket completely separating the mating surfaces. The gasket then contributes to the spring constant of the joint. The gasket's spring constant k_g can be combined with the spring constants of the mating parts in equation 14.2b (p. 787) to find an effective spring constant k_m for the assembly. The moduli of elasticity for several gasket materials are shown in Table 15-11.

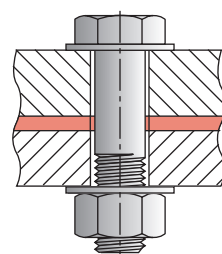
With the exception of the copper and copper-asbestos gasket materials in Table 15-11, typical gaskets' moduli are so low that they will dominate equation 13.2b and essentially determine the joint stiffness. In those cases it is not necessary to solve equa-



(a) Confined gasket



(b) Confined O-ring



(c) Unconfined gasket

FIGURE 15-32

Confined and
Unconfined Gaskets

Table 15-10 Young's Modulus for Some Gasket Materials

Source: Reference 12 with permission of McGraw-Hill, Inc., New York

Material	Modulus of Elasticity	
	psi	MPa
Cork	$12.5E3$	86
Compressed asbestos	$70E3$	480
Copper-asbestos	$13.5E6$	$93E3$
Copper (pure)	$17.5E6$	$121E3$
Plain rubber	$10E3$	69
Spiral wound	$41E3$	280
Teflon	$35E3$	240
Vegetable fiber	$17E3$	120

tion 13.2b and k_m can be set equal to k_g . With a copper-asbestos or copper gasket (or any other stiff, unconfined gasket) the gasket stiffness may be sufficiently high to warrant computing k_m from equation 13.2b. Use an area of gasket material consistent with the entire clamp zone at the level of the gasket to estimate k_g .

EXAMPLE 15-4

Determining the Gasket Stiffness and Joint Constant

Problem A pressure chamber is sealed by a gasketed cap fastened with eight preloaded bolts. Find the gasket stiffness and joint constants for two designs of the assembly as shown in Figure 15-33, one with a confined gasket and one with an unconfined gasket. Also determine the loads felt by bolts and material.

Given The cylinder diameter $D_p = 4$ in. Bolt circle diameter $D_{bc} = 5.5$ in. Outside flange diameter $D_f = 7.25$ in. The eight 3/8-16 UNC bolts are equispaced on the bolt circle. The flange on the steel chamber is 0.75 in thick. The aluminum cover thickness $l_c = 1.125$ in. The clamped length l of the joint is 1.875 in. The gasket thickness $t = 0.125$ in. The pressure in the cylinder is 1 500 psi.

Assumptions The gasket material is rubber.

Solution See Figure 15-33.

- Figure 15-33 shows two alternate designs of gasket for the joint on the same view to save space. Whichever design is used, its gasket configuration will be present on both sides of the centerline. Don't be confused by the depiction of different gaskets top and bottom; only one or the other will be used in the final assembly. We will deal first with the confined gasket configuration.
- The force on each bolt can be found from the known pressure and cylinder dimensions, assuming that all bolts share the load equally. The total force on the end cap is

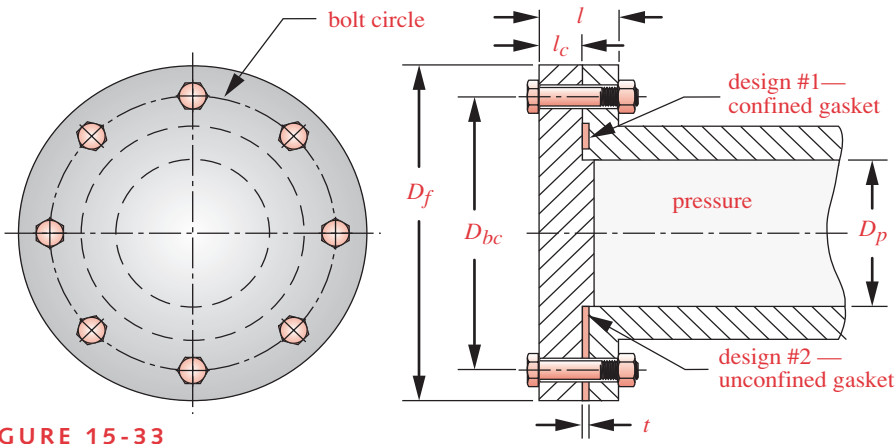


FIGURE 15-33

Pressure Vessel End Plate Secured with Preloaded Bolts on a Bolt Circle

$$P_{total} = pA = p \frac{\pi D_p^2}{4} = 1500 \frac{\pi(4)^2}{4} = 18850 \text{ lb} \quad (a)$$

and the applied force P on each bolt is

$$P = \frac{P_{total}}{N_{bolts}} = \frac{18850}{8} = 2356 \text{ lb} \quad (b)$$

- 3 First analyze the confined gasket case. A confined gasket allows the metal surfaces to contact just as if there were no gasket present. So the analysis of the material stiffness can ignore the confined gasket.
- 4 Determine the relevant ratios for this joint from equations 15-17. The joint aspect ratio is:

$$j = \frac{d}{l} = \frac{0.375}{1.875} = 0.200 \quad (c)$$

- 5 There are two plate to bolt moduli of interest here since we have different materials in the joint. We will call them r_H for the high modulus material (the steel cylinder flange) and r_L for the low modulus aluminum cover plate.

$$r_H = \frac{E_{material}}{E_{bolt}} = \frac{30E6}{30E6} = 1.0 \quad (d)$$

$$r_L = \frac{E_{material}}{E_{bolt}} = \frac{10.4E6}{30E6} = 0.347$$

- 6 The plate thickness ratio relates the thicknesses of the low and high modulus materials in the joint.

$$t = \frac{T_L}{T_L + T_H} = \frac{1.125}{1.125 + 0.750} = 0.600 \quad (e)$$

- 7 Calculate the C_r terms C_H and C_L for r_H and r_L , respectively, using equation 15.19 and the coefficients p_i from Table 15-8. For $j = 0.20$, they are: $p_0 = 0.6118$, $p_1 = -1.1715$, $p_2 = 1.0875$, and $p_3 = -0.3806$.

$$\begin{aligned} C_L &= C_r = p_3 r_L^3 + p_2 r_L^2 + p_1 r_L + p_0 \\ &= -0.381(0.347)^3 + 1.088(0.347)^2 - 1.172(0.347) + 0.612 = 0.321 \end{aligned} \quad (f)$$

Note that $r_H = 1$ so C_H is:

$$\begin{aligned} C_H &= C_r = p_3 r_H^3 + p_2 r_H^2 + p_1 r_H + p_0 \\ &= -0.381 + 1.088 - 1.172 + 0.612 = 0.147 \end{aligned} \quad (g)$$

- 8 Because $j > 0.1$ in this example, we need to use equation 15.20b to calculate C_t . The coefficients q_i are taken from Table 15-9 and for $j = 0.20$, they are: $q_0 = 0.101$, $q_1 = 8.547$, $q_2 = -24.166$, and $q_3 = 15.497$.

$$\begin{aligned} C_t &= q_3 t^3 + q_2 t^2 + q_1 t + q_0 \\ &= 15.497(0.60)^3 - 24.166(0.60)^2 + 8.547(0.60) + 0.101 = -0.124 \end{aligned} \quad (h)$$

- 9 Calculate the amplitude of the correction factor to the linearized estimate using equation 15.21.

$$a = e^{0.0598(\ln j)^3 + 0.1385(\ln j)^2 - 0.4350(\ln j) - 2.3516} = 0.214 \quad (i)$$

- 10 The joint stiffness factor for the confined-gasket design is calculated with equation 15.22.

$$\begin{aligned} C &= C_H + (t + aC_t)(C_L - C_H) \\ &= 0.321 + [0.60 + 0.214(-0.124)][(0.321 - 0.147)] = 0.247 \end{aligned} \quad (j)$$

- 11 The portions of the applied load P felt by the bolt and the material can now be found from equations 15.13.

$$\begin{aligned} P_b &= CP = 0.247(2356) \cong 581.1 \text{ lb} \\ P_m &= (1 - C)P = (1 - 0.247)(2356) \cong 1775.1 \text{ lb} \end{aligned} \quad (k)$$

- 12 We can estimate the bolt stiffness k_b' from equation 15.17 using its shank area = 0.110 in² and tensile stress area = 0.077 in² (Table 15-1), then estimate the material stiffness k_{m_1} for the confined gasket case by using equation 15.13c, given k_b' and C .

$$\text{length of thread : } l_{thd} = 2d + 0.25 = 2(0.375) + 0.25 = 1.0 \text{ in}$$

$$\text{length of shank : } l_s = l_{bolt} - l_{thd} = 2.25 - 1.0 = 1.25 \text{ in}$$

$$\text{length of clamped thread : } l_t = l - l_s = 1.875 - 1.25 = 0.625 \text{ in}$$

$$k_{b'} \cong \left(1 + \frac{d}{l}\right)^{-1} \frac{A_t A_b}{A_b l_t + A_t l_s} E_b$$

$$k_{b'} \cong \left(1 + \frac{0.375}{1.875}\right)^{-1} \frac{0.077(0.110)}{0.110(0.625) + 0.077(1.25)} 30E6 = 1.290E6 \text{ lb/in}$$

$$C = \frac{k_{b'}}{k_{m_1} + k_{b'}} \Rightarrow k_{m_1} = k_{b'} \frac{1 - C}{C} = 1.29E6 \left(\frac{1 - 0.247}{0.247} \right) = 3.940E6 \text{ lb/in} \quad (l)$$

- 13 Now we will address the unconfined-gasket case. The bolt stiffness is not affected by the gasket but the material stiffness is. We now have two springs in series, the

metal whose stiffness k_m is defined in equation (l) and the gasket which is calculated in equation (n) below. These combine according to equation 14.2b (p. 787). The portion of the unconfined gasket subjected to the clamp force can be assumed to be from the outside diameter of the flange shown in Figure 15-33 to the inside diameter of the vessel. The bolt hole should be subtracted from the gasket area. The area of the clamped gasket around one bolt is:

$$A_g = \frac{\pi}{4} \left[\frac{(D_f^2 - D_p^2)}{N_{bolts}} - d^2 \right] = \frac{\pi}{4} \left[\frac{(7.25^2 - 4^2)}{8} - 0.375^2 \right] = 3.479 \text{ in}^2 \quad (m)$$

- 14 The stiffness of this piece of gasket is found from equation 15.11c (p. 885).

$$k_{m_2} = k_g = \frac{A_g E_g}{t} = \frac{3.479(10E3)}{0.125} \cong 2.783E5 \text{ lb/in} \quad (n)$$

The modulus of elasticity E_g of the gasket material is found in Table 15-10 (p. 900).

- 15 The combined stiffness of the gasketed joint (from equation 14.2b, p. 787) is

$$k_m = \frac{1}{\frac{1}{k_{m_1}} + \frac{1}{k_{m_2}}} = \frac{1}{\frac{1}{3.94E6} + \frac{1}{2.783E5}} \cong 2.600E5 \text{ lb/in} \quad (o)$$

Note that the combined stiffness is essentially the same as that of the soft gasket alone, since it dominates the equation. We could have used the gasket stiffness k_g to represent the joint stiffness k_m with little error.

- 16 The joint constant with the unconfined gasket is now

$$C = \frac{k_b'}{k_m + k_b'} = \frac{1.290E6}{2.600E5 + 1.290E6} = 0.832 \quad (p)$$

and

$$(1 - C) = 0.168$$

- 17 The portions of the applied load P felt by the bolt and the material with a soft, unconfined gasket in the joint can now be found from equations 15.13 (p. 886).

$$P_b = CP = 0.832(2356) \cong 1961 \text{ lb} \quad (q)$$

$$P_m = (1 - C)P = (1 - 0.832)(2356) \cong 395 \text{ lb}$$

- 18 See what has happened as a result of introducing an unconfined soft gasket. Compare the value of C in equation (j) to C in equation (p). The bolt has gone from feeling only 25% of the applied load with no gasket (or a confined gasket) to feeling 83% of the applied load with a soft, unconfined gasket. In effect, the roles of the bolt and the material have been reversed by the introduction of the soft gasket. An unconfined, soft gasket severely limits the ability of the bolt to accommodate fatigue loads, as was accomplished in the previous example. The files EX15-04 can be found on the CD-ROM.

Note that to obtain the benefits of high preloads in terms of protecting the fasteners from fatigue loading, it is necessary to have a material stiffness greater than the bolt stiffness. Soft, unconfined gaskets reduce the material stiffness so severely that they

Table 15-11

Torque Coefficient K_i for
UNS Standard Threads
with Coefficients of
Friction $\mu = \mu_c = 0.15$

Bolt Size	K_i UNC	K_i UNF
0	0.22	
1	0.22	0.22
2	0.22	0.22
3	0.22	0.22
4	0.22	0.22
5	0.22	0.22
6	0.22	0.22
8	0.22	0.22
10	0.22	0.21
12	0.22	0.22
1/4	0.22	0.21
5/16	0.22	0.21
3/8	0.22	0.21
7/16	0.21	0.21
1/2	0.21	0.21
9/16	0.21	0.21
5/8	0.21	0.21
3/4	0.21	0.21
7/8	0.21	0.21
1	0.21	0.21
1 1/8	0.21	0.21
1 1/4	0.21	0.21
1 3/8	0.21	0.21
1 1/2	0.21	0.20
1 3/4	0.21	
2	0.21	
2 1/4	0.21	
2 1/2	0.21	
2 3/4	0.21	
3	0.21	
3 1/4	0.21	
3 1/2	0.21	
3 3/4	0.21	
4	0.21	

limit the effectiveness of preloading. For heavily loaded joints, unconfined gaskets should be made of high-stiffness material such as copper or copper-asbestos, or be replaced with confined gaskets.

Some rules of thumb regarding patterns of bolts such as used in Example 15-4 are

- 1 Bolt spacing around a bolt circle or in a pattern should not exceed about 6 bolt diameters between adjacent bolts for good force distribution.
- 2 Bolts should not be closer to an edge than about 1.5 to 2 bolt diameters.

15.9 CONTROLLING PRELOAD

The amount of preload is obviously an important factor in bolt design. Thus we need some means of controlling the preload applied to a bolt. The most accurate methods require that both ends of the bolt be accessible. Then the amount of bolt elongation can be directly measured with a micrometer, or an electronic length gage, and the bolt stretched to a length consistent with the desired preload based on equation 15.10a (p. 884). Ultrasonic transducers are sometimes used to measure change in bolt length when tightened, and these only need access to the head end. These methods are not as useful in high-production or field-service situations, since they require time, care, precision instruments, and skilled personnel.

A more convenient but less accurate method measures or controls the torque applied to the nut or to the head of a cap screw. A torque wrench gives a readout on a dial of the amount of torque applied. Torque wrenches are generally considered to give an error in preload of up to $\pm 30\%$. If great care is taken and the threads are lubricated (which is desirable anyway), this error can perhaps be halved, but it is still large. Pneumatic impact wrenches can be set to a particular torque level at which they stop turning. These give more consistent results than a manual torque wrench and are preferred.

The torque necessary to develop a particular preload can be calculated from equation 15.5a (p. 869), developed for the power screw. Substitute equation 15.3 (p. 868) in 14.5a to get it in terms of lead angle λ :

$$T_i = F_i \frac{d_p}{2} \frac{(\mu + \tan \lambda \cos \alpha)}{(\cos \alpha - \mu \tan \lambda)} + F_i \frac{d_c}{2} \mu_c \quad (15.23a)$$

The pitch diameter d_p can be roughly approximated as the bolt diameter d , and the mean collar diameter d_c can be approximated as the average of the bolt diameter d and a standard head or nut size of $1.5d$,

$$T_i \approx F_i \frac{d}{2} \frac{(\mu + \tan \lambda \cos \alpha)}{(\cos \alpha - \mu \tan \lambda)} + F_i \frac{(1+1.5)d}{4} \mu_c \quad (15.23b)$$

Factor out the force and bolt diameter to get

$$T_i \approx K_i F_i d \quad (15.23c)$$

where
$$K_i \approx \left[0.50 \frac{(\mu + \tan \lambda \cos \alpha)}{(\cos \alpha - \mu \tan \lambda)} + 0.625 \mu_c \right]$$

K_i is called the *torque coefficient*.

Note that the friction coefficient μ_c between the head or nut and the surfaces as well as the thread friction coefficient μ contribute to the torque coefficient K_i . If we assume a friction coefficient of 0.15 for both locations, and calculate the torque coefficients K_i for all standard UNC and UNF threads (using their correct pitch diameters d_p rather than the approximation of equation 15.23b), the value of K_i varies very little over the entire range of thread sizes, as shown in Table 15-11 (opposite page). Thus, the tightening torque T_i needed to obtain a desired preload force F_i in **lubricated threads** can be approximated (subject to the friction assumptions listed above) as

$$T_i \cong 0.21 F_i d \quad (15.23d)$$

The Turn-of-the-Nut Method

Another technique often used to control preload is called the *turn-of-the-nut* method. Since the lead of the fastener is known, turning the nut a specified number of turns will stretch the bolt a known amount provided that the starting point is such that all of the nut advance contributes to bolt stretch. The nut is first brought to a useful start point, called *snug-tight*, defined as the tightness obtained from a few strikes of an impact wrench or, if manually done, as tight as a person can make the nut with a standard wrench. Then the nut is turned (with a longer wrench) through an additional number of turns, or fractions thereof, calculated to stretch the bolt the desired amount based on equation 15.10a (p. 884).

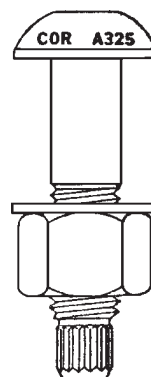
Torque-Limited Fasteners

The need for accurate preloads in high-strength bolts has caused bolt manufacturers to provide special “controlled-tension break-away” bolts, as shown in Figure 15-34. These bolts are provided with a splined extension on the end. This extension is designed with a shear area calculated to fracture when the proper torque is reached. Special sockets are provided that engage the spline as shown in Figure 15-35, which also details how they are used. These fasteners are often used in structural-steel construction, where their preload uniformity compared to a manual torque wrench or impact wrench is a big advantage in terms of minimizing operator error when tens of thousands of bolts must be properly installed to ensure that the skyscraper or bridge stays up.

Load-Indicating Washers

Another aid to proper bolt tensioning involves using special washers under the bolt head that either control the tension load or indicate when it is correct. Belleville-spring washers are sometimes used under bolt heads. The Belleville spring is designed to give the desired bolt force when it is compressed flat (see Section 14.9, p. 838). The bolt is simply tightened until the Belleville spring is flat.

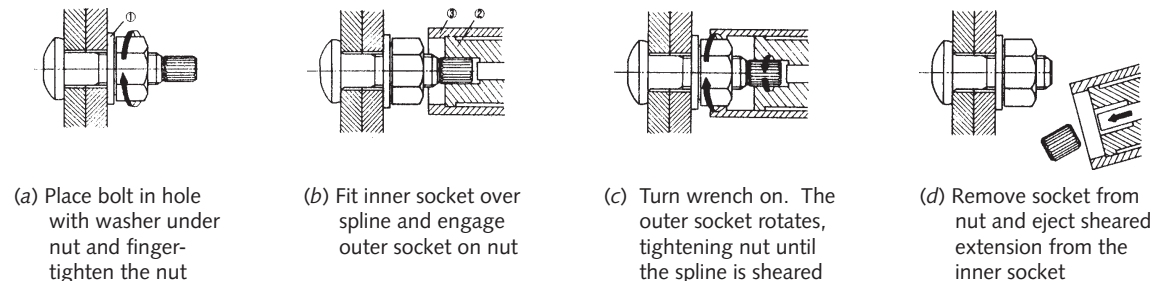
Load-indicator washers (also called direct tension indicators) are made with protrusions that crush under the desired preload as shown in Figure 15-36. The bolt is tightened until the height of the washer has been reduced to the proper dimension, as shown in the figure.



15

FIGURE 15-34

Controlled-Tension
Break-Away Bolt -
Courtesy of Cordova Bolt
Inc., Buena Park, CA 90621

**FIGURE 15-35**

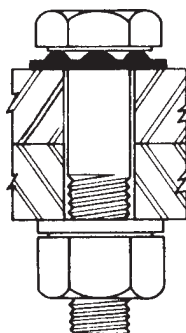
Instructions for Use of Break-Away Bolts Courtesy of Cordova Bolt Inc., Buena Park, Calif. 90621

Torsional Stress Due to Torquing of Bolts

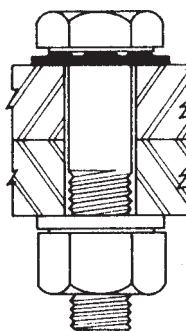
When a nut on a bolt is torqued to a preload, a torsional load is applied to the bolt through the threads. If the friction in the threads is large, the torsion in the bolt can be appreciable. This is the principal reason for lubricating the threads before assembling fasteners. If there were no thread friction, the torsion load on the bolt would be close to zero. A dry lubricant such as graphite powder with molybdenum disulfide added works well, as will a petroleum oil.



(a) Load indicator washer



(b) Before tightening



(c) After tightening

A torsional stress is generated in the bolt shank during tightening, as defined in equation 15.9 (p. 876). This torsional stress combines with the axial tensile stress in the shank to create a principal stress larger than the applied tensile stress, as shown in the Mohr's circle diagram of Figure 15-37a. If a reversed torque is applied to the nut after it is fully tightened, without actually loosening it, the torsional stress component can be relieved. Even if nothing is deliberately done to relieve the torsional stress after tightening, it will tend to relax over time, especially if there is any vibration present. When the torsional stress is relieved or goes away over time, the principal stress will be reduced by an amount $\Delta\sigma_1$, as shown in Figure 15-37b. This is the other reason, alluded to earlier, why a bolt that doesn't break when torqued to a high preload (near its proof strength) will probably not break under the applied loads for which it was designed.

EXAMPLE 15-5

Determining the Torque to Generate a Bolt Preload

Problem Find the torque required to preload the bolt in Example 15-3.

Given A 5/16-18 UNC-2A, grade 5.2 bolt, 2.5 in long, preloaded to 90% of proof strength with an axial force of 4 011 lb.

Assumptions The threads will be lubricated. Assume a coefficient of friction of 0.15.

Solution

- 1 The required tightening torque can be estimated with equation 15.23d:

$$T_i \approx 0.21F_id = 0.21(4011)(0.3125) = 263 \text{ lb-in} \quad (a)$$

- 2 The files EX15-05 can be found on the CD-ROM.

FIGURE 15-36Load Indicator Washers
Courtesy of Cordova Bolt Inc., Buena Park, CA 90621

15.10 FASTENERS IN SHEAR

Bolts are also used to resist shear loads, as shown in Figure 15-38, though this application is more common in structural design than in machine design. Structural-steel building and bridge frames are frequently bolted together with high-strength, preloaded bolts. (Alternatively, they may be welded or riveted together.) The tensile preload in this case serves the purpose of creating large frictional forces between the bolted elements, which can resist the shear loading. Thus, the bolts are still loaded in tension with high preloads. If the friction in the joint is not sufficient to support the shear loads, then the bolt(s) will be placed in direct shear.

In machine design, where the dimensional relationships between parts typically require much closer tolerances than in structural work, it is not considered good practice to use bolts or screws in shear to locate and support precision machine parts under shear loads. Instead, a combination of bolts or screws and **dowel pins** should be used, with the screws or bolts serving to clamp the joint in compression and the hardened-steel dowel pins providing accurate transverse location and shear resistance. The joint friction developed from the bolt-clamp force should be expected to sustain the shear loads in combination with the dowel pins loaded in direct shear. In effect, the task is split between these different types of fasteners. *Dowel pins support shear loads but not tensile loads, and bolts/screws support tensile loads but not direct shear loads.*

There are several reasons for this approach, all centering around the typical need for accurate positional location of the machine's functional parts (e.g., within ± 0.005 in {0.13 mm} or closer in most machinery). There are exceptions to this, of course, as in the case of a machine frame, which, other than its mounting surfaces, may be less accurately made and may even be an inherently inaccurate weldment.

Consider an assembly of two parts, loaded in shear as shown in Figure 15-38. There is a pattern of multiple bolts clamping the two parts together. Bolts and screws are not made to close tolerances. Holes for bolts or screws must be made oversize to provide some clearance for the bolt/screw insertion. Tapped holes for machine screws will have radial clearance versus the inserted screw, meaning that the concentricity of a screw in a tapped hole or a bolt in a clearance hole is not guaranteed. They will be eccentric.

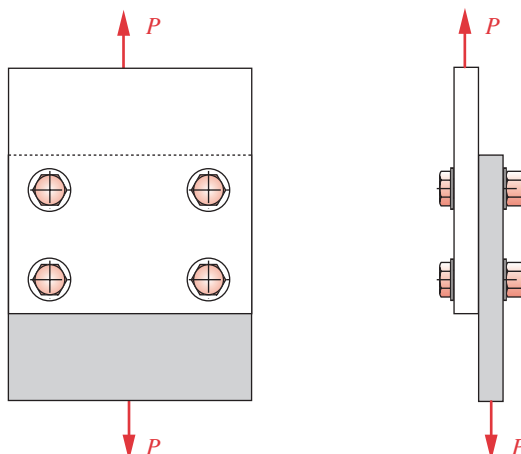


FIGURE 15-38

A Bolted Joint Loaded in Shear

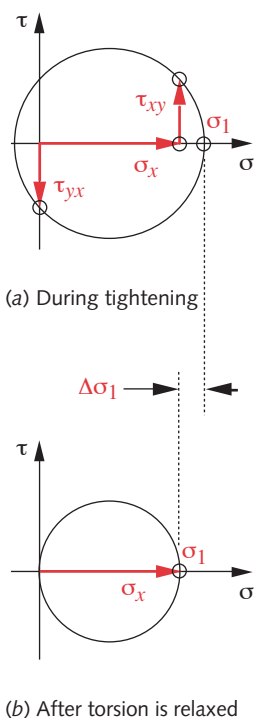


FIGURE 15-37

Mohr's Circles for a Preloaded Bolt Both During and After Tightening

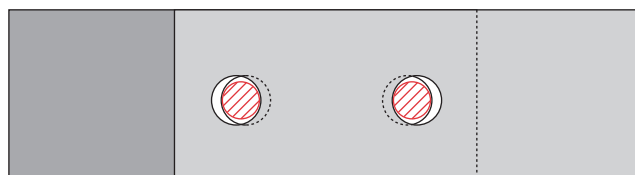
The above observations are true for any one bolt/screw in any one hole. When a pattern of fasteners is used as in Figure 15-38, the required clearances between bolts/screws and holes becomes significantly greater than for one hole because of the tolerances on the dimensions between the hole centerlines in the two mating parts. For reliable and interchangeable assembly, the holes will have to be significantly larger than the removable fasteners in order to accommodate all the variation possible within customary manufacturing tolerances. Figure 15-39 shows an exaggerated mismatch between a pair of holes in mating pieces and indicates why the holes have to be larger in diameter than the fasteners to allow assembly.

Now consider what will happen if we rely on the four bolts in Figure 15-38 to both locate the parts and take the shear loads without tensile preloading. The positional location of one part to the other is severely compromised by the needed clearances in the holes and by the variations in diameter of commercial bolts. The ability of the four bolts to share the loads in direct shear is also compromised by the clearances. At best, two bolts will probably take all the shear load, with the others not even contacting the appropriate sides of their holes on both parts in order to share the load.

So what is the solution to this problem? A better design is shown in Figure 15-40, which adds two hardened-steel dowel pins to the pattern of four bolts. More dowels could be added, but two is the minimum number needed in order to withstand a couple in that plane and is usually sufficient. A brief digression on the proper application of dowel pins is necessary at this point.

Dowel Pins

Standard straight dowel pins* are made to close tolerances (typically ± 0.0001 in variation in diameter), are hardened and ground to a fine finish, and are truly round. They are available in low-carbon steel, corrosion-resistant (chrome) steel, brass, and alloy steel hardened to 40-48 HRC, and are purchased to the required length. They are relatively inexpensive. Tapered dowel pins are also available. Other varieties of grooved, knurled, and spring-roll pins are available that do not require as close-toleranced holes for a press fit. We will limit our brief discussion to straight, solid dowel pins.



Note that holes in top and bottom plates are on different centers due to tolerances.

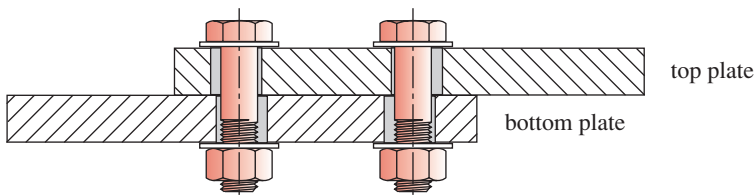
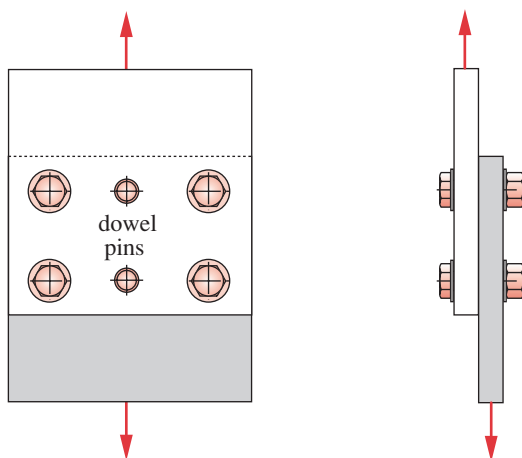


FIGURE 15-39

Clearance is Needed in Fastener Holes to Accommodate Manufacturing Tolerances

* ANSI Standard B18.8.2-1978 (R1989), American National Standards Institute, New York, 1989.

**FIGURE 15-40**

A Bolted and Doweled Joint Loaded in Shear

Dowel pins are typically press-fit into one part (the “bottom” part) and made to be a close slip fit in the other part (the “top” part). While tapped or clearance holes for the bolts or screws are machined into the separate parts prior to assembly, the dowel-pin holes are not drilled until after the assembly has been bolted or screwed together and aligned to its proper configuration. Then pilot holes for the dowels, smaller than the dowel-pin diameter, are drilled through both clamped parts in the specified locations. In some cases, the top part may have the pilot holes already in it, and it will be used as the jig to drill the holes through the bottom part, when assembled.

Once the (exactly concentric) pilot holes are in both parts, they can be reamed to the proper diameter for a press fit with the dowel pin while still clamped together. They are then disassembled and the pilot holes in the “top” part are reamed slightly larger for a slip fit with the dowel pin. The reamer will follow the hole, accurately keeping its center location. The dowels are then pressed into the bottom part, and the top part is carefully fitted over the protruding dowels. The screw fasteners are then replaced and torqued to the appropriate preload.

We now have an assembly that is **accurately relocatable** when disassembled and reassembled and one in which we have **essentially zero radial clearance** between some number of hardened pins, which can, if necessary, resist shear loads in a shared fashion. Eccentric loading is not a problem, since the two dowels can resist couples in the shear plane. Without dowels (or sufficient compressive preload to generate friction between the plates) applied couples will rack the bolts in their clearance holes, allowing relative motion between the top and bottom plate.

15

Centroids of Fastener Groups

When a group of fasteners is arranged in a geometric pattern, the location of the centroid of the fastener areas is needed for force analysis. With respect to any convenient coordinate system, the coordinates of the centroid are

$$\tilde{x} = \frac{\sum_1^n A_i x_i}{\sum_1^n A_i}, \quad \tilde{y} = \frac{\sum_1^n A_i y_i}{\sum_1^n A_i} \quad (15.24)$$

where n is the number of fasteners, i represents a particular fastener, A_i are the cross-sectional areas of the fasteners, and x_i, y_i are the coordinates of the fasteners in the selected coordinate system.

Determining Shear Loads on Fasteners

Figure 15-41a shows a shear joint with an eccentric load applied. Four bolts and four dowel pins are used to connect the two parts. Assume that the four dowels will take all the shear loading and will share the load equally. The eccentric load can be replaced with the combination of a force P acting through the centroid of the pin pattern and a moment M about that centroid, as shown in Figure 15-41b. The force through the centroid will generate equal and opposite reactions F_1 at each pin. In addition, there will be a second force F_2 at each pin, acting perpendicular to a radius from the centroid to the pin, due to the moment M .

The magnitude of the force component F_1 at each pin due to the force P acting through the centroid will be

$$|F_{1i}| = \frac{P}{n} \quad (15.25a)$$

where n is the number of pins.

To determine how much force each pin feels from the moment M , assume that one part is allowed to rotate slightly about the centroid with respect to the other part. The displacement at any hole will be proportional to its radius from the centroid. The strain developed in the pin will be proportional to that displacement. Stress is proportional to strain in the elastic region, and force is proportional to stress for constant shear area. The magnitude of the force component felt at any pin due to the moment M is:

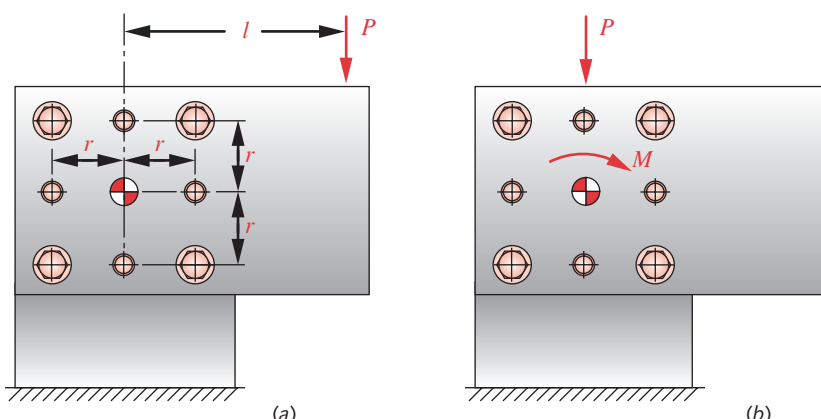
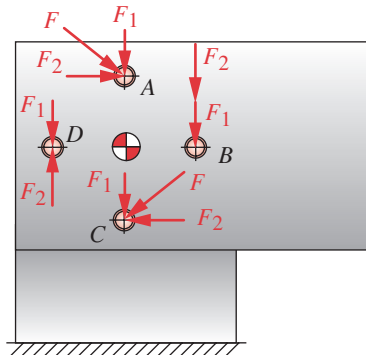


FIGURE 15-41

A Bolted and Dowelled Joint Eccentrically Loaded in Shear

**FIGURE 15-42**

Pin Forces in a Joint Eccentrically Loaded in Shear

$$|F_{2i}| = \frac{Mr_i}{\sum_{j=1}^n r_j^2} = \frac{Plr_i}{\sum_{j=1}^n r_j^2} \quad (15.25b)$$

The total force F_i at each pin is then the vector sum of the two components F_{1i} and F_{2i} , for that pin, as shown in Figure 15-42. The total force is greatest at pin B in the particular case shown.

The stress in the pin is found from equation 15.8c for direct shear stress. The shear yield strength can be estimated from the relationship in equation 5.9b, repeated here:

$$S_{ys} = 0.577 S_y \quad (5.9b)$$

The minimum shear yield strengths S_{ys} for several common dowel-pin materials can be found in Table 15-12. The data are for pins of 0.5-in dia and smaller. Recall from Section 14.3 (p. 790) that small-diameter drawn wire has high strength due to its cold working. These are essentially proof strengths as defined by ANSI standard.* Pins made to this standard will have at least the indicated strengths when loaded in shear.

Table 15-12

Minimum Strengths for Dowel Pins in Double Shear. Source: Drive-Lok, Inc., Sycamore, Ill.

Material	S_{ys} (kpsi)
Low-carbon steel	50
Alloy steel 40-48 HRC	117
Corrosion-resistant steel	82
Brass	40

EXAMPLE 15-6

Fasteners in Eccentric Shear

Problem Determine a size for the dowel pins in the bracket of Figure 15-41.

Given The static force $P = 1200$ lb is applied at $l = 5$ in. The radius to the dowel pins is $r = 1.5$ in.

Assumptions All pins share load equally. Use 40-48 HRC alloy steel for the pin material.

Solution See Figures 15-41 and 15-42.

- Calculate the moment of the applied force.

$$M = Pl = 1200(5) = 6000 \text{ lb-in} \quad (a)$$

* ANSI Standard B18.8.2-1995, American National Standards Institute, New York, 1995.

2 Calculate the magnitude of the force due to this moment at each pin.

$$F_M = \frac{M}{nr} = \frac{6\,000}{4(1.5)} = 1\,000 \text{ lb} \quad (b)$$

3 Find the amount of the direct force P felt at each pin.

$$F_P = \frac{P}{n} = \frac{1\,200}{4} = 300 \text{ lb} \quad (c)$$

4 Based on the vector diagram in Figure 15-42, pin B is the most heavily loaded and its resultant force is

$$F_B = F_P + F_M = 300 + 1\,000 = 1\,300 \text{ lb} \quad (d)$$

5 Assume a trial pin diameter of 0.375 in and calculate the direct shear stress in pin B .

$$\tau = \frac{F_B}{A_B} = \frac{1\,300(4)}{\pi(0.375)^2} = 11\,770 \text{ psi} \quad (e)$$

6 Find the shear yield strength of the material from Table 15-12 and calculate the safety factor against static shear failure.

$$N_s = \frac{S_{ys}}{\tau} = \frac{117\,000}{11\,770} = 10 \quad (f)$$

7 The files EX15-06 can be found on the CD-ROM.

15.11 CASE STUDY

Designing Headbolts for an Air Compressor

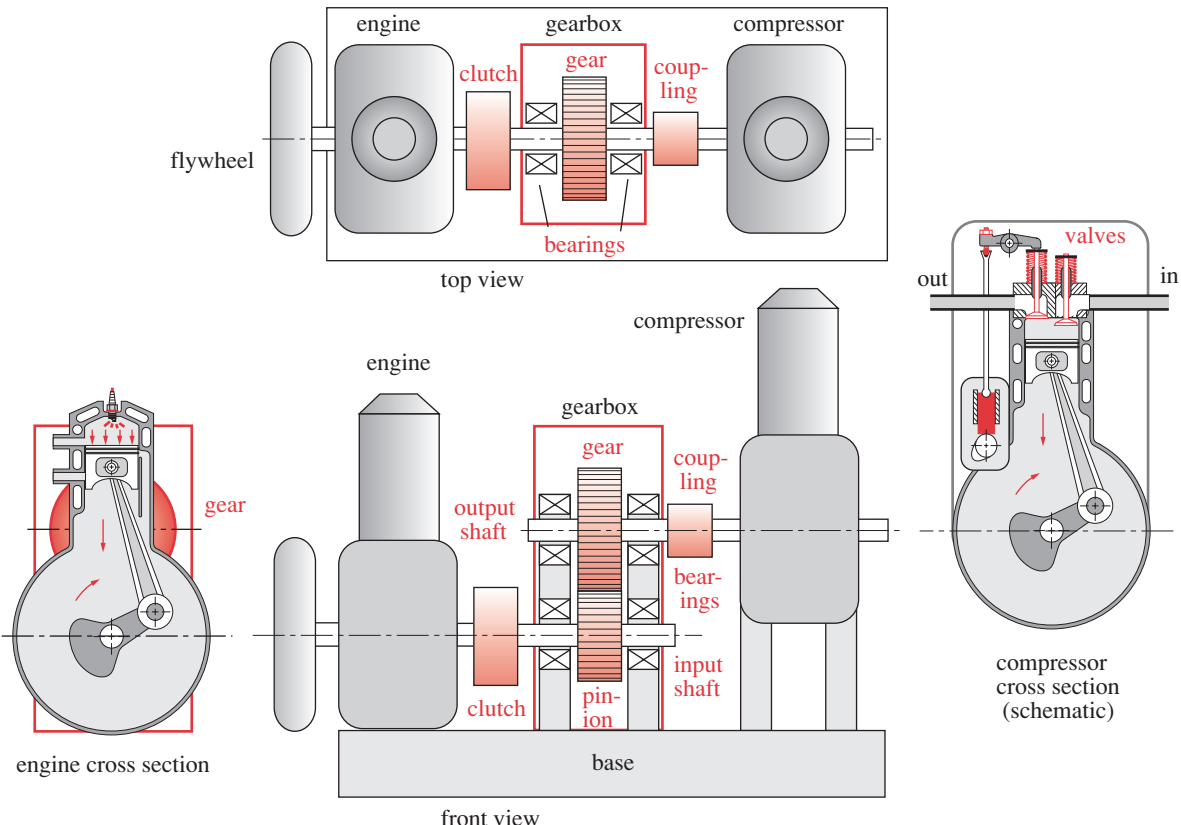
The preliminary design of this device is shown in Figure 9-1. The cylinder and head are cast aluminum. The head is fastened to the cylinder block with a number of cap screws that insert in tapped holes arranged on a bolt circle. The pressure generated in the cylinder creates a force-time function on the head, as shown in Figure 9-2.

CASE STUDY 8D

Design of the Headbolts for an Air Compressor

15

Problem	Design a set of cap screws to attach the head to the cylinder in Figure 9-1 based on the loads defined in Case Study 8A (p. 526).
Given	The compressor bore is 3.125-in diameter. The dynamic force acting on the head fluctuates from 0 to 1 000 lb each cycle from the 130-psi cylinder pressure. A 0.06-in-thick, unconfined copper-asbestos gasket covers the entire head-cylinder interface. The head thickness at the attachment points (exclusive of cooling fins) is 0.4 in.
Assumptions	Infinite life. Use standard hex-head cap screws without washers. The operating temperature is less than 350°F. Use 99.9% reliability.

**FIGURE 9-1** Repeated

Preliminary Design Schematic of Gasoline-Engine-Powered Portable Air Compressor, Gearbox, Couplings, Shafts, and Bearings

Solution

See Figures 9-1 and 9-2.

- 1 Choose a trial diameter d for the screws of 0.313 in. Use UNC threads to avoid stripping problems in the cast-aluminum cylinder. The trial fastener is then a 5/16-18 UNC-2A cap screw with rolled threads for fatigue resistance.
- 2 Choose a bolt circle and outside diameter based on the cylinder bore and the rule of thumb of *at least* $1.5d$ to $2d$ of distance between any screw and an edge. We will use $2d$ because of the need for sealing area against the cylinder pressure.

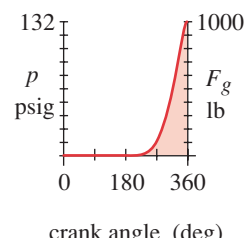
$$d_{bc} = 3.125 + 2(2)(0.313) = 4.375 \text{ in} \quad (a)$$

$$d_o = 4.125 + 2(2)(0.313) = 5.625 \text{ in}$$

- 3 To get the recommended maximum of 6-screw-diameters spacing between bolts we will need about 8 screws equispaced around the bolt circle. Calculate the spacing between screws in units of screw diameters.

$$\Delta b = \frac{\pi D_p}{n_b d} = \frac{\pi(4.375)}{8(0.313)} = 5.5 \text{ bolt diameters} \quad (b)$$

This is less than the maximum of 6 screw diameters so is acceptable. We will later calculate the gasket pressure to check for possible leakage.

**FIGURE 9-2** Repeated

Pressure and Force Within Cylinder During One Cycle

- 4 Assume a trial screw length of 1.25 in. The head thickness of 0.40 in at the screw holes plus the 0.1-in gasket will leave 0.75 in of thread penetration into the cylinder's tapped hole. This is $> 2 \times$ the screw diameter (10 threads), which is the minimum recommended length for a steel screw in aluminum threads. For U.S. standard bolts up to 6-in long, the thread length is $2d + 0.25 = 0.875$ in of this bolt's length,^[2] which allows the desired penetration. The trial clamp length for the stiffness calculations is then 1.25 in, since the entire cap screw is engaged.
- 5 Try an SAE grade 7 screw preloaded to 70% of its proof strength. Table 15-6 (p. 882) shows the proof strength of this screw to be 105 kpsi. The tensile-stress area from equation 15-1 (p. 863) is 0.052 431 in². The required preload is then

$$F_i = 0.7S_p A_t = 0.7(105\ 000)(0.052\ 431) = 3\ 853.66 \text{ lb} \quad (c)$$

- 6 Find the joint aspect ratio and plate to screw modulus from equations 15.18a and b:

$$j = \frac{d}{l} = \frac{0.313}{1.25} = 0.25 \quad (d)$$

$$r = \frac{E_{\text{material}}}{E_{\text{bolt}}} = \frac{10.4E6}{30E6} = 0.347$$

- 7 Since this joint has the same material (aluminum) throughout, equation 15.19 is all that is needed to calculate the joint constant C_{ng} for the metal without the gasket. The parameters needed for the equation are found by interpolating for $j = 0.25$ in Table 15-8. They are: $p_0 = 0.653$, $p_1 = -1.207$, $p_2 = 1.103$, and $p_3 = -0.383$.

$$\begin{aligned} C_{ng} &= p_3 r^3 + p_2 r^2 + p_1 r + p_0 \\ &= -0.383(0.347)^3 + 1.103(0.347)^2 - 1.207(0.347) + 0.653 = 0.351 \end{aligned} \quad (e)$$

- 8 We can approximate the stiffness of the screw k_b' with equation 15.17, then estimate material stiffness k_m with no gasket by using equation 15.13c, given k_b' and C_{ng} .

$$\text{length of thread : } l_{thd} = 2d + 0.25 = 2(0.313) + 0.25 = 0.875 \text{ in}$$

$$\text{length of shank : } l_s = l_{\text{bolt}} - l_{thd} = 1.25 - 0.875 = 0.375 \text{ in}$$

$$\text{length of clamped thread : } l_t = l - l_s = 1.25 - 0.375 = 0.875 \text{ in}$$

$$k_{b'} \cong \left(1 + \frac{d}{l}\right)^{-1} \frac{A_t A_b}{A_b l_t + A_t l_s} E_b$$

$$k_{b'} \cong \left(1 + \frac{0.313}{1.25}\right)^{-1} \frac{0.052(0.077)}{0.077(0.875) + 0.052(0.375)} 30E6 = 1.112E6 \text{ lb/in}$$

$$C_{ng} = \frac{k_{b'}}{k_{m_1} + k_{b'}} \Rightarrow k_{m_1} = k_{b'} \frac{1 - C_{ng}}{C_{ng}} = 1.112E6 \left(\frac{1 - 0.351}{0.351}\right) = 2.060E6 \text{ lb/in} \quad (f)$$

- 9 Now consider the gasket. The area of the unconfined gasket subjected to the clamp force can be assumed to be that of one "bolt's worth" of the total clamped area which extends from the outside diameter of the cylinder head to the bore:

$$A_{\text{total}} = \frac{\pi}{4} (D_o^2 - D_l^2) = \frac{\pi}{4} (5.625^2 - 3.125^2) \cong 17.18 \text{ in}^2 \quad (g)$$

Dividing by the number of bolts and subtracting the screw hole area gives the area of the clamped gasket around any one screw as:

$$A_g = \frac{A_{total}}{n_b} - \frac{\pi}{4} d^2 = \frac{17.18}{8} - \frac{\pi}{4} 0.313^2 = 2.071 \text{ in}^2 \quad (h)$$

10 The stiffness of this piece of gasket is then

$$k_{m_2} = \frac{A_g E_g}{l_g} = \frac{2.071(13.5E6)}{0.06} \cong 4.659E8 \text{ lb/in} \quad (i)$$

The modulus of elasticity of the gasket material is found in Table 15-10 (p. 900).

11 The material and gasket stiffness combine according to equation 14.2b (p. 787). The combined stiffness of the gasketed joint is then

$$k_{m_g} = \frac{1}{\frac{1}{k_{m_1}} + \frac{1}{k_{m_2}}} = \frac{1}{\frac{1}{2.060E6} + \frac{1}{4.659E8}} \\ k_{m_g} = 2.051E6 \text{ lb/in} \quad (j)$$

Note that the combined stiffness in this case is dominated by the aluminum because the copper-asbestos gasket is stiffer.

12 The joint constant with the unconfined gasket is

$$C = \frac{k_b}{k_{m_g} + k_b} = \frac{1.112E6}{2.051E6 + 1.112E6} \cong 0.352 \quad (k)$$

and

$$(1 - C) = 0.648$$

13 The 1 000-lb load is assumed to be divided equally among the 8 bolts at 125 lb each. The portions of the applied load felt by each screw and material (Eq. 15.13, p. 886) are:

$$P_b = CP = 0.352(125) \cong 43.95 \text{ lb} \quad (l)$$

$$P_m = (1 - C)P = 0.648(125) \cong 81.05 \text{ lb}$$

14 The resulting peak loads in screw and material are

$$F_b = F_i + P_b = 3853.66 + 43.95 = 3897.61 \text{ lb} \quad (m)$$

$$F_m = F_i - P_m = 3853.66 - 81.05 = 3772.61 \text{ lb}$$

15 The alternating and mean components of force on the screw are

$$F_{alt} = \frac{F_b - F_i}{2} = \frac{3897.61 - 3853.66}{2} \cong 21.98 \text{ lb} \quad (n)$$

$$F_{mean} = \frac{F_b + F_i}{2} = \frac{3897.61 + 3853.66}{2} \cong 3875.63 \text{ lb}$$

16 The nominal mean and alternating stresses in the screw are

$$\sigma_{a_{nom}} = \frac{F_{alt}}{A_t} = \frac{21.98}{0.052431} \cong 419.2 \text{ psi} \quad (o)$$

$$\sigma_{m_{nom}} = \frac{F_{mean}}{A_t} = \frac{3875.63}{0.052431} \cong 73919 \text{ psi}$$

- 17 The fatigue stress-concentration factor for this diameter thread is found from equation 15.15c and the mean stress-concentration factor K_{fm} is found from equation 6.17 (p. 364).

$$K_f = 5.7 + 0.6812d = 5.7 + 0.6812(0.313) = 5.9$$

$$\text{if } K_f |\sigma_{max_{nom}}| > S_y \text{ then :} \quad K_{fm} = \frac{S_y - K_f \sigma_{a_{nom}}}{|\sigma_{m_{nom}}|}$$

$$K_f |\sigma_{max_{nom}}| = K_f |\sigma_{a_{nom}} + \sigma_{m_{nom}}| = 5.9 |460.2 + 73\ 960| = 440\ 039 \text{ psi}$$

$$440\ 039 \text{ psi} > S_y = 115\ 000 \text{ psi}$$

$$K_{fm} = \frac{S_y - K_f \sigma_{a_{nom}}}{|\sigma_{m_{nom}}|} = \frac{115\ 000 - 5.9(460.2)}{73\ 960} = 1.52 \quad (p)$$

- 18 The local mean and alternating stresses in the screw are

$$\sigma_a = K_f \frac{F_{alt}}{A_t} = 5.9 \frac{21.98}{0.052\ 431} \cong 2478 \text{ psi} \quad (q)$$

$$\sigma_m = K_{fm} \frac{F_{mean}}{A_t} = 1.52 \frac{3\ 875.63}{0.052\ 431} \cong 112\ 522 \text{ psi}$$

- 19 The stresses at the initial preload and at the maximum screw force are

$$\sigma_i = K_{fm} \frac{F_i}{A_t} = 1.52 \frac{3\ 853.66}{0.052\ 431} \cong 111\ 883 \text{ psi} \quad (r)$$

$$\sigma_b = K_{fm} \frac{F_b}{A_t} = 1.52 \frac{3\ 897.61}{0.052\ 431} = 113\ 160 \text{ psi}$$

- 20 The endurance strength for this material is found using the methods of Section 6.6 (p. 327):

$$S_e^* = 0.5 S_{ut} = 0.5(133\ 000) = 66\ 500 \text{ psi} \quad (s)$$

$$\begin{aligned} S_e &= C_{load} C_{size} C_{surf} C_{temp} C_{reliab} S_e^* \\ &= 0.70(0.995)(0.739)(1)(0.753)(66\ 500) = 25\ 778 \text{ psi} \end{aligned} \quad (t)$$

where the strength-reduction factors are taken from the tables and formulas in Section 6.6 for, respectively, axial loading, the screw size, a machined finish, room temperature, and 99.9% reliability.

- 21 The corrected endurance strength and the ultimate tensile strength are used in equation 15.16 (p. 891) to find the fatigue safety factor from the Goodman line.

$$\begin{aligned} N_f &= \frac{S_e(S_{ut} - \sigma_i)}{S_e(\sigma_m - \sigma_i) + S_{ut}\sigma_a} \\ &= \frac{25\ 778(133\ 000 - 111\ 883)}{25\ 778(112\ 522 - 111\ 883) + 133\ 000(2478)} \cong 1.6 \end{aligned} \quad (u)$$

- 22 The static screw stress after initial local yielding and the yielding safety factor are:

$$\sigma_s = \frac{F_{bolt}}{A_t} = \frac{3897.61}{0.052431} = 74\,338 \text{ psi} \quad N_y = \frac{S_y}{\sigma_b} = \frac{115\,000}{74\,338} \cong 1.5 \quad (v)$$

- 23 The safety factor against joint separation is found from equation 15.14d (p. 887).

$$N_{separation} = \frac{F_i}{P(1-C)} = \frac{3853.66}{125(1-0.352)} \cong 47 \quad (w)$$

- 24 The joint will leak unless the clamping forces are sufficient to create more pressure at the gasket than exists in the cylinder. The minimum clamping pressure can be found from the total area of the gasketed joint and the minimum clamping force F_m .

$$p_{avg} = \frac{F_m}{A_j} = \frac{4F_m}{\pi(D_o^2 - D_i^2) - n_b A_b} = \frac{4(3\,772.6)}{\pi(5.625^2 - 3.125^2) - 8(0.077)} \cong 228 \text{ psi} \quad (x)$$

$$N_{leak} = \frac{p_{avg}}{p_{cyl}} = \frac{228}{130} \cong 1.7$$

This ratio of clamp pressure vs. cylinder pressure makes the screw spacing acceptable.

- 25 The torque required to obtain the preload of 3853.66 lb found in step 5 is:

$$T_i \cong 0.21F_id = 0.21(3\,853.66)(0.313) \cong 253 \text{ lb-in} \quad (y)$$

- 26 This design uses eight 5/16-18 UNC-2A, grade 7 hex-head cap screws, 1.25 in long, preloaded to 70% of proof strength and equispaced on a 4.375-in-dia bolt circle. This design has a safety factor against leakage of 1.7, a fatigue safety factor of 1.6, and can stand 47 times the operating pressure before joint separation will occur. These safety factors are acceptable. The files CASE8D can be found on the CD-ROM.

15.12 SUMMARY

This chapter has dealt with only a small sample of commercially available fasteners. An extremely varied collection of fasteners is produced by vendors. The “right” fastener can usually be found for any application, and if not (and the required quantity is high enough), some vendor will make a new one for you. Many standards exist that define the configurations, sizes, strengths, and tolerances of fasteners. Threaded fasteners are made to one or another of these standards, which provides good interchangeability. Unfortunately, metric and English threads are not interchangeable, and both are in wide use in the United States.

Power screws are threaded devices used primarily to move loads or accurately position objects. They have low efficiency due to their large friction losses unless the ball-screw variety is used, which lowers the friction significantly. However, low-friction screws give up one of their advantages, which is self-locking or the ability to hold a load in place with no input of energy (as in a jack). Back-drivable screws are the opposite of self-locking and can be used as a linear-to-rotary motion converter.

Threaded fasteners (bolts, nuts, and screws) are the standard means of holding machinery together. These fasteners are capable of supporting very large loads, especially

if they are preloaded. Preloading tightens the fastener to a high level of axial tension before any working loads are applied. The tension in the fastener causes compression in the clamped parts. This compression has several salutary effects. It keeps the joint tightly together and thus able to contain fluid pressure and resist shear loads with its interfacial friction. The compressive forces in the clamped material also serve to protect the fastener from fluctuating fatigue loads by absorbing most of the applied load oscillations. The high clamping forces also guard against vibratory loosening of the fastener by creating high friction forces in the threads.

Threaded fasteners are also capable of resisting shear loads and are used extensively in that manner in structural applications. In machine design it is more common to rely on close-fitted dowel pins to take shear loads and let the threaded fasteners provide the tension to hold the joint together. The interested reader is referred to the publications listed in the bibliography of this chapter for more information on the diverse and fascinating world of fasteners.

Important Equations Used in This Chapter

See the referenced sections for information on the proper use of these equations.

Torque Required to Raise the Load with a Power Screw (Section 15.2):

$$T_u = T_{s_u} + T_c = \frac{Pd_p}{2} \frac{(\mu\pi d_p + L \cos \alpha)}{(\pi d_p \cos \alpha - \mu L)} + \mu_c P \frac{d_c}{2} \quad (15.5a)$$

Self-locking of a Power Screw Will Occur if (Section 15.2):

$$\mu \geq \frac{L}{\pi d_p} \cos \alpha \quad \text{or} \quad \mu \geq \tan \lambda \cos \alpha \quad (15.6a)$$

Efficiency of a Power Screw (Section 15.2):

$$\epsilon = \frac{W_{out}}{W_{in}} = \frac{PL}{2\pi T} \quad (15.7c)$$

Spring Constant of a Threaded Fastener (Section 15.7):

$$\frac{1}{k_b} = \frac{l_t}{A_t E_b} + \frac{l - l_t}{A_b E_b} = \frac{l_t}{A_t E_b} + \frac{l_s}{A_b E_b} \quad \therefore \quad k_b = \frac{A_t A_b}{A_b l_t + A_t l_s} E_b \quad (15.11a)$$

$$k_{b'} = \left(1 + \frac{d}{l}\right)^{-1} k_b \quad (15.17alt)$$

Spring Constant of the Clamped Material if A_m is known (Section 15.7):

$$k_m = \frac{A_m E_m}{l} \quad (15.11c)$$

Load Taken by the Preloaded Material (Section 15.7):

$$P_m = \frac{k_m}{k_b + k_m} P = (1 - C)P \quad (15.13d)$$

Load Taken by a Preloaded Bolt and the Joint Constant C (Section 15.7):

$$P_b = \frac{k_b}{k_m + k_b} P \quad \text{or} \quad P_b = CP \quad \text{where } C = \frac{k_b}{k_m + k_b} \quad (15.13c)$$

Minimum Load in Material and Maximum Load in Bolt (Section 15.7):

$$F_m = F_i - (1 - C)P \quad (15.14a)$$

$$F_b = F_i + CP \quad (15.14b)$$

Load Required to Separate a Preloaded Joint (Section 15.7):

$$P_0 = \frac{F_i}{(1 - C)} \quad (15.14c)$$

Mean and Alternating Loads Felt by a Preloaded Bolt (Section 15.7):

$$F_{alt} = \frac{F_b - F_i}{2}, \quad F_{mean} = \frac{F_b + F_i}{2} \quad (15.15a)$$

Mean and Alternating Stresses in a Preloaded Bolt (Section 15.7):

$$\sigma_a = K_f \frac{F_{alt}}{A_t}, \quad \sigma_m = K_{fm} \frac{F_{mean}}{A_t} \quad (15.15b)$$

Fatigue Stress Concentration Factor in Threads:

$$K_f = 5.7 + 0.6812d \quad d \text{ in inches} \quad \text{or} \quad K_f = 5.7 + 0.02682d \quad d \text{ in mm} \quad (15.15c)$$

Preload Stress in a Bolt (Section 15.7):

$$\sigma_i = K_{fm} \frac{F_i}{A_t} \quad (15.15d)$$

Fatigue Safety Factor for a Preloaded Bolt (Section 15.7):

$$N_f = \frac{S_e(S_{ut} - \sigma_i)}{S_e(\sigma_m - \sigma_i) + S_{ut}\sigma_a} \quad (15.16)$$

Approximate Torque Needed to Preload a Bolt (Section 15.9):

$$T_i \approx 0.21F_id \quad (15.23d)$$

Centroid of a Group of Fasteners (Section 15.10):

$$\tilde{x} = \frac{\sum_1^n A_i x_i}{\sum_1^n A_i}, \quad \tilde{y} = \frac{\sum_1^n A_i y_i}{\sum_1^n A_i} \quad (15.24)$$

Forces on Fasteners Eccentrically Loaded in Shear (Section 15.10):

$$\left|F_{1i}\right| = \frac{P}{n} \quad (15.25a)$$

$$\left|F_{2i}\right| = \frac{Mr_i}{\sum_{j=1}^n r_j^2} = \frac{Plr_i}{\sum_{j=1}^n r_j^2} \quad (15.25b)$$

15.13 REFERENCES

- 1 *Product Engineering*, vol. 41, p. 9, Apr. 13, 1970.
- 2 **H. L. Horton**, ed. *Machinery's Handbook*, 21st ed. Industrial Press, Inc.: New York. p. 1256, 1974.
- 3 **ANSI/ASME Standard B1.1-1989**, American National Standards Institute, New York, 1989.
- 4 **ANSI/ASME Standard B1.13-1983 (R1989)**, American National Standards Institute, New York, 1989.
- 5 **T. H. Lambert**, Effects of Variations in the Screw Thread Coefficient of Friction on Clamping Force of Bolted Connections, *J. Mech Eng. Sci.*, **4**: p. 401, 1962.
- 6 **R. E. Peterson**, *Stress-concentration factors*. John Wiley & Sons: New York, p. 253, 1974.
- 7 **H. H. Gould and B. B. Mikic**, Areas of Contact and Pressure Distribution in Bolted Joints, *Trans ASME, J. Eng. for Industry*, **94**: pp. 864–869, 1972.
- 8 **N. Nabil**, Determination of Joint Stiffness in Bolted Connections, *Trans. ASME, J. Eng. for Industry*, **98**: pp. 858–861, 1976.
- 9 **Y. Ito, J. Toyoda and S. Nagata**, Interface Pressure Distribution in a Bolt-Flange Assembly, *Trans. ASME, J. Mech. Design*, **101**: pp. 330–337, 1979.
- 10 **J. F. Macklin and J. B. Raymond**, *Determination of Joint Stiffness in Bolted Connections using FEA*, Major Qualifying Project, Worcester Polytechnic Institute, Worcester, Mass., Dec. 31, 1994.
- 11 **B. Houle**, *An Axisymmetric FEA Model Using Gap Elements to Determine Joint Stiffness*, Major Qualifying Project, Worcester Polytechnic Institute, Worcester, Mass., Dec. 31, 1995.
- 12 **J. E. Shigley and C. H. Mischke**, *Mechanical Engineering Design*, 5th ed. McGraw-Hill: New York, p. 354, 1989.
- 13 **J. Wileman, M. Choudhury, and I. Green**, “Computation of Member Stiffness in Bolted Connections,” *Trans. ASME, J. Mech. Design*, **113**, pp. 432–437, 1991.
- 14 **T. F. Lehnhoff, K. I. Ko, and M. L. McKay**, “Member Stiffness and Contact Pressure Distribution of Bolted Joints,” *Trans. ASME, J. Mech. Design*, **116**, pp. 550–557, 1994.
- 15 **R. E. Cornwell**, “Computation of Load Factors in Bolted Connections,” *Proc. IMechE, J. Mech. Eng. Sci.*, **223c**, pp. 795–808, 2009.
- 16 **A. R. Kephart**, “Fatigue Acceptance Test Limit Criterion for Larger Diameter Rolled Thread Fasteners,” *ASTM Workshop on Fatigue and Fracture of Fasteners*, May 6, 1997, St. Louis, MO.
- 17 **C. Crispell**, “New Data on Fastener Fatigue,” *Machine Design*, pp. 71–74, April 22, 1982.

15.14 BIBLIOGRAPHY

American Institute of Steel Construction Handbook. AISI: New York.

Helpful Hints for Fastener Design and Application. Russell, Burdsall & Ward Corp.: Mentor, Ohio, 1976.

SAE Handbook. Soc. of Automotive Engineers: Warrendale, Pa., 1982.

“Fastening and Joining Reference Issue,” *Machine Design*, vol. 55, Nov. 17, 1983.

J. H. Bickford, *An Introduction to the Design and Behavior of Bolted Joints*, 2nd ed. Marcel Dekker, New York, 1990.

H. L. Horton, ed., *Machinery’s Handbook*, 21st ed. Industrial Press: New York, 1974.

R. O. Parmley, ed. *Standard Handbook of Fastening and Joining*. McGraw-Hill: New York, 1977.

H. A. Rothbart, ed., *Mechanical Design and Systems Handbook*. McGraw-Hill: New York, Sections 20, 21, 26, 1964.

15.15 PROBLEMS

- 15-1 Compare the tensile load capacity of a 5/16-18 UNC thread and a 5/16-24 UNF thread made of the same material. Which is stronger? Make the same comparison for M8 × 1.25 and M8 × 1 ISO threads. Compare them all to the strength of a 5/16-14 Acme thread.
- *15-2 A 3/4-6 Acme thread screw is used to lift a 2 kN load. The mean collar diameter is 4 cm. Find the torque to lift and to lower the load using a ball-bearing thrust washer. What are the efficiencies? Is it self-locking?
- 15-3 A 1 3/8-4 Acme thread screw is used to lift a 1-ton load. The mean collar diameter is 2 in. Find the torque to lift and to lower the load using a ball-bearing thrust washer. What are the efficiencies? Is it self-locking?
- *†15-4 The trailer hitch from Figure 1-1 (p. 11) has loads applied as shown in Figure P15-1. The tongue weight of 100 kg acts downward and the pull force of 4 905 N acts horizontally. Using the dimensions of the ball bracket in Figure 1-5 (p. 14), draw a free-body diagram of the ball bracket and find the tensile and shear loads applied to the two bolts that attach the bracket to the channel in Figure 1-1. Size and specify the bolts and their preload for a safety factor of at least 1.7.[‡]
- 15-5 For the trailer hitch of Problem 3-4, determine the horizontal force that will result on the ball from accelerating a 2 000-kg trailer to 60 m/s in 20 sec. Assume a constant acceleration. Size and specify the bolts and their preload for a safety factor of at least 1.7.[‡]
- *15-6 For the trailer hitch of Problem 3-4, determine the horizontal force that will result on the ball from an impact between the ball and the tongue of the 2 000-kg trailer if the hitch deflects 1 mm on impact. The tractor weighs 1 000 kg. The velocity at impact is 0.3 m/s. Size and specify the bolts and their preload for a safety factor of at least 1.7.[‡]
- *15-7 A 1/2-in-dia UNC, class 7 bolt with rolled threads is preloaded to 80% of its proof strength when clamping a 3-in-thick sandwich of solid steel. Find the safety factors against static yielding and joint separation when a static 1 000-lb external load is applied.[‡]

Table P15-0[†]

Topic/Problem Matrix

15.2 Power Screws

15-1, 15-2, 15-3, 15-37, 15-38

15.3 Stresses in Threads

15-15, 15-16, 15-39, 15-47

15.6 Strengths of Bolts

15-28, 15-29, 15-40, 15-41, 15-48

15.8 Joint Stiffness

Material Only

15-17, 15-18, 15-19, 15-31, 15-32, 15-33, 15-42, 15-43

No Gasket-Static Load

15-7, 15-8, 15-23, 15-30, 15-49

No Gasket-Dynamic Load

15-9, 15-10, 15-24, 15-25, 15-27

Unconfined Gasket

15-26, 15-42, 15-43, 15-44, 15-45, 15-46

Different Materials in Joint

15-42, 15-43, 15-44, 15-45, 15-46

15.9 Controlling Preload

Torque Only

15-11, 15-12, 15-13, 15-14,

No Gasket-Static Load

15-4, 15-5, 15-6, 15-50

No Gasket-Dynamic Load

15-22, 15-51, 15-52

Unconfined Gasket

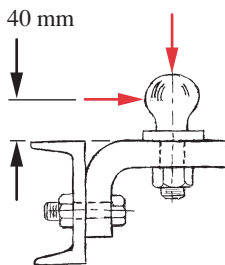
15-20, 15-21

15.10 Fasteners in Shear

15-34, 15-35, 15-36

* Answers to these problems are provided in Appendix D.

[†] Problem numbers in *italics* are design problems. Problem numbers in **boldface** are extended from similar problems in earlier chapters with the same dash no.

**FIGURE P15-1**

Problems 15-4 to 15-6

- 15-8 An M14 × 2, class 8.8 bolt with rolled threads is preloaded to 75% of its proof strength when clamping a 3-cm-thick sandwich of solid aluminum. Find the safety factors against static yielding and joint separation when a static 5-kN external load is applied.[‡]
- *15-9 A 7/16-in-dia UNC, class 7 bolt with rolled threads is preloaded to 70% of its proof strength when clamping a 2.75-in-thick sandwich of solid steel. Find the safety factors against fatigue failure, yielding, and joint separation when a 1000-lb (peak) fluctuating external load is applied.[‡]
- 15-10 An M12 × 1.25, class 9.8 bolt with rolled threads is preloaded to 85% of its proof strength when clamping a 5-cm-thick sandwich of aluminum. Find the safety factors against fatigue failure, yielding, and joint separation when a 2.5-kN (peak) fluctuating external load is applied.[‡]
- *15-11 Find the tightening torque required for the bolt in Problem 15-7.
- 15-12 Find the tightening torque required for the bolt in Problem 15-8.
- *15-13 Find the tightening torque required for the bolt in Problem 15-9.
- 15-14 Find the tightening torque required for the bolt in Problem 15-10.
- 15-15 An automobile manufacturer would like a feasibility study of the concept of building-in electric-motor-powered screw jacks at each end of the car to automatically jack the car wheels off the ground for service. Assuming a 2-ton vehicle with a 60/40 front/rear weight distribution, design a self-locking screw jack capable of lifting either end of the car. The jack body will be attached to the car frame and the screw will extend downward to engage the ground. Assume a minimum installed clearance of 8 in under the retracted screw in the up position. It must lift the car frame at least 8 additional inches. Use rolling-element thrust bearings. Determine a minimum screw size safe against column buckling. Determine its required lifting torque and efficiency and the power required to lift it to full height in 45 sec. What is your recommendation as to the feasibility of this idea?
- 15-16 Design a manual screw jack similar to that shown in Figure 15-4 (p. 866) for a 20-ton lift capacity and a 10-cm lift stroke. Assume that the operator can apply a 400-N force at the tip of its bar handle to turn either the screw or nut depending on your design. Design the cylindrical bar handle to fail in bending at the design load before the jack screw fails, so that one cannot lift an overload and fail the screw. Use rolling-element thrust bearings. Seek a safety factor of 3 for thread or column failure. State all assumptions.
- *15-17 Determine the effective spring constant of the following sandwiches of materials under compressive load. All are uniformly loaded over their 10-cm² area. The first- and third-listed materials are each 10 mm thick and the middle one is 1 mm thick, together making a 21-mm-thick sandwich.
- (a) aluminum, copper-asbestos, steel
 - (b) steel, copper, steel
 - (c) steel, rubber, steel
 - (d) steel, rubber, aluminum
 - (e) steel, aluminum, steel
- In each case determine which material dominates the calculation.
- *15-18 Determine the effective spring constant of the following sandwiches of materials under compressive load. All are uniformly loaded over their 1.5-in² area. The first and third-listed materials are each 0.4 in thick and the middle one is 0.04 in thick, together making a 0.84-in-thick sandwich.
- (a) aluminum, copper-asbestos, steel
 - (b) steel, copper, steel

* Answers to these problems are provided in Appendix D.

[†] Problem numbers in *italics* are design problems. Problem numbers in **boldface** are extended from similar problems in earlier chapters with the same dash number.

[‡] For these problems, assume that the nut and washer, together, have a thickness equal to the bolt diameter, and assume that bolts are available in length increments of either 0.25 in or 5 mm.

- (c) steel, rubber, steel
- (d) steel, rubber, aluminum
- (e) steel, aluminum, steel

In each case determine which material dominates the calculation.

- 15-19 A preloaded steel bolt similar to that shown in Figure 15-31a (p. 898) clamps two flanges of total thickness l . Using the data given in the rows assigned in Table P15-1, find the joint stiffness constant.[†]
- *15-20 A single-cylinder air-compressor head sees forces that range from 0 to 18.5 kN each cycle. The head is 80-mm-thick aluminum, the unconfined gasket is 1-mm-thick Teflon, and the block is aluminum. The effective clamp length of the cap screw is 120 mm. The piston is 75-mm dia and the cylinder is 140-mm outside dia. Specify a suitable number, class, preload, and bolt circle for the cylinder-head cap screws to give a minimum safety factor of 1.2 for any possible failure mode.
- 15-21 A single-cylinder engine head sees explosive forces that range from 0 to 4 000 lb each cycle. The head is 2.5-in-thick cast iron, the unconfined gasket is 0.125-in-thick copper-asbestos, and the block is cast iron. The effective clamp length of the cap screw is 3.125 in. The piston is 3-in dia and the cylinder is 5.5-in outside dia. Specify a suitable number, class, preload, and bolt circle for the cylinder-head cap screws to give a minimum safety factor of 1.2 for any possible failure mode.
- [†]15-22 The forged-steel connecting rod for the engine of Problem 15-21 is split around the 38-mm-dia crankpin and fastened with two bolts and nuts that hold its two halves together. The total load on the two bolts varies from 0 to 8.5 kN each cycle. Design these bolts for infinite life. Specify their size, class, and preload.[‡]
- *15-23 (See also Problem 4-33 on p. 233.) The bracket in Figure P15-2 (p. 924) is fastened to the wall by 4 cap screws equispaced on a 10-cm-dia bolt circle and arranged as shown. The wall is the same material as the bracket. The bracket is subjected to a static force F , where F and the beam's other data are given in the row(s) assigned from Table P15-1. Find the forces acting on each of the 4 cap screws due to this loading and choose a suitable cap screw diameter, length, and preload that will give a minimum safety factor of 2 for any possible mode of failure.[‡]
- *15-24 (See also Problem 6-33 on p. 412.) The bracket in Figure P15-2 is fastened to the wall by 4 cap screws equispaced on a 10-cm-dia bolt circle and arranged as shown. The wall is the same material as the bracket. The bracket is subjected to a sinusoidal force-time function with $F_{max} = F$ and $F_{min} = -F$, where F and the beam's other data are given in the row(s) assigned from Table P15-1. Find the forces acting on each of the 4 cap screws due to this fully reversed loading and choose a suitable cap screw diameter, length, and preload that will give a minimum safety factor of 1.5 for any possible mode of failure for $N = 5E8$ cycles.[‡]
- *15-25 (See also Problem 6-34 on p. 412.) The bracket in Figure P15-2 is fastened to the wall by 4 cap screws equispaced on a 10-cm-dia bolt circle and arranged as shown. The bracket is subjected to a sinusoidal force-time function with $F_{max} = F$ and $F_{min} = 0$, where F and the beam's other data are given in the row(s) assigned from Table P15-1. Find the forces acting on each of the 4 cap screws due to this fluctuating loading and choose a suitable cap screw diameter, length, and preload that will give a minimum safety factor of 1.5 for any possible mode of failure for $N = 5E8$ cycles.[‡]
- [†]15-26 (See also Problem 6-42 on p. 414.) A cylindrical, steel tank with hemispherical ends is required to hold 425 kPa of pressurized air at room temperature. The pressure cycles from zero to maximum. The tank diameter is 0.5 m and its length is 1 m. The hemispherical ends are attached by some number of bolts through mating flanges on each part of the tank. A 0.5-mm-thick, compressed asbestos, unconfined gasket is used between

Table P15-1
Data for Problem 15-19

Row	Bolt Thd	Member Mat'l	l (mm)
a	m8 x 1	steel	30
b	m8 x 1	alum	40
c	m14 x 2	steel	38
d	m14 x 2	alum	45
e	m24 x 3	steel	75
f	m24 x 3	alum	90

* Answers to these problems are provided in Appendix D.

[†] Problem numbers in *italics* are design problems. Problem numbers in **boldface** are extended from similar problems in earlier chapters with the same dash number.

[‡] For these problems, assume that the nut and washer, together, have a thickness equal to the bolt diameter, and assume that bolts are available in length increments of either 0.25 in or 5 mm.

Table P15-2 Data for Problems 15-23 through 15-25

Use Only Data Relevant to the Particular Problem—Lengths in mm, Forces in N

Row	<i>l</i>	<i>a</i>	<i>t</i>	<i>h</i>	<i>F</i>	<i>OD</i>	<i>ID</i>	<i>E</i>
a	100	400	10	20	50	10	4	steel
b	70	200	6	80	85	12	6	steel
c	300	100	4	50	95	15	7	steel
d	800	500	6	65	250	25	15	alum
e	85	350	5	96	900	40	30	alum
f	50	180	4	45	950	30	25	alum
g	160	280	5	25	850	45	40	steel
h	200	100	2	10	800	40	35	steel
i	400	150	3	50	950	45	38	steel
j	200	100	3	10	600	30	20	alum
k	120	180	3	70	880	60	55	alum
l	150	250	8	90	750	45	30	alum
m	70	100	6	80	500	20	12	steel
n	85	150	7	60	820	25	15	steel

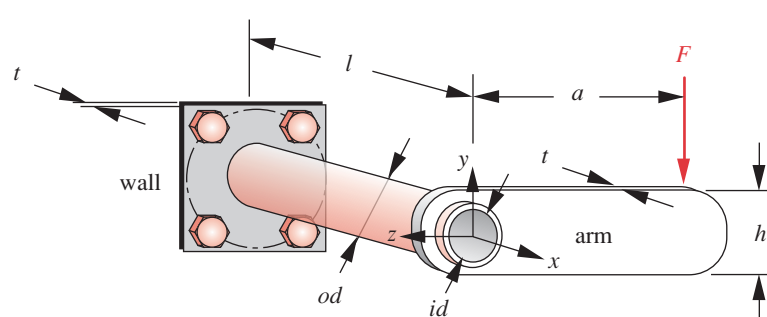
the 10-mm-thick steel flanges. Determine a suitable number, class, preload for, and size of bolts to fasten the ends to the tank. Specify the bolt circle and outside diameter of the flange needed to prevent leakage. A minimum safety factor of 2 is desired against leakage and a safety factor of 1.5 against bolt failure for infinite life.[‡]

- 15-27 Repeat Problem 15-26 using a confined O-ring gasket.[‡]
- 15-28 Calculate the proof load (load that causes a tensile stress equal to the proof strength) for 1/2-13 UNC bolts in each SAE grade listed in Table 15-6 (p. 882).
- 15-29 Calculate the proof load (load that causes a tensile stress equal to the proof strength) for M20 × 2.50 bolts in each class listed in Table 15-7 (p. 882).
- 15-30 Determine the joint stiffness constant for the bolt and members in Problem 15-7.[‡]
- 15-31 Determine the joint stiffness constant for the bolt and members in Problem 15-8.[‡]
- 15-32 Determine the joint stiffness constant for the bolt and members in Problem 15-9.[‡]
- 15-33 Determine the joint stiffness constant for the bolt and members in Problem 15-10.[‡]

* Answers to these problems are provided in Appendix D.

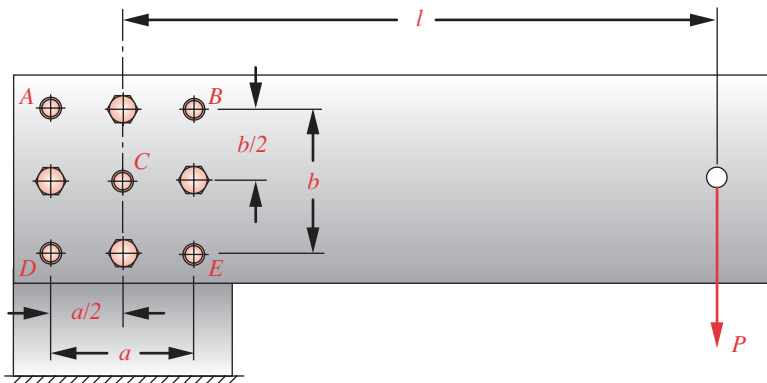
† Problem numbers in *italics* are design problems. Problem numbers in **boldface** are extended from similar problems in earlier chapters with the same dash number.

‡ For these problems, assume that the nut and washer, together, have a thickness equal to the bolt diameter, and assume that bolts are available in length increments of either 0.25 in or 5 mm.

**FIGURE P15-2**

Problems 15-23 through 15-25

- 15-34 Figure P15-3 (p. 925) shows a bolted and doweled joint eccentrically loaded in shear. The shear loads are taken by the dowel pins, the number and size of which are given in Table P15-3. Though the figure shows 5 dowel pins, that is not the case for every row in the table. For $a = 4$ in, $b = 4$ in, $l = 10$ in, $P = 2500$ lb, and the data in the row(s) assigned from Table P15-3 (p. 876), find the magnitude and direction of the total shear force acting on each dowel.
- 15-35 Figure P15-3 (p. 926) shows a bolted and doweled joint eccentrically loaded in shear. The shear loads are taken by the dowel pins, the number and size of which are given in Table P15-3. Though the figure shows 5 dowel pins, that is not the case for every row in the table. For $a = 4$ in, $b = 4$ in, $l = 10$ in, $P = 2500$ lb, and the data in the row(s) assigned from Table P15-3 (p. 926), find the total shear stress in each dowel.
- 15-36 Figure P15-3 (p. 926) shows a bolted and doweled joint eccentrically loaded in shear. The shear loads are taken by the alloy steel dowel pins, the number and size of which are given in Table P15-3. Though the figure shows 5 dowel pins, that is not the case for every row in the table. For $a = 4$ in, $b = 4$ in, $l = 10$ in, $P = 2500$ lb, and the data in the row(s) assigned from Table P15-3 (p. 926), find the factor of safety against yielding in shear for each dowel pin. See Table 15-12 (p. 911) for strength data.
- 15-37 The coefficient of friction for an oil-lubricated, single-start, power screw thread-nut combination is 0.10. Which of the American Standard Acme Threads in Table P15-3 (p. 926) will be self-locking for this thread-nut combination? Which will be the least likely to back down in the presence of dynamic loading? Which will be the most likely to back down in the presence of a dynamic load?
- 15-38 The coefficient of friction for an oil-lubricated, single-start, power screw thread-nut combination is 0.20. Which of the American Standard Acme Threads in Table P15-3 (p. 926) will have the greatest efficiency (neglecting thrust-collar friction)?
- *15-39 Determine the number of engaged screw threads required to make the total stripping-shear area of the engaged threads equal to twice the tensile stress area for each of the fine pitch screw threads in Table 15-2 (p. 865).
- 15-40 Calculate the ultimate tensile loads (load that causes a tensile stress equal to the tensile strength) for 1/2-13 UNC bolts in each SAE grade listed in Table 15-6, p. 882.
- *15-41 Calculate the ultimate tensile loads (load that causes a tensile stress equal to the tensile strength) for M20 x 2.50 bolts in each class listed in Table 15-7, p. 882.

**FIGURE P15-3**

Problems 15-34 through 15-36

15

* Answers to these problems are provided in Appendix D.

[†] Problem numbers in *italics* are design problems. Problem numbers in **boldface** are extended from similar problems in earlier chapters with the same dash number.

Table P15-3 Data for Problems 15-34 through 15-36

Dowels with Diameters of Zero Are Not Present

Row	Number of Dowels, n	d_A (in)	d_B (in)	d_C (in)	d_D (in)	d_E (in)
a	5	0.250	0.250	0.250	0.250	0.250
b	4	0.250	0.250	0	0.250	0.250
c	5	0.375	0.250	0.250	0.375	0.250
d	5	0.375	0.375	0.250	0.250	0.250
e	3	0.375	0.375	0	0.375	0
f	3	0.375	0	0	0.375	0.375

- 15-42 3/8-16 UNC bolts and nuts clamp 0.75-in-thick aluminum cover plate to a 0.50-in-thick steel flange. Determine the stiffness factor of the joint at each bolt.
- 15-43 M14 x 2.0 bolts and nuts clamp a 16-mm-thick aluminum cover plate to a 12-mm-thick steel flange. Determine the stiffness factor of the joint at each bolt.
- 15-44 M16 x 2.0 bolts and nuts clamp a 50-mm-thick aluminum cover plate to a 30-mm-thick steel flange. Determine the stiffness factor of the joint at each bolt.
- 15-45 5/16-18 UNC bolts and nuts clamp a 1.625-in-thick cast-iron cover plate to a 1.5-in-thick steel flange. Determine the stiffness factor of the joint at each bolt.
- 15-46 M16 x 1.5 bolts and nuts clamp an 8-mm-thick titanium cover plate to a 8-mm-thick stainless steel flange. Determine the stiffness factor of the joint at each bolt.
- 15-47 An M12 X 1.25 soft steel nut is assembled with a hardened steel bolt. The nut is 11 mm thick and has a shear yield-strength of 120 MPa. Determine the axial force that will cause stripping failure of the nut if the nut threads fail before the bolt fails.
- 15-48 Compare the yield loads (load that causes a tensile stress equal to the yield strength) to the proof loads (load that causes a tensile stress equal to the proof strength) for M12 x 1.25 bolts in each class listed in Table 14-7.
- 15-49 An M16 x 1.50, class 4.8 bolt with cut threads is preloaded to 85% of its proof strength when clamping a 20-mm-thick sandwich of solid steel. Find the safety factors against static yielding and joint separation when a static 3-kN external load is applied.
- 15-50 A 15-mm-thick steel cap is to be fastened to a 15-mm-thick steel flange with 6 bolts and nuts. The external load on the cap is 30 kN. Size and specify the bolts for a safety factor of at least 1.5 and specify the torque required on each bolt to obtain the preload if the threads are lubricated.
- 15-51 Repeat Problem 14-50 with a total external load on the six bolts that varies from 0 to 30 kN per cycle. Design these bolts for infinite life with a factor of safety of at least 1.5. Specify their size, class, preload, and tightening torque.
- 15-52 A 20-mm-thick aluminum cap is to be fastened to a 20-mm-thick aluminum flange with 8 bolts and nuts. The external load on the cap varies from 0 to 40 kN per cycle. Size and specify the bolts for infinite life and a safety factor of at least 1.5 and specify the torque required on each bolt to obtain the preload if the threads are lubricated.

16



WELDMENTS

*To invent, you need a good imagination and
a pile of junk.*

THOMAS A. EDISON

16.0 INTRODUCTION

Weldments (welded assemblies) are used in many applications such as machine frames, machine parts, building structures, bridges, ships, vehicles, construction equipment, and many other systems. Our focus here will be on their use in machine design rather than as structural elements in buildings and bridges, though the principles of weldment design are similar across applications. We also do not address welded pressure vessels that see elevated temperatures and can have corrosion issues. ASME publishes detailed codes for these applications. A half-century ago, machine frames were commonly made as grey-iron castings, which have good damping. Now it is as common to see machines with welded steel frames. One reason for the change is the superior stiffness of steel over grey cast iron (30E6 psi versus 15E6 psi.). A steel frame can then be lighter than a cast-iron casting and have equivalent stiffness or be the same weight and much stiffer.

Unlike structural steel applications such as buildings, which have relatively loose tolerances on their dimensions, machine frames and parts usually have to be made to tight dimensional tolerances. But it is difficult to hold tight tolerances when welding an assembly. This requires (as it does for castings) that the weldment be machined as an assembly once it is welded into the desired configuration on any surfaces whose dimensions are critical. Noncritical surfaces can be left in the as-welded condition.

Most metals can be welded though some are easier to weld than others. Low carbon steel is one of the easiest to weld. High carbon and alloy steels are more difficult to weld and, if parts are hardened or cold-rolled before welding to improve strength, the high localized heat of welding will tend to anneal it locally, reducing its strength. For these reasons, it is generally recommended to limit steel weldments to low carbon and low-alloy steels. Aluminum can be welded but requires proper attention to choice of

Table 16-0 Variables Used in This Chapter

Symbol	Variable	ips units	SI units	See
A	amplitude ratio	none	none	Eq. 6.1d
A_{shear}	shear area of weld	in ²	mm ²	Eq. 16.4
A_w	shear area per unit length of weld	in	mm	Eq. 16.4
C_f	Coefficient for S_{fr} equation	none	none	Table 16-4
E_{xx}	min. ultimate tensile strength of electrode	kpsi	—	Table 16-4
f_b	bending load per unit length of weld	lb/in	N/mm	Eq. 16-4
f_n	normal load per unit length of weld	lb/in	N/mm	Eq. 16-4
f_s	shear load per unit length of weld	lb/in	N/mm	Eq. 16-4
f_t	torsional load per unit length of weld	lb/in	N/mm	Eq. 16-4
F_r	torsional load per unit length of weld	lb/in	N/mm	Eq. 16-4
J_w	polar 2nd moment per unit length of weld	in ³	mm ³	Eq. 16.4
N	number of cycles	none	none	Ex. 16-2
N_f	fatigue stress safety factor	none	none	Ex. 16-4
N_{fr}	fatigue stress-range safety factor	none	none	Eq. 16.3
N_{yield}	static yield-stress safety factor	none	none	Eq. 16.3
R	stress ratio	none	none	Eq. 6.1d
S_{er}	tensile stress-range endurance strength	psi	MPa	Table 16-4
S_{ers}	shear stress-range endurance strength	psi	MPa	Ex. 16-2
S_{fr}	tensile stress-range fatigue strength	psi	MPa	Eqs. 16.2
S_{frs}	shear stress-range fatigue strength	psi	MPa	Ex. 16-4
S_w	section modulus per unit length of weld	in ²	mm ²	Eq. 16.4
t	weld throat dimension	in	mm	Fig. 16-4
w	weld leg dimension	in	mm	Fig. 16-4
Z	section modulus	in ³	mm ³	Eq. 4.11d
$\Delta\sigma$	stress range	psi	MPa	Eq. 6.1a
σ_x	normal stress	psi	MPa	Eq. 4.7
$\sigma_{1,2,3}$	principal stresses	psi	MPa	Ex. 16-4
σ_a	alternating normal stress	psi	MPa	Eq. 6.1b
σ_m	mean normal stress	psi	MPa	Eq. 6.1c
σ'	von Mises effective stress	psi	MPa	Ex. 16-4
σ_{max}	maximum applied normal stress	psi	MPa	Eq. 6.1a
σ_{min}	minimum applied normal stress	psi	MPa	Eq. 6.1a
$\Delta\tau$	shear stress range	psi	MPa	Ex. 16-2
τ_{xy}	shear stress	psi	MPa	Eq. 4.9
τ_{allow}	allowable shear stress	psi	MPa	Ex. 16-1, -2

process and technique. Machine frames are usually made of steel for strength and stiffness. Their large mass is not of concern since they are static. Machine parts that move, such as links, may be better made from aluminum if they experience large accelerations. Many links will nevertheless need to be of steel for strength, stiffness, or wear issues.

Opening page photograph A man gas metal arc welding by William M. Plate Jr., USAF (photograph is in public domain).

The reader should consider this chapter to be but a brief introduction into what is actually a quite fascinating and complicated technology. This short treatment will not make you an expert weldment designer by any means. But it will get you started and point you to the extensive literature and code publications available on the topic.* Several organizations do research in welding and publish recommendations and requirements. Some of these are:

American Association of State Highway and Transportation Officials (AASHTO)—
<http://www.transportation.org/>

American Institute of Steel Construction (AISC)—<http://www.aisc.org/>

American Petroleum Institute (API)—<http://www.api.org/>

American Society of Mechanical Engineers (ASME)—<http://www.asme.org/>

American Welding Society (AWS)—<http://www.aws.org/>

James F. Lincoln Arc Welding Foundation—<http://www.jflf.org/>

Welding Research Council—<http://www.forengineers.org>

See the references at the end of this chapter for some of their relevant publications.

16.1 WELDING PROCESSES

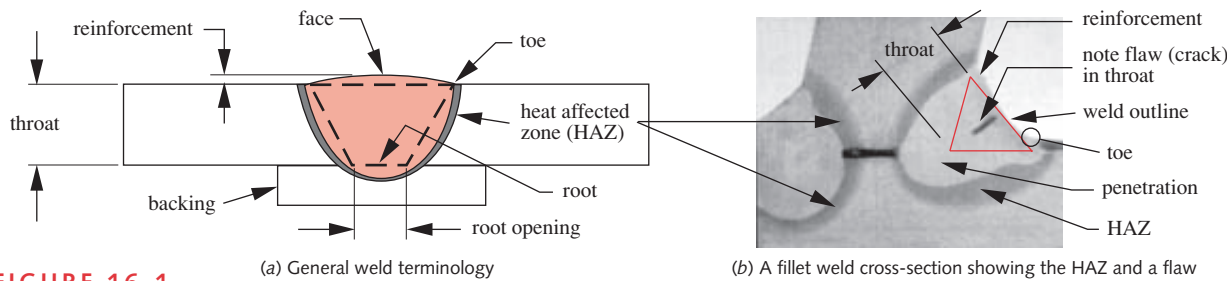
Arc welding of metals requires the localized application of sufficient heat to melt the base material while adding compatible filler material to join the two parts. A properly applied weld can be as strong as the material adjacent to it but if improperly done can leave the assembly severely weakened. The heat is typically supplied by bringing an electrode close to or in contact with the surface, causing an arc to jump between electrode and workpiece. The “arc-welding” machine supplies either DC or AC current at sufficient voltage to create the arc which has a temperature of 6000-8000 °F, well above the melting point of steel.[†] The weld filler metal is supplied either as the electrode itself or as a separate wire fed into the arc and are consumed in the process.

A good weld requires **fusion** of the metal on both sides of the joint with the added weld metal and fusion requires **atomic cleanliness**. The oxygen in air will contaminate the surface with metal oxide rapidly at these temperatures. The nitrogen in air also can compromise weld quality and trap bubbles in the molten metal as it cools causing porosity that weakens the weld. Moisture in the air or on the metal will cause hydrogen embrittlement and weaken the weld. To prevent contamination of the heated metal, either a flux material is supplied that covers the molten pool of metal with **slag** while it cools, or a stream of inert gas such as argon or helium is used to displace the air. If slag is present, it is chipped off when the weld cools. A good weld also requires that the molten mass **penetrate** into the parent metal, making the final **weld metal** a combination of the filler material and the parent material. There will also be a **heat affected zone** or **HAZ** formed at the edges of the weld as shown in Figure 16-1. This HAZ can be weaker than the parent material in higher strength steel (above 50 kpsi tensile strength), or stronger and harder than the parent in low-strength steel, which promotes crack formation. Aluminum strength is reduced up to 50% in the HAZ.

Figure 16-1 shows typical weld terminology. The toes are at the interface between the weld and the base material on the weld face. The root is at the base of the weld.

* The Lincoln Electric Company (www.lincolnelectric.com) offers a short course called “Blodgett’s Welding Design,” which is an excellent introduction to welding processes and weldment design for any engineer.

[†] Oxyacetylene gas welding is not generally used where high-strength welds are required. It is slow and the gas flame causes too much oxidation that contaminates and weakens the weld. It is sometimes used for field repairs but not generally for new work.

**FIGURE 16-1**

Weld cross section and terminology – Courtesy of Lincoln Electric Company, Cleveland, OH

Preparation of the parts for welding may involve contouring the edges and leaving a root opening to allow the heat and weld metal to penetrate fully. A root opening may require a backing strip be used to keep the molten puddle in place until it solidifies. The backing can be the same or different material. If the same, it will become welded to the joint. It can be left in place or removed by grinding. The latter is usually recommended if the joint is dynamically loaded as the backing creates stress concentrations. The reinforcement is the amount of weld material that protrudes above the surface of the base metal. This can be left in place for statically loaded joints but should be ground flush to remove the stress concentration at the toes if dynamically loaded. The material in the reinforcement is not considered to contribute to the strength of the weld regardless of loading. The throat dimension, which is used to determine the stress area excludes any weld material outside the part thickness or weld outline.

Types of Welding in Common Use

Shielded Metal Arc Welding (SMAW), also called “stick welding,” uses discrete lengths of electrode (sticks) that are coated with flux on the outside. As the arc melts the electrode, liquefied flux flows onto the pool to cover and protect it from air contact. This method is commonly used outdoors or for field repairs as it has no gas stream that could be blown away by wind.

Flux Cored Arc Welding (FCAW) uses hollow electrode wire with flux trapped in its hollow core. This allows it to be spooled in long lengths. The welding machine has a wire feeder that drives the wire through the welding head at a rate controlled by the welder, making it a continuous and more efficient process. FCAW wire electrodes are available for use either with or without an inert gas stream. The gas stream makes it easier to use indoors, but with the right electrode it can also be used without gas.

Gas Metal Arc Welding (GMAW), also called **MIG (Metal Inert Gas)** welding, uses a wire electrode with no flux. An inert gas is directed onto the weld to displace the air. This makes cleaner welds because of the absence of slag and its necessary cleanup but cannot be used outside if the wind blows over 5 m.p.h..

Gas Tungsten Arc Welding (GTAW), also called **TIG (Tungsten Inert Gas)** or **Heliarc** welding, uses a nonconsumable tungsten wire electrode. A separate metal filler rod or wire is fed into the molten pool. An inert gas such as argon is directed onto the weld to protect it. The original gas used was helium, which gave it the Heliarc name.

This method is often used on aluminum, titanium, and magnesium, and for fine repairs. It gives a clean weld but has the same wind limitation outside as does GMAW.

Submerged Arc Welding (SAW) uses powdered flux that is applied in such quantity as to bury or “submerge” the entire weld in a blanket so thick that the arc cannot be seen. The operator needs only untinted eye protection. The flux is delivered to the arc as a powder flowing through a tube adjacent to or concentric with the electrode. After the weld cools, the unmelted powder is brushed or vacuumed away and can be reused. The melted slag is chipped away to expose the weld. This process is limited to welds done on a top surface and is best suited to production welds in a shop where the motion and path of the electrode can be controlled automatically by a robot or semi-automatically by guides. It gives a good appearing weld that is free of spatter.

Resistance welds are created in thin sheet metal by a similar electrical process. Electrodes pinch the metal sandwich and a high current is passed through, fusing the two materials together in a “spot.” If the electrodes are moved along the parts with the current on, it will create a “seam” weld. A laser can be used to create the needed heat instead of electrodes. No filler material is added in these welds. They are commonly used to weld automotive bodies together as well as sheet metal enclosures and other thin-walled structures but are not used for thicker sections.

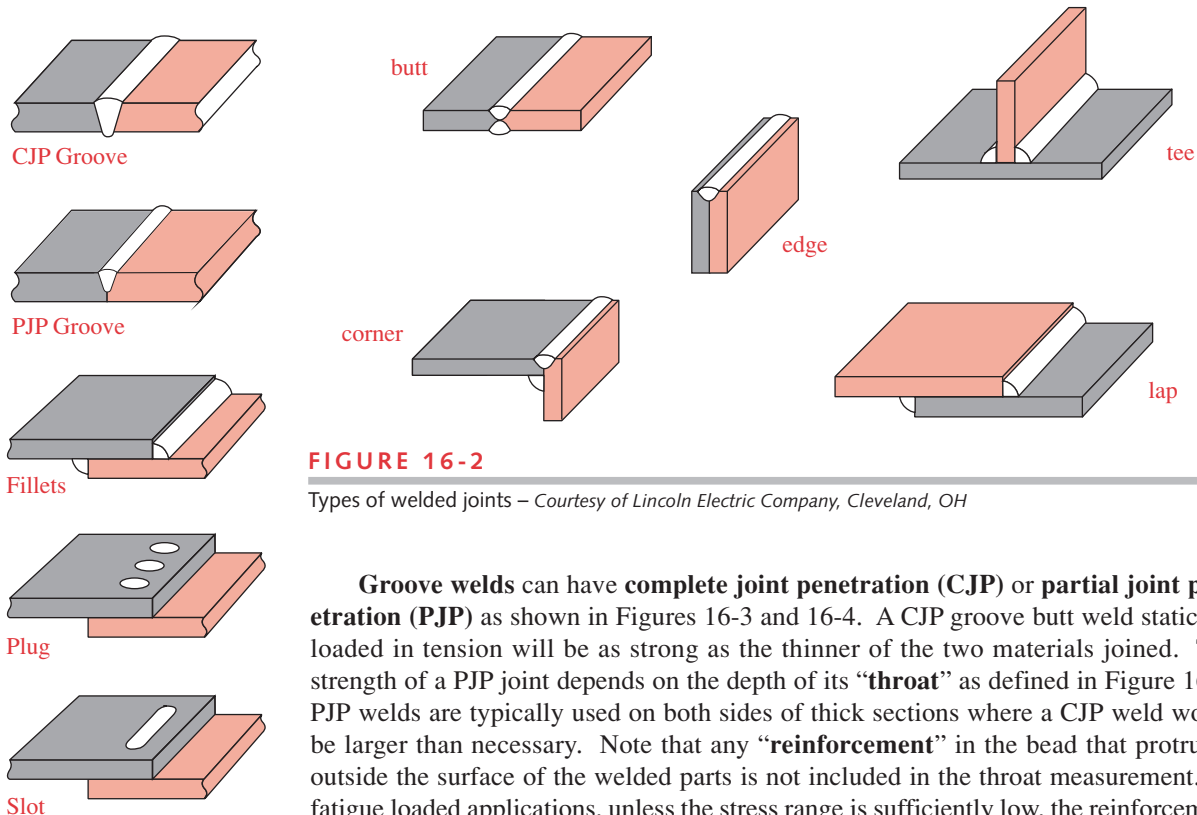
Why Should a Designer Be Concerned with the Welding Process?

It is useful for the design engineer to have a basic understanding of these welding processes and their limitations, just as one needs to understand how a part can (and cannot) be machined on a lathe or milling machine. But most design engineers are not also machinists nor are they often certified welders. So just as engineers don’t try to tell an expert machinist how to make the part, they should leave the detailed decisions on welding process to the expert welder. But they nevertheless must be familiar with its limitations. The design engineer’s task is to design the weldment according to good and accepted engineering practice, size the welds based on the techniques to be explained here (and in the references of this chapter) so that they are safe against failure in expected use, choose the needed strength of weld material, and specify this information on the drawing.

16.2 WELD JOINTS AND WELD TYPES

There are five types of weld joints as shown in Figure 16-2, butt, tee, corner, lap, and edge. The choice of joint type will to some degree be dictated by the desired geometry of the weldment and a given weldment may have several types within it.

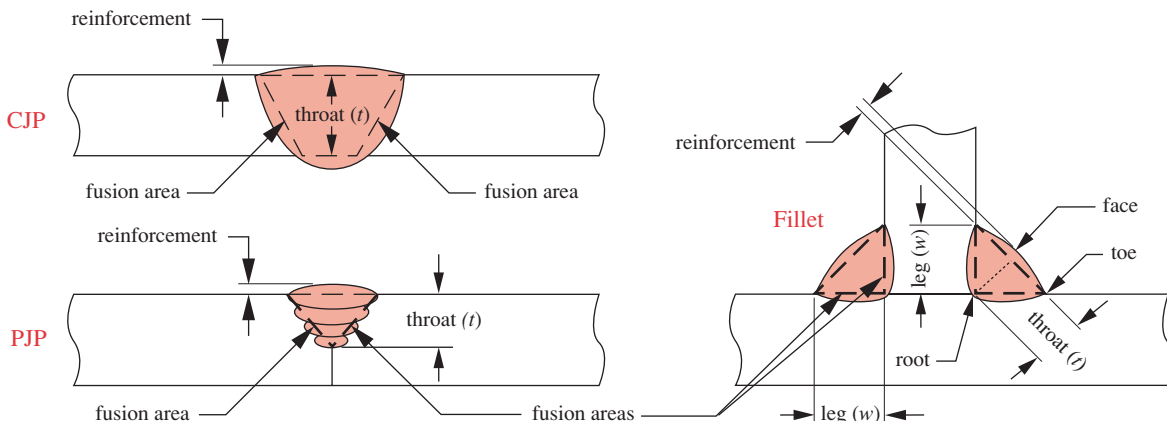
There are three general types of welds that can be used with one or more of the five joint types: groove welds, fillet welds, and plug/slot welds as shown in Figure 16-3. Groove welds break into two subcategories, having either complete or partial penetration. It is generally recommended that plug and slot welds be avoided as they tend to be weaker than the others. We will focus here on the two subtypes of groove welds and fillet welds. Groove welds are suitable for butt joints, outside corner joints, and edge joints in materials with sufficient thickness. Fillet welds are suitable for tee joints, lap joints, and inside corner joints.

**FIGURE 16-3**

Types of welds

Groove welds can have **complete joint penetration (CJP)** or **partial joint penetration (PJP)** as shown in Figures 16-3 and 16-4. A CJP groove butt weld statically loaded in tension will be as strong as the thinner of the two materials joined. The strength of a PJP joint depends on the depth of its “**throat**” as defined in Figure 16-4. PJP welds are typically used on both sides of thick sections where a CJP weld would be larger than necessary. Note that any “**reinforcement**” in the bead that protrudes outside the surface of the welded parts is not included in the throat measurement. In fatigue loaded applications, unless the stress range is sufficiently low, the reinforcement may need to be ground flush with the material to eliminate stress concentrations in the rippled surface of the weld and at the toes. The total weld throat area is the throat dimension times the length of weld. The fusion area is the area of the junction between the weld and the base material as shown in Figure 16-4.

Fillet welds are defined by their leg dimension w , but the weld strength is limited by the throat dimension t as shown in Figure 16-4. Fillet welds are typically at 45° be-

**FIGURE 16-4**

Throat dimensions of welded joints – Courtesy of Lincoln Electric Company, Cleveland, OH

tween two orthogonal parts but can join parts at any angle. If the pieces joined are orthogonal and the fillet at 45° , then the throat width t is 0.707 times the leg width w . Any reinforcement is ignored. The total **weld area** is the *throat width t times the length of weld* but the **fusion area** that determines whether the weld tears away from the base metal is the *leg width w times the length of weld* on each leg for a fillet weld. The stress on each leg's fusion area may be the same or different depending on part loading.

Joint Preparation

Better welds will result if the joint is properly prepared to allow the heat and weld metal to reach and fuse to all portions of the joint area. Unless the sections are thin, the weld joint should be prepared by removing metal from one or both sides of the joint. Several joint shapes are recommended, U, J, and V, as shown in Figure 16-5. The J or U joint detail leaves a small amount of base material in the bottom of the slot to prevent the molten weld metal from running out but is thin enough to allow good penetration. A V groove is easier to machine but may need to have a gap at the bottom to get good penetration. This gap can be closed with a backing strip of metal or ceramic to contain the weld metal until it cools. If the backing strip is the same material as the parts joined, it too will become welded to the joint. It can be removed, but if left in place it should be continuous over the entire length of the joint. If any splices are allowed in the backing strip and if they are not fully welded, high stress concentrations will be created that could cause failure. In like fashion, one can choose to weld a long seam only intermittently rather than put down a continuous bead over its length. But, it is often better to use a continuous weld because every interruption of the bead causes a stress concentration, undesirable especially with dynamic loading as is common in machine parts. Moreover, for the same strength a bead that runs only half the length of a joint must have twice the throat dimension, which quadruples its cross-sectional area. A longer, smaller cross-section bead will use less weld material and be more economical.

The designer needs to select and specify the size of the groove to be machined into the parts before welding. Recommended sizes based on part thickness can be found in welding handbooks and specifications such as references [1 – 4]. It is highly recommended that these handbooks and codes be used when designing weldments. If one is designing buildings or bridges, then the AISC and AWS codes must be adhered to. They contain very specific rules and procedures that must be followed when designing structures whose failure can put people's lives in danger. The machine designer is usually not required to follow these codes but would be wise to do so anyway to be sure of good results.

Weld Specification

Welds and their joint preparation are specified on a drawing using a standard form of welding symbol as shown in Figure 16-6a. At a minimum, it has a reference line and an arrow. There can also be an optional tail at the end opposite the arrow. The arrow points to the joint and the weld symbol defines the type of weld (fillet, CJP, PJP, etc.). Weld symbols above the reference line refer to the side opposite the arrow and those below the line refer to the arrow side. The arrow may point either up or down. The symbols are always read right to left regardless of which end the arrow is on. Figure 16-6b shows some of the possible weld symbols. Refer to AWS A2.4^[3] for details.

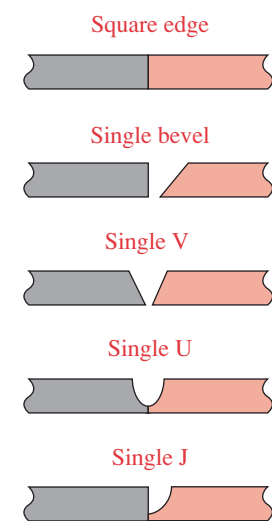


FIGURE 16-5

Joint preparation – Courtesy of Lincoln Electric Company, Cleveland, OH

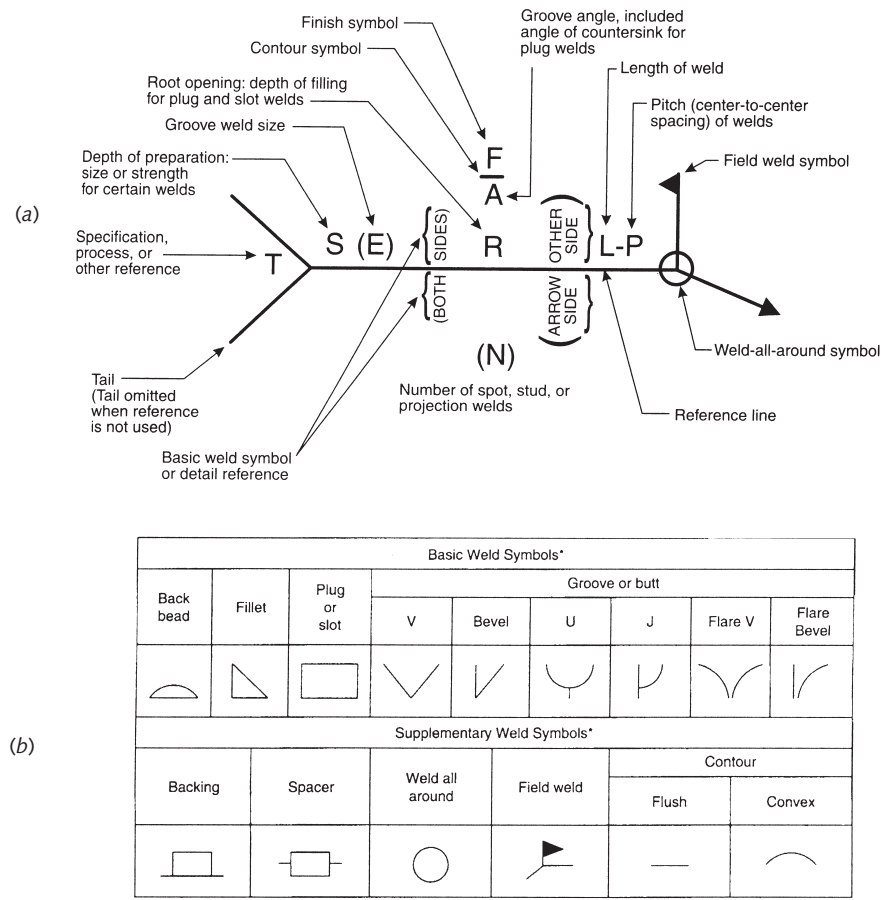


FIGURE 16-6
AWS Welding symbols^[3]

16.3 PRINCIPLES OF WELDMENT DESIGN

It is just as important to pay attention to the geometry of the weldment as it is to consider the sizes of the welds if one wants the design to succeed. It is also very important to arrange the welds so that a sensible and safe load path exists to take the applied loads to their reaction points. The “force-flow” concept introduced in Chapter 4 applies here. The following rules have been developed by welding design experts over many years and more detail on them can be found in reference [1].

- 1 Provide a path for applied forces to enter into the section(s) of the weldment that lie parallel to the direction of the applied force.
- 2 Forces will follow the stiffest path to ground so it is better to have relatively uniform stiffness to distribute reaction loads evenly in the weldment.
- 3 There are no secondary members in weldments. It is essentially one piece. But the welds can be either primary or secondary. A **primary** weld carries the entire load

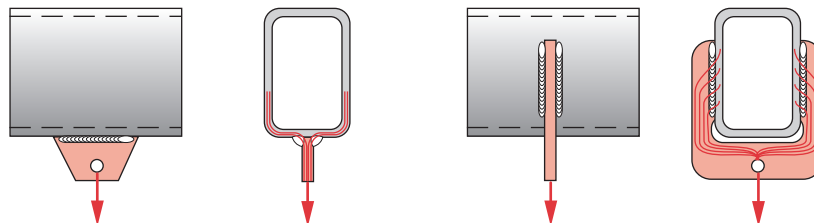
directly and its failure causes the weldment to fail. **Secondary** welds just hold the parts together and have low forces on them.

- 4 Do not put welds in bending if possible. If bending moments exist, try to place welds near locations of zero or low moment, or arrange the welds to handle shear or axial tension/compression.
- 5 Where possible, do not apply tensile loads across a transverse thickness of the parent material (i.e., “across the grain”). Wrought metals do have a grain in the direction of rolling and are slightly weaker across the grain than with the grain. (See Section 14.3, p. 790 for a discussion of grain in metals.) Welds loaded in tension on a transverse cross section (see Figure 16-10) may cause “lamellar tearing” of the material under the weld. Shear loads applied to such a surface through a weld are preferable.
- 6 Where section size changes across a joint, taper the material around the joint to improve force flow and reduce stress concentration.

Figure 16-7 shows alternate designs for a hangar welded to a beam. Part *a* shows an inferior arrangement in which the hangar is turned 90° and so loads the flange of the beam. Since the stiffest path will carry the bulk of the load, the small length of weld that spans the central web will handle most of the force. If the entire length of the weld is sized to have acceptable stress levels, it may fail because the nonuniform stress distribution across the flange overloads the center section of the weld. The flange compliance near its ends reduces its ability to transfer load to the central web. Note the force flow arrows for each design. Part *b* shows an acceptable arrangement wherein the load from the hangar is transferred directly into the web of the I-beam through the weld.

Figure 16-8 shows a similar assembly that uses a rectangular section beam. In part *a*, the solution that worked in Figure 16-7 is now inferior because the load applied to the center of the bottom surface of the section must travel across it to reach the side webs that carry the forces into the beam. This weld experiences bending. A better arrangement is shown in part *b* where the hangar is redesigned to weld directly to the side webs, put the welds in shear, and carry the forces into the sections that lie parallel to the load through the hangar, which is stiffer in bending than the section’s web. Note the force flow arrows for each design.

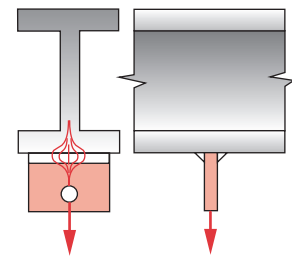
Figure 16-9 shows parts of differing width or thickness welded together. The AWS welding code D1.1 calls for a taper of at least 2.5:1 ($\leq 22^\circ$) be provided at all such junctions across nonuniform-size butt joints when cyclically loaded.



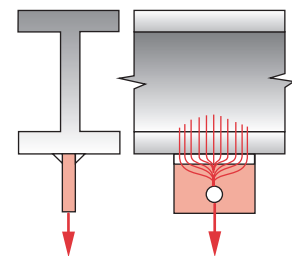
(a) Poor design - load taken through bottom into side webs (b) Good design - load taken directly into side webs

FIGURE 16-8

Examples of good and poor welded joints – Courtesy of Lincoln Electric Company, Cleveland, OH



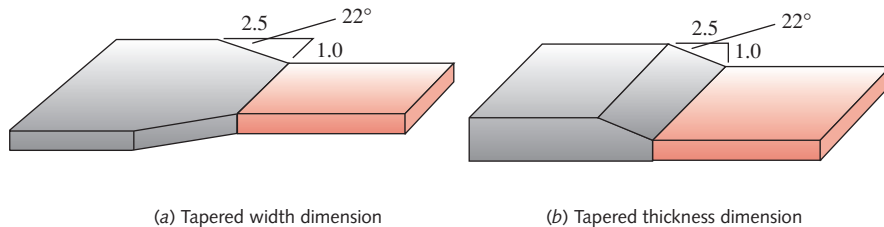
(a) Poor design - load taken through flange into web and the center of weld takes the brunt of load



(b) Good design - load taken directly into web and whole weld shares the load

FIGURE 16-7

Examples of good and poor welded joints – Courtesy of Lincoln Electric Company, Cleveland, OH

**FIGURE 16-9**

Mismatched joints must be tapered – Courtesy of Lincoln Electric Company, Cleveland, OH

16.4 STATIC LOADING OF WELDS

Compared to the calculation of stresses in general machine parts of complex geometry, calculation of weld stresses is fairly straightforward. If we can avoid loading welds in bending, the loading will typically be direct tension/compression or direct shear. In either case the equation for stress is simple. For axial tension or compression the normal stress was defined in equation 4.7 (p. 152) as:

$$\sigma_x = \frac{P}{A} \quad (4.7)$$

Direct shear, which is common in welds, is defined in equation 4.9 (p. 153) as:

$$\tau_{xy} = \frac{P}{A_{shear}} \quad (4.9)$$

In both cases P is the applied load and A or A_{shear} is the area of the weld. For a butt joint with a CJP weld in tension or compression, the weld throat area is equal to the cross section of the smaller part joined. For a PJP weld in tension or compression or a fillet weld in tension, compression, or shear, the area is simply the throat dimension t times the length of the weld. Figure 16-4 defines throat size for a variety of welds. Note that whether a fillet-welded tee joint is loaded in tension or shear, the weld will experience shear stress and may also have tensile stress. The fusion areas between weld and base metal may have one or both types of stresses applied depending on loading.

16.5 STATIC STRENGTH OF WELDS

In Chapter 5 we discussed static failure theories in depth and concluded that static failures were due to shear stress and that the distortion energy theory best defines a safe stress level for a ductile material using any desired safety factor. The metals used in welding and the weld filler materials are ductile, so this theory should apply, and it does. However, extensive testing done on welded assemblies over the last half-century by the welding industry has developed good data on allowable strengths of welds and weldments. An electrode's part number appears as E followed by 4 or 5 digits, the first 2 or 3 of which define its minimum ultimate tensile strength in kpsi and the rest indicate the position in which it can be used and its coating. We note its strength generally as Exx . For example, an E70 electrode has a minimum $S_{ut} = 70$ kpsi and E110 has a minimum $S_{ut} = 110$ kpsi.* Note that a given sample may actually exceed the stated value.

* The yield strength of steel electrode material is usually taken as 75% of S_{ut} .

It is recommended that the strength of the selected electrode be approximately matched to that of the base metal to be welded, and this is a requirement with CJP welds loaded in tension. It can be **undermatched** (*weld metal weaker than base metal*) in some cases, particularly if higher strength steels are welded or better crack resistance is needed. **Undermatching** is often done with fillet welds. **Overmatching** (*weld metal stronger than base metal*) is generally not recommended.

Residual Stresses in Welds

Welds will always have large residual tensile stresses in them. This is because weld metal expands to about six times its elongation at yield when melted. When it cools, it shrinks by that same factor. No solid metal has 600% elongation to yield, so this means that the weld material is guaranteed to yield in tension as it shrinks, since the solid base metal adjacent to the weld cannot move with it. There will be a balancing compressive stress formed in the adjacent base metal and the residual stress distribution will look like Figure 16-10 when cooled. Using an undermatched (i.e., weaker) weld metal will reduce the residual stress due to its lower yield strength. It is not recommended that a significantly overmatched weld metal be used in any case as this could result in a non-conservative design.

Direction of Loading

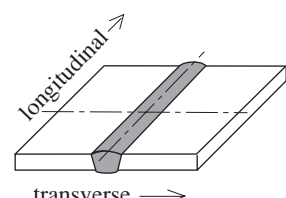
The direction of applied load versus the weld axis has a significant effect on fillet weld strength. Tests show that fillet welds loaded orthogonal (transverse) to the long axis of the weld, have 50% greater strength than the same weld loaded along (longitudinal to) the weld axis (see Figure 16-10a). This is due in part to the effective throat of a transversely loaded fillet weld between two orthogonal parts being at 67.5° versus 45° when loaded longitudinally. The 67.5° plane has 30% more shear area. Nevertheless, the AWS D1.1 code specifies that the effective throat area, defined by the shortest distance from root to weld face, be used for any direction of applied load.^[9] However, longitudinal welds have the advantage of allowing more deformation before yield than transverse welds do.^[9] Nevertheless, welds are designed against failure by rupture rather than yield because, even though ductile, the weld volume is so small compared to the entire part, the magnitude of weld deformation between yield and fracture is too small to provide any warning of incipient failure.

Allowable Shear Stress for Statically Loaded Fillet and PJP Welds

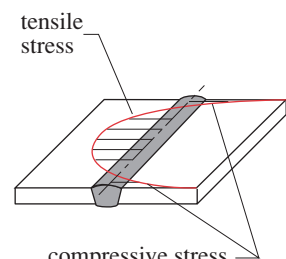
For static loading, the AWS^[3] recommends that shear stresses in fillet or PJP welds be limited to 30% of the electrode tensile strength, E_{xx} .

$$\tau_{allow} = 0.30E_{xx} \quad (16.1)$$

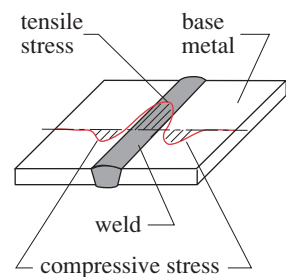
This value has a built-in **minimum** safety factor against **fracture** ranging from 2.21 to 4.06 for various weld loadings using electrode strengths from E60xx to E110xx in extensive testing.* Table 16-1 shows more detail on these safety factors. These safety factors and equation 16.1 are based on extensive testing done on welded assemblies by AISC^[6] and assume that the weld material strength approximately matches that of the base metal in each case.[†] Equation 16.1 is included in the AWS D1.1 Structural Welding Code.^[3] The nominal safety factor for equation 16.1 is usually stated as 2.5, which is within the range of longitudinal weld safety factor values in Table 16-1.



(a) CJP butt-welded plates



(b) Transverse residual stress



(c) Longitudinal residual stress

FIGURE 16-10

Residual Stresses in Welds

* Note that E60XX electrodes are now considered essentially obsolete and the lowest strength electrode now in common use is E70XX.

† Equation 16.1 has been verified by extensive FEA modeling that shows good correlation with this estimate.^[8]

Table 16-1 Safety Factors Against Static Failure When Using Equation 16.1^[6]

As reported by Testing Engineers, Inc., 1968

Base Metal	Electrode Class	Factor of Safety Using Stress on Throat Area Equal to 0.3 Tensile Strength of Electrode			
		Longitudinal Welds		Transverse Welds	
		Average	Minimum	Average	Minimum
A36	E60xx	2.88	2.67	—	—
A441	E70xx	2.95	2.67	4.62	4.06
A514	E110xx	2.41	2.21	3.48	3.30

Table 16-2

Minimum Fillet Weld Sizes*

Base Metal Thickness (T)	Minimum Weld Size
<u>sizes in inches</u>	
T ≤ 1/4	1/8
1/4 < T ≤ 1/2	3/16
1/2 < T ≤ 3/4	1/4
3/4 < T	5/16
<u>sizes in mm</u>	
T ≤ 6	3
6 < T ≤ 12	5
12 < T ≤ 20	6
20 < T	8

* Source: AWS D1.1 Table 5.8

Equation 16.1 is a bit unusual in that it compares applied shear stress to tensile ultimate strength as a reference value. It also appears to give a safety factor of 3.33 (the reciprocal of 0.30) rather than the stated 2.5. This anomaly is explained by the mixing of shear stress and tensile strength in the equation. Equation 2.5b (p. 37) gives an approximate ratio between ultimate shear strength and ultimate tensile strength of ductile metals of 0.75 to 0.8. Multiplying 0.75 by 3.33 gives 2.5 as a factor against shear rupture. But, it is more convenient to use the stated minimum tensile strength of the electrode and adjust the factor in the equation from $1 / 2.5$ to $1 / 3.33 = 0.30$.

The AWS D1.1 Structural Welding Code defines minimum sizes for welds based on thickness of the material being welded. Some of these data are shown in Table 16-2. The minimum weld size is to ensure that sufficient heat is applied to achieve good fusion.

EXAMPLE 16-1

Design of a Statically-Loaded Fillet Weld

Problem

A tee section of 0.5-in-thick by 4-in wide ASTM 36 hot-rolled steel on both legs as shown in Figure 16-11 is to be fillet welded on both sides. Determine the required weld throat size t .

Given

The tee is statically loaded in tension on the center web with $P = 16\ 800$ lb applied at the 1-in-dia hole. Strengths of ASTM steels are shown in Table 16-3.

Assumptions

Use matching strength electrode material and run the welds the full width of the parts. The weld is directly loaded and will fail in shear along a 45° plane in its throat.

Solution

- Table 16-3 gives the tensile strength of this material as 58-80 kpsi. Select an electrode with approximately the same strength as the average of the material strength. Electrodes come in increments of 10 kpsi and the closest available is an E70 with 70 kpsi tensile strength. (E60xx electrodes are now considered obsolete.)
- Determine the allowable strength based on 30% of the Exx value for this electrode using equation 16.1.

Table 16-3

Minimum Strengths of Some ASTM Structural Steels

ASTM Number	S_y kpsi (MPa)	S_{ut} kpsi (MPa)
A36	36 (250)	58-80 (400-500)
A572 Gr42	42 (290)	60 (415)
A572 Gr50	50 (345)	65 (450)
A514	100 (690)	120 (828)

$$\tau_{allow} = 0.30Exx = 0.30(70) = 21 \text{ kpsi}$$

- 3 Determine the shear area in the throat needed to limit the stress to this value.

$$\begin{aligned}\tau_{xy} &= \tau_{allow} = 21 \text{ kpsi} = \frac{P}{A_{shear}} = \frac{16\ 800}{A_{shear}} \\ A_{shear} &= \frac{16\ 800}{21\ 000} = 0.8 \text{ in}^2\end{aligned}$$

- 4 Determine the throat dimension of two full length fillet welds (one on each side of the joint) that will give the required area.

$$\begin{aligned}A_{shear} &= 2Lt = 2(4)t = 0.8 \text{ in}^2 \\ t &= 0.1 \text{ in}\end{aligned}$$

- 5 Convert this throat dimension t to a leg width w assuming an equal-leg fillet in a 90° tee joint.

$$w = \frac{t}{\cos(45^\circ)} = \frac{0.1}{0.707} = 0.141 \text{ in}$$

- 6 Check this against the recommended minimum weld size for this thickness part. Table 16-2 indicates that a 0.5-in-thick part needs at least a 3/16-in weld leg width, so increase the weld's leg width to 0.187 in.
- 7 Now check whether the part will fail in the fused base metal. There are two areas of concern, the areas between the welds and the base, labeled areas 'A', which are in tension, and the areas between welds and web, labeled areas 'B', which are in shear. Since both are the same total area and the shear strength of the base metal is about half that of its tensile strength, we need only check the shear areas 'B' against failure. The material's minimum tensile yield strength from Table 16-3 is 36 kpsi.

$$\tau_{xy} = \frac{P}{A_{fusion}} = \frac{P}{2Lw} = \frac{16\ 800}{2(4)(0.187)} = 11\ 230 \text{ psi}$$

$$N_{yield} = \frac{S_y}{\tau_{xy}} = \frac{36\ 000(0.577)}{11\ 230} = \frac{20\ 772}{11\ 230} = 1.85$$

This is acceptable, especially since the yield strength is a guaranteed minimum value.

- 8 Check the part's strength against tensile failure across the section at the centerline of the 1-in-dia hole.

$$\sigma_x = \frac{P}{A} = \frac{16\ 800}{3(0.5)} = 11\ 200 \text{ psi}$$

$$N_{yield} = \frac{S_y}{\sigma_x} = \frac{36\ 000}{11\ 200} = 3.2$$

The part is safe against yielding in tension at the hole and against failure in the weld, which limits the design. To complete the design, it needs to be checked for tearout and bearing failure at the hole, and preloaded bolts need to be designed to clamp the base of the tee. These tasks are left to the reader.

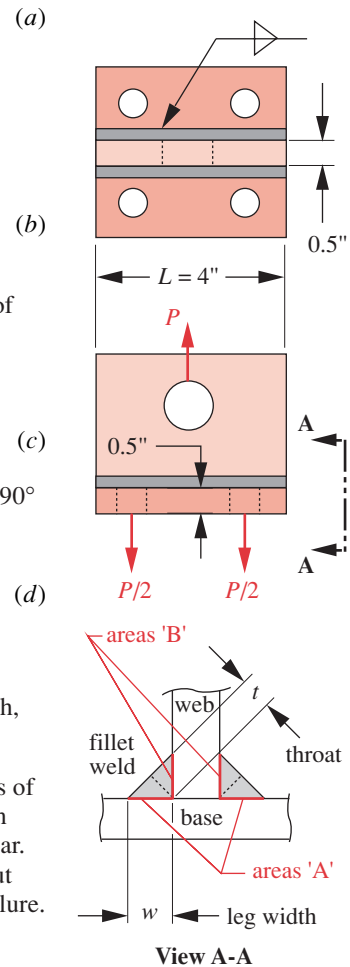


FIGURE 16-11

Examples 16-1 and 16-2

16.6 DYNAMIC LOADING OF WELDS

As described in Chapter 6, parts loaded dynamically fail at much lower stress levels than parts loaded statically. In that chapter we learned about fully reversed, repeated, and fluctuating stresses (see Figure 6-6) and also learned that the presence of a mean stress component in addition to an alternating stress component made the situation worse and required that a Goodman-, Gerber-, or Soderberg-line analysis be done. (Figures 6-42, 6-43, and 6-44.) The mean and alternating stress components σ_m and σ_a , the stress range $\Delta\sigma$, the stress ratio R , and the amplitude ratio A , were defined in equations 6.1a – 6.1d, repeated here for your convenience.

$$\Delta\sigma = \sigma_{max} - \sigma_{min} \quad (6.1a)$$

$$\sigma_a = \frac{\sigma_{max} - \sigma_{min}}{2} \quad (6.1b)$$

$$\sigma_m = \frac{\sigma_{max} + \sigma_{min}}{2} \quad (6.1c)$$

$$R = \frac{\sigma_{min}}{\sigma_{max}} \quad A = \frac{\sigma_a}{\sigma_m} \quad (6.1d)$$

Effect of Mean Stress on Weldment Fatigue Strength

Weldments loaded dynamically behave in a surprisingly different way than non-welded parts, which makes the mean stress irrelevant to their potential fatigue failure.* Figure 16-12 shows fatigue test data for both unwelded and welded test specimens. The unwelded specimens were rectangular cross-section, hot-rolled steel bars loaded in axial tension/compression. The welded specimens were pieces of the same bar cut, then joined with transverse CJP butt welds, making their overall geometry, material, and finish the same as the unwelded ones. Samples were tested with axial loading at stress ratios R of 1/4 (fluctuating), 0 (repeated), and -1 (fully reversed). The first two have nonzero mean stress and the last has zero mean stress. Note that nonzero mean stress reduces the strength of the unwelded parts as we saw in Figure 6-16. But, the data for the welded parts show no significant difference between the fully reversed data and the data with mean stress added. The stress range (equation 6.1a) is the single determining factor in failure of dynamically loaded weldments. This makes the calculation for dynamically loaded weldments simpler than for nonwelded machine parts. A Goodman-line analysis is not needed here. Instead, the **stress range** that a weldment sees in the cycle is compared to an acceptable stress-range fatigue strength S_{fr} obtained from test data.[†]

* The 2005 AISC specification^[2] states on p. 16.1-400:

Extensive test programs using full-size specimens, substantiated by theoretical stress calculations have confirmed the following general conclusions ... :

(1) Stress range and notch severity are the dominant stress variables for welded details and beams;

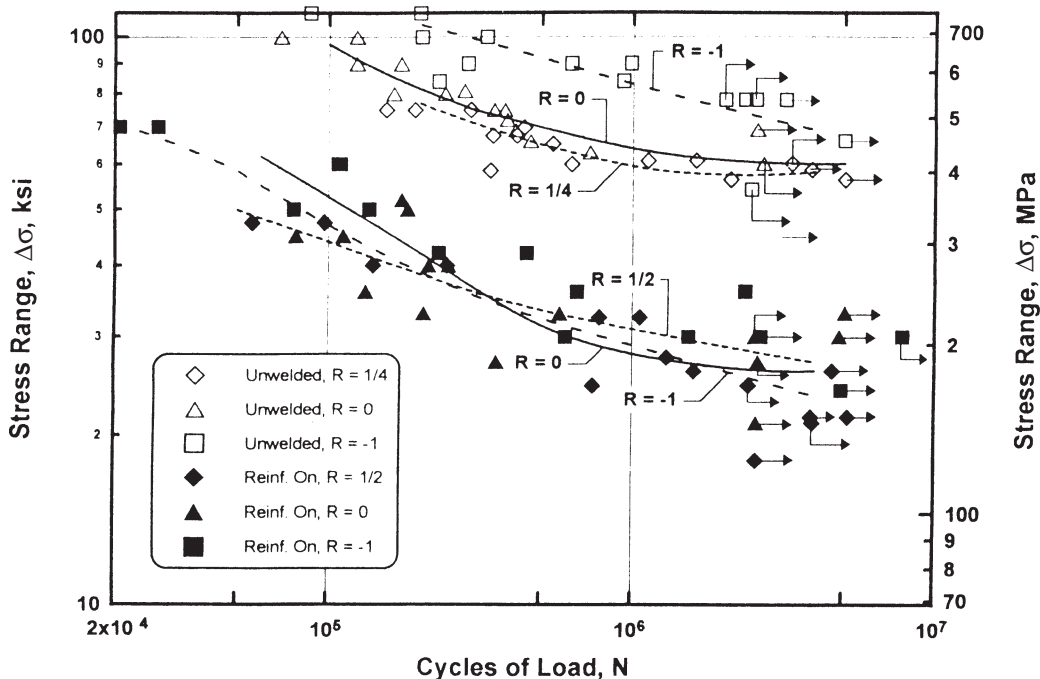
(2) Other variables such as minimum stress, mean stress, and maximum stresses are not significant for design purposes; and

(3) Structural steels with yield points of 36 to 100 ksi (250 to 690 MPa) do not exhibit significantly different fatigue strengths for given welded details fabricated in the same manner.

Are Correction Factors Needed For Weldment Fatigue Strength?

Recall from Chapter 6 that the fatigue strength S_f of a steel part is never more than 50% of its ultimate tensile stress S_{ut} and is usually much less due to a number of factors that involve its surface finish, size, type of loading, and other factors (equation 6.6, p. 330). The data that give the uncorrected endurance limit $S_{e'} = 0.5 S_{ut}$ come from testing small-diameter, rotating-beam specimens with polished surfaces and these are reported as average values. Thus the uncorrected value $S_{e'}$ must be reduced by the factors noted to account for differences in size, surface finish, etc. between the test specimen and your part and by a statistical reliability factor to obtain a corrected endurance strength S_e .

[†] Fatigue crack propagation and fatigue life of most weldments is proportional to the third power of the stress range^[10]

**FIGURE 16-12**

Fatigue-strength data for unwelded and welded parts at various stress ratios – Adapted from [4]

Fatigue and endurance strength data for weldments are not obtained from polished laboratory specimens but rather from actual welded assemblies in a variety of configurations. Also, these test specimens are large (think building- and bridge-sized parts) and are made from hot-rolled steel with rough surfaces, residual stresses from the rolling process, and real welds containing stress concentrations and tensile residual stress. So, we don't have to factor these fatigue test data down to match our parts on the basis of size, surface finish, etc., as our parts are similar to the test specimens in those respects.

Effect of Weldment Configuration on Fatigue Strength

The fatigue resistance of a weldment also will vary according to the presence or absence of interruptions in the geometry of the assembly and of weld beads, both of which create stress concentrations.* So, the test specimens were made with deliberate stress concentrations in the form of interrupted welds, added stiffeners, and all varieties of weld joints and welds listed above. AISc defined and tested many different welded configurations, and based on the fatigue strength of the base metal, grouped them into eight categories labeled A, B, B', C, D, E, E', and F in order of decreasing resistance to dynamic loading. Category A is most resistant and E' least resistant to fatigue. Note that F is the shear strength of the weld metal itself, and the others are for tensile strength of the fusion area between the weld and base material. Sketches of these configurations and their associated letter categories and fatigue strengths for various numbers of cycles for each letter category are all published in reference [2]. The chart is too large to reproduce here in its entirety, but a few selected examples are shown in Figure 16-13.

* According to Barsom and Rolfe^[10],

One of the most sensitive weld details is a fillet weld termination oriented perpendicular (transverse) to the applied cyclic stress field. In this case, fatigue cracking initiates from the toe of the fillet weld and propagates through the adjacent base metal. In fact, the majority of weld-related fatigue failures initiate at the surface, generally at the weld toe.

Note that several examples in this chapter have fillet welds loaded in this manner.

Figure 16-13a shows a category A part. Note that it has no welds. This is the strongest category and is in effect a reference against which the other categories can be compared. The relatively low fatigue strength of this specimen (24 kpsi) compared to a rotating beam specimen of the same material (about 30 kpsi) has to do with its much larger size, rough surface, residual stresses from the hot-rolling process, and flame cut edges. Figure 16-13b has uninterrupted welds running the full length or width of the part and is a category B. Figure 16-13c is similar to 16-13b but has attachments added. In the direction of stress, the attachments are short (just the thickness of the attached member), but some stress will flow from the main member into the attachment, creat-

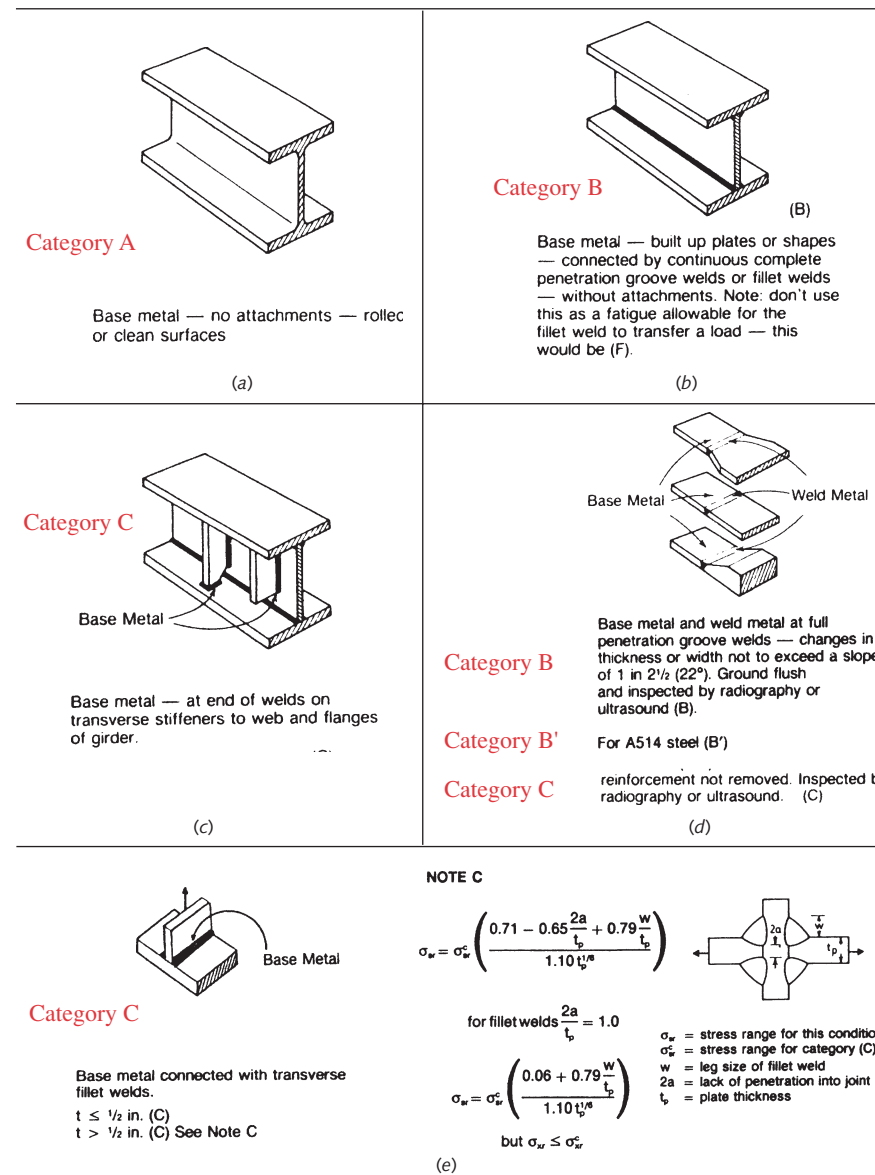


FIGURE 16-13

AISC Strength Categories for Welded Parts Subject to Fatigue Loading – Excerpted from [2]

ing a stress concentration and the stress category is therefore reduced to category **C**. Figure 16-13d can be any one of three categories depending on the base material and whether or not the weld reinforcement is ground flush. Figure 16-13e has very different geometry from 16-13c but is also a category **C** with a **Note C** attached that applies if the web size is larger than 0.5 in. **Note C** is also shown in Figure 16-13e. Note the level of detail in these test specimen types—there are many more in the AISC Specification.* The weld metal itself is nearly always category **F** except in the case of a transverse CJP weld, which can be a category **B** or **C** depending on reinforcement removal.

Extensive testing of weldments in each of these categories was done by the Highway Research Board in the 1960s.^[11] Testing of 374 beams of 10-foot span and depths of about 15 inches having various welded details were done at two separate university laboratories. The data from both labs had close statistical correlation. Figure 16-14a shows test data for category A beams and Figure 16-14b shows data for category E beams. The three sets of data in each plot are from loadings with different values of minimum stress but with the same stress range. All cluster together showing that the only stress parameter that had any effect was stress range. The maximum, mean and minimum stresses were not factors in the failures.

Regression lines are fitted to the data on log-log axes. The equations are shown on the plots. One has a slope of 3.372 and the other a slope of 2.877. The lines above and below the mean line represent ± 2 standard deviations, which includes 95% of the population. The lower band line is taken as the fatigue strength line. Exponential relationships for weldment fatigue strength as a function of number of cycles were developed from the data and are shown below. The average slope of all the data for categories A to E' was rounded to 1/3 for the design equation 16.2a below.

Figure 16-14c shows the *S-N* diagrams for each of the AISC weldment categories based on these test data. **These are different from the *S-N* diagrams in Chapter 6 in that the ordinate shows stress range $\Delta\sigma$ (labelled as *fatigue strength range* S_{fr}) rather than alternating stress σ_a (denoted as *fatigue strength* S_f) They also differ in that they do not show average fatigue strength values, but rather use values that are two standard deviations below the average.** While not truly minimum values, they are close to minimum because 95% of the population will be within plus or minus two standard deviations from the average, meaning only 2.5% lie below these values. **So it is not necessary to apply reliability factors to reduce them further unless one wants to have more than a 95% confidence level in the data,** then use Table 16-4.

All categories except **F** have the same slope of 1/3 and their intercepts decrease with each higher category letter. Category **F**, which is for the weld metal rather than the base metal near the weld, has a shallower slope of 1/6 and a low intercept. Note that the knees where infinite life begins also vary with the category from 2E6 to over 1E7 cycles. These curves are linear on a log-log plot up to the knee so exponential equations can be fitted to them. For all categories except **F** the allowable fatigue stress range S_{fr} is

$$S_{fr} = C_{reliab} \left(\frac{C_f}{N} \right)^{\frac{1}{3}} \geq S_{er} \quad (16.2a)$$

where N is the required number of stress cycles. C_f and S_{er} (*the stress range endurance strength*) are shown in Tables 16-5a and -b for U.S. and SI units, respectively. These values are for hot-rolled steels with tensile yield strengths from 36 to 110 kpsi.

Table 16-4

Reliability Factors Versus 95% for $S_d = 0.08 \mu$

Reliability %	C_{reliab}
50	1.152
90	1.033
95	1.000
99	0.938
99.9	0.868
99.99	0.809
99.999	0.759

Table 16-5a^[2]

U.S. Coefficient C_f and S_{er} for Equation 16.2

AISC Category	C_f ips	S_{er} kpsi
A	250 E08	24.0
B	120 E08	16.0
B'	61 E08	12.0
C	44 E08	10.0
D	22 E08	10.0
E	11 E08	4.5
E'	3.9 E08	2.6
F	150 E10	8.0

Table 16-5b^[2]

SI Coefficient C_f and S_{er} for Equation 16.2

AISC Category	C_f SI	S_{er} MPa
A	170 E10	165
B	83 E09	110
B'	42 E09	82
C	30 E09	69
D	15 E09	48
E	7.6 E09	31
E'	2.7 E09	18
F	10 E12	55

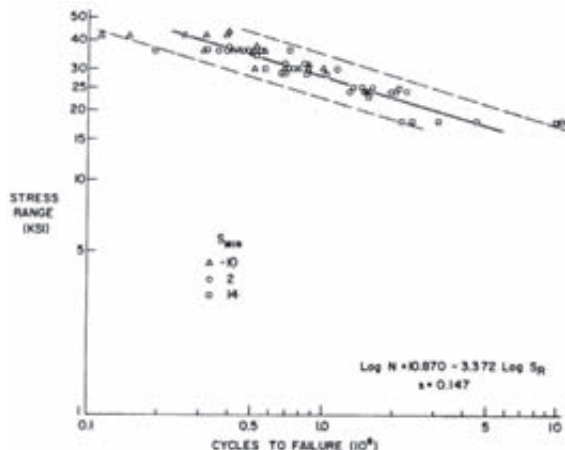
* The AISC Specification For Structural Steel Buildings is a free download from www.aisc.org.

For category F, which is for shear stress in the weld metal, it becomes:

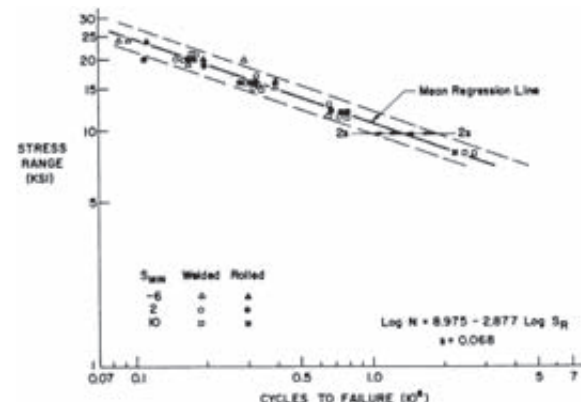
$$S_{frs} = C_{reliab} \left(\frac{C_f}{N} \right)^{\frac{1}{6}} \geq S_{ers} \quad (16.2b)$$

* The Welding Research Council^[12] recommends that the exponent in equation 16.2b be 1/5 rather than 1/6.

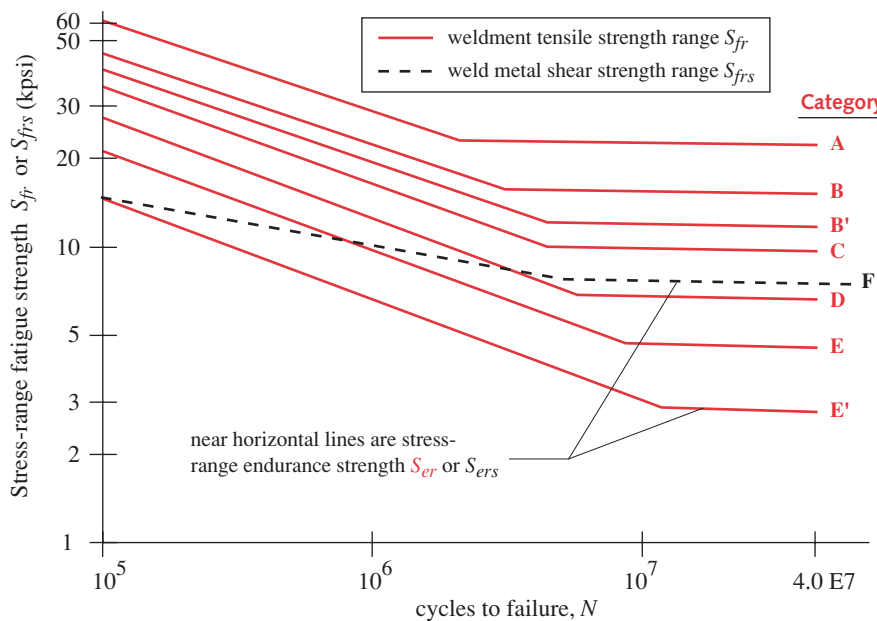
and C_F and S_{ers} for category F are also shown in Tables 16-5a and -b. C_{reliab} is given in Table 16-4.*



(a) Experimental data for Category A^[11]



(b) Experimental data for Category E^[11]



(c) Regression lines fitted to experimental fatigue strength data for all categories

FIGURE 16-14

Experimental Fatigue-Strength Data for Welded Parts^[11] in the AISC Categories^[2] and for Weld Metal^[3]

The values in Tables 16-5 can be reduced by a factor of three for use with aluminum. To use these strength data, calculate your applied stress range $\Delta\sigma$ or $\Delta\tau$ and determine the safety factor for the fusion area in tension or weld metal in shear, respectively, as:

$$N_{fr} = \frac{S_{fr}}{\Delta\sigma} \quad \text{or} \quad N_{frs} = \frac{S_{frs}}{\Delta\tau} \quad (16.3)$$

Is There an Endurance Limit for Weldments?

Until recently it was assumed that once the knee of a curve in Figure 16-14c was reached, the curve remained horizontal out to infinite cycles for steel and a few other materials such as titanium. This allowed one to use that value as an endurance limit for infinite life as was done in Chapter 6 for unwelded parts. More recent research^[12] indicates that the fatigue strength of weldments continues to decline beyond the knee.

Figure 16-15 shows sample stress-range fatigue curves for both steel and aluminum from reference 12. These data result from extensive testing done by the Welding Research Council (WRC) on weldment assemblies of various geometries. The WRC has defined categories similar to those of the AISC shown in Figure 16-13 except that WRC has many more categories that are denoted by numbers rather than letters. See reference 12 for their definitions. The numbers assigned to the symbols in Figure 16-15 refer to the strength of that number WRC welding category taken at 2 million cycles. The knee for steel and aluminum in tension is taken at $1E7$ cycles, but shear fatigue data (not shown) have the knee at $1E8$ cycles. These figures show the tensile-stress-range fatigue strength of steel and aluminum weldments declining with stress cycles beyond the curve's knee but with a much lower slope. The exponent of the curve's equation becomes $1/22$ beyond the knee.^[12] Figure 16-14 also reflects this fact by showing those lines with a small negative slope beyond the knee. We also avoid calling the value at the knee an endurance limit, instead referring to S_{ers} as an endurance strength.

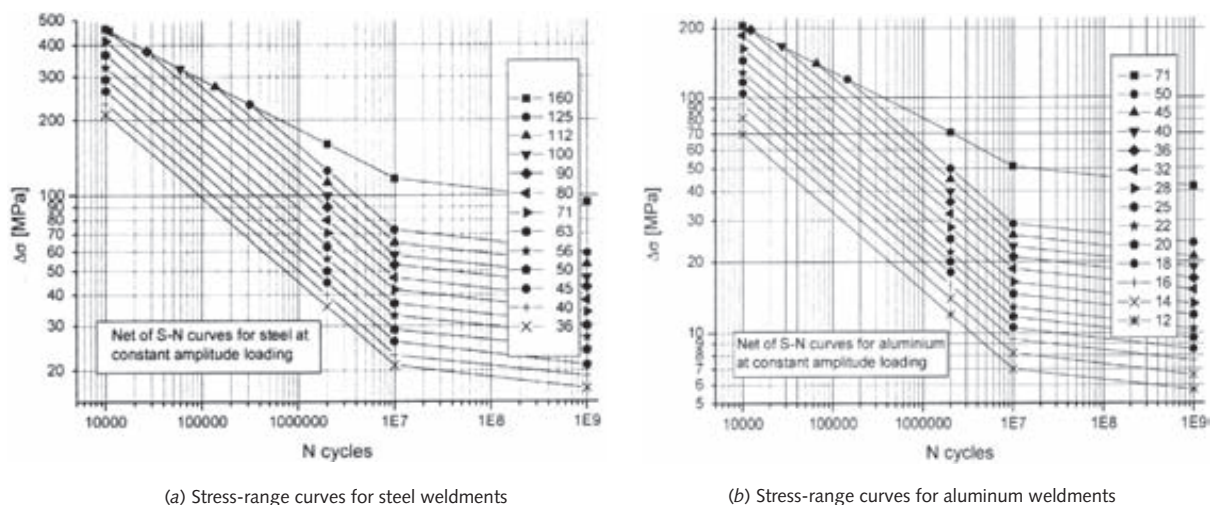


FIGURE 16-15

Experimental Tensile-Stress-Range Fatigue -Strength Data for Welded Parts in Various Welding Research Council Categories^[12]

Fatigue Failure in Compression Loading?

Another difference between unwelded and welded parts in fatigue has to do with the tensile residual stress in the welds. Recall from Chapter 6 that fatigue failures were stated to be due only to oscillating tensile stress. Compressive stress oscillations could be safely ignored. In fact, we saw in Chapter 15 how to use residual compressive stress in the clamp zone of preloaded bolts to partially “hide” the applied oscillating tensile stress from the tension-loaded bolt. We regard compressive stress as a friend in dynamically loaded, **unwelded** parts. When welds are introduced to a part this is no longer true. **Oscillating compressive stress can also cause fatigue cracks.** How can this be?

The answer is **residual tensile stress**. As described above and as depicted in Figure 16-10, *a weld will always have residual tensile stress at the material's yield point*. Consider two different loading cases on a given welded part whose yield strength is 50 kpsi. In the first case, an oscillating tensile stress that varies between zero and 10 kpsi is applied in the region of the weld. On the first cycle, the stress in the weld area will go above the yield strength. The material will yield locally relieving some of the residual stress, about 10 kpsi of it. When the load cycles back to zero it has only 40 kpsi of residual stress there. The next and all successive cycles will oscillate from 40 to 50 kpsi tensile stress at that point with a stress range of 10 kpsi.

Now get a fresh specimen with the same 50 kpsi residual stress in its weld and change the applied load to a compressive oscillation from zero to negative 10 kpsi. The local stress in the weld now goes from 50 to 40 kpsi tensile stress each cycle. Since the phase of the stress oscillation does not matter, this is the same tensile stress oscillation in both cases. Applied compression loading stresses that location with a varying tensile stress and so can develop cracks in the weld. These cracks only grow in the residual tensile stress zone and don't propagate into the base metal but they still weaken the weld and can cause failure there. Chapter 6 warned against allowing residual tensile stress in fatigue-loaded parts. Unfortunately, the nature of welds guarantees high tensile residual stress. This residual stress can be reduced by hammer-peening as discussed in Section 6.8, but shot peening is less effective on welds.

EXAMPLE 16-2

Design of a Dynamically-Loaded Fillet Weld

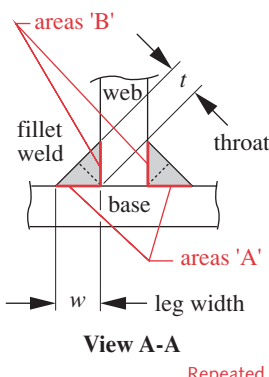


FIGURE 16-11

Examples 16-1 and 16-2

Problem

The welded tee section of Figure 16-11 is going to be loaded dynamically with repeated stress ranging from zero to a maximum. Determine the largest repeated tensile load that the welds can safely withstand for infinite life with a fatigue safety factor $N_{frs} = 1.5$.

Given

The tee is 0.5-in-thick by 4-in wide ASTM A36 hot-rolled steel on both legs, and has 3/16-in fillet welds full length on both sides. This matches the minimum weld size specified in Table 16-2.

Assumptions

Matching strength electrode material was used. Shear stress in the weld throat governs the design (see Example 16-1). The load is evenly distributed along the weld length.

- 1 A repeated stress will range from zero to a maximum value each cycle. Adapting equation 6.1a, the shear stress range $\Delta\tau$ is

$$\Delta\tau = \tau_{max} - \tau_{min} = \tau_{max} \quad (a)$$

- 2 The geometry of this weldment is similar to that of Figure 16-13e. Note C in Figure 16-13e indicates that this part is a category C based on its thickness. However, this design has the welds taking the load directly. In that case we must use the fatigue strength for category F, the weld metal itself, in the weld throat area. From Table 16-5, the tensile stress range endurance strength S_{ers} for category F and infinite life is 8000 psi.
- 3 Calculate an allowable shear stress range based on S_{ers} and the desired safety factor.

$$\tau_{allow} = \frac{S_{ers}}{N_{frs}} = \frac{8000}{1.5} = 5333 \text{ psi} \quad (b)$$

- 4 The part as designed has two 4-in-long 3/16-in-leg fillet welds. We need the throat area for this calculation which is 0.707 as wide as the leg. The load to create the allowable shear stress from equation 4.9 is then:

$$P_{max} = \tau_{allow} A_{shear} = 5333(2)(4)(0.187)(0.707) = 5641 \text{ lb} \quad (c)$$

- 5 Check that the fusion area of weld to base metal is safe. The most likely point of failure is at the weld toe. The weld leg area rather than throat area is used here.

$$\sigma_{toe} = \frac{P_{max}}{A_{fusion}} = \frac{5641}{2(4)(0.187)} = 3770 \text{ psi} \quad (d)$$

A category C weldment has $S_{er} = 10$ ksi from Table 16-5a, giving a safety factor of $10000/3770 = 2.65$. The weld throat limits the design, as is typical in fillet welds.

- 6 We still need to check that this repeated load will not fail the part statically or in fatigue at locations away from the welds. For example, a Goodman line analysis (Chapter 6) should be done for this repeated load applied to the smallest tensile area across the centerline of the 1-in-dia hole and for the tearout shear areas of the same hole. Any fasteners used to attach the base will need to be checked for fatigue under their applied preload (Chapter 15). These tasks are left to the reader.

16.7 TREATING A WELD AS A LINE

The designer is usually trying to determine the size of weld (cross-section and length) needed to withstand the applied loads. One approach is to assume a weld size, calculate the safety factor and if inadequate, change the weld size assumption, recalculate and iterate this process until satisfied with the result. A more direct and somewhat simpler approach as defined by Blodgett^[1] is to treat the weld as a line. Instead of stress, this calculation will give a load/length (lb/in or N/m) number which is easily converted to a required weld cross section area using the allowable stress for the weld from either equation 16.1 for static loads or equations 16.2 for dynamic loads. The weld area and the load are essentially normalized to one unit of weld throat length. Allowable unit load factors relating fillet weld leg width w to electrode strength for static loads are shown in Table 16-6. These are calculated as $0.707(0.30)Exx^{[5]}$ and so are for 90° corners.

Loading on a given weld location is typically one or a combination of direct tension or compression, direct shear, bending, and torsion. The stresses associated with

Table 16-6^[5]

Allowable Static Unit Force on Fillet Welds as a Function of Weld Leg Length w .

Electrode Number	Allowable Unit Force lb/in
E60	12 730 w
E70	14 850 w
E80	16 970 w
E90	19 090 w
E100	21 210 w
E110	23 330 w
E120	25 450 w

each of these loading conditions were defined in earlier chapters. The stress equations can be converted into $f_x = \text{load per length}$ of weld throat t as follows:

$$\begin{aligned} \text{direct tension or compression} \quad f_n &= \frac{P}{A_w} \\ \text{direct shear} \quad f_s &= \frac{V}{A_w} \\ \text{bending} \quad f_b &= \frac{M}{S_w} \\ \text{torsion} \quad f_t &= \frac{Tc}{J_w} \end{aligned} \quad (16.4)$$

The units of A_w are *area/length* = length. S_w is the **section modulus** $Z/\text{length} = \text{length}^2$ and J_w is the **polar area moment of inertia** $J/\text{length} = \text{length}^3$. This makes $f_x = \text{load per length}$ of weld throat in all cases.

Figure 16-16 shows nine configurations of weldments and equations for calculating the factors A_w , S_w , and J_w . Their application will be shown in an example.

EXAMPLE 16-3

Design of a Statically Loaded Weldment Assembly

Problem The weldment assembly in Figure 16-17 has fillet welds all around between the pipe and each end plate. Determine the weld size needed to withstand a static load $P = 2700$ lb.

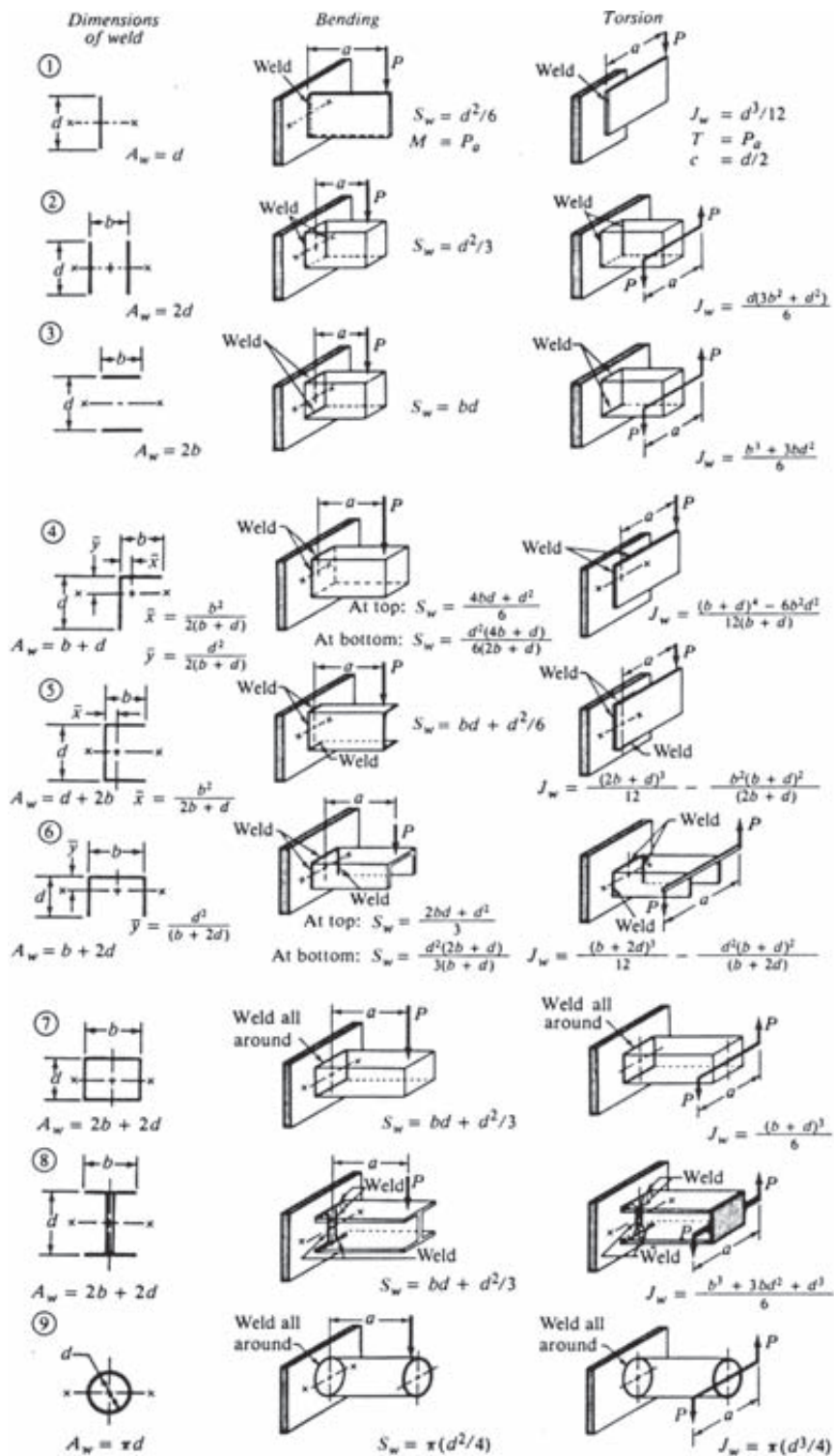
Given The material is ASTM A36 structural steel and an E70xx welding electrode is used. The Schedule 40 pipe is 4.5-in OD by 0.24-in wall. Dimension $a = 15$ in and $r = 10$ in.

Assumptions The weld takes the load directly. Stress in the weld will limit the design since the fusion areas for fillet welds are larger than their throat areas. Ignore weight of arm and pipe.

Solution See Figure 16-17 (overleaf).

- 1 The offset load puts the pipe section and weld in combined bending, torsion, and direct shear at the root of the cantilever beam where the moment and torque are both maximum. The torsion and direct shear are assumed to be uniformly distributed along the weld. The location of highest stress will be on the top of the pipe at the weld toe (labeled A) where the bending stress is maximum tensile. We first need to calculate the unit loads on the weld due to each mode of loading and then find their vector sum.
- 2 This is Case 9 in Figure 16-16, which shows the direct shear component factor $A_w = \pi d$. Use this to find the unit load f_s at point A due to direct shear.

$$f_s = \frac{P}{A_w} = \frac{P}{\pi d} = \frac{2700}{4.5\pi} = 191.0 \text{ lb/in} \quad (a)$$

**FIGURE 16-16**

Geometry Factors to Analyze a Weld as a Line (reprinted from [7])

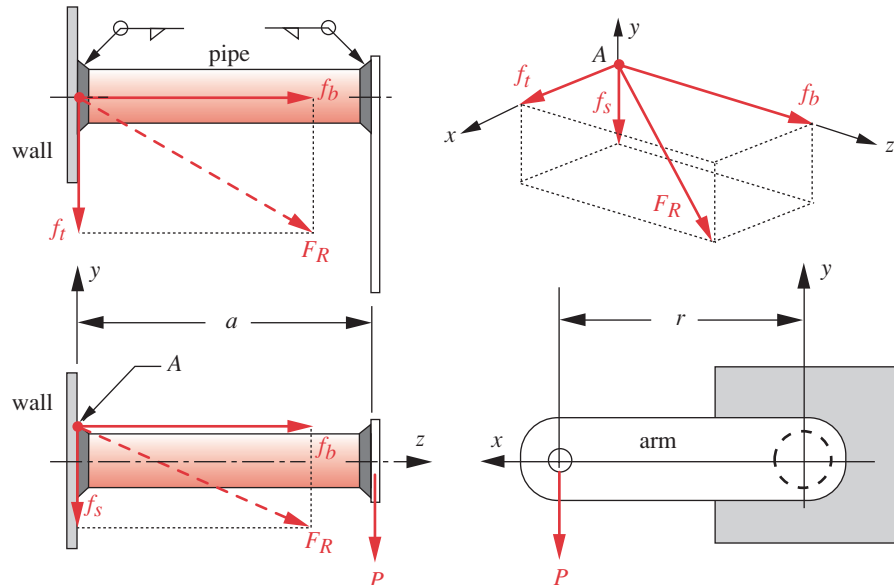


FIGURE 16-17

Examples 16-3 and 16-4

- 3 Find the unit load f_b at point A due to the bending moment using S_w from Case 9.

$$f_b = \frac{M}{S_w} = \frac{Pa}{\pi d^2/4} = \frac{2700(15)}{\pi(4.5^2/4)} = 2546.5 \text{ lb/in} \quad (b)$$

- 4 Find the unit load f_t at point A due to the torsional moment using J_w from Case 9.

$$f_t = \frac{Tc}{J_w} = \frac{Prd/2}{\pi d^3/4} = \frac{2700(10)(4.5/2)}{\pi(4.5^3/4)} = 848.8 \text{ lb/in} \quad (c)$$

- 5 Find the magnitude of the resultant force at point A (the maximum weld load).

$$|F_R| = \sqrt{f_s^2 + f_b^2 + f_t^2} = 2691 \text{ lb/in} \quad (d)$$

- 6 This is the load per inch of weld. The throat area of one linear inch of weld is equal to the throat dimension. So, if we set the throat stress equal to the allowable value from equation 16.1, use this unit load and calculate the area needed to achieve that allowable stress, we will define the required throat dimension. From equation 16.1, an E70 electrode has an allowable stress of $0.30(70\ 000) = 21\ 000 \text{ psi}$.

$$t = \frac{|F_R|}{\tau_{allow}} = \frac{2691 \text{ lb/in}}{21\ 000 \text{ lb/in}^2} = 0.128 \text{ in}^2/\text{in} \quad (e)$$

- 7 This is the throat dimension, but fillet welds are specified by their leg dimension. Assuming an equal-leg fillet in a 90° joint, the leg dimension will be:

$$w = 1.414t = 1.414(0.128) = 0.181 \text{ in} \quad (f)$$

- 8 Specify a $3/16''$ fillet weld. This meets the minimum weld size specified in Table 16-2 and will have a safety factor of approximately 2.5 based on equation 16.1.

- 9 The weld between the pipe and arm is stressed at a lower level than the weld at A because the bending moment is zero at the end of the cantilever. It sees only direct shear and torsional shear which are 32% of the stress at A. Use a 3/16" weld here also for consistency of fabrication. It is also the minimum for this wall thickness.

EXAMPLE 16-4**Design of a Dynamically Loaded Weldment Assembly****Problem**

The weldment assembly in Figure 16-17 has fillet welds all around between the pipe and each end plate. Determine the weld size needed to withstand a dynamic load that varies between $F_{min} = -80$ lb and $F_{max} = 600$ lb for infinite life with a fatigue safety factor $N_{fr} = 1.5$.

Given

The material is ASTM A36 structural steel and an E70xx welding electrode is used. The Schedule 80 pipe is 4.5-in OD by 0.337-in wall (3.83-in ID). Dimension $a = 15$ in and $r = 10$ in.

Assumptions

The weldment is a Category C but the weld may limit as Category F.

Solution

See Figure 16-17.

- Failure due to dynamic loading of weldments has been shown to depend only on the stress range or oscillation between the minimum and maximum values of stress seen during the cycle.^[2] The force range is $F_{max} - F_{min} = 600 - (-80) = 680$ lb.
- This is Case 9 in Figure 16-16, which shows the direct shear component factor $A_w = \pi d$. Use this to find the unit load f_s at point A due to direct shear.

$$f_s = \frac{P}{A_w} = \frac{P}{\pi d} = \frac{680}{4.5\pi} = 48.1 \text{ lb/in} \quad (a)$$

- Find the unit load f_b at point A due to the bending moment using S_w from Case 9.

$$f_b = \frac{M}{S_w} = \frac{Pa}{\pi d^2/4} = \frac{680(15)}{\pi(4.5^2/4)} = 641.3 \text{ lb/in} \quad (b)$$

- Find the unit load f_t at point A due to the torsional moment using J_w from Case 9.

$$f_t = \frac{Tc}{J_w} = \frac{Prd/2}{\pi d^3/4} = \frac{680(10)(4.5/2)}{\pi(4.5^3/4)} = 213.8 \text{ lb/in} \quad (c)$$

- Find the magnitude of the resultant unit force at point A.

$$|F_R| = \sqrt{f_s^2 + f_b^2 + f_t^2} = 678 \text{ lb/in} \quad (d)$$

This is the load per inch of weld length.

- From Table 16.2a, a Category F joint has a shear stress-range endurance strength $S_{ers} = 8000$ psi. Apply the safety factor to this strength to get an allowable stress.

$$\tau_{allow} = \frac{S_{ers}}{N_{fr}} = \frac{8000}{1.5} = 5333 \text{ psi} \quad (e)$$

- 7 The throat area of one linear inch of weld length is equal to the throat dimension. So, if we set the throat stress equal to the allowable value from equation (e), use this unit load and calculate the unit area needed to achieve that allowable stress, we will define the required throat dimension.

$$t = \frac{|F_R|}{\tau_{allow}} = \frac{678 \text{ lb/in}}{5333 \text{ lb/in}^2} = 0.127 \text{ in}^2/\text{in} \quad (f)$$

- 8 This is the throat dimension (in), but fillet welds are specified by their leg dimension. Assuming a 45° fillet, the leg dimension will be:

$$w = 1.414t = 1.414(0.127) = 0.180 \text{ in} \quad (g)$$

- 9 Specify a $3/16"$ (0.187") fillet weld to obtain the specified safety factor of 1.5. This meets the minimum weld size specified in Table 16-2.
- 10 The weld between the pipe and arm has lower stress than the weld at A because the bending moment is zero at the cantilever end. That weld sees only direct shear and torsional shear which are 32% of the stress at A. Table 16-2 gives a minimum $3/16"$ weld for this wall thickness—the same size as at A, which simplifies fabrication.
- 11 We also need to check that the stress in the fusion area between weld and pipe will not fail. Remember that only the stress range is of concern with weldments and it is due to the range of force oscillation, here 680 lb from step 1. Find the normal bending stress range and torsional shear stress range on point A using equations 4.11b (p. 156) and 4.23b (p. 177) respectively.

$$\sigma_x = \frac{Mc}{I} = \frac{(Pa)c}{I} = \frac{680(15)(2.25)}{\pi(4.5^4 - 3.83^4)/64} = 2388 \text{ psi} \quad (h)$$

$$\tau_{xz} = \frac{Tr}{J} = \frac{(Pr)c}{J} = \frac{680(10)(2.25)}{\pi(4.5^4 - 3.83^4)/32} = 796 \text{ psi} \quad (i)$$

- 12 Find the maximum shear stress, principal stresses, and von Mises stress that result from this stress combination using equations 4.6 (p. 145) and 5.7c (p. 249).

$$\begin{aligned} \tau_{max} &= \sqrt{\left(\frac{\sigma_x - \sigma_z}{2}\right)^2 + \tau_{xz}^2} = \sqrt{\left(\frac{2388 - 0}{2}\right)^2 + 796^2} = 1435 \text{ psi} \\ \sigma_1 &= \frac{\sigma_x + \sigma_z}{2} + \tau_{max} = \frac{2388}{2} + 1435 = 2629 \text{ psi} \\ \sigma_2 &= 0 \end{aligned} \quad (j)$$

$$\sigma_3 = \frac{\sigma_x + \sigma_z}{2} - \tau_{max} = \frac{2388}{2} - 1435 = -241 \text{ psi}$$

$$\sigma' = \sqrt{\sigma_1^2 - \sigma_1\sigma_3 + \sigma_3^2} = \sqrt{2629^2 - 2629(-24) + (-24)^2} = 2757 \text{ psi} \quad (k)$$

- 13 Assume this assembly is an AISC Category C. Table 16-5a shows the infinite-life fatigue strength for a Category C weldment as 10 000 psi. The safety factor is then:

$$N_f = \frac{S_f}{\sigma'} = \frac{10000}{2757} = 3.62 \quad (l)$$

The weld material limits this design.

16.8 ECCENTRICALLY LOADED WELD PATTERNS

Weldments are often used to support offset or eccentric loads as in Examples 16-3 and 16-4. There are many other common arrangements as shown in Figure 16-16. Some of these such as the one shown in Figure 16-18 require that the centroid of the weld pattern be found. This is the same procedure as was described in Section 15-10 and Example 15-6 where a pattern of bolts and dowels was used to support an eccentric load and its centroid was needed. The arrangement of Figure 16-18 is defined in part 5 of Figure 16-16. An equation for the location of the weld pattern's centroid is defined there as well as expressions for the unit loads due to direct shear and either bending or torsional loading depending on the location of the applied force being either in- or out-of-plane. This application will be shown in an example.

EXAMPLE 16-5

Design of an Eccentrically Loaded Weldment Assembly

Problem The weldment assembly in Figure 16-18 has fillet welds on three sides of the joint. Determine the weld size needed to withstand a static load of $P = 4000$ lb. Check for yielding in the beam also.

Given The material is ASTM A36 structural steel and an E70xx welding electrode is used. The plates are 1/2" thick. Dimension $a = 12"$, $b = 3"$, and $d = 6"$.

Assumptions Consider the weld as a line. The weld pattern matches that of part 5 of Figure 16-16. The weld will limit the design as Category F.

Solution See Figure 16-18.

- Find the centroid of the weld pattern with the equation given in Figure 16-16.

$$\bar{x} = \frac{b^2}{2b+d} = \frac{3^2}{2(3)+6} = \frac{9}{12} = 0.75 \text{ in} \quad (a)$$

- Find the radius from applied load to centroid.

$$r = a + b - \bar{x} = 12 + 3 - 0.75 = 14.25 \text{ in} \quad (b)$$

- The weld joint is loaded in direct shear and also has a torsional moment about its centroid. Find the unit load in the weld due to direct shear.

$$f_s = \frac{P}{A_w} = \frac{P}{2b+d} = \frac{4000}{6+2(3)} = 333.3 \text{ lb/in} \quad (c)$$

- As far as the weld is concerned, the torsional moment acts about its centroid which is at radius r from the applied load P .

$$T = Pr = 4000(14.25) = 57\,000 \text{ lb-in} \quad (d)$$

- The torsional geometry factor for this weld versus the centroid from Figure 16-16 is:

$$J_w = \frac{(2b+d)^3}{12} - \frac{b^2(b+d)^2}{2b+d} = \frac{(12)^3}{12} - \frac{9(9)^2}{12} = 83.25 \text{ in}^3 \quad (e)$$

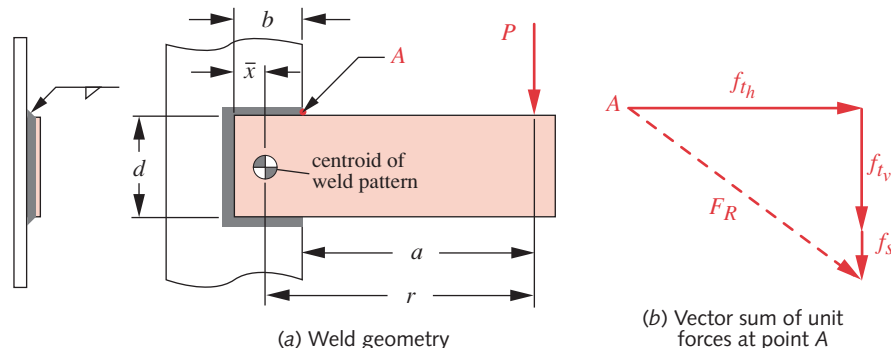


FIGURE 16-18

Example 16-5

- 6 The highest stress in the weld due to the torsional moment will occur at the point furthest from the centroid, labelled A in Figure 16-18. It will be simplest if we compute the horizontal and vertical components at point A and then resolve them in combination with the vertical direct shear component into a resultant unit force. For the horizontal component, the radius from the centroid is $d/2$. For the vertical component, the radius from the centroid is $r-a$.

$$\begin{aligned} f_{t_h} &= \frac{T d/2}{J_w} = \frac{57\,000 (6/2)}{83.25} = 2054.1 \text{ lb/in} \\ f_{t_v} &= \frac{T(r-a)}{J_w} = \frac{57\,000 (14.25 - 12)}{83.25} = 1540.5 \text{ lb/in} \\ F_R &= \sqrt{f_{t_h}^2 + (f_{t_v} + f_s)^2} = \sqrt{2054.1^2 + (1540.5 + 333.3)^2} = 2780 \text{ lb/in} \end{aligned} \quad (f)$$

- 7 The unit area of the throat will then be

$$t = \frac{|F_R|}{\tau_{allow}} = \frac{2780 \text{ lb/in}}{0.30(70\,000) \text{ lb/in}^2} = 0.132 \text{ in}^2/\text{in} \quad (g)$$

using the S_{ut} of E70 electrode and equation 16.1 for τ_{allow} . The leg dimension is

$$w = 1.414t = 1.414(0.132) = 0.187 \text{ in} \quad (h)$$

- 8 The minimum recommended weld size for 1/2-in plate is 3/16" which matches this number. Use a 3/16" fillet weld.

16.9 DESIGN CONSIDERATIONS FOR WELDMENTS IN MACHINES

Weldments can be a practical choice for odd-shaped subassemblies that locate and support machine parts. They may not prove to be an economic choice if not properly designed, however. A significant fraction of their cost is in fixturing and setup of the pieces to hold them in position while welded. In some cases, it can be less expensive to machine a complex part from solid billet with modern numerical control (CNC) machines, which can machine complex shapes defined with solid-modeling CAD systems rapidly and relatively inexpensively and can run unattended after being programmed, creating parts while you sleep. The CNC tool path information generated from the CAD model

can be sent directly to the machining center electronically and the part made in one or a few setups with very little operator interaction. Welded assemblies, on the other hand often are labor intensive. It may be worth seeking quotes on direct machining of parts from billet that were initially designed as weldments.

That said, what can be done during its design to reduce the cost of a weldment? It may be possible to design the weldment assembly to be fully or partially “self-fixturing.” The degree that the individual pieces to be welded are designed to fit together easily in the correct orientation and alignment for welding as opposed to requiring external fixtures to be made to hold them will reduce cost. Obviously, minimizing the number and size of welds will also reduce cost.

Be cautious about using weldments for parts subject to dynamic loading. Try to place welds in locations of lower stress when possible. The residual tensile stress in all welds is a danger when oscillating stress is applied to those regions. If that situation cannot be designed around, then weld reinforcements and any backing strips should be removed and weld surfaces ground smooth to reduce stress concentration at the toes and on the weld surface. Hammer peening the welds will reduce tensile residual stress and improve fatigue resistance, but this can add significant cost. Parts machined from solid billet will often prove less expensive than a weldment in these cases and should be investigated as an alternative. If quantities permit, forging will give parts with better fatigue resistance, but high tooling cost eliminates this option for small batches that are typical with custom machine parts.

If a weldment requires post-weld machining, it will probably be necessary to thermally stress relieve the weldment before machining it. This will relieve the residual stresses globally and improve part life. Otherwise the part will likely distort when metal removal during machining releases the residual stress locally where machining is done.

16.10 SUMMARY

This brief introduction to the design of weldments probably raises as many questions in the mind of the designer as it provides answers. Welding is a complex subject and is based on a large body of research and experimental data. It has advanced tremendously since its application to ship construction in World War II. Some of the problems encountered then are described in Chapters 5 and 6. If the reader needs to design weldments, they are strongly encouraged to delve more deeply into the subject than can be attempted here. See the references noted.

One of the most interesting results of extensive weldment fatigue testing is the independence of failure to the presence of mean stress, which is a serious issue in fatigue failure of unwelded parts. This simplifies the weldment designer’s task since it eliminates the need for a Goodman line analysis. Treating the weld as a line greatly simplifies the task of determining appropriate weld sizes for various loading situations.

The existence of design codes both simplifies and complicates the designer’s task. It simplifies by providing rules and guidelines for design. But it also complicates the situation because those rules are far from simple and require much effort to fully understand and use properly. The AISC provides design guidelines and failure stress data based on extensive experiment that should be used for weldment design. The AISC and AWS specifications and codes should be studied by the serious designer.

Weldments work best when made of low-carbon hot-rolled steel and statically loaded, which is typical of machine frames and structures. Parts that are highly stressed or loaded dynamically may not be good candidates for weldment design. One does not find engine crankshafts and connecting rods made as weldments, for example. Those highly loaded, dynamically stressed parts are usually hot forged.

Important Equations Used in This Chapter

Allowable Shear Stress in Statically Loaded Weldments (Section 16.5):

$$\tau_{allow} = 0.30Exx \quad (16.1)$$

Tensile Stress-Range Fatigue Strength - Cat. A-E (Section 16.6):

$$S_{fr} = C_{reliab} \left(\frac{C_f}{N} \right)^{\frac{1}{3}} \geq S_{er} \quad (16.2a)$$

Shear Stress-Range Fatigue Strength - Cat. F (Section 16.6):

$$S_{frs} = C_{reliab} \left(\frac{C_f}{N} \right)^{\frac{1}{6}} \geq S_{ers} \quad (16.2b)$$

See Table 16-5 for values of C_f and S_{er}, S_{ers} .

Safety Factor in Fatigue for Weldments

$$N_{fr} = \frac{S_{fr}}{\Delta\sigma} \quad \text{or} \quad N_{frs} = \frac{S_{frs}}{\Delta\tau} \quad (16.3)$$

16.11 REFERENCES

- 1 **O. Blodgett**, *Design of weldments*, J. F. Lincoln Foundation, Cleveland, OH, 1963.
- 2 **ANSI/AISC 360-05**, *Specification for Structural Steel Buildings*, p. 16-1-400, American Institute of Steel Construction, March 9, 2005.
- 3 **American Welding Society**, Miami, FL.
- 4 **SAE Fatigue Design Handbook AE-22** 3ed, p. 95, Society of Automotive Engineers, Warrandale, PA, 1997.
- 5 **O. Blodgett**, "Stress Allowables Affect Welding Design," J. F. Lincoln Foundation, Cleveland, OH, 1998.
- 6 **T. R. Higgins and F. R. Preece**, "Proposed Working Stresses for Fillet Welds in Building Construction," *AISC Engineering Journal*, Vol. 6, No. 1, pp. 16-20, 1969.
- 7 **R. L. Mott**, *Machine Elements in Mechanical Design*, 4ed., p. 786, Prentice-Hall, Upper Saddle Brook, NJ, 2004.
- 8 **M. A. Weaver**, "Determination of Weld Loads and Throat Requirements Using Finite Element Analysis with Shell Element Models—A Comparison with Classical Analysis," *Welding Research Supplement*, pp. 1s-11s, 1999.
- 9 **D. K. Miller**, "Consider Direction of Loading When Sizing Fillet Welds," *Welding Innovation*, Vol. XV, No. 2, 1998.

Table P16-0[†]

Topic/Problem Matrix

16.5 Static Strength of Welds

16-1, 16-2, 16-3

16.6 Dynamic Strength of Welds

16-5, 16-7, 16-9

16.7 Weld as a Line

16-6, 16-7, 16-8, 16-9

16.8 Eccentrically Loaded Weld Patterns

16-4, 16-5

- 10 **J. M. Barsom and S. T. Rolfe**, *Fracture and Fatigue Control in Structures*, 3ed., pp. 238, 269, Prentice-Hall, Upper Saddle Brook, NJ, 1999.
- 11 **J. W. Fisher et al.**, *Effect of Weldments on the Fatigue Strength of Steel beams*, National Cooperative Highway Research Program Report 102, Highway Research Board, National Research Council, 1970.
- 12 *Recommendations for Fatigue Design of Welded Joints and Components*, WRC Bulletin 520, The Welding Research Council Inc., 2009.

16.12 PROBLEMS

- *16-1 A submerged-arc complete joint penetration (CJP) butt weld was made between two sections of A36 hot-rolled steel plate. The plate is 10-in wide by 1/2-in-thick. E70 electrode was used. How much tensile load can the assembly withstand across the weld without yielding in either base metal or weld?
- 16-2 The plate of problem 16-1 has partial joint penetration welds applied from each side. Each weld throat is 1/4 in. What is the maximum allowable tensile load across the weld.
- *†16-3 A tee bracket similar to Figure 16-11 has 1/2-in-thick A572 Grade 42 steel welded with a 3/16 in fillet weld along both inside corners using an E70 electrode. It will be subjected to a 20 kip tensile load on the leg of the tee. Determine the minimum required length L of the bracket based on full-length welds.
- 16-4 Figure P16-1 shows a bar welded to a base with 3/16 in fillet welds on three sides using an E70 electrode. Material is A572 Grade 50 hot-rolled steel. What is your recommended maximum static load P that can safely be applied?
- *16-5 Figure P16-1 shows a bar welded to a base with 3/16 in fillet welds on three sides using an E70 electrode. Material is A572 Grade 50 hot-rolled steel. What is your recommended maximum dynamic repeated load, zero to P_{max} that can be applied for 10^8 cycles with a safety factor of 1.6?
- *†16-6 Figure P16-2 shows a bracket welded to a wall with a fillet weld using an E70 electrode. For the row(s) assigned in Table P16-1, determine the fillet weld size needed between the tube and wall for a static load F and $h = 1.2OD$, $a = 2OD$, and $l = 2.5OD$. The pipe and wall material are A36 steel.
- *†16-7 Figure P16-2 shows a bracket welded to a wall with a fillet weld using an E70 electrode. For the row(s) assigned in Table P16-1, determine the fillet weld size needed between the tube and wall for a dynamic load that varies from $-0.1F$ to $+0.2F$. The pipe and wall material are A36 steel, $h = 1.2OD$, $a = 2OD$, and $l = 2.5OD$. Use a safety factor of 1.5.

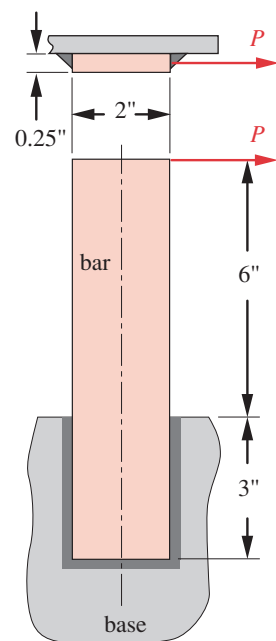


FIGURE P16-1

Problems 16-4 and 16-5

Table P16-1

Data for Problems 16-6 to 16-7
Lengths in inches, forces in kip.

Row	F	OD	ID	b
a	2.5	3.500	3.068	1/2
b	3.8	4.500	4.026	1/2
c	4.8	5.563	5.047	1/2
d	8.0	6.625	6.065	1/2
e	9.0	8.625	7.981	3/4
f	11.0	10.750	10.020	3/4

16

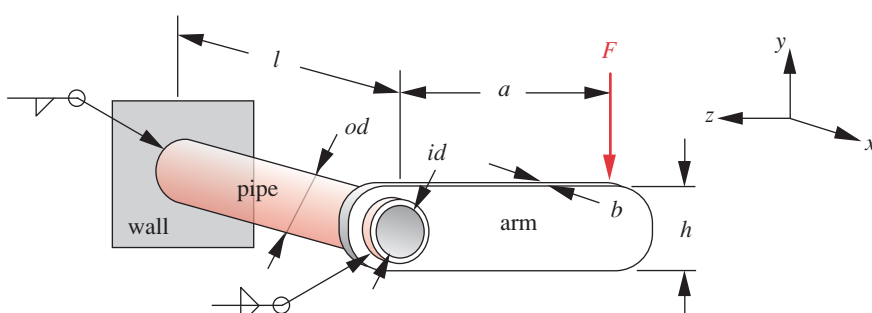
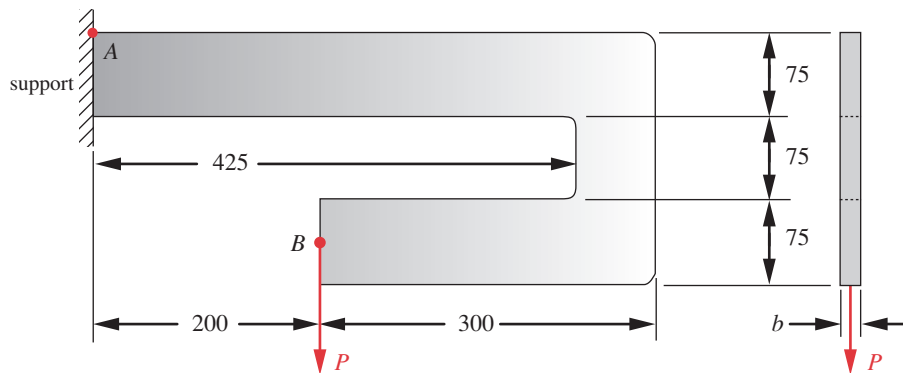


FIGURE P16-2

Problems 16-6 to 16-7

* Answers to these problems are provided in Appendix D.

† Problem numbers in *italics* are design problems.

**FIGURE P16-3**

Problems 16-8 and 16-9

[†]16-8 Figure P16-3 shows a bracket machined from 12-mm-thick A572 Grade 50 hot-rolled steel flat stock. It is welded to a support with a fillet weld all around using an E80 electrode. Determine the fillet weld size needed between the bracket and the support for a static load of $P = 12 \text{ kN}$.

*[†]16-9 Figure P16-3 shows a bracket machined from 12-mm-thick A572 Grade 50 hot-rolled steel flat stock. It is welded to a support with a fillet weld all around using an E90 electrode. Determine the fillet weld size needed between the bracket and the support for a dynamic load that varies from 0 to +3 kN using a safety factor of 1.8.

16-10 Two 8-mm-thick by 50-mm-wide A572 Grade 42 steel straps are welded together with fillet welds in a lap joint using E70 electrode. The tensile load of 45 kN on the straps is orthogonal (transverse) to the welds. What is your recommended weld size for the two full-length welds?

16-11 Two 8-mm-thick by 50-mm-wide A572 Grade 42 steel straps are welded together with fillet welds in a lap joint using E70 electrode. Determine the fillet weld size needed for a dynamic load that varies from 0 to +12 kN using a safety factor of 1.5 for infinite life of the two full-length welds.

16-12 Two 12-mm-thick by 50-mm-wide weldable aluminum straps are welded together with fillet welds in a lap joint using an aluminum electrode. Determine the fillet weld size needed for a dynamic load that varies from 0 to +5 kN using a safety factor of 2.0 for infinite life of the two full-length welds.

* Answers to these problems are provided in Appendix D.

[†] Problem numbers in *italics* are design problems.



CLUTCHES AND BRAKES

A big book is a big nuisance.

CALLIMACHAS, 260 BC

17.0 INTRODUCTION

Clutches and brakes are essentially the same device. Each provides a frictional, magnetic, hydraulic, or mechanical connection between two elements. If both connected elements can rotate, then it is called a clutch. If one element rotates and the other is fixed, it is called a brake. A clutch thus provides an interruptible connection between two rotating shafts as, for example, the crankshaft of an automobile engine and the input shaft of its transmission. A brake provides an interruptible connection between one rotating element and a nonrotating ground plane as, for example, the wheel of an automobile and its chassis. The same device may be used as either clutch or brake by fixing its output element to a rotatable shaft or by fixing it to ground.

Brakes and clutches are used extensively in production machinery of all types, not just in vehicle applications where they are needed to stop motion and allow the internal-combustion engine to continue turning (idling) when the vehicle is stopped. Clutches also allow a high-inertia load to be started with a smaller electric motor than would be required if it were directly connected. Clutches are commonly used to maintain a constant torque on a shaft for tensioning of webs or filaments. A clutch may be used as an emergency disconnect device to decouple the shaft from the motor in the event of a machine jam. In such cases, a brake will also be fitted to bring the shaft (and machine) to a rapid stop in an emergency. To minimize injuries, many U.S. manufacturers require their production machinery to stop within one or fewer revolutions of the main driveshaft if a worker hits the “panic bar” that typically spans the length of the machine. This can be a difficult specification to achieve on large machines (10 to 100 feet long) driven by multihorsepower electric motors. Manufacturers provide clutch-brake combinations in the same package for such applications. Applying power disengages the brake and engages the clutch, making it fail-safe. Fail-safe brakes are engaged

Table 17-0 Variables Used in this Chapter

Symbol	Variable	ips units	SI units	See
<i>a</i>	length	in	m	Sect. 17.6
<i>b</i>	length	in	m	Sect. 17.6
<i>c</i>	length	in	m	Sect. 17.6
<i>d</i>	diameter	in	m	various
<i>F</i>	force	lb	N	various
<i>F_a</i>	applied force	lb	N	Sect. 17.6
<i>F_f</i>	friction force	lb	N	Sect. 17.6
<i>F_n</i>	normal force	lb	N	Sect. 17.6
<i>R_x</i>	reaction force	lb	N	Sect. 17.6
<i>R_y</i>	reaction force	lb	N	Sect. 17.6
<i>K</i>	arbitrary constant	none	none	various
<i>l</i>	length	in	m	various
<i>M</i>	moment	lb-in	N-m	various
<i>N</i>	number of friction surfaces	none	none	Eq. 17.2
<i>P</i>	power	hp	Watts	Ex. 17-1
<i>p</i>	pressure	psi	N/m ²	Sect. 17.4
<i>P_{max}</i>	maximum pressure	psi	N/m ²	Sect. 17.4
<i>r</i>	radius	in	m	various
<i>r_i</i>	inside radius of disk lining	in	m	various
<i>r_o</i>	outside radius of disk lining	in	m	various
<i>T</i>	torque	lb-in	N-m	various
<i>V</i>	linear velocity	in/sec	m/sec	Eq. 17.4
<i>W</i>	wear rate	psi-in/sec	Pa-m/sec	Eq. 17.4
<i>w</i>	width	in	m	various
θ	angular position	rad (deg)	rad (deg)	Sect. 17.6
μ	coefficient of friction	none	none	Eq. 17.2
ω	angular velocity	rad/sec	rad/sec	Ex. 17-1

(typically by internal springs) unless power is applied to disengage them. Thus they “fail safe” and stop the load if the power fails. Highway truck and railroad-car air brakes are of this type. Air pressure releases the brake, which is normally engaged. If the railroad car or truck trailer breaks loose and severs its air-hose connection to the engine or tractor, the brakes automatically engage.

This chapter will describe a number of types of commercially available clutches and brakes and their typical applications, and will also discuss the theory and design of a few particular types of friction clutches/brakes. Table 17-0 lists the variables used in this chapter and indicates the equation or section in which they can be found.

Title page photograph courtesy of the Logan Clutch Corporation, Cleveland, Ohio.

17.1 TYPES OF BRAKES AND CLUTCHES

Brakes and clutches can be classified in a number of ways, by the *means of actuation*, the *means of energy transfer* between the elements, and the *character of the engagement*. Figure 17-1 shows a flow chart depicting these characteristics. The means of actuation may be **mechanical**, as in the pushing of an automobile's clutch pedal, **pneumatic or hydraulic**, in which fluid pressure drives a piston to mechanically engage or disengage as with vehicle brakes, **electrical**, which is typically used to excite a magnetic coil, or **automatic**, as in an antirunaway brake that engages by relative motion between the elements.

POSITIVE CONTACT CLUTCHES The means of energy transfer may be a **positive mechanical contact**, as in a toothed or serrated clutch, which engages by mechanical interference as shown in Figure 17-2. The character of engagement is mechanical interference obtained with jaws of square or saw-toothed shape, or with teeth of various shapes. These devices are not as useful for brakes (except as holding devices) because they cannot dissipate large amounts of energy as can a friction brake, and as clutches they can be engaged only at low relative velocities (about 60 rpm max for jaw

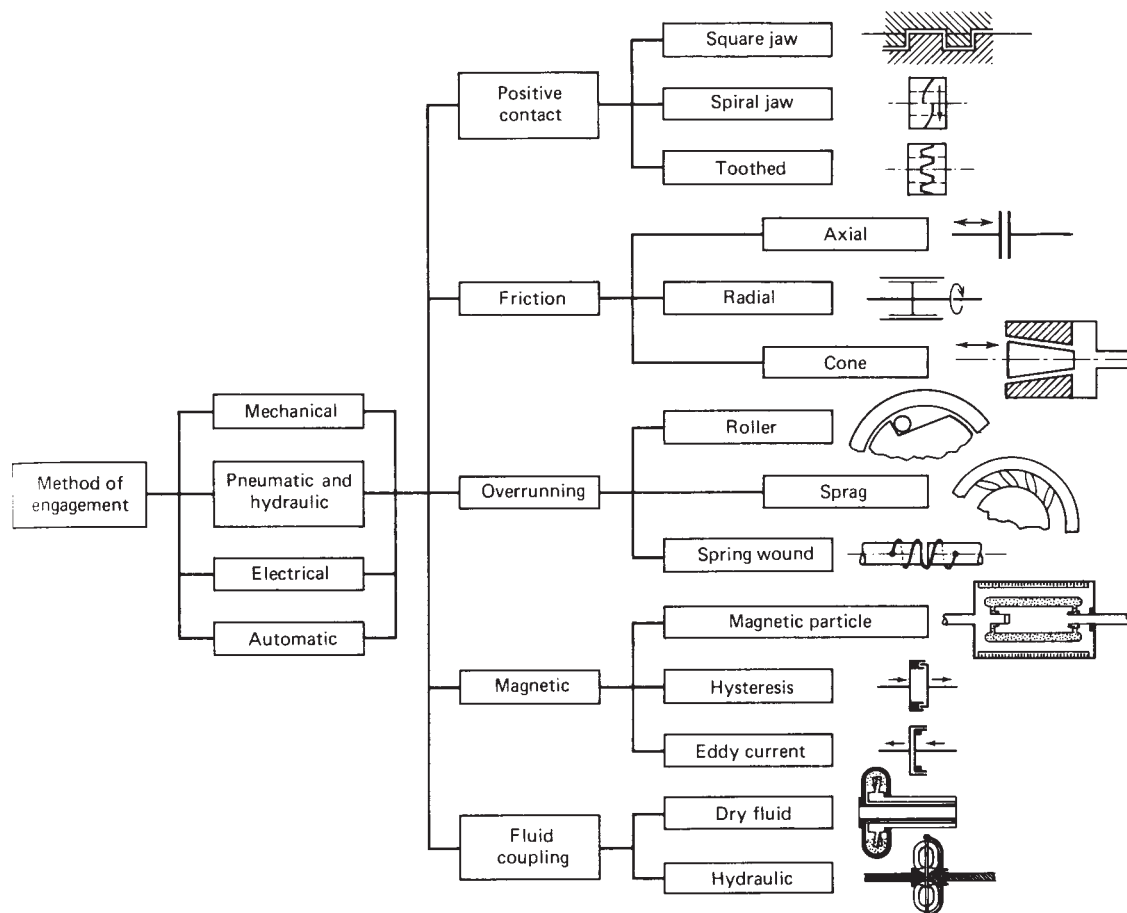
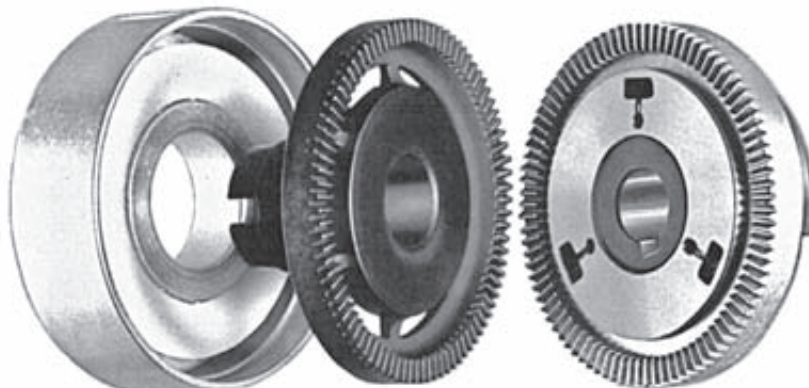


FIGURE 17-1

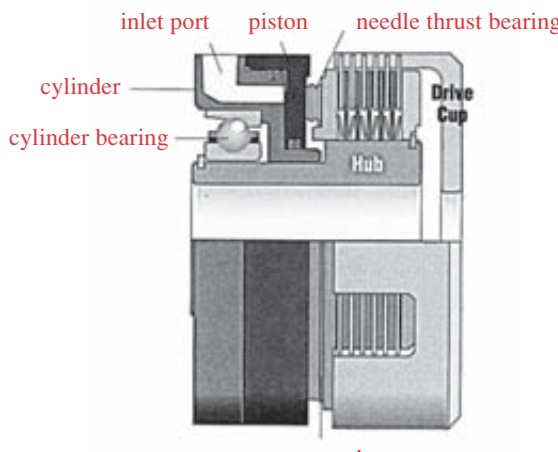
Classification of Clutches and Brakes Source: Z. Hinchliffe, *Machine Design Fundamentals: A Practical Approach*, Prentice-Hall, 1983, with permission

**FIGURE 17-2**Positive Contact Clutch *Courtesy of American Precision Industries, Deltran Division, Amherst, N.Y. 14228*

clutches and 300 rpm max for toothed clutches). Their advantage is positive engagement, and, once coupled, they can transmit large torque with no slip. They are sometimes combined with a friction-type clutch, which drags the two elements to nearly the same velocity before the jaws or teeth engage. This is the principle of a **synchromesh clutch** in a manual automotive transmission.*

FRICITION CLUTCHES AND BRAKES are the most common types used. Two or more surfaces are pressed together with a normal force to create a friction torque. The friction surfaces may be flat and perpendicular to the axis of rotation, in which case the normal force is axial (disk brake or clutch), as shown in Figure 17-3, or they may be cylindrical with the normal force in a radial direction (drum brake or clutch), as shown in Figures 17-9 and 17-10 (pp. 973, 975), or conical (cone brake or clutch). Cone clutches can tend to grab or refuse to release and are not now used very much in the United States, but are popular in Europe.^[1]

* Automotive transmissions typically use helical gears, for quiet operation, as was noted in Chapter 13. The helical gears cannot be easily shifted in and out of engagement in manual transmissions because of their helix angle. So, they are all kept in constant mesh and clutched/declutched from the transmission shaft to engage a particular ratio. Each gear has a synchromesh clutch connecting it to its shaft. This clutch actually consists of conical friction surfaces that drag the two elements (shaft and gear) into near zero relative velocity before the teeth of its companion positive-contact clutch engage. The shift lever moved by the driver is shifting these synchromesh clutches into and out of engagement, rather than moving gears around in the transmission.

**FIGURE 17-3**A Multiplate Disk Clutch Actuated by Fluid Pressure *Courtesy of Logan Clutch Corporation, Cleveland, Ohio*

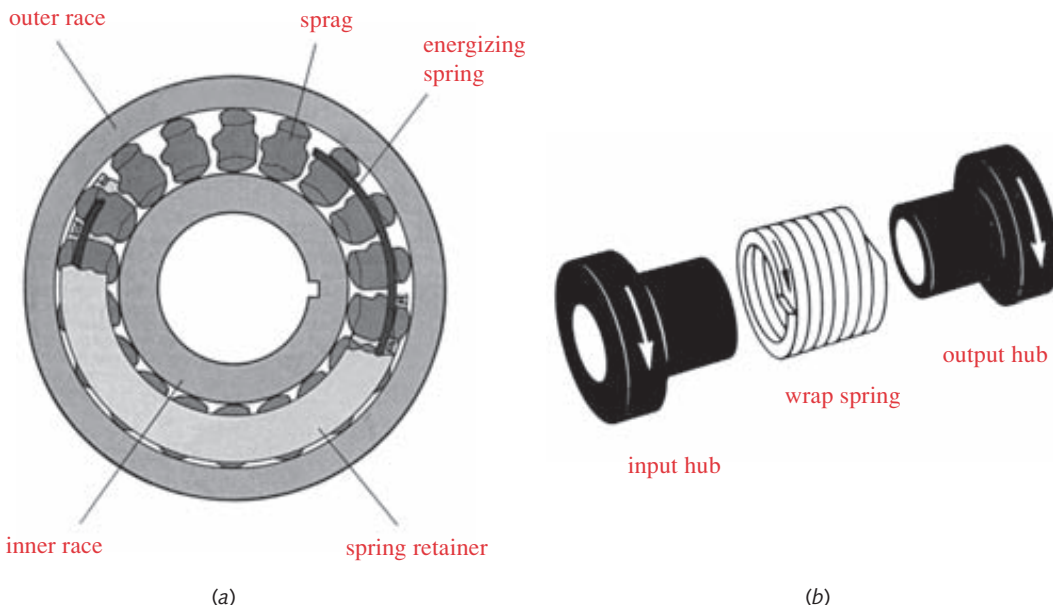
At least one of the friction surfaces is typically metal (cast iron or steel) and the other is usually a high-friction material, referred to as the lining. If there are only two elements, there will be either one or two friction surfaces to transmit the torque. A cylindrical arrangement (drum brake or clutch) has one friction surface, and an axial arrangement (disk brake or clutch) has one or two friction surfaces, depending on whether the disk is sandwiched between two surfaces of the other element or not. For higher torque capacity, disk clutches and brakes are often made with multiple disks to increase the number of friction surfaces (see Figure 17-3). A clutch or brake's ability to transfer the heat of friction generated can become the limiting factor on its capacity. Multidisk clutches are more difficult to cool so are appropriate for high-load, low-speed applications. For high-speed dynamic loads, fewer friction surfaces are better.^[1]

Friction clutches may be operated either dry or wet, the latter running in an oil bath. While the oil severely reduces the coefficient of friction, it greatly increases the heat transfer. Friction coefficients of clutch/brake material combinations typically range from 0.05 in oil to 0.60 dry. Wet clutches often use multiple disks to make up for the lower friction coefficient. Automatic transmissions for automobiles and trucks contain many wet clutches and brakes operating in oil that is circulated out of the transmission for cooling. Manual transmissions for off-road vehicles, such as motorcycles, use sealed, oil-filled, multidisk wet clutches to protect the friction surfaces from dust, water, and dirt. Manual-transmission automobiles and trucks typically use single-disk, dry clutches.

OVERRUNNING CLUTCHES (also called one-way clutches) operate automatically based on the relative velocity of the two elements. They act on the circumference and allow relative rotation in only one direction. If the rotation attempts to reverse, the internal geometry of the clutch mechanism grabs the shaft and locks up. These *backstop clutches* can be used on a hoist to prevent the load from falling back if power to the shaft is interrupted, for example. These clutches are also used as indexing mechanisms. The input shaft can oscillate back and forth but the output turns intermittently in only one direction. Another common application of an overrunning clutch is in the rear hub of a bicycle to allow freewheeling when the wheel speed exceeds that of the drive sprocket.

Several different mechanisms are used in one-way clutches. Figure 17-4a shows a **sprag clutch**, which has an inner and outer race like a ball bearing. But, instead of balls, the space between the races is filled with odd-shaped *sprags*, which allow motion in one direction but jam and lock the races together in the other, transmitting a one-way torque. A similar result is obtained with balls or rollers captured in wedge-shaped chambers between the races, then called a **roller clutch**. Figure 17-4b shows another type of one-way or overrunning clutch called a **spring clutch**, which uses a spring wrapped tightly around the shaft. Rotation in one direction wraps the spring tighter on the shaft and transmits torque. Counterrotation unwinds the spring slightly, allowing it to slip.

CENTRIFUGAL CLUTCHES engage automatically when the shaft speed exceeds a certain magnitude. Friction elements are thrown radially outward against the inside of a cylindrical drum to engage the clutch. Centrifugal clutches are sometimes used to couple an internal-combustion engine to the drive train. The engine can idle decoupled from the wheels and when the throttle is opened, its increased speed automatically engages the clutch. These are common on go-karts. Used on chain saws for the same purpose, they also serve as an overload release that slips to allow the engine to continue running when the chain jams in the wood.

**FIGURE 17-4**

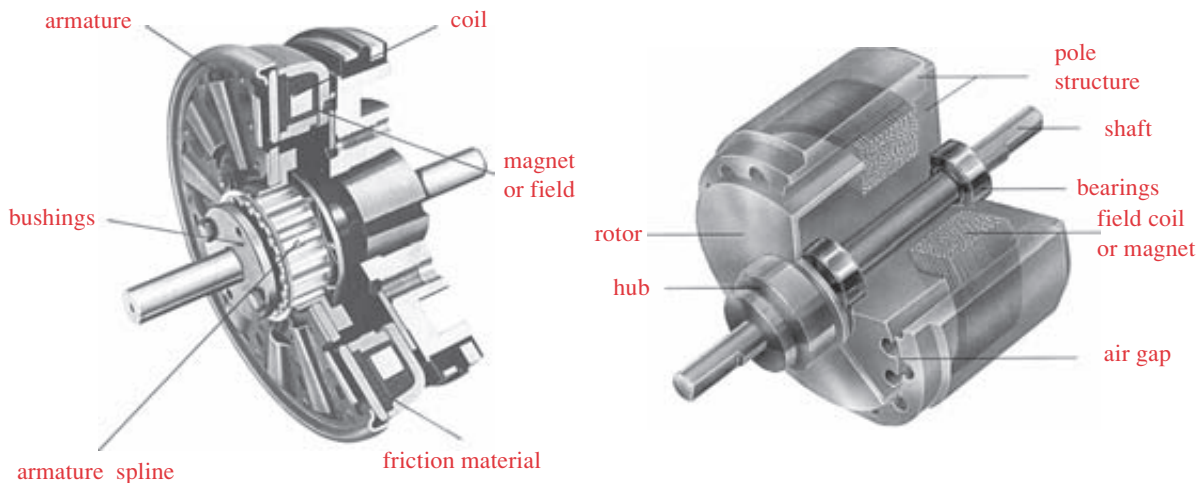
Overrunning Clutches (a) Sprag Clutch (b) Wrap-Spring Clutch Courtesy of Warner Electric, South Beloit, Ill. 61080

MAGNETIC CLUTCHES AND BRAKES are made in several types. **Friction clutches** are commonly electromagnetically operated, as shown in Figure 17-5a. These have many advantages, such as rapid response times, ease of control, and smooth starts and stops, and are available powered on or powered off (fail-safe). Both clutch and brake versions are supplied as well as combined clutch-brake modules.

Magnetic-particle clutches and brakes (not shown) have no direct frictional contact between the clutch disk and the housing and no friction material to wear. The gap between the surfaces is filled with a fine ferrous powder. When the coil is energized, the powder particles form chains along the magnetic field's flux lines and couple the disk to the housing with no slip. The torque can be controlled by varying the current to the coil and the device will slip when the applied torque exceeds the value set by coil current, providing a constant tension.

Magnetic hysteresis clutches and brakes (Figure 17-5b) have no mechanical contact between the rotating elements and so have zero friction when disengaged. The rotor, also called the drag cup, is dragged along (or braked) by the magnetic field set up by the field coil (or permanent magnet). These devices are used to control torque on shafts in applications such as winding machines, where a constant force must be applied to a web or filament of material as it is wound up. The torque on a hysteresis clutch is controllable independent of speed. These devices are extremely smooth, quiet, and long-lived, as there is no mechanical contact within the clutch except in its bearings.

Eddy-current clutches (not shown) are similar in construction to hysteresis devices in that they have no mechanical contact between rotor and pole. The coil sets up eddy currents, which magnetically couple the clutch together. There will always be some slip in this type of clutch, as there has to be relative motion between rotor and pole to gen-

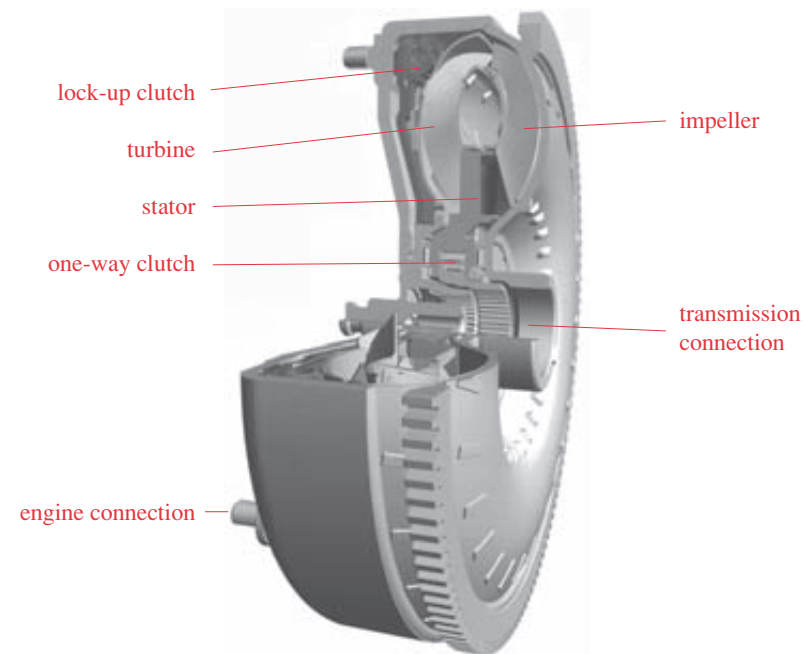
**FIGURE 17-5**

Magnetic Clutches (a) Magnetically Operated Friction Clutch (b) Hysteresis Clutch *Source: (a) Courtesy of Warner Electric, South Beloit, Ill. 61080, (b) Courtesy of Magtrol, Buffalo, N.Y. 14224*

erate the eddy currents that supply the coupling force; so an eddy-current brake cannot hold a load stationary, only slow it from one speed to another. These have similar advantages to the hysteresis devices and are used for similar applications, such as coil or filament winders, etc.

FLUID COUPLINGS transmit torque through a fluid, typically an oil. An impeller having a set of blades is turned by the input shaft and imparts angular momentum to the oil that surrounds it. A turbine (or runner) with similar blades is attached to the output shaft and is turned by the moving oil impinging on it. The principle of operation is similar to placing two electric fans face to face and turning only one on. The airflow from the powered fan blades will cause the facing, unpowered blades to windmill, passing power without any mechanical contact. Using incompressible oil in a confined volume is much more efficient than two open-air fans, especially when the impeller and turbine blades are optimally shaped to pump the oil. A fluid coupling provides extremely smooth starts and absorbs shocks, as the fluid simply shears when there is a speed differential, then gradually accelerates (or decelerates) the output turbine to nearly match the speed of the impeller. There will always be some slip, meaning the turbine can never reach 100% of the impeller's speed (0% slip), but it can operate at 100% slip when the turbine is stalled. All the input energy will then be converted to heat in shearing the oil. Heat transfer is an important consideration when designing a fluid coupling. The outside case is often finned to improve heat transfer. A fluid coupling transmits the input torque to the output shaft at any speed including stall, so it can never be totally decoupled like a friction clutch. The output must be braked to hold it stationary when the input shaft is turning.* The horsepower rating of a fluid coupling varies as the fifth power of its diameter. A 15% increase in diameter doubles its power capacity. If used as a brake, a fluid coupling can only provide a drag to slow a device, as in a dynamometer, but cannot hold a load stationary.

* This is why you must keep your foot on the brake when stopped at a traffic light in an automobile that has an automatic transmission if the engine is running and the transmission is in "drive." The fluid coupling between the engine and transmission is always transmitting torque and the car will creep forward at idle unless the brakes are applied.

**FIGURE 17-6**

Torque converter Courtesy of Mannesmann Sachs AG, Schweinfurt, Germany

If a third, stationary, element with a set of curved blades, called a **reactor** or **stator**, is placed between impeller and turbine, additional angular momentum is imparted to the fluid and the device is then called a **torque converter** as shown in Figure 17-6. Torque converters are used in vehicles to couple the engine to an automatic transmission. The engine can idle with the vehicle stopped (turbine stalled—100% slip). At stall the impeller and reactor blades create about a 2:1 torque multiplication, which is available to help accelerate the vehicle when the brakes are released and the engine speed increased. As the vehicle (and thus turbine) speed increases, the turbine will approach the impeller speed and the torque multiplication will decrease to essentially zero at a slip of a few percent. If more torque is needed momentarily (as in passing), the slip between impeller and turbine will automatically increase when the engine is sped up to provide more torque and power to accelerate the vehicle.

17.2 CLUTCH/BRAKE SELECTION AND SPECIFICATION

Manufacturers of specialty clutches and brakes such as those described above provide extensive information on the torque and power capacities of their various models in catalogs, many of which are as informative as a textbook on the particular subject. They also define procedures for selection and specification, usually based on the anticipated torque and power for the application plus suggested service factors that attempt to accommodate different loading, installation, or environmental factors than those under which the products were tested. For example, the manufacturer's standard rating for a clutch model may be based on a smooth driver such as an electric motor. If the particular application uses an internal-combustion engine of the same power, there will be impulse

loads, and a clutch or brake of larger capacity than dictated by the average power will need to be selected. This is sometimes referred to as *derating* the clutch (or brake), meaning that its actual capacity under the anticipated conditions is considered to be less than the rated capacity of the chosen device.

SERVICE FACTORS According to many clutch manufacturers, a common cause of clutch trouble is the designer's failure to properly apply adequate service factors to account for the particular conditions of the application.^[1] This may, in part, be due to confusion engendered by a lack of standardization for definitions of service factors. One manufacturer may recommend a service factor of 1.5 for a particular condition while another manufacturer recommends 3.0 for the same condition. Both will be correct for their particular clutch designs because, in one case, the manufacturer may have already built-in a safety factor while the other applies it in the service factor. The wise designer will carefully follow each manufacturer's recommended selection procedures for their products, realizing that they are typically based on extensive (and expensive) testing programs as well as on field-service experience with that particular product.

A clutch even slightly too small for the applied loading will slip and overheat. A clutch too large for the load is also bad, as it adds unnecessary inertia and may overload the motor that must accelerate it. Most manufacturers of machine parts are generous in providing engineering help to properly size and specify their products for any application. The machine designer's principal concern should be to accurately define the loading and environmental conditions that the device must accommodate. This may require extensive and tedious calculations of such things as the moments of inertia for all the elements in the drive train actuated by the clutch or brake. The load-analysis methods of Chapter 3 are applicable to such a task.

CLUTCH LOCATION When a machine has both high- and low-speed shafts (as it will whenever a speed reducer is used, such as in Case Studies 7 and 8), and a clutch is needed in the system, the question immediately arises, should the clutch be placed on the low- or high-speed side of the gear reducer? Sometimes the answer is dictated by function. For example, it would make little sense to put an automotive clutch on the output shaft of the transmission instead of the input side, since in this instance the principal purpose of the clutch is to interrupt the connection between engine and transmission, *ergo*, it must go on the high-speed side. In other cases, function does not dictate the clutch location, as, for example, in Case Study 8, where the coupling on either shaft could be replaced by a clutch if it were desired to decouple the compressor from the engine. (See Figure 9-1 on p. 525.) The choice is less clear in these situations, and there are two competing schools of thought.

The torque (and any shock load) is larger on the low-speed shaft than on the high-speed shaft by the gear ratio. The power is essentially the same at both locations (neglecting losses in the gear train), but the kinetic energy at the high-speed shaft is larger by the square of the gear ratio. A clutch on the low-speed side must be larger (and thus more expensive) in order to handle the larger torque. However, a smaller and cheaper clutch on the high-speed side must dissipate the greater kinetic energy at that location and thus may more readily overheat. Some manufacturers recommend always using the high-speed side for the clutch location if function allows, opting for its better initial economy. Other clutch manufacturers suggest that the higher initial cost of the larger, low-speed clutch will be counterbalanced by lower maintenance cost in the long run. The balance of expert opinion seems to tilt toward the high-speed location with the caveat that each situation should be individually evaluated on its own merits.^[1]

17.3 CLUTCH AND BRAKE MATERIALS

Materials for the structural parts of brakes and clutches such as the disks or drums are typically made of gray cast iron or steel. The friction surfaces are usually lined with a material having a good coefficient of friction and sufficient compressive strength and temperature resistance for the application. Asbestos fiber was once the most common ingredient in brake or clutch linings, but is no longer used in many applications because of its danger as a carcinogen. Linings may be molded, woven, sintered, or of solid material. Molded linings typically use polymeric resins to bind a variety of powdered fillers or fibrous materials. Brass or zinc chips are sometimes added to improve heat conduction and wear resistance and reduce scoring of drums and disks. Woven materials typically use long asbestos fibers. Sintered metals provide higher-temperature resistance and compressive strength than molded or woven materials. Materials such as cork, wood, and cast iron are sometimes used as linings as well. Table 17-1 shows some frictional, thermal, and mechanical properties of a few friction-lining materials.

17.4 DISK CLUTCHES

The simplest disk clutch consists of two disks, one lined with a high-friction material, pressed together axially with a normal force to generate the friction force needed to transmit torque, as shown in Figure 17-7. The normal force can be supplied mechanically, pneumatically, hydraulically, or electromagnetically and is typically quite large. The pressure between the clutch surfaces can approach a uniform distribution over the surface if the disks are flexible enough. In such cases, the wear will be greater at larger diameters because wear is proportional to pressure times velocity (pV) and the velocity increases linearly with radius. However, as the disks wear preferentially toward the outside, the loss of material will change the pressure distribution to a nonuniform one and the clutch will approach a uniform wear condition of $pV = \text{constant}$. Thus the two extremes are a **uniform-pressure** and a **uniform-wear** condition. A flexible clutch may be close to a uniform-pressure condition when new, but will tend toward a uniform-wear condition with use. A rigid clutch will more rapidly approach the uniform-wear condition with use. The calculations for each condition are different, and the uniform-wear assumption gives a more conservative clutch rating, so is favored by some designers.

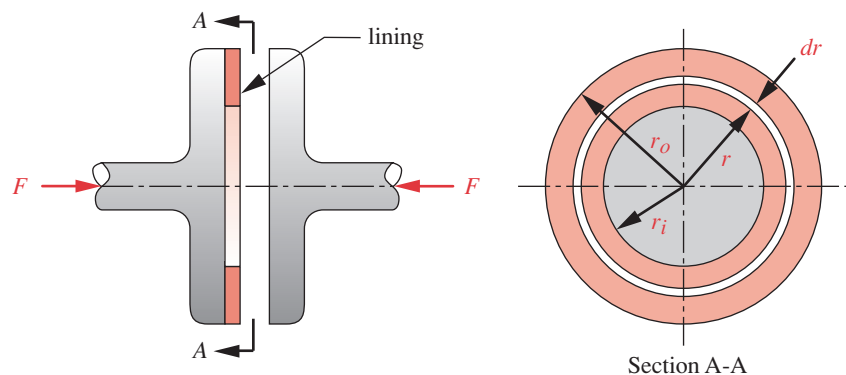


FIGURE 17-7

A Single-Surface Axial Disk Clutch

Table 17-1 Properties of Common Clutch/Brake Lining Materials

Friction Material Against Steel or CI	Dynamic Coefficient of Friction		Maximum Pressure		Maximum Temperature	
	dry	in oil	psi	kPa	°F	°C
Molded	0.25–0.45	0.06–0.09	150–300	1 030–2 070	400–500	204–260
Woven	0.25–0.45	0.08–0.10	50–100	345–690	400–500	204–260
Sintered metal	0.15–0.45	0.05–0.08	150–300	1 030–2 070	450–1 250	232–677
Cast iron or hard steel	0.15–0.25	0.03–0.06	100–250	690–720	500	260

Uniform Pressure

Consider an elemental ring of area on the clutch face of width dr as shown in Figure 17-7. The differential force acting on this ring is

$$dF = p\theta r dr \quad (17.1a)$$

where r is the radius, θ is the angle of the ring in radians and p is the uniform pressure on the clutch face. For a full circumference clutch as shown in Figure 17-7, θ will be 2π . The total axial force F on the clutch is found by integrating this expression between the limits r_i and r_o .

$$F = \int_{r_i}^{r_o} p\theta r dr = \frac{p\theta}{2} (r_o^2 - r_i^2) \quad (17.1b)$$

The friction torque on the differential ring element is

$$dT = p\theta\mu r^2 dr \quad (17.2a)$$

where μ is the coefficient of friction. The total torque for one clutch disk is

$$T = \int_{r_i}^{r_o} p\theta\mu r^2 dr = \frac{p\theta\mu}{3} (r_o^3 - r_i^3) \quad (17.2b)$$

For a multiple-disk clutch with N friction faces:

$$T = \frac{p\theta\mu}{3} (r_o^3 - r_i^3) N \quad (17.2c)$$

Equations 17.1b and 17.2c can be combined to give an expression for torque as a function of axial force.

$$T = N\mu F \frac{2}{3} \frac{(r_o^3 - r_i^3)}{(r_o^2 - r_i^2)} \quad (17.3)$$

Uniform Wear

The constant-wear rate W is assumed to be proportional to the product of pressure p and velocity V .

$$W = pV = \text{constant} \quad (17.4a)$$

And the velocity at any point on the face of the clutch is

$$V = r\omega \quad (17.4b)$$

Combine these equations, assuming a constant angular velocity ω .

$$pr = \text{constant} = K \quad (17.4c)$$

The largest pressure p_{max} must then occur at the smallest radius r_i .

$$K = p_{max}r_i \quad (17.4d)$$

Combining equations 17.4c and 17.4d gives an expression for pressure as a function of the radius r :

$$p = p_{max} \frac{r_i}{r} \quad (17.4e)$$

where the maximum allowable pressure p_{max} will vary with the lining material used. Table 17-1 shows recommended values of p_{max} and coefficients of friction for various clutch/brake lining materials.

The axial force F is found by integrating equation 17.1a for the differential force on the ring element of Figure 17-7 with equation 17.4e substituted for p .

$$F = \int_{r_i}^{r_o} p\theta r dr = \int_{r_i}^{r_o} \theta \left(p_{max} \frac{r_i}{r} \right) r dr = r_i \theta p_{max} (r_o - r_i) \quad (17.5a)$$

The torque is found by integrating equation 17.2a with the same substitution:

$$T = \int_{r_i}^{r_o} p\theta\mu r^2 dr = \frac{\theta}{2} \mu r_i p_{max} (r_o^2 - r_i^2) \quad (17.5b)$$

Combine equations 17.2a and b for an expression relating torque to axial force for the uniform-wear case:

$$T = N\mu F \frac{(r_o + r_i)}{2} \quad (17.6)$$

where N is the number of friction surfaces in the clutch.

From equations 17.5a and 17.5b, it can be shown that the maximum torque for any outside radius r_o will be obtained when the inside radius is:

$$r_i = \sqrt{1/3r_o} = 0.577r_o \quad (17.7)$$

Note that the uniform-wear assumption gives a lower torque capacity for the clutch than does the uniform-pressure assumption. The higher initial wear at the larger radii shifts the center of pressure radially inward, giving a smaller moment arm for the resultant friction force. Clutches are usually designed based on uniform wear. They will have a greater capacity when new but will end up close to the predicted design capacity after they are worn in.

EXAMPLE 17-1**Design of a Disk Clutch**

Problem Determine a suitable size and required force for an axial disk clutch.

Given The clutch must pass 7.5 hp at 1 725 rpm with a service factor of 2.

Assumptions Use a uniform-wear model. Assume a single dry disk with a molded lining.

Solution

- 1 The service factor of 2 requires derating the clutch by that factor, so we will design for 15 hp instead of 7.5. Find the torque required for that power at the design rpm.

$$T = \frac{P}{\omega} = \frac{15 \text{ hp}}{1725 \text{ rpm}} \left(\frac{6600 \frac{\text{in-lb/sec}}{\text{hp}}}{\frac{2\pi}{60} \frac{\text{rad/sec}}{\text{rpm}}} \right) = 548.05 \text{ lb-in} \quad (a)$$

- 2 Find the coefficient of friction and maximum recommended pressure for a dry, molded material from Table 17-1. Use the average of the ranges of values shown: $p_{max} = 225 \text{ psi}$ and $\mu = 0.35$.
- 3 Substitute equation 17.7 relating r_i to r_o for maximum torque into equation 17.5b to get

$$T = \pi \mu r_i p_{max} (r_o^2 - r_i^2) = \pi \mu (0.577 r_o) p_{max} \left(r_o^2 - \frac{1}{3} r_o^2 \right) = 0.3849 r_o^3 \pi \mu p_{max}$$

$$r_o = \left(\frac{T}{0.3849 \pi \mu p_{max}} \right)^{\frac{1}{3}} = \left(\frac{548.05}{0.3849 \pi (0.35)(225)} \right)^{\frac{1}{3}} = 1.79 \text{ in} \quad (b)$$

- 4 From equation 17.7:

$$r_i = 0.577 r_o = 0.577(1.79) = 1.03 \text{ in} \quad (c)$$

- 5 The axial force needed (from equation 17.5a) is:

$$F = 2\pi r_i p_{max} (r_o - r_i) = 2\pi(1.034)(225)(1.792 - 1.034) = 1108 \text{ lb} \quad (d)$$

- 6 The clutch specification is then a single disk with 3.6-in outside diameter and 2-in inside diameter, a molded lining with $\mu_{dry} \geq 0.35$, and an actuating force $\geq 1108 \text{ lb}$.
- 7 The files EX17-01 can be found on the CD-ROM.

17.5 DISK BRAKES

The disk clutch equations also apply to disk brakes. However, disk brakes are seldom made with linings covering the entire circumference of the face, because they would then overheat. Use the appropriate value of θ for the included angle of the brake pads in equa-

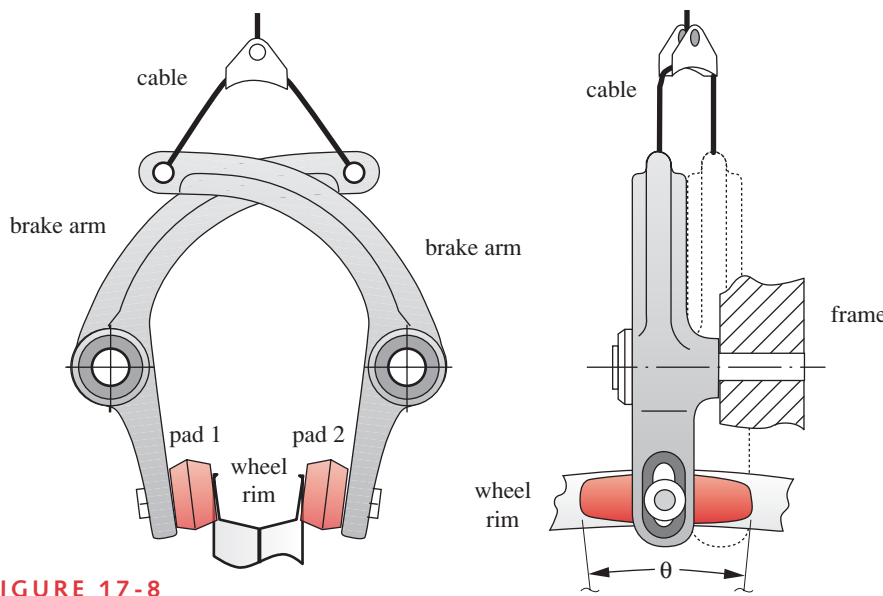


FIGURE 17-8

Bicycle Disk-Type Brake

tions 17-1 through 17-5 to calculate the force and torque in a disk brake. Note that N will be at least 2 for a disk brake as it has opposing pads in pairs as shown in Figure 17-8. While clutches are often used with light duty cycles (engagement time a small fraction of total time), brakes often must absorb large amounts of energy in repeated applications. Caliper disk brakes, such as those used on automobiles, use friction pads applied against only a small fraction of the disk circumference, leaving the rest exposed for cooling. The disk is sometimes ventilated with internal air passages to promote cooling. The caliper typically straddles the disk and contains two pads, each rubbing one side of the disk. This cancels the axial force and reduces axial loads on the bearings. The common bicycle caliper brake as shown in Figure 17-8 is another example in which the wheel rim is the disk and the calipers pinch against only a small fraction of the circumference. Disk brakes are now commonly used on automobiles, particularly on the front wheels, which provide more than half the stopping force. Some advantages of disk over drum brakes are their good controllability and linearity (braking torque is directly proportional to applied axial force).

17.6 DRUM BRAKES

Drum brakes (or clutches) apply the friction material to the circumference of a cylinder, either externally, internally, or both. These devices are more often used as brakes than as clutches. The part to which the friction material is riveted or bonded with adhesive is called the brake shoe, and the part against which it rubs, the brake drum. The shoe is forced against the drum to create the friction torque. The simplest configuration of a drum brake is the **band brake**, in which a flexible shoe is wrapped around a majority of the outer circumference of the drum and squeezed against it. Alternatively a relatively rigid, lined shoe (or shoes) can be pivoted against the outer or inner circum-

ference (or both) of the drum. If the shoe contacts only a small angular portion of the drum, it is a **short-shoe brake**, otherwise a **long-shoe brake**. The geometry of the short versus long shoe contact requires a different analytical treatment in each case. We will examine the cases of external short-shoe and external long-shoe drum brakes to illustrate their differences and features, particularly in contrast to disk brakes. The principles are the same for internal-shoe brakes as well.

Short-Shoe External Drum Brakes

Figure 17-9a shows a schematic of a short-shoe external drum brake. If the angle θ subtended by the arc of contact between shoe and drum is small (< about 45°), then we can consider the distributed force between shoe and drum to be uniform, and it can be replaced by the concentrated force F_n in the center of the contact area, as shown in Figure 17-9b. For any maximum allowable lining pressure p_{max} (Table 17-1, p. 969) the force F_n can be estimated as

$$F_n = p_{max}r\theta w \quad (17.8)$$

where w is the width of the brake shoe in the z direction and θ is the subtended angle in radians. The frictional force F_f is

$$F_f = \mu F_n \quad (17.9)$$

where μ is the coefficient of friction for the brake lining material (Table 17-1).

The torque on the brake drum is then

$$T = F_f r = \mu F_n r \quad (17.10)$$

Summing moments about point O on the free-body diagram of Figure 17-9b and substituting equation 17.9 gives

$$\sum M = 0 = aF_a - bF_n + cF_f \quad (17.11a)$$

$$F_a = \frac{bF_n - cF_f}{a} = \frac{bF_n - \mu cF_n}{a} = F_n \frac{b - \mu c}{a} \quad (17.11b)$$

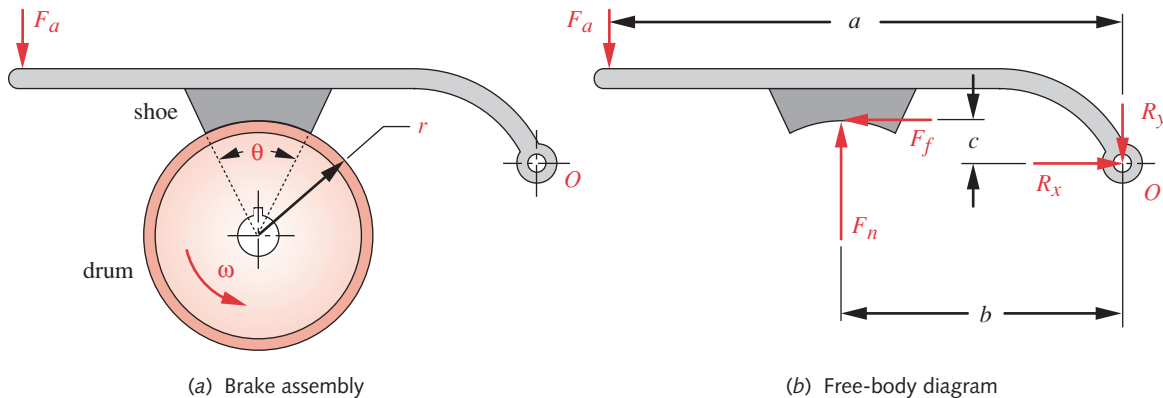


FIGURE 17-9

Geometry and Forces for a Short-Shoe External Drum Brake

The reaction forces at the pivot are found from a summation of forces.

$$\begin{aligned} R_x &= -F_f \\ R_y &= F_a - F_n \end{aligned} \quad (17.12)$$

SELF-ENERGIZING Note in Figure 17-9b that with the direction of drum rotation shown, the friction moment cF_f adds to the actuating moment aF_a . This is referred to as **self-energizing**. Once any application force F_a is applied, the friction generated at the shoe acts to increase the braking torque. However, if the brake-drum rotation is reversed from that shown in Figure 17-9a, the sign of the friction-moment term cF_f of equation 17.11a becomes negative, and the brake is then **self-deenergizing**.

This self-energizing feature of drum brakes is a potential advantage, as it reduces the required application force compared to a disk brake of the same capacity. Drum brakes typically have two shoes, one of which can be made self-energizing in each direction, or both in one direction. The latter arrangement is commonly used in automobile brakes to aid in stopping forward motion at the expense of stopping backward motion, which is normally at lower speeds.

SELF-LOCKING Note in equation 17.11 that if the brake is self-energizing and the product $\mu c \geq b$, the force F_a needed to actuate the brake becomes zero or negative. The brake is then said to be **self-locking**. If the shoe touches the drum, it will grab and lock. This is usually not a desired condition except in so-called *backstopping* applications, as were described under overrunning clutches above. In effect, a self-locking brake can function as an overrunning clutch to backstop a load and prevent it from running away if power is lost. Such brakes are sometimes used in hoists for that purpose.

EXAMPLE 17-2

Design of a Short-Shoe Drum Brake

Problem For the drum-brake arrangement shown in Figure 17-9, determine the ratio c / r that will give a self-energizing ratio F_n / F_a of 2. Also find the c / r ratio that will cause self-locking.

Given The dimensions are $a = b = 6$, $r = 5$.

Assumptions Coefficient of friction $\mu = 0.35$.

Solution* See Figure 17-9.

- Rearrange equation 17.11 to form the desired ratio.

$$\frac{F_n}{F_a} = \frac{a}{b - \mu c} \quad (a)$$

- Substitute the desired self-energizing ratio, the given dimensions, and solve for c .

$$\begin{aligned} \frac{F_n}{F_a} &= 2 = \frac{6}{6 - 0.35c} \\ c &= \frac{-3}{-0.35} = 8.571 \end{aligned} \quad (b)$$

- 3 Form the c / r ratio for a self-energizing ratio of 2 with the given brake geometry.

$$\frac{c}{r} = \frac{8.571}{5} = 1.71 \quad (c)$$

- 4 For self-locking to begin, F_a becomes zero, making $F_n / F_a = \infty$ and $F_a / F_n = 0$. The second of these ratios will need to be used to avoid division by zero. Rearrange equation 17.11 to form the desired ratio and solve for c .

$$\begin{aligned} \frac{F_a}{F_n} &= \frac{b - \mu c}{a} = \frac{6 - 0.35c}{6} = 0 \\ c &= 17.143 \end{aligned} \quad (d)$$

- 5 Form the c / r ratio for self-locking with the given brake geometry.

$$\frac{c}{r} = \frac{17.143}{5} = 3.43 \quad (e)$$

- 6 Note that these ratios are specific to the dimensions of the brake. The length a was set equal to b in this example in order to eliminate the effect of the lever arm ratio a / b , which further reduces the application force F_a required for any normal force F_n .

Long-Shoe External Drum Brakes

If the angle of contact θ between shoe and drum in Figure 17-9 exceeds about 45° , then the assumption of uniform pressure distribution over the shoe surface will be inaccurate. Most drum brakes have contact angles of 90° or more, so a more accurate analysis than the short-shoe assumption is needed. Since any real brake shoe will not be infinitely rigid, its deflections will affect the pressure distribution. An analysis that accounts for deflection effects is very complicated and is not really warranted here. As the shoe wears, it will pivot about point O in Figure 17-10, and point B will travel farther than point A because of its greater distance from O . The pressure at any point on the shoe will also vary in proportion to its distance from O . Assume that the drum turns

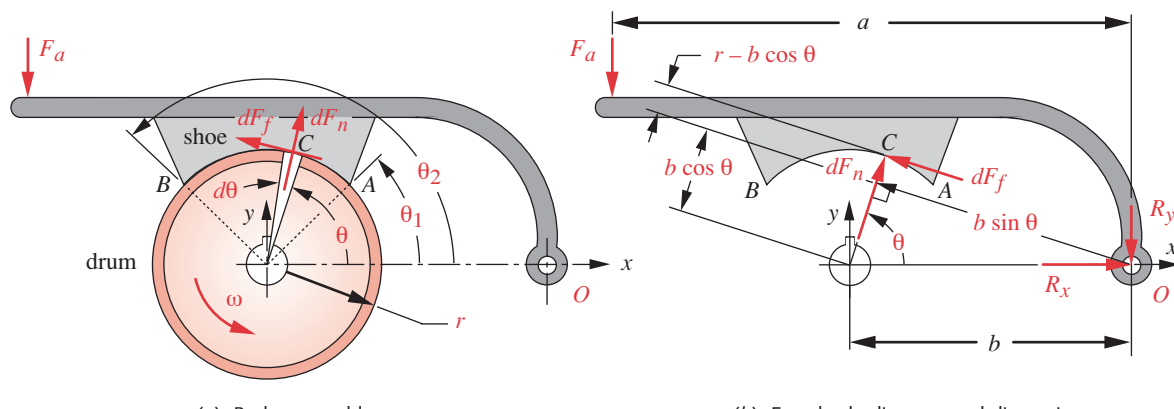


FIGURE 17-10

Geometry and Forces for a Long-Shoe External Drum Brake

at constant velocity and that wear is proportional to the friction work done, i.e., the product pV . Then, at any arbitrary point on the shoe, such as C in Figure 17-10, the normal pressure p will be proportional to its distance from point O .

$$p \propto b \sin \theta \propto \sin \theta \quad (17.13a)$$

Since the distance b is constant, the normal pressure at any point is just proportional to $\sin \theta$. Call its constant of proportionality K .

$$p = K \sin \theta \quad (17.13b)$$

If the maximum allowable pressure for the lining material is p_{max} (Table 17-1, p. 969) then the constant K can be defined as

$$K = \frac{p}{\sin \theta} = \frac{p_{max}}{\sin \theta_{max}} \quad (17.13c)$$

where θ_{max} is the smaller of θ_2 and 90° . Then

$$p = \frac{p_{max}}{\sin \theta_{max}} \sin \theta \quad (17.13d)$$

Equation 17.13d defines the normal pressure at any point on the shoe and it varies as $\sin \theta$, since p_{max} and θ_2 are constant for any particular brake. Thus, the friction force is small at small θ , is optimum at $\theta = 90^\circ$, and diminishes at angles larger than 90° . Little is gained by using $\theta_1 < 10^\circ$ or $\theta_2 > 120^\circ$.

To obtain the total force on the shoe, the pressure function must be integrated over the angular range of the shoe. Consider the differential element $d\theta$ shown in Figure 17-9. Two differential forces act on it, dF_n and dF_f . They have respective moment arms about point O of $b \sin \theta$ and $r - b \cos \theta$, as shown in Figure 17-10b. Integrating to create their moments about O for the entire surface gives, for the moment due to the normal force:

$$\begin{aligned} M_{F_n} &= \int_{\theta_1}^{\theta_2} pwr d\theta b \sin \theta = \int_{\theta_1}^{\theta_2} wrb p \sin \theta d\theta \\ &= \int_{\theta_1}^{\theta_2} wrb \frac{p_{max}}{\sin \theta_{max}} \sin^2 \theta d\theta \\ M_{F_n} &= wrb \frac{p_{max}}{\sin \theta_{max}} \left[\frac{1}{2}(\theta_2 - \theta_1) - \frac{1}{4}(\sin 2\theta_2 - \sin 2\theta_1) \right] \end{aligned} \quad (17.14a)$$

where w is the drum width in the z direction and the other variables are as defined in Figure 17-10. For the moment due to the frictional force:

$$\begin{aligned} M_{F_f} &= \int_{\theta_1}^{\theta_2} \mu pwr d\theta (r - b \cos \theta) \\ &= \int_{\theta_1}^{\theta_2} \mu wr \frac{p_{max}}{\sin \theta_{max}} \sin \theta (r - b \cos \theta) d\theta \\ M_{F_f} &= \mu wr \frac{p_{max}}{\sin \theta_{max}} \left[-r(\cos \theta_2 - \cos \theta_1) - \frac{b}{2}(\sin^2 \theta_2 - \sin^2 \theta_1) \right] \end{aligned} \quad (17.14b)$$

Summing moments about point O gives

$$F_a = \frac{M_{F_n} \mp M_{F_f}}{a} \quad (17.14c)$$

where the upper sign is for a self-energizing brake and the lower one for a self-deenergizing brake. Self-locking can occur only if the brake is self-energizing and $M_{F_f} > M_{F_n}$.

The torque for the brake is found by integrating the expression for the product of the friction force F_f and drum radius r .

$$\begin{aligned} T &= \int_{\theta_1}^{\theta_2} \mu pwr d\theta r \\ &= \int_{\theta_1}^{\theta_2} \mu wr^2 \frac{p_{max}}{\sin \theta_{max}} \sin \theta d\theta \\ T &= \mu wr^2 \frac{p_{max}}{\sin \theta_{max}} (\cos \theta_1 - \cos \theta_2) \end{aligned} \quad (17.15)$$

The reaction forces R_x and R_y are found by summing forces in the x and y directions (see Figure 17-10b):

$$\begin{aligned} R_x &= \int \cos \theta dF_n + \int \sin \theta dF_f \\ &= \int_{\theta_1}^{\theta_2} wrp \cos \theta d\theta + \mu \int_{\theta_1}^{\theta_2} wrp \sin \theta d\theta \\ &= \int_{\theta_1}^{\theta_2} wr \frac{p_{max}}{\sin \theta_{max}} \sin \theta \cos \theta d\theta + \mu \int_{\theta_1}^{\theta_2} wr \frac{p_{max}}{\sin \theta_{max}} \sin^2 \theta d\theta \\ R_x &= wr \frac{p_{max}}{\sin \theta_{max}} \left\{ \begin{array}{l} -\left(\frac{\sin^2 \theta_2}{2} - \frac{\sin^2 \theta_1}{2} \right) \\ + \mu \left[\frac{1}{2}(\theta_2 - \theta_1) - \frac{1}{4}(\sin 2\theta_2 - \sin 2\theta_1) \right] \end{array} \right\} \end{aligned} \quad (17.16a)$$

$$\begin{aligned} R_y &= \int \cos \theta dF_f + \int \sin \theta dF_n - F_a \\ &= \int_{\theta_1}^{\theta_2} \mu wr \frac{p_{max}}{\sin \theta_{max}} \sin \theta \cos \theta d\theta + \int_{\theta_1}^{\theta_2} \mu wr \frac{p_{max}}{\sin \theta_{max}} \sin^2 \theta d\theta - F_a \\ R_y &= wr \frac{p_{max}}{\sin \theta_{max}} \left\{ \begin{array}{l} -\mu \left(\frac{\sin^2 \theta_2}{2} - \frac{\sin^2 \theta_1}{2} \right) \\ + \left[\frac{1}{2}(\theta_2 - \theta_1) - \frac{1}{4}(\sin 2\theta_2 - \sin 2\theta_1) \right] \end{array} \right\} - F_a \end{aligned} \quad (17.16b)$$

EXAMPLE 17-3**Design of a Long-Shoe Drum Brake**

Problem For the drum-brake arrangement shown in Figure 17-10, determine the friction torque T , application force F_a , and reaction forces R_x, R_y .

Given The dimensions are $a = 180 \text{ mm}$, $b = 90 \text{ mm}$, $r = 100 \text{ mm}$, $w = 30 \text{ mm}$, $\theta_1 = 30^\circ$, $\theta_2 = 120^\circ$, $\theta_{max} = 90^\circ$.

Assumptions Coefficient of friction $\mu = 0.35$, maximum lining pressure $p_{max} = 1.5 \text{ MPa}$, and the brake is self-energizing.

Solution See Figure 17-10.

- 1 Convert the given angles θ_1 and θ_2 to radians: $\theta_1 = 0.524 \text{ rad}$, $\theta_2 = 2.094 \text{ rad}$.
- 2 Calculate the moment M_{F_n} about O due to the normal force using equation 17.14a.

$$\begin{aligned} M_{F_n} &= wrb \frac{p_{max}}{\sin \theta_{max}} \left[\frac{1}{2}(\theta_2 - \theta_1) - \frac{1}{4}(\sin 2\theta_2 - \sin 2\theta_1) \right] \\ &= 30(100)(90) \frac{1.5}{\sin(1.57)} \left[\frac{1}{2}(2.094 - 0.524) \right. \\ &\quad \left. - \frac{1}{4}(\sin\{2(2.094)\} - \sin\{2(0.524)\}) \right] \\ &= 493 \text{ N} \cdot \text{m} \end{aligned} \quad (a)$$

- 3 Calculate the moment M_{F_f} about O due to the friction force using equation 17.14b.

$$\begin{aligned} M_{F_f} &= \mu wr \frac{p_{max}}{\sin \theta_{max}} \left[-r(\cos \theta_2 - \cos \theta_1) - \frac{b}{2}(\sin^2 \theta_2 - \sin^2 \theta_1) \right] \\ &= 0.35(30)(100) \frac{1.5}{\sin(1.57)} \left[-100(\cos\{2.094\} - \cos\{0.524\}) \right. \\ &\quad \left. - \frac{90}{2}(\sin^2\{2.094\} - \sin^2\{0.524\}) \right] \\ &= 180 \text{ N} \cdot \text{m} \end{aligned} \quad (b)$$

- 4 Find the application force from equation 17.14c.

$$F_a = \frac{M_{F_n} \mp M_{F_f}}{a} = \frac{497 - 181}{0.180} = 1743 \text{ N} \quad (c)$$

- 5 Find the friction torque from equation 17.15.

$$\begin{aligned} T_f &= \mu wr^2 \frac{p_{max}}{\sin \theta_{max}} (\cos \theta_1 - \cos \theta_2) \\ &= 0.35(30)(100)^2 \frac{1.5}{\sin(1.57)} (\cos\{2.094\} - \cos\{0.524\}) \\ &= 215 \text{ N} \cdot \text{m} \end{aligned} \quad (d)$$

- 6 The reaction forces are found from equations 17.16.

$$\begin{aligned}
 R_x &= wr \frac{p_{max}}{\sin \theta_{max}} \left\{ \left(\frac{\sin^2 \theta_2}{2} - \frac{\sin^2 \theta_1}{2} \right) + \mu \left[\frac{1}{2}(\theta_2 - \theta_1) - \frac{1}{4}(\sin 2\theta_2 - \sin 2\theta_1) \right] \right\} \\
 &= 30(100) \frac{1.5}{\sin(1.57)} \left\{ \left(\frac{\sin^2 \{2.094\}}{2} - \frac{\sin^2 \{0.524\}}{2} \right) - 0.35 \left[\frac{1}{2}(2.094 - 0.524) - \frac{1}{4}(\sin \{2(2.094)\} - \sin \{2(0.524)\}) \right] \right\} \\
 &= 794 \text{ N} \tag{e}
 \end{aligned}$$

$$\begin{aligned}
 R_y &= -F_a + wr \frac{p_{max}}{\sin \theta_{max}} \left\{ -\mu \left(\frac{\sin^2 \theta_2}{2} - \frac{\sin^2 \theta_1}{2} \right) + \left[\frac{1}{2}(\theta_2 - \theta_1) - \frac{1}{4}(\sin 2\theta_2 - \sin 2\theta_1) \right] \right\} \\
 &= -2013 + 30(100) \frac{1.5}{\sin(1.57)} \left\{ -0.35 \left(\frac{\sin^2 \{2.094\}}{2} - \frac{\sin^2 \{0.524\}}{2} \right) + \left[\frac{1}{2}(2.094 - 0.524) - \frac{1}{4}(\sin \{2(2.094)\} - \sin \{2(0.524)\}) \right] \right\} \\
 &R_y = 4134 \text{ N} \tag{f}
 \end{aligned}$$

7 The files EX17-03 can be found on the CD-ROM.

Long-Shoe Internal Drum Brakes

Most drum brakes (and virtually all automotive ones) use internal shoes that expand against the inside of the drum. Typically two shoes are used, pivoted against the ends of an adjusting screw and forced against the drum by a double-ended hydraulic cylinder. Light springs hold the shoes against the pistons of the wheel cylinder and pull the shoes away from the drum when not activated. Typically, one shoe is self-energizing in the forward direction and the other is self-energizing in the reverse direction of drum rotation. The automobile wheel attaches directly to the brake drum. The analysis of an internal-shoe brake is the same as that of an external-shoe one.

17.7 SUMMARY

Clutches and brakes are used extensively in all kinds of machinery. Vehicles all need brakes to stop their motion, as do many stationary machines. Clutches are needed to interrupt the flow of power from a prime mover (motor, engine, etc.) to the load so the

load can be stopped (by a brake) and the prime mover continue running. A clutch and a brake are essentially the same device, the principal difference being that both sides of a clutch (input and output) are capable of rotation, but the output side of a brake is fixed to some nonrotating "ground plane," which itself may have some other motion, as in the case of an automobile chassis.

Many different styles of clutches/brakes are made, but the most common style uses frictional contact between two or more surfaces to couple the input and output sides together. The friction surfaces can be moved into and out of engagement by any of several means including direct mechanical, electromagnetic, pneumatic, hydraulic, or combinations thereof. Other styles include direct magnetic (magnetic particle, hysteresis, and eddy current), some of which have no mechanical contact (and thus zero drag) when disengaged, and fluid couplings, which are commonly used to couple vehicle engines to automatic transmissions.

Except for high-volume, specialized applications such as vehicle design, a machine designer seldom designs a clutch or brake from scratch. For the typical machine-design application, one usually selects a commercially available clutch or brake assembly from the many manufacturers' offerings. The design problem then becomes one of properly defining the torque, speed, and power requirements and the character of the load, whether smooth or shocky, continuous or intermittent, etc. The inertia of the rotating elements to be accelerated by a clutch or decelerated by a brake can have a significant effect on the required size of that device and must be carefully calculated. Any gear ratios present in the system will cause the reflected or effective inertia to vary as the square of the gear ratio and this effect must be carefully included when calculating the inertia. (See Chapter 3 or any text on dynamics of machinery.)

The clutch/brake manufacturers' catalogs contain extensive engineering data that rate each device on its torque and power capacity and also suggest empirical derating factors for situations with shock loads, high duty cycles, etc. Once the loading is well defined, a suitable device can be specified using the manufacturers' rating data modified by their suggested service factors. The designer's (nontrivial) task then becomes that of proper load definition for the application, followed by proper use of the manufacturers' rating data. Engineering assistance is usually available from the manufacturer for the latter task, but the result can be only as suitable to the design requirements as the accuracy of the load analysis allows. The mechanical configurations of several clutch designs are briefly described within this chapter. Manufacturers' catalogs and applications engineers can provide more detailed information on the capabilities and limitations of the various clutch/brake styles.

Commercial friction clutches and brakes are most often made in a single- or multiple-disk configuration. Vehicle brakes are typically made in either disk or drum configurations. Disk configurations provide a friction torque that is linearly proportional to the applied actuating force, and this can be an advantage from a control standpoint. Drum configurations can be designed to be self-energizing, meaning that once the brake or clutch is initially engaged, the friction force tends to increase the normal force, thus nonlinearly increasing the friction torque in a positive feedback fashion. This can be an advantage when braking large loads, as it decreases the required application force but it makes control of braking torque more difficult. The analysis of both friction disk devices and friction drum devices is developed in this chapter.

Clutches and brakes are essentially energy-transfer or energy-dissipation devices and as such generate a great deal of heat in operation. They must be designed to absorb and transfer this heat without damage to themselves or their surroundings. Often, the heat-transfer ability of a device rather than its mechanical torque-transmission ability limits its capacity. The thermal design of clutches and brakes is a very important consideration, but it goes beyond the scope of this text and space does not permit its treatment here. Nevertheless, the designer needs to be aware of the heat transfer aspect of clutch/brake design and take it into account. See any text on heat transfer for the theoretical background and see the references mentioned in the bibliography to this chapter as well as other manufacturers' catalogs for more specific information.

Friction clutches may be operated either dry or wet (typically in oil). Dry friction is obviously more effective, as the coefficient of friction is severely reduced with lubrication. However, running in oil can significantly improve the heat transfer situation especially when the oil is circulated and/or cooled. More friction surfaces (e.g., multiple disks) are needed to achieve the same torque capacity wet that can be obtained with a single dry disk, but the trade-off can be positive because of enhanced cooling. Modern vehicle automatic transmissions use many internal clutches and brakes to interconnect or stop various members of their epicyclic (planetary) gear trains in order to shift among gear ratios. These are either multidisk clutches or band brakes and are run immersed in the transmission oil that is continuously circulated through a heat exchanger in the vehicle's radiator for cooling.

Important Equations Used in This Chapter

Torque in a Disk Clutch with Uniform Pressure (Section 17.4):

$$T = N\mu F \frac{2}{3} \frac{(r_o^3 - r_i^3)}{(r_o^2 - r_i^2)} \quad (17.3)$$

Torque in a Disk Clutch with Uniform Wear (Section 17.4):

$$T = N\mu F \frac{(r_o + r_i)}{2} \quad (17.6)$$

Forces and Torque on a Short-Shoe Drum Brake (Section 17.6):

$$F_n = p_{max}r\theta w \quad (17.8)$$

$$F_a = \frac{bF_n - cF_f}{a} = \frac{bF_n - \mu cF_n}{a} = F_n \frac{b - \mu c}{a} \quad (17.11b)$$

$$T = F_f r = \mu F_n r \quad (17.10)$$

Forces and Torque on a Long-Shoe Drum Brake (Section 17.6):

$$M_{F_n} = wrb \frac{p_{max}}{\sin \theta_{max}} \left[\frac{1}{2} (\theta_2 - \theta_1) - \frac{1}{4} (\sin 2\theta_2 - \sin 2\theta_1) \right] \quad (17.14a)$$

$$M_{F_f} = \mu wr \frac{P_{max}}{\sin \theta_{max}} \left[-r(\cos \theta_2 - \cos \theta_1) - \frac{b}{2} (\sin^2 \theta_2 - \sin^2 \theta_1) \right] \quad (17.14b)$$

$$F_a = \frac{M_{F_n} \mp M_{F_f}}{a} \quad (17.14c)$$

$$T = \mu wr^2 \frac{P_{max}}{\sin \theta_{max}} (\cos \theta_1 - \cos \theta_2) \quad (17.15)$$

$$R_x = wr \frac{P_{max}}{\sin \theta_{max}} \left\{ \begin{aligned} & - \left(\frac{\sin^2 \theta_2}{2} - \frac{\sin^2 \theta_1}{2} \right) \\ & + \mu \left[\frac{1}{2} (\theta_2 - \theta_1) - \frac{1}{4} (\sin 2\theta_2 - \sin 2\theta_1) \right] \end{aligned} \right\} \quad (17.16a)$$

$$R_y = wr \frac{P_{max}}{\sin \theta_{max}} \left\{ \begin{aligned} & - \mu \left(\frac{\sin^2 \theta_2}{2} - \frac{\sin^2 \theta_1}{2} \right) \\ & + \left[\frac{1}{2} (\theta_2 - \theta_1) - \frac{1}{4} (\sin 2\theta_2 - \sin 2\theta_1) \right] \end{aligned} \right\} - F_a \quad (17.16b)$$

17.8 REFERENCES

- 1 J. Proctor, "Selecting Clutches for Mechanical Drives," *Product Engineering*, pp. 43–58, June 19, 1961.

17.9 BIBLIOGRAPHY

Mechanical Drives Reference Issue. Penton Publishing: Cleveland, Ohio,

Deltran, *Electromagnetic Clutches and Brakes*. American Precision Industries: Buffalo, N.Y., 716-631-9800.

Logan, *Multiple Disk Clutches and Brakes*. Logan Clutch Co.: Cleveland, Ohio, 216-431-4040.

Magtrol, *Hysteresis Brakes and Clutches*. Magtrol: Buffalo, N.Y., 800-828-7844.

MCC, *Catalog 18e*. Machine Components Corporation: Plainview, NY, 516-694-7222.

MTL, *Eddy Current Clutch Design*. Magnetic Technologies Ltd.: Oxford, Mass., 508-987-3303.

W. C. Orthwein, *Clutches and Brakes: Design and Selection*. Marcel Dekker: New York, 1986.

Placid, *Magnetic Particle Clutches and Brakes*. Placid Industries Inc.: Lake Placid, N.Y., 518-523-2422.

Warner, *Clutches, Brakes, and Controls: Master Catalog*. Warner Electric: South Beloit, Ill., 815-389-2582.

17.10 PROBLEMS

- *17-1 Find the torque that a 2-surface, dry disk clutch can transmit if the outside and inside lining diameters are 120 mm and 70 mm, respectively, and the applied axial force is 10 kN. Assume uniform wear and $\mu = 0.4$. Is the pressure on the lining acceptable? What lining material(s) would be suitable?
- 17-2 Repeat Problem 17-1 assuming uniform pressure.
- *17-3 Design a single-surface disk clutch to transmit 100 N·m of torque at 750 rpm using a molded lining with a maximum pressure of 1 MPa and $\mu = 0.25$. Assume uniform wear. Find the outside and inside diameters required if $r_i = 0.577r_o$. What is the power transmitted?
- [†]17-4 Repeat Problem 17-3 assuming uniform pressure.
- *17-5 How many surfaces are needed in a wet disk clutch to transmit 120 N·m of torque at 1 000 rpm using a sintered lining with a maximum pressure of 1.8 MPa and $\mu = 0.06$? Assume uniform wear. Find the outside and inside diameters required if $r_i = 0.577r_o$. How many disks are needed? What is the power transmitted?
- 17-6 Repeat Problem 17-5 assuming uniform pressure.
- *17-7 Figure P17-1 shows a single short-shoe drum brake. Find its torque capacity and required actuating force for $a = 100$, $b = 70$, $e = 20$, $r = 30$, $w = 50$ mm, and $\theta = 35^\circ$. What value of c will make it self-locking? Assume $p_{max} = 1.3$ MPa and $\mu = 0.3$.
- 17-8 Repeat Problem 17-7 with the drum rotating clockwise.
- 17-9 Figure P17-1 shows a single short-shoe drum brake. Find its torque capacity and required actuating force for $a = 8$, $b = 6$, $e = 4$, $r = 5$, $w = 1.5$ in, and $\theta = 30^\circ$. What value of c will make it self-locking? Assume $p_{max} = 250$ psi and $\mu = 0.35$.
- 17-10 Repeat Problem 17-9 with the drum rotating clockwise.
- *17-11 Figure P17-2 shows a double short-shoe drum brake. Find its torque capacity and required actuating force for $a = 90$, $b = 80$, $e = 30$, $r = 40$, $w = 60$ mm, and $\theta = 25^\circ$. What value of c will make it self-locking? Assume $p_{max} = 1.5$ MPa and $\mu = 0.25$. Hint: Calculate the effects of each shoe separately and superpose them.
- 17-12 Figure P17-2 shows a double short-shoe drum brake. Find its torque capacity and required actuating force for $a = 12$, $b = 8$, $e = 3$, $r = 6$ in, and $\theta = 25^\circ$. What value of c

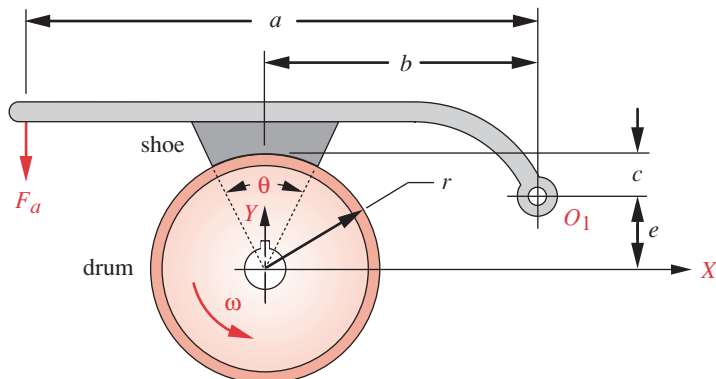


FIGURE P17-1

Geometry for a Short-Shoe External Drum Brake

Table P17-0[†]

Topic/Problem Matrix

17.4 Disk Clutches

17-1, 17-2, 17-3, 17-4, 17-5,
17-6, 17-27, 17-28

17.5 Disk Brakes

17-29, 17-30, 17-31,
17-32, 17-33, 17-34

17.6 Drum Brakes

Short Shoe

17-7, 17-8, 17-9, 17-10, 17-11,
17-12, 17-21, 17-22

Long Shoe

17-13, 17-14, 17-15, 17-16,
17-17, 17-18, 17-19, 17-20,
17-23, 17-24, 17-25, 17-26

* Answers to these problems are provided in Appendix D.

[†] Problem numbers in *italics* are design problems.

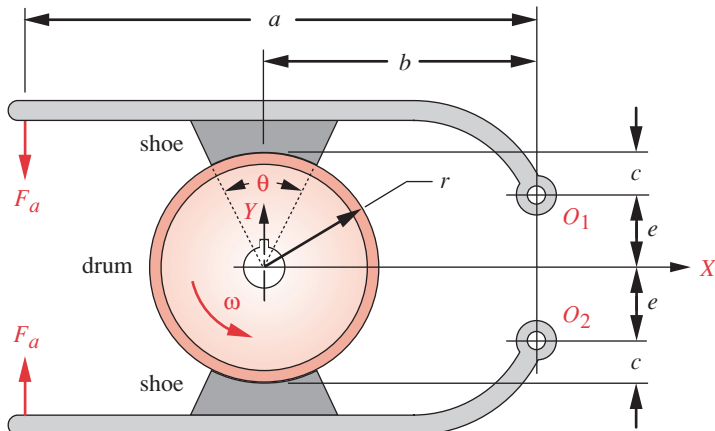


FIGURE P17-2

Geometry for a Double Short-Shoe External Drum Brake

will make it self-locking? Assume $p_{max} = 200$ psi, width = 2 in, and $\mu = 0.28$. Hint: Calculate the effects of each shoe separately and superpose them.

- *17-13 Figure P17-3 shows a single long-shoe drum brake. Find its torque capacity and required actuating force for $a_X = 100$, $b_X = 70$, $b_Y = 20$, $r = 30$, $w = 50$ mm, and $\theta_1 = 25^\circ$, $\theta_2 = 125^\circ$. Assume $p_{max} = 1.3$ MPa and $\mu = 0.3$.
- 17-14 Figure P17-3 shows a single long-shoe drum brake. Find its torque capacity and required actuating force for $a_X = 8$, $b_X = 6$, $b_Y = 4$, $r = 5$, $w = 1.5$ in, and $\theta_1 = 35^\circ$, $\theta_2 = 155^\circ$. Assume $p_{max} = 250$ psi and $\mu = 0.35$.
- *17-15 Figure P17-4 shows a double long-shoe drum brake. Find its torque capacity and required actuating force for $a_X = 90$, $b_X = 80$, $b_Y = 30$, $r = 40$, $w = 30$ mm, and $\theta_1 = 30^\circ$, $\theta_2 = 160^\circ$. Assume $p_{max} = 1.5$ MPa and $\mu = 0.25$. Hint: Calculate the effects of each shoe separately and superpose them.
- 17-16 Figure P17-4 shows a double long-shoe drum brake. Find its torque capacity and required actuating force for $a_X = 12$, $b_X = 8$, $b_Y = 3$, $r = 6$, $w = 2$ in, and $\theta_1 = 25^\circ$, $\theta_2 = 145^\circ$. Assume $p_{max} = 200$ psi and $\mu = 0.28$. Hint: Calculate the effects of each shoe separately and superpose them.

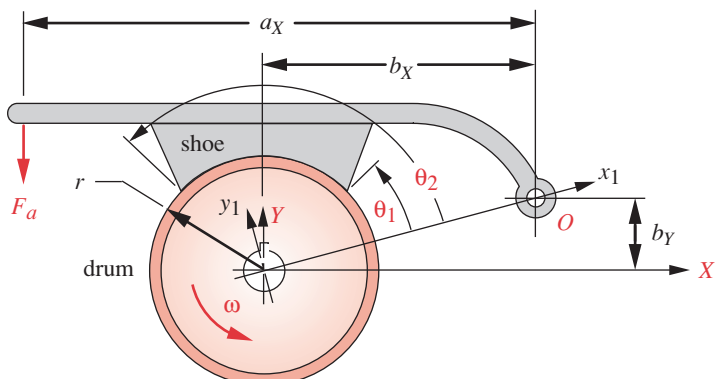
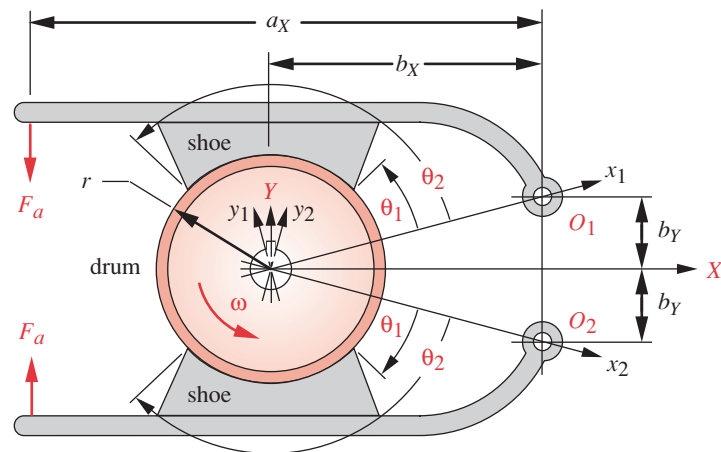


FIGURE P17-3

Geometry for a Long-Shoe External Drum Brake

* Answers to these problems are provided in Appendix D.

**FIGURE P17-4**

Geometry for a Double Long-Shoe External Drum Brake

- *17-17 The short-shoe approximation is considered to be valid for brake shoes with an included angle of up to about 45° . For the brake shown in Figure P17-3, calculate its torque capacity and required force by both the short-shoe method and the long-shoe method and compare the results for the following data: $a_X = 90$, $b_X = 80$, $b_Y = 30$, $r = 40$, $w = 30$ mm. Assume $p_{max} = 1.5$ MPa and $\mu = 0.25$. Note that $\theta = \theta_2 - \theta_1$ for the short-shoe approximation.
- $\theta_1 = 75^\circ$, $\theta_2 = 105^\circ$.
 - $\theta_1 = 70^\circ$, $\theta_2 = 110^\circ$.
 - $\theta_1 = 65^\circ$, $\theta_2 = 115^\circ$.
- *17-18 Repeat Problem 17-17 for the brake design shown in Figure P17-4.
- 17-19 The short-shoe approximation is considered to be valid for brake shoes with an included angle of up to about 45° . For the brake shown in Figure P17-3, calculate its torque capacity and required force by both the short-shoe method and the long-shoe method and compare the results for the following data: $a_X = 8$, $b_X = 6$, $b_Y = 4$, $r = 5$, $w = 2$ in. Assume $p_{max} = 250$ psi and $\mu = 0.35$. Note that $\theta = \theta_2 - \theta_1$ for the short-shoe approximation.
- $\theta_1 = 75^\circ$, $\theta_2 = 105^\circ$.
 - $\theta_1 = 70^\circ$, $\theta_2 = 110^\circ$.
 - $\theta_1 = 65^\circ$, $\theta_2 = 115^\circ$.
- 17-20 Repeat Problem 17-19 for the brake design shown in Figure P17-4.
- *17-21 Find the reaction forces at the arm pivot in the global XY system for the brake of Problem 17-11.
- 17-22 Find the reaction forces at the arm pivot in the global XY system for the brake of Problem 17-12.
- *17-23 Find the reaction forces at the arm pivot in the global XY system for the brake of Problem 17-13.
- 17-24 Find the reaction forces at the arm pivot in the global XY system for the brake of Problem 17-14.

* Answers to these problems are provided in Appendix D.

- *17-25 Find the reaction forces at the arm pivot in the global XY system for the brake of Problem 17-15.
- 17-26 Find the reaction forces at the arm pivot in the global XY system for the brake of Problem 17-16.
- [†]17-27 A clutch is needed for an electric motor that transmits 20 kW at 1 100 rpm. The clutch will attach directly to the motor housing faceplate and is to have the same housing diameter as the motor, which is 125 mm. The minimum radial clearance between the housing *OD* and the clutch disk *OD* is 5 mm. The clutch output shaft will have the same diameter as the motor shaft, which is 15 mm. Design a multiple disk clutch for this application. State all assumptions and design choices. Specify the clutch material, outside disk radius, inside disk radius, and the required actuation force.
- 17-28 A clutch is needed for an electric motor that transmits 25 hp at 800 rpm. The clutch will attach directly to the motor housing faceplate and is to have the same housing diameter as the motor, which is 5.5 in. The minimum radial clearance between the housing *OD* and the clutch disk *OD* is 0.25 in. The clutch output shaft will have the same diameter as the motor shaft, which is 0.625 in. Design a multiple disk clutch for this application. State all assumptions and design choices. Specify the clutch material, outside disk radius, inside disk radius, and the required actuation force.
- *17-29 Find the torque that a dual-pad, caliper disc brake with pad angle of 60deg can transmit if the outside and inside lining diameters are 160 mm and 90 mm, respectively, and the applied axial force is 3 kN. Assume uniform wear and $m = 0.35$. Is the pressure on the lining acceptable? What lining materials would be suitable?
- 17-30 Repeat Problem 17-29 assuming uniform pressure.
- ^{*}17-31 Design a dual-pad caliper disc brake to provide a braking force of 240 N at the periphery of a 750-mm-dia wheel that is rotating at 670 rpm. Use an inside radius to outside radius ratio of 0.577. Assume uniform wear. State all assumptions and design choices. Specify the brake material, outside pad radius, inside pad radius, pad angle, and the required actuation force.
- 17-32 Repeat Problem 17-31 assuming uniform pressure.
- 17-33 An ultra-light solar racecar weighs 500 lb with driver. It has two 20-in-dia bicycle wheels in front that are to have dual-pad caliper disk brakes on each wheel. The brakes must be capable of bringing the car to a stop in a distance of 150 feet from a speed of 45 mph. Neglecting aerodynamic and rolling resistance forces, design dual-pad caliper disc brakes for the car. Use an inside radius to outside radius ratio of 0.577. Assume uniform wear. State all assumptions and design choices. Specify the brake material, outside pad radius, inside pad radius, pad angle, and the required actuation force.
- 17-34 Repeat Problem 17-33 assuming uniform pressure.

* Answers to these problems are provided in Appendix D.

[†] Problem numbers in *italics* are design problems.

Appendix A

MATERIAL PROPERTIES

The following tables contain approximate values for strengths and other specifications of a variety of engineering materials compiled from various sources. In some cases the data are minimum recommended values and in other cases they are from a single test specimen. These data are suitable for use in the engineering exercises contained in this text, but should not be considered as statistically valid representations of specifications for any particular alloy or material. The designer should consult the materials' manufacturers for more accurate and up-to-date strength information on materials used in engineering applications, or conduct independent tests of the selected materials to determine their ultimate suitability to any application.

Much more information on material properties is available on the world-wide-web. Some sites are:

<http://www.matweb.com>
<http://metals.about.com>

Table No.	Description
A-1	Physical Properties of Some Engineering Materials
A-2	Mechanical Properties for Some Wrought-Aluminum Alloys
A-3	Mechanical Properties for Some Aluminum Casting Alloys
A-4	Mechanical Properties for Some Wrought- and Cast-Copper Alloys
A-5	Mechanical Properties for Some Titanium Alloys
A-6	Mechanical Properties for Some Magnesium Alloys
A-7	Mechanical Properties for Some Cast Iron Alloys
A-8	Mechanical Properties for Some Stainless Steel Alloys
A-9	Mechanical Properties for Some Carbon Steels
A-10	Mechanical Properties for Some Alloy and Tool Steels
A-11	Mechanical Properties for Some Engineering Plastics

Table A-1 Physical Properties of Some Engineering Materials

Data from Various Sources.* These Properties Are Essentially Similar for All Alloys of the Particular Material

Material	Modulus of Elasticity <i>E</i>		Modulus of Rigidity <i>G</i>		Poisson's Ratio <i>v</i>	Weight Density <i>γ</i>	Mass Density <i>ρ</i>	Specific Gravity
	Mpsi	GPa	Mpsi	GPa				
Aluminum Alloys	10.4	71.7	3.9	26.8	0.34	0.10	2.8	2.8
Beryllium Copper	18.5	127.6	7.2	49.4	0.29	0.30	8.3	8.3
Brass, Bronze	16.0	110.3	6.0	41.5	0.33	0.31	8.6	8.6
Copper	17.5	120.7	6.5	44.7	0.35	0.32	8.9	8.9
Iron, Cast, Gray	15.0	103.4	5.9	40.4	0.28	0.26	7.2	7.2
Iron, Cast, Ductile	24.5	168.9	9.4	65.0	0.30	0.25	6.9	6.9
Iron, Cast, Malleable	25.0	172.4	9.6	66.3	0.30	0.26	7.3	7.3
Magnesium Alloys	6.5	44.8	2.4	16.8	0.33	0.07	1.8	1.8
Nickel Alloys	30.0	206.8	11.5	79.6	0.30	0.30	8.3	8.3
Steel, Carbon	30.0	206.8	11.7	80.8	0.28	0.28	7.8	7.8
Steel, Alloys	30.0	206.8	11.7	80.8	0.28	0.28	7.8	7.8
Steel, Stainless	27.5	189.6	10.7	74.1	0.28	0.28	7.8	7.8
Titanium Alloys	16.5	113.8	6.2	42.4	0.34	0.16	4.4	4.4
Zinc Alloys	12.0	82.7	4.5	31.1	0.33	0.24	6.6	6.6

* *Properties of Some Metals and Alloys*, International Nickel Co., Inc., N.Y.; *Metals Handbook*, American Society for Metals, Materials Park, Ohio.**Table A-2 Mechanical Properties for Some Wrought-Aluminum Alloys**

Data from Various Sources.* Approximate Values. Consult Material Manufacturers for More Accurate Information

Wrought-Aluminum Alloy	Condition	Tensile Yield Strength (0.2% offset)		Ultimate Tensile Strength		Fatigue Strength at 5E8 cycles		Elongation over 2 in %	Brinell Hardness -HB
		kpsi	MPa	kpsi	MPa	kpsi	MPa		
1100	sheet annealed	5	34	13	90			35	23
	cold rolled	22	152	24	165			5	44
2024	sheet annealed	11	76	26	179			20	-
	heat treated	42	290	64	441	20	138	19	-
3003	sheet annealed	6	41	16	110			30	28
	cold rolled	27	186	29	200			4	55
5052	sheet annealed	13	90	28	193			25	47
	cold rolled	37	255	42	290			7	77
6061	sheet annealed	8	55	18	124			25	30
	heat treated	40	276	45	310	14	97	12	95
7075	bar annealed	15	103	33	228			16	60
	heat treated	73	503	83	572	14	97	11	150

* *Properties of Some Metals and Alloys*, International Nickel Co., Inc., N.Y.; *Metals Handbook*, American Society for Metals, Materials Park, Ohio.

Table A-3 Mechanical Properties for Some Aluminum Casting Alloys

Data from INCO.* Approximate Values. Consult Material Manufacturers for More Accurate Information

Aluminum Casting Alloy	Condition	Tensile Yield Strength (0.2% offset)		Ultimate Tensile Strength		Elongation over 2 in %	Brinell Hardness -HB
		kpsi	MPa	kpsi	MPa		
43	permanent mold casting—as cast	9	62	23	159	10	45
195	sand casting—as cast	24	165	36	248	5	-
220	sand casting—solution heat treated	26	179	48	331	16	75
380	die casting—as cast	24	165	48	331	3	-
A132	permanent mold casting—heat treated + 340°F	43	296	47	324	0.5	125
A142	sand casting—heat treated + 650°F	30	207	32	221	0.5	85

* Properties of Some Metals and Alloys, International Nickel Co., Inc., New York.

Table A-4 Mechanical Properties for Some Wrought- and Cast-Copper Alloys

Data from INCO.* Approximate Values. Consult Material Manufacturers for More Accurate Information

Copper Alloy	Condition	Tensile Yield Strength (0.2% offset)		Ultimate Tensile Strength		Elongation over 2 in %	Brinell or Rockwell Hardness
		kpsi	MPa	kpsi	MPa		
CA110—Pure Copper	strip annealed	10	69	32	221	45	40HRF
	spring temper	50	345	55	379	4	60HRB
CA170—Beryllium Copper	strip annealed plus age	145	1 000	165	1 138	7	35HRC
	hard plus age	170	1 172	190	1 310	3	40HRC
CA220—Commercial Bronze	strip annealed	10	69	37	255	45	53HRF
	spring temper	62	427	72	496	3	78HRB
CA230—Red Brass	strip annealed	15	103	40	276	50	50HB
	hard temper	60	414	75	517	7	135HB
CA260—Cartridge Brass	strip annealed	11	76	44	303	66	54HRF
	spring temper	65	448	94	648	3	91HRB
CA270—Yellow Brass	strip annealed	14	97	46	317	65	58HRF
	spring temper	62	427	91	627	30	90HRB
CA510—Phosphor Bronze	annealed	19	131	47	324	64	73HRF
	spring temper	80	552	100	689	4	95HRB
CA614—Aluminum Bronze	soft	45	310	82	565	40	84HRB
	hard	60	414	89	614	32	87HRB
CA655—High Silicon Bronze	annealed	21	145	56	386	63	76HRF
	spring temper	62	427	110	758	4	97HRB
CA675—Manganese Bronze	soft	30	207	65	448	33	65HRB
	half-hard	60	414	84	579	19	90HRB
Leaded-Tin Bronze	as cast	19	131	34	234	18	60HB
Nickel-Tin Bronze	as cast	20	138	50	345	40	85HB
	cast and heat treated	55	379	85	586	10	180HB

* Properties of Some Metals and Alloys, International Nickel Co., Inc., New York.

Table A-5 Mechanical Properties for Some Titanium Alloys

Data from INCO. * Approximate Values. Consult Material Manufacturers for More Accurate Information

Titanium Alloy	Condition	Tensile Yield Strength (0.2% offset)		Ultimate Tensile Strength		Elongation over 2 in	Brinell or Rockwell Hardness
		kpsi	MPa	kpsi	MPa		
Ti-35A	sheet annealed	30	207	40	276	30	135HB
Ti-50A	sheet annealed	45	310	55	379	25	215HB
Ti-75A	sheet annealed	75	517	85	586	18	245HB
Ti-0.2Pd Alloy	sheet annealed	45	310	55	379	25	215HB
Ti-5 Al-2.5 Sn Alloy	annealed	125	862	135	931	13	39HRC
Ti-8 Al-1 Mo-1 V Alloy	sheet annealed	130	896	140	965	13	39HRC
Ti-8 Al-2 Sn-4 Zr-2 Mo Alloy	bar annealed	130	896	140	965	15	39HRC
Ti-8 Al-6 V-2 Sn Alloy	sheet annealed	155	1 069	165	1 138	12	41HRC
Ti-6 Al-4 V Alloy	sheet annealed	130	896	140	13	2.5	39HRC
Ti-6 Al-4 V Alloy	heat treated	165	1 138	175	1 207	12	-
T1-13 V-11 Cr-3 Al Alloy	sheet annealed	130	896	135	931	13	37HRC
T1-13 V-11 Cr-3 Al Alloy	heat treated	170	1 172	180	1 241	6	-

* Properties of Some Metals and Alloys, International Nickel Co., Inc., New York.

Table A-6 Mechanical Properties for Some Magnesium Alloys

Data from INCO. * Approximate Values. Consult Material Manufacturers for More Accurate Information

Magnesium Alloy	Condition	Tensile Yield Strength (0.2% offset)		Ultimate Tensile Strength		Elongation over 2 in	Brinell or Rockwell Hardness
		kpsi	MPa	kpsi	MPa		
AZ 31B	sheet annealed	22	152	37	255	21	56HB
	hard sheet	32	221	42	290	15	73HB
AZ 80A	as forged	33	228	48	331	11	69HB
	forged and aged	36	248	50	345	6	72HB
AZ91A & AZ91B	die cast	22	152	33	228	3	63HB
AZ91C	as cast	14	97	24	165	2.5	60HB
	cast, solution treated and aged	19	131	40	276	5	70HB
AZ92A	as cast	14	97	25	172	2	65HB
	cast, solution treated	14	97	40	276	10	63HB
	cast, solution treated and aged	22	152	40	276	3	81HB
EZ33A	cast and aged	16	110	23	159	3	50HB
HK31A	strain hardened	29	200	37	255	8	68HB
	cast and heat treated	15	103	32	221	8	66HRB
HZ32A	cast - solution treated and aged	13	90	27	186	4	55HB
ZK60A	as extruded	38	262	49	338	14	75HB
	extruded and aged	44	303	53	365	11	82HB

* Properties of Some Metals and Alloys, International Nickel Co., Inc., New York.

Table A-7 Mechanical Properties for Some Cast-Iron Alloys

Data from Various Sources.* Approximate Values. Consult Material Manufacturers for More Accurate Information

Cast Iron Alloy	Condition	Tensile Yield Strength (0.2% offset)		Ultimate Tensile Strength		Compressive Strength		Brinell Hardness -HB
		kpsi	MPa	kpsi	MPa	kpsi	MPa	
Gray Cast Iron—Class 20	as cast	—	—	22	152	83	572	156
Gray Cast Iron—Class 30	as cast	—	—	32	221	109	752	210
Gray Cast Iron—Class 40	as cast	—	—	42	290	140	965	235
Gray Cast Iron—Class 50	as cast	—	—	52	359	164	1 131	262
Gray Cast Iron—Class 60	as cast	—	—	62	427	187	1 289	302
Ductile Iron 60-40-18	annealed	47	324	65	448	52	359	160
Ductile Iron 65-45-12	annealed	48	331	67	462	53	365	174
Ductile Iron 80-55-06	annealed	53	365	82	565	56	386	228
Ductile Iron 120-90-02	Q & T	120	827	140	965	134	924	325

* Properties of Some Metals and Alloys, International Nickel Co., Inc., N.Y.; Metals Handbook, American Society for Metals, Materials Park, Ohio.

Table A-8 Mechanical Properties for Some Stainless Steel Alloys

Data from INCO.* Approximate Values. Consult Material Manufacturers for More Accurate Information

Stainless Steel Alloy	Condition	Tensile Yield Strength (0.2% offset)		Ultimate Tensile Strength		Elongation over 2 in %	Brinell or Rockwell Hardness
		kpsi	MPa	kpsi	MPa		
Type 301	strip annealed	40	276	110	758	60	85HRB
	cold rolled	165	1 138	200	1 379	8	41HRC
Type 302	sheet annealed	40	276	90	621	50	85HRB
	cold rolled	165	1 138	190	1 310	5	40HRC
Type 304	sheet annealed	35	241	85	586	50	80HRB
	cold rolled	160	1 103	185	1 276	4	40HRC
Type 314	bar annealed	50	345	100	689	45	180HB
Type 316	sheet annealed	40	276	90	621	50	85HRB
Type 330	hot rolled	55	379	100	689	35	200HB
	annealed	35	241	80	552	50	150HB
Type 410	sheet annealed	45	310	70	483	25	80HRB
	heat treated	140	965	180	1 241	15	39HRC
Type 420	bar annealed	50	345	95	655	25	92HRB
	heat treated	195	1 344	230	1 586	8	500HB
Type 431	bar annealed	95	655	125	862	25	260HB
	heat treated	150	1 034	195	1 344	15	400HB
Type 440C	bar annealed	65	448	110	758	14	230HB
	Q & T @ 600°F	275	1 896	285	1 965	2	57HRC
17-4 PH (AISI 630)	hardened	185	1 276	200	1 379	14	44HRC
17-7 PH (AISI 631)	hardened	220	1 517	235	1 620	6	48HRC

* Properties of Some Metals and Alloys, International Nickel Co., Inc., New York.

Table A-9 Mechanical Properties for Some Carbon Steels

Data from Various Sources. * Approximate Values. Consult Material Manufacturers for More Accurate Information

SAE / AISI Number	Condition	Tensile Yield Strength (0.2% offset)		Ultimate Tensile Strength		Elongation over 2 in	Brinell Hardness -HB
		kpsi	MPa	kpsi	MPa		
1010	hot rolled	26	179	47	324	28	95
	cold rolled	44	303	53	365	20	105
1020	hot rolled	30	207	55	379	25	111
	cold rolled	57	393	68	469	15	131
1030	hot rolled	38	259	68	469	20	137
	normalized @ 1 650°F	50	345	75	517	32	149
	cold rolled	64	441	76	524	12	149
	quench & temper @ 1 000°F	75	517	97	669	28	255
	quench & temper @ 800°F	84	579	106	731	23	302
	quench & temper @ 400°F	94	648	123	848	17	495
1035	hot rolled	40	276	72	496	18	143
	cold rolled	67	462	80	552	12	163
1040	hot rolled	42	290	76	524	18	149
	normalized @ 1 650°F	54	372	86	593	28	170
	cold rolled	71	490	85	586	12	170
	quench & temper @ 1 200°F	63	434	92	634	29	192
	quench & temper @ 800°F	80	552	110	758	21	241
	quench & temper @ 400°F	86	593	113	779	19	262
1045	hot rolled	45	310	82	565	16	163
	cold rolled	77	531	91	627	12	179
1050	hot rolled	50	345	90	621	15	179
	normalized @ 1 650°F	62	427	108	745	20	217
	cold rolled	84	579	100	689	10	197
	quench & temper @ 1 200°F	78	538	104	717	28	235
	quench & temper @ 800°F	115	793	158	1 089	13	444
	quench & temper @ 400°F	117	807	163	1 124	9	514
1060	hot rolled	54	372	98	676	12	200
	normalized @ 1 650°F	61	421	112	772	18	229
	quench & temper @ 1 200°F	76	524	116	800	23	229
	quench & temper @ 1 000°F	97	669	140	965	17	277
	quench & temper @ 800°F	111	765	156	1 076	14	311
1095	hot rolled	66	455	120	827	10	248
	normalized @ 1 650°F	72	496	147	1 014	9	13
	quench & temper @ 1 200°F	80	552	130	896	21	269
	quench & temper @ 800°F	112	772	176	1 213	12	363
	quench & temper @ 600°F	118	814	183	1 262	10	375

* SAE Handbook, Society of Automotive Engineers, Warrendale, Pa.; Metals Handbook, American Society for Metals, Materials Park, Ohio.

Table A-10 Mechanical Properties for Some Alloy and Tool Steels

Data from Various Sources.* Approximate Values. Consult Material Manufacturers for More Accurate Information

SAE / AISI Number	Condition	Tensile Yield Strength (0.2% offset)		Ultimate Tensile Strength		Elongation over 2 in %	Brinell or Rockwell Hardness
		kpsi	MPa	kpsi	MPa		
1340	annealed	63	434	102	703	25	204HB
	quench & temper	109	752	125	862	21	250HB
4027	annealed	47	324	75	517	30	150HB
	quench & temper	113	779	132	910	12	264HB
4130	annealed @ 1 450°F	52	359	81	558	28	156HB
	normalized @ 1 650°F	63	434	97	669	25	197HB
	quench & temper @ 1 200°F	102	703	118	814	22	245HB
	quench & temper @ 800°F	173	1 193	186	1 282	13	380HB
	quench & temper @ 400°F	212	1 462	236	1 627	10	41HB
4140	annealed @ 1 450°F	61	421	95	655	26	197HB
	normalized @ 1 650°F	95	655	148	1 020	18	302HB
	quench & temper @ 1 200°F	95	655	110	758	22	230HB
	quench & temper @ 800°F	165	1 138	181	1 248	13	370HB
	quench & temper @ 400°F	238	1 641	257	1 772	8	510HB
4340	quench & temper @ 1 200°F	124	855	140	965	19	280HB
	quench & temper @ 1 000°F	156	1 076	170	1 172	13	360HB
	quench & temper @ 800°F	198	1 365	213	1 469	10	430HB
	quench & temper @ 600°F	230	1 586	250	1 724	10	486HB
6150	annealed	59	407	96	662	23	192HB
	quench & temper	148	1 020	157	1 082	16	314HB
8740	annealed	60	414	95	655	25	190HB
	quench & temper	133	917	144	993	18	288HB
H-11	annealed @ 1 600°F	53	365	100	689	25	96HRB
	quench & temper @ 1 000°F	250	1 724	295	2 034	9	55HRC
L-2	annealed @ 1 425°F	74	510	103	710	25	96HRB
	quench & temper @ 400°F	260	1 793	290	1 999	5	54HRC
L-6	annealed @ 1 425°F	55	379	95	655	25	93HRB
	quench & temper @ 600°F	260	1 793	290	1 999	4	54HRC
P-20	annealed @ 1 425°F	75	517	100	689	17	97HRB
	quench & temper @ 400°F	205	1 413	270	1 862	10	52HRC
S-1	annealed @ 1 475°F	60	414	100	689	24	96HRB
	quench & temper @ 400°F	275	1 896	300	2 068	4	57HRC
S-5	annealed @ 1 450°F	64	441	105	724	25	96HRB
	quench & temper @ 400°F	280	1 931	340	2 344	5	59HRC
S-7	annealed @ 1 525°F	55	379	93	641	25	95HRB
	quench & temper @ 400°F	210	1 448	315	2 172	7	58HRC
A-8	annealed @ 1 550°F	65	448	103	710	24	97HRB
	quench & temper @ 1 050°F	225	1 551	265	1 827	9	52HRC

* Machine Design Materials Reference Issue, Penton Publishing, Cleveland Ohio; Metals Handbook, ASM, Materials Park, Ohio.

Table A-11 Mechanical Properties of Some Engineering Plastics

Data from Various Sources.* Approximate Values. Consult Material Manufacturers for More Accurate Information

Material	Approximate Modulus of Elasticity E		Ultimate Tensile Strength		Ultimate Compressive Strength		Elongation over 2 in	Max Temp	Specific Gravity
	Mpsi	GPa	kpsi	MPa	kpsi	MPa			
ABS	0.3	2.1	6.0	41.4	10.0	68.9	5 to 25	160–200	1.05
20–40% glass filled	0.6	4.1	10.0	68.9	12.0	82.7	3	200–230	1.30
Acetal	0.5	3.4	8.8	60.7	18.0	124.1	60	220	1.41
20–30% glass filled	1.0	6.9	10.0	68.9	18.0	124.1	7	185–220	1.56
Acrylic	0.4	2.8	10.0	68.9	15.0	103.4	5	140–190	1.18
Fluoroplastic (PTFE)	0.2	1.4	5.0	34.5	6.0	41.4	100	350–330	2.10
Nylon 6/6	0.2	1.4	10.0	68.9	10.0	68.9	60	180–300	1.14
Nylon 11	0.2	1.3	8.0	55.2	8.0	55.2	300	180–300	1.04
20–30% glass filled	0.4	2.5	12.8	88.3	12.8	88.3	4	250–340	1.26
Polycarbonate	0.4	2.4	9.0	62.1	12.0	82.7	100	250	1.20
10–40% glass filled	1.0	6.9	17.0	117.2	17.0	117.2	2	275	1.35
HMW Polyethylene	0.1	0.7	2.5	17.2	—	—	525	—	0.94
Polyphenylene Oxide	0.4	2.4	9.6	66.2	16.4	113.1	20	212	1.06
20–30% glass filled	1.1	7.8	15.5	106.9	17.5	120.7	5	260	1.23
Polypropylene	0.2	1.4	5.0	34.5	7.0	48.3	500	250–320	0.90
20–30% glass filled	0.7	4.8	7.5	51.7	6.2	42.7	2	300–320	1.10
Impact Polystyrene	0.3	2.1	4.0	27.6	6.0	41.4	2 to 80	140–175	1.07
20–30% glass filled	0.1	0.7	12.0	82.7	16.0	110.3	1	180–200	1.25
Polysulfone	0.4	2.5	10.2	70.3	13.9	95.8	50	300–345	1.24

* Modern Plastics Encyclopedia, McGraw-Hill, New York; Machine Design Materials Reference Issue, Penton Publishing, Cleveland, Ohio.

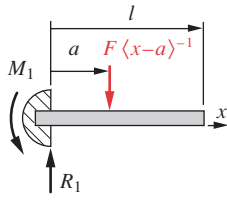
Appendix B

BEAM TABLES

Loading, shear, moment, slope, and deflection functions for a selection of common beam configurations and loadings are presented in these tables. **Cantilever**, **simply supported**, and **overhung** beams with either a **concentrated load** at any point or a **uniformly distributed load** across any portion of the span are defined. A general set of equations is derived for each beam. Special cases, such as those with the load at center span, are accommodated by appropriate choice of dimensions in the general formulas. In all cases, singularity functions are used to write the beam equations, which gives a single expression for the entire span for each function. See Section 3.9 (p. 112) for a discussion of singularity functions. The equations for the beam cases in this appendix have been encoded in computer files, which are provided on the CD included with this text. In some cases, the computer files allow multiple loads to be applied at different locations on the beam, but the derivations in this appendix each accommodate only one load per beam. *Use superposition to combine various beam cases when more than one type of load is present on a beam.* For a more complete collection of beam formulas see Roark and Young, *Formulas for Stress and Strain*, 6th ed., McGraw-Hill, New York, 1989. A key to the figures in this appendix and their related files follows.

Figure No.	Case	File Name
B-1a	Cantilever beam with concentrated load	CANTCONC
B-1b	Cantilever beam with uniformly distributed load	CANTUNIF
B-2a	Simply supported beam with concentrated load	SIMPCONC
B-2b	Simply supported beam with uniformly distributed load	SIMPUNIF
B-3a	Overhung beam with concentrated load	OVHGCONC
B-3b	Overhung beam with uniformly distributed load	OVHGUNIF

(a) Cantilever beam with concentrated loading

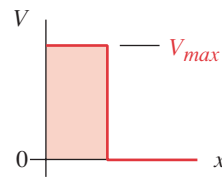


Loading

$$R_1 = F$$

$$M_1 = Fa$$

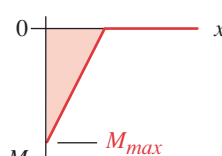
$$q = M_1 \langle x \rangle^{-2} + R_1 \langle x \rangle^{-1} - F \langle x - a \rangle^{-1}$$



Shear

$$V_{max} = R_1 = F$$

$$\begin{aligned} V &= M_1 \langle x \rangle^{-1} + R_1 - F \langle x - a \rangle^0 \\ &= F(1 - \langle x - a \rangle^0) \end{aligned}$$

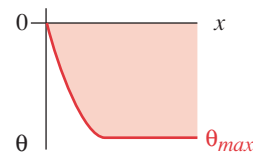


Moment

$$M_{max} = -Fa$$

$$\text{when } a = l : M_{max} = -Fl$$

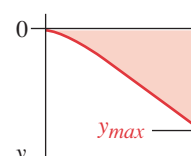
$$\begin{aligned} M &= -M_1 + R_1 x - F \langle x - a \rangle^1 \\ &= F(-a + x - \langle x - a \rangle^1) \end{aligned}$$



Slope

$$\theta = \frac{1}{EI} \begin{pmatrix} -M_1 x + \frac{R_1}{2} x^2 \\ -\frac{F}{2} \langle x - a \rangle^2 \end{pmatrix}$$

$$\theta = \frac{F}{2EI} (-2ax + x^2 - \langle x - a \rangle^2)$$



Deflection

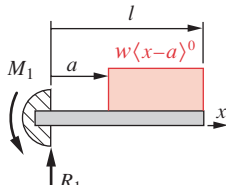
$$y_{max} = \frac{Fa^2}{6EI} (a - 3l)$$

$$\text{when } a = l : y_{max} = -\frac{Fl^3}{3EI}$$

$$y = \frac{1}{EI} \left(-\frac{M_1}{2} x^2 + \frac{R_1}{6} x^3 - \frac{F}{6} \langle x - a \rangle^3 \right)$$

$$= \frac{F}{6EI} (x^3 - 3ax^2 - \langle x - a \rangle^3)$$

(b) Cantilever beam with uniformly distributed loading

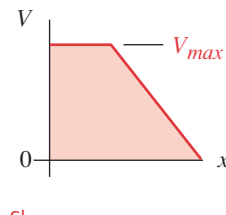


Loading

$$R_1 = w(l - a)$$

$$M_1 = \frac{w}{2} (l^2 - a^2)$$

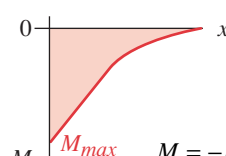
$$q = M_1 \langle x \rangle^{-2} + R_1 \langle x \rangle^{-1} - w \langle x - a \rangle^0$$



Shear

$$V_{max} = R_1 = w(l - a)$$

$$\begin{aligned} V &= M_1 \langle x \rangle^{-1} + R_1 - w \langle x - a \rangle^1 \\ &= w[(l - a) - \langle x - a \rangle^1] \end{aligned}$$

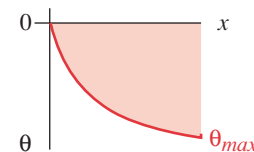


Moment

$$M_{max} = M_1 = \frac{w}{2} (l^2 - a^2)$$

$$\text{when } a = 0 : M_{max} = \frac{wl^2}{2}$$

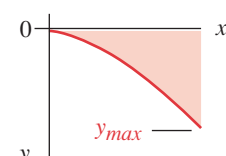
$$\begin{aligned} M &= -M_1 + R_1 x - w \langle x - a \rangle^2 \\ &= \frac{w}{2} [2(l - a)x - (l^2 - a^2) - 2\langle x - a \rangle^2] \end{aligned}$$



Slope

$$\theta = \frac{1}{EI} \begin{pmatrix} -M_1 x + \frac{R_1}{2} x^2 \\ -\frac{w}{6} \langle x - a \rangle^3 \end{pmatrix}$$

$$\theta = \frac{w}{6EI} (3(l - a)x^2 - 3(l^2 - a^2)x - \langle x - a \rangle^3)$$



Deflection

$$y_{max} = \frac{w}{24EI} (-3l^4 + 4a^3l - a^4)$$

$$\text{when } a = 0 : y_{max} = -\frac{wl^4}{8EI}$$

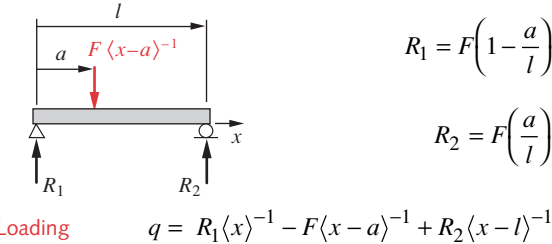
$$y = \frac{1}{EI} \left(-\frac{M_1}{2} x^2 + \frac{R_1}{6} x^3 - \frac{w}{24} \langle x - a \rangle^4 \right)$$

$$= \frac{w}{24EI} (4(l - a)x^3 - 6(l^2 - a^2)x^2 - \langle x - a \rangle^4)$$

FIGURE B-1

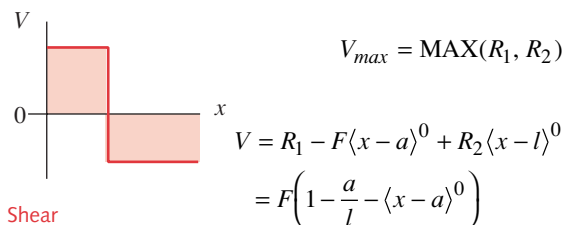
Cantilever Beams with Concentrated or Distributed Loading. Note: $\langle \rangle$ Denotes a Singularity Function

(a) Simply supported beam with concentrated loading

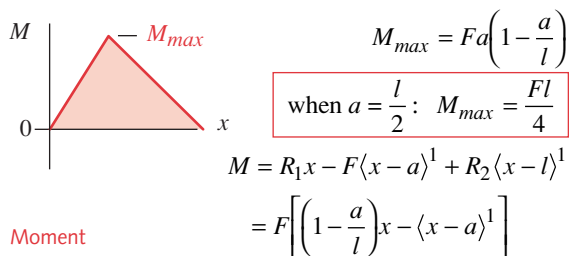


$$R_1 = F \left(1 - \frac{a}{l} \right)$$

$$R_2 = F \left(\frac{a}{l} \right)$$

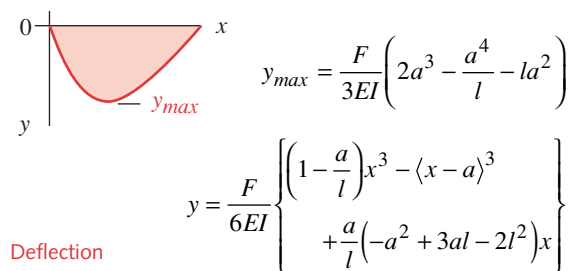
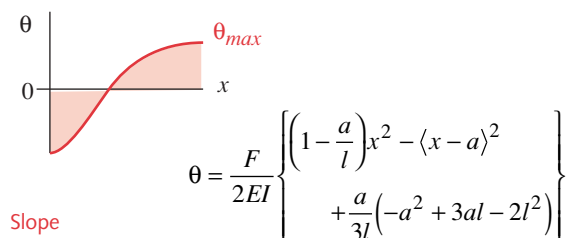


$$V_{max} = \text{MAX}(R_1, R_2)$$



$$M_{max} = Fa \left(1 - \frac{a}{l} \right)$$

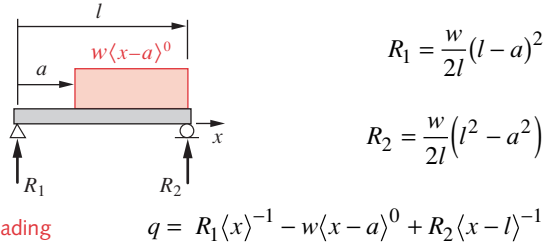
$$\text{when } a = \frac{l}{2} : M_{max} = \frac{Fl}{4}$$



$$y_{max} = \frac{F}{3EI} \left(2a^3 - \frac{a^4}{l} - la^2 \right)$$

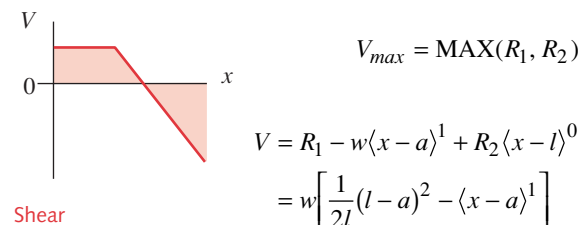
$$y = \frac{F}{6EI} \left\{ \left(1 - \frac{a}{l} \right) x^3 - \langle x - a \rangle^3 + \frac{a}{l} (-a^2 + 3al - 2l^2) x \right\}$$

(b) Simply supported beam with uniformly distributed loading

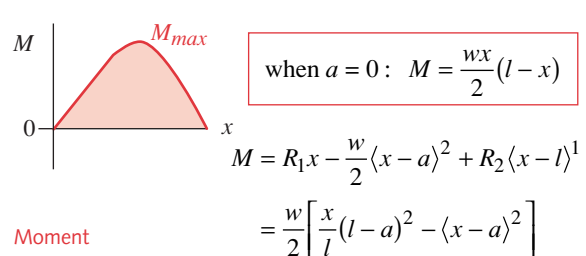


$$R_1 = \frac{w}{2l} (l - a)^2$$

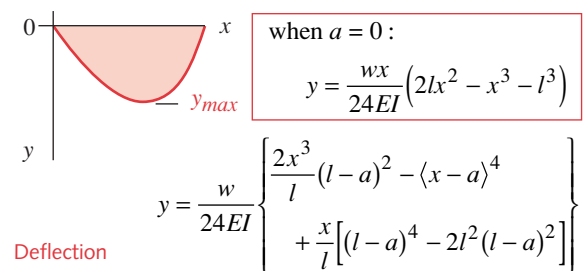
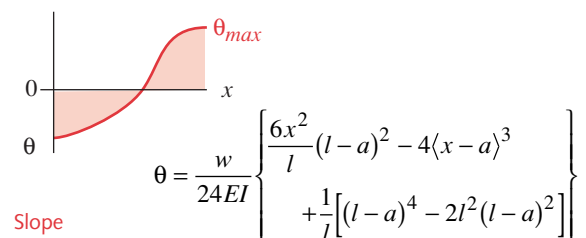
$$R_2 = \frac{w}{2l} (l^2 - a^2)$$



$$V_{max} = \text{MAX}(R_1, R_2)$$



$$\text{when } a = 0 : M = \frac{wx}{2} (l - x)$$

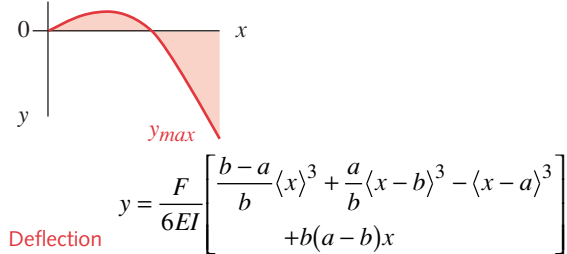
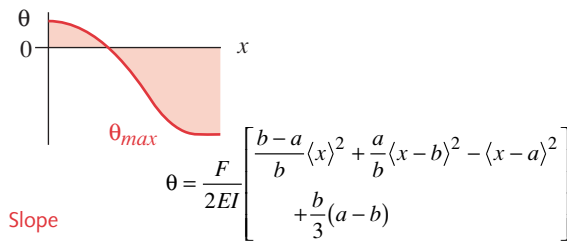
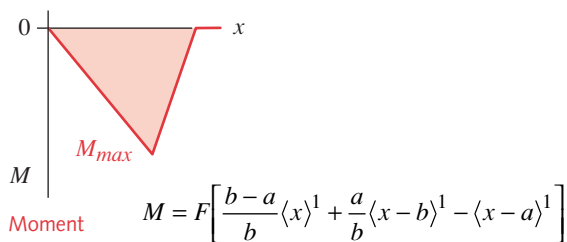
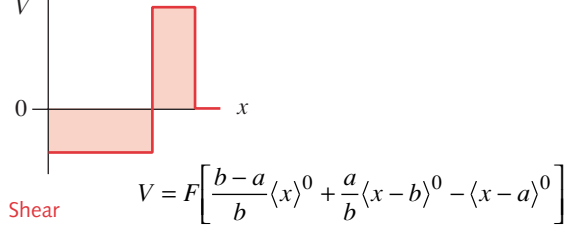
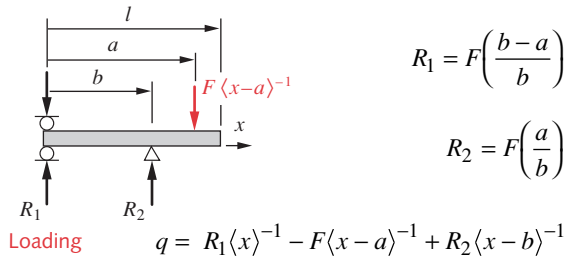


$$\text{when } a = 0 : y = \frac{wx}{24EI} (2lx^2 - x^3 - l^3)$$

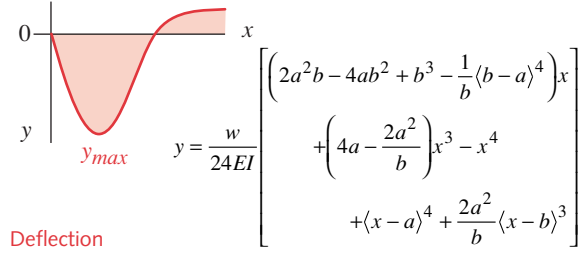
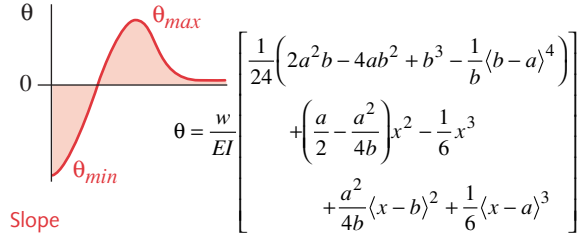
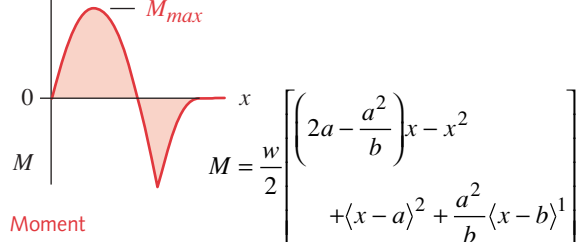
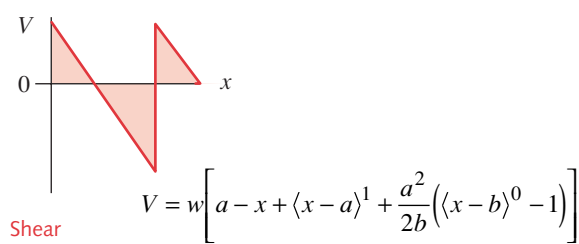
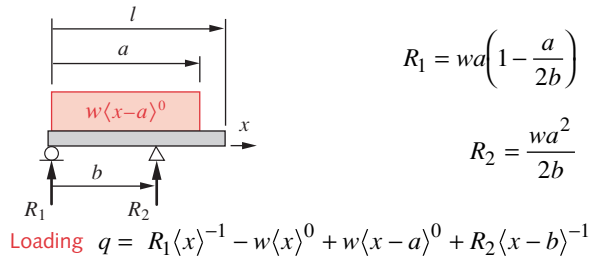
FIGURE B-2

Simply Supported Beams with Concentrated or Distributed Loading. Note: $\langle \rangle$ Denotes a Singularity Function

(a) Overhung beam with concentrated loading



(b) Overhung beam with uniformly distributed loading

**FIGURE B - 3**

Overhung Beams with Concentrated or Distributed Loading. Note: $\langle \rangle$ Denotes a Singularity Function

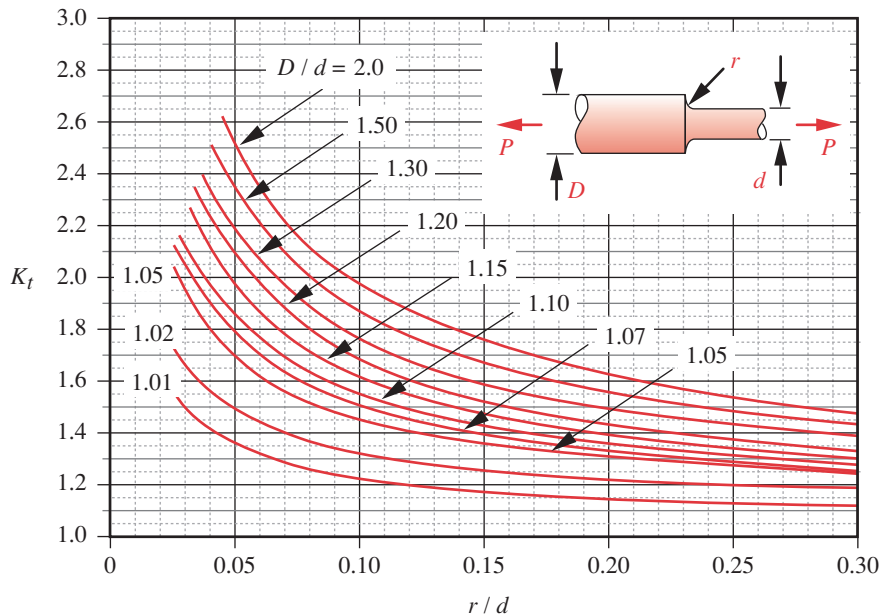
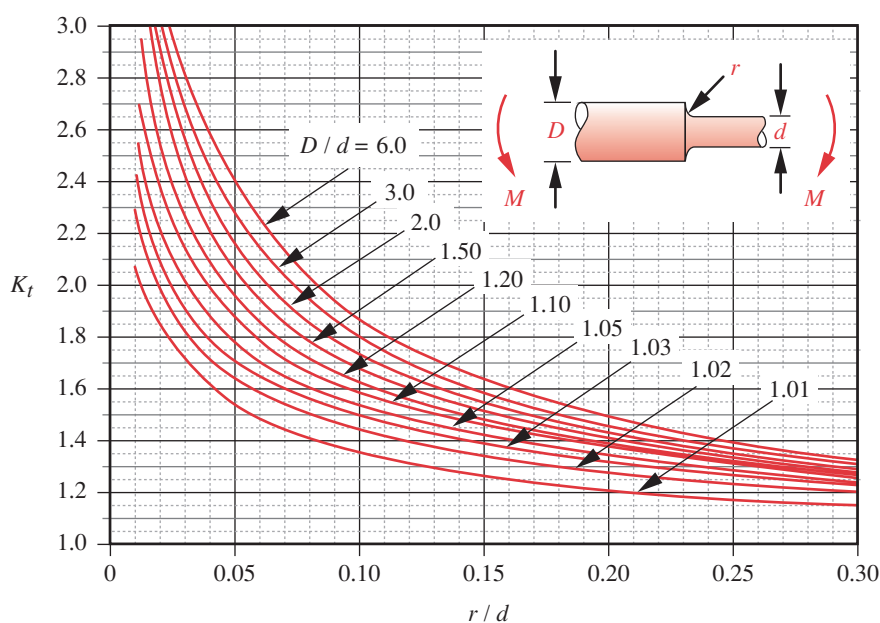
Appendix

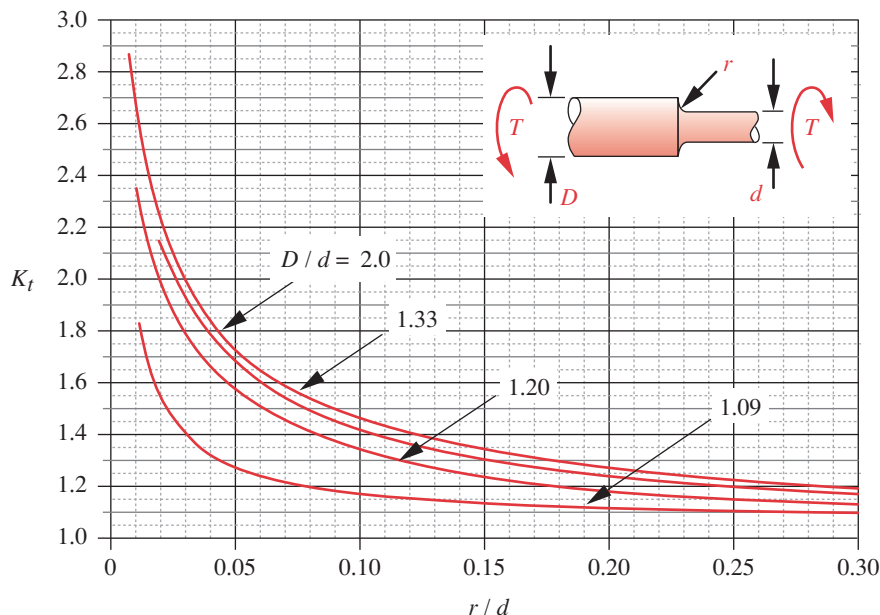
C

STRESS- CONCENTRATION FACTORS

Stress-concentration factors for 14 common cases are presented in this appendix as listed below. All curves are taken from R. E. Peterson, "Design Factors for Stress Concentration, Parts 1 to 5," *Machine Design*, February–July, 1951, Penton Publishing, Cleveland, Ohio, with permission. Approximate equations for these curves have been fitted and are defined in each figure. These equations have been encoded as computerized functions (noted below) that can be incorporated in computer models to allow automatic generation of approximate stress-concentration factors during calculations.

Figure	Case	File Name
C-1	Shaft with Shoulder Fillet in Axial Tension	APP_C-01
C-2	Shaft with Shoulder Fillet in Bending	APP_C-02
C-3	Shaft with Shoulder Fillet in Torsion	APP_C-03
C-4	Shaft with Groove in Axial Tension	APP_C-04
C-5	Shaft with Groove in Bending	APP_C-05
C-6	Shaft with Groove in Torsion	APP_C-06
C-7	Shaft with Transverse Hole in Bending	APP_C-07
C-8	Shaft with Transverse Hole in Torsion	APP_C-08
C-9	Flat Bar with Fillet in Axial Tension	APP_C-09
C-10	Flat Bar with Fillet in Bending	APP_C-10
C-11	Flat Bar with Notch in Axial Tension	APP_C-11
C-12	Flat Bar with Notch in Bending	APP_C-12
C-13	Flat Bar with Transverse Hole in Axial Tension	APP_C-13
C-14	Flat Bar with Transverse Hole in Bending	APP_C-14

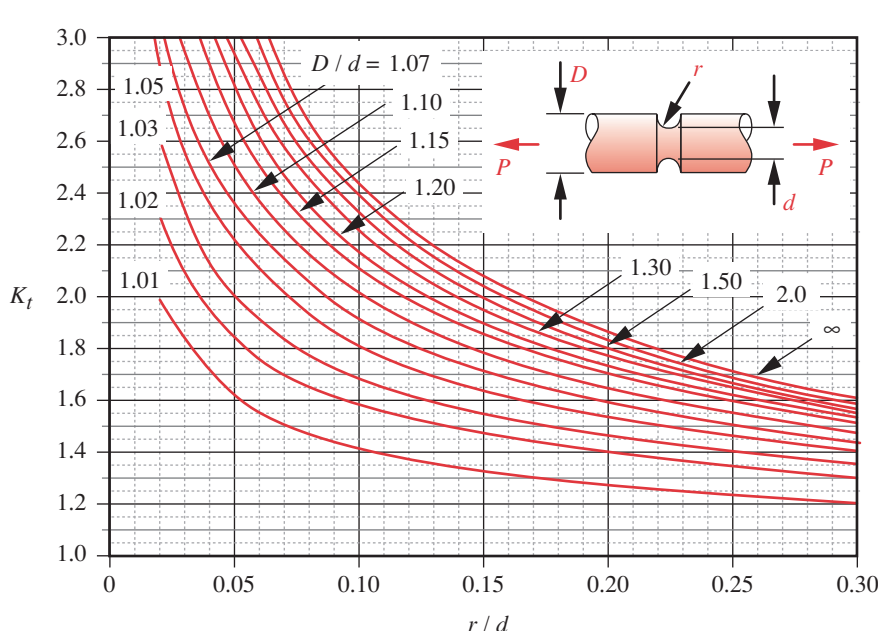
**FIGURE C-1**Geometric Stress-Concentration Factor K_t for a Shaft with a Shoulder Fillet in Axial Tension**FIGURE C-2**Geometric Stress-Concentration Factor K_t for a Shaft with a Shoulder Fillet in Bending

**FIGURE C-3**Geometric Stress-Concentration Factor K_t for a Shaft with a Shoulder Fillet in Torsion

$$K_t \cong A \left(\frac{r}{d} \right)^b$$

where :

D/d	A	b
2.00	0.863 31	-0.238 65
1.33	0.848 97	-0.231 61
1.20	0.834 25	-0.216 49
1.09	0.903 37	-0.126 92

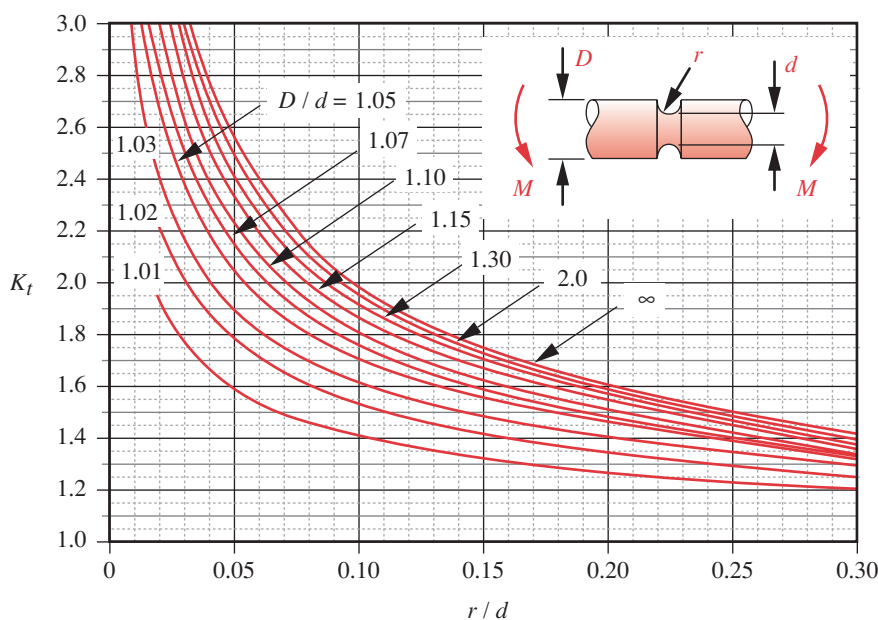


$$K_t \cong A \left(\frac{r}{d} \right)^b$$

where :

D/d	A	b
∞	0.993 72	-0.393 52
2.00	0.993 83	-0.382 31
1.50	0.998 08	-0.369 55
1.30	1.004 90	-0.355 45
1.20	1.010 70	-0.337 65
1.15	1.026 30	-0.316 73
1.10	1.027 20	-0.294 84
1.07	1.023 80	-0.276 18
1.05	1.027 20	-0.252 56
1.03	1.036 70	-0.216 03
1.02	1.037 90	-0.187 55
1.01	1.000 30	-0.156 09

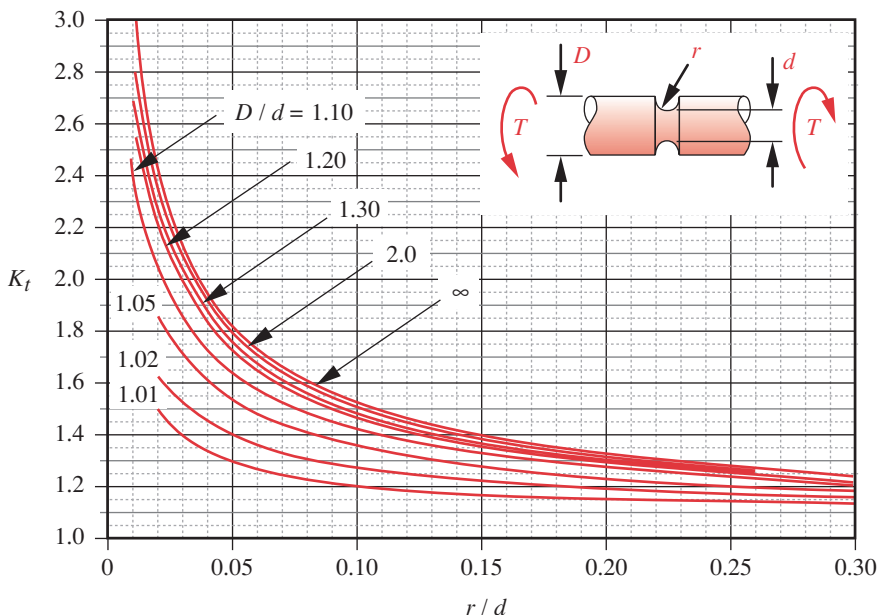
FIGURE C-4Geometric Stress-Concentration Factor K_t for a Grooved Shaft in Axial Tension

**FIGURE C-5**Geometric Stress-Concentration Factor K_t for a Grooved Shaft in Bending

$$K_t \approx A \left(\frac{r}{d} \right)^b$$

where :

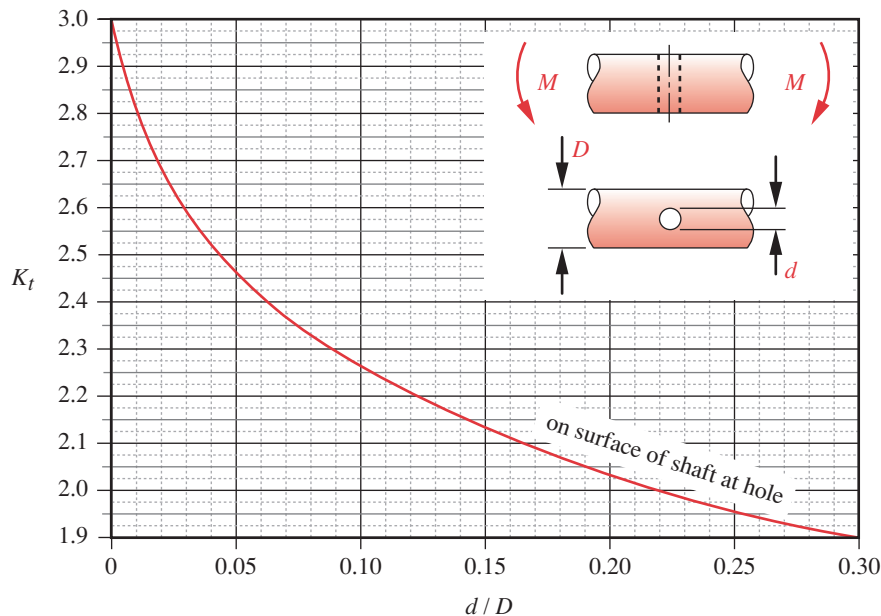
D/d	A	b
∞	0.948 01	-0.333 02
2.00	0.936 19	-0.330 66
1.50	0.938 94	-0.323 80
1.30	0.942 99	-0.315 04
1.20	0.946 81	-0.305 82
1.15	0.953 11	-0.297 39
1.12	0.955 73	-0.288 86
1.10	0.954 54	-0.282 68
1.07	0.967 74	-0.264 52
1.05	0.987 55	-0.241 34
1.03	0.990 33	-0.215 17
1.02	0.977 53	-0.197 93
1.01	0.993 93	-0.152 38

**FIGURE C-6**Geometric Stress-Concentration Factor K_t for a Grooved Shaft in Torsion

$$K_t \approx A \left(\frac{r}{d} \right)^b$$

where :

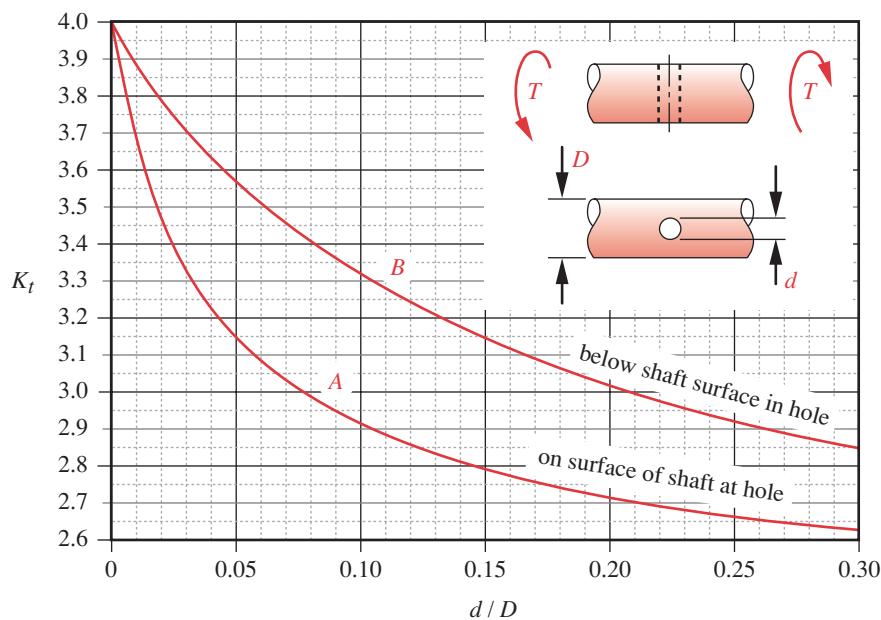
D/d	A	b
∞	0.881 26	-0.252 04
2.00	0.890 35	-0.240 75
1.30	0.894 60	-0.232 67
1.20	0.901 82	-0.223 34
1.10	0.923 11	-0.197 40
1.05	0.938 53	-0.169 41
1.02	0.968 77	-0.126 05
1.01	0.972 45	-0.101 62



$$K_t \approx 1.58990 - 0.63550 \log\left(\frac{d}{D}\right)$$

FIGURE C-7

Geometric Stress-Concentration Factor K_t for a Shaft with a Transverse Hole in Bending

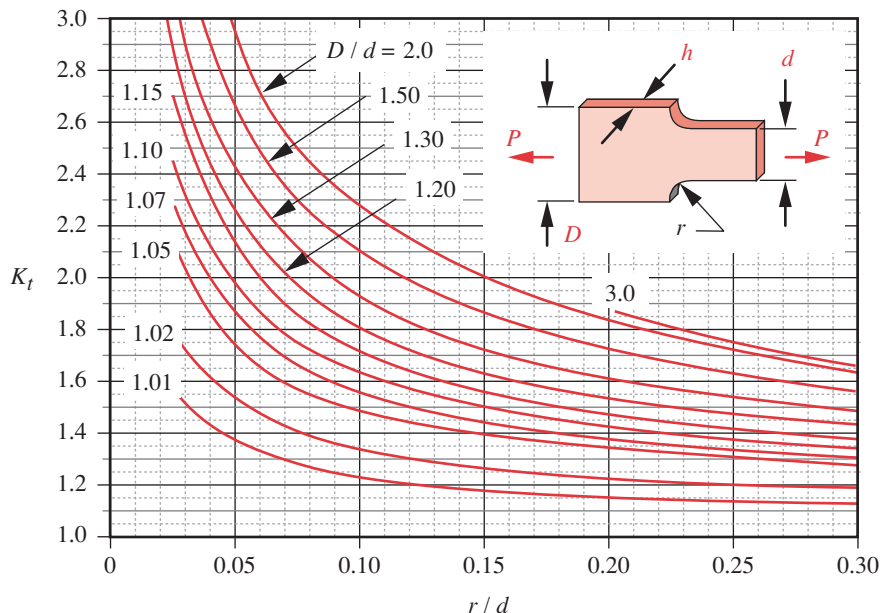


$$K_{t_B} \approx 3.9702 - 9.292 \frac{d}{D} + 27.159 \left(\frac{d}{D}\right)^2 + 30.231 \left(\frac{d}{D}\right)^3 - 393.19 \left(\frac{d}{D}\right)^4 + 650.39 \left(\frac{d}{D}\right)^5 + 15.451 \left(\frac{d}{D}\right)^6$$

$$K_{t_A} \approx 3.92150 - 24.435 \frac{d}{D} + 234.06 \left(\frac{d}{D}\right)^2 - 1200.5 \left(\frac{d}{D}\right)^3 + 3059.5 \left(\frac{d}{D}\right)^4 - 3042.4 \left(\frac{d}{D}\right)^5$$

FIGURE C-8

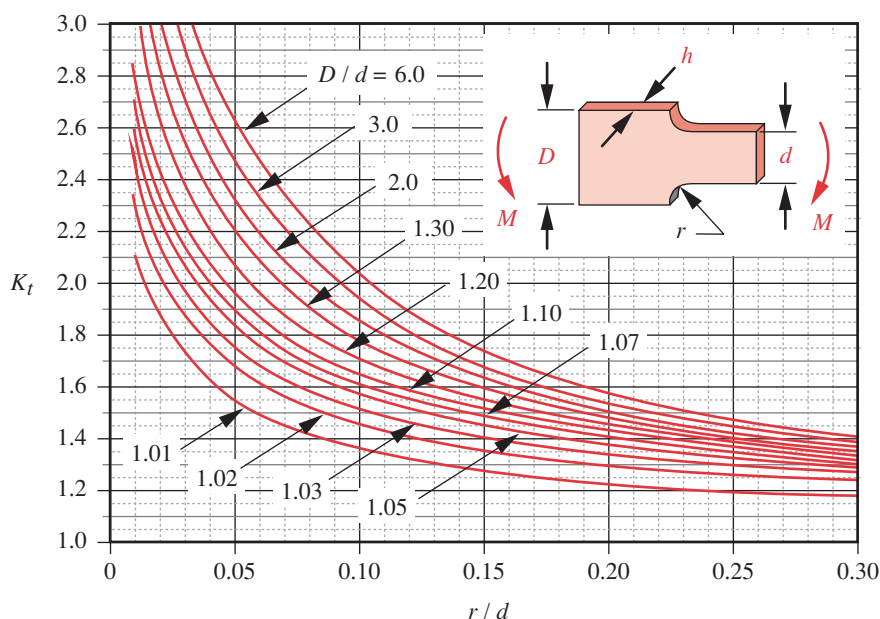
Geometric Stress-Concentration Factor K_t for a Shaft with a Transverse Hole in Torsion

**FIGURE C-9**Geometric Stress-Concentration Factor K_t for a Filleted Flat Bar in Axial Tension

$$K_t \approx A \left(\frac{r}{d} \right)^b$$

where :

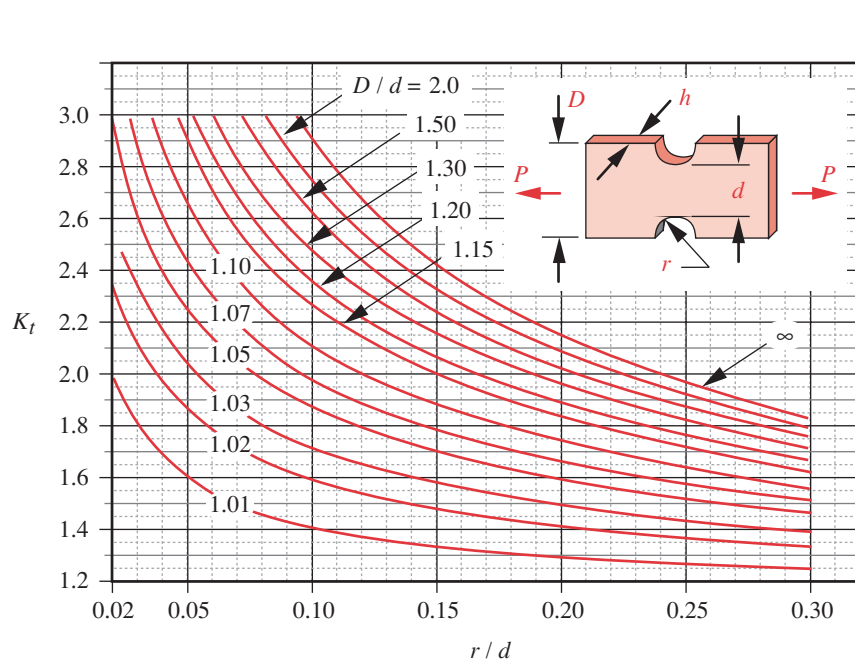
D/d	A	b
2.00	1.099 60	-0.320 77
1.50	1.076 90	-0.295 58
1.30	1.054 40	-0.270 21
1.20	1.035 10	-0.250 84
1.15	1.014 20	-0.239 35
1.10	1.013 00	-0.215 35
1.07	1.014 50	-0.193 66
1.05	0.987 97	-0.138 48
1.02	1.025 90	-0.169 78
1.01	0.976 62	-0.106 56

**FIGURE C-10**Geometric Stress-Concentration Factor K_t for a Filleted Flat Bar in Bending

$$K_t \approx A \left(\frac{r}{d} \right)^b$$

where :

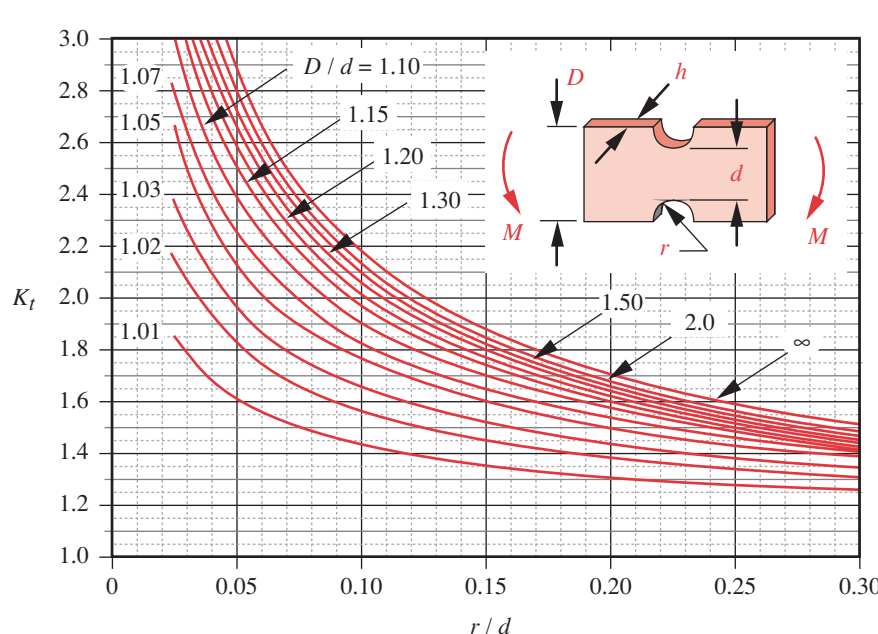
D/d	A	b
6.00	0.895 79	-0.358 47
3.00	0.907 20	-0.333 33
2.00	0.932 32	-0.303 04
1.30	0.958 80	-0.272 69
1.20	0.995 90	-0.238 29
1.10	1.016 50	-0.215 48
1.07	1.019 90	-0.203 33
1.05	1.022 60	-0.191 56
1.03	1.016 60	-0.178 02
1.02	0.995 28	-0.170 13
1.01	0.966 89	-0.154 17

**FIGURE C-11**Geometric Stress-Concentration Factor K_t for a Notched Flat Bar in Axial Tension

$$K_t \equiv A \left(\frac{r}{d} \right)^b$$

where :

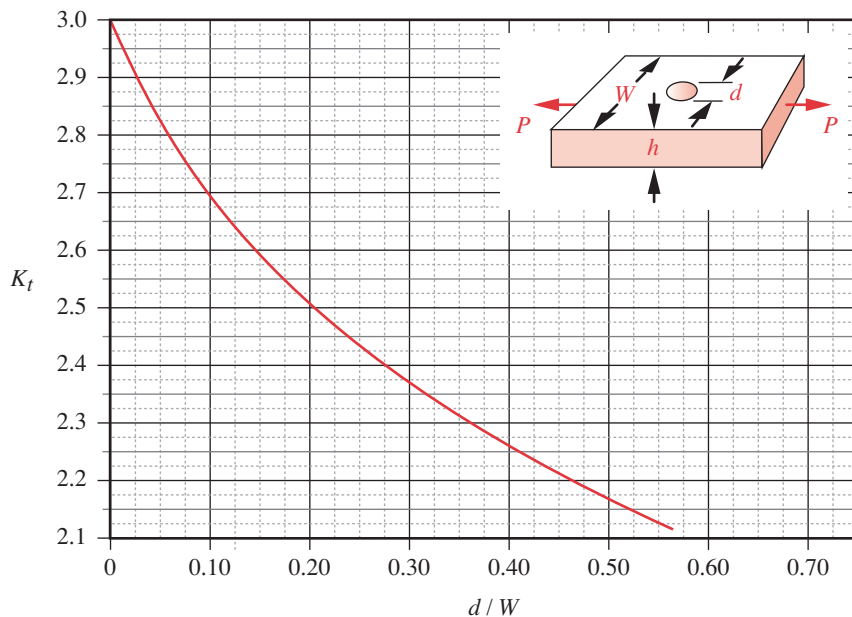
D/d	A	b
∞	1.109 50	-0.417 12
3.00	1.113 90	-0.409 23
2.00	1.133 90	-0.385 86
1.50	1.132 60	-0.365 92
1.30	1.158 60	-0.332 60
1.20	1.147 50	-0.315 07
1.15	1.095 20	-0.325 17
1.10	1.085 10	-0.299 97
1.07	1.091 20	-0.268 57
1.05	1.090 60	-0.241 63
1.03	1.051 80	-0.222 16
1.02	1.054 00	-0.188 79
1.01	1.042 60	-0.141 45

**FIGURE C-12**Geometric Stress-Concentration Factor K_t for a Notched Flat Bar in Bending

$$K_t \equiv A \left(\frac{r}{d} \right)^b$$

where :

D/d	A	b
∞	0.970 79	-0.356 72
3.00	0.971 94	-0.350 47
2.00	0.968 01	-0.349 15
1.50	0.983 15	-0.333 95
1.30	0.982 88	-0.326 06
1.20	0.990 55	-0.313 19
1.15	0.993 04	-0.302 63
1.10	1.007 10	-0.283 79
1.07	1.014 70	-0.261 45
1.05	1.025 00	-0.240 08
1.03	1.029 40	-0.211 61
1.02	1.037 40	-0.184 28
1.01	1.060 50	-0.133 69

**FIGURE C-13**Geometric Stress-Concentration Factor K_t for a Flat Bar with Transverse Hole in Axial Tensionfor $\frac{d}{W} \leq 0.65$:

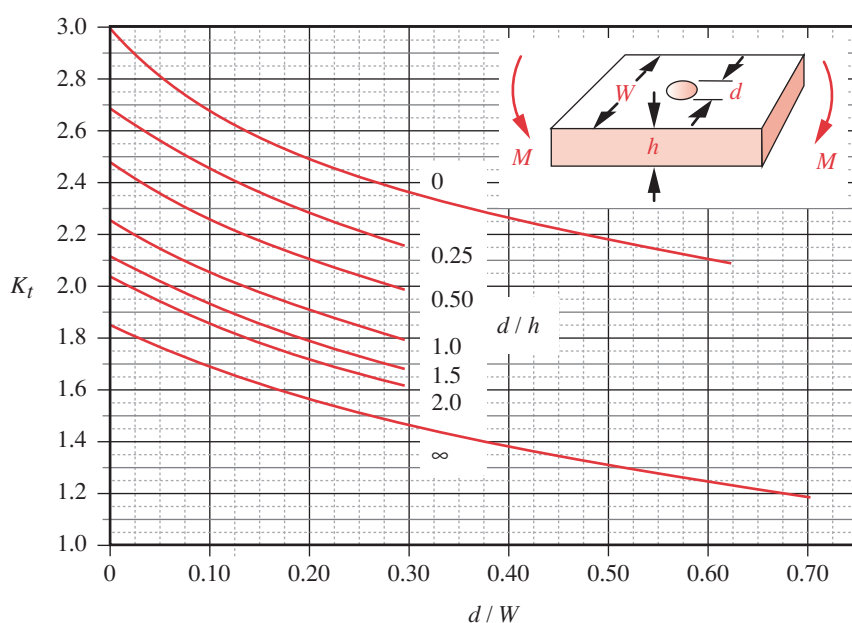
$$K_t \cong 3.0039 - 3.753 \frac{d}{W}$$

$$+ 7.9735 \left(\frac{d}{W} \right)^2$$

$$- 9.2659 \left(\frac{d}{W} \right)^3$$

$$+ 1.8145 \left(\frac{d}{W} \right)^4$$

$$+ 2.9684 \left(\frac{d}{W} \right)^5$$

**FIGURE C-14**Geometric Stress-Concentration Factor K_t for a Flat Bar with Transverse Hole in Bendingfor $\frac{d}{h} = 0$ and $\frac{d}{W} \leq 0.65$:

$$K_t \cong 2.9947 - 3.4833 \frac{d}{W}$$

$$+ 5.8268 \left(\frac{d}{W} \right)^2 - 4.1986 \left(\frac{d}{W} \right)^3$$

for $\frac{d}{h} \geq 0.25$: $K_t \cong A e^{[b(d/W)]}$

where :

d/h	A	b
0.25	2.68750	-0.75128
0.50	2.46620	-0.77215
1.00	2.24000	-0.78739
1.50	2.02430	-0.80821
2.00	2.10560	-0.79878
∞	1.80820	-0.66702

Appendix D

ANSWERS TO SELECTED PROBLEMS

The solutions manual (pdf) and a complete set of *Mathcad* problem-solution files are downloadable from <http://www.prenhall.com/> under the **Instructor Support** option. Both *Mathcad* and *TK Solver* solutions are also available to instructors from the author's website at <http://www.designofmachinery.com/registered/professor.html>. A family tree of related problems in various chapters is shown in the solutions manual.

CHAPTER 1 INTRODUCTION TO DESIGN

- 1-4 1 000 lb_f, 31.081 slug, 2.59 blob, 453.592 kg, 4 448.2 N.
- 1-5 25.9 lb_f.
- 1-6 220.5 lb_f, 220.5 lb_m, 6.85 slug, 0.571 blob, 980.7 N.

CHAPTER 2 MATERIALS AND PROCESSES

- 2-6 $E = 207 \text{ GPa}$, $U = 2.7 \text{ N-m}$, steel.
- 2-8 $E = 207 \text{ GPa}$, $U = 1.3 \text{ N-m}$, magnesium.
- 2-9 $E = 16.7 \text{ Mpsi}$, $U_{el} = 300 \text{ psi}$, titanium.
- 2-12 $U_T = 82.7 \text{ MPa}$, $U_R = 0.41 \text{ MPa}$.
- 2-14 $S_{ut} = 170 \text{ kpsi}$, 359HV, 36.5HRC.
- 2-16 Iron and carbon, 0.95% carbon, can be through hardened or surface hardened without carburization.
- 2-27 $S_y = 88.1 \text{ kpsi}$, $S_y = 607 \text{ MPa}$.
- 2-34 The most commonly used metal is zinc. The process is called "galvanizing" and it is accomplished by electroplating or hot dipping.

CHAPTER 3 LOAD DETERMINATION

- 3-3 $T = 255 \text{ N-m}$ on sprocket, $T = 90 \text{ N-m}$ on arm, $M = 255 \text{ N-m}$ on arm.
- 3-6 55 114 N.
- 3-7 12 258 N.
- 3-8 $\omega_h = 31.6 \text{ rad/sec}$, $\omega_d = 30.1 \text{ rad/sec}$.
- 3-10 $R_1 = V = -1821 \text{ N}$ @ 0 to 0.7 m, $R_1 = 2802 \text{ N}$, $M = -1275 \text{ N-m}$ @ 0.7 m.
- 3-11 3 056-N dynamic force and 408-mm deflection. $V = -5677 \text{ N}$ @ 0 to 0.7 m, $M = -3973 \text{ N-m}$ @ 0.7 m, $R_1 = 5676 \text{ N}$, $R_2 = 8733 \text{ N}$.
- 3-15 $\mu = 0.025$.
- 3-18 Tipover begins at 18.7 mph, load slides at 14.8 to 18.3 mph.
- 3-22 (a) 897 N, (b) 3 592 N.
- 3-23 (a) $R_1 = 264 \text{ N}$, $R_2 = 316 \text{ N}$, $V = -316 \text{ N}$, $M = 126 \text{ N-m}$.
- 3-24 (a) $R_1 = 620 \text{ N}$, $M_1 = 584 \text{ N-m}$, $V = 620 \text{ N}$, $M = -584 \text{ N-m}$.
- 3-25 (a) $R_1 = -353 \text{ N}$, $R_2 = 973 \text{ N}$, $V = 580 \text{ N}$, $M = -216 \text{ N-m}$.
- 3-27 (a) $R_1 = 53895 \text{ N}$, $V = 53895 \text{ N}$, $M = -87040 \text{ N-m}$.
- 3-34 Row (a) $V_{max} = 1000 \text{ lb}$ at $x = 16$ to 18 in, $M_{max} = 2000 \text{ lb}$ at $x = 16$ in.
- 3-48 $\omega_h = 10.1 \text{ Hz}$.

CHAPTER 4 STRESS, STRAIN, AND DEFLECTION

- 4-1 $\sigma_1 = 1207 \text{ psi}$, $\sigma_2 = 0$, $\sigma_3 = -207 \text{ psi}$, $\tau_{max} = 707 \text{ psi}$.
- 4-4 (a) $\sigma_1 = 114 \text{ MPa}$, $\sigma_2 = 0$, $\sigma_3 = 0 \text{ MPa}$, $\tau_{max} = 57 \text{ MPa}$.
 (b) 9.93 MPa.
 (c) 4.41 MPa.
 (d) $\sigma = 53.6 \text{ MPa}$, $\tau = 1.73 \text{ MPa}$.
 (e) $\sigma_1 = 72.8 \text{ MPa}$, $\sigma_2 = 0$, $\sigma_3 = 0$, $\tau_{max} = 36.4 \text{ MPa}$.
- 4-6 (a) $\sigma_1 = 1277.8 \text{ MPa}$, $\sigma_2 = 0$, $\sigma_3 = 0$, $\tau_{max} = 639 \text{ MPa}$.
 (b) 111.6 MPa.
 (c) 49.6 MPa.
 (d) $\sigma = 540 \text{ MPa}$, $\tau = 1.7 \text{ MPa}$.
 (e) $\sigma_1 = 636 \text{ MPa}$, $\sigma_2 = 0$, $\sigma_3 = 0$, $\tau_{max} = 318 \text{ MPa}$.
- 4-7 OD = 0.375 in, ID = 0.230 in.
- 4-8 199 mm.
- 4-10 24.5-MPa principal stress, -128-mm deflection.
- 4-11 76-MPa stress, -400-mm deflection.
- 4-15 4.5-mm-dia pin.

- 4-18 13 254-lb force per rod, 132 536-lb force total, 0.36-in deflection.
- 4-19 2.125-in-dia pin, 2.375-in outside radius.
- 4-22 (a) 5.72 MPa. (b) 22.87 MPa.
- 4-23 Row (a) $R_1 = 264 \text{ N}$, $R_2 = 316 \text{ N}$, $V = -316 \text{ N}$ over $b \leq x \leq l$, $M = 126 \text{ N-m}$ @ $x = b$, $\theta = 0.33 \text{ deg.}$, $y = -1.82 \text{ mm}$, $\sigma_{max} = 88.7 \text{ MPa}$.
- 4-24 Row (a) $R_1 = 620 \text{ N}$, $M_1 = 584 \text{ N-m}$, $V = 620 \text{ N}$ @ $x = 0$, $M = -584 \text{ N-m}$ @ $x = 0$, $\theta = -2.73 \text{ deg.}$, $y = -32.2 \text{ mm}$, $\sigma_{max} = 410 \text{ MPa}$.
- 4-25 Row (a) $R_1 = -353 \text{ N}$, $R_2 = 973 \text{ N}$, $V = 578 \text{ N}$ @ $x = b$, $M = -216 \text{ N-m}$ @ $x = b$, $\theta = -0.82 \text{ deg.}$, $y = -4.81 \text{ mm}$, $\sigma_{max} = 152 \text{ MPa}$.
- 4-26 Row (a) $R_1 = 112 \text{ N}$, $R_2 = 559 \text{ N}$, $R_3 = -52 \text{ N}$, $V = -428 \text{ N}$ @ $x = b$, $M = 45 \text{ N-m}$ @ $x = a$, $\theta = 0.06 \text{ deg.}$, $y = -0.02 \text{ mm}$, $\sigma_{max} = 31.5 \text{ MPa}$.
- 4-29 Row (a) 307.2 N/mm.
- 4-30 Row (a) 17.7 N/mm.
- 4-31 Row (a) 110.6 N/mm.
- 4-32 Row (a) 2 844 N/mm.
- 4-33 Row (a) $\sigma_1 = 21.5 \text{ MPa}$ @ A, $\sigma_1 = 16.1 \text{ MPa}$ @ B.
- 4-34 Row (a) $y = -1.62 \text{ mm}$.
- 4-35 Row (a) $k = 31 \text{ N/mm}$.
- 4-37 $e = 0.84 \text{ mm}$, $\sigma_i = 410 \text{ MPa}$, $\sigma_o = -273 \text{ MPa}$.
- 4-41 (a) 38.8 MPa, (b) 11.7 MPa.
- 4-49 Row (a) Johnson—part: (a) 1.73 kN, (b) 1.86 kN, (c) 1.94 kN, (d) Euler 676 N.
- 4-50 Row (a) Euler—part: (a) 5.42 kN, (b) 8.47 kN, (c) 12.8 kN, (d) 1.23 kN.
- 4-51 Row (a) Johnson—part: (a) 57.4 kN, (b) 58.3 kN, (c) 58.9 kN, (d) 48.3 kN.
- 4-52 Row (a) part: (a) 18.6 kN, (b) 18.7 kN, (c) 18.8 kN, (d) 17.9 kN.
- 4-69 $\sigma_i = 132 \text{ MPa}$, $\sigma_o = -204 \text{ MPa}$.
- 4-75 Row (a) $\sigma_{nom} = 40 \text{ Mpa}$, $K_t = 1.838$, $\sigma_{max} = 73.5 \text{ Mpa}$.

CHAPTER 5 STATIC FAILURE THEORIES

- 5-1 Row (a) $\sigma_1 = 1 207 \text{ psi}$, $\sigma_2 = 0 \text{ psi}$, $\sigma_3 = -207 \text{ psi}$, $\tau_{13} = 707 \text{ psi}$, $\sigma' = 1 323 \text{ psi}$.
Row (h) $\sigma_1 = 1 140 \text{ psi}$, $\sigma_2 = 250 \text{ psi}$, $\sigma_3 = 110 \text{ psi}$, $\tau_{13} = 515 \text{ psi}$, $\sigma' = 968 \text{ psi}$.
- 5-4 (a) $N = 2.6$, (b) $N = 30.2$, (c) $N = 39.3$, (d) $N = 5.6$, (e) $N = 4.1$.
- 5-6 (a) $N = 0.23$, (b) $N = 2.7$, (c) $N = 3.5$, (d) $N = 0.56$, (e) $N = 0.47$.
- 5-7 for $N = 3.5$, $OD = 0.375 \text{ in}$, $ID = 0.281 \text{ in}$.
- 5-8 $ID = 198 \text{ mm}$.
- 5-10 $N = 5.3$.
- 5-11 $N = 1.7$.

- 5-15 $N = 1.0$ by definition if stress = strength.
- 5-17 $N = 3.5$.
- 5-19 2.250-in-dia pin and 2.250-in outside radius.
- 5-22 (a) $N = 40.4$ (b) $N = 10.1$.
- 5-23 Row (a)—part: (a) $N = 3.4$, (b) $N = 1.7$.
- 5-24 Row (a)—part: (a) $N = 0.73$, (b) $N = 0.37$.
- 5-25 Row (a)—part: (a) $N = 2$, (b) $N = 1$.
- 5-26 Row (a)—part: (a) $N = 9.5$, (b) $N = 4.8$.
- 5-27 (a) $a = 166$ mm, $b = 94$ mm, $N = 1.5$, (b) $a = 208$ mm, $b = 70$ mm, $N = 1.5$.
- 5-32 Modified-Mohr, $N = 1.6$.
- 5-33 Row (a) $\sigma' = 30.2$ MPa at point A, $\sigma' = 27.9$ MPa at point B.
- 5-34 Row (a) Distortion-energy theory: $N = 13.2$ at point A, $N = 14.3$ at point B, Max shear theory: $N = 11.6$ at point A, $N = 12.4$ at point B, Max normal stress theory: $N = 18.6$ at point A, $N = 24.8$ at point B.
- 5-35 Row (a) Coulomb-Mohr theory: $N = 13.4$ at point A, $N = 16.1$ at point B, Modified-Mohr theory: $N = 16.3$ at point A, $N = 21.7$ at point B.
- 5-37 (a) $N = 1.7$ at inner fiber, $N = 2.6$ at outer fiber; (b) $N = 1.0$ at inner fiber, $N = 4.4$ at outer fiber.
- 5-38 $N = 1.5$.
- 5-39 Crack half-width = 0.216 in.
- 5-41 (a) $N = 9.4$, (b) $N = 24.5$.
- 5-65 (a) $N_a = 1.8$, (b) $N_b = 2.6$.
- 5-68 $d = 1.500$ in.

CHAPTER 6 FATIGUE FAILURE THEORIES

- 6-1 Row (a) $\Delta\sigma = 1\,000$, $\sigma_a = 500$, $\sigma_m = 500$, $R = 0$, $A = 1.0$.
 Row (c) $\Delta\sigma = 1\,000$, $\sigma_a = 500$, $\sigma_m = 1\,000$, $R = 0.33$, $A = 0.50$.
 Row (e) $\Delta\sigma = 1\,500$, $\sigma_a = 750$, $\sigma_m = -250$, $R = -2.0$, $A = -3.0$.
- 6-3 $N_f = 0.31$.
- 6-6 (a) 0.14, (b) 1.17, (c) 1.6, (d) 0.24, (e) 0.25.
- 6-7 for $N_f = 1.5$, $OD = 0.375$ in, $ID = 0.299$ in. Round to $ID = 0.281$ in for $N_f = 1.8$.
- 6-8 $ID = 190$ mm assuming machined, 99.9% reliability, and room temperature.
- 6-10 $N_f = 2.4$.
- 6-11 $N_f = 0.79$.
- 6-15 Row (a) $a = 0.062$ in $^{0.5}$, $q = 0.89$, $K_f = 3.05$.
- 6-17 $N_f = 2.7$ assuming forged, 99.99% reliability, and room temperature.
- 6-19 2.750-in-dia pin and 2.625-in outside radius (machined, 90% reliability, and 100 °F).

- 6-22 (a) $N_f = 21.3$, (b) $N_f = 5.3$ assuming machined, 99.999% reliability, and 37 °C.
- 6-23 Row (a) Use a material with $S_{ut} = 468$ MPa (assuming $C_{temp} = C_{surf} = C_{reliab} = 1$).
- 6-24 Row (a) Use a material with $S_{ut} = 676$ MPa (assuming $C_{temp} = C_{surf} = C_{reliab} = 1$).
- 6-25 Row (a) Use a material with $S_{ut} = 550$ MPa (assuming $C_{temp} = C_{surf} = C_{reliab} = 1$).
- 6-26 Row (a) Use a material with $S_{ut} = 447$ MPa ($C_{temp} = C_{reliab} = 1$, $C_{surf} = 0.895$).
- 6-27 (a) $a = 190$ mm, $b = 100$ mm, $N = 2.1$, (b) $a = 252$ mm, $b = 100$ mm, $N = 2$ (both assuming machined, 90% reliability, and 40 °C).
- 6-29 $N_f = 2.6$ assuming machined, 99.999% reliability, and 37 °C.
- 6-31 $N_f = 1.8$ assuming machined, 99.999% reliability, and 37 °C.
- 6-33 Row (a) Use a material with $S_{ut} = 362$ MPa (machined, 50% reliability, and 37 °C).
- 6-34 Row (a) Use a material with $S_{ut} = 291$ for $N_f = 1.5$ MPa (machined, 50% reliability, and 37 °C).
- 6-37 (a) $N_f = 1.8$, (b) $N_f = 0.92$ assuming machined, 90% reliability, and 37 °C.
- 6-39 $N_f = 1.9$ using SEQA method and assuming ground shaft, 50% reliability, and 37 °C.
- 6-41 (a) $N_f = 3.3$, (b) $N_f = 8.6$ assuming machined, 99.999% reliability, and 37 °C.
- 6-47 $N_f = 1.5$ assuming machined, 90% reliability, and 60 °C.
- 6-52 $t_{min} = 3.2$ mm.
- 6-64 Row (a) $\sigma_m = 0.0$ MPa, $\sigma_a = 251.9$ MPa.

CHAPTER 7 SURFACE FAILURE

- 7-1 $A_r = 0.333$ mm².
- 7-2 $\mu = 0.4$.
- 7-3 $N = 4.6E6$.
- 7-4 $\sigma_1 = -61$ kpsi, $\sigma_2 = -61$ kpsi, $\sigma_3 = -78$ kpsi.
- 7-8 64.4-mm total width.
- 7-10 0.15-mm total width.
- 7-13 (a) 19.6 min dry, (b) 9.8 min wet.
- 7-16 1-mm dia contact patch, $\sigma_{zball} = -1\ 900$ MPa, $\sigma_{zplate} = -1\ 900$ MPa.
- 7-18 0.166-mm total contact width, $\sigma_{zcylinder} = \sigma_{xcylinder} = -123$ MPa, $\sigma_{zplate} = \sigma_{xplate} = -123$ MPa.
- 7-20 Contact-patch half-dimensions: 0.933 × 0.713 mm, $\sigma_1 = -5.39$ GPa, $\sigma_2 = -5.81$ GPa, $\sigma_3 = -7.18$ GPa.
- 7-22 (a) $\sigma_1 = -66.9$ MPa, $\sigma_2 = -75.2$ MPa, $\sigma_3 = -79.0$ MPa, (b) $\sigma_1 = -106$ MPa, $\sigma_2 = -119$ MPa, $\sigma_3 = -125$ MPa.
- 7-23 $\sigma_1 = -24\ 503$ psi, $\sigma_2 = -30\ 043$ psi, $\sigma_3 = -57\ 470$ psi.
- 7-39 $t = 4.7$ min.
- 7-42 The principal stresses are maximum at the surface. They are: $\sigma_1 = -276.7$ MPa, $\sigma_2 = -393.3$ MPa, $\sigma_3 = -649.0$ MPa. The maximum shear stress is $\tau_{13} = 186.1$ MPa.

CHAPTER 10 SHAFTS, KEYS, AND COUPLINGS

- 10-1 Row (a) $d = 1.188$ in, assuming machined, 99% reliability, and 100°F.
- 10-2 Row (a) $d = 48.6$ mm, assuming machined, 99% reliability, and 30°C.
- 10-4 Row (a) $y = 0.003$ 6 in, $\theta = 0.216$ deg.
- 10-5 Row (a) $y = -5.7$ μm , $\theta = 1.267$ deg.
- 10-6 Row (a) 3/8-in square key, 0.500 in long, $N_f = 2.1$, $N_{bearing} = 2.1$.
- 10-8 Shaft ID = 191 mm, assuming machined, 99.9% reliability, and 30°C.
- 10-9 Row (a) $d = 1.188$ in, assuming a notch radius of 0.015 in, machined, 99% reliability, and 100°F.
- 10-11 Row (a) 0.0007 to 0.0021 in of interference over tolerance range.
- 10-13 Row (a) 2 102 rad/sec or 20 075 rpm, or 334.5 Hz.
- 10-15 Row (a) min = 0, avg = 11.9 hp, max = 23.8 hp.
- 10-16 Row (a) min = 0, avg = 5.2 kW, max = 10.5 kW.
- 10-17 Row (a) $N = 0.61$ at key on right end of roller, $\theta = 0.20$ deg, $f_n = 1\ 928$ Hz.
- 10-18 Row (a) $y = -30.0$ μm to 22.9 μm .
- 10-19 Row (a) $d = 1.337$ in, $N_A = 2.0$, $N_B = 3.1$.
- 10-37 $\delta_{min} = 0.06$ mm, $\delta_{max} = 0.12$ mm.
- 10-38 $r_i = 1.00$ in, $r_o = 14.66$ in, $t = 0.800$ in.

CHAPTER 11 BEARINGS AND LUBRICATION

- 11-1 Row (a)—part (a) $d = 1.188$ in, $l = 1.485$ in, $C_d = 1.8E-3$ in, $R_L = 125$ lb, $R_R = 1125$ lb, $\eta_L = 0.204$ μreyn , $\eta_R = 1.84$ μreyn , $p_{avgL} = 71$ psi, $p_{avgR} = 638$ psi, $T_{rL} = 0.15$ lb-in, $T_{rR} = 1.38$ lb-in, $\Phi_L = 0.004$ hp, $\Phi_R = 0.033$ hp.
Part (b) #6300 bearing at left end gives $1.4E9$ cycles L_{10} life on left bearing and #6306 bearing at left end gives $8.8E7$ cycles L_{10} life on right bearing.
- 11-3 267 cP.
- 11-5 0.355 in-lb.
- 11-6 10.125 μm .
- 11-7 $T_r = 3.74$ N-m, $T_0 = 2.17$ N-m, $T_s = 2.59$ N-m, $\Phi = 979$ W.
- 11-8 $d = 220$ mm, $l = 165$ mm, $C_d = 0.44$ mm, $R_L = R_R = 26.95$ kN, $\eta = 181$ cP, $p_{avg} = 743$ kPa, $T_r = 12.9$ N-m, $\Phi = 67.7$ W.
- 11-10 $h_{min} = 4.94$ μm .
- 11-14 $\eta = 13$ cP, $T_s = 519$ N-mm, $T_0 = 325$ N-mm, $T_r = 699$ N-mm, $\Phi = 183$ W, $P = 19.222$ kN.
- 11-17 Row (a)—part (a) $d = 40$ mm, $l = 30$ mm, $C_d = 0.04$ mm, $R_L = 6\ 275$ N, $R_R = 7\ 525$ N, $\eta_L = 20.7$ cP, $\eta_R = 24.8$ cP, $p_{avgL} = 5\ 229$ kPa, $p_{avgR} = 6\ 271$ kPa, $T_{rL} = 468$ N-m, $T_{rR} = 561$ N-m, $\Phi_L = 88.2$ W, $\Phi_R = 106$ W.
Part (b) #6308 bearing at left end gives $1.41E8$ cycles L_{10} life on left bearing and #6309 bearing at left end gives $1.58E8$ cycles L_{10} life on right bearing.

11-20 Specific film thickness = 0.53—boundary lubrication.

11-33 Row (a) left, #6300; right, #6314.

11-36 Row (a) left, #6300; right, #6320.

CHAPTER 12 SPUR GEARS

12-1 $d_p = 5.4$ in, addendum = 0.2 in, dedendum = 0.25 in, $OD = 5.8$ in, $p_c = 0.628$ in.

12-3 1.491.

12-5 30.33 deg.

12-7 7.159 : 1.

12-9 96:14 and 96:14 compounded give 47.02:1.

12-11 $N_{ring} = 75$ t, ratio between arm and sun gear = 1 : 3.273.

12-14 7 878 in-lb on pinion shaft, 19 524 in-lb on gear shaft.

12-16 $p_d = 3$ and $F = 4.25$ in gives $N_{pinion} = 5.4$ and $N_{gear} = 2.0$.

12-18 $p_d = 4$, $F = 4.125$ in, gives $N_{pinion} = 3.5$ and $N_{gear} = 2.0$.

12-20 202 N-m (1 786 in-lb) on sun shaft, 660 N-m (5 846 in-lb) on arm shaft.

12-23 $p_d = 3$, $F = 3.500$ in, gives $N_{pinion} = 7.7$ and $N_{gear} = 2.8$.

12-25 $p_d = 4$, $F = 4.000$ in, gives $N_{pinion} = 4.8$ and $N_{gear} = 1.8$.

12-27 $T_1 = 1\ 008$ N-m, $T_2 = 9\ 184$ N-m, $T_3 = 73\ 471$ N-m, $T_4 = 661\ 236$ N-m.

12-28 $p_d = 3$, $F = 4.500$ in.

12-29 $p_d = 1.5$, $F = 9.375$ in.

12-30 $p_d = 0.75$, $F = 17$ in.

12-31 104:12 and 144:16 compounded give exactly 78:1.

12-52 $T_1 = 40.9$ N-m, $T_2 = 295$ N-m, $T_3 = 2172$ N-m.

12-53 $F = 1.250$ in, $p_d = 8$.

CHAPTER 13 HELICAL, BEVEL, AND WORM GEARS

13-1 $d_p = 5.4$ in, addendum = 0.200 in, dedendum = 0.250 in, $OD = 5.8$ in, $p_t = 0.628$ in, $p_h = 0.544$ in, $p_a = 1.088$ in.

13-3 $m_p = 1.491$, $m_F = 0.561$.

13-5 $\alpha_g = 83.66^\circ$, $\alpha_p = 6.34^\circ$, $d_g = 21$ in, $d_p = 2.33$ in, $W_{ag} = W_{rp} = 25$ lb, $W_{rg} = W_{ap} = 2.8$ lb.

13-7 $\alpha_g = 78.69^\circ$, $\alpha_p = 11.31^\circ$, $d_g = 11.429$ in, $d_p = 2.286$ in, $W_{ag} = 60.5$ lb, $W_{ap} = -169.64$ lb, $W_{rp} = 136.28$ lb, $W_{rg} = 209.01$ lb.

13-9 $l = 20$ mm, $\lambda = 7.26^\circ$, λ per tooth = 3.63° , $d_g = 140$ mm, $c = 95$ mm, self-locking.

13-11 $l = 5$ mm, $\lambda = 2.28^\circ$, λ per tooth = 2.28° , $d_g = 130.5$ mm, $c = 85.3$ mm, self-locking.

13-12 $T_w = 22.4$ N-m, $T_g = 492$ N-m rated, $W_t = 7\ 028$ N, friction = 215 N, output power available = 2.34 kW, rated input power = 2.91 kW.

- 13-14 7 878 in-lb on pinion, 19 524 in-lb on gear.
- 13-16 $p_d = 3$ and $F = 3.25$ in gives $N_{pinion} = 5.6$ and $N_{gear} = 2.0$.
- 13-18 $p_d = 4$ and $F = 2.75$ in gives $N_{pinion} = 2.8$ and $N_{gear} = 1.6$.
- 13-20 $p_d = 18$ and $F = 1$ in gives $N_{pinion} = 2.0$ —bending, with $N_{gear} = 13.6$ —bending.
- 13-23 $p_d = 16$ and $F = 1$ in gives $N_{pinion} = 1.4$ —surface failure which limits the design.
- 13-27 Rated input power = 2.11 hp, output power available = 1.69 hp, rated output torque = 1 290 lb-in.
- 13-49 $F = 1.375$ in, $p_d = 10$.

CHAPTER 14 SPRING DESIGN

- 14-1 $k = 1.6$ N/mm.
- 14-3 $S_{ys} = 110\ 931$ psi, $S_{us} = 148\ 648$ psi.
- 14-4 $S_{fs} = 85.6$ kpsi.
- 14-6 $C = 10$, $k = 1.01$ N/mm.
- 14-7 $f_n = 363.4$ Hz.
- 14-10 $k = 7\ 614$ N/m, $f_n = 1.39$ Hz.
- 14-11 $d = 0.125$ in, $D = 0.94$ in, $L_f = 3.16$ in, $k = 36$ lb/in, 13.75 coils RH, music wire, squared and ground ends, unpeened, set.
- 14-13 $N_a = 19.75$, $D = 1.37$ in, $L_f = 7.84$ in, $L_{shut} = 6.79$ in, $k = 266.6$ lb/in, $y_{initial} = 0.19$ in, hole = 1.75 in.
- 14-17 $d = 3.5$ mm, $D = 28$ mm, $L_f = 93.63$ mm, $k = 5876$ N/m, 12.75 coils, music wire, std. hooks. $N_y = 2.2$ torsion fatigue in hook, $N_f = 1.7$ bending fatigue in hook, $N_{surge} = 5.5$.
- 14-19 $d = 6.5$ mm, $D_o = 65$ mm, $L_f = 171$ mm, $N_{tot} = 10.75$ coils, $N_y = 1.6$ shut, $N_f = 1.3$, $N_{surge} = 9.3$.
- 14-21 $d = 5$ mm, $D = 40$ mm, $L_f = 116.75$ mm, $k = 8\ 967$ N/m, 13 coils RH, music wire, S&G ends, unpeened, set.
- 14-22 $d = 16$ mm, $D = 176$ mm, $k = 1\ 600$ N-m/rev, 4.5 coils RH, 40-mm straight ends, A229 oil-tempered wire, unpeened, relieved.
- 14-24 $d = 15$ mm, $D = 124.5$ mm, $k = 248$ N-m/rev, 31 coils RH, 40-mm straight ends, A229 oil-tempered, unpeened, relieved.
- 14-26 $d_o = 39.55$ mm, $d_i = 19.77$ mm, $t = 0.76$ mm, $h = 1.075$ mm, $h/t = 1.414$, 1-mm working deflection, $S_{ut} = 1\ 700$ MPa, $N_s = 1.11$.
- 14-42 $D_o = 3.000$ in, $D_i = 1.500$ in, $t = 0.125$ in, $h = 0.050$ in.
- 14-44 A228 wire, $d = 0.125$ in, $D_o = 1.000$ in, $N_t = 15$, $L_f = 3.600$ in.

CHAPTER 15 SCREWS AND FASTENERS

- 15-2 Lifting torque = 42.68 lb-in, lowering torque = 18.25 lb-in, lifting efficiency = 27.95%, lowering efficiency = 65.36%, screw is self-locking.

- 15-4 Two M12 × 1.75 bolts, ISO class 8.8, $F_{preload} = 59\%$ proof strength, $N_y = 1.7$. $N_{sep} = 2.5$.
- 15-6 Two M24 × 3 bolts, ISO class 12.9, $F_{preload} = 55\%$ proof strength, $N_y = 1.7$, $N_{sep} = 1.6$.
- 15-7 $N_y = 1.4$, $N_{sep} = 13.7$.
- 15-9 $N_f = 1.3$, $N_y = 1.5$, $N_{sep} = 8.9$.
- 15-11 1 252 in-lb.
- 15-13 718 in-lb.
- 15-17 (a) $K_{eff} = 5.04E9$ N-m, aluminum dominates.
 (b) $K_{eff} = 9.52E9$ N-m, steel dominates.
 (c) $K_{eff} = 2.73E8$ N-m, rubber dominates.
 (d) $K_{eff} = 2.66E8$ N-m, rubber dominates.
 (e) $K_{eff} = 9.04E9$ N-m, no one material dominates.
- 15-18 (a) $K_{eff} = 2.74E7$ N-m, aluminum dominates.
 (b) $K_{eff} = 5.18E7$ N-m, steel dominates.
 (c) $K_{eff} = 3.73E5$ N-m, rubber dominates.
 (d) $K_{eff} = 3.70E5$ N-m, rubber dominates.
 (e) $K_{eff} = 4.92E7$ N-m, no one material dominates.
- 15-20 Use 10 M12 × 1.75, ISO class 8.8 cap screws, torqued to 90% of proof strength on a 107.5-mm-dia bolt circle. $N_f = 1.3$, $N_{sep} = 34$, $N_y = 1.2$ dynamic and 1.2 static.
- 15-23 Row (a)—Four M5 × 0.8 × 20-mm-long cap screws, class 4.6, $F_{preload} = 1.72$ kN, (54% of proof), load on top bolt: 1.73 kN, $N_{sep} = 58$, $N_y = 2.0$.
- 15-24 Row (a)—Four M4 × 0.7 × 20-mm-long cap screws, class 4.8, $F_{preload} = 2.04$ kN, (75% of proof), load on top bolts when force is maximum and on bottom bolts when force is minimum: 2.05 kN, load on top bolts when force is minimum and on bottom bolts when force is maximum: 2.05 kN, $N_y = 1.5$, $N_{sep} = 69$, $N_f = 10$.
- 15-25 Row (a)—Four M4 × 0.7 × 20-mm-long cap screws, class 4.8, $F_{preload} = 2.04$ kN, (75% of proof), load on top bolts when force is maximum and on bottom bolts when force is minimum: 2.05 kN, load on top bolts when force is minimum and on bottom bolts when force is maximum: 2.05 kN, $N_y = 1.5$, $N_{sep} = 69$, $N_f = 10$.
- 15-39 $d = 8$ mm: number of threads = 4.6.
- 15-41 Class 4.6: $F_{ut} = 98$ kN.

CHAPTER 16 WELDING

- 16-1 A CJP butt weld in tension develops the full strength of the section: $P_{max} = 180\,000$ lb.
- 16-3 Bracket (weld) length = 3.592 in.
- 16-5 Maximum dynamic load = 525 lb.
- 16-6a Weld size required = 3/16 in.
- 16-7a Weld size required = 1/4 in.
- 16-9 Weld size required = 10 mm.

CHAPTER 17 CLUTCHES AND BRAKES

17-1 $T = 380 \text{ N-m}$, $p_{max} = 1.819 \text{ MPa}$, molded or sintered metal lining will work.

17-3 $d_o = 140 \text{ mm}$, $d_i = 80 \text{ mm}$, $\Phi = 7.85 \text{ kW}$.

17-5 $N = 7$, $d_o = 104 \text{ mm}$, $d_i = 60 \text{ mm}$, $\Phi = 12.6 \text{ kW}$.

17-7 (a) $T = 10.7 \text{ N-m}$, $F_a = 798 \text{ N}$,
 (b) Will self-lock when $c = 233 \text{ mm}$.

17-11 (a) $T = 30.5 \text{ N-m}$ (15.7 top shoe, 14.8 bottom shoe), $F_a = 1353 \text{ N}$,
 (b) Will self-lock when $c = 320 \text{ mm}$.

17-13 $T = 26 \text{ N-m}$, $F_a = 1689 \text{ N}$.

17-15 $T = 56.5 \text{ N-m}$ (32.5 top shoe, 24 bottom shoe), $F_a = 2194 \text{ N}$.

17-17 (a) short shoe: $T = 11.3 \text{ N-m}$, $F_a = 806 \text{ N}$,
 long shoe: $T = 11.2 \text{ N-m}$, $F_a = 750 \text{ N}$.

(b) short shoe: $T = 15.1 \text{ N-m}$, $F_a = 1075 \text{ N}$,
 long shoe: $T = 14.8 \text{ N-m}$, $F_a = 982 \text{ N}$.

(c) short shoe: $T = 18.8 \text{ N-m}$, $F_a = 1344 \text{ N}$,
 long shoe: $T = 18.3 \text{ N-m}$, $F_a = 1197 \text{ N}$.

17-18 (a) short shoe: $T = 21.8 \text{ N-m}$, $F_a = 806 \text{ N}$,
 long shoe: $T = 19.6 \text{ N-m}$, $F_a = 750 \text{ N}$.

(b) short shoe: $T = 29.1 \text{ N-m}$, $F_a = 1075 \text{ N}$,
 long shoe: $T = 25.8 \text{ N-m}$, $F_a = 982 \text{ N}$.

(c) short shoe: $T = 36.3 \text{ N-m}$, $F_a = 1344 \text{ N}$,
 long shoe: $T = 31.9 \text{ N-m}$, $F_a = 1197 \text{ N}$.

17-21 Top pivot: $R_x = -392.7 \text{ N}$, $R_y = -218.2 \text{ N}$,
 bottom pivot: $R_x = -368.9 \text{ N}$, $R_y = -123.0 \text{ N}$.

17-23 $R_x = 1005 \text{ N}$, $R_y = -808 \text{ N}$.

17-25 Top pivot: $R_x = 1694 \text{ N}$, $R_y = -45.3 \text{ N}$,
 bottom pivot: $R_x = 325 \text{ N}$, $R_y = -147.7 \text{ N}$.

17-29 $T = 131 \text{ N-m}$.

17-31 Sintered metal, $m = 0.30$, $r_i = 40 \text{ mm}$, $r_o = 70 \text{ mm}$, $q = 90 \text{ deg}$, $F = 2.83 \text{ kN}$.